PIERS 2011 Marrakesh

Progress In Electromagnetics Research Symposium

Abstracts

March 20–23, 2011
Marrakesh, MOROCCO

www.emacademy.org
www.piers.org

PIERS 2011 Marrakesh Abstracts

Published by

The Electromagnetics Academy
777 Concord Avenue, Suite 207
Cambridge, MA 02138

www.emacademy.org
www.piers.org

ISSN: 1559-9450
ISBN: 978-1-934142-15-8

Progress In Electromagnetics Research Symposium

March 20–23, 2011

Marrakesh, MOROCCO

PIERS 2011 MARRAKESH ORGANIZATION

PIERS Founding Chair

J. A. Kong, MIT, USA

PIERS Chair

L. Tsang, University of Washington, USA

PIERS 2011 Marrakesh General Chair

S. Zouhdi, University Paris-Sud, France

PIERS 2011 Marrakesh General Vice Chairs

A. Priou, University Paris Ouest, France

L.-W. Li, National University of Singapore, Singapore

PIERS 2011 Marrakesh International Advisory Committee

D. Aboutajdine	Y. M. Antar	D.-C. Chang	W. C. Chew
H. T. Chua	P. de Maagt	S. El-Ghazali	N. Engheta
R. D. Graglia	T. M. Habashy	Y. Hao	S. He
M. Inggs	Y. Kivshar	K. Kobayashi	D. Lesselier
K. M. Luk	J. Mosig	M. Ney	A. I. Nosich
B. Perlman	Y. Rahmat-Samii	A. Razek	A. B. Samokhin
H. W. Schürmann	Y. V. Shestopalov	A. Sihvola	M. Sorolla
A. Vinogradov	J. Vrba	W. X. Zhang	N. Zheludev

PIERS 2011 Marrakesh Technical Program Committee

T. Akalin	I. Akduman	F. Bouillault	A. de Lustrac
H. El Hennawy	Y. Fan	D. Felbacq	Y. Guo
W. Hong	J. Hu	Z. Hu	S. Iqbal
J.-M. E. Lopez	B. Lukỳanchuk	S. Maier	C. Marchand
F. Medina-Mena	H. Ouslimani	P. Pampaloni	R. Plana
E. Pottier	O. Ramahi	M. Saillard	J. T. Sri Sumantyo
R. Staraj	S. Tedjini	S. Trabelsi	D. P. Tsai
A. Urbas	S. Weiss	G. Xie	A. I. Zaghloul

PIERS 2011 Marrakesh Organizing Committee

Y. Bernard	L. Daniel	O. Dubrunfaut	L. Santandrea
H. Talleb			

PIERS 2011 Marrakesh Local Organizing Committee

N. Adnet
H. Belyamoun
R. Corcolle
P. P. Ding
C. Gilbert
M. Gueye
X.-K. Han
O. Hubert
L. Idoughi
F.-H. Meng
T. T. Nguyen
C. Pareige
A. Rabhi
T.-J. Yuan
T. Zhang
L.-Y. Zhou
Y. Zhu

PIERS 2011 MARRAKESH SESSION ORGANIZERS

I. Abdulhalim
Y. Bernard
L. R. Cander
L. Capineri
D. A. Cardimona
X. D. Chen
Y. F. Chen
I.-S. Choi
F. Choubani
C. Craeye
L. Crocco
L. Daniel
E. DelRe
D. Diallo
R. Doebbelin
M. Drissi
A. P. Duffy
M. D'Urso
M. I. Dyakonov
M. El Hachemi Benbouzid
N. Ayuso
F. J. Falcone
Y. Fan
D. Felbacq
G. Franceschetti
E. Gescheidtová
H. W. Giessen
A. A. Glazunov
P. Grelu
B. Guizal
H. Hafdallah-Ouslimani
H.-E. Horng
J. H. Hu
T. Isernia
K. Iwatsuki
S. Kabir
Y. H. Kerr
A. A. Kishk
M. Klemm
W. Knap
K. Kobayashi
P. Kosmas
I. Kypraios
D. Lesselier
J. Lettl
J.-C. S. Levy
J. H. Li
A. Litman
Y. L. Lu
S. A. Maier
A. Massa
F. Medina
A. F. Morabito
G. V. Morozov
M. Nadi
L. Nowosielski
J. Ojeda-Castañeda
M. Oristaglio
A. Ourir
P. Paillou
F. Rachidi
V. Ramos
S. Residori
J.-E. Rhazi
P. Rocca
M. Rubinstein
A. Sharaiha
Y. V. Shestopalov
O. Sidek
G. Sonnino
R. Staraj
M. Taki
R. Talhi
S. Tedjni
M. M. Tentzeris
G. Tissoni
M. Tlidi
H. Trabelsi
D. Trinchero
L. Udpa
P. Virtic
A. G. Vladimirov
J. Vrba
S. D. Wall
S. Weiss
C. G. Windsor
C.-J. Wu
G. Q. Xie
T.-J. Yang
A. Zaghloul
B. Zolesi
M. Zribi

PIERS 2011 MARRAKESH SPONSORS

- ☐ EPL
- ☐ CST
- ☐ DIRECTEVENT
- ☐ CNRS
- ☐ SUPELEC
- ☐ University Paris West
- ☐ National University of Singapore
- ☐ University of Electronic Science & Technology of China
- ☐ Zhejiang University
- ☐ Laboratoire de Genie Electrique de Paris (LGEP)
- ☐ Energy, Mechanics and Electromagentics Lab
- ☐ The Electromagnetics Academy at Zhejiang University
- ☐ The Electromagnetics Academy

PIERS 2011 SESSIONS

Session 1A1
Advances in Nonlinear Optical Cavity Dynamics

Noise-induced Pulse Interaction in Mode-locked Lasers

Omri Gat
The Hebrew University of Jerusalem, Israel

Abstract— Ultrashort pulses in multi-pulse passively mode locked lasers exhibit rich dynamics, behaving as a system of interacting particle-like entities. An important mechanism for the inter-pulse interactions is continuum light radiated and absorbed by the pulses. Statistical light-mode dynamics (SLD) is the established method for analyzing the fluctuating dynamics of the pulse-continuum optical field of the mode locked laser. We use a non-steady state formulation of SLD where the laser waveform is decomposed in three parts, pulse, continuum and overlap, to study the pulse fluctuations in an environment made inhomogeneous by gain dynamics. We show that the drift induced by the inhomogeneity is expressed effectively as a long-range attractive interaction between pulses. When the distance between the pulses becomes smaller than the width of dispersive-wave pedestals, also known as Kelly sidebands, the interaction becomes repulsive, thus yielding the first complete theory of the formation of steady-state pulse 'molecules' with stable inter-pulse spacings in multi-pulse mode locked lasers.

Experimental Study of the 1D Kerr Cavity Soliton

François Leo[1], **Stéphane Coen**[2], **Pascal Kockaert**[1], **Simon-Pierre Gorza**[1], **Philippe Emplit**[1], **and Marc Haelterman**[1]

[1]Service OPERA-Photonique, Université libre de Bruxelles (U.L.B.)
50 Avenue F. D. Roosevelt, CP 194/5, B-1050 Bruxelles, Belgium
[2]Department of Physics, The University of Auckland, Private Bag 92019, Auckland, New Zealand

Abstract— Temporal cavity solitons are packets of light persisting in a continuously driven nonlinear resonator. They are robust attracting states, readily excited through a phase-insensitive and wavelength-insensitive process. As such, they constitute an ideal support for bits in an optical buffer that would seamlessly combine three critical telecommunication functions, namely all-optical storage, all-optical reshaping and wavelength conversion. Here, with standard silica optical fibres, we report the first experimental observation of temporal cavity solitons. The cavity solitons are 4 ps long and are used to demonstrate storage of a data stream for more than a second. We also observe interactions of close cavity solitons, revealing for our set-up a potential capacity of up to 45,000 bits at 25 Gbit s21. More fundamentally, cavity solitons are localized dissipative structures. Therefore, given that silica exhibits a pure instantaneous Kerr nonlinearity, our experiment constitutes one of the simplest examples of self-organization phenomena in nonlinear optics.

High Repetition-rate Passively Mode-locked Fiber Lasers

F. Sanchez, F. Amrani, M. Salhi, H. Leblond, and A. Komarov
Laboratoire de Photonique d'Angers EA 4644, Université d'Angers
2 Bd Lavoisier, Angers Cedex 49000, France

Abstract— Fiber lasers have today numerous applications from the industry to research. The problem related to the relatively small power supported by optical fibers has been overcome thanks to double-clad structures and, more recently, to large area microstructured fibers. The increase of the optical power delivers by fiber lasers has allowed the realization of passively mode-locked fiber lasers with still increasing pulse energy when operating in the normal dispersion regime. The anomalous dispersion regime strongly limits the energy per pulse because it favours multipulsing behaviour. In this case, several pulses coexist in the cavity. Although such regime can be detrimental for some applications, it is essential for the realization of high repetition-rate fiber laser for which the repetition-rate is much higher than the fundamental frequency of the cavity (typically about 10 MHz in fiber lasers). Actually the quantum dots semiconductor lasers allow reaching high frequency rates. However, the average power remains small. Passively mode-locked double-clad fiber lasers could be a promising alternative. In this communications, we will present two ways to considerably increase the frequency rate of a cavity. The first case is the harmonic mode-locking [1]. This operating regime starts spontaneously but suffers from a large temporal jitter. The second case is based on bound-states resulting from soliton interaction. A bound state is a group of identical and equidistant solitons which are phase locked resulting in a very high stability. When the pumping power increases, the number of pulses in the cavity also increases leading, under specific conditions, to the formation of a soliton crystal [2]. Numerical simulations demonstrate that if the pumping power is high enough, the soliton crystal can fill the entire cavity resulting in a very high repetition-rate [3]. The remarkable point is the very high stability of such state in comparison to the harmonic passive mode-locking.

REFERENCES

1. Amrani, F., A. Haboucha, M. Salhi, H. Leblond, A. Komarov, P. Grelu, and F. Sanchez, "Passively mode-locked erbium-doped double-clad fiber laser operating at the 322nd harmonic," *Opt. Lett.*, Vol. 34, 2120–2122, July 15, 2009.
2. Haboucha, A., H. Leblond, M. Salhi, A. Komarov, and F. Sanchez, "Analysis of soliton pattern formation in passively mode-locked fiber laser," *Phys. Rev. A*, Vol. 78, 043806(12), October 2008.
3. Komarov, A., A. Haboucha, and F. Sanchez, "Ultrahigh repetition rate bound-soliton harmonic passive mode-locked laser," *Opt. Lett.*, Vol. 33, 2254–2256, October 1, 2008.

Complex Self-organized Multi-pulse Dynamics in a Fiber Laser: The Rain of Solitons

S. Chouli and Ph. Grelu
Laboratoire Interdisciplinaire Carnot de Bourgogne, UMR 5209 CNRS, Université de Bourgogne
9 Avenue A. Savary, 21000 Dijon, France

Abstract— Passively mode-locked fiber lasers are mature technology that lead to the manufacturing of compact, robust and versatile short and ultrashort pulsed sources for numerous market applications. They also constitute an ideal platform for the exploration of new areas of nonlinear dynamics in an open, dissipative environment, since under moderate pumping power, significant interplays between various physical effects can be experienced.

A common understanding is that mode locking appears as an abrupt transition from a noisy cw operation to a *clean* short-pulsed laser operation. However, there can be significant deviations to such scenario. The existence of dispersive waves that are radiated by the pulse as it travels through the discontinuities of the laser cavity medium can significantly alter the spectral and temporal pulsed features [1]. The observation of noiselike pulses is an example of puzzling dynamics that does not fall in the conventional picture of mode-locked operation [2]. Such intriguing is the recent finding of the *soliton rain* dynamics, which corresponds to an intermediate regime where soliton pulses and cw components of comparable strengths not only coexist, but also interact in a dramatic way [3, 4].

Rains of solitons constitute a novel class of nonlinear dynamics of dissipative soliton ensembles. This dynamics results from the complex and dramatic self-organization between large numbers of solitons and radiation, and was observed in a fiber laser operated in highly-pumped but weakly mode-locked regime. The existence of a relatively intense noisy background together with several tens of soliton pulses aggregated in a condensed soliton phase constitutes a necessary condition for their appearance. New soliton pulses form spontaneously from the background fluctuations and drift until they reach the condensed soliton phase.

In this presentation, we relate in details the experimental conditions under which soliton rains manifest and their key features, demonstrate ways to control their appearance, describe related dynamics observed in their vicinity. Finally, we propose an explanation for the soliton rain dynamics.

REFERENCES

1. Gordon, J. P., "Dispersive perturbations of solitons of the nonlinear Schrodinger equation," *J. Opt. Soc. Am. B*, Vol. 9, 91, 1992.
2. Horowitz, M., Y. Barad, and Y. Silberberg, "Noiselike pulses with a broadband spectrum generated from an erbium-doped fiber laser," *Opt. Lett.*, Vol. 22, 799, 1997.
3. Chouli, S. and P. Grelu, "Rains of solitons in a fiber laser," *Opt. Express*, Vol. 17, 11776, 2009.
4. Chouli, S. and P. Grelu, "Soliton rains in a fiber laser: An experimental study," *Phys. Rev. A*, Vol. 81, 063829, 2010.

Ultralong Raman Fiber Lasers and Their Applications: An Overview

Juan Diego Ania-Castañón
Instituto de Óptica "Daza de Valdés", CSIC, Serrano 121, Madrid 28006, Spain

Abstract— Since their inception in 2004, ultralong Raman fiber lasers have attracted much attention thanks to their unique properties and potential technological impact. The extreme length of these resonant cavities makes their physical behaviour genuinely different from that of traditional fiber lasers and, more importantly, makes it possible to shift away from the traditional paradigm of lasers as light sources to a much richer one in which the cavity itself can be seen as a reliable medium for the transmission of dense information over long distances. This has enabled the development of multiple applications, including but not limited to low-noise high bit-rate transmission, soliton propagation, secure key distribution, signal processing, gain clamping in amplification systems and enhanced distributed sensing.

In this paper we will review the basics of ultralong Raman fiber lasers theory, their experimental applications, their current limitations and the expected immediate future of this technology.

Bistability of Soliton Molecules in Mode-locked Fiber Lasers

A. Zaviyalov, R. Iliew, O. Egorov, and F. Lederer
Institute of Condensed Matter Theory and Optics, Friedrich-Schiller-Universität Jena, Germany

Abstract— Meaningful progress in mode-locked fiber laser technology allows to routinely access different operation regimes. Operation in the single soliton, vectorial soliton, dark soliton and multi-soliton regime can be achieved in the anomalous and/or the normal dispersion domain. In particular, both from the practical and theoretical side multi-pulse localization as the formation of bound states (BSs) or so-called dissipative soliton molecules, soliton trains, patterns and gases attract a great deal of interest. Usually, the simplest unit of any multi-pulse structure is a soliton pair (molecule) which defines the common properties of the structure.

In fiber lasers three kinds of robust soliton molecules are known. The first kind is referred to as stationary molecules with invariant phase between both pulses [1]. For slightly detuned parameters these two pulse solutions oscillate around such a stationary state [2]. Second, robust molecules with flipping phase exist [3] which are infinitely alternating between two unstable stationary invariant phase solutions (in-phase and out-of-phase states). And thirdly there are robust soliton molecules with independently evolving phase [3], which are characterized by a significant amount of nonlinear interaction between the pulses.

In the present contribution we numerically investigate the properties of such robust molecules with independently evolving phase in normal dispersion mode-locked fiber laser. We demonstrate that the internal interaction of these twin-pulse solutions has a bistable nonlinear nature. This property manifests itself in a hysteretic behavior of the dependence of the separation between the pulses on the pump level. The upper and lower branch of the hysteresis loop correspond to a chaotic or periodic behavior, respectively. Moreover, we detect period doubling phenomena on the route to chaos and between chaotic regions. Beyond a critical value of the gain saturation energy, however, the hysteresis disappears.

These results reveal nonlinear and memory properties of dissipative soliton molecules which can be applied for optical information storage, optical logic systems and communication lines.

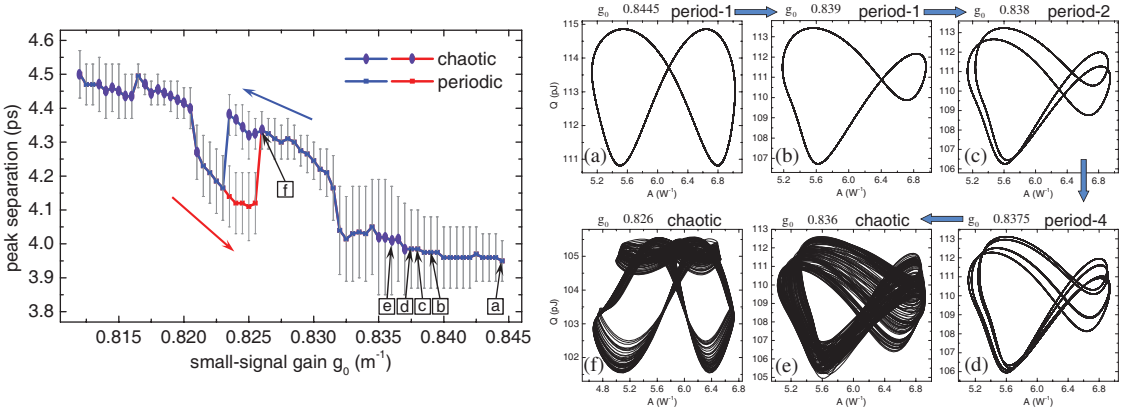

Figure 1: Left: separation distance between pulses in a soliton molecule as function of the small-signal gain. Right: single period transformation followed by period-doubling phenomena in evolution to chaos on the phase plane; correspond to points a-e in the left figure.

REFERENCES

1. Akhmediev, N. N., A. Ankiewicz, and J. M. Soto-Crespo, "Multisoliton solutions of the complex Ginzburg-Landau equation," *Phys, Rev. Lett.*, Vol. 79, 4047, 1997.
2. Soto-Crespo, J. M., P. Grelu, N. N. Akhmediev, and N. Devine, "Soliton complexes in dissipative systems: Vibrating, shaking, and mixed soliton pairs," *Phys. Rev. E*, Vol. 75, 016613, 2007.
3. Zavyalov, A., R. Iliew, O. Egorov, and F. Lederer, "Dissipative soliton molecules with independently evolving or flipping phases in mode-locked fiber lasers," *Phys. Rev. A*, Vol. 80, 043829, 2009.

Oscillating and Self-pulsing Laser Cavity Solitons and Indications for 3D Light Localization

T. Ackemann, **N. Radwell**, **Y. Noblet**, **C. McIntyre**, **W. J. Firth**, **and G.-L. Oppo**
SUPA, Department of Physics, University of Strathclyde, Glasgow, Scotland, UK

Abstract— Light bullets or three-dimensional solitons were intensively pursued in propagational schemes without feedback, for example in [1], but to our knowledge there is no experimental demonstration, yet. For Kerr media this is due to the fact that solitons are unstable in more than one dimension [2]. Saturation might stabilize solitons, e.g., [3], but the parameter range seem to be very dicult to reach experimentally. The dissipative dynamics of a cavity relax the requirements on the material to sustain CS, e.g., [4]. Indeed light bullets were found in a model for a driven cavity with a two-level nonlinearity [5].

The last years have seen rapid progress in the generation of *laser cavity solitons* (LCS) in broad-area semiconductor lasers [4, 6, 7]. We aim on combining the concepts of spatial laser solitons and mode-locking to create cavity light bullets (CLB). If an LCS operates on multiple, phase-locked cavity modes, a pulse is formed which has a duration shorter than the cavity round-trip time and is hence also spatially localized along the longitudinal (cavity) axis, forming a CLB. They would share the intrinsic feature of dissipative solitons to be bistable and could serve as the source of optically-controllable pulse trains in communication systems for multiplexing, de-multiplexing, routing and regeneration.

The experimental system is based on a broad-area vertical-cavity surface-emitting laser (VCSEL) with bistability induced by frequency-selective feedback (FSF) [6]. The VCSELs used are bottom-emitting devices (Ulm Photonics), emitting at 980 nm and electrically pumped through a 200 µm diameter circular oxide aperture. Frequency-selective feedback is provided by a self-imaging external cavity closed by a VBG with a bandwidth of about 20 GHz. The temporal dynamics are measured with an AC-coupled amplified fast detector with a bandwidth of 12 GHz.

We find two types of dynamics, both characterized by excitation of multiple modes in the external cavity and excitation of a radio-frequency spectrum dominated by multiples of the external cavity round-trip frequency. The first case is characterized by noisy, irregular oscillations extending more or less symmetrically below and above the baseline, thus indicating oscillations around a DC offset. LCS can be switched from the off-state to this oscillating state. This regime reminds of coherence collapse in semiconductor lasers with feedback [8] and is typical for 'long' cavities (about 1 ns round-trip time).

In a shorter cavity (about 0.6 ns round-trip time), this irregular regime is also observed but in addition fairly regular, pronounced pulsing at the cavity-round trip time with smaller pulses in between is obtained. It is strongly asymmetric compared to the baseline indicating pulsing from a DC-level, which is unknown but estimated to be low by comparison with switch-on experiments. The envelope has a low frequency envelope on the time scale of about 50 ns. The FWHM of a peak is about 120 ps, i.e., considerably shorter than a cavity round-trip. The width of the radio-frequency peak is smaller than the linewidth of a single optical mode under single-frequency operation (6 MHz) supporting the notion of at least partial mode-locking.

Both types of dynamics are reproduced qualitatively by numerical simulation of a class B VCSEL model taking into account feedback terms to all orders (see [9] for the moel). Pulsing at the cavity round-trip time is found from zero offset in narrow parameter intervals.

We conclude on the observation of temporally irregularly shaped light structures with an extent certainly shorter than the round-trip time, i.e., on the participation of CLB in the dynamics, probably on an irregular non-zero background. The FSF does not have an obvious mechanism as saturable absorption to induce mode-locking, but, for example, four-wave mixing is argued to support mode-locking in lasers [10]. Regular pulse packages known from semiconductor lasers with feedback [11] are discussed as an alternative mechanism.

REFERENCES

1. Wise, F. W. and P. Di Trapani, *Opt. Photon. News*, Vol. 13, 28, 2002.
2. Silberberg, Y., *Opt. Lett.*, Vol. 15, 1282, 1990.
3. Soto-Crespo, J. M., P. Grelu, and N. Akhmediev, *Opt. Exp.*, Vol. 14, 4013, 2006.
4. Ackemann, T., G.-L. Oppo, and W. J. Firth, *Adv. Atom. Mol. Opt. Phys.*, Vol. 57, 323, 2009.

5. Brambilla, M., T. Maggipinto, G. Patera, and L. Columbo, *Phys. Rev. Lett.*, Vol. 93, 203901, 2004.
6. Tanguy, Y., T. Ackemann, W. J. Firth, and R. Jäger, *Phys. Rev. Lett.*, Vol. 100, 013907, 2008.
7. Genevet, P., S. Barland, M. Giudici, and J. R. Tredicce, *Phys. Rev. Lett.*, Vol. 101, 123905, 2008.
8. Petermann, K., *IEEE J. Selec. Top. Quantum Electron.*, Vol. 1, 480, 1995.
9. Scroggie, A. J., W. J. Firth, and G.-L. Oppo, *Phys. Rev. A*, Vol. 80, 013829, 2009.
10. Renaudier, J., et al., *Electron. Lett.*, Vol. 41, 1007, 2005.
11. Heil, T., et al., *Phys. Rev. E*, Vol. 67, 066214, 2003.

Towards Light Bullets in Dissipative Systems: Fast Pulsation and Localised Structures in a Cavity Soliton Laser

P. Genevet, **S. Barland**, **M. Giudici**, **and J. R. Tredicce**

INLN, Universite de Nice Sophia Antipolis
1361 route des lucioles, Valbonne 06560, France

Abstract— Three dimensional localisation of light is still an open challenge of non-linear optics [1]. Alternatively to propagative schemes, light bullets can also be sought in dissipative systems where these structures would be a stable solution towards which the system would spontaneously evolve. In this context, localisation of light is meant with respect to some temporal/spatial scale of the system [2]. For example, in the case of a laser resonator, light can be time localised with respect the round trip time and spatial localised with respects the transverse size of the cavity.

In this contribution we report on progress towards the observation of light bullets in a Cavity Soliton Laser. A cavity soliton laser is a device able to generate single-peak stationary localized structures, also called cavity solitons (CS), without the injection of an external coherent beam. We realized experimentally a cavity soliton laser by mutually coupling in face to face configuration two broad-area vertical cavity surface emitting lasers (VCSELs), one set to work as amplifier while the second, biased below transparency, plays the role of a saturable absorber [3].

Beyond the possibility of forming CS, the two VCSELs resonators define a compound cavity whose longitudinal modes can be mode-locked by saturable absorption. In single transverse mode devices this scheme is successfully implemented in edge-emitting devices using intracavity saturable absorber [4] and in vertical external cavity surface emitting lasers (VECSEL) [5]. In both cases short laser pulses are obtained at a repetition rate corresponding to the free spectral range. These mode-locked laser pulses are time localised with respect the round trip time of the electromagnetic field and therefore they are considered dissipative temporal solitons.

Then, we build on the existence of 2D stationary localized structures in our system and we try to set proper conditions in order to get these localized structures pulsing according to a mode-locking condition. We report on the observation of spatial structures pulsing at the round trip-time of the compound cavity defined by the two devices. The pulsing is enveloped in a low-frequency amplitude modulation; we interpret these dynamics in terms of Q switch mode-locking instability. Possible improvements and solutions for achieving a stable mode-locking emission will be discussed.

REFERENCES

1. Wise, F. and P. Di Trapani, "Spatiotemporal solitons," *Optics and Photonics News*, Feb. 2002.
2. Akhmediev, N. and A. Ankiewicz (eds.), "Dissipative solitons," *Lectures Notes in Physics*, Vol. 661, Springer, New York, 2005.
3. Genevet, P., et al., *Phys. Rev. Lett.*, Vol. 101, 123905, 2008.
4. Haus, H. A. and Y. Silberberg, *IEEE J. Quantum Electron.*, Vol. 22, 325, 1986.
5. Keller, U., *Physics Reports*, Vol. 429, 67, 2006.

On the Study of Giant Chirp Oscillators

E. J. R. Kelleher[1], C. E. S. Castellani[1], J. C. Travers[1], Z. Sun[2], A. C. Ferrari[2], S. V. Popov[1], and J. R. Taylor[1]

[1]Femtosecond Optics Group, Photonics, Department of Physics, Blackett Laboratory
Prince Consort Road, Imperial College London, London SW7 2AZ, UK
[2]Department of Engineering, University of Cambridge, Cambridge CB3 0FA, UK

Abstract— We review recent progress in a class of normally dispersive mode-locked laser that has become known as a giant chirp oscillator. We discuss spectral and temporal versatility and consider the pulse formation dynamics, both using numerical simulation and experimental investigation.

Introduction: Passively mode-locked fiber lasers have become a ubiquitous tool in both the research domain and for many commerical applications requiring a source of ultrashort light pulses. Recently, researchers have become interested in mode-locked laser systems with normal dispersion maps because such systems can support pulses with energies in excess of the limits imposed by the soliton regime [1]. As well as the obvious practical significance, a modified dispersion profile gives rise to a rich complex of associated dynamics. In this contribution we consider a specific class of normally dispersive mode-locked laser that has become known as a giant chirp oscillator (GCO) because of the large, predominatly linear, chirp carried by the pulse structures that evolve is such systems with ultralarge normal dispersion [2, 3]. This property has allowed us to move to a new regime of pulse parameters, with nanosecond pulses now routinely generated from all-fiber oscillators [4].

Discussion: We will discuss aspects of temporal and spectral versatility, showing experimental results using well established rare-earth-doped fiber amplfiers as well as more exotic gain media, such as Bismuth and Raman, where the limits of the gain bandwidth are somewhat relaxed, leading to spectrally exible systems. To gain insight and understanding of the pulse evolution and the cavity dynamics we have performed detailed numerical simulations, based on a modified nonlinear Schrödinger equation, and analytical studies using the Haus master equation [5]. We will present simulation results, in particular to explore the start-up dynamics and the role the spectral filter plays in the pulse shaping mechanism, and experimental measurements of the pulse properties. The predominantly linear nature of the chirp carried by the pulse structures in GCOs makes them a potentially useful candidate for seeding a simplified chirp-pulse amplification scheme. Issues with compression will be considered.

ACKNOWLEDGMENT

FOG is supported by the UK Engineering and Physical Sciences Research Council (EPSRC) and Royal Society. JCT holds an Imperial College Junior Research Fellowship, SVP is a Royal Society Industry Fellow and JRT is a Royal Society Wolfson Research Merit Award holder.

REFERENCES

1. Chong, A., et al., *Opt. Express*, Vol. 14, 10095, 2006.
2. Renninger, W. H., et al., *Opt. Lett.*, Vol. 33, 3025, 2008.
3. Kelleher, E. J. R., et al., *Opt. Lett.*, Vol. 34, 3526, 2009.
4. Kelleher, E. J. R., et al., *Appl. Phys. Lett.*, Vol. 95, 111108, 2009.
5. Haus, H. A., et al., *J. Opt. Soc. Am. B*, Vol. 8, 2068, 1991.

Principal Component Analysis for Low-dimensional Modeling of Mode-locked Lasers

J. N. Kutz, **M. Williams**, **E. Shlizerman**, **and E. Ding**
Department of Applied Mathematics, University of Washington, Seattle, WA 98195, USA

Abstract— Mode-locked lasers are one of the most successful commercial devices which are based fundamentally on nonlinear optics. Commercially available pulsed mode-locked lasers are compact, cheap, reliable and robust and have a wide range of applications from optical communications to medical devices. The mode-locking in these packaged lasers are commonly based upon nonlinear polarization rotation, saturable absorbers, nonlinear interferometry, or acouto-optic modulators. Here, we present a radically new mode-locking technique which is based upon the nonlinear mode-coupling (NLMC) produced by semiconductor waveguide arrays (WGA). From a theoretical and simulation standpoint, the resulting mode-locking is highly robust and self-starting, making it a viable candidate for the ever-maturing technology of mode-locked lasers. Indeed, this new WGA technology in conjunction with mature fiber optics technology presents a promising candidate for consideration as a high-energy, mode-locked laser source. Given the promising theoretical predictions achieved, and the agreement between the theory and experiment, the WGA based laser technologies warrants significant development as there are a variety of techniques we proposed that can potentially lead to high-energy, robust laser sources for a wide range of applications. Key to developing an underlying theoretical framework for characterizing the mode-locking dynamics is low-dimensional modeling effort that results from a principal component (proper orthogonal decomposition) analysis. The entire mode-locking process can be understood from a simple two- to four-degree of freedom system. Using a low-dimensional reduction constructed by the method of proper orthogonal decomposition (principal components), a complete characterization of the multi-pulsing transition is given, including the onset of periodic (Hopf) solutions and a period doubling and Neimark-Sacker (torus) bifurcation route to chaos. This is the first low-dimensional construction of the entire multi-pulsing transition from N to $N+1$ pulses per round trip. The reduced model qualitatively reproduces the dynamics observed in the multi-pulse transition of the mode-locked laser and confirms recent experimental observations of periodic and chaotic behavior preceding the multi-pulsing transition.

Session 1A2
Extraordinary Transmission: Theory and Experiments

Extraordinary Transmission for the "Wrong" Polarization

M. Navarro-Cía[1], M. Beruete[1], V. Lomakin[2], S. A. Kuznetsov[3], and M. Sorolla[1]

[1]Millimeter and Terahertz Waves Laboratory, Universidad Pública de Navarra, Spain
[2]Department of Electrical and Computer Engineering, University of California-San Diego, USA
[3]Novosibirsk State University, Budker Institute of Nuclear Physics SB RAS, Russia

Abstract— The phenomenon of strongly enhanced transmission through metal plates perforated with arrays of subwavelength holes led to an increased interest to the area of plasmonics [1, 2]. There is general consensus that the physical mechanism behind the enhanced transmission phenomena is a strong resonance caused by the excitation of a surface wave [3, 4], which becomes leaky through the interaction with the periodic structure. In the optical regime such leaky waves are typically associated with surface plasmon polariton, which are TM (p) polarized waves [3, 4]. However, other realizations of surface waves are possible in the optical as well as microwave and terahertz regimes.

One of less commonly known mechanisms is through the interaction with grounded slab modes, which can be of conventionally considered TM (p) polarization or of (anomalous) TE (s) polarization [4, 5]. Enhanced transmission of TE polarized waves is a clear manifestation of the underlying physics of the general leaky wave nature of the phenomenon. Recently, we reported measurements of TE transmission in the millimeter-wave [6, 7].

In this work, we present a complete analytical, numerical, and experimental study of the conditions for anomalous TE enhanced transmission. These results can find uses in interesting applications such as sensing in the THz regime.

REFERENCES

1. Ebbesen, T. W., H. J. Lezec, H. Ghaemi, T. Thio, and P. A. Wolf, "Extraordinary optical transmission through sub-wavelength hole arrays," *Nature*, Vol. 391, 667–669, 1998.
2. Maier, S. A., *Plasmonics — Fundamentals and Applications*, Springer, New York, 2007.
3. Pendry, J. B., L. Martín-Moreno, and F. J. García-Vidal, "Mimicking surface plasmons with structured surfaces," *Science*, Vol. 305, 847–848, 2004.
4. Lomakin, V. and E. Michielssen, "Enhanced transmission through metallic plates perforated by arrays of subwavelength holes and sandwiched between dielectric slabs," *Phys. Rev. B*, Vol. 71, 235117-1-10, 2005.
5. Moreno, E., L. Martín-Moreno, and F. J. García-Vidal, "Extraordinary optical transmission without plasmons: The s-polarization case," *J. Opt. A: Pure Appl. Opt.*, Vol. 8, S94–S97, 2006.
6. Kuznetsov, S. A., M. Navarro-Cía, V. V. Kubarev, A. V. Gelfand, M. Beruete, I. Campillo, and M. Sorolla, "Regular and anomalous extraordinary optical transmission at the THz-gap," *Opt. Express*, Vol. 17, 18184–18195, 2009.
7. Beruete, M., M. Sorolla, M. Navarro-Cía, F. Falcone, I. Campillo, and V. Lomakin, "Extraordinary transmission and left-handed propagation in miniaturized stacks of doubly periodic subwavelength hole arrays," *Opt. Express*, Vol. 15, 1107–1114, 2007.

Anisotropy in Extraordinary Transmission Fishnet Structures

M. Navarro-Cía, M. Beruete, and M. Sorolla
Millimeter and Terahertz Waves Laboratory, Universidad Pública de Navarra, Spain

Abstract— After the first realization of a Negative Refractive Index Metamaterial (NIM) in the microwave regime [1], most research efforts were directed towards a NIM working at optical frequencies. To date, the most promising structure is the so-called fishnet structure, which consists in two perforated plates separated by a dielectric [2]. In parallel, other strategies to get negative refraction aside from the traditional combination of doubly negative metamaterials were investigated. It was found that with anisotropic media, called indefinite media, negative refraction was feasible [3].

Our contribution here was twofold: firstly, we could demonstrate that fishnet structures are equivalent to stacked Extraordinary Transmission [4, 5] hole arrays, extending the study to a stack larger than two plates and, besides, showed negative refraction in a prism of stacked hole arrays [6]. Secondly, we showed that this structure is strongly anisotropic and has complex two-dimensional dispersion diagram [7, 8] that can be analyzed with the theory of indefinite media of Ref. [3]. In Ref. [7], we reported intrinsic negative refraction in stacked hole arrays and in Ref. [8] extended the analysis for the two principal polarization states, with negative or positive refraction depending on the wave polarization.

In this work, we will analyze in depth the anisotropy characteristic of fishnet structures and will link it with the rich variety of refraction angles obtained with them. These results could be of interest both from a fundamental as well as practical point of view and could lead to interesting applications such as unconventional beam steerers.

REFERENCES

1. Shelby, R. A., D. R. Smith, and S. Schultz, "Experimental verification of a negative index of refraction," *Science*, Vol. 292, 77–79, 2001.
2. Dolling, G., C. Enkrich, M. Wegener, C. M. Soukoulis, and S. Linden, "Simultaneous negative phase and group velocity of light in a metamaterial," *Science*, Vol. 312, 892–894, 2006.
3. Smith, D. R. and D. Schurig, "Electromagnetic wave propagation in media with indefinite permittivity and permeability tensors," *Phys. Rev. Lett.*, Vol. 90, 077405, 2003.
4. Ebbesen, T. W., H. J. Lezec, H. Ghaemi, T. Thio, and P. A. Wolf, "Extraordinary optical transmission through sub-wavelength hole arrays," *Nature*, Vol. 391, 667–669, 1998.
5. Beruete, M., M. Sorolla, and I. Campillo, "Left-handed extraordinary optical transmission through a photonic crystal of subwavelength hole arrays," *Opt. Express*, Vol. 14, 5445–5455, 2006.
6. Navarro-Cía, M., M. Beruete, M. Sorolla, and I. Campillo, "Negative refraction in a prism made of stacked subwavelength hole arrays," *Opt. Express*, Vol. 16, 560–566, 2008.
7. Beruete, M., M. Navarro-Cía, M. Sorolla, and I. Campillo, "Negative refraction through an extraordinary transmission left-handed metamaterial slab," *Phys. Rev. B*, Vol. 79, 195107-1-6, 2009.
8. Beruete, M., M. Navarro-Cía and M. Sorolla, "Strong lateral displacement in polarization anisotropic extraordinary transmission metamaterial," *New J. Phys.*, Vol. 12, 063037-1-15, 2010.

Extraordinary Transmission and Light Confinement in Subwavelength Metallic Films Apertures

R. Ortuño, C. García-Meca, F. J. Rodríguez-Fortuño, and A. Martínez
Nanophotonics Technology Center, Universidad Politécnica de Valencia, Spain

Abstract— Light-matter interactions in a metal layer patterned at the subwavelength scale give rise to a wide variety of optical resonances. Since the discovery of extraordinary light transmission, numerous experiments on such subwavelength apertures of opaque metallic films have demonstrated the ability to control light confinement and light propagation at the subwavelength scale.

The pattern in periodic structures allows coupling mechanisms between impinging light and surface plasmon waves. The excitation of horizontal coupled surface plasmons on the surfaces of the grating is pointed out to explain the extraordinary transmission of light trough periodic arrays of subwavelength apertures in metallic films. However, other mechanisms are also responsible for the high transmission and huge confinement of light in metallic gratings. For instance, waveguide modes, which appear in one-dimensional gratings made of narrow slits, also play an important role in the onset of extraordinary transmission. In addition, when the patterned metallic film is surrounded by a dielectric material, the excitation of cladding modes by the incoming light also cause extraordinary transmission resonances.

Moreover, cascading extraordinary transmission structures leads to a magnetic resonance response which yields a left-handed behavior and a negative refraction over a specific frequency range. By properly adjusting the separation distance among the cascaded metallic layers the negative refractive index can be extended over a larger frequency range.

These phenomena allow us to design planar optical elements having different refractive indices and spectral dispersion properties. This is very attractive for many optical applications in fundamental optics and in optoelectronics, like lenses and filters, and open up new possibilities in controlling and manipulating light by a wide range of plasmonic materials. In this sense, we have designed subwavelength structures for filtering purposes in the mid-infrared frequency range with high transmission levels. In addition, one advantage of such filters is their simple and compact implementation by comparison with conventional multilayer filters due to their huge number of layers and their large thicknesses required in the mid-infrared domain.

Transmission Properties of Dual-period Arrays of Cylinders

D. C. Skigin[1] and M. Lester[2]

[1]Applied Electromagnetics Group, Physics Dept., FCEN, University of Buenos Aires
and IFIBA (CONICET), Argentina
[2]Grupo Optica de Sólidos-Elfo, Instituto de Física Arroyo Seco, Facultad de Ciencias Exactas
Universidad Nacional del Centro de la Provincia de Buenos Aires, Argentina

Abstract— We investigate the potential of dual-period structures to control and manipulate the transmitted intensity. We consider supergratings (periodic arrays with a compound unit cell) in which each period comprises several cylinders with circular cross section.

Three different configurations are considered: (i) all the cylinder axes are contained in the same plane; (ii) the cylinder axes in each unit cell are aligned in a plane which is tilted with respect to the periodicity direction; (iii) evanescent wave illumination.

For case (i) we show that this kind of structure permits one to control the diffracted response, regardless of the cylinder material and the incident polarization. A given diffraction order can either be enhanced or suppressed by appropriately choosing the geometrical parameters of the structure. Our numerical results suggest that the effect produced by wire gratings with dual-period characteristics is basically a geometric effect, and it can be present for other shapes of individual scatterers within each subarray. If the cylinder diameters are much smaller than the incident wavelength (subwavelength cylinders), and their axes are aligned in a plane tilted with respect to the periodicity direction (case (ii)), this structure behaves like a blazed grating in the sense of its capability to enhance the intensity in a pre-designed direction. This blazed-like behavior is found for both incident polarization modes, and for dielectric as well as for metallic cylinders. We also consider dual-period arrays illuminated by an evanescent wave generated by total internal reflection in a close interface. For particular wavelengths, the system exhibits resonances and the inhomogeneous wave is converted into propagating waves that radiate to the far field. This effect can be controlled by varying the geometrical parameters of the structure, such as the period and the inclination angle. Therefore, the transmitted intensity can be sent to a predesigned direction. If we consider the quick evolution of manufacturing techniques of nanogratings, such structures constitute a realizable alternative not only for the microwave and millimeter wave regions but also for optical devices, and they could be used in highly sensitive detection devices, among other applications.

Bulk Metamaterial under Front Illumination at Terahertz Frequencies

J. Carbonell[1], **S. Wang**[2], **E. Lheurette**[2], **and D. Lippens**[2]

[1]Wave Phenomena Group, Departamento de Ingeniería Electrónica
Universidad Politécnica de Valencia, Camino de Vera, s/n, E-46022 Valencia, Spain
[2]IEMN, Université des Sciences et Technologies de Lille
Av. Poincaré B.P. 60069, 59652 Villeneuve d'Ascq Cedex, France

Abstract— Front side illuminated devices operating at terahertz and even higher frequencies have become a very active field of research owing to their wide range of possible applications. In particular, devices exhibiting a negative refractive index may open the path to obtain high-resolution lenses, super scatters, and other challenging purposes. Several routes have been explored to fulfill a normal incidence requirement such as the ones based on the so-called nanorod or fishnet approaches. Nevertheless, the Terahertz spectral range still raises some issues. The first and perhaps the most important difficulty stems from the requirement of generating (virtually or de facto) of a resonant current loop, as in the generic so-called split ring resonator technology. This loop will induce an artificial magnetic moment under grazing incidence. This key issue explains why most of the present works in the Terahertz frequency range have addressed preferably metasurfaces based on resonant electrical dipoles rather than bulk metamaterials. Clearly the scaling of the underlying concept for artificial magnetism from microwaves to Terahertz frequencies requires developing other excitation techniques under front side illumination. The so-called sub-wavelength holes array and fishnet technologies are two suitable routes towards this goal. Recent demonstrations of left-handedness at millimeter, sub-millimeter wavelengths and in the infrared spectral region have been proposed.

We have investigated several bulk metamaterial prototypes under front illumination at Terahertz frequencies [1, 2]. To this aim we have fabricated several stacked structures of slab- and wedge-types. The devices are constituted of holes arrays etched in gold thin films, which are stacked according to a sequential mask with benzocyclobutene (BCB) spacer polymers. We have characterized them with a measurement setup based on angle-resolved time domain spectroscopy (TDS) carried out at operating frequencies around 0.5 THz. Analysis of these experimental data is carried out in conjunction with numerical simulations, effective parameters retrieval methods and equivalent circuit analysis. In terms of the experimental results, a favorable comparison can be established with a broad-band equivalent circuit. Also, the dispersion of refractive index retrieved from the Snell law on these measured data shows comparable trends with the dispersion deduced from numerical simulations. Complex transmission and reflection measurements we have performed on slab- and wedge-type samples permit to confirm the findings regarding the effective retrieved parameters.

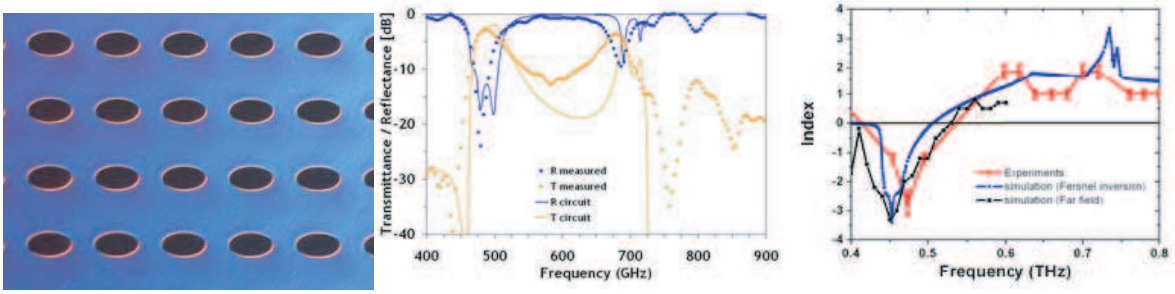

(a) (b) (c)

Figure 1: (a) Optical microscope view of the surface of a fabricated prototype, (b) transmittance and reflectance for a five layer stacked structure in magnitude (equivalent circuit response compared to measured data), and (c) frequency dependence of effective refractive index extracted for a 10-layer wedge type device (far field).

REFERENCES

1. Carbonell, J., C. Croënne, F. Garet, E. Lheurette, J. L. Coutaz, and D. Lippens, "Lumped elements circuit of terahertz Fishnet-like arrays with composite dispersion," *Journal of Applied Physics*, Vol. 108, 014907, 2010.
2. Wang, S., F. Garet, K. Blary, C. Croënne, E. Lheurette, J. L. Coutaz, and D. Lippens, "Composite left/right-handed stacked hole arrays at submillimeter wavelengths," *Journal of Applied Physics*, Vol. 107, 074510, 2010.

Holey Structured Metamaterials

Francisco J. Garcia-Vidal
Departamento de Física Teórica de la Materia Condensada (C-05), Facultad de Ciencias
Universidad Autónoma de Madrid, Spain

Abstract— The interest in the optical properties of metallic films perforated with periodic arrays of subwavelength holes was revitalized after the discovery of the phenomenon of extraordinary optical transmission (EOT), reported by Ebbesen and co-workers in 1998 [1, 2]. This phenomenon is characterized by the emergence of some transmission resonances that appear at wavelengths slightly larger than the period of the array. It is now well-established that the origin of this intriguing behaviour is associated with the excitation of surface plasmon polaritons (SPPs) by the incident light. Here in this summary, we will demonstrate how a single holey metal film (or several holey metal films stacked together) can present interesting optical and acoustic properties when it behaves as a metamaterial, i.e., in the effective medium limit in which the operating wavelength is much larger than the size of the holes and period of the array.

The concept of spoof surface plasmon was firstly introduced in 2004 by Pendry, Martin-Moreno and Garcia-Vidal [3]. In that paper, it was demonstrated how the optical response of a holey perfect conductor can be effectively mapped into a Drude-like formula in which the plasma frequency of the real metal is replaced by the cutoff frequency of the hole waveguide. The first theoretical studies on the concept of spoof surface plasmons were done for planar geometries [3, 4], i.e., periodic arrays of holes and periodic arrays of dimples. Experimental verification of this concept was firstly reported in the microwave regime by Hibbins and co-workers by looking at the angle-dependent transmission spectrum through periodic arrays of holes [5]. Very recently, the subwavelength (vertical) confinement of these geometrically induced surface electromagnetic modes was verified in the terahertz regime [6].

Recently, Zhang and co-workers [7] have proposed and demonstrated a negative index metamaterial working at near infrared frequencies with a design very similar to the structure showing EOT. This metamaterial is composed by a two-dimensional array of holes penetrating completely in a metal-dielectric-metal film stack. This double-fishnet (DF) structure has received a lot of attention for its negative refractive index (NRI) at visible and near infrared frequencies. A theory is presented of the negative refractive index observed in the double-fishnet structures [8]. We find that the electrical response of these structures is dominated by the cutoff frequency of the hole waveguide whereas the resonant magnetic response is due to the excitation of gap surface plasmon polaritons propagating along the dielectric slab. Associated with this origin, we will show how the negative refractive index in these metamaterials presents strong dispersion with the parallel momentum of the incident light.

We will also analyze the distinct behaviour observed for acoustic waves [9]. We will show how the physics of the acoustic double-fishnet is quite different to its electromagnetic counterpart. This metamaterial structure exhibits a tuneable attenuation band but does not present negative-index behaviour. The blockage of acoustic radiation originates from a negative effective bulk modulus, associated with the excitation of a gap mode in the region between the two holey plates. Importantly and as a difference with the electromagnetic case, the acoustic gap mode presents a weak dispersion with parallel momentum and its bandwidth can be tuned at will by varying the thickness of the separating layer.

Finally we will analyze possible superlensing effects in holey metal films. We will show that within the effective-medium limit and at some resonant frequencies, holey perfect conductor films make perfect endoscopes, i.e., are capable of transforming an image from the input to the output surface of the film with very deep subwavelength resolution [10]. To corroborate our finding in a realistic structure, a full numerical calculation including diffraction and losses is presented for a one-dimensional perforated metal film in the terahertz regime. However, the practical implementation of these endoscopes for three-dimensional objects using a two-dimensional array of holes instead of a one-dimensional array of slits is limited due to the existence of a cutoff wavelength inside the holes. Importantly, this limitation is lifted in the case of acoustic waves. We have recently demonstrated a three-dimensional holey structured metamaterial that achieves acoustic imaging down to a feature size of $\lambda/50$ [11]. The evanescent field components of a subwavelength object are efficiently transmitted through the structure thanks to their strong coupling with Fabry-Perot resonances inside the holey plate. This capability of acoustic imaging at a very deep subwavelength scale brings promising perspectives for broad applications in medical ultrasonography, underwater sonar and ultrasonic non-destructive evaluation.

REFERENCES

1. Ebbesen, T. W., H. J. Lezec, H. F. Ghaemi, T. Thio, and P. A. Wolff, "Extraordinary optical transmission through sub-wavelenght hole arrays," *Nature*, Vol. 392, 667, 1998.
2. For a recent review on EOT phenomenon: F. J. Garcia-Vidal, L. Martin-Moreno, T. W. Ebbesen, and L. Kuipers, "Light passing through subwavelength apertures," *Rev. Mod. Phys.*, Vol. 82, 729, 2010.
3. Pendry, J. B., L. Martín-Moreno, and F. J. García-Vidal, "Mimicking surface plasmons with structured surfaces," *Science*, Vol. 305, 847, 2004.
4. García-Vidal, F. J., L. Martín-Moreno, and J. B. Pendry, "Surfaces with holes in them: New plasmonic metamaterials," *J. Opt. A (Pure Appl. Opt.)*, Vol. 7, 597, 2005.
5. Hibbins, A. P., B. R. Evans, and J. R. Sambles, "Experimental verification of designer surface plasmons," *Science*, Vol. 308, 670, 2005.
6. Williams, C. R., S. R. Andrews, S. A. Maier, A. I. Fernandez-Dominguez, L. Martin-Moreno, and F. J. Garcia-Vidal, "Highly confined guiding terahertz surface plasmon-polaritons on structured metal surfaces," *Nature Photonics*, Vol. 2, 175, 2008.
7. Zhang, S., et al., "Experimental demonstration of near-infrared negative-index metamaterial," *Phys. Rev. Lett.*, Vol. 95, 137404, 2005.
8. Mary, A., Sergio G. Rodrigo, F. J. Garcia-Vidal, and L. Martin-Moreno, "Theory of negative-refractive index response of double-fishnet structures," *Phys. Rev. Lett.*, Vol. 101, 103902, 2008.
9. Christensen, J., L. Martin-Moreno, and F. J. Garcia-Vidal, "Broadband all-angle blockage of sound by an acousticdouble-fishnet metamaterial," *Appl. Phys. Lett.*, in press.
10. Jung, J., F. J. García-Vidal, L. Martín-Moreno, and J. B. Pendry, "Holey metal films make perfect endoscopes," *Phys. Rev. B*, Vol. 79, 153407, 2009.
11. Zhu, J., J. Christensen, J. Jung, L. Martin-Moreno, X. Yin, L. Fok, X. Zhang, and F. J. Garcia-Vidal, "A holey structured metamaterial for acoustic deep subwavelength imaging," *Nature Physics*, in press.

Anomalous Band Formation in Terahertz Nanoresonators

J. Bravo-Abad[1], **L. Martin-Moreno**[2], **F. J. Garcia-Vidal**[1], **Y. M. Park**[3], **H. R. Park**[3], **K. J. Ahn**[3], **H. S. Kim**[3], **Y. H. Ahn**[4], **and D.-S. Kim**[3]

[1]Departamento de Fisica Teorica de la Materia Condensada
Universidad Autonoma de Madrid, E-28049 Madrid, Spain
[2]Instituto de Ciencia de Materiales de Aragon (ICMA)
Departamento de Fisica de la Materia Condensada, CSIC-Universidad de Zaragoza
E-50009 Zaragoza, Spain
[3]Center for Subwavelength Optics, Department of Physics and Astronomy
Seoul National University, Seoul 151-747, Korea
[4]Division of Energy Systems Research, Ajou University, Suwon 433-749, Korea

Abstract— Light transmission through subwavelength apertures in metal films has been extensively studied since the phenomenon of Extraordinary Optical Transmission was reported over a decade ago [1]. In this context, it was shown that the collective response of an array of subwavelength holes perforated in a metallic screen is strongly influenced by the shape of the apertures forming the array [2]. It was also found that this strong dependence is already present in a single isolated hole [3, 4]. In particular, cutoff transmission resonances were reported in single rectangular holes, which enable dramatic enhancements of the corresponding normalized-to-area transmission just by increasing the ratio between the long and short sides of the aperture.

In this talk, we describe our recent analysis of band formation in periodic arrays of rectangular holes [5]. Specifically, we consider one-dimensional arrays formed by rectangular apertures tailored to work as resonators in the THz frequency regime, each aperture being characterized by nanoscale width but a length of a hundred microns. First, we present THz time-domain spectroscopy measurements of the transmission amplitude through this class of systems. From these measurements two unexpected observations emerge: on one hand, in contrast to what it is expected from a canonical tight-binding picture of band formation in periodic systems, the linewidth and the position of the resonant peak observed in the transmission spectra do not show a monotonic behavior as the period of the array is changed. On the other hand, the maximum normalized-to-area transmitted amplitude decreases as more apertures are added to the sample.

In the second part of this talk, we discuss the physical origin of these findings in terms of both numerical calculations based on a theoretical coupled-mode formalism and a minimal model that captures the main features observed experimentally. Thus, we show in detail how the considered array of coupled THz nanoresonators displays unique features stemming from both the oscillating behavior of the electromagnetic coupling between holes and its long-range character.

REFERENCES

1. Ebbesen, T. W., H. J. Lezec, H. F. Ghaemi, T. Thio, and P. A. Wolff, *Nature*, Vol. 391, 667, 1998.
2. Koerkamp, K. J. K., S. Enoch, F. B. Segerink, N. F. van Hulst, and L. Kuipers, *Phys. Rev. Lett.*, Vol. 92, 183901, 2004.
3. Degiron, A., H. J. Lezec, N. Yamamoto, and T. W. Ebbesen, *Opt. Commun.*, Vol. 239, 61, 2004.
4. Garcia-Vidal, F. J., E. Moreno, J. A. Porto, and L. Martin-Moreno, *Phys. Rev. Lett.*, Vol. 95, 103901, 2005.
5. Park, Y. M., H. R. Park, K. J. Ahn, H. S. Kim, Y. H. Ahn, D.-S. Kim, J. Bravo-Abad, L. Martin-Moreno, and F. J. Garcia-Vidal, *Phys. Rev. Lett.*, accepted for publication.

Analytical Modeling of Extraordinary Transmission in the Presence of Dielectric Slabs

R. Rodríguez-Berral[1], **F. Medina**[2], **and F. Mesa**[1]

[1]Microwaves Group, Department of Applied Physics 1, University of Seville, Spain
[2]Microwaves Group, Department of Electronics and Electromagnetism, University of Seville, Spain

Abstract— The phenomenon of extraordinary transmission of electromagnetic waves through electrically small apertures is nowadays well understood and several authorative reviews are available [1–4]. The basic idea is that surface waves can be strongly excited over the structured surface (surface plasmon polaritons, SPP) at some critical frequencies close to the onset of the first diffraction order of the grating. Although the plasma behavior of metals at optical frequencies influences the detailed shape of the transmission spectrum, it is the periodic distribution of holes or slits the main cause behind the phenomenon. The analysis of this type of structures can be reduced to the study of a single unit cell [5]. Moreover, the analysis of this unit cell straightforwardly leads to reduced order circuit models such as those reported in [6] and [7] to deal with 2D arrays of holes and 1D simple/compound slit gratings respectively. However, most of the structures studied in the previous references are free standing metallic surfaces. The presence of dielectric slabs on which the metal structure is deposited or printed is essential due to fabrication requirements. From the point of view of SPP theory, it is more or less obvious that the transmission spectrum is expected to experience important modifications with respect to the free-standing holey metal screen: The presence of dielectric slabs adds new opportunities to surface waves to propagate along the structure. The consequences of adding dielectric slabs to the holey metallic surface has been explored by several authors [8–10]. These authors make use of different approaches but emphasis is given to the role of the surface waves. The aim of the present work is to show how the impedance matching point of view adopted in [6, 7] can be extended to deal with slit–like dielectric coated metallic perforated stuctures. This approach provides an alternative explanation to the appearence of new peaks and dips in the transmission spectrum (with respect to the free–standing structure). The behavior of these systems, under certain restrictions, can be modeled using a few circuit parameters, which are enough to describe the transmission and reflection spectra over a very wide frequency band.

REFERENCES

1. Genet, C. and T. W. Ebbesen, "Light in tiny holes," *Nature*, Vol. 445, 39–46, 2007.
2. García-de-Abajo, F. J., "Colloquium: Light scattering by particle and hole arrays," *Rev. Mod. Phys.*, Vol. 79, 1267–1290, 2007.
3. García-Vidal, F. J., L. Martín-Moreno, T. W. Ebbesen, and L. Kuipers, "Light passing through subwavelength apertures," *Rev. Mod. Phys.*, Vol. 82, 729–787, 2010.
4. Gordon, R., A. G. Brolo, D. Sinton, and K. L. Kavanagh, "Resonant optical transmission through hole-arrays in metal films: Physics and applications," *Laser & Photon. Rev.*, Vol. 4, No. 2, 311–335, 2010.
5. Beruete, M., I. Campillo, M. Navarro-Cía, F. Falcone, and M. Sorolla, "Molding left- or right-handed metamaterials by stacked cutoff metallic hole arrays," *IEEE Trans. on Antennas and Propagat.*, Vol. 55, No. 6, 1514–1521, 2007.
6. Medina, F., F. Mesa, and R. Marqués, "Extraordinary transmission through arrays of electrically small holes from a circuit theory perspective," *IEEE Trans. Mic. Theory Tech.*, Vol. 56, No. 12, 3108–3120, 2008.
7. Medina, F., F. Mesa, and D. C. Skigin, "Extraordinary transmission through arrays of slits: A circuit theory model," *IEEE Trans. Mic. Theory Tech.*, Vol. 58, No. 1, 105–115, 2010.
8. Lomakin, V. and E. Michielssen, "Enhanced transmission through metallic plates perforated by arrays of subwavelength holes and sandwiched between dielectric slabs," *Phys. Rev. B*, Vol. 71, 235117, 2005.
9. Moreno, E., L. Martín-Moreno, and F. J. García-Vidal, "Extraordinary optical transmission without plasmons: The *s*-polarization case," *J. Opt. A: Pure Appl. Opt.*, Vol. 8, S94–S97, 2006.
10. Ortuño, R., C. García-Meca, F. J. Rodríguez-Fortuño, J. Martí, and A. Martínez, "Multiple extraordinary optical transmission peaks from evanescent coupling in perforated metal plates surrounded by dielectrics," *Opt. Express*, Vol. 18, No. 8, 7893–7898, 2010.

Enhanced Transmission through Deep Subwavelength Apertures Using Metamaterials

Ekmel Ozbay
Nanotechnology Research Center, Bilkent University, Bilkent, Ankara 06800, Turkey

Abstract— We obtained enhanced transmission of electromagnetic waves through a single subwavelength aperture by making use of the resonance behavior of a split ring resonator (SRR) at microwave frequencies. By placing a single SRR at the near-field of the aperture, strongly localized electromagnetic fields were effectively coupled to the aperture with a radius that is twenty times smaller than the resonance wavelength ($r/\lambda = 0.05$). We obtained 740-fold transmission enhancement by exciting the electric resonance of SRR. We have recently extended this transmission enhancement performance to even higher values. The respective design parameters of the connected SRRs (Sample A&B) are depicted in Fig. 1(a). We have demonstrated the extraordinary transmission by using these samples. Fig. 1 illustrates how we incorporate the samples with the aperture. We drilled an opening on a large metal plate of 1 m × 1 m. The opening on our metal screen constituted the subwavelength aperture. The area of the subwavelength aperture is $3 \times 7.5\,\mathrm{mm}^2$ (width × height). The connected SRRs are inserted inside the aperture. Transmission measurements were performed with conventional horn antennas operating around the frequency band of our interest. The antennas were located 8 cm away from each other and the metal plate was positioned in between these antennas.

The enhancement results are calculated by dividing the transmission values obtained from the apertures with the samples to the only aperture case for every frequency. The measured transmission results are portrayed in Fig. 2(a) and Fig. 2(d) in linear scale. The peaks are the evidence of the transmission enhancement in the presence of the samples. Single aperture transmission results were multiplied with 10 to be able to visualize both results on the same graph. Likewise, Fig. 2(b) and Fig. 2(e) depict the simulation results. The simulation results agree well with the experimental results. The enhancement peaks are spotted at similar frequencies. The minor discrepancies are due to the difficulty of the exact manual alignment of the samples in the experiments as well as the small variations in the manufacturing processes and the crude modeling of the materials used in the experiments. Finally, the measured enhancement figures are plotted in Figs. 2(c) and (f). We experimentally observed a more than 70,000 times transmission enhancement for Sample A, whereas a higher than 5,300-fold transmission improvement was achieved with Sample B.

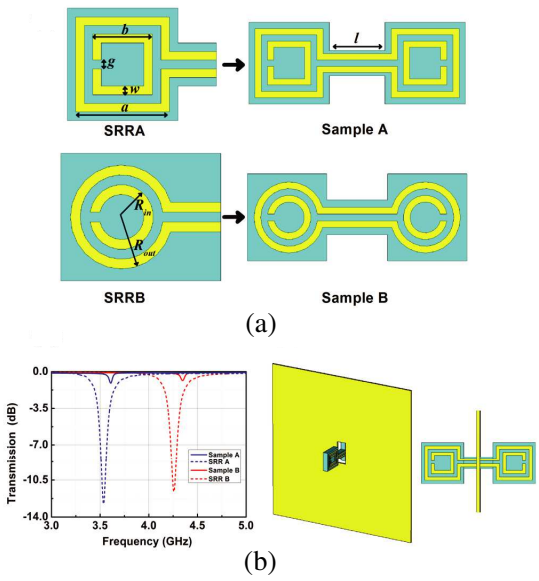

Figure 1.

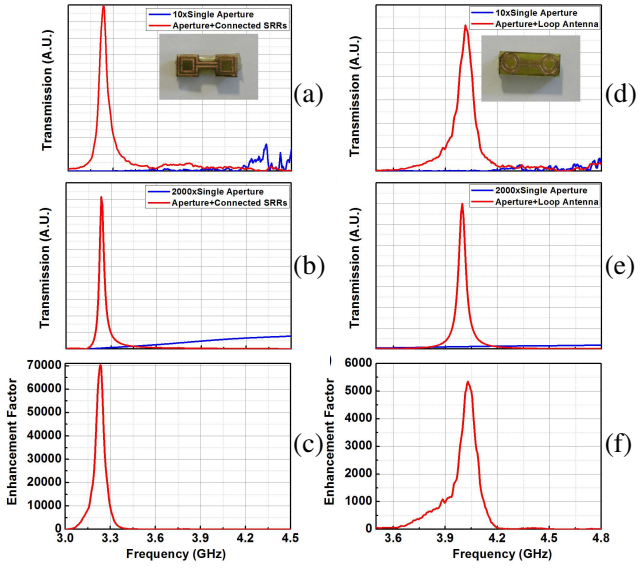

Figure 2.

Extraordinary Kerr Effect in Transmission in Magnetoplasmonic Nanostructured Films

V. I. Belotelov[1, 2], I. A. Akimov[3], M. Pohl[3], V. A. Kotov[1, 4], A. S. Vengurlekar[5], A. V. Gopal[5], D. Yakovlev[3], A. K. Zvezdin[1], and M. Bayer[4]

[1]A. M. Prokhorov General Physics Institute RAS, Moscow 119991, Russia
[2]M. V. Lomonosov Moscow State University, Moscow 119992, Russia
[3]Dortmund University, Dortmund 44221, Germany
[4]V. A. Kotelnikov Institute of Radio Engineering and Electronics RAS, Moscow 125009, Russia
[5]Tata Institute of Fundamental Research, Mumbai 400005, India

Abstract— Nowadays, much effort is being made in the area of nanophotonics, which demands materials with outstanding optical performance and tunability at the femtosecond time scale. For these purposes, magnetooptical materials hold great potential since their optical properties can be easily altered via magnetic field. However, the magnetooptical effects are usually not sufficiently strong. Until recently, the streamline in the magnetooptical effects enhancement was on chemical side. In this paper we propose a new concept. It was revealed recently that surface plasmons lie at the root of the extraordinary optical transmission phenomenon in the metallic films periodically perforated with subwavelength hole or slit arrays. Surface plasmons also remain decisive in the proposed here nanoscale magnetooptical material. In this material a thin magnetic dielectric film is attached to the perforated metal, thus constituting a kind of metal-dielectric heterostructure with nanoscaled pattern. Unique features of the proposed material are high value of the magnetooptical constant and low optical losses. We demonstrate experimentally a significantly enhanced the transverse Kerr effect in transmitted light. Observation of this effect in transmission in smooth ferromagnets is extremely difficult because of its small value and/or ultra low detected light intensity. The new magnetoplasmonic material allowed to make the effect several orders larger and to observe it near the extraordinary transmission peaks. Furthermore, the effect is very sensitive to the properties of the surface plasmons and is shown to be an efficient method for in-depth studies of plasmonic systems. The other magnetooptical effects can be also enhanced by the same structure. It is possible to switch among the effects by applying magnetic field in different directions. It is of great importance for applications in the fields of telecommunication, computing and sensing.

Session 1A3a
Near-field Techniques Applied to Based Metamaterial Devices

Engineering Near Field Coupling in Metamaterials

Abdelwaheb Ourir, **Redha Abdeddaim**, **and Julien de Rosny**
Institut Langevin, ESPCI Paris Tech., UMR 7587, CNRS, Laboratoire Ondes et Acoustique (LOA)
10 rue Vauquelin, 75231 Paris Cedex 05, France

Abstract— A Left-handed material (LHM), is a composite material characterized by simultaneous negative values of the real parts of electrical permittivity (ε) and magnetic permeability (μ). The most common and well known approach to realize a LHM is the combination of two distinct meta-atoms with respectively negative ε and negative μ, like the association of continuous wires and split-ring resonators (SRRs) [1]. Since then, other types of unit-cell have been proposed [2–4]. All these configurations require the application of a magnetic field perpendicularly to the resonator plane. Consequently, large number of planes has to be stacked laterally which is difficult to realize in the optical domain. Recently, a novel way to generate a negative index was demonstrated [5–8]. It consists in the inversion of the hybridization of two plasmon modes. The hybridization results from the stacking of two identical atoms. These two atoms are twisted or shifted regarding one another. With this novel coupling configuration, it has become possible to realize a thin metafilm which exhibits a negative index [8–11]. Breaking the geometrical symmetry between the two stacked meta atoms leads to the inversion of the hybridization modes. The negative index is present when the two modes coming from hybridization resonate around the same frequency. This hybridization inversion by a geometrical asymmetry is due to the modification of the Coulomb interactions between the two stacked meta atoms. Metamaterials obtained in such ways are called stereometamaterials in reference to the stereochemistry consisting in materials with the same chemical formula but different spatial arrangements of atoms [11].

In this work, we propose a new kind of stereometamaterials by engineering the near field coupling between the meta atoms. By this way, we control the hybridization of the produced resonant modes. The aim is to overlap two resonant hybrid modes with negative m and negative e, respectively. We show that a negative index can be achieved thanks to this method.

REFERENCES

1. Smith, D., W. Padilla, D. Vier, S. Nemat-Nasser, and S. Schultz, *Phys. Rev. Lett.*, Vol. 84, 4184, 2000.
2. Huangfu, J., L. Ran, H. Chen, X.-M. Zhang, K. Chen, T. M. Grzegorczyk, and J. A. Kong, *Appl. Phys. Lett.*, Vol. 84, 1537, 2004.
3. Chen, H., L. Ran, J. Huangfu, X. Zhang, K. Chen, T. M. Grzegorczyk, and J. A. Kong, *Appl. Phys. Lett.*, Vol. 86, 1, 2005.
4. Chen, H. S., L. X. Ran, J. T. Huangfu, X. M. Zhang, and K. S. Chen, "Magnetic properties of S-shaped split-ring resonators," *Progress In Electromagnetics Research*, Vol. 51, 231–247, 2005.
5. Podolskiy, V. A., A. K. Sarychev, and V. M. Shalaev, *Nonlinear Opt. Phys. Mater.*, Vol. 11, 65, 2002.
6. Dolling, G., C. Enkrich, M. Wegener, J. F. Zhou, C. M. Soukoulis, and S. Linden, *Opt. Lett.*, Vol. 30, 3198, 2005.
7. Zhang, S., W. Fan, N. C. Panoiu, K. J. Malloy, R. M. Osgood, and S. R. J. Brueck, *Phys. Rev. Lett.*, Vol. 95, 137404, 2005.
8. Linden, S., M. Decker, and M. Wegener, *Phys. Rev. Lett.*, Vol. 97, 083902, 2006.
9. Christ, A., O. J. F. Martin, Y. Ekinei, N. A. Gippius, and S. G. Tikhodeev, *Nano Lett.*, Vol. 8, 2171, 2008.
10. Kante, B., A. de Lustrac, and J.-M. Lourtioz, *Photonics and Nanostructures — Fundamentals and Applications*, Vol. 8, 112, 2010.
11. Liu, N., H. Liu, S. Zhu, and H. Giessen, *Nat. Photon.*, Vol. 3, 157, 2009.

Metamaterials: An Enabling Technology for Wireless Communications

Omar M. Ramahi, **Muhammad S. Boybay**, **Omar Siddiqui**, **Leila Yousefi**, **Ali Kabiri**, **Hussein Attia**, **Mohammad Bait-Suwailam**, **and Zhao Ren**
Electrical and Computer Engineering Department, University of Waterloo
Waterloo, Ontario, N2L 3G1, Canada

Abstract— Metamaterials are structures that provide electromagnetic properties not found in naturally occurring media; properties such as negative index of refraction, negative permittivity, or negative permeability. Since the appearance of Pendrys seminal work in the year 2000 on the feasibility of creating material with negative refractive index, a deluge of papers were published on metamaterials proposing the existence of phenomena and applications never conceived before. So why would such excitement about something that was not intended to be present naturally? The answer is simple. We tend to design or envision applications based on what we believe to exist. It is fair to argue that many applications were not envisioned simply because they would have to be based on materials that do not exist. With the realization of metamaterials, new phenomena and applications became not only possible, but even practical. In this paper, we discuss metamaterial applications that our group at the University of Waterloo has focused on. These applications are mostly related to wireless communication systems including sensing.

Metamaterials are in essence electrically-small resonators. A structure that is electrically small implies that the size of the structure is much smaller than the wavelength in free space. The resonance that takes place in these structures is the result of an applied field that generates either a magnetic dipole moment, electric dipole moment or both in the small resonators. This resonance phenomenon is in sharp contrast to the constructive interference between waves bouncing back and forth along or within a traditional resonator such as a transmission line or cavity. For instance, in the artificial magnetic material type of metamaterials, the frequency range of interest will be immediately before the resonance frequency, whereas for single-negative type of metamaterials, the interest would be in the frequency range immediately above resonance.

In addition to providing enhanced magnetic or dielectric properties, metamaterials are fundamentally dispersive due to the inherent laws of physics governing the magnetization and polarization of materials or structures. So the question arises as to how such new interesting structures with properties not found in naturally available material provide engineering value, especially in the area of wireless communications? Here, the definition of wireless communications embodies hardware such as transmitters, receivers, antennas used for point-to-point communications, devices for RF, microwave, THz and optical frequencies transmission, and devices used for non-invasive detection or monitoring.

While metamaterial have seen applications in wide area of engineering disciplines, here, we focus on engineering applications related to the important area of wireless communications. We address how metamaterial can have a strong impact on the performance of planar antennas, Multi-Input Multi- Output antenna systems, electromagnetic interference in printed circuit boards and packages, microwave non-invasive detection using near-field microscopy, and, finally, biosensing.

Simulation and Measurement and of a Negative Refractive Index in Resonators Planar Medium

Z. Djeffal, H. Talleb, D. Lautru, and V. Fouad Hanna
UPMC Université Paris 06, EA 4436, L2E, F-75005, Paris, France

Abstract— So far, there have been very few successfully realized engineering applications making use of materials that can exhibit backward-wave propagation phenomenon most of them utilizing planar microwave circuits. This paper gives results of measurements in X band demonstrating the presence of a negative refractive index in magneto-electric medium composed of split ring resonators (SSR). The experiment has been performed using a prism. The obtained results concerning the steering beam angle as well as the relative negative index value show a good agreement with those obtained by full-wave simulations extraction method. Thus, these results show that magnetoelectric activities inside a bianistropic medium can lead to the establishment of a relative negative refractive index supported by a backward-wave propagation phenomenon. The non use of metallic wires medium to obtain a negative index should provide many potential opportunities to reduce and improve the performance of the planar structure. A direct application can be the insertion of localized circuit elements inside the structure to control electronically a specific reconfigurable resonator planar medium.

REFERENCES

1. Sievenpiper, D., et al., "High-impedance electromagnetic surfaces with a forbidden frequency band," *IEEE Trans. on Microwave Theory and Techniques*, Vol. 47, No. 11, 2059–2074, November 1999.
2. Grbic, A. and G. V. Eleftheriades, "Experimental verification of backward-wave radiation from a negative refractive index metamaterial," *Journal of Applied Physics*, Vol. 92, No. 10, November 15, 2002.
3. Cummera, S. A. and B.-I. Popa, "Wave fields measured inside a negative refractive index metamaterial," *Applied Physics Letters*, Vol. 85, No. 20, November 15, 2004.
4. Mahmoudi, A., A. Semnani, R. Alizadeh, and R. Adeli, "Negative refraction of a three-dimensional metallic photonic crystal," *Eur. Phys. J. Appl. Phys.*, Vol. 39, 27–32, 2007.
5. Sudhakaran, S., Y. Hao, and C. G Parini, "Negative-refraction phenomenon at multiple frequency bands from electromagnetic crystals," *Microwave and Optical Technology Letters*, Vol. 45, No. 6, June 20, 2005.
6. Notomi, M., "Theory of light propagation in strongly modulated photonic crystals: Refraction like behavior in the vicinity of the photonic band gap," *Phys. Review B*, Vol. 62, No. 16, October 15, 2000.
7. Luo, C., S. G. Johnson, and J. D. Joannopoulos, "All-angle negative refraction without negative effective index," *Phys. Review B*, Vol. 65, 201104(R), 2002.
8. Grzegorczyk, T. M. and J. A. Kong, "Electrodynamics of moving media inducing positive and negative refraction," *Phys. Review B*, Vol. 74, 033102, 2006.
9. Simovski, C. R. and B. Sauviac, "Role of wave interaction of wire and split-ring resonators for the losses in a left-handed composite," *Phys. Review E*, Vol. 70, 046607, 2004.
10. Marques, R., F. Medina, and R. Rafii-El-Idrissi, "Role of bianisotropy in negative permeability and left-handed metamaterials," *Phys. Rev. B*, Vol. 65, 144440-1–6, 2002.
11. Tretyakov, S. A., C. R. Simovski, and M. Hudlička, "Bianisotropic route to the realization and matching of backward-wave metamaterial slabs," *Phys. Review B*, Vol. 75, 14504, 2007.
12. Qiu, C. W., H. Y. Yao, L. W. Li, S. Zouhdi, and T. S. Yeo, "Routes to left-handed materials by magnetoelectric couplings," *Phys. Review B*, Vol. 75, 245214, 2007.
13. Qiu, C. W., H. Y. Yao, L. W Li, S. Zouhdi, and T. S. Yeo, "Backward waves in magneto-electrically chiral media: Propagtion, impedance, and negative refraction," *Phys. Review B*, Vol. 75, 155120, 2007.
14. Markel, V. A., "Correct definition of the poynting vector in electrically and magnetically polarizable medium reveals that negative refraction is impossible," *Optics Express*, Vol. 17, No. 17, 15170–15172, 2009.

15. Chen, X., et al., "Robust method to retrieve the constitutive effective parameters of metamaterials," *Phys. Review E*, Vol. 70, 2004.
16. Born, M. and E. Wolf, *Principle of Optics*, 7th Edition, 190–192, 1999, ISBN 0521642221.
17. Kong, J. A., *Electromagnetic Wave Theory*, 1986, ISBN 0-471-82823-8.

Characterization of High Impedance Surface (HIS) Properties for Low Profile Antenna Application

C. T. Manh, **H. Hafdallah Ouslimani**, **and A. C. Priou**
Laboratory of Énergétique Mécanique et Électromagnétisme
University of Paris West Nanterre la Défense, 50 Rue de Sèvres, Ville d'Avray 92410, France

Abstract— The millimeter-wave domain is always important for high speed wireless and high bit rate optical (> 40 Gbits/s) communications systems. In this paper, we introduce a number of HIS structures with various metallic unit cells motifs optimized for the millimeter-wave domain. Those electromagnetic structures become nowadays very attractive in particular in low profile antenna applications and mutual coupling reduction. Various experimental, numerical and simulation techniques are used to characterize the resonant property of HIS structures. In particular, the method of suspended microstrip line is used to obtain the transmission coefficients and determine the resonant region of HIS. The experimental and simulated results are in good agreement.

Microstrip antennas based on High Impedance Surface reflectors are designed at 40 GHz. The measurement as well as simulation results demonstrate the advantages of the metamaterial structure. Enhancements of their performances including gain, directivity, and bandwidth and reducing back radiation [1, 2] are demonstrate. Furthermore, one can use a combination of HIS with antenna by inserting them between array elements to reduce the mutual coupling for application in array antenna [1–6].

REFERENCES

1. Sievenpiper, D., L. Zhang, R. F. J. Broas, N. G. Alexopoulos, and E. Yablonovitch, "High Impedance electromagnetic surfaces with a forbidden frequency band," *IEEE Trans. on Microwave Theory and Tech.*, Vol. 47, 2059–2074, 1999.
2. Yang, F. R., K. P. Ma, Y. Qian, and T. Itoh, "A uniplanar compact photonics bandgap structure and its applications for microwave circuits," *IEEE Trans. on Microwave Theory and Tech.*, Vol. 47, No. 8, 1999.
3. Yang, F. and Y. R. Samii, "Microstrip antennas intergrated with electromagnetic bandgap structure: A low mutual coupling design for array applications," *IEEE Trans. Ant. Appl.*, Vol. 51, 2003.
4. Xin, H., K. Matsugatani, M. Kim, J. Hacker, J. A. Higgins, M. Rosker, and M. Tanake, "Mutual coupling reduction of low-profile monopole antennas on high impedance ground plane," *E. Lett.*, Vol. 38, No. 16, August 2002.
5. Yang, L., M. Fan, F. Chen, J. She, and Z. Feng, "A novel compact electromagnetic-bandgap (EBG) structure and its applications for microwave circuits," *IEEE Trans. on Microwave Theory and Tech.*, Vol. 53,183–190, 2005.
6. Ziolkowski, R. W. and A. Erentok, "Metamaterial-based efficient electrically small antennas," *IEEE Transactions on Antennas and Propagation*, Vol. 57, 2113–2130, 2006.

Session 1A3b
Metamaterials and Their Applications 1

Scattering Properties of Elliptical Cylinder Coated by Lossy DNG Metamaterial

M. I. Hussein
Department of Electrical Engineering, United Arab Emirates University, Al-Ain, UAE

Abstract— This document gives formatting instructions for authors preparing papers for publication in the Proceedings of an IEEE conference. The authors must follow the instructions given in the document for the papers to be published. You can use this document as both an instruction set and as a template into which you can type your own text.

Ferromagnetic Resonances in Single and Two-phase Magnetic Microwires

G. Infante[1], **L. Kraus**[2], **V. Raposo**[3], **R. El Kammouni**[4], **M. Britel**[4], **and M. Vázquez**[1]

[1]Institute of Materials Science of Madrid, CSIC, Madrid 28049, Spain
[2]Institute of Physics, ASCR, Prague 18221, Czech Republic
[3]Dpto. de Física Aplicada, Universidad de Salamanca, 37071, Spain
[4]Faculty of the Sciences and Techniques, UAE, BP 418, Tangier, Morocco

Abstract— Magnetic microwires are composed of a metallic core coated by an insulating glass layer and have a remarkable magnetic behaviour [1]. Further improvement of their properties can be achieved by electroplating an outer magnetic outer shell onto the glass layer, obtaining a so-called two-phase microwire [2].

Despite that the ferromagnetic resonance (FMR) in these wires has been extensively studied [3–5], the interpretation of their FMR spectra is far from being unanimous. The aim of this work is therefore to present experimental results showing that geometry, shape of the driving microwave field and skin depth should be considered as a whole for a correct understanding of their microwave absorption. Various resonance modes can be excited in single phase microwires [4]. Bulk samples satisfy the Kittel's condition for a tangentially magnetized thin film (FMR_1). However, for wires with diameters close to 1 µm (Figure 1) placed in zero microwave electric field ($e = 0$) a second absorption mode (FMR_2) is excited with a weak resonance peak at magnetic field close to the Kittel's condition for an axially magnetized cylinder. Finally, for wires with diameters much less than the electromagnetic penetration depth (i.e., nanoscale) FMR_1 disappears and only FMR_2 is observed [6].

Two phase microwires are micro coaxial lines displaying multiple FMR absorptions [5]. Experiments performed on fully saturated samples (Figure 2) reveal the presence of 3 resonance peaks. It will be shown that the two ones appearing at higher frequencies correspond to FMR of the two magnetic phases, while the intrinsic capacitive character of the microwire structure is the responsible for the low-frequency resonance via a the measuring circuit.

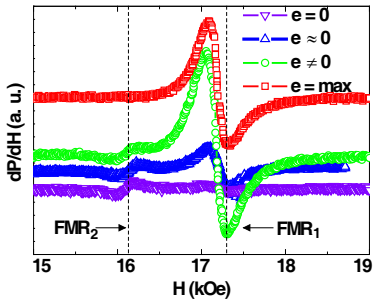

Figure 1: Ferromagnetic absorption derivative vs static applied field at 69.7 GHz for an $Fe_{76}Si_9B_{10}P_5$ microwire with a 1.5 µm thick metallic nucleus (total diameter is 30 µm). Microwave magnetic field intensity e as a parameter.

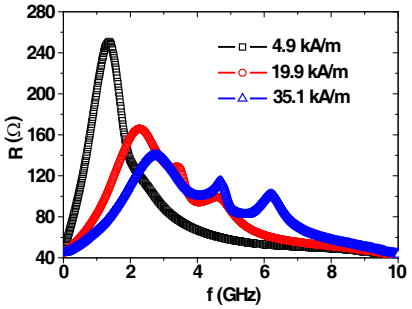

Figure 2: Evolution of the multipeak resonance spectra (real part of impedance) with static magnetic field for a saturated CoFe/FeNi composite microwire. CoFe core and FeNi shell are 16 and 2.5 µm thick, respectively. Insulating Pyrex layer is 13 µm thick.

REFERENCES

1. Vázquez, M., *Handbook of Magnetism and Advanced Magnetic Materials*, Vol. 4, 2193, Wiley, 2007.
2. Torrejón, J., L. Kraus, G. Badini-Confalonieri, and M. Vázquez, *Acta Materialia*, Vol. 56, 292, 2008.
3. Menard, D., M. Brittel, P. Ciureanu, and A. Yelon, *J. Appl. Phys.*, Vol. 84, 2805, 1998.
4. Kraus, L., *Czech. J. Phys. B*, Vol. 32, 1264, 1982.
5. Torrejón, J., G. A. Badini-Confalonieri, and M. Vázquez, *J. Appl. Phys.*, Vol. 106, 023913, 2009.
6. Arias, R. and D. L. Mills, *Phys. Rev. B*, Vol. 63, 134439, 2001.

Enhanced Ferromagnetic and Ferroelectric Properties of La Doped Multiferroic $Bi_5Fe_{0.5}Co_{0.5}Ti_3O_{15}$ Ceramics

Xiangyu Mao[1], **Wei Wang**[1], **Xiaobing Chen**[1], **and Yalin Lu**[2]

[1]College of Physics Science and Technology, Yangzhou University, Yangzhou 225002, China
[2]Department of Physics, Laser and Optics Research Center, U.S. Air Force Academy, Colorado 80840, USA

Abstract— The samples of $Bi_{4.25}La_{0.75}Fe_{0.5}Co_{0.5}Ti_3O_{15}$ (BLFCT) were processed in two steps: Firstly making $Bi_{3.25}La_{0.75}Ti_3O_{12}$ powders using multi-calcination-method and secondly synthesizing BLFCT samples in a traditional solid state reaction route.

The evaluated lattice parameters of BLFCT are $a = 0.5343\,\text{nm}$, $b = 0.5359\,\text{nm}$, and $c = 3.9881\,\text{nm}$, slightly smaller form the BFCT samples. The BLFCT sample exhibits a typical ferromagnetic M-H loop, with remnant magnetization ($2M_r$) of $\sim 49.7\,\text{memu/g}$ and coercive field ($2H_c$) of $\sim 475\,\text{Oe}$, respectively. The M_{FC} and M_{ZFC} curve decreases when increasing temperature and good reversibility is maintained until the temperature about 143°C below which an obvious difference between ZFC and FC magnetization appeared and the phenomenon might be suggest a relaxation process [24]. The magnetic Curie temperature (T_{cM}) is thus estimated to be $\sim$ 210°C. Under the electric field of $180\,\text{kV/cm}$, the remnant polarization ($2P_r$) and the coercive field ($2E_c$) were about $15.4\,\mu\text{C/cm}^2$ and $129\,\text{kV/cm}$, respectively. The $2P_r$ of BLCFT samples increase with increasing the driving field (shown inset (a) of Fig. 4.). It is still far from saturation even at the used field of $180\,\text{kV/cm}$ (limited by sample breakdown). This result indicates that La-doping at A — site with $Bi_5Fe_{0.5}Co_{0.5}Ti_3O_{15}$ sample was also improved the FE, the $2P_r$ of BLFCT is above 2 times larger than that of BFCT ceramics ($2P_r \approx 7.1\,\mu\text{C/cm}^2$, under $E = 180\,\text{kV/cm}$). The advantage of BLFCT samples comes mainly from the two factors: (1) Many investigations of bismuth layer-structured ferroelectrics (BLSFs), the doping of lanthanum was effective to the reduced oxygen vacancy by the stabilized oxygen octahedron. (2) It is known that the BFO and BCO crystals are rhombohedrally distorted.

Enhanced Absorption in Si Solar Cells via Adding Thin Surface Plasmonic Layers and Surface Microstructures

Yalin Lu[1], **W. J. Mandeville**[2], **M. K. Shaffer**[1], **R. J. Knize**[1], **and Kitt Reinhardt**[3]

[1]Laser and Optics Research Center, Department of Physics
U.S. Air Force Academy, CO 80840, USA
[2]MITRE Corporation, 1155 Academy Park Loop, Colorado Springs, Colorado 80910, USA
[3]AFOSR/NE, 875 North Randolph Street, Ste 326, Arlington, VA 22203, USA

Abstract— Theoretically, large, broadband, and polarization-insensitive light absorption enhancement can be realized via integrating with unique metallic nanostructures either at the surface or buried inside the structures, and with surface microstructures created by lasers. In order further to understand the mechanisms and to reduce the fabrication cost, experimental demonstrations of light absorption affection by adding thin metallic plasmonic layers and laser-created surface microstructures to the thin film a-Si solar cells was performed. For adding the plasmonic layer, by adjusting those structural parameters such as thicknesses of the a-Si thin layer and the thin plasmonic layer's thickness, and the incident angle, light absorption enhancement by cavity resonances and by the planar plasmonic coupling was carefully analyzed. For creating the dense microstructures on silicon surface, frequency doubled, nanosecond (*nsec*) Nd:YAG laser pulses in the SF_6 ambient, were used. The infrared absorption is increased to near unity and extends well below the original bandgap far into the infrared. These results are interesting to making advanced solar cells on both efficiency and cost, as comparing to previous results reported using more complicated and less economical femotosecond (*fsec*) titanium sapphire and picosecond (*psec*) and nanosecond excimer lasers.

Layer-structured $Bi_5F_{0.5}Co_{0.5}Ti_3O_{15}$ Thin Films Grown by Pulsed Laser Deposition

Yalin Lu[1], **Gail Brown**[2], **Gregory Kozlowski**[3], **and Xiaobing Chen**[4]

[1]Laser and Optics Research Center, Department of Physics, U.S. Air Force Academy, CO 80840, USA
[2]AFRL/RXPSO, 3005 Hobson Way Bldg 651, Wright-Patterson AFB, OH 45433, USA
[3]Department of Physics, Wright State University, Dayton, OH 45435, USA
[4]College of Physics Science and Technology, Yangzhou University, Yangzhou 225002, China

Abstract— Thin films of Layer-structured $Bi_{0.5}Fe_{0.5}Co_{0.5}Ti_{0.3}O_{0.15}$ with the potential as metatmaterials for many functional photonic devices were fabricated by using pulsed laser deposition (PLD). In a search of optimal conditions to achieve epitaxial thin films, different substrate temperatures and different partial pressures of oxygen in the PLD chamber were used during deposition of the films on $LaAlO_3$, LSAT, MgO and STO single crystal substrates with (100) surface orientations. Combination of 100 mTorr of oxygen partial pressure and substrate temperature of 650°C gives the best crystallinity of the thin films. Thorough structural and chemical studies of these BFCTO films were done by using SEM, HRTEM, AFM, XPS and Electron Probe Microanalyser measurements. Dielectric and other properties of these films were measured and their correlations with structural and chemical properties were established.

Homogenization of Metallic Metamaterials in the Visible Range

B. Guizal[1], **D. Felbacq**[1], **and F. Zolla**[2]

[1]UMR-CNRS 5650, University of Montpellier 2, 34095 Montpellier Cedex 05, France
[2]Institut Fresnel, 13397 Marseille Cedex 20, France

Abstract— The famous mixtures formulas (Bruggeman, Lorentz-Lorenz...) used to derive relative effective permittivities of dielectric compounds have been show to experience some difficulties when applied to metal-insulator structures. The difficulty seems to stem from the fact that the constituents have positive and negative permeabilities. This situation is, for example, that encountered with metamaterials in the visible range. In the present work, we use a rigorous electromagnetic model and a homogenization tool to derive the effective permittivites and compare them with the aforementioned formulas.

In this work we focus on the behavior of periodic structures made of metallic wires embedded in a dielectric host. We use a rigorous formalism [1] based on a two-scale developpements of the fields in order to derive the exact effective permittivity of the compound. The homogeneization process is conducted through two steps: first a partial differential equation is derived from the two scale expansion and then solved numerically to obtain the effective permittivity. Equipped with this tool, we perform a systematic test of the validity of the classical formulas and their sturdiness when applied to metallic structures. As an application, we consider subwavelength structures made of gold or siver rods embedded in a dielectric matrix and focus on the consequences of their effective permittivity on the colour that would be really observed. To that purpose, we use a rigorous modal method [2] to compute the spectral (in the visible) reflection cefficient of such structures and then convert them into real observable colour by using the standard international data linked to the behavior of human eyes. We show that the filling ratio has a crutial importance in this process.

ACKNOWLEDGMENT

This work was realized in the framework of the ANR contract SCOP ANR-07-NANO-053-01. Support from the Institut Universitaire de France is gratefully acknowledged.

REFERENCES

1. Felbacq, D., B. Guizal, G. Bouchitte, and C. Bourel, "Resonant homogenization of metamaterials," *Microwave and Optical Technology Letters*, Vol. 51, 2695–2701, Nov. 2009.
2. Guizal, B., H. Yala, and D. Felbacq, "Fourier modal method with spatial adaptive resolution for structures comprising homogeneous layers," *JOSA A*, Vol. 26, 2567–2570, Dec. 2009.

Light Trapping within the Grooves of Diffraction Gratings

Mario M. Jakas and Francisco Llopis
Departamento de Física Fundamental y Experimental, Electrónica y Sistemas
Universidad de La Laguna, E-38205 La Laguna, Tenerife, Spain

Abstract— The possibility of using the rectangular-shaped grooves of a perfectly conducting diffraction grating as a light-trapping structure is analyzed. To this end a numerical code, which calculates the electromagnetic field produced by a well collimated, monochromatic light using the Rayleigh-Bloch method is developed. This code is then used to calculate the mean-square electric field amplitude over the groove volume, resulting from a beam of light which arrives to the grating within a cone, having all polarization states and within a small, but not negligible range of wavelengths. It is found that the average electromagnetic energy within the groove is considerably larger than that one finds far away above the grating. No such large peaks as those previously reported for well-collimated, monochromatic light are observed. However, figures in this paper show that diffraction gratings can be successfully used for producing light-confinement in photovoltaic and optoelectronic devices.

Session 1A4
Emerging Modalities and Novel Applications of Inverse Problems in Electromagnetics

3D Tomographic Approach for Microwave Breast Cancer Detection

Elia A. Attardo[1], **Andrea Borsic**[2], **Giuseppe Vecchi**[1], **and Paul M. Meany**[2]

[1]Electronic Department (DELEN), Polytechnic of Turin, C.so Duca degli, Abruzzi, 24, Turin 10144, Italy
[2]Thayer School of Engineering, Dartmouth College, 8000 Cummings Hall, Hanover, NH 03755-8000, USA

Abstract— Recently, Microwave Imaging (MI) has grown as a promising technique in breast cancer detection. In fact, it is possible observe a different response for the normal and malignant breast tissue when an electromagnetic wave (at microwave frequency) impinges the breast. Unlike the proposed radar based technique, when a inhomogeneous scenario is involved, which is the case of breast tissue, a tomographic one can better detect the presence of small tumor inside the breast. In this work, we present some preliminary results on breast phantom obtained processing the data from the tomographic system developed at Dartmouth College, Microwave Imaging System (MIS), by using a tomographic method. Basically, it is a crucial aspect having a reliable representation of the working scenario. In order to accomplish this task a full-wave approach, 3D, is used related to the electromagnetic forward solution while a 2D inversion procedure is taken into account to reconstruct the electric properties of the phantom. We present our results analyzing separately the two aspect, forward and inverse. In modelling the forward problem we will consider a discretization of the Helmhotz's equations by a finite element method (FEM), double curl. In doing this we have selected as basis function the zero order Whitney form, edge element. Also, noting that MIS uses an array of resistively-loaded monopole antenna immersed in a lossy medium, a FEM model for the aforementioned antenna is presented. Additionally, the entire domain under investigation is truncated by several layers of Perfectly Matched Layer (PML) terminated by a Perfect Electric Conductor (PEC), metal-backed PML. In order to correctly implement the PML all equations involved are recast in a tensorial way. Moreover, a new attenuation rule for the PML is presented. Using this rule allows us to reduced the number of elements for each layer and consequently to speed up the solution of the direct problem. Concerning the 2D inversion procedure a Gauss-Newton iterative method using a Tikhonov regularization for solving for the updates (GN-T) is applied. Naturally, in each step of the iterative process we need to construct the Jacobian matrix, and solve the direct problem in order to update the sought dielectric properties. The efficiency of the numerical tomographic approach presented here will be tested on phantoms.

Nondestructive Evaluation of Extended Scatterers Using Phaseless Data Subspace-based Optimization Method in the Framework of the Method of Moments

L. Pan, X. Chen, and S. P. Yeo
Department of Electrical and Computer Engineering, National University of Singapore, 117576, Singapore

Abstract— The electromagnetic inverse scattering technique has attracted much interest in a diversity of imaging-related applications, such as remote sensing, biomedical diagnosis, nondestructive testing and military surveillance. One of the main challenges in the practical application of inverse scattering technique lies in the fact that that the phase is generally more difficult to measure than the amplitude. As a matter of fact, accurate knowledge of the phase information involves far more sophisticated measurement equipments, especially as the working frequency increases. Furthermore, researchers have reported that the accuracy of phase measurements cannot be guaranteed for operating frequencies approaching the millimeter-wave band and beyond, due to the fact that the phase data is more prone to noise corruption during measurement than the amplitude data. Consequently, the adoption of phaseless (intensity-only) inverse scattering techniques is mandatory at optical frequencies, and strongly suggested at microwave frequencies.

In this paper, we propose the Phaseless Data Subspace-based Optimization Method (PDSOM) in the framework of the Method of Moments (MoM) so as to reconstruct the relative permittivity profiles of extended scatterers in Transverse Electric case, by utilizing only phaseless measurements (i.e., intensity data of the total field with no phase information). The numerical result demonstrates that the proposed method is capable of reconstructing complicated patterns with rapid rate of convergence and robust immunity to noise; and, more importantly, the comparison unravels the framework-dependence of PDSOM, i.e., PDSOM in the framework of MoM outperforms PDSOM in framework of coupled dipole method (CDM), which supplies a new way of improving the capability of reconstruction.

REFERENCES

1. Chen, X., "Application of signal-subspace and optimization methods in reconstructing extended scatterers," *J. Opt. Soc. Am. A*, Vol. 26, 1022–1026, 2009.
2. Pan, L., K. Agarwal, Y. Zhong, S. P. Yeo, and X. Chen, "Subspace-based optimization method for reconstructing extended scatterers: Transverse electric case," *Journal of the Optical Society of America*, Vol. 26, 1932–1937, 2009.
3. Pan, L., X. Chen, and S. P. Yeo, "Application of the subspace-based optimization method in the framework of the method of moments: Transverse electric case," *Asia-Pacific Microwave Conference*, 980–983, Singapore, Dec. 2009.

Two-step Inversion Procedure for Microwave Breast Imaging

T. Moriyama[1], **Z. Meng**[2], **and T. Takenaka**[1]

[1]Nagasaki University, Nagasaki 852-8521, Japan
[2]Fukuoka University, Fukuoka 814-0180, Japan

Abstract— The breast cancer is a leading cause of cancer death among women all over the world. The number of breast incidence cases is 45,716 in 2003 and the death toll is 11,323 in 2007 in Japan. Since breast cancer has a high recovery rate by detection and treatment at early stage, mass screening is recommended. An X-ray mammography is currently considered as the most effective detection modality for a front-line mass screening. However, shortcoming in conventional X-ray mammography for breast cancer screening, such as lack of sensitivity (missing up to 15% of tumors) and an unreasonably large amount of false positive readings, especially for dense breast, have led to the search for viable complementary and/or alternative approaches for breast imaging.

Over the last two decades, a number of researchers have been working on the early detection of breast cancer by microwave imaging. Microwave breast imaging methods are roughly classified into two groups. Radar-based imaging techniques detect existence and location of an abnormality different from surrounding tissue with short processing time from amplitude and arrival time of reflected pulse from the abnormality. Inverse-scattering-based approaches give not only the location of the abnormality but also the size, shape and dielectric properties, which characterizes the abnormality more precisely, although they require intensive computational burden. We have proposed a time-domain inverse scattering imaging technique referred to as forward-backward time-stepping (FBTS) algorithm based on a gradient optimization to reconstruct the electrical parameters profiles of scattering objects and applied it to breast cancer detection. One of the reasons which attract researchers to work on microwave beast imaging is the significant contrast between malignant tumor and normal breast tissues. However, recently, the permittivity and conductivity of fibroglandular breast tissue was shown to be much higher than previously imagined. This makes microwave imaging of a dense breast more challenging.

In this paper, we consider microwave tomographic imaging of internal structure of a breast model with low contrast between fibroglandular and tumor tissues. A combination of the FBTS method and a genetic algorithm (GA) is introduced as a time-domain inversion method for the nonlinear inverse scattering problem. When inverse scattering problems are solved using optimization techniques, it is important to choose a proper initial guess to avoid the local minima problem and obtain the solution with less computation time. To this end, in the first step we find a rough geometrical data about the size and location of a fibroglandular tissue region inside a breast by assuming that both fibroglandular and fat tissue regions are homogeneous. In order to extract the rough geometrical data, it is sufficient to express the fibroglandular region by a simple shape. This greatly reduces the number of parameters to be estimated and make GA feasible. Before the second step, the roughly estimated fibroglandular tissue region was enlarged a little bit, followed by filtering to smooth the abrupt change at the boundary of the region. After obtaining rough image of the breast inside, detailed reconstruction in the second step is efficiently carried out applying the FBTS method. The proposed two-step reconstruction algorithm was applied to imaging of 2D breast numerical phantom based on a MR image and was shown to successfully detect 5 mm diameter tumor in the breast model.

Can Tissue Oxygenation be Non-invasively Assessed Using Microwave Tomography?

S. Semenov[1], **J. Kellam**[2], **T. Williams**[2], **M. Quinn**[2], **and B. Nair**[1]

[1]School of Medicine, ISTM, Keele University, Stoke-on-Trent, ST4 7QB, UK
[2]Carolinas Medical Center, Charlotte, NC, 28203, USA

Abstract— Microwave Tomography (MWT) is approaching its pre-clinical evaluation stage when the technology is assessed for its imaging potentials of various functional and pathological conditions of biological tissues. The examples are: tissue malignancies, with recent major focus on breast cancer detection, tissue blood content, ischemia, infarction, stroke and others.

Early in non-imaging experiments we have demonstrated the feasibility of the technology for an assessment of tissue oxygenation status. Those studies were conducted on live animals (canine) when blood oxygenation was decreased by 10% having the same myocardial blood flow. We used a contact, probe method to measure changes in myocardial dielectric properties. The dielectric properties of tissues are the ones imaged by MWT. In recent research we study an applicability of MWT for a noninvasive assessment of tissue oxygenation. We focus of skeletal muscle and used our fast 2D MWT system, presented elsewhere.

Five Yorkshire domestic cross/farm pigs, males and females, were used in this study. Animals were cared for under an Institutional Animal Care and Use Committee approved research protocol and the NIH guidelines for laboratory research. Top portion of left front swine extremity was position inside of an imaging chamber filled with matching solution. Frequency was 1.05 GHz. We used a full system electronic scanning and control with 133 frames acquired and with 12 msec data acquisition at each frame.

Since the system has 24 antennas capable for operation in either transmitting or receiving modes, after electronic san we obtained a raw measured data matrix $(24 * 23)$ of complex scattered electromagnetic fields. Then inversion approaches were used for image reconstruction of the raw data from each frame. We used a nonlinear Newton based approaches as well as Born approximation. Images obtained at different stages of tissues oxygenation demonstrate potential applicability of MWT for an assessment of tissue oxygenation status.

The Linear Sampling Method as a Synthesis Strategy: A Simple Approach to Focusing in Unknown Media

I. Catapano[1], **L. Crocco**[1], **D. Iero**[2], **and T. Isernia**[2]

[1]CNR, IREA, Institute for Electromagnetic Sensing of the Environment, National Research Council, Italy
[2]DIMET, Mediterranea University of Reggio Calabria, Italy

Abstract— The linear sampling method (LSM) [1] is an imaging approach capable of retrieving the shape of an unknown target from a simple processing of the field it scatters. Given its robustness and low computational burden is nowadays very popular in the inverse scattering community both as an effective tool to retrieve the morphology of an object (qualitative imaging) and as a valuable preprocessing step for the quantitative characterization of a scatterer.

The authors of this contribution have proposed a physical interpretation of the LSM [2], which enlightens the analogy existing among the linear inverse problem underlying LSM and the problem of focusing waves in presence of a target. While such an interpretation has proved to be an useful tool to assess and foresee the performances of LSM in several (canonical and non-canonical) configurations [3–7], we instead take it here as the starting point to propose a novel exploitation of the LSM in a different inverse electromagnetic problem, that is the synthesis of a source (actually an array of antennas) capable of focusing the field it radiates onto a target located in an unknown environment.

The problem can be stated as follows: determine the excitation coefficients of the array elements in such a way that the radiated field is focused in a target point located in a medium of unknown characteristics. Notably, this kind of problem cannot be handled with usual antennas synthesis techniques, that implicitly require the knowledge of the electromagnetic features of the medium in which the target point is hosted. Similarly, time-reversal techniques are not suitable as well, since they need a knowledge of the medium into which the waves are "reversed", in order to properly focus them on the target point.

The recalled physical interpretation [2] suggests that the LSM provides a simple way to pursue the desired task. The key idea is that, for a given target point belonging to the region under test, the solution of the LSM integral equation corresponds to a linear combination of the incident fields able to create a point source induced current in the selected point. Hence, the proposed focusing method consists of two steps: first, the unknown region where the target point is located is probed by plane waves and the resulting scattered field processed in order to achieve the solution of the LSM equation in the target point, second, the (possibly scaled) LSM coefficients are adopted as excitations coefficients for the array elements to achieve the desired focused field.

REFERENCES

1. Cakoni, F. and D. Colton, *Qualitative Methods in Inverse Scattering Theory: An Introduction*, Springer, Berlin Heidelberg, New York, 2006.
2. Catapano, I., L. Crocco, and T. Isernia, "On simple methods for shape reconstruction of unknown scatterers," *IEEE Trans. Antennas Propagat.*, Vol. 55, No. 5, 1431–1436, 2007.
3. Catapano, I., L. Crocco, and T. Isernia, "Improved sampling methods for shape reconstruction of 3D buried targets," *IEEE Trans. Geosci. Rem. Sens.*, Vol. 46, No. 10, 3265–3273, 2008.
4. Catapano, I., L. Crocco, M. D'Urso, and T. Isernia, "3D Microwave Imaging via preliminary support reconstruction: Testing on the fresnel 2008 database," *Inv. Problems*, Vol. 25, No. 4, 024002, 2009.
5. Catapano, I. and L. Crocco, "An imaging method for concealed targets," *IEEE Trans. Geosci. Rem. Sens.*, Vol. 47, No. 5, 1301–1309, 2009.
6. Catapano, I. and L. Crocco, "Linear sampling method for time-lapse qualitative through-the-wall imaging," *Proc. European Radar Conference 2009, EuRAD 2009*, 613–616, Rome, Italy, Sept. 2009.
7. Di Donato, L., I. Catapano, F. Soldovieri, and L. Crocco, "Imaging of 3D magnetic targets from multiview multistatic GPR data," *Proceedings of 13th Int. Conf. Ground Penetrating Radar, GPR2010*, 1–6, Lecce, Italy, Jun. 2010.

Exploiting Inverse Scattering Theories for Real-time Tracking in Homeland Security Applications

F. Viani[1], **P. Rocca**[1], **M. Donelli**[1], **D. Trinchero**[2], **and A. Massa**[1]

[1]ELEDIA Research Group at DISI, University of Trento, via Sommarive 14, I-38123, Trento, Italy
[2]iXem Labs at DELEN, Politecnico di Torino, corso Duca degli Abruzzi, 24, I-10129, Torino, Italy

Abstract— Recent developments in wireless and embedded systems brought to a wide and rapid diffusion of Wireless Sensor Networks (WSNs) [1]. There are many applications for WSN ranging from everyday life practical solutions to military applications. One of the most attractive feature of sensor networks is localization and tracking capability. In such a framework, the main efforts have been devoted to the development of ad-hoc systems, that require each target to be equipped with a radio transmitting device, which is then located processing the signal received from other anchor nodes such as the time of arrival (TOA) or the direction of arrival (DOA) [2, 3] or exploiting dedicated sensors measuring quantities as light, infrared or sound energy to infer the position of targets [4, 5]. However, when dealing with people, the need of wearable active devices limits the reliability of the tracking system because of privacy issues or damages caused by noncooperative subjects (such as elderly people).

The aim of this work is to present an inversion procedure for the localization and tracking of passive targets measuring only the strength of the RF signals transmitted among the nodes of the WSN. The easily available RSS index gives the opportunity to measure the arising electromagnetic radiations that can be exploited to sense the environment. The objects lying within the monitored area interact with RF electromagnetic waves and the perturbations are processed by a suitable inversion strategy to determine the equivalent source modeling the presence and the position of the target. In order to have a flexible methodology and real-time estimates, a customized learning-by-examples (LBE) strategy based on a support vector machine (SVM) classifier is exploited. The proposed approach has been experimentally validated in presence of single and multiple targets lying in outdoor and indoor environments.

REFERENCES

1. Chong, C. Y. and S. P. Kumar, "Sensor networks: Evolution, opportunities, and challenges," *Proc. IEEE*, Vol. 91, 1247–56, 2003.
2. Latsoudas, G. and N. D. Sidiropoulos, "A fast and effective multidimensional scaling approach for node localization in wireless sensor networks," *IEEE Trans. Geosci. Remote Sens.*, Vol. 55, 5121–5127, 2007.
3. Huang, C. T., C. H. Wu, Y. N. Lee, and J. T. Chen, "A novel indoor RSS-based position location algorithm using factor graphs," *IEEE Trans. Wirel. Commun.*, Vol. 8, 3050–3058, 2009.
4. Boukerche, A., H. Oliveira, E. F. Nakamura, and A. Loureiro, "Localization systems for wireless sensor networks," *IEEE Wireless Comm.*, Vol. 14, No. 6, 6–12, Dec. 2007.
5. Zappi, P., E. Farella, and L. Benini, "Tracking motion direction and distance with pyroelectric IR sensors," *IEEE Sensor Journal*, Vol. 10, No. 9, 1486–1494, Sep. 2010.

A Diagnostic Toolbox for Large Arrays Combining Different Spectral Estimation Techniques

Aniello Buonanno[1], **Michele D'Urso**[1], **Marco Donald Migliore**[2], **and D. Pinchera**[2]

[1]Innovation Team, Intangible Capital Directorate Managment, SELEX Sistemi Integrati S.p.A.
Via Circumvallazione Esterna, Loc. Pontericci Zona ASI, I-80014 Giugliano, Napoli, Italy
[2]Dipartimento di Automazione, Elettromagnetismo, Ingegneria dell'Informazione e Matematica Industriale
Università degli Studi di Cassino, Via G. di Biasio, 43, 03043 Cassino, Frosinone, Italy

Abstract— In many applications there is the need of developing accurate toolbox for the fast and accurate diagnosis of very large arrays. These have several hundreds of active radiating elements, and the possibility of their failure strongly increases, with negative effect on the overall array performances. To solve the problem, many active antennas often include calibration systems. These tools make an easy control of the overall system components, but they can fail if the calibration system is damaged too. These systems are often rejected because its inclusion means a critical increase in array volume, weight and costs. An alternative solution is to localize the faulty elements starting from a proper set of near-field measures, as in [1–5].

In this contribution, thanks to a proper re-interpretation of the Multiple Signal Classification (MUSIC) technique published in [6] mainly used to estimate the direction of arrival of multiple plane waves, a novel diagnostic tool is proposed and discussed by means of experimental data. The main idea is to assume that the incident signals and noise are uncorrelated, thus properly allowing to consider the subspace spanned by the noise orthogonal to the one spaced by the incident signals. By evaluating the eigenvalues of the covariance matrix of the waveforms measured at the probe positions, and then the eigenvectors belonging to the noise subspace, an estimate of both positions and actual weights of each radiating elements can be achieved by plotting a proper indicator derived by the spatial domain spectrum function. Different from traditional approaches [1, 5], where the problem is outlined as an inverse source one, here, similarly to [7], the problem has been outlined as an inverse scattering one.

Note that a proper set of near field measurements (both amplitude than phase) are required for an accurate estimation of the faulty elements by using the above MUSIC based approach. Due to the large dimensions of the considered radiating systems, this means that a very long time is required for acquiring the near-field data, with very high costs. To overcome such a limitation, the proposed toolbox herein proposed is also equipped with a further diagnostic procedure which only allows to detect (and not to localize, as above) the presence of faulty elements in the considered arrays starting from a very reduced set of near field measurement. The procedure can be applied when the number of faulty elements is much lower than the number of radiating elements, which, of course, is hopeful. The further technique is based on the Compressed Sensing theory of [8], and exploits the *a priori* knowledge of the failure-free excitation vector to allow an equivalent sparse array discarding the pieces of information not of interest for the failure identification problem.

REFERENCES

1. Patnaik, A., B. Choudhury, P. Pradhan, R. K. Mishra, and C. Christodoulou, "An ANN application for fault finding in antenna arrays," *IEEE Trans. on Antennas and Propag.*, Vol. 55, 775–777, Mar. 2007.
2. Castaldi, G., V. Pierro, and I. M. Pinto, "Efficient faulty element diagnostics of large antenna arrays by discrete mean field neural nets," *Progress In Electromagnetics Research*, Vol. 25, 53–76, 2000.
3. Yeo, B. and Y. Lu, "Array failure correction with a genetic algorithm," *IEEE Trans. on Antennas and Propag.*, Vol. 47, 823–828, May 1999.
4. Rodriguez, J. A., F. Ares, H. Palacios, and J. Vassal'lo, "Finding defective elements in planar arrays using genetic algorithms," *Progress In Electromagnetics Research*, Vol. 29, 25–37, 2000.
5. *IEEE Antennas and Wireless Propagation Letters*, Vol. 8, 375–378, May 2009.
6. Schmidt, R. O., "Multiple emitter location and signal parameter estimation," *IEEE Trans. on Antennas and Propag.*, Vol. 34, 276–280, Mar. 1986.
7. Buonanno, A., M. D'Urso, M. Cicolani, and S. Mosca, "Large phased arrays diagnostic via distributional approach," *Progress In Electromagnetics Research*, Vol. 92, 153–166, 2009.

8. Candes, E. J. and T. Tao, "Near-optimal signal recovery from random projections: Universal encoding strategies?" *IEEE Trans. on Information Theory*, Vol. 52, No. 12, 5406–5425, Dec. 2006.

Theoretical Model for Optical Sensing of a Random Monolayer of Particles

A. García-Valenzuela[1], **C. Sánchez-Pérez**[1], **E. Gutiérrez-Reyes**[2], **and R. G. Barrera**[2]

[1]Centro de Ciencias Aplicadas y Desarrollo Tecnológico
Universidad Nacional Autónoma de México, Apartdo Postal 70-186, Distrito Federal 04510, México
[2]Instituto de Física, Universidad Nacional Autónoma de México
Apartado Postal 20-364, Distrito Federal 01000, México

Abstract— In this work, we derive a theoretical model for the coherent reflection of light from a random monolayer of particles adsorbed on a flat surface. The coherent component of reflected light corresponds to the ensemble average of the scattered light and easily resolved from the diffuse one in practice because of its directionality. First, we consider a plane wave incident to a "free standing" random monolayer at an oblique angle of incidence. We set up a multiple scattering formalism to obtain the scattered field by the ensemble of particles. We average formally the integral equations and adapt to the monolayer problem the so called "effective field" approximation commonly used in light propagation through random colloidal systems. We establish a self consistent integral equation to solve for the average exciting field seen by the particles. Then we calculate the average scattered field giving rise to the so called "coherent" reflection. The derived model is expressed in terms of the elements of the amplitude scattering matrix of an isolated particle and is valid for monolayers with a low surface coverage fraction but for all angles of incidence. This model is a rigorous extension of more empirical models derived a few years ago [1, 2]. Then we introduce in the model the effects of a flat substrate of different refractive index supporting the monolayer. The numerical evaluation of the model is fast, rendering the model suitable for real time analysis. The derived model is suitable for its use in reflectometry experiments and optical sensing of monolayers either in an external or an internal configuration. We simulate numerically several possible sensing applications in a multi-angle reflectometry scheme for monitoring physical or chemical processes of adsorbed monolayers of nanoparticles on a flat surface.

REFERENCES

1. Van Der Zeeuw, E. A., L. M. Sagis, G. J. M. Koper, E. K. Mann, M. T. Haarmans, and D. Bedeaux, "The suitability of angles scanning reflectometry for colloidal particle sizing," *J. Chem. Phys.*, Vol. 105, No. 4, 1646–1653, 1996.
2. Peña-Gomar, M. C., J. J. F. Castillo, A. García-Valenzuela, R. G. Barrera, and E. Pérez, "Coherent optical reflectance from a monolayer of large particles adsorbed on a glass surface," *Applied Optics*, Vol. 45, No. 4, 626–632, 2006.

Session 1A5
SMOS Satellite CAL/VAL: CAROLS L Band Radiometer Airborne Campaigns

SMOS Mission and Related Airborne Carols Cal/Val Activities

Yann H. Kerr
Centre d'Etudes Spatiales de la BIOsphere (CESBIO (CNRS/IRD/CNES/UPS)), France

Abstract— SMOS, a L Band radiometer using aperture synthesis to achieve a good spatial resolution, was successfully launched on November 2, 2009. It was developed and made under the leadership of the European Space Agency (ESA) as an Earth Explorer Opportunity mission. It is a joint program with the Centre National d'Etudes Spatiales (CNES) in France and the Centro para el Desarrollo Teccnologico Industrial (CDTI) in Spain. SMOS carries a single payload, an L band 2D interferometric,radiometer in the 1400–1427 MHz h protected band. This wavelength penetrates well through the vegetation and the atmosphere is almost transparent enabling to infer both soil moisture and vegetation water content. SMOS achieves an unprecedented spatial resolution of 50 km at L-band maximum (43 km on average) with multi angular-dual polarized (or fully polarized) brightness temperatures over the globe and with a revisit time smaller than 3 days.

SMOS as been now acquiring data and undergoing the commissioning phase. The data quality exceeds what was expected, showing very good sensitivity and stability. The data is however very much impaired by man made emission in the protected band, leading to degraded measurements in several areas including parts of Europe and of China. However, many different international teams are now addressing cal val activities in various parts of the world, with notably large field campaigns either on the long time scale or over specific targets to address the specific issues. These campaigns take place in various parts of the world, in different environments from the Antarctic plateau to the deserts, from rain forests to deep oceans. Actually SMOS is a new sensor making new measurements paving the way to new applications. However it also requires a very fine analysis of the data so as to validate both the approach and the retrieval quality, as well as for monitoring the evolution of the sensor. To achieve such goals it is very important to link efficiently ground measurement to satellite measurements through field campaigns and related airborne acquisitions. It is in this framework that the CAROLS campaigns were organized in France and Spain, over the ocean and over land. This paper thus gives an overview of the science goals of the SMOS mission, a description of the main mission elements, and a foretaste of the first results including performances at brightness temperature as well as at geophysical parameters. It will include how the CAROLS campaigns were elaborated to address the main cal Val activities accounting for SMOS specificities and in what context they were organized.

CAROLS SMOS CAL/VAL Campaigns

M. Zribi[1, 2], M. Pardé[2], J. Boutin[3], P. Fanise[2], D. Hauser[2], M. Dechambre[2], Y. Kerr[1], M. Leduc-Leballeur[2], G. Reverdin[3], N. Skou[4], S. S. Søbjærg[4], C. Albergel[5], C. Calvet[5], J. P. Wigneron[6], E. Lopez-Baeza[7], K. Saleh[7], A. Ruis[8], and J. Tenerelli[9]

[1]CESBIO (CNRS/IRD/CNES/UPS), Toulouse, France
[2]LATMOS, Guyancourt, France
[3]LOCEAN, Paris, France
[4]DTU-Space, Lyngby, Denmark
[5]CNRM/GAME, Toulouse, France
[6]INRA-Bordeaux, Cestas, France
[7]Facultat de Fisica, Valencia, Spain
[8]IEEC/ICE-CSIC, Bellaterra, Spain
[9]National Institute of Marine Research, Brest, France

Abstract— SMOS satellite mission is based on an aperture synthesis L-band radiometer, designed and developed by the European Space Agency (ESA). In the context of the validation activity for the SMOS mission, the authors proposed to design, build and operate the CAROLS L-Band radiometer from an aircraft. Because the sensitivity of L-band brightness temperature to salinity is very small (-0.45° K/psu at a physical temperature equal to 15° K), it was necessary to build a very accurate, sensitive, and stable system. The CAROLS, an L-band radiometer (1400–1427 MHz), was built and designed as a copy of EMIRAD II radiometer of DTU team by the LATMOS. It is a Correlation radiometer with direct sampling and fully polarimetric (i.e., 4 Stockes) which shows sensitivity equal to 0.1 K for 1 s integration time (300 K target) and with stability better than 0.1 K over 15 min. This radiometer could be used in conjunction with other airborne instruments (in particular the C-Band scatterometer (STORM), one visible camera), in coordination with in situ field campaigns for SMOS CAL/VAL.

An airborne campaign was realized during spring 2010 over south west of France, Valencia (Spain), and Bay of Biscay (Atlantic Ocean). Twenty two flights are proposed with CAROLS radiometer, using two antennas, one looking at nadir and the other at 33.5° incidence angle. Simultaneously to flights, different ground measurements were made over continental surfaces and ocean. First results show a good quality of data over ocean and continental surfaces. For continental surfaces, Radio-Frequency Interferences (RFI) were observed particularly over south west of France. Different approaches are proposed to correct RFI. The ability of the CAROLS radiometer to measure the brightness temperature of the surface was evaluated and then we compared measurements with ocean emission models outputs for different configurations. These estimations were performed for different view angles — using wing and nose wags movements and circles done by the aircraft over ocean — and for different dates. First comparisons between CAROLS data and SMOS products are realized.

Radio Frequency Interferences Investigation Using the Airborne L-band Full Polarimetric Radiometer CAROLS

M. Pardé[1], **P. Fanise**[1], **M. Zribi**[2], **and M. Dechambre**[1]

[1]UVSQ-CNRS, LATMOS, Guyancourt, France
[2]CESBIO-IRD, Toulouse, France

Abstract— The CAROLS radiometer is a correlation radiometer based on direct sampling and fully polarimetric (the 4 Stokes parameters are measured) which sensitivity and stability are better than 0.5 K. We used CAROLS data sets acquired during the airborne CAROLS campaigns done in 2008 and 2009 in the South West of France, to study Radio Frequency Interferences (RFI). In this paper, we propose to evaluate the capability of various algorithms to detect and mitigate RFI in airborne radiometric measurements. First we tested the commonly used Kurtosis parameter and we also used various criteria based on the Brightness Temperatures standard deviation: using a simple threshold we masked data supposed to be disturbed. Finally, we tested new algorithms based on the 3rd and 4th Stokes parameters measurements. Based on the estimation of the mean brightness temperature on a large transect (approximately 30 minutes of measurements), we have shown that all algorithms have the capability to detect Radar pulsed signals. However, algorithms based on Kurtosis are not able to correctly mitigate RFI appearing like strong permanent emissions. We have shown that the combination of STD-based algorithms with Kurtosis measurements can significantly improve the detection of RFI. The use of the 3rd and 4th Stokes parameters appears to be a quite good substitute to the Kurtosis algorithms.

Airborne Radar Measurements during the CAROLS Campaign

M. Dechambre[1], **D. Hauser**[1], **M. Zribi**[2], **and L. Baggio**[1]

[1]LATMOS (UVSQ/CNRS/UPMC), 11 Boulevard d'Alembert, Guyancourt 78280, France
[2]CESBIO (CNRS/IRD/CNES/UPS), 18 avenue Edouard Belin, 31401 Toulouse Cedex 9, France

Abstract— Airborne radar measurements have been carried out during the CAROLS campaign in conjunction with the L-band CAROLS radiometer, with the aim of testing the synergy between active and passive measurements. More specifically, the radar can provide a description of the surface roughness conditions useful to separate moisture and roughness effects (land surface) or salinity and roughness effects (ocean surface) on the radiometric signal. This information is expected to improve direct and inverse radiometric modelling. The operating instrument is the C-band full polarimetric ranging radar STORM, which has already participated to several field campaigns.

First we propose to present the experimental setup and the backscattering coefficient behaviour over different land surface moisture and roughness conditions (vegetated, areas, bare soils and forested areas). Secondly an estimate of the surface moisture is obtained by means of a simple semi-empirical modelling and compared with in situ and/or CAROLS measurements.

Sea Surface and Soil Moisture Remote Sensing with GNSS-R in the Frame of CAROLS Campaigns

Fran Fabra, **Estel Cardellach**, **and Antonio Rius**
Institut de Ciències de l'Espai (ICE-IEEC/CSIC), Spain

Abstract— CAROLS 2009 and 2010 (CNES/ESA) campaigns pursued the main objective of studying the science and calibration/validation of the Soil Moisture and Ocean Salinity (SMOS) mission, an ESA space-based experiment launched in November 2009 that performs soil moisture and ocean salinity measurements with a L-band radiometer. For that purpose, the campaigns comprised a set of flights over different experimental sites: the mouth of Garonne river into the Bay of Biscay, the South of France and Monegros (Zaragoza) and Valencia Anchor Station sites from Spain. The main payload of the aircraft was composed by a L-band radiometer (CAROLS), a C-band radar (STORM), and a GNSS-R instrument. In this work, we will present the analysis and results obtained with the latter instrument.

During the last years, the use of GNSS signals reflected off the Earth's surface has been proved as a valid method for remote sensing purposes. First appeared in 1993 (PARIS concept), the approach works as a L-band multistatic radar and has been motivated by the availability of the GPS, GLONASS and future GALILEO and COMPASS constellations of navigation satellites. Initially conceived for sea surface altimetry, GNSS-R offers many other potential applications, such as ocean wind speed, sea surface state determination, soil moisture changes and sea ice detection and classification. In the CAROLS campaigns context, the L-band roughness from both sea and soil surfaces affects the radiometric measurements and its retrieval with GNSS-R would improve the salinity and moisture estimations.

The instrument employed has been the GOLD-RTR, a dedicated reflectometry receiver designed, developed and tested at the IEEC with the aim of collecting GPS signals reflected off the Earth's surface. Three different radio front-ends generate the complex cross-correlation function (waveform) in realtime. Input 1 is fed by an up-looking antenna for reference signal (direct), and either one or two other antennas (down-looking for reflected signals, either polarization) fed inputs 2 and 3. Ten configurable correlation channels running in parallel give an output of ten waveforms every millisecond, with a length of 64 lags (delay resolution of 15 meters). The GOLD-RTR has been widely used since 2005, and nowadays it has been replicated (3 GOLD-RTR available).

The retrieval of L-band roughness with GNSS-R is based on the analysis of the shape of reflected waveforms. Over smooth surfaces, the peak of the waveform would correspond to the location of the specular reflection; however the roughness introduces multi-path like contributions at larger delays, shifting the peak in time-delay. For the sea surface and a given geometry, the delay between the specular point and the peak has a near-linear relationship with the variance of the slopes of the surface, a parameter usually known as MSS (mean square slopes). The same behavior is detected over soil surfaces, but further empirical modeling is needed to determine the contribution of scattering processes (roughness, vegetation canopy) from the content of the waveform.

The presence of salinity in the sea modifies its dielectric properties, resulting in different phase for the co- and cross-polar components of the complex Fresnel coefficients. This difference is captured as the POlarimetric Phase Interferometry (POPI), the phase difference between the received co- and cross-polarized fields. Its correct determination would enable an additional mean for the determination of sea surface salinity.

In this paper, we will show the results obtained with the data collected with GOLD-RTR during CAROLS campaigns towards sea surface and soil moisture remote sensing, including L-band roughness determination and evaluation of the POPI method for the retrieval of salinity.

Interpretation of CAROLS L-band Measurements in the Gulf of Biscay (September 2007)

J. Boutin[1], **M. Leduc-Leballeur**[2], **M. Pardé**[2], **M. Zribi**[3], **P. Fanise**[2], **G. Reverdin**[1], **J. Tenerelli**[4], **and N. Reul**[5]

[1]LOCEAN (CNRS/UPMC/IRD/MNHN), France
[2]LATMOS (UVSQ/CNRS/UPMC), France
[3]CESBIO (CNRS/IRD/CNES/UPS), France
[4]CLS, France
[5]LOS/IFREMER, France

Abstract— The L-band Cooperative Airborne Radiometer for Ocean and Land Studies (CAROLS) radiometer flew four times over the Gulf of Biscay between September 24 to September 28, 2007 around 20UTC. These flights were the first ones over the ocean of this new instrument. Brightness temperatures (Tb) of the surface were measured by one antenna looking at 33° on the right hand side of the aircraft and optionally by a nadir antenna. Measurements are compared with simulations conducted with the Terrestrial Radiometry Analysis Package (TRAP) (Tenerelli et al., 2008) software run for CAROLS geometry and different observed geophysical conditions. Concomitant ship campaign and drifter deployments provide in situ ground truths for sea surface salinity (between 34.6 and 35.8 pss) and temperature (between 15°C and 17°C). Wind speed (between 2 and 10 m/s) and direction are estimated from the QSCAT scatterometer.

TRAP uses the physical modelling of atmospheric radiative transfer, sea surface emissivity and galactic glint foreseen for the processing of the Soil Moisture and Ocean Salinity satellite data. The circle flights and wing-wags movements of the CAROLS aircraft (The French research ATR42 aircraft) allow to explore a wide range of incidence angles (from 0° to about 60°) and of galactic signals reflected by the sea surface.

On a whole, simulated and observed variations of Tb with incidence angle are very consistent, demonstrating a good sensitivity of CAROLS instrument. During the wing-wags, differences between observations and simulations occur in some azimutal directions possibly linked to imperfect knowledge of the galactic signal in some parts of the sky close to the Milky Way. During circle flights, observed azimutal variations are consistent with the galactic noise signal scattered by the sea surface as simulated with the model of (Tenerelli et al., 2008) and the signal due to rough sea assymmetry as simulated by a two-scale model using the Durden and Vesecky x2 wave spectrum (Dinnat et al., 2003). On September 28, a more than 1 K increase of Tb over 2° longitude is observed, mainly linked to an increase of wind speed from 2 to 8 m/s.

Sea Surface Salinity Retrieval from CAROLS L-Band Measurements

A. Martin[1], **J. Boutin**[1], **D. Hauser**[2], **G. Reverdin**[1], **M. Pardé**[2], **M. Zribi**[3], **P. Fanise**[2], **J. Tenerelli**[4], **and N. Reul**[5]

[1]LOCEAN/IPSL, Paris, France
[2]LATMOS/IPSL, Paris, France
[3]CESBIO, Toulouse, France
[4]CLS, Brest, France
[5]LOS/IFREMER, Brest, France

Abstract— The L-band Cooperative Airborne Radiometer for Ocean and Land Studies (CAROLS) radiometer [1] flew seven times over the Gulf of Biscay between May 04 and May 26, 2009 around 20UTC. These flights followed two airborne campaigns with the same instrument in September 2007 and November 2008. Brightness temperatures (Tb) of the surface were measured by one antenna looking at 33° on the right hand side of the aircraft and optionally by a nadir antenna. The nadir antenna is sometimes exchanged with the radar scatterometer STORM in order to get a measurement of surface roughness, related to wind, coincident in space and time with the radiometric measurement.

Measurements are compared with simulations conducted with the Terrestrial Radiometry Analysis Package (TRAP) (Tenerelli et al., 2008) software run for CAROLS geometry and different observed geophysical conditions. Concomitant ship campaign and drifter deployments provide in situ ground truths for sea surface salinity and temperature. Wind speed and direction are either estimated from the QSCAT scatterometer or from the STORM scatterometer and complemented with in situ observation.

TRAP uses the physical modelling of atmospheric radiative transfer, sea surface emissivity and galactic glint foreseen for the processing of the Soil Moisture and Ocean Salinity satellite data. The circle flights and wing-wags movements of the CAROLS aircraft (The French research ATR42 aircraft) allow to explore a wide range of incidence angles (from 0° to about 60°) and of galactic signals reflected by the sea surface.

Previous flights in 2007 and 2008 have demonstrated that on a whole, simulated and observed variations of Tb with incidence angle are very consistent, demonstrating a good sensitivity of CAROLS instrument. In this presentation we will focus on the correlation between L-band radiometer measurements and scatterometer measurements, especially in a case of strong spatial gradient of wind speed (1 to 10 m/s) observed in 2007 and on the signature of coastal salinity gradients on the L-band radiometer observed in 2009 during which we observed SSS variations between roughly 32 and 35.6 pss.

New CAROLS flights in the Gulf of Biscay are foreseen in November 2010 under the track of the SMOS satellite.

REFERENCES

1. Zribi, M., et al., *IGARSS*, 2008.

Retrievals of Soil Moisture and Optical Depth from CAROLS

M. Pardé[2], J.-P. Wigneron[1], M. Zribi[3], Y. Kerr[3], P. Fanise[2], J.-C. Calvet[4], C. Albergel[4], A. Albitar[3], F. Cabot[3], F. Demontoux[3], E. Jacquette[3], E. Lopez-Baeza[5], A. Mialon[3], C. Moisy[3], N. Novello[1], P. Richaume[3], K. Saleh[6], M. Schwank[3], P. Waldteufel[3], E. Zakharova[4], and M. Dechambre[2]

[1]INRA, EPHYSE, Bordeaux, France
[2]UVSQ-CNRS, LATMOS, Guyancourt, France
[3]CESBIO, Toulouse, France
[4]Météo-France, CNRM, Toulouse, France
[5]Universitat de Valencia, Valencia, Spain
[6]Cambridge University, Cambridge, England, UK

Abstract— The SMOS (Soil Moisture and Ocean Salinity) mission was launched on November 2, 2009. It is the second Earth Explorer Opportunity mission to be developed as part of ESA's Living Planet Programme. It aims to improve our understanding of the Earth's water cycle by making global observations of soil moisture over land and salinity over oceans. Over the land surfaces, the principle of the SMOS Level 2 retrieval algorithm is to exploit multi-angular data in order to retrieve simultaneously several surface parameters including surface soil moisture and vegetation characteristics. The L-MEB (L-band Microwave Emission of the Biosphere) forward model was selected to simulate the microwave signatures of the various soil and vegetation types which are present in the mixed SMOS pixel, which is larger than about 30×30 km generally.

The CAROLS (Combined Airborne Radio-instruments for Ocean and Land Studies) campaigns were carried out in 2007–2010 in the context of the validation of the SMOS measurements and products (mainly soil moisture and optical depth over the land surfaces). The CAROLS L-band radiometer was implemented on board the French research airplane ATR42. Over terrestrial ecosystems, the measurements were made over the south western region of France (Smosmania site and Les Landes forest) and over the VAS site (Smos validation site south-west of Valencia).

This communication will present first results of the soil moisture (SM) and optical depth (Tau) retrievals carried out from the CAROLS data. The 2-parameter inversion of L-meb (the model used in the Level 2 algorithm of the Smos mission) was made from four CAROLS observations made at two polarisations and two angles (nadir and 35° from a side-looking antenna). The measurements were obtained from two slightly-shifted flight lines, so that each nadir footprint under the first or second flight line could be seen by the side-looking antenna from the second or first flight. A single calibration of the roughness effects was used for all measurement dates over each site. The effective surface temperature was computed from estimations of soil temperature at depth (~ 50 cm) and from measurements of the surface temperature acquired by a CIMEL thermal radiometer concurrently with the CAROLS observations. The retrievals could be compared with *in situ* measurements obtained from either teams collecting observations (of SM and vegetation characteristics) on the date of the flights or from automatic Meteo-France meteorological stations. Within the Smosmania (soil moisture observing system — meteorological automatic network integrated application) network, 12 automatic stations were modified to provide continuous profiles of soil temperature and SM at four depths (5, 10, 20 and 30 cm) along a Mediterranean-Atlantic gradient.

A good spatial (along the Smosmania gradient) and temporal (from the beginning to the end of the Carols campaigns, e.g., 3 and 4 months, respectively, in 2009 and 2010) agreement was obtained from the retrievals and the *in situ* measurements of SM. Further comparisons of the SM retrievals could be also attempted against the SMOS observations and the SIM products. The retrieved values of Tau were compared against *in situ* and satellite (MODIS) estimations of the vegetation development in spring. The obtained values of the b' parameter (relating Tau to LAI) was close to 0.06, the default value used within the L2 algorithm over agricultural areas.

A First Assessment of the SMOS Data in Southwestern France Using in Situ, Airborne and Model Soil Moisture Estimates

Clément Albergel[1], **Elena Zakharova**[1], **Jean-Christophe Calvet**[1], **Mehrez Zribi**[2], **Mickaël Pardé**[4], **Jean-Pierre Wigneron**[4], **Nathalie Novello**[4], **and Yann Kerr**[2]

[1]CNRM-GAME, Météo-France, CNRS, 42 avenue Gaspard Coriolis, Toulouse, France
[2]CESBIO, CNES/CNRS/IRD/UPS(UMR5126), Toulouse, France
[3]LATMOS, Paris, France
[4]INRA, EPHYSE, Villenave d'Ornon, France

Abstract— Passive microwave remote sensing of soil moisture has been at the center of attention of many research programs, for several decades. Various airborne and in situ radiometers have been developed, showing the high potential of L-band measurements for the estimation of surface parameters. The Soil Moisture and Ocean Salinity (SMOS) satellite mission, based on an aperture synthesis L-band radiometer was successfully launched on November 2009. In the context of a validation campaign for the SMOS mission, intensive airborne and in situ observations were performed in southern France for the SMOS CAL/VAL, from April to May 2009 and April to July 2010. The CAROLS "Cooperative Airborne Radiometer for Ocean and Land Studies" L band radiometer was designed, built and installed on board a dedicated French ATR42 research aircraft. In spring 2010, soil moisture observations from 12 stations of the SMOSMANIA network of Météo-France were complemented by airborne observations of the CAROLS L-band radiometer, following an Atlantic-Mediterranean transect in southwestern France.

The first CAL/VAL results include a comparison between the surface soil moisture retrieved from the brightness temperatures measured during the CAROLS flights with either in situ (SMOSMANIA network and additional measurements) or synthetic soil moisture simulated by the SIM (Safran-Isba-Modcou) hydrometeorological model. It also includes a comparison between L-band brightness temperatures from CAROLS and SMOS, and between soil moisture values retrieved from CAROLS and SMOS. The latter are compared with the in situ observations of soil moisture. Also, simulated soil moisture estimates produced by the ISBA land surface model are used in the cross-evaluation and the biophysical variables produced by ISBA are used as input to the CMEM microwave emission model to simulate brightness temperatures.

CNES and ESA CAROLS Airborne Campaigns at the Valencia Anchor Station and Los Monegros Site in the Framework of SMOS Validation

E. Lopez-Baeza[1], **M. C. Antolin**[2], **C. Bouzinac**[3], **E. Carbo**[2], **C. Castaneda**[4], **M. Davidson**[3], **M. Drusch**[3], **J. Herrero**[5], **S. Juglea**[6], **Y. H. Kerr**[6], **S. Mecklenburg**[7], **C. Millan-Scheiding**[2], **N. Novello**[8], **M. Parde**[9], **K. Saleh**[1, 10], **J.-P. Wigneron**[8], **and M. Zribi**[6, 9]

[1]Department of Earth Physics and Thermodynamics, University of Valencia, Burjassot, Valencia, Spain
[2]Center for Desertification Research, Territorial Planning, Albal, Spain
[3]ESA-ESTEC, Earth Observation Programmes, Noordwijk, The Netherlands
[4]Agrifood Research and Technology Centre of Aragon, Zaragoza, Spain
[5]Estacion Experimental de Aula Dei (EEAD), CSIC, Zaragoza, Spain
[6]Centre d'Etudes Spatiales de la BIOsphere (CESBIO), Toulouse, France
[7]Directorate of Earth Observation Programmes, ESA-ESRIN, Frascati, Italy
[8]Institut National de la Recherche Agronomique, Villenave d'Ornon, France
[9]LATMOS-IPSL, Vélizy, France
[10]Centre for the Development of Industrial Technology (CDTI), Ministry for Science and Innovation Madrid, Spain

Abstract— This communication will present the main results of a series of airborne campaigns conducted at the *Valencia Anchor Station* (VAS) and *Los Monegros* site using the CAROLS (*Combined Airborne Radio-instruments for Ocean and Land Studies*) radiometer on board the ATR 42 aircraft from Météo-France. The main objective was to contribute to the implementation of the SMOS emission model L-MEB (*L-band Microwave Emission model of the Biosphere*) in the framework of the validation of SMOS land data and products. Specifically, the objectives of the CAROLS campaigns were the following:

Soil Moisture Validation Studies: Previous flights at the VAS area took place in 2008 in the context of the ESA *SMOS Validation Rehearsal Campaign* 2008 (EMIRAD radiometer, L-band) over a control area of 10 km × 10 km where intensive soil moisture data was acquired concurrently to airborne L-band measurements. One of the objectives of that campaign was to establish homogeneous units to characterize the average soil moisture of that area, and to investigate the possibility of extending the methodology to the whole SMOS validation pixel at the VAS site. The 'homogeneous units' characterisation was studied and extended further in the context of CAROLS 2009, and validated during the CAROLS 2010 campaign.

Radiometric Characterisation & SMOS Data Validation: The 10km × 10 km mentioned above is part of a larger area of ∼ 50 km × 50 km within the VAS SMOS validation pixel. For CAROLS 2009, flights were performed over a 30 km × 50 km area in order to examine the radiometric signature of other surfaces that are present in the VAS SMOS pixel but not in the 10 km × 10 km control area examined in 2008 (mostly dense forests, matorral, and non-flat surfaces). Main results of CAROLS 2009 will be presented in this communication, and the emphasis will be on comparing local to regional scale results given that CAROLS flights were performed at 4000 m above the surface. For 2010, lower altitude flights (∼ 2200 m a.s.l.) over an area of 20 km × 20 km containing a large number of homogeneous units ('environmental units'), were used for validation of SMOS microwave model L-MEB. The preliminary results of this campaign will be presented in this communication, and the emphasis will be on the validation of the L-MEB model.

In addition to the activities at the VAS site, flights over *Los Monegros*' salt pans near Zaragoza were performed in the 2010 CAROLS Campaign to study their emissivity at L-band. Three playa-lakes (Guallar, La Playa, and Salineta) were sampled to measure gravimetric soil moisture and electrical conductivity.[1]

[1]This paper is also with the collaboration of B. Abalos, M. Alcantara, C. Andres, S. Asensi, A. Buil, M. A. Coll, C. Narbon, F. Requena (University of Valencia, Spain) and E. Torre (Center for Desertification Research, Territorial Planning, Albal, Spain).

Session 1A6a
Small Antennas

A Compact Single Feed, Low Cost Broadband Switched-beam Antenna for Mobile Wimax Applications

C. D. Nikolopoulos, C. I. Tsitouri, T. D. Dimousios, and C. N. Capsalis
Division of Information Transmission Systems and Material Technology
School of Electrical and Computer Engineering, National Technical University of Athens, Greece

Abstract— With the growing demand for wideband mobile communications, more and more attention is being paid to the design of new handsets. A broadband and low cost switched beam antenna suitable for wimax applications is presented in this paper. The present mobile terminal antenna is expected to show increased bandwidth as well as low-loss impedance matching while maintaining low-profile geometry. The proposed structure consists of a conductive top plate (four planar inverted F antennas-PIFA's connected forming a cross) lying over a finite sized ground plane which is interconnected through four wires (feeding wires-only one active at the time), and four other elements as shorting strips, in a configuration designed for symmetrical coverage of the horizontal plane. The radiation characteristics and performance of the array can be adjusted by altering the dimensions of the structure. Also due to the structures symmetry, by electrically controlling the active (feeding wire) and passive (shorting strips) elements, the array's beam pattern may be steered through the azimuth plane. A custom Genetic Algorithm is used in order to optimize the array parameters regarding resonation frequency and radiation

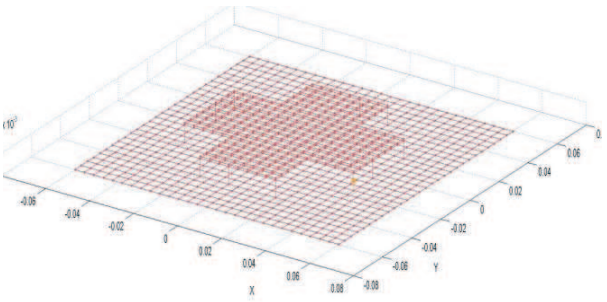

Figure 1: Implementation and analysis of the Switched-Beam array using wire segments and the SNEC platform.

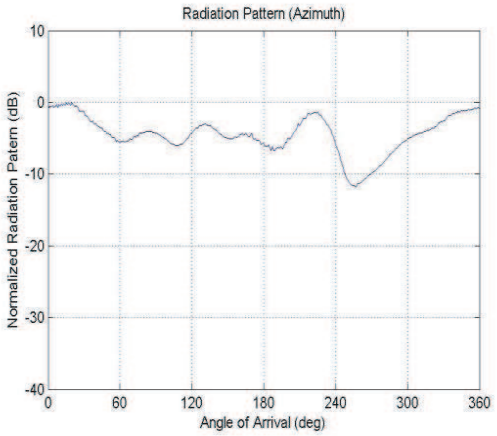

Figure 2: Radiation patterns of the antenna at xy plane at 3500 MHz.

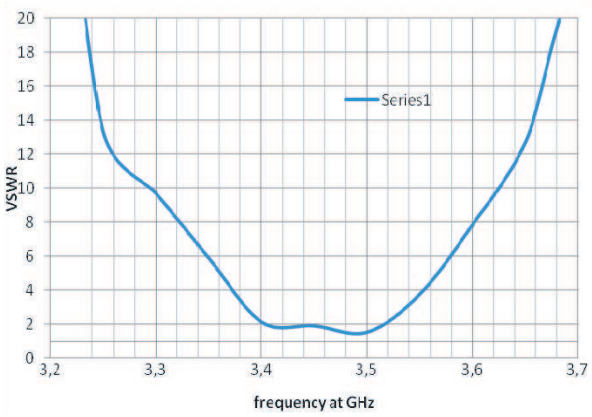

Figure 3: VSWR of the optimized switched-beam array around the frequency band of 3.5 GHz.

pattern orientation angle. The optimized antenna exhibits small size (dimensions $12 \times 12\,\text{cm}$), satisfactory directivity for mobile terminal applications of 6.2 dB over an operation bandwidth of 120 MHz. Simulation results and parameters range are exposed below followed by the according radiation pattern and variation of the simulated VSWR.

Table 1: Genetic Algorithm parameters range and results. (Wavelength equal to $\lambda_o = 0,0857\,\text{m}$ corresponding to an operating freq. of 3.5 GHz)

Element	**Range of Variation**	**Step**	**Results**	**Physical Dimentions**
Length of top plate (UpLen)	$0.05\lambda_o$–$0.5\lambda_o$	$0.05\lambda_o$	$0.9\lambda_o$	7.7 cm
Width of top plate (UpWid)	$0.05\lambda_o$–$0.5\lambda_o$	$0.05\lambda_o$	$0.9\lambda_o$	7.7 cm
Length of ground plate	UpLen + 2*($0.05\lambda_o$–$0.5\lambda_o$)	$0.05\lambda_o$	UpLen + $0.25\lambda_o$	12 cm
Width of ground plate	UpWid + 2*($0.05\lambda_o$–$0.5\lambda_o$)	$0.05\lambda_o$	UpWid + $0.25\lambda_o$	12 cm
Height of wires/shorting strips	$0.05\lambda_o$–$0.2\lambda_o$	$0.05\lambda_o$	$0.05\lambda_o$	0.42 cm
Width of shorting strips	$0.05\lambda_o$–$0.4\lambda_o$	$0.05\lambda_o$	$0.25\lambda_o$	2.14 cm

Compact MIMO Microstrip Antenna with Defected Ground for Mutual Coupling Suppression

Fitri Yuli Zulkifli and Eko Tjipto Rahardjo
Antenna Propagation and Microwave Research Group (AMRG)
Center for Information and Communication Engineering Research (CICER)
Electrical Engineering Department, Faculty of Engineering
Universitas Indonesia, Depok 16424, Indonesia

Abstract— A compact four triangular shape microstrip antenna with defected ground for multiple input multiple ouput (MIMO) systems is presented in this paper. The multi-feed four triangular patches are placed uniquely without any distance to each other; however the mutual coupling reduction is achieved by adding slots on the antenna's ground.

The antenna is designed to operate at 3.3 GHz WiMAX application and studied experimentally regarding mutual coupling reduction. Details of the antenna design, simulated and measured results on the return loss and mutual coupling reduction of the proposed antenna are presented.

A New Compact Tri-band Antenna for MIMO Applications

Shaya Karimkashi and Ahmed A. Kishk
Department of Electrical Engineering, University of Mississippi, University, MS 38677, USA

Abstract— A new tri-band printed inverted F antenna (PIFA) working at the frequencies, 2.45, 5.25, and 5.8 GHz is presented. This antenna can be used as a single element or an element of a compact array in MIMO applications. The tri-band PIFA consists of three parallel arms each resonates at a single frequency. The resonant frequencies can be tuned by changing the length of each arm. A schematic of the PIFA mounted on a ground plane is shown in Fig. 1(a). Fig. 1(b) shows the measured reflection coefficient of the tri band PIFA.

The tri-band PIFA is replaced with a set of infinitesimal electric dipoles, producing the same electric field as the actual antenna. Infinitesimal dipole model (IDM) is obtained by minimizing the near-fields due to the antenna and the IDMs in each resonant frequency of the antenna. Therefore, three IDMs, each representing the PIFA in one resonant frequency are obtained. After replacing each PIFA with its IDMs in a two antenna array system mounted on a 90×40 mm PCB ground plane, the location and orientation of the second antenna is optimized to obtain the minimum cross correlation at each frequency. The measured S parameters of the compact tri-band two element PIFA array are indicative of a dual array with very good isolations and return losses at three MIMO frequencies. It should be mentioned that optimization of multi element arrays using commercial software may be extremely time consuming.

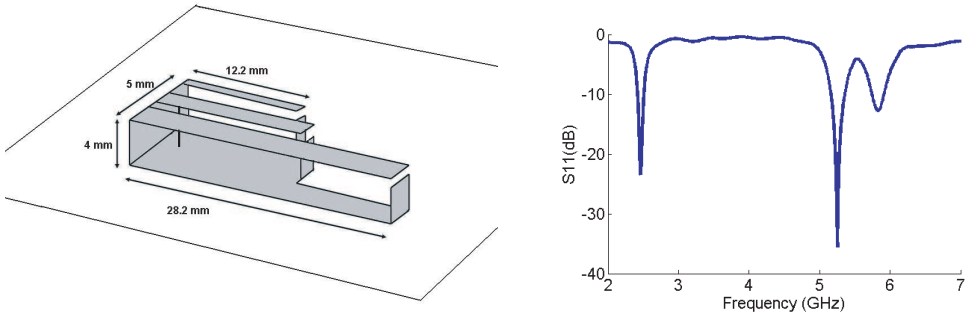

(a) (b)

Figure 1: The tri band PIFA, (a) schematic, (b) reflection coefficient.

Performance and Capacity Analysis of Compact MIMO Aided OFDM-SDMA Systems

Mostafa Hefnawi
Department of Electrical and Computer Engineering, Royal Military College of Canada, Kingston, Canada

Abstract— This paper investigates antenna array coupling effects on the symbol error rate (SER) performance and system capacity of compact MIMO aided multiuser OFDM-SDMA systems. The results show that at close antenna separation the mutual coupling degrades the SER performance and reduces the system capacity.

Wide-Band Rectangular Dielectric Resonator Antenna for Wireless Applications

Achraf Jaoujal, **Noura Aknin**, **and Ahmed El Moussaoui**
Information and Telecommunications Systems Laboratory, Faculty of Sciences
Abdelmalek Essaadi University, Tetouan, Morocco

Abstract— The world of the wireless communication has known a very significant progress in the two last decades, and one of the essential components which contributed to this development is the antenna. For this reason very intense studies were realized to improve and develop the antennas performances. One kind of antennas is the dielectric resonator antenna (DRA) which was proposed for the first time by the Professor S. A. Long in 1983, and it has received increasing attention in the last two decades. The DRA has many common advantages to microstrip antennas (MSA) such small size, low cost, low loss, light weight, and ease of excitation. Additionally, DRAs have wider bandwidth ($\sim 10\%$ for dielectric constant ~ 10) than conventional MSA since they don't use metallic radiators. As consequence, DRAs radiation efficiency (more than 98%), radiation pattern performances and antennas directivity become higher compared to those of microstrip antennas operating in the same frequencies in millimetre wave band or in microwave range.

In this letter, we proposed a dual-band rectangular DRA using Alumina (Al_2O_3, $\varepsilon_r = 9.8$) as radiating element and fed by a simple network technique, named the strip-fed method (coax + conducting strip). As a result, this work presents the characteristics of a new dual-band antenna operating at 2.879 (2.81–3.09 GHz)/3.506–3.941 (3.09–4.69 GHz) GHz providing higher gain values (more than 8 dBi), and a fractional bandwidth of 50.19%.

A Very Small UWB Dielectric Resonator Antenna for Mobile and Wireless Communications Systems

M. Aoutoul[1], **N. Healey**[1], **J. Kiwan**[1], **F. Bourzeix**[1], **B. Lakssir**[1], **and M. Essaaidi**[2]

[1]Moroccan Foundation for Advanced Science, Innovation and Research — Microelectronics Rabat, Morocco
[2]Faculty of Science, Abdelmalek Essaadi University, Tetuan, Morocco

Abstract— UWB antennas, the key elements of any ultra wideband systems, has become a competitive academic and industrial topic after 2002 date of the first standards ruling the commercial use of ultra wideband technology reported by the FCC.

Recently, dielectric resonator antennas (DRA) have attracted a steady increasing attention during the last decade due to their main advantages such as wider bandwidth, better radiation efficiency [1–4] compared to those of their microstrip antennas counterparts and due to other additional characteristics such as light weight and low size, and their ability to support harsh environment conditions (i.e., high temperature degree). In the last few years, UWB DRAs have been designed for high data rate local wireless communication systems, radars and imaging systems, in microwave and milliliter wave frequency ranges, responding to the extensive demand of wideband application and benefiting from their higher efficiency performance. However broad band and ultra wideband DRA structures are still suffering from some designing disadvantages making them less competitive such as complex geometries, higher dielectric constant material involved and/or the incompactness of proposed DRAs.

In this work we propose an extremely compact UWB DRA having a simple rectangular geometry, simple feeding technique and wider bandwidth (more than 5 GHz) which makes it low cost and, hence, practical for fabrication and integration into hand held devices. The working principle of this antenna is similar to that we have reported in [5] but the actual topology size is enormously reduced by about 74% compared to the original one. A parametric study has been done to reach the optimum structure to meet exactly the characteristics of the DS-UWB higher band, involving the principal geometrical and physical parameters, using the commercial EM simulator CST MWS and Ansoft HFSS to validate the optimum results obtained by CST MWS.

The proposed antenna has a very low prole, a very small size, $10 \times 10 \times 2.5\,\mathrm{mm}^3$, and low permittivity constant (10.2). The simulated impedance bandwidth, achieved is about 65%, from 5.47 GHz to 10.83 GHz (Fig. 1). The considered DRA radiation pattern is quasi-omni directional and has a simulated gain values up to 5 dB, which makes it suitable for higher band DS-UWB communication systems applications.

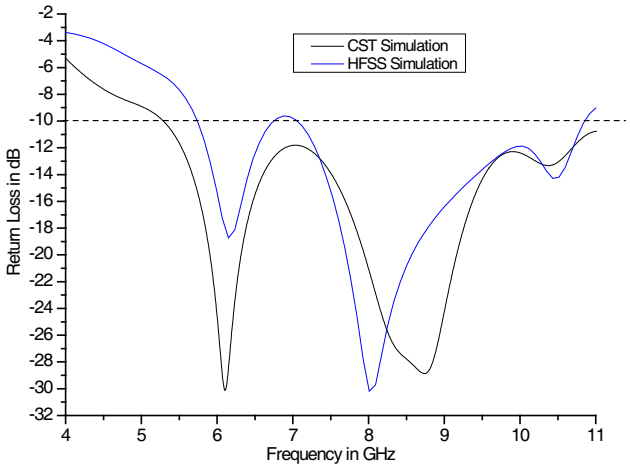

Figure 1: DRA simulated return loss of the optimised structure.

REFERENCES

1. Long, S. A., M. W. Mcallister, and L. C. Shen, "The resonant cylindricaldielectric cavity antenna," *IEEE Trans. Antennas Propagat.*, Vol. 31, 406–412, 1983.
2. Petosa, A., A. Ittipiboon, Y. M. M. Antar, D. Roscoe, and M. Cuhaci, "Recent advances in dielectric resonator antenna technology," *IEEE Antennas and Propagation Magazine*, Vol. 40, No. 3, 35–48, 1998.
3. Mongia, R. K. and P. Bhartia, "Dielectric resonator antennas — A review and general design relations for resonant frequency and bandwidth," *Internaional Journal of Microwave and Millimeter-Wave Computer-Aidel Engineering*, Vol. 4, No. 3, 230–247, 1994.
4. LuK, K. M. and K. W. Leung, *Dielectric Resonator Antennas*, Research Studies Press LTD., 2002.
5. Aoutoul, M., O. El-Mrabet, M. Essaaidi, and A. El Moussaoui, "A compact rectangular dielectric resonator antenna for UWB wireless communication systems," *Microwave and Optical Technology Letters*, Vol. 51, No. 10, 2281–2286, October 2009.

Session 1A6b
Electrically Small Antennas for Military Applications

A Super-miniaturized Low Profile Antenna on a Substrate of Rose Curve Resonators

A. Kabiri[1], **L. Talbi**[1], **and O. M. Ramahi**[2]

[1]Universite du Quebec Outaouais, Canada
[2]University of Waterloo, Canada

Abstract— Reducing the size and encapsulating the multifunctionality in wireless hand-held devices are of the highest priority in the wireless industry. This kind of demand is very challenging for antenna designers because smaller devices need smaller antennas. The smaller size antennas should retain their capability to fulfill the ever-shrinking system requirements. Recently, an influx of research has been devoted to antenna miniaturization using artificial magnetic materials (AMMs) [1, 2].

In this work, the performance of a patch antenna while lying on an AMM substrate composed of Rose curve resonators (RCRs) is analyzed. The RCR is a generic inclusion for AMMs, and can be formulated in polar coordinates in a parametric form of $R_n(r_0, a) : r(\theta) = r_0 + a\cos(n\theta)$ [3], where $r(\theta)$ represents the position of a inclusion's contour in the polar coordinate and θ is the polar angle which sweeps the contour aside the slit. The parameters r_0 and a are constants and n is an integer representing the order of the curve. These parameters are tuned in a design procedure so that the produced AMM fulfills a desired magnetic properties [4]. An AMM composed of RCRs can be designed to operate over a desired frequency bandwidth with a specific frequency dispersion. The AMM can be used as a substrate of a microstrip patch antenna. Therefore, the designer, by choosing a suitable artificial magneto-dielectric substrate, has the opportunity of designing an antenna with a desired performance. Next, the designer can configure the AMM to respond based on the substrate chosen in the antenna design procedure. Moreover, a substrate composed of RCRs can be used in design of highly miniaturized microstrip patch antennas. In fact, increasing the effective substrate parameters results in antenna size reduction.

Let consider a half-wavelength resonant patch antenna operating at an angular frequency $f_{op} = 600\,\text{MHz}$. The size of the antenna ℓ_a is proportional to the wavelength in the substrate, i.e., $\ell_a \propto \lambda = \lambda_0/\sqrt{\epsilon_{\text{eff}}\mu_{\text{eff}}}$, where λ_0 is the wavelength of the radiation in the free space, and ϵ_{eff} and μ_{eff} are the effective permittivity and permeability of the substrate. The AMM is designed to provide $\mu_{\text{Re}} = 9 \pm 5\%$ over a frequency bandwidth of 2 MHz and with a magnetic loss tangent of less than 0.05. The AMM provides an effective permittivity of 6.795 with a dielectric loss tangent of 0.0095 at the operating frequency. The patch antenna is designed with the coax-probe feeding line and the quarter-wavelength microstrip feeding line. The numerical results were compared with similar patch antenna designs with substrates composed of various AMM's inclusions' geometry. The numerical calculations show a maximum gain of 1.5 dB and 59% radiation efficiency for the miniaturized antenna. According to the design dimensions, the resonant length of antenna is 28.6 mm which is 1/17.4 of $\lambda_0 = 50\,\text{cm}$. Thus, a miniaturization factor of 8.7 is achieved using artificial magnetic substrate composed of RCRs. The simulated S_{11} shows a relative bandwidth ($S_{11} < -10\,\text{dB}$) of 0.67%. The bandwidth of the antenna is relatively low compared to other counterparts proposed in the literature, and is useful for narrow band antenna applications. The antenna were fabricated and the numerical and experimental results were compared in a good agreement.

REFERENCES

1. Ikonen, P., S. I. Maslovski, C. R. Simovski, and S. A. Tretyakov. "On artificial magnetodielectric loading for improving the impedance bandwidth propertiesof microstrip antennas," *IEEE Transactions on Antenna and Propagation*, Vol. 54, No. 6, 1654–1662, June 2006.
2. Wang, R., Y. Bo, G. Wang, and F. Yi, "Efficient design of directive patch antennas in mobile communications using metamaterials," *International Journal of Infrared and Millimeter Waves*, Vol. 28, No. 8, 639–649, 2007.
3. Kabiri, A. and O. M. Ramahi, "Metamaterials composed of rose curve inclusions," *Proceeding of Antenna and Propagation Symposium*, Toronto, Canada, July 2010.
4. Kabiri, A. and O. M. Ramahi, "A simple approach for synthesizing of multipurpose metamaterials," *Proceeding of Antenna and Propagation Symposium*, Toronto, Canada, July 2010.

Ultra Compact VHF Vertically Polarized Antenna for Aircraft

Tangjie Yuan[1], **Luyang Zhou**[1], **Habiba Hafdallah Ouslimani**[1], **Alain Priou**[1], **Gérard Collignon**[2], **and Aurélien Marteau**[2]

[1]University Paris-Ouest Nanterre-La Defense, LEME 50 rue de Sèvres, 92410 Ville d'Avray, France
[2]INEO Defense, Route Militaire Nord-ZA Louis Bréguet, CS 80526, 78140 Velizy Villacoublay, France

Abstract— A very efficient miniaturized VHF antenna with dimensions of $0.15\lambda_o \times 0.15\lambda_o$ etched on 0.8 mm and $\varepsilon_r = 4.4$ dielectric FR-4 substrate is presented. The total height of the designed antenna is below $0.01\lambda_o$. It is inspired from the Sarabandi and co-authors works. The antenna is vertically polarized and behaves like a vertical dipole antenna used for Civil Aviation. It is composed by a great number of folded slots arranged in circular loop geometry and has a total length of a half-wave. The numerical simulations show a resonance frequency in the desired VHF frequency range with a narrow bandwidth $\sim 1.3\%$ and an omnidirectional radiation patterns.

Electrically Small Antennas for Military Applications

S. Weiss and A. Zaghloul
U.S. Army Research Lab, USA

Abstract— Electrically small antennas are very desirable for both military and commercial applications. The driving force for the electrically small antenna is due to the wavelengths of many terrestrial communications systems (HF, VHF, and UHF.) There is an enormous body of work addressing fundamental limitations dating for at least 70 years. The primary issues are usually directivity (gain) versus aperture size and bandwidth versus volume (Chu limit.) Recent advances in ordered structures (e.g., metamaterials) have made some progress in getting closer to limits on both aperture size and bandwidth and are of great interest to both the military and commercial sectors.

We present what are seen as realistic benchmarks to be used for claims of antenna performance when the antenna is electrically small. Often such "small" antennas are placed on a large metamaterial-realized ground plane. The question then becomes what is the antenna size that takes into account the minimal real estate needed to support the antenna's enhanced characteristics? Some modeled and measured results will be presented. Additionally, the placement of the antenna on the platform (commercial or military) can significantly impact the antenna's performance. By understanding the in-situ effects, a sensible goal will be to use materials to make the antenna's performance as insensitive to placement as possible. Additionally, the inherent loss of the antenna should be well understood for any application mounted on a platform.

Finally, we discuss the large body of work that exists for electrically small antenna designs that have been know for many years. As claims are made for enhanced performance (e.g., using metamaterials), it is fair to make comparisons to established designs and quantify the performance improvements.

Gain Improvement of Dual Band Patch Antenna Based on Complementary Rectangular Split-ring Resonators

N. Ortiz, **F. Falcone**, **and M. Sorolla**
Departamento de Ingeniería Eléctrica y Electrónica
Universidad Pública de Navarra, Spain

Abstract— Microstrip antennas are commonly used for wide applications, because of its compact size and low profile. Up to now, the use of metamaterial concepts in practical miniaturized antennas is a very challenging research topic which is in its very infancy [1–7] and the achieved results [7] exhibit very low efficiencies driving to low gain antennas designed by metamaterial concepts. In this sense, the use of a complementary rectangular split ring resonator etched in the patch of a conventional patch antenna allows us to design a dual band patch antenna with enhanced gain comparing to previous works. Furthermore, a miniaturization of the conventional rectangular patch antenna is achieved.

Besides, in this work a parametric study of the location of the complementary rectangular split ring resonator has been carried out to show the improvement of the radiation efficiency depending on the excitation of the particle inside the patch. Within these results, radiation efficiencies up to 50% are achieved for both frequency bands. The presented design in this work is a simple design, as the only parameters comparing to a conventional patch antenna are the ones of the complementary split ring resonator particle. This kind of antenna can not be achieved replacing the complementary split ring resonator by a rectangular iris (or rectangular slot) because its resonance will be placed for the same dimensions of the complementary split ring resonator at higher frequencies from the patch antenna. These slots should produce dynamic resonances and not quas-static resonances. Thus, the origin of the radiation is different. Also, this design opens the way to design in a similar way multiband antennas adding different complementary split ring resonators in the patch. As a final remark, depending on the location of this particle and its dimensions, the bandwidth of a conventional patch antenna can be increased.

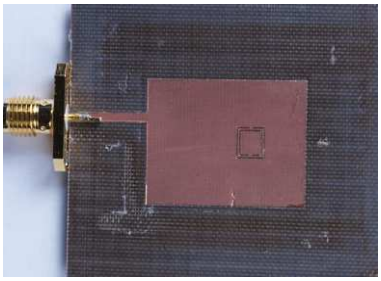

Figure 1: Dual band patch antenna based on complementary split ring resonators.

REFERENCES

1. Ziolkowski, R. W. and A. D. Kipple, "Application of double negative materials to increase the power radiated by electrically small antennas," *IEEE Transactions on Antennas and Propagation*, Vol. 51, No. 10, 2626–2640, Oct. 2003.
2. Qureshi, F., M. A. Antoniades, and G. V. Efeftheriades, "A compact and low-profile metamaterial ring antenna with vertical polarization," *IEEE Antennas and Wireless Propagation Letters*, Vol. 4, 2005.
3. Baeel, R. K., G. Dadashzadehl, and F. G. Kharakhilil, "Using of CSRR and its equivalent circuit model in size reduction of microstrip antenna," *Proceedings of Asia-Pacific Microwave Conference 2007*, 1–4, Dec. 11–14, 2007.
4. Lee, Y., S. Tse, Y. Hao, and C. G. Parini, "A compact microstrip antenna with improved bandwidth using complementary split-ring resonator (CSRR) loading," *2007 IEEE Antennas and Propagation International Symposium*, 5431–5434, Jun. 9–15, 2007.
5. Li, M., M. Lu, and T. J. Cui, "Novel miniaturized dual band antenna design using complementary metamaterial," *International Workshop on Metamaterials*, 374–376, Nov. 9–12, 2008.

6. Liu, J., S. Gong, Y. Xu, X. Zhang, C. Feng, and N. Qi, "Compact printed ultra-wideband monopole antenna with dual band-notched characteristics," *Electronics Letters*, Vol. 44, No. 12, 710–711, Jun. 5, 2008.
7. Zhang, H., Y.-Q. Li, X. Chen, Y.-Q. Fu, and N.-C. Yuan, "Design of circular/dual frequency linear polarization antennas based on the anisotropic complementary split ring resonators," *IEEE Transactions on Antennas and Propagation*, Vol. 57, No. 10, 3352–3355, Oct. 2009.

Session 1A7
Biosensing with Nanoplasmonics

Single Molecule Spectroscopy and Sensing Using Coherent Plasmons — Part I

Peter Nordlander
Laboratory for Nanophotonics, Department of Physics, Rice University
Houston, TX 77005, USA

Abstract— The resonant excitation of plasmons in metallic nanostructures can generate large electromagnetic field enhancements in localized regions around the surfaces of the partices, "hotspots". While quantum mechanical effects can introduces a significant screening of the local electric fields in such hotspots [1, 2], the field intensities can still be sufficiently large to enable single molecule surface enhanced Raman scattering (SERS) [3] and localized surface plasmon resonance (LSPR) sensing [4]. In the first part of the talk, I will discuss several different approaches to biomolecular sensing, including SERS, LSPR, surface enhanced infrared absorption (SEIRA), and a novel method for optical sensing of conductive molecules sandwiched in narrow plasmonic gaps [5].

REFERENCES

1. Zuloaga, J., et al., *Nano Lett.*, Vol. 9, 887, 2009.
2. Zuloaga, J., et al., *ACS Nano*, Vol. 4, 2010, 10.1021/nn101589n.
3. Ward, D. R., et al., *Nano Lett.*, Vol. 8, 919, 2008.
4. Mayer, K. M., et al., *Nanotechnology*, Vol. 21, 255503, 2010.
5. Perez, O., et al., *Nano Lett.*, Vol. 10, 3090, 2010.

Single Molecule Spectroscopy and Sensing Using Coherent Plasmons — Part II

Peter Nordlander
Laboratory for Nanophotonics, Department of Physics, Rice University
Houston, TX 77005, USA

Abstract— In the second part of the talk, I will discuss how plasmonic radiative interference and coherence effects such as subradiance and Fano resonances can be exploited for ultrasensitive LSPR sensing. I will present a general framework for the description of radiative interference effects in plasmonic systems and illustrate the concepts with examples from recent applications to symmetry broken nanoshells, Fanoshells [1], small nanoparticle clusters of D6h symmetry (Heptamers) [2, 3], planar ring-disk systems (Fanocavities) [4], plasmonic heterodimers [5]. Apart from their fundamental importance, such phenomena are also of practical interest in metamaterial and chemical and sensing applications because of the extraordinarily narrow linewidths and strong sensitivities to the dielectric properties of the environment [6].

REFERENCES

1. Mukherjee, S., et,al., *Nano Lett.*, Vol. 10, 2694, 2010.
2. Fan, J. A., et al., *Science*, Vol. 328, 1135, 2010.
3. Fan, J. A., et al., *Nano Lett.*, Vol. 10, 3184, 2010.
4. Sonnefraud, Y., et al., *ACS Nano*, Vol. 4, 1664, 2010.
5. Brown, L., et al., *ACS Nano*, Vol. 4, 819, 2010.
6. Lukyanchuk, B., et al., *Nature Mat.*, Vol. 9, 712, 2010.

Plasmons and DNA: Label-free Sensing and Nanoscale Actuation (Part 1)

N. J. Halas
Rice University, Houston, TX, USA

Abstract— Detection of DNA using surface-enhanced Raman spectroscopy has typically relied upon the use of Raman active molecules, such as dyes, for recognition of DNA hybridization events. This type of detection requires that the target analyte to be detected be functionalized with the Raman-active tag molecule, an expensive and time-consuming process. The target DNA binds to its complementary probe DNA on a sensor platform, and the SERS signal reports the hybridization/recognition event. Recently we have shown that plasmonic substrates such as nanoshells, with strong and highly uniform enhancements, enable us to detect biomolecules such as DNA, in a label-free manner. The naturally occurring variation in Raman cross section for the constituent nucleic acids of DNA (adenine>guanine>cytosine, thymine) is clearly evident in the SERS spectrum, such that a random DNA sequence will feature primarily the Stokes modes of adenine. This provides an easily recognizable SERS reporter signal for the target DNA without the need for a molecular label. To detect a hybridization event between the target and complementary probe DNA, however, requires the suppression of the adenine SERS signal from the complement probe DNA strand. By substituting the nucleic acid 1-aminopurine for adenine in the probe DNA strand, DNA hybridization events between the substituted probe complement and the target DNA analyte can be detected easily and unmistakably, in a label-free manner.

REFERENCES

1. Barhoumi, A., O. Neumann, D. Zhang, and N. J. Halas, "Surface enhanced raman spectroscopy of DNA," *Journal of the American Chemical Society*, Vol. 130, 5523–5529, 2008.
2. Barhoumi, A., D. Zhang, and N. J. Halas, "Correlation of molecular orientation and packing density in a dsdna self-assembled monolayer observable with surface enhanced raman spectroscopy," *JACS*, Vol. 130, 14040–1, 2008.
3. Barhoumi, A. and N. J. Halas, "Label free detection of DNA oligonucleotides using surface enhanced Raman spectroscopy," *Journal of the American Chemical Society*, Vol. 132, 12792–3, 2010.

Plasmons and DNA: Label-free Sensing and Nanoscale Actuation (Part 2)

N. J. Halas
Rice University, Houston, TX, USA

Abstract— It has recently been shown that the dehybridization of DNA can occur in response to illumination of a plasmon resonant nanoparticle or nanostructure substrate at its resonant wavelength. DNA configured with one strand bound to the nanoparticle surface and the complement bound only to the DNA and not to the substrate, will, when illuminated, release the non-substrate bound ssDNA. This process is of intense interest for applications such as intracellular drug and gene therapy. DNA can also incorporate other, smaller molecules within its double-helix framework, which upon plasmon resonant illumination and subsequent DNA dehybridization can be released into living cells. We have recently shown that plasmon-triggered release of the bright blue fluorescent dye DAPI (4', 6-diamidino-2-phenylindole), that binds reversibly to dsDNA, can be used to visualize the light-triggered molecular release process. In living cells, the released DAPI diffuses to the cell nuclei and intercalates within the cell's endogenous DNA. DNA+DAPI-laden nanoshells were prepared and incubated with H1299 human lung cancer cells. Upon resonant illumination, a large increase in blue fluorescence within the cell nuclei was observed, where the nonilluminated control showed no measurable increase in fluorescence from the cell nuclei. An assay was performed to determine whether this process affected cell viability, and not significant changes in cell viability occurred following illumination.

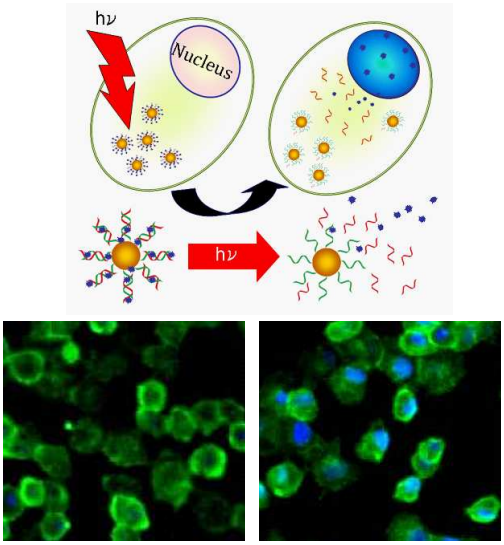

Figure 1: Top: Schematic of light-triggered release of DAPI from DNA molecules bound to nanoshells. Bottom left: H1299 lung cancer cells before light-triggered DAPI release; Bottom right: after DAPI release.

REFERENCES

1. Barhoumi, A., R. Huschka, R. Bardhan, M. Knight, and N. J. Halas, "Characteristics of light-controlled release of DNA from plasmon resonant nanoparticle vectors," *Chemical Physics Letters*, Vol. 482, 171–179, 2009.
2. Huschka, R., O. Neumann, A. Barhoumi, and N. J. Halas, "Visualizing light-controlled release of molecules in living cells," *Nano Letters*, articles ASAP.

Optical Spectroscopy of Conductive Molecular Junctions in Plasmonic Cavities

J. Aizpurua[1], **O. Pérez-González**[1, 2], **N. Zabala**[1, 2], **A. Borisov**[3], **N. J. Halas**[4], **and P. Nordlander**[5]

[1]Donostia International Physics Center (DIPC)
Centro Mixto de Física de Materiales (CSIC-UPV/EHU), Donostia-San Sebastián, Spain
[2]Departamento de Electricidad y Electrónica, Univ. of the Basque Country (UPV/EHU), Bilbao, Spain
[3]Lab. des Collisions Atomiques et Moleculaires, CNRS-Université Paris-Sud, Orsay CEDEX, France
[4]Chemistry Department, Laboratory for Nanophotonics, Rice University, Houston, USA
[5]Physics Department, Laboratory for Nanophotonics, Rice University, Houston, USA

Abstract— In the last decade fundamental advances have been achieved in the fields of molecular electronics and plasmonics. In particular, the optical properties of adjacent nanoshell pairs have been explained using exact numerical calculations and hybridization models [1]. Recent simultaneous measurements of electronic conduction and Raman spectroscopy in molecular junctions have suggested the possibility of sensing individual molecules [2], connecting both fields.

We study theoretically this connection between molecular electronics and plasmonics in a system composed of a molecular junction bridging a plasmonic cavity. The conductivity of the junction, σ, is related to its conductance, G, through the geometrical parameters of the system. We modify the conductivity of the junction by varying the number n of quanta of conductance, nG_0 ($G0 \equiv 2e^2/h \cong 77.5\,\mathrm{mS}$). Maxwell's equations are solved via a boundary element method (BEM) [5] to obtain the electromagnetic fields and the optical extinction spectra.

Two regimes in the optical response are found (see Figure) [3]. For the short wavelength regime, we first notice a broadening of the plasmon resonance as conductance is increased, followed by a slight blue-shift. We call this plasmon resonant mode the Bonding Dimer Plasmon (BDP). For very large values of conductance, a new highly red-shifted resonance emerges. We call this resonance the Charge Transfer Plasmon (CTP). We identify a threshold value of the conductance when the optical properties of the junction start being affected by the transport properties. This threshold conductance relates the time of flight of the electrons involved in the transport process with the time of the optical cycle of the plasmonic resonances of the cavity. The study of this kind of spectral changes in plasmonic cavities might serve as a probe of molecular conductance and transport processes in the visible part of the spectrum, a range which is not accessible through electrical measurements.

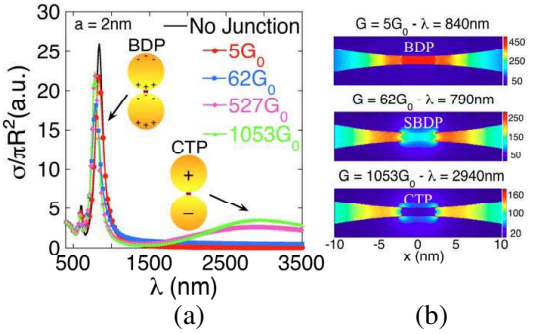

Figure 1: (a) Optical extinction spectra of a metallic dimer bridged by a conductive molecular junction of radius $a = 2\,\mathrm{nm}$ as conductance in the bridge is increased. A bonding dimer plasmon (BDP) is observed for low conductances, whereas a charge transfer plasmon (CTP) is observed for larger conductances. (b) Near-fields patterns corresponding to the short wavelength regime (*top and middle*) and to the long wavelength regime (*bottom*).

REFERENCES

1. Lassiter, J. B., et al., *Nano Lett.*, Vol. 8, 1212, 2008.
2. Ward, D. R., et al., *Nano Lett.*, Vol. 8, 919, 2008.
3. Pérez-González, O., et al., *Nano Lett.*, Vol. 10, 3090, 2010.

Hybrid Plasmonic-dielectric Waveguide Platform for Biosensing and Fluorescence Detection

Björn Agnarsson, **Hamid Keshmiri**, **and Kristjan Leosson**
Department of Physics, Science Institute, University of Iceland, Iceland

Abstract— Plasmonic waveguides are promising for biosensing applications but unsuitable for transmitting optical signals over large distances due to their inherently large propagation loss. In the present work, we have studied high-index-contrast polymer waveguides that were partially coated with metal film, resulting in a hybrid plasmonic-dielectric waveguide structure. The substrate material was selected to provide a good match to the refractive index of water, resulting in a close-to-symmetric dielectric waveguide structure when probing aqueous samples. We find that for the correct value of the metal thickness, the energy of the fundamental TM mode of the dielectric waveguide is coupled efficiently into a primarily plasmonic mode in the metal-coated region, resulting in a substantial increase of the evanescent field intensity near the waveguide surface. With suitable mode conversion for the fiber-to-waveguide coupling, the plasmonic mode can thus be excited with close to 100% efficiency using a single-mode fiber-coupled source. Furthermore, the dielectric-plasmonic mode coupling ensures that the intensity distribution in the propagation direction is more uniform than in the case of an exponentially decaying surface plasma wave on a single metal-dielectric interface. We have studied this effect experimentally by monitoring emission from fluorescent beads in solution, excited at 633-nm wavelength by end-fire coupling into the dielectric waveguide. An enhancement in fluorescence intensity above the metal surface is observed. Near-surface fluorescence is also partly absorbed (quenched) into the plasmonic mode and subsequently coupled to the dielectric waveguide, allowing for a purely planar excitation and detection platform. In order to explain the experimental findings, mode structure and mode coupling were studied numerically using finite-element and finite-difference time domain methods.

Plasmonic Modes of Gold Nano-particle Arrays on Thin Gold Films

A. Hohenau and J. R. Krenn
Karl-Franzens University, Graz, Austria

Abstract— Regular arrays of metal nanoparticles on metal films have tuneable optical resonances that can be applied for surface enhanced Raman scattering or biosensing. With the aim of developing more surface selective geometries we investigate regular gold nanoparticle arrays on 25 nm thick gold films, which allow to excite asymmetric surface plasmon modes featuring a much better field confinement compared to the symmetric modes used in conventional surface plasmon resonance setups. By optical extinction spectroscopy we identify the plasmonic modes sustained by our structures [1]. Furthermore, the role of thermal treatment of the metal structures is investigated, revealing the role of modifications in the crystalline structure of gold on the optical properties.

REFERENCES

1. Hohenau, A. and J. R. Krenn, "Plasmonic modes of gold nano-particle arrays on thin gold films," *Phys. Stat. Sol. RRL*, 2010, doi: 10.1002/pssr.201004260.

Enhanced Optical Transmission and Improved Spatial Resolution Image through a Plasmon Film Lens with Roughness

Kung-Hau Ding[1], **Quinn Bagley**[2], **and Leung Tsang**[2]

[1]Air Force Research Laboratory, Hanscom AFB, MA 01731-2909, USA
[2]Department of Electrical Engineering, University of Washington, Seattle, WA 98195-2500, USA

Abstract— Nano-optics is a rapidly developing research field in recent years, which studies the phenomena and manipulation of light on the nano scale and investigates potential applications in versatile disciplines, such as imaging, sensing, and communications. The resolving capability of conventional optical imaging systems is limited by the diffraction limit due to the loss of evanescent waves that contain the sub-wavelength spatial information of an object. Recently, the development of superlens or perfect lens using metamaterial, or left-handed material (LHM), to overcome the diffraction limit has attracted great attention. The perfect image achieved by superlens is based on, theoretically, reproducing both propagating and evanescent components of the wave spectrum. Metamaterials is the engineered nanostructures that can control the propagation of electromagnetic waves inside themselves, however, the fundamental challenge is the high loss encountered in the current metamaterials. The idea of perfect lens has been extended to use a negative permittivity material (NPM), e.g., noble metal. The NPM superlens is comprised of a flat silver film and the imaging with resolution below the diffraction limit can be achieved by the excitation of surface plasmons. The surface plasmon is an electromagnetic wave confined to the interface between two materials with real parts of their dielectric functions of opposite signs The idea of NPM slab superlens has been extended to silver films with natural roughness or with various grating schemes. Recently, we applied the fast-all-modes (FAM) method and the numerical modified steepest-descent-path (NMSP) method to solve for the electric field below a metal film and verified the existence of superlensing of the electric field.

In this paper we investigate the effects of rough surface on the transmission properties of an optical plasmon film lens. We investigate the effects of random roughness and periodic roughness of various rms heights and correlation lengths. We show that the silver film lens with small periodic roughness can provide additional enhancement of the superlensing effect. We further show that by using multiple sources over a periodic roughness with small rms heights and correlation lengths, that the enhanced images are close to translational invariant. This shows that the images of small roughness have enhanced resolution and yet the spatial separations of multiple images are preserved. On the other hand, the random roughness on the film may cause image shift and distort the image. For random roughness, the images of multiple sources do not obey translation invariant.

Session 1A8a
EM Interactions in Biomedical Engineering

Analyse of Dispersion of Ex Vivo Electric Properties Measurements of Female Breast Tissues between 1 MHz and 1 GHz

Nadi Mustapha, Gagny Camille, Djilali Kourtiche, Patrice Roth, and Pierre Schmitt
Faculty of Sciences and Techniques, L.I.E.N., Nancy University
BP 239, Vandoeuvre les Nancy 54506, France

Abstract— Interactions between electromagnetic field and biological tissue find applications in many therapeutic and diagnosis methods. On the other hand, development of devices radiating electromagnetic field, like mobile phone, led to the questions of their possible biological effects. These so called EM bio-effects have led to controversial models for EM dosimetry simulation because they are depending on the knowledge of the dielectric properties. Electromagnetic properties of biological tissues appears thus as fundamental parameters that are necessary for any research in these domains.

This paper summarize and discuss results measured ex vivo on mamallian tissue two hours after excision in a surgery department at the Nancy Cancer Center (France). Dielectric permittivity and electrical conductivity of female breast human tissues in the frequency range from 1 MHz to 1 GHz are compared to previously published results and discussed according to the influencing parameters.

A systematic spectroscopic measurements were done for different samples and compared to the previous results obtained by others. The samples were classified according to their nature (muscle, fat) and dimensions. Measurements for permittivity and conductivity of breast muscle and breast fat samples are presented and compared to previous results.

The main goal being to compare the measurement in a large frequency band to the disseminated results found in the previous works in order to evaluate how great is the dispersion when measuring on ex vivo samples.

Thermographic Analysis of Swiss Albino Mice Exposed to 1.8 GHz GSM Frequency

A. D. Usman[1], **W. F. Wan Ahmad**[1], **M. Z. A. Ab Kadir**[1], **M. Mokhtar**[2], **and A. Rusnani**[3]

[1]Centre of Excellence on Lightning Protection (CELP), Faculty of Engineering
Universiti Putra Malaysia, UPM Serdang, Selangor 43400, Malaysia
[2]Wireless and Photonic Networks (WiPNET), Research Center of Excellence
Faculty of Engineering, Universiti Putra Malaysia, UPM Serdang, Selangor 43400, Malaysia
[3]Faculty of Electrical Engineering, Universiti Teknologi Mara (UiTM) Pulau Pinang
Permatang Pauh 13500, Pulau Pinang, Malaysia

Abstract— Exposure to radio frequency electromagnetic field has been a subject of debate for many years. Currently, related regulations provided were meant to safeguard occupational and general public for short term thermal effect only. This study was designed to investigate the long term thermal effect of electromagnetic field exposure of 1.8 GHz GSM frequency. 72 unrestrained Swiss albino mice were used as surrogate for this study and were divided into two groups of 1.8 GHz and control groups. The cage for the 1.8 GHz group was placed at far field distance from the directional antenna, and the exposure were for seven hours per day, seven days in a week and for four weeks. Thermographic pictures were taken daily to obtain temperature of the mice brain before and after being exposed to the 1.8 GHz GSM down-link frequency. The highest and lowest mice brain temperatures recorded for 1.8 GHz group are on day 20 and day 6 for 37.0°C and 33.9°C, respectively. While, the highest and lowest mice brain temperatures recorded for control group are on day 1 and day 24 for 36.9°C and 32.7°C, respectively. Daily rise in temperature for 1.8 GHz and control groups range from 0.3°C to 2.1°C and 0.3°C to 2.8°C, respectively. The mice weight taken on weekly basis shows a decrease for 1.8 GHz expose group as compared to the mice in control group. The death rate was also found to be higher for 1.8 GHz group compared to control group.

Prenatal and Postnatal Cell-phone Exposure and Migraine and Other Headaches in Children

Madhuri Sudan[1], **Leeka Kheifets**[1], **and Jorn Olsen**[2]

[1]Department of Epidemiology, University of California, Los Angeles (UCLA), USA
[2]The Danish Epidemiology Science Centre, University of Aarhus, Denmark

Abstract— With the rapid growth of cellular communication technology, children are increasingly exposed to cell phones beginning at very early ages. As cellular telephones are an immediate, common source of radiofrequency (RF) fields, concerns from parents and the scientific community are increasing as to whether this technology could have negative neurological health effects. Results of previous studies of the effects of RF exposure have been inconsistent, but indicate a need to further investigate its association with various reported outcomes, including migraines and other headaches [1–3]. To address this need, we will explore the potential association between prenatal and age-seven cell phone exposure and reports of migraines and other headaches in children.

The Danish National Birth Cohort (DNBC) enrolled over 90,000 pregnant women (over 100,000 total pregnancies) between 1996 and 2002. Detailed information about the child's lifestyle, dietary habits, environmental exposures, and health has been collected since enrollment. Most recently, mothers were interviewed after their child turned seven years of age, and this interview included questions about the mother's cell phone use during pregnancy as well as her child's cell phone use at the age of seven. We currently have data on 52,680 children from singleton births and their mothers from the DNBC Age-7 interview. We also have diagnostic data from hospitalizations for all children in the DNBC from the Danish National Hospital Register.

Given that mothers in the DNBC were pregnant when cell phone use was increasing in popularity but not fully pervasive, our data include a naturally high exposure contrast. Approximately 39% ($n = 20,842$) of mothers reported using a cell phone while they were pregnant (prenatal exposure), leaving a large proportion unexposed. Similarly, while most children at the age of seven are unlikely to own their own cell phone, about 36% ($n = 18,935$) of mothers reported that their child used a cell phone to some degree at the age seven (postnatal exposure). These large proportions of exposed and unexposed children results in greater statistical efficiency and power to detect even small associations.

We will employ a number of analysis techniques to study the association between cell phone exposure and migraine/headache. One percent ($n = 523$) of mothers reported that their child had migraines. Our main analysis will use logistic regression to investigate the association between prenatal exposure only, postnatal exposure only, and both prenatal and postnatal exposure with mothers' reports of migraine in children. Childhood migraines are often complicated to diagnose and difficult to distinguish from other types of headache, causing medical diagnosis to be missed until the child is several years older [4]. Not surprisingly, while a large number of mothers reported migraines, only 64 children were medically diagnosed with migraine during hospitalization. As a second approach, we will use sparse data techniques to look at the association between cell phone exposure and diagnosis of migraine and other headache in children. We will also consider mothers' reports of headaches in general as an outcome. For all analyses, we will consider several potential confounding factors for adjustment, including sex of the child, gestational age at birth, birth weight, breastfeeding, physical activity, fever during pregnancy, prenatal smoking, prenatal alcohol use, mother's age, and social-occupational status.

As cell phones are extremely prevalent, even a very small effect of this exposure on development of migraines and headaches in children could have a large public health impact. Whether we find an effect or not, our results are likely to have a significant impact in public health, policy, and technology.

REFERENCES

1. Hillert, L., et al., "The effects of 884 MHz GSM wireless communication signals on headache and other symptoms: An experimental provocation study," *Bioelectromagnetics*, Vol. 29, No. 3, 185–196, 2008.
2. Soderqvist, F., M. Carlberg, and L. Hardell, "Use of wireless telephones and self-reported health symptoms: A population-based study among Swedish adolescents aged 15–19 years," *Environ Health*, Vol. 7, 18, 2008.

3. Thomas, S., et al., "Personal exposure to mobile phone frequencies and well-being in adults: A cross-sectional study based on dosimetry," *Bioelectromagnetics*, Vol. 29, No. 6, 463–470, 2008.
4. Bigal, M. E. and M. A. Arruda, *Migraine in the Pediatric Population-evolving Concepts*, Headache, 2010.

FDTD Cell Size Study for SAR Evaluation for Human Head Exposure to Near EM Field

Hiroshi Shirai and Jun Ohisa
Department of Electrical, Electronic, and Communication Engineering
Faculty of Science and Engineering, Chuo University
1-13-27 Kasuga, Bunkyo, Tokyo 112-8551, Japan

Abstract— As the usage of the portable wireless equipments has been increased dramatically, public concerns more on the bio-electromagnetic effect to the human body. Governments or international committees have been set guidelines for human protection from electromagnetic waves. Radio wave dosimetric evaluation has usually been done in terms of the Specific Absorption Rates (SARs) calculated by the internal electric field and tissue properties.

In order to analyze the electromagnetic wave scattering by a complex structure, such as a human body, one must first know the fine details of the internal organ and tissue properties, then the field calculation will be made by numerical solutions. The Finite Difference Time domain (FDTD) method is the one of the powerful tools for such task, and there are many papers on the dosimetric evaluation by FDTD. In order to accomplish the reliable numerical simulation by FDTD, cell size is one of the critical parameters, and it should be sufficiently smaller than the wavelength to compute the mutual interaction between the different media. Accordingly, the required memory size becomes larger for high frequency calculation.

In this paper, two dimensional FDTD calculation error due to an insufficient cell division has been estimated for inhomogeneous numerical head phantom, which identifies 11 different human organs and tissues in 2 mm × 2 mm cells. The evaluation has been made for analyzing two dimensional human head exposure to the near EM field radiated by a line source. Each cell (2 mm × 2 mm) has been subdivided, and electrical field and specific absorption rate (SAR) inside the head have been calculated for each subdivision. It has found that the numerical error due to the insufficient cell sub-division of has little effect on assessing maximum SAR value in the human head.

Influence of a Dielectric Insert of High Permittivity on the Transmit Performance of a 300 MHz Multi-channel MRI Loop Array

M. Kozlov and R. Turner
Max Planck Institute for Human Cognitive and Brain Sciences, Leipzig, Germany

Abstract—

Purpose: Recently several reports have been published suggesting that the transmit performance of a given MRI RF coil can be enhanced by incorporating suitable dielectric materials. However these reports, which are mostly based on experimental results, do not provide detailed analysis of the power balance of the coil with and without such high permittivity dielectric materials nor data regarding the transmit field homogeneity for different slices of the object. To analyse this proposed approach more fully, we investigated the effect of dielectric inserts with varying size and permittivity on loop array power balance, transmit performance and homogeneity. We have created a multidimensional database by varying load shape, distance between array and load, axial length of the loop array, and the size of loop elements.

Method: We investigated 8 channel loop-type array coils with different diameters (160, 200, 240, 280 mm) and lengths (80, 100 and 120 mm). To eliminate the influence of RF shimming (adjustment of amplitude and phase for excitation signals) on coil performance, we used only cylindrical loads with different diameters (80, 120, 155 and 190 mm) and two 80 and 120 mm diameter spherical phantoms. By defining a cylindrical load as long as 375 mm, we removed the influence of load length on transverse slice homogeneity. The electrical properties of all loads were close to those of average human tissue at 300 MHz — permittivity 52 and conductivity 0.55 s/m.

A high permittivity hollow dielectric insert, with permittivity ranging from 10 to 79, and with cylindrical or spherical geometries, was placed between the coil and load. The length, thickness, outer diameter, and permittivity of the insert were varied. In all cases, there was no air gap between the insert and load.

Our investigation was performed using RF circuit and 3-D EM co-simulation [1]. The RF circuit simulator was Agilent ADS software, and Ansoft HFSS was chosen as the 3-D EM tool for its robustness in handling complex coil geometry. For all geometries the array was tuned/matched/decoupled using capacitor and inductor based decoupling networks, and also tuned by minimization of power reflected by the entire array. The effect of the insert on array performance and transmit magnetic field homogeneity was analyzed at three transverse slices (center and $+/-25$ mm from the load center). The array was excited in circular polarization mode, applying the same power to each port and using sequential 45 degree phase increments.

Results: In most cases, the insert increases both the coupling between elements, and the effective resistance that is seen by each loop coil. The first effect makes array decoupling more complicated, while the second makes it easier. Which effect dominates depends on the array and geometries, and the dielectric material.

For a spherical load and a cylindrical insert with length comparable to or larger than the load, it is impossible to decrease inter-element coil coupling by any decoupling approach that can reduce power reflected by entire array to below 40% of delivered power. As a result array performance drops significantly. For other cases investigated, where it is possible to minimize power reflected by entire coil, use of the insert increases the fraction of the power absorbed by the load. This is because other losses are decreased relative to load losses. The higher the permittivity of the dielectric material, the larger the increase of resistance that is seen by loop coil.

If the insert is longer than the array, the magnetic field propagates more strongly in parts of the load outside the array. In this case array performance is decreased by 5–30%. If the insert is shorter or equal to the array length, performance is improved by 10–25% in the central slice, and decreased in the two offset slices studied. Simple modification of the insert geometry by splitting it and inserting a 50 mm long air gap at the centre slice position improves neither the performance in all slices nor their homogeneity, relative to these without the insert.

Our study suggests that no configuration exists where use of the high permittivity dielectric material improves homogeneity by more than 10%. Usually we obtained the same or decreased homogeneity. With or without the insert, the array transmit field homogeneity is strongly dependent on the distance between array and load, and also the load diameter and shape. Inhomogeneity increases with load diameter.

Use of a high permittivity insert does not affect the choice of decoupling method. Both capacitance and inductance based decoupling circuitry allow similar decoupling levels. For all cases investigated, coupling between second neighbors was larger than between first neighbors.

Conclusion: Use of the high permittivity dielectric material insert is not a general recipe to improve array performance and homogeneity. For loop based array with relative long distance between array and load, the insert can improve performance within the central slice without greatly affecting its homogeneity. To improve transmit performance in other slices needs investigation of much more sophisticated insert designs (both shape and variable permittivity).

REFERENCES

1. Kozlov, M. and R. Turner, *Journal of Magnetic Resonance*, Vol. 200, 147–152, 2009.

Laser Surface Modification of Alloys for Reduced Heating in an MRI Environment

O. Benafan[1], **S.-Y. Chen**[2], **A. Kar**[2], **and R. Vaidyanathan**[1]

[1]Advanced Materials Processing and Analysis Center (AMPAC)
Mechanical, Materials, and Aerospace Engineering
University of Central Florida, Orlando, FL 32816, USA
[2]Laser-Advanced Materials Processing Laboratory
Center for Research and Education in Optics and Lasers (CREOL)
College of Optics and Photonics, University of Central Florida, Orlando, FL 32816, USA

Abstract— Magnetic resonance imaging (MRI) has become an indispensable noninvasive medical imaging technique in medical diagnostics of the human body. However millions of patients worldwide with active and passive implanted metallic medical devices such as cardiac pacemakers, implantable cardioverter-defibrillators (ICDs), deep brain stimulators (DBSs), stents, bone implants and devices, etc., are prevented from MRI scans due to potential hazards. One such hazard is tissue heating in the vicinity of the metallic alloy due to induction heating of the alloy by the pulsed radio frequency (RF) magnetic field during a typical MRI sequence, e.g., at the tip of a lead wire electrode.

In this study, nanoscale surface modification of medical grade metallic alloys was conducted using a Nd : YAG laser-based dopant diffusion technique. The objective of this approach was to reduce induction heating by reducing the absorbed RF field. Such an approach is advantageous in that the dopant is diffused into the alloy and is not susceptible to detachment or spallation as would an externally applied coating. Furthermore, the dopant distribution is controlled so as to not deteriorate the mechanical and electrical properties of the base alloy or device. Experiments were conducted using a controlled environment laser system with the ability to control laser properties (i.e., laser power, spot size and irradiation time) and dopant characteristics (i.e., temperature, concentration and pressure). The reflective and transmissive properties of both the doped and untreated samples were measured in a RF (63.86 MHz) magnetic field using a system comprising a high power signal generator, a localized magnetic field source and sensor, and a signal analyzer. The results indicate an increase in the reflectivity of the laser-treated samples compared to untreated samples. The effect of reflectivity on the heating of the alloys is investigated through a mathematical model involving Maxwell's equations and heat conduction.

Modeling Electromagnetic Interference in Medical Implants Exposed to Uniform Magnetic Fields

Juliano Katrib[1], **Mustapha Nadi**[1], **Pierre Schmitt**[1], **Djilali Kourtiche**[1], **and Isabelle Magne**[2]

[1]L.I.E.N., Nancy University, Vandoeuvre les Nancy 54506, France
[2]EDF — R&D, Site des Renardières, Ecuelles, Moret sur Loing 77250, France

Abstract— This paper presents a finite integral method to evaluate electromagnetic interference in active medical implant (Implantable Cardiovertor Defibrillator (**ICD**)), exposed to uniform magnetic fields, at power lines frequencies. An analysis of the standards regarding interferences in ICD is carried out to determine the level of induced voltage which may cause the malfunction of such devices. A uniform magnetic field at 50 and 60 Hz was generated by Helmholtz coil. Three irradiations were considered: above (up to down), front (chest to back) and side (right to left).

In the first approach, a homogenous model was used to validate our physical models with analytical equation and to estimate the relative error. Field strengths, based on the recommendations of ICNIRP, were selected and additional fields exceeding these limits were also used. Results show strong agreement with the literature for the induced electric field and current, therefore we investigate the induced electric field and current density in ICDs with bipolar detection (2 electrodes for sensing and stimulating). These results made a good base to investigate the induced electric field and current in a real human body.

Secondly, an anatomical model based on MRI scan of a 34 years old male, 1.74 m in height, was used. This phantom structure is composed of more than 70 tissues, thus the inhomogeneity of the human body is taken into account. Dielectrics properties values were based on the Gabriel database. Induced current density, averaged over 1 cm^2, was calculated for each organ and compared to ICNIRP level. The next step will be to insert a detailed CAD model of an ICD with the help of a scanner, to provide a more realistic configuration. The induced voltage U will be calculated (1). This voltage will be evaluated for bipolar electrodes (distal and proximal) arriving to the heart passing the aorta. This distance will be fixed to 16 mm in this study as it is the average for constructers.

$$U = \int_{dist}^{prox} \vec{E} \cdot dl \tag{1}$$

Table 1 presents the induced voltage/1 µT for the three irradiations. The electric field distribution near the medical implant and its probe were simulated and the results will be discussed according to the different parameters of influence. The role of the interface between the electrodes and human tissues is discussed when they are exposed to such magnetic fields. Investigations are underway to determine the role of anisotropy on induced voltage.

Table 1: Induced voltage at the input of ICD.

Position	Induced voltage @ 50 Hz (µV/µT)	Induced voltage @ 60 Hz (µV/µT)
Above	0.0988	0.1185
Front	0.1527	0.1832
Side	0.3512	0.4214

Electromagnetic Compatibility between Implantable Cardiac Pacemakers and RFID Systems: Experimental Set-up, Test Protocol and Preliminary Results

E. Mattei[1], **G. Calcagnini**[1], **F. Censi**[1], **M. Triventi**[1], **C. Desantis**[2], **P. Menna**[2], **and P. Bartolini**[1]

[1]Italian National Institute of Health (ISS), Italy
[2]"Sapienza" University of Rome, Italy

Abstract— RFID emissions have the potential to affect electronic devices. Particular care has to be paid for the electromagnetic interference (EMI) to implantable pacemakers and implantable cardioverter-defibrillators (ICDs). A recent study conducted by the Food and Drug Administration in collaboration with major implantable pacemaker and ICD manufacturers, demonstrates the effects of emissions from RFID readers on common implantable cardiac devices. Significant effects were observed especially for low frequency RFID readers, and the authors concludes that "are concerned that the continued proliferation of RFID without taking electromagnetic interference into consideration could cause clinically significant events for patients", even if they "do not believe the current situation reveals an urgent public health risk".

In this paper, an experimental set-up for the evaluation of the EMI between implantable cardiac pacemaker and RFID readers operating in the low-frequency (LF — 125 kHz) and high frequency (HF — 13.56 MHz) range is described. The set-up and the test protocol are derived from the standard ANSI/AAMI PC69 : 2007, and modified to better take into account the coupling mechanisms in a frequency range lower than the one adopted in the standard (< 400 MHz). A human torso simulator filled with a saline solution appropriate for each frequency is used to host the pacemaker and its leads. Two couples of stainless steel plates are mounted at the center of each of the 4 inner walls of the torso simulator. The first couple is used to monitor the pacemaker activity; the second couple is used to simulate the electrical activity of the heart, in such a way that the pacemakerrecognizes as an inhibition signal. For each pacemaker, two tests are performed, one with and one without the simulated heart signal. Two development kits were used to generate the RFID signal at 125 kHz and 13.56 MHz. Since some studies on the EMI between RFID and medical devices highlighted that a degradation of the performances of the devices occurred only when the tag was placed close the device under test, the functioning of the pacemaker has to be tested also when a closed-loop is established in the communication between the reader and the tag.

Before the EMI tests, the magnetic fields generated by the two RFID emitters were measured at 1 cm from the RFID antenna: peak values of 35.3 A/m at 125 kHz and 0.024 A/m at 13 MHz, were found.

Eight pacemakers from 6 manufactures were tested. The programming parameters were left as the default setting chosen by the manufacturer. Six pacemakers were tested in the unipolar pacing/sensing modality, whereas 2 in the bipolar modality. In all the EMI tests, no significant degradations of the basic performances of the device were observed. Noteworthy, the field strength generated by the RFID readers used in this study is lower than the maximum values allowed by the RFID international standards.

The adopted experimental set-up and test protocol is suitable for further investigations, using other types of RFID readers and higher values of field.

Session 1A8b
EMC and Mitigation Techniques: Theory and Practice 1

Impedance Variation of an Equipment under Test in a GTEM Cell

David Pouhè
Technical University Berlin, Einsteinufer 25, Berlin 10587, Germany

Abstract— In a recent paper [1], the interaction between an equipment under test (EUT) and the cell reflecting metal walls as represented by images of the EUT has been investigated by restricting the scope of the study to the total incident field and its subsequent deviation from the primary excited TEM field, to the current on the EUT and its deviation when compared to the induced current in free space. The impedance variation of the EUT was set arbitrary as being constant and equal to 10% the value of the impedance the EUT would have in free space. It was essentially shown that strong and weak test conditions may occur since the overall impinging field on the EUT generally deviates from the primary TEM field. In addition to that, the deviations in field and the errors in induced current were quantified. The role plays by excited evanescent modes was neglected. At high frequencies however, the role of evanescent modes in both the impedance variation and the change in current on the EUT might be of no less importance and can therefore no longer be ignored. Hence, it is expedient to know which influence these waves can have on the overall impedance and on the surface current on an EUT placed in the cell. We address this issue in the present work. Especially a generalized approach for investigating the reactive effects of the GTEM cell is provided using the MoM. The method is applied to thin dipoles as canonical EUTs to capture even small changes in the characteristics of the antenna by providing a basic understanding of the effects of the mutual coupling between the cell and EUT. Although the approach allows deep investigations of the deviation in field and the error in induced current, emphasis has been put on the impedance variation and the overall current distribution on the EUT, as they are a measure par excellence of this coupling. The impact of the phenomenon of illumination an re-illumination along with the influence of evanescent modes on the capacitive or inductive behavior of the EUT is demonstrated. It is shown that even for small EUTs the contribution of the fields excited by induced currents on the EUT and scattered back from cell walls cannot be ignored. The appeal of the method resides in its simplicity and in imparting deep insights into the physic behind the mutual influence between the cell and the EUT.

REFERENCES

1. Pouhè, D. and G. Mönich, "On the interplay between equipment under test and TEM cells," *IEEE Trans. EMC*, Vol. 50, No. 1, 3–12, Feb. 2008.
2. Pouhè, D., "Spherical waves in conical TEM cells," *Progress In Electromagnetics Research*, Vol. 57, 209–236, 2006.
3. Harrington, R. F., *Field Computation by Moment Methods*, R. E. Krieger Publishing Compagny, INC., Krieger Drive, Malabar, Florida, 1968.
4. Stutzman, W. L. and G. A. Thiele, *Antenna Theory and Design*, 2nd Edition, John Wiley and Sons, New York, 1998.
5. Simonyi, K., *Theoretische Elektrotechnik*, 10. Auflage, Dt. Verlag der Wissenschaft, Leipzig, Berlin, Heidelberg, 1993.

Design Optimisation to Reduce the Magnetic Fields Propagated from DC Light Rail Transit Systems

A. Ogunsola[1, 2] and A. Mariscotti[3]

[1]Department of Electrical and Electronics Engineering, Faculty of Engineering
University of Lagos, Lagos, Nigeria
[2]Rail Transit Division, Parsons Group International, London, United Kingdom
[3]Naval and Electrical Engineering Department, University of Genoa
Via all' Opera Pia 11A, 16145 Genoa, Italy

Abstract— The increasing implementation of Light Rail Transit System (LRTS) as an integrated form of public transportation, with the rail corridor running through city centers and connecting major commercial centers, presents a unique electromagnetic coupling scenario between sensitive installations and the dc magnetic field propagated from the LRTS. It is not surprising therefore, that there has been increasing interest in the prediction and mitigation of the magnetic fields propagated from such light rails. Numerous measurements have been performed, such as those by Lowes [1], Hsaio and Lin [2], Yamazaki [3, 4] with the view of quantifying the magnetic field from dcrailways, however differences in Light Rail Vehicles restrict the use of measurement data across differing LRTS. Measurement data however has contributed to the development of numerical and computational analysis as applied to dc electrified railway. Waki et al. [5] investigated the use of magnetic shields, installed along the alignment, to attenuate the magnetic field propagated by the railway; this solution is feasible where the railway does not share the right of way with an existing road network. Schepper and Rabl [6], analysed a Compensation Conductor (CC) arrangement using resistance network approach and reporting a 42% improvement in the magnetic field due to the CC. Mariscotti and Ogunsola in [7] investigated the effectiveness of a mitigating technique based on the installation of CCs that can either be installed to be at the same potential of either the Overhead Contact Wire (OCW) or Running Rail (RR); the authors were able to demonstrate a 10 dB attenuation of the propagating magnetic field. In this paper, the work of Mariscotti and Ogunsola is furthered by optimising the CCs arrangement with a view of maximising the attenuation of the propagated magnetic field.

The approach to optimization is based on the minimization of either the mutual impedance term in the loop impedance expression or the weighted sum of magnetic field intensity in selected points. Computational results of the induction field computation is reported by means of contour curves, showing the achieved attenuation of the propagated magnetic field.

REFERENCES

1. Lowes, F. J., "Magnetic monitoring of dc electric railways," *Physics in Technology*, Vol. 18, 209–14, 1987.
2. Hsiao, Y.-T. and K.-C. Lin, "Measurement and characterization of harmonics on the Taipei MRT DC system," *IEEE Trans. Industry Applications*, Vol. 40, 1700–1704, 2004.
3. Yamazaki, K., K. Kato, K. Kobayashi, Y. Uchikawa, Y. Kumagai, A. Haga, and K. Fujiwara, "Characteristics and prediction of magnetic noise due to DC electric railcars for biomagnetic measurements," *IEEE Trans. Magnetics*, Vol. 37, No. 4, 2884–2887, 2001.
4. Yamazaki, K., K. Kato, K. Kobayashi, K. Kawamata, A. Saga, N. Goto, S. Minegishi, and A. Haga, "Environmental low frequency magnetic field due to direct current electric railcars," *Electrical Engineering in Japan*, Vol. 137, No. 3, 10–21, 2001.
5. Waki, H., H. Igarashi, and T. Honma, "An analysis of shielding against dc magnetic fields generated by electric railways — Evaluation of effective permeability of fine structures," *Electrical Engineering in Japan*, Vol. 160, No. 4, 309–316, 2005.
6. Schepper, W. and C. R. Rabl, "Electromagnetic field emissions of electrified railways," *Computer Theoretikum und Praktikum für Physiker*, Vol. 11, 85–105, Fachbereich Physik der Martin-Luther-Universität Halle-Wittenberg, Hall, Germany, 1996.
7. Mariscotti, A. and A. Ogunsola, "Prediction and mitigation of magnetic fields propagated from dc light rail transit system," *Intern. Conf. on Electrical Systems for Aircraft, Railway and Ship Propulsion*, Bologna, Italy, Oct. 19–21, 2010.

Noise Coupling Reduced by Using Non Uniform Transmission Lines for Power Bus Design in Active RF Circuits

M. Boussalem[1, 2], F. Choubani[1], J. David[2], Tan Hoa Vuong[2], and R. Crampagne[2]

[1]Equipe de Recherche 6'Tel SUPCOM, Tunis, Tunisia
[2]Laboratoire Laplace, ENSEEIHT, Toulouse, France

Abstract— Diminishing and controlling the coupling noise of power bus design in RF circuit is a major issue because it reduces the interference with RF circuit. In our paper we expose an original technique to minimize this noise coupling induced by power bus in RF circuits. This technique is based on the non uniform transmission lines (LNUT).

The analysis and design of non uniform transmission lines have been largely explored in the literature [1, 2]. Various applications of these transmission lines have been of a great importance for both microwave and power engineering [3, 4].

It is well known that non uniform transmission lines have specific frequency behaviour [5] which strictly depends on their profiles. A non homogeneity adds some degree of freedom compared to uniform transmission lines. Whereas uniform transmission structures resonate at frequencies that are multiple of fundamental frequency, the non uniform lines resonate at frequencies which are different.

Usually power bus is designed with uniform microstrip lines that are used as power lines, its represents the supply of voltage and currents to the circuit. This uniform elements induce a noise coupling witch disturbs the functioning of the circuit.

Our methodology consists in replacing a uniform structure by their equivalent based on non uniform parts in order to reduce or control the noise coupling and improve functioning of RF active circuit.

Our paper provides a methodology that minimizes a noise coupling using a non uniform transmission lines. We have demonstrated by ADS simulation that noise is sharply reduced by such use of NUTL in the case of RF oscillator design, and it will be experimentally explored. Moreover, we have optimised the profiles of different elements of power circuits in order to get better frequency response.

REFERENCES

1. Khalaj-Amirhosseini, M., "Analysis of coupled or single non uniform transmission lines using step-by-step numerical integration," *Progress In Electromagnetic Research*, Vol. 58, 187–198, 2006.
2. Khalaj-Amirhosseini, M., "Analysis of coupled or single non uniform transmission lines using Taylor series expansion," *Progress In Electromagnetic Research*, Vol. 60, 107–117, 2006.
3. Boussalem, M., F. Choubani, J. David, and R. Crampagne, "Harmonic suppression in low pass filter designed by non uniform transmissions lines," *12th IEEE International Conference on Electronics, Circuits and Systems*, Gammarth, Tunisia, December 11–14, 2005.
4. Boussalem, M., J. David, F. Choubani, and R. Crampagne, "Intelligence use of the non uniform transmissions lines to design actives and passive microwave circuits," *Progress In Electromagnetic Research Symposium*, Tokyo, Japan, August 2–5, 2006.
5. Boussalem, M., H. Gaha, J. David, F. Choubani, and R. Crampagne, "Analysis of the non uniform transmission lines using the direct numerical resolution of Hill's equation," *Progress In Electromagnetic Research Symposium*, 229, Prague, Czech Republic, August 27–30, 2007.

Session 1A9
Poster Session 1

Experimental Dynamical Evolution of Impulse and Delta Pulses through Dispersive Vegetation in Remote Sensing Frequency Bands

Ana V. Alejos[1, 2], **Luis Medina**[1], **Muhammad Dawood**[1], **Luis Rodríguez**[1], **and Paula Gomez**[2]

[1]EMAG and Wireless Group, New Mexico State University, Las Cruces, NM, USA
[2]University of Vigo, Campus Universitario, Maxwell St, Vigo 36310, Spain

Abstract— In this contribution we introduce an approach to analyze and detect the formation of Brillouin precursor in a signal propagated through a dispersive vegetation for the frequency band of 2.4 GHz.

One important effect of the dispersive propagation is the evolution of signals called Brillouin precursor. One main distinguishing property of the precursors is the algebraic peak amplitude attenuation compared to the conventional exponential decay of the original signal. The former is important for optimum transmitter and receiver design, demanding further research in that direction. The latter property leads to the optimal penetration depth in a given media and is of great interest for remote sensing applications involving soil, water, and foliage.

An experimental method has been developed in the frequency domain that gives as a result the frequency transfer function of the medium under study. This transfer function acts as a filter allowing as input signal any kind of waveform. In the outcome signal we can detect the formation of the Brillouin precursor superimposed to the rising and leading signal edges.

Herein, we introduce the experimental data obtained with the target of analyzing the time and spatial propagation of an input signal formed by an impulse and a delta pulse, and a sequence of delta pulses, through dispersive vegetation consisted of a single tree. We present the experimental results achieved for both pulses as input waveforms, which modulate a sine carrier at 2.4 GHz.

A Concave-hexagonal Dual-band Antenna with Defected Ground Structure

Yuta Tahara and Toshiaki Kitamura
Faculty of Engineering Science, Kansai University, Osaka, Japan

Abstract— Wireless local area network (WLAN) has experienced rapid growth due to their merit such as cost effectiveness, high-speed data connectivity, and user mobility. Integration of 2.4/5.2/5.8 GHz frequency bands into one device has become an increasing demand. Accordingly, development of a compact antenna providing a dual-band operation has been gained much attention. Various kinds of dual-band antennas have been proposed so far.

In this study, a dual-band antenna for 2.4/5.2/5.8 GHz WLAN applications is proposed. The proposed antenna has a single layer metallic structure on FR4 substrate with a dielectric constant of 4.4 and substrate thickness of 1.6 mm. It is formed by a concave-hexagonal monopole antenna that consists of a combination of an equilateral triangle patches and an inverted equilateral triangle ones. A side of the triangle is 12.1 mm for both patches. A 50-ohm CPW transmission line, in which a center strip width 2.0 mm and a gap distance between the strip and the coplanar ground plane is 0.25 mm, is used for a feed line. Defected ground structure (DGS) is introduced into the coplanar ground planes in order to improve radiation loss between two operating bands at 2.4 and 5.2 GHz. To investigate the performance of the proposed antenna, electromagnetic simulator HFSS is used. Dual-band operations covering 2.4/5.2/5.8 GHz are shown from the frequency characteristics of return loss. An affect of the dimensional parameters of DGS to the return-loss characteristics is studied. Electromagnetic fields and radiation patterns at each resonant frequency are also shown.

Investigation on a Ladder-shaped Frequency Selective Surface for Dual-band Operation

Keisuke Morimoto, **Toshiaki Kitamura**, **and Daigo Yonetsu**
Faculty of Engineering Science, Kansai University, Osaka, Japan

Abstract— Frequency selective surfaces (FSSs) have attracted much attention due to their widespread applications as spatial microwave filters. Their practical applications can be found in electromagnetic-interference (EMI) protection, selective electromagnetic (EM) shielding, and EM absorbers. A typical FSS is composed of planar metallic patterns that are periodically arranged on a dielectric substrate. Various types of FSS have been proposed so far.

In this study, a ladder-shaped FSS is proposed. The proposed FSS, whose equivalent circuit is expressed as a combination of parallel and series LC circuits, shows dual stopband characteristics. Indoor shielding application for 2.4/5.2 GHz wireless local area network (WLAN) is assumed and the shielding effect when the FSS is placed on the window grass is investigated. The structure of the unit cell is composed of a metal patch ($44.0 \times 44.0\,\mathrm{mm}^2$) in which five parallel slots are arranged. The slot size is $28.0 \times 4.0\mathrm{mm}^2$ and the gap between two adjacent slots is 4.0 mm. The unit cell surrounded by symmetric planes is analyzed by using an EM simulator HFSS. The equivalent circuit is also analyzed and the results are compared with the simulation results. Finally, the proposed FSS is fabricated by arranging the arrays of the proposed unit cells on both side of the glass substrate whose relative permittivity is 5.5. Aluminum sheet is used for forming metallic patterns. A shield box (WaveLaboratory Co., Ltd.) and a spectrum analyzer N1996A (Agilent Technology) are used for the experiment. The experimental results are compared with the numerical ones.

Study on a Quad-band Microstrip Bandpass Filter Using Quarter-wavelength Resonators

S. Murata[1], **T. Kitamura**[1], **and Y. Horii**[2]

[1]Faculty of Engineering Science, Kansai University, Osaka, Japan
[2]Faculty of Informatics, Kansai University, Osaka, Japan

Abstract— Recently, multi-band operation for RF devices has been gaining much attention in order to incorporate multiple frequency bands of wireless communication systems such as GPS (1.57 GHz), WLAN (2.4/5.2 GHz) and WiMAX (3.5 GHz). Multi-band RF devices have been strongly demanded and dual-band, tri-band, and quad-band filters have been studied extensively.

In this study, a quad-band microstrip bandpass filter is proposed. The proposed filter consists of a combination of quarter-wavelength resonators. They are composed of two long resonators (resonators 1 and 2) and two short ones (resonator 3 and 4). The resonators 1 and 2 form a kind of coupled hair-pin resonators and one part of each resonator is terminated to the ground plane through a via hole. They create the first, third, and forth passbands. The resonators 3 and 4, which are arranged between the resonators 1 and 2, construct coupled resonators and they create the second passband. The resonators are arranged on the substrate with a dielectric constant of 10.2 and substrate thickness of 1.27 mm. As an I/O ports, a microstrip line is directly connected to each of the resonators 1 and 2, respectively. To investigate the performance of the proposed filter, electromagnetic simulator HFSS is used. The results when the operation frequencies are designed for the applications of GPS, WLAN and WiMAX systems are shown.

Evaluation of a Planar Coil Model Using Shell Elements

A. Ospina, **L. Santandrea**, **Y. Le Bihan**, **and C. Marchand**
Laboratoire de Génie Electrique de Paris, CNRS UMR8507; SUPELEC
UPMC Univ. Paris 06; Univ. Paris-Sud 11
11 Rue Joliot-Curie, Plateau de Moulon, 91192 Gif-sur-Yvette Cedex, France

Abstract— Planar printed coils are increasingly used in many applications: eddy-current non-destructive testing (EC-NDT) [1, 2], Magnetic Resonance Imaging (MRI) [3, 4], Micro Electromechanical Systems (MEMS) [5, 6]... The recourse to numerical methods allows to finely study these kinds of devices.

Among the numerical methods for the study of planar coils, the finite element method (FEM) is one of the most adapted. However, the discretization stage (meshing), leads to a considerable increase of the number of unknowns or to deformed elements in this thin area and its vicinity (ill-conditioned system). Consequently, the computation time became very expensive. In order to eliminate these problems a kind of degenerated elements (shell elements) is used in this paper [7–9].

In the meshing process, the planar coil is considered as a surface, and thus deformation of elements are avoided and their number remains limited. Then, in the problem formulation, the degenerated elements are introduced in order to model the planar coil. Finally, a linear equation system is solved and the fields are calculated in the "real" geometry. In this paper a comparison is established between this planar coil model and analytical results [10] in order to find a range of validity.

REFERENCES

1. Fava, J. O. and M. C. Ruch, "Calculation and simulation of impedance diagrams of planar rectangular spiral coils for eddy-current testing," *NDT & E International*, Vol. 39, 414–424, 2006.
2. Ditchburn, R. J. and S. K. Burke, "Planar rectangular spiral coils in eddy-current non-destructive inspection," *NDT & E International*, Vol. 38, 690–700, 2005.
3. Massin, C., G. Boero, F. Vincent, J. Abenhaim, P.-A. Besse, and R. S. Popovic, "High-Q factor RF planar microcoils for micro-scale NMR spectroscopy," *Sensors and Actuators A: Physical*, Vol. 97–98, 280–288, 2002.
4. Eroglu, S., B. Gimi, B. Roman, G. Friedman, and R. L. Magin, "NMR spiral surface microcoils: Design, fabrication, and imaging," *Concepts in Magnetic Resonance Part B: Magnetic Resonance Engineering*, Vol. 17B, 1–10, 2003.
5. Liu, Y., H. Lee, R. M. Westervelt, and D. Ham, "IC/microfluidic hybrid system for biology: Review (Invited Paper)," *Proceedings of the IEEE Bipolar/BiCMOS Technology Meeting (BCTM)*, 174–179, Oct. 2005.
6. Massin, C., F. Vincent, A. Homsy, K. Ehrmann, G. Boero, P.-A. Besse, A. Daridon, E. Verpoorte, N. F. de Rooij, and R. S. Popovic, "Planar microcoil-based microfluidic NMR probes," *Journal of Magnetic Resonance*, Vol. 164, No. 2, 242–255, Oct. 2003.
7. Ren, Z., "Degenerated Whitney prism elements — General nodal and edge shell elements for field computation in thin structures," *IEEE Transactions on Magnetics*, Vol. 34, No. 5, 2547–2550, Sept. 1998.
8. Ospina Vargas, A., L. Santandréa, Y. Le Bihan, and C. Marchand, "Electromagnetic field computation in magnetic and conductive thin sheets," *Sensor Letters*, Vol. 7, No. 3, 480–485, Jun. 2009.
9. Ospina, A., L. Santandrea, Y. Le Bihan, and C. Marchand, "Modeling of thin structures in eddy current testing with shell elements," *The European Physical Journal Applied Physics*, Vol. 52, No. 2, Nov. 2010.
10. Dodd, C. V. and W. E. Deeds, "Analytical solutions to eddy-current probe-coil problems," *J. Appl. Phys.*, Vol. 39, No. 6, 2829–38, 1968.

Maxwell's Motor Equation and the Mechanical Power

S. L. Vesely[1], **A. A. Vesely**[2], **and C. A. Dolci**[3]

[1]I.T.B.-C.N.R., Italy
[2]Via L. Anelli 13, Milano, Italy
[3]Liceo Einstein, Milano, Italy

Abstract— Ever since our first acquaintance with electric power yield there have been good reasons, including marketability, to endow it with a unit of measurement. In the beginning, that requirement was blended with the problem of interpreting the electrical phenomena themselves. Subsequently, energy-balance linear equations have prevailed over the quest for detailed mechanisms explanation. Nowadays, the impressive technological advance in ICs miniaturization has created high expectations centered on using solid state devices as sensors, actuators, and MEMS, as well as extending large scale integration down to the molecular level. Since the relationship between quantum mechanics and the classical world is not yet fully established, one may still hope that large scale integration technology will eventually unveil the primary energy conversion mechanisms. Thus, there are various, possibly conflicting, objectives: the electro-mechanical performance, a theoretical explanation of the involved mechanisms, and the fixing of the quantum measurement problem. Here we focus on the first one. In particular, we wish to call attention to two points: 1) Transduction power gain differs from signal magnification. High efficiency electromechanical power transduction exploits specific couplings, that can hardly be explained by linear models. For instance, a stepper motor can be used to explain a system-on-a-chip actuator, but not to evaluate its mean efficiency. 2) The power delivered by an electric engine cannot be ascertained by electrical means only. Hence, the mean power intensity drawn by a given engine during its functioning at steady conditions would tell less about the overall conversion efficiency than the start-up peaks.

To delve into the origin of points 1) and 2), we review the illustration given by Maxwell of the electromagnetic force (A treatise on electricity and magnetism, Vol. 2, Part IV, Chap. I) and compare it with his treatment of Faraday's induction (*ibid.*, Chap. III). They are in fact the empirical basis of the two equations of electromagnetism, named after Ampère-Maxwell and Faraday, that introduced innovative conceptions with respect to the Newtonian way of thinking.

Chapter one illustrates the equation $\mathbf{rotH} = \mathbf{I}_{total}$ by dint of the *unipolar motor*, a current-carrying arm capable of revolving about one of its polar expansions, but developing a negligible amount of power. Maxwell was able to explain that motion in a geometrical fashion by way of *electromagnetic* force, that he kept well distinct from *electromotive* force (emf). His description involves no electrically supplied power, and thus is as linear as any small signal linearization. This suggests that electro-mechanical performance is not covered by his approach, according to point 1 above.

Chapter three introduces Faraday's induction as an emf. In fact, a *transient* emf; actually, an hybrid between the linearized output of a sort of stabilized generator and a carrierless induction signal. Possibly, confusing the signal and the generator's output might have undermined Maxwell's intent. Nowadays, even the want for a distinction between electromagnetic force and emf is deemed a trait of pre-relativistic electromagnetism. Dynamo generators and motors are considered reciprocal devices, in principle. In order to elaborate on point 2, and to approach efficiency considerations according to the intended applications, we propose to distinguish a generator's emf from the signal recorded during power conversion.

In summary, we think that, since today's concern with small scale sensors and actuators arouses not only from the desire to test existing general theories, but also from technological production needs, a clear-cut distinction between transferred power and electrically measured parameters is in order.

Analysis of Light-beam Scattering from DWDD Disk with Control Layer under Considering Rear Process

Yuya Matsunami and Toshiaki Kitamura
Faculty of Engineering Science, Kansai University, Osaka, Japan

Abstract— The magneto-optical (MO) disks are used as rewritable media of information. Recently, various technologies of higher density version that exceed optical resolution have been proposed for MO disk, and put to practical use. In those technologies, the domain wall displacement detection (DWDD) is one of the excellent readout methods, which utilizes the characteristic of magnetic film called wall-displacement phenomenon by temperature gradient. This method has no limit of resolution in principle. However, it has a problem that ghost signals are caused by so-called rear process (RP) due to continuously recorded marks.

In this study, we deal with a DWDD disk model that has a control layer to suppress ghost signals. We use FDTD method for the analysis. So far, we have applied FDTD method to the analysis of light-beam scattering and detected signal characteristics from various types of optical disks such as digital versatile disks (DVD) and MO disks and demonstrated that it can be a powerful tool for the numerical simulation of light-beam diffraction from conventional DVD and MO disk structures.

We analyze light-beam scattering from the disk model. We also investigate main-polarized and cross-polarized components of scattered far field and phase differences between them. We show how the rear process affect the characteristics of the main-polarized and cross-polarized components of the light-beam scattering.

Electromagnetic Wave Propagating in Gyroelectric Slab in the Perpendicular Configuration

Hui Huang[1, 2], **Bo Yi**[2], **and Bo Huang**[3]

[1]School of Electrical Engineering, Beijing Jiaotong University, Beijing 100044, China
[2]State Key Laboratory of Millimeter Waves, Nanjing 210096, China
[3]School of Electronics Engineering and Computer Science, Peking University, 100871, China

Abstract— This paper present the characteristics of electromagnetic wave propagating in gyroelectric slab with an external magnetic field perpendicular to the interface between gyroelectric medium and a perfect conductor. First, using KDB coordinate system, we decomposed an electromagnetic wave in infinite gyroelectric medium into 2 types and got the dispersion relation respectively. Second, we discuss the reflection from the interface between gyroelectric medium and a perfect conductor for inclined incidence case. The conclusion that the reflected wave has the same ellipticity but the opposite rotate direction to the incident wave is proofed theoretically. Finally, the characteristics of metallic waveguide in Perpendicular Configuration have been discussed, and the guidance condition has been derived. And we found the main mode is zero mode, which is similar to the ordinary wave in infinite gyrotropic medium.

A Simple Algorithm for Multiple Reflection of Rays from a Smooth Surface

P. Bruscaglioni[1] **and A. Ismaelli**[1, 2]

[1]University of Florence, Italy
[2]ASPER, Florence, Italy

Abstract— A simple algorithm is presented. It allows one to follow trajectories of optical radiation which undergoes multiple reflections on a smooth surface described by a net of points, placed at equal distances with respect to the x, y co-ordinates and whose z co-ordinates are specified. The x, y projected surface is divided in equal area squares, and the z co-ordinate of the vertexes are defined. In order to model the surface continuously each plane square is divided into two triangles by a diagonal. The figure shows a square (A) where the diagonal line c-b divides it. The possible points of intersection of the rays with the surface and the directions of reflection are obtained by geometrical considerations. Polarization can be dealt with by considering Fresnel coefficients. A series of decisions are made in order to find the first incidence triangle, and the subsequent ones The figure shows the first incidence square A and the surrounding squares B, C, D, E where a possible subsequent incidence occurs.

The square A is divided into two triangles as indicated above.

A couple of examples showing broken trajectories determined by the algorithm will be given. Polarization and intensity of the reflected beams, changing during the trajectories, have to be inserted in the programme.

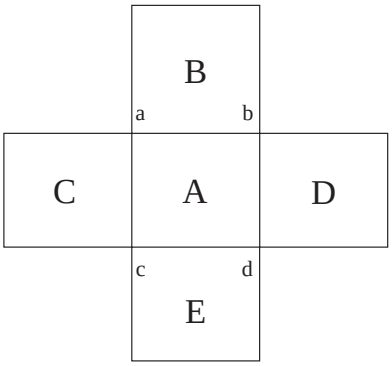

Table 1: VERTEXES OF A: m=integer $(x_0/H)+1$, n=integer $(y_0/H)+1$.

x	x	y	z
a	$m-1$	n	za
b	m	n	zb
c	$m-1$	$n-1$	zc
d	m	$n-1$	zd

Effects of Non-Sphericity of Scatterers on Polarization of Lidar Returns. Cases of Chebyshev Particles

P. Bruscaglioni and A. Mannoni
Department of Physics, University of Florence, Italy

Abstract— As is well known lidar returns from non spherical particles shows particular effects of polarization even for single scattering.

The effect depends much on the type of scatterers. To understand how even a simple deviation from sphericity may produce such effects, for this note we have considered Chebyshev particles. We have chosen these particles, though one can observe that they do not represent atmospheric particles in a very realistic way. However they are easily dealt with, since calculations of scattered radiation can be carried out by means of analytic procedures such as that of the Extended Boundary Conditions [1–3], which allows us to obtain the Mueller matrices and the extinction properties of the medium.

Thus some polarization effect on the lidar returns is the object of our numerical study, It extends a previous one which referred on received power [4].

The Chebyshev particles with rotational shape, case T2, are described by the radius r as given by:

$$r(\theta) = r_0(1 + \varepsilon \cos(2\theta))$$

ε "deformation parameter" (Sphere for $\varepsilon = 0$).
The Mueller matrix was considered for two simplifying situation.
Random-3d orientation (**R3**): the axes are distributed at random in the three directions with respect to the direction of the incident beam.
Random-2d orientation (**R2**): the symmetry axes of the particles are uniformly distributed in a plane normal to the direction of the incident beam.
The latter geometry was considered for backscattering only of first order.
In both cases the Mueller matrix assumes a simpler form.

All the numerical results obtained refer to particles with real refractive index $n = (1.33, 0.0)$ in a medium with the property of vacuum.

Wavelength of incident radiation $\lambda = 0.532\,\mu$m.

Comparisons were made with spheres of fixed radii with volumes equal to the central one of the polydispersion.

To simplify the calculations a Gaussian polydipersion of the radii has been taken with standard deviation 'sd' of 4% uniformly distributed in 200 steps within $a + / - 3\,$sd.

The elements of the Mueller matrix were evaluated at 91 values, with interpolation in the intervals between them.

The geometrical situation is that of a medium with homogeneous density of particles. The medium is at a distance of 1000 m from the emitter-receiver position. The total depth of the medium is 300 m.

The assumed total depth, relative to the equivalent sphere, is 6 for the extinction linear coefficient $\sigma = 0.02m^{-1}$.

Our Monte Carlo code for dealing with polarization uses the phase function for determining the scattering angle θ. The azimuthal angle ϕ is first considered to be equiprobable, and determined from a random number routine as $\phi = 2\pi R$ (R equiprobable between 0 and 1). Then a correction for the "photon" energy is multiplied by an opportune "weight" factor taking into account the elements a11, a12, a21, a22 of the Mueller matrix.

The results refer to a (fictitious) medium with extinction coefficients: $\sigma_e = 0.02m^{-1}$ (total optical depth 6). Receiver field of view of 1.5, 5, 15, 30 mrad (half aperture).

Single Backscattering: If one chooses linear polarization of the emitted beam. the calculated polarization ratio in backscattering will be shown by some examples. The obtained results show a great amount of variation with a complex dependence on size parameter and deformation parameter, showing a greater variability for the case of Random-2d distribution.

This feature does not appear to be casual, since it is maintained for the range of size parameter.

Multiple Scattering: Random-3d orientation of scatterers. For multiple scattering a version of a Monte Carlo code was used, whose description will be given, The geometrical situation is that of a homogeneous layer, width 300 m, at a distance from the source of 1000 m.

Some figures will present results obtained for multiple scattering up to 15th order. As expected, a comparison with the case of the sphere shows that at small optical depths the polarization effect is much different.

No substantial change of polarization is present for the sphere at small optical depth. But, as is well known, when the optical depth increases for the sphere the polarization change also increases. In general one observes that, at least for large FOV, polarization effect for the sphere tends to become similar to that for the Chebishev particles when the sounded optical depth increases.

ACKNOWLEDGMENT

Work carried on in the framework of Contract 05-100000-8024, INTAS PROGRAM.

REFERENCES

1. Waterman, P. C., *Proc. IEEE*, Vol. 53, 805–812, 1965.
2. Barber, P. and C. Yeh, *Applied Optics*, Vol. 14, 2864–2872, 1975.
3. Mugnai, A. and W. J. Wiscombe, *Applied Optics*, Vol. 25, 1235–1244, 1989.
4. Mannoni, A., C. Flesia, P. Bruscaglioni, A. Ismaelli, et al., *Applied Optics*, Vol. 34, 7151–7164, 1996.

Three Dimensional FDTD Analysis of Near-field Optical Disk

Shingo Iwata and Toshiaki Kitamura
Faculty of Engineering Science, Kansai University, Osaka, Japan

Abstract— The capacity of optical storage system has been improved by shortening wavelength, or increasing the numerical aperture of an objective lens. However, the recording density has a limitation due to optical diffraction limit. Recording methods based on near-field optical principles are one of the candidates that can overcome the limitation. Many researchers have been interested nano-apertures for the method to obtain near-field light and many types of apertures have been proposed so far. In order to obtain high emission intensity and small spot size simultaneously, they have discussed various aperture shapes such as triangular, H, I or C shaped, figure-eight or bow-tie shaped, ridge waveguide type, rectangular holes with a metallic slit, and so on.

In this paper, we analyze a phase change disk illuminated by near-field optical light through a metallic nano-aperture by means of finite-difference time-domain (FDTD) method. We deal with a three-dimensional structure. Here, we assume that metallic materials are silver, gold, and so on. In the analysis, we use FDTD method into which motion equations of free electrons are installed to analyze a metallic material. We show that the field intensity of near-field light can be increased by changing the aperture shapes. We also investigate the influence of the near-field light output through the recorded marks.

Mapping Technique of Basic Magnetic Field in MR Tomography

M. Hadinec[1], **P. Fiala**[1], **and K. Bartušek**[2]

[1]Department of Theoretical and Experimental Electrical Engineering
Brno University of Technology, Kolejní 2906/4, Brno 612 00, Czech Republic
[2]Institute of Scientific Instruments of the ASCR, v.v.i
Královopolsk 147, Brno 612 64, Czech Republic

Abstract— The paper presents a mapping method, which is used to obtain boundary conditions on desired volume. The process of obtaining the magnetic flux density from NMR spectral characteristics is explained. The spherical functions are used for magnetic flux density approximation. The discussion of suitable degree and order for approximation is made. Then maps of magnetic flux density inside measured volume are computed. These maps are compared to measured phase images. Phase images are gained by mapping technique based on MRI methods. The comparison algorithm in Matlab is made and results are discussed.

ACKNOWLEDGMENT

The work described in the paper was financially supported by the research project GA102/09/0314, research plan MSM 0021630513 and project of the BUT Grant Agency FEKT-S-10-13.

REFERENCES

1. Stratton, J. A., *Teorie Elektromagnetického Pole*, STNL, Praha, 1961.
2. Haacke, E. M., R. W. Brown, M. R. Thomson, and R. Venkatesan, *Magnetic Resonance Imaging — Physical Principles and Sequence Design*, John Wiley & Sons, 2001, ISBN 0-471-48921-2.
3. Dědek, L. and J. Dědková, *Elektromagnetismus*, Vol. 2, 232, Vutium, Brno, 2000, ISBN 80-214-1548-7.
4. Bartušek, K., Z. Dokoupil, and E. Gescheidtová, "Magnetic field mapping using an asymmetric spin echo MRI sequence around metal implants," *Measurement Science and Technology*, Vol. 17, No. 12, 2006, ISSN 0957-0233.

EMHD Effects Come through at Linear Moving Objects Analysis

Pavel Fiala and Zoltán Szabó
FEEC, BUT, UTEE, Kolejní 2906/4, Brno 612 00, Czech Republic

Abstract— The paper provides an insight into the issues of measurement methods for accuracy obtain information velocity objects. One of the measurement method used for its problems is based on electromagnetic field measurement. The accuracy measurement method is focused to use of EMHD effects analysis and results applied to the experimental measurement. This results and measurement method decrease lethality of wrong measurements of non-ballistics projectile velocity. The paper describe comparison numerical analysis and experimental data.

From the formal point of view, several perspectives are utilized to facilitate the topic analysis, and these aspects of evaluation can be identified within the regions of legal ethics, medicine, or military tactics as well as engineering and technology. In relation to the problem of protection against undesirable phenomena like terrorism, it is necessary to mention the fact that there exists long-term research focused on the institution of NATO and its member armies; this research mainly pertains to the determination and practical use of non-lethal or wounding methods and means in all constituent parts of protection and defence. The armies of European countries participate systematically in the process of non-lethal weapons development and integration within the respective armament systems.

ACKNOWLEDGMENT

The funding of the project was supported by the Ministry of Defence of the CR and Ministry of Industry and Trade of the CR (Diagnostics of superfast objects for safety testing, FR-TI1/368), Ministry of Education, Youth and Sports of the CR, and by insitutional resources from the Research Design — Electronic Communication Systems and New Generation Technologies (ELKOM) MSM0021630513, GAČR 102/09/0314.

REFERENCES

1. Krüger-Sprengel, F., "Legal adaptation of non-lethal capabilities in new conflict scenarious," *2nd European Symposium on Non-Lethal Weapons*, Ettlingen, SRN, May 13–15, 2003.
2. Kim, B., "Between principles and absolutes: Non-lethal weapons and the law of armed conflict," *2nd European Symposium on Non-Lethal Weapons*, Ettlingen, SRN, May 13–15, 2003.
3. Janssen, W. J. H. and E. J. M. Jansen, "Decision-making processes: The choice between lethal an non-lethal force," *2nd European Symposium on Non-Lethal Weapons*, Ettlingen, SRN, May 13–15, 2003.
4. David, E., "An effectiveness and risk during application of NLW from the medical point of view," *4nd European Symposium on Non-Lethal Weapons*, Ettlingen, SRN, May 10–12, 2005.
5. David, E., A. Fretz, and J. Reissenweber, "Mortality following taser exposure," *4nd European Symposium on Non-Lethal Weapons*, Ettlingen, SRN, May 21–23, 2007.
6. Wolf, F., "Multi-spectral measurement of NLW effects," *4nd European Symposium on Non-Lethal Weapons*, Ettlingen, SRN, May 21–23, 2007.
7. Fiala, P., "Finite element method analysis of a magnetic field inside a microwave pulsed generator," *2nd European Symposium on Non-Lethal Weapons*, Ettlingen, SRN, May 13–15, 2003.
8. Fiala, P. and P. Drexler, "Measurement methods of pulsed power generators," *4nd European Symposium on Non-Lethal Weapons*, Ettlingen, SRN, May 21–23, 2007.
9. Stratton, J. A., *Teorie Elektromagnetického Pole*, STNL, Praha, 1961.

GPGPU Acceleration of the Finite-difference Time-domain Program

Hideaki Taniyama[1], **Takashi Shimokawabe**[2], **Takayuki Aoki**[3], **and Masaya Notomi**[1]

[1]NTT Basic Research Laboratories, NTT Corporation, Japan
[2]Interdisciplinary Graduate School of Science and Engineering, Tokyo Institute of Technology, Japan
[3]Global Scientific Information and Computing Center, Tokyo Institute of Technology, Japan

Abstract— Finite-Difference Time-Domain (FDTD) method of Maxwell equation is widely used and is a powerfull tool in the study of optical nanostructures. Especially, photonic crystal (PhC) cavities attract many researchers interests because of large Q-factor. Generally, FDTD simulation of PhC structures requires large amount of memories and long computing time but the computing speed is essentialy limited by memory bandwidth. Multi core processor, which is these day's trend of CPU, does not solve this problem. To overcome this limitaion, one of widely used techniques is parallel computing on such as PC cluster. However, for large number of clusters, data transfer between computing nodes limits the computation speed instead. Recent GPUs achieve very high memory bandwidth and peak computation power, compared to conventional CPUs. Programming tools have been provided from GPU venders these days. Then application of GPU computation is rapidly expanding to many fields.

In this work, we report the result of acceleration of computing the FDTD algorithm. The program is double-precision 3D calculation of Maxwell's equation. Yee's algorithm and PML technique are implimented in the program.

We use CUDA 3.1, which is an integrated development environment for NVIDIA's GPGPU. For GPU, we use NVIDIA's GPUs, Tesla C1060 and GeForce GTX 480 and Xeon/W3580 CPU for the reference. We calculate the confined electromagnetic field profile in one hole missing photonic crystal slab cavity (see Fig. 1). Fig. 2 shows evaluation of the performance on GPUs and CPU for several amount of simulation size. The elapsed time for calculation of 1351MB is 2429 s for the CPU version and 337s for C1060, and 136s for GeForce GTX 480. On GPU, our algorithm achieves about 20x speedup over CPU implementation, on average.

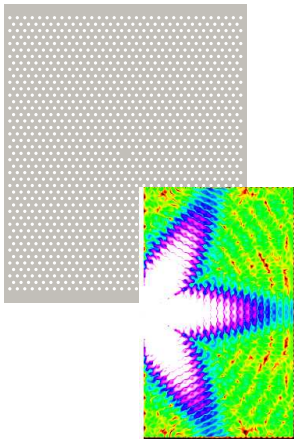

Figure 1: Photonic crystal cavity and hexagonal-mode field profile.

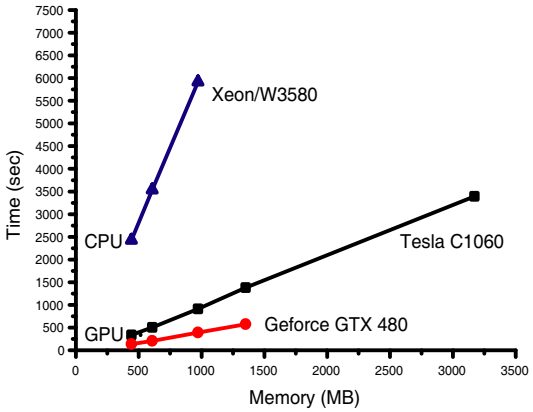

Figure 2: Elapsed time of GPUs and CPU.

Modelling of 3D Thin Regions in Magnetostatic NDT Using Overlapping Elements in Dual Formulations

H. Zaidi, **L. Santandréa**, **G. Krebs**, **and Y. Le Bihan**
Laboratoire de Génie Electrique de Paris
(CNRS UMR 8507, Supelec, Univ. Paris-Sud 11, UPMC Paris 6)
11 rue Joliot Curie, 91192 Gif-sur-Yvette, France

Abstract— The finite element method is widely used for the simulation of non-destructive testing. In this context, the modelling of thin regions which are currently found in this kind of problem (lift-off, thin flaw, thin coil ...) with classical finite elements results in numerical problems (very fine mesh or very deformed elements, illconditioned matrix, poor convergence, ...). To overcome these numerical problems, a solution can consist in the use of the overlapping element method.

This method was originally introduced in [1] and [2] to simulate the motion of electrical machines. Considering two non-conform meshes facing each other, the principle of the approach consists in the projection of the nodes of one boundary on the other and reversely. This projection creates overlapping elements. Theses elements are support of shape functions and permit to assure the continuity of the interpolated values but do not introduce new nodal degrees of freedom. Once the double projection is done, integration areas are created allowing to evaluate the different integral terms of the FEM formulation.

This paper proposes to evaluate the overlapping elements with a low frequency 3D NDT problem using the classical dual magnetic formulations with nodal and edge Whitney elements. Indeed the combined use of these formulations exhibits interesting features for mesh refinement and energy calculation. As an example, an air coil probe characterizing the magnetic permeability of a plate is considered and its inductance computed. The overlapping element method is used to take into account the low lift-off between the coil and the plate.

REFERENCES

1. Tsukerman, I. A., "Overlapping finite element for problems with movement," *IEEE Transactions on Magnetics*, Vol. 28, No. 5, 2247–2249, Sep. 1992.
2. Krebs, G., S. Clenet, A. Abakar, F. Locment, and F. Piriou, "Method to connect non-conforming mesh in 3D with the overlapping method," *IEEE Transactions on Magnetics*, Vol. 45, No. 3, 1420–1423, Mar. 2009.

Design and Study of a Permanent Magnet Synchronous Motor for an Electric Compressor

M. Khanchoul[1], **G. Krebs**[1], **C. Marchand**[1], **F. Alves**[1], **A. Battelier**[2], **and M. Roze**[3]

[1]Laboratoire de Génie Electrique de Paris
CNRS UMR 8507, Supelec, Univ. Paris-Sud 11, UPMC Paris 6
11 rue Joliot Curie, 91192 Gif-sur-Yvette, France
[2]EDC Project, VALEO Compressor, La Verrière 78321, France
[3]Phenix International, Route de Noiron, Gray 70100, France

Abstract— Nowadays, electrical vehicles present a technological solution to reduce gas emissions. To preserve the autonomy and also maintain the lifetime of the battery, it is necessary to regulate the temperature inside. Air conditioner compressors are consequently used to assure this function. Mechanical air compressors are now substituted by electrical devices in order to improve the efficiency, compactness and flexibility.

In this paper, a permanent magnet synchronous motor is designed to drive an electrical air compressor. Design constraints require a power of 6 kW (torque of $5\,\mathrm{N}\cdot\mathrm{m}$) at a speed of 10000 rpm. Volume and mass of the motor are imposed. Torque oscillations must not exceed 3% of the rated torque. Furthermore, the supply voltage is limited and dependant on the battery level. A last design aspect concerns the cooling gas that has to flow through the motor.

The studied structure for the air compressor is a surface-mounted permanent magnet motor with concentrated coils. It permits to have very low values for the cogging torque and, due to the constant winding inductance [1], for the load torque oscillations also. Due to different pole numbers of the stator and rotor, this kind of structure can present a higher mass/volume ratio than conventional motors [2]. Concentrated coils permit to reduce the motor length and also Joules losses [3].

The first part of the paper deals with analytical and numerical models (reluctance networks and 2D finite element methods). The second part of the paper is dedicated to the procedure used for the design of the motor geometry. The designed motor is finally studied in a third part in terms of electrical, mechanical and thermal behaviours.

REFERENCES

1. Zhu, T. Q. and D. Howe, "Electrical machines and drives for electric, hybrid, and fuel cell vehicles," *Proc. IEEE*, Vol. 95, No. 4, 746–765, 2007.
2. Matt, D. and J. F. Llibre, "Performance comparées des machines à aimants et à réluctance variable. Maximisation du couple massique ou volumique," *Journal de Physique*, Vol. 3, 1621–1641, 1995.
3. Magnussen, F. and C. Sadarangani, "Winding factors and Joule losses of permanent magnet machines with concentrated winding," *Electric Machines and Drives Conference, IEMDC'03*, Vol. 1, 333–339, 2003.

On Modeling the Near-field Coupling between an Electronic Device and a Transmission Line in the Presence of a Ground Plane

Elagiri-Ramalingam Rajkumar, **Abhishek Ramanujan**, **Mohamed Bensetti**, **and Anne Louis**
Institut de Recherche en Systémes Electroniques Embarqués (IRSEEM)
76801 Saint Etienne du Rouvray, France

Abstract— The development of electromagnetic simulation tools has become critically important in the design and development of embedded systems. This work is focused in modeling the near-field electromagnetic coupling between an electronic component and a transmission line when placed at proximity. The induced coupling on a transmission line due to an external plane wave has been reported in [1–3]. Based on the radiated emission model developed in IRSEEM, the work in [4] reports a coupling model, but the radiated electromagnetic field by the dipole network is analytically computed. It neglects the possible electromagnetic coupling that could exist between the dipoles and the transmission line when they are close to each other. The problem is addressed with the use of a hybrid method associating analytical and numerical methods.

A wire of radius 0.1 mm, length 8 mm above a ground plane at a height of 2.1 mm is used as the target device and an elementary electric dipole placed between the ground plane and the wire is used as the radiating source. Both the terminals of the wire are terminated with matched 221 Ω impedance. An integrated simulation (numerical modeling) in Ansoft HFSS and CST Microwave Studio gave encouraging results for the coupled voltage at both ends of the wire at 1 GHz. The coupling between the dipoles and the wire/ground plane is considered in our simulations. Alternatively, a hybrid model based on the Agrawal method [2] is built from HFSS simulated results (with open ended wire). The modeled terminal voltage correlates well with those of numerical simulations, with about 3–4% relative error. Interestingly our model gives better results than that in [4] for the same configuration. As a next step, an active device placed between the ground plane and the wire is used as the perturbing source. The model developed in [5] is used to simulate the EM fields radiated by the component. The dipole network is integrated into HFSS and simulated along with the transmission line. The hybrid model is constructed as before and good correlation was found between the model and HFSS simulations.

As perspective, a PEEC model [6] could be developed from the current model. Preliminary tests proved that the model does not consider the capacitive coupling between the devices. Currently, work is in progress to improvise and complete the PEEC coupling model.

REFERENCES

1. Rachidi, F., "Formulation of the field to transmission line coupling equations int of magnetic excitation field," *IEEE Tran. EMC*, Vol.35, No. 3, 404–407, Aug. 1993.
2. Agrawal, A. K. and H. J. Price, "Transient reponse of multiconductor transmission lines excited by a non uniform electromagnetic field," *Mission Research Corporation*, Albuquerque, NM 87108.
3. Atrous, S., D. Baudry, E. Gaboriaud, A. Louis, B. Mazari, and D. Blavette, "Near-field investigation of the radiated susceptibility of printed circuit boards," *Proc. EMC Europe 2008, Int. Symp.*, Hamburg, Germany, Sept. 8–12, 2008.
4. Leseigneur, C., P. F. Lopez, C. Arcambal, D. Baudry, and A. Louis, "Near-field coupling model between electronic systems and transmission line," *IEEE Int. Symp. EMC Ft.*, 22–27, Lauderdale, USA, Jul. 25–30, 2010.
5. Ramanujan, A., Z. Riah, A. Louis, and B. Mazari, "Modeling the electromagnetic radiations of passive microwave components using a near-field scanning method," *IEEE Trans. EMC*, accepted, 2010.
6. Ruehli, A. E. and A. C. Cangellaris, "Application of the partial element equivalent circuit (PEEC) method to realistic printed circuit board problems," *Proc. IEEE Int. Symp. EMC*, 182–187, Aug. 1998.

Full-wave Mode Analysis of Asymmetric Coupled Microstrip Structures: Particular Case of Quasi-symmetric Lines

A. Khodja[1], **R. Touhami**[1], **M. C. E. Yagoub**[2], **and H. Baudrand**[3]

[1]Instrumentation Laboratory, Faculty of Electronics and Informatics
U.S.T.H.B University, Algiers, Algeria
[2]SITE, University of Ottawa, 800 King Edward, Ottawa, Ontario, K1N 6N5, Canada
[3]ENSEEIHT, 2 rue Charles Camichel 31071, Toulouse Cedex 7, France

Abstract— The aim of this paper consists to highlight in which case asymmetric coupled microstrip structures can be studied by symmetric line model in order to use the quasi-symmetric approach. For this purpose, a rigorous formulation was developed; trial functions of C and π modes were obtained from the quasi-symmetric case, and thus proposed for the asymmetric case. A comparative study of dispersion parameters demonstrated the limits of the quasi-symmetric model validity with respect to asymmetries due to influence of shielding and metal strips widths difference.

In order to efficient full-wave analysing the quasi-symmetric coupled line model, transverse resonance technique combined with the electromagnetism (EM) operators formalism is used. This technique consists in more easily formulating the boundary conditions by considering the fictitious propagation in the transverse direction.

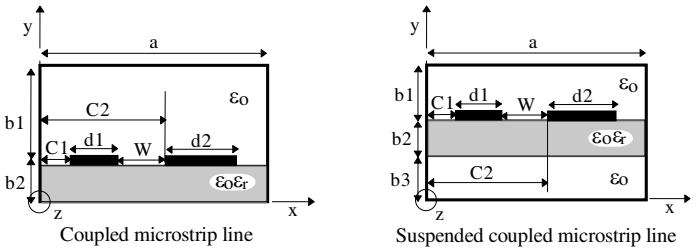

Figure 1: Transverse section of the shielded asymmetric coupled microstrip transmission lines.

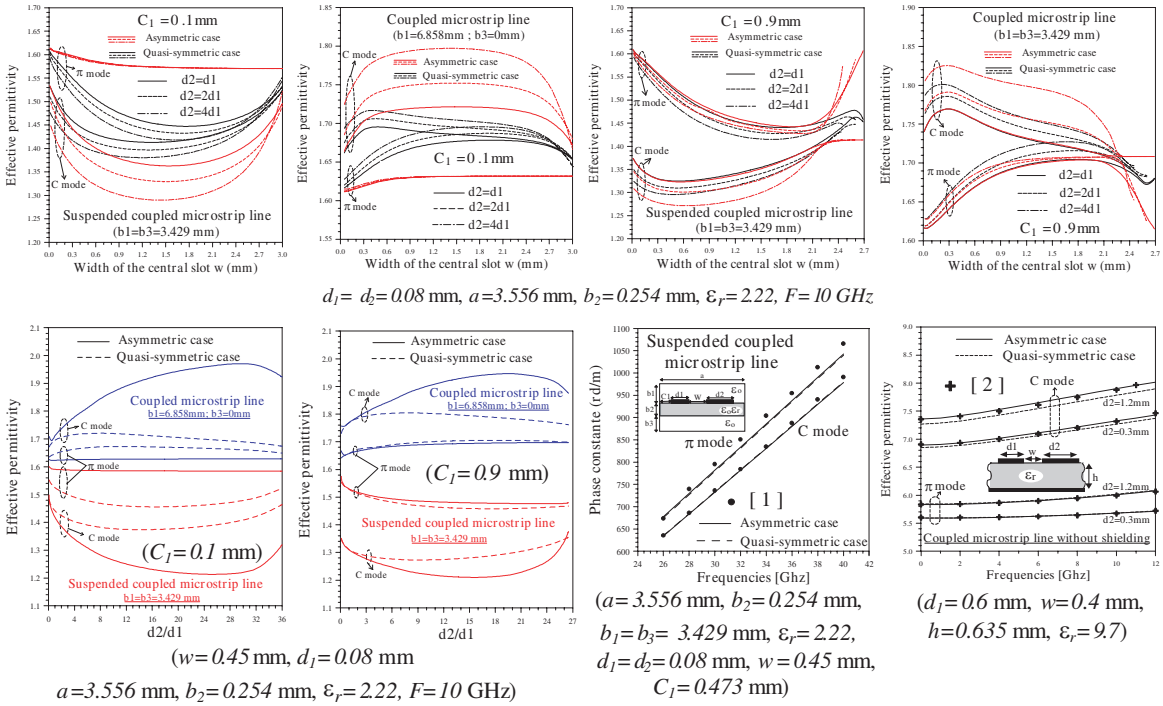

Figure 2: Variation of dispersion parameters versus physical parameters and frequencies.

The obtained results show a good agreement of our results with those published in the literature [1, 2]. However, when the line is without shielding, the asymmetric model is more accurate than the quasi-symmetric case.

REFERENCES

1. Achkar, J., O. Picon, V. F. Hanna, and J. Citerne, "Analysis of symmetric and asymmetric coupled suspended striplines and some associated discontinuities," *20th EMC*, Budapest, Hungary, 1990.
2. El-Deeb, N. A., E. A. F. Abdellah, and M. B. Saleh, "Design parameters of inhomogeneous asymmetrical coupled transmission lines", *IEEE Transactions on Microwave Theory and Techniques*, Vol. 31, No. 7, 592–596, July 1983.

2D PIM Simulation Based on COMSOL

Xinbo Wang[1], **Wanzhao Cui**[1], **Jingyu Wang**[2, 3], **Jingnan Pan**[2], **Xiaocheng Zheng**[2], **Jiangtao Huangfu**[2], **and Lixin Ran**[2]

[1]National Key Lab of Science and Technology on Space Microwave Technology
Xi'an 710000, China
[2]Department of Information and Electronic Engineering, Zhejiang University
Hangzhou 310027, China
[3]Department of Photonics Engineering, Technical University of Denmark
Copenhagen, DK-2800, Denmark

Abstract— Passive Intermodulation (PIM) is notoriously known for its detrimental effect on performance of base stations used in the space, military and civil telecommunications. PIM products, resulting from nonlinear frequency mixing by passive components, occur in the reception band of antenna and degrade the system signal integrity. Recently, more and more efforts have been devoted to PIM simulations. However, most of them require a very good comprehension of computational electromagnetic.

In this paper, the domain wave equation for PIM simulation was derived form Maxwell equations accomplished with nonlinear constitutive relations. And the well-known commercial software COMSOL Multiphysics was employed. Those who are not familiar with computational techniques but have a solid background in electromagnetic should find it extremely beneficial. A 2D nonlinear model was established as an example. Two carriers, whose frequencies were close to each other, were set to be the input signals. And a probe was used to monitor the field strength at the output terminal. After the numerical simulation in time domain, the data were transformed into frequency domain by COMSOL script. As a result, the 3rd order PIM products were observed in the output spectrum.

The contribution of this paper is to make the PIM simulation more convenient and more efficient. And this type of analysis should aid in the development of the means for PIM mitigation. The further research will focus on the effective determination methods for nonlinear coefficient. In addition, the effect of device geometry and system level simulation will also be taken into consideration in the future.

A Novel Approach for Modeling Diodes into FDTD Method

Hsin-Hsiang Su[1], **Chih-Wen Kuo**[1], **and Toshihide Kitazawa**[2]

[1]Department of Electrical Engineering, National Sun Yat-San University, Taiwan
[2]Department of Electrical and Electronic Engineering, Ritsumeikan University, Kusatsu 525-8777, Japan

Abstract— A novel technique is proposed to incorporate diodes into the finite difference time domain (FDTD) method. The equivalent circuit of the diode is combined with Yee's time-stepping equations to update the fields without using the time-consuming iterative method at each time step. Two types of diodes are investigated by being connected at the end of a microstrip transmission line to demonstrate the validity of this method. Stability of the proposed method is demonstrated numerically and the accuracy is verified by comparison with commercial software ADS. The numerical results agree well with ADS. In these two cases, the numerical results show no sign of instability after a long simulation time (number of time steps = 10^5).

Magnetic Susceptibility Modelling Using ANSYS

K. Bartusek[1], **M. Cap**[2], **P. Marcon**[2], **and J. Mikulka**[2]

[1]Institute of Scientific Instruments, Academy of Sciences of the Czech Republic
Kralovopolska 147, Brno 612 64, Czech Republic
[2]Department of Theoretical and Experimental Electrical Engineering, Brno University of Technology
Kolejni 2906/4, Brno 612 00, Czech Republic

Abstract— The paper deals with modeling of magnetic induction in close to the paramagnetic materials. NMR based method for material susceptibility measuring give as variable results which need to be verified by other reliable method. ANSYS model based on Finite Element Method makes verification of measured results possible. ANSYS is the suitable system for multiphysics modeling and simulation, anisotropic materials and for possible use of special programming language APDL. Therefore, is the use of this program for results verification advantageous.

The samples were experimentally tested in a static field flux density $B_0 = 4,7\,\mathrm{T}$. This field matches the real magnetic field in the MR tomograph at the Institute of Scientific Instruments, Academy of Sciences of the Czech Republic (ISI ASCR).

Paramagnetic and diamagnetic material samples as s aluminum, copper, glass, and water are used. The samples are cylinders, 3 cm in length and 0.5 cm in diameter. In model the cylinder is placed in an air filed cube with side length 4 cm. Simulation results of designed models are used for magnetic.

ACKNOWLEDGMENT

The research described in the paper was financially supported by FRVS (a fund of university development) by research plan No. MSM 0021630513 ELCOM, No. MSM 0021630516, grant of Czech ministry of industry and trade No. FR-TI1/001, Czech Science Foundation (102/09/0314) and project of the BUT Grant Agency FEKT-S-10-13.

REFERENCES

1. Vladingerbroek, M. T. and J. A. Den Boer, *Magnetic Resonance Imaging*, Springer-Verlag, Heidelberg, Germany, 1999, ISBN 3-540-64877-1.
2. Dedek, L. and J. Dedková, *Elektromagnetismus*, 2nd Edition, 232, VITIUM, Brno, 2000, ISBN 80-214-1548-7.
3. Steinbauer, M., "Měření magnetické susceptibility technikami tomografie magnetické resonance," VUT v Brně, FEKT, Brno, 2006.
4. Fiala, P., "Finite element method analysis of a magnetic field inside a microwave pulsed generator," *2nd European Symposium on Non-Lethal Weapons*, Ettlingen, SRN, May 13–15, 2003.

Statistics of the Shielding Effectiveness of Metallic Enclosures

J. Benoit[1,2], **P. Bonnet**[1,2], **C. Chauvire**[1,3], **and B. Pecqueux**[4]

[1]Clermont University, Blaise Pascal University, LASMEA, Clermont-Ferrand, France
[2]CNRS, UMR 6602, LASMEA, Aubière, France
[3]CNRS, UMR 6620, LM, Aubière, France
[4]CEA/DAM/CEG Centre d'études de Gramat, France

Abstract— The shielding effectiveness (SE) characterizes the ability of a shielding enclosure to reduce the emissions or improve the immunity of electronic equipment to high frequency interferences. Electromagnetic shielding is an important and challenging problem since the influence of many parameters has to be studied. In this paper, a rectangular metallic cavity whose surface has a fine aperture illuminated by a plane wave will be considered.

Shielding effectiveness can be estimated by analytical techniques [1] based on simplifying assumptions. However, with more complex enclosure structures, numerical methods may be the only practical way to calculate SE. The major limitation of existing codes is that they require significant computer resources and it may take several hours to get a solution. This is a real problem when there are many variables to consider (length, width, depth of the enclosure and the slot, position of the probe, polarization of the incident field, conductivity of the walls of the box ...). In order to evaluate the impact of each of them, the thousands of runs required by standard Monte Carlo simulation is unfeasible for most practical cases.

Recently, to obtain statistical information such as the mean or the variance, new methods have emerged [2, 3]. In this paper, we propose to adapt an original non intrusive stochastic collocation method based on Lagrange polynomials which presents the simplicity Monte Carlo simulation, but with higher rates of convergence [3]. The mean, variance, kurtosis and skewness of SE will be computed by both analytical and numerical methods considering up to five random variables following different probabilistic laws.

Thanks to the high efficiency of the stochastic collocation method, the final work will discuss the physical behavior of the SE relatively to the impact of the different parameters of the enclosure.

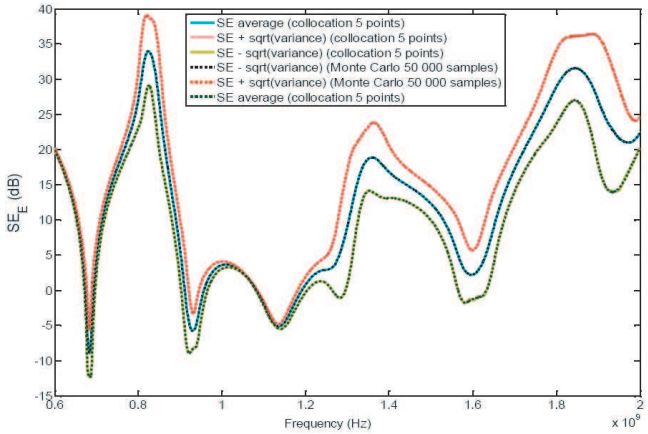

Figure 1: SE for 2 uniform random variables: uncertainty of 3% on the enclosure width and uncertainty of 4% on the slot length. Results are shown with the mean SE as well as ± one standard deviation.

REFERENCES

1. Mendez, H. A., "Shielding theory of enclosures with apertures," *IEEE Trans. Electromagn. Compat.*, Vol. 20, 296–305, May 1978.
2. De Menezes, L., D. Thomas, C. Christopoulos, A. Ajayi, and P. Sewell, "The use of the unscented transforms for statistical analysis in EMC," *EMC Europe 2008*, Hamburg-Germany, Sep. 2008.
3. Chauvière, C., J. S. Hesthaven, and L. Wilcox, "Efficient computation of RCS from scatters of uncertain shapes," *IEEE Trans. on Antennas and Propagation*, Vol. 55, No. 5, 1437–1448, 2007.

Paradigm for Time Reversal Numerical Experiments in Reverberation Chamber: Focusing Fields and Mode Stirrers' Impact

I. El Baba[1,2], **S. Lalléchère**[1,2], **and P. Bonnet**[1,2]

[1]LASMEA, Clermont University, Blaise Pascal University, Clermont-Ferrand, France
[2]CNRS, UMR 6602, LASMEA, Aubiere, France

Abstract— This communication deals with the application of Time Reversal (TR) Technique in the ElectroMagnetic Compatibility (EMC) domain. This technique was originally developed in acoustics [1], and more recently in electromagnetism [2]. In this work we are interested in the capacity of the method to focus field in both time and space and with all polarizations. Previous studies [3] have proven how reverberating medium, especially Mode Stirred Reverberation Chamber (MSRC), may supply an ideal environment to work with TR.

Theoretically, TR requires two steps, firstly a source emitting an electromagnetic radiation and secondly a number of antennas forming a Time Reversal Mirror (TRM) used to back propagate inversed recorded fields allowing time (Fig. 1(a)) and space (Fig. 1(b)) focusing at the original source location. From an experimental point of view (Fig. 2), necessary signals for the second phase of TR may be obtained by injecting signals straightforward on the TRM antennas one by one. Those impulse responses are recorded by a field sensor, and then back propagating them from the TRM involves space and time focusing over the probe both due to the principle of reciprocity and the reverberating behavior.

The foundations and numerical experiments are carried out with the Finite Difference Time Domain (FDTD) method, where the walls of the MSRC are designed with Perfect Metallic Conductors (PEC) conditions jointly with lossy materials to model MSRC losses.

In the final work, we will detail theoretical and numerical aspects of the TR technique discussed in this summary; we will precise how to improve focusing in terms of Signal To Noise (STN) ratio. The numerical results (FDTD simulations) regarding the impact of the excitation source and the

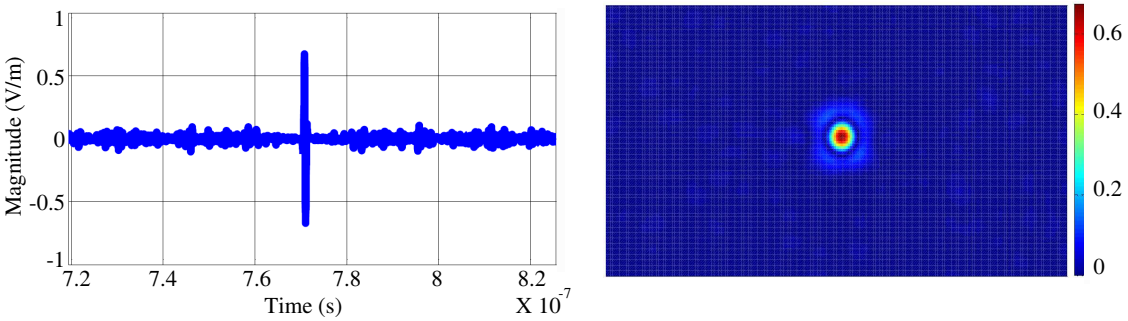

Figure 1: Time (a) and space (b) focusing.

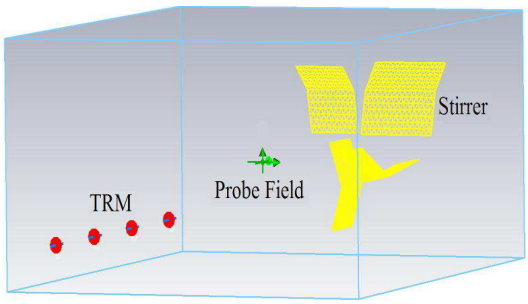

Figure 2: TR set-up in MSRC.

number of TRM antenna will be validated by commercial software (CST Studio suite). Finally, the impact of the mode stirrer for TR numerical experiments in reverberating environment will be demonstrated.

REFERENCES

1. Fink, M., "Time reversal of ultrasonic fields — Part I: Basic principles," *IEEE Trans. Ultras. Ferro-electr.*, Vol. 39, No. 5, 555–566, 1992.
2. De Rosny, J., G. Lerosey, A. Tourin, and M. Fink, "Time reversal of electromagnetic waves," *Modeling and Computations in Electromagnetics*, Vol. 59, 187–202, 2008, ISSN 1439–7358.
3. El Baba, I., S. Lalléchère, and P. Bonnet, "Electromagnetic time-reversal for reverberation chamber applications using FDTD," *Int. Conf. on Adv. In Comp. Tools for Eng. App.*, 157–162, Zouk Mosbeh, Lebanon, July 2009, ISBN 978-1-4244-3833-4.

Simulation of Defects in Photonic Band Gap Structures

Laurent Oyhenart and Valérie Vignéras
Laboratoire IMS, UMR CNRS 5218, 16 Avenue Pey-Berland, Pessac 33607, France

Abstract— The modelling of defects in photonic band gap structures [1] by traditional numerical methods is a complex problem because requiring much memory and computing time [2]. An analytical method of multiple-scattering solves this typical problem for spherical objects. Only this method allows studying lattices with a great number of spheres.

The multiple-scattering method is separated in two parts. The first part allows the calculation of the scattered wave by one sphere by using the Mie scattering theory. The incident and scattered fields are developed on a spherical harmonics basis. Then one writes the transfer matrix between the incident field and the scattered field.

The second part of the method is an iterative algorithm which turns the scattered field calculation from one sphere to N spheres. For the first order, we calculate the diffraction of the incident field for each sphere. For the second order, the scattered field of first order for one sphere becomes the incident field for the $N-1$ others spheres. With this new incident field, the scattered field is calculated as at first order and so on for higher orders. This iterative process stops when a criteria of residual is satisfied. The total scattered field is the contribution of all spheres and all orders used.

In our code of multiple-scattering, no condition of symmetry is required. We can choose the diameters, the dielectric properties and the positions of all spheres. This characteristic is very important for the defects study. We studied various defects, displacement of one layer of sphere, random variation of spheres radii and spheres positions. An example of this study is presented above.

We chose a photonic crystal composed of dielectric spheres in simple cubic lattice. On Fig. 1, we calculate the transmittance of the signal when operating a random variation on the spheres positions around the initial value.

We keep constant the average and the standard deviation of spheres positions. The first forbidden band goes up gradually by increasing the random variation of the lattice constant. This band gap has a classical behaviour. The lattice is disorganized as the random variation increases.

On the other hand, the second band almost does not vary. The first two bands have a radically different behaviour. By modifying the lattice gradually, the first forbidden band will become complete whereas it is not the case for the second. The second band does not result from constructive or destructive interferences between all the layers of the cubic lattice. Various other kind of defects will be presented during the conference.

REFERENCES

1. Joannopoulos, J. D., R. D. Meade, and J. N. Winn, *Photonic Hooks*, 2nd Edition, Princeton University, 2008.
2. Mittra, R., "A look at some challenging problems in computational electromagnetics," *IEEE Ant. Prop. Mag.*, Vol. 46, No. 5, 18–32, 2004.

Simulations of Eigenmodes and Dispersion Relations of 2D Magneto-photonic Crystals

Roman Antos and Martin Veis
Institute of Physics, Faculty of Math. & Phys., Charles University, Czech Republic

Abstract— We present numerical simulations of space distributions of eigenmodes and energy dispersion relations of two-dimensional (2D) magneto-photonic crystals (MPhCs) by using the plane wave expansion (PWE) method. The PWE method is reformulated by using the complex Fourier factorization (CFF) method, which is a new, simple, and numerically effective way of applying the fast Fourier factorization rules [1]. The approach is based on solving the eigen-equation of a MPhC in the reciprocal space, where the anisotropy of the permittivity tensor is determined by the orientation of magnetization vector. In the Fourier space the multiplication of the components of the permittivity tensor and the electric field can be treated by the Laurent rule, which is a numerically ineffective method (here referred to as model A), because the functions of permittivity and electric field have, in general, concurrent discontinuities. Various methods of Fourier factorization are techniques of transforming those quantities to obtain functions without concurrent discontinuities, for which the Laurent rule would be valid. The principle of the CFF method follows the normal vector method [2], where the polarization basis was distributed within the periodic cell so that the normal and tangential components of electric field were treated independently, which enabled the correct application of the Fourier factorization (model B). To improve the method even further, the CFF method (model C) uses generally elliptic polarization bases, so that the matrix of transformation between polarization bases becomes completely continuous. This yields remarkably efficient convergence properties compared to the other methods, which are demonstrated on several 2D MPhC samples with various geometries.

REFERENCES

1. Li, L., *J. Opt. Soc. Am. A*, Vol. 13, 1870, 1996.
2. David, A., et al., *Phys. Rev. B*, Vol. 73, 075107, 2006.

Using Functional Programming for the Parallelization of the Finite Element Method

Laurent Santandréa
Laboratoire de Génie Electrique de Paris, France

Abstract— The majority of computers have now multi-core architectures. In finite element programming, the mostly used solutions to exploit this kind of architecture is based on the methods of domain decomposition. This article proposes a different approach based on Functional Programming. The benefits of this programming paradigm in a finite element method (FEM) implementation context to obtain a parallelized program are shown.

The most advantage of this programming paradigm is that the side effects are avoided and this property is welcomed to have a good parallelization. To illustrate this approach Python language is used. Although this language is usually considered as a procedural and an object oriented language, it contains everything you need for a functional approach to programming. With the modules Numpy et Scipy, it is a very powerful language to implement numerical methods. The module Parallel Python will be used for the parallelization process.

In this work, after having explained the concepts of the FP, the parallelization of the finite element method for the resolution of a 2D magnetostatic problem is proposed. Our approach is based on the following observation: A very expensive time part of a FEM program is used to build the finite element matrix. Our approach consists to apply the functional programming concepts to obtain this matrix. A linear speedup is obtained in function of the CPU number.

Microstrip Ultra-Wide-Band Filter

Abdel-Fattah Sheta and Ibrahim Elshafiey
Electrical Engineering Department, College of Engineering
King Saud University, P. O. Box 800, Riyadh 11421, Saudi Arabia

Abstract— Since the Federal Communications Committee (FCC) authorized the unlicensed use of the ultra-wideband (UWB) frequency spectrum for short-range and high-speed wireless communication in 2002, remarkable research interests in the analysis and design of various microwave devices have been investigated. UWB bandpass filters (BPFs) with low insertion loss, high out-of-band rejection, and a flat group delay performance within that band, are highly needed to meet the required UWB frequency mask (3.1 to 10.6 GHz). Several prototype UWB filters based on different techniques have been studied. One method based on circuit model for an optimum distributed high pass filter (HPF) [1] has been implemented in various techniques [2, 3]. The filter structure in its simplest form consists of cascaded short circuit stubs separated by connecting lines. The electrical length of the connecting lines is twice that of the length of the short circuited stubs at the lower cutoff frequency. The characteristic impedances of the short-circuited stubs and the connecting lines are calculated based on the HPF model [1].

In this paper, a filter consists of four shunt short circuit stubs separated by three connecting lines is designed and implemented based on modified HPF concept. The filter bandwidth can be controlled by the selection of the characteristics impedances of the stubs as well as the connecting lines. The connecting lines herein are similar. The filter in this case can be designed to cover either the entire UWB-band (3.1 to 10.3 GHz) or some groups of the sub-bands of the entire UWB-band. UWB-filter with more bandwidth can also be achieved. The filter was realized using microstrip technique on a substrate with a relative dielectric constant of 2.2 and thickness of 0.78 mm. The filter is designed and implemented to cover the entire band from 3.1 to 10.3 GHz. The characteristic impedance of the connecting lines is 60 Ω. The characteristic impedance of the two stubs located at the edge is 80 Ω while the characteristic impedance of stubs in the middle is 40 Ω. The electrical lengths of the connecting lines and shunt stubs at 3.35 GHz are 45° and 90°, respectively. Fig. 1 shows the simulation results. More details as well as the experimental results will be available in the full paper version.

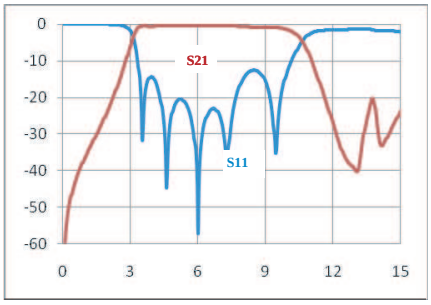

Figure 1: Simulation results of the proposed filter.

ACKNOWLEDGMENT

This research is funded by The National Plan for Science & Technology under project No. 08-ELE262-2.

REFERENCES

1. Hong, J. S. and M. J. Lancaster, *Microstrip Filters for RF/Microwave Applications*, Wiley, New York, 2001.
2. Razalli, M. S., A. Ismail, M. A. Mahdi, and M. N. Hamidon, "Ultra-wide band microwave filter utilizing quarter-wavelength short-circuited stubs," *Microwave and Optical Technology Letters*, Vol. 50, No. 11, 2981–2983, Nov. 2008.
3. Shaman, H. and J. S. Hong, "A novel Ultra-Wideband (UWB) Bandpass Filter (BPF) with pairs of transmission zeroes," *IEEE Microw. Wireless Compon. Lett.*, Vol. 17, No. 2, 121–123, Feb. 2007.

Study on Electromagnetic Properties of Reinforced Concrete Construction Wall

A. Pruksanubal
King Mongkut's University of Technology North Bangkok, Thailand

Abstract— Nowadays, everyday life is concerned with IT devices such as PDAs, mobile phones, laptops, etc., both directly and indirectly. These devices can be used to send or receive the information to or from the large distance. By this reason, our devices can also be disturbed during working in this electromagnetic environment. The elimination or attenuation of the disturbances can be done by shielding the sensitive area. An excellent design of a room or building structure can provide an excellent shielding effectiveness (SE). The application of materials, which offer better shielding properties, can increase SE or reduce the disturbing signals.

In the scope of this work, the properties of around 20 construction materials, such as Gypsum boards, Aluminum blinds, etc., are studied. However in this paper, the setup of an example of reinforced concrete construction wall with metal grid structure (grid size of 10×10 cm.) in the frequency range of 30 MHz–3 GHz are shown. The results from the calculations with Schelkunoff's Model for metal grid structure, the 3D MoM simulations and measurements are compared and discussed. The comparison results show that the calculation results are agreed with the measurement ones at the frequency below resonance frequency, which is caused by the cabinet. The metal grid structure offers the SE of around 20–40 dB at the frequency below 600 MHz.

Effect of Friction Layer Creep Deformation on Dynamic Behavior of Traveling Wave Rotary Ultrasonic Motor

Chao Chen, Huafeng Li, Fan Li, and Kang Yang
Nanjing University of Aeronautics and Astronautics, Nanjing, Jiangsu 210016, China

Abstract— Depending on its piezoelectrically generated vibration and contact mechanism, a traveling wave rotary ultrasonic motor (TRUM)'s shaft can produce considerable torque while the rotor is pressed on the stator. The contact mechanism of TRUM provides us with numerous advantages, including: breaking without power supply, a high torque-to-mass ratio, and high torque/low speed characteristics. Usually polymer friction material is bonded on the contact surface of the rotor, in order to obtain extra excellent mechanical characteristics, such as high efficiency, long life and so on. Unfortunately, the creep deformation happens for the friction layer made of polymer material, due to the large pressure at the contact interface between the stator and rotor. In this case, poor mechanical characteristics of TRUM can be obtained, and the prototype cannot even operate under some conditions.

In this paper the creep of the friction layer made of polymer material is taken into account at the contact interface, especially the startup characteristics of TRUM in storage for rather long time. First the mathematical model representing the electromechanical system of TRUM is derived. Moreover the creep deformation of polymer material in the friction layer is investigated at the contact interface between the stator and rotor. Then the contact problem is numerically analyzed at length to calculate the resulting change of natural frequency of the stator. With the creep deformation of the friction layer considered, we tried to explain how the normal preload force applied on the rotor affect the operation frequency of stator and startup characteristics of TRUM, as is shown in our experiments.

A Single Balanced Quadruple Subharmonical Mixer with a Compact IF Extraction

Yeong-Hsiang Chang, **Wei-Chi Chien**, **Chih-Ming Lin**, **Chun-Chi Su**, **Chia-Chin Hung**, **and Yeong-Her Wang**
Institute of Microelectronics, Department of Electrical Engineering
National Cheng-Kung University, Tainan 70101, Taiwan

Abstract— A novel 21–35 GHz single balanced quadruple subharmonic monolithic passive mixer is fabricated using the 0.15 µm GaAs pHEMT process. This mixer consists of a LO spiral balun and a RF band pass filter possessed of IF extracted feature utilizing a pair of anti-parallel Schottky barrier diode to achieve quadruple subharmonic mixing mechanism. The RF band pass filter formed with a interdigital coupler and a low-pass network is used to reduce the chip dimension while operating at low frequency band and to improve the isolation between the RF and IF ports with a broadband operation. From the measured results, the mixer exhibits a 11.3–15.1 dB conversion loss, a 28.8 dB high RF-to-IF isolation, a 40 dB high LO-to-RF isolation, a 60 dB high 4LO-to-RF isolation over 21–35 GHz RF bandwidth, and an input 1 dB compression power of 3 dBm. The compact IF extraction circuit supports an IF frequency ranging from DC to 3.1 GHz. The chip size is as small as $0.67 \times 0.75\,\mathrm{mm}^2$.

Doorway State Mechanism with Electromagnetic Waves in the Optical Regime

Celia Sánchez-Pérez[1], **Karen Volke-Sepúlveda**[2], **and Jorge Flores**[2]

[1]Centro de Ciencias Aplicadas y Desarrollo Tecnológico, Universidad Nacional Autónoma de México
Apdo. Postal 70-186, 04510 México D. F., México
[2]Instituto de Física, Universidad Nacional Autónoma de México
Apdo. Postal 20-364, 01000 México D. F., México

Abstract— Giant dipole resonances were discovered in the 40's in the form of collective oscillations of protons and neutrons in a nucleus [1]. However, as a wave phenomenon, its ubiquity has manifested in many other areas of physics since then. For example, giant resonance has been observed in the cases of mechanical waves and electromagnetic waves in the microwave regime [2]. In general, giant resonances appear whenever two oscillating systems, one of them having a low density of eigenmodes and the other one having a much larger density of eigenmodes, couple together. The output of the coupled system is an important enhancement of the oscillation amplitude, and therefore of the energy, for the frequencies of the high density eigenmodes around the frequencies of the low density eigenmodes, the latter usually referred to as the doorway states. We experimentally analyse the case of two resonators fabricated by means of two thin layers of metal oxides that satisfy the condition of high optical contrast. The films are deposited on a glass substrate, which is isolated from the coupled resonators by a previous deposition a partially reflective aluminium metallic layer. We also discuss the case of including another ultrathin aluminium metallic layer between the two resonators in order to improve the finesse of the coupled system. Theoretical and experimental results are presented. Potential applications of our system, such as a highly-selective filter, are also discussed.

REFERENCES

1. Goldhaber, M. and E. Teller, *Phys. Rev.*, Vol. 74, 354, 1948.
2. Aberg, S., et al., *Phys. Rev. Lett.*, Vol. 100, 204101, 2008.

A Hemi-directional Antenna Array Concept for Automotive Radar

S. A. Askeland, T. Cella, and J. Hjelmstad
Norwegian University of Science and Technology (NTNU), Norway

Abstract— New advances in mm-wave technologies [1] are making phased array antenna systems feasible for automotive radar systems. In this paper, we introduce a new automotive radar system capable of wide angle traffic monitoring. A narrow radar beam that is scanned over a wide field of view makes it possible to detect imminent collisions from vehicles approaching our vehicle head on or slantingly, and to monitor traffic from the sides when our vehicle has stopped at a crossing road. The system will ultimately use a multidomain approach (angular, frequency, temporal) to achieve target detection and classification. In order to obtain both wide angle coverage and narrow beam width we employ a phased array antenna consisting of three 15 elements planar arrays mounted in three sectors. Each sector has 15 patch antenna elements. The sectors are placed at a 120° angle with each other, see Figure 1(a). When scanning out to angles larger than ±60° from broadside only the elements in the respective side sectors are used. When the scan angle is $< \pm 60°$ the elements in the front sector are used together with the elements in either the left or right sector (depending on which side the array is scanned to). For broadside direction, all elements are used. This means that the elements on the side sectors are scanned ±60° relative to their broadside directions. By using all elements the array looks electronically larger, and hence a narrower beam width can be achieved. To evaluate the performance of the array antenna, radiation pattern simulations were run for 0°, 45° and 90° scan angle. The single element pattern and the pattern for the linear arrays in each sector were simulated in CST Studio Suite [2] using a transient time domain solver, while the simulations for angles including elements from multiple sectors were simulated in Matlab Phased Array Design Toolbox [3] by importing the single element pattern from CST Studio Suite and using conformal array theory. The simulation results (see Figure 1(b)) show that the 3 dB-beamwidths and the side lobe levels or the individual beams are sufficient to obtain good target detection and classification over a more than 180° coverage when used with the multidomain approach. Hence, imminent collisions from head-on, front-side or straight from the sides at intersections can be detected and avoided.

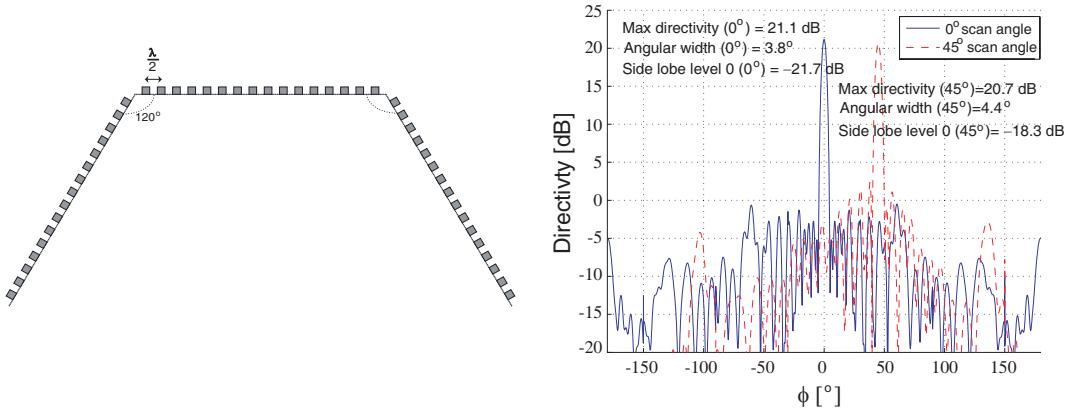

(a) (b)

Figure 1: (a) Array configuration and (b) simulated directivity for 0° and 45° scan angle.

REFERENCES

1. Stemme, G., N. Somjit, and J. Oberhammer, "Binary-coded 4.25-bit W-band monocrystalline-silicon MEMS multi-stage dielectric-block phase shifters," *IEEE/MTT-S Transactions on Microwave Theory and Technology*, Vol. 57, 2834–2840, 2009.
2. CST Studio Suite 2010^{TM}, www.cst.com.
3. Tucker, N., "Phased array design toolbox V2.3 for matlab," Technical Report, 2009.

A Dual Polarization Bow-tie Slot Antenna for Broadband Communications

Chang-Ju Wu, I-Fong Chen, and Chia-Mei Peng
Graduate Institute of Computer and Communication, Jinwen University of Science and Technology
23154 No. 99, An-Chung Road, Hsin-Tien City, Taipei, Taiwan, R.O.C.

Abstract— A dual polarization bow-tie slot antenna for broadband communications is proposed in this paper. This antenna consists of two bow-tie slot antennas which is perpendicular to each another and with coplanar waveguide (CPW)-fed. The proposed antenna has a very simple antenna structure and wide impedance bandwidth ($\sim$ 400% for S_{11}| and $|S_{22}| \geqq 10$ dB) which can cover the $1.5 \sim 6$ GHz frequency band for Global Positioning System (GPS, 1575 MHz) and dual ISM band (2.4 GHz and 5.8 GHz) applications. Good isolation between the two input ports ($|S_{21}| \geqq 20$ dB) is also achieved at the operating band. The radiation pattern and efficiency of the proposed antenna are also measured, and radiation pattern data are compared with simulation results.

Broadband Fractal Circular-monopole Antenna

Wen-Yi Tsai, **I-Fong Chen**, **Chia-Mei Peng**, **Pei-Cheng Hu**,
Hsu-Hung Tung, **and Hsuan-Chi Lin**
Department of Electronic Engineering, Institute of Computer and Communication Engineering
Jinwen University of Science and Technology, No. 99, An-Chung Rd., Hsien Tien, Taipei, Taiwan, R.O.C.

Abstract— In this paper, a novel broadband Fractal circular-monopole antenna is presented. This antenna consists of printed circular iteration with two iterating level and ground-plane with radius 25 mm, making it easy to making it easy to combine directional, high gain and wide bandwidth. A prototype is designed to operate at 1.5 GHz–5.86 GHz, the measured 10 dB bandwidth is nearly 1 : 2 at the center frequency of 3.68 GHz. Experimental results are shown to verify the validity of theoretical work.

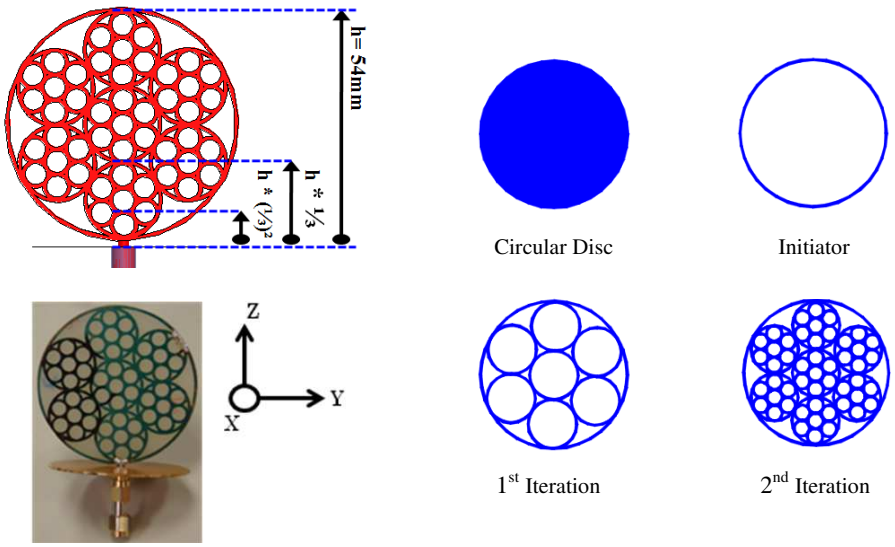

Characterization Under Probe of Integrated Antennas at Millimeter-wave Frequencies

Y. Fu[1], **T. P. Vuong**[1], **L. Dussopt**[2], **and F. Ndagijimana**[1]

[1]IMEP-LAHC, Grenoble, France
[2]CEA, LETI, MINATEC, Grenoble, France

Abstract— Test of Millimeter-wave Antennas: Millimeter-wave integrated antennas have typical dimensions smaller than 1 mm, and therefore are much smaller than modern probing devices. Their radiation performances are difficult to characterize as they are perturbed by their testing environment such as RF probes, connecting bond wires and transmission lines. Classical feeding techniques use RF probes with 1 mm coaxial lines of 5–10 mm length connected to a probe body of 2–3 cm. One consequence is the masking effect caused by the probe body on a significant angular sector of the radiation pattern. Another consequence is the reflection and scattering effects of the waves radiated by the antenna on the body of the probe. These cause significant interference and degradation of the radiation pattern. Other feeding methods exist. For instance, it is possible to use bond wires connected to a transmission line. This leads to less degradation of the radiation pattern since the connector or RF probe is moved away from the antenna; however the bond wires cause additional noise in the pattern and it is difficult to calibrate the gain due to the transmission line losses and transition mismatches.

Use of a Long Coaxial Probe: In this work, we have investigated and compared the performances of several RF probes at 60 GHz. More specifically, we have tested several custom RF probes with a long (5 cm) coaxial extension between the body and the probe tip. The references of the tested probes are I67-A-GSG-100 supplied by CASCADE Microtech (7 mm between probe tip and body) and 67A-GSG-100 supplied by PICOPROBE (50 mm between probe tip and body). The antenna-under-test (AUT) is a dual-arm Archimedean spiral integrated antenna realized on 130 nm CMOS SOI technology. It is a circularly-polarized wideband antenna, designed to operate in the 50–85 GHz region with a reflection coefficient under −10 dB.

Within our equipment's capabilities, we were able to prove that the reflection coefficient satisfies this constraint in the range from 50 GHz to 65 GHz. Figure 1 shows the measurement setup and the gain in the E-plane at 60 GHz. We compared measurement results obtained with the two probes. They show that the angular sector with valid measurements extends to $[-50°; 90°]$ with the extended probe rather than $[-10°; 90°]$ with the short probe: thus the masked zone is reduced by 40°. Furthermore, fewer fluctuations are observed and the gain curve is closer to the simulation result in the scanning zone. For the H-plane, there is no masked zone, but the proposed probe managed to improve in terms of fluctuation and the gain curve is closer to the simulation result.

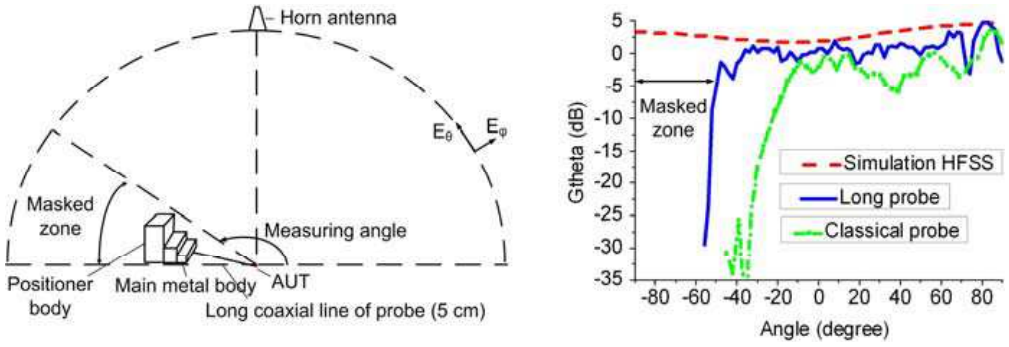

Figure 1: Setup and radiation pattern in E-plane.

A Monopole Antenna with CPW-fed for Digital Video Broadcasting Applications

Mau-Phon Houng[1], **Yu-Jen Chou**[1], **Ding-Bing Lin**[2], **and I-Tseng Tang**[3]

[1]Institute of Microelectronics, National Cheng Kung University, Tainan, Taiwan
[2]Institute of Computer and Communication Engineering, National Taipei University of Technology Taipei, Taiwan
[3]Department of Greenergy, National University of Tainan, Tainan, Taiwan

Abstract— This paper is to design the miniaturized Digital video broadcasting (DVB) antenna. The miniaturized consideration must be paid attention in DVB antenna design, because many consumer products and communication facilities are integration with the DVB. The monopole antenna is designed in the paper. The antenna characteristics including return loss and radiation patterns were analyzed and discussed. In this thesis, a monopole antenna conformed standard (470 $\sim$ 862 MHz) is proposed. The obtained results show that the impedance bandwidth, determined by -6 dB return loss. The radiation E-plane patterns are displayed with traditional 8-shaped patterns, and H-plane patterns are shown omnidirectional.

Introduction: Recently, the trend of personal wireless communications is growing thin, light, and relatively miniature. Consequently, the area of antennas should be ease integration. Printed coplanar waveguide (CPW) fed antenna have attracted much attention due to its ease of integration with monolithic microwave integrated circuits (MMIC). The content of this paper is focused on the analysis and investigation based on the band suppression of a novel DVB antenna. We apply many solutions for those considerations We proposed a novel notion of printed monopole antenna for DVB (470 $\sim$ 862 GHz) applications.

Antenna Design: Antenna structure and design: Fig. 1 shows the geometry and configuration of the proposed antenna. The proposed antenna is to fabricate on a low-cast FR-4 substrate with dielectric constant $\varepsilon_r = 4.4$, loss $\tan\delta = 0.02$, and thickness $h = 1.6$ mm. The proposed planar coplanar waveguide fed antenna is easy to be integrated for low manufacturing cost. The CPW-fed line is fixed at 4.6 mm and the distance of the gap between the line and the symmetric ground planes is fixed at 0.4 mm to achieve 50 Ω, characteristics impedance. Fig. 2 shows that the stub length L_4 mainly influences the impedance at higher frequencies. The simulated return loss against frequency for various length $L_4 = 29,\ 31$ and 33 mm, where the optimal bandwidth is obtained when the length is about 33 mm. The input impedance is well matched as the -6 dB return loss bandwidth covers the entire DVB band (470 $\sim$ 862 MHz).

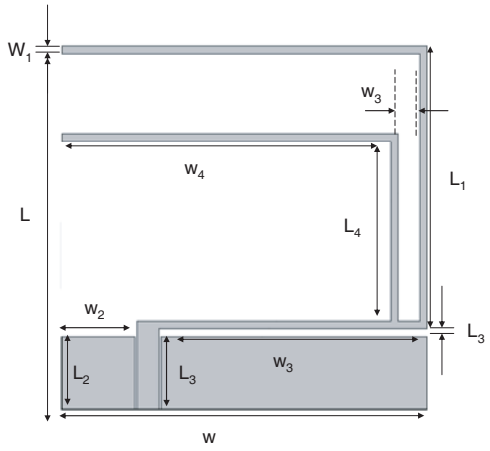

Figure 1: Geometry and configuration of the proposed antenna.

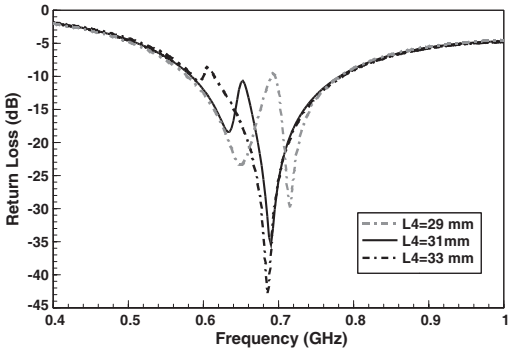

Figure 2: Effects of the stub length L_4 on the return loss.

REFERENCES

1. Kim, Y. and D.-H. Kwon, "CPW-fed planar ultra wideband antenna having a frequency band notch function," *Electronics Letters*, Vol. 40, No. 7, 403–405, April 2004.
2. Chen, H.-D. and H.-M. Chen, "Planar CPW-fed sleeve monopole antenna for ultra-wideband operation," *IEE Proc. — Microw. Antenna Propag.*, Vol. 152, No. 6, December 2005.

Reflection Characteristics of Microstrip Base on Finite Element Method

Qi Liu[1], **Hui Huang**[1, 2], **and Xin Wang**[1]

[1]School of Electrical Engineering, Beijing Jiaotong University, Beijing 100044, China
[2]State Key Laboratory of Millimeter Waves, Nanjing 210096, China

Abstract— A detailed study on the reflection characteristics of the single-line microstrip on the Printed Circuit Board (PCB) base on Finite Difference Time Domain (FDTD) method is presented. Using Mur first-order function as an absorbing boundary condition and Gaussian pulse signal as an excited source, we focused on reflection characteristics of the microstrip bended on the PCB in 90 degree. We calculated two cases: one is the microstrip bended without any cutting; the other is that cut in 45 degree at the bend position. Keeping the microstrip width as constant, we studied the effect of tangent plane width on the reflection characteristics. The characteristics curves of reflection parameter for several cases are presented, which can provide theory basis for optimum design of microstrip.

Circularly Polarized Rectangular Microstrip Antenna Using Ring Slots on the Ground Plane

Jeung-Keun Park, **Dang-Oh Kim**, **and Che-Young Kim**
School of Electronics Engineering, Kyungpook National University
Sankyuk-dong, Buk-gu, Daegu 702-701, South Korea

Abstract— In this paper, a single-feed circularly polarized rectangular microstrip antenna with a slotted ground plane is proposed. To obtain a circularly polarized operation, two ring slots are etched on the ground plane. These slots are optimally placed below the diagonal corner of radiating rectangular patch. Additionally, with the optimum position of the ring slots, either of right-handed CP (RHCP) or left-handed CP (LHCP) operation is worked out. By embedding the two ring slots on the ground plane and generated electric field from the patch, a magnetic resonance can be established in the operating bandwidth of the proposed antenna. By this phenomenon, two orthogonal near degenerate resonant modes for circular polarization (CP) radiation can be excited. In order to demonstrate this phenomenon, surface current distributions on the ground plane for proposed antenna and reference antenna are simulated by using the simulated software SEMCAD and HFSS. The structure and size of the proposed antenna are the same as those of the reference antenna without ring slots on ground plane. The proposed antenna shows more improvements on the directivity, gain, and radiation efficiency than the reference antenna. Comparisons between the simulated and measurement results are given, and in particular the role of two ring slots is fully explained during the descriptive illustrations.

Resonance of Rectangular Microstrip Patch over Ground Plane with Rectangular Aperture in the Presence of High-permittivity Dielectric Layer below the Aperture

S. Benkouda and T. Fortaki
Electronics Department, University of Batna, Algeria

Abstract— In recent years, microstrip patches have aroused great interest in both theoretical research and engineering applications due to their low profile, light weight, conformal structure and ease in fabrication and integration with solid state devices. Because of the inherent narrow bandwidth of microstrip patch resonators, many attempts have been made to improve their bandwidth characteristics. In general, there are two efficient approaches to broaden the bandwidth of the microstrip resonators, i.e., by increasing the substrate thickness and by combining several patches with similar resonance frequencies on the same or different layers of a microstrip structure. Since the bandwidth of microstrip patch resonators around their operating resonant frequencies is very narrow, it is important to develop accurate algorithms for the prediction of those resonant frequencies [1].

When a microstrip patch resonator acts as an antenna, it can be fed by a microstrip line located below the ground plane of the antenna through an aperture in the ground plane. This feeding configuration has been found very advantageous for several reasons [2]. For instance, it makes it possible to use a high dielectric-constant substrate for the feeding network and a low dielectric-constant substrate for the antenna element, which yields optimal performance for both the feeding network and antenna element. Also, the radiation arising from the feeding network cannot interfere with the main radiation pattern generated by the antenna since the ground plane separates the two radiation mechanisms. In addition, the presence of apertures in the ground planes of microstrip patches adds new design parameters that can be used as a way to tune their resonant frequencies without modifying the patch itself. A rectangular aperture introduces two physical parameters-its length and width. Since the presence of apertures in the ground planes of microstrip patches affects the resonant properties of microstrip-patch antennas and microstrip-patch circuit components, the development of an accurate theoretical method for predicting the aperture effect is of considerable interest.

In this paper, the authors analyze how the resonant frequencies of rectangular microstrip patch resonators with rectangular apertures in the ground planes are affected by the presence of a high-permittivity dielectric layer below the apertures. To the best of our knowledge, this subject has not been reported in the open literature; the only published results on full-wave analysis of rectangular microstrip-patch resonators over ground planes with rectangular apertures refer to apertures in contact with air [1]. The effect of substrate thickness on the resonant frequency of rectangular microstrip patch over ground plane with rectangular aperture is also investigated.

REFERENCES

1. Fortaki, T. and A. Benghalia, "Rigorous full-wave analysis of rectangular microstrip patches over ground planes with rectangular apertures in multilayered substrates that contain isotropic and uniaxial anisotropic materials," *Microwave Opt. Technol. Lett.*, Vol. 41, No. 6, 496–500, 2004.
2. Losada, V., R. R. Boix, and M. Horno, "Resonant modes of circular microstrip patches over ground planes with circular apertures in multilayered substrates containing anisotropic and ferrite materials," *IEEE Trans. Microwave Theory Tech.*, Vol. 48, 1756–1762, 2000.

Tag Antennas Using Differentially-connected UC-PBG Elements

The-Nan Chang
Tatung University, Taipei, Taiwan

Abstract— Radio Frequency Identification (RFID) technology is widely applied to object identification. An RFID tag is composed of an RFID chip and an antenna. Maximum power can be transferred to the antenna when impedances of the chip and the antenna are conjugative matched. As the tag is possibly attached to a metal material, tag antenna on metallic object has caused much attention in recent years.

To design an RFID on-metal tag, a possible choice for the antenna is a microstrip patch antenna as it inherently has a conductive ground. In [1], a tag antenna consists of two symmetrical patches. They are also electrically connected through vias to the ground plane. The tag can be made very compact. However, the use of vias may increase the cost of the tag. Since the design is based on a high-impedance unit cell, the cell may be replaced by a UC-PBG structure. In [2], the UC-PBG element is used in an efficient antenna.

In this paper, we differentially connect two symmetrical UC-PBG elements as shown below. Each UC-PBG element has a specific metallic pattern etched on a grounded dielectric substrate. In the metallic pattern, there are four strips; each has a dimension of h by s, extended from four sides of a central square pad. In [2], adjacent UC-PBG elements in a large periodic structure are connected by those strips. In this paper, two UC-PBG units are uniquely and differentially excited. Investigate on whether it can be a useful RFID antenna will be studied.

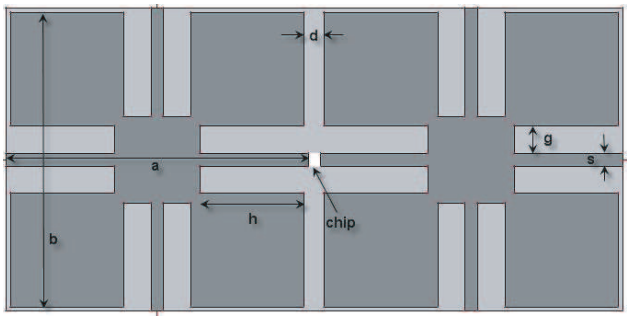

Figure 1: AUC-PBG pair as a tag antenna.

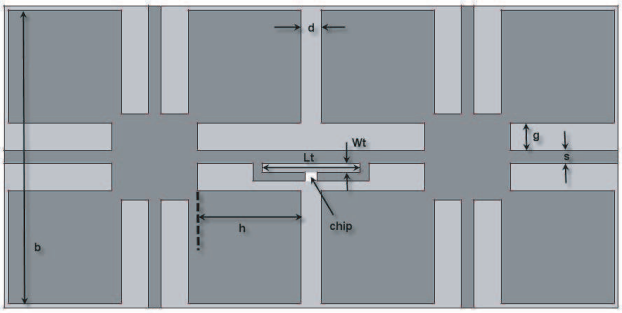

Figure 2: AUC-PBG pair with a tuning element.

REFERENCES

1. Chen, S. L. and K. H. Lin, "A slim RFID tag antenna design for metallic object applications," *IEEE Antennas and Wireless Propagation Letters*, Vol. 7, 729–732, 2008.
2. Coccioli, R., K.-P. Ma, and T. Itoh, "UC-PBG substrate for planar antennas," *29th European Microwave Conference-Munich*, 159–161, 1999.

Session 1P1
Advances in Phase — Space Optics

Generalized Wigner Functions for Evanescent Waves

Jonathan C. Petruccelli[1], **Se Baek Oh**[2], **Lei Tian**[2], **and George Barbastathis**[1, 2]

[1]Singapore-MIT Alliance for Research and Technology (SMART) Centre
3 Science Drive 2, 117543, Singapore
[2]Department of Mechanical Engineering, Massachusetts Institute of Technology
77 Massachusetts Avenue, Cambridge, MA 02139, USA

Abstract—

Introduction: Radiometric models describe the propagation of optical wave fields using rays. The set of all rays propagating from an initial plane is naturally described in an optical phase space, where each point in phase space denotes a ray's position in that plane, and its direction of propagation. The radiance is a function that assigns weights to rays that are conserved in propagation. In addition, the intensity at any point is given by the sum of the weights of all rays passing through that point. In free space propagation of fields with no evanescent components, these properties are satisfied by the Wigner function for paraxial propagation [1, 2], or by its nonparaxial generalization [3].

Generalized Wigner Functions for Fields with Evanescent Components: Consider the case of monochromatic, scalar fields in two dimensions for simplicity. These fields may be described in a half-space, taken without loss of generality to be $z \geq 0$, in the form of an angular spectrum representation,

$$U(\mathbf{r}) = \int_C A(\xi) \exp[\mathrm{i}k\mathbf{r} \cdot \mathbf{u}(\xi)] \mathrm{d}\xi, \tag{1}$$

where $\mathbf{u}(\xi) = [\sin(\xi), \cos(\xi)]$ is a direction unit vector, and the integration contour, C, consists of three segments, one which describes propagating plane waves $[\xi \in (-\pi/2, \pi/2)]$ as well as two which describe evanescent waves $[\xi = \pm(\pi/2 - \mathrm{i}\beta),$ where $\beta \in [0, \infty)]$ [4].

We propose a generalization of the nonparaxial Wigner function to include evanescent components, such that this generalized Wigner function is described by a phase space in which one coordinate is position and the other is a (possibly complex) angle. This generalized Wigner function is given by the sum of five terms, each of which has the form

$$W(\mathbf{r}, \xi) = \int A^*[\xi_1(\xi, \alpha)] A[\xi_2(\xi, \alpha)] \exp(\mathrm{i}k\{\mathbf{u}[\xi_2(\xi, \alpha)] - \mathbf{u}[\xi_1(\xi, \alpha)]\} \cdot \mathbf{r}) \mathrm{d}\alpha, \tag{2}$$

where the domain of ξ and the changes of variables, $\xi_{\mathrm{i}}(\xi, \alpha)$, differ for each term. The contribution of each term to the field's intensity at any point is given by integration over ξ.

When the $\xi_{1,2}(\xi, \alpha)$ are both real-valued, W is exactly the nonparaxial Wigner function. When one of the angles given by $\xi_{1,2}(\xi, \alpha)$ is real and the other is complex, W is defined over real-valued angles, although it decays upon propagation along these rays due to the influence of the evanescent waves. When both $\xi_{1,2}(\xi, \alpha)$ are complex-valued, W describes rays oriented along the z axis whose weights decay rapidly in z. As application of these generalized Wigner functions, we extend previous work on the propagation of the nonparaxial Wigner function past interfaces [5] to include evanescent components, such as might arise in the case of total internal reflection.

REFERENCES

1. Dolin, L. S., "Beam description of weakly inhomogeneous wave fields," *Radiofizika*, Vol. 7, 559–562, 1964.
2. Walther, A., "Radiometry and coherence," *Journal of the Optical Society of America*, Vol. 58, 1256–1259, 1968.
3. Alonso, M. A., "Radiometry and wide-angle wave fields. I. Coherent fields in two dimensions," *Journal of the Optical Society of America A*, Vol. 18, 902–909, 2001.
4. Born, M. and E. Wolf, *Principles of Optics*, 7th Edition, 639–643, Cambridge University Press, 2001.
5. Petruccelli, J. C. and M. A. Alonso, "Propagation of partially coherent fields through planar dielectric boundaries using angle-impact Wigner functions I. Two dimensions," *Journal of the Optical Society of America A*, Vol. 24, 2590–2603, 2007.

Generalized Wigner Functions in Classical Optics: Achieving Exact Conservation

Miguel A. Alonso[1, 2] **and Jonathan C. Petruccelli**[3]

[1]Department of Applied Physics, Aalto University, P. O. Box 13500, FI-00076 Aalto, Finland
[2]The Institute of Optics, University of Rochester, Rochester, NY 14627, USA
[3]SMART Centre, 3 Science Drive 2, 117597, Singapore

Abstract— Phase space distributions like the Wigner function are mathematical representations that describe a function in terms of both its original variables and the Fourier conjugate ones. In classical optics, Wigner functions have been used both in the time-frequency and the space-spatial frequency domains. In the latter case, the Wigner function has been employed mostly in the paraxial regime to describe a monochromatic (or stationary) field as a function of both position and direction. That is, the Wigner function takes the role of a weight distribution for all the rays travelling through the medium or system. This interpretation is supported by the following two properties:

i) at any given position, the integration of the Wigner function over all directions (i.e., over all rays through the prescribed point) gives the local intensity;
ii) for paraxial propagation through free space, homogeneous media, or more general ABCD systems, the Wigner function is conserved along rays.

These two properties make the Wigner function a useful conceptual tool for visualizing wave propagation in a ray-like fashion. It must be noted, however, that the weights assigned to certain rays by this description can be negative. These "negative" rays are necessary for this description to account for destructive interference effects.

It turns out, however, that property ii above is not rigorously satisfied beyond the paraxial regime. In this talk, we give a simple geometric interpretation that explains the conservation property in the paraxial approximation. We then give a generalized geometric prescription for the definition of generalizations of the Wigner function that are exactly conserved along rays away from the paraxial limit for propagation in homogeneous transparent media, including anisotropic and/or chiral ones. These extensions can be used to give a numerically-efficient model of the propagation of partially coherent electromagnetic fields. We also discuss propagation across medium interfaces.

Based on similar ideas, we propose new representations for the description of pulses propagating in 1D transparent dispersive media with arbitrary dispersion relations (neglecting absorption). The standard Wigner function has also been applied in this context, but its description of propagation is only exact in the limiting case where the dispersion relation is quadratic over the region of the spectrum occupied by the pulse. By using the geometric interpretation mentioned earlier, we propose generalizations of the Wigner function tailored for the dispersion relation in question. The pulse is represented as a function of position, time and velocity, in a fashion similar to a statistical-mechanical particle distribution:

i) at any position and time, the intensity is given by the integral of the function over all velocities;
ii) the distribution is exactly conserved, i.e., for a given velocity v, it only depends on position z and time t as the combination z-vt.

Detailed Modified Iwasawa Decomposition of Ray Transformation Matrix and Its Applications

T. Alieva
Facultad de Ciencias Físicas, Universidad Complutense de Madrid
Avda. Complutense, s/n, Madrid E-28040, Spain

Abstract— The formalism of ray transformation matrices allows establishing a close relation between the geometric and wave paraxial optics and providing their description in phase space. The modified Iwasawa decomposition of ray transformation matrix is crucial for classification of phase space transformations. Moreover further concretization of its components significantly simplifies system design, beam synthesis and characterization. The applications of the detailed ray transformation matrix decomposition are considered on several examples: design of optical set up for phase space tomography, generation of stable, spiral and auto-reciprocal beams, characterization of optical signals.

Radon-Wigner Display Implemented by Spatial Light Modulators

A. Cámara[1], **J. A. Rodrigo**[2], **T. Alieva**[1], **and M. L. Calvo**[1]

[1]Facultad de Ciencias Físicas, Universidad Complutense de Madrid
Avda. Complutense, s/n, Madrid E-28040, Spain
[2]Imaging and Vision Department, Instituto de Optica (CSIC)
Serrano 121, Madrid E-28006, Spain

Abstract— The Radon-Wigner transform (RWT) is a useful tool for signal analysis and synthesis. Moreover, since it corresponds to a set of projections of the Wigner distribution (WD), the application of tomographic methods allows reconstructing the WD and, therefore, the phase or mutual intensity of the signal.

Several optical schemes based on the application of varifocal glass lenses or combination of Fresnel zone plates have been considered to obtain the RWT of one dimensional signals. Here we propose the use of two spatial light modulators (SLMs) for the implementation of the Radon-Wigner Display. The discussed setup does not need rescaling of the measured intensity distribution. Furthermore, the application of the SLMs makes the system flexible, in the sense that it allows a higher resolution mapping of a chosen interval of the projections, if necessary. Several experimental examples demonstrate the feasibility of the proposed setup.

Correlation Digital System Invariant to Position and Rotation

Josué Álvarez-Borrego
Departamento de Óptica, División de Física Aplicada, Cicese
Carretera Ensenada-Tijuana 3918, Fraccionamiento Playitas, Ensenada, B. C., C. P. 22860, México

Abstract— Recently a correlation digital system invariant to position and rotation was presented [1]. In this work a deeper analysis of this system is shown. We analyze both the real and the imaginary part of the Fourier transform of the input image to obtain the binary mask to have rotation invariance. In addition, to obtain the one-dimensional signature of the input image, the module of the Fourier transform of the image to different exponents is analyzed in order to see if influences in the recognition of objects using a phase only filter and a nonlinear filter in the correlation process. The results show that the signature of each image varies depending if the real or imaginary part of the Fourier transform of the input image is used. Average signature filters were done considering 10 and 18 input images. Nonlinear correlations gave better results it does not matter if we are using the real or the imaginary part of the Fourier transform of the input image to make the binary mask in the system.

REFERENCES

1. Solorza, S. and J. Álvarez-Borrego, "Digital system of invariant correlation to position and rotation," *Optics Communications*, Vol. 283, No. 19, 3613–3630, 2010.

Orbital Angular Moment Density of Beam Given as a Superposition of Hermite-Laguerre-Gauss Functions

A. M. Caravaca Aguirre and T. Alieva
Universidad Complutense de Madrid, Madrid, Spain

Abstract— Orbital angular moment (OAM) is an important global parameter of beam which can be found from its second order moments. Nevertheless often, for example for the description of the interaction of light with microparticles, the knowledge of the OAM density is required. Hermite-Laguerre-Gauss (HLG) modes which form a complete orthonormal basis are frequently used for beam design. In this contribution we derive the expression for the OAM density of beam given as a superposition of the HLG modes. The result is useful for the design and characterization of stable, spiral, rotating beams and their application for micro particle manipulation.

Light Propagation in Tapered Optical Fibers: Spatial Light Confinement and Generation of Plasmonic Waves

A. Hartung, F. Wirth, and H. Bartelt
Institute of Photonic Technology, Albert-Einstein-Str. 9, Jena 07743, Germany

Abstract— Light propagation in optical waveguides is fundamentally different from free space propagation since light spreading by diffraction is avoided. The light is confined to modes which stay constant in shape along perfect waveguides and which can propagate with low attenuation for long propagation lengths. In the case of rotationally symmetric fiber waveguides the fundamental mode is, in principle, existent for any core diameter, i.e., also for small core diameters even below the scale of the optical wavelength. However, the shape of the modes is changing strongly in this range of core diameters and coupling to non-guiding modes becomes possible. Under realistic assumptions concerning the homogeneity of the waveguide a cutoff condition for the guided wave propagation can be derived theoretically and observed experimentally. Additional reflective coatings (metallic layers) on the outside of the fiber guiding structure would support better confinement of the modes, but such metallic components as part of a waveguide are connected with stronger attenuation. Therefore the possibilities of further light confinement are limited. At the metallic-dielectric interface plasmonic waves (plasmonic surface polaritons) can be generated under specific conditions, which can be observed as wavelength dependent attenuation peaks in the transmitted light spectrum. Such plasmonic wave generation is well-known from planar metallic-dielectric interfaces. For the circular fiber waveguide geometry specific conditions apply. The strength of such attenuation peaks is strongly dependent not only on the refractive index conditions but also on the geometrical parameters of the waveguide.

The characteristics of propagating modes and their coupling under the conditions of small scale fiber diameters and in combination with additional metallic layers will be discussed theoretically and supported by experimental results.

First-order Optical Systems: Radon-Wigner Transform Approach

Genaro Saavedra and Walter D. Furlan
Optics Department, Universitat de València, c/ Dr. Moliner 50, E46100 Burjassot, Spain

Abstract— Phase-space representation of signals is a well-established tool for describing physical systems. Although the use of phase-space joint distributions is widely spread, when they are interpreted as joint probability densities some difficulties arise, namely: their conjugate coordinates are non commutative and cannot be simultaneously specified with absolute accuracy, they present complex or negative values, and they may spread in regions of the phase space where either the signal or its Fourier transform vanish. As an alternative, the projections (*marginals*) of the phase-space distributions are strictly positive and they give information about the signal on both phase-space variables. These projections can be formally associated with probability functions, avoiding all interpretation ambiguities associated with the original phase-space distributions. This is the case of the Radon-Wigner transform (RWT), defined by the complete set of projections of the Wigner distribution function in phase-space.

In this contribution, the RWT is presented as a tool for the description of 1st-order optical systems. The input/output relationships for this phase-space representation are obtained and their application in analysis and design tasks is pointed out. In particular, the use of this representation in the analysis of optical signals and systems is developed in several aspects, namely, the computation of diffraction intensities, the optical display of Fresnel patterns, the amplitude and phase reconstruction of optical fields and the calculation of merit functions in imaging systems. A review of design techniques, based on the utilization of the RWT, for these imaging systems is also presented, along with some techniques for optical signal processing.

Wigner Based Analysis of Geometric Related Resolution Degradation and Geometric Super Resolution Configurations

Zeev Zalevsky
School of Engineering, Bar-Ilan University, Ramat-Gan 52900, Israel

Abstract— Geometric related resolution limitations of an imaging system can be divided into two bounds. The first is related to the density of the spatial sampling, i.e., how densely the analog spatial distribution of the intensity is being sampled by the detector. This is directly affected by the pitch of the pixels in the detection array. According to Nyquist criteria the maximal spectral bandwidth that may be reconstructed is inversely proportional to this pitch. Higher spectral bandwidths are being spectrally overlapped due to under sampling effect.

The second bound is related to the fact that the sampling is not ideal, i.e., it is not done with a two dimensional train of delta functions but rather with pixels performing spatial averaging of the light impinging on their area. The larger the fill factor of each pixel is the less ideal is the sampling. The non ideal sampling is resulted in low pass filtering in the spectral domain.

Geometric super resolving approaches aim to overcome both limitations by proper encoding and decoding of the spatial information or its spectrum prior to being sampled by the detector. The under sampling effect by itself may also be reduced by performing spatial micro scanning procedure.

In this paper we use the Wigner transform to represent the two above mentioned geometric resolution limits. Then, we discuss how the usage of Wigner may assist in understanding several geometric super resolving approaches that are applying random masks to encode the spatial as well as the spectral information of the analog distribution prior to its being sampled by the detector.

Partially Coherent Ambiguity Functions for Depth-variant Point Spread Function Design

Roarke Horstmeyer[1], **Se Baek Oh**[2], **Otkrist Gupta**[1], **and Ramesh Raskar**[1]

[1]Media Lab, MIT, 75 Amherst St., Cambridge, MA 02139, USA
[2]Department of Mechanical Engineering, MIT, 77 Massachusetts Avenue, Cambridge, MA 02139, USA

Abstract— The joint design of a digital imaging system with its image post-processing algorithms can enhance camera performance in a variety of domains. Additional modalities like depth detection, extended depth-of-field, object tracking and super-resolution can be realized by modifying a conventional imaging system with a phase or amplitude mask placed at the pupil plane. This aperture mask re-defines the point spread function (PSF) response of the camera at any plane of defocus, which is then exploited by a matched post-processing step to gain additional scene information. Determining an optimal mask pattern for a given system is connected with the specifics of the required functionality, camera parameters and imaging environment.

Recently, an iterative "mode-selective" method of designing aperture masks using a sparse set of desired PSF intensity distributions at different planes of focus was presented [1]. The set of desired PSFs are used to generate a desired ambiguity function (AF), which can completely represent a camera's response to defocus. The desired AF iteratively converges to determine a mask's optimal amplitude and phase distribution to place at the camera's pupil plane. If the set of desired PSFs are not physically realizable from a thin mask (i.e., do not obey the constraints of propagation), the algorithm converges to a nearby solution that is realizable.

The mode-selective algorithm is among a class of techniques, including phase retrieval, phase space tomography and transport-of-intensity, which determine the amplitude and phase of a wavefront from multiple intensity measurements along the direction of propagation. Unlike other methods, mode-selection applies a global constraint to the solution set in the mutual intensity (MI) domain. As the PSFs are defined as a camera's response to an ideal point source, a spatially coherent MI function is used as a constraint each iteration. A spatially coherent MI function can be defined as a single orthogonal mode of propagation. A convenient way to obtain a single mode is by taking the singular value decomposition (SVD) of the desired MI function, and selecting the first mode with the largest singular value. This single mode can then generate a physically valid AF, which is a nearby solution to the desired AF created from the desired PSF set.

In this paper, we explore what types of 3D PSF intensity distributions are possible when more than one mode from a coherent-mode decomposition is selected during algorithm iteration. From a mathematical viewpoint, this is a shift from a rank-1 to a rank-n MI outer-product algorithm restriction. Since the Eckert-Young Theorem guarantees that the first n-modes of a function's SVD yields it's lowest MSE rank-n approximation, the selection of more than one mode (i.e., a partially coherent MI) almost always provides a closer solution to an arbitrarily desired PSF set than 1 mode. The use of a time-varying aperture mask, with several mask patterns displayed during the integration time of one image, is investigated as an experimental method of realizing such a partially coherent MI function [2]. Additionally, due to fabrication constraints aperture masks are often limited to amplitude-only or phase-only distributions. Thus, we also investigate the concept of a constrained coherent mode decomposition, which attempts to determine the optimal decomposition of a desired MI into multiple outer-products of amplitude-only or phase-only content.

REFERENCES

1. Horstmeyer, R., S. B. Oh, and R. Raskar, "Iterative aperture mask design in phase space using a rank constraint," *Optics Express*, Vol. 18, 2010.
2. Desantis, P., F. Gori, G. Guattari, and C. Palma, "Sythesis of partially coherent fields," *JOSA*, Vol. 3, No. 8, 1986.

Complex Amplitude Filters for Extended Depth of Field

J. Ojeda-Castañeda, E. Yepez-Vidal, and E. Ayala
University of Guanajuato, Salamanca, Guanajuato 36885, México

Abstract— We present a complex amplitude transmittance filter that reduces the impact of focus errors, on the modulation transfer function. We use linear regression for identifying the associated inverse filter. We report digital images for illustrating the use of the new complex amplitude filter, and its associated inverse filter, for extending the depth of field.

Introduction: Certain nonconventional phase masks, as well as some amplitude variations, can reduce the influence of focus error on the Modulation Transfer Function (MTF) [1–3]. Here we unveil an optical element that uses both amplitude and phase variations for generating a MTF with low sensitivity to defocus.

Phase-space Representations: For visualizing the impact of focus error on the MTF, it is convenient to employ the ambiguity function of an optical filter. Low sensitivity to focus error is related to an ambiguity functions with polar symmetry. For reducing the oscillations of ambiguity function, here we propose the use a weak Gaussian filter. We consider that the several values of the MTF are points on a scatter diagram, for identifying the associated inverse filter. Computer simulated images illustrate the depth of field that can be achieved, when using both the new complex amplitude filter and its associated inverse filter.

REFERENCES

1. Ojeda-Castañeda, J., R. Ramos, and A. Noyola-Isgleas, "High focal depth by apodization and digital restoration," *Applied Optics*, Vol. 27, 2583–2586, 1988.
2. Dowski, Jr., E. R. and W. T. Cathey, "Extended depth of field through wavefront coding," *Applied Optics*, Vol. 34, 1859–1866, 1995.
3. Ojeda-Castañeda, J., J. E. A. Landgrave, and C. M. Gómez-Sarabia, "Conjugate phase plate use in analysis of the frequency response of optical systems designed for extended depth of field," *Applied Optics*, Vol. 47, E1–E7, 2008.

Temporal Similarity for Short Pulses

Jorge Ojeda-Castañeda, Cristina M. Gómez-Sarabia, and Helena E. López-Aviléz
University of Guanajuato, Salamanca, Guanajuato 36885, México

Abstract— We use a temporal cross-correlation for analyzing the similarity between the complex amplitude envelopes of two short pulses. We unveil a relationship between temporal similarity and the expectation value, as used in quantum physics. We apply this relationship for analyzing the temporal version of the fractional Talbot effect.

Introduction: For analyzing the propagation of modes in an optical fiber, often it is convenient to compare the near field diffraction patterns against the far field diffraction pattern. One can do a quantitative comparison of similarity, by performing a spatial cross-correlation between two diffraction patterns [1]. Lohmann et al. have developed a definition for Fresnel similarity, which is defined as a cross-correlation between an initial complex amplitude distribution and its Fresnel diffraction pattern [2]. This definition finds practical applications for setting array illuminators.

Temporal Similarity: Our aim here is to analyze the temporal similarity between the complex amplitude envelopes of two short pulses. The first short pulse is at the input of a dispersive medium, and the second short pulse is at the output of a dispersive medium. The length of the dispersive medium is z.

Next, we define temporal similarity as a cross-correlation between the complex envelopes of the two short pulses. And then, we relate the above definition with the concept of expectation value, as used in quantum physics. We apply this relationship for analyzing the temporal, fractional Talbot effect.

REFERENCES

1. Feit, M. D. and J. A. Fleck, "Calculation of dispersion in graded-index multimode fibers by a propagating-beam method," *Applied Optics*, Vol. 18, 2843–2851, 1979.
2. Lohmann, A. W. and J. Ojeda-Castañeda, "Fresnel similarity," *Optics Communications*, Vol. 249, 397–405, 2005.

Lens Arrays with Tunable Power and Variable Depth of Focus

Jorge Ojeda-Castañeda and Cristina M. Gómez-Sarabia
University of Guanajuato, Salamanca, Guanajuato 36885, México

Abstract— We present the use of a phase conjugate pair of screens for setting an array of lenses. We show that by introducing a lateral displacement between the phase conjugate pair, one can change the focal length of the lenses in the array. We discuss the use of this type of arrays for optical sensing.

Introduction: By using a suitably pair of optical elements, it is possible to set a lens, whose focal length can be modified [1–3]. This nonconventional approach can be extended for setting optical devices with specific amounts of wave aberrations [4, 5]. Recently, it has been shown that the same approach can be used to implement spatial filters that extend the depth of field, in a tunable fashion [6]. Our aim here is to propose an optical method for setting an array of lenses, which can vary either its focal length or its depth of focus.

Display of the Ambiguity Function: To our end, we present the use of a phase conjugate pair of screens for setting an array of lenses. We apply the formalism of the ambiguity function for showing that the proposed pair of screens can change the focal length of the array of lenses. Furthermore, we show that it is possible to control the depth of focus without using pupil apertures. We discuss the use of this novel array of lenses for optical sensing.

REFERENCES

1. Alvarez, L. W., U.S. Patent 3,305,294, Dec. 3, 1964.
2. Lohmann, A. W., Italian Patent 727,848, Jun. 19, 1964.
3. Lohmann, A. W., *Appl. Opt.*, Vol. 9, 1669, 1970.
4. Palusinski, I. A., J. M. Sasián, and J. E. Greivenkamp, *Appl. Opt.*, Vol. 38, 86, 1999.
5. López-Gil, N., H. C. Howland, B. Howland, N. Charman, and R. Applegate, *J. Opt. Soc. Am. A*, Vol. 15, 2563, 1998.
6. Ojeda-Castaneda, J., J. E. A. Landgrave, and C. M. Gómez-Sarabia, *Appl. Opt.*, 47, 2008.

Conditions for Photon-particle Interactions

Tibor Berceli
Budapest University of Technology and Economics, Hungary

Abstract— The conditions of photon-particle interactions are presented. In an atomic process the processing energy has to be utilized (or delivered) during the processing time. The processing time and the processing energy are strictly connected to each other.

Introduction: Photon-particle interaction means the photon energy is transferred to a particle. Recently the emission of a single photon or a series of individual photons is feasible [1, 2], therefore the investigation of the individual cases is also possible.

Photon Duration: The photon being an energy burst or pulse has a length in time called photon duration. That is equal to the photon generation time τ_{ph} [3]:

$$\tau_{ph} = \frac{h}{2E_b} = \frac{1}{2f_{ph}} \tag{1}$$

where E_b is the band gap energy and h is the Planck constant. That relationship is in agreement with the Mandelstam-Tam uncertainty relation between energy and time [4].

Processing Time and Processing Energy: The time interval during which a process is carried out is called processing time. That is an inherent property of a process. The energy utilized (or delivered) in a process is called the processing energy.

Conditions for Interactions: The processing time and the processing energy are strongly connected to each other. In an atomic process the processing energy has to be utilized or delivered during the processing time. By other words the processing energy and the processing time have to be matched. That relationship has many consequences.

As it was mentioned a process can only be carried out if the photon energy is equal to the energy needed for the specific process and the duration of the photon is equal to the processing time of the specific process. A good example is the photosynthesis in the leaves of the trees or vegetation. If the vegetation is in a dark room the photosynthesis cannot work although the room can be warm enough which means heat energy is available. The reason is: the infrared photons have neither sufficient energy nor proper duration needed for the photosynthesis process.

Photon Power: The instantaneous photon power is proportional to the square of the electric field component multiplied by the factor K:

$$P_{ph}(t) = KE_0^2 \sin^4(\omega_{ph} t) \quad \text{if} \quad 0 \le t \le \tau_{ph} \tag{2}$$

This relationship shows a smooth transition from zero to a maximum and then back to zero in the time period from 0 to τ_{ph}.

Limit on Optical Pulse Length: The lower limit (τ_{op}) for the optical pulse length at a specific frequency is:

$$\tau_{op} \ge \frac{\tau_{ph}}{2} = \frac{1}{4f_{ph}} \tag{3}$$

If we want to generate a shorter optical pulse it only can be done at a higher frequency.

REFERENCES

1. Jacques, V., et al., "Experimental realization of Wheeler's delayed-choice gedanken experiment," *Science*, Vol. 315, 966–968, 2007.
2. Darquie, B., et al., "Controlled single-photon emission from a single trapped two-level atom," *Science*, Vol. 309, 454–456, 2005.
3. Berceli, T., "Processing time of photon generation," *PIERS Online*, Vol. 5, No. 6, 541–545, 2009.
4. Mandelstam, L. and I. Tamm, "The uncertainty relation between energy and time in nonrelativistic quantum mechanics," *J. Phys. USSR*, Vol. 9, 249–254, 1945.

Session 1P2a
Ionospheric Radio Propagation and Effects with Special Emphasis on the Mediterranean and North African Areas

The European COST (European Cooperation in Scientific and Technology) Actions: An Important Chance to Cooperate and to Grow for All the International Ionospheric Community

Bruno Zolesi[1] **and Ljiljana R. Cander**[2]

[1]Istituto Nazionale di Geofisica e Vulcanologia, Rome, Italy
[2]STFC Rutherford Appleton Laboratory, Chilton, OX11 0QX, UK

Abstract— The last COST (European Cooperation in Scientific and Technology) Action 296 on Mitigation of Ionospheric Effects on Radio Systems, along with previous COST238 (Prediction and Retrospective Ionospheric Modelling over Europe), COST251 (Improved Quality of Service in Ionospheric Telecommunication Systems Planning and Operation) and COST271 (Effects of the Upper Atmosphere on Terrestrial and Earth-Space Communications) Actions have addressed investigations of the different effects of the ionosphere on terrestrial telecommunication systems and on Earth-space systems. Throughout their lifetime of 20 years, these COST actions have achieved a great deal in long-term archiving of synoptic soundings of the state of the European mid-latitude ionosphere, in enhancing understanding of the morphology of the ionosphere and its dependence on space weather and in producing ionosphere-plasmasphere as well as propagation models for terrestrial radio services available to variety of radio users. Besides the formal contributions to ITU-R and the contributions to international organisations such as URSI, COSPAR, EGU and ESA, these COST Actions have provided a forum for the establishment of collaborative European initiatives, a centre of expertise and excellence in ionosphere knowledge when none other equivalent in Europe or elsewhere exists.

In this paper, we briefly review the main achievements of the COST 238, 251, 271 and 296 actions as developed in the past studies and discuss the application of their methods to South Mediterranean and North African ionospheric region that has a special importance for modern telecommunication and navigation systems.

FORMOSAT/COSMIC foE Observations and IRI Model Predictions

A. V. Mikhailov[1] and L. Perrone[2]

[1]Institute of Terrestrial Magnetism, Ionosphere and Radio Wave Propagation
Troitsk, Moscow Region 142190, Russia
[2]Istituto Nazionale di Geofisica e Vulcanologia, Via di Vigna Murata 605, Rome 00143, Italy

Abstract— International Reference Ionosphere (IRI) has been created for some decades by the efforts of many researches and monthly median foE values in particular at middle latitudes are known with a good accuracy. However recent FORMOSAT/COSMIC E-region observations (Chu et al., 2009) cast doubts on IRI model indicating much larger daytime foE values at low-middle latitudes. Some more morphological discrepancies with IRI in foE variations have been obtained from FORMOSAT/COSMIC observations. But a direct comparison of monthly foE medians observed at Rome ionosonde shows that they coincide with IRI predictions. However according to Rome ionosonde observations sporadic E (Type C) takes place $\geq 90\%$ of daytime hours in summer and $\approx 60\%$ in winter. Electron concentration in such Es (fbEs) is larger than NmE (foE) and the fbEs/foE ratio is close to foECOSMIC/foE. This means that FORMOSAT/COSMIC in fact observes Es in the areas of abnormal E-layer. This is real electron concentration in the low-middle daytime E-layer, but Es is not present in IRI where only regular E-layer is described.

International Reference Ionosphere 2010 and Application to the Mediterranean and North African Areas

Dieter Bilitza[1, 2]

[1]Space Weather Laboratory, George Mason University, Fairfax, Virginia, USA
[2]Heliophysics Science Division, GSFC, Greenbelt, Maryland, USA

Abstract— The International Reference Ionosphere (IRI) is an international project sponsored by the Committee on Space research (COSPAR) and the International Union of Radio Science (URSI) that has as its goal the development and improvement of a data-based model of ionospheric densities, temperatures, and velocities using all available and reliable data sources for these ionospheric parameters. The model is widely recognized as the international standard for the specification of ionospheric parameters and recently was accepted by the International Standardization Organization (ISO) as Technical Specification TS 16457. This presentation will discuss the new version of the model, IRI-2010, with special emphasis on improvements and additions that will affect the Mediterranean and North African sectors. Most notably, the electron and ion densities in the lower ionosphere were significantly improved by using a large volume of ionosonde data as well as photochemical considerations. At the F2 peak Neural Network based models for the peak density and the propagation factor M3000F2, which is related to the F2 peak height, are introduced as new options. Regarding the electron temperature, IRI-2010 now models variations with solar activity. For the first time the model will include the representation of auroral boundaries at high latitudes and their variation with magnetic activity. The 2010 version also introduces the increased ionization in the auroral E-region during magnetic storms.

Annual IRI Workshop are the prime venue for the discussion of model comparisons with new data, improvements based on thes comparisons, and applications of the model in science, engineering, and education. This presentation will report on the latest workshops and their results including a recently launched new task force activity that is focusing on assimilating IRI with real-time data to establish ionospheric conditions in real-time. The IRI homepage is at http://IRI.gsfc.nasa.gov/.

Investigation of Ionospheric Slab Thickness Behaviour over Cyprus during Minimum Solar Activity

Haris Haralambous
Frederick University, 7 Y. Frederickou St., Palouriotisa, Nicosia 1036, Cyprus

Abstract— The ionospheric slab thickness (τ) is a parameter which provides information about the nature of the distribution of ionization at a specific location and is defined as the ratio of the vertical Total Electron Content (TEC) measured in TEC units (1 TECu = 10^{16} electrons m^{-3}) to the maximum ionospheric electron density in the F-region (NmF2). Slab thickness measurements offer substantial information on the shape of the electron density profile, the neutral and ionospheric temperatures/gradients and on the ionospheric composition and dynamics. Hourly values of TEC and NmF2 collected at Cyprus (coordinates: 35°N, 33°E geographic), are used in the study of slab thickness characteristics during a low solar activity period. The slab thickness database used in this study consists of measurements from January 2009 to August 2010, i.e., covering more than one year of data. Climatology of the slab thickness is described by the diurnal and seasonal variations. Examining the variations of τ, during the different seasons of solar minimum, they are generally characterised by higher night-time values compared to the daytime values. The yearly mean value of τ obtained in this study is 249 km during daytime and 384 km during night-time. Another important feature of the slab thickness presented in this study is its large day-to-day variability. As τ represents the ratio of TEC to NmF2, the day-to-day variability of τ reflects the combined effect of the variability of the individual parameters. The night-time day-to-day variability of slab thickness is higher compared to the daytime variability during most of the year. Our results show, percentage standard deviation changes from 10% to 48%.

A Study of Es Layer Characteristics over Cyprus

Photos Vryonides[1], **Lefteris Economou**[2], **and Haris Haralambous**[1]

[1]Frederick University, 7 Y. Frederickou St., Nicosia 1036, Cyprus
[2]Intercollege, Ayias Phylaxeos St., Limassol 3507, Cyprus

Abstract— Sporadic E is an ionospheric phenomenon classified as an E-region (90–150 km) irregularity characterised by a thin layer of extremely dense ionization patches around Eregion altitudes which can significantly affect radio wave propagation. Sporadic E can occur during daytime or nighttime, and its characteristics vary with latitude. Sporadic E has been correlated in literature with solar activity, geomagnetic activity and associated to thunderstorms and meteor showers. In this study manually scaled digital ionosonde ionograms obtained in Cyprus (coordinates: 35°N, 33°E geographic) have been analysed to study the diurnal and seasonal occurrence of Sporadic E layer during a low solar activity period (January 2009 to August 2010). Processing of ionograms and scaling of Sporadic E parameters was carried out in accordance with the URSI Handbook of Ionogram Interpretation and Reduction (Second Edition, 1972, Report UAG-23). Statistics of Sporadic E layer parameters, which include the critical (foEs), blanketing (fbEs) frequencies and the layer height (hoEs) as well as Sporadic E layer classification types are also analysed in an effort to identify systematic seasonal and diurnal patterns. The seasonal occurrence of blanketing Sporadic E layer over Cyprus is much more frequent during summer months (June-August). The Sporadic E diurnal occurrence pattern is generally high during morning hours (starting around 0700 LT) with a strong blanketing character, diminishes during noon and the afternoon and then reappears again during evening hours sometimes persisting through the night. Regarding sporadic E classification the most typical types observed over Cyprus are the f, l, c and h types.

Ionosphere Storms, Waves and Irregularities in Mediterranean Area

Ljiljana R. Cander
STFC, Rutherford Appleton Laboratory, Chilton, OX11 0QX, UK

Abstract— Modern radio communication and navigation systems are applications most affected by the ionosphere space weather in action. Therefore, they could benefit significantly from accurate specification of ionospheric conditions when storms, waves and irregularities are in progress. Even with current improvements in modelling techniques and increased quality and amounts of ground- and space-based data assimilation, ionospheric nowcasting and forecasting remain difficult. This paper intends to provide a review of the latest key links between solar activity and the various physical processes, which govern disturbed ionospheric plasma structure that has been under scientific examination over past several decades but has lately received considerable importance in relation to the ionospheric space weather services. Specific examples during high and recent extremely low solar activity will be used to show how modelling and observing techniques could be incorporated in different ionospheric specification and prediction models for real-time operational applications in Mediterranean area.

Electromagnetic Ionospheric Anomalies Related to the Central Italy Earthquakes

L. Perrone[1], **L. Korsunova**[2], **and A. Mikhaylov**[2]

[1]Istituto Nazionale di Geofisica e Vulcanologia, Via di Vigna Murata 605, Rome 00143, Italy
[2]Pushkov Institute of Terrestrial Magnetism, Ionosphere and Radio Wave Propagation (IZMIRAN) Troitsk, Moscow 142190, Russia

Abstract— Crustal earthquakes with magnitude $6.0 > M \geq 5.5$ observed in Italy for the period 1979–2009 including the last one at L'Aquila on 06.04.09 were considered to check if the earlier obtained relationships for ionospheric precursors for strong Japanese earthquakes are valid for the Italian moderate earthquakes. The ionospheric precursors are based on the observed variations of the sporadic E-layer parameters (h'Es, fbEs) and foF2 at the ionospheric station Rome. Empirical dependencies for the seismo-ionospheric disturbances relating the earthquake magnitude and the epicenter distance are obtained and they have been shown to be similar to those obtained earlier for Japanese earthquakes. The dependences indicate the process of spreading the disturbance from the epicenter towards periphery during the earthquake preparation process.

Session 1P2b
Biomedical Electromagnetic Instruments, EM Condensed Materials and Imaging

Contact-less Concentration Measurements in Aqueous Glycine Solution Using Microwaves

Akio Oota, **Touru Katou**, **Tatsunori Uchida**, **and Ryoji Inada**
Department of Electrical and Electronic Information Engineering,
Toyohashi University of Technology, Tempaku-cho, Toyohashi, Aichi 441-8580, Japan

Abstract— Glycine $C_2H_5NO_2$ and its solution with various solvents are widely used as antioxidants, moisturizing agents, disinfectants and additives in foods, medicines and toiletries etc. The grade and the concentration therein are mostly measured by chemical methods, and the contact-less measuring methods haven't been established yet.

It is well known that dramatic dielectric relaxation phenomena occur in glycine and its solution with various solvents in the microwave range, resulting from rotational motions of glycine molecules and/or its macro-molecules via hydrogen bonds. This causes significant energy absorption in passing through microwaves therein, and leads to developments of new microwave contact-less testing (MCLT) system for the grade and the concentration in glycine and its solution with various solvents.

As a first step, we measure the complex dielectric constant $\varepsilon^* = \varepsilon' - \mathrm{j}\varepsilon''$ of aqueous glycine solution in the microwave range between 0.2 and 20 GHz using a network analyzer to obtain the basic data necessary for developments of MCLT system. In parallel, we construct the experimental apparatus to measure the transmitted power of microwaves into aqueous glycine solution, which consists of a pair of antennas, a signal generator with a power amplifier, a spectrum analyzer and a sample holder. Using this, we measure the transmitted power of microwaves into aqueous glycine solution as a function of glycine concentration. We elucidate a relationship between the transmitted power and the dielectric loss factor ε'' in $\varepsilon^* = \varepsilon' - \mathrm{j}\varepsilon''$ as a parameter of glycine concentration to examine the possibility for realization of MCLT system.

Integral Localized Approximation Description of v-th Order Bessel Beams in the Generalized Lorenz-Mie Theory and Applications to Optical Trapping

L. A. Ambrosio and H. E. Hernández-Figueroa
School of Electrical and Computer Engineering (FEEC)
Department of Microwaves and Optics (DMO)
University of Campinas (Unicamp), Campinas 13083-970, SP, Brazil

Abstract— In this work, we present theoretical derivations and numerical calculations of the beam shape coefficients (BSCs) of the generalized Lorenz-Mie theory (GLMT) by adopting the integral localized approximation and assuming, for the first time in the literature, an arbitrary and ideal v-th order Bessel beam. It is shown that, although this approximation was first derived for azimuthally symmetric laser beams (Gaussian and sheet laser beams) and is easily extendable to zero-order Bessel beams, higher order Bessel beams can also be successfully described within its framework with great accuracy, even though closed-form solutions are not readily found. Numerical comparisons between our new approach and other time-consuming methods, such as quadratures, are performed, and it is revealed that the integral localized approximation provides a fast and efficient code for numerically evaluating the BSCs of Bessel beams and their associated electromagnetic field components. New symmetry relations are outlined for the BSCs and the scattered fields, due to the incident field profile assumed, and it is seen that their numerical implementation can significantly decrease the computation time of the full set of BSCs regardless of the method used to evaluate them. This approach is further applied in calculating the radiation pressure cross sections and the torque components exerted on simple (homogeneous, isotopic and linear) lossless and lossy dielectric spherical particles by linearly and circularly polarized Bessel beams, comparing our results with those obtained by previous authors in both the ray optics and Rayleigh-Gans regime, where the GLMT is still applicable. Finally, we conclude that this new fast and robust approach can be advantageously used in the analysis of scattering problems involving incident Bessel beams, such as in the case, for example, of optical trapping systems.

Genetic Algorithms Application for the Optimal Design of Magnetic Vagus Nerve Stimulator

M. Chojnowski and J. Starzyński
Warsaw University of Technology, Poland

Abstract— Stimulation of human vagus nerve with use of electromagnetic field is intensively developing since late 1980's. The method pioneered by J. K. Penry and J. C. Dean is based on surgical implantation of electric device into human body and owes its prosperity to very promising results in various therapies. Its contemporary field of clinical applications stretches from epilepsy through depression and anxiety to migraines and still widens. Vagus nerve stimulation (VNS) was the initial trigger for authors to undertake the challenging research towards design of magnetic stimulator. Unlike the already well known electric VNS stimulator, the magnetic one (MVNS) is supposed to operate externally instead of being implanted into patient's body. The realistic, three-dimensional numerical model was prepared to begin with, in order to estimate the feasibility of the concept. One of the problems that emerged soon after the initial calculations were made, was to improve the basic design of the stimulator model. Having a complex, 3D model at hand to deal with a number of calculations required for an inverse problem meant a considerably long time of analysis and high demands for computational capacity. At that point, the need of model simplification became apparent and the most evident measure of bringing it into effect was to reduce the space of analysis into two dimensions. That assumption has conceived and brought to life a 2D model that proved to be less time and capacity consuming, compared to the three-dimensional one. At last, but not least, authors had to decide on the type of optimization method to address the problem and eventually employed the genetic algorithms for the job. Was it a wise choice and what was its yield, one can acknowledge from this paper along with more details of the research.

REFERENCES

1. Nemeroff, C. B., et al., "VNS therapy in treatment-resistant depression: Clinical evidence and putative neurobiological mechanisms," *Neuropsychopharmacology*, Vol. 31, No. 7, 1345–1355, 2006.
2. Stuchly, M. A. and T. W. Dawson, "Interaction of low-frequency electric and magnetic fields with the human body," *Proceedings of the IEEE TM*, Vol. 88, No. 5, 643–664, 2000.
3. Sawicki, B., et al., "Scalar potential applied to magnetic stimulation modelling," *Electrical Review*, Vol. 83, No. 7/8, 143–147, 2007.

Near-field Radar for Prostate Cancer Detection: Principles and Clinical Evidence

C. Bellorofonte[1] and U. Spagnolini[2]

[1]Urology Department, Columbus Clinic, via M. Buonarroti 38, Milano, Italy
[2]Dipartimento di Elettronica e Informazione
Politecnico di Milano, P. zza L. da Vinci 32, Milano, Italy

Abstract— Cancer is the major public health problem worldwide, 25% of deaths are due to cancer, and over 50% for each sex are due to prostate/breast, lung, and colon rectum. Early diagnostic methods for massive screening need to comply with reliability, simplicity, and costs constraints. Purpose of this paper is to investigate a new diagnostic device that is based on interaction between low-frequency (approx 434 MHz) electromagnetic (EM) field and tumors for massive firstscreening. Preliminary clinical results on prostate tumors on 107 patients show very encouraging negative predictive values (better than 97%).

Tumor tissues have a significant different electrical conductivity and permittivity from the normal surrounding tissues, this property is used in several diagnostic tools mostly based on providing the clinicians with the EM imaging of the locally altered anatomy. This is the basis of researches on imaging method where quantitative analysis is obtained by solving (non-linear) inverse problems with microwave excitation ($>$ 1 GHz). Scientific community focuses on breast cancer for the fairly simple geometry and the translucent properties of normal breast tissues. Prostate cancer has the same incidence (approx. 24–29%) but the anatomy of the perineum area is more complex and heterogeneous.

Main Contribution: In this paper we propose to exploit the peak of absorption around 300–500 MHz (namely due to the increase of water and sodium in malignant tissues) to define a new diagnostic method based on multiple bistatic radar. One transmitting (TX) antenna is placed in close contact to the skin of the patient and operated by the clinician that places and moves the antenna in the perineum region, at minimal distance from prostate. The antenna generates a modulated narrowband signal $s(t) = a(t)\exp(j2\pi f_o t)$ with carrier frequency $f_o = 434$ MHz, the wavelength in the body is approx. 19–25 cm. Prostate size is 3 cm (or 20 cc) and it is embedded within 3–4 cm from the perineum position where the clinician places the TX antenna. The backscattered field is the combination of all the scattering contributions that arise from the interaction between the radiating antenna and the body. The backscattered field is measured by a set of receiving antennas arranged over a 2D planar array so as to act as a multiple bistatic radar system. Differently from EM tomography methods where multiple views are obtained by changing both the orientation of the 2D array and the TX antenna, here the TX antenna is freely operated by the clinician in search of the best coupling with tumor from backscattered field measured with fixed 2D array. Once again, the diagnostics is obtained by the analysis of the corresponding backscattered field measured from the receiving antennas array in static position.

Experimental Results and Clinical Evidence: The preliminary experimental setting is based on linearly polarized TX antenna with on/off modulation $a(t)$ at 434 MHz. The TX antenna is operated by the clinician in the perineum region with patient standing and normally dressed. Signals from receiving antennas are gathered from the processing unit that is synchronized with modulation signal. Signal processing of the backscattering field is based on the analysis of the nulls in radiation pattern as this is simple enough to distinguish between low (no-tumor) or high (tumor) interference pattern. Clinical validations are in progress but the first available data are based on 107 patients with different prostatic pathologies (i.e., not all with prostate cancer), preliminary results shows more than encouraging negative predictive values (better than 97%), sensitivity better than 95%, specificity approx 75%. A complete description of the experimental setting and other clinical evidence will be provided in the full paper.

Optical Detection of Hepatitis in Liver Tissue Using Polarization Technique

M. Ikram, **M. Umair**, **A. Rahat**, **S. Ali**, **and S. Firdous**
Department of Physics and Applied Mathematics
Pakistan Institute of Engineering and Applied Sciences, Islamabad 45650, Pakistan

Abstract— Biological tissues are optically active, its size, external-internal structure, and refractive index of the material affects the polarization properties of the incident light and can reveal the information about the objects. The polarization state of the input and output light has been observed using Mueller matrix polarimeter. Lu-Chipman and symmetric decomposition techniques has been applied for obtaining physical parameters e.g., diattenuation, depolarization, polarizance, retardance against the wavelength range from 400–800 nm. A good contrast (ratio of nearly 10 in retardance, 6 in depolarization and 2 in diattenuation at 600 nm) between control and the infected tissue showed the potential application of the technique not only in hepatitis but other diseases.

Session 1P3
Metamaterials and Their Applications 2

Slow Light Phenomena in Stacked Metasurfaces

M. Aznabet[1], **M. Navarro-Cía**[2], **M. Beruete**[2], **F. Falcone**[2], **O. El Mrabet**[1], **M. Essaaidi**[1], **and M. Sorolla**[2]

[1]Electronics and Microwave Group, Abdelmalek Essaadi University, Tétouan, Morocco
[2]Millimeter and Terahertz Waves Laboratory, University of Navarre, Pamplona, Spain

Abstract— Recently, a new topic has emerged in metamaterials research: scientists and Engineers are looking to slow down the speed of light by using metamaterials structures. Indeed, several groups [1–3] have reduced the speed of light by using left handed metamterials. The major fascination of metamaterials (MMs) over the classical approaches [4–8] is that their effective parameters can be engineered artificially. Such ability seems to provide more degrees of freedom. Also, properties shown by photonic crystals can be achieved in principle in more compact structures as a result of the subwavelength dimension of their unit cell. For example, the lattice constant in graded metallic gratings tends to be slightly larger than that of metamaterials and, in addition, those structures are not applicable to free-space configurations. In this work, we report experimentally a delay of more than 2 orders of magnitude (with respect to freespace) of a microwave beam through a metamaterial composed of alternative layers of split-ring-resonators [9] and complementary-split-ring-resonators [10] at the two first transmission bands. The study is developed for 3 stacked functional layers, where one functional layer comprises one split-ring-resonators- and one complementary-split-ringresonators-metasurface. The slow light effect described here may resemble to that reported in [11] based on coupled resonators, which is reminiscent of electromagnetically induced transparency in terms of dark and radiative states/elements [12]. However, in our case both resonators are coupled directly to the incident electromagnetic field via the electric (split-ring-resonator) and the magnetic field (complementary-split-ring-resonator) due to the bianisotropy of these particles [13], and thus both can be considered radiative elements.

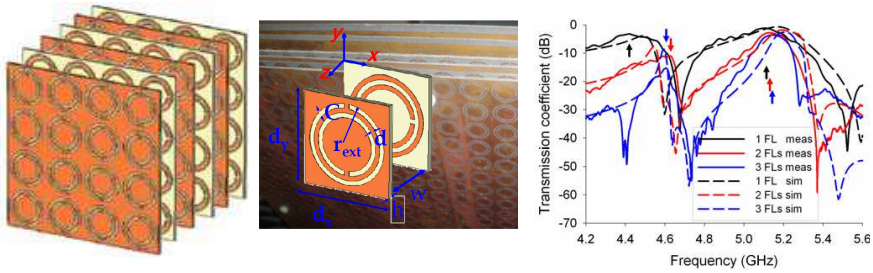

(a) (b) (c)

Figure 1: (a) Schemtaic of the functional layers. (b) Picture of the fabricated prototype. The front layer is a complementary-split-ring-resonators metasurface. Inset: unit cell with its parameters. (c) Transmission coefficient through a stack of 1 (black), 2 (red) and 3 functional layers (blue): measurements (solid lines) and numerical calculations (dashed lines). Arrows point out experimental maxima at each transmission band and for each number of functional layers.

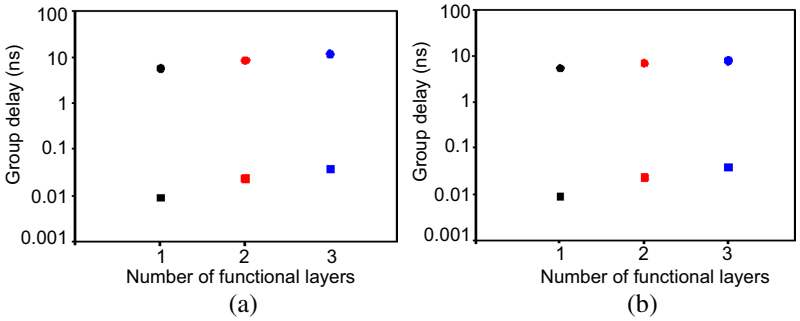

Figure 2: Experimental group delay in metamaterial (circular) and in free space propagating the same distance (rectangular) as a function of the number of functional layers for the first (a) and second propagating band (b).

REFERENCES

1. Tsakmakidis, K. L., A. D. Boardman, and O. Hess, "Trapped rainbow storage of light in metamaterials," *Nature*, Vol. 450, 397–401, 2007.
2. Lu, W. T., S. Savo, B. D. F. Casse, and S. Sridhar, "Slow microwave waveguide made of negative permeability metamterials," *Microwave Opt. Tech. Lett.*, Vol. 51, 2705–2709, 2009.
3. Dong, J. W. and H. Z. Wang, "Slow electromagnetic propagation with low group velocity dispersion in an all-metamaterial-based waveguide," *Appl. Phys. Lett.*, Vol. 91, 111909, 2007.
4. Krauss, T. F., "Why do we need slow light?," *Nat. Photon.*, Vol. 2, 448–450, 2008.
5. Kasapi, A., M. Jain, G. Y. Yin, and S. E. Harris, "Electromagnetically induced transparency: Propagation dynamics?," *Phys. Rev. Lett.*, Vol. 74, 2447–2450, 1995.
6. Hau, L. V., S. E. Harris, Z. Dutton, and C. H. Behroozi, "Light speed reduction to 17 meters per second in an ultracold atomic gas," *Nature*, Vol. 397, 594–598, 1999.
7. Heebner, J. and R. Boyd, "Slow and fast light in resonator-coupled waveguides," *J. Modern Opt.*, Vol. 49, 2629–2636, 2002.
8. Baba, T., "Slow light in photonic crystals," *Nat. Photon.*, Vol. 2, 465–473, 2008.
9. Pendry, J. B., A. J. Holden, D. J. Robbins, and W. J. Stewart, "Magnetism from conductors and enhanced nonlinear phenomena," *IEEE Trans. Microwave Theory and Techniques*, Vol. 47, No. 11, 2075–2084, 1999.
10. Falcone, F., T. Lopetegi, M. A. G. Laso, J. D. Baena, J. Bonache, M. Beruete, R. Marqués, F. Martín, and M. Sorolla, "Babinet principle applied to metasurface and metamaterial design," *Phys. Rev. Lett.*, Vol. 93, 197401-1–4, 2004.
11. Tassin, P., L. Zhang, T. Koschny, E. N. Economou, and C. M. Soukoulis, "Planar designs for electromagnetically induced transparency in metamaterials," *Opt. Express*, Vol. 17, 5595–5605, 2009.
12. Papasimakis, N. and N. I. Zhedulev, "Metamaterial-induced transparency: Sharp fano resonances and slow light," *Opt. Photonics News*, Vol. 20, 22, 2009.
13. Marqués, R., F. Martin, and M. Sorolla, *Metamaterials with Negative Parameter: Theory, Design, and Microwave Applications*, Wiley, New York, 2008.

Asymmetrical Stripline Based Method for the Electromagnetic Characterization of Metamaterials

S. Gómez, A. Chevalier, and P. Quéffélec
Lab-STICC, UMR-CNRS 3192, UEB, Université de Bretagne Occidentale, France

Abstract— Metamaterials are artificial composite structures that exhibits electromagnetic properties not observed in their constituent materials or in nature. These types of material are generally dispersive, anisotropic and heterogeneous.

Many factors must be considered in the characterization of metamaterials, as the frequency band, the geometry and the orientation and distribution of the metallic inclusions. This last point is fundamental because the response of the material is determined by the way the electromagnetic field interacts with the inclusions. The appropriated behavior, in the case of a metamaterial type SRR or similar, is obtained when the direction of the magnetic field is normal to the surface of the structure, and the electric field is tangent to the spirals.

There are some experimental methods used for extracting the constitutive parameters of metamaterials. The main objective of these methods is to obtain the S parameters of a sample of material and then determine the permittivity and permeability using different analytical inverse procedures. Free space methods allow us to perform measurements in high frequencies, but it is not recommended for frequencies below 10 GHz because big samples are required. Other methods based in resonant cavities are not convenient because of the dispersive nature of the metamaterials. The transmission line based methods, such as waveguide or microstrip line, do not present the field distribution that produces a representative response of the metamaterial because the direction and strength of the EM field are not constant over all the volume of the metamaterial.

The method proposed in this work utilizes an asymmetric stripline that has been developed in our laboratory for the broadband characterization of magnetic materials. In the region below the central conductor where the sample is set, the electric field is parallel to the metal strips and the magnetic field is perpendicular to them. The amplitude of both fields is constant for the entire sample and it is possible to consider the propagation of a quasi-TEM mode.

Due to the heterogeneous character of metamaterials, the response may change depending on the number of inclusions or unit cells added to the sample. That makes necessary to find the elementary volume of the material that will produce a representative result.

This point was solved simulating different types of metamaterials using HFSS software. The number of inclusions was increased in the direction of electric and magnetic field to analyze how the response changed. This analysis showed us that only one unit cell of metamaterial does not have the same behavior than a more complex structure. Otherwise, if the number of cells was increased until a certain minimum value, we obtained a convergence in the response. In this case, we can consider the metamaterial as a homogeneous medium and the effective permittivity and permeability do not longer depend on the size of the structure.

This work presents the stripline cell and its application for the measurement of metamaterials, the convergence analysis based on HFSS simulations and a comparison between some experimental and simulated results.

Dielectric-resonator-like Response of a Metamaterial Particle Composed of a Multi-layered CRLH Transmission Line

Yasushi Horii
Kansai University, 2-1-1 Ryozenji, Takatsuki, Osaka 569-1095, Japan

Abstract— Left-handed (LH) metalaterals, defined by simultaneously negative permittivity ε and permiability μ, has dawn considerable interest in microwave engineering because of its unique properties such as negative refractive index, backward-wave propagation and phase-advanced microwave response. In addition, handling capability of material parameters, ε and μ, is attractive for production of new artificial electromagnetic materials.

In this presentation, a dielectric-resonator-like metamaterials particle is proposed. This particle is structured by a multi-layered (ML) composite right/left-handed (CRLH) transmission line (TL) with three LH unit cells, each of which is configured by a pair of parallel plates, a meander line and a connecting wire between them. Both end of the TL is open-terminated so as to couple to electric field outside the particle. To confirm the dielectric-resonator-like response, a particle with dimensions of $5.0 \times 5.0 \times 2.85\,\mathrm{mm}^3$ is mounted on a microstrip line, and coupling characteristics are studied theoretically by using commercial software Ansoft HFSS Ver. 9. It is clearly observed from the simulated results that a deep transmission zero is created around 5.5 GHz, which frequency corresponds to the transition frequency (zero phase constant: $\beta = 0$) of balanced CRLH TL. This frequency can be tuned widely by changing CRLH circuit parameters, and fine-tuned by scraping the dielectric surface of the particle.

Design and Fabrication of Random Optical Surfaces by a Modified Speckle-based Method

V. Brissonneau[1], **L. Escoubas**[2], **G. Soriano**[3], **F. Flory**[2], **G. Maire**[3], **and G. Berginc**[1]

[1]Thalès Optronique S.A., 2 Avenue Gay-Lussac, 78995 Elancourt Cedex, France
[2]Institut Matériaux Microélectronique Nanosciences de Provence — IM2NP CNRS UMR 6242
Aix-Marseille University, Campus de Saint-Jérôme, Avenue Escadrille Normandie Niemen — Service 231
F-13397 Marseille Cedex 20, France
[3]Institut Fresnel, Aix-Marseille University, Campus de Saint-Jérôme
Avenue Escadrille Normandie Niemen, Marseille, France

Abstract— Random optical surfaces are of primary interest for several applications such as anti-reflective surfaces, scattering surfaces allowing enhanced performances of photonic sensors, exalted absorption of solar cells, stealth, etc ....

In this paper, we describe how random optical surfaces with tuned statistical properties can be modeled and fabricated using a diffracted laser field registered in a photoresist. The two main parameters characterizing a random surface are the correlation function and the height distribution.

Our study is mainly focused on the correlation function of the surface which is governed by the correlation function of the diffracted laser beam registered in the photoresist.

Based on the Kirchhoff approximation and considering that the laser beam dimensions are larger than the roughness of the diffracting element we derive the equation linking the correlation function of the diffracted field to that of the generated surface:

$$Icorr \propto |FT(E0^2)|^2 \tag{1}$$

where $Icorr$ is the light intensity registered in the photoresist and $E0$ the field amplitude distribution of the laser beam.

Thus, by adjusting the field amplitude distribution, one is able to tune the correlation function of the surface.

The original method described by Gray [1], allows the generation of Gaussian height distribution with Gaussian correlation.

A modified experimental Gray method, comprising a spatial light modulator (SLM) to control the laser beam shape is proposed to fabricate the random optical surfaces having controlled statistics: An argon laser beam shaped by the SLM is scattered by a diffusing element on the photoresist deposited at the surface of an optical substrate. The realized surface is then transferred by reactive ion etching (RIE) on the substrate.

Experimental parameters (insolation time, diffusing element position, annealing and etching process to transfer the pattern into the surface) will also be discussed.

Theoretical results are shown and compared with first experiment.

REFERENCES

1. Gray, P. F., "Method of forming optical diffusers of simple known statistical properties," *Optica Acta*, Vol. 25, No. 8, 765–775, 1978.

Bifurcated Permittivity in a Field-dependent Metamaterial via Discharge Plasma Generation

Osamu Sakai and Satoshi Iio
Kyoto University, Japan

Abstract— Bifurcation of permittivity and corresponding electromagnetic wave propagation is analytically and numerically investigated in a field-dependent metamaterial composed of discharge plasmas and magnetic resonators.

In a metamaterial, which has a functional micro structure in its internal spatial periodicity to control permittivity and permeability, sign of permittivity at a constant permeability determines a state of a wave which is either propagating or evanescent. Here, when the permittivity depends on the local electric field of the propagating electromagnetic wave, self consistency in a system of the permittivity and the electric field is maintained. Furthermore, if the dependence is not monotonous with dissipation, the system becomes nonlinear with possible bifurcated solutions.

Such a situation is found in a microwave plasma, in which the microwave propagates and electric fields of the microwave induce breakdown and generation of plasma; its electron density depends on the local electric field and also determines local permittivity. By changing sign of permeability, dispersion relation varies drastically; we find one stable solution at positive permeability, but bifurcated solutions are observed at negative permeability. Bifurcation of the permittivity takes place at a constant electric field, and two saddle-node points determines these bifurcation criteria.

In the case with negative permeability, numerical results show that microwaves can propagate in a medium with negative permittivity in which the wave frequency is less than the electron plasma frequency by generation of high-electron-density plasma; this is a negative-refractive-index state [1, 2]. On the other hand, the results indicate that the microwaves cannot propagate if the permittivity is positive and the electron density is low, in which the refractive index is purely imaginary. Using evolution equations of electron density in a discharge plasma which is generated by the electric field of propagating microwaves, analytical results show that bifurcation of the permittivity takes place as a function of the electric field beyond the propagation-prohibited range with positive permittivity. In summary, a state with negative permeability in a field-dependent metamaterial triggers bifurcation of permittivity between positive and negative values, and such a dynamic feature can be observed in a metamaterial with discharge plasmas generated by the electromagnetic waves.

REFERENCES

1. Sakai, O., T. Naito, T. Shimomura, and K. Tachibana, *Thin Solid Films*, Vol. 518, 3444, 2010.
2. Sakai, O., T. Naito, and K. Tachibana, *Phys. Plasmas*, Vol. 17, 057102, 2010.

Anisotropic Composite Right/Left-handed Transmission Line Metamaterials with Ferrite Substrate

T. Zhou[1,2], **M. Le Berre**[1,2], **F. Calmon**[1,2], **D. Vincent**[1,3], **F. Boukchiche**[1,3], **and B. Payet-Gervy**[1,3]

[1]Université de Lyon, France
[2]Institut des Nanotechnologies de Lyon, INL-UMR5270, CNRS, INSA de Lyon
Villeurbanne, F-69621, France
[3]Laboratoire DIOM, Université de Saint-Etienne
25 rue du Dr. Rémy Annino, Saint-Etienne, F-42000, France

Abstract— Metamaterials are macroscopic composites whose function is determined by both the cell structure and the chemical composition [1]; they can be realized by resonant structures and non-resonant structures. As a kind of non-resonant metamaterial structure, the composite right/left-handed (CRLH) transmission line (TL) is based on TL approaches; they have lower loss and wider bandwidth and can be applied to develop novel microwave devices [2]. Yttrium iron garnet (YIG) is a ferrite material that can be easily magnetized by a D.C. magnetic field; it plays an important role in microwave circuits.

A metamaterial combining CRLH TL and YIG substrate is proposed, the metamaterial is realized by embedding series interdigital capacitors and shunt inductors in a coplanar waveguides on a ferrite substrate. The microwave characteristics of these structures are experimentally measured up to 20 GHz: the S parameters are measured and propagation constant is calculated; the influence of YIG substrate with in-plane magnetization is studied.

A prototype of CRLH TL metamaterial is successfully implemented. The thickness of YIG and conductor gold is around 900 µm and 1 µm respectively. The center conductor width W is 400 µm, the slot width S is 150 µm, the prototype length Ls is 6280 µm, the dimensions for the capacitors and inductors lie between 10 µm and 650 µm.

The experiments are performed with an applied field 140 kA/m. From measured S parameters, the gyroresonance frequency is about 6 GHz, the difference between S_{21} and S_{12} is 10 dB at 8.2 GHz, and non-reciprocal effect is obtained. The propagation constant is given: the difference between α^+ and α^- is 1 Neper around 8.2 GHz; for 2 frequency bands, the phase velocities (β) and group velocities are opposite, a left-handed behavior is obtained. The structure has properties such as non reciprocity, and backward waves. These properties are very attractive for isolators, filters, resonators and other future novel active components.

REFERENCES

1. Cui, T. J., H. F. Ma, R. P. Liu, B. Zhao, Q. Cheng, and J. Y. Chin, "A symmetrical circuit model describing all kinds of circuit metamaterials," *Progress In Electromagnetics Research B*, Vol. 5, 63–76, 2008.
2. Caloz, C. and T. Itoh, *Electromagnetic Metamaterials: Transmission Line Theory and Microwave Applications*, John Wiley & Sons, New York, 2004.

A New Multi-ring SRR Type Metamaterial Design with Multiple Magnetic Resonances

O. Turkmen[1, 2], **E. Ekmekci**[1, 3], **and G. Turhan-Sayan**[1]

[1]Department of Electrical and Electronics Engineering
Middle East Technical University, Ankara, Turkey
[2]Department of Electronics and Telecommunications Engineering
Kocaeli University, Kocaeli, Turkey
[3]Department of Electronics and Communication Engineering
Suleyman Demirel University, Isparta, Turkey

Abstract— Metamaterials are specially designed periodic structures which can show unique properties such as having negative values of permeability and/or negative values of permittivity over finite frequency bands. Theoretical aspects and many important applications of metamaterials in microwave, terahertz and optic regions have been investigated in detail in a vast amount of publications for the last decade. Split ring resonator (SRR) type magnetic resonators are among the most popular metamaterial structures having negative permeability over narrow frequency bandwidths. Although various forms of SRR structures have been found useful in many narrowband applications, research on metamaterials has been focused recently on the design of multiband and/or frequency tunable metamaterials.

In this study, we propose a new SRR unit cell design for multi-band metamaterial applications. The suggested unit cell structure consists of N number of split rings with aligned gaps as described in Figure 1 to obtain magnetic resonances at N distinct frequencies. The schematic view of the proposed unit cell for the case of $N = 3$ is shown in this figure together with the excitation details where the incident $\bar{H}$ field is perpendicular to the SRR plane and the $\bar{E}$ field is perpendicular to the gap containing edges of the SRR rings. It is well known that, this type of excitation will yield magnetic LC resonances. In this design, the value of each distinct resonance frequency can be adjusted by choosing design parameters properly. For a given substrate material, design parameters are the side lengths, widths and gap distances for each ring, and the separation distances between the rings. As the proof of concept, we will design and simulate our multi-band SRR arrays for three different cases (i.e., for $N = 1, 2$ and 3) by using CST Microwave Studio. The complex transmission and reflection characteristics (i.e., the complex S-parameters S_{21} and S_{11}) of the SRR arrays computed by CST will also be used to extract the effective medium parameters μ and ε of the designed metamaterials to verify the nature of resulting resonances. It should be noted that this multi-SRR structure is also capable to display multiple electrical resonances under proper excitation conditions. We believe that the proposed multi-ring SRR design will provide an electrically small and easy-to-fabricate alternative to the present multi-band metamaterial structures.

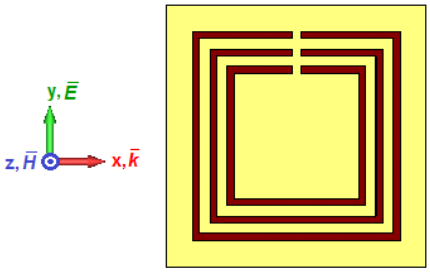

Figure 1: The multiple split ring resonator configuration with $N = 3$.

Additive Digital Assembly of Metamaterials

Rehmi Post, **David Cranor**, **Maxim Lobovsky**, **Jonathan Ward**, **and Neil Gershenfeld**
MIT Center for Bits and Atoms, 20 Ames Street, E15-401 Cambridge, MA 02139, USA

Abstract— The state of the art of photonic crystal [1] and negative-index metamaterial [2] fabrication is dominated by inherently planar additive and subtractive lithographic techniques such as those common to the semiconductor industry. Here we propose instead to fabricate metamaterials via additive digital assembly [3], a class of rapid-prototyping technologies which utilize intrinsically digital processes and materials, based on mechanically bistable reversible joints to assemble primitive voxels into complex 3D structures. Using these methods, we will demonstrate the fabrication and characterization of a negativeindex metamaterial lens through simulation and experiment.

Digital assembly is distinct from additive 3D printing in that it assembles discrete unit cells into composite structures. These units or voxels are designed to mate at specific sites and orientations via press-fit junctions, and may comprise either homogeneous or composite media with varied properties. This inherent quantization of form and fit reduces the cumulative error that would otherwise develop during assembly and enforces a constant lattice spacing. The ability to place voxels of arbitrary materials and properties (e.g., conducting, insulating, dielectric, ferromagnetic) at each lattice site enables the precise definition of three-dimensional circuit interconnects, as well as waveguides, resonators, and other electromagnetic circuit elements.

Going one step further, electromagnetic metamaterial fabrication is an exemplary application for digital assembly. Such materials typically comprise a collection of repeated elements designed to have a strong reponse to applied fields [4]. If the size and spacing of the elements is much smaller than the wavelengths of interest, the collection is indistinguishable from a homogeneous material. In order to reap the benefits provided by digital assembly, the voxel shapes are designed for assembly into arbitrary three dimensional structures as a lattice of various materials, thus facilitating the creation of metamaterials of any shape. To demonstrate feasibility, we will show that it is possible to fabricate structures such as a planoconcave lens [5] with these methods and materials. In addition, we will demonstrate other electromagnetic structures whose fabrication is (perhaps uniquely) enabled by additive digital assembly.

REFERENCES

1. Joannopoulos, R. M. and J. Winn, *Photonic Crystals: Molding the Flow of Light*, 2nd Edition, Princeton Univ. Press, Princeton, NJ, 2008.
2. Shelby, R. A., D. R. Smith, S. C. Nemat-Nasser, and S. Schultz, "Microwave transmission through a two-dimensional, isotropic, left-handed metamaterial," *Appl. Phys. Lett.*, Vol. 78, No. 4, 489–491, January 2001.
3. Popescu, G. A., "Digital materials for digital fabrication," S.M. Thesis, Massachusetts Institute of Technology, School of Architecture and Planning, Program in Media Arts and Sciences, 2007. URI: http://hdl.handle.net/1721.1/41754.
4. Pendry, J. B. and D. R. Smith, "Reversing light with negative refraction," *Physics Today*, Vol. 57, No. 6, 37–44, 2004.
5. Vodo, P., P. V. Parimi, W. T. Lu, and S. Sridhar, "Focusing by planoconcave lens using negative refraction," *Appl. Phys. Lett.*, Vol. 86, 201108, 2005, doi:10.1063/1.1927712.

VLSI Photonics Using Plasmonic Wires and Rings

El-Hang Lee[1, 2]

[1]Optics and Photonics Elite Research Academy (OPERA)
National Research Center for VLSI Photonic Integration Technology, INHA University
253 YongHyun-Dong, Nam-Ku, Incheon, South Korea
[2](μ-PARC) Micro/Nano-Photonics Advanced Research Center, Graduate School of Information Technology
INHA University, 253 YongHyun-Dong, Nam-Ku, Incheon, South Korea

Abstract— We report on the design and integration of nano-scale surface plasmonic polariton (SPP) wires and dielectric wires for VLSI photonic integrated circuit applications. We first analyze the propagation characteristics of the plasmonic lightwaves, either fast or slow. We then design and integrate coupled structures of plasmonic nanowires and examine the optical mismatch problem between two plasmonic wires for "very large scale integrated" VLSI nano-photonic circuit applications. The plasmonic nano-wires are also integrated with other micro/nanoscale dielectric wires and devices, such as silicon wires and devices. We analyze the effective index of the silicon waveguides and the SPP waveguides and design a guided directional coupler based on the matching of the effective refractive indices between two waveguides. We use polymer or silicon wires for dielectric wires and the silver or gold for plasmonic wave generation. We investigate three kinds of plasmonic coupled structures: Strip wires, slot wires, and stripe wires. Strip wires are constituted with two identical plasmonic wires. Slot wires consist of two plasmonic wires separated by a dielectric material of a narrow gap. Stripe wires consist of a thin plasmonic wire and a semi-infinite metal plate. We calculate the mode fields of the individual SPP nanowaveguides. We then calculate the coupled eigen-modes of even and odd eigen-modes directly to analyze the coupling between two nano-waveguides. In the case of the strip wire coupling, we find that, for the even mode, the magnetic field has the same direction in all the position while the odd mode has opposite field direction on the two nano-waveguides. In terms of energy transfer, we find that the lightwave coming into a no-wire is transferred to the SPP wire due to the refractive index matching or the optical impedance matching. We study both the single SPP and the slot SPP wire excited by the electrical filed component normal to metal-dielectric interface. For a single SPP waveguide we find that the SPP modes are not excited by TE mode but by TM mode in the lateral guided wave coupler. In the slot SPP waveguide, we find that the SPP modes are not excited by TM mode but by TE mode in the lateral guided wave coupler. We also used surface plasmon-polaritons (SPPs) formed on a flat metal surface like silver or gold for micro/nano-photonic circuits and networks. Using the results of the above mismatch characteristics, we have been able to design plasmonic devices, such as micro-ring switches, splitters, modulators, including the basic blocks such as horizontal directional couplers, vertically integrated directional couplers, multimode interference devices, switches, and modulators. We use these building blocks to form VLSI photonics. We will present some of the recent examples of our progresses along with the global and historical perspectives of micro/nano-photonics and VLSI photonics.

From Millimeter-waves to Terahertz Metamaterials by Stacking Frequency Selective Surfaces

M. Navarro-Cía[1], **M. Beruete**[1], **M. Aznabet**[1, 2], **S. A. Kuznetsov**[3], **F. Falcone**[1], **M. Sorolla**[1]

[1]Millimeter and Terahertz Waves Laboratory, Universidad Pública de Navarra, Spain
[2]Electronics and Microwave Group, Abdelmalek Essaadi University, Tétouan, Morocco
[3]Budker Institute of Nuclear Physics SB RAS, Novosibirsk State University, Russia

Abstract— Metamaterials are becoming the engine that is powering the revolution on the reinterpretation of many propagation phenomena [1]. Examples are the negative refraction [2], perfect lensing [3] to name a few. In addition, the ability of having transmission through sub-wavelength holes, both under the so-called extraordinary transmission (ET) [4] and the recently termed anomalous ET [5] is expect to make significant contribution to electromagnetism and to the burgeoning area of plasmonics.

Among others approaches, the stacking of surfaces has proven to be flexible as well as interesting route to build up bulk or even 3D metamaterials. These surfaces range from subwavelength hole arrays [6] to 2D array of SRRs and CSRRs [1]. Moreover, some of these stacks (those based on subwavelength hole arrays [6] and CSRRs [7]) lead to negative refractive metamaterials as a result of the electro-inductive-wave phenomenon [7] supported by electrically-coupled resonant unit cells.

This work is another step forward in the rapidly evolving field of metamaterials. The breadth and utility of these stacks at millimeter-waves and THz must be questioned from the perspective of losses. Therefore, we study in-depth the properties of different substrates to reduce losses. We also present results of single layer and multi-layer structures based on metasurfaces of SRRs and CSRRs as well as subwavelength hole arrays. Particular attention is put on the effect of the stacking on the propagation and on the unusual phenomena supported by dielectric-backed surfaces such as the anomalous ET [5].

REFERENCES

1. Solymar, L. and E. Shamonina, *Waves in Metamaterials*, Oxford University Press, New York, 2009.
2. Veselago, V. G., "The electrodynamics of substances with simultaneously negative values of ε and μ," *Soviet Physics Uspekhi.*, Vol. 10, 509–514, 1968.
3. Pendry, J. B., "Negative refraction makes a perfect lens," *Physical Review Letters*, Vol. 85, 3966–3969, 2000.
4. Ebbesen, T. W., H. J. Lezec, H. Ghaemi, T. Thio, and P. A. Wolf, "Extraordinary optical transmission through sub-wavelength hole arrays," *Nature*, Vol. 391, 667–669, 1998.
5. Kuznetsov, S. A., M. Navarro-Cía, V. V. Kubarev, A. V. Gelfand, M. Beruete, I. Campillo, and M. Sorolla, "Regular and anomalous extraordinary optical transmission at the THz-gap," *Optics Express*, Vol. 17, 18184–18195 , 2009.
6. Beruete, M., M. Sorolla, and I. Campillo, "Left-handed extraordinary optical transmission through a photonic crystal of subwavelength hole arrays," *Optics Express*, Vol. 14, 5445–5455, 2006.
7. Beruete, M., M. Aznabet, M. Navarro-Cía, O. El Mrabet, F. Falcone, N. Aknin, M. Essaaidi, and M. Sorolla, "Electroinductive waves role in left-handed stacked complementary split ring resonators," *Optics Express*, Vol. 17, 1274–1281, 2009.

Electric Field Thermography for Metamaterial Characterization

T. Crépin, F. Issac, S. Bolioli, and D. Prost
ONERA — The French Aerospace Lab, France

Abstract— We present an original characterization technique for measuring metamaterial electric field patterns. This is based on the use of a conductive and thermoemissive thin film located in the near field domain of the metamaterial. The microwave electric field radiated by the antenna induces currents in the film which therefore exhibits ohmic losses. The corresponding heating is recorded using an infrared camera. The microwave field source is modulated, as well as the camera image processing, in order to avoid an average heating of the film and to increase image accuracy. This allows getting sub-wavelength details of the field pattern.

Composite right/left-handed transmission lines (CRLH TLs) — or *zeroth* order resonator (ZOR) antennas — consisting in structures periodically loaded by series capacitances and shunt inductances, have thus been characterized. Then, the electric field distributions of a 4-cell and of a 10-cell ZOR microstrip antennas, at frequencies corresponding to longitudinal modes above 4 GHz and up to 12 GHz, have been recorded. These field frames are in accordance with experimental and numerical results exposed in the literature. Numerical simulations (using finite element analysis) also give coherent results, but the computation cost is not negligible, due to the small dimensions and wavelengths combined with finite element modeling meshing rules ($\lambda/10$ for element sizes).

We thus demonstrated that the electromagnetic infrared (EMIR^{TM}) method is well suited to efficiently characterize metamaterials by getting accurate electric field patterns. We exhibited the different longitudinal modes arising on CRLH TLs, in the particular case of compact ZOR antennas, and we proved that the inductances radiate major part of the energy, and also that ground plane coupling capacitors participate to the antenna radiation.

Session 1P4a
Theoretical Issues and Experimental Constraints in Active Microwave Imaging

Experimental Choices and Measurements Accuracy: Their Influences on the Inversion Results

J.-M. Geffrin, **C. Eyraud**, **and A. Litman**
Institut Fresnel, UMR-CNRS 6133, France

Abstract— The anechoic chamber of the CCRM has been used by the Institut Fresnel researchers for a while to measure scattered fields and to offer these fields to the inverse community to test their inversion algorithms (see the special sections of the *Inverse Problems* journal [1–3]). Several research lines are currently being followed: an increase of the complexity of the considered targets [4], the possibility to measure more data points, and, at the same time, the possibility to segregate between the most relevant measurement points.

Measuring the scattered field of a target, with the aim of reconstructing it, is not a trivial problem [5]. Indeed, when the scattered fields are not directly measurable, as it is often the case, one possibility is to perform the measurements in two steps: firstly, by measuring a reference field (the incident field) without any target, and secondly, by measuring the field in presence of the target (the total field). Then, in ideal conditions, the subtraction of these two measured fields should only contain the contribution of the target due to the underlying scattering process. Unfortunately, in the real world, as the scattered field is very small compared to the measured ones (30 or 40 dB below the measured fields is rather common), any change in the experimental conditions might lead to strong perturbations in the deduced scattered field.

In this presentation, we will show how the scattering theory can be exploited at full length to pre-process the data using very basic *a-priori* information on the target. By simply taking into account that the considered targets are of finite extent and that the scattering phenomenon is a low-pass filter in far-field, we developed a pre-processing procedure which allows to correct one of the major experimental problems, that is, the drift effects [6]. We will show how very small drifts, on the order of a few hundredth of radian in phase and of 0.1% in amplitude, can be compensated efficiently with this procedure.

The scattering theory can be also useful to optimize the sampling of the fields. We will show how we have taken advantage of the limited spatial bandwidth of the scattered fields, to define an optimal sampling criterion and therefore to limit the overall measurement time.

Even if the scattering theory may allow to predict the number of measurements necessary to extract all available information for a given configuration [7], it does not answer to all the practical constraints which must be considered when handling a real experimental set-up. These considerations concern the fact that: (i) all the source/receiver couples may not physically be reached, (ii) the accuracy of all the measurements is not everywhere the same, (iii) the measurement time has to be reasonable, ... On the other hand, these considerations can be exploited to improve the inversion results. Indeed, we will show how we can take benefit of the knowledge of the characterized experimental random noise to improve the reconstructed permittivity maps thanks to a maximum likelihood approach [8].

To summarize, the construction and the exploitation of a microwave imaging instrument, i.e., an experimental set-up combined with the ad-hoc processing tools, necessarily implies a tight collaboration between theoretical and experimental considerations, where the constraints on one side can be transformed into advantages on the other side.

REFERENCES

1. Belkebir, K. and M. Saillard, "Special section on testing inversion algorithms against experimental data: Inhomogeneous targets," *Inverse Problems*, Vol. 21, S1–3, 2005.
2. Geffrin, J.-M., P. Sabouroux, and C. Eyraud, "Free space experimental scattering database continuation: Experimental set-up and measurement precision," *Inverse Problems*, Vol. 21, S117–S130, 2005.
3. Geffrin, J.-M. and P. Sabouroux, "Continuing with the Fresnel database: Experimental setup and improvements in 3D scattering measurements," *Inverse Problems*, Vol. 25, 035012, 2009.
4. Merchiers, O., et al., "Microwave measurements of the full amplitude scattering matrix of a complex aggregate: A database for the assessment of light scattering codes," *Optics Express*, Vol. 18, 2056–2075, 2010.

5. Geffrin, J.-M., C., Eyraud, A. Litman, and P. Sabouroux, "Optimization of a bistatic microwave scattering measurement setup: From high to low scattering targets," *Radio Science*, Vol. 44, RS2007, 2009.
6. Eyraud, C., et al., "Drift correction for scattering measurements," *Applied Physic Letters*, Vol. 89, 2006.
7. Bucci, O. M. and T. Isernia, "Electromagnetic inverse scattering: Retrievable information and measurement strategies," *Radio Science*, Vol. 32, 2123–37, 1997.
8. Eyraud, C., et al., "Microwave imaging from experimental data within a Bayesian framework with realistic random noise," *Inverse Problems*, Vol. 25, 024005, 2009.

Compressive Sensing Strategies for Active Microwave Imaging

G. Oliveri, L. Poli, M. Carlin, P. Rocca, and A. Massa
ELEDIA Research Group at DISI, University of Trento, via Sommarive 14, I-38123, Trento, Italy

Abstract— Conventional sampling techniques follow Shannon/Nyquist theorem which relates the bandwidth (spatial and temporal) of a signal with the minimum number of samples required to reliably reconstruct it. Such a fundamental assumption yields to both theoretical issues as well as experimental constraints in microwave imaging systems. As a matter of fact, there is a relation among the number of measurements (complexity of the acquisition setup), the degrees of freedom of the field (spatial bandwidth), and the achievable reconstruction accuracy.

The new paradigm of Compressive Sensing (CS) is allowing a total re-visiting of such issues, introducing the concepts of informative content of phenomena and relating it to their "sparsity" rather than to their bandwidth. CS theory, against common wisdom, asserts that one can recover certain signal/phenomena *exactly* from far fewer measurements than indicated by Nyquist frequency. To make this possible, CS relies on [2].

(a) the principle of sparsity, that is on the fact that most natural phenomena can be represented by few non-zero coefficients by selecting a suitable basis [1];

(b) the exploitation of non-uniform sampling strategies, which can guarantee, under suitable conditions (i.e., the sensing matrix satisfies the restricted isometry property [1]) a perfect recovery of the signal.

Several interesting results have already been obtained by exploiting CS to solve inverse problems arising, for example, in MRI [3] as well as radar imaging [4]. However, few results have been obtained in the field of microwave imaging.

Therefore, the aim of this work is to investigate the theoretical and experimental advances allowed by the CS paradigm in inverse problems arising in active microwave imaging. Towards this end, the exploitation of sparse representation of the investigated objects will be coupled with suitable field sampling strategies to assess on the one hand the achievable accuracy of CS retrieval algorithms if compared to standard inversion techniques, and on the other to deduce suitable guidelines to overcome the limitations of bandwidth-based imaging systems.

REFERENCES

1. Candes, E. J. and M. B. Wakin, "An introduction to compressive sampling," *IEEE Signal Processing Magazine*, Vol. 25, No. 2, 21–30, March 2008.
2. Oliveri, G. and A. Massa, "Bayesian compressive sampling for pattern synthesis with maximally sparse non-uniform linear arrays," *IEEE Trans. Antennas Propagat.*, in press.
3. Lustig, M., D. L. Donoho, J. M. Santos, and J. M. Pauly, "Compressed sensing MRI," *IEEE Signal Processing Magazine*, Vol. 25, No. 2, 72–82, March 2008.
4. Potter, L. C., E. Ertin, J. T. Parker, and M. Cetin, "Sparsity and compressed sensing in radar imaging," *Proc. IEEE*, Vol. 98, No. 6, 1006–1020, June 2010.

Microwave Imaging in Cluttered Media with an Ultrawideband Time Reversal-based Prototype

L. Bellomo[1], M. Saillard[1], S. Pioch[1], K. Belkebir[2], and P. Chaumet[2]

[1]LSEET, UMR CNRS 6017, Universit du Sud Toulon-Var, Bât. F, BP 20132, La Garde 83957, France
[2]Institut Fresnel, UMR CNRS 6133, Campus de Saint Jérôme, case 162, Marseille Cedex 20, France

Abstract— In any application where one wants to reconstruct the electromagnetic properties of objects embedded in a cluttered medium [1, 2], it is mandatory to improve the signal-to-clutter ratio as much as possible before processing the scattered field data. If this is not done, non-linear inverse algorithms — which are known to be very sensitive to noise and clutter — are more easily trapped into local minima of the cost function, giving insatisfactory results.

One way to achieve this task is to illuminate the scene with a wave focusing onto the relevant targets, so that the scattered field coming from the surrounding cluttered medium is reduced. One of the Time Reversal-issued methods known as DORT method [3] allows to easily generate such waves provided the time-harmonic multistatic data matrix associated to an array of antennas is measured. In fact, *via* a simple Singular Value Decomposition of the matrix, it has been shown [4] that the resulting singular vector(s) contain the complex amplitude law(s) needed to properly "bias" the array antennas. The idea is then to include the response to such DORT wave(s) within the inversion process in order to increase the robustness of the algorithm with respect to clutter.

To prove and explore this concept, we have built a microwave-range RADAR prototype working in the [2–4] GHz band with an array of 8 ultrawideband linearly polarized Exponentially Tapered Slot Antennas (ETSA) [5]. Since each antenna channel is equipped with a couple of digitally controlled attenuator and phase shifter, we can experimentally build and transmit the focusing wave by coding the complex amplitudes of the DORT singular vectors into the prototype.

Before inversing the 2D scattered field data, a fine antenna calibration procedure based on the same experimental data is run in order to properly model the incident field of the antennas. This step is delicate since a wrong or imprecise model could undermine the inversion results, and we solve it by applying a multipolar expansion of the incident field [6] combined with a separation between transmitting and receiving antenna patterns.

Finally, the non-linear, iterative Modified^2 Gradient Algorithm [7] is run to retrieve the features of the targets. It is here that we introduce DORT data as a regularization term of the "traditional" cost function.

At the conference we will show experimental data and results proving the whole concept.

REFERENCES

1. Devaney, A. J., "Geophysical diffraction tomography," *IEEE Transactions on Geoscience and Remote Sensing*, Vol. 22, 3–13, 1984.
2. Dubois, A., K. Belkebir, and M. Saillard, "Localization and characterization of two-dimensional targets buried in a cluttered environment," *Inverse Problems*, Vol. 20, S63–S79, 2004.
3. Prada, C. and M. Fink, "Eigenmodes of the time reversal operator: A solution to selective focusing in multiple-target media," *Wave Motion*, Vol. 20, 151–163, 1994.
4. Micolau, G. and M. Saillard, "D.O.R.T. method as applied to electromagnetic subsurface sensing," *Radio Science*, Vol. 38, 1038, 2003.
5. Guillanton, E., J. Y. Dauvignac, C. Pichot, and J. Cashman, "A new design tapered slot antenna for ultra-wideband applications," *Microwave and Optical Technology Letters*, Vol. 19, 286–289, 1998.
6. Franceschini, D., M. Donelli, and A. Massa, "On the effects of the electromagnetic source modeling in the iterative multiscaling method," *Radio Science*, Vol. 42, RS3020, 2007.
7. Belkebir, K. and A. G. Tijhuis, "Modified^2 gradient method and modified Born method for solving a two-dimensional inverse scattering problem," *Inverse Problems*, Vol. 17, 1671–1688, 2001.

The Linear Sampling Method as a Focusing Strategy: Available Implicit Information and Hybrid Inversion Approaches

L. Crocco[1], **I. Catapano**[1], **M. Bevacqua**[1], **L. Di Donato**[2], **and T. Isernia**[2]

[1]CNR, IREA, Institute for Electromagnetic Sensing of the Environment, National Research Council, Italy
[2]DIMET, Mediterranea University of Reggio Calabria, Italy

Abstract— The sampling methods [1] are widely adopted *qualitative* imaging approaches, which are able to retrieve the shape of a target by means of a simple processing of the field it scatters. Due to their robustness against uncertainty and their computational effectiveness, they are also often adopted as a pre-processing for *quantitative* imaging methods aimed at retrieving not only the morphology, but also the electromagnetic parameters of the target [2, 3]. As a matter of fact, the estimation of the target's support is helpful to reduce the non-linearity of the inverse scattering problem, as well as its computational burden [2].

In the framework of these *hybrid* inversion approaches, the existing analogy between the linear inverse problem underlying sampling methods and the problem of focusing an electromagnetic wave in presence of an obstacle [4] suggests that it is possible to move a step further, going beyond the somehow straightforward exploitation of the estimated morphology achieved from the qualitative preprocessing as a starting guess for the quantitative inversion.

As a matter of fact, this physical interpretation shows that solving the sampling methods equation is indeed equivalent to enforce an induced current having peculiar features (that is, focused in the sampling point as long as it belongs to the target). Hence, not only the methods give information on the shape of the target, but also on the current which is induced in it. We shall refer to this as the *implicit* information provided by methods, as opposed to *explicit* one represented by the method's output in terms of estimated shape.

Therefore, a new hybrid approach which exploits both the explicit and implicit information arising from the sampling methods will be discussed in this contribution.

REFERENCES

1. Cakoni, F. and D. Colton, *Qualitative Methods in Inverse Scattering Theory: An Introduction*, Springer, Berlin Heidelberg, New York, 2006.
2. Catapano, I., L. Crocco, M. D'Urso, and T. Isernia, "On the effect of support estimation and of a new model in 2-D inverse scattering problems," *IEEE Trans. Antennas Propagat.*, Vol. 55, No. 6, 1895–1899, 2007.
3. Catapano, I., L. Crocco, M. D'Urso, and T. Isernia, "3D microwave imaging via preliminary support reconstruction: Testing on the Fresnel 2008 database," *Inv. Problems*, Vol. 25, No. 4, 024002, 2009.
4. Catapano, I., L. Crocco, and T. Isernia, "On simple methods for shape reconstruction of unknown scatterers," *IEEE Trans. Antennas Propagat.*, Vol. 55, No. 5, 1431–1436, 2007.

Fisher Information in Inverse Scattering

Mats Gustafsson[1] and Sven Nordebo[2]

[1]Electrical and Information Technology, Lund University, Sweden
[2]School of Computer Science, Physics and Mathematics, Linnaeus University, Sweden

Abstract— This paper discusses the use of Fisher information to analyze optimal measurement setups and to construct preconditioners for various inverse scattering problems. The Fisher information is used to quantify the quality of the inversion data. Its associated Cramer-Rao bound gives a priori bounds on the resolution. This provides a methodology to compare and optimize measurement setups in inverse scattering problems. Here, we analyze three dimensional microwave tomography setups and discuss the effects of different object functionals, such that the determinant, trace, and Cramer-Rao bound.

The convergence of gradient based inverse scattering algorithms can be greatly improved with preconditioners. Here, we discuss preconditioners based on the Fisher information and their use in time-domain inverse scattering problem. The inverse scattering problem is formulated as a least-squares optimization problem and the gradients are computed with an adjoint formulation. The Fisher information analysis estimates the Hessian of the least-squares error functional. The preconditioner is implemented by the parameter scaling that gives a Fisher information matrix with unit diagonal. It is shown that this greatly improves the convergence rate of the used conjugate gradient algorithm in the considered examples. Numerical results in microwave tomography and ground penetrating radar are used to illustrate the results.

ACKNOWLEDGMENT

The research leading to these results has received funding from the European Community's Seventh Framework Programme (FP7/2007-2013) under Grant Agreement No. 225663 Joint Call FP7-ICT-SEC-2007-1.

Dielectric Permittivity Estimation via Localization of a Reference Target

Adriana Brancaccio and Giovanni Leone
Dipartimento di Ingegneria dell'Informazione, Seconda Universita' di Napoli, Italy

Abstract— One of the challenges in ground penetrating radar applications is the estimation of the electromagnetic properties of the host medium (i.e., the dielectric permittivity and the conductivity), whose knowledge is crucial for a successful data processing. Several procedures for the estimation of such parameters have been proposed in the literature.

In this contribution, we propose to exploit an approach founded on an algorithm developed and tested for cylinders localization. In fact, in [1] the localization of perfectly electrically conducting (PEC) circular cylinders of known radius by multimonostatic-multifrequency backscattered field measurements is successfully performed by linear inversion of an appropriate integral operator. The goal of the localization approach consists in determining the center of the cylinder so appearing as a spot in the reconstructed image of the investigation domain. The analysis of the involved operator allows to predict that a defocalization occurs in the reconstructed image when the assumed radius is wrong. So, a procedure for the focalization, based on the minimization of a proper defined functional, is set-up to estimate the radius when it is not a priori known (providing that the background medium permittivity is known) [2].

We now suggest to apply the same focalization procedure in the opposite conditions, that is when the radius is known (so using the PEC cylinder as a reference target) and the background permittivity is unknown.

The problem is formulated as follows. We consider a circular cylinder of known radius a embedded into a homogeneous medium of permittivity ε_r and residing within the investigation domain D, illuminated by the field radiated by a filamentary source placed at the cylindrical coordinates $(r, \theta) = \underline{r}$. The multimonostatic-multifrequency far zone scattered field collected at the same coordinates at the backscattering direction can be recast as a linear integral operator [1]:

$$E_s(k, r, \theta) = \left[\sum_{p=-P}^{+P} \frac{J_p(ka)}{H_p^{(2)}(ka)} \right] \int_D \gamma(\underline{r}') \frac{e^{-j2k|\underline{r}-\underline{r}'|}}{|\underline{r}-\underline{r}'|} d\underline{r}' \quad \underline{r} \in \Sigma,\ k \in [k_{\min}, k_{\max}]$$

where $k = k_0\sqrt{\varepsilon_r}$ is wavenumber of the background medium, $P \sim [ka]$ and $\gamma(\underline{r}')$ is a distributional function peaked in the cylinder's center position. The multiplicative factor in square brackets provides the information about the scatterer's shape. A correct knowledge of such a factor provides the localization of the cylinder's center as a spot via the normalization of the scattered field, the regularized operator inversion via truncated singular values decomposition and a threshold procedure. Otherwise defocusing occurs [2].

Accordingly, the proposed estimation procedure consists in evaluating the area of the image resulting from the inversion for each tentative permittivity value: The minimum is obtained for the focused image corresponding to the correct permittivity. It has to be pointed out that the whole procedure does not require to know the actual position of the cylinder, provided it is located within the investigation domain.

REFERENCES

1. Brancaccio, A., C. Di Dio, and G. Leone, "Localization of cylinders by near field multibistatic measurements," *IEEE Geoscience and Remote Sensing Letters*, Vol. 7, No. 3, 525–529, 2010, ISSN 1545-598X.
2. Brancaccio, A., C. Di Dio, and G. Leone, "Localization of cylinders by reflection mode multibistatic near zone measurements data," *International Workshop on Advanced GPR*, Granada, Spain, May 27–29, 2009, ISBN: 978-84-692-2661-2.

Some Considerations on Embedded Microwave Imaging Systems

L. Crocco[1] and A. Litman[2]

[1]CNR, IREA, Institute for Electromagnetic Sensing of the Environment
National Research Council, Italy
[2]Institute Fresnel, UMR-CNRS 6133, France

Abstract— In several electromagnetic diagnostics applications, such as for instance medical imaging, the target under test is surrounded by a coupling medium, which is meant to improve the matching between the probing wave and the target itself [1–3]. In such a configuration, the overall system (probes−coupling medium-target) is confined in a casing. Therefore, such an embedding, which is usually metallic [4, 5] in order to shield from the surrounding environment, has to be taken into account when modeling the scattering phenomenon [6].

On the other hand, besides increasing the complexity of the wave-target interaction, the presence of the embedding also affects the results of the imaging process. In particular, as recently shown by the authors through an analysis of the spectral properties of the integral radiation operator [7], the presence of a casing modifies the "quality" of the permittivity profile that can be reconstructed, while leaving the "quantity" of retrievable information unchanged.

Indeed, a thorough examination of the properties of this linear operator enables to investigate the number of degrees of freedom pertaining to the set-up at hand. This theoretical tool is particularly adapted to provide interesting guidelines for the following issues: (i) the minimum number of independent measurements needed to correctly perform the experiment; (ii) the amount of parameters which can be reliably extracted from the inversion of data (in the lack of any other a priori information); and (iii) the class of unknown functions which can be reconstructed in the imaging process.

Starting from the results of this analysis, in this contribution we will discuss how these peculiar features can be exploited to improve the capabilities of the imaging process and how they can be taken into account in the design of an embedded system for microwave imaging applications.

ACKNOWLEDGMENT

This research has been partially supported by the 2010 Short Term Mobility action of National Research Council.

REFERENCES

1. Meaney, P., M. Fanning, D. Li, S. Poplack, and K. Paulsen, "A clinical prototype for active microwave imaging of the breast," *IEEE Trans. Microwave Theory and Tech.*, Vol. 48, 1841–1853, 2000.
2. Catapano, I., L. Di Donato, L. Crocco, O. M. Bucci, A. F. Morabito, T. Isernia, and R. Massa, "On quantitative microwave tomography of female breast," *Progress In Electromagnetics Research*, Vol. 97, 75–93, 2009.
3. Salvador, S., E. Fear, M. Okoniewski, and J. Matyas, "Exploring joint tissues with microwave imaging," *IEEE Trans. Microwave Theory and Tech.*, Vol. 58, 2307–2313, 2010.
4. Lencrerot, R., A. Litman, H. Tortel, and J.-M. Geffrin, "Measurement strategies for a confined microwave circular scanner," *Inverse Problems Sci. Eng.*, Vol. 17, 787–802, 2010.
5. Mojabi, P. and J. Lo Vetri, "Eigenfunction contrast source inversion for circular metallic enclosures," *Inverse Problems*, Vol. 26, 025010, 2010.
6. Van den Berg, P. M. and J. T. Fokkema, "Removal of undesired wavefields related to the casing of a microwave scanner," *IEEE Trans. Microwave Theory and Tech.*, Vol. 51, 187–192, 2003.
7. Crocco, L. and A. Litman, "On embedded microwave imaging systems: Retrievable information and design guidelines," *Inverse Problems*, Vol. 25, 065001, 2009.

Session 1P4b
Time Reversal Methods for Electromagnetic Applications

Time Reversal and Resonant Subwavelength Scaled Media: Beating the Diffraction Limit

Geoffroy Lerosey, **Fabrice Lemoult**, **Abdelwaheb Ourir**,
Julien de Rosny, **Arnaud Tourin**, **and Mathias Fink**
Institute Lagevin, CNRS, ESPCI Paris Tech., 10 rue Vauquelin, Paris 75005, France

Abstract— Time reversal is a well know principle that allows to focus waves in time and space. It is based on the reversibility of the wave equation, and its basics are quite simple. First a point source emits a pulse in a media, and after propagation, an array of sensors measure the impulse response between the source and the sensor's locations. Then those signals are flipped in time and sent in a reversed order. If the sensors form a closed surface containing the source, the waves created converge towards the source point and focus both in space and time, achieving an instantaneous focal spot at the source location. In a homogeneous media, the size of this focal spot equals half of the wavelength.

It has been shown that in a very reverberating media, one can use only one sensor in order to perform a time reversal experiment, and focus in space and time a wave. In this paper we will start by explaining how this focusing occurs, taking the example of a complex cavity. We will show that time reversal permits to take advantage of all the modes of the cavity, ensuring that they all interfere constructively at the source location, hence producing the diffraction limited focal spot.

The next question is: can time reversal be used for focusing under the diffraction limit? Recently, we have shown that it is indeed possible to use TR for this purpose [1]. Here, we will explain theoretically this phenomena [2]. We will describe how one can create materials that have the capability to convert evanescent waves into propagating ones, hence allowing far field TR under the diffraction limit. We will show that this result can be understood in terms of subwavelength modes which are excited coherently thanks to TR, and we will make the link with the principles described for the chaotic cavity. We will exemplify our concept through various examples of media that we have studied, such as resonant wire arrays, split ring arrays, or mie resonator arrays, demonstrating focal spots much smaller than the diffraction limit. Finally we will mention the difference between TR and inverse filtering in those media, and underline that such media can be used for other purpose such as subwavelength imaging from the far field.

REFERENCES

1. Lerosey, G., J. de Rosny, A. Tourin, and M. Fink, "Focusing beyond the diffraction limit with far-field time reversal," *Science*, Vol. 315, 1120, 2007.
2. Lemoult, F., G. Lerosey, J. de Rosny, and M. Fink, "Resonant metalenses for breaking the diffraction barrier," *Physical Review Letters*, Vol. 104, 203901, 2010.

A Time Reversal based Spatial Inverse Filter Exploiting Temporal Degrees of Freedom

F. Lemoult, G. Lerosey, and M. Fink
Institut Langevin, ESPCI Paris Tech. & CNRS, France

Abstract— The principle of information transport within a medium for imaging, focusing, communication or detection lies in electromagnetic wave propagation. Obviously, performances strongly depend on the behavior of the wave in the medium of interest. Within the last decades, complex and random media have gathered a lot of interest since physics associated with them offer more possibilities than their homogeneous counterparts. Time reversal, which uses broadband waves and multiple sensors, has been proved to be a powerful principle to focus wave through a random medium. Usually multiple reflexions degrade the focusing ability, while time reversal takes advantage of them to increase the focusing quality. It takes advantage of all the spatio-temporal degrees of freedom of the random medium, but does not distinguish between spatial and temporal ones, which results in a focusing that is equivalent spatially and temporally [1]. The question that arises is: can one make use of temporal degrees of freedom in order to obtain spatial information, or vice versa?

We have recently shown [2] that it is indeed possible to make use of all the spatio-temporal degrees of freedom in order to increase the spatial focusing. We have demonstrated that all of them can be "converted" into spatial information, hence allowing spatial inversion, at a single time, on multiple locations using a single sensor. Based on iterations of Time Reversal we invert the field at the focusing time: we decrease the instantaneous spatial side lobes at this time using the information contained in the bandwidth. We first performed an experimental single sensor spatial inversion using ultrasound. As shown on the figure a significative gain of the side lobes level is attainable, and we do not lose too much the temporal focusing (inset). We have also experimentally verified that this concept is applicable to polarized waves and obtained the same results with microwaves.

Moreover, we analytically study the convergence of the iterative process. According to calculation, an interesting result is that the convergence gives us information about the medium. Actually, if the number of degrees of freedom is high enough it ensures the inversion feasibility. For a given number of sensors, decreasing the available bandwidth of signals (i.e., the number of temporal degrees of freedom) a minimum value is reached when the inversion no longer converges. Thus we are able to build the evolution of the statistical parameter describing the medium like its elastic mean free path.

We believe that this work will have applications within the fields of imaging, detection in scattering media, sensing techniques, and telecommunications.

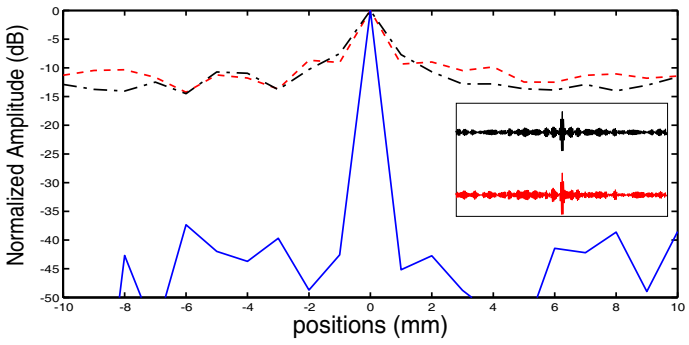

Figure 1: Focal spot obtained for Time Reversal (black dashed-dotted line) and emission of iterative signals (red dashed line) with one transducer source. The blue line represents the instantaneous spot with emission of the iterative signals. The focused pulses for TR and iterative signals emissions are represented in the inset.

REFERENCES

1. Fink, M., "Time reversed acoustics," *Physics Today*, Vol. 50, 34–40, 1997.

2. Lemoult, F., G. Lerosey, J. de Rosny, and M. Fink, "Manipulating spatiotemporal degrees of freedom of waves in random media," *Physical Review Letters*, Vol. 103, 173902, 2009.

Performance Assessment of DORT-based Methods for Microwave Breast Imaging

P. Kosmas[1] and Y. Chen[2]

[1]Division of Engineering, King's College London, Strand, London, WC2R 2LS, UK
[2]School of Electrical, Electronic and Computer Engineering, Newcastle University
Newcastle upon Tyne, NE1 7RU, UK

Abstract— The application of time reversal (TR) methods for ultra-wideband (UWB) breast cancer detection has recently been an active topic of research [1–3]. In this talk, we review and extend our work on TR breast imaging based on the decomposition of the time reversal operator (DORT). We also relate our hybrid DORT-method [3] to space-frequency TR (SF-TR) imaging, which has been proposed for subsurface sensing applications [4]. Instead of recovering the full time-domain eigenvectors, our hybrid DORT method employs temporally windowed versions of the scattered signal in the TR process . These signals encode spatial information responsible for selective focusing onto each scatterer, and can be related to the space-frequency (SF)-TR approach presented in [4]. We show that the difference in our implementation lies in the use of a Gaussian pulse as our time-domain function in SF-TR implementation rather than the signals obtained by the right eigenvectors of the SF-MDM [4]. To test our methods, we use a realistic two-dimensional (2-D) numerical breast model, and produce simulated data for TM_x polarization using the finite-difference time-domain (FDTD) algorithm, which also implements numerical backpropagation of the TR input signals. A possible application of interest is contrast-enhanced differential imaging, where the tumor signal can become available from data obtained before and after the injection of the agents [5, 6]. We investigate the use of DORT-based methods in this context for lesion detection and classification, and examine our approach's robustness to various assumptions in the simulated data. Our analysis aims to provide useful insight on the potential of applying such techniques to microwave breast imaging and similar problems.

REFERENCES

1. Kosmas, P. and C. M. Rappaport, "A matched filter FDTD-based time reversal algorithm for microwave breast cancer detection," *IEEE Trans. Antennas Propag.*, Vol. 54, No. 4, 1257–1264, Apr. 2006.
2. Chen, Y., E. Gunawan, K. S. Low, S. C. Wang, C. B. Soh, and T. C. Putti, "Time-reversal ultra-wideband breast imaging: Pulse design criteria considering multiple tumors with unknown tissue properties," *IEEE Trans. Antennas Propag.*, Vol. 56, No. 9, 3073–3077, Sep. 2008.
3. Kosmas, P., "Application of the DORT technique to FDTD-based time reversal for microwave breast cancer detection," *Proc. European Microw. Conf.*, 306–308, Munich, Oct. 2007.
4. Yavuz, M. E. and F. L. Teixeira, "Space-frequency ultrawideband time-reversal imaging," *IEEE Trans. Geosc. Remote Sens.*, Vol. 46, No. 4, 1115–1124, Apr. 2008.
5. Mashal, A., J. H. Booske, and S. C. Hagness, "Toward contrast-enhanced microwave-induced thermoacoustic imaging of breast cancer: An experimental study of the effects of microbubbles on simple thermoacoustic targets," *Phys. Med. Biol.*, Vol. 54, 641–650, 2009.
6. Shea, J. D., P. Kosmas, S. C. Hagness, and B. D. Van Veen, "Contrast-enhanced microwave imaging of breast tumors: A computational study using 3D realistic numerical phantoms," *Inverse Problems*, Vol. 26, 074009, 2010.

Session 1P5
Remote Sensing

Impact of Measurement System Characteristics on Advanced Sounder Information Content

Allen M. Larar, Xu Liu, and Daniel K. Zhou
NASA Langley Research Center, Hampton, VA, USA

Abstract— Advanced satellite sensors are tasked with improving global observations of the Earth's atmosphere, clouds, and surface to enable enhancements in weather prediction, climate monitoring capability, and environmental change detection. Achieving such an improvement in geophysical information inferred from these observations requires optimal usage of data from current systems as well as instrument system enhancements for future sensors. This presentation addresses results of tradeoff studies evaluating the impact of spectral resolution, spectral coverage, instrument noise, and a priori knowledge on remote sensing system information content, with a specific emphasis on thermodynamic state and trace species information obtainable from advanced atmospheric sounders. Particular attention will be devoted toward information achievable from the Atmospheric InfraRed Sounder (AIRS) on the NASA EOS Aqua satellite in orbit since 2002, the Infrared Atmospheric Sounding Interferometer (IASI) aboard MetOp-A since 2006, and the Cross-track Infrared Sounder (CrIS) instrument to fly aboard the NPP and JPSS series of satellites expected to begin in late 2011. While all of these systems cover nearly the same infrared spectral extent, they have very different number of channels, instrument line shapes, coverage continuity, and instrument noise. AIRS is a grating spectrometer having 2378 discrete spectral channels ranging from about 0.4 to 2.2 cm^{-1} resolution; IASI is a Michelson interferometer with 8461 uniformlyspaced spectral channels of 0.5 cm^{-1} (apodized) resolution; and CrIS is a Michelson interferometer having 1305 spectral channels of 0.625, 1.250, and 2.50 cm^{-1} (unapodized) spectral resolution, respectively, over its three continuous but non-overlapping bands. Results of tradeoff studies showing information content sensitivity to assumed measurement system characteristics will be presented.

Transmission and Total Reflection of Subhertz Electromagnetic Waves at the Earth-Atmosphere Interface

Toshiyuki Shiozawa
Department of Electronics and Information Engineering, Chubu University, Japan

Abstract— In recent years, electromagnetic signals with extremely low frequencies generated months, days, or hours before large-magnitude earthquakes have been observed here and there on the earth. Many scientists around the world have been systematically monitoring these electromagnetic phenomena and trying to correlate them to earthquakes for establishing accurate and reliable short-term earthquake predictions. Among others, the frequency range around 0.01 Hz has attracted many experts' attention. This is because in this particular frequency range, lower propagation loss for electromagnetic waves is expected and the main background noises due to geomagnetic pulsation and lightning remain at lower levels. For the purpose of providing for a theoretical background for the study of electromagnetic fields generated by precursory effects of earthquakes, the problem of transmission and total reflection at the earth-atmosphere interface is investigated in detail for a subherz plane electromagnetic wave incident from the earth's crust. The term "subhertz" means "below 1 Hertz". First, for the special case of normal incidence, the overall power transmission coefficient at the earth-atmosphere interface is found to take a maximum value at a definite frequency which is inversely proportional to the square of the depth of a virtual hypocenter. A typical value of this frequency falls around 0.01 Hz. For the general case of oblique incidence as well, this feature of the overall power transmission coefficient is retained except in the vicinity of the critical angle of incidence for the H-wave. At the critical angle of incidence, the power flow carried by a surface wave along the interface becomes anomalously large for the H-wave. However, over a wide range of angles of incidence greater than the critical angle, the power flow carried by the surface wave remains at much lower levels. Finally, the energy conservation relations for the incident, reflected, and transmitted waves at the earth-atmosphere interface are discussed. For an incident wave coming from the earth's crust, the interactive power between the incident and reflected waves plays a crucial role for the conservation of electromagnetic energy at the interface.

Active Earth Observation from Unmanned Aerial System

C. E. Lin[1], **Y.-C. Huang**[1], **Y.-H. Lai**[1], **Y.-L. Yeh**[1], **C.-C. Cheng**[2], **and C.-C. Nien**[3]

[1]Department of Aeronautics and Astronautics, National Cheng Kung University, Tainan 701, Taiwan
[2]EOL, Industrial Technology Research Institute, Chu-Tong, Hsin-Chu 310, Taiwan
[3]ISTC, Industrial Technology Research Institute, Chu-Tong, Hsin-Chu 310, Taiwan

Abstract— Earth observation may also be carried by low altitude photo acquisition using flying vehicles. The unmanned aerial system (UAS) includes unmanned aerial vehicle (UAV), flight operation and control, payloads for image acquisition, and communication for data downlink. This paper presents a UAS implementation project using high resolution camera set to capture earth images in remote operation. The high resolution camera set includes a wide angle camera and a twin camera. The wide angle camera is located in front of the UAV to guide ground search and flight control. The twin camera set is constructed inside the UAV with two lenses of 200 mm and 1000 mm (135 format equivalent) on each side of a reflecting mirror. This camera is viewed from the UAV bottom and it reflects input images in either direction of the two lenses. Their FOV (field of view) angles are 11.5° and 2.5°, respectively. The fast zoom-in mechanics turns the mirror by switching twin cameras to perform a 25 times zoom-in. The adopted UAV is remotely operated or autopilot to the targets. The earth observation is implemented from low altitude UAV flights by setting target waypoints. The proposed UAS is applied in disaster surveillance before rescue force is evolved.

Remote Sensing for Climate and Environmental Change

Diane L. Evans and Duane E. Waliser
Jet Propulsion Laboratory, California Institute of Technology, USA

Abstract— Satellite and aircraft remote sensing data from instruments spanning the electromagnetic spectrum are used to varying degrees for decision support. For example, data from infrared and microwave instruments are used operationally for weather and short-term climate forecasting (e.g., ENSO). However, their use for longer- term climate projections generally remains research rather than operationally focused. Similarly, while a variety of instruments routinely monitor the effectiveness of the Montreal protocol in regulating ozone-destroying chlorofluorocarbons, there is no operational framework in which to quantify adherence to treaties regulating greenhouse gas emissions and verifying potential offsets. Finally, many sensors are tasked for emergency response, with recent examples being the eruption of Eyjafjallaj?kull volcano in Iceland, the earthquake on the U.S./Mexican border, and the oil spill in the U.S. Gulf of Mexico. While data from these sensors is made widely available, only a small amount is used operationally.

Several current efforts are focused on creating a structured approach that will increase the use of remote sensing data for decision-making and policy development. One example is the more comprehensive use of satellite observations spanning the electromagnetic spectrum within the context of the Intergovernmental Panel on Climate Change (IPCC) Assessment Reports. Specifically, satellite-measured quantities that are analogs to variables output from climate models are being identified, sampled, formatted and web-disseminated in a manner parallel to the model outputs to facilitate their use by the IPCC model evaluation community. This effort will provide for multi-sensor evaluations and constraints of the models which in turn can be used for quantitative scoring/weighting of the models' climate projections based on their skill at representing the historical record.

A second effort is focused on the use of satellite, aircraft, and in situ measurements leading to "Greenhouse Gas Information Systems (GHGIS)", recommended by the U.S. National Academy of Science in a recent report. There are several active and passive instruments operating in the infrared currently flying and being planned to make direct measurements of carbon dioxide. These will be augmented by measurements of ocean color, land cover, biomass and carbon stocks based on visible, near infrared, lidar and synthetic aperture radar data. When combined with in situ measurements into inversion models, much more accurate monitoring of greenhouse gases will be possible.

The third effort is the development of a prototype system to provide rapid response after natural disasters, with an initial focus on earthquakes. The emphasis of this activity is to use synthetic aperture radar interferometry to determine regions of strain buildup near and along faults for improved hazard forecasts, and to identify regions of ground disturbance and destruction for use in earthquake response.

ACKNOWLEDGMENT

This work was done under contract to NASA.

Undersampled Digitally Heterodyned SFGPR with Variable Sampling Frequency

D. Adirosi[1], **G. Alberti**[2], **and G. Galiero**[2]

[1]Thales Alenia Space Italia, Italy
[2]Consortium for Research on Advanced Remote Sensing Systems — CO.RI.S.T.A., Italy

Abstract— In this paper, a new architecture of an Undersampled Digitally Heterodyned SFGPR with variable sampling frequency is presented. This design starts by the technical knowledge and on field experience achieved during the design of a SFGPR developed in the framework of the ARCHEO project; it was funded by the Italian Ministry of the scientific research and industry whose main aim was the development of tools to aid the archeoloogists in their on field researches [1].

The key aspects and the advantages of the new architecture here presented are discussed: signal generation by means of DAC; undersampling of the echoes by means of a large bandwidth ADC with a planned step by step varying sampling frequency; digital quadrature demodulation of the undersampled echoes.

The SFGPR architecture presented has not only the well known advantages of the heterodyne GPRs but also peculiar ones related to the choices made and described in this paper:

- Absence of a synchronism chain, generally used in SFGPR to get a phase reference of the transmitted signal [1];
- Simplified RF front end: both Tx and Rx chains are substantially constituted by an amplifier and a filter; this is allowed by the undersampling of the received echoes;
- Simplified Frequency Generation Unit;
- Substantial reduction of the power consumption and weight due to the great simplification brought in the RF front end;
- Flexible architecture with respect of the possible frequency bands to use. In fact the constraints on which bands to use are mainly due to DAC and ADC 3-dB bandwidths; nowadays are present on the market DACs capable to generate frequencies even in the second and third Nyquist zone as well as ADC with input bandwidth as large as 3 GHz. This allows the employment of the same SFGPR in large band of investigation frequencies and with very large synthesized bandwidth. This peculiarity of the architecture presented will be even more enhanced in the near future with the advent of integrated circuits with increased input/output banwidths as the trend of the last years has indicated.

The achievement of the mentioned goals has been possible by moving SFGPR complexities from the analog domain into the digital one.

The digital section implemented in the FPGA includes a synchronism detector circuit also. In fact because the sampling frequencies are different between them and they are not integer multiple of the FPGA reference clock frequency, it is necessary a circuit that determine when both are phase alligned. Because the characteristic of the FGU is to generate the clocks of the ADC, DAC and FPGA reference clock in a phase locked way and because they are integer multiple of the same reference clock (a very low phase noise master oscillator), it is possible to recover the phase reference in each frequency step by means of the calibration phase usually performed in GPR.

The mentioned synchronism detector circuit has been designed by starting from phase detector circuits of digital PLLs [3] and adapted to the needs of the presented architecture. The design has been made in VHDL and simulations have been performed in order to test its behaviour by means of standard VHDL simulation tools. Main results of these simulations will be presented.

As explained before, the knowledge of the sampling frequencies to use as well as the frequencies to be generated in each step must be known in advance to correctly program both the FGU and the digital local oscillator of the quadrature downconverter. A software tool has been developped in order to perform automatically such choice once the input parameters (step frequency, first frequency to generate, number of steps, ...) are provided.

The whole post-processing chain, from the undersampling of the step frequencies to their quadrature demodulation and processing to synthesize simulated target has been performed by developing an ad hoc simulator in a high level language (LabView^{TM}). This simulator use as input the data generated by the mentioned frequency planner. The main results of this simulator are reported. These results show that the architecture proposed performs as foreseen.

REFERENCES

1. Alberti, G., L. Ciofaniello, G. Galiero, R. Persico, and M. Sacchettino, "An Italian experience on stepped frequency GPR," *PIERS Proceedings*, Pisa, Italy, March 28–31, 2004.
2. Noon, D. A., "Stepped-frequency radar design and signal processing enhances ground penetrating radar performance," Ph.D. Thesis, Department of Electrical & Computer Engineering, University of Queensland, Australia, 1996.
3. Best, R. E., *Phase-locked Loops: Design, Simulation and Aplications*, McGraw-Hill Professional, 2007.

Advanced Tools for Leak Detection in the Urban Water Distribution Networks

Giancarlo Prisco[1], **Michele D'Urso**[1], **Gabriella Bernardi**[1], **Gabriella Bernardi**[2], **and Fulvio Schettino**[3]

[1]Innovation Team, Intangible Capital Directorate Managment, SELEX Sistemi Integrati S.p.A.
Via Circumvallazione Esterna, Loc. Pontericci Zona ASI, I-80014 Giugliano, Napoli, Italy
[2]Laboratorio di Ingegneria delle Acque, Università degli Studi di Cassino
Via G. di Biasio, 43, 03043 Cassino, Frosinone, Italy
[3]Dipartimento di Automazione, Elettromagnetismo, Ingegneria dell'Informazione e Matematica Industriale
Università degli Studi di Cassino, Via G. di Biasio, 43, 03043 Cassino, Frosinone, Italy

Abstract— This paper focuses on the leakage detection of the *urban water distribution networks*, that is the portion of the water distribution system, underlying the urban streets that provides the water to the community. Since from the earliest water distribution systems were built, the control of water losses has represented a critical and crucial point for the water system administrators. In particular, the lost of a significant percentage of water, due to the leakage from the distribution pipes, requires to the operators a cost expensive system maintenance, causing a rise in the service prices for the end-users. As an example, in Italy the lost percentage is around 40%, and the majority of the services are over 50 years old and unmapped. There is, therefore, a growing demand for improved utility mapping, characterization and monitoring technologies. A particular interest is turned to non-invasive techniques, the best candidates to realize cost-effective and flexible investigation tools. Actually, leaks are detected by using acoustic equipment [1]. These ones are considered to be satisfactory for metallic pipes; for plastic pipes, instead, (whose use is always increasing in the water distribution systems) its effectiveness has not at all been demonstrated. In each case such a method allows to obtain an accurate result only when a very large leak is present, due to the intrinsic limitations on the achievable sensitivity and resolution. For this reason a growing attention is paid to non-invasive electromagnetic techniques, like Ground Penetrating Radar (GPR) [2]. However, standard GPR techniques are strongly dependent on the interpretation of the collected data, that can be affected by the lack of information about the investigated structure; as a consequence, innovative model based data processing techniques are required such that the results can be uniquely interpreted [3].

Aim of this contribution is to provide reliable processing tools that can make quick and easy the interpretation of the GPR collected data as applied to the location of the services, to the leak detection, its shape reconstruction and its spatial evolution prediction. It is worth to note that a small percentage of the leaks is physiological in a distribution system; this means that the intervention is necessary when the leak is already significant and when the leak is rapidly expanding. Therefore, besides locating the leak, it is very important to evaluate its entity and its evolution.

The proposed tool uses a data acquisition scheme like GPR and an imaging algorithm, based on Compressed Sensing (CS) [4], that also takes into account the actual Tx/Rx system by performing a full-wave numerical evaluation of its radiating properties, thus including coupling effects.

The developed tools and algorithms have been tested on experimental data, in different controlled scenarios with appropriate instruments, developed in the laboratory of water engineering (LIA) of University of Cassino. In particular, the presented processing procedures detect and characterize the leaks in different types of soil, both homogeneous and stratified (typical of realistic scenarios), in different conditions of moistures. Concerning the test instrumentation, an array of two antennas at 2 GHz provided by IDS — Ingegneria dei Sistemi S.p.A., Pisa, Italy has been used to perform both monostatic and bistatic acquisitions.

REFERENCES

1. http://www.subsurfaceleak.com.
2. Hunaidi, O. and P. Giamou, "Ground Penetrating Radar for detection of leaks in buried plastic water distribution pipes," *Seventh International Conference on Ground-penetrating Radar*, 783–786, Lawrence, Kansas, 1998.
3. Crocco, L., G. Prisco, F. Soldovieri, and N. J. Cassidy, "Early-stage leaking pipes GPR monitoring via microwave tomographic inversion," *Journal of Applied Geophysics*, Vol. 67, No. 4, 270–277, April 2009.

4. Donoho, D. L., "Compressed sensing," *IEEE Transactions on Information Theory*, Vol. 52, No. 4, 1289–1306, April 2006.

Mapping Snow Cover with X-band Cosmo-Skymed SAR

S. Pettinato[1], **E. Santi**[1], **M. Brogioni**[1], **G. Macelloni**[1], **S. Paloscia**[1], **P. Pampaloni**[1], **and Chuan Xiong**[2]

[1]Institute of Applied Physics, IFAC, CNR
Via Madonna del Piano 10, Sesto Fiorentino, Firenze 50019, Italy
[2]Institute for Remote Sensing Applications, Beijing, China

Abstract— Production of snow cover maps is very important in the study of global changes, in water resource management, as well as in flood and avalanche risk prevention. The potential of radar systems in mapping the extent of wet snow has been demonstrated in several works. However, the effect of dry snow on the backscattering of the C- band satellite SARs is too small to reliably detect dry snow cover, and the estimation of SWE with the present available satellite SAR systems is still a challenge. With the launch of the new X band SAR systems (Cosmo-Skymed and TerraSAR-X) some improvements are expected; the aim oth this paper is to evaluate the potential of these SAR sensors, and Cosmo-Skymed in particular, in providing information on snow cover in different physical conditions. The Cosmo-Skymed project includes four satellites equipped with SAR. The system was mostly designed to enhance the monitoring and management of environmental hazards, but it also addresses scientific and commercial applications. A significant characteristic of the constellation is that, utilizing more satellites, the scene can be almost simultaneously observed at different polarization and incidence angle.

The study has been performed in two phases:

- First of all a classical approach used at C-band and based on a change detection analysis was extended to X-band images. A temporal sequence of COSMO SAR images was studied by comparing the backscattering of specific sub-areas of interest with in-situ snow and meteo data, and with model simulations. As for C-band images both experimental data and model simulations showed a clear decrease in backscattering as snow melted. The multi-temporal analysis of SAR images, combined with some auxiliary information on the topography of the area and the air vertical temperature, made it possible generate snow cover maps. This approach was validated with snow data collected on the Cordevole watershed in North Italy.
- In the second phase the sensitivity of X-band backscattering, measured at different polarizations and incidence angles, to dry snow was exploited by means of a theoretical model based on the Dense Medium Radiative Transfer Theory (DMRT). Several configurations of dry snow-pack with different values of depth, density, and crystal dimension were tested. Simulations showed that an appreciable sensitivity of X-band backscattering to dry snow can be found for Snow Water Equivalent higher than 70–100 mm and relatively high values of snow density and crystal dimensions. On the basis of these encouraging results a retrieval algorithm based on a Neural Network was implemented and tested with experimental data collected on Cordevole.

Neural Network Adaptive Algorithm Applied to High Resolution C-band SAR Images for Soil Moisture Retrieval in Bare and Vegetated Areas

C. Notarnicola[1], **E. Santi**[2], **M. Brogioni**[2], **S. Paloscia**[2], **S. Pettinato**[2], **G. Preziosa**[3], **and B. Ventura**[3]

[1]Institute for Applied Remote Sensing, EURAC, Viale Druso 1, Bolzano, Italy
[2]CNR-IFAC, Via Madonna del Piano 10, Florence 50019, Italy
[3]Dipartimento Interateneo di Fisica, Via Amendola 173, Bari, Italy

Abstract— This paper presents the application of an innovative approach for the detection of soil moisture from high resolution SAR images. One of the main drawbacks of the existing algorithms for soil moisture retrieval from high resolution satellite data is that they cannot be easily extended to areas where they have not been calibrated and validated.

In order to overcome these limitations and understand the effect of the different environmental and seasonal conditions on the SAR measurements, extensive sets of ENVISAT/ASAR images have been collected along with the related ground truth and analyzed on three areas characterized by very different surface features.

The first area is characterized by long periods of drought and high vulnerability to fire and placed in the outskirts of Matera town in Southern Italy. The area is mainly covered by agricultural fields devoted to wheat cultivation. The second area is a fairly large plateau in at the top of Mount Cherz (2000 m asl), free of forests, mainly covered by grassland, located in the middle of the Cordevole watershed at the foothill of Mount Sella in Northern Italy (Veneto region). It was selected because of its relatively smooth topography and availability of historical and topographic data. The third area is located in the Scrivia basin, a flat agricultural area close to Alessandria, in northern Italy. It is a flat alluvial plain measuring about 300 km^2 and situated close to the confluence of the Scrivia and Po rivers. This area is characterized by large, homogeneous agricultural fields of wheat, alfalfa, fodder crops, corn, and sugarbeet.

From a preliminary analysis, the comparison of the backscattering coefficients in dependence of soil moisture values for all the analyzed datasets indicates the same sensitivity to soil moisture variations but with different biases, which may depend on soil characteristics, vegetation presence and roughness effect. A further comparison with historical data collected on bare soils with comparable roughness at the same frequency, polarization and incidence angle, confirmed that the different surface features affect the bias of the relationship, while the backscattering sensitivity to the SMC remains quite constant.

These different bias values have been used to introduce an adaptive term in the electromagnetic formulation of the backscattering responses from natural bare surfaces, in the formulation of the Advanced Integral Equation Model (AIEM). The simulated data from this new model have been then used to train a neural network to be used then as an inversion algorithm.

The paper will present the results from this new technique and compare them to neural network and Bayesian algorithms outputs trained on one area and then tested on the other one.

Forward Models and Retrieval of Soil Moisture of Radar Remote Sensing of Bare Soil at L Band Based on 3D Numerical Simulations of Maxwell Equations Using both Like Polarization and Cross Polarization

Xiaolan Xu[1], **Tien-Hao Liao**[1], **Leung Tsang**[1], **Shaowu Huang**[1], **J. C. Shi**[2], **and Kuan Shan Chen**[3]

[1]Department of Electrical Engineering, University of Washington
185 Stevens Way, Seattle, WA 98195-2500, USA
[2]Institute for Computational Earth System Science, University of California
6808 Ellison Hall, Santa Barbara, CA 93106, USA
[3]Center for Space and Remote Sensing Research, National Central University, Chung-Li, Taiwan

Abstract— The NASA Soil Moisture Active/Passive (SMAP) Mission at L band will enable the mapping of soil moisture with unprecedented resolution. The SMAP is a combined active and passive sensor with 40° incident angle. For the radar sensors, there will be three measurements at 1.26 GHz, VV, HH and VH. Thus both co-polarization and cross polarization measurements will be made. In this paper, we study the forward models of these 3 signatures from bare soils using numerical methods of 3D simulations of Maxwell Equations. For bare soil, assuming exponential correlation functions, there are 3 parameters, the soil moisture, the rms heights and the correlation lengths. The retrieval algorithm has been studied by making use of all three measurements.

In studying backscattering from soil surfaces, empirical formulas of Dubois's method, Oh's method and analytical models of the AIEM model were used. Dubois and AIEM only have co-polarization results. In 3D simulations, the height function $z = f(x, y)$ of the rough surface varies in both horizontal directions. Fast computation methods have been developed, including the Sparse Matrix Canonical Grid (SMCG) method the Physical Based Two Grid (PBTG) method and the multilevel UV method. Recently, with computation resources and the UV/PBTG/SMCG method, the UW Group computed a total of close to 200 cases for incidence angle equal to 40 degrees and by varying rms height, correlation lengths and soil permittivity Both co-polarizations and cross polarizations were computed. The area was up to 32 by 32 square wavelengths. Since the maximum rms height calculated was 0.21 wavelength ($kh = 1.32$ which is about 5 cm at L band), thus the cases covered and the interpolations used can be applied to cover a wide range of interests for SMAP. In this paper, we make detailed comparisons of backscattering scattering from bare soils of analytical models of AIEM, and 3D numerical simulations of Maxwell equations. We also make comparisons with Oh et al. truck mounted experiments.

In soil moisture retrieval, we made a comparison between the Oh's method, Dubois Method, Kim's method and Shi's method using Michigan data. All these methods are based on inversion of parameters using 2 measurements to retrieval 2 parameters. In this paper, we study the retrieval algorithm using the 3 to 3 inverse problem of rms heights, correlation and soil moisture to VV, HH and VH. We first validate the retrieval algorithm using the Michigan data. Next, we use NMM3D to generate a set of testing data which contains large combination of rms height and testing data to validate the 3 to 3 retrieval algorithm. We show the performance of the 3 to 3 algorithm using these test data from NMM3D.

Using of Multi-angular Radiometric Measurements for Short Wind Wave Parameters Estimate

M. N. Pospelov, **A. V. Kuzmin**, **and I. N. Sadovsky**
Space Research Institute, Russia

Abstract— Short gravity and gravity-capillary waves play very important role in ocean-atmosphere interaction affecting momentum exchange through wind waves generation and dissipation. At the same time, short waves affect the electromagnetic waves emission and scattering from a sea surface, and this effect is used in satellite radiometers and scatterometers for remote measurements of winds over ocean. The relations between wind, waves and emitted/scattered signal are extremely complicated and can hardly be described unambiguously by any theoretical model. Therefore experimental measurements of the ocean-atmosphere interaction parameters under various meteorological conditions are of high importance.

The paper presents the results of the experimental measurements performed on an offshore oceanographic platform in the Black Sea in June 2005. The experiment aimed on investigations of air-sea interaction by means of direct and remote measurements was carried out in framework of the INTAS project "Combined Active/Passive Microwave Measurements of Wind Waves for Global Ocean Salinity Monitoring (CAPMOS)". The project united experienced research teams from Russia, Ukraine and Italy.

A specialized research platform managed by the Marine Hydrophysical Institute provided a unique opportunity of long-term measurements of sea and atmosphere parameters using remote and contact sensors. The following remote sensors were used: Ku-band scatterometer (polarizations VV, HH or cross); L-band radiometer; S-band radiometer (V-pol.); K-band radiometer (3 Stokes parameters); Ka-band radiometer (3 Stokes parameters); W-band radiometer (V- and H-pol.); IR-radiometer (8–12 mkm); optical digital camera. List of contact sensors for atmosphere and sea parameters measurements included: three 3-component sonic anemometers at 1.5, 4 and 21 meters above the surface; air pressure and humidity sensors; three air temperature sensors; water vapor and carbon dioxide sensor; 6-strings wave gauge; two CTDs; five current meters at a depth of 3, 5, 10, 15 and 10 meters; water turbulence sensor.

The measurements on a platform were carried during June 1–20 round a clock. The weather conditions during the experiment were favorable for the measurements. The mean wind speed ranged from 0 to 13 m/s; two episodes of high wind speeds were observed, with gusts well above 20 m/s.

The parameters of gravity wave spectrum were measured by a wave gauge. The curvature spectrum of gravity-capillary waves and gravity waves slope variance were retrieved from remote radiometric measurements using an original algorithm developed recently. The dynamics of short surface waves at different bands of spectrum under the conditions of variable winds was investigated. It was found that short gravity-capillary waves are the most sensitive to the wind velocity variations. This assumption was supported by both remote sensing and traditional means.

ACKNOWLEDGMENT

The study was supported by INTAS Grant 03-51-4789 and RFBR Grant 09-02-00780.

Performance Improvement of OFDM UWB Synthetic Aperture Radar

I. Elshafiey[1], **A. Hossain**[1], **M. Elnamaky**[1], **A. Mabrouk**[2], **M. A. Alkanhal**[1], **A. Sheta**[1], **A. Alsanie**[1], **and A. Alsuwailem**[1]

[1]Electrical Engineering Department, Prince Sultan Advanced Technologies Research Institute (PSATRI)
King Saud University, Riyadh 11421, P. O. Box 800, Saudi Arabia
[2]Computer Science Department, KICT, International Islamic University
Kuala Lumpur 50728, P. O. Box 10, Malaysia

Abstract— Synthetic aperture radar (SAR) techniques have been used in various civilian and military applications to obtain detailed information about particular targets. Challenges that arise to such systems include the continuous search for increasing the imaging resolution and improving the system ability to cancel interference signals. Recent technology advances allow rapid progress of some of the SAR concepts. For example, ultra-wideband (UWB) techniques are suggested to enhance the imaging resolution. Waveform shaping using Orthogonal Frequency Division Multiplexing (OFDM) algorithms is proposed to enhance the anti-jamming capabilities of SAR systems. OFDM implementation also allows the design of SAR systems that operate in multi-function radar/communication scenario. In UWB-OFDM SAR system, the signal is originally created as random numbers representing the OFDM sub-bands in the frequency domain. The digital time domain signal is obtained using an IFFT block which can be implemented using a Field Programmable Gate Arrays (FPGAs). The discrete time domain signal is then transformed into an analog signal that is heterodyned to obtain the continuous time domain RF signal, which is amplified and finally transmitted through a UWB antenna. Reflected signal is received by another UWB antenna and then amplified by a low noise amplifier. The signal is transformed to baseband and digitized to obtain one row of the SAR raw data matrix.

The objective of this paper is to introduce an adaptive SAR system based on UWB-OFDM architecture for three different scenarios: high resolution imaging for friendly environment, anti-jamming proficient for hostile environment and bandwidth adaptive for multi-function system. A tool is developed to analyze the performance of SAR systems. Computational modeling is performed for different scenarios of system operation. Performance of multi-function radar/communication system is investigated. Adaptive techniques are suggested to automate the optimization process of system parameters in accordance to the operation environment. The paper also addresses one of the common challenges to UWB SAR algorithms in terms of their need for huge computational complexity. Investigation is performed of the SPECAN SAR algorithm under FPGA environment. Results are presented of analysis of this algorithm under FPGA Viertex-6 platform.

ACKNOWLEDGMENT

This research is funded by *The National Plan for Science & Technology* under project No. 08-ELE262-2.

Glacier Parameters Estimation and Snow Classification Integrated nterferometric and Polarimetric SAR

Zhen Li, **Jianmin Zhou**, **Ping Zhang**, **Bangsen Tian**, **and Ding Shen**
Center for Earth Observation and Digital Earth, Chinese Academy of Sciences
Post Box 9718, Beijing 100101, China

Abstract— Snow and glacier are sensitive indicators of climate fluctuations. The effects of climate warming are for instance evident in the continuous retreat of glaciers and decrease of snow area. In the paper, methods of snow classification, snow line identification and moving velocity for glacier are presented integrated interferometric and polarimetric SAR from ALOS/PALSAR and RadarSat/SAR data in the Qinhai-Tibetan Plateau. Utilizing repeat two-pass D-InSAR approach, with an external DEM, we extracted the motion of the glacier surface. The amount of "glacier surface" decorrelation is increased by the longer spatial baseline of the interferometric pair, the longer time separation of the SAR images acquisition, more complex terrain, and more noise sources. The longer wavelength SAR data (ALOS L-band) are better to avoid decorrelation phenomenon. Also, SAR interferometry is used to obtain the coherence coefficients. The coherence coefficients can be used to classify the glacier from background.

The movement parameter of the Dongkemadi glacier is resolved using a 46 day-separation ALOS InSAR pair acquired from ascending orbit at Dec. 10, 2007 and Jan. 25, 2008 in the Dongkemadi Glacier (33.08N, 92.09E) in Qinghai-Tibet Plateau. The snow and ice classification are carried out integrated full polarization RADARSAT-2 SAR imagery at same area in Aug. 30, 2009.

With combination interferometric parameters and polarimetric parameters from SAR targets decomposition, several classification method were compared, which are the decision tree method, SVM (Support Vector Machine) classifier, maximum likelihood classifier, minimum distance classifier and Wishart classifier. From the classification map at the end of melt season, the snow line at glacier area can be identification. Polarimetric and interferometric coherence data are complementary in classification. The combination of the two kind data gets very high classification accuracy in glacial areas. It's an effective way to identify the snow line on glaciers in later summer using new SAR data.

Development of Circularly Polarized Synthetic Aperture Radar (CP-SAR) Onboard Small Satellite

Josaphat Tetuko Sri Sumantyo
Center for Environmental Remote Sensing, Chiba University
1-33, Yayoi-cho, Inage-ku, Chiba-shi 263-8522, Japan

Abstract— Synthetic Aperture Radar (SAR) is a multipurpose sensor that can be operated in all-weather and day-night time. Conventionally, the SAR sensor has been operated in linear polarization with limited retrieved information. In this research, we are developing Circularly Polarized Synthetic Aperture Radar (CP-SAR) onboard small satellite to retrieve the physical information of Earth surface. Comparing to linear polarized systems, the CP-SAR sensor has the advantage of compactness and low power requirement, since the transmission of CP microwave is not affected by the Faraday rotation effect in the ionosphere. In this paper, the CP-SAR onboard UAV is also introduced.

Session 1P6a
Advances in Nano-antennas

Nano Particles, Wires and Helical Wires for Sub-wavelength Energy Transport

Ergun Simsek and Can Boran Akdal
Bahcesehir University, Istanbul, Turkey

Abstract— It has been shown both theoretically and experimentally that the light can be coupled to metallic nano structures and transferred from one point to another based on the surface plasmon phenomenon [1]. An important outcome of this phenomenon is that using structures with dimensions much less than the wavelength allows us to beat the diffraction and miniaturize plasmonic/photonic devices. This is why there has been an enormous amount of interest in plasmonic waveguides and optical antennas in the last two decades. The ultimate goal of these studies is designing such structures that guide the light towards a specific direction as efficiently as possible and the main focus of this partly theoretical — partly numerical work is to answer a very basic question: which one is better to transport and confine the energy: nano particle chains (NPCs), nano wires (NWs) or nano helical wires (NHWs)?

Theoretically obtained dispersion relation [2] of a plasmonic waveguide consisting periodically aligned gold nano cylinders embedded on top of an indium tin oxide coated glass slide agreed well with the experimental result presented in [3]. Even though the coupled dipole approximation (CDA) based theoretical models can predict the propagation length of the resonance surface plasmon modes, there has been no experimental evidence supporting these theoretical predictions [4, 5]. The main reason behind lacking of experimental evidence is the difficulty of measuring power in nano scale. This is why we study the propagation length of NPCs, NWs and NHWs and their ability for sub-wavelength energy transfer as follows.

We assume a perfectly electrical conductor (PEC) wall with a width of $\lambda/10$ on the xy-plane and open a cylindrical hole along the z-axis at the center with a radius of $\lambda/4$. We first numerically demonstrate the diffraction limit, such that the incident plane electromagnetic (EM) wave cannot pass through the other side. Then we place a gold NPC along the z-axis. The main motivation of placing a NPC chain through a cavity is to numerically proof the sub-wavelength energy transport. It should be also noted that PEC wall is preferred to a metallic wall in order to prevent secondary plasmonic effects of the wall itself. By optimizing the size, material type and inter-particle spacing, we achieve to demonstrate the sub-wavelength energy transport with $10\,\mathrm{dB}/\mu\mathrm{m}$ loss in the visible. Note that this result is close to the prediction of the finite CDA theory [2, 4] but much less than the prediction of [5]. At the conference, we will discuss/explain the possible reasons for this dramatic difference.

In the second part of our study, we replace NPC with metal NWs and NHWs and compare their power transfer and field confinement capabilities. We will present some interesting results (for example, single or multiple NW arrangements can provide more efficient energy transfer and stronger confinement than NPCs) and discuss their performance (gain, directivity, bandwidth, etc.) under different illuminations.

REFERENCES

1. Brongersma, M. L., J. W. Hartman, and H. A. Atwater, "Electromagnetic energy transfer and switching in nanoparticle chain arrays below the diffraction limit," *Phys. Rev. B*, Vol. 62, No. 24, R16356–R16359, 2000.
2. Simsek, E., "Full analytical model for obtaining surface plasmon resonance modes of metal nanoparticle structures embedded in layered media," *Opt. Express*, Vol. 18, No. 2, 1722–1733, 2010.
3. Crozier, K., E. Togan, E. Simsek, and T. Yang, "Experimental measurement of the dispersion relations of the surface plasmon modes of metal nanoparticle chains," *Opt. Express*, Vol. 16, 13070, 2008.
4. Weber, W. H. and G. W. Ford, "Propagation of optical excitations by dipolar interactions in metal nanoparticle chains," *Phys. Rev. B*, Vol. 70, No. 12, 125429, 2004.
5. Koenderink, A. F. and A. Polman, "Complex response and polariton-like dispersion splitting in periodic metal nanoparticle chains," *Phys. Rev. B*, Vol. 74, No. 3, 033402, 2006.

Optical Nanoantennas: Correlative Electron Beam and Optical Spectroscopies and Design of a Broadband Response

Stefan A. Maier[1], **Ai Leen Koh**[1], **Dave McComb**[1], **and Joel Yang Kwang Wei**[2]

[1]Imperial College London, London SW7 2AZ, UK
[2]IMRE A*Star, Singapore

Abstract— The optical response of a metallic nanoantenna is determined by the interplay between the intrinsic bright and dark plasmon modes supported. A complete characterization hence requires a means to excite dark modes, which do not couple efficiently to far-field optical radiation. We demonstrate that electron energy loss spectroscopy (EELS) is a powerful tool allowing the complete determination of the plasmonic mode spectrum, with nanometre-scale spatial resolution facilitated by the scanning electron beam. Correlations with optical measurements and full-field electrodynamic simulations will be presented for a variety of top-down fabricated nanoantennas supported by ultrathin silicon nitride membranes, as well as for colloidal assemblies based on core/shell structures. A particular focus will lie on different nanofabrication strategies suitable for use with the thin substrates (30–50 nm thickness) required for EELS investigations. Furthermore, we present a comparison of the experimentally acquired data with numerical simulations based on calculations of both optical extinction and electron energy loss. Additionally, the influence of dark modes on the emission properties of nearby single emitters will be discussed.

Finally, we will outline a new strategy for the design of optical nanoantennas showing a broadband optical response while maintaining sub-wavelength size, based on the tools of transformation optics.

Directional Control of Field Enhancement by Two Strongly Coupled Nanoantennas

A. Locatelli and C. De Angelis
Dipartimento di Ingegneria dell'Informazione, Università degli Studi di Brescia, Brescia, Italy

Abstract— The field of optical antennas is one of the hottest research topics nowadays, with a large variety of applications (ranging from microscopy to dense data storage) that could benefit from the possibility to confine light at the nanoscale well beyond the diffraction limit [1].

In this context, the capability to shape the radiation pattern in order to tailor the interaction between nanoantennas and the surrounding objects will definitely be an important tool for designers of plasmonic circuits. Nevertheless, up to now the scientific community has mainly focused the attention on the analysis of simple wire antennas, such as the optical dipole [2], which are characterized by an omnidirectional radiation pattern. The optical version of the well known Yagi-Uda antenna has also been studied [3], and a strong analogy between the behavior of this structure at radio frequency and at optical frequencies was demonstrated. Anyway, conventional Yagi-Uda antennas are quite complicated structures that require the usage of many elements to achieve an appreciable boost of directivity [4], with a corresponding increase of the occupied space.

In this work, we analyze the radiative properties of two strongly coupled nanoantennas. One of the two nanorods hosts a feeding gap region, whereas the other one is placed in the near-field with the goal of increasing the front-to-back ratio (defined as the ratio between field enhancement in the feed-gap achievable by launching light from opposite directions) of the whole system. We demonstrate that this simple arrangement permits to obtain a tremendous increase of directionality with respect to a single dipole. Moreover, we show that surface integral equations for coupled nanorods and theory of antenna arrays can be used in order to predict the behavior of the two-element array in a straightforward way.

REFERENCES

1. Bharadwaj, P., B. Deutsch, and L. Novotny, "Optical antennas," *Advances Optics Photon.*, Vol. 1, No. 3, 438–483, 2009.
2. Novotny, L., "Effective wavelength scaling for optical antennas," *Phys. Rev. Lett.*, Vol. 98, No. 26, 266802(1–4), 2007.
3. Kosako, T., Y. Kadoya, and H. F. Hofmann, "Directional control of light by a nano-optical Yagi-Uda antenna," *Nature Photon.*, Vol. 4, No. 5, 312–315, 2010.
4. Balanis, C. A., *Antenna Theory: Analysis and Design*, Wiley, New York, 2005.

Spin-orbit Coupling of Light in Surface Plasmonic Cross Nano-antennas

A. C. T. Thijssen[1,2], **M. J. Cryan**[2], **M. Klemm**[2], **M. R. Dennis**[1], **J. B. Götte**[1], **J. G. Rarity**[1], **J. L. O'Brien**[1,2], **and R. Oulton**[1,2]

[1]Department of Electrical and Electronic Engineering, University of Bristol
Woodland Road, Bristol, BS8 1UB, UK
[2]H.H. Wills Physics Laboratory, Tyndall Avenue, BS8 1TL, UK

Abstract— We report the first simulation of spin-orbit coupling of light in the far-field of a dipole emitter in photonic structure. A linearly-polarized dipole emitter in the feedgap of a cross-shaped plasmonic nano-antenna gives rise to a longitudinal optical vortex in the far-field.

Circular polarized light is used for many applications, including electron spin manipulation for quantum dot memories and nano-magnetic data storage. Many of these applications require focusing of the beam onto a small area and therefore require photonic nanostructures. However, the paraxial ray approximation on which circular polarization is based becomes invalid in nanophotonics. It is only recently that spin-orbit angular momentum coupling was observed in free-space optics [2], and almost no studies have been made of circular polarization and angular momentum of emitters in photonic structures.

Here, we study spin to orbital angular momentum coupling in a nano-antenna. FDTD simulations are used to analyze a plasmonic cross-antenna as presented in [1]. The two vertical nano-rods of the antenna differ by a quarter plasmon wavelength, generating a phase delay between the x and y components of the electric field, which converts a linearly-polarized plane wave into a circularly polarized near field spot.

Here we study the complimentary case. A linearly-polarized dipole is inserted into the feedgap, and we examine the far-field. Naively, one expects the far-field to be circularly-polarized in this case. What we find, however, is while that the E_x and E_y fields are out of phase by 90° in the far-field as expected, an E_z component of the same order of magnitude also exists. This component has a ring-shaped intensity, and a phase vortex consistent with an orbital angular momentum description. This result implies that the polarization behavior of dipole emitters in photonic structures requires a new formalism that goes beyond the simple paraxial approximation.

Such considerations become important for a quantum interface between single electron qubits and single photon qubits in photonic structures. Although the total angular momentum will be conserved in the system, the Poincare and Bloch sphere representations of light and spin do not have a one-to-one equivalence in this case, and a different formalism needs to be found.

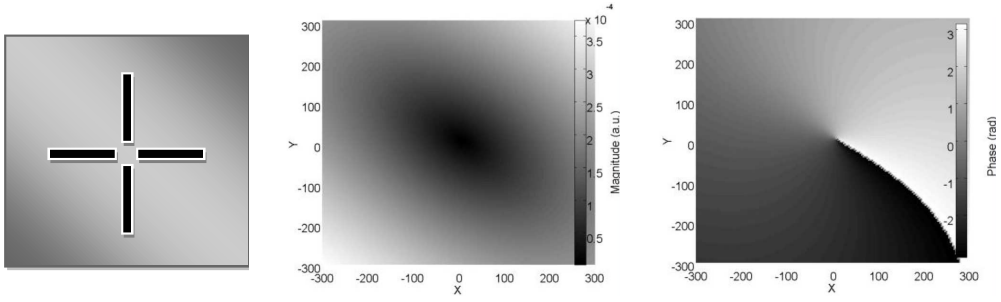

(a) (b) (c)

Figure 1: (a) Cross-shaped gold nanoantenna, (b) Magnitude and (c) Phase of the E_z component 1 µm above the antenna. Note phase singularity in the centre and phase discontinuity of 2π.

REFERENCES

1. Öğüt, E., G. Kiziltaş, and K. Şendur, *Appl. Phys. B*, Vol. 99, 1, 2010.
2. Nieminen, T. A., A. B. Stilgoe, N. R. Heckenberg, and H. Rubinsztein-Dunlop, *J. Opt. A: Pure Appl. Opt.*, Vol. 10, 115005, 2008.

Coherent Excitation of Single Emitters with Optical Antennas and Ultrashort Laser Pulses

Xue-Wen Chen[1], **Amir Baradaran Ghasemi**[1, 2], **Vahid Sandoghdar**[1], **and Mario Agio**[1]

[1]Laboratory of Physical Chemistry, ETH Zurich, Zurich 8093, Switzerland
[2]Laser and Plasma Research Institute, Shahid Beheshti University, Teheran 63113, Iran

Abstract— The enhancement of light emission with metal nanostructures has gained considerable attention in the recent years across a broad range of areas from biophotonics to quantum optics. Under continuous weak excitation, it is well established that the fluorescence signal is proportional to the field intensity and to the apparent quantum yield. The latter accounts for the competition between the radiative and non-radiative decay rates, which are strongly modified by the presence of an optical antenna. Extensive investigations have shown that huge field enhancements can coexist with large quantum efficiencies, making these systems appealing for quantum optical applications and single-molecule spectroscopy. On the other hand, time-resolved techniques, such as pump-probe spectroscopy, coherent control and triggering single-photon sources, to mention a few, rely on (ultrafast) pulsed excitation. The immediate question that arises is thus how an optical antenna affects the response of a molecule under laser pulses of various widths, at room and cryogenic temperatures. Here the important points of concern are the competition between decay times, dephasing and pulse width, the increased interaction strength due to field enhancements, and the dispersion occurring when the pulse duration becomes comparable with the lifetime of the antenna resonance. We have performed a detailed analysis of these phenomena and found that pulsed excitation discloses new challenges and opportunities for optical antennas. We present our findings in a context that ties ultrafast nano-optics with quantum-optics.

Travelling-wave Directional Optical Nanoantennas Integrated with Plasmonic Waveguides

M. Klemm
Department of Electrical and Electronic Engineering, University of Bristol
Woodland Road, Bristol, BS8 1UB, United Kingdom

Abstract— Optical nanoantennas are emerging as one of the key components in the future nanophotonic and plasmonic circuits. The first optical nano-antennas were in a form of simple spherical nanoparticles. Currently more complex Uda-Yagi nanoantenna structures were demonstrated [1, 2]. These nanoantennas enhance radiation of single emitters and provide well defined directional radiation. However unlike at the RF/microwave frequencies, these directional nanoantennas were excited either by near-field coupling of the dipole source (quantum dot in [1]) or by far-field laser radiation [2]. In this contribution we present the novel design of the directional nanoantenna, which is excited from the propagating mode of the plasmonic waveguide. The nanoantenna design is based on the *traveling wave* principle, well known at RF/microwave frequencies. By properly designing the propagating parts of the nanoantenna, a very efficient coupling to free space wave impedance can be achieved. Radiation efficiency achieved is better than 80%. Furthermore, the control over the radiation direction and beam width is relatively easy with this nanoantenna. Finally, for the nanoantenna on the high index material (e.g., glass) we will present a strategy for modifying the basic design in order to achieve a directional radiation into the low index material.

REFERENCES

1. Curto, A. G., G. Volpe, T. H. Taminiau, M. P. Kreuzer, R. Quidant, and N. F. van Hulst, "Unidirectional emission of a quantum dot coupled to a nanoantenna," *Science*, Vol. 329, No. 5994, 930–933, August 20, 2010.
2. Kosako, T., Y. Kadoya, and H. F. Hofmann, "Directional control of light by a nano-optical Yagi-Uda antenna," *Nature Photonics*, Vol. 4, 312–315, 2010.

Field-enhancement and Control in Optical Nanoantennas

Javier Aizpurua[1], **Aitzol Garcia-Etxarri**[1], **Nicolas Large**[1], **Martin Schnell**[2], **Martina Abb**[3], **Otto L. Muskens**[3], **and Rainer Hillenbrand**[2, 4]

[1]Center for Materials Physics CSIC-UPV/EHU and DIPC, Donostia-San Sebastin 20018, Spain
[2]CIC NanoGUNE CONSOLIDER, Donostia-San Sebastián 20018, Spain
[3]School of Physics and Astronomy, University of Southampton, SO17, 1BJ, United Kingdom
[4]IKERBASQUE, Basque Foundation for Science, Bilbao 48011, Spain

Abstract— Similar to their radiowave counterpartners, linear $\lambda/2$ optical and infrared nanoantennas show the capability to tune their electromagnetic response when the impedance loading at the antenna nanogap is modified using a dielectric or metallic medium. We show this concept in infrared metallic antennas, where we connect two micron-sized metallic arms of an antenna by means of a metallic bridge of different sizes. When the metallic bridge is inexistent or its size is very small, a capacitive coupling between both antenna arms produces a large Coulomb interaction at the gap, yielding a strongly red-shifted response (dashed bottom line in Fig. 1(a)). As the diameter of the metallic bridge connecting both arms becomes larger, the inductive nature of the gap dominates, allowing for a new electromagnetic mode distribution (dashed top line). The change from capacitive to inductive behavior can be observed directly in the near field by scattering-type near-field microscopy, providing direct evidence that local near-field amplitude and phase can be controlled by antenna loading [1].

We also propose and explore theoretically this concept for application in ultrafast optical switches based on nonlinear plasmonic nanoantennas. The antenna nanoswitch operates on the transition from the capacitive to conductive coupling regimes between two closely spaced metal nanorods (see schematics in Fig. 1(b)). By filling the antenna gap with amorphous silicon, progressive antenna-gap loading is achieved due to variations in the free-carrier density in the semiconductor [2]. Strong modification of the antenna response is observed both in the far-field response and in the local near-field intensity. The large modulation depth, low switching threshold, and potentially ultrafast time response of antenna switches holds promise for applications ranging from integrated nanophotonic circuits to quantum information devices.

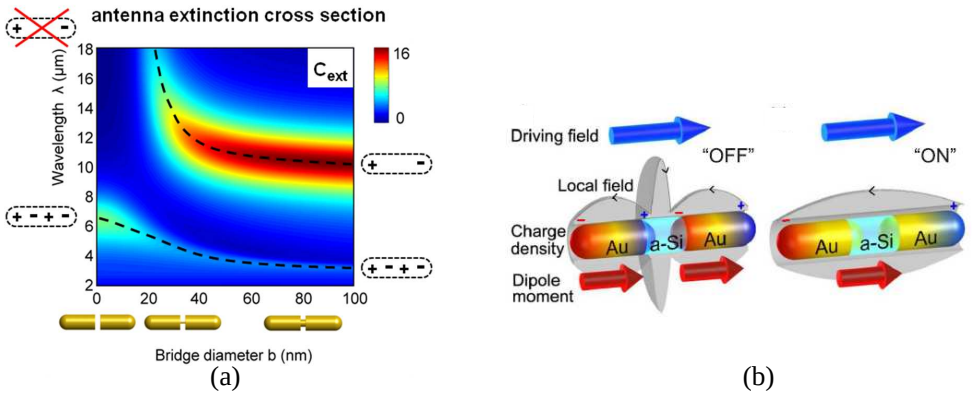

Figure 1: (a) Extinction cross section of a nanoantenna progressively loaded with a metallic bridge of diameter b. (b) Concept of optical switch (OFF/ON situations) based on photoconductive load ing of an optical antenna.

REFERENCES

1. Schnell, M., et al., *Nature Photonics*, Vol. 3, 287, 2009.
2. Large, N., et al., *Nano Lett.*, Vol. 10, 1741, 2010.

Controlling Light with Nanoantennas

Alexis Devilez[1], **Brice Rolly**[1], **Sebastien Bidault**[2], **Brian Stout**[1], **and Nicolas Bonod**[1]

[1]Institut Fresnel, Domaine Universitaire de Saint Jérôme, Marseille 13013, France
[2]Institut Langevin, UMR 7587 ESPCI ParisTech, 10 rue Vauquelin, 75231 Paris Cedex 05, France

Abstract— We show that it is possible to design ultracompact nanoantennas combining radiative properties and directionality.

Metallic nanostructures have been thoroughly investigated for their ability to focus light into tiny volumes, and also to drastically alter the spontaneous decay rates of quantum emitters [1, 2]. More recently, attention was focused on the control of the angular emission of quantum emitters by metallic nanoparticles [3]. The Yagi-Uda antenna has been downscaled into the optical range of frequencies [4–7]. But the fabrication of such an antenna remains a technical challenge, and the chain of nanoparticles is rather large.

We show that a single dielectric particle 500 nm in diameter, made of titania, exhibits excellent directivity in a wide spectral range. And a judicious combination with a metallic dimer permits to provide excellent directivity together with high radiative decay rates and good quantum efficincy (Fig. 1). The fluorescent gain can experiment an increase of 4 orders of magnitudes [8].

In order to design ultracompact metallic antennas, we first investigated the angular emission properties of a dipolar emitter coupled with a single metallic dipolar particle. The collection or reflection properties of the nanoparticle are showed to depend on the dephasing between the exciting and induced dipoles. This dephasing can be tuned by varying the distance between the emitter and the metallic surface at a scale around $\lambda/30$, a distance achievable with biological linkers (Fig. 2). We demonstrate analytically a counter-intuitive result: when the exciting and induced dipoles are perfectly in opposite phase, the diagram of emission of the emitter is perfectly symmetric while the environment is highly asymmetric since the emitter is coupled with a metallic particle. Also, by suitably positioning the dipolar emitter, the reflection efficiency of a single metallic particle can be optimized up to 90%, with an angular opening around 40°. When a second particle is added, the reflection efficiency can be increased up to 98% and the angular opening is reduced down to 30°, suitable for commercial microscope objectives [9].

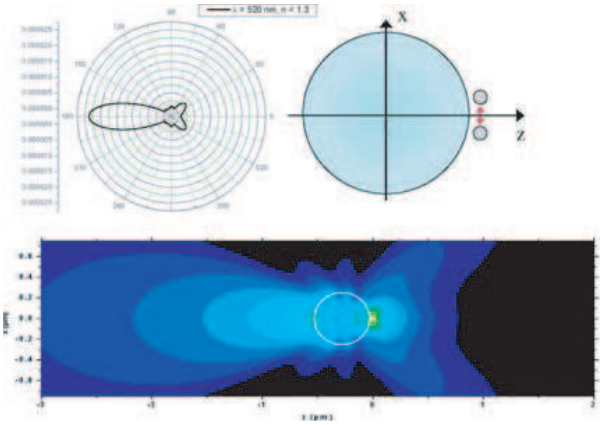

Figure 1: Metallo-dielectric antenna [8].

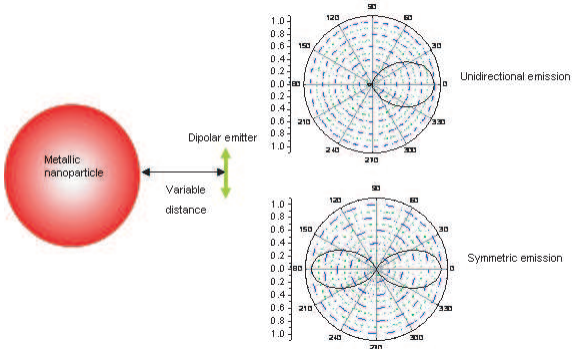

Figure 2: Ultracompact metallic antenna [9].

REFERENCES

1. Gerard, D., et al., "Nanoaperture-enhanced fluorescence: Towards higher detection rates with plasmonic metals," *Phys. Rev. B*, Vol. 77, 045413, 2008.
2. Mertens, H., et al., "Plasmon-enhanced luminescence near noble-metal nanospheres: Comparison of exact theory and an improved Gersten and Nitzan model," *Phy. Rev. B*, Vol. 76, 115123, 2007.
3. Taminiau, T. H., et al., "Optical antennas direct single molecule Emission," *Nature Photon.*, Vol. 2, 234–237, 2008.

4. Li, J., et al., "Shaping light beams in the nanometer scale: A Yagi-Uda nanoantenna in the optical domain," *Phys. Rev. B*, Vol. 76, 245403, 2007.
5. Hofman, H. F., et al., "Design parameters for a nano-optical yagi-uda antenna," *New J. Phys.*, Vol. 9, 217, 2007.
6. Kosako, T., et al., "Directional control of light by a nano-optical Yagi-Uda antenna," *Nature Photon.*, Vol. 4, 312, 2010.
7. Curto, A. G., et al., "Unidirectional emission of a quantum dot coupled to a nanoantenna," *Science*, Vol. 329, 930–933, 2010.
8. Devilez, A., et al., "Compact metallo-dielectric optical antenna for ultra directional and enhanced radiative emission," *ACS Nano*, Vol. 4, 3390–3396, 2010.
9. Bonod, N., et al., "Ultracompact and unidirectional metallic antennas," *Phys. Rev. B*, Vol. 82, 115429, 2010.

Session 1P6b
Platform Effects and Mutual Coupling in Large Complex Array Systems

Mutual Coupling in Large Complex ADS-based Arrays

G. Oliveri, P. Rocca, and A. Massa
ELEDIA Research Group at DISI, University of Trento, via Sommarive 14, I-38123, Trento, Italy

Abstract— Several modern applications including radar, microwave imaging, remote sensing, radio astronomy, satellite and ground communications require large and light antenna arrays with low sidelobes [1]. In order to meet these goals, thinned arrays have been proposed, and several design techniques have been introduced [1].

In this framework, random arrays were among the first techniques able to efficiently achieve low PSL levels [1]. More recently, their performances have been overcome by those of stochastic approaches based on genetic algorithms (GAs), simulated annealing (SA), or particle swarm optimizers (PSOs) [1]. However, it has been shown that their computational complexity rapidly grows with the aperture size, and that no predictors are available to a-priori estimate their performances [1].

In order to overcome these limitations, thinning techniques exploiting analytic sequences such as Difference Sets or Almost Difference Sets (ADSs) have been proposed [2, 3]. These techniques have been shown to provide low and predictable PSL values, as well as to allow the design of large layouts with a reduced computational effort [2, 3].

However, the analytic bounds for the PSL behavior of such layouts are actually applicable only for ideal arrays (i.e., in the absence of mutual coupling) [2, 3]. Indeed, neither a-priori estimates exist nor simple extensions of the ADS array theory have been deduced in the presence of nonideal radiators when mutual coupling (MC) effects between the array elements arise.

The aim of this work is to analyze the performances in terms of PSL control of ADS-based linear thinned arrays when mutual coupling effects are taken into account. Towards this end, an extensive numerical analysis aimed at showing the PSL behavior of non-ideal arrays versus the predicted PSL bounds for various aperture sizes, inter-element spacing, and thinning factor is presented. Both linear [4] and planar apertures will be taken into account. The presented result will be aimed at providing suitable design guidelines for ADS thinned arrays in the presence of MC effects, as well as at assessing the reliability of the PSL bounds yielded in [2, 3].

REFERENCES

1. Haupt, R., *Antenna Arrays: A Computational Approach*, IEEE Press, New York, 2010.
2. Oliveri, G., M. Donelli, and A. Massa, "Linear array thinning exploiting almost difference sets," *IEEE Trans. Antennas Propagat.*, Vol. 57, No. 12, 3800–3812, Dec. 2009.
3. Oliveri, G., L. Manica, and A. Massa, "ADS-based guidelines for thinned planar arrays," *IEEE Trans. Antennas Propagat.*, Vol. 58, No. 6, 1935–1948, June 2010.
4. Oliveri, G., L. Manica, and A. Massa, "On the impact of mutual coupling effects on the PSL of ADS thinned arrays," *Progress in Electromagnetic Research B*, Vol. 17, 293–308, 2009.

System Aspects of Mutual Coupling in Reconfigurable Active Phased Array

S. Celentano[1], **L. Infante**[1], **S. Sabatini**[1], **M. R. Toma**[1], **and T. Johansson**[2]

[1]SELEX Sistemi Integrati, Italy
[2]SAAB Electronic Defence Systems, Sweden

Abstract— In a MAESA (Multifunction/multirole Active Electronically Steered Array) system performing simultaneously different TX and RX functions with different sub-apertures there are unwanted effects due to the interferences of a transmitting sub-aperture on the receiving one. This type of interference is called "mutual coupling".

The sub-apertures dedicated to different activities (Radar, ECM, ESM, and COM) can interfere among one and another by means of:

- direct coupling due to direct free-space radiation and to substrate-conduced waves;
- reflection from platform structure;
- clutter reflections due to the close returns from environment.

An analysis of the direct coupling effect has been carried out to determine if two given system functions can be executed with an acceptable amount of mutual interference or not.

The result of this type of analysis is crucial within a MAESA system, since the implementation of multi-functionality requires a good understanding and description of interference between functions.

The scope of this paper is to present the mutual interference model and evaluation method for the interference between functions serving as a knowledge base for future design of MAESA applications.

The analysis of the mutual interference is performed through the following steps:

1. evaluate if saturation occurs in the different stages of the receiver from TRM to A/D converter;
2. evaluate the interfering signal at the output of the receiver when no saturation occurs;
3. analyse the consequences of the interference signal in terms of performances evaluation for the selected system functions.

An analysis of the system impact from the mutual coupling will be performed and a functional description of model for the interference levels between TX and RX system functions operating simultaneously will be given.

Active Element Pattern in CP Array Synthesis Strategy

Gabriella Bernardi[1], **Michele D'Urso**[1], **Maurizio Felaco**[1], **and Ettore Flavio Meliado**[2]

[1]Innovation Team, SELEX Sistemi Integrati S.p.A.
Via Circumvallazione Esterna di Napoli, Loc. Pontericcio zona ASI
I-80014 Giugliano di Napoli, Napoli, Italy
[2]OPTEL Consorzio Nazionale di Ricerca per le Tecnologie Optoelettroniche dell'InP
Centro Ricerche Giugliano, SELEX S.I.
via Circumvallazione Esterna di Napoli, Loc. Pontericcio zona ASI
I-80014 Giugliano di Napoli, Napoli, Italy

Abstract— In this paper the mask power pattern array synthesis problem is faced. Modern radar systems are called to satisfy strict requirements in terms of beam-width, side-lobe level, jammer rejection, etc. [1]. The today's technical literature is rich of contributions about this subject, but in the most of them the non-ideal effects of coupling between array elements and platform are neglected. This is a crucial problem instead, since these phenomena affect significantly the radiating performance. Herein an effective method is proposed to achieve the desired requirements accounting for all the mentioned coupling effects.

The first aspect treated in this study has been the choice of the synthesis procedure. Among the most effective techniques the ones based on global research algorithms arise; these ones ensure in principle the global maximum achievement but are very time consuming; so in the most of practical cases, the results obtained are suboptimal (according to a fixed tolerance accepted) [2, 3]. This problem can be solved in a better way by observing its intrinsic convexity properties [5]; this allows to adopt convex programming (CP) procedures that guarantee a faster convergence to the optimum, assured to be the global one due to the convexity. The strengths of the power pattern synthesis procedures based on CP are the flexibility respect to the array geometry and the effectiveness in solving the kinds of synthesis problems considered in this paper.

The second aspect here treated is related to the coupling effects, existent between the array antennas as well as between the array and the platform. The most of the synthesis procedures available in technical literature do not provide a useful practical design instrument because they consider the radiated pattern of each array element as isolated. In some cases, instead, the coupling effects are somehow dealt with, but all the proposed methods show some weak points, like the beamforming strategy [6], as before mentioned, or the adopted coupling evaluation technique [7, 8]. Concerning this second class, in fact, it is well known that the Pattern Multiplication method cannot be applied when not well-behaved [9] radiating elements are used, or when arrays are mounted on complex platforms; in these cases the most flexible techniques are based on the Active Element Pattern (AEP) method [9]; in this paper, the CP synthesis includes the coupling effects via AEP, where the single active pattern are computed numerically by means of a full-wave simulator [10], with the maximum achievable accuracy. This method has been applied to an interesting practical study case, with encouraging results.

REFERENCES

1. Farina, A., *Antenna-based Signal Processing Tecniques for Radar Systems*, Artech House, Ed. Boston, London, 1992.
2. Boeringer, D. W. and D. H. Werner, "Particle swarm optimization versus genetic algorithms for phased array synthesis," *IEEE Trans. on Antennas and Propagation*, Vol. 52, 771–779, Mar. 2004.
3. Guney, K. and S. Basbug, "Interference suppression of linear antenna arrays by amplitude-only control using a bacterial foraging algorithm," *Progress In Electromagnetics Research*, Vol. 79, 475–497, 2008.
4. Bevalaqua, P. J. and C. A. Balanis, "Minimum sidelobe levels for linear arrays," *IEEE Trans. on Antennas and Propagation*, Vol. 55, 3442–3449, Dec. 2007.
5. Bucci, O., M. D'Urso, and T. Isernia, "Some facts and challenges in array antenna synthesis problems," *Applied Electromagnetics and Communications International Conference*, 1–4, Dubrovnik, Sept. 24–26, 2007.
6. Demarcke, P., H. Rogier, R. Goossens, and P. De Jaeger, "Beamforming in the presence of the mutual coupling based on constrained particle swarm optimization," *IEEE Trans. on Antennas and Propagation*, Vol. 57, 1655–1666, Jun. 2009.

7. Oliner, A. A. and R. G. Malech, "Mutual coupling in infinite scanning arrays," *Microwave Scanning Antennas*, 195–335, R. C. Hansen, Ed., Academic Press, New York, 1996.
8. Allen, J. L., "Gain and impedance variation in scanned dipole arrays," *IRE Trans. Antennas Propagat.*, Vol. 10, 556–573, Sept. 1962.
9. Kelley, D. F. and W. L. Stutzman, "Array antenna pattern modelling methods that include mutual coupling effects," *IEEE Trans. on Antennas and Propagation*, Vol. 41, No. 12, 1625–1632, Dec. 1993.
10. CST Microwave Studio tool for 3D EM simulation of high frequency components in CST Studio Suite. Official website: http://www.cst.com.

Platform Effect in Circular Arrays with Polarization Diversity

R. Sarkis and C. Craeye
Ecole Polytechnique de Louvain, ICTEAM, UCL, Belgium

Abstract— This communication presents the ground plane effect on a circular antenna array, with polarization diversity, of connected wideband taper slot antennas. The Array Scanning Method is then applied in a Method-of-Moments approach in order to simulate efficiently the behavior of this array of 8 novel 3D Vivaldi antennas which are electrically connected to each other in octagonal shape. The method allows the inclusion of the finite ground plane in the fast analysis. A parametric study of the ground plane dimension will be analyzed to conclude on its effect over the radiation pattern and its spherical wave decomposition.

We propose such a novel Vivaldi antenna with 3D aluminum elements that contains the feeding cable so as to avoid a balun circuit [1]. Then, using the fact that the currents obtained from infinite-array simulations [2] with the help of the Array Scanning Method becomes the exact solution when the array is uniformly circular, we reduce the MoM system of equations to N systems of $(M \times M)$ where N is the number of antennas and M the number of basis function on each antenna element. After we studied the effect of the ground plane size over the radiation pattern and we found that the number of spherical modes needed to reconstruct the radiation pattern increases faster than linearly with the size of the ground plane. New methods, based on localized spherical modes are under study.

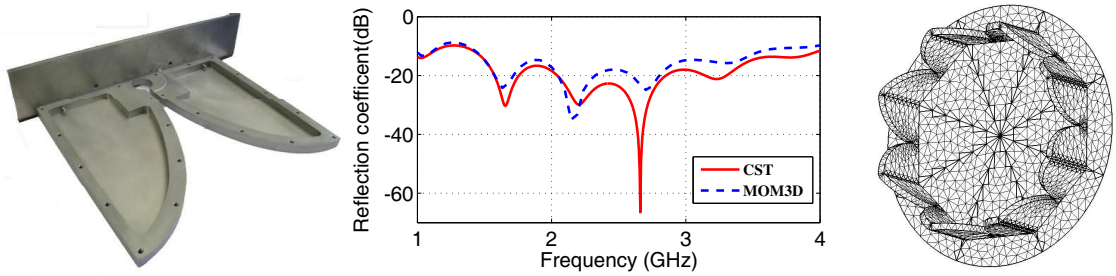

Figure 1: Single antenna design (left) reflection coefficient results (center) and antenna array layout (right).

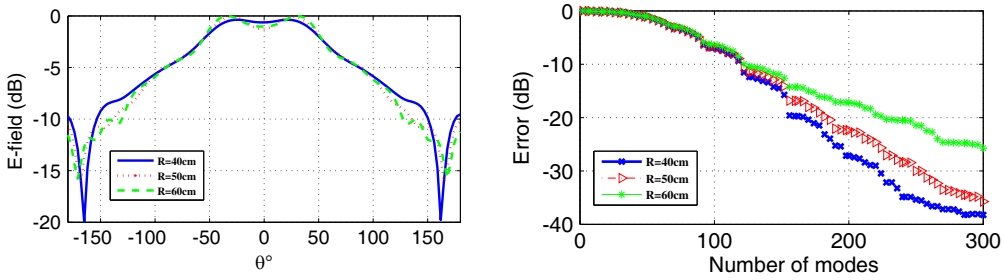

Figure 2: E-field in E plane (left) and spherical wave decomposition error (right) for different ground dimensions.

REFERENCES

1. Munk, B. A. and G. A. Burrell, "Plane-wave expansion for arrays of arbitrarily oriented piecewise linear elements and its application in determining the impedance of a single linear antenna in a lossy half-space," *IEEE Trans. Antennas Propagat.*, Vol. 27, No. 5, 331–343, May 1979.
2. Sarkis, R. and C. Craeye, "Simulation of large circular antenna arrays using array scanning method," *EuCAP2010*, Barcelona, Spain, 2010.

On the Relationship between Finite and Infinite Arrays in the Context of Radiation and Scattering Problems

S. N. Jha, N. A. Ozdemir, and C. Craeye
Université Catholique de Louvain, ICTEAM, Belgium

Abstract— A fast technique for Finite Array analysis applicable to metallic as well as printed antennas is proposed using an Infinite Array approach. In view of that, the Dyadic form of Periodic Array Green's function for the case of dielectric medium are computed in spectral domain. The extraction of the periodic singularities is carried out by subtracting the contribution from an Infinite Array solution for an average medium in space-spectral domain with exponential convergence, where the computational acceleration is based on the work in [1]. Then, the Infinite Array solution is generated and is further used to analyse finite arrays. The Array Scanning Method (ASM) [2], which is a DFT transformation applied to the infinite-array results, is developed for the case of antennas printed on dielectrics, which allows one to obtain fields in infinite arrays for non-periodic excitation. Those results are then considered as "Macro Basis Functions (MBF) [3]", i.e., as expansions of the fields at the unit-cell level in the Finite Array. This generally allows the reduction of the total number of unknowns by one to two orders of magnitude, while preserving accuracy far beyond engineering requests.

A preliminary validation of the proposed approach is carried out through an analysis of a 12×12 finite array of resonant printed dipoles on dielectrics at 1 GHz. Here, Fig. 1(a) shows an example of Method of Moment (MoM) matrix computed with the Dyadic approach for Periodic Green's function for dielectrics in the infinite array case within a unit cell to ensure the periodicity of the result. However, it should be noted that the total MoM matrix of the Infinite Array approach is given by the sum of the MoM matrix as shown in Fig. 1(a) and the MoM matrix contribution from the Infinite Array solution for average medium. Fig. 1(b) shows the comparisons between the solutions obtained with Infinite and Finite array approaches in terms of absolute values of the port current, where one can see that the finite array solution is oscillating around the infinite array solution.

Examples will be shown on the use of the combined ASM-MBF [2] method to analyse bigger arrays with higher antenna complexity. The effect of array truncation will be also addressed through the ASM-MBF technique. Finally, the accuracy of the results will be assessed through the comparison with data generated with the help of Krylov sub-space [4] based iterative techniques.

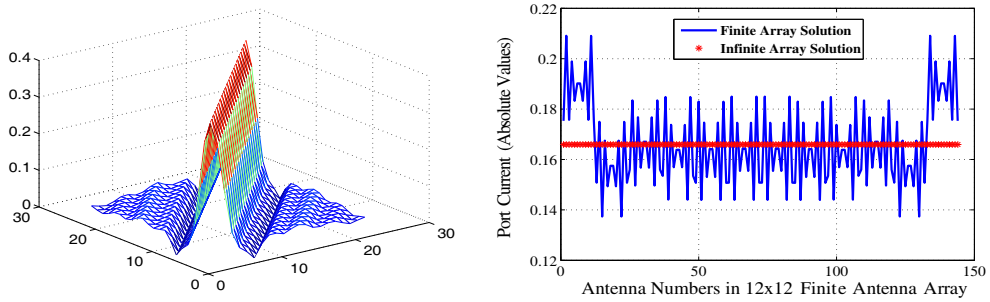

(a) An Example of Periodic MoM Matrix.

(b) Infinite Array vs. Finite Arrays Solution.

Figure 1: Results related to the proposed approach.

ACKNOWLEDGMENT

The authors are grateful to the Région Wallone for financial support through the project RADIANT.

REFERENCES

1. Guérin, N., C. Craeye, and X. Dardenne, "Accelerated computation of the free space Green's function gradient of infinite phased arrays of dipoles," *IEEE Transaction on Antenna and Propagation*, Vol. 57, No. 10, 2009.
2. Craeye, C. and R. Sarkis, "Finite array analysis through combination of Macro basis functions and array scanning methods," *Journal of the Applied Computational Electromagnetics Society*, 256–261, 2008.

3. Mittra, R. and K. Du, "Characteristic basis function method for iteration free solution of large method of moments problems," *Progress In Electromagnetics Research B*, Vol. 6, 307–336, 2008.
4. Craeye, C., "Further comparison between Macro basis functions and Krylov subspace iterative methods," *Progress In Electromagnetics Research Symposium Abstracts*, 191, Xi'an, China, March 22–26, 2010.

Session 1P7
Novel Mathematical Methods in Electromagnetics

An Interpretation of Maxwell Equation by Using the Formalism of Gravitational Waves

Patrick Vaudon
Xlim, Mixt Research Unit CNRS-University No. 6172, 123 rue Albert Thomas, Limoges 87000, France

Abstract— Maxwell equations are known to be fully compatible with the special theory of relativity, but have no representation in terms of space-time perturbations, in opposition with gravitational waves which are described as the propagation of small perturbations in the metric of space-time.

This paper propose to interprete Maxwell equations and electromagnetic waves by using the formalism now well established to describe gravitational waves. This formalism is grounded on the general relativity which seems a priori non adequate to describe electromagnetism since Einstein's equations are non linear. However, for very small perturbations, a linearised frame has been derived, and gravitational waves are studied in this frame.

After deriving a momentum-energy tensor T^{ij} for electromagnetic sources different from the electromagnetic field's one which is used in the so called Maxwell-Einstein equations [1–3], we can apply Einstein equations in their linearised form. We introduce this new momentum-energy tensor in the Maxwell-Einstein equations and we obtain a wave propagation equation on the metric coefficients which is usually used to explain the propagation of gravitational waves.

Since this propagation equation is identical as the electromagnetic one with currents in the second member, we examine how electromagnetic waves can be interpreted as the propagation of small perturbations in the space-time metric. We show that in such an interpretation, the electromagnetic potential plays an equivalent role as the gravitationnal potential, and then, can be represented by the metric coefficients. We give the explicite relation between electromagnetic potentials and the metric coefficients which are obtained in this approach. We show that this allow to define a whole electromagnetic energy associated with a point charge as a function of the Planck units.

REFERENCES

1. Dolan, P., "A singularity free solution of the Maxwell-Einstein equations," *Communications in Mathematical Physics*, Vol. 9, No. 2, 161–168, 1968.
2. Caricato, G., "Sur le problème de Cauchy intrinsèque pour les équations de Maxwell-Einstein dans le vide," *Annales de l'I. H. P*, Section A, Vol. 11, No. 4, 373–392, 1969.
3. McGuire, P. and R. Ruffini, "Some magnetic and electric monopole one-body solutions of the Maxwell-Einstein equations," *Phys. Rev.*, Vol. 12, 3019–3025, 1975.

Optical Soliton Perturbation with Full Nonlinearity in Non-Kerr Law Media

Anjan Biswas
Department of Mathematical Sciences, Delaware State University
1200 N. DuPont Highway, Dover, DE 19901-2277, USA

Abstract— The dynamics of optical solitons is studied in presence of perturbation terms, with full nonlinearity. The study is conducted in presence of Kerr law as well as non-Kerr law nonlinearity. These nonlinear media are power law, parabolic law, dual-power law and log law. The fixed points are also obtained that leads to soliton cooling.

Low-frequency Electromagnetic Scattering by Two PEC Spheres Buried in Conductive Medium

P. Vafeas[1], **P. K. Papadopoulos**[1], **and D. Lesselier**[2]

[1]Division of Applied Mathematics and Mechanics, Department of Engineering Sciences
School of Engineering, University of Patras, Greece
[2]Laboratoire des Signaux et Systèmes UMR8506, Département de Recherche en Electromagnétisme
CNRS, SUPELEC, Univ. Paris Sud, France

Abstract— Analytical approaches of low-frequency electromagnetic scattering [1] by simple bodies remain a subject of worthwhile investigation, even if there exist computational tools that could directly provide numerical data. Indeed, whenever analytical solutions are found, one is expected to get (i) accurate means to check the suitability of these most probably computationally demanding solutions, and (ii) fast means to invert scattered field data that could be collected around similar bodies to yield some information on them. This is particularly true in exploration of the Earth's subsurface and possibly highly conducting bodies embedded in it for which the frequency range is often quite low due to its conductive character, meaning that low-frequency models are pertinent. Those involve expanding all fields into positive integral powers $(jk)^n$, k wavenumber of the embedding medium at frequency ω, $k = \sqrt{j\omega\sigma\mu_0}$, σ conductivity, μ_0 permeability, and calculating the real-valued vector coefficients at each n. They are the Rayleigh term $n = 0$, and, typically, the first dynamic ones $n = 2$ and $n = 3$, the $n = 1$ being trivial due to absence of primary field term for a magnetic dipole (current loop sources are generally employed, assimilated to dipoles). The magnetic field then comprises an in-phase (real) component (essentially from $n = 0$) and a quadrature (imaginary) component (from $n = 2$).

Previous studies in this framework have been led on single bodies, sphere, and recently spheroid and ellipsoid [2, 3]. Here, two simple bodies are modeled as perfectly conducting (PEC) spheres, of arbitrary radii and distance from one another (contact excepted), with the limit case of one sphere collapsed to a plane, the magnetic dipole being of arbitrary location and orientation. The boundary value problem is faced in the bispherical system of coordinates (attached to the spheres) and scalar/vector Laplace equations handled via harmonic eigenfunction expansions and using R-separability, plus boundary conditions on the two surfaces. Infinite series expansions of the Rayleigh term as the gradient of a scalar potential in vacuum with Neumann boundary condition have already been provided (in the same line of analysis, refer to [4]). The $n = 3$ term can be calculated likewise, as the gradient of another scalar potential. The cumbersome construction of the series expansion of the $n = 2$ terms of both magnetic and electric fields has just been achieved (it involves the solution of a vector Laplace equation whose source is the Rayleigh term to calculate the magnetic term, taking in account the electric term proportional to its curl).

Only magnetic terms need to be simulated in practice. Each of the three expansions appears to have every coefficient, after proper ordering, being inter-related to a number of other coefficients that are emerging before or after it via involved sets of recurrence relationships (like in [4] to give an example). So, one is left with an infinite sequence of non-homogeneous systems of equations solved by a cut-off method, starting from small-sized systems and increasing their sizes to convergence. The main points of the analytical works carried out will be sketched while numerical results obtained at low computational cost, even if the spheres almost touch one another, will illustrate the investigation.

REFERENCES

1. Dassios, G. and R. E. Kleinman, *Low Frequency Scattering*, Oxford University Press, Oxford, 2000.
2. Vafeas, P., G. Perrusson, and D. Lesselier, "Low-frequency scattering from perfectly conducting spheroidal bodies in a conductive medium with magnetic dipole excitation," *International Journal on Engineering Sciences*, Vol. 47, 372–390, 2009.
3. Perrusson, G., P. Vafeas, and D. Lesselier, "Low-frequency dipolar excitation of a perfect ellipsoidal conductor," *Quarterly of Applied Mathematics*, Vol. 68, 513–536, 2010.
4. Dassios, G., M. Hadjinicolaou, G. Kamvyssas, and N. Kandili, "On the polarizability potential for two spheres," *International Journal of Engineering Science*, Vol. 44, 1520–1533, 2006.

An Efficient Algorithm for the Analysis of a Nano Wire in Homogeneous or Layered Media

Ergun Simsek[1], **Jianguo Liu**[2], **and Qing H. Liu**[3]

[1]Bahcesehir University, Istanbul, Turkey
[2]Schlumberger Doll Research, Cambridge, MA, USA
[3]Duke University, Durham, NC, USA

Abstract— Recently, metal and carbon nano wires (NWs) have received a serious amount of interest due to their potential in confining light transversally to sub-wavelength dimensions and yet to be used as an optical waveguide or an antenna in the visible [1]. Oulton et al. have shown that a hybrid optical waveguide, which consists of a dielectric NW separated from a metal surface by a nano scale dielectric gap, can provide an extremely long propagation length (dozens of wavelengths) and strong mode confinement [2]. Experimental and theoretical results reveal a huge potential for realistic nano scale semiconductor-based plasmonics and photonics. This is why it is extremely important to develop efficient and robust algorithms for the analysis and design of such structures, especially for the ones embedded in a layered medium.

In [3], Hochman and Leviatan developed a source model technique for the analysis of NW chains. They calculated periodic Green's functions analytically as a sum of Floquet harmonics and determined the complex propagation constants of the NW chain modes directly and accurately. Their approach is mathematically correct but requires at least 10 current filaments per wavelength in order to obtain accurate results. More importantly, their approach assumes a homogeneous background, so cannot handle NWs embedded in a multilayered medium, which is a more realistic scenario. This problem can be solved more efficiently using a spectrally accurate algorithm, namely the Spectral Integral Method (SIM).

SIM is related to the fast method originally developed by Bojarski [4] for sound-soft circular cylinders, and extended by Hu [5] to sound-soft or sound-hard smooth cylinders. Liu et al. developed its surface integral equation solver version for homogeneous background [6] and Simsek et al. brought similar approach for multilayered background for microwave problems. The idea behind this method is the use of fast Fourier transform (FFT) algorithm and the subtraction of singularities in Green's functions to achieve spectral accuracy in the integral.

In this work, we further improve SIM to handle 2D optical scattering problems with materials and/or layers of negative permittivity. To describe the metals in the visible, Lorentz-Drude model is implemented. For the NWs embedded in a multilayered medium, surface integral equation is formulated with layered medium Green's functions (LMGFs). Advantages of this approach are as follows: The usage of FFT algorithm provides exponentially accurate results and approximately three points per wavelength guarantees an error less than 1%. The method can be extended to periodic structures easily by implementing with periodic LMGFs and to inhomogeneous scatterers by using SIM as a radiation boundary in a hybrid boundary integral-volume integral equation solver as it is done in [8].

REFERENCES

1. Bharadwaj, P., B. Deutsch, and L. Novotny, "Optical antennas," *Adv. Opt. Photon.*, Vol. 1, No. 3, 438–483, 2009.
2. Oulton R. F., V. J. Sorger, D. A. Genov, D. F. P. Pile, and X. Zhang, "A hybrid plasmonic waveguide for subwavelength confinement and long-range propagation," *Nat. Photonics*, Vol. 2, 496–500, 2008.
3. Hochman, A. and Y. Leviatan, "Rigorous modal analysis of metallic nanowire chains," *Opt. Expr.*, Vol. 17, No. 16, 13561–13575, 2009.
4. Bojarski, N. N., "Scattering by a cylinder: A fast exact numerical solution," *J. Acoust. Soc. Amer.*, Vol. 75, No. 2, 320–323, 1984.
5. Hu, F. Q., "A spectral boundary integral equation method for the 2D Helmholtz equation," *J. Comp. Phys.*, Vol. 120, 340–347, 1995.
6. Liu, J. and Q. H. Liu, *IEEE Microwave and Wire. Comp. Lett.*, Vol. 13, 97–99, 2004.
7. Simsek, E., J. Liu, and Q. H. Liu, "A spectral integral method (SIM) for layered media," *IEEE Trans. Antennas Propag.*, Vol. 54, No. 6, 1742–1749, Jun. 2006.
8. Simsek, E., J. Liu, and Q. H. Liu, "A spectral integral method and hybrid SIM/FEM for layered media," *IEEE Trans. Microwave Theory Tech.*, Vol. 54, No. 11, 3878–3884, Nov. 2006.

Velocity Curl and Spin in Electromagnetic Fields

Zi-Hua Weng
School of Physics and Mechanical & Electrical Engineering
Xiamen University, Xiamen 361005, China

Abstract— J. C. Maxwell described first the electromagnetic field theory with the algebra of quaternions, which was invented by W. R. Hamilton in 1843. Nowadays the gravitational field and electromagnetic field both can be demonstrated by quaternions, although these two fields are distinct from each other. Combining the quaternion space of electromagnetic field with that of gravitational field, the octonion space can illustrate simultaneously the features of gravitational field and electromagnetic field.

In the octonion space, the radius vector and the integral of field potential can be combined together to become the compounding radius vector, which can be considered as the vector in the function space or the compounding space. In this compounding space we can define similarly the field strength, field source, linear momentum, and angular momentum etc. It is found that the velocity curl has an influence on these compounding physical quantities. And the weightlessness condition is equivalence to that the compounding field strength is equal to zero.

In the compounding space, the gravitational strength possesses two parts. One is the electric-like component, which is the expansion of Newtonian gravitational strength and similar to the electric strength, while the other is to the magnetic strength. In the gravitational field two component equations of weightlessness can be derived from zero compounding field strength. As well as the zero vector sum of the acceleration and the electric-like component of gravitational strength, it is equal to zero the vector sum of the angular velocity and the magnetic-like component.

Similarly two component equations for the 'weightlessness' state in electromagnetic fields can be derived from zero compounding field strength. One is the zero vector sum of the electric strength and one acceleration-like quantity, the other is the zero vector sum of the magnetic strength and the velocity curl in the electromagnetic quaternion space. The latter can be considered as the spin angular velocity with the non-quantum explanation. The research claims that the spin angular velocity is necessary when the charged particle is on 'weightlessness' state.

ACKNOWLEDGMENT

The author is grateful for the financial support from the National Natural Science Foundation of China under grant number 60677039.

Theorem for the Identity of the $L(c,n)$ and $\hat{L}(\hat{c},\hat{n})$ Numbers and Its Application in the Theory of Waveguides

Georgi Nikolov Georgiev[1] **and Mariana Nikolova Georgieva-Grosse**[2]

[1]Faculty of Mathematics and Informatics
University of Veliko Tirnovo "St. St. Cyril and Methodius", BG-5000 Veliko Tirnovo, Bulgaria
[2]Meterstrasse 4, D-70839 Gerlingen, Germany

Abstract— $L(c,n)$ numbers are called the common limits of the infinite sequences of positive real numbers: i) $\{K_-(c,n,k_-)\}$ and $\{M_-(c,n,k_-)\}$ for $k_- \to -\infty$ [1], $(K_-(c,n,k_-) = |k_-|\zeta^{(c)}_{k_-,n}$, $M_-(c,n,k_-) = |a_-|\zeta^{(c)}_{k_-,n}$, $\zeta^{(c)}_{k_-,n}$ — nth positive purely imaginary zero of the Kummer confluent hypergeometric function $\Phi(a,c;x)$ [2] in x $(n = 1,2,3,\ldots)$ with $a \equiv a_-$, $a_- = c/2 - jk_-$ — complex, $c = 2\mathrm{Re}a$ — real $(c \neq l,\ l = 0,-1,-2,\ldots)$, $x = jz$, k_-, z — real, $k_- < 0$, $z > 0, c, n$ — fixed); ii) $\{L(l-\varepsilon,n)\}$ and $\{L(l+\varepsilon,n+1)\}$ for $\varepsilon \to 0$ when $c = l$, (ε — infinitesimal positive real number). In this instance it holds: $L(l,n) = L(2-l,n)$ [1]. The notion $\hat{L}(\hat{c},\hat{n})$ number is determined likewise [3]. To distinguish both cases, however, it is accepted in the second one to introduce hats "$\hat{}$" above all the symbols involved. Besides, unlike previously, now the quantities $\hat{a}$, $\hat{c}$, $\hat{x}$ are real, $\hat{\zeta}^{(\hat{c})}_{\hat{k}_-,\hat{n}}$ stands for the $\hat{n}$th positive real zero of the function $\Phi(\hat{a},\hat{c};\hat{x})$ [2] in $\hat{x}$, $\hat{x} > 0$, $\hat{n} = 1,2,\ldots,\hat{p}$, $\hat{p} = abs[\hat{a}]$, if $\hat{a} < 0$, $\hat{c} > 0$, $(\hat{n} = 1,2,\ldots,\hat{s}$, $\hat{s} = \hat{p} - \hat{q}$, $\hat{p} = abs[\hat{a}]$, $\hat{q} = abs[\hat{c}]$, $\hat{q} = 1,2,\ldots,\hat{p}-1$, provided $\hat{a} < 0$, $\hat{c} < 0$, $\hat{c} \neq \hat{l}$, $\hat{l} = 0,-1,-2,\ldots,\hat{a} < \hat{c} < 0)$, $\hat{a} \equiv \hat{a}_-$, $\hat{a}_- = \hat{c}/2 + \hat{k}_-$, $\hat{k}_-$ — real, negative, ($[\hat{a}]$ denotes the greatest integer less than or equal to $\hat{a}$) and $\hat{\varepsilon}$ is real, positive, $\hat{\varepsilon} \to 0$ [3].

In this study a theorem is proved numerically, stating that if $c \neq l$ and $\hat{c} \neq \hat{l}$ $(l = \hat{l})$, on condition that $c = \hat{c}$, $n = \hat{n}$ and $k_- = \hat{k}_-$ — large negative, it is fulfilled: i) $\zeta^{(c)}_{k_-,n} \approx \hat{\zeta}^{(\hat{c})}_{\hat{k}_-,\hat{n}}$; ii) $K_-(c,n,k_-) \approx M_-(c,n,k_-) \approx \hat{K}_-(\hat{c},\hat{n},\hat{k}_-) \approx \hat{M}_-(\hat{c},\hat{n},\hat{k}_-)$; iii) $L(c,n) \equiv \hat{L}(\hat{c},\hat{n})$. Moreover, in the vicinity of points $l = \hat{l}$, assuming that $\varepsilon = \hat{\varepsilon} \to 0$, it is true: $L(l-\varepsilon,n) = \hat{L}(\hat{l}-\hat{\varepsilon},\hat{n})$, $L(l+\varepsilon,n+1) = \hat{L}(\hat{l}+\hat{\varepsilon},\hat{n}+1)$, or $L(l,n) \equiv \hat{L}(\hat{l},\hat{n})$.

The identity iii) with $c = \hat{c} = 3$ finds application in the theory of the circular waveguide, entirely filled with azimuthally magnetized ferrite that supports rotationally symmetric TE modes [1, 3, 4]. The physical interpretation of its truthfulness is the coincidence in case of negative magnetization of the structure's filling of the envelope curves of the phase characteristics, restricting the propagation of normal TE_{0n} modes from the side of the higher frequencies [4] and of slow $\hat{TE}^{(1)}_{0\hat{n}}$ waves $(n = \hat{n})$ from that of the lower ones [3]. Thus, there exists a curve of equation, written in parametric form as: $\bar{r}_{0en-} = L\,(c,\,n)\,/\,[\,|\,\alpha_{\,en-}|\,(1-\alpha^2_{en-})\,]^{\,1/2}$, $\bar{\beta}_{en-} = (\,1-\alpha^2_{en-}\,)^{\,1/2}$ [1, 3–5], separating the transmission area for the magnetization mentioned in two regions: a left and a right one in which normal TE_{0n}, resp. slow $\hat{TE}^{(1)}_{0\hat{n}}$ mode is sustained, ($\bar{r}_0$ and $\bar{\beta}$ are the normalized in an appropriate way guide radius and phase constant and α is the off-diagonal ferrite permeability tensor element, $|\alpha| < 1$, and the subscript "$en-$" distinguishes the quantities, relevant to the envelopes). The same is connected with the upper boundary of the domain of phase shifter operation of the configuration for the first set of fields [5].

REFERENCES

1. Georgiev, G. N. and M. N. Georgieva-Grosse, "The $L(c,n)$ numbers and their application in the theory of waveguides," *Proc. Int. Conf. Days Diffr. 2008, DD'08*, 44–57, St. Petersburg, Russia, June 3–6, 2008.
2. Tricomi, F. G., *Funzioni Ipergeometriche Confluenti*, Edizioni Cremonese, Rome, Italy, 1954.
3. Georgiev, G. N. and M. N. Georgieva-Grosse, "Theory of the $\hat{L}(\hat{c},\hat{n})$ numbers and its application to the slow wave propagation in the circular ferrite waveguide," *PIERS Proceedings*, 976–980, Cambridge, USA, July 5–8, 2010.
4. Georgiev, G. N. and M. N. Georgieva-Grosse, "A new property of the complex Kummer function and its application to waveguide propagation," *IEEE Antennas Wireless Propagat. Lett.*, Vol. 2, 306–309, December 2003.
5. Georgieva-Grosse, M. N. and G. N. Georgiev, "Advanced studies of the differential phase shift in the azimuthally magnetized circular ferrite waveguide," *PIERS Proceedings*, 841–845, Cambridge, USA, July 5–8, 2010.

Electromagnetic Sources and Observers in Motion VI — New Motional Optics

S. E. Wright
Moor Lane Laboratory, ECASS Technologies Ltd., Kirkburton, Huddersfield, HD8 0QS, UK

Abstract— In paper V, the first of the two papers given at this symposium, the arguments for revising Einstein's relativity were discussed. In this paper VI, the new motional properties resulting from the revision are considered. It appears from paper V that Einstein's Special Relativity (SR) has three aspects: 1) An ether-less aspect whose properties have not been observed. To simulate the medium removal, oblique transform axes were effectively used. This implied simultaneity, no absolute time and space, and no causality, where the future can be observed before it occurs. None of these ether-less, oblique axes claims appear to have been established or shown to have any scientific foundation. 2) A medium based aspect whose properties are causal and have been observed, but are incomplete. Amazingly, in spite of his rejecting the medium, Einstein's 1905 analysis (motional electrodynamics), actually solves the wave equation based on a reference medium. Einstein's SR therefore appears to be medium based not ether-less as he claimed. It satisfies the rectangular axes, medium based Lorentz Transform (LT), not the ether-less oblique axes one, and 3) A medium based aspect whose properties are complete, but cannot be predicted by SR. To describe the complete radiation, propagation and reception processes, the LT has to be extended to include source and observer motion relative to the medium.

Through the assumed lack of a propagation medium, the complete electromagnetic (EM) motional wave equation solution, for sources and observers in motion relative to the medium, has not been attempted previously. The only additional features compared with the classical motional solution, are that time and space contract with motion relative to the medium, where the contraction does not affect causality. However, it does make the speed of light and Maxwell's (1865) wave equation invariant in the moving frame. Also, it makes the Doppler Effect (1842), identical between directly approaching and receding sources and observers. The propagation time perpendicular to the direction of motion becomes invariant, whereas the propagation time in and against the direction of motion remains variant and asymmetrical. This new medium based theory supports Fresnel's (1818) light convection, transverse Doppler, changes in time, space, mass, momentum, Einstein's energy equation, relativistic quantum mechanics and quantum electro-dynamics. Assuming the medium to be homogeneous and isotropic, the Robertson-Walker metric in cosmology is obtained. There is nothing in any of these theories to doubt the existence of the propagation medium. In fact none of the motional properties could be accounted for without a medium.

In addition to the above motional properties, the new motional wave equation solution predicts additional relationships. It is shown that the observed source events depend on the individual motion of the source and observer, relative to the medium. This motional event time transform clearly establishes astronauts who go travelling and their twins who stay at home. The medium acknowledgement resurrects the medium moving with the Earth (entrainment) model, proposed by Stokes (1845). The LT explains why the speed of light is invariant in the moving frame, supporting Einstein's ether-less explanation of the Michelson and Morley experiment (1887), but not the propagation time which is asymmetrical. The unity refractive index explains, why Bradley's (1725) stellar aberration in telescopes, is unchanged passing from the 'stationary' universal medium at rest in 'space', to that orbiting with the Earth. Light propagation cannot be altered by the universal medium refractive index $n = 1$ changing velocity or direction at its boundary. Although the medium has finite permeability μ and permittivity ε, it has no matter, no moving atomic structure to deflect the light. This moving medium based theory explains the observations of the universe quite naturally. Einstein, not aware of the detailed moving medium model, tried to unify (simplify) the situation by removing the medium altogether, resulting in ambiguities and paradoxes.

Time in this new theory is predicted (defined) through the visual solution of the EM motional wave equation. It is an observed effect, requiring a medium to provide the observations and a reference to compare an ordered sequence of events, creating the direction of time. Material time travel to the future and past, a manifestation of no medium, is not a solution of the wave equation, it is therefore irrational (non causal). It creates the absurdity that the future can be observed/experienced before it occurs. Causally, only visual time travel to the past is allowable in the medium based theory, but it is not possible to influence or interact with past events, they have already happened. In the case of space travel, it is legitimate to measure the slower time in

the moving astronauts frame and regular space (propagation medium) in the stationary frame, then the same distance is covered in less time, or more distance for the same time, in the moving frame. By measuring time and space across hybrid reference frames, the traveller's effective speed can exceed that of light. Thus vast distances across the universe are achievable at super-'lightic' speeds, whilst maintaining sub-'lightic' speed in the propagation medium. Without a medium, Einstein's ether-less relativity cannot distinguish between source and observer motion or satisfy causality.

Electromagnetic Sources and Observers in Motion V — A Revised Theory of Relativity

S. E. Wright[1]
Moor Lane Laboratory, ECASS Technologies Ltd., Kirkburton, Huddersfield, HD8 0QS, UK

Abstract— In paper I-II, given in Xi'an China, March 2010, the evidence for the existence of the propagation medium (ether) was established, and the differences between Einstein's ether-less relativity and the medium based Lorenz transform considered. In papers III-IV, given in Boston USA, in July 2010, a new medium based theory involving both source and observer motion relative to the medium was derived, and the effect of gravity on the medium investigated. In this paper the case for revising Einstein's theory of relativity is considered.

Einstein believed that there was no propagation medium (ether) needed to transmit light. Einstein's ether-less model considered only relative motion between objects, not their motion with respect to the medium. This lack of a medium and its associated non causal, ether-less relativity appears not to have been measured or verified theoretically. Researchers claiming the verification have usually verified Lorentz's time and space contraction through motion, not the medium's absence. An extensive investigation, both historic and modern, reveals that the medium very much exists. In fact no light transmission data could be found that could be explained without a propagation medium. It is shown that Einstein's Special Relativity (SR) (1905), without a medium, cannot satisfy the Lorentz Transform (LT), the motional wave equation and causes a discontinuity between classical and modern physics. Although Einstein denied the medium's presence, close examination of SR shows that Einstein's 1905 motional electrodynamics is in fact based on a propagation medium, in agreement with the medium based LT. SR therefore has an ether-less relativity prediction, which has not been observed, and a medium based prediction that has. However, Einstein's medium based aspect is incomplete, it cannot predict the complete radiation processes of sources and observers in motion relative to the medium. The medium based LT is extended to include source and observer motion. Besides predicting Lorentz's motional properties, the extension predicts additional measurable observations, which SR cannot predict.

Newton (1687), based his mechanics on the assumption that time and space can be judged with respect to an absolute reference (propagation medium) at rest in the universe. Maxwell (1865), developed his EM field equations based on a propagation medium. Also, Lorentz (1899) based his transform (LT) on the medium's existence. Whereas, Einstein (1905) declared that there was no need for a medium (ether) to transmit EM waves (light). The Michelson and Morley experiment (MMX) (1887) appeared to support, at first, Einstein's ether-less claim. However, rejecting the medium, as discussed in reference [1], causes fundamental problems, including the inability to transmit light, no distinction between source and observer motion and no causal prediction of time. This is in spite of data establishing the medium's existence, documented in reference [2]. A revised theory described in reference [3] completes the radiation process not covered by SR. The new theory extends the LT to describe (for the first time) both source and observer motion with respect to the medium. It removes the ether-less aspect of SR and the ether-less explanation for the MMX, it restores a rational universe and common sense. The theory predicts new (measured) motional optics in addition to those predicted by the LT. At that time (1905), Einstein's SR was a good, but an inconsistent attempt to fit existing measurements into his theory. However, his conclusion that there is no medium when obviously there is one, and the fact that he uses one in his analysis is a major inconsistency. Einstein fails also to distinguish between source and observer motion, making his analysis incomplete.

An extensive study into EM source and observer motion has been carried out in the references listed. In summary, the main points from these investigations are:

- Indisputable data shows that the propagation medium for the transmission of light exists.
- Considerable evidence indicates that the medium moves with gravitational bodies (Earth).
- Einstein's ether-less claim is simulated through oblique transform axes.
- These ether-less, oblique axes aspects of SR have not been measured, they have no physical reality.
- A new medium based, rectangular axes, source and observer motion theory has been developed.

[1]Professor Wright contact details are: selwyn.wright@ntlworld.com.

It is the ether-less aspect of SR that appears to make relativity incomprehensible. Its properties are non causal (irrational, non predictable) and non observable (cannot be observed or measured). The new theory completes the analysis for systems in motion generally, with respect to the medium, restoring the continuity between classical and modern physics. There appears to be nothing mysterious (irrational) about light propagation, it has a medium and satisfies the wave equation, exactly like all other wave forms, predicting causal observations.

REFERENCES

1. Wright, S. E., "Electromagnetic sources and observers in motion II — Einstein's ether-less relativity versus Lorentz's medium based theory," *Progress In Electromagnetics Research Symposium Proceedings*, 77–81, Xi'an, China, March 22–26, 2010.
2. Wright, S. E., "Electromagnetic sources and observers in motion I — Evidence supporting the EM propagation medium for the transmission of light," *Progress In Electromagnetics Research Symposium Proceedings*, 71–76, Xi'an, China, March 22–26, 2010.
3. Wright, S. E., "Electromagnetic sources and observers in motion III — Derivation and solution of the electromagnetic motional wave equation," *Progress In Electromagnetics Research Symposium Proceedings*, 1151–1155, Cambridge, USA, July 5–8, 2010.

Generalized Eigenfunction Method and Resonances for Time-dependent Scattering

Michael Meylan
Department of Mathematics, University of Aucklan, Private Bag 92019, Auckland, New Zealand

Abstract— The generalized eigenfunction method is a technique for solving linear wave problems in the time domain. It was originally applied to Schrödinger's equation [1] and has been extended to various wave scattering problems [2, 3]. The generalized eigenfunction method allows the solution in the time domain to be found in terms of the solution in the frequency domain. This has some computational advantages, for example methods to solve in the frequency domain already exist and radiation conditions at infinity need only be satisfied in the frequency domain. The principal advantage of the generalized eigenfunction method is that it gives a formula for the solution which is exact up to the determination of the frequency domain solutions and which has the same accuracy for all times (since the formula does not involve any time stepping).

The generalized eigenfunction method has been recently applied to wave scattering by cylinders in the context of wave waves [4]. However, this problem essentially solved the wave equation in the time domain using solutions for Helmholtz equation. The theory behind the method is applicable to bodies of arbitrary geometry, but the computations were greatly facilitated by the use of multiple expansions and addition theorems to solve the frequency domain problem. These methods only apply only to cylinders.

The generalized eigenfunction method gives the solution in the time domain as an generalized Fourier integral. If we close this contour in the upper half plane and consider only the contributions from the poles of the analytic continuation we can approximate the solution as a sum over the resonances. This is an analogous method to the *singularity expansion method* except it is derived from the generalized eigenfunction method rather than the Laplace transform. This method has proved to give simple formulas for the long time asymptotics [4], but there are many open mathematical questions about this method because it relies on many assumptions, for example that the resonance modes are near orthogonal and that the contribution from branch cuts can be ignored. However, if we compare the approximate and exact solutions we find remarkable agreement, at least in the case where there are strong resonances [4].

We show here how the solution given for water waves (but essentially for the wave equation) can easily be extended to electromagnetic scattering and show that exactly the same formulas for the solution in the time domain and asymptotic expansion can be found. Numerical results will also be presented for the case of scattering by groups of small number of cylinders.

REFERENCES

1. Povzner, A. Y., "On the expansions of arbitrary functions in terms of the eigenfunctions of the operator Du + Cu," *Mat. Sbornik*, Vol. 32, No. 74, 109–156, 1953 (in Russian).
2. Wilcox, C. H., *Scattering Theory for the d'Alembert Equation in Exterior Domains*, Springer-Verlag, 1975.
3. Hazard, C. and F. Loret, "Generalized eigenfunction expansions for scattering problems with an application to water waves," *Proc. R. Soc. Edinburgh*, Vol. 137A, 995–1035, 1975.
4. Meylan, M. H. and R. Eatock Taylor, "Time-dependent water-wave scattering by arrays of cylinders and the approximation of near trapping," *J. Fluid Mech.*, Vol. 631, 103–125, 2009.

General Vector Formulation for the EFIE and MFIE Applied to Arbitrary Sheets and Exact Expression for the Sum of Fields on Both Sides of a Flat Perfectly Conducting Sheet

Thierry Gilles and Marc Piette
Ecole Royale Militaire, Laboratoire d'Electromagnétisme Appliqué (LEMA)
Avenue de la Renaissance 30, Bruxelles 1000, Belgium

Abstract— The Electric Field Integral Equation (EFIE) and Magnetic Field Integral Equation (MFIE) are well established and demonstrated for volumic regions, but it has been found that this is not the case for zero volume bodies, namely sheets. In this work, the most general vector form of the EFIE and the MFIE is therefore given for arbitrary sheets. They are obtained through a complete and original derivation, with special attention for the sharp edges that are always present in the case of sheets. These two integral formulations are then applied and particularized to dielectric and perfectly conducting sheets. Starting from the general vector formulations, it is also made clear when and how the tangential component of the EFIE and MFIE can or cannot be used to obtain the equivalent current densities in the framework of the Method of Moments. Finally, two closed form expressions for the sum of the fields on both sides of a flat perfectly conducting sheet are demonstrated and supported by several exact analytical examples.

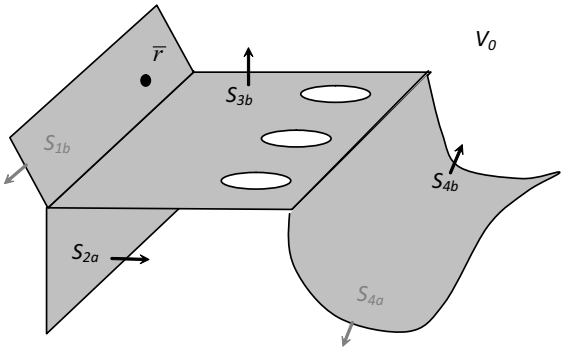

Figure 1: Zero volume sheet.

Session 1P8
EMC and Mitigation Techniques: Theory and Practice 2

Efficient Use of "White Spaces" in the UHF Band (470–862 MHz) Employing Genetic Algorithms

Nikolaos C. Kapsalis and Panayotis G. Cottis
Division of Information Transmission Systems and Material Technology
School of Electrical and Computer Engineering, National Technical University of Athens, Greece

Abstract— The recent evolution of traditional mobile voice services to multimedia oriented communications necessitates the efficient use of the limited spectrum resources. The advent of Digital Terrestrial Television (DTT), and in particular the Digital Video Broadcasting-Terrestrial (DVB-T) standard which is currently used in Europe, may offer additional spectrum. According to the DVB-T standard, digital TV may be accommodated within a considerably reduced frequency range compared to analogue TV. Hence, after the migration of analog broadcasting services to digital operation, a significant part of the 470–862 MHz UHF spectrum, currently occupied by analog TV, will become available for new services. This part of the UHF spectrum — referred to as the "Digital Dividend" and still to be specified in many countries — will provide additional spectrum resources. In addition to the careful assignment of the Digital Dividend, the full exploitation of the spectral opportunities arising from "white spaces" dispersed all over the freed UHF spectrum will result in a more efficient spectrum usage. It seems challenging to assure that the new services destined to operate in the "white spaces" will be free from interference. The present work employs Genetic Algorithms (GAs) to implement a dynamic channel reallocation scheme for DTT networks destined to operate in "white spaces" dispersed along the Digital Dividend.

In order to formulate the problem, two kinds of matrices are introduced: the allocation matrix denoting how spectrum is allocated to the broadcasters, and the interference matrix representing possible interference from the cellular network. **A** is a matrix representing interference between broadcasters. **B** is a matrix representing the interference caused by the cellular network. The first step of the proposed GA scheme is the creation of an initial population definining a set of random allocations of every available frequency to a broadcaster. Every possible allocation of frequency channels to non interfered broadcasters will be appropriately represented as a matrix. Initially, the proposed scheme randomly allocates frequency i to broadcaster n and then creates a matrix **C** representing the allocation of frequency i, to the broadcasters taking into account both Intrabroadcasters Interference and Broadcasters Interference. As the proposed GA scheme unfolds, the members of the initial population are combined and possibly mutated and finally reallocate frequency i to all non interfered broadcasters.

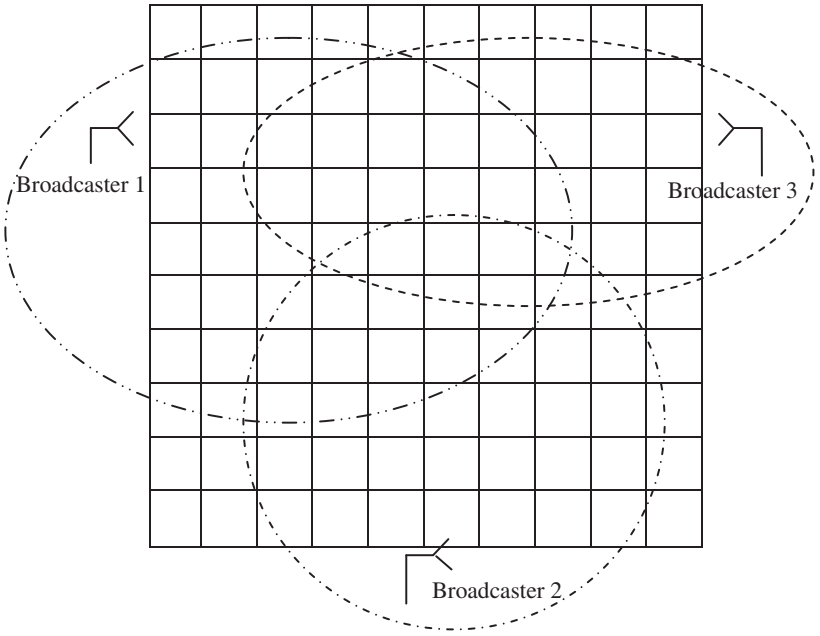

Figure 1: Typical cellular network subjected to BI. Overlapping broadcasters.

A Planar Parabolic Patch Antenna for UWB Applications

Mohamed Hayouni[1], **Nabil Dakhli**[1], **Fethi Choubani**[1], **Tan Hoa Vuong**[2], **and Jacques David**[2]

[1]6'tel Research Unit, Higher School of Communications of Tunis, Sup'Com
University 7th November at Carthage, Tunisia
[2]High School of Electronic, Electro Technical, Hydraulic and Telecommunications of Toulouse, France

Abstract— For the purpose of wideband operations, partial grounded substrate planar patch antenna is investigated. The antenna consisted of a parabolic planar monopole antenna printed on a thin dielectric FR4_epoxy substrate with a dielectric constant of 4.4 and of 35 mm by 30 mm dimensions. It is fed through a partial grounded substrate microstrip line. A lot of prototypes with different parabolic contours equations with the same length $l = 69$ mm have been simulated using commercial computer software package, Ansoft HFSS witch is based on the finite element method and have been measured using a vector network analyser Anritsu 37369C (40 MHz to 40 GHz) where the calibration plane is the SMA connector jack used to connect the antenna.

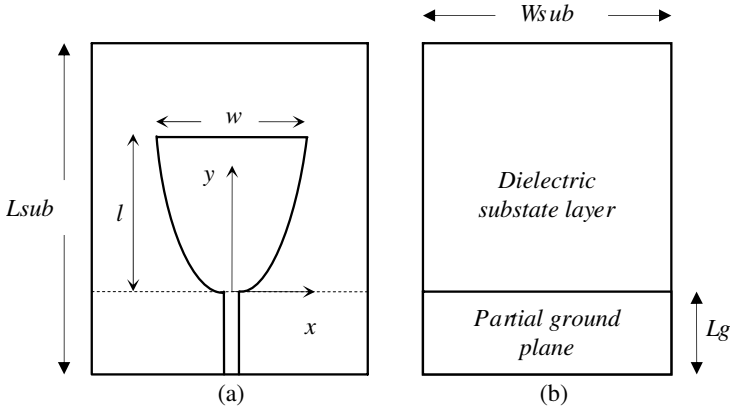

Figure 1: Antenna geometry design. (a) Top view of the design. (b) Bottom view.

Antenna parameter	Value
Peak directivity	3.443
Peak gain	2.7186
Peak realized gain	2.6865
Radiated power	0.78026 W
Accepted power	0.98818 W
Incident power	1 W
Radiation efficiency	0.78959
Front to back ratio	5.732

Table 1: Antenna parameters at 9.5 GHz frequency.

Figure 2: Photograph of the realised planar patch parabolic antenna of $y = 0.044x^2$ equation.

Table 2: Maximum field datas at 9.5 GHz frequency.

E field	Value	At phi (°)	At theta (°)
Total	340	12.696 V	280
X	7.489 V	60	90
Y	11.521 V	160	90
Z	360	6.1848 V	60
Phi	12.291 V	340	280
Theta	360	7.1416 V	60

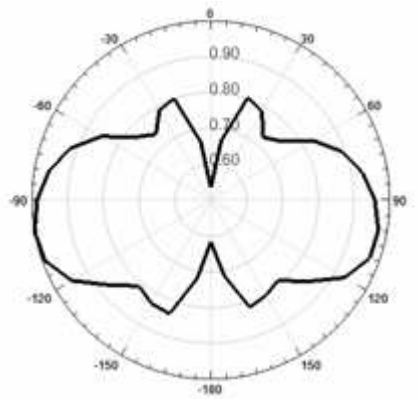

Figure 3: Normalised E field in the XY plane at 9.5 GHz.

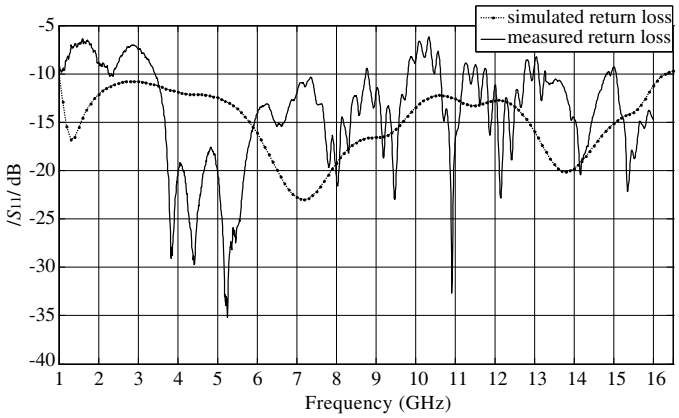

Figure 4: Measured and simulated return loss of the parabolic planar patch antenna.

The best antenna simulated and measured results were obtained from a parabolic planar patch monopole antenna defined by the geometrical equation $y = 0.044x^2$. Indeed, it have proved the ultra wide band behaviour that allowed it to be suitable candidate for wireless, satellite and mobile applications. Nevertheless measured and simulated results in terms of return loss coefficient concord on a bandwidth that ranges from 3.5 GHz to 16 GHz for a VSWR < 2.

A Novel Compact Ultra-wideband Rectangular Shaped Antenna

Mohamed Hayouni[1], **Fethi Choubani**[1], **Mohsen Denden**[1],
Tan Hoa Vuong[2], **and Jacques David**[2]

[1]6'tel Research Unit, Higher School of Communications of Tunis, Sup'Com
University 7th November at Carthage, Tunisia
[2]ENSEEIHT, France

Abstract— In this paper novel Compact Ultra Wideband (UWB) antennas are proposed. It consisted of printed planar monopoles structures that are based on a modified rectangular patch with some geometrical inserted and removed shapes at its two coins witch are circled concave and convex profiles. All the prototypes are printed on a partial grounded FR4_epoxy substrate of 30 mm by 35 mm dimensions. Both of these inserted geometrical shapes provide different electric lengths with smoothly variations witch are adjusted to enhance the impedance bandwidth and reduce the VSWR between the main resonance frequencies of the rectangular patch. A compact

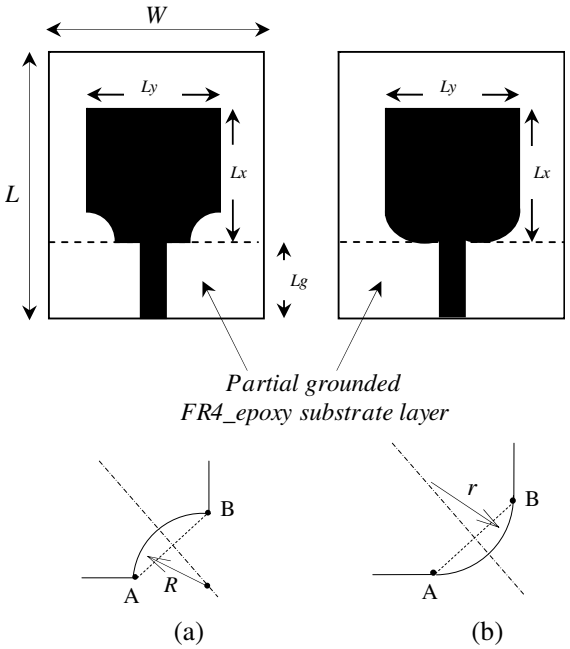

Figure 1: Geometry of the proposed UWB antenna with removed concave and convex profiles (a) antenna with concave form (b) antenna with convex form.

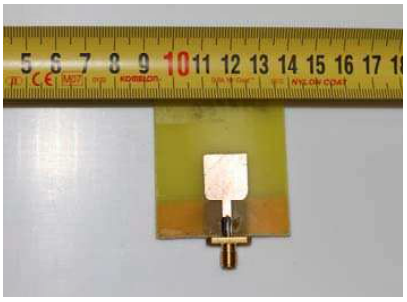

Figure 2: Photograph of the realised rectangular patch with two inserted convex circled curves of $R = 3$ mm radius.

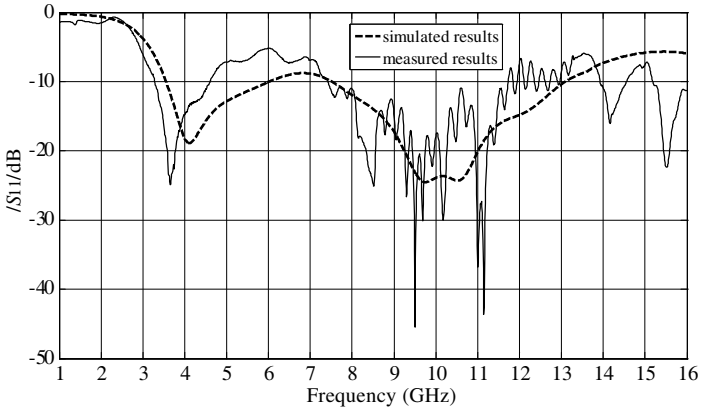

Figure 3: Measured and simulated return loss of the rectangular patch with two inserted convex circled curves of $r = 3$ mm radius.

modified rectangular patch of 14.5 mm∗15 mm dimensions with two inserted convex circled curves of 3 mm radius has been measured using a vector network analyser Anritsu 37369C (40 MHz to 40 GHz) where the calibration plane is the SMA connector jack used to connect the antenna and the measured results in terms of reflexion coefficient show good agreement with simulated ones using commercial computer software package, Ansoft HFSS witch is based on the finite element method. It proved the ultra wide band behaviour of this antenna that allowed it to be suitable candidate for wireless, satellite and mobile applications. Nevertheless, the bandwidth is ranging from about 3.55 GHz to 4.6 GHz and from 7.4 GHz to 11.7 GHz for $S_{11} < -10$ dB.

A Novel Printed Circular Antenna for Ultra Wideband Applications

Mohamed Hayouni[1], **Mohsen Denden**[1], **Fethi Choubani**[1], **Tan Hoa Vuong**[2], **and Jacques David**[2]

[1]6'tel Research Unit, Higher School of Communications of Tunis, Sup'Com
University 7th November at Carthage, Tunisia
[2]ENSEEIHT, France

Abstract— In this paper, we present a new Half Hollow cylindrical monopole antenna for ultra-wide band applications. The proposed antenna gives a bandwidth ranging from 2.3 to 6.1 GHz for $S_{11} < -10$ dB. It consists of a half-disc of 10 mm radius associated with a rectangular patch of 10.4 mm by 1 mm dimensions printed on a half hollow cylindrical substrate shape with dielectric permittivity of 2.05, 1.5 mm tick and of 46 mm by 32 mm dimensions. At the bottom of the substrate, a partial ground plane of 36 mm by 18 mm is mounted as depicted by Figure 1. The excitation is launched through a 50 Ω microstrip feed line. Design and performances are analysed using Ansoft HFSS electromagnetic simulator based on the finite element method and measured using a vector network analyser Anritsu 37369C (40 MHz to 40 GHz) where the calibration plane is the SMA connector jack used to connect the antenna as showed by Figure 3. Compared to the monopole planar antenna case as depicted by Figure 2, the half hollow cylindrical geometry antenna has reduced the space occupied by the antenna of about 36,28%. The bandwidth frequency of the proposed antenna makes this conformal antenna suitable for some radio frequencies applications. Nevertheless, it include the wireless local area (WLAN) band such as IEEE802.11, wireless personnel area network (WPAN) such as Bluetooth and it contains the two ranges of the ISM (Industrial, Scientifics, and Medical band) bands defined by the ITU-R (International Telecommunication Union-Radio communication sector) witch are [2.4 GHz, 2.5 GHz] and [5.725 GHz, 5.875 GHz]. The proposed UWB antenna can be also used in the biomedical

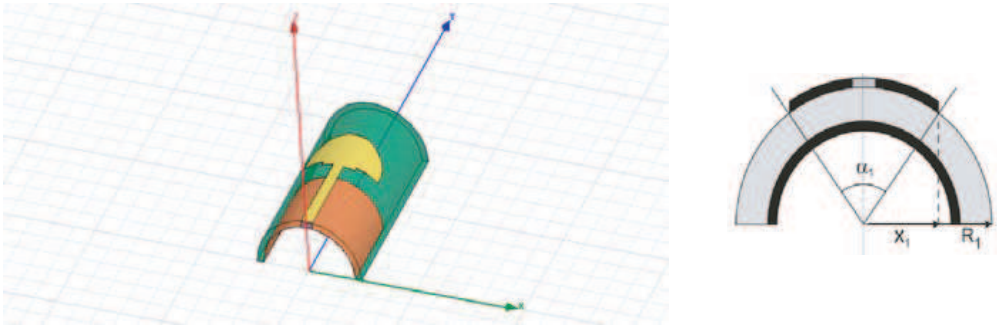

(a) (b)

Figure 1: The proposed hollow half cylindrical antenna design: (a) perspective drawing and (b) side view.

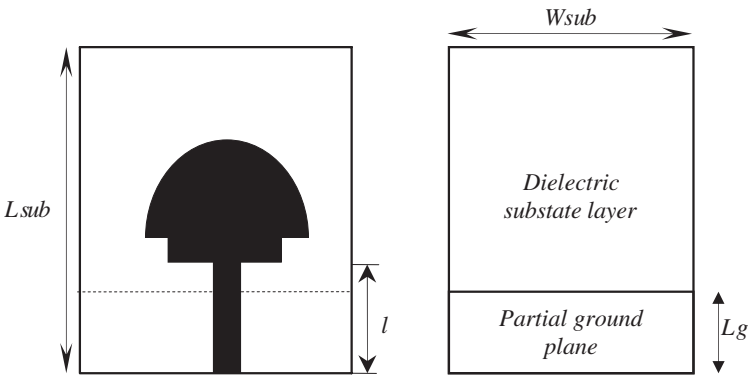

(a) (b)

Figure 2: UWB planar patch monopole antenna: (a) top view and (b) bottom view.

systems where it can be mounted on medical devices. All the measured and simulated results in terms of VSWR, radiation parameters of the conformal and planar monopole antennas will be presented in the full paper.

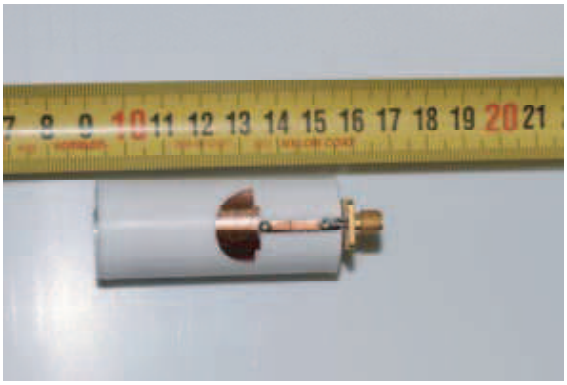

Figure 3: Photograph of the realised half hollow cylindrical UWB antenna.

Circular Patch Antenna Directivity Enhanced by Left-handed Material Cavity

Mondher Labidi, **Nabil Dakhli**, **Jamel Belhadj Tahar**, **and Fethi Choubani**
6'Tel Research Unit, Higher School of Communications of Tunis, Sup'Com
University 7th November at Carthage, Tunisia

Abstract— During the past few year, many investigation have been proposed for designing patch antennas. Feresidis [1] and Zhou [2] showed that the half wavelength restriction of a Fabry-Perot cavity antenna can be reduced to respectively a quarter wavelength and a tenth (10th) wavelength by using a novel type of metamaterial-based resonant cavity in order to design compact directive electromagnetic sources based on a single radiating antenna.

In the present work, we study the properties and characterization of an optimized cavity of a patch antenna at about 10 GHz. The cavity is composed of a substrate, a high impedance surface (HIS) and a partially reflective surface (PRS).

The high impedance surface (HIS) consists of periodic metallic patterns printed on a dielectric substrate, they have very interesting electromagnetic properties, because they allow the propagation of electromagnetic waves along the surface only for certain frequency bands.

Moreover the HIS has very important property of resonant impedance surface. This resonance leads to the zero crossing of the phase coefficient reflection. The HISs creates a current in phase with the surface source. Therefore, these surfaces behave as artificial magnetic conductors (AMC).

In this study we use an artificial magnetic conductor (AMC) surface with reflection phase zero instead of a perfect electric conductor (PEC) surface and a partially reflective surface (PRS) with a frequency dependent reflection phase. In addition, we utilize Left Handed Materials (LHM) composed of HIS-AMC and PRS-AMC in the near environment of a circular patch antenna in order to enhance its performances. Using LHM technique, the gain and directivity of the patch antenna are greatly improved and the results obtained from the numerical simulations using CST Microwave show an enhancement of ~ 26 dB for the gain and a better directivity of the antenna in order of 16° instead of 85.5°.

Coupled Non Uniform Transmission Lines: Modeling and Crosstalk Performances

Mnaouer Kachout, **Jamel Bel Hadj Tahar**, **and Fethi Choubani**
6'Tel Research Unit, Higher School of Communications of Tunis, Sup'Com
University of the 7th November at Carthage, Ghazala Technopark, Ariana 2083, Tunisia

Abstract— In this paper we propose a rigorous method to evaluate the crosstalk performance for coupled non uniform transmission lines. Single and coupled non uniform transmission lines (NTLs) are widely used in RF and microwave circuits as resonators, impedance matching, delay equalizers, filters, wave shaping, analog signal processing, VLSI interconnect and etc.. MTL is a system consisting of N conductors and a conducting shield or common return conductor and serving to transmit signals via guided electromagnetic waves-mostly of transverse electromagnetic (TEM) or quasi-TEM type. Such a system is further called $N+1$ MTL. From telecommunication cables (of the lengths of meters or kilometers) through interconnects of equipment modules (of the lengths of centimeters) down to the micrometer scale for micrometer integrated circuit (MMIC) interconnects, all can be treated as MTL. Modern trends in circuit designs such as operating at higher frequencies, lowering threshold voltages, and shrinking device geometries have made accurate prediction of electromagnetic (EM) compatibility an indispensable component in the design cycle. Susceptibility to electromagnetic interference (EMI) can severely degrade the signal integrity of the system. One of the main sources for the EMI is the coupling between the electrical interconnects, which serve as antennas at high frequencies. Many researches about MTL are conducted, such as multi-pin connector characteristic, crosstalk prediction of cable bundle, field analysis of digital bus. In this method, the width of the non uniform line is subdivided into a large number of rigorously coupled narrow lines. So, non uniform lines can be considered as a coupled multi-conductor transmission line. An electric equivalent model is developed to calculate the crosstalk between coupled non uniform transmission lines. Determination of the per-unit length capacitance and inductance parameters of the model is introduced. Finally, we demonstrate that coupled non uniform lines give the best performance in term of crosstalk compared to coupled microstrip lines.

Design of Non Uniform Meander Line Antennas for Passive RFID Tags in the UHF Band

Karim Bentaher[1], **Fethi Choubani**[1], **Tan-Hôa Vuong**[2], **and Jacques David**[2]

[1]6'tel Research Unit, High School of Communications, Sup'Com
University 7 Novembre of Carthage, Tunisia
[2]ENSEEIHT, University of Toulouse, France

Abstract— Since their first commercial use in 1970, barcodes are still the main automatic identification system. What makes barcodes so famous is their low cost. But the optic technology used to capture the data needs physical proximity, and makes the scanner unable to read more than one label at a time. This is the major limitation of the barcodes, and the reason why RFID was introduced. This novel technology uses radio frequency (RF) signals to enable wireless communication between the reader (interrogator) and the tags (transponders). Obviously, RFID systems can read data from multiple tags, simultaneously, within a short time interval.

Development of far-field passive tags occurred during the first half of the twentieth century thanks to technological advances in the field of low power consumption integrated circuits. Passive tags are essentially composed of a chip and an antenna laying on a substrate. They are actually seen as the "future wireless barcodes". But further research aiming at lowering manufacturing cost is still needed. This makes dipole based antennas so popular commercially, and an attractive choice for passive tags designers. In the UHF band, the dipole length ($\sim 16.5\,\mathrm{cm}$) is above standard label dimensions (10×5, 10×10, $10 \times 15\,\mathrm{cm}$). This size constraint is solved using different miniaturization techniques. The most known method is meandering.

In this paper, we study the effect of line width on non-uniform meandered antenna with inductively coupled feed. The performance is explored in terms of power transfer efficiency and tag free space read range (dmax).

Design of Composite Electromagnetic Wave Absorber Made of Fine Spherical Metal Particles Dispersed in Polystyrene Resin

Y. Guan, **K. Sakai**, **Y. Sato**, **and S. Yoshikado**
Department of Electronics, Doshisha University, Japan

Abstract— Development of an electromagnetic wave absorber suitable for frequencies above 1 GHz is required with the increasing use of wireless telecommunication systems or electronic toll collection system. In this study, the frequency dependences of the relative complex permeability μ_r^*, the relative complex permittivity ε_r^* and the absorption characteristics for composite electromagnetic wave absorbers made of fine spherical metal particles, such as aluminum or copper dispersed in polystyrene resin were investigated in the frequency range from 1 to 40 GHz. Theoretical calculation method of μ_r^* considering the particle size distribution of spherical metal is also proposed based on the theoretical calculation for single particle size to predict the frequency dependences of μ_r^* precisely and design an electromagnetic wave absorber.

The real part μ_r' of μ_r^*, must be less than unity to satisfy the non-reflective condition for electromagnetic wave in the high frequency region above several GHz. In an electromagnetic wave absorber dispersed metal particles, an eddy current flows on the particle surface and a reverse magnetic moment appears. Thus, μ_r' becomes less than unity. Furthermore magnetic loss arises by eddy current loss. Thus, electromagnetic wave power can be absorbed by the composite made of polystyrene and metal particles which satisfies the non-reflective condition.

The spherical particle of three kinds of diameter was prepared using atomizing method. The frequency where μ_r' became less than unity depend on the size of metal particle and this frequency sifted to high frequency side with decreasing the particle size. The measured values of the real μ_r' and imaginary μ_r'' parts of μ_r^* approached to the calculated results considering the particle size distribution. The relative complex dielectric constant for an electromagnetic wave absorber made of spherical particles was much smaller than that made of non-spherical particles, because spherical particles cannot contact each other easily. Thus, the composite made of polystyrene and spherical metal particles absorbed more than 99% of electromagnetic wave power at frequencies above 1 GHz.

Identifying EMC Interference Sources of a Microwave Transmission Module in Order to Locate Them

P. Descamps[1], **G. Ngamani-Njomkoue**[2], **D. Pasquet**[1], **C. Tolant**[2], **D. Lesénéchal**[1], **and P. Eudeline**[1]

[1]LaMIPS, Laboratoire Commun CRISMAT, UMR 6508 CNRS
6 boulevard Maréchal juin, CAEN, France
[2]Thales Air Systems SA, Technical Unit Radio Frequency (TU-RF)
Technology & Innovation (REIRI-Y), Z.I. du Mont Jarret, Ymare 76520, France

Abstract— In the design of microwave transmitter modules, many signals of different types coexist in a small space. It is possible that module dysfunctions occur due to the presence of electromagnetic disturbance type. It's the reason why it is important to understand and quantify these disturbances and in what form they spread in the structure. To do this we have studied a microwave simplified demonstrator placed in a shielded box by reducing the complex electromagnetic study of the complete transmission module taking into account a maximum of electromagnetic effects with and without shield. The electromagnetic (EMC) measurements of the demonstrator were conducted in a GTEM cell to isolate the demonstrator from all external interference and to compare to the 3D electromagnetic simulations, allowing to locate parts of the sensitive circuit to disturbances and to determine the sources of disturbances of the module. The simulation of the demonstrator using electromagnetic simulator allowed us to obtain a real internal mapping of the demonstrator. This mapping was used to characterize the electromagnetic behavior of the overall structure issue and identify sources of disturbance. This study should be complemented by measurements to scan the surface of the circuit using appropriate probes and serve to validate the method.

Low Frequency Monopole-like Small Metamaterial Antenna

Nabil Dakhli[1], **Mohamed Hayouni**[1], **Fethi Choubani**[1], **and Jacques David**[2]

[1]Research Unit of Telecommunication Systems (6'Tel) at Sup'COM, Tunisia
[2]ENSEEIHT, France

Abstract— Components based on artificial structures called metamaterials have received much attention these last years because of a number of advantages such as its small size, low design complexity and high performances for radiating or guiding structures Antenna size reduction is due to resonance property at the infinite wavelength which corresponds also to 0° phase shift. A general model for a CRLH/DNG TL unit cell consists of a series capacitance, a series inductance, a shunt capacitance, and a shunt inductance. By modifying either shunt capacitance and/or shunt inductance circuit parameters, the infinite wavelength frequency is changed independently from the physical size of the antenna. Thus a small size antenna can be designed. In this paper, we propose a monopole-like small antenna resonating at low frequency based on LC loaded transmission line (TL). The main radiating elements of the antenna are the two vias which are connected in series to an inductor at each edge of a transmission line in between. The inductance values are tuned in order to calibrate the flowing currents in the posts to be in phase so that the radiated fields are constructive in the far field region. Full-wave simulations were carried in order to study the properties of the antenna at 434 MHz. The antenna is compact; it has $\frac{\lambda_0}{230} \times \frac{\lambda_0}{25} \times \frac{\lambda_0}{14}$ volume, offers a fractional bandwidth of 1.3%, a radiation efficiency exceeding 50%, and a monopole-like radiation pattern.

Accurate Approximation of Error Probability for Two Types of Adaptive Antenna-based Receivers over Fading Channels

R. Haddad and R. Bouallèguee
Laboratory Research in Telecommunication 6'Tel, High School of Communication of Tunis, Tunisia

Abstract— Multipath fading and Multiple Access Interference (MAI) are the major constraints on the performance of wireless communication systems. Antenna arrays have been considered to increase the system capacity through mitigation of such impairments. In this paper, we focused our research on the performance of two kinds of smart antenna receivers in order to gain from the enhancements of both: multiuser detection and adaptive antenna.

In principle, a multiuser receiver allows constructive combination of multipath signals received by an array of antennas while minimizing the MAI's effect. In this contribution, an accurate average Bit Error Rate (BER) formula is derived in the context of asynchronous transmissions for two types of smart antenna receivers: The BPSK smart antenna receiver and the OQPSK smart receiver. The proposed model is shown to provide the performance of the complex smart antenna receivers in Rayleigh as well as Ricean fading channels under different conditions.

In fact, the physical channel model incorporates parameters such as: user mobility, azimuth angle of arrival, angle spread and Doppler frequency, which have critical influence on the performance of smart antennas. The proposed model is implemented in software using Matlab. The simulated channels are analysed to confirm that the proposed channel model is able to accurately simulate Rayleigh and Ricean fading environments.

Simulation results presented for the two types of receivers, under varying a variety of user, antenna and channel scenarios, confirm the validity and accuracy of the analytical results.

Our analysis is based on modeling the angular gain of the spatial filter that approximates the passband (or in-beam) and the stop-band (or out-beam) with an equivalent attenuation. The proposed model confirms the benefits of adaptive antennas in reducing the overall interference level (intercell/intracell) and to find an accurate approximation of the error probability.

In the two kinds of receivers, we assessed the impact of smart antenna systems and we considered the case of conventional single antenna receiver model as reference (single user/single antenna).

Optimization of a Patch Antenna Performances Using a Left Handed Metamaterial

Akram Boubakri and Jamel Bel Hadj Tahar
Graduate School of Communications of Tunis, Sup'Com
University of 7 November of Carthage
Route de Raoued, Cité Elghazela, Ariana 2083, Tunisia

Abstract— There are many design adopted in the literature to improve antenna properties (gain, directivity and size...) for instance antenna array, Yagi antenna and patch antenna... However this design leads to improve one property in detriment of others and provide also bulk size and high cost.

In few past years the use of metamaterials gives the opportunity to achieve many enhancements at once thanks to the unusual properties of metamaterials either with metamaterial built antenna or with placing such a medium in the near antenna environment.

In this second solution we find two categories, the first which consist of placing a superstrate of high permittivity or permeability above the patch antenna (suggested by Jackson and Alexópoulos) and the second solution proposed by Nakano et al. is to sandwich the patch antenna by dielectric layers of the same permittivity.

Here, the work is based on the use of a LHM in the near environment of a patch antenna in order to enhance its performances. For this study, a circular patch antenna has firstly been designed on a dielectric board of relative permittivity and permeability of 2.5 for a working frequency of about 10 GHz. Then, a LHM considered to be characterized by an effective permittivity and permeability of -2.5 is placed above the patch antenna. The results obtained from numerical simulations using Ansoft's *HFSS* show that an improvement of the gain by 4.7 dB is achieved, more directional antenna, less backward radiation and inter-element coupling problems obtained by the use of a LHM in the near environment.

Compared to the method used by Jackson and Alexópoulos, we do not require high values of permittivity or permeability of the superstrate. Also simulations show's that sandwitch method lead to performances better than superstrate one's.

Simulation and Measurement Techniques to Estimate the High Power Electromagnetic Coupling into Small Casings

Florian Brauer, **Tobias Dyballa**, **and Jan Luiken ter Haseborg**
Institute of Measurement Technology and EMC, Hamburg University of Technology
Hamburg, Germany

Abstract— With the growing number of electromagnetic interferences (EMI), especially high power electromagnetics (HPEM), such as UWB-(ultra wideband), DS-(damped sinusoids) or HPM-(high power microwave) sources, communication systems are more and more vulnerable. In supposable scenarios it is already possible, that HPEM sources could be used by terrorists to disturb electronic systems on purpose. This threat is known as intentional electromagnetic interferences (IEMI) [1]. IT-components are spread out widely on the market and are already used in huge areas of current applications. An error or a momentary breakdown of the data transfer can be extremely critical for some applications. Especially the coupling of HPM signals can be critical, since the high power pulses in the RF region can easily couple through the small apertures of casings (e.g., Ethernet switches), which results in a considerable interior field strength disturbing sensitive system parts [2].

In this contribution different methods are presented to determine the shielding effectiveness of the casing of a small Ethernet switch. Simulations are performed with a CST model of the casing and measurements are carried out with a small optical sensor. With the help of a special 2-D scanning system the sensor can be placed directly inside the casing also with parts of the interior electronic circuitry to achieve space-resolved measurement results [3]. In Figure 1, the simulation model and results for the empty casing and the measurement setup as well as results for the casing with interior electronic circuitry for one position of the sensor in the center inside for each case are presented.

In the simulation sharper resonances and partially different characteristics can be seen depending on the interior electronic circuitry.

With the help of variations in the simulation model and the space-resolved measurement method an evaluation of the different methods is possible. Additionally the results provide the basis for the estimation of the electromagnetic coupling of HPEM signals into the casing. In the final presentation additional results for coupled time domain HPEM signals will be shown. Therefore predictions about the susceptibility and the need for protection concepts for IT systems are possible. Moreover the used methods should have the potential to be used also for other applications.

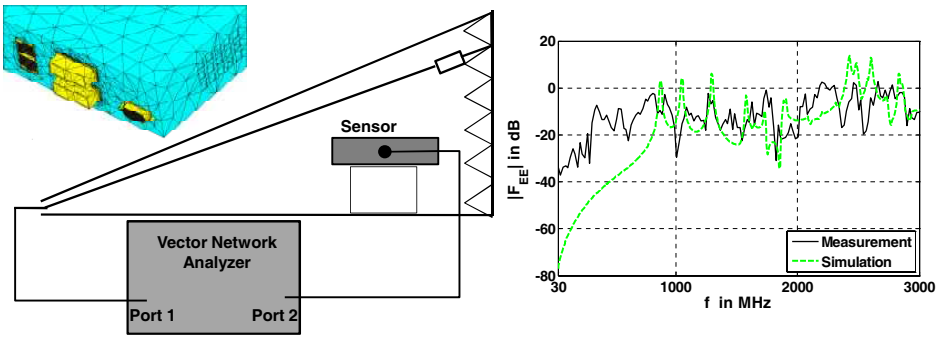

(a) (b)

Figure 1: (a) Simulation model and measurement setup to determine the transfer function of an Ethernet Switch's casing. (b) Results for the simulated and measured transfer function.

REFERENCES

1. Radasky, W. A., C. E. Baum, and M. W. Wik, "Introduction to the special issue on high-power electromagnetics (HPEM) and intentional electromagnetic interference (IEMI)," *IEEE Transactions on Electromagnetic Compatibility*, Vol. 46, No. 3, 314–321, August 2004.

2. Brauer, F., F. Sabath, and J. L. ter Haseborg, "Susceptibility of IT network systems to interferences by HPEM," *IEEE EMC Symposium*, Austin, Texas, USA, August 17–21, 2009.
3. Dyballa, T. and J. L. ter Haseborg, "Investigations of the EM-coupling in the near and far field of a transmitting antenna according to EUROCAE ED-130," *IEEE EMC Symposium*, Fort Lauderdale, Florida, USA, July 25–30, 2009.

Matching Technique Design for Multi-fed Full Wave Dipole Antenna

Yahya S. H. Khraisat[1, 2], **Khedher A. Hmood**[3], **and A. Anwar**[3]

[1]Electrical and Electronics Department, Al-Huson University College, Al-Balqa Applied University, Jordan
[2]Hijjawi Faculty for Engineering Technology, Telecommunications Engineering Department
Yarmouk University, P. O. Box 1375, Irbed 21110, Jordan
[3]School of Electrical and Electronic Engineering, Engineering Campus
Universiti Sains Malaysia, Seri Ampangan, Nibong Tebal 14300, Penang, Malaysia

Abstract— This paper is focused on the derivation of equations for a full-wave dipole antenna based on feeding techniques. The current distribution was measured, followed by the measurement of parameters of antenna like gain, radiation patterns and input impedance. Based on these observations four equations for current distribution were eventually formulated. These equations were then used to compute the values of the same parameters of the antenna. Finally, the values of parameters obtained practically and theoretically were compared to analyse the validity of the developed equations.

Session 1P9
Poster Session 2

Global Maps of TEC and Conditions of Radio Wave Propagation in the Mediterranean Area

O. A. Maltseva, N. S. Mozhaeva, and G. M. Glebova
Institute of Physics, Southern Federal University, Russia

Abstract— Global maps of TEC are a huge array of TEC data provided by various centers: JPL, CODE, UPC, ESA over the Internet, covering a period exceeding the cycle of solar activity. According to many experts, this array can be used both for physical investigations and for modeling and predicting conditions of radio wave propagation, despite some limitations of determination of the TEC (2 hour interval mapping, conversion of STEC into VTEC using a constant height, failures of phase and others). For the problems of radio wave propagation is often necessary to have absolute values of TEC. However, as is known, the values of various maps differ from each other and from the values obtained at individual stations due to differences in methods of determining the TEC and mapping. Differences can reach a factor of 1.5–2, so the question might arise, which card to choose in certain circumstances. Using the values of the IGS to some extent solves the problem, but these weighted average values are often far from the values of the best cards. Moreover, despite the existence of these values, in many studies the specific card is used without giving any reason for which one or another card is selected. In this paper the choice of map is associated with the assessment of the possibility to determine the values NmF2 (foF2) from an array of cards TEC. The main role is played by the coefficient of proportionality between NmF2 and TEC (the equivalent slab thickness of the ionosphere TAU). It is shown that the use of regression TAU (NmF2) allows to: 1) choose a card which provides the best fit of calculated foF2 into experimental values, 2) fill the gaps of foF2 data of vertical sounding, 3) increase correspondence between the values of foF2 calculated from the TEC and experiment in the area, exceeding the radius of spatial correlation of foF2, in comparison with other methods. The results are illustrated by the data of stations in the Mediterranean region. Since this region is characterized by increased activity of the layer Es, the features of the map usage to determine foF2 from TEC in the presence of Es are discussed.

Analysing the Attenuation at Mobile Phone Bands Provided by Vegetation Supported by Lattice Structures

Paula Gómez, Iñigo Cuiñas, and Ana V. Alejos
Dept. Teoría do Sinal e Comunicacións, Universidade de Vigo, Spain

Abstract— Population in many countries is afraid of the presence of radioelectric antennas transmitting in the surroundings of their houses or workplaces. Although most of the medical research indicates that there is no risk for the human health exposed to controlled electromagnetic fields, under some restrictions defined by the ICNIRP, the WHO also recognises a lack in the research in some fields: long-term exposure, or children and elderly exposure. Trying to mitigate the human contact to electromagnetic fields, a proposal involving the construction of vegetation walls to provide shadowed areas has been previously done.

This contribution goes beyond: the wall or barrier could be constructed by means of a lattice structure (as the supports of climbing plants in parks and gardens) holding some foliated plants or bushes.

A mathematical parameterization for the attenuation induced by rows of trees and shrubs supported by lattice structures is here proposed with the aim of obtaining an empirical method to approach the surplus attenuation induced by this architecture for GSM and UMTS bands.

Models obtained are based on measurement campaigns with lattices of different material (metallic, plastic, wood) and pattern design for both vertical and horizontal polarization at 900, 1800 and 2100 MHz. Empirical results have shown that the presence of the lattice supporting structure enhances the attenuation provided by the vegetation fence, becoming a rather homogeneous value mathematically parameterizable.

Equations presented connect lattice parameters (material and pattern design), vegetation specie characteristics (canopy diameter, density, foliage) and shrubs and trees layouts to obtain the attenuation induced by these barrier configurations. Results show a simple method to obtain an accurate value for the excess attenuation provided when designing vegetation fences supported with lattice structures to reduce electromagnetic pollution in sensitive areas.

GPS-Galileo Antenna with Circular Polarization

M. Silva Pimenta, **F. Ferrero**, **J. M. Ribero**, **and R. Staraj**
Laboratoire d'Electronique, Antennes et Télécommunications, CNRS UMR 6071
Université de Nice-Sophia Antipolis, Bât. 4, 250 rue Albert Einstein, Valbonne 06560, France

Abstract— Textile antennas are emerging as an interesting solution for improving the security for persons in dangerous area. Firemen in mission could be localized in real time, for example. There are also a lot of military applications for the soldiers...

Low profile GPS and Galileo antennas are needed for this kind of applications. These antennas have to be as thin as possible, flexible and easy to integrate in clothes. There are many restrictions on the desired types of antennas but the most important are certainly the thickness, the low permittivity material, the total size, and the right hand circular polarization desired in all the bands. This work is a pre-work for a later integration of antennas in clothes for the two standards GPS and Galileo. The work presented in this paper is based on the dual-band planar antenna, in view to reduce the total thickness of structure. The design of the antenna was done with low permittivity material like foam, and using thin sheets of Duroid of 0.127 mm thickness in view to print the antenna. Circular polarization in printed antennas can be obtained as well using a single or a dual feed. Single feed structures have a limitation over the circular polarization. Obtained circular polarization axial ratios AR bandwidths are in average closed to 2%. The use of dual feeds in quadrature is then more appropriate for GPS-Galileo bands.

The antenna is a dual band antenna. The dual frequency behavior is obtained using slots well placed on a simple square patch feed with a 90° wideband coupler. Compared to [1] which uses lumped elements, our coupler is composed of a power divider and a phase adjusting network using a CRLH (Composite Right Left Handed) line with printed elements. The patch is printed on a 0.127 mm thick Duroid substrate of permittivity 2.2. The antenna is separated from the ground plane by a foam layer of 6 mm thickness. The wideband coupler is printed on a 0.762 mm thick Duroid substrate of permittivity 2.2. It is placed at the bottom of the ground plane, and thus the overall antenna height is 6.88 mm. The ground plane is drilled for the feeding of the patch.

The antenna was simulated and designed using HFSS software, and the coupler was designed with ADS software. A prototype was realized. The antenna work in the E1-E2-L1 bands (central frequency 1.575 GHz) and in the other band E5a-E5b-L5-L2 (central frequencies 1.176-1.202-1.176-1.227 respectively) with −6 dB return loss, the circular polarization is obtained in all bands and also with good radiation pattern.

REFERENCES

1. Tseng, C. H. and C. L. Chang, "A broadband quadrature power splitter using metamaterial transmission line," *IEEE Microwave and Wireless Components Letters*, Vol. 18, No. 1, January 2008.

Microstrip Antenna for Microwave Imaging Application

S. Adnan, **R. A. Abd-Alhameed**, **H. I. Hraga**, **I. T. E. Elfergani**, **J. M. Noras**, **and R. Halliwell**
Mobile and Satellite Communications Research Centre, University of Bradford
Bradford, West Yorkshire, BD7 1DP, UK

Abstract— Breast cancer is the most common form of cancer found in women; early detection is the best protection for long time survival. X-ray mammography is currently the popular screening method which is X-ray imaging of a compressed breast. According to the reports limitation of X-ray mammography provide clear motivation for the development of new imaging tool to assist in early detection. For long time microwave engineers try to implement non-ionizing electromagnetic waves to image human body to detect cancer. Over the past several years significant progress has been made to use the microwave for breast cancer detection. Microwave imaging can be defined as seeing the internal structure of an object by illuminating the object with low power electromagnetic wave at microwave frequencies. In microwave frequency range Passive, Hybrid and Active approaches to breast cancer have been considered for research. The methods seem very attractive for patients because both ionizing radiation and breast compression are avoided.

Active method using radiation of microwave frequency band to detect the presence of tumour cancer in women breast is most widely adopted method. This method is well classified into tomography and radar-base approaches [1]. In tomography a single transmitter is radiating into the breast while a number of antenna placed around the breast to receive any scattered wave. The procedure is repeated for various position of transmitter. Depending on the acquisition of data these data will be processed to produce a 2-dimensional or 3-dimensional image of the breast [2]. For radar base microwave imaging short-pulsed signal is transmitted from a single UWB antenna into the breast tissue and receives any back-scattered wave from the same antenna. This process will be repeated for different location around the breast. Much energy is reflected back with the presence of tumor and this may significantly affect the response to predict the location of tumour. The travel time of the signals at various locations are recorded and computed [1]. This system does not require complex image reconstruction algorithms similar to any radar-based system and hence offer detailed information than the tomography microwave imaging method.

The antenna which is used as transceiver front end as radiating and sensor element, should exhibits ultra-wideband response to alter signals of high level of resolution. Such requirements thus limit the class of antenna that can be utilized. Large fractional bandwidth, low side lobes

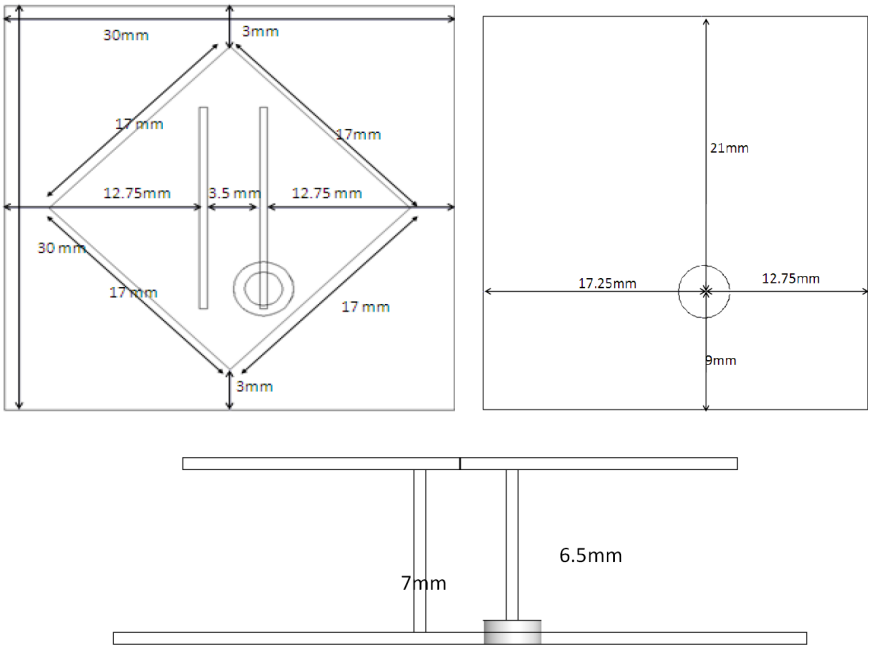

Figure 1: Geometry of the Antenna. (a) Top view, (b) Ground plane, (c) Side view.

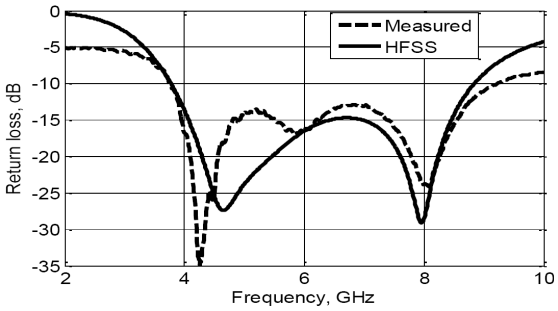

Figure 2: The input return loss of the proposed antenna.

and low level of mutual coupling when two antennas are considered to operate in a short range of a complex medium. This paper presents a microstrip antenna design process to improve the operation of detection system of a possible existence of cancer cells inside the human breast tissue. Figure 1 shows the overall dimensions of the proposed compact antenna. Dimension and other design parameters are obtained by performing several parametric studies. The simulated and the measured of input return loss of the proposed antenna are shown in Figure 2, and found in good agreement.

REFERENCES

1. Fear, E. C., "Microwave imaging of the breast," *Technology in Cancer Research & Treatment*, Vol. 4, 69–82, February 2005.
2. Meaney, P. M., M. W. Fanning, D. Li, S. P. Poplack, and K. D. Paulsen, "A clinical prototype for active microwave imaging of the breast," *IEEE Trans. Microwave Theory Tech.*, Vol. 48, 1841–1853, 2000.

Propagation Characteristics of 24 GHz Frequency Band for Automotive Collision Avoidance Radar

Deock-Ho Ha[1], **Yeon-Wook Choe**[2], **Jee-Youl Ryu**[1], **and Sung-Un Kim**[1]

[1]Department of Telecommunication Engineering, Pukyong National University, Busan, Korea
[2]Department of Control and Measurement Engineering, Pukyong National University, Busan, Korea

Abstract— In this paper, we describe the propagation characteristic of 24 GHz frequency band used for automotive collision avoidance radar (ACAR). To investigate the radio propagation characteristic of ACAR signals, we used 24 GHz UMCW (Un-Modulated Continuous Wave) signals using by several polarized antenna combinations. To detect the accurate message data for safety guiding ACAR, we analyzed and investigated the optimum receiving condition from the short range UMCW signal. From the measurement analysis, it can be clearly seen that the short range UMCW signal can be encountered to multipath interference due to scattering rays from the ground plane and adjacent moving vehicles. In addition, it was also found that the received signal strength of circularly co-polarized antenna shows the most strong envelopes and best fading reduction effect.

Introduction and Measurement Results: In this paper, we investigate which is best propagation condition to reduce the multipath fading when the combinations of transmitting and receiving polarized waves are adopted. In the narrowband signal measurement, the signal generator transmits the 24 GHz UMCW radio frequency band. And also, we examined the broadband signal which show the characteristic of amplitude fluctuation within broad bandwidth which the transmitting frequency is sweeping from 23.9 GHz to 24.1 GHz. In order to obtain maximum power transfer between two antennas, we used several polarized antenna which generate the vertical, horizontal, and circular polarized waves. From the measurement analysis, it was found that the circular co-polarization combination shows better fading reduction result than the cases of circular cross-polarization, vertical polarization, and horizontal polarization combination, respectively. Fig. 1 shows the results of fading reduction effects for the polarization combinations. Fig. 2 shows the broadband signal strengths received by frequency sweeping with 200 MHz wideband.

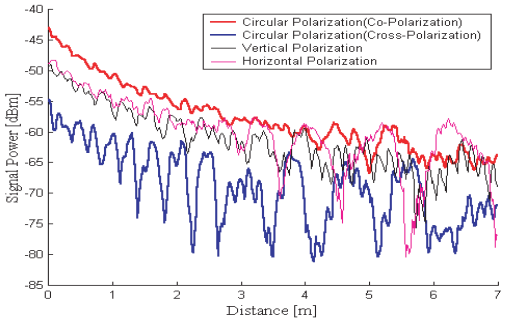

Figure 1: Signal envelops of each polarized waves.

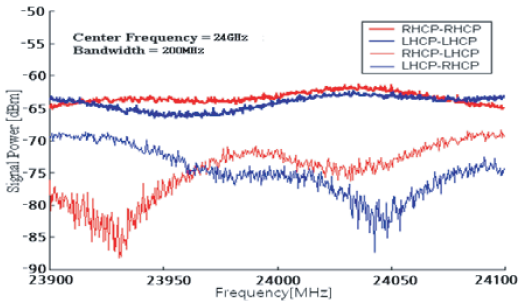

Figure 2: Wideband characteristics of circular polarization combinations.

Swept Versus Real-time Spectrum Analyzer Ability to Accurately Asses Electromagnetic Exposure due to Wireless Communications Signals in the Environment: An Analysis

Paul Bechet and Simona Miclaus
Land Forces Academy, Sibiu, Romania

Abstract— There is a need to increase precision of field level assessment of stochastic signals like those in wireless local area networks (WLAN) used for data communication in indoor areas. No standardized procedure exists yet, so as highest technological available equipment may represent a suitable reference for best available accuracy to be obtained by measurements. Present study aimed to identify optimal settings of a swept spectrum analyzer (SSA) used to measure the electric field level around WLAN sources by comparison to the results obtained when using a real-time spectrum analyzer (RTSA), which is highly advanced but prohibitive for many metrological labs (Fig. 1). Measurement sessions in present work investigated both stable WLAN signals produced in the lab in ideal conditions by a vector signal generator and realistic WLAN signals produced by an access point, in various operational conditions, with the scope of procedure validation. There are a group of settings of major importance for achieving high precision assessment in case of routine labs analyzers, like the SSA, and they are: resolution bandwidth, video bandwidth, sweep time, number of sweeps, etc..

The major problem is that WLAN signals are pulsed, short duration and wide-banded, so that one of the key aspects when using a SSA is establishment of proper sweep time in connection to the time when signal source is active. When the propagation environment is unstable and the SNR is low, averaging to get the active time may be troublesome and it becomes necessary to involve powerful statistic techniques before proceeding to field assessment. Solutions given in present paper start from a classical analysis in Zero span mode with the SSA and go to advanced time-frequency analysis with the RTSA. Signal's spectrogram obtained by proper temporal windowing offers a better precision in active time evaluation (Fig. 2). Obtained results sustain the conclusion that SSA may be successfully used for exposure assessment of stochastic-like signals when specific care and adequate procedure is applied.

Figure 1: Spectrum analyzers used for field assessment and the WLAN acces point.

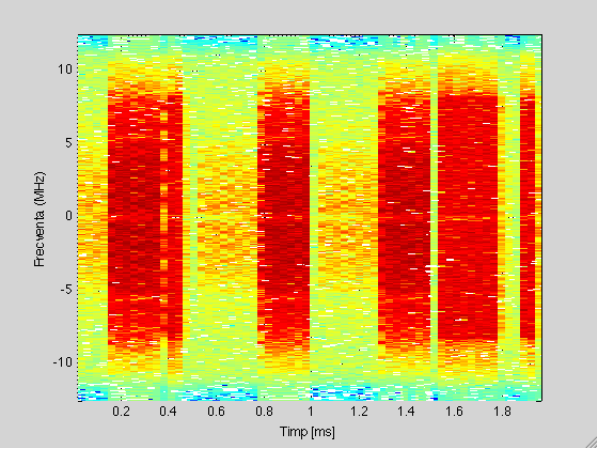

Figure 2: Spectrogramm of the WLAN signal: signal is active between 0.2–04 ms; 0.8–1 ms; 1.3–1.5 ms and 1.6–1.8 ms.

A Compact Dual-band Reconfigurable Frequency Selective Reflectors for Pattern Diversity Antenna Application

Chih-Hsiang Ko, I-Young Tarn, and Shyh-Jong Chung
Department of Communication Engineering, National Chiao Tung University
1001 Ta Hsueh Rd., Hsinchu 300, Taiwan, R.O.C.

Abstract— For the IEEE 802.11 a/b/g/n, it is one of the most crowded bands in wireless communications since they are unlicensed by any international agreement or government authority so there are lots of devices working in this band. Therefore, efficiently utilizing the limited spectrum in such bands and solving the severe interference between devices are very crucial nowadays. There are many solutions in relative research fields proposed or under development. A pattern diversity antenna is a good candidate to solve the problem and reduce the multi-path effects around our usage environment. In a pattern diversity antenna, its radiation pattern can be shaped to concentrate the power to the directions of targets and minimize the power emission in unwanted directions. On the other hand, in reality, an omni-directional pattern is also needed to communicate in all directions. The most suitable pattern can be configured on demand with the pattern reconfigurable antenna.

In this study, a novel dual-band pattern diversity antenna is simulated, fabricated, and measured. Dual-band reconfigurable frequency selective reflectors are designed on each side of the proposed antenna. Only one switch is used on each reflector, and the reconfigurable frequency selective reflector can be controlled to be transmissive or reflective to vertically polarized waves at 2.45 GHz and 5.25 GHz. By the different combinations of the switch states, multiple patterns are achieved. In addition, a dual-band feeding antenna is essential because of the different electromagnetic conditions caused by the various switch states. Well-matching conditions in all situations at two different frequency bands can be obtained by using the coupling effect to excite the lower-band resonance. The dimensions of the proposed antenna are very small ($60 \times 60 \times 40.8\,\mathrm{mm}^3$). The size in each dimension is less than $\lambda/2$ of the lower frequency. The simulation results are obtained by using Ansoft HFSS and they agree well with the measurement results.

Frequency Tuned Planar Inverted F Antenna with L Shaped Slit Design for Wide Frequency Range

I. T. E. Elfergani[1], **Abubakar Sadiq Hussaini**[1, 2], **R. A. Abd-Alhameed**[1], **C. H. See**[1], **M. M. Abusitta**[1], **H. I. Hraga**[1], **A. G. Alhaddad**[1], **and Jonathan Rodriguez**[2]

[1]Mobile and Satellite Communications Research Centre, University of Bradford
Bradford, West Yorkshire, BD7 1DP, UK
[2]Instituto de Telecomunicações, Aveiro, Portugal

Abstract— PIFA designs tend to be low profile, light weight and efficient space filling structures, and as such, are particularly attractive for handset and terminal applications. Conventional PIFA designs have constrained bandwidth; however, it is possible to realize novel structures which are electronically tuneable over most of the wireless communication bands. Tuneable multifunctional handset modules employ the same basic design aims to provide favourable trade-offs in terms of volume, weight and performance. Many interesting PIFA, and more general tuned printed antennas, have been proposed [1]. Various switching technologies, such as RF switches, MEMs switches, PIN diodes and varactor diodes have been used in reconfigurable antenna designs [2–4]. The varactor diodes in particular seem to offer a rich possibility for future designs over a wide frequency range, due to their excellent DC voltage controlled reactance property.

The design optimisation for this study requires an antenna structure compatible with contemporary handset chassis dimensions. In this present work, the structural and lumped element parameters were simulated using the general electromagnetic analysis packages HFSS [5]. The prototype radiator patch is suspended over a 50 mm×80 mm (W_{board}, L_{broad}) ground plane with a 2 mm×7 mm shorting pin, and the antenna is fed by means of a vertical plate, of maximum height 6.5 mm and width 2 mm as shown in Fig. 1. It is connected to the feeding probe through the slot in the ground plane and the effective substrate is air. The rectangular patch dimensions, (L_{ant}, W_{ant}), are 14 mm×50 mm. The L-slot has a uniform width (S_s) of 1 mm, and the lateral dimensions, (L_S, W_S, and W_{gap}), are 8 mm, 17.5 mm, and 15 mm. Initial frequency tuning is tested and evaluated by placing lumped capacitors in the range of 0.5 to 3.3 pF along the slot of the radiator. This process is equivalent to replace the varactor operation. Fig. 2 illustrates both simulated and measured return loss; the measurement was made using a HP 8510C VNA. Five frequencies were selected: 1750 MHz, 1850 MHz, 2040 MHz, 2200 MHz, and 2400 MHz, respectively. The results show a satisfactory agreement between both the simulation and measurement.

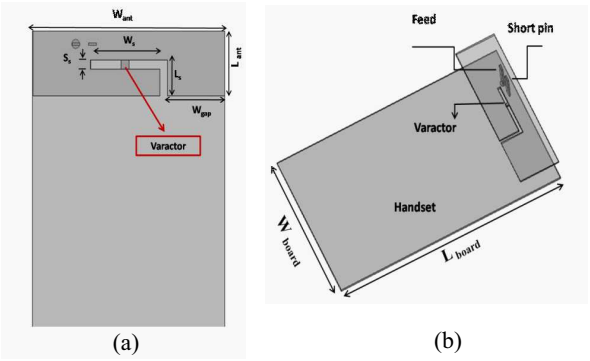

Figure 1: Basic antenna structure; (a) Top view, (b) 3D.

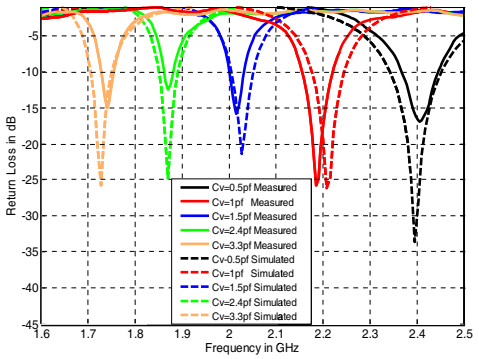

Figure 2: Measured and simulated return loss.

REFERENCES

1. Wu, J., C. J. Panagamuwa, P. McEvoy, J. C. Vardaxoglou, and O. A. Saraereh, "Switching a dual band PIFA to operate in four bands," *IEEE Antennas and Propagation Society International Symposium*, 2675–2678, 2006.
2. Chiu, C. W. and F. L. Lin, "Compact dual-band PIFA with multi-resonators," *Electronics Letters*, Vol. 38, No. 12, 538–540, Jun. 2002.

3. Behdad, N. and K. Sarabandi, "A varactor-tuned dual-band slot antenna," *IEEE Transactions on Antennas and Propagation*, Vol. 54, No. 2, Part 1, 401–408, Feb. 2006.
4. Panaia, P., C. Luxey, G. Jacquemod, R. Staraj, G. Kossiavas, L. Dussopt, F. Vacherand, and C. Billard, "MEMS-based reconfigurable antennas," *IEEE Int. Symp. on Industrial Electronics*, Vol. 1, 175–179, 2004.
5. Ansoft High Frequency Structure Simulator v10 Uses Guide, CA, USA.

Beam Steering of Time Modulated Antenna Arrays Using Particle Swarm Optimization

M. M. Abusitta[1], **R. A. Abd-Alhameed**[1], **I. T. E. Elfergani**[1], **A. D. Adebola**[1], **and P. S. Excell**[2]

[1]Mobile and Satellite Communications Research Centre, University of Bradford, UK
[2]Centre for Applied Internet Research, Glyndŵr University, Wrexham, Wales, UK

Abstract— A simple switching process is employed to steer the beam of a vertically polarised circular antenna array. This is a simple method, in which the difference resulting from the induced currents when the radiating/loaded element is connected/disconnected from the ground plane. A time modulated switching process is applied through particle swarm optimisation.

The current growth in the wireless communications industry has brought about the need for greater performance through improved capacity, data rates and reduce interference [1, 2]. The application of beam forming techniques on multiple-antenna arrays has increased in importance in the commercial wireless sector [3, 4]. Most previous research on beam steering has been for linear [5], circular or planar arrays, although it may be applied to other geometries. The uniform linear array provides the simplest array geometry, and the array processing is straight forward, however, it does not provide full view in the azimuthal range because of its use of edge elements Although adaptive beam-forming may be the preferred method, there are issues in the multi-criteria optimisation required to steer the main-lobe of the array in the desired direction(s), in a dynamically changing signal environment. This optimisation will operate through the amplitude and phase of each element, either continuously, or in discrete steps. The performance of the array is affected principally by its geometry and radiation pattern.

This paper describes a simple beam steering exercise for a circular array, using time modulated elements, through switching the conducting current from each radiator to the ground plane as shown in Fig. 1. The differenced values of the currents for switch states are used to fully generate

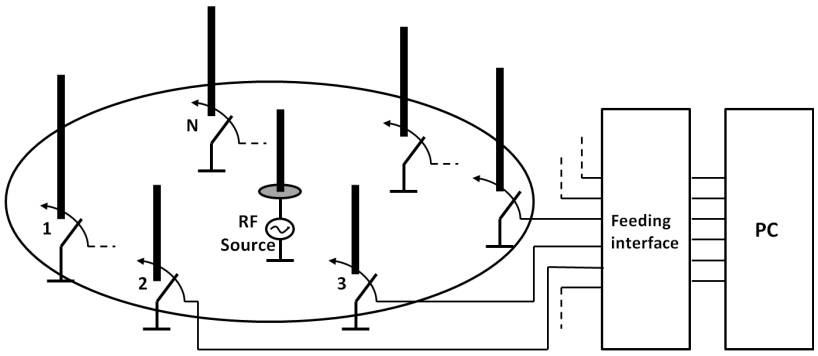

Figure 1: Beam steering ring antenna array; using simple time switches.

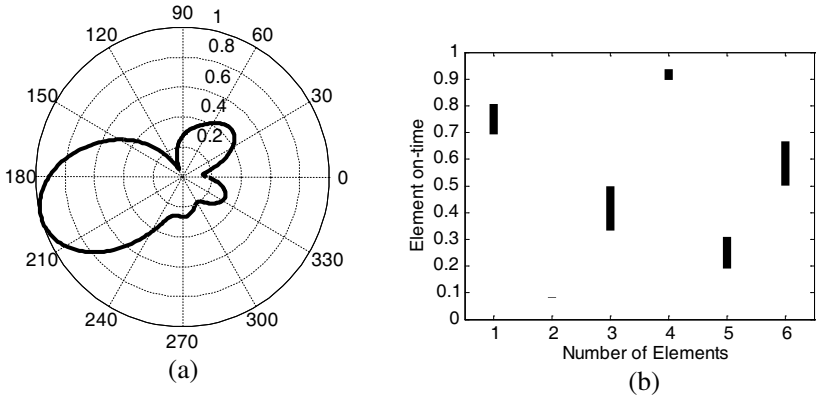

Figure 2: (a) The far field steered beam. (b) The time switching sequence of the antenna elements.

the required radiation pattern, with beam steering control facilitated by particle swarm optimisation (PSO). The present work demonstrates the method by simply connecting one element at a short time of one harmonic cycle, and leaving the others disconnected to ground plane. Several results are presented to validate the concept of this method, sample of which is shown in Fig. 2.

REFERENCES

1. Li, G., S. Yang, Y. Chan, and Z.-P. Nie, "A novel electronic beam steering technique in time modulated antenna arrays," *Progress In Electromagnetics Research*, Vol. 97, 391–405, 2009.
2. Tong, Y. and A. Tennant, "Simultaneous control of sidelobe level and harmonic beam steering in time-modulated linear arrays," *Electronics Letters*, Vol. 46, No. 3, 201–202, 2010.
3. Tennant, A. and B. Chambers, "A two-element time-modulated array with direction-finding properties," *IEEE Antennas Wirel. Propag. Lett.*, Vol. 6, 64–65, 2007.
4. Tennant, A., "Experimental two-element time-modulated direction finding array," *IEEE Trans. Antennas Propag.*, Vol. 58, No. 3, 986–988, 2010.
5. Abusitta, M. M., R. A. Abd-Alhameed, D. Zhou, C. H. See, S. M. R. Jones, and P. S. Excell, "New approach for designing beam steering uniform antenna arrays using genetic algorithms," 617–620, Loughborough, UK, November 16–17, 2009.

The Compact Design of Dual-band and Wideband Planar Inverted F-L-antennas for WLAN and UWB Applications

H. I. Hraga, **C. H. See**, **R. A. Abd-Alhameed**, **S. Adnan**, **I. T. E. Elfergani**, **and F. Elmegri**
Mobile and Satellite Communications Research Centre, University of Bradford, Bradford, UK

Abstract— Two planar inverted-F-L antennas (PIFLA) with a broadband rectangular feeding structure are proposed for lower-band and dual-band ultra-wideband applications. The antenna design model applied for these two models is the planar inverted F-L antenna (PIFLA) [1, 2]. The design optimization is carried out using a frequency domain finite element analysis (Ansoft HFSS [3]); the final model is also cross validated through the time domain using a conformal FDTD method (SEMCAD [4]). A working prototype is constructed and tested on this basis.

The design model of the PIFLA antenna was implemented on a finite volume size of 30 mm × 15 mm × 8 mm in which the magnetic wall concept was applied to reduce the antenna size. As a result a reduced size dual-band and a wideband half PIFLAs for WLAN (2.4 GHz/5.2 GHz) and UWB applications were achieved. The dual-band antenna shows a relative bandwidth of 12% and 10.2% at ISM2400 and IEEE802.11a frequency bands respectively for input return loss less than 10dB. By carefully tuning the geometry parameters of the dual-band proposed antenna, the two resonant frequencies can be merged to form a wide bandwidth characteristic PIFLA, to cover 3000 MHz to 5400 MHz bandwidth (57%) for a similar input return loss, that is fully covering the upper band UWB (3.1–4.8 GHz) spectrum. The initial geometry parameters of the proposed antenna as shown in Fig. 1 are stated as follows: $L1 = 18.6$ mm, $L2 = 10$ mm, $h1 = 8$ mm, $h2 = 4.5$ mm, $d = 3.5$ mm and $w = 0$ mm and ground plane have been cropped to half, which are 7.5 mm, 8.5 mm and 15 mm respectively. The copper metal plate thickness of the proposed antenna and the gap distance for feeding are 0.5 mm.

Two antenna prototypes were fabricated. Fig. 2 illustrates the typical measured and computed antenna performance in term of impedance bandwidth for both full-size and half-size PIFLAs of the dual band PIFLA. Two adjacent resonant frequencies in the range of return loss ≤ -10 dB are observed, i.e., (2450 and 5350) MHz. The lower and upper mode provides 12% and 10.2% relative bandwidth from 2350 MHz to 2650 MHz and 5100 MHz to 5650 MHz, at a minimum return loss of −10 dB or less, completely satisfying the desired IEEE802.11b/g frequency band (2400–2485 MHz) and IEEE 802.11a (5.15–5.35 GHz) band respectively. As can be observed, simulated and measured results for half-size PIFLA were found to be in excellent agreement. The half-size and full-size PIFLA seem to show identical measured impedance bandwidth at two resonant modes. By merging the two bands of the dual band antenna a lower band of the UWB was achieved over 3000 MHz to 5200 MHz.

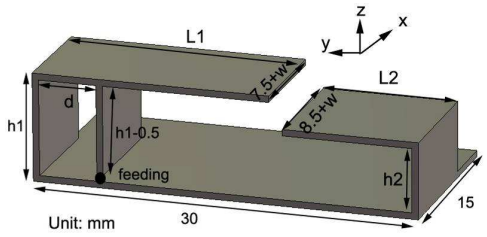

Figure 1: Geometry of the proposed miniature PIFLA.

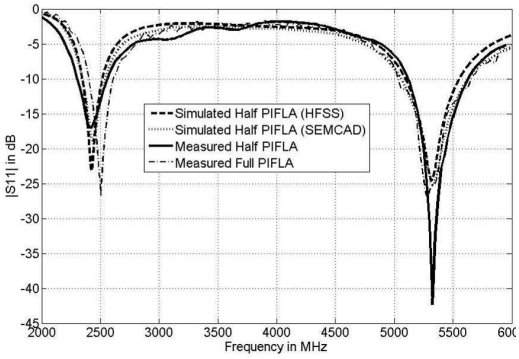

Figure 2: Measured and simulated return losses for the proposed dual-bands PIFLA.

REFERENCES

1. Taga, T. and K. Tsunekawa, "Performance analysis of a built-in planar inverted-F antenna for 800 MHz band radio units," *IEEE J. Select. Areas Commun.*, Vol. 5, 921–929, June 1987.
2. Liu, Z. D. and P. S. Hall, "Dual-frequency planar inverted-F antenna," *IEEE Trans. Antennas Propagation*, Vol. 45, 1451–1458, 1998.
3. HFSS ver.11, Ansoft. Ltd.
4. SEMCAD X ver.14, Schmid & Partner Engineering AG, Zeughausstrasse 43, 8004 Zurich, Switzerland.

The Application in Spacecraft of High Temperature Superconducting Magnetic Energy Storage

Bo Yi[1] **and Hui Huang**[1, 2]

[1]School of Electrical Engineering, Beijing Jiaotong University, Beijing 100044, China
[2]State Key Laboratory of Millimeter Waves, Nanjing 210096, China

Abstract— This paper present application feasibility of High Temperature Superconducting Magnetic Energy Storage technology (HTSMEST) in spacecraft. We analyzed the requirement of energy storage devices in spacecraft, and introduced the present development situation of HTSMEST, then conceived the application of HTSMEST in spacecraft. Also, a comprehensive comparison among the HTSMEST and the other existing energy storage technologies such as flywheel energy storage technology, battery energy storage technology, are presented. The conclusion that the HTSMEST has more advantages than other existing energy storage technologies in application of aerospace technology is reached. Finally, from the perspective of the volume and the mass of such a device of HTSMEST in spacecraft, the preliminary feasibility is testified theoretically, and a model has been given out.

Comparison Study of Eddy Current Losses of Induction Motors Fed by SPWM and SVPWM Inverters

Jingjing Han[1], **Ruifang Liu**[1], **and Hui Huang**[1, 2]

[1]School of Electrical Engineering, Beijing Jiaotong University, Beijing 100044, China
[2]State Key Laboratory of Millimeter Waves, Nanjing 210096, China

Abstract— PWM (pulse width modulation) inverters are widely applied in speed control of motor devices. SPWM (Sinusoidal pulse width modulation) and SVPWM (voltage space vector pulse width modulation) are two common modulation methods. Normally, there are high-order harmonics in the output voltage of PWM inverter, which increase the motor losses. The paper compared and analyzed the eddy current losses of induction motors fed by SPWM inverter and SVPWM inverter, which has significance in improving motor operating efficiency and designing of control method.

Firstly, the principles of SVPWM and SPWM were introduced in this paper. Matlab/simulink software was used to establish the simulation model of SPWM and SVPWM inverter respectively. The harmonic spectrums of inverter output voltage were obtained. It showed that the lower-order harmonics in SVPWM inverter were less than that in SPWM inverter. The distribution of harmonic was related with the carrier wave ratio and modulation ratio.

Secondly, the eddy current losses of induction motors fed by PWM inverter were analyzed under superposition principle. The losses are equal to the sum of iron losses produced by fundamental voltage and all other orders harmonic voltages. Based on this assumption, the relationships between eddy current losses of and modulation ratio as well as carrier wave ratio of PWM were discussed. Eddy current losses discrepancy in SPWM and SVPWM was also compared.

Finnaly, taking into account the influence of nonlinearity of magnetic materials, the paper analyzed eddy current losses of induction motors fed by PWM inverter with electromagnetic field numerical method. The electromagnetic field finite element model of PWM-fed induction motor was established. The model was directly coupled with the external PWM control circuit. After time-stepping finite element calculation, the rules between the eddy current losses and control parameters in SPWM and SVPWM were obtained. The research showed that high-order harmonics had large influence to motor losses and decreased the efficiency. Comparing with SPWM, SVPWM control method could effectively decrease harmonic components and thus reduce the iron losses.

An Investigation into the Effects of the Location of via on Mushroom-like EBG Structure

Hsin-Hsiang Su[1], **Chih-Wen Kuo**[1], **and Toshihide Kitazawa**[2]

[1]Department of Electrical Engineering, National Sun Yat-San University, Taiwan
[2]Department of Electrical and Electronic Engineering, Ritsumeikan University, Kusatsu 525-8777, Japan

Abstract— The mushroom-like electromagnetic bandgap structures are usually consisted of a rectangular patch and connected via through to the ground plane. Usually, the via is at the center of the patch. To implement a broad bandgap, the previous studies cascaded the EBG structures might by different radius vias, a single patch with numbers of vias, or different patch sizes. This study investigated the effects of the via at different locations on the patch. The center frequency changes with the location of via on the same patch size. By moving the location of via, the bandgap of the mushroom-like structure will increase at same time.

Comparative Reliability Evaluation on TVS diode Made by Domestic Products and Foreign Advanced Products

Soon-Mi Hwang, **Chul-Hee Kim**, **Kwan-Hun Lee**, **and Byeong-Jin Ma**
Korea Electronics Technology Institute (KETI)
#68, Yatap-Dong, Bundang-Gu, Sungnam-Si, KyungGi-Do, Republic of Korea

Abstract— In this paper, the level of quality and reliability of TVS diodes, EMI protection devices, was compared and assessed precisely with other advanced products so as to find out the technological position of the domestic products.

TVS diodes are used mainly on the signal input or output of portable devices such as notebook PC, cellular phone and PDA, and these take the role to suppress the ESD and over-voltage that income into the device.

The sample used in the evaluation was selected as the products similar in capability and usage. Moreover, for the accurate comparison, products of each type from 2 domestic companies and 1 foreign company were selected. The comparative evaluation item and method followed the RS C 0144' Bridge Diode rated, up to 100 A, 2008' and RS C0089' Chip Varistor for Electronic Equipment, 2006' that are the reliability evaluation standards and performed the failure rate examinations for the capability examination and the reliability confirmation. The electrical test items are three items; reverse breakdown voltage test, reverse leakage current test and capacitance test, while the environmental test items are five items; high-temperature test, low-temperature test, temperature cycle test, vibration test and electrostatic discharge immunity test. The failure rate test item is electro static discharge test.

As a result of the tests, the domestic products showed comparatively more stable than the foreign products in all of three test items; reverse breakdown voltage test, reverse leakage current test and capacitance test. After the environmental test, none of the domestic or foreign products was failed. However, the domestic products showed a phenomenon that variation rate increased more after the environmental test in all of the test items; reverse breakdown voltage test, reverse leakage current test and capacitance test.

As a result of the failure rate test, both the domestic and foreign products satisfy the failure rate standard(reliability standard 90%) of 1.0×10^{-6}/h within the presented environment condition. However, the domestic products showed a phenomenon that variation rate increased more after the failure rate test in all of the test items; reverse breakdown voltage test, reverse leakage current test and capacitance test.

The level of the production technology of the domestic manufacturers is relatively high in comparison with other advanced countries but the global competitiveness is still weak due to low reliability of the products. Although it is difficult to conclude the supremacy of reliability and quality of domestic and foreign products merely with the evaluation processed within the comparative evaluation, it will be possible to verify that the domestic products hold the technical standards of equal or higher in comparison to the products of technically advanced countries with the results of the comparative evaluation.

Reliability Analysis of Low Noise Amplifier Using Radio Communication

Soon-Mi Hwang, Chul-Hee Kim, and Kwan-Hun Lee
Korea Electronics Technology Institute (KETI)
#68, Yatap-Dong, Bundang-Gu, Sungnam-Si, KyungGi-Do, Republic of Korea

Abstract— Low-noise amplifier is a component that amplifies the signal while lowering the noise figure of high-frequency signal so that it is widely used for telecommunication. Even though there have been a lot of domestic developments because this component holds a very important position in RF system, as a matter of fact, most of integrated module types were imported from overseas. This is not only because the RFIC module for telecommunication is highly dependent on a specified company due to compatibility issue but also because the product reliability is lower than that of the advanced foreign products.

In this paper, the test criteria for the reliability assessment on the IC type low-noise domestic amplifier were developed and a product reliability analysis was executed according to these criteria. The low-noise amplifiers that were selected as the subjects of the reliability assessment were chip-on-board products that have gallium arsenide semiconductor (GaAs Phemt) on a ceramic substrate. High-frequency signal loss can be reduced by using an amplifier transistor in bare chip and directly mounting the components around the circuit connected with the bare chip transistor on a ceramic substrate. Moreover, thermal stability and reliability, which are weakest points of active modules, can be improved because bare transistor chip is 10 times better in thermal conductivity than existing plastic packaging type transistor and easier in heat sink dissipation to ceramic substrate.

The development for the reliability evaluation was based on the IEC 510-2-3 to reference the standards of domestic and foreign advanced companies and reflected upon the opinions of experts through working group conferences for its preparation.

For the reliability certification, the performed test is largely divided into the quality test and the failure rate test. The items of evaluating the capabilities of the subject parts and the environment were included within the quality test and the item of evaluating the failure rate was included within the failure rate test. Within the quality test, only the evaluation of whether the subject part satisfies the quality related capability condition (capability and environment related) is accomplished and the failure rate test guarantees the fixed reliability standards for the product's failure rate.

The items of the developed capability test are 6 items of degree of 1 dB Gain Compression Point, Third Order Intercept Point, Operating Current, Return Loss, Gain, Noise Figure with the items of the environment test to be a total of 9 items of high temperature and high humidity test, high temperature test, surge test, temperature cycle test, low temperature test, high temperature pressure test, sine wave vibration test and electro static discharge test.

The main failure mode and failure mechanism of the LNA is the random failure form of changes in the interior balance and lines according to the sudden high temperatures and temperature changes. Accordingly, the failure rate was determined as the reliability evaluation scale to postulate the failure distribution as exponential distribution. The time of examination and the sample size was determined by referencing the KS C 6032.

Reliability test was executed on two models of low-noise amplifier for mobile phone in accordance with the criteria developed and both of the models passed the test. However, there was a fluctuation that the noise figure was increasing after surge test and ESD test as well as after failure rate test. This means that low-noise amplifier is vulnerable to a momentary overpower such as surge or static electricity and can be changed in performance in case of long-time exposure to high temperature and high humidity.

Regulatory Analysis of the Intermodulation Interference between the PCS Receiver and the Low-power Radio Devices

D. O. Kim and C. Y. Kim
School of Electronics Engineering, Kyungpook National University, South Korea

Abstract— In this paper, the regulatory radiation level emanated from the low-power radio devices has been predicted. From a radio interference point of view, the personal communication services (PCS) receiver is chosen as a victim wireless device. And the low-power radio devices is offender ones. This paper primarily focuses on the intermodulation interference by unmodulated signal in adjacent channel. A theoretical analysis has been proposed using the well-known intermodulation interference theory. That method of analysis includes amplitude of interference corresponding signal-to-interference ratio (SIR) and transformation process of the electric field strength. The calculated electric field strength level becomes the quantified upper limit to avoid the intermodulation interference on the victim device, and it was 75.96 dBμV/m. To show the validity on the suggested value, the simulation was conducted by the Advanced Design System (ADS) tool for the commercial PCS receiver model. The resultant numerals show a good match between two values within less than 5%. In addition, we discussed the relation between our conclusion and the Federal Communication Commission (FCC) regulation of the low-power radio device. The outcomes of the paper may be applicable to any other wireless devices with nonlinear characteristics in many ways.

Tuning Microwave Devices and Systems

Mateusz Mazur, **Jerzy Michalski**, **Jacek Gulgowski**, **and Tomasz Kacmajor**
Telemobile Electronics Ltd., Gdynia 81-451, Poland

Abstract— The process of fabrication may, and usually causes undesirable negative influence on device or system properties. Pre- and post-fabricating actions are possible to reduce influence of fabrication errors. Proper design should be focused not only on achieving assumed characteristics of product, but requires to take into account such aspects like bottlenecks of technological processes in manufacturing causing usually systematical errors. Tolerances in fabrications (e.g., while milling and drilling) may be utilized in design process allowing to estimate and finally reduce errors. For example using Monte-Carlo method allow getting information about scatter of parameters. CAD methods are continuously developed but there are still differences between project and final device parameters. Very often post fabricated actions must be undertaken. When batch of products is very small, usually experienced man's work is sufficient to solve problems and tune device. In case of sophisticated solutions or large volume of products automated tuning is recommended. The reasons are different in these two cases. Where we have to correct parameters depended on many variables the human abilities are limited. It is not possible to remember all relations between variables and system/device properties. As an example the antenna system with phase shifters will be presented. In case where there are a few variables (< 10) the device may be tuned with experienced worker, but it is time consuming procedure. A huge production volume of this same product may require automatic tuning as time and money savings are easy to calculate. Waveguide filters are good examples in that case. There will be also described a limiter where scattering parameters depend on diodes polarization. Mechanically tuned elements will be fixed, but good parameters must be achieved during transmission state and limiting state. As the last example the slotted waveguide antenna with tuning screws will be presented as an example, where there is no ability to measure all parameters after every tuning step so parameters must be extracted from other measurements. So, the variety of devices that may be tuned and practical problems in tuning processes are described and illustrated by some chosen examples.

Low Field Microwave Absorption in Ni-Zn Ferrite Nanoparticles in Different Aggregation States

R. Valenzuela[1], **S. Ammar**[2], **F. Herbst**[2], **and R. Ortega-Zempoalteca**[1]

[1]Departamento de Materiales Metálicos y Cerámicos, Instituto de Investigaciones en Materiales
Universidad Nacional Autónoma de México, México 04510, México
[2]ITODYS, UMR-CNRS 7086, Université Paris-Diderot, Paris 75205, France

Abstract— Magnetic nanoparticles (MNPs) have a strong technological interest and also a fundamental importance in basic science. Most of this importance is due to the substantial changes in macroscopic magnetic properties associated with the change in dimensions, down to the nanometric scale. Virtually all materials show such differences due to the increase in the fraction of atoms on the surface when particle dimensions decrease. In the case of magnetic nanoparticles, the effects of mutual magnetic interactions have to be added, in a complex way, to the effects of decreasing dimensions.

Ferrite NPs of composition $Ni_{0.5}Zn_{0.5}Fe_2O_4$ were prepared by the polyol method [1] (forced hydrolysis of corresponding metal acetates in diethylenglycol). By changing the synthesis parameters, we obtained two states of aggregation: monodispersed NPs of about 5 nm, and clusters of a few tens of nm, formed also by NPs about 5 nm. X-ray diffraction patterns showed pure a spinel phase, and high-resolution electron microscopy revealed an epitaxial arrangement of crystal planes between NPs in the clustered samples.

The NPs were investigated by Low-Field Microwave Absorption [2] (LFMA). In addition to useful information about long-range order and total anisotropy field as a function of the aggregation state, the LFMA technique revealed features than can be associated with changes in the spin arrangement between crystal sites in the spinel structure. In particular, evidence of the spin-canted structure known as Yafet-Kittel triangular arrangement has been observed in Ni-Zn ferrites. Non-resonant microwave absorption methods can become a sensitive and powerful characterization technique.

We also present an investigation of the character of magnetic interactions between nanoparticles using the δ-M magnetization reversal method [3]. Monodispersed samples exhibited a dipolar interaction between NPs, while clustered NPs led to exchange interactions.

REFERENCES

1. Beji, Z., L. Smiri, T. B. Chabane, S. Ammar, N. Jouini, F. Fiévet, and J.-M. Grenèche, *Phys. Stat. Solidi. A*, Vol. 203, 504, 2006.
2. Valenzuela, R., et al., *J. Magn. Magn. Mater.*, Vol. 320, 1961, 2008.
3. Garcia-Otero, J., M. Porto, and J. Rivas, *J. Appl. Phys.*, Vol. 87, 7376, 2000.

Micromachined Suspended Band-stop Resonator for Frequency Tuning

Yun-Ho Jang[1], **Ignacio Llamas-Garro**[2], **Zabdiel Brito-Brito**[3], **Yong-Kweon Kim**[1], **and Jung-Mu Kim**[4]

[1]Seoul National University, South Korea
[2]Centre Tecnologic de Telecomunicacions de Catalunya (CTTC), Barcelona, Spain
[3]ESIME, Instituto Politécnico Nacional, C. P. 04430, D. F., Mexico
[4]Chonbuk National University, South Korea

Abstract— We firstly propose the concept of a frequency tuning method using a micromachined suspended resonator. The structure consists of a freestanding half-wavelength ($\lambda/2$) resonator connected with large displacement comb actuators. The lateral movement of the $\lambda/2$ resonator over the main transmission line produces different electromagnetic decoupling values from the main transmission line. The decoupled energy leads to center frequency tuning of the band-stop resonator circuit. The freestanding $\lambda/2$ resonator plays the role of a loading capacitor as well as a decoupling resonator in the structure.

The resonator is formed on a high resistivity silicon shuttle that moves towards the main transmission line by the comb actuators. The comb actuators have been designed to provide a 60 μm back-and-forth total displacement. One end of the resonator is overlapping the transmission line to form a variable loading capacitor. As the resonator moves back-and-forth over the transmission line, the decoupling energy can be controlled in such a way that center frequency of the resonator can be tuned. When no potential is applied to the stators, center frequency and rejection ratio are 19.5 GHz and −7.42 dB, respectively. When voltages are applied to the rotor, the overlapped area increases leading to move the center frequency and the rejection ratio at that moment. In case of 50 V, the center frequency moves to 18.3 GHz with a rejection ratio of −11.02 dB. The center frequency tuning ratio is 6.2%.

The preliminary result for the proposed resonator successfully showed the possibility of tunable micromachined band-stop resonators.

Statistical Characteristics of Region Propagation of Decametric Radiowaves in Time of Heliogeophysical Disturbanses

N. P. Sergeenko and M. V. Rogova
Pushkov Institute of Terrestrial Magnetism, Ionosphere and Radio-waves Propagation
Russian Academy of Sciences, Troitsk, Russia

Abstract— The concept of use of an artificial satellite for over-the horizon information transfers was essentially added with concept about use ionosphere information transfer channels as reserve. In some cases (over-the horizon radar, positionometry of remote radio sources etc.) ionosphere channels are fundamental. In this aspect interest to properties the ionosphere channels directly connected with properties of an ionosphere has increased. However level of researches in a part of statistics of variations of critical frequency essentially did not change for last years.

The way of overcoming of limitation of applicability of Gauss distribution as model of casual variability of critical frequency of F2 layer of an ionosphere is generalized in this work. As initial experimental data daily samples of relative variability of critical frequency F2 layer received on various ionosphere stations, entering into a world network are used. It is supposed that each sample is characterised by values selective statistical invariants, skewness A and kurtosis E. In according to the first remarkable limit and the scheme of casual pulse process usage for modelling Poisson casual process which in a limiting case $A \to 0$, $E \to 0$ passes in Gauss process is proved.

Basis of a procedure is the construction of analytical model of a random quantity, determined on all axis of ordinates and defined by four statistical invariants: medial, variance, skewness and kurtosis. The generalization on an unsymmetrical case is achieved by use of nonholomorphic functions.

The mathematical model of function of density of probability $W(x)$ is applicable in all area of experimentally observable values A and E, i.e., for various heliogeophysical activity and various geographical conditions.

Remote Pipeline Inspection with a Millimetre Wave SAR

Helmut Essen[1], **Thorsten Brehm**[1], **and Carl Strübbe**[2]

[1]Fraunhofer FHR, Germany
[2]P-Systems, Germany

Abstract— Pipeline inspection is a very important topic for the prevention of intentional and unintentional disruptions of pipeline operation. Disturbances may be induced by terroristic attacks in remote regions or due to thefts of oil. Also in a peaceful environment construction machines operating in the vicinity of buried pipeline may cause danger. At the time beeing airborne inspection is done visually on board of helicopters flying at low altitude. This regular service is due to limitations by bad weather, darkness or other environmental shortcomings. A high flying sensor system capable to penetrate clouds and rain would be in a state to deliver a 24 hour inspection period per day.

An airborne system is suggested, which uses a Synthetic Aperture Radar operating at millimeterwave frequencies. The radar approach offers all-weather capability and the millimetre wave region a high sensitivity on small scale changes of the ground. Thus, oil leakage, even with a low penetration into the ground, can be detected by the evaluation of the indirect signature of a modified plant cover manifesting as a different surface roughness. Millimetre wave SAR is especially sensitive to small scale changes of surface roughness due to the short wavelength in this frequency region. An even better performance can be expected if a polarimetric system is used and change detection algorithms are employed.

The paper describes the general outline of the experimental airborne SAR inspection system and discusses its advantages and shortcomings. Frst results from 94-GHz and 35-GHz flights with the high resolution MEMPHIS SAR onboard a C-160 aircraft over terrain with buried pipelines are shown.

Millimeter Wave Radar Network for Foreign Object Detection on Runways

Helmut Essen[1], **Paul Warok**[1], **Martin Schröder**[1], **Rüdiger Zimmermann**[1], **Wolfgang Koch**[2], **and Marek Schikora**[2]

[1]Fraunhofer FHR, Germany
[2]Fraunhofer FKIE, Germany

Abstract— Incidents arising from Foreign Objects & Debris (FOD) on runways have been a major concern for a long time, as flight delays and accident claims as well as aircraft repairs are very costly. The problem came into public knowledge with the Air France Concorde crash in July 2000. A few systems have been developed but are not yet widely in use.

In forthcoming years traffic on airports will even increase. To maintain a secure handling of the air traffic the runway and taxiways have to be permanently in undisturbed condition and have to be cleared rapidly if any disturbance is encountered.

Currently following the recommendations of the ICAO the inspection of runways is done at a period of 6 hours visually by security personnel. This is not only costly and may be subject to human failure, but is also highly dependent on weather and daylight conditions. Especially at adverse weather the visual inspection cannot guarantee the detection of small metallic particles like screws. Moreover the traffic density on airports has been considerably increasing, and a secure inspection between consecutive take-offs and landings by human visual inspection is not possible. This shortcoming can be reduced by the use of radars, which permanently inspect the traffic areas and generate an alarm whenever the state of the runway is changed in comparison to the standard condition. An advantage of radar is the all-weather and day-and-night capability in combination with a high range resolution, defined by a wide signal bandwidth, which is easy to achieve at higher frequencies.

The 220 GHz band is used, which in addition to a wide bandwidth allows considerably smaller antennas with high directivity.

The paper describes the distributed radar sensor approach which demands sensor data fusion algorithms. Measurements on typical small scale targets are discussed and the conclusions for an implementation on a typical airport are drawn.

Soil Parameters Retrieval Using a Neural Network Algorithm Trained by a Two Layers Multi-scale Bi-dimensional SPM Model

L. Bennaceur Farah[1], **I. Hosni**[1], **I. R. Farah**[2], **R. Bennaceur**[3], **and M. R. Boussema**[1]

[1]LTSIRS, ENIT, Tunisia
[2]RIADI, ENSI, Tunisia
[3]LMPC, FST, Tunisia

Abstract— Although significant progress has been made in the ability to acquire remotely sensed data, extracting soil moisture and roughness parameters of natural surfaces from this data has been problematic for many reasons. In fact, many previous studies have dealt with model-based retrieval algorithm and have encountered many problems like the lack of information about the characteristics of natural surface roughness as well as the range of roughness parameters to use in one hand. In another hand, the uncertainties concerning the validity of the scattering models when applied to natural roughness conditions reduces the accuracy of the retrieval procedure. In addition, the relation-ship between the backscattering coefficient is non linear and the problem of retrieving parameters may be ill-posed.

In the context of radar remote sensing application, surface roughness has been usually described as single gaussian stationary processes which processes a characteristic vertical and horizontal spatial scale summarized by two statistical parameters, the profile height root mean square and the correlation length. Recent studies have shown that in natural conditions the agreement between experimental measurements and theoretical values is usually poor due to the large variability of the correlation function and as a consequence backscattering models have often failed to predict correctly backscattering. Many mathematical works dealing with natural surfaces description have shown that they are better described as self-affine random processes than as stationary processes. Thus, in this study, surfaces are considered as band limited fractal random processes which corresponds to a superposition of a finite number of one-dimensional gaussian processes each one having a spatial scale. We described the multi-scale bi-dimensional surfaces with the bi-dimensional wavelet transform using the Mallat algorithm giving us respectively the horizontal wavelet component, the vertical wavelet component and the diagonal wavelet component of the height z. Multi-scale roughness is characterized by two parameters, the first one is proportional to the standard deviation and the other one is related to the fractal dimension. Soil moisture is related to the complex dielectric constant. A second step in this study has consisted in adapting the small perturbation model (direct model) to this multi-scale surface description to investigate the impact of this description on radar backscattering through a sensitivity analysis of backscattering coefficient to the multi-scale roughness parameters, dielectric constant related to soil moisture and radar parameters like the incident angle and the frequency. In this present work, we characterize the soil surfaces and subsurfaces by a two layer geo-electrical model. The upper layer is described by its dielectrical constant, thickness, a multi-scale bi-dimensional surface roughness model by using the wavelet transform and the Mallat algorithm, and volume scattering parameters. The lower layer is described by its dielectric constant and multi-scale surface roughness.

The principal aim of this present work is to find an inverse model to retrieve roughness geometric and dielectric parameters of natural rough surfaces from radar backscattering data.

To perform the inversion the small perturbation multi-scale scattering model (MLS SPM) we used a multi-layer neural network (NN) architecture trained by a backpropagation learning rule. The inversion technique has been realized in four basic steps. The first one has consisted in selecting the bounds of the scattering model, the MLS SPM, through a sensitivity analysis. In a following step, we have generated the NN training data consisting in a set of input-output pairs using the MLS SPM model. The inputs to the scattering model have been randomly selected within the bounds determined in step 1. The third step has consisted in training the NN using the backpropagation learning algorithm. The last step consisted to use the trained algorithm to retrieve our parameters of interest, the dielectric complex constant and soil roughness multi-scale parameters. Once the NN was trained, we have tested it to multi-frequency and multi-incident radar data. The inversion leads to satisfactory results with a good relative uncertainty.

Accuracy of Wind Field Deduced from Envisat WSM SAR Images along the Range

P. Trivero, W. Biamino, M. Borasi, and M. Cavagnero
Dipartimento di Scienze dell'Ambiente e della Vita
Università del Piemonte Orientale "Amedeo Avogadro", Italy

Abstract— Since several years the Synthetic Aperture Radar (SAR) is used as a reliable tool for sea surface observation. SAR provides information about the sea surface roughness generated by wind. In order to extract wind field from SAR images the direction and the intensity of the wind vector must be considered separately. Particularly the well-established methods for determining the wind intensity required the wind direction as input. We analyzed the Envisat WSM images: The wind direction has been deduced applying the Continuous Wavelet Transform (CWT) analysis to the periodic structures of the image. The obtained direction has been used as input of the CMOD5 model to calculate the intensity. The large swath width of a Envisat WSM image corresponds to incidence angles ranging from 15 to 45, involving specular and Bragg scatter mechanisms; the Normalised Radar Cross Section (NRCS) depends on the position along the range, on the wind intensity as well as on the angle between the radar beam and the wind direction. Here we present an analysis concerning the accuracy of the wind field deduced from Envisat WSM SAR images as a function of the position along the range. We have compared the data obtained in different position along the range, of about 100 images, with external data of wind. The accuracy of the outputs of the wind as a function of the different zones of the range are presented and the backscatter mechanisms concerning both the structures of the image and the values of the NRCS are discussed.

Imaging Permittivity Measurements for Automated Material Inspection

Nadia Fatihi, Sebastian Hantscher, Jasmin Rubart, Christian Krebs, Dirk Nüβler, and Helmut Essen

Department of Millimetre Wave Radar and High Frequency Sensors
Fraunhofer Institute for High Frequency Physics and Radar Techniques
Neuenahrer Straβe 20, Wachtberg 53343, Germany

Abstract— In the last decade, in many fields the non-destructive material inspection has become more and more of great interest. One application is the detection and localisation of impurities in dielectric materials. Transmission measurements in millimetre or sub-millimetre wave band are particularly suitable for this purpose. However, the exact knowledge of the permittivity of the material under test is essential for obtaining precise and distortion-free microwave images. That is why, an iterative method for the relative dielectric constant determination is proposed taking into account the 2π ambiguities of the measured transmissions phase, moving average based noise suppression as well as the refraction caused differences between physical and electrical lengths. Among others, starting with an estimated value for ε_r, the resulting electrical length of the material is calculated whose result is used for updating the relative dielectric constant. This iterative process is carried out until reaching an appropriate termination condition.

The permittivity measurement can be also performed for two-dimensional data sets. An object under test is scanned in two dimensions by a network analyser measuring the transmission characteristics in amplitude and phase. A critical step during the data processing are the two-dimensional unwrapping of the phase, in x- and y-direction, as well as taking into account the radiation characteristic of the antenna. After correcting the data, based on a phase derivative variance map, the permittivity contribution can be displayed by an image showing false-coloured the relative dielectric constant of each measurement position. For demonstrating the proposed procedure, 24 pieces of chocolate were measured at 110 GHz. Before the measurement started, we impured some of them with a glass splinter, a piece of plastic and a screw which should be detected by the measurement. All the objects could be easily identified in the obtained image such that this package of chocolate would have failed the quality testing.

Combined Direct and Remote Sensing Measurements of Wave Parameters at the off-shore Research Platform in the Black Sea

N. Y. Komarova[1], **F. De Biasio**[2], **A. S. Kuznetsov**[3], **M. N. Pospelov**[1], **and S. Zecchetto**[2]

[1]Space Research Institute, Moscow, Russia
[2]Institute of Atmospheric Sciences and Climate, Italy
[3]Marine Hydrophysical Institute, Ukraine

Abstract— Air-sea interaction in coastal areas reveals some features resulted from non-stationary character of wind and waves there. To study these features in details, combined remote sensing and in situ measurements are desired. Among other means of in situ measurements like research vessels or buoys, the oceanographic platforms are of particular importance because they provide a unique opportunity of long-term measurements of sea and atmosphere parameters in a fixed point using various kinds of sensors, both remote and contact.

The paper presents some results of the experiments CAPMOS'05 and CAPMOS'07 performed on an offshore oceanographic platform in the Black Sea. The experiments aimed at investigations of air-sea coupling by means of direct and remote measurements were carried out in frames of the INTAS project "Combined Active/Passive Microwave Measurements of Wind Waves for Global Ocean Salinity Monitoring (CAPMOS)". The project joined several research teams from Russia, Ukraine and Italy involved in long-term experimental study of ocean and atmosphere.

A specialized research platform managed by the Marine Hydrophysical Institute is located on the shelf slope approximately 600 m to the south of Crimea coast, Ukraine. The sea depth at the site is about 30 m, so the deep water and long fetch conditions were ensured for prevailing winds from the south, south-east and south-west. The measurements on a platform were carried during June 1–20, 2005 and August 10–22, 2007 round a clock. The weather conditions during the experiment permitted to observe various phenomena of air-sea interaction in a coastal area. The mean wind speed ranged from 0 to 13 m/s; several episodes of high wind speeds were observed, with gusts well above 20 m/s.

List of research equipment used in the experiment included a set of sensors for direct measurements of atmosphere and sea parameters (3-component sonic anemometers, air temperature and humidity sensors, current meters, CTD sensors, string wave gauge) as well as a set of remote sensing instruments (microwave and IR radiometers, microwave scatterometer). Direct measurements of wave parameters were compared with remote sensing data. The spectral peak frequency of gravity waves varied in the range from 0.2 to 0.7 Hz that corresponded to dominating wave lengths from 50 down to several meters. Comparison of two different techniques of wave spectrum retrieval from scatterometer data, and also comparison of scatterometer and radiometric data shows satisfactory agreement.

ACKNOWLEDGMENT

The study was supported by INTAS Grant 03-51-4789 and RFBR Grant 09-02-00780.

Geophysical Parameter Retrieval Algorithm for CrIS and Testing Results

Daniel K. Zhou, **Xu Liu**, **and Allen M. Larar**
NASA Langley Research Center, Hampton, VA 23681, USA

Abstract— Retrieval algorithm development in conjunction with its performance validation is critical for the production of useful atmospheric and surface geophysical parameters as well as for the development of data processing algorithms for future satellite instruments. The NPOESS Cross-track Infrared Sounder (CrIS) is scheduled to launch in the near future. The CrIS is a Fourier Transform Spectrometer (FTS) making infrared hyperspectral measurements. This paper presents atmospheric profile results based on the single field-of-view retrieval system for all-weather conditions applied to the CrIS spectral radiance measurements, the proxy data generated from the Infrared Atmospheric Sounding Interferometer (IASI) measurements during the Joint Airborne IASI Validation Experiment (JAIVEx). An advanced retrieval algorithm with a fast radiative transfer model, including cloud effects, is used for atmospheric profile and cloud parameter retrieval. This physical inversion scheme has been developed, dealing with cloudy as well as cloud-free radiance observed with ultraspectral infrared sounders, to simultaneously retrieve surface, atmospheric thermodynamic, and cloud microphysical parameters. A fast radiative transfer model is used for atmospheric profile and cloud parameter retrieval. A one-dimensional (1-d) variational multi-variable inversion solution is used to improve an iterative background state defined by an eigenvector-regression-retrieval. The solution is iterated in order to account for non-linearity in the 1-d variational solution. Profile retrievals with the CrIS are validated through comparisons with profiles observed with dedicated dropsondes, radiosondes, and those determined from the NPOESS Airborne Sounder Testbed — Interferometer (NAST-I) airborne FTS system. The capability of satellite ultraspectral IR remote sensors to observe fine-scale horizontal thermodynamic features with high vertical resolution is demonstrated.

Hyperspectral Remote Sensing of Atmosphere and Surface Properties

Xu Liu[1], **Daniel K. Zhou**[1], **Allen M. Larar**[1], **and Ping Yang**[2]

[1]NASA Langley Research Center, Hampton, VA 23681, USA
[2]Department of Atmospheric Sciences, Texas A & M University, College Station, TX 77843, USA

Abstract— Atmospheric Infrared Sounder (AIRS), Infrared Atmospheric Sounding Interferometer (IASI), and Cross-track Infrared Sounder (CrIS) are all hyper-spectral satellite sensors with thousands of spectral channels. Top of atmospheric radiance spectra measured by these sensors contain high information content on atmospheric, cloud, and surface properties. Exploring high information content contained in these high spectral resolution spectra is a challenging task due to computation effort involved in modeling thousands of spectral channels. Usually, only very small fractions (4–10 percent) of the available channels are included in physical retrieval systems or numerical weather forecast (NWP) satellite data assimilations.

We will describe a method of simultaneously retrieving atmospheric temperature, moisture, cloud, and surface properties using all available spectral channels without sacrificing computational speed. The essence of the method is to convert channel radiance spectra into super-channels by an Empirical Orthogonal Function (EOF) transformation. Because the EOFs are orthogonal to each other, about 100 super-channels are adequate to capture the information content of the radiance spectra. A Principal Component-based Radiative Transfer Model (PCRTM) developed at NASA Langley Research Center is used to calculate both the super-channel magnitudes and derivatives with respect to atmospheric profiles and other properties. There is no need to perform EOF transformations to convert super channels back to spectral space at each iteration step for a one-dimensional variational retrieval or a NWP data assimilation system. The PCRTM forward model is also capable of calculating radiative contributions due to multiple-layer clouds. The multiple scattering effects of the clouds are efficiently parameterized. A physical retrieval algorithm then performs an inversion of atmospheric, cloud, and surface properties in super channel domain directly therefore both reducing the computational need and preserving the information content of the IASI measurements. The inversion algorithm is based on a non-linear Levenberg-Marquardt method with climatology covariance matrices and a *priori* information as constraints. One advantage of this approach is that it uses all information content from the hyper-spectral data so that the retrieval is less sensitive to instrument noise and eliminates the need for selecting a sub-set of the channels.

RCS Simulations on Wet Corner Reflectors with SBR Code SIGRAY

E. Kemptner
DLR, Microwaves and Radar Institute, Germany

Abstract—

Introduction: Corner reflectors play a major role in the calibration of radar systems. The influence of geometry deformations, caused by insufficient production accuracy or outside exposure, and of dirt, water film, snow or snow slush on the RCS is often neglected. This topic has been investigated by applying the 'Shooting & Bouncing of Rays' (SBR) code SIGRAY which has been developed at DLR. In this work simulation results on trihedral corner reflectors with a wet base area are presented.

RCS Model SIGRAY: SIGRAY is based on the 'Shooting & Bouncing of Rays' method [1] and models multiple reflections by using a combination of Geometrical Optics (GO) and Physical Optics (PO). This high frequency approximation method is well suited for RCS calculations on 50λ corner reflectors. In the framework of SIGRAY the triple reflection of rays, which is the dominant reflection order on electrically large corner reflectors, is simulated by twofold application of GO and single-use of PO which leads to good results on the mentioned radar targets. SIGRAY can separate scattering contributions corresponding to the order of reflection.

A great number of rays are shot towards the reflector corresponding to a fine grid. The propagation lengths are measured from and back to a virtual plane, which is a kind of substitute for the antenna in infinity, perpendicular to the viewing direction. All reflected rays interfere at this receiving plane and accumulate to the total scattered field.

SIGRAY has been successfully applied in the past to deformed dry corner reflectors [2] and to several other targets.

Simulations: A trihedral corner reflector with an edge length of 1.5 m at a frequency of 10 GHz was investigated. Typically more than 10 million rays hit the target and are tracked.

The base panel of the reflector was assumed to be wet, several thicknesses of the water film have been investigated. The polarization dependent Fresnel's reflection coefficients have been applied.

Results: The dependence of Fresnel's reflection coefficients on the incidence angle at 10 GHz is very strong. According to this the RCS of the corner reflector changes dramatically. The RCS for E- and H-polarization differ heavily (Fig. 1).

Because of cohesion a thin water film occurs not only on a roughly horizontal base panel of the corner reflector but also on slightly tilted ones. This results in the need to account for a water film on the base panel of corner reflectors in radar calibration.

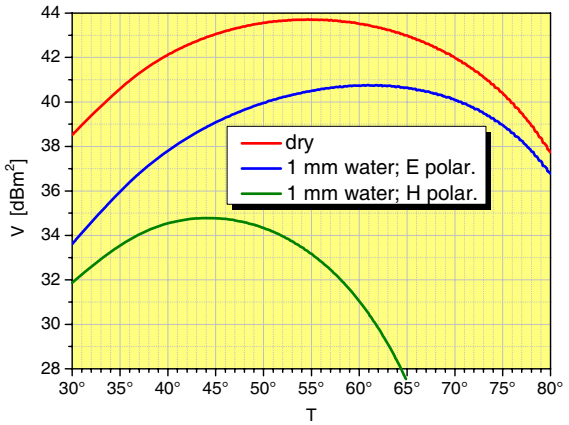

Figure 1: RCS of a 1.5 m corner reflector at 10 GHz with and without a water film on the base panel.

REFERENCES

1. Ling, H., R. Chou, and S. Lee, "Shooting and bouncing rays: Calculating RCS of an arbitrary cavity," *IEEE Trans. on Antennas and Propagation*, Vol. 37, 605–607, May 1987.
2. Kemptner, E., "RCS simulations on deformed corner reflectors applying SBR code SIGRAY," *EuCAP 2010*, Barcelona, Spain, April 12–16, 2010.

Design of Q-band Polarizer Having Excellent Polarity

Soon-Mi Hwang[1] and Bierng-Chearl Ahn[2]

[1]Korea Electronics Technology Institute (KETI)
#68, Yatap-Dong, Bundang-Gu, Sungnam-Si, KyungGi-Do, Republic of Korea
[2]Department of Radio Engineering, Chungbuk National University, Republic of Korea

Abstract— Recently multi-band antenna feeds for satellite communication is used as frequency band number increases. Waveguide polarizer is used making circularly polarized wave feeds of antenna.

There are many different types of polarizer. For example, dielectric insertion type, septum insertion type, iris type, etc. Of many different types of polarizer, the iris polarizer in the square waveguide finds widespread applications due to the simplicity in structure, design and fabrication. It also has such desirable properties at wide or multi band operation, compactness and simple interfacing requirements.

In this paper, we present design method for a square iris polarizer to be used in Q-band (33.0 GHz $\sim$ 50.0 GHz) antenna feeds.

The design of the square waveguide iris polarizer starts with the choice of the waveguide size. For a broad-band operation, the size of the waveguide is made larger than the standard rectangular waveguide. Next spacing between iris, iris thickness and height, the number of iris are optimized to satisfy design specifications. The iris height is properly tapered to realize a low reflection.

For design example, we design a square iris polarizer having the broadband and good polarity to be used in Q-band (33.0 GHz $\sim$ 50.0 GHz) antenna feed. The widely used commercial software HFSS® is employed in the analysis of the polarizer structure. The design result show that the phase difference less than 10°, the axial ratio is within 1.1 dB and return loss is below 30 dB in full band. This polarizer has a good possibility at antenna feeds for satellite communication. And according to suggestion in this paper, easily we will design iris polarizer having excellent polarity characterization and broadband.

REFERENCES

1. Uher, J., J. Bornemann, and U. Rosenberg, *Waveguide Components for Antenna Feed Systems: Theory and CAD*, Artech House, Boston, 1993.
2. Kitsuregawa, T., *Satellite Communication Antennas*, Artech House, Boston, 1990.
3. Simmons, A. J., "Phase shift by periodic loading of waveguide and its application to broadband circular polarization," *IRE Transcations Microwave Theory and Techniques*, Vol. 3, No. 6, 18–21, December 1955.
4. Pozar, D. M., *Microwave Engineering*, 2nd Edition, John Wiley & Sons, New Work, 1998.
5. Tucholke, U., F. Arndt, and T. Wriedt, "Field theory design of square waveguide Iris polarizers," *IEEE Transactions on Microwave Theory and Techniques*, Vol. 34, No. 1, 156–160, Januray 1986.
6. James, G. L., "Design of wide-band compact corrugated horns," *IEEE Trans. on Antennas and Propagation*, Vol. 32, No. 10, 1134–1138, October 1984.

Reconfigurable Amplifier for Wifi/Wimax Applications Using RF MEMS

N. Otegi, **A. Anakabe**, **J. Portilla**, **and J. M. Collantes**
Electricity and Electronics Department, University of the Basque Country
Apdo. 644, Bilbao 48080, Spain

Abstract— Wireless communication systems are oriented to 'always best connected and served' ABC&S philosophy. In this context, multiband multistandard RF front ends (MMRR: Multiband Multistandard Reconfigurable Radio) are fundamental. In particular, power amplifiers with multiband operation capabilities and adaptability to different applications are required. RF MEMS have shown to be one of the most promising technologies for low cost, high performance tunable subsystems. Particularly, RF MEMS switches provide low insertion losses, low consume, better linearity and high integrability at high frequencies.

In this work a reconfigurable amplifier for WiFi/WiMAX applications (2.4/3.5 GHz) intended to be integrated with a MEMS Single Pole Double Throw (SPDT) is presented. The reconfigurability is achieved by means of two parallel input matching networks that will be externally switched by the MEMS SPDT.

The amplifier has been designed maximizing the robustness against stability problems and technological dispersion. Due to the multi-band character of the design and the presence of multiresonant networks, the integration in the design process of a careful stability analysis has been a key factor in the final design achievement. It is worthwhile to point out that a multi-band design makes the detection of spurious signals as well as stabilization process more demanding. While different MEMS based reconfigurable options can be found in the literature [1–4], stability issues have not been deeply treated. In this work a rigorous small and large signal stability analysis based on pole-cero identification [5–8] has been applied to ensure and maximize device stability versus unavoidable post-integration MEMS SPDT dispersion.

The amplifier makes use of a SiGe BFP650 transistor and has been fabricated in hybrid microstrip technology. Coming to the design, several a priori restrictions have had to be met. For instance, the source impedance seen by the input networks varies approximately from matched to open-circuit when commuting the SPDT. Therefore, the effect of the open-circuited branch has to be carefully taken into account. Besides, the presence of the MEMS SPDT imposes strict size and geometry restrictions. However, the most limiting factor comes from integration issues, which will require coplanar to microstrip transitions and wire bonding. The final effect of this bonding on the amplifier is difficult to be simulated with precision. Thus, different network topologies have been analyzed by means of Monte Carlo method to select the most robust against dispersion from bonding wires, transistor parameters, or deviations from models. In addition to maximizing robustness, the possibility of fine tuning by means of discrete elements was also one of the goals.

As above mentioned, stability issues have also been critical in the multi-band design. On the one hand, the transistor selected presents a high tendency to generate low frequency oscillations that have been avoided with a careful design of the bias networks. On the other hand, in large-signal operation two different spurious oscillations have been detected: a parametric frequency division by two versus the input power at 3.5 GHz port and a spurious oscillation at around 1 GHz versus the input power at 2.4 GHz port. Thanks to the information provided by the pole-cero identification and Monte Carlo analyses, all these unwanted oscillations have been successfully eliminated ensuring an adequate stability margin against expected dispersion.

A prototype of the amplifier has been fabricated and measured to validate the proposed design before SPDT integration. Fine tuning has been achieved by changing a single capacitor. Measurement results show a very good agreement with simulation and absence of any unwanted oscillation.

REFERENCES

1. Fukuda, A., H. Okazaki, T. Hirota, and Y. Yamao, "Novel 900 MHz/1.9 GHz dualmode power amplifier employing MEMS switches for optimum matching," *IEEE Microw. Wirel. Comp. Lett.*, Vol. 14, No. 3, 121–123, March 2004.
2. Fukuda, A., H. Okazaki, T. Hirota, and Y. Yamao, "A 900/1500/2000-MHz triple-band reconfigurable power amplifier employing RF-MEMS switches," *IEEE IMS2005*, WE2E-4, 2005.

3. Fukuda, A., T. Furuta, H. Okazaki, and S. Narahashi "A 0.9-5-GHz wide-range 1WClass reconfigurable power amplifier employing RF-MEMS switches," *IEEE IMS2006*, 1859–1862, 2006.
4. Vaha-Heikkila, T. and G. M. Rebeiz, "A 20–50 GHz reconfigurable matching network for power amplifier applications," *2004 IEEE MTT-S Microwave Symposium Digest*, 717–720, June 2004.
5. Jugo, J., J. Portilla, A. Anakabe, A. Suárez, and J. M. Collantes, "Closed-loop stability analysis of microwave amplifiers," *IEE Electronics Letters*, Vol. 37, 226–228, February 2001.
6. Anakabe, A., J. M. Collantes, J. Portilla, J. Jugo, A. Mallet, L. Lapierre, and J. P. Fraysse, "Analysis and elimination of parametric oscillations in monolithic power amplifiers," *2002 IEEE MTT-S International Microwave Symposium Digest*, Vol. 3, 2181–2184, Seattle, June 2002.
7. Anakabe, A., J. M. Collantes, J. Portilla, S. Mons, and A. Mallet, "Detecting and avoiding odd-mode parametric oscillations in microwave power amplifiers," *International Journal of RF and Microwave Computer-Aided Engineering*, Vol. 15, No. 5, 469–478, Wiley, September 2005.
8. Anakabe, A., N. Ayllón, J. M. Collantes, A. Mallet, G. Soubercaze-Pun, and K. Narendra, "Automatic pole-zero identification for multivariable large-signal stability analysis of RF and microwave circuits," *40th European Microwave Conference*, Paris, France, September 2010.

Design of Super-compact Multi-layered CRLH Transmission Lines Using the Latest Low-temperature Co-fired Ceramics (LTCC) Technology

Shinya Ueno, Naohiro Inoue, Takuya Kaneko, and Yasushi Horii
Kansai University, 2-1-1 Ryozenji, Takatsuki, Osaka 569-1095, Japan

Abstract— Over the last decade, left-handed (LH) metamaterials, characterized by anti-parallel phase and group velocity, have drawn considerable interest in the microwave community due to their potential for novel types of devices and components. Nowadays, however, most of the one dimensional metamaterials are treated as a relic of the past saying that "the first stage metamaterials". In fact, they do not exhibit particularly small dimensions comparing with the latest miniaturized components used in mobile communication systems.

In order to reduce the dimensions of metamaterial applications toward miniaturization, we developed a multi-layered (ML) composite right/left-handed (CRLH) transmission line (TL) with vertically stacked three LH unit cells. This architecture, which supports propagation in the vertical direction perpendicular to the planes of the substrates, presents the advantage of providing large electrical length over an extremely short TL length and small transverse footprint.

In this study, we develop a super-compact ML CRLH architecture by applying the latest low-temperature co-fired ceramics (LTCC) technology to the conventional ML CRLH TL models. In the theoretical demonstration by using commercial software Ansoft HFSS 9, an LTCC ML CRLH TL, having a wide LH passband from 5 GHz to 15 GHz with small insertion loss of less than 1 dB, is obtained with dimensions of $1.6 \times 1.6 \times 1.0\,\mathrm{mm}^3$.

Study of Microwave Circuits Using the FDTD Method. Example of Multiconductor Transmission Lines Loaded by Diodes and Transistors Mesfet Modeled by Their Non-linear Equivalent Schemes

Amine Amharech and Hassane Kabbaj
Laboratoire LCEMINAS, Equipe de Recherche CEM et Composants Microondes, FST de Fès, France

Abstract— This paper deals with electromagnetic compatibility domain and coupling in microwave circuits.

Multiconductor transmission lines loaded by nonlinear elements are handled by a purely temporal method. This type of circuit is usually studied by a combination of method using several techniques as the MNA (Modified Nodal Analysis) method or the state variables. In this communication we use a computational approach based upon the centered-points finite-difference time-domain (FDTD) technique for evaluating voltages and currents along multiconductor transmission lines terminated with complex nonlinear devises.

The primary advantage of the FDTD method over many existing methods is that nonlinear terminations may be readily incorporated into the algorithm and the analysis. Add to this the gain in simulation time and memory space is very important.

We have considered several scenarios, including that of a transmission line with three coupled conductors loaded by a metal semiconductor field-effect transistor (MESFET). The MESFETs are modeled by their equivalent circuit large signal.

Other examples are studied in that of a coupled transmission line loaded by diodes and an other one case of a coupled transmission line loaded by two MESFETs and a resistor.

In this context, a pattern seems interesting: the case of a transmission line with two conductors (plus ground) in which the transistors of the load are mutually influenced by electromagnetic coupling. Here we show the effects of coupling on the performance of these transistors.

We also show, in the case of a multiconductor transmission line loaded with two MESFET transistors (on passive conductors) and resistance (on the active conductor), the effects of electromagnetic coupling on the circuit.

In a final section, we present a thorough analysis of circuit parameters that can limit the risk of drift performance.

Optimum Design of Wave Absorber for Milli-meter Band Based on Alumina Ceramic Containing Carbon Black

H. Terasaki[1], **T. Yasuzumi**[1], **Y. Maeda**[2], **M. Uno**[2], **and O. Hashimoto**[1]

[1]Aoyama Gakuin University, Japan
[2]Wicera Co., Ltd., Japan

Abstract— Wave absorbers are well known as a key component to solve electromagnetic compatibility problems. Recent years, various types wave absorbers with dielectric-loss material have been investigated for milli-meter frequency band. Relative permittivity might change when designed frequency or width of lossy material is different value.

In this paper, optimum design of one layered wave absorber milli-meter band is studied by changing width and contained amount of lossy material. The wave absorber consists of almina ceramic containing carbon black which is used for controling relative permittivity. Figure 1 shows measured relative permittivity when width d changes from 1.0 to 3.0 mm as plots for each frequency band. The approximate lines are calculated and also shown in Figure 1 as solid lines. Figure 2 illustrates relative permittivity when contained rate of carbon black changes from 1.0 to 1.5% with no-reflection curves. As shown in Figure 2, the relative permittivity moves for higher amount when the rate increases. Table 1 and Figure 3 show the optimized parameter for each frequency band and measured absorption characteristics. As the results, the fabricated absorbers has a good absorption characteristics and peak-frequencies show the good agreement with designed ones.

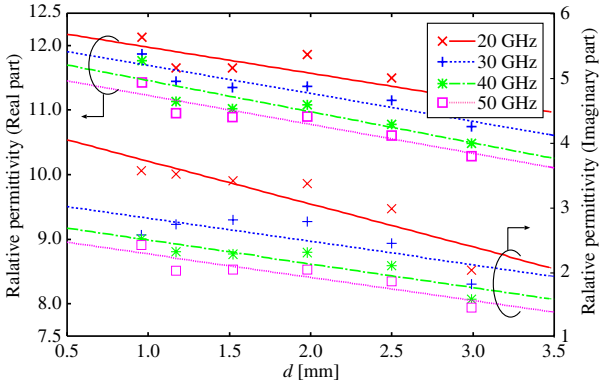

Figure 1: Relative permittivity when width change.

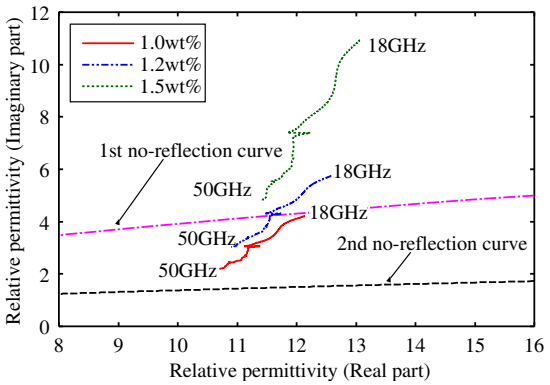

Figure 2: Relative permittivity with no-reflection curve.

Frequency f [GHz]	Rate of content [wt%]	Width d [mm]
20	1.2	1.11
30	1.2	0.75
40	1.5	0.55
50	1.5	0.45
60	1.5	0.38
60	1.0	1.17

Table 1: Optimized width for each frequency band.

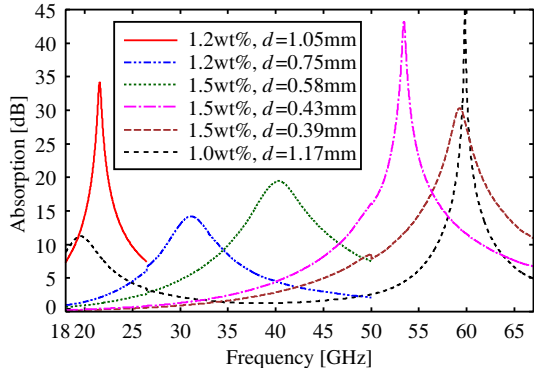

Figure 3: Measured absorption characteristics of designed wave absorbers.

Lowpass and Bandstop Filters Using CSRRs and SRRs in Finline Configurations

A. Casanueva[1], **A. León**[2], **J. Herrero**[3], **A. Mediavilla**[1], **Abelwahed Tribak**[1], **and J. Cagigas**[1]

[1]Dpto. Ingeniería de Comunicaciones, Universidad de Cantabria
Avda los castors, S/N 39005 Santander, Cantabria, Spain
[2]Facultad Eléctrica, Instituto Superior Politécnico José Antonio Echeverría, CUJAE
Ciudad de la Habana, Cuba
[3]Estacion Experimental de Aula Dei (EEAD), Zaragoza, Spain

Abstract— Two compact filters in finline configurations, a low pass filter (LPF) in unilateral finline and a stop band filter (SBF) in bilateral finline are presented. The low pass filter in unilateral finline waveguide consists of a uniplanar finline loaded, on the upper side, by narrow wires shunting periodically the two metal plates and in the same side for additional Complementary Split Ring Resonators (CSRRs). The stop band pass filter (SBF) in bilateral finline consists in a bilateral finline loaded, on both sides, with Split Ring Resonators. The transition from metal waveguide to finline is achieved by tapering the finline slot to the waveguide. Further in the present work, the width of the finline contour itself has been varied according to the finline configuration. Filters at millimetre-wave frequencies require accurate theoretical design and precision fabrication. Finline technology has been established as a practical approach in the design and construction of mm-wave components and subsystems. The electromagnetic wave is guided by slots in a metallization printed on a thin dielectric substrate. All passive circuit functions are realized by these slot-line structures. These circuits are correctly known as E-plane circuits. During recent years, various finline filters have been widely analyzed. However they cannot provide wide stop band with high attenuation level. The discontinuities involved have to be included in the design procedure. Higher order modes occur between the discontinuities. For better band attenuation, bilateral finline or several metal inserts side-by-side are used. These arrangements strongly suppress higher order mode coupling and therefore improve stop-band behaviour. Due to this, reducing the discontinuities is crucial in the function of the filter. To this end, this paper aims to find alternatives to conventional filters based mainly on finline slot sharp discontinuities. For this purpose, split-ring resonators (SRRs) coupled to finline structures is investigated. Specifically, the development of SRRs, originally proposed by Pendry et al. [1] was a major breakthrough for implementing lefthanded techniques in planar circuit technology. Split-ring resonators (SRRs) together with complementary split-ring resonators (CSRRs) contribute to maintaining the smaller size of filter pass band performance as the sub wavelength dimension enables sharp rejection [2]. CSRRs were used to design band pass filters [3], and improved performances were demonstrated in low pass filters [4]. By incorporating CSRRs, has been positive proof that it is feasible to produce a filter that performs with no ripples in the pass band, while producing a sharp stop band rejection in the vicinity of its resonant frequency. This paper expands the above procedure to finline filter design. SRRs are sub wavelength resonators that are able to inhibit signal propagation in a narrow band in the vicinity of their resonant frequency, provided that the magnetic field is polarized along the ring's axis and the finline structures present an appropriate magnetic field distribution for this purpose. A low pass filter in asymmetrical unilateral finline and a stop band filter in symmetrical bilateral finline configurations are designed, simulated, and tested. The results obtained using a resonant ring set suggests that these elements and their duals could provide tools that would dramatically improve the response of filters in planar technology. Experimental results of the SRR-loaded filters are presented to demonstrate feasibility of the proposed structures. The theoretical and experimental results were obtained using the fullCwave EM simulator Ansoft HFSS and HP8510 network analyzer respectively.

REFERENCES

1. Pendry, J. B., A. J. Holden, D. J. Robbins, et al., "Magnetism from conductors and enhanced nonlinear phenomena," *IEEE Trans. Microwave Theory Tech.*, Vol. 47, No. 11, 2075–2084, 1999.
2. Bonache, J., F. Martin, F. Falcone, et al., "Application of complementary split-ring resonators to the design of compact narrow band-pass structures in microstrip technology," *Microwave and Optical Technology Letters*, Vol. 46, No. 5, 508–512, 2005.

3. Garcia-Garcia, J., F. Martin, F. Falcone, J. Bonache, J. D. Baena, I. Gill, E. Amat, T. Lopetegi, M. A. G. Laso, J. A. M. Iturmendi, M. Sorolla, and R. Marques, "Microwave filters with improved stopband based on sub-wavelength resonators," *Microwave and Optical Technology Letters*, Vol. 46, No. 3, 283–286, 2005.
4. Casanueva, A., A. León, O. González, A. Mediavilla, M. Arias, and N. Amar, "Improved compact microstrip low pass filter with novel distributions of complementary split ring resonators (CSRRs)," *Asia-Pacific Microwave Conference (APMC 2009)*, 1450–1453, Singapore, December 7–10, 2009.

Development of THz Coherent Sources Using Quantum Cascade Lasers

S. Shiba[1,2], **N. Sekine**[2], **Y. Irimajiri**[2], **I. Hosako**[2], **T. Koyama**[2,3], **H. Maezawa**[3], **and S. Yamamoto**[1]

[1]Department of Physics, Faculty of Science, The University of Tokyo, Japan
[2]National Institute of Information and Communications Technology, Japan
[3]Solar-Terrestrial Environment Laboratory, Nagoya University, Japan

Abstract— We are developing THz quantum cascade lasers (QCLs) and hot-electron bolometer (HEB) mixers for a THz heterodyne receiver system. THz-QCLs are promising THz radiation sources as a local oscillator for heterodyne receivers because of their high output power and high frequency purity. So far we have successfully fabricated which can be operated in a continuous oscillation mode at the frequency around 3.1 THz up to a heat-shink temperature of 60 K. The QCLs are made of a GaAs/$Al_{0.15}Ga_{0.85}$ as material system using a resonant LO phonon scattering depopulation scheme, and processed in a double metal waveguide with the size of 40 μm wide and 1.5 mm long by using gold-gold thermo compression wafer bonding technique and a dry-etching method. We have also succeeded in detecting the QCL output power with an HEB mixer. The HEB mixer using an NbTiN ultra thin film as the superconducting material is coupled with the THz radiation by a quasi-optics twin slot antenna, and the THz radiation is detected as a change in the I-V characteristic curve. In this experiment, the QCL and the HEB mixer are installed in a different liquid helium cryostat respectively. The operating temperature of the QCL in continuous wave operation is around 15 K. Heterodyne mixing experiments using the QCL as a local oscillator are in progress toward establishing the PLL technique in THz region. We report the current results of our development and discuss the possibilities of THz-QCLs for heterodyne sensing applications in various research fields.

Modeling by FDTD of Some Optical Properties of Photonic Crystals Based on a Nanocomposite of Silver in TiO_2

A. Labbani and A. Benghalia
Laboratoire Hyperfréquences et Semi-conducteurs, Faculté des Sciences de l'ingénieur
Université Mentouri Constantine, Route d'Ain El Bey Constantine 25000, Algérie

Abstract— Photonic crystals (PCs) provide an effective way to control and manipulate electromagnetic radiation because they can affect the properties of photons in much the same way as a crystal semiconductor affects the properties of electron. Electromagnetic waves propagating in photonics crystals can be inhibited for a certain frequency range resulting in the formation of a photonic band gap. This ability is the basis of many applications of PCs, such as waveguides, microcavities and communication components.

In this work, we have demonstrated that it is possible to modify and tune the optical properties of TiO_2 in presence of silver nanoparticles. Changes in dielectric permittivity allow as to obtain a new material witch can have tunable photonic band gaps. To describe the optical properties of composite material, TiO_2 doped with Ag aggregates of various volume fractions f, using his dielectric permittivity, one can use the Maxwell-Garnett theory. In this approach the metallic nano-objets are considered as spherical and very small compared to the wavelength of the incident light.

We have calculated the photonic band gaps and the reflectivity for a system of one-dimensional (1D) photonic crystals $(Ag+TiO_2)/SiO_2$ using FDTD method (Figure 1). The characteristics of these bands are adjustable according to size and the volume factor occupied by the metallic nanoparticles in the host matrix (Figure 2).

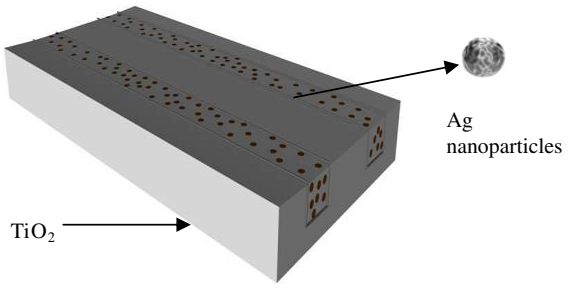

Figure 1: TiO_2 matrix doped with Ag nanoparticles.

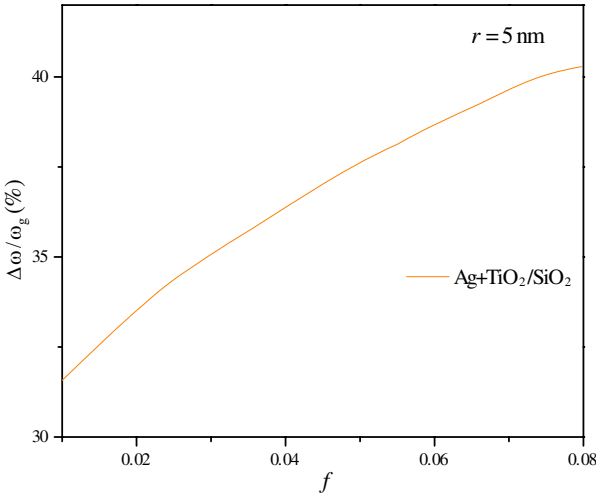

Figure 2: Gap width to midgap frequency ratio of the Bragg mirrors (Ag + TiO_2)/glass as a function of the filling factor f. The radius of the nanoparticles $r = 5\,\text{nm}$.

Materials Adsorption Characterization by Random Coherent Electromagnetic Waves

C. I. Cabello[1], **G. Bertolini**[1], **M. J. González**[2], **I. L. Botto**[2], **R. Arizaga**[3], **and M. Trivi**[3]

[1]Centro de Investigación y Desarrollo en Ciencias Aplicadas Dr. J. Ronco
(CINDECA-CONICET La Plata-UNLP), Calle 47 No. 257, (1900) La Plata, Argentina
[2]Centro de Investigaciones en Química Inorgánica
(CEQUINOR-CONICET La Plata-UNLP), Calle 47 y 115, (1900) La Plata, Argentina
[3]Centro de Investigaciones Ópticas (CIC-CONICET La Plata) and UID Optimo
Dpto. Ciencias Básicas, Facultad de Ingeniería, Universidad Nacional de La Plata
Casilla de Correo 3, (1897) Gonnet, La Plata, Argentina

Abstract— A random interference pattern of the electromagnetic waves is observed when a coherent laser beam illuminates a rough surface of an object. If this surface does not remain rigid, but it presents some type of local movement, then the intensity pattern evolves in time. This phenomenon, well known as *dynamic speckle*, is characteristic of biological samples. This behavior can also be observed in non-biological industrial processes, including the drying of paint, corrosion and heat exchange.

This activity takes place when the sample changes its properties due to movement of the scattering centers, changes in the optical path due to variations of refractive index, configuration changes or combination of these situations.

The study of the temporary evolution of the speckle patterns may provide an interesting tool to characterize the parameters involved in these processes.

The present work addresses the implementation of dynamic laser speckle technique to the hydro-adsorption analysis of the natural silica-aluminates (kaolinite, zeolites, original bentonite clay and chemically modified clays such as PILCs "pillared clays" and PCHs "porous clays heterostructured") with different chemical composition, surface area and pore volume. Experimental results show the temporal evolution of the materials speckle patterns during the process of water adsorption. Studies with commercial silica (SiO_2) with different textural properties show the correlation of the speckle activity with the hydro-adsorption process.

Also we found that it is possible to correlate the dynamic speckle stabilization time of each species with the Si/Al ratio and the Si-OH groups availability.

This analysis can be considered as a potential new method to study different porous materials of interest such as absorbents or catalysts supports.

A Proposal for a Low-cost TO-can 25-Gb/s Laser Diode Package

Tien-Tsorng Shih[1], **Pei-Hao Tseng**[2], **Yung-Yu Lai**[1], **Yaw-Dong Wu**[1], **and Wood-Hi Cheng**[2]

[1]Electronic Engineering Department, National Kaohsiung University of Applied Sciences
Kaohsiung, Taiwan
[2]Department of Photonics, National Sun Yat-sen University, Kaohsiung, Taiwan

Abstract— 25-Gb/s laser diode package is very essential for optical fiber communication networks, such as 21 GBaud fiber channel (20GFC) and 100-Gb/s Ethernet (100 GbE). TO-can package is a low-cost solution and is capable of mass production. However, the transmission rate of a TOcan laser diode package nowadays is limited to 10-Gb/s. Therefore, a modified TO-can laser diode package is proposed and demonstrated theoretically. A simulation method composed by a three dimension electromagnetic field simulation and a time-domain simulator is developed to investigate the electrical package performance of a TO-can laser diode package. The frequency-domain S-parameter characteristics and time-domain eye-diagrams are obtained through the simulation. The TO-can header structure, parasitics of bonding wire, and the builtin matching resistor are investigated and designed to an optimum condition. In contrast with a conventional TO-56 header, the transmission 3-dB bandwidth of the proposed TO-can header is improved from 17-GHz to over 40-GHz. After the wire bonding process, the transmission bandwidth is degraded to 36-GHz and 28-GHz for different numbers of bonding wire. The resistance of a laser diode is usually a few Ohms and forms a big impedance discontinuity. Without a proper built-in matching resistor to achieve the impedance-matching condition, the transmission bandwidth is deteriorated to only 12-GHz. With a built-in matching resistor of 20-Ohm and 45-Ohm, the transmission bandwidth is restored to 35-GHz and 36-GHz, respectively. The time-domain simulation shows a clear eye-diagram with a rise time and a fall time of 13.9-ps and 13.86-ps, respectively, under 25-Gb/s modulation.

Light Coupling from Optical Fiber to Silicon Nano-waveguide Using Si-SiO_2 Dielectric Metamaterial Structure

Shinmo An, **Beom-Hoan O**, **Seung-Gol Lee**, **Se-Geun Park**, **and El-Hang Lee**
Optics and Photonics Elite Research Academy (OPERA)
Micro Photonics Advanced Research Center (MPARC)
Department of Information and Communication Engineering, Inha University, Incheon, Korea

Abstract— We report, for the first time, on a novel scheme of coupling light from an optical fiber to nano-size optical waveguide using Si-SiO_2 dielectric metamaterial structure. As silicon material cannot generate light, an external light source is generally used to couple the light into a singlemode waveguide. However, the waveguide size for 1.55 μm wavelength is normally around $400 \times 250\,\mathrm{nm}^2$ in width and height, which is much smaller than conventional singlemode optical fiber with a 9 μm in diameter. Therefore, an efficient light coupling mechanism is needed. Most of the conventional coupling methods such as grating coupler, 3D taper, and 2D inverse taper [1–3] use either diffraction phenomenon or gradual mode field change to couple the out-of-plane light into a thin Si slab. In this paper, however, we have used a Si-SiO_2 dielectric metamaterial structure for light coupling from optical fiber to Si nano waveguide. The matamaterial system consists of an array of $50 \times 250\,\mathrm{nm}^2$ Si waveguides embedded in SiO_2 with a certain spacing. A Si waveguide having the size of $50 \times 250\,\mathrm{nm}^2$, has no TE mode, and therefore, it cannot be used as a waveguide. However, the simulation study shows that when Si waveguides are placed in an array, the light feels the whole piece as one unit medium and that the array generates a propagation mode. This is because most of the light power exists in the SiO_2 surrounding Si waveguide and and because that the effective index of the waveguide is closer to SiO_2 than to Si. The simulation also shows that the effective index can be precisely controlled by the number of Si waveguide and the inter-waveguide spacing. By extending the spacing, the intensity of the light around the Si pieces can be made weaker as a result of decreased refractive index. Although the decreased effective index causes the mode field diameter to increase, the nano waveguide maintains the singlemode condition. In the presentation, we will discuss the theory and the principle of this phenomena along with the simulation results. We will also duscuss the advantages of this metamaterial structure in nano-scale lightwave coupling.

REFERENCES

1. Taillaert, D., W. Bogaerts, P. Bienstman, et al., "An out-of-plane grating coupler for efficient butt-coupling between compact planar waveguides and single-mode fibers," *IEEE Journal of Quantum Electronics*, Vol. 38, No. 7, 949–955, 2002.
2. Fritze, M., J. Knecht, C. Bozler, et al., "Fabrication of three-dimensional mode converters for silicon-based integrated optics," *Journal of Vacuum Science & Technology B: Microelectronics and Nanometer Structures*, Vol. 21, No. 6, 2897, 2003.
3. Almeida, V. R., R. R. Panepucci, and M. Lipson, "Nanotaper for compact mode conversion," *Optics Letters*, Vol. 28, No. 15, 1302–4, 2003.

Session 2A1
Instabilities and Solitons in Nonlinear Photonics: Part 1

Difference Differential Equations for a Resonator with a Very Thin Nonlinear Medium

L. A. Lugiato and F. Prati
Dipartimento di Fisica e Matematica, Università dell'Insubria, Via Valleggio 11, Como 22100, Italy

Abstract— The last 30 years witnessed a flourishing development of theoretical and experimental activities in the area of temporal and spatial instabilities in general and in nonlinear optical systems in particular. Complete models which include time +3D in space are extremely difficult to handle numerically even when the nonlinear medium is enclosed in an optical cavity. A tractable configuration, which has been extensively studied, is that of ring cavity models in the single-longitudinal model approximation, because one can neglect the longitudinal variable z and therefore reduce to time +2D.

The case of Fabry-Perot (FP) cavity is, however, substantially more complex than that of ring cavity, because one must take into account the left- and the right-propagating fields and the standing wave effects which arise from their superposition.

We derive [1] from the classic Maxwell-Bloch equations a set of difference-differential equations valid, in general, when the length of the nonlinear medium in the optical cavity is much smaller than a wavelength. Such equations provide an elegant and simple framework in which the case of Fabry-Perot and ring cavity can be discussed in a unified way. We outline a complete scenario for the multimode laser instability in the Fabry-Perot case, illustrating the results for parameter values appropriate to quantum cascade lasers. Our approach can have a relevant impact also on the study of dynamical instabilities in external cavity semiconductor lasers, including multiple quantum well or quantum-dot structures.

Especially relevant for the future development of our result is the case of three spatial dimensions, in the study of phenomena of outstanding interest for applications, e.g., the generation of pulses localized in 3D and time (light bullets). The substantial reduction in computer time allowed by our delay — difference equations, represents in this case the crucial step which enables one to engineer the parameters to obtain the desired spatiotemporal behavior.

REFERENCES

1. Lugiato, L. A. and F. Prati, "Difference differential equations for a resonator with a very thin nonlinear medium," *Phys. Rev. Lett.*, Vol. 104, 233902, 2010.

One-dimensional Wave Turbulence in Framework of Generalized Nonlinear Schrodinger Equation

Dmitry Agafontsev[1] **and V. Zakharov**[2]

[1]Lebedev Institute of Physics, RAS, Moscow, Russia
[2]Department of Mathematics, University of Arizona, Tucson, USA

Abstract— We solve numerically the focusing generalized Nonlinear Schrodinger equation

$$i\Psi_t + \Psi_{xx} + |\Psi|^2\Psi + \alpha|\Psi|^4\Psi - \beta|\Psi|^6\Psi = 0 \qquad \alpha > 0, \quad \beta > 0, \quad \alpha/\beta \gg 1,$$

in the box $0 < x < 2\pi$ with periodically boundary conditions and the initial data

$$\Psi|_{t=0} = \psi(x) + \epsilon f(x),$$

where $\psi(x)$ is a solution of the stationary equation

$$-\lambda^2\psi + \psi_{xx} + \psi^3 + \lambda\psi^5 - \beta\psi^7 = 0.$$

Here $f(x)$ is a stochastic noise and $\epsilon \ll 1$ is a parameter. Function $\psi(x)$ could be either a stationary monochromatic wave ($\psi = A = \text{const}$) or a periodic chain of solitons. We are interested only in the cases when the stationary wave is unstable and a number of unstable modes is large. In these cases the development of modulational instability leads to formation of one-dimensional wave turbulence. In the integrable case $\alpha = \beta = 0$ the turbulence is called integrable and relaxes to one of infinite possible stationary states. In a general non-integrable case the turbulence must turn in a long run to combination of one soliton and Bose-gas at zero temperature, however to reach this final equilibrium one needs to perform calculation during very long time. In a finite time, the development of non-integrable turbulence is a slow evolution of integrable turbulence.

We measured evolution of spatial spectra $I_k = \langle|\Psi_k|^2\rangle$ and the PDF of $|\Psi|^2$, concentrating special attention on formation of "fat tails" in the PDF. Integrable turbulence appearing as a result of modulational instability of the stationary monochromatic wave leads to an almost Gaussian PDF, while instability of the soliton-like knoidal wave leads to formation of heavy fat tails, which can be interpreted as "freak waves". Adding even small higher order terms enhance this effect dramatically.

Finite-size Effects and Information Capacity of Cavity Solitons

G. Kozyreff[1] and L. Gelens[2]

[1]Université Libre de Bruxelles (ULB), Belgium
[2]Vrije Universiteit Brussels (VUB), Belgium

Abstract— We analyze the influence of boundaries on cavity solitons in a large but finite optical cavity. Analytical results are first derived in a general context in the frame of the Swift-Hohenberg, where cavity solitons stand as stable localized patterns produced by a Turing bifurcation. For almost any boundary conditions, we find that they can only be stably located in a discrete set of locations. Multi-peak solutions are rapidly constrained to sit in the middle of the domain as their size increase. Moreover, single-peak solutions only exist sufficiently far from the edges of the domain. These features are predicted and confirmed numerically on the Lugiato-Lefever model. We show how this restricts the information capacity associated to cavity solitons.

Logical Operations Using Cavity Solitons

D. Gomila, A. Jacobo, M. A. Matías, and P. Colet
IFISC (CSIC-UIB), Campus Universitat Illes Balears, 07122 Palma de Mallorca, Spain

Abstract— Optical computing, via photons instead of electrons, has long appealed researchers as a way of achieving ultrafast performance. Photons travel faster than electrons and do not radiate energy, even at fast frequencies. Despite the constant advances and miniaturization of conventional electronics, optical computing remains as an alternative to overcome the heat generation and bandwidth limitations of conventional electronics. Many of the systems studied in optical computing applications imply light propagation, for example in optical correlators, already commercially used in optical processing applications, or using spatial solitons to create all-optical logic gates. Dissipative solitons (DS), also known as cavity solitons, have been suggested as a potentially useful strategy for information storage, that is specially attractive after DS have been shown in semiconductor lasers, a very compact and widespread technology. Within this approach a DS describes a bit of information. Here we will take this idea a step further and discuss the potential of DS for carrying out computations, not merely information storage, benefiting from the excitability property exhibited by some DS. In particular, we will consider DS in an optical cavity filled with a self-focusing Kerr medium, and we will show how three basic logic gates can be designed using these structures, namely the AND, OR and NOT gates. These three logic gates provide complete logic functionality, as by combination of them one can construct any other logical operation including the NOR and NAND universal gates. We will also discuss how this approach can fulfill the basic criteria for practical optical logic.

Control and Managing of Optical Localized States and Spatial Solitons in Liquid Crystal Light-valves

S. Residori[1], **U. Bortolozzo**[1], **F. Haudin**[1], **R. Rojas**[2], **M. G. Clerc**[3], **A. Piccardi**[4], **A. Alberucci**[4], **and G. Assanto**[4]

[1]INLN, CNRS, Université de Nice-Sophia Antipolis, 1361 route des Lucioles, Valbonne 06560, France
[2]Instituto de Fisica, Pontificia Universidad Catolica de Valparaiso, Casilla, Valparaiso 4059, Chile
[3]Departamento de Fisica, FCFM, Universidad de Chile, Casilla, Santiago 487-3, Chile
[4]NooEL, University "Roma Tre", Via della Vasca Navale 84-00146, Rome, Italy

Abstract— During the last years optical spatial solitons, or self-trapped beams, and localized structures in the transverse profile of spatially extended wavefronts have been the subject of a wealth of theoretical and experimental works, not only for their fundamental interest but also for their potential applications in optical wave-guiding and all-optical signal processing. Controlling and managing the dynamical features of such nonlinear states of light propagation is nowadays one of the main experimental challenges, constituting a complex task which often lacks theoretical supports, especially when we deal with localized structures in systems with more than one spatial dimension. In this context, we will show here that liquid crystal light-valves offer unique potentialities for studying and managing optical localized state dynamics, providing at the same time a high nonlinear response, leading to the stable formation of spatial solitons and optical localized structures of different types, and the possibility of photo-addressing the localized states by an external control beam or by a spatially structured input beam. We will present two prototype experimental setups: the liquid crystal light-valve (LCLV) with optical feedback and the propagation of solitons, also called "nematicons", along the thickness of the nematic liquid crystal layer inside the LCLV. In the first setup we realize a two-dimensional spatial forcing by suitable spatial modulations of the input beam. By changing the forcing parameters, we show a stable family of localized structures of different size and shape, resulting from the front pinning-depinning phenomenon that occurs in spatially modulated media. In the second setup we show that all-optical deviations of solitons can be realized by the presence of external beams illuminating the LCLV, thereby entailing complete optical control of the soliton trajectory. With a proper design of shape, intensity and location of the optical perturbations on the soliton path, we show that elementary Boolean architectures can be effectively implemented in a fully reconfigurable manner by means of external optical-addressing beams.

REFERENCES

1. Haudin, F., R. G. Elìas, R. G. Rojas, U. Bortolozzo, M. G. Clerc, and S. Residori, "Driven front propagation in 1-D spatially periodic media," *Phys. Rev. Lett.*, Vol. 103, 128003–128006, 2009.
2. Clerc, M. G., F. Haudin, S. Residori, U. Bortolozzo, and R. G. Rojas, "Control and managing of localized states in two-dimensional spatially periodic media," *Eur. Phys. J. D*, Vol. 59, 43, 2010.
3. Piccardi, A., U. Bortolozzo, S. Residori, and G. Assanto, "Optical spatial solitons in liquid crystal light valves," *Opt. Lett.*, Vol. 34, 737–739, 2009.
4. Piccardi, A., A. Alberucci, U. Bortolozzo, S. Residori, and G. Assanto, "Soliton gating and switching in liquid crystal light valve," *Appl. Phys. Lett.*, Vol. 96, 071104–071106, 2010.

Spatio-temporal Characteristics of Spatial Solitons in Molecular Reorientational Kerr Media with Sharp Raman Resonance

H. Maillotte, G. Fanjoux, J. Michaud, M. Delqué, and T. Sylvestre
Département d'Optique, P.M. Duffieux, Institut FEMTO-ST, UMR CNRS 6174
Université de Franche-Comté, UFR Sciences, 16 route de Gray, Besançon Cedex 25030, France

Abstract— Kerr materials exhibiting inertial molecular reorientation at the picosecond time scale and sharp Raman resonance give rise to a range of specific spatio-temporal effects that enrich the dynamical behavior of spatial solitons. In these materials, multi-component (in polarization and/or frequency) bound vector Kerr solitons can be generated and exhibit slow-light effect, spectral energy transfer, symmetry-breaking instability, and polarization rotation. During this presentation, we will give an overview of such effects and propose potential applications.

Experimental Solitons and Fronts in a Transverse One-dimensional Optical Kerr Cavity

E. Louvergneaux, V. Odent, S. Coulibaly, P. Glorieux, and M. Taki
Laboratoire de Physique des Lasers, Atomes et Molécules, CNRS, UMR 8523, Université Lille 1
Villeneuve d'Ascq Cedex 59655, France

Abstract— Passive Kerr resonators have been extensively studied theoretically for their transverse patterns, solitons as well as e.g., their excitable regimes [1–6] in "ideal" configurations. The latter assume an instantaneous medium without diffusion and a high finesse ring cavity that allow for mean field approximation. However, no experiments on Localized Structures (LSs) in such passive cavities have been given up to now so that the agreement between theory and experiments still remain to be achieved. Here, to investigate experimentally the formation and dynamics of solitons and fronts, we use a transverse one-dimensional Fabry-Prot cavity filled with an ultra-thin slice of liquid crystal (LC) as nonlinear Kerr medium. The features of our setup such as the non-instantaneous response time of the nonlinear medium, the finesse of the cavity (around 10) and the non-locality of the medium render our system far from the "ideal" configuration and its mean field model [1]. However, we show that the localized states still survive experimentally in our conditions. Indeed, using a cavity linear phase shift stabilization, we have experimentally shown the existence of solitons and fronts in our specific system. Then, we study the influence of the spatial profile of the pump beam and of the diffraction sign on these localized structures. For positive diffraction, we demonstrate the formation of stable spatial solitons with oscillating tails being either independent or locked. For negative diffraction associated with negative optical cavity length [7], fronts are generated. In this latter configuration, our nonlinear medium can be viewed as a left-handed material. Using the Gaussian profile of the input beam as forcing spatial conditions, we control the distance between the two fronts defining the localized pattern and so its transverse extension. The numerical simulations carried out on the infinite-dimensional map of the intra-cavity field fully agree with the experimental observations.

REFERENCES

1. Lugiato, L. A. and R. Lefever, *Phys. Rev. Lett.*, Vol. 58, 2209, 1987.
2. Scroggie, A., W. Firth, G. McDonald, M. Tlidi, R. Lefever, and L. A. Lugiato, Special issue on "Nonlinear optical structures, patterns and chaos," *Chaos, Solitons and Fractals*, Vol. 4, 1323, 1994.
3. Firth, W. J., G. K. Harkness, A. Lord, J. M. McSloy, D. Gomila, and P. Colet, *J. Opt. Soc. Am. B*, Vol. 19, 747, 2002.
4. Gomila, D., M. A. Matas, and P. Colet, *Phys. Rev. Lett.*, Vol. 94, 063905, 2005.
5. Gomila, D. and P. Colet, *Phys. Rev. E*, Vol. 76, 016217, 2007.
6. Gelens, L., D. Gomila, G. Van Der Sande, J. Danckaert, P. Colet, and M. A. Matas, *Phys. Rev. A*, Vol. 77, 033841, 2008.
7. Kockaert, P., *J. Opt. Soc. Am. B*, Vol. 26, 1994, 2009.

The Dynamics of a Stabilized Nonlinear Fiber Ring Resonator: from CW Pumping to Synchronously Pumped Regime

P. Emplit[1], **S. Coen**[2], **F. Leo**[1], **P. Kockaert**[1], **S.-P. Gorza**[1], **M. Taki**[3], **A. Mussot**[3], **E. Louvergneau**[2], **and M. Haelterman**[1]

[1]Service OPERA-Photonique, Université Libre de Bruxelles
CP 194/5, Avenue F. D. Roosevelt 50, B-1050 Brussels, Belgium
[2]Department of Physics, The University of Auckland, Private Bag 92019, Auckland, New Zealand
[3]Laboratoire PhLAM, UMR CNRS 8523, IRCICA, FR CNRS 3024, Université Lille 1
Villeneuve d'Ascq Cedex 59655, France

Abstract— During the last 10 years, we investigated theoretically and experimentally the nonlinear dynamics of an all-fiber passive ring cavity, alternatively pumped by a CW monochromatic source, or synchronously pumped by a mode-locked laser.

Depending on the relative influences of the dispersion map of the cavity, its finesse and its Kerr-induced nonlinearities, a wide range of temporal dynamics of the intra-cavity signal has been observed and explained. This paper is willing to review and analyze our main results, and their potential applications in the frame of all-optical information processing systems.

The core of our studies is the use of a passive single-mode silica-fiber ring-resonator [1], including a specially designed piezo stretcher stabilization system, that allows for interferometric and reproducible control of the cavity length, at a submicron scale.

While synchronously pumped by a 82-MHz repetition rate picosecond Ti:Sapphire laser at a wavelength around 800 nm, the fiber cavity exhibits normal dispersion. Pulses propagate into the cavity, and interact, after each roundtrip, with the launched pumping pulse train. Besides the expected fundamental nonlinear behaviors such as optical bistability and period doubling instabilities, dissipative modulational instability, resulting from the interplay between dispersion and Kerr nonlinearity, is observed [2]. Through the analysis of the output pulse spectra we show, in excellent agreement with our theoretical predictions, that modulational instability plays an unexpected role in the dynamics of the cavity (in particular, in the period-doubling route to chaos).

Such a cavity constitutes an extraordinary "laboratory device" for the study of the fundamental dynamical properties of nonlinear optical dissipative systems.

When moving towards a CW single-line pumping scheme, around 1550 nm, the fiber dispersion becomes anomalous and, in this configuration, modulational instability is able to induce the generation of soliton trains [3]. A fine tuning of the dispersion, around the zero-dispersion value, constitutes the key element governing the outgoing pulse train repetition-rate. The precise characterization of the pulse train in the spectral and in the temporal domain, confirms the ability of such a simple passive fiber device to generate pulse-trains at repetition-rates far above 1 THz.

In such a configuration, the fiber cavity can be considered as a very promising pulse spatially and temporally coherent source

More recently [4], we launched, in a similar passive standard single-mode fiber ring cavity, on one hand a CW pump beam at a wavelength around 1550 nm, and separately, isolated seeding 4-ps 1535 nm pulses. In such a configuration, the cavity supports stable sets of temporal cavity solitons that behave as coded sequences of on-off optical bits, circulating quasi-indefinitely in the ring cavity, as in an all-optical buffer memory. These type of solitons are robust attracting states, that can be excited through a phase-insensitive and wavelength-insensitive process.

As such, cavity temporal solitons constitute an ideal support for bits in a 25 Gbit/s optical buffer that would seamlessly combine three critical telecommunication functions, namely all-optical storage, all-optical reshaping, and wavelength conversion.

In conclusion, depending on the relative importance of dispersive and nonlinear properties of light interaction into its fiber components, a passive waveguiding ring cavity is able to deliver pulse trains at Tbit/s repetition rate, to store and handle large sequences of ultrashort bits for a long time, and to offer an unequaled simple experimental platform for nonlinear dynamics studies of dissipative or non dissipative 1-D systems. Major breakthroughs have been demonstrated by using this device, while room still remains for major improvements.

ACKNOWLEDGMENT

This work was partially supported by the Belgian Science Policy Office (BelSPO) under grant IAP6-10. Additional supports of the Fonds de la Recherche Scientifique (FRS-FNRS, Belgium) and the Fonds pour la formation a la Recherche dans l'Industrie et dans l'Agriculture (FRIA, Belgium) are acknowledged as well.

REFERENCES

1. Coen, S., M. Tlidi, P. Emplit, and M. Haelterman, *Phys. Rev. Lett.*, Vol. 83, No. 12, 2328–2331, 1999.
2. Coen, S., M. Haelterman, P. Emplit, L. Delage, L. M. Simohamed, and F. Reynaud, *J. Opt. Soc. Am. B*, Vol. 15, No. 8, 2283–2293, 1998.
3. Leo, F., A. Mussot, P. Kockaert, M. Taki, E. Louvergneau, P. Emplit, and M. Haelterman, *Proc. of IEEE/LEOS Symposium Benelux Chapter*, 19–22, 2008.
4. Leo, F., S. Coen, P. Kockaert, S.-P. Gorza, P. Emplit, and M. Haelterman, *Nature Photonics*, Vol. 4, No. 7, 471–476, 2010.

Optical Similaritons and Their Collisions inside Fiber Amplifiers

Govind P. Agrawal[1] and Sergey A. Ponomarenko[2]

[1]Institute of Optics and Department of Physics, University of Rochester, Rochester, NY 14627, USA
[2]Department of Electrical and Computer Engineering, Dalhousie University, Halifax, NS, B3J 2X4, Canada

Abstract— Optical similaritons represent pulses or beams that preserve their shape while their widths and peak powers change in a self-similar fashion. A decade ago, such parabolic-shape pulses were found to form in optical amplifiers exhibiting normal dispersion [1]. Recently, exact self-similar solutions in the form of hyperbolic secant shape have been discovered for optical pulses propagating inside fiber amplifiers with distributed dispersion and gain [2–4]. It turns out that there exists a one-to-one correspondence between such self-similar waves and solitons of the standard, homogeneous, nonlinear Schrödinger equation if a certain compatibility condition is satisfied [4]. As this correspondence guarantees the stability, we have studied the collision of two or more fundamental and higher-order similaritons [5].

Although both the bright and dark kinds of similaritons can exist, in this presentation we focus on the bright similaritons that form when short optical pulses propagate inside fiber amplifiers whose gain and anomalous dispersion vary along the fiber length. We first focus on the situation in which two similaritons propagate with the same velocity inside a fiber of constant anomalous dispersion but they are spaced closely enough to overlap. Each similariton has an initial chirp that can be positive or negative and it broadens in the former case but is compressed in the later case as it propagates down the fiber. Similar to the soliton case, the similariton interaction occurs through cross-phase modulation; the similaritons attract or repel each other depending on their relative phase difference. The main difference from the soliton case is that the similariton width, chirp, and the amplitude scale upon the interaction and the subsequent propagation along the fiber. We have found evidence of a substantial energy transfer between two similaritons when their relative phase lies between 0 and π. We also consider the case of three higher-order similaritons moving with different velocities and colliding inside the fiber. We find that the nonlinear interaction of closely spaced similaritons exhibits a variety of interesting features that are different from those typical of the soliton case [5]. In particular, we show that the similariton interactions can under certain conditions lead to the formation of molecule-like bound states of two similaritons [4].

REFERENCES

1. Kruglov, V. I., A. C. Peacock, J. M. Dudley, and J. D. Harvey, "Self-similar propagation of high-power parabolic pulses in optical fiber amplifiers," *Opt. Lett.*, Vol. 25, 1753–1755, 2000.
2. Kruglov, V. I., A. C. Peacock, and J. D. Harvey, "Exact self-similar solutions of the generalized nonlinear Schrödinger equation with distributed coefficients," *Phys. Rev. Lett.*, Vol. 90, 113902(1–4), 2003.
3. Ponomarenko, S. A. and G. P. Agrawal, "Do solitonlike self-similar waves exist in nonlinear optical media?," *Phys. Rev. Lett.*, Vol. 97, 013901(1–4), 2006.
4. Ponomarenko, S. A. and G. P. Agrawal, "Interactions of chirped and chirp-free similaritons in optical fiber amplifiers," *Opt. Express*, Vol. 15, 2963–2973, 2007.
5. Ponomarenko, S. A. and G. P. Agrawal, "Nonlinear interaction of two or more similaritons in loss- and dispersion-managed fibers," *J. Opt. Soc. Am. B*, Vol. 25, 983–989, 2008.

An Optical Instability Phenomena in The Optical Emission of InGaN Devices

K. Oikawa[1] and R. Micheletto[2]

[1]Graduate School of Nanobioscience, Yokohama City University, Japan
[2]Nanoscience and Technology, International Graduate School of Art and Sciences
Yokohama City University, Japan

Abstract— Recent advances in studies for InGaN/GaN have led to high-brightness green and blue light emitting diodes (LED). These wide band gap materials are currently used for many applications, for example full color displays, white (RGB) light sources or for the creation of shorter wavelength devices for optical data storage.

In this presentation, we will report our observations of intriguing optical instability (blinking phenomenon) in the photoluminescence of InGaN single quantum well devices. Similar uorescence blinking has been observed in three dimensional confined systems (quantum dots) as CdSe, ZnCdSe, InP and GaAs, however the phenomenon is difficult to be explained in our case where the photoluminescence is generated in a system that is quantum confined only in a single direction (quantum well).

We will describe in detail the optical phenomena observed, characterize its chaotic behavior with Fourier and correlation anlysis. Also, we give a tentative theoretical explanation of the optical instability by the use of a turbulent model of carrier propagation that results in an optical unstable photon emission that is compatible with our results.

We believe that the elucidation of the phenomena will contribute to the effort of understanding fundamental phenomena of photon emission and pave the way for the realization of new and more efficient optical devices.

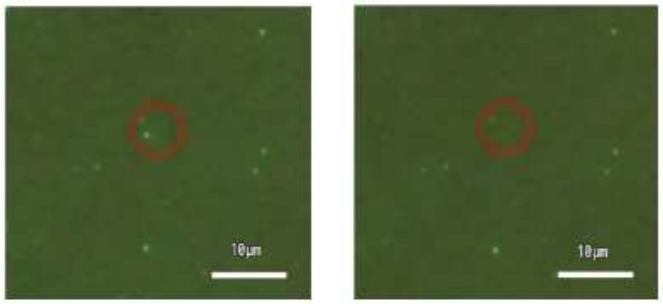

(a) (b)

Figure 1: Optical microscope PL images of a 510 nm InGaN sample. A instability blinking point is circled in two figures (a) and (b) taken about a few second apart. The sample was excited by Ultra violet Hg lamp (about 425 nm).

REFERENCES

1. Micheletto, R., M. Allegrini, and Y. Kawakami, "Near-field evidence of local polarized emission centers in InGaN/GaN materials," *Applied Physics Letters*, Vol. 95, 211904, 2009.
2. Micheletto, R., M. Abiko, A. Kaneta, and Y. Kawakami, "Observation of optical instabilities in the photoluminescence of InGaN single quantum well," *Applied Physics Letters*, Vol. 88, 61118–61120, 2006.
3. Feldmeier, C., M. Abiko, U. T. Schwarz, Y. Kawakami, and R. Micheletto, "Transient memory effect in the photoluminescence of InGaN single quantum wells," *Optical Express*, Vol. 17, No. 25, 22855, 2009.

Session 2A2
Electromagnetic Modeling, Inversion and Applications

Novel Analytic Method Based on Differential Geometry and Perturbation Theory for Electromagnetic Wave Problems

Morten Willatzen
Mads Clausen Institute for Product Innovation, University of Southern Denmark
Alsion 2, DK-6400 Sønderborg, Denmark

Abstract— A combination of differential geometry and perturbation theory is used to obtain novel analytic expressions for waveguide eigenmode changes due to general curvature effects in the case of general boundary conditions, i.e., encompassing the important and application-relevant cases of Dirichlet and Neumann boundary conditions [1].

The Laplacian is recast in curved coordinates t, p, and q, where t is the local tangent vector along the nano-waveguide centerline coordinate x and p, q span the local cross section. Further, using the so-called Minimal Rotating Frame and assuming small cross sectional dimensions relative to the waveguide length, allows the problem to be solved effectively.

For circular-shaped and helix-shaped structures, the perturbative expressions yield the same result as independent analytical results.

A selection of complicated wave problems is solved quasi-analytically using differential geometry arguments. Our method allows arbitrarily shaped complex-geometry problems to be addressed as a set of three ordinary differential equations rather than solving the three-dimensional wave equation problem. Hence the presented method vastly simplifies the complexity of the problem. Some examples will be demonstrated for Maxwell's and Schrödinger's equations corresponding to applications in photonics and nanoelectronics [2, 3].

REFERENCES

1. Willatzen, M., J. Gravesen, and L. C. Lew Yan Voon, "Analytic theory of curvature effects for wave problems with general boundary conditions," *Phys. Rev. A Rapid Communication*, Vol. 81, 060102(R), 2010.
2. Gravesen, J. and M. Willatzen, "Eigenstates of Möbius nanostructures including curvature effects," *Physical Review A*, Vol. 72, 032108, 2005, also Published in *Virtual Journal of Nanoscale Science & Technology*, October 3, 2005.
3. Willatzen, M., "Electromagnetic-wave propagation along curved surfaces," *Phys. Rev. A*, Vol. 80, No. 4, 043805, 2009.

1D Inversion of Multi-component and Multi-frequency Low-induction Number EM Device (PROMIS) for Near-surface Exploration

C. Schamper and F. Rejiba
UMR 7619 Sisyphe, University of Paris 6, France

Abstract— Most of the low-induction number ElectroMagnetic sensors measure only the vertical magnetic field component for a vertical magnetic dipole source. We propose here to present the results of a sensitivity analysis of a slingram device, named PROMIS (Iris Instruments), which allows the measurement of ten frequencies ranging from 110 Hz to 56 kHz and the three components of the magnetic field. The main objective is to analyze how the radial component Hr, which varies during a profiling acquisition above a horizontally-layered ground, could improve the inversion process of the usual Hz, by essentially decreasing the number of equivalences as well as improving the convergence.

First results coming from separated sensitivity analysis of Hr and Hz have shown that Hr is more sensitive to the variation of the thickness of a near-surface conductive layer. Analysis of the RMS error in the parameters' space (resistivity and thickness of the conductive layer) indicates less dispersion associated to equivalences for Hr rather than for Hz. The inversion process involving both Hr and Hz components have been performed using several methods (gradient and Monte Carlo types) including a Marquardt-Levenberg-like approach. The sensitivity analysis shows a "narrow banana" distribution of equivalences for the parameters' pair thickness/resistivity of the conductive layer, which leads to convergence problems that cannot be solved easily by the lone use of a damping factor. In order to improve significantly the convergence rate, we have implemented a two step inversion process that includes an intermediary random search step, associated to the Marquardt-Levenberg technique. This helps to circumvent the issue of equivalences in the "narrow banana" zone. Synthetic tests demonstrate clearly that, at least for thicknesses larger than few meters, the joint inversion of Hr and Hz measured with the PROMIS improves the estimation of the physical parameters.

3D Laser Imaging

Gerard Berginc and Michel Jouffroy
THALES, 2 avenue Gay Lussac, Elancourt Cedex 78995, France

Abstract— This paper addresses 3D laser imaging. There is a considerable interest in the development of new optical imaging systems that are able to give three-dimensional images. Potential applications range across medical imaging, surveillance and robotic vision. Identifying targets or objects concealed by foliage or camouflage is a critical requirement for operations in public safety, law enforcement and defense. The most promising techniques for these tasks are 3D laser imaging techniques. Active imaging systems using a near-infrared laser and a suitable detector are used for most long range imaging applications. We propose a method to enable a superresolution 3D reconstruction from several intensity images. The laser illuminates the scene and the reflected radiation is collected by a detector to give a two-dimensional image. We obtain a three-dimensional image owing to a tomographic process taking into account 2D images with different angles of view. This technique utilizes properties of the target to perform the identification function (geometry, surface, absorption, scattering and depolarization of the electromagnetic waves).

In this paper, we present the 3D laser imaging simulation, the physics based model and the reconstruction algorithm. The model includes all of the electromagnetic interaction mechanisms. The surface of hard objects is considered as randomly rough surfaces and we compute the laser signature (laser cross-section) of these objects. To estimate the laser interaction with the randomly rough surface, we use the second order Small-Slope Approximation method. Because the problem, we consider in this paper, is three-dimensional, all the scattering coefficients (coherent and incoherent component of the electromagnetic field) are functions of the azimuth angles, and the cross-polarized terms do not vanish. We define, in this case, the Mueller matrix, which gives all the combinations of the polarization states of the scattered electromagnetic waves. The randomly rough surfaces of the complex object are characterized by electromagnetic parameters (permittivity ...) and roughness parameters (standard deviation of rough surface height and autocorrelation function). We obtain the three-dimensional reconstruction by a cone-beam algorithm, which is a convolution-backprojection algorithm deduced from the Radon transform. In this paper, we study the robustness of this algorithm and analyze the 3D reconstruction algorithm with added Gaussian noises.

We also give experimental proof of the theory. We develop a 3D imaging system based upon a two-dimensional imaging device with high pixel density in the visible band.

A Hessian Based Numerical Convergence Analysis of a Dual-grid Tikhonov Regularized Gauss-Newton Reconstruction Approach to Electromagnetic Tomography

Naren Naik[1] and Jerry Eriksson[2]

[1]Department of Electrical Engineering, Indian Institute of Technology-Kanpur, Kanpur-208016, India
[2]Department of Computing Science, Umea University, S-901, 87 Umea, Sweden

Abstract— We present a numerical study of convergence of a Tikhonov regularized Gauss Newton (TRGN) optimization scheme used to solve a dual-grid nonlinear reconstruction problem of subsurface electromagnetic tomography. Due to the ill-posed (almost rank-deficient) nature of this reconstruction problem, it is typically very difficult to know whether we have stopped the iterations at a best possible solution, and hence our attempt at a better quantification.

Basically a local iteration matrix for the TRGN iterates is derived (using Hessian information) [1], whose spectral radius needs would be less than one close to convergence. This matrix is further decomposed so as to yield distinct contributions to the rate of convergence from data and parameter spaces. The utility of the nature of the decomposition is evident, in that, rather than only the total iteration matrix we now have information regarding the separate effects of the objective-function and parameter-space errors, as well as that of the regularization parameter and center, on the convergence of the iterates.

Thus, the iterates obtained from the dual-grid regularized Gauss-Newton scheme are subjected to this analysis that yields Hessian based estimates of convergence rates in the residual and parameter spaces. This helps in numerically quantifying whether a given iterate sequence is a part of a convergent subsequence (helping to choose a stopping iterate), and, to give an insight into sources of non-convergence from parameter and residual spaces.

For test cases in a GPR tomography setting of mine like objects embedded in the ground, the convergence analysis is numerically demonstrated by computing these convergence-rates for a medium size dual-grid reconstruction and then used to interpret the reconstructions obtained by the iterative scheme. Importantly also, the response of the reconstructions to changes of regularization parameter and center of the Tikhonov functional have been attempted to be quantified in these post-reconstruction numerical studies; to the best of our knowledge these are unique studies in this respect.

REFERENCES

1. Naik, N. and J. Eriksson, "A Hessian based analysis of a Tikhonov regularized Gauss-Newton approach to subsurface electromagnetic tomography," Submitted.

A Fully Automatic Model Predicting the Electromagnetic Radiations of High Frequency Electronic Devices

Abhishek Ramanujan, Zoheir Riah, Anne Louis, and Bélahcène Mazari
Institut de Recherche en Systèmes Electroniques Embarqués (IRSEEM)
76801 Saint Etienne du Rouvray, France

Abstract— As electromagnetic compatibility (EMC) gains ground in today's world of electronics, testing tools and modeling methods are of paramount importance to develop EMC compliant products. A simple and practical model to predict the radiated emissions of passive microwave devices [1] and on-chip RF devices [2] has been developed in IRSEEM in this context. It is built with an array of miniature electric dipoles and the dipole orientations, and currents are extracted from magnetic field measurements (or simulations) with the use of an optimization procedure. Though the model considers the physical effect of the dielectric present in the device under test, its value should be known before hand. Moreover, the position of every dipole in the model is prefixed. To overcome these limitations, a new extraction procedure is developed incorporating phenomenal improvements: detect the dipole positions automatically and extract the model parameters: dipole orientations, their currents and the effective relative dielectric constant of the device under test. Only the dipole lengths are prefixed.

The dipole positions are determined from the tangential components of the magnetic field (H_x, H_y) with the use of the intensity thresholding technique [3]. The user is allowed to interactively select the intensity level. The default value is determined with the use of the global image thresholding technique based on the Otsu's method pre-coded in MATLAB. The dipole lengths are however pre-fixed. Only the dipoles contributing significantly to the radiated field are considered and thus optimum number of dipoles is used in contrast to the previous model. This improves the model's computational performance considerably. Another significant advancement is made in the model extraction procedure. The three model parameters are extracted with a two-step procedure implemented in MATLAB: the initial parameter vector is first determined and then a two-level non-linear optimization procedure is used to accurately obtain the "bestavailable" solution. The E_z field is used in addition to H_x and H_y to aid in extraction. A graphical user interface is developed to facilitate the use of the model. The model is validated on a Wilkinson power divider operating at 5.6 GHz from electromagnetic field simulations made in Ansoft HFSS. The fields at 500 µm above the device were used for model construction with 478 dipoles automatically detected. This is about 36% less than the minimum number of dipoles needed with the manual model. An excellent correlation was found between the modeled and simulated electromagnetic fields at 500 µm and 1.5 mm above the device. The extracted effective relative dielectric constant correlates well with that of empirical calculations.

ACKNOWLEDGMENT

This work was performed under the CoSiP (Chip/Package-System Co-Design) project, funded by French government via the DGCIS and supported by the European commission via MEDEA+.

REFERENCES

1. Ramanujan, A., Z. Riah, A. Louis, and B. Mazari, "Modeling the electromagnetic radiations of passive microwave components using a near-field scanning method," *IEEE Trans. EMC*, 2010, Accepted for Publication.
2. Ramanujan, A., Z. Riah, A. Louis, and B. Mazari, "On the radiated emission modeling of on-chip microwave components," *IEEE Int. Sym. EMC*, Florida, USA, Jul. 2010.
3. Sezgin, M. and B. Sankur, "Survey over image thresholding techniques and quantitative performance evaluation," *Journal Electronic Imaging*, Vol. 13, No. 1, 146–165, Jan. 2004.

Session 2A3
Microwave/Terahertz Photonics Technologies and Their Applications

Amplified Stimulated Terahertz Emission from Optically Pumped Graphene

T. Otsuji[1,4], **S. A. Boubanga Tombet**[1,4], **S. Chan**[2], **T. Watanabe**[1], **A. Satou**[1,4], **and V. Ryzhii**[3,4]

[1]Research Institute of Electrical Communication, Tohoku University, Japan
[2]Nano-Japan Program, University of Pennsylvania, USA
[3]Computational Nano-Electronics Laboratory, University of Aizu, Japan
[4]JST-CREST, Japan

Abstract— Graphene, a one-atom-thick planar sheet of carbon atomic honeycomb lattice crystal [1], has attracted attention [2, 3] owing to the massless and gapless energy spectra. The gapless and linear energy spectra of electrons and holes lead to nontrivial features such as negative dynamic conductivity in the terahertz (THz) spectral range [4], which may lead to the development of a new type of THz laser [5]. A series of work searching for application of graphene in terahertz science and technology have been carried out and suggest that graphene can be used in building innovative devices for terahertz optoelectronics [4–6]. In this communication we report on THz stimulated emission from optically pumped graphene.

We measure the carrier relaxation and recombination dynamics in optically pumped exfoliated graphene using THz time-domain spectroscopy based on an optical pump/THz-and-optical-probe technique [6]. The time-resolved field emission properties are measured by an electro-optic sampling method in total-reflection geometry. The pumping photon energy (wavelength) is selected to be around 800 meV (1550 nm). The exfoliated graphene sample was placed on the stage and a 0.12-mm-thick (100)-oriented CdTe crystal was placed on the sample; the CdTe crystal acts as a THz probe pulse emitter as well as an electro-optic sensor. The single femtosecond fiber laser beam is split into two beams: One for optical pumping and generating the THz probe beam in CdTe crystal, and one for optical probing. The pumping laser, which is linearly polarized, was simultaneously focused at normal incidence from the back surface on graphene sample to induce population inversion and the CdTe, to induce optical rectification and emission of THz pulse (the first pulse in Fig. 1). This THz beam reflecting back at CdTe surface stimulates THz emission in grapheme (the seconde pulse in Fig. 1). The probing laser, which is cross-polarized to the pumping beam, was focused from the top surface (See Fig. 1). The time-resolved resulting electric field intensity generated by this coherent terahertz emission was detected as polarization change of the optical probe beam.

Figure 1 shows the temporal response measured in the EOS set up. The red curve is the response measured on the SiO_2/Si substrate (without graphene) took as the reference spectra and the black curve is the response obtained on graphene + substrate. The second pulse obtained on graphene is more intense compared with that obtained on the SiO_2/Si substrate. This indicates the grapheme act as an amplifying medium.

These experiments were done for different pumping beam intensity. Fig. 2 shows the emission spectra from graphene after normalisation by dividing the emission spectra with that of the substrate. The inset in Fig. 2 shows the measured gain as a function of the pumping power. A

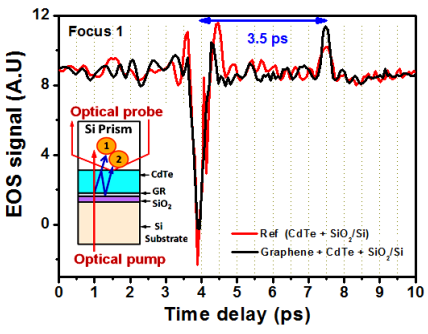

Figure 1: Measured temporal response.

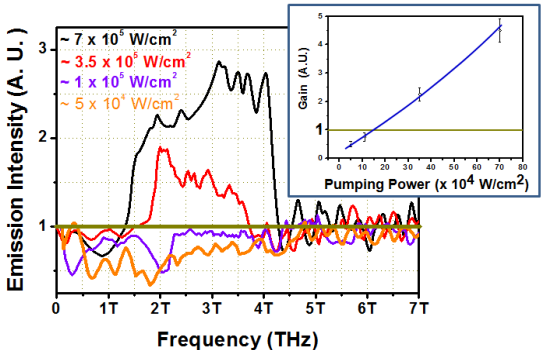

Figure 2: Normalized fourier spectra and gain profile.

threshold like behaviour can be seen testifying the occurrence of the negative conductivity and inversion population in optically pumped graphene.

REFERENCES

1. Novoselov, K. S., A. K. Geim, S. V. Morozov, D. Jiang, Y. Zhang, and S. V. Dubonos, *Science*, Vol. 306, 666, 2004.
2. Zhang, Y., Y. W. Tan, H. L. Stormer, and P. Kim, *Nature*, Vol. 438, 201, London, 2005.
3. Geim, A. K. and K. S. Novoselov, *Nature Mater.*, Vol. 6, 183, 2007.
4. Ryzhii, V., M. Ryzhii, and T. Otsuji, *J. Appl. Phys.*, Vol. 101, 083114, 2007.
5. Ryzhii, V., M. Ryzhii, A. Satou, T. Otsuji, and A. A. Dubinov, *J. Appl. Phys.*, Vol. 106, 084507, 2009.
6. Karasawa, H., T. Komori, T. Watanabe, A. Satou, H. Fukidome, M. Suemitsu, V. Ryzhii, and T. Otsuji, *J. Infrared Milli. Terhz. Waves*, Online, 2010, doi:10.1007/s10762-010-9677-1.

Nano/micro Semiconductor Devices for Optical Communications

R. Katouf[1, 2], **N. Yamamoto**[1], **K. Akahane**[1], **and T. Kawanishi**[1]

[1]National Institute of Information and Communications Technology
4-2-1 Nukui-kitamachi, Koganei, Tokyo 184-8795, Japan
[2]Graduate School of Engineering, Yokohama National University
79-5 Tokiwadai, Hodagaya-Ku, Yokohama 240-8501, Japan

Abstract— Nano/micro scale photonic devices bring the promise to vastly increase the efficiency of future communication networks with the advantages of high density integration and the potential of cost reduction. Advances in fabrication technology over the last decade have made it possible to fabricate semiconductor devices with micron and nano-scale dimensions. Which opens up new possibilities for the realization of ultra-compact and highly efficient photonic devices and components required for advanced optical communication systems.

Among our research in microwave photonics we have carried special interest to nanowire waveguides, micro-ring resonators and quantum dots (QD) based devices.

Nanometer-scale waveguides, known as nano-wire waveguides, provide extremely strong light confinements and thus enhanced optical nonlinearity that offers relevant interesting functionalities. In our recent research an effective and practical fabrication procedure toward III-V compound semiconductor on silica nano-wire waveguide devices have been developed, and operational device in mW class have been demonstrated.

Microring resonator-based photonic devices, the device is typically in the form of a microring closely coupled to a waveguide, offers unique properties such as narrow bandwidth filtering, high-quality factor, and compactness, which can lead to high integration densities of up to 10^5 devices per square centimeter. Moreover, the field build-up inside the ring cavity can be used to enhance nonlinear effects to the fourth power of ring resonator finesse, and thus lowering the operational power of the device.

Quantum dots (QDs) have some unique advantages over their QW counterparts for nonlinear optics applications, mainly due to the nonlinearity enhancement by the quantum confinement in three dimensions, which will allow for another means of highly efficient devices.

In this invited talk we will provide some research results in III-V compound semiconductor based nanowire waveguides, QD based devices and an introduction to semiconductor microring resonators and their applications.

Amplitude Modulation of Terahertz Quantum Cascade Laser by External Photon Injection with a Photon Energy above or below the Bandgap of Host Material

Iwao Hosako and Norihiko Sekine
National Institute of Information and Communications Technology, Japan

Abstract— The quantum cascade laser (QCL) is an unipolar device in which only electrons are traveling through the device. And the life time of the electrons in the terahertz QCLs (THz-QCL) are about few picoseconds. Based on these facts, one can estimate that the relaxation oscillation frequency becomes to be over one hundred giga-hertz. In a word, very high-speed modulation operation can be possible. THzQCLs are highly desired to be used as light sources in short-range ultra high-speed wireless communications. Theoretically, THz-QCLs are predicted to have the modulation bandwidth of more than 100 GHz. However, due to the electrical limit (arising from parasitic electrical components) of the modulation speed, the modulation frequency of several GHz has been experimentally shown One way to overcome the difficulty is the modulation by external lightpulse injection to the THz-QCL device which was made of a GaAs/Al015Ga085As material system using a resonant LO phonon scattering depopulation scheme. In our study, we have investigated modulation characteristics of THz QCLs by injecting external laser light into the front facet of the THz-QCLs. We have investigated the light-current characteristics of THz-QCLs using an external light whose photon energy is above or below the bandgap energy of the host material. We have found that light injection, below the bandgap energy of the host material, induces a large modulation depth, up to 100%.

In this study, we also discussed a modulation mechanisms caused by the external light injection. If the photon energy of the injected-light is bigger than the band gap of GaAs, the injectedphoton generates electrons and holes, then changing electronic distribution of the THz-QCL active layer greatly to stop the laser operation. Moreover, it is possible to modulate the THz-QCL by feeding a light with smaller photon energy than the band gap of GaAs. In this case, only a distribution of electrons in the conduction subband is thought to be greatly modified.

High-speed Electro-optic Modulation Devices for Coherent Systems

T. Kawanish
National Institute of Information and Communications Technology
4-2-1 Nukui-kitamachi, Koganei, Tokyo 184-8795, Japan

Abstract— Modulation technologies play important roles in lightwave transmission systems, where digitized information should be described by some parameters of lightwave, such as amplitude, phase, frequency, etc. As well known, lightwave state can be mathematically expressed by a point on a two-dimensional complex plane which has a real and imaginary axes. If the real and imaginary components of the lightwave can be manipulated independently, we can generate arbitrary lightwave-states. This technique is called vector modulation, which is commonly used in wireless radio communication systems. The significant difference in carrier frequencies causes difficulties in precise lightwave control on the complex plane. The linewidths of light sources are much larger than radio wave sources, so that it is very difficult to fix a lightwave state on the complex plane. Thus, precise and high-speed lightwave control is very important in transmitter side, while high-performance lightwave estimation is needed in receivers, to achieve vector modulation based high-speed transmission systems.

An optical phase modulator can be constructed with an optical waveguide and an electrode on EO material. Various types of modulators for advanced modulation formats can be built with optical phase modulators. Mach-Zehnder interferometer based modulators (MZMs) consisting of two high-speed optical phase modulators can control lightwave amplitude, precisely. Dual-parallel MZMs (DPMZMs), which can control the real and imaginary components independently, are commonly used for high-speed DQPSK signal generation. A quad-parallel MZM (QPMZM) can synthesize 4-level signals optically both in the real and imaginary components, so that a 16-QAM signal can be generated from four electric binary data streams. In this presentation, we describe lightwave modulation techniques for high-speed signal generation based on integrated MZMs using lithium niobate. EO effect on lithium niobate provides very precise optical phase modulation, so that we can achieve almost pure intensity or amplitude modulation using Mach-Zehnder interferomenters (MZIs). Impact of extinction-ratio (ER) of MZMs on advanced modulation formats is also discussed. ER which describes preciseness of the lightwave modulation depends on error in fabrication of the modulators.

Terahertz-wave Imaging Using Photonics-based Noise Source

Tadao Nagatsuma and Takuto Kumashiro
Graduate School of Engineering Science, Osaka University
1-3 Machikaneyama, Toyonaka, Osaka 560-8531, Japan

Abstract— Terahertz-wave imaging has been extensively studied and deployed in numerous areas such as material inspection, non-destructive testing, and security applications [1]. Between continuous-wave (CW) and pulsed-wave imaging systems, the CW imaging can be faster, more compact, cost-effective and simpler to operate. However, mono-chromatic waves cause interference effect and/or speckles due to reflection of waves at any boundary in the materials under inspection and components used such as lenses and mirrors, which leads to significant degradation in image quality and effective spatial resolution [2].

In this paper, we present a new approach to achieving high-quality image with use of photonically-generated incoherent terahertz-wave noise signals. To generate the noise, a high-frequency photodiode is pumped by the amplified spontaneous emission (ASE) noise from Er-doped fiber amplifier. Spatial resolution and degree of speckles in addition to noise-generation efficiency are dependent upon the bandwidth of the optical noise injected into the photodiode. We discuss several methods to optimize the above items, and show the effectiveness of controlled terahertz noise in the imaging applications.

REFERENCES

1. Chan, W. L., et al., *Rep. Prog. Phys.*, Vol. 70, 1325–1379, 2007.
2. Sanches, A. R., et al., *Proc. 4th Intern. Workshop on Ultrasonic and Advanced Methods for Nondestructive Testing and Material Characterization*, 67–77, June 2006.

Recent R&D Trends in Broadband Optical Access System Technologies towards the Second-generation FTTH Era in Japan

Naoto Yoshimoto
NTT Access Network Service Systems Laboratories, Japan

Abstract— This paper first describes a historical overview of technical trends in especially passive optical network (PON) systems which have widely deployed all over the world. Taken the trend into consideration, the author indicates some R&D trends and activities with regards as PON technologies in the next decade named as "the second-generation FTTH era", from the telecom operator's viewpoint.

First, to meet continuous bandwidth requirement for providing attractive new services such as high-definition video distribution services, the way to smoothly migrate from the current 1G-class system through future 10G-class systems must be considered. The author introduces 10G-EPON and its co-existence technology with the current 1G-EPON. And then, to reduce the operational expenditure of these systems, not only number increasing in accommodated user within one system, but also widespread coverage area are effective solutions. As a typical example for these solutions, various expanded PON systems by using large splitting-ratio techniques as well as reach-extension techniques have been investigated. Next, from a social requirement to reduce carbon dioxide, the power consumption of network system equipments is mandatory, especially optical network unit (ONU) because its power consumption accounts for approximately half of that of total network equipments. Various methods of ONU power-saving control techniques have therefore been discussed. Finally, such advanced PON system in future should be positively utilized for other network services such as broadband ubiquitous and cloud services. The author briefly introduces an example of wired-wireless conversion network system by using advanced PON technologies as well as the distributed antenna network technologies.

Ultra High-speed Optical OFDM for Future BroadBand Applications

Ting Wang
NEC Labs America, Inc., 4 Independence Way, Princeton, NJ 08540, USA

Abstract— The ever-increasing bandwidth demand in access systems is catalyzing research and development activity in future ultra high-speed 100 Gb/s broadband networks. In this article, we discuss the principles, key advantages and most recent demonstrations of record 100 Gb/s Orthogonal Frequency Division Multiplexing (OFDM)-based access as a future broadband network architecture. Moreover, we provide an analysis of primary cost factors in a practical digital signal processing (DSP)-based OFDM optical implementation, and survey the most recent achievements in this domain. Due to the combination of highly-attractive advanced features and favorable related trends in optical long-haul 100G/400G and Terabit fiber transmission, OFDMA Passive Optical Network can be regarded as a very promising solution for future broadband access.

A New Configuration of Broadband Wireless Access in Heterogeneous Ubiquitous Antenna and Its Experimental Investigation

T. Higashino[1], **K. Miyamoto**[1], **K. Tsukamoto**[1], **S. Komaki**[1], **T. Tashiro**[2], **K. Hara**[2], **J. Kani**[2], **N. Yoshimoto**[2], **and K. Iwatsuki**[3]

[1]Graduate School of Engineering, Osaka University, Japan
[2]NTT Access Network Service Systems Laboratories, Japan
[3]NTT Service Integration Laboratories, Japan

Abstract— In the next generation wireless access network, various kind of high-throughput internet services are provided at any time and any place. It is requested that throughput is equivalent of the optical fiber internet access service up to Gigabit per second.In addition to the radio regulation (RR) strictly limits the transmitting power and bandwidth of RF signal. The higher radio frequencies will be assigned to new wireless services because of the lack of bandwidth at present.

The higher radio frequency band such as microwave-band, millimeter wave band, and terahertz band is promising resource of the high-throughput wireless local/personal area network. Then, not only a lot of radio base stations, but also broadband entrance network to backbone IP network are required.

This paper proposes a new architecture to multiplex/de-multiplex of plural base stations in order to fully utilize optical wavelength resources. Radio on fiber technology is adopted in order to realize different kind of air interface.

In the MIMO technology, multiple data bit-streams are transferred between transceivers with sharing radio bandwidth. To communicate MIMO system on the optical entrance network, multiplexing schemes for multiple data bit-streams sharing single wavelength resource is required. In this paper, a new multiplexing method of MIMO antenna element based on the bandpass sampling theory is proposed. The enhancement in the channel capacity and required number of radio base stations at various kind of cell-topologies are shown by the numerical analysis. A first experiment of WDM/TDM RoF MIMO network is conducted, and their evaluations are presented as a fundamental experiment.

Radio Agents Technologies for Wireless-as-a-service Network

Katsutoshi Tsukamoto, **Takeshi Higashino**, **and Shozo Komaki**
Division of Electrical, Electronic and Information Engineering, Graduate School of Engineering
Osaka University, Japan

Abstract— Current and next generation wireless access such as 3.9G, 4G, and WiMAX, will provide full internet services with IP networks as a core network. In addition, the flexible and effective use of radio frequency spectrum will accelerate the convergence of fixed optical broadband access and heterogeneous wireless access via femtocell architecture. Mobile users will be able to utilize a large variety of application services from cloud network, and also one of various types of wireless service should be provided from wireless cloud according to users' preference or their location. The latter is able to be realized by use of Wireless over IP technology, and its concept is called "Wireless as a Service (WIaaS)".

Radio Agents technologies in the WIaaS networks have been proposed to achieve a good balance between users demands in charge, QoE, or so on, operators' demands in penetrations, investments, or so on, and regulation demands for radio regulations and frequency efficiency. Radio agents, that are middleware implemented at several locations like mobile terminals, AP, and proxy/application servers on the application layer of the network, will tend to realize user centric wireless services.

This paper will classify radio agents in terms of time and objective scale, and describe our proposed user utility function, that is derived from subjective experiments for mobile internet services or AHP method. Radio agents will decide the assignment of frequency or network resources to user on the basis of these utility functions.

Next Generation Free Space Optics System for Ubiquitous Communications

Pham Tien Dat[1], **Chedlia Ben Naila**[1], **Peng Liu**[1], **Kazuhiko Wakamori**[1], **Mitsuji Matsumoto**[1], **and Katsutoshi Tsukamoto**[2]

[1]GITS/GITI, Waseda University, Tokyo, Japan
[2]Graduate School of Engineering, Osaka University, Osaka, Japan

Abstract— Light wave communications with high speed and large bandwidth capacity has been become an attractive means for broadband wireless access and HDTV broadcasting services. Optical communication systems using optical fibers can reach even beyond 1 Terabit/s capacity thanks to dense wavelength division multiplexing (DWDM) technology. However, in practice it is not always possible to use and install fiber cables, especially in the remote and rural areas. Recently, the other kind of optical communications without necessity to use fiber cables i.e., Free Space Optics (FSO) has been realized and considered as an alternative means to compensate and/or replace the traditional optical communications in many applications. The currently deployed FSO systems use 0.8 μm wavelength band and able to provide 1.5 Gbps communications. However, the use of optical devices at 0.8 μm wavelength makes the FSO systems incompatible with current high capacity optical fiber systems. In addition, these systems need to perform optical-electrical (O/E) and electrical-optical (E/O) conversions before emitting/coupling optical signals from/into an optical fiber thus depends on the protocol and data rate of transmission signals. Consequently, it is not being considered as a suitable and practical solution for very high-speed and heterogeneous wireless communications such as those of terrestrial WDM optical networks.

To overcome such technical barriers, devices and components being used in optical fiber communications should be effectively utilized to achieve high-speed, improved capacity FSO communication systems. Longer wavelength like the 1.5 μm band should also be used. Particularly, the Er-doped fiber amplifier (EDFA) which is considered as one of the most important devices to achieve wide bandwidth, high power transmitters and sensitive receivers also operates in 1.5-μm wavelength band. To employ EDFAs in FSO communications, we must efficiently couple a free-space optical beam after transmission over atmosphere into a single-mode fiber (SMF) which has a diameter of approximately 10 μm. By realizing this technology, a protocol and data rate transparent FSO link can be achieved, thus the system can be utilized for heterogeneous wireless transmission without necessity to reconfigure the terminals. However, the signal transmitted over the atmosphere is highly affected by environment especially turbulence due to the random change in the air temperature gradient, resulting in difficulty to focus directly the received signal into the fiber core. The system thus needs specially designed terminals and tracking scheme in order to receive as much as possible the signal and mitigate the effects of atmospheric environment.

From 2004, we have been engaged in various research activities to realize such a FSO system with the aim to develop a universal platform for future ubiquitous communication networks. We developed and successfully demonstrated a next generation FSO system capable of WDM transmission and capacity of each channel up to 10 Gbps. Recently based on this technology, we extended and demonstrated successfully an advanced Radio on FSO (RoFSO) system capable of transferring multiple wireless signals using DWDM FSO channel. The developed systems have many advantages compared to the currently available systems especially in transmission of the heterogeneous radio signals, however, they are affected by larger impacts from environment, especially atmospheric turbulence due to using seamless connection at the terminals. To our best knowledge, there is no current work so far both in theory and experiment describing these characteristics. In this paper, we thus describe these effects and compare to that of a conventional system co-located at the same experiment field and to classical theories which were developed for describing conventional systems. The newly derived characteristics and models will be helpful in theoretical evaluation of the system and its further optimization. In the paper we also review some other research activities with the aim to optimize and develop a FSO system capable of maintaining a carrier-grade performance, resilient to link failure. These activities include optimizing the system on transceiver aperture size, pre-amplifier gain and optical modulation index (OMI) of the radio-optical interfaces and enhancing the performance using some atmospheric turbulence mitigation techniques like time and reception diversity. The results confirm that the system performance can be further significantly improved by using appropriately optimal design parameters and the enhancement techniques.

Session 2A4
Electromagnetic Nondestructive Evaluation (NDE) 1

Application of Volume-integrals to Nondestructive Evaluation: (1) Overview of the Method

Harold A. Sabbagh[1], **R. Kim Murphy**[1], **Elias H. Sabbagh**[1], **John C. Aldrin**[2], **Jeremy Knopp**[3], **and Mark P. Blodgett**[3]

[1]Victor Technologies, LLC, P. O. Box 7706, Bloomington, IN 47407-7706, USA
[2]Computational Tools, Gurnee, IL 60031, USA
[3]Air Force Research Laboratory (AFRL/RXLP), Wright-Patterson AFB, OH 45433-7817, USA

Abstract—

Derivation of the Volume-Integral Equation: This is the first of a series of papers that are designed to demonstrate the applicability of modern computational electromagnetics to the discipline of nondestructive evaluation (NDE). This paper outlines the method by starting with the computation of electromagnetic Green's functions in layered media, and then deriving the volumeintegral equation for the anomalous currents, which are the unknowns in the problem. By an anomalous current, we mean the departure of known currents flowing in a layered medium with no anomalies, such as a crack or flaw, present. Thus, the anomalous currents generate the scattered field due to these anomalies. Because the layered media may contain electrically conducting as well as magnetically permeabile materials, the anomalous currents will, in general, be of electric or magnetic type.

Discretization via the Galerkin Method of Moments: The anomalous currents are expanded in facet (electric) or edge (magnetic) elements, which are generated from higher-order splines that are defined on a uniform grid. The Galerkin variant of the method of moments is obtained by testing the integral equation with the same expansion functions.

Solution of the Discretized Equations: Because the discretization grid is uniform, it follows that the discretized system of linear equations has a matrix that is either Töplitz or Hankel, the former being a three-dimensional convolution, and the latter being a convolution in two dimensions and a correlation in the third. This allows a very speedy computation of iterative methods, such as the conjugate-gradient, by resorting to three-dimensional FFTs for performing vector-matrix products.

Special Algorithms: The volume-integral method allows special algorithms to be easily implemented. Two such algorithms that will be important in later discussions of NDE are the spatial-decomposition algorithm, which is used whenever the anomaly extends over several layers of different materials, and the multiscale algorithm, which is used when there are anomalies of different sizes, such as a crack in the presence of a fastener or corrosion.

Application of Volume-integrals to Nondestructive Evaluation: (2) The Forward Problem

Harold A. Sabbagh[1], **R. Kim Murphy**[1], **Elias H. Sabbagh**[1], **John C. Aldrin**[2], **Jeremy Knopp**[3], **and Mark P. Blodgett**[3]

[1]Victor Technologies, LLC, P. O. Box 7706, Bloomington, IN 47407-7706, USA
[2]Computational Tools, Gurnee, IL 60031, USA
[3]Air Force Research Laboratory (AFRL/RXLP), Wright-Patterson AFB, OH 45433-7817, USA

Abstract—

The Cessna Sandwich: This is the second paper in a series dealing with the application of computational electromagnetics to nondestructive evaluation, using the vehicle of volume-integral equations (VIE), as developed in the preceding paper in this volume. A challenge-problem in the field of nondestructive evaluation is the inspection of fastener sites for fatigue cracks in multilayer structures. Using the volume-integral equation approach, problems comprising multilayer structures, ferromagnetic fastener sites, gaps between materials interfaces, and the presence of fatigue cracks are accurately modeled. Simulated studies are presented with **VIC-3D©**, a proprietary volume-integral code, and comparisons are made with the finite-element method (FEM) highlighting performance advantages of the VIE approach. Further, the role that volume-integral equations play in the context of other well-known computational-electromagnetic algorithms is discussed.

Validation With Benchmark Tests: We continue the discussion of validation of the forward model by acquiring benchmark data for a 'simple' tilted notch in a homogeneous half-space. The issues raised here include the question of estimating grid requirements *a priori*, and handling electrically large problems. The problem of gridding is attacked by using a simple version of the Whittaker-Shannon sampling theorem, but is complicated by the fact that two distinct features contribute to the spatial-frequency response that must be determined in order to apply the theorem. The first feature has to do with the anomalous conductivity distribution throughout the 'bounding box' of the volume-integral algorithm, and the second involves the spatial distribution of the incident electromagnetic field of the probe. Thus, we perform an analysis of the 'conductivity scene' and 'electromagnetic scene', using straightforward spatial Fourier Transforms, obtaining an estimate of the maximum spatial frequency extent produced by the combined scenes. Upon using the sampling theorem, we can estimate the number of cells required to accurately solve the problem. The estimates are validated with benchmark data taken on the tilted notch.

Application of Extrapolation Theory to Large Problems: The problem of the tilted notch, though simple in geometry, requires a large number of cells, because the bounding box is large and the conductivity scene has a broad spatial-frequency extent. Furthermore, the electromagnetic scene will have a broad spatial-frequency content if the bounding box is large relative to the skin-depth parameter, and the convolution of the Fourier Transforms of both scenes will then yield a large gridding requirement. We apply extrapolation theory to get accurate solutions, and these model solutions are validated against the benchmark data.

Fast Imaging of Void Defects in Conductive Half-space

T. Henriksson, **M. Lambert**, **and D. Lesselier**
Département de Recherche en Electromagnétisme, Laboratoire des Signaux et Systèmes UMR8506
CNRS, SUPELEC, Univ Paris Sud, France

Abstract— In line with preliminary studies [1] and in harmony with a set of investigations led on fast, non-iterative MUSIC-type imaging algorithms in electromagnetics, acoustics and elasticity, by the authors' research group and others, e.g., [2], among many references, we are presently considering such an approach in the case of diffusive electromagnetic fields.

That is, let us assume that some thick highly-conductive horizontal plate has been somehow damaged, the resulting defects being a small collection of isolated 3-D bounded voids, hidden inside the plate or opening in air at the top interface of the plate (top, as seen vs. the position of the sources, described next), which might also get close to one another in limit cases, e.g., in crack-like fashion. A time-harmonic, eddy-current probe array, which consists of a small number (say, a few tens at best) of identical electric current loops that are either closely packed or well separated from one another within a given planar surface is placed close to and parallel with the plate, above the zone where the defects are assumed to be found; each current loop (assimilated with an ideal magnetic dipole orientated vertically) is excited one after another, the anomalous vertical magnetic field observed at all loop centers (in effect, it is proportional to the variation of impedance which is traditionally measured) being collected, yielding us a multi-static response matrix in a rather restricted polarization mode (vertical magnetic dipoles and vertical components of the magnetic fields) however.

The method of imaging itself relies on a first-order asymptotic formulation of the anomalous magnetic field as is induced by the defects. The latter is valid when those appear small enough with respect to the skin-depth at the frequency of operation, yet we still expect to get some useful information when sizes are not so small (but always well smaller than the skin-depth, which is a realistic hypothesis in eddy-current non-destructive testing). Then, a singular value decomposition of the multistatic response matrix collected as indicated in the above is carried out. Discrete singular values and vectors emerge in so doing, which can be separated into quantities respectively associated to a signal subspace and a noise subspace; from that distinction, which means also that the level of noise is not such that the singular spectrum is too corrupted, we can compute a MUSIC indicator (in effect, several indicators can be introduced, as it will be shown in the presentation) expected to peak at the location of the defects.

After a brief presentation of the mathematical formulation behind the approach, and some reminder of the validity and limits of the asymptotic field formulation via a comparison with results provided by means of the modeling CIVA platform from CEA, we will exhibit singular value patterns and MUSIC images. Here, a high-level Gaussian distributed noise is added to the data, and a number of arrangements of the source array and locations and distributions of the defects, at various frequencies (usually a low, median and high one, in effect allowing close-to-surface, median and deep imaging), will be considered. This will enable us to highlight pros and cons of the approach, as well as signaling paths of further research, notably in terms of thin perfectly-isolating cracks, for which so far only 2-D models in the frame of scalar scattering and for propagative fields appear to have been dealt with via non-iterative methods similar to the one herein, refer, e.g., to [3].

REFERENCES

1. Henriksson, T., M. Lambert, and D. Lesselier, "Non-iterative MUSIC-type algorithm for eddy-current nondestructive evaluation of metal plates," *Proc. 15th International Workshop on Electromagnetic Non-destructive Evaluation*, 151–152, Szcecin, June 2010.
2. Ammari, H., E. Iakovleva, D. Lesselier, and G. Perrusson, "MUSIC-type electromagnetic imaging of a collection of small three-dimensional inclusions," *SIAM Journal on Scientific Computing*, Vol. 29, 674–709, 2007.
3. Park, W. K and D. Lesselier, "Electromagnetic MUSIC-type imaging of perfectly conducting, arc-like cracks at single frequency," *Journal of Computational Physics*, Vol. 228, 8093–8111, 2009.

Semi-analytical Simulation of Eddy Current Testing Signals Due to Narrow Cracks Embedded in a Multilayered Planar Medium

R. Miorelli[1], **C. Reboud**[1], **D. Lesselier**[2], **and T. Theodoulidis**[3]

[1]CEA LIST, France
[2]Laboratoire des Signaux et Systèmes UMR8506, Département de Recherche en Electromagnétisme
CNRS, SUPELEC, Univ Paris-Sud, France
[3]Department of Mechanical Engineering, University of Western Macedonia, Greece

Abstract— Fast and accurate simulation of eddy current testing (ECT) of thin cracks in conductive pieces, e.g., [1] for an earlier investigation, using standard numerical or semi-analytical volumetric models is still a matter of concern nowadays, due to the small — compared to the skin depth — dimension of the cracks in their opening direction.

The formalism of the boundary elements method (BEM) has been proposed in the literature to treat the case of an ideal crack. A recent improvement on this method carries out the evaluation of the dyadic Green function analytically in the spatial domain by using the well-known Sommerfeld identity combined with the Generalized Pencil Of Function method (GPOF). This approach has shown to considerably improve the performance in terms of computation time since the fill-time of the moment matrix involved is drastically reduced, a very good degree of precision being still achieved.

Starting from these results obtained in the case of a plate, refer among other references to [2], a collaborative work by the authors has been started that aims at developing a quite general semi-analytical model dedicated to the simulation of ECT signals that are due to multiple thin cracks embedded in multilayered planar structures. Two developments are presented in this contribution: the medium containing the crack is first generalized to a non-magnetic multilayered structure. The global performance of the model appears very satisfactory in comparison to volumetric models, as only the flawed region needs to be meshed in two dimensions. Synthetic results obtained in so doing are compared to measurements from well-known benchmark cases as well as to numerical results obtained with volumetric models. The modelling of problems involving multiple cracks in a planar layered medium is also introduced. First results, as well as further improvements of the model currently in progress, are discussed.

REFERENCES

1. Bowler, J. R., "Eddy-current interaction with an ideal crack. I. The forward problem," *Journal of Applied Physics*, Vol. 75, 8128–8137, 1994.
2. Theodoulidis, T., "Developments in efficiently modelling eddy current testing of narrow cracks," *NDT-E International*, Vol. 43, 591–598, 2010.

Surface Impedance Boundary Conditions in Eddy Current NDT Models

T. Theodoulidis
University of Western Macedonia, Greece

Abstract— Approximate boundary conditions are frequently used to obtain solutions to various field problems in the presence of given objects by only analyzing the field outside these objects. Applicability of this simplified approach depends on the type of excitation, material properties, and the geometric shape of the objects under consideration [1, 2]. In eddy current nondestructive testing, if we take into account the usual combination of materials and excitation coil dimensions we can deduce that SIBC is well suited for the analysis of specific configurations at excitation frequencies of the order of several kHz. Moreover, when the material is ferromagnetic and hence the skin depth is even smaller the frequency can be lowered even further.

Up to now, SIBC have been used for modeling eddy current testing but the method was purely numerical [3]. In this paper, we introduce SIBC and specifically the Leontovich condition in analytical models of eddy current testing. Combined with a recently devised approach that involves the truncation of the solution domain [4], we can greatly extend the class of problems that are treated analytically.

First, we first evaluate the SIBC applicability in the simple configuration of a coil above a planar conductor and then a coil inside a cylindrical domain. We also evaluate the SIBC performance in geometries that include edges. Finally, we provide an analytical solution and results for the case of a bobbin coil inside a tube with a support plate. This axisymmetric configuration is of extreme interest in the power industry and so far was only treated numerically [3]. Solution of the three dimensional problem of a rotary pancake coil inside the tube with a support plate is also possible as well as the construction of the appropriate Green's function that will take into account the support plate geometry.

REFERENCES

1. Jayasekera, K. A. S. N. and I. R. Ciric, "Evaluation of surface impedance models for axisymmetric eddy-current fields," *IEEE Trans. Magn.*, Vol. 43, No. 5, 1991–2000, 2007.
2. Yuferev, S. V. and N. Ida, *Surface Impedance Boundary Conditions*, CRC Press, 2009.
3. Badics, Z., Y. Matsumoto, K. Aoki, and F. Nakayasu, "Effective probe response calculation using impedance boundary condition in eddy current NDE problems with massive conducting regions present," *IEEE Trans. Magn.*, Vol. 32, No. 3, 737–740, 1996.
4. Theodoulidis, T. P. and E. E. Kriezis, *Eddy Current Canonical Problems (with Applications in Nondestructive Evaluation)*, Tech Science Press, 2006.

Numerical Modeling of Crack in Ferromagnetic Material by Eddy Current Testing

A. Tamburrino[1, 2] **and S. Ventre**[1]

[1]EURATOM/ENEA/CREATE, DAEIMI, Università di Cassino, Cassino 03043, Italy
[2]Department of Electrical & Computer Engineering, Michigan State University
East Lansing, Michigan 48824, USA

Abstract— Ferrous materials such as steel are commonly employed in the manufacturing industry, in mechanical industry, in oil and gas pipelines and in many other fields. However, the detection of cracks in such materials by means of time-harmonic eddy current testing (ECT) poses severe challenges because of the strong skin-effect that shields the internal volumes. Even the presence of small ferrous subcomponents, such as steel fasteners applied to nonmagnetic conducting structure, may mask the signals arising from defects emanating near the fastener site in the nonmagnetic region. Therefore, particular care must be paid in developing experimental system as well as processing/inversion algorithms.

The present contribution is about the numerical modeling of such critical cases where magnetic materials play a relevant role. Nowadays, the numerical modeling of eddy current testing in the presence of magnetic conductive materials is not yet mature as for non magnetic materials. For penetrable cases (skin-depth non negligible with respect to the thickness of the sample) we mention [1, 2] where finite element models based on differential formulations are presented [3], where a surface integral equation is proposed (Indirect Boundary Integral Equation Method) and [4] where a finite element method based on sources (the eddy current and the magnetization vector) is proposed. For non-penetrable case (skin-depth negligible with respect to the thickness of the sample and all relevant sizes) we mention [4] that cast the forward problem in term of the Laplace equation on the crack surface and [5] where, in the same approximation, the problem is cast in term of a boundary integral equation for the scalar magnetic potential produced by the sources induced on the ferromagnetic body. Finally, we mention [7] where benchmark problems are described in detail.

In this contribution we propose a finite element method based on an integral formulation in term of the induced eddy current $\mathbf{J}$ and magnetization $\mathbf{M}$. With respect to past work we relaxed the assumption that the magnetic material is nonconductive and we consider crack that may occur also in the magnetic material (in [4] we considered a probe with a magnetic but nonconductive ferrite core). As in [8] we consider volumetric defects and we develop an ad-hoc fast numerical method for efficiently computing the signals they produce.

REFERENCES

1. Huang, H., T. Takagi, and T. Uchimoto, "Fast numerical calculation for crack modeling in eddy current testing of ferromagnetics materials," *J. of Applied Physics*, Vol. 94, No. 9, 5866–5872, 2003.
2. Tanaka, M., K. Ikeda, and H. Tsuboi, "Fast simulation method for eddy current testing," *IEEE Trans. on Magnetics*, Vol. 36, No. 4, 1728–1731, 2000.
3. Lee, H.-B. and D.-H. Kim, "Impedance calculation for a plate with crack in eddy current NDT using indirect BIEM," *IEEE Trans. on Magnetics*, Vol. 36, No. 5, 3131–3133, 2000.
4. Rubinacci, G., A. Tamburrino, and S. Ventre, "An efficient numerical model for a magnetic core eddy current probe," *IEEE Trans. on Magnetics*, Vol. 44, No. 6, 1306–1309, June 2008.
5. Harfield, N. and J. R. Bowler, "Theory of eddy-current interaction with surface crack in ferromagnetic steels," *Electromagnetic Nondestructive Evaluation*, 59–66, T. Takagi, et al. (Eds.), IOS Press, 1997.
6. Grimberg, R., H. Mansir, J. L. Muller, and A. Nicolas, "A surface impedance boundary condition for 3-D non destructive testing modeling," *IEEE Trans. on Magnetics*, Vol. 22, No. 5, 1272–1274, 1986.
7. Takagi, T., et al., "Benchmark model of eddy current testing for steam generator tube: Experiment and numerical analysis," *Int. Journal of Applied Electromagnetics in Materials*, Vol. 5, No. 2, 149–162, 1993.
8. Morozov, M., G. Rubinacci, A. Tamburrino, and S. Ventre, "Numerical models with experimental validation of volumetric insulating cracks in eddy current testing," *IEEE Trans. on Magnetics*, Vol. 42, No. 5, 1568–1576, 2006.

Detection of Subsurface Defects in Multilayer Structures with Steel Fasteners

G. Yang[1], **Z. Zeng**[2], **Y. Deng**[3], **X. Liu**[3], **L. Udpa**[1], **and S. S. Udpa**[1]

[1]Department of Electrical & Computer Engineering, Michigan State University
East Lansing, Michigan 48824, USA
[2]Department of Aeronautics, Xiamen University, Xiamen, Fujian 361005, China
[3]Electrical Engineering and Radiology, University of Colorado Denver, Denver, CO 80217-3364, USA

Abstract— The inspection of deep embedded cracks under fastener heads (CUF) in multi-layer structures has contributed to the development of several variations of eddy current based techniques [1]. Although, the main difficulty is due to skin depth or penetration depth of the fields, eddy current testing methods combined with magnetoresistive (MR) sensors have improved their effectiveness in detecting 2nd and 3rd layer defects around fastener heads. An eddy currentgiant magnetoresistive (EC-GMR) sensor system has been developed and shown to be reliable in detection of subsurface cracks at Aluminum fastener sites in a multilayer structure [2]. With linear multiline excitation currents, and GMR sensor mounted on the line of symmetry the normal magnetic field associated with the induced currents can be measured In the presence of fasteners and/or cracks, the normal magnetic field (B_z) caused by induced currents is picked up by the GMR sensor and the asymmetry of the normal component signal is analyzed for crack inspection [2, 3]. However, in the presence of steel fasteners the conventional GMR signal (normal field component) due to steel fastener is dominant and completely masks the presence of defect signal.

This paper presents the feasibility study of detecting cracks under steel fasteners using the tangential components of the induced fields B_x and B_y components of induced magnetic field. Simulation results in Figure 1 show that B_x and B_y components carrying significant information regarding presence of 2nd layer cracks at steel fastener sites of three layers sample. Experimental validation of the concept will be presented along with signal analysis methods combining information in all 3 components B_z, B_x and B_y for automated defect detection.

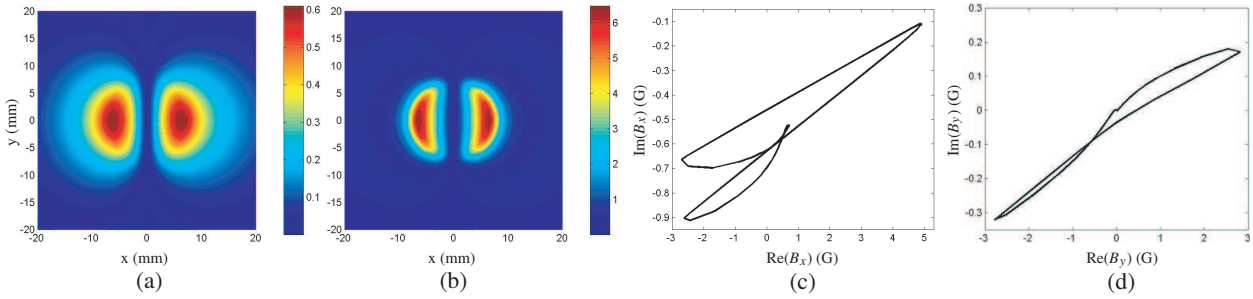

Figure 1: Image of $|B_z|$ and complex trajectory with 8 mm notch. (a) B_z — Aluminum fastener. (b) B_z — Steel fastener. (c) B_x — Steel fastener. (d) B_y — Steel fastener.

REFERENCES

1. Knopp, J. S., J. C. Aldrin, and K. V. Jata, "Computational methods in eddy current crack. Detection at fastener sites in multilayer structures," *Nondestructive Testing and Evaluation*, Vol. 24, No. 1–2, 103–120, Mar. 2009.
2. Nair, N. V., V. R. Melapudi, H. R. Jimenez, X. Liu, Y. Deng, Z. Zeng, L. Udpa, T. J. Moran, and S. S. Satish, "A GMR-based eddy current system for NDE of aircraft structures," *IEEE Trans. Magn.*, Vol. 42, No. 10, 3312–3314, Oct. 2006.
3. Zeng, Z., X. Liu, Y. Deng, L. Udpa, L. Xuan, W. C. L. Shih, and G. L. Fitzpatrick, "A parametric study of magneto-optic imaging using finite-element analysis applied to aircraft rivet site inspection," *IEEE Trans. Magn.*, Vol. 42, No. 11, 3737–3744, Nov. 2006.

Checking of Combustion Chamber of Rocket Using ECT with AMR Sensor

D. F. He[1], **M. Shiwa**[1], **J. Takatsubo**[2], **and S. Moriya**[3]

[1]National Institute for Materials Science, 1-2-1 Sengen, Tsukuba 305-0047, Japan
[2]Advanced Industrial Science and Technology, 1-2-1 Namiki, Tsukuba 305-8564, Japan
[3]Japan Aerospace Exploration Agency, 2-1-1 Sengen, Tsukuba 305-8505, Japan

Abstract— Eddy current testing (ECT) system with high sensitive AMR sensor was developed. To reduce the influence of experimental noise and the influence of lift off variance, a differential AMR sensor was used in this system, which was composed of two AMR sensors in parallel and their outputs were subtracted. The sensing direction of the AMR sensor was along Z direction and the distance between two sensors was about 3 mm. The AMR sensor was mounted with an X-Y stage for the scanning. In our experiments, a specimen of cooper plate with grooves and slits was used to simulate the cooling grooves of the combustion chamber of liquid rocket and the defect in it. Three defects, with the width of 0.2 mm, the length of 4 mm and the depth of 0.2 mm, 0.5 mm and 0.8 mm respectively, were made in the bottom of the grooves. With a Φ 4.5 mm and 30 turn circular excitation coil to produce the excitation field, the frequency of about 2 kHz, and the current amplitude of about 50 mA, ECT experiments were done and the defects could be successfully detected.

Observation of Defects in Polymer and Composite Materials Using Terahertz Waves

K. Fukunaga[1], **M. Mizuno**[1], **I. Hosako**[1], **and M. Suzuki**[2]

[1]National Institute of Information and Communications Technology, Tokyo 184-8795, Japan
[2]Takenaka Corporation, Chiba 270-1395, Japan

Abstract— Terahertz (THz) imaging technology has been progressed in these ten years, and number of practical applications have been realised, especially in security systems. THz waves can penetrate opaque materials and preparation layers, and THz spectroscopy shows fingerprint-like spectra that are similar to infrared bands. The time domain reflection imaging uses THz pulses that act as a probe and propagate through an artwork to obtain its internal structure without requiring the sampling of the specimen. Such information cannot be obtained by other well-established methods such as X-ray observation.

Most polymer insulating materials used in high voltage apparatus have high transmission characteristics in THz region. Thus internal defects and ageing phenomena are expected to be observed non-destructively. We observed a semi-transparent plastic sample with three types of artificial defects; air (separation), metal (contamination), and water (invasion). The defects were clearly distinguished by THz imaging as shown in Fig. 1. When there is a void, in particular, reflection signals come from both top and bottom sides of the void, resulting in two layers in a cross-section image. In addition, contamination of ceramics in plastics, vice versa can be detected because the refractive index highly depends on materials. These results suggest that THz imaging can be a new nondestructive tool to detect defects in insulation systems.

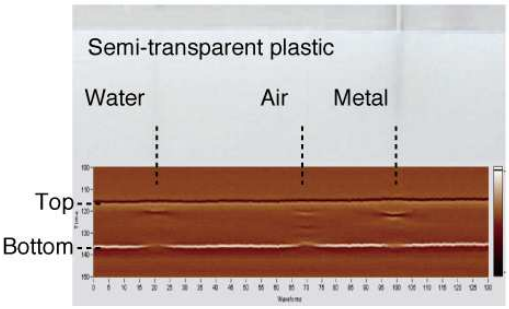

Figure 1: THz imaging of three defects in a plastic sheet.

Magnetic Flux Leakage NDE Using Statistical Copulas

Ameet V. Joshi
608 Strohm Road, Traverse City, MI-49696, USA

Abstract— Nondestructive evaluation (NDE) often involves solution of ill-posed inverse problems. In the context of magnetic flux leakage (MFL) inspection of the ferromagnetic materials, the associated inverse problem is to estimate the geometry of defects in the material using the recorded MFL signal. Recorded MFL signal is segmented to identify the regions of interest (ROI's). Useful features are extracted from the ROI and are used to estimate the defect geometry in the form of length, width and depth. As the relationship between the extracted features and defect geometry parameters is complex and nonlinear, simple curve fit type of methods cannot be used. Neural networks have been used widely for this purpose [1]. However, careful regularization is required to be applied while developing the neural networks to avoid over-fitting and loss of generalization. Neural networks need large amount of training data in order to produce good results. In many practical situations, training data is limited and neural networks fail to produce generic mapping that will produce reasonable results when we encounter test data that is substantially different than the training data.

In this paper, we propose a novel approach towards solution of this problem using the statistics of copulas. Copulas were introduced fairly recently [2] and have been successfully used in the financial applications [3]. Copulas present certain distinct advantages over neural networks with respect to regularization and generalization because the marginal distributions of the input parameters are intrinsically bounded from both sides and can be made continuous and differentiable throughout the limits of operations. These properties make the solution robust and provide a built-in regularization framework. The algorithm is proposed and described with reference to MFL NDE; however, it can be easily adapted for any other similar application involving inverse problem or nonlinear regression.

The problem of predicting the geometrical parameters of the defect from the MFL ROI can be recast in the context of copulas as follows:

(1) Estimate the marginal distributions of the features extracted from the MFL ROI.
(2) Estimate the marginal distributions of the corresponding geometrical parameters from training data.
(3) Develop a copula using all the marginal distributions.

Once such copula is developed, it can be used to predict the marginal distributions of the geometrical parameters for test data. Further using Bayesian analysis the actual values of the parameters can be estimated. The details of the algorithm will be described in the final full paper.

REFERENCES

1. Joshi, A. V., "Wavelet transform and neural network based 3D defect characterization using magnetic flux leakage," *International Journal of Applied Electromagnetics and Mechanics*, 2008.
2. Nelson, R. B., *An Introduction to Copulas*, 2nd Edition, Springer, 2006.
3. Bouyé, E., V. Durrleman, A. Nikeghbali, G. Riboulet, and T. Roncalli, "Copulas for Finance — A reading guide and some applications," March 7, 2000, available at SSRN: http://ssrn.com/abstract=1032533.

Detecting Material Change in Rectangular Cavities Using Neural Networks and Signal Processing Techniques

Matthew Pillar and Omar M. Ramahi
Electrical and Computer Engineering Department, University of Waterloo
Waterloo, Ontario, N2L 3G1, Canada

Abstract— We present a method to detect material change in a rectangular cavity using Neural Networks and various signal processing techniques. Our method is based on the theoretical knowledge that a change in the resonant frequencies of the cavity is directly proportional to the dielectric constant of the inserted material. This premise allows for the possibility of detection of material change using the resonant frequencies. The physical dimensions and position of the inserted material will also affect resonance, but due to the fact that the dielectric constant of most materials changes with frequency, a change in the inserted material will have a different effect compared to a change in the dimensions of the material. Therefore it should be possible to determine the position of the object in the cavity as well. However, our focus in this work is to detect material change only. A rectangular cavity test fixture was constructed and excited with a monopole antenna with the reflection coefficient measured over various frequencies. Different materials were inserted into the cavity including metal, water, wood and air. Signal processing techniques including Wavelet transforms, Sigma filters and M-Smoothing are then applied to the experimentally obtained reflection coefficient to determine the resonant frequencies. The first six resonant frequencies are then used as inputs to a Neural Network for training purposes. Various types of Neural Networks are examined by varying the number of internal nodes, and by using different activation functions. Data sets are individually excluded for the purposes of testing the Neural Network accuracy. Under ideal conditions, the neural network correctly identifies the contents of the rectangular cavity with an accuracy of over 90%.

Session 2A5
Emerging Strategies and Innovative Algorithms for the Solution of Inverse Scattering Problems 1

Target Property Assessment without Inversion — Measurement Data Observations

Paul M. Meaney[1], **Amir Golnabi**[1], **Neil Epstein**[1], **Tomasz Grzegorczyk**[2], **Shireen D. Geimer**[1], **and Keith D. Paulsen**[1]

[1]Thayer School of Engineering, Dartmouth College, Hanover, NH, USA
[2]Delpsi LLC, Newton, MA, USA

Abstract— As microwave tomographic imaging has generated increased interest worldwide, it is noteworthy that the preponderance of effort has been exerted in developing and applying new numerical algorithms. However, only minimal attention has been paid to visualizing and studying trends of the actual data. And even within the realm of studying the data, there are two principle styles employed — observing the phase and log amplitude, or the real and imaginary field components. In this paper we investigate the measurement field patterns for our tomographic imaging system (focusing primarily on the phase and log amplitude) for a controlled series of phantoms to understand the baseline behavior and then describe examples where we have explicitly utilized only the data as a means of characterizing a target and in a clinical study develop strategies for choosing the optimal matching liquid.

For our system, we have long observed that when the average composite permittivity of a target is lower than that of the surrounding bath, the phase projections (differences between the case where an object is present and not present) are well behaved and increase in the depth of the projection as a function of target size and contrast. However, for the situation where the properties are higher, while there are recognized patterns with respect to projection characteristics, the behavior is less obviously exploited. The overall behavior is noticeable for a lossy bath configuration and slightly less so for a low loss setting. While this characteristic has proven to be beneficial for the tomography reconstruction problem, we have also applied this data characteristic in other settings. For instance, we have been able to use this for a simple and fast screening technique for contraband liquids at airports simply by looking at these measurements [1]. In addition, the data could also be characterized as a function of frequency because the data processing time was so much less than that for actual tomographic images. In a more prominent example, we used this approach to optimize the best dielectric bath properties for our breast imaging system [2]. While there were certainly variations in the overall projections with respect to breast size and radiographic density, the overall patterns were quite obvious. From a clinical perspective, it was important to be able to select the optimal liquid based on direct measurements without the indirect, possibly confusion posed by the reconstruction process. In addition, it was also highly beneficial to choose a liquid based on our actual clinical measurement data versus extrapolating ex vivo tissue property measurements which could have involved their own set of confounding issues.

In summary, examining the actual measurement data and the general behavior is extremely useful with respect to understanding a tomographic measurement system. This process can potentially guide the imaging system development and even open up avenues for novel interrogation applications without having to implement computationally costly inverse algorithms.

ACKNOWLEDGMENT

This work was sponsored by NIH/NCI grant # PO1-CA080139.

REFERENCES

1. Meaney, P. M., E. M. Godshalk, T. Raynolds, and G. C. Burke, "Microwave detection of flammable materials in an airport screening environment," *Spring IEEE Conference on Technologies for Homeland Security*, Cambridge, MA, 2006.
2. Meaney, P. M., M. W. Fanning, T. Raynolds, C. J. Fox, Q. Fang, C. A. Kogel, S. P. Poplack, and K. D. Paulsen, "Initial clinical experience with microwave breast imaging in women with normal mammography," *Academic Radiology*, Vol. 14, 207–218, 2007.

Estimation of Reinforcing Bars by Using Real GA with Discrete Chromosomes

Toshiyuki Tanaka, **Takahiro Matsuoka**, **Takashi Takenaka**, **and Toshifumi Moriyama**
Nagasaki University, Japan

Abstract— As for concrete structures, it is expected the long durability. It is necessary to make a close investigation of the condition of concrete structures with respect to cracks, cavities, and corrosion of reinforcing bars in order to prevent dangerous accidents such as drop of a mass of concrete. Important factors of the strength investigation of the concrete structure are position and size of the reinforcing bars. The existence of reinforcing bars in the concrete structure can be confirmed by conventional concrete radars easily. However, the exact position and the radius of the reinforcing bar in concrete structure cannot be presumed with conventional concrete radars. Then we use Real-corded GA (RGA) to estimate the exact position and the radius of the reinforcing bar in concrete structure. In RGA, the chromosome for a reinforcing bar is composed of three genes. These genes are radius, location and depth of the reinforcing bar. The fitness is defined by the norm which is the summation of the absolute value of the difference between the observation field and the estimate field. The estimate field is calculated by using FDTD method. We succeed in estimation of the position and the radius of reinforcing bars by using RGA. But, an enormous computing time is necessary for RGA.

The gene updated by RGA is a real number. On the other hand, it is necessary for the investigation field to be divided at the cell size of the FDTD method. Therefore, even if the gene of the real number is defined, the discrete gene rounded by the size of the sell will actually be used when FDTD is executed. Therefore, the calculated electromagnetic field with the chromosome with only a difference that is smaller than the size of the cell will have the same value. In this paper, we propose RGA with discrete chromosome divided at the sell size of the FDTD method. The crossing-over and the mutation are calculated by the same computational method as gene of the real number, and the obtained gene is discretized. Numerous chromosomes of real number arise during evolution, but many of them are same discrete chromosome. So the discretized chromosome is numbered and the chromosome and the value of the fitness are memorized. Because the fitness to the same discrete chromosome is not calculated, the computing time until the investigation is completed can be greatly shortened.

The effectiveness of the presented method has been confirmed using calculated data.

Efficient Inverse Scattering Solutions Using the Distorted Born Iterative Method and the Multilevel Fast Multipole Algorithm on Regular Grids

Andrew J. Hesford[1] **and Weng C. Chew**[2, 3]

[1]Department of Electrical and Computer Engineering, University of Rochester, USA
[2]Department of Electrical and Electronic Engineering, University of Hong Kong, USA
[3]Department of Electrical and Computer Engineering, University of Illinois, USA

Abstract— The distorted Born iterative method (DBIM) computes iterative solutions to nonlinear inverse scattering problems through successive linear approximations. By decomposing the scattered field into a superposition of scattering by an inhomogeneous background and by a material perturbation, large or high-contrast variations in medium properties can be imaged through iterations that are each subject to the distorted Born approximation. However, the need to repeatedly compute forward solutions still imposes a very heavy computational burden. To ameliorate this problem, the multilevel fast multipole algorithm (MLFMA) has been applied as a forward solver within the DBIM. The MLFMA computes forward solutions in linear time for volumetric scatterers.

Because the distribution of the scattering medium is unknown in an inverse scattering problem, the optimal meshing for an imaging domain is regular. The use of regular grids of scattering elements in inverse problems allows the MLFMA to take advantage of data redundancy and reduce the computational demands of the normally expensive MLFMA setup. Additional benefits are gained by employing Kaczmarz-like iterations here dubbed the round-robin approach. In the round-robin approach, the overall solution is represented as a composition of solutions from individual transmissions. The scattering distribution is updated more frequently than in traditional, full-view distorted Born iterations, resulting in much faster convergence rates. An added benefit to the roundrobin approach is the built-in regularization that results from computing minimum-norm solutions to severely underdetermined linear systems.

Numerical results demonstrate both efficiency of the solution method and illustrate the benefits of the round-robin approach for imaging problems with dimensions in the neighborhood of ten wavelengths.

Potentialities and Effectiveness of the IMSA-FBTS Strategy for the Solution of Inverse Scattering Problems

G. Oliveri[1], **F. Carmanica**[1], **T. Moriyama**[2], **A. Massa**[1], **and T. Takenaka**[2]

[1]ELEDIA Research Group at DISI, University of Trento, via Sommarive, I-38123, Trento, Italy
[2]Department of Electrical and Electronic Engineering, Nagasaki University, 852-8521, Japan

Abstract— Microwave inverse scattering techniques have several applications in biomedical diagnosis, subsurface imaging, non-destructive testing/non-destructive evaluation, and material probing. Despite such important applications, general purpose inversion techniques are still subject of research. This is due to the fact that the arising scattering problem is usually very difficult to solve because of its nonlinearity, the ill-posedness, and the non-uniqueness of the solution [1]. To solve such problems, both frequency-domain and time-domain techniques have been proposed. Although frequency-based techniques have been successfully applied [1], they present some drawbacks in terms of accuracy and collectable information. To properly address these issues, broadband probing fields have been proposed due to the achievable resolution, reliability and accuracy [2]. However, such advantages are achieved at the expenses of a larger computational complexity for the inversion [2]. To limit the computational burden of time-domain inversions and enhance the achievable spatial resolution, this work presents an innovative approach based on the time-domain application [2] of the iterative multiscaling methodology [3, 4]. More in detail, a multi-focusing scheme is employed to iteratively apply the Forward-Backward Time Stepping method [2] according to the identified Regions-of-Interest. Thanks to such an approach, a high resolution is selectively achieved only around the identified scatterers [Fig. 1].

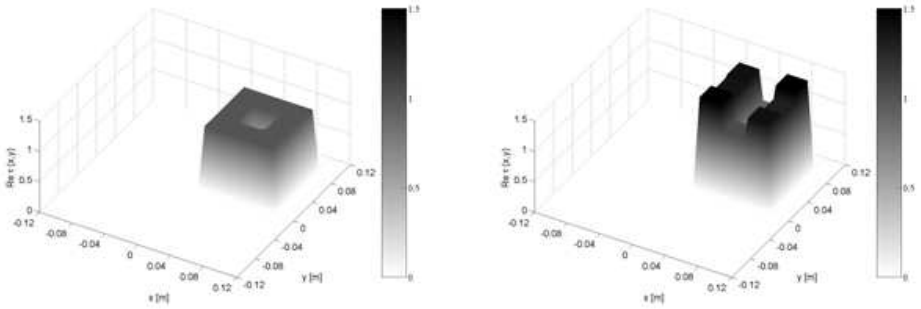

(a) (b)

Figure 1: Reconstruction of a dielectric hollow square cylinder with $\varepsilon_r = 2.0$ illuminated by band-pass Gaussian incident pulse with center frequency $f_0 = 2\,[\mathrm{GHz}]$ and band-width $1.3\,[\mathrm{GHz}]$. (a) True object; (b) IMSA-FBTS.

REFERENCES

1. Donelli, M. and A. Massa, "A computational approach based on a particle swarm optimizer for microwave imaging of two-dimensional dielectric scatterers," *IEEE Trans. Microwave Theory Techn.*, Vol. 53, No. 5, 1761–1776, May 2005.
2. Takenaka, T., H. Jia, and T. Tanaka, "Microwave imaging of electrical property distributions by a forward-backward time-stepping method," *Journal of Electromagnetic Waves and Applications*, Vol. 14, No. 12, 1609–1626, 2000.
3. Caorsi, S., M. Donelli, D. Franceschini, and A. Massa, "A new methodology based on an iterative multiscaling for microwave imaging," *IEEE Trans. Antennas Propagat.*, Vol. 51, No. 4, 1162–1173, Apr. 2003.
4. Caorsi, S., M. Donelli, and A. Massa, "Detection, location and imaging of multiple scatterers by means of the iterative multiscaling method," *IEEE Trans. Microwave Theory Techn.*, Vol. 52, No. 4, 1217–1228, Apr. 2004.

On the Role and Exploitation of the Information in Inverse Scattering Problems

M. Donelli, **G. Oliveri**, **P. Rocca**, **and A. Massa**
ELEDIA Research Group at DISI, University of Trento
Via Sommarive 14, I-38050 Trento, Italy

Abstract— Dealing with inverse scattering problem, the main theoretical difficulties are concerned with the ill-posedness and nonlinearity of the arising inverse scattering problem. These critical issues are correlated and strongly connected to the "information" content of the scattering data. In view of this, the role of the data information as well as its exploitation are key-topics to be carefully analyzed for yielding reliable and efficient inverse solutions.

A "golden rule" for addressing inverse scattering problems is the search for approximate solutions satisfying additional (besides the knowledge of the scattered field collected at the receivers) constraints coming from different (when available) information 'source': (i) the physics of the problem, (ii) the *a-priori* information on some features on the scenario/scatterers at hand, (iii) the knowledge of input-output samples of data and reference solutions, (iv) the acquired-information during the inversion process, (v) the fuzzy-knowledge on some characteristics of the solution/scenario.

As for the nonlinearity arising from the multiple-scattering effects, a nonlinear model of the electromagnetic interactions between scatterers and probing fields is usually considered and suitable nonlinear inversion approaches are used. Dealing with the spatial domain framework, the problem solution is generally recast as the minimization of a properly-defined cost function that presents local minima (i.e., wrong solutions or artifacts). In order to reduce/minimize/overcome the presence of local minima, the addition of more information is still an effective countermeasure. In view of this, the use of multiple-agents evolutionary strategies (EAs) [1] as "information-acquisition" techniques is also justified.

In this talk, starting from an analysis of the key characteristics of an inversion problem, the role of information in inverse scattering is thoroughly discussed and some inversion strategies based on information exploitation and retrieval are presented. Finally, some indications on future trends are envisaged.

REFERENCES

1. Barrière, P.-A., F. Caramanica, M. Benedetti, and A. Massa, "Multi-resolution approaches for inverse scattering problems," *Proc. ACES 2010*, 102–107, Tampere, Finland, Apr. 25–29, 2010.
2. Caorsi, S., A. Massa, and M. Pastorino, "A crack identification microwave procedure besed on a genetic algorithm for nondestructive testing," *IEEE Trans. Antennas Propagat.*, Vol. 49, 1812–1820, Dec. 2001.
3. Caorsi, S., M. Donelli, and A. Massa, "Detection, location and imaging of multiple scatterers by means of the iterative multiscaling method," *IEEE Trans. Microwave Theory Techn.*, Vol. 52, 1217–1228, Apr. 2004.
4. Massa, A., A. Boni, and M. Donelli, "A classification approach based on SVM for electromagnetic sub-surface sensing," *IEEE Trans. Geoscience Remote Sens.*, Vol. 43, 2084–2093, Sept. 2005.
5. Benedetti, M., A. Casagranda, M. Donelli, and A. Massa, "An adaptive multi-scaling imaging technique based on a fuzzy-logic strategy for dealing with the uncertainty of noisy scattering data," *IEEE Trans. Antennas Propagat.*, Vol. 55, 3265–3278, Nov. 2007.
6. Rocca, P., M. Benedetti, M. Donelli, D. Franceschini, and A. Massa, "Evolutionary optimization as applied to inverse problems," *Inverse Problems (Invited Topical Review)*, Vol. 25, 123003, 1–41, Dec. 2009, doi: 10.1088/0266-5611/25/12/123003.

The Subspace-based Optimization Method in Reconstruction of Perfectly Electric Conductors

Xiuzhu Ye and Xudong Chen
National University of Singapore, Singapore 117576, Singapore

Abstract— A new method of solving perfectly electric conductors (PEC) inverse scattering problem by usage of subspace-based optimization method (SOM) is presented. No *a prior* information such as the number of the objects, the approximate locations and centers is required except for the information that the unknown object is PEC.

Due to the boundary condition on the PEC scatterer, the methods for solving the PEC inverse scattering problems are significantly different from those for the dielectric scatterers. In dielectric case, both scatterers and the background medium can be represented by permittivities such that the Lippmann-Schwinger equation can be applied to the whole domain of interest. Therefore the objective function can be constructed into the function of the permittivity which can represent both the background medium and the scatterers. In the case of PEC, the electric-field-integral-equation (EFIE) is only applicable to the boundary of PEC scatterer which is however unknown in inverse problem. There exists no physical parameter to represent both the PEC scatterers and the background medium. Therefore the objective function for the PEC case is much more difficult to build up than the dielectric case.

In this paper the whole domain is discretized into segments of current lines and both the background medium together with scatterers of arbitrary number and arbitrary shapes are expressed as a vector, which performs similarly as the scattering strength vector that is used in SOM [1]. This process effectively enables us to build up the objective function which is the key point in applying SOM.

Numerical result shows that this method performs well in solving PEC inverse scattering problems and also inherits the merits of its counterpart in dielectric case.

REFERENCES

1. Chen, X., "Application of signal-subspace and optimization methods in reconstructing extended scatterers," *J. Opt. Soc. Am. A*, Vol. 26, 1022–1026, 2009.

Microwave NDE of Brain Tissues: Exploiting Geometrical A-priori Information

H. Tortel[1], **A. Litman**[1], **M. Luong**[2], **G. Ferrand**[2], **and A. France**[2]

[1]Institute Fresnel, UMR-CNRS 6133, France
[2]CEA Saclay, France

Abstract— In magnetic field MRI imaging, the next generation apparatuses are actually being designed to provide images with improved spatial resolution. Increasing the resolution directly comes with an increase of the amplitude of the magnetic field and therefore of the amplitude of the electric field. Threshold guidelines of the specific absorption rate (SAR) in human head have been specified by the medical community. The challenge here is to provide the highest magnetic field while keeping the SAR below the thresholds. As SAR is directly linked to the permittivity value distribution in the patient head, one way of tuning the electromagnetic field is to "measure" in advance these permittivity maps and adapt consequently the field distribution within the head.

The idea proposed here is to use the antennas circularly located around the head, which bring the RF signal of the MRI system, as an array of microwave emitters and receivers. By exploiting the multi-static response matrix captured with a low magnetic field MRI system and combining it with advanced inverse scattering techniques, a non-destructive microwave imaging setup for determining the permittivity maps of the brain tissues can be devised.

Unfortunately, the expected spatial resolution of this first-stage setup is low, as the working frequency is fixed at 500 MHz and the brain tissues have high permittivity values. To overcome this drawback and provide permittivity maps with increased spatial resolution, we take advantage of some *a-priori* knowledge on the brain topologies. We have thus introduced these geometrical pieces of information into an up-to-date inversion algorithm. This inversion scheme is coupled to a fast forward FEM solver, yielding the ability of managing complex shaped objects. We will present the gain obtained in terms of resolution, by means of different reconstructions examples. The sensitivity of the inversion algorithm with respect to the various parameters involved (noise, geometrical offset between different zones ...) will also be discussed.

ACKNOWLEDGMENT

This research has been supported by the Commissariat l'Energie Atomique et aux Energies Alternatives (CEA Saclay), in the framework of the Iseult/Inumac project.

Joint Petrophysical Inversion of Electromagnetic, Seismic and Gravity Data

Aria Abubakar, **Guozhong Gao**, **and Tarek M. Habashy**
Schlumberger-Doll Research, Cambridge, USA

Abstract— Inversion methods are widely used in geophysics to derive the Earth geophysical properties from physical measurements in an automated manner. Seismic inversion has been a powerful tool in reconstructing complex geologic structures of the Earth subsurface by inverting for compressional velocity, shear velocity and mass-density distributions from seismic data. Electromagnetic inversion has been a useful tool to derive the resistivity distribution of the Earth subsurface. These two methods have complimentary information, for example: seismic method is very effective in distinguising between gas and liquid while electromagnetic data is very sensitive to the difference between hydrocarbon (oil and gas) and water. Hence, the joint interpretation of these two data sets is expected to bring a tremendous value in the oil and gas industry.

However, because seismic inversion reconstructs seismic velocity and mass density distributions, while electromagnetic inversion inverts for the resistivity distribution, the joint interpretation of these two types of data is not straightforward. One way of performing joint data interpretation is through imposing the structural similarity constraints between resistivity and seismic velocity distributions of the targeted regions [1, 2]. The alternative approach is to use petrophysical links between the resistivity and the seismic velocities. The petrophysical relationship, such as Archie's equations [3] and Waxman and Smits' equations [4], establishes the relation between resistivity, porosity, and water saturation, while the fluid substitution model [5] links the seismic velocity to porosity and saturations. These relationships are derived from core analysis, which are usually only meaningful in the region where core samples were collected. In this presentation, we present a method to jointly invert seismic and electromagnetic measurements to directly obtain porosity and fluid saturation distributions using these petrophysical relationships. We will also discuss advantages and disadvantages of adding an additional measurement such the gravity data. Our inversion method is based on the Gauss-Newton minimization framework described in Habashy and Abubakar [6] and the regularization approach described in Abubakar et al. [7].

We applied this joint inversion for integrating the marine controlled source electromagnetic (CSEM) data with surface seismic data for sub-sea reservoir exploration applications and also in integrating the cross-well electromagnetic and seismic data for reservoir monitoring and evaluation applications. We show that both joint inversion approaches implemented in this work may reduce the ambiguity on the data interpretaion, thus leading to improved reservoir characterization.

REFERENCES

1. Gallardo, L. A. and M. A. Meju, "Characterization of heterogeneous near-surface materials by joint 2D inversion of DC resistivity and seismic data," *Geophysical Research Letters*, Vol. 30, 1658, 2003.
2. Hu, W., A. Abubakar, and T. M. Habashy, "Joint inversion algorithm for electromagnetic and seismic data," *77th Annual International Meeting, SEG Expanded Abstracts*, 1745–1749, 2007.
3. Archie, G. E., "The electrical resistivity log as an aid in determining some reservoir characteristics," *Petroleum Transactions of AIME*, Vol. 146, 54–62, 1942.
4. Waxman, M. H. and M. J. L. Smits, "Electrical conductivities in oil-bearing shaly sands," *Society of Petroleum Engineers Journal*, Vol. 8, 107–122, 1968.
5. Gassmann, F., "Uber die elastizitat poroser medien," *Vierteljahrsschrift der Naturforschenden Gesellschaft*, Vol. 96, 1–23, 1951.
6. Habashy, T. M. and A. Abubakar, "A general framework for constraint minimization for the inversion of electromagnetic measurements," *Progress In Electromagnetic Research*, Vol. 46, 265–312, 2004.
7. Abubakar, A., T. M. Habashy, V. Druskin, D. Alumbaugh, and L. Knizhnerman, "2.5D forward and inversion modeling for interpreting low-frequency electromagnetic measurements," *Geophysics*, Vol. 73, F165–F177, 2008.

The Linear Sampling Method as a Focusing Strategy: A Generalized Formulation Using Multipoles Expansion

I. Catapano[1], **L. Crocco**[1], **and T. Isernia**[2]

[1]CNR, IREA, Institute for Electromagnetic Sensing of the Environment, National Research Council, Italy
[2]DIMET, Mediterranea University of Reggio Calabria, Italy

Abstract— The linear sampling method (LSM) [1] is a qualitative inverse scattering approach able to retrieve the shape of a target by means of a simple processing of the field it scatters. As a matter of fact, the presence of the target is associated to the lowest values achieved by an indicator function, given by the energy of the solution of a linear inverse problem as computed in each point of the domain under test. Such a low implementation and computational complexity, paired with a remarkable robustness against uncertainties has motivated the wide adoption of this method, not only as a tool for rapidly estimating the target's shape, but also, in the framework of the so-called *hybrid* methods, as an effective and reliable pre-processing for a complete characterization (i.e., morphologic and electromagnetic) of the target [2, 3].

The physical interpretation of the LSM recently proposed by the authors of this contribution [4] has shown that the integral equation which casts the linear inverse problem underlying LSM corresponds to the attempt of enforcing, in each point of the investigated domain, an induced current focused in (sampling) point itself. Excluding some cases related to special symmetries of the targets, no current can be induced in sampling points which do not belong to the target, thus motivating why focusing the induced current is indeed a way to estimate the target's support (that is the sampling point which belong to the target).

This paper explores the idea of a generalized version of the LSM in which different right-hand side terms for the LSM integral equation are considered. In particular, since the standard LSM formulation considers the zero-th order term of the multipole expansion series, higher order terms are adopted in the modified formulation. As a matter of fact, the physical interpretation in terms of focusing proposed for standard LSM suggests that the cooperative adoption of the indicators arising from zero-th and higher order terms as right-hand sides of equation may improve the estimation of the target's features, (and in particular of its borders) by taking advantage from the different spatial distribution of the induced currents pertaining to the different multipoles.

These concepts will be illustrated at the conference, together with the formulation and the description of the performances of the generalized LSM.

REFERENCES

1. Cakoni, F. and D. Colton, *Qualitative Methods in Inverse Scattering Theory: An Introduction*, Springer, Berlin Heidelberg, New York, 2006.
2. Catapano, I., L. Crocco, M. D'Urso, and T. Isernia, "On the effect of support estimation and of a new model in 2-D inverse scattering problems," *IEEE Trans. Antennas Propagat.*, Vol. 55, No. 6, 1895–1899, 2007.
3. Catapano, I., L. Crocco, M. D'Urso, and T. Isernia, "3D microwave imaging via preliminary support reconstruction: Testing on the Fresnel 2008 database," *Inv. Problems.*, Vol. 25, No. 4, 024002, 2009.
4. Catapano, I., L. Crocco, and T. Isernia, "On simple methods for shape reconstruction of unknown scatterers," *IEEE Trans. Antennas Propagat.*, Vol. 55, No. 5, 1431–1436, 2007.

A Comparison of Focusing Algorithms for Ground Based SAR System

C. Ozdemir, E. Yiğit, and Ş. Demirci
Department of Electrical-Electronics Engineering, Mersin University, Mersin, Turkey

Abstract— Synthetic Aperture Radar (SAR) is an important remote sensing technique for ground monitoring and many mapping applications. Although SAR system is generally installed on an airplane or a satellite, because of the cheapness and applicability's of the ground based SAR systems have been developed in recent years. There are several techniques and algorithms for focusing the SAR data. For more than a decade, the *range-Doppler algorithm* (RDA) [l] has been the basis of most precision SAR systems. In traditional SAR imaging based on RDA processing, a space-variant interpolation scheme is required to compensate the effect of range cell migration problem. Phase perturbations, aliasing effects, complication of the processing due to extra interpolation burden are the main disadvantages of the RDA process. New algorithms have been developed to avoid this type of interpolation [2, 3] that makes SAR processing computationally ineffective. On the other hand, *chirp scaling algorithm* (CSA) allows the high precision SAR processing without applying such interpolation procedures [4]. Therefore, CSA is inherently phase preserving and its focusing quality is not limited by large swath width and/or high squint angle cases.

In this work, two common and reliable algorithms; namely RDA and CSA are implemented and compared with each other in terms of their focusing and processing abilities. A part of RADARSAT-1 [5] data was used to examine the focusing performances of the algorithms. The resultant focused images are shown in Fig. 1 which fairly presents the effectiveness and differences of the RDA and CSA.

These two algorithms were also applied and tested with a ground based system where the synthetic aperture is formed by sliding the SAR antenna on a straight rail. Some selected targets have been randomly distributed within the SAR imaging area. The resultant SAR images of the site obtained by RDA and CSA are presented and compared.

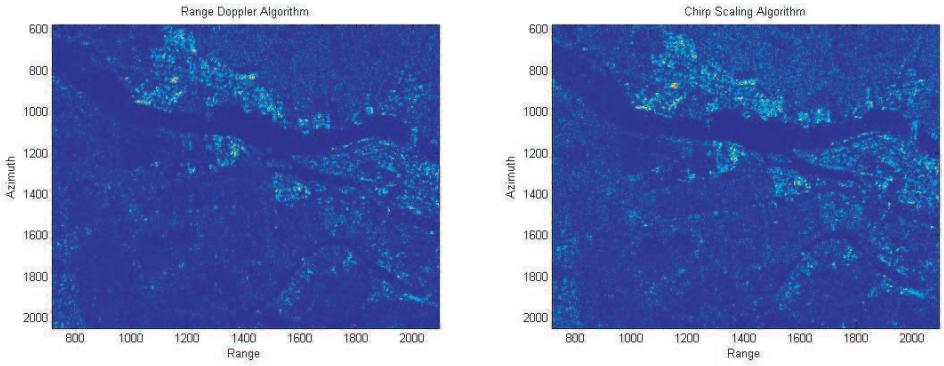

(a) (b)

Figure 1: A Processed and improved scene using (a) RDA, (b) CSA.

REFERENCES

1. Bennett, J. R. and I. G. Cumming, "A digital processor for the production of Seasat synthetic aperture radar imagery," *Proc. SURGE Workshop*, ESA-SP-154, Frascati, 1979.
2. Cumming, I., F. Wong, and K. Raney, "A SAR processing algorithm with no interpolation," *Proc. IGARSS'92*, 376–379, Houston, 1992.
3. Runge, H. and R. Bamler, "A novel high precision SAR focussing algorithm based on chirp scaling," *Proc. IGARSS'92*, 372–375, Houston, 1992.
4. Raney, R. K., H. Runge, R. Bamler, I. Cumming, and F. Wong, "Precision SAR processing without interpolation for range cell mgration correctlon," *IEEE Trans. Geosci. Remote Sensing*, Vol. 32, 786–799, July 1994.
5. RADARSAT International, "RADARSAT data products specifications," May 2000.

Imaging of Wide-angle Near-field Inverse Synthetic Aperture Radar Data Using Back-projection Algorithm

Şevket Demirci[1], **Deniz Üstün**[2], **and Caner Özdemir**[1]

[1]Department of Electrical-Electronics Engineering, Mersin University, Mersin, Turkey
[2]Department of Electronic and Computer Education, Mersin University, Mersin, Turkey

Abstract— Inverse Synthetic Aperture Radar (ISAR) systems generally use narrow angular integration widths that may typically extent only a few degrees while collecting the reflectivity data from the target. This is mainly due to the fact that using narrow look-angle apertures provide major simplifications in data collection and image formation processes. The plane-wave illumination assumption can be made under most narrow-angle situations and therefore direct Fourier transformation procedure can be efficiently employed in forming the final ISAR images. Besides these benefits, noting that the cross-range resolution is inversely proportional to the look-angle width, high resolution ISAR image formation of targets which have large cross-range extents cannot be possible with narrow-angle data. Therefore, collecting the backscattered data over a wide angular aperture will improve the cross-range resolution [1]. Furthermore, wide-angle measurement is also required in achieving improved range resolutions when desirable narrow-band waveforms are used [2]. On the other hand, wide-angle systems significantly face with the problem of unfocused images. Plane-wave illumination assumption is no longer valid in the wide-angle case and hence the imaging algorithm must take wavefront curvature effects into account. One possible solution is the sub-aperture approach which assumes planar wavefronts in smaller apertures [3]. This procedure exhibits resolution degradations because of not using the whole angle aperture at the same time.

In this work, an imaging procedure based on back-projection algorithm [4] with near-field corrections is developed to be able to get a focused image out of the wide-angle data. The proposed algorithm is then validated by using two-dimensional monostatic/bistatic wide-angle, near-field ISAR simulation data. For this goal, a point scatterer model of a prototype aircraft is constructed as shown in Fig. 1(a). In a monostatic configuration, antenna is located at 10 m distance from the target center and near-field data is acquired for an angular span of 90° at 361 points and a frequency span of 6 GHz to 12 GHz for 201 stepped frequencies. The focused image is shown in Fig. 1(b) which clearly demonstrates the effectiveness and the success of the algorithm.

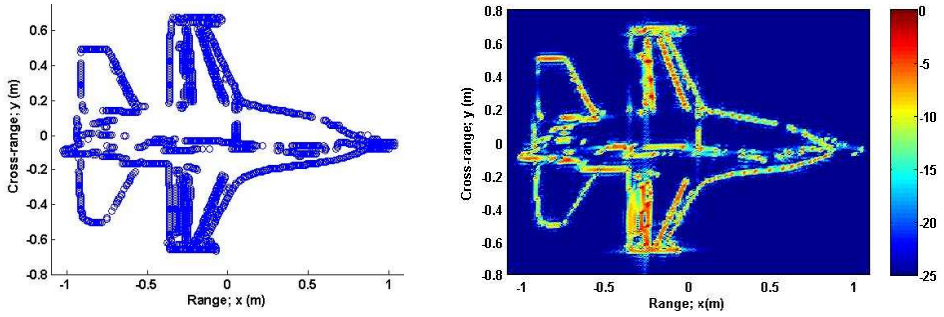

(a) (b)

Figure 1: (a) Point scatterer model of an aircraft. (b) Focused image of the wide-angle ISAR data.

REFERENCES

1. Wehner, D. R., *High Resolution Radar*, Artech House, Norwood, Mass, USA, 1997.
2. Wu, Y. and D. C. Munson, Jr., "Wide-angle ISAR passive imaging using smoothed pseudo wigner-ville distribution," *Proceedings of the IEEE National Radar Conference*, 363–368, Atlanta, GA, USA, May 2001.
3. Ozdemir, C., O. Kırık, and B. Yılmaz, "Sub-aperture method for the wide-bandwidth wide-angle Inverse synthetic aperture radar imaging," *Int. Conf. Electric. and Electron. Engin. — ELECO*, Vol. 2, 288–292, Bursa, Turkey, 2009.
4. Munson, Jr., D. C. and R. L. Visentin, "A signal processing view of strip-mapping synthetic aperture radar," *IEEE Trans. Acoust. Speech Signal Processing*, Vol. 37, No. 12, 131–2147, Dec. 1989.

Session 2A6
Antenna and Array 1

A Quasi-static Theory for Dielectric-coated Thin-wire Antenna Structures

A. I. Mowete[1], **A. Ogunsola**[1, 2], **and L. Sandrolini**[3]

[1]Department of Electrical and Electronics Engineering, Faculty of Engineering
University of Lagos, Lagos, Nigeria
[2]Rail Transit Division, Parsons Group International, London, United Kingdom
[3]Department of Electrical Engineering, University of Bologna
Viale del Risorgimento 2, I-40136 Bologna, Italy

Abstract— Analytical investigations of the problem of dielectric-coated thin-wire antenna structures have invariably focused on the physics of developing appropriate models for the dielectric insulation on the thin-wire conductors that serve as antenna for the structure. These include the frequency domain moment-method-based approaches described by Richmond and Newman [1], Lee and Balmain [2], and More and West [3], in which the dielectric insulation is replaced by equivalent volume polarization currents; and the time-domain analysis due to Bretones et al. [4], and based on the 'equivalent radius' concept developed by Popovic and Nesic [5]. Adekola et al. [6], gave a physical interpretation to the solutions provided by [1] and [2], to suggest that the volume polarization currents derive from an equivalent static charge distribution, which excites an essentially radially-directed quasi-static field, confined to the region associated with the dielectric insulation. In a related development, Mowete and Ogunsola [7], advanced arguments to suggest that the field described in [6], not only has an axially directed component as suggested by Bretones et al. [4], but also that it is this axial component that dominates. The main objective of this paper is to investigate the veracity of the claims in [5, 6] and [7], as they concern the physics of the model for the dielectric insulation in terms of the electric field excited in the dielectric region. And to that end, simulation experiments were carried out, using a commercial Transmission Line Matrix (TLM) Method code, in which the radial and axial component of the electric field within the dielectric region was investigated. The simulation results obtained from the experiments suggest that the field in question is not only of the quasi-static variety, but that it is also characterized by an axial component that meets the boundary condition of vanishingly small values on the surface of the conducting wire, to support the theory proposed in [6] and [7].

REFERENCES

1. Richmond, J. H. and E. H. Newman, "Dielectric coated wire antenna," *Radio Science*, Vol. 11, 13–20, 1976.
2. Lee, J. P. Y. and K. G. Balmain, "Wire antennas coated with magnetically and electrically lossy material," *Radio Science*, Vol. 14, No. 3, 437–445, May–June 1979.
3. Moore, J. and M. A. West, "Simplified analysis of coated wire antennas and scatterers," *Proc. IEE Microw. Antennas Propag.*, Vol. 142, No. 1, 14–18, February 1995.
4. Bretones, A. R., A. Martin, R. Gomez, A. Salinas, and I. Sanchez, "Time domain analysis of dielectric coated wire antennas and scatterers," *IEEE Trans. Antennas Propag.*, Vol. 42, No. 6, 815–819, June 1994.
5. Popovic, B. D. and A. Nesic, "Generalisation of the concept of equivalent radius of thin cylindrical antenna," *IEE Proc.*, Vol. 131, No. 3, 153–158, 1984.
6. Adekola, S. A., A. I. Mowete, and A. Ogunsola, "On the problem of dielectric coated wire antenna," *PIERS Proceedings*, 431–437, Moscow, Russia, August 18–21, 2009.
7. Mowete, A. I. and A. Ogunsola, "Plane wave scattering by a coated thin wire," *PIERS Proceedings*, 743–749, Xi'an, China, March 22–26, 2010.

Novel Symmetrical EH-horn Antennas Based on EBG Technology

I. Khromova, **I. Ederra**, **and R. Gonzalo**
Public University of Navarra, Spain

Abstract— The scientific and technological interest towards electromagnetic band gap (EBG) structures has been growing rapidly since their discovery. The essence of any EBG structure, a periodical dielectric structure with certain geometry and dimension, is that it is a resonance structure. Due to this funda-mental property different interesting well-known effects, such as band gaps, controllable dispersion, defect-based waveguiding, field localization or resonant transmission are observed [1, 2].

In recent years EBGs have been widely exploited for the purpose of shaping and improving the radiation characteristics of antennas of different types. In particular, EBG resonator cavities and defects [1–3] have been used to create antennas with large directivities and high efficiencies. Finally, following the analogy with classical metallic horn antennas, introducing a horn-shaped hollow defect can make the EBG-based system work as a horn antenna [4–6].

However, EBG-based horn antennas in their present form despite offering a wide spectrum of applications still have several fundamental gaps and drawbacks. Up to now only H-horns embedded in one layer of rods in a woodpile structure have been designed. The reason for this is the lack of understanding of electromagnetic processes inside such structures. The other principal drawback of the woodpile horn antennas is the absence of mirror symmetry in the stacking direction of a woodpile structure, which results in non-symmetrical radiation patterns of the antennas.

This paper presents the design of a novel symmetric EH-horn antenna based on EBG structures. The main concept of the design lies in turning the EBG structure at the antenna flare angle and thus forming the EBG "walls" of the horn. The main difficulty in creating an EH-antenna or even an H-antenna embedded in various adjacent layers of a woodpile structure, lies in the fundamental difference between the processes of mode formation in metallic and EBG waveguides and horns. This research is aimed at better understanding of the phenomena, observed in 3D EBG defects. Basing on careful modal analysis, this paper explains the fundamental difference between a gradual transition in metallic and EBG waveguides. It is shown that unlike the analogous situation in metallic horns, forming a horn antenna by cutting out a pyramidal shaped defect results in creating abrupt transition between effective EBG waveguides (the local waveguides in each cross-section of the horn antenna). Using the proposed concept of rotating the woodpile structure and thus shifting the EBG lattice nodes provides the real adiabatic transition between en EBG waveguide and the free space.

This paper presents a novel pyramidal woodpile-based horn antenna possessing a symmetric radiation pattern and competitive parameters. Such antennas can substitute metallic horns in certain circumstances, which is especially valuable for millimeter and THz devices. In this paper the design of a woodpile horn antenna operating at frequencies around 110 GHz is presented.

REFERENCES

1. Meade, R. D., et al., *Phys. Rev. B*, Vol. 44, No. 24, 13772–12774, 1991.
2. Noda, S., A. Chutinan, and M. Imada, *Nature*, Vol. 407, No. 6804, 608–610, 2000.
3. Khromova, I., et al., *J. Appl. Phys.*, Vol. 106, 014901–01498, 2009.
4. Moore, R. L., M. P. Kesler, J. G. Maloney, and B. L. Shirley, US Patent 5,689,275, 1997.
5. Weily, A. R., K. P. Esselle, and B. C. Sanders, *Phys. Rev. E*, Vol. 70, 037602–4, 2004.
6. Khromova, I., I. Ederra, J. Teniente, R. Gonzalo, and K. Esselle, submitted to *IEEE Transactions on Antennas and Propagation 2010*.

Rain and Ka-band Antennas

M. Kharadly
University of British Columbia
1766 West 68th Ave, Vancouver, B. C., V6P 2W1, Canada

Abstract— This paper describes the development and characteristics of a reflector antenna that circumvents the problem of wet-antenna attenuation when operating in a rainy environment.

The propagation experiment of NASA's Advanced Communications Satellite (ACTS) was intended to explore the feasibility of Ka-band satellite communications by measuring rain attenuation along the propagation path. Several receiving sites were selected for this purpose including the University of British Columbia (UBC).

Because of some anomalies in the reported rain attenuation data at one of the sites, it was decided to conduct additional experiments on the ACTS receiving antenna at UBC. Thus, antenna-wetting experiments with simulated rain were conducted on clear days. The observations were quite remarkable and may be summarized in the following points [1].

1. Signal attenuation due to surface wetting could reach values of the order of 10 dB at the Ka-band.
2. Rapid and deep fluctuations in antenna gain could occur depending on the type of precipitation and other meteorological conditions.
3. Wet radome surfaces result in much higher signal attenuation than that caused by wet reflector surfaces.
4. The antenna attenuation during rain at any instant of time is essentially related to the amount of water accumulated on the antenna surfaces. It is, however, largely independent of the instantaneous rain rate.

It became quite clear at that time that for efficient Ka-band satellite communications there was a need to develop new types of antennas which would not suffer from this problem.

Our initial approach was to develop antennas whose radiating surfaces would not get wet at all during rain events. One such antenna, a slot array, was developed and it performed quite satisfactorily [2]. In this antenna the radiation surface faced downward while the radiation from the antenna pointed upwards toward the satellite. There were, however, some stringent requirements concerning the precision needed in its construction.

The fact that most of the wet-antenna attenuation (90% or greater) resulted from the wetting of the feed-horn radome led us in another direction. A new type of reflector antenna (the main subject of this paper) was developed using a spherical reflector with its feed-horn always pointing vertically downwards [3, 4]. In this paper the design, testing and performance of such an antenna are described. The antenna's simplicity makes its production quite inexpensive, and its performance in a rainy environment has shown it to be most effective in alleviating the problem of wet antenna attenuation.

REFERENCES

1. Kharadly, M. M. Z. and R. Ross, "Effect of wet antenna attenuation on propagation data statistics," *IEEE Trans. on Ant. and Prop.*, Vol. 49, 1183–1191, August 2001.
2. Kharadly, M. M. Z. and A. Chan, "New antenna concept for efficient Ka-band terminal operation," *Proc. 4th Ka-Band Utilization Conference*, 223–230, Venice, Italy, November, 1998.
3. Kharadly, M., T. Street, and R. Ross, "A refector antenna for operation in rain at mm wavelengths," *Proc. 11 Ka- and Broadband and Communications Conference*, 73–80, Rome, Italy, September, 2005.
4. Kharadly, M. M., U.S. Patent No: 7733282 B2, June 2010.

Compact and High Gain Array Using Printed Dipole Array with Reflector and Directors

Jean-Marie Floc'h and Jean-Michel Denoual
IETR, URM CNRS 6164, 20 Avenue Buttes des Coësmes, 35043 Rennes, France

Abstract—

Introduction: In this paper, we propose a technique to reduce the back side radiation in antenna array. This technique allows very simple way for feeding network of the array by using a reflector in each element array like it is done with Yagi antenna. This new structure permits to avoid metallic reflector in back side of the array and then it reduces the size of the antenna [1–6] with good performances. In the first part of the conference, we present antenna without and with reflectors. In the second part, we present a four element antenna with a non uniform distribution and a director in each antenna element in order to increase the gain performances and the side lobe level. We use after this array to built 2×4 array and 4×4 array in order to increase the gain and the directivity. We plan also to present another type of arrays with different elementary printed dipole. All arrays are optimized by using HFSS Ansoft software.

Example of Four-element Dipole Array: The Figure 1 presents the photography of the both sides of the 4-element dipole array. Each dipole is now fitted with a reflector and also with one director. A non-uniform distribution current is used on each dipole in order to reduce the side lobe level (below −20 dB) and increase the gain.

The Figure 2 presents the results for the simulated and measured reflection coefficient. We can note a very good agreement between the two reflection coefficients.

The simulated gain is 12.5 dBi in the 0° direction and −6 dBi in the 180° direction (Figure 11), the measured gain is 11.5 dBi in 0° direction and −9 dB in 180° direction at the design frequency 3 GHz. The difference between gain in the 0° and 180 ° direction is around −20 dB, and this, without adding ground plane or metallic reflector behind the whole array.

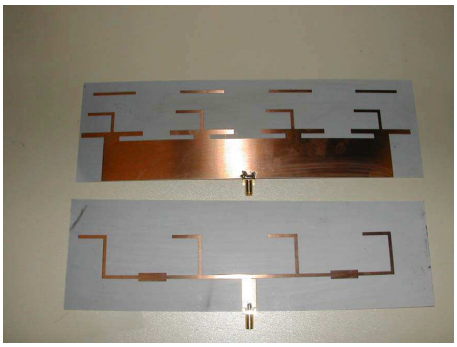

Figure 1: Photo of the two sides of the four-element array.

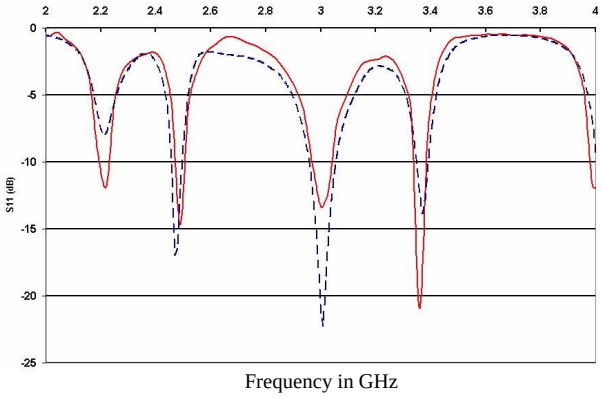

Figure 2: Simulated (----) and measured (—) reflection coefficient of the four-element array with reflectors and directors.

REFERENCES

1. Floc'h, J. M., F. Queudet, and E. Fourn, "Design of printed dipole with reflector," *EUCAP*, Birmingham, UK, 2007.
2. IETR Communications and Internal Reports — 2000–2009.
3. Avila-navarro, E., J. A. Carrasco, and C. Reig, "Desing of yagi-like printed antennas for wlan applications," *Microwave and Optical Technology Letters*, Vol. 49, No. 9, September 2007.
4. Floc'h, J. M. and H. Rmili, "Desing of multiband printed dipole antennas using parasitic elements," *Microwave and Optical Technology Letters*, Vol. 48, No. 8, August 2006.
5. Kaneda, N., W. R. Deal, Y. Qian, R. Waterhouse, and T. Itho, "A broad-band planar quasi-yagi antenna," *IEEE Transaction on Antennas and Propagation*, Vol. 50, No. 8, August 2002.
6. Floc'h, J. M., J. M. Denoual, and K. Sallem, "Design of printed dipole with reflector and multi directors," *LAPC*, Loughborough, UK, November 16–17, 2009.

Developments Low Cost Probe Compensated Cylindrical Near Field Measurement for Antenna Radiation Wave

E. T. Rahardjo, **F. Y. Zulkifli**, **M. D. Firmansah**, **and C. Apriono**
Antenna propagation and Microwave Research Group (AMRG), Department of Electrical Engineering
Universitas Indonesia, Kampus Baru UI Depok, Depok 16424, Indonesia

Abstract— Antenna radiation wave measurement is needed to ensure that the design of an antenna is in accordance with the expected performance. Far field antenna measurement, however, require a large real estate and high cost. In the far field method, when the antenna has a large size, a problem occurs concerning the large distance needed to measure the radiation pattern of the antenna. As for the limited space availability in our laboratory, the measurement of the antenna then mostly can only be done with near field method.

A low cost near field measurement technique for antenna radiation pattern has been developed in our laboratory. Firstly the measurement equipment was design by means of rectangular scanner to pick up the cylindrical near field antenna radiation wave. The Fast Fourier Transform (FFT) method is then utilized to transform near field to far field data. The developed near field measurement technique is then compared with the available simulation of the commercial software to validate the result. Furthermore, a probe compensation technique is used to improve the radiation pattern. Details of the developed measurement technique, simulated and measured results on the antenna radiation pattern are presented.

A Circularly Polarized Microstrip Antenna Array with a Binomial Power Distribution

N. R. Rishani, A. Ramadan, M. Al-Husseini, K. Y. Kabalan, and A. El-Hajj
ECE Department, American University of Beirut, Beirut 1107 2020, Lebanon

Abstract— The design of a four-element circularly polarized microstrip antenna array, which is based on Binomial power distribution, is presented in this paper. For a (1-3-3-1) power distribution, the elements' coefficients are (1-1.73-1.73-1). This is the distribution of a four-element Bessel, or better called a Taylor one-parameter, array with a sidelobe level of −20 dB. The pro- posed printed-type array is based on a 1.6 mm-thick FR4-epoxy substrate with dimensions 200 mm × 120 mm, has a microstrip-line-formed Binomial power distribution-based feeding network using equal/unequal Wilkinson power dividers, and features four identical circularly polarized patch antenna elements. Each array element incorporates two opposite 0.65 mm-wide 90° sectoral slots to achieve circular polarization at 3 GHz. The proposed antenna array is designed and simulated using Ansoft HFSS. The computed peak gain of the antenna, at 3 GHz, is 5.75 dB. A prototype of the antenna is fabricated and measured. A credible analogy between measured and simulated results is attained as shown in Figure 1(a). As illustrated in Figure 1(b), the axial ratio of the proposed antenna is 2.42 dB at 3 GHz. Compared to the Uniform-based array, the Bessel-based one's radiation pattern reveals lower side-lobes and a wider half power beam-width (HPBW), as depicted in Figure 1(c), over the operating frequency band.

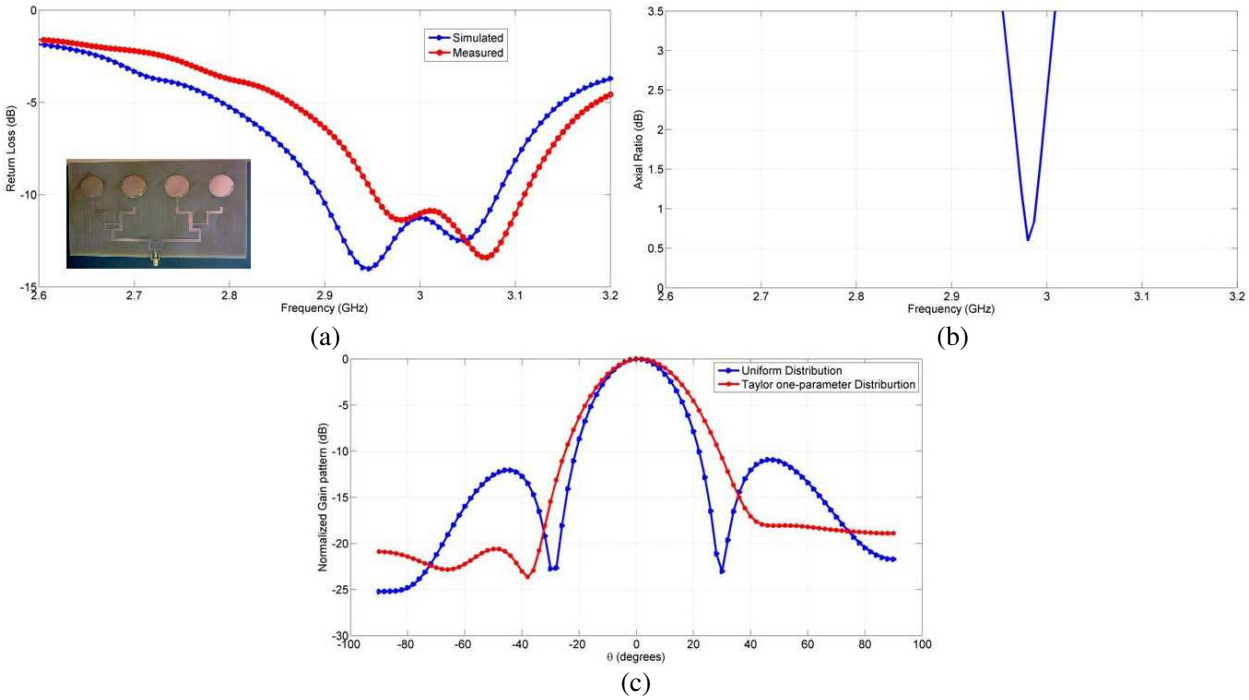

Figure 1: (a) Return loss, (b) axial ratio and (c) normalized gain pattern of the proposed antenna array, compared to a uniform array's pattern.

Performance Characteristics of a Dual-sense Helical-beam Antenna

S. A. Adekola[1, 2], **A. Ike Mowete**[1], **and A. A. Ayorinde**[1]

[1]Department of Electrical and Electronics Engineering, Faculty of Engineering
University of Lagos, Lagos, Nigeria
[2]Department of Electrical and Electronics Engineering, Niger Delta University
Wilberforce Island, Yenegoa, Nigeria

Abstract— Several years ago, Coleman and Wright, [1], experimentally demonstrated the feasibility of exciting a dual-sense circularly polarized field, using a single-element helical antenna. The results obtained and described by [1] suggest that good on-axis axial ratios then become available, and that the off-axis axial ratios may be rated 'reasonable'. It was discovered [1], in particular, that the off-axis axial ratio for the added port of the antenna's feed arrangement was significantly worse on account of an imbalance in the feed as well as currents excited along the axially located outer coaxial conductor.

This paper, using a moment-method analytical approach earlier developed for elliptical cylindrical thin-wire helical antenna [2], investigates the possibility of improving off-axis ratios for the dual-sense helical antenna through an informed location of the added port and choice of amplitude and relative phase of feed point excitation voltage. Computational results obtained suggest that both choice of location and magnitude and relative phase of feed point excitation voltage can lead to significant improvements in both on-axis and off-axis axial ratios for the dual-sense helical antenna. In addition to offering possibilities for compensating for the imbalance in the feed and effects of currents excited in the outer coaxial conductor alluded to in [1], the proposals described in this paper indicate such other antenna parameters as polarization sense of radiated field, of interest to optimum energy transfer can be controlled through the use the dual-feed arrangement of the type proposed in [1].

REFERENCES

1. Coleman, H. P. and B. D. Wright, "An orthogonal mode (dual-sense) helical antenna," *IEEE Transactions on Antennas and Propagation*, Vol. 32, No. 4, 414–415, April 1984.
2. Adekola, A., A. I. Mowete, and A. A. Ayorinde, "Compact theory of the broadband elliptical helical antenna," *European Journal of Scientific Research*, Vol. 31, No. 3, 446–490, 2009.

Analytical Prediction of Feed Efficiency in Offset Gregorian Reflector Antennas with Non Planar Log-periodic Type Feeds

D. I. L. de Villiers
University of Stellenbosch, South Africa

Abstract— Non planar log-periodic antennas are finding increasing application in wide band reflector antenna systems due to their excellent wide band performance in terms of input impedance and pattern stability. However, due to the physical operation and configuration of these antenna types the phase center position is frequency dependent and will cause defocusing and therefore a loss in aperture efficiency when they are used in a wide band reflector antenna system. This loss can be substantial, and will dominate the efficiency of the system in wide band applications.

The offset Gregorian reflector antenna configuration is popular in high performance systems such as radio telescopes due to the high levels of efficiency that can be obtained by eliminating feed or subreflector blockage from the system. Unfortunately, using an offset configuration will not eliminate subreflector edge diffraction effects, which also cause a loss in efficiency, and these should be included to obtain accurate performance predictions.

This paper presents a technique to get an initial estimate of the performance of an offset Gregorian reflector antenna fed by a non planar log-periodic antenna by using closed form expressions and simple one dimensional integration of analytical functions. An analytical function is used to approximate the radiation pattern of the feed antenna, and this approximated pattern is used to calculate the efficiency of the reflector antenna system. The frequency dependent phase center position of the feed antenna as well as subreflector edge diffraction is included in the calculations. The results compare favorably with full wave simulations of the structure, and some simple design guidelines are derived. These design guidelines can now provide an initial value for further optimization of a design to also include effects such as spillover, cross-polarization, side lobe levels, and other secondary effects.

Study of Microstrip Patch Resonator Printed on Anisotropic Substrate Characterized by Permittivity and Permeability Tensors

S. Benkouda and T. Fortaki
Electronics Department, University of Batna, Algeria

Abstract— Some dielectric substances exhibit anisotropy due to their natural crystal structures or as the result of their production processes [1]. Isotropic substances may also exhibit anisotropy at high frequencies. In the design of microwave integrated circuit components and microstrip patch antennas, anisotropic substances have been increasingly popular. Especially the effects of uniaxial type anisotropy have been investigated [1–3] due to availability of this type of substances such as Sapphire, Magnesium fluoride and Epsilam-10. In the previous studies the uniaxially anistropic substrates considered are nonmagnetic. In this paper, we extend the theoretical analysis presented in [2] to investigate microstrip patch resonators printed on anisotropic substrates, which are characterized by both permittivity and permeability tensors. The paper is organized as follows. In Section 2, using a matrix representation of the dielectric anisotropic layer, a new approach to derive the dyadic Green's function of the problem is proposed. Although a single-layer microstrip antenna is considered in this paper, we show that it is quite straightforward to extend the analysis presented to structures involving stratified substrates, which are characterized by both permittivity and permeability tensors. In Section 3, the validity of the solution is tested by comparing the computed results with previously published data. The effects of the permittivity and permeability variations on the operating frequency are also investigated in Section 3. Both variations in the permittivity as well as in the permeability perpendicular to the optical axis of the dielectric and along this axis are considered. Finally, concluding remarks are summarized in Section 4.

REFERENCES

1. Gurel, C. S. and E. Yazgan, "Characteristics of a circular patch microstrip antenna on a uniaxially anisotropic substrate," *IEEE Trans. Antennas Propagat.*, Vol. 52, No. 10, 2532–2537, 2004.
2. Fortaki, T. and A. Benghalia, "Rigorous full-wave analysis of rectangular microstrip patches over ground planes with rectangular apertures in multilayered substrates that contain isotropic and uniaxial anisotropic materials," *Microwave Opt. Technol. Lett.*, Vol. 41, No. 6, 496–500, 2004.
3. Fortaki, T., L. Djouane, F. Chebara, and A. Benghalia, "On the dual-frequency behavior of stacked microstrip patches," *IEEE Antennas Wireless Propagat. Lett.*, Vol. 7, 310–313, 2008.

Design of Flat Gain UWB Tapered Slot Antenna for on-body Concealed Weapons Detections

Ali Atiah and N. Bowring
Electrical Engineering Department, Manchester Metropolitan University, UK

Abstract— The standoff detection of on-body concealed weapons is one of the great challenges. Successful late time response LTR extraction to identify the target signature and its correct interpretation requires specific UWB antenna, which can cover the fundamental complex natural resonance (CNR) frequency of the on-body concealed weapons such as guns and knives. This antenna should be capable to have flat gain across all frequencies in the desired spectrum and must be able to pass very narrow distortion less monocycle time pulse. This criterion is required to enable effective de-convolution of the antenna response from the received scattered signal. Nevertheless, having a less than desirable antenna response, may lead to have unauthentic resonances, which could contribute to mask the LTR of concealed on-body objects.

In this paper, we present a compact flat gain UWB tapered slot antenna with operating frequency bandwidth 0.25 to 3GHz. An optimum antenna achieved by the adjustment of the following parameters: flare angle, cavity radius and throat width to reduce the antenna ringing as much as possible. The ultra wideband antenna designed based on closed form equations, and it is manufactured using FR4 epoxy ($\varepsilon_r = 2.33$, $h = 0.125\,\text{cm}$) as substrate. The taper rate was 0.18 cm and radial stub angle(θ) = 105°. Antenna measurements done in the anechoic chamber room. Figure 1 illustrates the simulated and measured −10 dB return loss. The measured −10 dB return loss bandwidth is from 0.2 to more than 3 GHz, the simulated results closely resemble the measured result confirming the design procedure of the antenna. It is very critical that the gain across the operating bandwidth to be comparatively flat, resulting in an around unity VSWR across the broadband spectrum specifically in the affected frequencies, leading to a very low late time ringing resonances needed for on-body weapon detection. Both the measured and simulated results show that the designed antenna achieves these requirements.

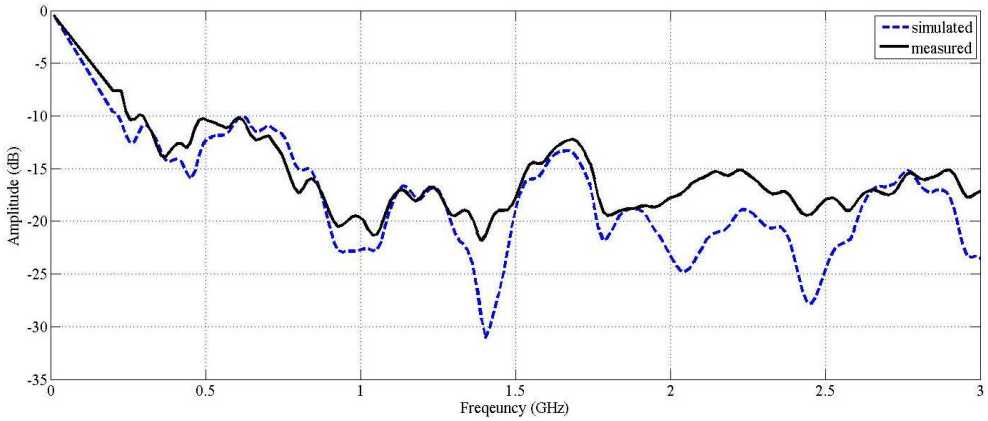

Figure 1: Measured and simulated S_{11} return loss.

Surface Wave Enhancement Using HF Metamaterials

L. Petrillo[1], **F. Jangal**[1], **M. Darces**[2], **J.-L. Montmagnon**[2], **and M. Hélier**[2]

[1]The French Aerospace Lab, ONERA, France
[2]L2E, UPMC Univ. Paris 06, France

Abstract— HF Surface Wave Radar (HFSWR) seems to be the most relevant and lowest cost solution for the surveillance of the Exclusive Economic Zone [1]. The HFSWR is a land based system that can watch over large maritime areas and detect low-altitude aircrafts and surface vessels beyond the electromagnetic horizon [2]. However, one of its major problems lies in the emitting antennas: since HF wavelength extend between 10 m and 100 m (most often in the order of 30 m), antenna dimensions can become a restraint for radar deployment. For this reason, equivalent quarter-dipole antennas are usually employed. This simple solution lacks in directivity and therefore causes energy dispersion towards the sky. As a consequence, ionospheric clutter corrupts radar data. We aim to solve those problem (i.e., energy wasting and clutter corruption) right from the conception. We are of the opinion that the design of a radiator dedicated to surface wave excitation cannot be achieved if the electromagnetic problem is ill-posed. In a recent paper [3] we have introduced the modal decomposition method [4] to study the influence of the Zenneck wave on the field excited by any vertical source placed at the sea surface. It has been found that the Zenneck wave contribution is masked by an infinite spectrum of bulk waves that are not confined at the sea surface. The excitation of the bulk waves does not permit to concentrate the radiated power at the interface between sea and air and therefore it lowers HFSWR performances. An interesting solution could come from the domain of negative parameters materials: an interface between air and a material having a negative permittivity can support a complex mode that may be not masked by the bulk waves. In this paper, with a similar approach of [5], we propose two different structures capable of sustaining a guided complex wave and of concentrating the radiated power at lower elevation angles.

REFERENCES

1. Menelle, M., G. Auffray, and F. Jangal, "Full digital high frequency surface wave radar: French trials in the biscay bay," *2008 International Conference on Radar*, 224–229, 2008.
2. Sevgi, L., A. Ponsford, and H. C. Chan, "An integrated maritime surveillance system based on high-frequency surface-wave radars. 1. Theoretical background and numerical simulations," *IEEE Antennas and Propagation Magazine*, Vol. 43, No. 4, 28–43, 2001.
3. Petrillo, L., F. Jangal, M. Darces, J.-L. Montmagnon, and M. Hélier, "Towards a better excitation of the complex wave," *Progress In Electromagnetics Research M*, Vol. 13, 17–28, 2010.
4. Kistovich, Y. V., "Possibility of observing Zenneck surface wave in radiation from a source with a small vertical aperture," *Sov. Phys. Tech. Phys.*, Vol. 34, No. 4, 391–394, 1989.
5. Jangal, F., L. Petrillo, and F. Darces, "Towards HF metamaterials," *2009 Loughborough Antenna and Propagation Conference, LAPC 2009*, 629–632, 2009.

Session 2A7
Statics and Dynamics of Magnetic Nanostructures: Vortices and Nanomagnonics

Spin-dynamics Simulations of Vortex Precession in 2-D Magnetic Dots

Philippe Depondt
University of Paris 6, France

Abstract— The precession of vortices was simulated in two-dimensional magnetic plots of finite size. The Landau-Lifshitz equation for the isotropic Heisenberg model with dipole-dipole interactions of various strengths, was integrated at a low temperature with initial conditions consisting in a single vortex situated aside from the central position. This vortex precesses around the center of the sample and is, in some cases, expelled from the sample, in others converges towards the middle of the sample. The frequencies and drift rates (towards or away from the center) depend on the size of the sample and on the Heisenberg versus dipolar interactions ratio. The drift rate usually shows different regimes for a given vortex and also exhibits vortex pinning before arrival at the center of the sample.

Probing GHz Dynamics of Double Vortex Metastable State in Circular Nanomagnet: Micromagnetic Simulations and Experiment

Farkhad G. Aliev, **Dennis Dieleman**, **and Ahmad A. Awad**
Departamento de Fisica de la Materia Condensada, CIII
Universidad Autonoma de Madrid, Madrid 28049, Spain

Abstract— Single or multi vortex states are present in many systems. Circular nanoscale ferromagnets (nanomagnets) with a curling magnetization, can also have a single vortex ground state with an extremely small core of about 10 nm. The magnetic vortex is created at high current densities in spin torque devices. The microwave dynamics of the single magnetic vortex has been actively investigated as a new basic element of spin torque oscillators and novel magnetic memories [1–3]. Recent reports show that thin circular dots may also accommodate two magnetic vortices as metastable state [4]. In this talk we present our recent experimental results and simulations of magnetization dynamics of pair vortex state circular Permally dots where pinning of the vortex cores prevents the system from attaining the ground state. Measurements were done using Vector Network Analyser based broadband magnetometer while numerical simulations with OOMMF code. We identify a novel type of quasi one-dimensional localized spin wave modes. These spin excitations are confined along diamond-shape domain walls connecting each of two vortex cores with edge magnetic charges. Our findings provide first insight into dynamics of remanent metastable states in highly symmetric magnetic elements and could be relevant for exploration of excitations in other cylindrically confined multivortex states.

REFERENCES

1. Dussaux, A., et al., *Nature Communicatons*, Vol. 1, 1, 2010.
2. Aliev, F. G., et al., *Phys. Rev. B*, Vol. 79, 174433, 2009.
3. Awad, A., et al., *Appl. Phys. Lett.*, Vol. 96, 012503, 2010.
4. Vaz, C. A. F., et al., *Phys. Rev. B*, Vol. 72, 224426, 2005.

The Effect of the Damping on the Stability of the In-plane Vortex State in 2D Magnetic Nanodots

S. Mamica[1], **J.-C. S. Lévy**[2], **Ph. Depondt**[3], **and M. Krawczyk**[1]

[1]Surface Physics Division, A. Mickiewicz University, ul. Umultowska 85, Poznań 61-614, Poland
[2]Lab. MPQ, UMR CNRS 7162, Université Paris 7, 10 r. A. Domon, Paris 75013, France
[3]INSP, UMR CNRS 7588, Université Paris 6, 75252 Paris Cedex 05, France

Abstract— The aim of this study is to analyze the stability of the single in-plane vortex state and the spin-wave excitations in two-dimensional magnetic nanodots with a damping. Small square and circular dots including up to a few thousand of spins are studied by means of a microscopic theory with nearest-neighbor exchange interactions, dipolar interactions and Gilbert damping taken into account.

We calculate the spin-wave frequencies versus the dipolar-to-exchange interaction ratio d to find the values of d for which the assumed ground state is stable. The transition to different ground state and its dependence on model parameters are investigated. We also elucidate the role of the spin-waves localization in the destruction of the assumed ground state. Spin-wave profiles of the excitations which are responsible for the transition suggests new ground state. We found two types of transition: vortex core formation for small d (strong exchange interactions) and in-plane reorientation of spins for large d (strong dipolar interactions).

For the transition to the core-vortex critical value d_1 is size-independent for large enough dots. Moreover, d_1 is independent on the shape of the dot. These are due to the fact, that core formation is local phenomenon forced by exchange interactions. While damping increases the critical value d_1 remains almost unchanged. Also the profile of the lowest spin-wave excitation for $d \approx d_1$ does not change with variation of the damping. It means that damping has very weak influence on the out-of-plane spins movement. In contrary in-plane reorientation is very sensitive to the damping. Its increasing changes the type of localization and lower the strength of dipolar interactions necessary to the transition which results in weaker stability of the assumed ground state.

ACKNOWLEDGMENT

The research leading to these results has received funding from the European Community's Seventh Framework Programme (FP7/2007-2013) under Grant Agreement No. 233552 for DYNAMAG project.

Consequences of Localization of Non-linear Effects in Magnetic Dots

Jean-Claude Serge Levy
Laboratoire Matériaux et Phénomènes Quantiques, Université Paris 7 Denis Diderot, UMR 7162 CNRS
75201 Paris Cedex 13, France

Abstract— In the recent years, polar vortices were observed in magnetic dots [1], in perfect agreement with theoretical and numerical investigations based on the competition between local exchange and long-ranged dipole-dipole interactions [3]. This is a new property of nanostructures. And recently some authors observed a frequency doubling of spin waves in such nanostructures [6]. This highly non-linear effect is precisely located at domain walls of which positions are determined from geometrical constraints.

The localization of non-linear effects is explained from a Taylor expansion of dipolar interactions into a local non-linear interaction [7]. And non linear terms occur only at the places where static magnetization is not uniform. Thus the present step is to propose to observe the occurrence of non-linear effects in magnetic dots where vortices are formed. This will bring new geometrical constraints for induced high frequency magnons. Applications of non-linear effects to ferroelectric materials and to other vortex structures are also suggested.

REFERENCES

1. Shinjo, T., T. Okuno, R. Hassdorf, K. Shigeto, and T. Ono, "Magnetic vortex core observation in circular dots of permalloy," *Science*, Vol. 289, 930, 2000.
2. Li, J. and C. Rau, *Phys. Rev. Lett.*, Vol. 97, 107201, 2006.
3. Vedmedenko, E. Y., et al., *Surf. Sci.*, Vol. 391, 402–404, 1998.
4. Elhajal, M., B. Canals, R. Sunyer, and C. Lacroix, *Phys. Rev. B*, Vol. 59, 3329, 1999.
5. Cowburn, R. P., "Spintronics: Change of direction," *Nature Materials*, Vol. 6, 255, 2007.
6. Hermsdoerfer, S. J., H. Schultheiss, C. Rausch, S. Schäer, B. Leven, S.-K. Kim, and B. Hillebrands, "A spin-wave frequency doubler by domain wall oscillation," *Appl. Phys. Lett.*, Vol. 94, 223510, 2009.
7. Levy, J.-C. S., "Dipolar induced magnetic anisotropy and magnetic topological defects in ultrathin films," *Phys. Rev. B*, Vol. 63, 104409, 2001.

Non-autonomous Dynamics of a Spin-torque Oscillator in a Wide Frequency Range: Fractional and Hysteretic Synchronization to External Periodic Signals

S. Urazhdin[1], **V. S. Tiberkevich**[2], **and A. N. Slavin**[2]

[1]Department of Physics, West Virginia University, Morgantown, WV 26506, USA
[2]Department of Physics, Oakland University, Rochester, MI 48309, USA

Abstract— We experimentally demonstrate a series of fractional synchronization regimes (Devil's staircase [1]) characterized by rational relations between the driving frequency and the frequency of the oscillation, in a spin-torque nano-oscillator driven by a microwave magnetic field. Analysis based on the phase model of an auto-oscillator indicates that fractional synchronization becomes possible when the driving signal breaks the symmetry of the oscillation, while the synchronization ranges are determined by the geometry of the oscillation orbit. Therefore, fractional synchronization can be utilized for the analysis of oscillation in nanoscale systems not accessible to direct imaging techniques.

We also report the observation of hysteretic synchronization predicted in [2] in a point contact spin torque nano-oscillator driven by a microwave magnetic field. The hysteresis is asymmetric with respect to the frequency detuning of the driving signal, and appears in the region of a strong dependence of the oscillation frequency on the bias current. Theoretical analysis based on the formalism [3] shows that hysteretic synchronization occurs when the width of the synchronization range, enhanced by the oscillator's nonlinearity, becomes comparable to the dissipation rate, while the observed asymmetry is a consequence of the nonlinear dependence of frequency on the bias current. Hysteretic synchronization is a general property of strongly nonlinear oscillators, and can, therefore, be expected to manifest itself in the dynamics of a variety of auto-oscillating systems.

REFERENCES

1. Pikovsky, A., M. Rosenblum, and J. Kurths, *Synchronization: A Universal Concept in Nonlinear Sciences*, Cambridge University Press, England, 2001.
2. Bonin, R., G. Bertotti, C. Serpico, I. D. Mayergoyz, and M. d'Aquino, *Eur. Phys. J. B*, Vol. 68, 221, 2009.
3. Slavin, A. and V. Tiberkevich, *IEEE Trans. Magn.*, Vol. 45, 1875, 2009.

Spin Waves in [Co_x Pd_y] Multilayers and Layered Nanograins

S. Mamica[1], **M. Krawczyk**[1], **P. Manchanda**[2], **A. Kashyap**[2], **and A. Barman**[3]

[1]Surface Physics Division, Faculty of Physics, Adam Mickiewicz University
ul. Umultowska 85, Poznań 61-614, Poland
[2]The LNM Institute of Information and Technology, Jaipur, India
[3]Department of Material Sciences and Unit for Nanoscience and Technology
S. N. Bose National Centre for Basic Sciences, Salt Lake, Kolkata 700098, India

Abstract— Layered magnetic nanograins with out-of-plane anisotropy are of much scientific interest because of their potential application in magnetic high-density mass data storage. Materials with strong anisotropy of this type include Co/Pd multilayers, in which the anisotropy mainly stems from the interfaces. If the Pd layer between adjacent Co planes only comprises a few atomic planes, a nonzero magnetic moment is induced at every Pd plane. As a result, a magnetic superlattice composed of two different magnetic materials is formed.

We focus on the spectrum of spin waves in such Co/Pd systems. The magnitude of magnetic moments at individual Co and Pd planes, the average magnetocrystalline anisotropy and the nearest- and next-nearest-neighbor exchange integrals are determined from first principles calculations performed for fcc multilayers with surface cut [111] for different numbers of Pd monoplanes (y) between adjacent Co planes (x). The parameter values determined in this way, in agreement with the available literature data, are used for the determination of the spin-wave spectrum, calculated for thin films first. Based on the Heisenberg model, our calculations take into account the exchange interactions between nearest and next-nearest neighbors, and the single-ion anisotropy. The results are confirmed by calculations using the discretized Landau-Lifshitz equations. This approach is extended to layered nanograins, but with parameters of the infinite system. The obtained spin-wave spectrum is analyzed versus exchange interactions, anisotropy and magnetostatic interactions. We show how these parameters and the structural assumptions can be expected to alter the SWR. Thereby, we present an indirect method of verification of the internal nanograin structure by measurement of the spin-wave spectrum.

ACKNOWLEDGMENT

The research leading to these results has received funding from the European Community's Seventh Framework Programme (FP7/2007-2013) and from Department of Science and Technology, Govt. of India under the India-EU collaborative project "DYNAMAG": Grant Agreement No. 233552 and INT/EC/CMS(24/233552), respectively.

Electric Field Control of Surface Spin Waves

R. L. Stamps, **V. Gunawan**, **and K. Livesey**
School of Physics, University of Western Australia, M013, 35 Stirling Hwy, Crawley, WA 6010, Australia

Abstract— We discuss how magnetic excitations in linear magnetoelectric media can be affected by applied electric fields. Previous calculations have shown that magnetic polaritons in bulk media can display interesting and potentially useful properties [1, 2], but little has been discussed regarding surface excitations until now. We show that, for single phase materials whose magnetic structure is canted antiferromagnetic, surface magnetic polaritons can exist in the GHz range and that the magnetoelectric interaction leads to "leaky" surface modes (pseudosurface waves that dissipate energy into the bulk). Most significantly, we show that the surface mode nonreciprocity, where $\omega(k) \neq \omega(-k)$, can be controlled with an applied *electric* field. Results are presented for propagation in TM and TE polarisations using parameters appropriate for $BaMnF_4$. Possibilities for *dynamic* magneto-electric coupling in superlattices are also discussed. We show that it is possible to obtain electric field induced frequency shifts of several GHz in ferromagnet/$BiFeO_3$ multilayers [3]. Lastly, we discuss the nature of spin correlations in multiferroic materials and how these can lead to thermal hysteresis [4].

REFERENCES

1. Tilley, D. R. and J. F. Scott, *Phys. Rev. B*, Vol. 25, 3251, 1982.
2. Barnas, J., *J. Phys. C: Solid State Physics*, Vol. 19, 419, 1986.
3. Livesey, K. and R. L. Stamps, *Phys. Rev. B*, in press.
4. Livesey, K. and R. L. Stamps, *Phys. Rev. B*, Vol. 81, 064403, 2010.

Switching of the Polarity of Vortices in Magnetic Nanodots by a Spin-polarized Electric Current

Franz G. Mertens[1], **D. Sheka**[2], **V. Kravchuk**[3], **and Yu. Gaididei**[3]

[1]Theoretical Physics, University of Bayreuth, Postfach, Bayreuth 95440, Germany
[2]National Taras Shevchenko University of Kiev, Ukraine
[3]Bogolyubov Institute for Theoretical Physics, Kiev, Ukraine

Abstract— The ground state of a flat cylindrical ferromagnetic nanodot is a non-planar vortex, if the radius of the dot is large enough. A non-planar vortex is characterized by two topolocigal charges: vorticity q and polarity $p = \pm 1$ (the spins in the vortex core are parallel or antiparallel to the cylinder axis). Both q and p are constants of motion in the continuum limit. However, in discrete spin systems the polarity can be switched in different ways: scattering with spin waves, thermal noise, a magnetic field pulse, a rotating magnetic field, or a spin-polarized electrical current.

We investigate the latter effect. We perform spin-lattice simulations for a nanodot using a spin model with Heisenberg exchange and dipole-dipole interactions. A spin-polarized dc current produces a spin torque (Slonczewski-Berger term) in the Landau-Lifshitz equation, which is solved numerically. The initial condition is an up-vortex ($p = +1$) in the middle of the system. The vortex center moves away from the middle and certain magnon modes are excited. Thereby a negative peak (a dip) in the out-of-plane spin structure appears close to the vortex. When this peak has reached its maximal depth, it splits into a vortex and an antivortex which both have polarity $p = -1$. Then the new antivortex and the original vortex annihilate and the new vortex with $p = -1$ remains. Thus effectively an up-vortex is replaced by a down-vortex. Using typical parameters for a Permalloy disk (radius 100 nm, thickness 20 nm), we find much faster switching times (about 50 ps) than in the rotating field method (about 200 ps). The critical current density is about $0.1\,\mathrm{A}/\mu\mathrm{m}^2$.

Interestingly, the above scenario is generic, because it has been observed both experimentally and numerically using different switching methods. As the formation of the dip close to the vortex seems to be essential for the switching process, we study in detail under which conditions the dip appears and how it is created.

To this end we perform spin-latttice simulations for different situations: A fixed planar vortex at the center of the system, and a planar vortex at the center of a small ring, situated either at the system center or at a distance from the center. One of the results is that the out-of-plane structure of the vortex core is not essential for the dip formation. This is confirmed by micromagnetic simulations.

Effective Magnetic Parameters of One-dimensional Magnonic Crystals in the Long-wavelength Limit

M. Mruczkiewicz, **M. Krawczyk**, **J. W. Kłos**, **and M. Sokolovskyy**
Surface Physics Division, Faculty of Physics, Adam Mickiewicz University
ul. Umultowska 85, Poznań 61-614, Poland

Abstract— Magnonic crystals (MCs) are the magnetic equivalent of photonic crystals, with spin waves as the counterpart of electromagnetic waves, playing the role of information carriers. One of the fundamental characteristics of wave propagation in periodic structures, which include magnonic crystals, is the occurrence of band gaps, or frequency ranges forbidden to propagating waves. The existence of magnonic gaps in the spectrum of spin waves, has already been verified experimentally in one-dimensional magnonic crystals. Controlling the propagation of spin waves is a very important application of magnonic crystals. It can be achieved also by modeling the dispersion relation, and consequently, the group velocity or the density of states available to spin waves. These possibilities are studied in this paper.

We present the results of the calculation of spin-wave spectra in thin films of one-dimensional magnonic crystals consisting of alternating nanoscale stripes of different ferromagnetic materials (such as Co/Py or Fe/Ni). Based on the plane wave method with exchange and magnetostatic interactions taken into account, numerical calculations have been performed for magnetic field of different magnitude and for different values of structural parameters. We demonstrate that effective values of material parameters, such as static magnetization, exchange constant or thickness of the MC, can be determined for the first band in the structures considered. The introduction of effective values of magnetic parameters allows the description of linear dynamic properties of the MC in the long-wavelength limit with the use of a homogeneous film. The effective parameters of the homogeneous film can differ significantly from the corresponding parameter values in known ferromagnets, which opens the way for even more practical applications of MCs in spin-wave devices. The effective parameter values are determined by a numerical procedure of fitting the analytical formulae describing the dispersion in the homogeneous film to numerical results obtained by the plane wave method.

ACKNOWLEDGMENT

The research leading to these results has received funding from the European Community's Seventh Framework Programme (FP7/2007-2013) under Grant Agreement No. 233552 (MAGNONICS).

Investigation of Spin Dynamics in Planar Two-dimensional Magnonic Crystals Using the Plane Wave Method and Micromagnetic Simulations

M. L. Sokolovskyy[1], M. Krawczyk[1], M. O. Dvornik[2], and V. V. Kruglyak[2]

[1]Surface Physics Division, Faculty of Physics, Adam Mickiewicz University
Umultowska 85, Poznan 61-614, Poland
[2]School of Physics, University of Exeter, Stocker Road, Exeter EX4 4QL, United Kingdom

Abstract— Investigation of the spin-wave spectrum in nanoscale magnetic materials has recently attracted significant attention because the possibility of miniaturization of the present microelectronic devices. Materials with periodic modulation of one or more structural parameters are promising for future applications. There are plenty of methods that describe multilayered structures. A popular analytical method for investigating the spin-wave spectrum of such kind of systems is the plane-wave method [1]. At the same time, it still remains a challenge to fabricate samples due to a small modulation length. However, the increase of computing power makes it possible to use programs to create numerical experiments — micromagnetic simulations (e.g., OOMMF, nmag, etc.) for rather complicated structures.

In this work we extend our previous calculations [2] to the case of two-dimensional magnonic crystals with a finite thickness. Both, the static and the dynamic demagnetizing fields are included in the calculations. In the case of one-dimensional periodic magnetic structure we obtain a good agreement with published Brillouin Light Scattering measurements [3]. Surface character of the spin waves in the Permalloy nanostripes is shown and the magnetostatic nature of the observed spin waves is justified. Sensitivity to boundary conditions on the surfaces of the magnetostatic modes in thin films [4] gives new possibilities for shapening dispersion relations of spin waves and magnonic band gaps in 1D MCs of nanoscale thickness, just by putting metallic overlayers on the top of it. In the case of two-dimensional magnonic crystals we perform also micromagnetic simulations using OOMMF. A good agreement between our calculations and numerical experiments in OOMMF is obtained.

ACKNOWLEDGMENT

The research leading to these results has received funding from the European Community's Seventh Framework Programme (FP7/2007-2013) under Grant Agreement No. 228673 MAGNONICS.

REFERENCES

1. Krawczyk, M. and H. Puszkarski, "Plane-wave theory of three-dimensional magnonic crystals," *Phys. Rev. B*, Vol. 77, No. 5, 054437, 2008.
2. Sokolovskyy, M. L. and M. Krawczyk, "A new treatment of the demagnetizing field for the plane-wave method," *JEMS, Magnonic-poster*, 104, 2010.
3. Wang, Z. K., et al., "Nanostructured magnonic crystals with size-tunable bandgaps," *ACS Nano*, Vol. 4, No. 2, 643–648, 2010.
4. Gurevich, A. G. and G. A. Melkov, *Magnetization Oscillations and Waves*, CRC Press, Boca Raton, 1996.

The Magnonic Spectra of Finite-thickness Slabs with Inclusions Forming 2D Lattices of Different Symmetry

J. W. Kłos, **M. Sokolovsky**, **and J. Romero-Vivas**
Surface Physics Division, Faculty of Physics, Adam Mickiewicz University
Umultowska 85, Poznań 61-614, Poland

Abstract— Using the Landau-Lifshitz (L-L) equation we calculate the spin-wave spectra of magnonic crystals in the shape of a single slab of finite thickness. The slab consists of two components: a ferromagnetic matrix and ferromagnetic inclusions ordered in a 2D lattice. Having the form of a prism of arbitrary shape of the in-plane cross section, the inclusions extend between the opposite surfaces of the slab and are arranged in three sorts of lattice: (i) a triangular lattice, (ii) a square lattice and (iii) a honey-comb lattice. We investigate the effect of the lattice symmetry on the magnonic spectrum by comparing the three structures with either the filling fraction f or the lattice constant a fixed. Separate investigations for the filling fraction and the lattice constant are necessary because of the different values of the a/f ratio for the considered lattice types.

We use the linear approximation of the L-L equation in the spin-wave regime and apply the Fourier transformation to convert the set of differential equations into an algebraic eigenproblem [1]. An in-plane external magnetic field is assumed in the calculations. The finite thickness of the slab is included in the model by taking into account the demagnetizing field. We use the analytical formulas given by Kaczer [2]. The dynamic and static components of the demagnetizing field are only assumed to be constant in the out-of-plane direction.

ACKNOWLEDGMENT

The research leading to these results has received funding from the European Community's Seventh Framework Program (FP7/2007-2013) under Grant Agreement No. 233552 (DYNAMAG).

REFERENCES

1. Krawczyk, M. and H. Puszkarski, *Phys. Rev. B*, Vol. 77, 054437, 2008.
2. Kaczer, J. and L. Murtinova, *Phys. Stat. Sol. (A)*, Vol. 23, 79, 1974.

Session 2A8
Antenna Channel Interactions in Multipath Wireless Channels

Evidence of Ducting Mode Electromagnetic Wave Propagation in the Indoor Environment

A. Draganov, J. Weinfield, L. Haas, and M. Harlacher
Argon ST, Wholly Owned Subsidiary of the Boeing Company, USA

Abstract— Wireless communication and radio-frequency navigation are converging to use similar signals and even sharing same devices. Both are adversely affected by multipath propagation of the signal, especially in the urban and indoor environment. While in the communications field the primary effect of multipath is the intersymbol interference and signal fading, navigation applications require a discernible line of sight to determine the user position. The next great frontier in radio navigation is accurate indoor positioning, where the line of sight signal may not exist or is corrupted by small delay (fraction of the symbol) multipath. Thorough understanding of signal propagation delays in indoor environments is therefore important for these emerging applications.

This paper presents results from three experiments on RF signal propagation in a multi-story office building. In the first experiment, we measured and analyzed fading patterns of an RF signal in the ISM band (915 MHz). We compute autocorrelation of the signal power as a function of the spatial separation between receiving antenna locations in the hallway. We compare this autocorrelation function with those derived from two analytical models. The first model is the classic Rician distribution. The second model assumes existence of one distinct mode of ducted wave propagation in the hallway in each direction, in addition to random multipath. We show that experimental results are in good agreement with the second model.

In the second experiment, we measure the time difference of arrival of a signal at two receiving antennas in the building. The transmitted spread-spectrum signal in the ISM band (915 MHz) has large bandwidth ($20 \cdot 10^6$ symbols per second), which gives us a relatively fine time resolution. The two receiving antennas are connected to the same two-channel receiver via cables of calibrated length, so that the time difference of arrival can be measured accurately and there is no need for a precise synchronization of receivers. In each setup, measurement results are compared with geometric lengths of two possible signal paths: 1) The line of sight and 2) the combined length of hallways between the two receive antennas. The latter is a crude model for the ducted propagation of the signal along hallways of the building. For half of scenarios, results for time difference of arrival are consistent with the hypothesis of ducted wave propagation along building hallways, and not with the line of sight hypothesis.

In the third experiment, we measured accumulated phase variations between a transmitter and a receiver as the receiver moved along a hallway. Variations in the phase of the arriving signal qualitatively correspond to the change in the distance between the transmitter and the receiver, but their magnitude is not consistent with the hypothesis of the phase velocity being equal to the speed of light. Rather, these variations can be explained if the major mode of propagation is ducted by the hallway.

Results of our experiments suggest that ducted propagation may be a common phenomenon in indoor environments. This fact may have important implications for RF navigation and positioning indoors.

Some Examples of Uncorrelated Antenna Radiation Patterns for MIMO Applications

A. Alayon Glazunov[1] and J. Zhang[2]

[1]Electromagnetic Engineering Lab, KTH — Royal Institute of Technology, Sweden
[2]Centre for Wireless Network Design, University of Bedfordshire, UK

Abstract— The radiation pattern is one of the most important figures of merit of an antenna for all applications. For example, together with the propagation channel, it determines the signal-to-noise ratio (SNR) of a wireless link and the correlation between antenna elements. Furthermore, both the SNR and the correlation have a great impact on the spectral efficiency of Multiple-Input Multiple-Output (MIMO) links over multipath wireless channels. Hence, an accurate account for the interactions between antennas and channels is essential to a successful implementation of MIMO technologies for 4G and beyond wireless systems. Although this topic has been extensively researched, a unified approach for the characterization of antenna-channel interactions has been introduced only recently. This method is based on the spherical vector waves expansion of the fields of the antennas and the propagation channel. In this paper we provide some examples of the approach resulting in uncorrelated antenna radiation patterns at both ends of a MIMO wireless link in a given propagation channel. The patterns of antennas exciting a few TE, TM or both modes are analyzed as a function of the angle spread of the angle-of-arrivals (AoA) and the cross-polarization ration of the channel.

Clustering Impact on the Statistics of the Multipole Expansion Coefficients of a Wireless Channel

A. Alayon Glazunov[1] and J. Zhang[2]

[1]Electromagnetic Engineering Lab, KTH Royal Institute of Technology, Sweden
[2]Centre for Wireless Network Design, University of Bedfordshire, UK

Abstract— It has been widely known that experimental results show that multipath components seem to arrive at the receiver in concentrated groups. These groups of multipath components, or clusters, are usually a result of scattering from large physical structures. Their impact on the capacity of Multiple-Input Multiple-Output (MIMO) systems has been widely studied. However, their impact on the spherical vector waves (SVW) expansion of the propagation channel has not yet been addressed in the literature. As we have recently shown, a SVW expansion, i.e., a multimode expansion provides a compact and straightforward representation of both antennas and channels. This can potentially facilitate the design of antennas that are tailored to take advantage of the spatial and polarimetric characteristics of the propagation environment. This is essential to the deployment of efficient wireless networks. Therefore, in this paper, we study the impact of clustering on the first and second order statistics of the multimode exapansion coefficients. We adopt the simulation approach to exemplify this behavior by numerical examples.

Space Diversity Evaluation in Millimeter Band Wireless Communication Systems

Mehran Atamanesh and Forouhar Farzaneh
School of Electrical Engineering, Sharif University of Technology, Iran

Abstract—

Introduction: In recent years, an ever-increasing growth of the demand for the new broadband communications services such as video conferencing, multi-media and high data-rate transmission has been observed. All these services need a higher data rate transmission than the conventional voice service and hence, need higher bandwidth [1]. Because of congestion in the frequency bands below 2 GHz, the attention of radio systems designers has tended to the higher frequency bands especially the unlicensed frequencies around 60 GHz [2–4]. Besides, in a typical wireless environment, the received signal is subjected to the fading phenomena and consequently quality degradation. One of the most effective methods to combat these phenomena is using diversity reception techniques [5].

In this paper, a software tool for predicting signal level in millimeter wave bands has been implemented which uses ray tracing method. In Section 2, the validation of this tool with the measurements will be presented. The space diversity will be studied in Section 3 with a proposed analytical expression and finally Section 4 draws the conclusion.

Computational Results and Validation: A good agreement between the simulated results with the ray tracing method and the measurements in an urban environment has been already

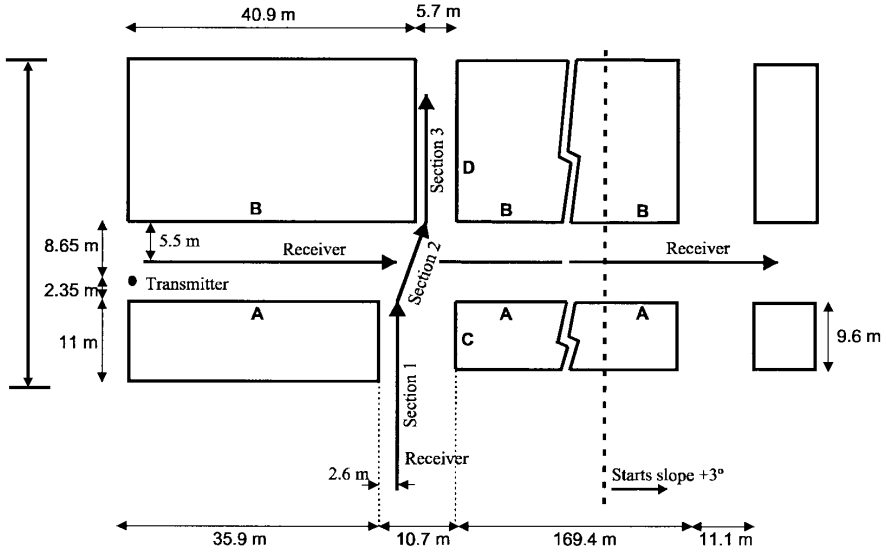

Figure 1: Measurement environment of [9].

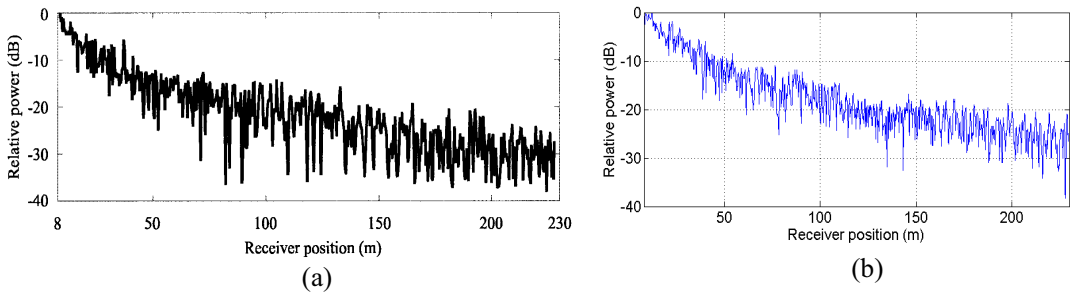

Figure 2: Relative power (dB) for LOS path. (a) Measured [9]. (b) Simulated.

shown [6, 7]. In ray tracing based on image method [8], the ray path will be determined when the position of the transmitter, receiver and objects causing propagation phenomenon are known. The objects have commonly flat surfaces (walls, ground). This method is useful for not too complicated environment, i.e., the propagation area with a relatively small number of reflecting surfaces. In this method, the first step is to find the virtual image of the transmitter relative to the surface, then by connecting the receiver and virtual image of the transmitter, it can be determined if the line intersects the object or not. If the answer is 'yes', the whole trajectory can be considered as a path from the transmitter, to the receiver. This procedure which takes into account the virtual image and determines the point of reflection on the surfaces is valid for multiple reflections of order N.

A program using MATLAB® has been written for predicting the signal level using image ray tracing method. For validation of this program we have chosen the measurement data of [9] at 62.4 GHz. Figure 1 shows the environment of measurements.

Measurements were made in two paths: LOS path along the street and equally spaced from the walls and the other path which includes LOS and NLOS parts. Simulation was made considering a permittivity and a conductivity of 6.81 and 0.95 s/m for the walls and 10 and 0.005 s/m for the ground, respectively. Figure 2 shows the measured and simulated relative power of the LOS path. In the simulation, maximum number of reflections was set to two. Because of strong attenuation of edge diffraction in millimeter wave, no diffracted ray was included in calculation of the relative received power. The walls were considered to be smooth. By comparing the measurement data with the simulation result, a good agreement can be concluded.

Antenna Height Compensation for an Indoor to Outdoor Channel Model Based on a 2D Finite Difference Model

G. de la Roche[1], D. Umansky[2], Z. Lai[1], G. Villemaud[2], J.-M. Gorce[2], and J. Zhang[1]

[1]University of Bedfordshire, Luton, UK
[2]INSA, University of Lyon, France

Abstract— It has been recently shown that a finite difference model (e.g., based on an approach similar to FDTD) combined with a ray optical approach (e.g., based on ray launching) can be efficient to compute the simulation of Outdoor to Indoor radio wave propagation [1]. Such model was based on 2D Finite Difference for the indoor part, which efficiently takes into account the propagation into the floors of the buildings since they can be well approximated with a 2D model, combined with a ray launching model for the outdoor part.

However, for the Indoor to Outdoor case [2] and depending on the height where the antenna is located inside the building, it is important to be able to launch the outdoor rays in the correct directions. Therefore, this paper proposes a new approach where the vertical cut of the building is simulated, in order to extract the directions of the outdoor rays to be computed.

The new method we proposed works as follows:

- The horizontal indoor radio coverage is simulated inside the building with the finite difference model (see Figure 1).
- The vertical indoor radio coverage is simulated inside the building with the finite difference model (see Figure 2).
- From these two radio coverage predictions, the directions of the rays to be launched outside are extracted based on the SAGE algorithm. In this approach, the electrical fields on the border of the building are used in order to estimate the angles of arrival.
- The outdoor rays are launched using the ray optical based model, and the reflections/diffractions on the neighbouring buildings are computed.

A measurement campaign was performed in order to evaluate the performance of the new combined model. For this purpose an emitter is deployed inside a building and radio measurements are performed both indoors and outdoors.

The indoor scenario, where the MRFDPF (Multi Resolution Frequency Domain ParFlow) method is used, is the CITI building whose size is approximately 110×100 meters. The outdoor rays are launched in the whole outdoor scenario (800×560 meters).

It is shown that, compared to [2] where only the horizontal indoor field is taken into account, this approach is efficient to take into account the height of the antenna in the building.

Future work include the realization of more measurements in order to validate this combined model in other scenarios and frequency bands.

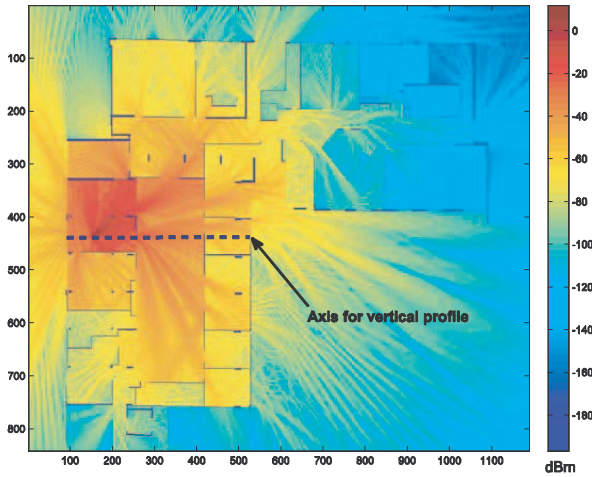

Figure 1: Horizontal indoor radio coverage (with line for vertical cut), from red (−40 dBm to blue (−100 dBm).

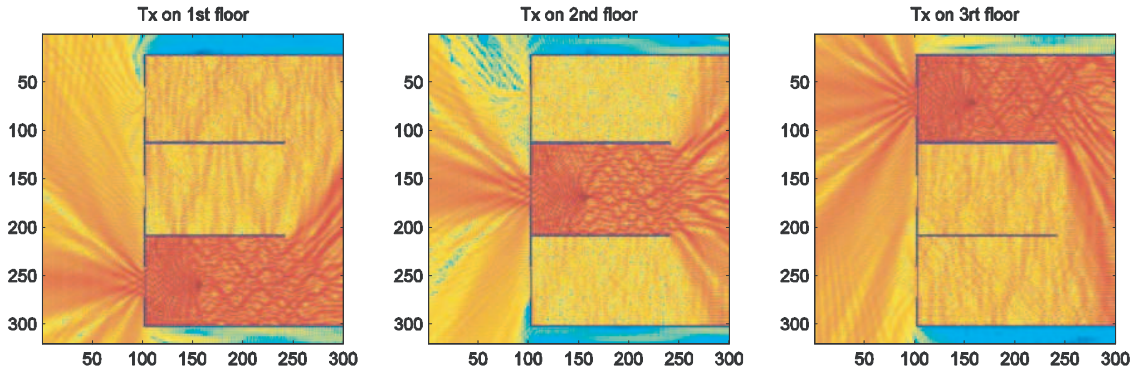

Figure 2: Vertical indoor radio coverage (for antennas located at 3 different floors), from red (−40 dBm to blue (−100 dBm).

ACKNOWLEDGMENT

This work is funded by the FP7 project "IPLAN".

REFERENCES

1. De La Roche, G., P. Flipo, Z. Lai, G. Villemaud, J. Zhang, and J.-M. Gorce, "Implementation and validation of a new combined model for outdoor to indoor radio coverage predictions," *EURASIP Journal on Wireless Communications and Networking*, 2010.
2. Umansky, D., G. de la Roche, Z. Lai, G. Villemaud, J.-M. Gorce, and J. Zhang, "A new deterministic hybrid model for indoor-to-outdoor radio coverage prediction," *European Conference on Antennas and Propagation (EuCAP 2011)*, 2011.

Angle of Arrival and Doppler Spectrum in the Presence of Generalized Two-dimensional Anisotropic Scattering

Petros Karadimas and Jie Zhang
Centre for Wireless Network Design (CWIND), Department of Computer Science and Technology
University of Bedfordshire, LU13JU, Luton, UK

Abstract— In this paper, we present a generalized theoretical model for the angle of arrival (AOA) in wireless channels when the scattering is two-dimensional (2-D) anisotropic. This model can constitute a platform for creating new angular distributions for the propagating multipath power and as such, a new distribution accounting for multi-modal arrival will be presented. The latter will represent the case that multipath power arrives into four angular sectors being parametrically defined with respect to the direction of the receiver motion. From the AOA, the power spectral density (PSD) of the received complex signal is analytically derived. Further generalization with multi-modal arrival into an arbitrary number of angular sectors can be treated similarly.

A New Approach for Measurements of Signal Level Contents in a Real Wireless System in the City of Curitiba, Brazil

H. Tertuliano Filho[1], G. D. Patriota[1], C. Alves[1], J. Carvalho[1], W. H. Fiorese[1], R. Schumacher[1], C. A. Dartora[1], and J. R. Descardeci[2]

[1]Department of Electrical Engineering, Federal University of Parana, Curitiba 81531-990, PR, Brazil
[2]Center of Engineerings, Federal University of Tocantins, Palmas 77020-210, TO, Brazil

Abstract— This paper describes a study of the attenuation of the mobile radio signal due the environment in the central and urban building-up area of Curitiba's downtown, a Brazilian city in the South of the country with more than two million inhabitants. The original results presented in this work are real life data collected from a major mobile operator in the city with gave for the project the real database drive test for the downtown area including shapes of buildings in the region under study. The propagation model used for mobile radio channels differently of the usual (COST 239, Lee, Okumura-Hata and so on) was a free and adjustable model without diffraction. Being a model designed to obtain predictions with few adjustments to converge to the signal's ideal level the comparison with the collected real signal show excellent approaches. Finally, the morphology, the topography, the real images of the downtown and all technical parameters of the used radio-base channel ERBCTRF01A are presented, explained and justified in this study. Only Omni-directional antennas were used and frequency hope was also considered. The analysis of the simulated results obtained using a PRORAD* software with practical database, 1) proven that the proposed technique that uses one free propagation model enable the detection of the interference points in a system and uses this technique to avoid critical points, because in big cities, a physical free spaces for antennas are hard to find, 2) enable to cover a wide range of frequencies and technologies (FDMA, GSM, CDMA ONE . . .) and 3) the provided average value of adjacent and co-channel interference over this single propagation model used appears to be viable in the-4G technology, giving appropriate solutions and offering advantages over existing usual techniques. Figure 1 below summarized the idea of the proposed simulation model's prediction in Curitiba downtown using the PRORAD software and also shows the chosen morphology of the region where the drive-test was used.

An important aspect must be noted. The free and reconfigurable propagation model used to measure the attenuation of the above specified radio-base channel due the environment and in function of the one specified level of frequency 1800 MHz proves that the intents to obtain a prediction without adjustments in view to measure the signal's ideal level in one specified channel is possible and suitable in big cities. Finally, it must be observed that the environment attenuations effects were obtained for each channel and linearized in view to obtain the medium value of the attenuation in function of the desired frequency.

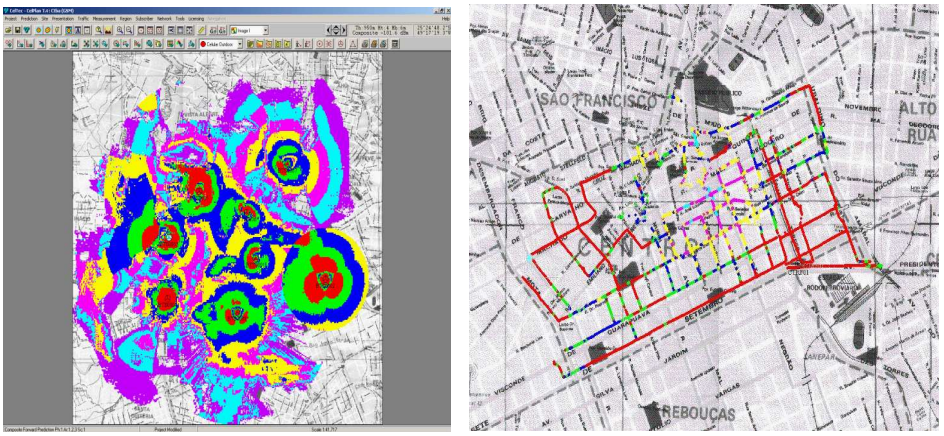

Figure 1.

Session 2A9
Poster Session 3

All-optical Technique to Measure the Pyroelectric Coefficient in Electro-optic Crystals

Jacopo Parravicini[1], **Jassem Safioui**[1], **Mathieu Chauvet**[1], **Paolo Minzioni**[2], **and Vittorio Degiorgio**[1]

[1]Département d'Optique "P.M. Duffieux", Institut FEMTO-ST, Université de Franche-Comté 16 route de Gray, Besançon 25030, France
[2]CNISM and Dipartimento di Elettronica, Università di Pavia, Via Ferrata 1, Pavia 27100, Italy

Abstract— A ferroelectric crystal exhibiting variation of spontaneous polarization as a function of the temperature is called *pyroelectric*; such a change of polarization is expressed by the *pyroelectric coefficient* p. As a consequence of this physical phenomenon, an electric field arises in the crystal, which in lithium niobate was recently found to be able to modify the refractive index generating bright solitons, so called *pyrolitons*. A precise knowledge of the pyroelectric coefficient of such crystals is therefore fundamental for an adequate theoretical treatment of this kind of solitons. The present work is then motivated by the quest of a technique, different from the usual ones, which can give specific information on the pyroelectric properties of a crystal. The aim of our all-optical method is to provide a measurement of the pyroelectric coefficient p of an electro-optic crystal. Through this technique we firstly acquire the birefringence variation $\delta\Delta n$ of the crystal as a function of its temperature T, both in closed and open-circuit conditions, using a Sénarmont phase-compensation configuration. Then the pyroelectric field is deduced from the difference between these two measurements and leads to the material spontaneous polarization change, whose derivative with respect to the temperature finally gives p. This method is alternative to the usual (quasi) static dielectric measurements, which in many conditions present great experimental difficulties. The proposed technique can be used to evaluate the pyroelectric properties of a ferroelectric crystal without need to place any electrodes. An advantage of this technique is that, since a localized beam is employed, a mapping of the pyroelectric coefficient can be obtained by scanning the beam over the crystal. This feature can provide the pyroelectricity distribution, not accessible with usual dielectric techniques that only provide a global value of p. Our technique is applied to both congruent and stoichiometric lithium niobate samples, for which a spreading of the measured values of p can be found in the literature.

Design of Lightning Systems with Usage Sensitivity Analysis for Improvement of Numerical Model

T. Kriz
Department of Theoretical and Experimental Electrical Engineering
Brno University of Technology, Kolejni 2906/4, Brno 612 00, Czech Republic

Abstract— Paper presents usage of the R-FEM method in the CFX environment. There is describes usage of the sensitivity analysis for improvement of numerical model and change dimensions of numerical model according to radiation pattern and required light distribution. The R-FEM method was used for modeling of special light sources and to compute lighting of surfaces from these sources with very good results. Basic description of the R-FEM method is described below. For modeling of the light sources in the CFX environment was used combination of the Finite Volume Method and the radiation method which are included with the CFX (The Discrete Transfer Model and The Monte Carlo Model). Numerical results are presented by model of head-lamp. Sensitivity analysis was used to change dimensions of numerical model according to lighting distribution.

The R-FEM method is a new way in the modeling of lighting systems. It utilizes the similarity between physical models. This paragraph demonstrates the usage of analogy between different physical models for the modeling of light problems. The R-FEM method is able to solve tasks that fulfill the condition $\lambda_S \ll \max(D) \wedge \lambda_S < 10 \cdot \max(D)$, where λ_S is the source of light wavelength and D is one of the geometrical dimensions of the modeling task. It can be used for models with more complicated physical structures than the methods mentioned up to now. An example of a more complicated physical problem, which we can solve by the R-FEM method, is the modeling of light intensity distribution in interior or exterior spaces with non-homogeneous environment, where the light has passed through some impure air (e.g., filled with smoke, fog, mist, vapour, dust, etc.).

ACKNOWLEDGMENT

The research described in the paper was financially supported by the project of the BUT Grant Agency FEKT-S-10-13.

REFERENCES

1. Fiala, P., E. Kroutilova, and T. Kriz, "Numerical modelling of the special light source with novel R-FEM method," *PIERS Proceedings*, 822–826, Cambridge, USA, July 2–6, 2008
2. Kroutilova, E., "Zpusob návrhu odrazných ploch reflexních zařızení pomocí analogie teplotního pole-radiace a vlnové rovnice a zař'ızení v podobě světelné soustavy určené pro numerickou optimalizaci požadovaných světelných parametru odrazných ploch," Patent No. PV 2008-65, Leden, Czech Republic, 2008.
3. Kadlecova, E., "Automated system of calculation of reflecting surface of light sources," Ph.D. thesis, VUT v Brně, FEKT, Srpen, Brno, 2004.

Microwave Photonic Signal Processing with Multiple Sagnac Loop Structures

Xudong Wang, **Erwin H. W. Chan**, **and Robert A. Minasian**
School of Electrical and Information Engineering, Institute of Photonics and Optical Science
University of Sydney, NSW, 2006, Australia

Abstract— The processing of microwave signals using optical delay lines is a powerful technique for conditioning high bandwidth signals. Photonic signal processing can overcome the inherent bottlenecks caused by limited sampling speeds in conventional electrical signal processors [1]. The advantages of this approach, including its EMI immunity, its high time-bandwidth product capabilities and its ability to process high-speed signals directly within the optical fibre transport system, have attracted significant interest.

Recently, several techniques for realizing microwave photonic filters using delay lines have been proposed. However, the operation of these structures with a single-wavelength, which is particularly attractive for fibre optic links, is significantly more demanding because of the requirements to overcome coherent interference effects, and to avoid the generation of phase-induced intensity noise which can dominate.

In this paper, we present a new photonic signal processor that can solve the problem of achieving single-wavelength, coherence-free microwave photonic filter operation. It has the ability to generate a narrow notch response with operation to high frequencies. The concept is based on a multiple Sagnac loop structure that functions with a new principle in which the loops operate with different free spectral ranges (FSR), and in which non-commensurate taps are generated. Each loop, comprising an optical intensity modulator at an off-centre location functions with a different FSR, has its output extracted from the reflective port [2] of the loop, and is connected via an optical circulator to form a multiple loop series structure.

We present an analytical model to examine the electric field of each of the counter-propagating and co-propagating light waves in the various path permutations of the multiple loops. The finite interconnect length between the loops and the length difference between the RF drive paths, are also included. Since the light propagating inside the loops travel different lengths after modulation occurs due to the fact that the modulators are off-loop-centre, and since the optical signals are also re-modulated following the delay time that occurs in reaching the second modulator, the modulated optical signals have different RF phases when they arrive at the photodetector. We examine several designs based on selecting the optimum differential delays for the loop FSRs, the interconnect and RF drive path lengths, and the optical modulation indexes. We introduce a new concept that is based on generating non-commensurate taps, which is different to conventional delay line signal processors where the delayed optical signals have the same separation, and which has the advantage of enabling the efficient realisation of a high-resolution notch filtering while only requiring a few taps.

Experiments have been conducted to verify these concepts. Measured results on a dual-Sagnac loop structure, as an example, designed to have an FSR ratio of 3 for the frequency responses of the two Sagnac loops and an optical modulation index ratio of 2, have demonstrated the ability to generate a notch filter with a narrow notch width, a flat passband, and high stopband attenuation of over 40 dB. The results also showed excellent agreement with theoretical predictions.

This offers high-resolution, high frequency all-optical notch filtering for interference mitigation applications.

ACKNOWLEDGMENT

This work was supported by the Australian Research Council.

REFERENCES

1. Minasian, R. A., "Photonic signal processing of microwave signals," *IEEE Trans. Microwave Theory & Tech.*, Vol. 54, 832–846, 2006.
2. Ning, G. and P. Shum, "Coherence-free microwave photonic notch filter with a single driver intensity modulator in a Sagnac fiber loop," *App. Opt.*, Vol. 46, 7179–7183, 2007.

Inhabitation of Proinflammatory Cytokine Release from Microglia Cells Using Static Magnetic Field

Che-Tong Lin[1], **Po-Chieh Yang**[2], **Chien-Wu Yeh**[3], **Shu-Li Lin**[3], **Jen-Chang Yang**[2], **and Haw-Ming Huang**[2]

[1]School of Dentistry, Taipei Medical University, Taipei, Taiwan
[2]Graduate Institute of Biomedical Materials and Engineering, Taipei Medical University Taipei, Taiwan
[3]Dental Department, Cathay General Hospital, Taipei, Taiwan

Abstract— Proinflammatory cytokine release from microglia cells are the major cause lead to various neurodegenerative diseases, such as Parkinson's disease, Alzheimer's disease and multiple sclerosis. Thus, inhibitions of inflammatory response of neural cells and reduction of proinflammatory cytokine release from microglia cells are two major strategies for prevention of neurodegenerative disease. Previous reported indicated that static magnetic field (SMF) has capability to reduce the excess inflammatory response in cellular level by changing the orientations of lipid molecular on the cellular membrane. This effect results in a reduction of binding capability between proinflammatory cytokine and its receptor. Accordingly, microglia cells, BV-2, were cultured with 4000 Gauss SMF. The effects of SMF on BV-2 proliferation were evaluated using MTT technique. In addition, the microglia cells were co-cultured with immune response initiators (β-Amyloid (Aβ) and LPS) and static magnetic fields. Then proinflammatory cytokine, IL-1, released by BV-2 cells were tested. Our results showed that the cell number of SMF-exposed BV-2 cells significantly decrease to 88% ($p < 0.05$) when compared to the unexposed group. In addition, the released IL-1form SMF-exposed BV-2 cells was also significantly reduced compared to the sham-exposed cells. These results are significantly larger than the sham-exposed cells (37.73 ± 7.89). Our finding suggests that indicate that SMF has potential to become a useful non-invasive physical therapeutic tool for neurodegenerative diseases.

Development and Biocompatibility Tests of a Novel Paramagnetic Nano-membrane for Wound Dressing

Sheng-Wei Feng[1], **Ya-Hui Chan**[1], **Wan-Hong Lan**[2], **Yuh-Yuan Shiau**[2, 3], **Che-Tong Lin**[1], **and Haw-Ming Huang**[4]

[1]School of Dentistry, Taipei Medical University, Taipei, Taiwan
[2]School of Dentistry, National Taiwan University, Taipei, Taiwan
[3]School of Dentistry, China Medical University, Taichung, Taiwan
[4]Graduate Institute of Biomedical Materials and Engineering
Taipei Medical University, Taipei, Taiwan

Abstract— Autologous skin grafts are the best choice for the treatment of extensively burns and chronic wound. However, the autologous skin grafts are always lack and expensive. Therefore, it is important to develop a functional and cheap artificial dressing. Several studies have demonstrated that static magnetic fields (SMF) stimulation can promote wound healing process. However, artificial dressing combined with SMF is still unavailable. With this regard, the aim of this study is to develop a novel magnetic dressing material. The Fe_3O_4 nano-particles were prepared by the chemical-precipitation method. The electrospinning method was carried out to manufacture nanofiber membrane with a concentration of 3g/3g (Fe_3O_4/PLLA). The physical properties of the nano-membrane were characterized by contact angle and XRD analysis. After magnetizing the new-developed PLLA-Fe_3O_4 membrane, the average residual magnetic intensity was 0.28 ± 0.06 G, and an approximate linear relationship was found between the magnetic intensity and membrane thickness ($R = 0.82$, $p < 0.05$). The nano-membrane displayed the paramagnetism at room temperature and the saturation magnetization was 0.08 emu/g under an applied field of 3000 Oe. The results of MTT assay and blood coagulation tests demonstrated that our PLLA-Fe_3O_4 membrane has excellent biological compatibility. These results can serve as a reference for future animal studies.

Neurogenerative Effects of Static Magnetic Field on Neurite-elongation of NGF-induced PC12 Cells

Haw-Ming Huang[1], **Chien-Wu Yeh**[2], **Shu-Li Lin**[2], **Yuh-Yuan Shiau**[3, 4], **and Wei-Jen Chang**[5]

[1]Graduate Institute of Biomedical Materials and Engineering
Taipei Medical University, Taipei, Taiwan
[2]Dental Department, Cathay General Hospital, Taipei, Taiwan
[3]School of Dentistry, National Taiwan University, Taipei, Taiwan
[4]School of Dentistry, China Medical University, Taichung, Taiwan
[5]School of Dentistry, Taipei Medical University, Taipei,Taiwan

Abstract— Several investigations indicated that pulse electromagnetic field (PEMF) can be a useful non-invasive physical therapeutic tool for stroke and traumatic injuring patients. Recent reports indicated that, similar to PEMF, static magnetic field (SMF) can promote osteoprogenitors to differentiate into a more mature phenotype. With this regard, we tested the effect of SMF on neurogeneration. In this study, PC12 cells were carried out for in vitro experiments. The cells were pre-induced to express neural characteristics with 50 ng/ml nerve growth factor (NGF). Then the induced cells were continuously exposed to 4000G-SMF for 15 days. Cell morphologies were monitored by optical microscope. The morphology changes of the differentiated PC12 cells treated with and without SMF exposure were compared by counting the length and branching degree of dendrites. Our results showed that SMF-treatment has neurite-elongation effect for the NGF-induced PC-12 cells. The population of PC-12 cells with more than four branching dendrites for SMF treated group is $100 \pm 0\%$ which is significantly larger ($p < 0.05$) than the analogous value of sham-exposed group (78.57 ± 10.38). In addition, for SMF exposed group, the population of PC-12 cells with a dendrite length longer than three-folds of the cell diameter is $61.06 \pm 6.36\%$. This value is also significantly larger ($p < 0.05$) than the sham-exposed cells (37.73 ± 7.89). These results indicate that SMF can affect neurogenerative process at neurite elongation stage. According to these findings, it is reasonable to suggest that static magnetic field has potential to become a useful non-invasive physical therapeutic tool for neural diseases.

Static Magnetic Files Affect Fibroblast Cell Proliferation via Changing the Binding Capability of Growth Factors and Their Receptors

Sheng-Yang Lee[1], **Kon-Shien Fan**[2], **Yuh-Yuan Shiau**[3, 4], **Wei-Jen Chang**[1], **and Haw-Ming Huang**[1]

[1]School of Dentistry, Taipei Medical University, Taipei,Taiwan
[2]Department of Dentistry, En-Chu Kong Hospital, Taipei Country, Taiwan
[3]School of Dentistry, National Taiwan University, Taipei, Taiwan
[4]School of Dentistry, China Medical University, Taichung, Taiwan
[5]Graduate Institute of Biomedical Materials and Engineering
Taipei Medical University, Taipei, Taiwan

Abstract— It was reported that static magnetic field (SMF) can increase the healing rate of burned skin. However, the mechanism of SMF on fibroblastic cell remains unclear. The aim of this study is to determine how the static magnet affects NIH-3T3 fibroblast cell. NIH3T3 cells were exposed to 0.4-T static magnetic fields. The cell cycle effects were tested by flow cytometry. The differentiation of the cells was assessed by detecting the changes in prostaglandin E2, osteocalcin, and extracellular matrix expression. Cell number assay was also conducted to test the effects of SMF on the proliferative activity of insulin-like growth factor-I (IGF-I), platelet-derived growth factor (PDGF), transforming growth factor-β (TGF-β). After 24 hr, there were significant differences in cell number comparing the 0.4-T SMF exposed and control groups ($p < 0.05$). The number of cell doublings for the former was also significantly lower than for the controls ($p < 0.05$). When PDGF was added to the serum-free medium, the number of 0.4 T SMF-exposed cells was 12.38% lower than without it. ($p < 0.05$). Results were similar in the IGF-I and TGF-β tests. The cell proliferation effects were also significantly decreased to 13.95% and 15.38% in the IGF-I and TGF-β tests, respectively ($p < 0.05$). According to these findings, it is reasonable to suggest that the interaction between SMF and cells may affect growth factor receptors. When the growth factors cannot bind to its receptor, the proliferation rates of the cells decrease. These effects may cause the cells to mature, which then, accelerate the wound healing.

Static Magnetic Fields Affect Red Blood Cells in Cryopreservation

Chun-Yen Lin[1], **Jen-Chang Yang**[2], **Wei-Jen Chang**[1], **Wan-Hong Lan**[3], **Sheng-Yang Lee**[1], **Yung-Kai Huang**[4], **and Haw-Ming Huang**[2]

[1]School of Dentistry, Taipei Medical University, Taipei, Taiwan
[2]Graduate Institute of Biomedical Materials and Engineering, Taipei Medical University, Taipei, Taiwan
[3]School of Dentistry, National Taiwan University, Taipei, Taiwan
[4]School of Oral Hygiene, Taipei Medical University, Taipei, Taiwan

Abstract— Since cell therapy has become an important treatment for various diseases, cryopreservation technology for biological cells frozen become a core issue for biomedical investigation. In this study, red blood cells (RBC) were frozen via a computer controlled programmed freezer. During the freezing process, the RBC samples were exposed to static magnetic fields up to 0.8 T which was supplied by a custom-designed chamber made with NdFeB permanent magnets. Before freezing process, glycerol 20% (w/v) was slowly added into the samples as a cryoprotectant. The cooling rate was set at -1°C/min and the finial temperature for cryopreservation is set at -80°C. After freezing for one day, the samples were thawing quickly in a 37°C water bath. Then, survival rate, morphology changes and biofunctions of the RBC samples were tested. Our results showed that the static magnetic field has a protective effect for RBC cryopreservation with a flux-intensity dependent manner. The mean hemolysis of 0.8 T-SMF exposed RBC samples is 9.03% lower than the sham-exposed analogue. The survival rate of the 0.8 T-SMF exposed RBC after thawing is 1.23-fold higher than that value of the sham-exposed controls. In addition, our data demonstrated freezing process combined with SMF exposure does not affect the RBC morphology and bio-functions of ATP and 2, 3-DPG. These results suggested that this technology has potential for low-temperature storage of blood sample.

Artifact Removal Algorithms for Microwave Imaging of the Breast

Martin O'Halloran, **Martin Glavin**, **and Edward Jones**
Electrical and Electronic Engineering, National University of Ireland, Galway, Ireland

Abstract— One of the most important components of any Confocal Microwave Imaging (CMI) system for breast cancer detection is the early-stage artifact removal algorithm. This early-stage artifact is composed of the incident pulse combined with the reflection from the skin-breast interface and residual antenna reverberation, and must be removed from the received signal at each antenna before further processing can take place. If the early-stage artifacts are not removed, they could potentially mask energy reflected from shallow tumors located close to the surface of the skin, and also hinder the identification of tumors located deeper within the breast.

Many existing artifact removal algorithms are based on variants of the assumption that the artifact in a particular channel can be estimated and effectively removed by creating a reference waveform. This reference waveform is typically based on the average of the artifact in all channels. The artifact in a particular channel is then removed by subtracting this reference waveform from the recorded signal. More sophisticated algorithms estimate the artifact in each channel as a filtered combination of all the artifacts, and have been shown to be more robust to normal variations in skin thickness. However, increased underlying dielectric heterogeneity, as highlighted by Lazebnik et al., could result in greater variation in the early-stage artifact, making the artifact removal process much more difficult. In this paper, several existing artifact removal are examined in this context of increased dielectric heterogeneity, and based on these results, suggestions for future work are discussed.

An Algorithm of Action Potential Duration Distribution with 3D Biventricular Heart Model

E. Ryzhii and M. Ryzhii
University of Aizu, Japan

Abstract— The distribution of M-cell regions within ventricular wall is not well determined. Experimental data suggest that M-cells are located in the layers with variable depth in the myocardium.

In this study we investigate the influence of different configurations of midmyocardial layer allocation on the action potential duration (APD) and surface electro-cardiogram (ECG). For this purpose we proposed an algorithm for APD spatial distribution and implemented it together with the combined ion-channel and 3D biventricular heart model to calculate body surface ECG.

Our simulations demonstrated that the thickness of M-cell layer affected in maximal and minimal APD within ventricular wall and also reflected in T-wave amplitude and QT interval on ECG increasing with the thickness of midmyocardial layer.

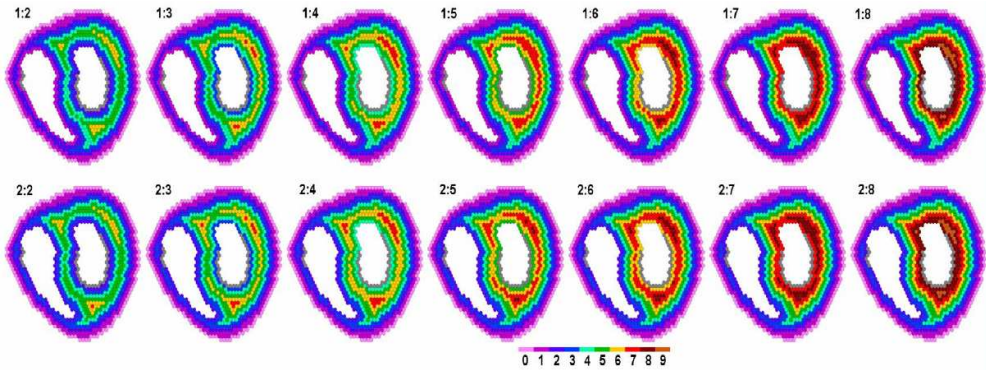

Figure 1: Distributions of cell layers with different APD for various moments of stimulation of right and left ventricular epicardium (RV : LV).

Influence of Weak Electromagnetic Fields on Cerebrovascular System of the Person

Yu. Ya. Varakin[1], **V. G. Ionova**[1], **G. V. Gornostaeva**[1], **E. A. Sazanova**[2, 3], **and N. P. Sergeenko**[2]

[1]Scientific Center of Neurology RAMS, Moscow, Russia
[2]Pushkov Institute of Terrestrial Magnetism, Ionosphere and Radio Wave Propagation RAS
Troitsk, Moscow Region, Russia
[3]Clinical Hospital of Russian Academy of Sciences, Troitsk, Moscow Region, Russia

Abstract— In recent decades it was accumulated many new facts indicating on effect of disturbances of a natural electromagnetic field on cerebrovascular system of the person, developing due to active processes at the Sun and in the Earth magnetosphere. In the article the statistical analysis of influence heliogeomagnetic factors on frequency of occurrence of strokes is presented. Data of the Moscow register of a stroke (1255 cases) including the population during the various periods of heliogeomagnetic activity were studied. The observation period included 730 days (2 years for 365 days). 334 days corresponded to quiet heliogeomagnetic background. During these days according to the register there were 342 strokes that corresponded on the average 1.02 strokes in a day. 112 days preceded development of the main phase of a geomagnetic storm. For this period there were 227 strokes that correspond 2.03 strokes in a day, i.e., twice more than in quiet days. 284 days corresponded to the active periods of geomagnetic storms. At this time there were 686 strokes — 2.41 strokes in a day. Frequency of cases of death from a stroke in quiet days was 0.37 in a day. In days before the beginning of a magnetic storm it increased to 0.90 in a day, and in a magnetic storm — to 1.01 cases.

Thus, during geomagnetic disturbances it is noted more than double, statistically significant increase in number of strokes and death rate. These effects can be caused by the occurrence of instability in a thrombocyte — vascular component of a hemostasis under the influence of physical processes during geomagnetic storms. This hypothesis which has been put forward by authors, has been confirmed by dynamics analysis of rheological parameters of human blood and catecholamines. It has been shown, that in the conditions of geomagnetic indignations:

- The most part of rheological parameters begin to fall outside the limits norm already before the beginning of a magnetic storm, the others — in day of the beginning of disturbances. In blood deterioration aggregation and deformation properties of erythrocytes is observed.
- Increased blood catecholamine concentration (adrenaline, noradrenalin, dofamin) is observed, and these changes is noted two days prior to a storm and remains during a storm.

The mentioned effects indicate to presence of direct influences of physical processes during indignations on blood cells and can be caused by:

- The influence of an electromagnetic field on cell membranes and the subsequent changes of their electric mobility that can impact on dynamics of process of aggregation — disaggregation of erythrocytes in a blood stream;
- The synchronisation of rhythms of electromagnetic fluctuations of cells of the central nervous system by external electromagnetic fields. In the process of development of the resonant phenomena as a result of stressful reaction there is an increase of catecholamine concentration in blood, that also increases activation of curtailing system.

Interpolation of 3D Magnetic Resonance Data

J. Mikulka[1], **E. Gescheidtova**[1], **and K. Bartusek**[2]

[1]Department of Theoretical and Experimental Electrical Engineering, Brno University of Technology
Kolejni 2906/4, 612 00 Brno, Czech Republic
[2]Institute of Scientific Instruments, Academy of Sciences of the Czech Republic
Kralovopolska 147, 612 64 Brno, Czech Republic

Abstract— This article deals with three-dimensional reconstruction methods of nuclear magnetic resonance images. The testing images were observed by tomography with basic magnetic field of 4.7 T at the Institute of Scientific Instruments (Academy of Sciences of the Czech Republic). There were acquired 20 slices of the testing phantom. There were found methods with the aim of getting utmost information about the shape of the testing phantom. One possible way is to increase the count of the sensed slices, but it implies decreasing of the signal to noise ratio. The second approach is finding the compromise between the effective count of slices and the following interpolation of other slices between the sensed ones. The both approaches were compared. There were used only 10 slices to compute the in-between others slices. It is better to use this approach because the computed slices can be compared with the real slices obtained by MR tomography. The results are described in the article. The images were interpolated in order to improve the following three dimensional model creation.

REFERENCES

1. Aubert, G. and P. Kornprobst, *Mathematical Problems in Image Processing: Partial Differential Equations and the Calculus of Variations*, 2nd Edition, 377, Springer Science + Business Media, LLC, New York, 2006, ISBN 0-387-32200-0.
2. Mikulka, J. and K. Bartusek, "3D reconstruction in magnetic resonance imaging," *PIERS Online*, Vol. 6, No. 7, 617–620, 2010.
3. Gonzales, R. C., R. E. Woods, and S. L. Eddins, *Digital Image Processing Using Matlab*, Gatesmark Publishing, 2009, ISBN 978-0-9820854-0-0.

Homogeneous Phantom Model vs. Visible Human Dataset: Impact on MRI-induced Heating of Metal Implants

Eugenio Mattei, **Giovanni Calcagnini**, **Federica Censi**, **Michele Triventi**, **and Pietro Bartolini**
Department of Technology and Health, Italian National Institute of Health, Roma, Italy

Abstract— Today, Magnetic Resonance Imaging (MRI) is strongly contraindicated for people with metal implants, such as a pacemaker or an implantable cardioverter/defibrillator. However, given the rapid expansion of technology in the fields of both MRI and device arrhythmia management, there is increasing interest in the issue of implantable device safety in the MRI environment. Considering the impressive progress in the use of diamagnetic material, the most important safety problem associated with MRI and medical implantable devices is the potential tissue heating induced by the radiofrequency (RF) fields. A large body of excellent work has been published in the past few years dealing with MRI induced heating of various kind of metallic implants. The majority of these works have used in vitro phantoms to characterize interaction with the RF fields and highlight the technical difficulty of the experimental assessment of the compatibility of implantable devices with MRI units. In this field, computational techniques represent a favorable choice for the evaluation of implantable devices with the MRI environment.

In this paper, numerical simulations were performed to evaluate the Specific Absorption Rate (SAR) induced at the tip of a pacemaker lead by the radiofrequency field used in MRI procedures (SEMCAD X, Speag). A realistic 34-tissue human model (Visible Human Dataset — VHD, ITIS Foundation) was used and both right and left pectoral implant locations were reproduced. The local SAR pattern computed for the VHD was then compared to the one of a homogeneous human-shaped phantom, a wide used numerical phantom, since it reproduces the in-vitro experimental set-up adopted for MRI safety studies. The local SAR at the pacemaker lead tip was −11.3% for the right implant and +0.3% for the left one in the homogeneous phantom, compared to the complete VHD. Other simplification of the HVD, in terms of anatomical structures modelling, were also studied. In particular, a homogeneous phantom with inside just the air cavities (lungs, trachea, upper airways, stomach and intestine lumens) and a homogenous phantom with inside the heart, the blood and the blood vessels. These partial simplifications of the complete VHD gave less accurate results than the fully homogeneous phantom. In particular, when air cavities are modelled inside the human trunk phantom, a significant overestimation of the local SAR induced at the lead tip was observed (+60.2% for the right implant and +136.0% for the left one, compared the complete VHD).

In conclusions, we showed that a homogeneous phantom with constant dielectric properties represents a reliable simplification of the anatomical structure of human body tissues, in the evaluation of the RF induced local heating on metallic implants. Partial simplifications of the complete VHD generally give less accurate results. This finding suggests that in the design of human trunk phantoms for experimental measurements of RF induced SAR, homogeneous gel-filled phantom with dielectric properties chosen as the weighted average of those of human body tissues, represents a suitable choice.

Design and Fabrication of Planar Magnetoinductive Resonator Arrays for MRI System Field Shaping

P. Drexler, **D. Nespor**, **P. Fiala**, **R. Kubasek**, **and K. Bartusek**
Department of Theoretical and Experimental Electrical Engineering
Brno University of Technology, Kolejni 2906/4, 612 00 Brno, Czech Republic

Abstract— A possibility of manipulation of magnetic field distribution in magnetic resonance (MR) systems has been shown in recent works [1]. Some approaches consider this phenomenon as a subwavelength imaging which can be observed with metamaterial slabs [2]. The main goal of manipulation of magnetic field distribution in MR systems is to increase the received MR signal which is a response to radiofrequency sample excitation. A suitable shaped resonant device is placed in the MR system cavity close to the examined specimen. Coil radiated RF magnetic field pulse in the cavity excites the specimen nuclei in order to obtain the nuclei response. The resonant device affects the field distribution close to the specimen in order to increase the excitation field and response field in the area of the specimen. Published papers have show a significant signal level increasing and the image quality improvement in medical type of magnetic resonance imaging (MRI) system [3]. The resonant device is configured as two coupled arrays of planar capacitance loaded ring resonators.

For the application in the experimental MRI system we need to design a coupled resonator arrays with considerably smaller dimension, which is restricted by the tomograph cavity. Further, the operational frequency of the MR tomograph is $f \sim 200\,\mathrm{MHz}$, which is higher in compare to the medical type tomograph. In previous work [4] the theoretical approach to resonator arrays design has been presented. There has been presented some issues of the resonators fabrication and component selections. Early results have shown the need to careful resonators assembly. The suggested points of the design have been taken into the account in the next resonator arrays fabrication. The improved resonator arrays fabrication approach will be presented in the paper. There will bee shown the measured resonant characteristics of the arrays and the results of device application in the MR system will be shown also.

ACKNOWLEDGMENT

The work described in the paper was financially supported by the research project GA102/09/0314, research plan MSM 0021630513 and project of the BUT Grant Agency FEKT-S-10-13.

REFERENCES

1. Wiltshire, M. C. K., J. V. Hajnal, J. B. Pendry, D. J. Edwards, and C. J. Stevens, "Metamaterial endoscope for magnetic field transfer: Near field imaging with magnetic wires," *Optic Express*, Vol. 11, No. 7, 2003.
2. Wiltshire, M. C. K., J. B. Pendry, and J. V. Hajnal, "Sub-wavelength imaging at radio frequency," *Journal of Physics: Condensed Matter*, Vol. 18, No. 22, 2006.
3. Freire, M. J., R. Marques, L. Jelinek, and V. Delgado, "Potential applications of a $\mu = -1$ metamaterial superlens for magnetic resonance imaging," *Proceedings of 3rd International Congress on Advanced Electromagnetic Materials in Microwaves and Optics*, 138–140, London, UK, 2009.
4. Bartusek, K., P. Drexler, P. Fiala, R. Kadlec, and R. Kubasek, "Magnetoinductive lens for experimental mid-field MR tomograph," *PIERS Online*, Vol. 6, No. 7, 621–624, 2010.

Measurement of Concentration and Mobility Spectrum of Air Ions in the Natural Environment

Z. Roubal[1], **K. Bartušek**[2], **Z. Szabó**[1], **and P. Drexler**[1]

[1]Department of Theoretical and Experimental Electrical Engineering, Brno University of Technology
Kolejní 2906/4, Brno 612 00, Czech Republic
[2]Institute of Scientific Instruments, Academy of Sciences of the Czech Republic
Kralovopolska 147, Brno 612 64, Czech Republic

Abstract— It was confirmed that concentration of light air ions has positive influence on the human health. For objective appraisal of the influence of synthetic sources of negative air ions the comparison with natural environment is necessary. The concentration of air ions and their mobility spectrum can be found out by aspiration condenser. When measure with the condenser, the spectrum mobility can be calculated from measured saturation characteristics. It will be discussed the most advantageous approximation of saturation characteristics from point of view of minimal numeric error. The saturation characteristic approximation will be made in Matlab. Using this method, the comparison of air ion spectra in various environments will be done, as natural deciduous forest, coniferous forest, meadow, contaminated industrial environment on one side and generated by synthetic source of negative air ions on the other side.

ACKNOWLEDGMENT

The work described in the paper was financially supported by the research project GA102/09/0314, research plan MSM 0021630513 and project of the BUT Grant Agency FEKT-S-10-13.

REFERENCES

1. Charry, J. M. and R. Kavet, *Air Ions: Physical and Biological Aspects*, CRC Press, Inc., Boca Raton, Florida, 1987.
2. Kondrashova, M. N., E. V. Grigigorreko, A. N. Tikhonov, T. V. Sirota, A. V. Temnov, I. G. Stavrovskaya, N. I. Kosyakova, N. V. Lange, and V. P. Tikonov, "The primary physic-ochemical mechanism for the beneficia biological/medical effects of negative air ions," *IEEE Trans. Plasma Scien.*, Vol. 28, No. 1, 230–237, 2000.
3. Vojtek, T., T. Skoupil, P. Fiala, and K. Bartušek, "Accuracy of air ion field measurement," *PIERS Online*, Vol. 2, No. 4, 412–415, 2006.
4. Steinbauer, M., P. Fiala, K. Bartušek, and Z. Szabó, "Experiments with accuracy of air ion field measurement," *PIERS Proceedings*, 1062–1066, Hangzhou, China, March 24–28, 2008.
5. Roubal, Z. and M. Steinbauer, "Design of electrometric amplifier for aspiration condenser measurement," *PIERS Proceedings*, 1430–1434, Xian, China, March 22–26, 2010.

Service Oriented Modular System for Modeling of the Human Body Stimulation

Robert Szmurło, **Bartosz Sawicki**, **Jacek Starzyński**, **and Stanisław Wincenciak**
Warsaw University of Technology, IETiSIP PW, ul. Koszykowa 75, Warsaw 00-661, Poland

Abstract— The paper presents a distributed system allowing quantitative evaluation of electric or magnetic stimulation of the organs or tissue on the basis of advanced, realistic numerical models of the electromagnetic field inside the human body.

The fundamental idea of the system is to be highly available to wide range of users — medical staff, designers of new stimulators, students, researchers, etc.. It is obtained by means of an internet-based service sending user's requests to a CUDA GPU accelerated computational cluster and delivering results of simulations to the client computers. The system is seen as the result *obtained as a service*.

The system is build of several components: the graphical user interface working on the client computer, the proxy server to which the clients can connect and the computational kernel build of several modules for preprocessing, numerical simulation [1] and postprocessing.

The graphical user frontend working on the client computer allows one to select the type of stimulation and its parameters and to build a parametric description of the personalized model of the stimulated body-part [2, 3]. These data are transferred to the computational center where simulations are carried out. Results of simulations are sent back to the client computer, where using the GUI a user can visualize and measure the quantitative results like energy absorbtion, stimulation efficiency, stimulation threshold levels and field quantities (electric and magnetic field intensity, flux density, etc.).

The paper will present the technical architecture of the system and the algorithms for rapid creation of patient-specific model used for simulations. The latter is one of the most important innovations introduced in the system.

REFERENCES

1. Sawicki, B., et al., "Scalar potential applied to magnetic stimulation modelling," *Electrical Review*, Vol. 83, No. 7/8, 143–147, 2007.
2. Borysiak, M., Z. Krawczyk, J. Starzyński, and R. Szmurło, "Speeding up a guided stretching Mesh Morpher with GPGPU," *Proceedings of the Computational Problems of Electrical Engineering*, 82, 2010.
3. Starzyński, J. and R. Szmurło, "Specimen-specific finite element models of human head obtained with mesh morphing," *Electrical Review*, No. 4, 47–49, 2009.

White Light Reflexion near the Critical Angle for Refractive Index Dispersion Measurement

Celia Sanchez-Perez and Augusto Garcia-Valenzuela
Centro de Ciencias Aplicadas y Desarrollo Tecnológico, Universidad Nacional Autónoma de México
Apartado Postal 70-186, México Distrito Federal 04510, México

Abstract— The refractive index of a material and its dispersion behavior are of special importance in several optical applications [1]. Many refractometric techniques have been developed to date for the measurement of the refractive index with hi resolution. Nevertheless, the determination of the dispersion of the refractive index requires different laser sources or a white light source with a monochromator, resulting in costly and time consuming systems [1, 2].

In this work, we describe a spectroscopic method for determining the refractive index dispersion of transparent and highly absorbing solutions. The method is based on the measurement of angular reflectance curves of a white light beam near the critical region defined by the refractive index of the prism and that of the solution to be characterized. The reflected beam is analyzed by a spectrophotometer so the reflectance can be obtained at many wavelengths within an angular range around the critical zone simultaneously; rendering an accurate and faster device than those already reported. The refractive index is calculated from the inflexion point of the reflectance curve near the critical angle for each wavelength within the spectral range of the white light lamp. The refractive index at each wavelength is obtained adjusting the complex Fresnel reflectance to the experimental data instead of calculating the inflexion point commonly used in critical angle refractometers also called process refractometers. We discuss the limitation coming from the use of an optical beam not a plane wave considered in Fresnel reflexion [3]. We present experimental results for Rhodamine 6G and methylene blue solutions.

REFERENCES

1. Eickhoff, M. L. and J. L. Hall, "Real-time precision refractometry: New approaches," *Appl. Opt.*, Vol. 36, No. 6, 1223–1234, 1997.
2. McClimans, M., C. LaPlante, D. Bonner, and S. Bali, "Real-time differential refractometry without interferometry at a sensitivity level of 10^{-6}," *Applied Optics*, Vol. 45, No. 25, 6477–6486, 2006.
3. Peña-Gomar, M. C. and A. Garcia-Valenzuela, "Reflectivity of a Gaussian beam near the critical angle with external optically absorbing media," *Appl. Opt.*, Vol. 39, No. 28, 5131–5137, 2000.

Cryogenic Technique for Cancer Destroying Optimalization

J. Hrozek and J. Mikulka
Department of Theoretical and Experimental Electrical Engineering, Brno University of Technology
Kolejni 2906/4, Brno 612 00, Czech Republic

Abstract— This paper deals with heat distribution in human tissues. The Bioheat equation is used for modelling of heat transfer in tissues. Software application Cryomodel is described in this paper. The Cryomodel is realized in Matlab software for simulation of cryosurgery operation. Simulation is realized in 3D space of tissue. The Cryomodel contains many adjustable parameters like: Temperature and diameter of cryoprobe and properties of tissue. The Cryomodel considers four layers of tissue and one centre of cancer. Layers of epidermis, dermis, subcutaneous fat and muscle for example. Optimization of cancer destroying is the main aim of this study. The Optimization is based on increasing of thermal conduction in cancer. This software application should be a good planning tool for doctors in practise.

ACKNOWLEDGMENT

The research described in the paper was financially supported by FRVS (a fund of university development) by research plan No. MSM 0021630513 ELCOM, No. MSM 0021630516, grant of Czech ministry of industry and trade No. FR-TI1/001, GACR 102/09/0314 and project of the BUT Grant Agency FEKT-S-10-13.

REFERENCES

1. Rabin, Y. and A. Shitzer, "Numerical solution of the multidimensional freezing problem during cryosurgery," *Journal of Biomechanical Engineering*, Vol. 120, No. 1, 32–37, 1998.
2. Polanka, M., "Technical experiment based inverse tasks in mechanics," *Vedoucí dizertační práce Doc. Ing. Miroslav Raudenský*, 141, CSc, 2006.
3. Akay, M., *Biomedical Engineering*, Vols. 1 and 5, John Wiley and Sons, Hoboken, 2006, ISBN-13: 978-0-471-24967-2.
4. Schmid, G., et al., "Bestimmung der expositionsverteilung von HF feldern im menschlichen Köper, unter Berüksichtigung kleiner strukturen und thermophysiologisch relevanter parameter," *Bundesamtes fur Stratenschutz 38201*, 129, ARC-IT-0174, Salzgitter, Deutschland, 2008.
5. Habif, T. P., *Clinical Dermatology: A Color Guide to Diagnosis and Therapy*, 4th Edition, 78, 816, 923–25, Mosby, London, 2004.

Image Reconstruction by EIT with Usage NMR

T. Kriz, J. Dedkova, and K. Bartusek
Department of Theoretical and Experimental Electrical Engineering, Brno University of Technology
Kolejni 2906/4, Brno 612 00, Czech Republic

Abstract— This paper presents a conductivity reconstruction inside an investigated sample. Here is described using of the standard Electrical Impedance Tomography (EIT) with added complementary data from Nuclear Magnetic Resonance (NMR) measurement of a sample to an inner conductivity reconstruction. Standard EIT use a set of voltage measurements is acquired from the boundaries of an investigated volume, whilst this is subjected to a sequence of low-frequency current patterns. In principle, measuring both the amplitude and the phase angle of the voltage can result in images of the electric conductivity and permittivity in the interior of a body. Alternating current patterns are preferred to DC to avoid polarization effects. In the usual frequency range (below 1 MHz) the field can be considered a steady current field, which is governed by the Laplace equation. An image reconstruction of EIT is an inverse problem, which is usually presented as minimizing the suitable objective function $\Psi(\sigma)$ relative to conductivity σ. To minimize the objective function $\Psi(\sigma)$ we often use a deterministic approach based on the Least Squares method. To solve the inverse EIT problem the standard Tikhonov regularization method has to be used because of the ill-posed nature of the problem. So it is necessary to minimize the objective function $\Psi(\sigma)$

$$\Psi(\sigma) = \frac{1}{2}\sum \|U_{\mathrm{M}} - U_{\mathrm{FEM}}(\sigma)\|^2 + \alpha\|L\sigma\|^2.$$

Here σ is the unknown conductivity distribution vector in the object, U_{M} is the vector of measured voltages on the object boundary, $U_{\mathrm{FEM}}(\sigma)$ is the vector of computed peripheral voltages in respect to σ which can be obtained using the FEM, α is a regularization parameter and L is a regularization matrix connecting adjacent elements of the different conductivities. The basic principle of NMR is the interaction between nucleus of an atom place in a static magnetic field B_0 and the hf magnetic field B_1 which have frequency near nuclear spin frequency. Nucleus of an atom radian frequency is direct proportional to a static magnetic field B_0

$$\omega = \gamma B_0.$$

Here ω is Larmor's frequency, γ is the gyro magnetic ration of spins and B_0 is static magnetic field. The 2D numerical model will used for a conductivity reconstruction. The current source will appended to the sample for measurement by NMR. A current that flows in a conductive sample creates a magnetic field that is measured by NMR. Magnetic field can be measured at each parts of a sample by NMR. Measured magnetic field can by convert to current density. The current density is use for EIT reconstruction as complementary data. If we use complementary data from NMR measurement at each of parts of a sample we can obtain better results (higher quality of reconstructed conductivity image) than if we use these describe methods separated.

ACKNOWLEDGMENT

The research described in the paper was financially supported by the project of the BUT Grant Agency FEKT-S-10-13.

REFERENCES

1. Vladingerbroek, M. T. and J. A. Den Boer, *Magnetic Resonance Imaging*, Springer-Verlag, Heidelberg, Germany, 1999, ISBN 3-540-64877-1.
2. Borsic, A., "Regularization methods for imaging from electrical measurement," Ph.D. Thesis, Oxford Brookes University, 2002.
3. Ziya Ider, Y. and O. Birgul, "Use of the magnetic feld generated by the internal distribution of injected currents for electrical impedance tomography (MR-EIT)," *Elektrik*, Vol. 6, No. 3, 1998.

Utilization of Boundary Conditions in MR Image Reconstruction

K. Ostanina, J. Dedkova, and T. Kriz
Department of Theoretical and Experimental Electrical Engineering, Brno University of Technology
Kolejni 2906/4, Brno 612 00, Czech Republic

Abstract— This article discusses two-dimensional reconstruction of the internal conductivity distribution for a tissues imaging of the human head and for the determination of corresponding brain tissue changes with the help of the Magnetic Resonance Electrical Impedance Tomography (MREIT) method. MREIT is a bio-imaging modality providing cross-sectional conductivity images with a high spatial resolution from measurements of internal magnetic flux densities produced by externally injected currents.

The new algorithm for the image conductivity reconstruction, which uses the internal current vector information with respect to corresponding boundary conditions, was developed. This algorithm was applied to the several computer simulations to demonstrate the feasibility, and to assess the performance of the proposed MREIT algorithm in estimating head tissue conductivity values. Obtained conductivity reconstruction results will be presented and compared with reconstruction results, which were obtained after applying algorithm based on the combination of the Tikhonov Regularization method and the Level Set technique. All reconstruction process properties will be also discussed.

ACKNOWLEDGMENT

The research described in the paper was financially supported by the project of the BUT Grant Agency FEKT-S-10-13.

REFERENCES

1. Kwon, O., J.-Y. Lee, and J.-R. Yoon, "Equipotential line method for magnetic resonance electrical impedance tomography," *Inverse Problems*, Vol. 18, 1–12, 2002.
2. Zhang, X., D. Yan, S. Zhu, and B. He, "Noninvasive imaging of head-brain conductivity profiles," *IEEE Engineering in Medicine and Biology Magazine*, Vol. 27, No. 5, 78–83, 2008.
3. Jeon, K., C.-O. Lee, E. J. Woo, H. J. Kim, and J. K. Seo, "MREIT conductivity imaging based on the local harmonic Bz algorithm: Animal experiments," *J. Phys.: Conf. Ser.*, IOP Publishing, 2010.

The Vagarious Dispersive Behavior in a Magnetically Uniaxial Metamaterial around the Plasma Frequency

Dexin Ye[1], **Shan Qiao**[2], **Jiangtao Huangfu**[1], **and Lixin Ran**[1]

[1]Department of Information and Electronic Engineering, Zhejiang University, Hangzhou 310027, China
[2]Zhejiang University City College, Hangzhou 310015, China

Abstract— Dispersion relationship describes the electromagnetic (EM) characteristics of a medium at different frequencies, and the group velocity and phase velocity of an EM wave are the most important physical quantities characterizing the dispersion. For most inartificial material, the phase velocity and group velocity are positive and are always lower than c, c is the speed of light in free space. Whereas, we also know that the phase velocity can be faster than c without violating any known physical laws, for example, in a plasma medium with a relative permeability $1-\omega_p^2/\omega^2$, the phase velocity will be large than c when the frequency is larger and approaching to ω_p, where ω_p is known as the plasma frequency. Meanwhile, the group velocity also can be superluminal or negative in the region of anomalous dispersion, such as in a magnetically uniaxial metamaterial. We focus on the vagarious group velocity in an anisotropic metamaterial, whose permeability along its optical axis exhibits a plasma-like frequency dependence at a certain microwave frequency band.

In this letter, the dispersive behavior around the plasma frequency in a magnetically uniaxial metamaterial is investigated. We show by theoretical analysis, parameter retrieval and simulation that when material loss is considered and the EM wave is oblique incidence, the negative group velocity of electromagnetic wave will be observed. Since the proposed magnetically uniaxial metamaterial can be constructed in the GHz frequency easily, the abnormal group velocity will be experimentally validated in the future, which provide an alternative way to the investigation of the abnormal group velocity.

A Novel Preconditioner Based on CSL Operator for Solving the Helmholtz Equations

Yue Hui Li[1, 2], **Zai-Ping Nie**[1], **Xiang Qian Zhang**[1], **and Xiang Yang Sun**[1]

[1]School of Electronic Engineering, UESTC, Chengdu, Sichuan 610054, China
[2]School of Mathematics and Computer Engineering, Xihua University, Chengdu 610039, China

Abstract— A novel preconditioner followed by the conjugate orthogonal conjugate gradient (COCG) iterative method is proposed for solving the large complex symmetric and highly indefinite systems of linear equations, which resulting from the Helmholtz equation discretized by edge-based finite element method (FEM). The proposed preconditioner is based on the complex shifted Laplace (CSL) operator and the modified AINV algorithm (MAINV), which derived from the basic AINV process with pivots compensation to avoid the breakdowns. Numerical tests on 3D waveguide discontinuity problem demonstrate the effectiveness of the proposed preconditioner,by comparison with other conventional onditioners.

The Characteristics of 116 Ore Belt in the Shihu Gold Deposit of Western Hebei — Based on the EH-4, China

Liu Yang, **Songling Chen**, **Tagen Dai**, **and Haiyang Zou**
School of Geosciences and Environmental Engineering, Central South University
Changsha, Hunan 410083, China

Abstract— This paper studies the ore controlling law and metallogenic law of depth and margin of 116 ore belt in Shihu Gold Deposit based on the methods combining geological and geophysics, and submit a new prospecting targets, providing the basis for further geological exploration. It also provides guidance both theoretical and practical by studying the 116 ore belt in Shihu gold deposit geological features, geochemistry, genesis and metallogenic regularity, to the edge of Shihu gold prospecting prediction of deep, but also the production tried to explore the resource crisis mines how quickly and effectively search for known blind ore bodies of deep vein edge. EH4 is widely used in solid minerals, especially in finding concealed ore deposit. In this paper, the author adopted EH-4 method to make a synthetic study on 116 ore belt in Shihu gold deposit of western Hebei. The result showed that the geophysical method was quite useful in the exploration of concealed ore deposit.

Application of EH4 in the Yuquanling Iron Deposit of Hebei, China

Liu Yang[1], **Songling Chen**[1], **Tagen Dai**[1], **Haiyang Zou**[1], **and Chaozhuang Xi**[2]

[1]School of Geosciences and Environmental Engineering, Central South University
Changsha, Hunan 410083, China
[2]Hunan Jinxin Gold Group Co., Ltd., Changsha, Hunan 410007, China

Abstract— Yuquanling iron deposit is under the administrative divisions of Wuji town of Wuan city in Hebei Province. The authors have reached the conclusion that the iron ore bearing horizon is the middle of Ordovician limestone, magmatic rocks in this area is for acid diorite, along with invasive structural vulnerability. EH4 is widely used in solid minerals, especially in finding concealed ore deposit. In this paper, the author adopted EH4 method to make a synthetic study on Yuquanling iron deposit in Hebei. The result showed that the geophysical method was quite useful in the exploration of concealed ore deposit.

Application of EH4 in the II Forecast Area of Yushiwa Iron Mine of Hanxing Area, China

Gaofeng Du, **Tagen Dai**, **and Liu Yang**
School of Geosciences and Environmental Engineering, Central South University
Changsha, Hunan 410083, China

Abstract— Yushiwa iron mine is under the administrative divisions of Xixu town of She city in Hebei Province. The authors have reached the conclusion that the iron ore bearing horizon is the middle of Ordovician limestone, magmatic rocks in this area is for acid diorite, along with invasive structural vulnerability. EH4 is widely used in solid minerals, especially in finding concealed ore deposit. In this paper, the author adopted EH-4 method to make a synthetic study on the II forecast area of Yushiwa iron deposit in Hanxing area.The result showed that the geophysical method was quite useful in the exploration of concealed ore deposit.

Validity of Image Theorems under Spherical Geometry

Shaolin Liao[1], **Sasan Bakhtiari**[1], **and Henry Soekmadji**[2]

[1]Argonne National Laboratory, USA
[2]Hamilton Sundstrand, USA

Abstract— This paper deals with different image theorems, i.e., Love's equivalence principle, the induction equivalence principle and the physical optics equivalence principle, in the spherical geometry. The deviation of image theorems approximation is quantified by comparing the modal expansion coefficients between the electromagnetic field obtained from the image approximation and the exact electromagnetic field for the spherical geometry. Two different methods, i.e., the vector potential method through the spherical addition theorem and the dyadic Green's function method, are used to do the analysis. Applications of this work include metal mirror design and other electrically-large object scattering.

A Novel and Simple Analytical Method for Analysis of AMC and EBG Properties of Lossless Artificial Impedance Surfaces

Mohsen Fallah, **Farrokh H. Kashani**, **and S. H. Mohseni Armaki**
Iran University of Science and Technology (IUST), Tehran, Iran

Abstract— In this paper, a novel and simple analytical method for analysis of AMC and EBG properties of a typical lossless artificial impedance surface (AIS) is investigated. The main contribution of the paper is to demonstrate that AMC and EBG behaviors of an artificial impedance surface can be characterized analytically with using reflection coefficient for both TE and TM polarized oblique incidence plane waves. It is shown that the AMC properties (when the reflection phase varies in between +90 and −90 degrees) of an impedance surface can be obtained from reflection phase and EBG properties (stop bands for TE and TM surface wave modes) from poles of reflection coefficient. We have derived closed analytical formulas for the impedance surface and reflection coefficient for TE and TM waves for two conventional impedance surfaces such as: grounded dielectric slab and grounded dielectric slab with embedded metallic vias (wired media). The analytical results are verified with numerical simulations.

Introduction: Artificial impedance surfaces have been extensively investigated and proposed as ground planes for many active and passive planar microwave circuits and antennas during the last decade. Nearly all of the articles about high impedance surfaces (HISs) [1], Frequency selective surfaces (FSSs) [2], electromagnetic bandgap (EBG or PBG) structures [3], reactive impedance surfaces (RISs) [4], Artificial magnetic conductors (AMCs) [5] and etc, are examples of artificial impedance surfaces.

In this paper, it is presented that the electromagnetic properties of AISs such as AMC and EBG can be achieved analytically from reflection coefficient for TE and TM polarized oblique incidence plane waves. When incident plane wave is a propagating wave, AMC characteristics can be achieved from the phase of reflection coefficients of TE and TM modes. On the other hand, when incident plane wave is an evanescent wave (exponentially decaying from the surface), poles of reflection coefficient for TE and TM waves represents the surface wave modes. Indeed, dispersion characteristics of the surface wave modes are obtained by equating the denominator of reflection coefficient to zero [6]. As a result, analytical formulas for reflection coefficients of TE and TM modes are necessary and sufficient to AMC and EBG characterization of impedance surface.

To validate our analytical model, accurate analytical formulas for two conventional AISs (grounded dielectric slab and grounded dielectric slab with embedded metallic vias) are extracted and compared with numerical results.

REFERENCES

1. Sievenpiper, D., L. Zhang, R. J. Broas, and N. G. Alexopolous, "High-impedance electromagnetic surfaces with a forbidden frequency band," *IEEE Trans. on MTT*, Vol. 49, No. 11, 1999.
2. Monoricho, A., G. Manara, and L. Lanuzza, "Synthesis of artificial magnetic conductors by using multilayerd FSS," *IEEE Antenna and Wireless Prop. Letters*, Vol. 1, No. 11, 2002.
3. Yang, F. and Y. Rahmat Samii, "Microstrip antennas integrated with EBG structures: A low mutual coupling design for array applications," *IEEE Trans. AP*, Vol. 51, No. 10, 2003.
4. Mosallaei, H. and K. Sarabandi, "Antenna miniaturization and bandwidth enhancement using a reactive impedance substrate," *IEEE Trans. AP*, Vol. 52, No. 9, 2004.
5. Luukkonen, O., C. R. Simovski, and S. A. Tretyakov, "Grounded uniaxial material slabs as magnetic conductors," *Progress In Electromagnetics Research B*, Vol. 15, 267–283, 2009.
6. Silveirinha, M. G., C. A. Fernandes, and J. R. Costa, "Electromagnetic characterization of textured surfaces formed by metallic pins," *IEEE Trans. AP*, Vol. 56, No. 2, 2008.
7. Luukkonen, O., M. G. Silveirinha, and A. B. Yakovlev, "Effects of spatial dispersion on reflection from mushroom-type artificial impedance surfaces," *IEEE Trans. MTT*, Vol. 57, No. 11, 2009.

Investigation of the Metallic Cavity Influence on the Electromagnetic Behavior of the Setup Used in Studying the Ratchet Effect

D. Medhat[1,2], **A. Takacs**[1,2], **H. Aubert**[1,2], **and J.-C. Portal**[2,3]

[1]LAAS, CNRS, 7 Avenue du Colonel Roche, F-31077 Toulouse, France
[2]University of Toulouse, UPS, INSA, INP, ISAE, LAAS, F-31077 Toulouse, France
[3]LNCMI, CNRS, BP 166, F-38042, Grenoble, Cedex 9, France

Abstract— Ratchet effect [1] has been recently proven in a high mobility two-dimensional electron gas system, based on a semiconductor heterojunction sample with a periodic array of asymmetric semi-discs shaped antidots. The sample has been illuminated by a microwave source and a directed electron motion can be obtained, under some conditions, at low temperature. As a result, an induced photovoltage of few mV is generated and measured between the sample extremities. A simplified simulation model of the experimental setup used was created using full-wave Ansoft HFSS software. This model helped us to calculate three descriptors [2–4]; the uniformity of the linear polarization of the incident microwave electric field, the uniformity of the incident power density and the amount of the electromagnetic incident power on the semiconductor sample surface, which clarify the behavior of the system. These descriptors were computed when the model was surrounded by a vacuum box with radiation boundaries approximating thus the free space. Actually, a cryogenic system is used and the sample is not totally exposed to free space, as simulated before, but it is surrounded by a metallic cavity to keep it at low temperature. Therefore, to be closer to the real case, the setup has to be simulated with the presence of this cavity. Our aim is to compare the simulation results of the model with and without cavity in order to investigate its influence on the three descriptors and hence on the generated voltage.

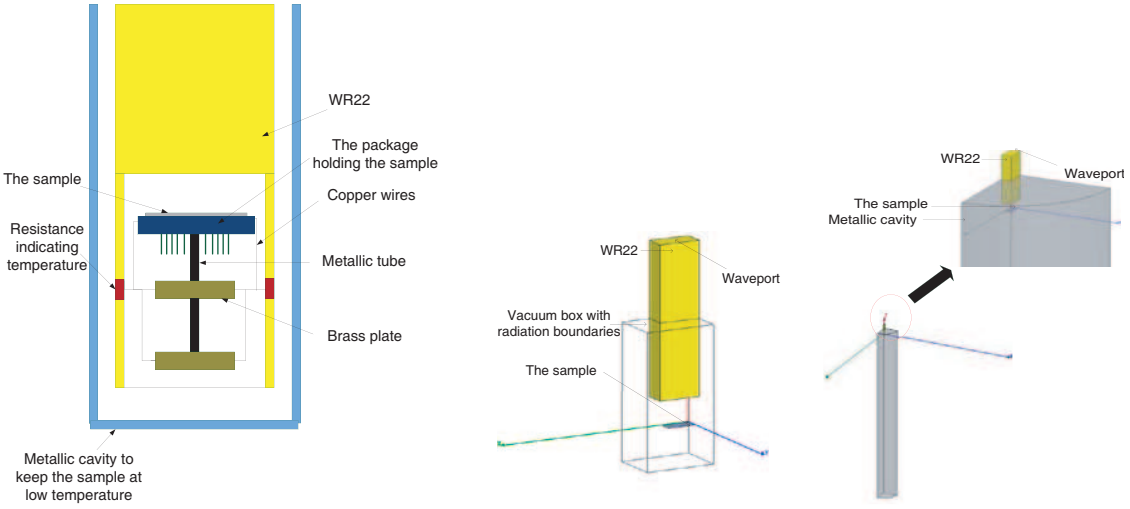

Figure 1: (a) Schema of the detailed experimental setup used to measure the photovoltage at low temperature; (b) simplified simulation model of the setup with the vacuum box (left) and with the metallic cavity (right).

REFERENCES

1. Sassine, S., Yu. Krupko, J.-C. Portal, Z. D. Kvon, R. Murali, K. P. Martin, G. Hill, and A. D. Wieck, "Experimental investigation of the ratchet effect in a two-dimensional electron system with broken spatial inversion symmetry," *Phys. Rev. B*, Vol. 78, No. 4, 54311–54315, Jul. 2008.
2. Takacs, A., D. Medhat, H. Aubert, and J. C. Portal, "Electromagnetic analysis of the experimental setup used to investigate the ratchet effect in two-dimensional electron system under microwave radiation," *Proceedings of CAS'2009*, Vol. I, 337–340, Oct. 2009.

3. Medhat, D., A. Takacs, H. Aubert, and J.-C. Portal, "Comparative analysis of different techniques for controlling ratchet effect in a periodic array of asymmetric antidots," *Proceedings of APMC'2009*, 1711–1714, Dec. 2009.
4. Takacs, A., D. Medhat, H. Aubert, and J.-C. Portal, "A method for estimating the electromagnetic power delivered by the front-end module used to investigate the ratchet effect in two-dimensional electron gas system under microwave radiation," Sep. 2010, Accepted at EuMC'2010.

Synthesis of Electromagnetic Sources by Reversed-TLM Method

A. Ungureanu, **T. P. Vuong**, **and F. Ndagijimana**
IMEP-LAHC, 3 Parvis Louis Néel, Grenoble, France

Abstract— Traditional methods for radiating electromagnetic structure design typically begin by defining the architecture of the source distribution. Iterative procedure is then developed to ensure that the design process converges to an optimal solution. Even if performance of such techniques in the frequency domain is good, convergent procedure is not efficient in the time domain.

The main advantage of time-domain methods and of the TLM (Transmission-Line Matrix) method in particular consists in the possibility of working with transient phenomena, which is essential in characterizing the radiation behavior of wide-band structures, especially when innovative radiating architectures are required. Therefore, our purpose is to introduce an innovative algorithm for source synthesis by *reversed*-TLM method.

Our new algorithm based on 3-D wave retro-propagation, permits the reconstruction of an unknown source distribution from its far-field radiation. Despite the fact that the solution to inverse problems is not unique, we are proving the feasibility of this method under some circumstances. Thus, some a *priori* information about the solution of the initial inverse problem is added. Knowledge of the initial transmitted waveform transforms the initial ill-posed problem in a well-posed one with a unique and steady solution. We develop a two-step reversed approach to determine the position and the dimensions of the sources from measured- or theoretically-computed far-field values. Following Huygens's principle, the knowledge of the radiated field on a closed surface surrounding the sources is sufficient to recreate the field inside the entire volume. We exploit this method as follows.

In a first step, the sampled values of the desired radiated field are injected in the 3-D TLM network, in a plane-parallel surface enclosing the volume supposed to contain the sources. In order to create the proper wave recomposition during the time-reversed process, the excitation of the TLM nodes in the external surfaces needs delay compensation. This first step gives a coarse determination of the source distribution. The spatial resolution depends on the transmitted signal wavelength, via the well known diffraction-limit. The second step is almost identical to the first one, the difference being that a reversed version of the initial signal is excited in the sources probable position as well. The addition of this reversed excitation, during the second step of the method, in order to ameliorate the resolution, can be explained by using wave-field formalism.

Our method is first applied to lumped wide band sources, in the frequency range [26 GHz–34 GHz], placed in a lossless, homogeneous and non-dispersive 3-D free-space. Results show that by using this method, the "classical" resolution limit of $\lambda/2$ is solved.

These encouraging results let us conclude that the reversed-TLM method may provide a useful and important new tool in the electromagnetic source synthesis.

Full Wave Analysis of Finite Uniform Metallic Grid FSS under Oblique Incidence Using Scale Changing Technique

Euloge B. Tchikaya[1,2], **Farooq A. Tahir**[1,2], **and Hervé Aubert**[1,2]

[1]CNRS, LAAS, 7 avenue du colonel Roche, F-31077 Toulouse, France
[2]UPS, INSA, INP, ISAE, LAAS, Université de Toulouse, F-31077 Toulouse, France

Abstract— The accurate prediction of the plane wave scattering by finite size arrays is of great practical interest in the design and optimization of modern frequency selective surfaces, reflectarrays and transmittarrays. A complete full-wave analysis of these structures demands enormous computational resources due to their large electrical dimensions which would require prohibitively large number of unknowns to be resolved. Thus the unavailability of efficient and accurate design tools for these applications limits the engineers with the choice of low performance simplistic designs that do not require enormous amount of memory and processing resources. The electromagnetic simulation of large and complex planar structures with fine-scale patterns by conventional numerical methods based on a spatial meshing (finite element method, finite difference method, method of moments) leads often to poorly conditioned matrices, numerical convergence problems or/and excessive computation time. In order to overcome the above-mentioned theoretical and practical difficulties, an original monolithic formulation for the electromagnetic modeling of multi-scale planar structures has been proposed [1]. The power of this technique called the *Scale-changing Technique (SCT)* comes from the modular nature of its problem formulation. Instead of modeling the whole planar-surface as a single large discontinuity problem, it is split into a set of many small discontinuity problems each of which can be solved independently using modematching variational methods [2]. Each of the sub-domain discontinuity solution can be expressed in the matrix form characterizing a multiport-network called *Scale-Changing Network* (SCN). SCT models the whole structure by interconnecting all scale-changing networks, where each network models the electromagnetic coupling between adjacent scale levels. The scale-changing networks are calculated independent of each other and are cascaded only at the final step to obtain the complete solution. Therefore SCT effectively computes a complex problem by scaling it in many simpler problems than can be solved independently. This leads to smaller sized matrices with much better condition numbers which translates to a significant reduction in terms of computational time and memory space as compared to conventional numerical methods that use linear meshing over the complete discontinuity plane.

In this communication, Scale Changing Technique has been applied for Full Wave Analysis of Finite Uniform Metallic Grid FSS Under Oblique Incidence Using Scale Changing Technique (Fig. 1(a)). Modeling of these structures is performed using SCT and Ansoft HFSS®. An excellent agreement between the HFSS- and SCT-results can be observed.

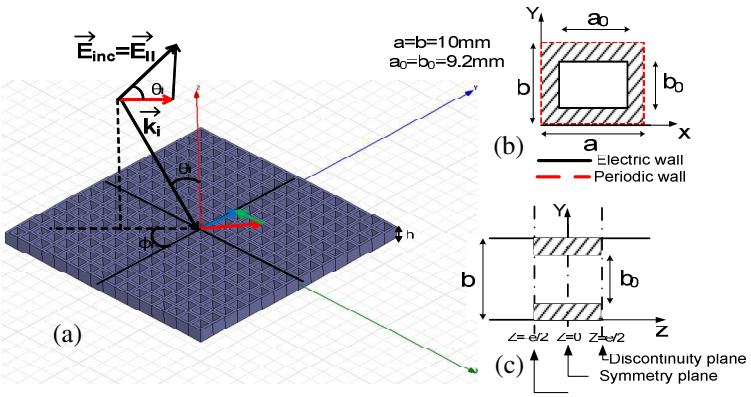

Figure 1: (a) Finite Frequency selective surface. (b) Cross section of the elementary cell. (c) Side-view of the cell (all the cells present the same thickness h).

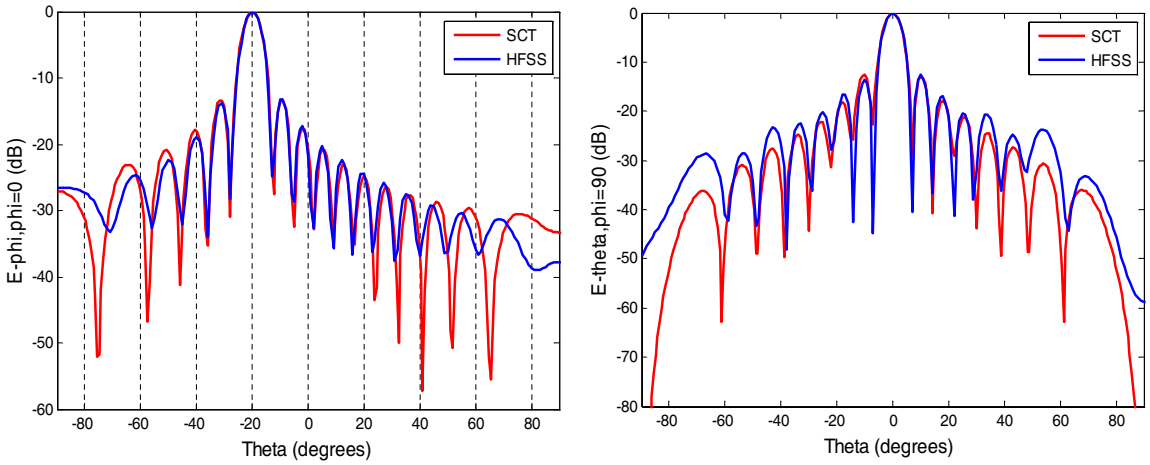

Figure 2: Co-polarization in (a) H-plane, and (b) E-plane @ 20 GHz ($\theta = 20°$, $\varphi = 0$).

REFERENCES

1. Aubert, H., "The concept of scale-changing network in the global electromagnetic simulation of complex structures," *Progress In Electromagnetics Research B*, Vol. 16, 127–154, 2009.
2. Tao, J. W. and H. Baudrand, "Multimodal variational analysis of uniaxial waveguide discontinuities," *IEEE Transactions on Microwave Theory and Techniques*, Vol. 39, No. 3, 506–516, March 1991.

A Study of the VLF Electric Field Spectra in Titan's Atmosphere Using TLM Method

S. Toledo-Redondo[1], **J. A. Morente**[2], **A. Salinas**[1], **J. A. Portí**[2], **E. A. Navarro**[3], **A. Méndez**[2], **and J. F. Fornieles**[1]

[1]Dpto. de Electromagnetismo y Física de la Materia. Universidad de Granada, Granada 18071, Spain
[2]Dpto. de Física Aplicada, Facultad de Ciencias, Universidad de Granada, Granada 18071, Spain
[3]Dpto. de Física Aplicada, Universidad de Valencia, Burjassot, Valencia 46100, Spain

Abstract— A study of the VLF electric field spectra in the Titan's atmosphere is carried out using the Transmission Line Matrix (TLM) method. As observed on the Earth, solar photons and galactic cosmic rays penetrating the upper layers of Titan's atmospheres increase the ionization and contribute to forming an electrical conductivity profile that, starting from low values near the surface, rises with altitude and generates an electromagnetic cavity for waves propagating in the ELF-VLF range. Due to high losses conferred by the electrical conductivity to Titan's atmosphere, the direct numerical and experimental spectra are decreasing functions of the frequency without resonances or other special forms. However, a procedure based on analysis of the late-time response extracts the expected VLF modes with successive peaks and a mean between adjacent resonances of 0.68 kHz, in agreement with the late-time analysis of the experimental measurements sent by Huygens probe, when the conductivity profile with aerosols is introduced in the numerical model.

Dielectric Properties of Semiconducting YBaCuO Thin Films for Future Uncooled THz Bolometers: Characterization Using a Coaxial-discontinuity Technique

Aurélie Gensbittel[1], **Alireza Banisadr**[1], **Olivier Dubrunfaut**[1], **Jean-Claude Badot**[2], **Alain Kreisler**[1], **and Annick Degardin**[1]

[1]Laboratoire de génie électrique de Paris
SUPELEC/LGEP; CNRS/UMR 8507; UPMC Univ. Paris 06; Univ. Paris-Sud 11
11 rue Joliot Curie, 91192 GIF SUR YVETTE Cedex, France
[2]Laboratoire de Chimie de la Matière Condensée de Paris (CNRS-UMR 7574)
Chimie-Paris Tech., 11 rue P. et M.Curie, 75231 Paris Cedex 05, France

Abstract— The material properties of $YBa_2Cu_3O_{\delta-7}$ (YBCO) vary with the oxygen content. The compound is superconducting at $\delta < 0.5$ and becomes semi-conductor at lower oxygen ratio ($0.6 < \delta \leq 1$) [1]. The temperature coefficient of resistance (TCR) of semiconducting YBCO ($TCR : (1/R)(dR/dT)$) is about 3 to $4\% \cdot \mathrm{K}^{-1}$ [1]. The TCR value is higher than that of semiconductor materials commonly used for infrared detection, such as VO_x ($2\% \cdot \mathrm{K}^{-1}$) and amorphous SiH ($2.5\% \cdot \mathrm{K}^{-1}$). Moreover, this material can be deposited at low temperature on different substrates including silicon, allowing the integration of the YBCO thermal detector to a reading circuit based on silicon CMOS technology.

This makes YBCO semiconducting an ideal candidate for the development of bolometers in the region of infrared and THz wave (500 GHz to 5 THz) [2]. These thermal detectors are studied in this frequency range for imaging applications in biomedical, civil security or quality control in industry. Our team has developed a first demonstrator THz imager consisting of a $2 * 2$ matrix of semiconductor bolometers in YBCO [2]. To understand pyroelectric effect of YBCO films, optimize the geometry of the system and increase sensitivity, better knowledge of dielectric and thermal characteristics of the material is necessary.

Hence, we performed the dielectric characterization of semiconducting YBCO thin films using a coaxial discontinuity technique. The characterizations were made in the frequency range 4 Hz–2 GHz and the temperature range 213 to 428 K. The material to be measured (substrate +film) is inserted into the cell between the inner conductor of the coaxial line and a short circuit. The principle is to relate discontinuity S-parameters caused by the cell containing the sample to material's constitutive parameters [3]. The complex relative dielectric permittivity $\varepsilon = \varepsilon' - i\varepsilon''$, real part ε' and complex part ε'', is computed from the admittance $Y = G + iB$, which is determined from the measurement of the reflection coefficient. The thin films of YBCO were deposited by off-axis DC magnetron sputtering. Deposition was made at 100°C under atmosphere of argon and oxygen on MgO single crystal substrates [1].

At all temperatures, the real part ε' of the dielectric permittivity as well as the imaginary part ε'' decrease with increasing frequency. ε' reaches a stable value around 1000 after 1 MHz, that is a typical value for YBCO semiconducting films [4]. Inflexions in the dielectric spectra indicate a dielectric relaxation in the material. We used the Debye model and the decomposition procedure of Nyquist diagram for complex permittivity (ε'' vs ε') to determine the relaxation frequency. The relaxation frequency f_{rel} increases with increasing temperature: f_{rel} evolves from 836 Hz at 228 K to 660 kHz at 428 K the 800 nm thick YBCO film. This dielectric relaxation may be associated with the presence of grains in the material and the time constant characterizing the dipole orientation of these grains. The presence of grains in our thin films of YBCO semiconductors has been shown by the characterization of atomic force microscope (AFM). The evolution of f_{rel} with the temperature follows an Arrhenius' law. The associated activation energy is 0.26 eV for the 800 nm thick YBCO film.

Another dielectric relaxation appears at low frequency for temperatures higher than 330 K. f_{rel} increases from 529 Hz at 330 K to 7.18 kHz at 428 K. This relaxation could be attributed to interfaces effects in the sample. The interfacial polarisation due to grain boundaries could give rise to relaxation in this low frequency domain.

REFERENCES

1. Longhin, M., A. J. Kreisler, and A. F. Degardin, *Materials Science Forum*, Vol. 587–588, 273–277, 2008.

2. Jagtap, V. S., A. F. Dégardin, M. Longhin, M. Aurino, and A. J. Kreisler, *Proc. SPIE*, Vol. 7117, 71170P, 2008.
3. Belhadj-Tahar, N., O. Meyer, and A. Fourrier-Lamer, *IEEE Trans. on Microwave Theory and Tech.*, Vol. 45, No. 2, 260–267, 1997.
4. Gray, J. E., Z. Çelik-Butler, D. P. Butler, and A. Jahanzeb, *Ferroelectrics*, Vol. 209, No. 1, 517–539, 1998.

Rapid Idea of Located Defects on Grounding Systems

Moussa Lefouili[1], **Kamel Kerroum**[2],
Khalil El Khamlichi Drissi[2], **and Vesna Arnautovski-Tosera**[2, 3]

[1]LAMEL Laboratory, University of Jijel, B.P. 98 Ouled Aissa, Jijel 18000, Algeria
[2]LASMEA Laboratory, Blaise Pascal University, 24 Avenue des Landais, Aubière 63177, France
[3]Electrical Engineering and IT, University Ss. Cyril and Methodius, Skopje, Macedonia

Abstract— The principal task of such grounding systems is to ensure the safety of personnel and prevent damage of installations and equipment. Defect on grounding systems may cause operation error, malfunction and destruction of components in electric and electronic systems connected to the grounding systems. As a consequence, electromagnetic compatibility (EMC) studies require the knowledge of the grounding systems performance.

For modeling the transient behavior of grounding system, the most rigorous methods is electromagnetic field approach, because it solves full Maxwell's equations with minimum approximations.

This method can be implemented either by Method of moment (MoM) [1, 2] or by Finite Element Method (FEM) [3]. However, their methods are more complicated to understand, because they are not directly solving the Maxwell's equations and they are too complex to be implemented [4]. Further, when the grounding structure is large, the computation time is very large. Another disadvantage of electromagnetic field approach is that, because of its frequency domain solution procedure, it cannot be easily modified to include non-linearity.

The injection of a transient current on the wire grid radiates electromagnetic fields at the surface. For modeling transient behavior grounding systems, instead of using complex method, we prefer an approach that summarizes each of three methods [5, 6]: analytical formula, based on electrical dipole theory for determining radiated magnetic field in infinite conductive medium, modified images theory for taking into account the interface in the half space, and transmission line approach for determining the longitudinal and leakage currents.

This study gives an original way to have a rapid idea of the position of the located defects on grounding systems. For determining electromagnetic fields' radiation, we use an easy method, based on: analytical formula; transmission line theory; and modified images theory, instead of complex method of Summerfield's integrals. The cartography of the electromagnetic fields radiated at the interface soil-air, by energized grounding systems (electrode or grid), can be used to detect and localize a defect on this systems. This model is aimed to help in electromagnetic compatibility (EMC) and lightning protection studies.

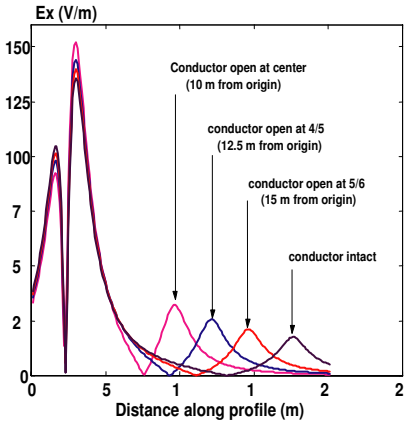

Figure 1: Electric Field radiated by Electrode (simple injection).

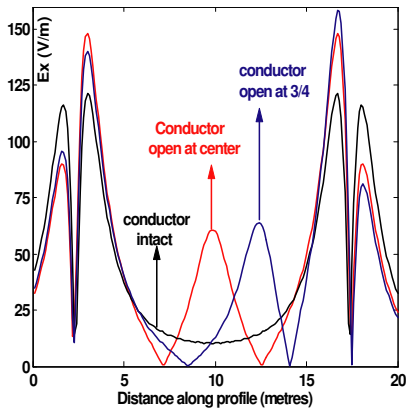

Figure 2: Electric Field radiated by electrode (double injection).

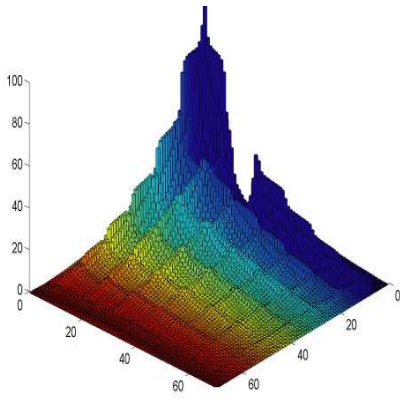

Figure 3: Magnetic Field radiated by Buried grid.

REFERENCES

1. Grcev, L. and F. Dawalibi, "Electromagnetic model for transients in grounding systems," *IEEE Transactions on Power Delivery*, Vol. 5, 1773–1781, 1990.

2. Grcev, L. D., "Computer analysis of transient voltages in large grounding systems," *IEEE Transactions on Power Delivery*, Vol. 11, No. 2, April 1996.
3. Brunotte, X., G. Meunier, and J. P. Imhoff, "Finite element solution of unbounded problems using transformation: A rigorous powerful and easy solution," *IEEE Transactions on Magnetic*, Vol. 25, No. 2, 1970–1975, March 1992.
4. Liu, Y., N. Theethay, and R. Thottappillil, "An engineering model for transient analysis of grounding systems under lightning strikes: non uniform transmission-line approach," *IEEE Transactions on Power Delivery*, Vol. 20, No. 2, 722–730, April 2003.
5. Lefouili, M., B. Nekhoul, B. Harrat, K. Kerroum, and K. E. K. Drissi, "Transient EM fields generated by buried conductor," *International Review of Electrical Engineering (IREE)*, Vol. 1, No. 1, Praise Worthy Prise, Marsh, April 2006.
6. Lefouili, M., B. Nekhoul, B. Harrat, K. Kerroum, and K. E. K. Drissi, "Detection et localisation par rayonnement électromagnétique d'un défaut sur une électrode enterrée," *Revue Internationale de Génie Electrique (RIGE)*, Vol. 9, No. 2–3, 2006.

Model to Predict Losses in the Permanent Magnets for Dynamic Applications

Z. Belli, **I. Boutana**, **and M. R. Mekideche**
Laboratoire d'études et de modélisation en électrotechnique (LAMEL)
Université de Jijel, Algérie

Abstract— Rare earth permanent magnets are very sensitive to temperature as an overheating can lead to a partial or a total demagnetization. It is then necessary to determine the losses in the permanent magnets to design with accuracy an electromagnetic system. The dynamic behaviour of permanent magnets can be easily studied through a simple model witch consist to replace the magnet by a conductor bulk verifying Ohm's law. The validity of the model was improved in several previous works [1].

In this paper, we applied this model in the context of finite element method to estimate loses in permanent synchronous machine.

REFERENCES

1. Benabou, A., S. Georges, and S. Clenet, "Permanent magnet modelling for dynamic applications," *Journal of Magnetism and Magnetic Materials*, 830–835, 2008.

Analytical Model of TeraHertz Frequency Voltage Noise in Schottky-barrier Diodes and Heterostructure Barrier Varactors

F. Z. Mahi[1], **L. Varani**[2], **P. Shiktorov**[3], **E. Starikov**[3], **and V. Gruzhinskis**[3]

[1]Physics of Semiconductor Devices Laboratory (LPDS), University of Bechar, Algeria
[2]Institute of Electronics of the South (IES, CNRS UMR 5214), University of Montpellier II, France
[3]Semiconductor Physics Institute, Vilnius, Lithuania

Abstract— One of the most important electronic devices used in terahertz systems as frequency multipliers is the Schottky-barrier diode (SBD) and the heterostructure barrier Varactor (HBV). The physical property at the basis of the frequency multiplication is a strongly nonlinear current-voltage and/or capacitance-voltage characteristics, which is typical of nanometric GaAs SBD [1]. On the other hand, the HBV is a unipolar device presenting a symmetric capacity-voltage and an asymmetric current-voltage characteristics [2], which lead to produce only odd harmonics compared to the SBD. Under high frequency large signal operation, the intrinsic current noise constitutes a critical limit for the extraction of the high-order harmonics at the basis of terahertz generation. This intrinsic noise is described by the spectrum of current fluctuations which has been recently investigated using an analytical model [1]. To extract the high-order harmonics generated, we consider the SBD or HBV operating in series with a parallel output resonant circuit when a high-frequency large-signal voltage is applied [3].

In this contribution we present a critical analysis and an extension of this analytical model for the calculation of the spectral densities of current and voltage fluctuations in SBD as well as HBV which enables to interpret the different resonances appearing in the terahertz frequency region.

REFERENCES

1. Shiktorov, P., E. Starikov, V. Gruzinskis, L. Reggiani, L. Varani, and J. C. Vaissiere, "Analytical model of high-frequency noise spectrum in Schottky-barrier diodes," *IEEE Electron Dev. Letters*, Vol. 26, No. 1, 2–4, 2005.
2. Melique, X., C. Mann, P. Mounaix, J. Thornton, O. Vanbesien, F. Mollot, and D. Lippens, "5-mW and 5% efficiency 216 GHz InP-based heterostucture barrier varactor tripler," *IEEE Microwave and Guided Wave Letters*, Vol. 8, No. 11, 384–386, 1998.
3. Shiktorov, P., E. Starikov, V. Gruzinskis, S. Pérez, T. Gonzàlez, L. Reggiani, L. Varani, and J. C. Vaissière, "Theoretical ivestigation of Schottky-brrier diode noise performance in external resonant circuits," *Semicond. Sci. Technol.*, Vol. 21, 550–557, 2006.

Application of EH4 in the Zhayaoku Area of Fushan Iron Mine of Hebei, China

Gaofeng Du, **Tagen Dai**, **and Liu Yang**
School of Geosciences and Environmental Engineering, Central South University
Changsha, Hunan 410083, China

Abstract— Fushan iron mine is under the administrative divisions of Xixu town of She city in Hebei Province. The authors have reached the conclusion that the iron ore bearing horizon is the middle of Ordovician limestone, magmatic rocks in this area is for acid diorite, along with invasive structural vulnerability. EH4 is widely used in solid minerals, especially in finding concealed ore deposit. In this paper, the author adopted EH4 method to make a synthetic study on the Zhayaoku area of Fushan iron deposit in Hebei.The result showed that the geophysical method was quite useful in the exploration of concealed ore deposit.

Terahertz Current and Voltage Noise in Nanometric Schottky-barrier Diodes

A. H. Mahi[1], **F. Z. Mahi**[1], **and L. Varani**[2]

[1]Physics of Semiconductor Devices Laboratory (LPDS), University of Bechar, Algeria
[2]Institute of Electronics of the South (IES, CNRS UMR 5214), University of Montpellier, France

Abstract— Schottky-barrier diodes (SBD) are among the most efficient electronic devices used in terahertz systems as frequency multipliers. The physical property at the basis of the frequency multiplication is a strongly nonlinear current-voltage and/or capacitance-voltage characteristics, which is typical, for instance, of nanometric GaAs SBD [1].

Under high frequency large signal operation, the intrinsic cyclostationary current noise constitutes a critical limit for the extraction of the high-order harmonics at the basis of terahertz generation. This intrinsic noise is described by the spectrum of current fluctuations which has been recently investigated using an analytical model [1]. To extract the high-order harmonics generated by the SBD, we consider these devices operating in series with a parallel output resonant circuit when a high-frequency large-signal voltage is applied [2].

In this contribution we present a critical analysis and an extension of this analytical model for the calculation of the spectral densities of current and voltage fluctuations in SBD enables to interpret the different resonances appearing in the spectrum densities.

REFERENCES

1. Shiktorov, P., E. Starikov, V. Gruzinskis, L. Reggiani, L. Varani, and J. C. Vaissiere, *IEEE Electron Dev. Letters*, Vol. 26, NO. 1, 2, 2005.
2. Shiktorov, P., E. Starikov, V. Gruzinskis, S. Pérez, T. Gonzàlez, L. Reggiani, L. Varani and J. C. Vaissière, *Semicond. Sci. Technol.*, Vol. 21, 550, 2006.

A Set of New SDA Basis Functions with Strongly Decaying Properties

F. Z. Siabah, **M. Bouchaour**, **M. T. Benhabiles**, **and M. L. Riabi**
Laboratory of Electromagnetism and Telecommunications, University Mentouri
Route Ain-El-Bey, Constantine 25000, Algeria

Abstract— Four smooth pulses with a strongly decaying spectrum are investigated as piecewise basis functions suitable for the SDA analysis of open microstrip lines, such that the integral tail slow convergence problem is canceled. These pulses are the Raised Cosine and three original pulses called $G(x)$, $T(x)$, and $Q(x)$.

Beyond the construction of such pulses, the challenge was at the same time to fulfill all of the SDA requirements.

Furthermore, the proposed functions yield a continuous current density profile, as the first order discontinuity at the cell transitions, which is commonly called the stairs aspect, is reduced with no further curve fitting nor post-processing treatment, see Figure 2. We believe that these profiles restitute the most accurate current density ever obtained in the literature.

The SDA impedance matrix spectra are plotted in Figure 1 in Logarithmic real magnitude. The rooftop spectrum is shown for reference as the most decaying state-of-the-art SDA basis function.

Computational validation is held by reference to the canonical data from [1]. The basis functions introduced in the present work verify a secure threshold of integrals convergence for $(\alpha^2+\beta^2)^{1/2}$ below $360k_o$, whereas this bound is located above $460k_o$ for the rooftop pulse, keeping all parameters identical, see Table 1.

Table 1: Comparative computed data.

Basis Functions	Number of Cells	Computed ε_{eff}	Integration Bound $(\alpha^2+\beta^2)^{1/2}$
Ref. [1 — Table 2]	99	8. 8097	$466.95k_o$
Raised Cosine	31	8.8071	$270.75k_o$
$G(x)$	31	8.8086	$264.66k_o$
$T(x)$	31	8.8093	$257.02k_o$
$Q(x)$	31	8.8108	$356.27k_o$

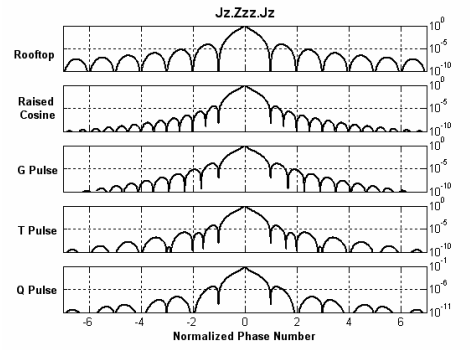

Figure 1.

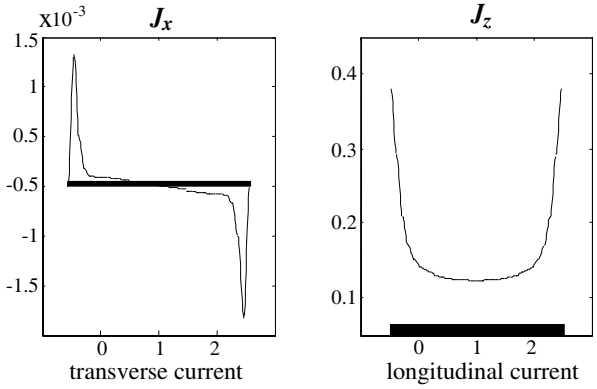

Figure 2.

REFERENCES

1. Coen, G., N. Faché, and D. De Zutter, "Comparison between two sets of basis functions for the current modeling in the galerkin spectral domain solution for microstrips," *IEEE Trans. MTT*, Vol. 42, No. 3, 505–513, March 1994.

Novel FDTD Method with Low Numerical Dispersion and Anisotropy

Xiang-Qian Zhang, **Zai-Ping Nie**, **Ming-Yao Xia**, **Shi-Wen Qu**, **and Yue-Hui Li**
School of Electronic Engineering, University of Electronic Science and Technology of China, China

Abstract— The numerical dispersion and stability analysis of the standard finite-difference time-domain (FDTD), six point lattice FDTD and high order FDTD (2, 4) are studied. A new FDTD method with low numerical dispersion and anisotropy are developed. The method of confirming the weighting factor and the optimal factor in this method are given. The numerical dispersion and anisotropy of the proposed method are studied. The amended method of the numerical dispersion of the proposed method and the amend factor are given. The numerical experiment shows that the numerical dispersion and anisotropy of the proposed method are greatly reduced and the accuracy of the FDTD method is improved greatly by using the proposed scheme.

Session 2P1
Instabilities and Solitons in Nonlinear Photonics: Part 2

Two-dimensional Cavity Polariton Solitons

F. Lederer[1], **O. Egorov**[1], **A. V. Yulin**[2], **and D. V. Skryabin**[2]

[1]Institute of Condensed Matter Theory and Optics, Friedrich-Schiller-Universität Jena, Germany
[2]Centre for Photonics and Photonic Materials, Department of Physics, University of Bath, United Kingdom

Abstract— While most of the recent experimental results and theoretical studies on wave localization have been dealing with optical or matter waves, there is a growing body of research on collective nonlinear dynamics of hybrid objects, i.e., half-light, half-matter exciton-polaritons in semiconductor microcavities [1]. Recently, the existence of moving 1D bright [2] and 2D dark solitons [3] have been studied in the context of cavity polaritons. It is essential for the bright polariton soliton existence that they have a sufficiently large momentum, so that the effective mass along the direction of motion may change sign and thus allows for the compensation of the exciton-exciton repulsion. The effective mass along the orthogonal direction remains positive and therefore the dispersive spreading of the 2D dimensonal polariton wavepacket in this direction is expected. However, recent experiments [4] addressing the superfluidity of cavity polaritons reported some evidence of a moving 2D cavity polariton localized object. In this presentation, we disclose the complex physics behind the formation of moving 2D cavity polariton solitons.

This is so far a unique example where the existence of self-localized states in a non-equilibrium (dissipative) optical or condensed matter system with opposite dispersion signs along the two orthogonal directions is supported experimentally and theoretically [5]. Our hypothesis is that parametric interaction can actually support the stable localization of cavity polaritons along the direction where the effective mass is negative. The coupled dynamics of the linearly polarized photon E and of the quantum well exciton Ψ field amplitudes is governed by the dimensionless system of equations [1, 2]

$$\begin{aligned} &\partial_t E - i(\partial_x^2 + \partial_y^2)E + (\gamma_{ph} - i\Delta)E = i\Psi + E_p e^{ik_p x}, \\ &\partial_t \Psi + (\gamma_{ex} - i\Delta)\Psi + i|\Psi|^2\Psi = iE, \end{aligned} \tag{1}$$

where E_p and k_p are amplitude and momentum of the external pump beam, respectively, and Δ is the detuning of the pump frequency from the identical exciton and cavity resonance frequency. Cavity and exciton damping constant are designated by $\gamma_{\rm ph}$ and $\gamma_{\rm ex}$, respectively. This system has been used for our numerical studies. The results support our hypothesis that two different nonlinear effects are required to evoke the formation of stable 2D cavity polarton solitons. Localization is promoted by the phase shifts generated by either the repulsive excitonic nonlinearity

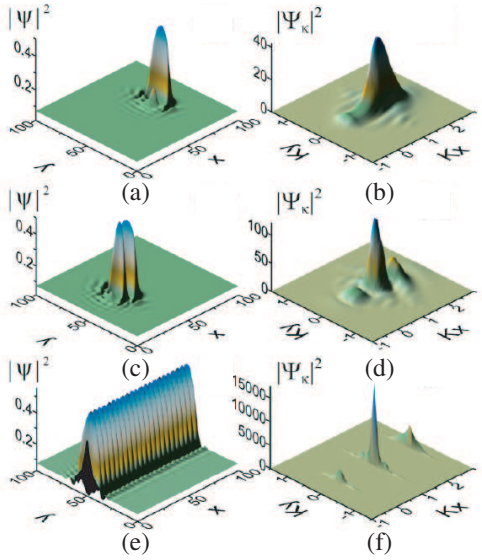

Figure 1: (a)–(c) Spatial and (d)–(f) spectral profiles of the excitonic components of stable bright polariton solitons. (a), (b), (d), (e) correspond to the single- and double-hump 2D solitons, whereas (c), (f) shows the parametric soliton localized only along the y coordinate.

(along x direction) or the parametric 4-wave mixing (along y direction). Fig. 1 shows both the spatial and spectral profiles of stable single and double hump 2D solitons. Moreover, in Fig. 1 the localization in y is demonstrated due to parametric interaction as proved by the respective spectrum (Fig. 1(f)). These results imply that, indeed, the parametric process promotes localization of polaritons along the direction with a positive effective mass.

REFERENCES

1. Kavokin, A., et al., *Microcavities*, Oxford University Press, 2007.
2. Egorov, O. A., et al., *Phys. Rev. Lett.*, Vol. 102, 153904, 2009.
3. Yulin, A. V., et al., *Phys. Rev. A*, Vol. 78, 061801, 2008.
4. Amo, A., et al., *Nature*, Vol. 457, 291, 2009.
5. Egorov, O. A., et al., *Phys. Rev. Lett.*, Vol. 105, 073903, 2010.

Chromatic Dispersion Slope Strongly Impacts Parametric Gain in Birefringent Photonic Crystal Fibers

S. Coulibaly[1], **Z. Liu**[1], **M. Taki**[1], **and G. P. Agrawal**[2]

[1]Laboratoire de Physique des Lasers, Atomes et Molécules, CNRS UMR 8523
Centre d'Etudes et de Recherches Lasers et Applications, Université des Sciences et Technologies de Lille
59655 Villeneuve d'Ascq Cedex, France
[2]The Institute of Optics, University of Rochester, Rochester, New York 14627, USA

Abstract— When a continuous-wave optical field propagates inside an ideal optical fiber (whose two orthogonally polarized modes are degenerate), it exhibits an modulational instability (MI) such that small amplitude perturbations at well-defined frequencies grow exponentially [1] provided the fiber provides anomalous group-velocity dispersion (GVD). In practice, this simplification of ideal fiber results from random changes in the magnitude and the orientation of modal birefringence. In especially designed photonic crystal fibers, the built-in birefringence can be made much larger than random birefringence variations, and one must consider the vectorial nature of wave propagation in such strongly birefringent fibers. In this case, the copropagating orthogonally polarized fields are found to exhibit the MI in both cases of normal and anomalous GVD [1].

The previous work on vectorial MI treats it as an absolute instability. We have recently shown that the inclusion of third-order dispersion (TOD) renders MI to be convective for pulses perturbations even in the scalar case [2]. Here, we investigate the effects of the third-order dispersion (TOD) on the polarization MI in a birefringent optical fiber and reveal the convective nature of MI for localized perturbations. In the linear regime, we have computed the output polarization state for an input Gaussian-shape perturbation near the maximum of the MI gain curve. We show that the MI gain decreases when the magnitude of TOD increases. This diminution increases with the frequency separation between the input perturbation and that of the maximum of the MI gain. We also report that the output signal displays a linear chirp which is proportional to the TOD magnitude. These predictions are in a very good agreement with full numerical simulations.

REFERENCES

1. Agrawal, G. P., *Nonlinear Fiber Optics*, 4th Edition, Academic Press, Boston, 2007.
2. Mussot, A., A. Kudlinski, E. Louvergneaux, M. Kolobov, and M. Taki, "Impact of the third-order dispersion on the modulation instability gain of pulsed signals," *Opt. Lett.*, Vol. 35, 1194–1196, 2010.

Multimode Localized Structures Far from Equilibrium

Ehud Meron
Institute for Dryland Environmental Research, BIDR & Physics Department
Ben-Gurion University, Sede Boqer Campus, 84990, Israel

Abstract— Localized spatial structures, such as defects in periodic patterns, fronts and vortices, are ubiquitous in non-equilibrium systems. Understanding the mechanisms by which they form, their stability and how to manipulate them, is significant for exploiting them in technological applications.

A localized structure may involve a single mode, e.g., a spiral wave in an oscillating medium (showcasing a Hopf mode), but quite often richer structures appear. This is particularly true when a system is driven far from thermal equilibrium and the number of growing modes increases. The system may still be governed by a single dominant mode that damps all other modes by means of nonlinear mode coupling. However, localized structures of the dominant mode, where its amplitude vanishes or becomes sufficiently small, can host the hidden damped mode, giving rise to multimode structures.

We studied structures of this kind in systems that go through dual instabilities, such as Hopf-Turing and cusp-Hopf instabilities. Among our findings are defect lines acting as self-organized wave-guides for traveling pulses and dual-mode spiral waves, which can destabilize to form a novel form of spatio-temporal chaos.

REFERENCES

1. Lampert, A. and E. Meron, "Localized structures as spatial hosts for unstable modes," *Europhys. Lett.*, Vol. 78, 14002(1–5), 2007.
2. Mau, Y., A. Hagberg, and E. Meron, "Dual-mode spiral vortices," *Phys. Rev. E*, Vol. 80, 065203R, 2009.

Light Propagation and Localization in Modulated Optical Waveguides

Yuri S. Kivshar
Nonlinear Physics Centre, Research School of Physics and Engineering
Australian National University, Canberra, 0200 ACT, Australia

Abstract— Photonic structures with a periodic modulation of the optical refractive index open many novel possibilities for engineering the fundamental aspects of optical wave dynamics. The physics of light propagation in periodic photonic structures is governed by the scattering of waves from the high refractive index regions and the subsequent interference of the scattered waves. This is a resonant process, which is sensitive to both frequency and propagation angle. As such, periodic photonic structures find various applications, including spatial beam control and manipulation of beam refraction and diffraction. These applications, however, are primarily optimized for beam shaping and deflection in a narrow-frequency range. In many practical cases, including ultra-broad bandwidth optical communications or propagation of ultra-short (sub-10 fs) pulses, the bandwidth of optical signals can span over a wide frequency range.

In this talk, we will overview our recent theoretical and experimental results on the tunable control of the supercontinuum light beams by employing photonic lattices. In particular, we report on the experimental observation of higher-order and mixed dynamic localization resonances in both one- and two-dimensional photonic lattices. New features such as spectral broadening of the dynamic localization resonances and localization-induced transformation of the lattice symmetry are demonstrated. These phenomena could be used to shape polychromatic beams emitted by supercontinuum light sources.

Our results demonstrate novel fundamental features of the effect of dynamic localization based on higher-order and mixed resonances in one- and two-dimensional lattices. Polychromatic dynamic localization and localization-induced transformation of lattice geometry, which we observe for the first time to our knowledge, open up new avenues for applications of the dynamic localization effect in various physical contexts. In particular, our work suggests new approaches for flexible shaping of polychromatic light with ultrabroadband or supercontinuum spectra, which can be enhanced further through the introduction of structure tunability and optical nonlinearities.

Impact of Light Polarization and Optical Feedback on Spatially Localized Structures in Vertical-cavity Surface-emitting Lasers

Krassimir Panajotov[1,2], **Xavier Hachair**[1], **Giovanna Tissoni**[3], **and Mustapha Tlidi**[4]

[1]1Department of Applied Physics and Photonics (IR-TONA)
Vrije Unversiteit Brussels, Pleinlaan 2, B-1050 Brussels, Belgium
[2]Institute of Solid State Physics, 72 Tzarigradsko Chaussee Blvd., Sofia 1784, Bulgaria
[3]INFM-CNR and CNISM, Dipartimento di Fisica e Matematica
Università dell'Insubria, Via Valleggio 11, Como 22100, Italy
[4]Optique Nonlinéaire Théorique, Université Libre de Bruxelles (U.L.B.)
CP 231, Campus Plaine, B-1050 Bruxelles, Belgium

Abstract— Broad area Vertical-Cavity Surface-Emitting Lasers (VCSELs) are most suitable for studying and utilizing Cavity Solitons (CS), i.e., localized spots of light in the transverse plane of a broad area nonlinear cavity or laser. Typically the VCSEL diameter is d∼150–200 μm in order to guarantee an independence on the transverse boundaries. In medium size VCSELs (d∼40–50 μm) emission of a single high order mode or a combination of several such modes prevents the existence of localized structures. We however, demonstrate hereby that a spontaneous pattern and localized structures in the nonlasing, orthogonal linear polarization can still exist. Due to current crowding, the laser emission in medium size VCSELs starts at threshold in a linearly polarized "flower mode" concentrated at the laser aperture periphery. Introducing a holding beam with orthogonal liner polarization we observe localized structure in the center of the device in the orthogonal polarization while the VCSEL keeps lasing in the same flower-mode. We support theoretically our experimental findings using two different VCSEL models, which account for both polarization and spatial dynamics.

We next consider theoretically the impact of optical feedback on cavity soliton behaviour. To this aim we introduce a rate equation model describing broad area VCSELs subject to injection and to time-delayed optical feedback. We show that the inclusion of an external cavity affects dramatically the space-time behavior of this system by modifying the instability threshold as well as the wavelength of the turing instability. We show also that the delayed feedback is responsible for the appearance of traveling wave instability. Finally, we demonstrate that a single cavity soliton exhibits a spontaneous motion with a constant velocity.

An Exploration of Ring Semiconductor Lasers and Alternative Mechanisms for Localized Light Emission

S. Barland, **M. Dufay**, **and L. Gil**

INLN, Universite de Nice Sophia Antipolis
1361 route des lucioles, Valbonne 06560, France

Abstract— Localized structures in dissipative optical systems have been explored in a variety of configurations and several mechanisms leading to their stability and mutual independence have been disclosed. Among well established results, one can mention the formation of localized states when a liquid crystal light valve or a sodium vapor cell with optical feedback receives a coherent optical injection. Similarly, broad area semiconductor microcavities either in amplifying or absorbing configurations have been shown to support localized structures. In all of these cases, a phase reference is provided to the system by the injection of a coherent field.

More recently, several laser-like configurations have been explored and localized laser emission has been reported both theoretically and experimentally in a laser with frequency selective feedback and in a system of semiconductor lasers coupled in an absorber/amplifier configuration. Contrary to the previous cases, no phase reference exist in these systems.

The difference is important in several aspects, in particular when considering the interaction between localized structures. In presence of an injection beam in a sodium vapor for example, structures have been shown to interact (albeit preserving their stability and independence) via their exponentially decaying oscillatory tails, leading to a nonmonotonous force between them. In the case of a laser with staurable absorber, while experimental data remain scarce, numerical works often underline that localized states may detrimentally interact even at rather large distances via the wings of the spatial distribution of the field. In this case, the mechanism by which two distant structures can remain independent consists in the existence of a spatial region of zero amplitude of the optical field separating the two structures.

In the present contribution, we explore the possibility of generating localized states in a bistable ring laser. In this configuration, no phase reference exists and the two coexisting solutions of the plane wave problem, left-and right-travelling wave, both have nonvanishing amplitudes. We suggest the existence of sources and sinks of waves (a phenomenon previously observed in hydrodynamics) in a ring laser and we study the stability of pairs of such defects as a mechanism for the formation of localized states in a semiconductor ring laser.

Dark Localized Structures near the Zero-diffraction Regime of a Nonlinear Optical Cavity Containing a Left-handed Material

Pascal Kockaert[1], **Mustapha Tlidi**[1], **and Lendert Gelens**[2]

[1]OPERA-photonique, Université libre de Bruxelles (U.L.B.)
CP194/5, 50 Av. F.D. Roosevelt, B-1050 Brussels, Belgium
[2]Optique Nonlinéaire, Université Libre de Bruxelles (U.L.B.)
CP 231, Campus Plaine, B-1050 Brussels, Belgium
[3]Department of Applied Physics and Photonics (IR-TONA)
Vrije Universiteit Brussel (V.U.B.), Pleinlaan 2, B-1050 Brussels, Belgium

Abstract— Recent works on nonlinear optical cavities filled with both a left-handed and a right-handed material, have shown that it was possible to design a cavity with tunable diffraction [1]. The zerodiffraction regime in such systems is of particular interest as it would, in principle, remove all limits on the minimal size of patterns arising from the interplay between the nonlinear Kerr effect and the diffraction.

Infinitely small patterns would however correspond to an infinite energy density. A more complete description is therefore needed near the zero-diffraction regime. Such a model was proposed in [2], where the nonlinear dynamics in the optical cavity is described with the help of a Lugiato-Lefever equation with an additional bi-Laplacian term describing higher order diffraction effects. The imaginary part of the bi-Laplacian coefficient arises from the spatial dispersion of the left-handedmaterial, i.e., it disappears when the spatial dispersion is turned off.

In this work, we assume that the left-handed material belongs to the 4/mmm group symmetry, as the structure presented in [3], and we make use a homogeneous nonlocal model [4] to estimate the range of realistic values of the spatial dispersion coefficient. This allows to study the dynamics of the nonlocal nonlinear optical resonator near the zero-diffraction regime within a realistic range of parameters.

With the help of numerical simulations, we showed the existence of stable single and multiple 1-D and 2-D dark localized structures. We could also plot the snaking bifurcation diagram in the 1-D case. It is important to mention that the dark localized structures become unstable when the coefficients of the higher order diffraction terms are canceled.

REFERENCES

1. Kockaert, P., P. Tassin, G. Van der Sande, I. Veretennicoff, and M. Tlidi, "Negative diffraction pattern dynamics in nonlinear cavities with left-handed materials," *Phys. Rev. A*, Vol. 74, No. 3, 033822, September 2006.
2. Kockaert, P., P. Tassin, I. Veretennicoff, G. Van der Sande, and M. Tlidi, "Beyond the zero-diffraction regime in optical cavities with a left-handed material," *J. Opt. Soc. Am. B*, Vol. 26, No. 12, B148–B155, December 2009.
3. Ding, P., E. J. Liang, W. Q. Hu, L. Zhang, Q. Zhou, and Q. Z. Xue, "Numerical simulations of terahertz doublenegative metamaterial with isotropic-like fishnet structure," *Photonics and Nanostructures — Fundamentals and Applications*, Vol. 7, No. 2, 92–100, May 2009.
4. Ritschel, U. L. Wilets, J. J. Rehr, and M. Grabiak, "Non-local dielectric functions in classical electrostatics and QCD models," *Journal of Physics G: Nuclear and Particle Physics*, Vol. 18, No. 12, 1889, 1992.

Dynamical Behavior in the Complex Swift-Hohenberg Equation

Lendert Gelens[1] **and Edgar Knobloch**[2]

[1]Department of Applied Physics and Photonics, Vrije Universiteit Brussel
Pleinlaan 2, Brussel B-1050, Belgium
[2]Department of Physics, University of California, Berkeley, CA 94720, USA

Abstract— The complex Swift-Hohenberg equation (CSHE) models pattern formation arising from an oscillatory instability with a finite wavenumber at onset. More in particular, it can model pattern formation in lasers, optical parametric oscillators and photorefractive oscillators. In most of these examples a trivial spatially homogeneous state loses stability with increasing forcing but the instability saturates at small amplitude. Systems of this type are referred to as supercritical. In general, the resulting supercritical CSHE has complex coefficients and hence time-dependent solutions. In this work, we study the dynamical behavior in such a supercritical CSHE in one spatial dimension.

Firstly, before tackling the complete problem, we restrict attention to an important but special case of this equation, namely the case of *real coefficients*. This case admits stationary solutions and for large times these are the only persistent states of the system. Simulations of this equation in one spatial dimension reveal that much of the observed dynamics can be understood in terms of the properties of exact solutions of phase-winding type. With real coefficients these states take the form of time-independent spatial oscillations with a constant phase difference between the real and imaginary parts of the order parameter and may be unstable to a long-wave instability. Depending on parameters the evolution of this instability may or may not conserve phase. In the former case the system undergoes *slow coarsening* described by a Cahn-Hilliard equation; in the latter it undergoes repeated phase-slips leading either to a stable phase-winding state or to a faceted state consisting of an array of *frozen defects* connecting phase-winding states with equal and opposite phase. The transitions between these regimes are studied and their location in parameter space is determined.

Secondly, we consider the supercritical CSHE with *complex coefficients*, which admits timedependent solutions in the form of traveling waves. The properties of these waves are systematically analyzed and the more involved dynamics associated with sources and sinks of such waves are investigated numerically. A number of distinct dynamical regimes is identified.

REFERENCES

1. Gelens, L. and E. Knobloch, "Coarsening and frozen faceted structures in the supercritical complex Swift-Hohenberg equation," *Eur. Phys. J. D*, Vol. 59, 23–36, 2010.

Disorder and Phase-locking in a Cavity Soliton Laser

T. Ackemann[1], **N. Radwell**[1], **Y. Noblet**[1], **C. McIntyre**[1], **W. J. Firth**[1], **G.-L. Oppo**[1], **and P. Paulau**[2, 3]

[1]SUPA, Department of Physics, University of Strathclyde, Glasgow, Scotland, UK
[2]IFISC (CSIC-UIB), Campus Universitat Illes Balears, Palma de Mallorca, Spain
[3]Institute of Physics, NASB, Minsk, Belarus

Abstract— In a cavity soliton laser (CSL), a broad transverse area (transverse indicates the plane orthogonal to the cavity axis) is pumped in a marginally stable plano-planar cavity. Emission does not take place over the whole aperture but on filaments which are much smaller than the pumped aperture and which are stabilized by nonlinearities, in the simplest case by self-lensing. Hence they are referred to as laser cavity solitons (LCS) and were recently realized in semiconductor microcavities (see [1–3]). They represent small coherent emitters, or microlasers. As such their optical phase, location (spatial phase) and polarization (phase between x- and y-components) are undetermined [1] and can dynamically evolve [4, 5]. This is in strong contrast to coherently driven systems [6, 7], which show intriguing interaction behavior, but the phase is fixed by the driving. The interaction of propagating spatial solitons in conservative systems is known to be phase-sensitive and at the origin of a wealth of intriguing phenomena of spatial dynamics. However, here the phases are fixed by the launching conditions. Hence the CSL is expected to combine properties of both systems and to provide new features.

On the other hand, the fact that a self-sustained oscillator has the freedom to choose phase and frequency makes it vulnerable to spatial disorder and indeed LCS at different locations are typically found to be incoherent. Synchronization of nonlinear self-sustained oscillators via frequency and phase locking is a basic paradigm of Nonlinear Science and it seems to be a very interesting question to ask whether these self-localized states show frequency and phase locking behavior as conventional lasers, with the long term vision of studying the interaction of a complex network of self-sustained oscillators which have freedom of choosing frequency, phase (possibly polarization) and location simultaneously.

The experimental system is based on a vertical-cavity surface-emitting laser (VCSEL) emitting at 980 nm with a diameter of 200 µm. It is coupled to a volume Bragg grating (VBG) providing narrow-band frequency-selective feedback via a self-imaging cavity [8]. We review disorder phenomena in VCSELs [9, 10] and discuss their manifestation and relevance in the feedback system in leading to different thresholds and threshold frequencies for LCS.

Tuning current and alignment of the VBG, we can observe fringes in the far field plane of the VCSEL, the spacing of which corresponds to the separation of the LCS in near field. The fringes can have essentially perfect as well as incomplete visibility, which is interpreted as complete and partial locking (corroborated by the behavior of the optical spectra). Indications for hysteresis are found.

A (minute) tilting of the VBG controls the detuning conditions. It is a global control parameter and hence cannot be adapted to the local disorder responsible for the frequency spread of the LCS but locking of three LCS can be also obtained in some situations. In contrast to conventional arrays of lasers, also other locking phases than π are observed.

The obvious mechanism of coupling via evanescent fields is likely to be enhanced by nonlocal coupling arising from a slight misalignment of the self-imaging condition. This feature could be utilized to provide a controllable amount of nonlocality in the system.

Phase-locking is studied in class B and simplified class A models as described in [11, 12] and reproduced numerically.

REFERENCES

1. Tanguy, Y., T. Ackemann, W. J. Firth, and R. Jäger, *Phys. Rev. Lett.*, Vol. 100, 013907, 2008.
2. Genevet, P., B. Barland, M. Giudici, and J. R. Tredicce, *Phys. Rev. A*, Vol. 79, 033819, 2009.
3. Ackemann, T., G.-L. Oppo, and W. J. Firth, *Adv. Atom. Mol. Opt. Phys.*, Vol. 57, 323, 2009.
4. Vladimirov, A. G., G. V. Khodova, and N. N. Rosanov, *Phys. Rev. E*, Vol. 63, 056607, 2001.
5. Turaev, D., A. G. Vladimirov, and S. Zelik, *Phys. Rev. E*, Vol. 75, 045601(R), 2007.
6. Barland, S., et al., *Nature*, Vol. 419, 699, 2002.
7. Schäpers, B., M. Feldmann, T. Ackemann, and W. Lange, *Phys. Rev. Lett.*, Vol. 85, 748, 2000.

8. Radwell, N. and T. Ackemann, *IEEE J. Quantum Electron.*, Vol. 45, 1388, 2009.
9. Babushkin, I., et al., *Phys. Rev. Lett.*, Vol. 100, 213901, 2008.
10. Schulz-Ruhtenberg, M., Y. Tanguy, R. Jäger, and T. Ackemann, *Appl. Phys. B*, 2009.
11. Scroggie, A. J., W. J. Firth, and G.-L. Oppo, *Phys. Rev. A*, Vol. 80, 013829, 2009.
12. Paulau, P. V., et al., *Phys. Rev. E*, Vol. 78, 016212, 2008.

Self-pulsing Localized Structures in a Semiconductor Laser with Saturable Absorber

L. Columbo[1], **F. Prati**[2], **M. Brambilla**[1], **and T. Maggipinto**[1]

[1]Dipartimento Interateneo di Fisica, Politecnico e Università di Bari, Via Amendola 173, Bari 70123, Italy
[2]Dipartimento di Fisica e Matematica, Università dell'Insubria, Via Valleggio 11, Como 22100, Italy

Abstract— Self-localization of light has been predicted in the plane orthogonal to the propagation direction in a broad-area VCSEL (Vertical Cavity Surface Emitting Laser) coupled with a saturable absorber. It occurs in the form of stationary, stable, structures named cavity solitons (CSs). On the other hand small aspect ratio monolithic semiconductor resonators made of alternating amplifying and absorbing layers show the formation of light pulses in the propagation direction through passive mode-locking.

The motivation of our work stems from the interest of joining the two previous phenomena of pulsing regimes and transverse self-confinement by predicting the existence of structures localized in the three spatial dimensions which travel in the resonator with a regular period. To this aim we consider a monolithic broad-area hetero-structured semiconductor laser with an integrated saturable absorber and we extend beyond the single-longitudinal mode approximation the CS model [1]. In the parametric regimes where CSs are stable, we show that the combination of transverse and longitudinal multimode competition can break the CSs along the axial coordinate leading to the formation of parallel trains of transverse localized structures that propagate endlessly within the resonator with a period equal to the resonator roundtrip time. We call these structures self-pulsing localized structures (SPLSs). Like CSs, they can simultaneously and independently coexist in different transverse locations.

A SPLS would be of remarkable applicative interest for the possibility of adding a periodicity to the encoding of information associated with 2D self-localization. The latter has proved to be exploitable for serial to parallel conversion, optical buffering and material scanning.

REFERENCES

1. Columbo, L., F. Prati, M. Brambilla, and T. Maggipinto, "Self-pulsing localized structures in a laser with saturable absorber," *Eur. Phys. J. D*, Vol. 59, 115–120, 2010.

Applications of Cavity Solitons in VCSELs with Optical Injection

C. McIntyre[1], **G. L. Oppo**[1], **F. Prati**[2], **and G. Tissoni**[1, 3]

[1]SUPA and Department of Physics, University of Strathclyde, Glasgow, UK
[2]CNISM and Dip. di Fisica e Matematica, Università dell'Insubria, Como, Italy
[3]INLN, Université de Nice-Sophia Antipolis, Nice, France (from Jan. 2011)

Abstract— Cavity solitons (CS) are controllable localized light peaks on a low-intensity, homogeneous (or quasi homogeneous) background and offer a variety of applications from optical memories to all-optical delay lines [1,2]. All-optical delay lines based on CS have thus far been demonstrated experimentally in passive configurations [1,2] although recent theoretical and computational work has extended them to the case of VCSELs above threshold with optical injection [3].

We show here that CS in models of VCSELs with optical injection have properties like stability, robustness, velocity, and merging that are important in optical memories and delay lines. In particular we demonstrate large velocities of CS propagation in the transverse space due to an injected frequency tuning and 2D CS merging in the presence of modulated injected phase for the optimization of memory operations.

The model used is based on VCSEL Maxwell-Bloch equations with injection and transverse effects originally described in [4] but after a reduction procedure as sketched in [3]. The full and reduced models correctly describe CS above and below the lasing threshold in the presence of an optical driving. When a linear gradient of slope K is introduced in the phase of the injected beam the CS speed v depends linearly on K over a large range, and then it saturates [1]. For higher values of K, the moving CS solution becomes unstable and the low-intensity homogeneous state is reached. In the presence of a phase gradient, we propose to change the detuning parameter form the value where stationary CS exist to a new one obtained by adding a term proportional to K^2. We progressively adapt the value of the cavity detuning parameter when K is increased, in such a way to compensate the variation introduced in the detuning by the phase gradient. This amounts to a blue-shift of the injected frequency by a term proportional to K^2. Numerical simulations of the Maxwell-Bloch equations for VCSELs with optical injections with a phase gradient have been performed in the parameter range where CS exist and are stable.

One of the most difficult operations in an optical memory based on CS is that of collecting the information stored in a CS. We propose an alternative readout operation based on the self-erasing mechanism of CS merging at the peaks of a background phase modulations. To investigate the CS merging, extensive simulations of the CS interactions around the maxima of phase modulations of the injected field have been performed in both 1D and 2D cases. CS were found to merge with existing CS at the modulation peaks. This is clearly useful for optical memories, but CS merging is also of practical use in all-optical delay lines, where the merging simultaneously erases the CS and releases a short pulse of light that can be used to re-transmit the delayed input data [3].

REFERENCES

1. Pedaci, F., et al., *Appl. Phys. Lett.*, Vol. 92, 011101, 2008.
2. Ackemann, T., W. J. Firth, and G.-L. Oppo, *Adv. in Atomic, Molecular, and Optical Physics*, Vol. 57, 323, 2009.
3. McIntyre, C., A. M. Yao, G.-L. Oppo, F. Prati, and G. Tissoni, *Phys. Rev. A*, Vol. 81, 13838, 2010.
4. Hachair, X., et al., *IEEE J. Sel. Top. Quantum Electron.*, Vol. 12, 339, 2006.

Session 2P2
Electromagnetic Theory and Design on the Optical Dispersive Materials, Invisible Cloak and Photonic Crystals

Investigation of Receiver Sensitivity in Notebook Platform with Multimode Functions

Yao Huang Kao[1] and Hui Chun Yang[2]

[1]Department of Communication Engineering, Chung Hua University
Hsin-chu, Taiwan 30050, China
[2]Department of Communication Engineering, National Chiao Tung University
Hsin-chu, Taiwan 30050, China

Abstract— In this study, electromagnetic interferences (EMI) of digital noises in notebook on wireless receiving are discussed. Four types of digital noises are investigated. Due to the small volume and multi-services as shown in Fig. 1, the weak rf signals are easily deteriorated. Among the digital signals the Low voltage differential signal (LVDS) for display and camera is the most concerned due to nearness to 3G antenna. Another point for noisy coupling is at the small hinge, which controls the cables from processor to the LCD panel board. The practical solutions of spreading spectrum, filtering, shielding, and grounding, which may be conventional but effective, are also proposed to minimize the interferences. The other problems, which occur to the manufacture of notebook platform, are also discussed. Those noises are from switching power supply for backlight inverter, camera, hard disk, MIC, and DDRII. With the above efforts, the ground floor for sensitivity measurement reaches to −99 dBm, which is ready for 2G/3G testing. TIS (Total Isotropic Sensitivity) is recently accepted as the receiver' sensitivity for 3D concern. It is normally around −100 dBm as demonstrated in Table 1. Ten dB improvements are obtained.

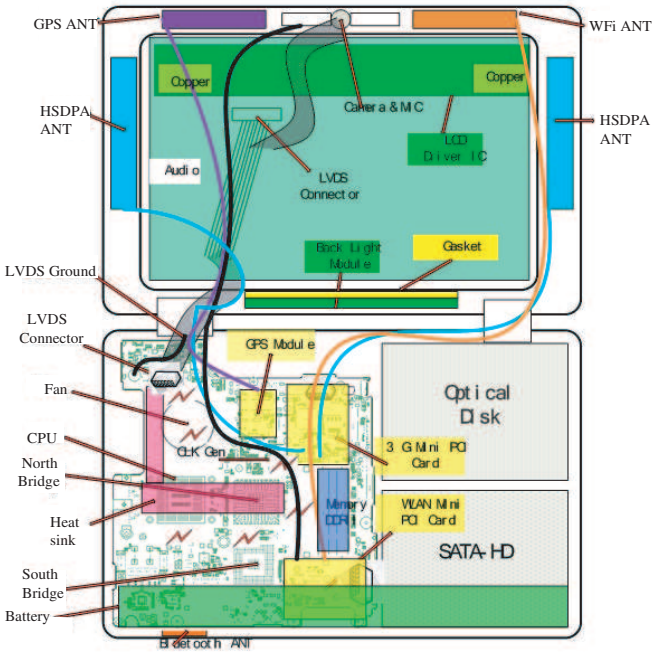

Figure 1: Key components arrangement in the notebook with antenna and panel in upper part and transceiver in lower part.

Test / Position	TRS / Free Space		
Communication System	GSM900		
Channel	975	38	124
Cond. Sensitivity (dBm)	-109.60	-108.20	-109.10
Original TIS (dBm)	-89.20	-90.00	-90.28
Original Min. EIS (dBm)	-92.37	-94.78	-93.51
Final TIS (dBm)	-99.70	-100.50	-99.78
Final Min. EIS (dBm)	-102.67	-104.48	-102.94
Spec.	-100.00	-100.00	-100.00

Table 1: Improved sensitivity in GSM900 Band.

The Equivalent Rest-mass of Photon

Antonio Puccini
Department of Neurophysiology, Order of Malta, Naples, Italy

Abstract— The photon (P), one of the elementary particles of the *Standard Model*, is considered massless. The Universal Gravitation Law states that the gravity force (GF) takes place only between bodies having a mass. Einstein's prediction, based on the Theory of General Relativity, provides that the light is conditioned by the action of the GF. However observations showed that the P *feels* GF. Lord Eddington, with his famous observation in 1919, confirmed completely what Einstein had said. During a sun eclipse, indeed, it was possible to observe that the light coming from far away stars, when passing next to the sun rather than propagate in straight line, followed a trajectory bended towards the sun.

We know that two massless Ps, meeting, *materialise* in a couple of quark-antiquark, or even in a couple muon-antimuon which, summed up, have a mass of 400 electrons.

The P is the *light quantum*, the electromagnetic radiation (*EMR*) *quantum*, which energetic value is represented by the *Planck's constant* (h) — equal to $6.625 \cdot 10^{-27}$ [erg $\cdot$ sec] — times the number of oscillations the P makes in a second, that is times its frequency (f):

$$E = hf \tag{1}$$

As we learn from the electromagnetic spectrum the number of oscillations (10^n) of a *EMR quantum* can be considerably different. It starts from 10^{27} c.s. (or more) of a highly energetic gamma P, to an *extremely low frequency* P, which may have few oscillations per second, or just one cycle per second (we cannot exclude it). Thus the value of f in Eq. (1) is not defined, but extremely variable, according to the EM band we consider. Thus we should indicate f with 10^n [1/s], where n can start from 0, that is one oscillation per second (since $10^0 = 1$), to 27 [c/s] of a very high frequency γP, or even a bit further. Thus it is possible to represent the energy of a P as follows:

$$E = h \cdot 10^n \text{ [1/s]}$$

If we apply the Principle of Equivalence Mass-Energy ($E = mc^2$) to the P, our calculations show that the P has a minimum *equivalent rest-mass* (*Zero Point Mass*) equal to 10^{-48} [g].

A Mechanical Effect Induced by Electromagnetic Radiation May Explain the Wave Function Collapse of a Quantum Object

Antonio Puccini
Department of Neurophysiology, Order of Malta, Naples, Italy

Abstract— When we try to observe a quantum object ($|\psi\rangle$) during its unitary evolving phase (*Uphase*), the Wave Function Collapse of the measured quantum object (QO) set up. The latter undergoes a jump of the quantum state: $|\langle\psi|\phi\rangle|^2$. We have that before the measurement the QO is *delocalised* and behaves almost as a wave. In fact in the experiment of the two holes (if we do not make any measurement) the QO leaves on the screen an interference figure, typical of waves. In the same experiment, if we try to see where the QO passes, we have that it is *localized* and leaves on the screen only point like marks, as a corpuscle.

The experiment shows clearly that as we light the QO, the light modifies its behaviour, going from an undulating-like behaviour to a corpuscular-like one. What makes the differences in the observed QO? What induces the Wave Function Collapse, that is the reduction of the state vector in the QO? We need to remember that the *momentum* (p) of any particle, including the photon (P), is given by the well known formula $p = h/\lambda$, where h is Planck's constant and λ (along with de Broglie's intuitions) corresponds to wave length of the considered particle. Thus a single visible P of a mean wave length has *a momentum* of $p = h/5 \cdot 10^{14}$ [c/s].

Our calculations show that this P has: $p = 1.1623 \cdot 10^{-22}$ [g · cm/s], that is one hundred times bigger than the mass of a proton. We think that it is this huge impact force, carried out by the P, to induce the Wave Function Collapse of the QO hit by the electromagnetic radiation.

Quantum Mechanics Suggests that Photons with Different Energy Do Not Travel at the Same Speed

Antonio Puccini
Department of Neurophysiology, Order of Malta, Naples, Italy

Abstract— Heisenberg's Uncertainty Principle states that time (Δ_T) and energy (Δ_E) are two parameters *canonically conjugated* and each other correlated by the well known Heisenberg's equation: $\Delta_E \cdot \Delta_T \geq h/2\pi$, where h is the Planck's constant. Hence we know that the members on the left are inversely proportional, thus as one of them increases the other will have to decrease proportionally. Besides if we consider photons (Ps) with different energy, those having a bigger energy will travel in a shorter time, and vice versa. As we know the P also carries a *momentum* (p), divided by the wavelength (λ): $p = h/\lambda$. Therefore, p is not constant for the electromagnetic waves, but is inversely proportional to λ.

Let us calculate the p of the P travelling with a radio wave, where λ is equal to 1 cm:

$$p = 6.625 \cdot 10^{-27}\,[\mathrm{erg} \cdot \mathrm{s}]/1\,[\mathrm{cm}].$$

Since $1\,\mathrm{erg} = \mathrm{g} \cdot \mathrm{cm/s^2} \cdot \mathrm{cm}$, we can write:

$$\begin{aligned} p &= 6.625 \cdot 10^{-27}\,[\mathrm{g} \cdot \mathrm{cm^2/s}]/1\,[\mathrm{cm}], \\ p &= 6.625 \cdot 10^{-22}\,[\mathrm{g} \cdot \mathrm{cm/s}]. \end{aligned}$$

The mean P's p of the visible light will be:

$$\begin{aligned} p &= 6.625 \cdot 10^{-27}\,[\mathrm{erg} \cdot \mathrm{s}]/5 \cdot 10^{-5}\,[\mathrm{cm}], \\ p &= 1.325 \cdot 10^{-27}\,[\mathrm{g} \cdot \mathrm{cm^2/s}]/10^{-5}\,[\mathrm{cm}], \\ \text{we have:}\quad p &= 1.325 \cdot 10^{-22}\,[\mathrm{g} \cdot \mathrm{cm/s}]. \end{aligned}$$

whereas, let us calculate the p of a P travelling with a γ ray, with $\lambda = 10^{-12}$ [cm]:

$$p = 6.625 \cdot 10^{-27}\,[\mathrm{erg} \cdot \mathrm{s}]/10^{-12}\,[\mathrm{cm}] = 6.625 \cdot 10^{-15}\,[\mathrm{g} \cdot \mathrm{cm/s}].$$

That is, the p of a γP is ten millions bigger than the p of a mean P of visible light, and 1000 billiards bigger of the p of a radio P!

We should consider that the p is a *motion* magnitude, thus the bigger a P's p the bigger the *motion*: that is the P's *motion* is not the same for all Ps, it is inversely proportional to the λ of the considered band, along with the well known equation: $p = mv$, hence we know that the velocity (v) of a particle, in a given direction, is directly proportional to its p.

Low Frequency Surface Plasmon Polaritons on a Periodically Structured Metal Strip with High Confinement of Fields

Jin Jei Wu[1], **Her-Lih Chiueh**[3], **Tzong-Jer Yang**[1], **Di Chi Tsai**[1], **Hung Erh Lin**[2], **Bear Hu**[1], **Ricardo Wu**[1], **Daniel Wang**[1], **Hung Jung Chang**[1], **Chun Cheng Li**[1], **and Ing-Jar Hsieh**[1]

[1]Department of Electrical Engineering, Chung Hua University, Hsinchu 30012, Taiwan, R.O.C.
[2]College of Engineering, Chung Hua University, Hsinchu 30012, Taiwan, R.O.C.
[3]Department of Electronic Engineering, Lunghwa University of Science and Technology
Kueishan, Tayouan 333, Taiwan, R.O.C.

Abstract— One novel conception is proposed in this report to reduce the crosstalk between transmission lines. We developed a new kind of microstrip line on which the spoof surface plasmon polaritons (SPPs) can propagate in the microwave regime. The microstrip line structure is designed by introducing periodical subwavelength hairpin structure on the lateral surface of conventional microstrip lines. The dispersion relation and bandwidth in the microwave regime are calculated by numerical methods. On the other hand, such periodically structured microstrip lines are fabricated and experimentally verified to support spoof SPPs in the frequency range between 200 MHz and 8 GHz. To take a comparison with the quasi-TEM modes on conventional microstrip lines, the spoof SPPs can be highly localized on the surface of the structured microstrip lines, so the crosstalk between the conventional and the structured microstrip lines is very weak. Hence this new kind of periodically structured microstrip line will be high potential application in the high density microwave circuits or high speed systems.

Inconsistencies on the Measurement of the Effective Refractive Index of Turbid Colloids and How to Avoid Them

R. G. Barrera[1], **E. Gutiérrez-Reyes**[1], **Augusto García-Valenzuela**[2], **and Celia Sánchez-Pérez**[2]

[1]Instituto de Física, Universidad Nacional Autónoma de México
Apartado Postal 20-364, Distrito Federal 01000, México
[2]Centro de Ciencias Aplicadas y Desarrollo Tecnológico, Universidad Nacional Autónoma de México
Ciudad Universitaria, Apartado Postal 70-186, Distrito Federal 04510, México

Abstract— Colloids are usually defined as systems composed by a disperse phase (colloidal particles) within a homogeneous one (matrix). The electromagnetic field traveling through these systems can be split into: (i) An average field (coherent beam) plus a fluctuating field (diffuse field) and turbidity arises, due to scattering, when the size of the colloidal particles is comparable to the wavelength of the incident radiation. Nevertheless, an effective refractive index (ERI) can be assigned to the propagation of only the coherent beam. On one hand, its measurement is usually done by using standard techniques based on fitting the measured reflectance (and transmittance) to Fresnel's relations. This is possible because one assumes that there is no magnetic response. On the other hand, its theoretical determination has been performed by using multiple-scattering theory together with a specific model for the colloidal particles and regarding that an electromagnetic wave in the bulk of the system propagates with an effective wave-vector [1]. This is the case of the popular expression derived by van de Hulst [2] in terms of the forward scattering amplitude of the colloidal particles, and valid in the dilute limit. Here we briefly review, first, a recently developed theory asserting that the effective electromagnetic response of turbid colloids is spatially dispersive (non-local) [3], and furthermore, that it has an effective magnetic response even if the colloidal particles do not. Within this theory the ERI is precisely defined from the non-local dispersion relation for transverse modes and it is shown that the expression obtained by van de Hulst can be also derived from a dispersion relation with a non-local character. Since for spatially dispersive media Fresnel's relations are not valid, the determination of the ERI based on them is inconsistent and leads to measurable errors. We show this explicitly through a direct comparison of the predictions obtained from Fresnel's relations together with the ERI given by van de Hulst, with actual reflectance measurements and with expressions for the reflectance based on multiple-scattering theory [4]. These expressions are given in terms of elements of the scattering matrix of the isolated particles and not in terms of the ERI, therefore one cannot use them to obtain the ERI directly from reflectance measurements. Under these circumstances and recalling that Snell's law is still valid even in the presence of spatial dispersion, we propose, for an accurate determination of the ERI, an spectroscopy based on the measurement of the angle of refraction. An specific experimental arrangement for colloidal suspensions is presented as well as preliminary experimental results. We also comment about the care that has to be taken to perform and to analyze these experiments. Finally, very definite ideas about the equivalence between the effective-medium approach and multiple-scattering theory are discussed.

REFERENCES

1. Tsang, L. and J. A. Kong, *Scattering of Electromagnetic Waves Advanced Topics*, John Wiley & Sons, Inc., NY, 2001.
2. Van de Hulst, H. C., *Light Scattering by Small Particles*, John Wiley & Sons, Inc., NY, 1957.
3. Barrera, R. G., A. Reyes-Coronado, and A. García-Valenzuela, "Non-local nature of the electromagnetic response of colloidal systems," *Physical Review*, Vol. 75, No. 18, Art. 184202, 1–19, 2005.
4. Reyes-Coronado, A., A. García-Valenzuela, C. Sánchez-Pérez, and R. G. Barrera, "Measurement of the effective refractive index of a turbid colloidal suspension using light refraction," *New Journal of Physics*, Vol. 7, Art. 89, 1–22, 2005.

Nonlocal Homogenization Theory of Multilayered Metal-dielectric Nanostructured Metamaterials

A. V. Chebykin[1], **A. A. Orlov**[1], **and P. A. Belov**[2]

[1]Department of Photonics and Optical Informatics
St. Petersburg State University of Information Technologies, Mechanics and Optics, Russia
[2]Department of Electronic Engineering, Queen Mary University of London
Mile End Road, London E1 4NS, UK

Abstract— In our presentation we consider an optical metamaterial consisting of spatially periodically repeated nanolayers of metal and dielectric. Such the metamaterial possess plenty of unique electromagnetic properties. For instance, it can transmit evanescent waves from one of its surfaces to another one. This property could be used to create superlenses, which is capable of transforming evanescent waves to propagating ones. Also, the metamaterial under consideration could be applied in subwavelength microscopy, as image magnification possibility recently was demonstrated in a number of works [1–5]. Another useful applications include nanolithography [6], as well as cloaking [7].

In order to describe such metamaterials method of local homogenization is in widely use. However, we will show that in the multilayered metal-dielectric nanostructure there are effects of strong spatial dispersion, which cannot be avoid. As expected, a local model does not provide satisfactory description of the metamaterial's electromagnetic behaviour because it does not depend on the wave vector. The latter is necessary for description of spatially dispersive effects. Thus we need nonlocal homogenization theory.

A method of nonlocal homogenization has been proposed by Mario Silveirinha in 2007 [8]. The main idea consists in excitation of system by an external electric current with certain field distribution. Solving Maxwell's equations with such a continuous source, it is possible to calculate average electric fields and then find the effective nonlocal dielectric permittivity $\varepsilon_{\text{eff}}(\omega, \mathbf{k})$ depending on a wave vector $\mathbf{k}$ by means of the following expression:

$$D_{av} = \varepsilon_0 E_{av} + P_g = \bar{\bar{\varepsilon}}_{\text{eff}}(\omega, \mathbf{k}) E_{av},$$

where D_{av}, E_{av} — average electric displacement and electric field, and P_g polarization.

We apply the given method to the special case of a multilayered metamaterial. Solutions of Maxwell's equations are written in the form of the sum of three components: direct and backward waves (eigenmodes of the structure), and the induced component caused by an external current, which is the solution of the equations for infinite space. Amplitudes of direct and backward waves are found by solving the system of the linear equations. Then from expressions for these amplitudes average electric fields are calculated. Finally we obtain analytical expressions for components of the nonlocal dielectric permittivity tensor $\bar{\bar{\varepsilon}}_{\text{eff}}$ of the multilayered metamaterial in directions along the layers and normal to the layers. Expressions obtained are fully spatial dispersive as they depend on the wave vector $\mathbf{k}$.

REFERENCES

1. Belov, P. and Y. Hao, *Phys. Rev. B*, Vol. 73, 113110, 2006.
2. Pendry, J. B. and S. A. Ramakrishna, *Physica B*, Vol. 338, 329, 2003.
3. Shamonina, E., V. A. Kalinin, K. H. Ringhofer, and L. Solymar, *Elect. Lett.*, Vol. 37, 1243–1244, 2001.
4. Salandrino, M. and N. Engheta, *Phys. Rev. B*, Vol. 74, 075103, 2006.
5. Zubin, J., L. Alekseyev, and E. Narimanov, *Opt. Express*, Vol. 14, 2006.
6. Xiong, Y., Z. Liu, and X. Zhang, *Appl. Phys. Lett.*, Vol. 93, 111116, 2008.
7. Cai, W., U. K. Chettiar, A. V. Kildishev, and V. M. Shalaev, *Opt. Express*, Vol. 16, 5444, 2008.
8. Silveirinha, M. G., *Phys. Rev. B*, Vol. 75, 115104, 2007.

Low Loss Optical Meta Material Implemented in Photonic Quasi Crystal

Kaisar R. Khan and Trevor J. Hall
School of Information Technology and Engineering (SITE), University of Ottawa
Ottawa, Ontario, K1N6N5, Canada

Abstract— Photonic crystal shows interesting physical characteristics due to its ability to engineer the dispersion by adjusting the crystal lattice. The dispersion calculations have been reported by several research groups. Some of them even claim to achieve negative refraction by dispersion engineering or by introducing metal like material in the crystal [1, 2]. But these periodic structures with translational symmetry experiences very high loss at negative refraction regime. People generate quasi periodic pattern in the photonic quasi crystal (PQC) that seems disorderly arranged in the short range but actually orderly arrange at long range. PQC is actually the rotational analogy of photonic crystal [3]. It provides the rotational extended states which appear as defect states because they are localized to certain sites within the photonic quasi crystal pattern [3]. Using the eigen-mode expansion (EME) method the photonic band gap of PQC has been evaluated. Here negative refraction can be achieved by means of dispersion engineering. The dispersion engineering can be done either by adjusting the appropriate lattice geometry or by changing the material. Fig. 1 shows PQC pattern implemented in GaAs with its band diagram for both TE and TM polarization. This PQC has six fold rotational symmetries that mean it is symmetrical at every 60° angle. A design effort was made to adjust the lattice constant and the air hole diameter to achieve the desired dispersion profile (dispersion less flat band for negative refractive index).

The transmission through PQC has been evaluated by the finite-difference time-domain (FDTD) method to determine the propagation loss. Plane or Gaussian wave excitation have been used to see the spectral features of the transmission. Two sensors were placed in both horizontal and vertical direction to differentiate the transmission properties from the two polarizations (TE/TM). Transmission has been evaluated at each angle to correlate the wavelength dependent loss with the dispersion along the k-path.

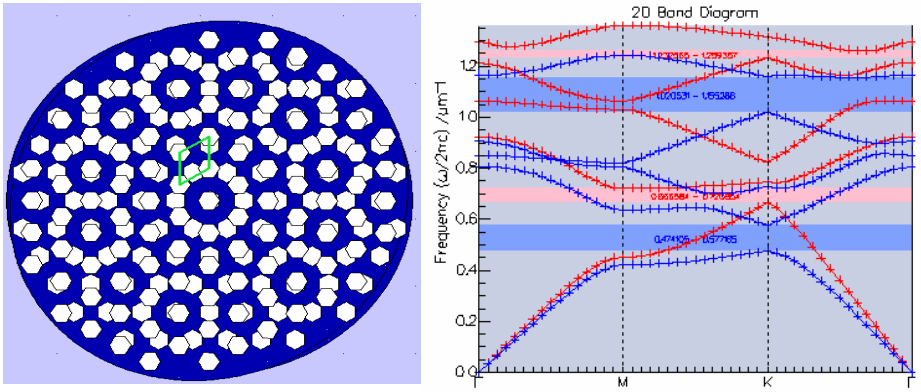

(a) (b)

Figure 1: (a) Photonic quasi crystal (PQC) pattern implemented in GaAs substrate and (b) band diagram from both TE and TM wave.

REFERENCES

1. Duque, C., N. Porras-Montenegro, S. Cavalcanti, and L. Oliveira, "Photonic band structure evolution of a honeycomb lattice in the presence of an external magnetic fields," *Journal of Applied Physics*, 105, 2009.
2. Khan K. and T. Hall, "Tuning the photonic band structure of lattices with cylindrical shell rod," *Proc. SPIE*, 7750–99, 2010.
3. Mnaymneh, K. and R. C. Gauthier, "Mode localization and band-gap formation in defect-free photonic quasicrystals," *Opt. Express*, Vol. 15, 5089–5099, 2007.

Session 2P3
Transformation Optics, Metamaterials and Plasmonics

Selective and Collaborative Optimization Methods for Plasmonics: A Comparison

S. Kessentini[1], **D. Barchiesi**[1], **T. Grosges**[1], **and M. Lamy de la Chapelle**[2]

[1]Project Group for Automatic Mesh Generation and Advanced Methods
Gamma3 Project (UTT-INRIA), University of Technology of Troyes, France
[2]CSPBAT CNRS-FRE3043, UFR SMBH, University of Paris 13, France

Abstract— Plasmonics has become a rapidly expanding interdisciplinary field with the development of numerous highly sensitive transducers which take advantage of acute resonances in the interaction between light and metallic nanostructures. The engineering of such sensors which involves numerous degrees of freedom for fabrication parameters therefore requires efficient optimization methods as well as accurate models whose numerical behavior is well known. Among the various classifications of the meta-heuristics optimization methods, that may help to find the best candidates of parameters to improve the sensor, the orientation process toward this optimum is based either on the crude selection of the best element or on the collaborative search of a way to reach it.

In this contribution we analyze the numerical properties of the electromagnetic models in plasmonics [1] and we propose some bench functions having such typical properties. Mainly, we consider analytical models: Mie theory for coated spheres and multilayer models, as they provide controlled benches for the multimodal optimization in a multidimensional space of parameters. The goal is to develop optimization schemes that would be able to involve some more complex and time consuming models like the Finite Element which are used to describe, in particular, more complex problems.

The investigated optimization methods are the classical Evolutionary Method (EM), using elitist or non-elitist selection, and the standard Particle Swarm Optimization (PSO), using collaborative algorithm. Some modifications of these conventional methods are proposed [2, 3], through the motivation of the specific search of plasmon singularity, enabling a faster convergence.

Practical applications are dedicated to improve the planar plasmonic biosensors sensitivity and to coated nanospheres with biological burning purpose, whereas the previous studies were focused on imaging improvement [4, 5]. The sensitivity of planar biosensor is described by a non analytic function, measuring the decay of the plasmon resonance, under a constraint of minimum visibility. The sensitivity is therefore far from the pure plasmonic efficiency [5]. On the other hand, the target of the optimization of the burning nanoparticle is the maximum of electromagnetic intensity in the vicinity of the nanoparticle and not the scattering cross section [4]. The topology of these two target functions differs from the classical intensity or scattering cross-section functions and the corresponding search of poles. Therefore, the optimization methods have to be adapted to this class of problems.

REFERENCES

1. Barchiesi, D., E. Kremer, V.-P. Mai, and T. Grosges, "A Poincaré's approach for plasmonics: The plasmon localization," *J. Microscopy*, Vol. 229, No. 3, 525–532, 2008.
2. Kessentini, S., D. Barchiesi, T. Grosges, L. Giraud-Moreau, and M. Lamy de la Chapelle, "Adaptive non-uniform particle swarm application to plasmonic design," *International Journal of Applied Metaheuristic Computing (IJAMC) Special Issue on: Metaheuristics and Their Applications to Industrial Engineering*, 2010, to appear.
3. Barchiesi, D., "Adaptive non-uniform, hyper-ellitist evolutionary method for the optimization of plasmonic biosensors," *International Conference on Computers & Industrial Engineering (CIE39)*, Vol. 1–3, 542–547, 2009.
4. Grosges, T., D. Barchiesi, T. Toury, and G. Gréhan, "Design of nanostructures for imaging and biomedical applications by plasmonic optimization," *Opt. Lett.*, Vol. 33, No. 23, 2812–2814, 2008.
5. Barchiesi, D., D. Macías, L. Belmar-Letellier, D. van Labeke, M. Lamy de la Chapelle, T. Toury, E. Kremer, L. Moreau, and T. Grosges, "Plasmonics: Influence of the intermediate (or stick) layer on the efficiency of sensors," *Appl. Phys. B*, Vol. 93, 177–181, 2008.

Electromagnetic Heat-induced in Meso-structures: Computation of Temperature in Metallic Dimers

D. Barchiesi[1], **T. Grosges**[1], **E. Kremer**[2], **and M. Lamy de la Chapelle**[3]

[1]Project Group for Automatic Mesh Generation and Advanced Methods
Gamma3 Project (UTT-INRIA), University of Technology of Troyes, France
[2]XLIM, Department of OSA, CNRS-UMR 6172, University of Limoges, France
[3]CSPBAT CNRS-FRE3043, UFR SMBH, University of Paris 13, France

Abstract— The plasmon resonance is known to produce high electromagnetic field confinement. This physical effect can be used as a intense nanosource of light for various applications (sensors, medical applications...). Moreover, this optical source can also be used for chemical reaction control and for biological purposes, acting as a secondary thermic source. Among the applications, a small burning oriented device could be also of interest. Therefore, the computation of the optically induced variations of temperature is necessary to design proper devices [1].

In this context, the spectral properties of "bowtie" nanoantennas can make them to be good candidates for these type of applications [2, 3]. We propose a multiphysics finite element model to solve both the electromagnetic and thermic problems. We discuss the validity of the heat equation and the influence of a non linear correction of the thermal conductivity of the two metallic parts of the nanoantenna [4, 5]. The computation of the electric field is obtained from the Finite Element Galerkin formulation of the Helmholtz' equation with complex permittivity. The electric field is then used to compute a heat source in the nanoantenna, which is the source term of the heat equation. The heat equation is then solved with the previous method, assuming constant or non linear thermal conductivity, in order to include the mesoscopic correction related to the hypothesis of phonon diffusion and of electron-phonon interaction [4, 5].

The critical point of convergence of the electromagnetic model is addressed owing to the target of temperature computation. The mesh quality and refinement, and the accuracy of the whole numerical procedure are investigated to control the error on the temperature computation [6]. In this first approach, we find some conditions, so that the above mentioned applications could be feasible and we propose some experiments that may help to improve the model.

REFERENCES

1. Grosges, T., S. Petit, D. Barchiesi, and S. Hudlet, "Numerical modeling of the subwavelength phase-change recording using an apertureless scanning near-field optical microscope," *Opt. Express*, Vol. 12, No. 24, 5987–5995, 2004.
2. Fischer, H. and O. J. F. Martin, "Engineering the optical response of plasmonic nanoantennas," *Opt. Express*, Vol. 16, No. 12, 9144–9154, 2008.
3. Yang, L., C. Du, and X. Luo, "Numerical study of optical properties of single silver nanobowtie with anisotropic topology," *Appl. Phys. B*, Vol. 92, 53–59, 2008.
4. Kazantseva, D., G. Guttroff, M. Bayer, and A. Forche, "Sample temperature measurement in a scanning near-field optical microscope," *Appl. Phys. Lett.*, Vol. 72, No. 6, 689–691, 1998.
5. Ju, Y. S., "Impact of nonequilibrium between electrons and phonons on heat transfer in metallic nanoparticles suspended in dielectric media," *J. Heat Transfer*, Vol. 127, 1400–1402, 2005.
6. Borouchaki, H., T. Grosges, and D. Barchiesi, "Improved 3D adaptive remeshing scheme applied in high electromagnetic field gradient computation," *Finite Elem. Anal. Des.*, Vol. 46, No. 1–2, 84–95, 2010.

Generation of Encryption Keys from Plasmonics

M. François[1], **T. Grosges**[1], **D. Barchiesi**[1], **and R. Erra**[2]

[1]Project Group for Automatic Mesh Generation and Advanced Methods, Gamma3 Project (UTT-INRIA) STMR CNRS UMR 6279, University of Technology of Troyes, France
[2]Network & Information Security, Ecole Supérieure d'Informatique, Electronique, Automatique (ESIEA) France

Abstract— The study of plasmon resonances has shown the possibility to produce complex electromagnetic field patterns, with strong gradients and high confinement, superimposed with interference patterns. These physical effects have open the experimental and theoretical way of designing efficient systems in various new applications (sensors, imaging and burning biomedicine applications, security...) [1–3]. In this contribution, we introduce a new method to generate encryption keys, from the computation of electromagnetic field produced through a plasmonic device.

The proposed method is based on a classical computation of the interaction between light and metallic nanomaterials. The computed field is the basis of the production scheme of encryption keys. The cryptographic quality of such a key is related to the number of degrees of freedom of the model and to the description of a resonant phenomenon, involving high sensitivity to numerous parameters [4]. This system is also quantified in term of complexity within the information theory.

Here, the key generator consists in an analytical model deduced from the Mie theory for spherical metallic particle including a mesh postprocessing of the whole domain of computation, in order to control spatial positions of the nodes where the field is computed, as well as the spatial distribution of intensity levels [5]. This meshing process is used not only to control the accuracy in the space of representation, but also to homogenize the occurrences of the electromagnetic intensities through a spatial redistribution of intensity levels in respect to criterium of maximum entropy distribution. This whole process assures the key to respect the maximum Shannon's entropy and the statistical characteristics of randomness.

REFERENCES

1. Barchiesi, D., D. Macías, L. Belmar-Letellier, D. van Labeke, M. Lamy de la Chapelle, T. Toury, E. Kremer, L. Moreau, and T. Grosges, "Plasmonics: Influence of the intermediate (or stick) layer on the efficiency of sensors," *Appl. Phys. B*, Vol. 93, 177–181, 2008.
2. Grosges, T., D. Barchiesi, T. Toury, and G. Gréhan, "Design of nanostructures for imaging and biomedical applications by plasmonic optimization," *Opt. Lett.*, Vol. 33, No. 23, 2812–2814, 2008.
3. Grosges, T. and D. Barchiesi, "Toward nano-world based secure encryption for enduring data storage," *Opt. Lett.*, Vol. 35, No. 14, 2421–2423, 2010.
4. Barchiesi, D., E. Kremer, V.-P. Mai, and T. Grosges, "A Poincaré's approach for plasmonics: The plasmon localization," *J. Microscopy*, Vol. 229, No. 3, 525–532, 2008.
5. Borouchaki, H., T. Grosges, and D. Barchiesi, "Improved 3D adaptive remeshing scheme applied in high electromagnetic field gradient computation," *Finite Elem. Anal. Des.*, Vol. 46, No. 1–2, 84–95, 2010.

Second and Third Harmonic Generation in Induced Photonic Crystals

P. Godard, F. Zolla, and A. Nicolet
Institut Fresnel UMR CNRS 6133, Aix-Marseille Université, Ecole Centrale de Marseille
Campus de Saint-Jérôme, F-13013 Marseille, France

Abstract— In this paper, we present a multiharmonic model able to allow for general nonlinear optical media [1]. As a particular example, two- and three-photon processes are considered here. The numerical model is based on the finite element method that allows to take into account the inhomogeneities of the refraction index due to the nonlinearities [2, 3]. It consists of several harmonic equations at various frequencies coupled via some nonlinear terms. As an illustration we propose a simple homogeneous uniform slab made of non- linear material but illuminated by three plane waves in order to create an artificial periodic structure with a fictitious permittivity. By so doing, an artificial metamaterial is created whose physical properties are determined by the incident field. This system exhibits a non trivial and quite complex behavior because of the induced photonic crystal as depicted on Figure 1.

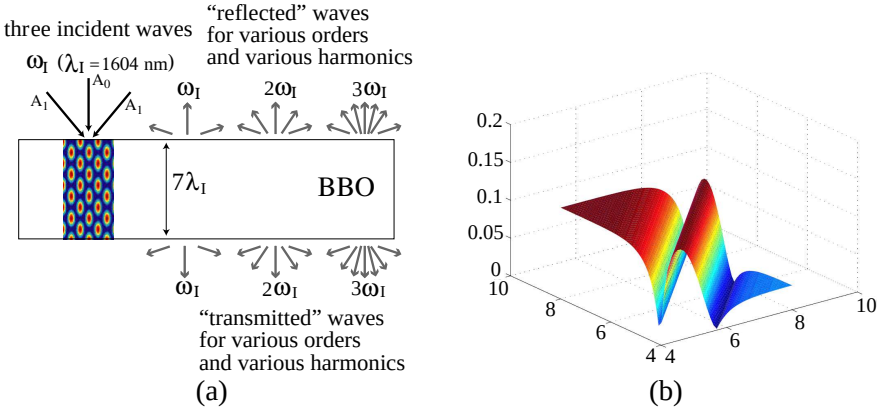

Figure 1: (a) The geometry of the system is an infinite slab. It is infinite along the z-axis, the invariance direction of the chosen incident field, and along the x-axis, the horizontal direction of the cross section shown here. Made up of β Barium Borate (BBO), it is illuminated by three plane waves, one with a normal incidence (amplitude A_0) and two with a symmetric oblique incidence (amplitude A_1) of 0.439 rad with respect to the normal. Along the finite dimension, the thickness is equal to $7\lambda_I$. Harmonics are generated in the nonlinear medium. Due to the interferences of the different waves oscillating at ω_I (the pattern of the field intensity of the incident waves is shown in color inside the slab), a structure (periodic along the x-axis and, therefore, equivalent to a diffraction grating or a finite photonic crystal) is induced in the cross section of the slab. This induced photonic crystal generates several orders for the fundamental frequency ω_I and for the higher harmonics [4, 5]. (b) The square of the modulus of coefficient $|b_{3,3}^{(t)}|^2$ of the order 3 transmitted propagating waves at the frequency $3\omega_I$ (vertical axis) as a function of the amplitude of the inclined incident field (left axis) and of the incident field orthogonally impinging on the slab (right axis).

REFERENCES

1. Boyd, R. W., *Non Linear Optics*, 2nd Edition, Academic Press, Amsterdam, 2003.
2. Godard, P., F. Zolla, and A. Nicolet, "Scattering by a 2-dimensional doped photonic crystal presenting an optical kerr effect photonic crystal," *COMPEL*, Vol. 28 , No. 3, 656–667, 2009.
3. Zolla, F., P. Godard, and A. Nicolet, "Virtual antenna method as applied to the study of the scattering by 2-dimensional non-linear metamaterials," *PIERS Proceedings*, 1204–1207, Beijing, China, March 23–27, 2009.
4. Demésy, G., F. Zolla, A. Nicolet, M. Commandré, and C. Fossati, "The finite element method as applied to the difiraction by an anisotropic grating," *Optics Express*, Vol. 15, 18089–18102, 2007.
5. Petit, R. and al., *Electromagnetic Theory of Gratings*, Springer, Berlin, 1980.

Probing Optical Modes on Disordered Metal Films with Spontaneous Decay Rate Fluctuations

V. Krachmalnicoff, E. Castanié, Y. De Wilde, and R. Carminati
Institut Langevin, ESPCI ParisTech, CNRS, 10 rue Vauquelin, 75231 Paris Cedex 05, France

Abstract— The study of light scattering and transport in disordered media is stimulated by fundamental issues in mesoscopic physics, including Anderson localization, and by the development of imaging techniques in complex media using multiply scattered light. Disordered semi-continuous metallic films are a particularly striking example of complex photonic systems. They exhibit peculiar optical properties that cannot be explained from the behavior of bulk metals or ensembles of isolated nanoparticles [1]. The interplay between surface-plasmon excitations and scattering by multiscale (fractal) metallic clusters leads to spatial localization of the electromagnetic field in subwavelength areas (hot spots). A feature of these "hot-spots modes" is the expected coexistence of both localized and delocalized modes at the same frequency [2, 3].

We have shown recently that the statistical distribution of the local density of optical states (LDOS) in disordered media carry information on the photon transport regime [4]. The distribution of the LDOS can be obtained experimentally from measurements of the spontaneous decay rate (inverse of fluorescence lifetime) of nanosources dispersed inside the medium. In this work, we present an experimental study of LDOS fluctuations on disordered fractal metallic films, using nanoscale fluorescent emitters [5]. Since the LDOS fluctuations are expected to be sensitive to changes of the structure of electromagnetic modes, one can expect to get a signature of the coexistence of localized and delocalized modes in the LDOS statistics. We show that the LDOS exhibits large fluctuations at the threshold corresponding to the appearance of fractal clusters. We interpret the measurements in terms of the inverse participation ratio, a parameter that measures the spatial extent of eigenmodes, and we show that the large fluctuations are a signature of localized surface-plasmon modes. These experiments seem to confirm the concept of inhomogeneous localization on self-similar disordered structures. They also show that localized plasmon modes can substantially modify the LDOS, on a scale in the range of tenth of nanometers. Semi-continuous metal films are samples that combine ease of fabrication and light localization in nanoscale bright modes, and that could be used for studies of light-matter interaction at the single-emitter level.

REFERENCES

1. Shalaev, V. M., *Nonlinear Optics of Random Media*, Springer, Berlin, 2000.
2. Stockman, M. I., S. V. Faleev, and D. J. Bergman, "Localization versus delocalization of surface plasmons in nanosystems: Can one state have both characteristics?," *Phys. Rev. Lett.*, Vol. 87, 167401, 2001.
3. Seal, K., et al., "Coexistence of localized and delocalized surface plasmon modes in percolating metal films," *Phys. Rev. Lett.*, Vol. 97, 206103, 2006.
4. Pierrat, R. and R. Carminati, "Spontaneous decay rate of a dipole emitter in a strongly scattering disordered environment," *Phys. Rev. A*, Vol. 81, 063802, 2010.
5. Krachmalnicoff, V., E. Castanié, Y. De Wilde, and R. Carminati, "Fluctuations of the local density of states probe localized surface plasmons on disordered metal films," *Phys. Rev. Lett.*, 2010, arXiv:1007.3691, in Press.

Disordered Semiconductor Strongly Coupled to Surface Plasmons

J. Bellessa, **S. Aberra Guebrou**, **C. Symonds**, **J. C. Plenet**, **and E. Homeyer**
LPMCN, Université de Lyon, Université Lyon 1 and CNRS, UMR 5586
F-69622, Villeurbanne, France

Abstract— The modification of the emitting properties of molecules or nanoparticles due to the proximity of a metallic surface is a subject of a large number of researches. Enhancement of the radiative rate can be for example obtained. When the particles present high oscillator strength a strong coupling regime can be reached inducing dynamical but also spectral modifications of the emission. The emitters hybridize with the metal surface plasmons leading to polaritonic states. This strong coupling has been observed with a large number of materials, in particular disordered materials. These materials are constituted by a collection of independent emitters (molecules, semiconductor quantum dots...). It has been show theoretically for systems in strong coupling that the excitations are not localised in a single particle but delocalised on a large number of particle due to the formation of an extended hybridised state.

We have investigated these extended polaritonic states by studying the spatial coherence of the emission. For this purpose, interferences between two different regions of the sample are measured with a Young interference experiment. We show that the strong coupling with the surface plasmon induces a cooperative emission of molecules otherwise independent. The typical coherence distances are a few microns and can be associated with a diffusion of the luminescence. On the same sample, incoherent states spatially localised can also be observed in agreement with theoretical predictions at the energy of the bare exciton states. The plasmon induced coherence can be used to create new type of optical materials, for example by ordering periodically different materials (dyes or semiconductors) on a metal surface, with a period smaller than the coherence length.

Nonlinear and Tunable Metamaterials

Yuri S. Kivshar
Nonlinear Physics Centre, Research School of Physics and Engineering
Australian National University, Canberra, 0200 ACT, Australia

Abstract— We will review recent theoretical and experimental results on tunability of periodic photonic structures and metamaterials, in particular the results obtained at our Nonlinear Physics Center at the Australian National University in Canberra (http://wwwrsphysse.anu.edu.au/nonlinear/). The simplest way to achieve direct tunability of metamaterials based on split-ring resonator (SRR) varieties is through a mechanical adjustment of the metamaterial lattice structure. The general principle of this tunability scheme lies in the essential dependence of the effective properties of metamaterials on the lattice structure, easily observable through near-field SRR interactions provided that the density of structural elements is sufficiently high.

More elaborated approach is based on nonlinear response of metamaterial elements, and we demonstrate both theoretically and experimentally the dynamic tunability of the magnetic resonance of a single SRR with a varactor diode at microwave frequencies. In particular, we demonstrate different tuning regimes with and without an inductive coil in parallel with the varactor. We show that the coil changes the sign of the nonlinearity and eliminates the memory effect caused by charge accumulation across the varactor. In addition, at higher powers the nonlinear response of the split-ring resonator becomes multivalued, paving a way for creating bistable tunable metamaterials.

Based on the properties of single SRRs, we fabricate and study nonlinear tunable magnetic metamaterials operating at microwave frequencies. We fabricate the nonlinear metamaterial composed of double split-ring resonators where a varactor diode is introduced into each resonator so that the magnetic resonance can be tuned dynamically by varying the input power. We demonstrate that at higher powers the transmission of the metamaterial becomes powerdependent and, as a result, such metamaterial can demonstrate various nonlinear properties. In particular, we study experimentally the power-dependent shift of the transmission band and demonstrate nonlinearity-induced enhancement (or suppression) of wave transmission.

In addition, we hope to discuss a variety of other intriguing effects and phenomena associated with the negative index of refraction and the specific properties of backward waves, including (i) appearance of two- and three-dimensional bandgaps in low-symmetry periodic strcutures, (ii) dramatic suppression of Anderson localisation, (iii) unusual dynamics of Bloch oscillations in metamaterial and metal-dielectric superlattices, (iv) backward-wave second-harmonic generation and nonlinear quadratic perfect lens, (v) nonlinear tunable electric metamaterials, (vi) nonlinear plasmonic structures and parametric effects for plasmon frequency conversion.

Bulk Micro-resonances and Artificial Magnetism — A full 3d-framework

G. Bouchitté[1], **C.Bourel**[1], **and Didier Felbacq**[2]

[1]Departement of Mathematics, Université de Toulon, BP 20132, 83957 La Garde Cedex, France
[2]GES UMR 5650, Place Bataillon, 34095 Montpellier Cedex 05, France

Abstract— In [1–3] , a theory for artificial magnetism in two-dimensional photonic crystals has been developed for large wavelength (homogenization). The main idea was that a periodic crystal with high permittivity inclusions shows up micro-resonance effects from which an effective permeability law with anomalous dirpersion could be evidenced in a explicit way. The main drawback was however that in this model we assumed magnetic parallel polarization so that merely infinite photonic crystals (invariants in one direction) could be considered.

In this work we propose a full 3d generalization of previous results: the diffraction of a finite 3d- dielectric crystal is considered at a fixed wavelength and a limit analysis as the period tends to zero is performed. We evidence a new microscopic vector spectral problem which turns out to rule the macroscopic behavior of the crystal. We obtain then an extension to the 3D-case of the results in [1, 2] by proving rigorously that permeability tensor laws can be reached where the effective tensor exhibits negative eigenvalues in appropriate range of frequencies. This suggests that periodic bulk dielectric inclusions could be an efficient alternative to the very popular metallic split-ring structure proposed by Pendry [4].

REFERENCES

1. Bouchitté, G. and D. Felbacq, "Homogenization near resonances and artificial magnetism from dielectrics," *C. R. Math. Acad. Sci. Paris*, Vol. 339, No. 5, 377–382, 2004.
2. Felbacq, D. and G. Bouchitté, "Homogenization of wire mesh photonic crystals embdedded in a medium with a negative permeability," *Phys. Rev. Lett.*, Vol. 94, 183902, 2005.
3. Felbacq, D. and G. Bouchitté, "Negative refraction in periodic and random photonic crystals," *New J. Phys.*, Vol. 7, 159, 10.1088, 2005.
4. O'Brien, S. and J. B. Pendry, "Magnetic activity at infrared frequencies in structured metallic photonic crystals," *J. Phys. Condens. Mat.*, Vol. 14, 6383–6394, 2002.

Broadband Free-space Characterization of Metamaterials

M. H. Belyamoun, O. Dubrunfaut, C. Pareige, Y. Zhu, S. Zouhdi, and F. Ossart
Laboratoire de Génie Électrique de Paris, CNRS UMR 8507, SUPELEC, UPMC
Univ Paris 6, Univ Paris-Sud, 11 rue Joliot-Curie, Plateau de Moulon, 91192, France

Abstract— We present in this paper the free-space measurements of several metamaterials in the 6–18 GHz frequency range, obtained with a free-space focused beam system. The system is calibrated with a Thru Reflect Line procedure, and the measured data is filtered in the time domain. We compute the effective electromagnetic parameters of High Impedance Surfaces and split-ring based metamaterials, and compare them to the simulation results obtained by original homogenization techniques. With our system, we obtain a good agreement between measurements and simulations with a 3% deviation.

Metamaterials characterization in free-space have benefit of a great interest [1]. Our measurements were done between two quad-ridged antenna, that operate in the 2–18 GHz frequency range. The beam is focused by Rexolite ($\varepsilon_r = 2.54$) lenses, in order to obtain a planar wave front on the sample. Thank to the specific properties of the gaussian beam, we calculate the lens geometry to keep a plane wave front at the same position on the sample. This is effectively the case in the 6–18 GHz frequency range, and the waist of the beam at the sample position is $w = 4.5$ cm. We ensure the sample's dimensions exceed $3w$ to limit the diffraction effects.

The S-parameters are retrieved by an Agilent PNA 8364C. The twelve errors of measure are described in transmission-reflexion by the full two ports model, that require three standard measurements. We choose the Thru Reflect Line procedure to calibrate our system. We start the calibration by measuring the S-parameters of the Thru standard: the reference planes are considered at the same distance of the two horn antennas. Thanks to the micrometric positioning stages, we move the second antenna by the sample thickness. Indeed, the standards Reflect (a metallic plate) and Line (an air line) are measured.

To eliminate all the signal noise, we use the FFT and an appropriate window and filter the S-parameters in the time domain. Several shapes of windows are considered, but some of them, as the rectangular, induce an important signal ringing. We choose the Blackman window that eliminates the signal noise of the multiple reflexions on the focused-beam system environment.

In this configuration, we characterized several arrays of copper inclusions, hosted in epoxy ($\varepsilon_r = 4.4$). We first study the effective impedance of a "mushroom" structure and obtain a very good agreement with the analytical model [2, 3]. The calculus of the effective impedance, which only depends on the S_{11} parameter, is immediate. The effective permittivity and permeability of individual split-ring based metamaterials [4] are determined by the Nicholson-Ross-Weir inversion method [5]. The arrays are characterized both in parallel and perpendicular polarizations, and we obtain a very good agreement with an homogenization technique based on the Floquet-Bloch decomposition [6, 7].

REFERENCES

1. Li, K., S. J. McLean, R. B. Greegor, C. G. Parazzoli, and M. H. Tanielian, "Free-space focused-beam characterization of left-handed materials," *Applied Physics Letters*, Vol. 82, No. 15, 2535–2537, 2003.
2. Sievenpiper, D. F., L. Zhang, R. F. J. Broas, N. G. Alexopolous, and E. Yablonovitch, "High-impedance electromagnetic surfaces with a forbidden frequency band," *IEEE Transaction on Microwave Theory and Techniques*, Vol. 47, No. 11, 2059–2074, 1999.
3. Zhu, Y., A. Bossavit, and S. Zouhdi, "Calculation of surface impedance for high impedance surfaces," *META'10, 2nd International Conference on Metamaterials, Photonic Crystals and Plasmonics*, 2010.
4. Gay-Balmaz, P. and O. J. F. Martin, "Electromagnetic resonances in individual and coupled split-ring resonators," *Journal of Applied Physics*, Vol. 92, No. 5, 2929–2936, 2002.
5. Weir, W. B., "Automatic measurement of complex dielectric constant and permeability at microwave frequencies," *IEEE Proceedings*, Vol. 62, 4, 33–36, 1974.
6. Bossavit, A., "Effective frequency-dependent permeability of split-ring metamaterials via homogenization," *IEEE Transactions on Magnetics*, Vol. 45, 1276–1279, 2009.
7. Belyamoun, M. H., A. Bossavit, and S. Zouhdi, "Effective parameters of split-ring arrays, numerically determined by frequency-dependent homogenization," *SPIE*, Vol. 7711, 77110W, 2010.

Nonlocality and Additional Extraordinary Waves in Multilayered Metal-dielectric Nanostructures

A. A. Orlov[1], **P. M. Voroshilov**[1], **A. V. Chebykin**[1], **and P. A. Belov**[1,2]

[1]St. Petersburg State University of Information Technologies, Mechanics and Optics
St. Petersburg, Russia
[2]Queen Mary University, London, UK

Abstract— Strong spatial dispersion effects are observed in the multilayered metal-dielectric structures at the long wavelength limit. The analysis of dispersion curves and isofrequency contours shows that the classical local effective medium model is not applicable for description of such structures. The metamaterials under consideration exhibit strong non-local properties.

The multilayered metal-dielectric structures are widely used in optics for manipulation of fields on the subwavelength scale. Their applications include subwavelength imaging [1–5], creation of subwave-length patterns [6] and achieving negative index of refraction [7]. In the most of the cases, the effective medium model is applied for description of the metal-dielectric structures. At the long-wavelength limit, it is assumed that the one-dimensional photonic crystal can be described as a uniaxial dielectric with the permittivity tensor of the following form:

$$\overline{\overline{\varepsilon}} = \begin{pmatrix} \varepsilon_\perp & 0 & 0 \\ 0 & \varepsilon_\parallel & 0 \\ 0 & 0 & \varepsilon_\parallel \end{pmatrix}, \qquad \varepsilon_\parallel = \frac{\varepsilon_1 d_1 + \varepsilon_2 d_2}{d_1 + d_2}, \qquad \varepsilon_\perp = \left[\frac{\varepsilon_1^{-1} d_1 + \varepsilon_2^{-1} d_2}{d_1 + d_2} \right]^{-1},$$

where d_1 and d_2 are thicknesses, ε_1 and ε_2 are permittivities of the constituent layers, respectively.

The effective medium model is widely used for explanation of various phenomena in multilayered metal-dielectric nanostructured optical metamaterials. However, its applicability for description of such structures was not verified yet, up to our knowledge.

We performed detailed full-wave study of dispersion properties of a typical multilayered metal-dielectric structure and compared the obtained results with ones predicted by effective medium model. The comparison of dispersion curves and isofrequency contours revealed very strong spatial dispersion effects in the structure at the frequencies near the resonance of transverse component of permittivity. At these frequencies the local effective medium model is not applicable. For example, the local model predicts existence of the only propagating extraordinary wave, whereas the full-wave results demonstrate two or even more waves at certain directions at some frequencies.

The observed effects are closely related to existence of hybrid plasmon-polariton waves travelling predominantly along interfaces of the layers. These travelling waves causes the spatial dispersion effects in multilayered optical metamaterials in the same manner as magneto-inductive waves causes the spatial dispersion effects in microwave metamaterials consisting of split-ring resonators [8, 9].

REFERENCES

1. Shamonina, E., V. A. Kalinin, K. H. Ringhofer, and L. Solimar, *Electronics Letters*, Vol. 37, 1243–1244, 2001.
2. Ramakrishna, S. A. and J. B. Pendry, *Phys. Rev. B*, Vol. 67, 201101 (1–4), 2003.
3. Ramakrishna, S. A., J. B. Pendry, D. Schurig, D. R. Smith, and S. Schultz, *J. Mod. Opt.*, Vol. 49, 1747–1753, 2002.
4. Belov, P. A. and Y. Hao, *Phys. Rev. B*, Vol. 73, 113110 (1–4), 2006.
5. Li, X., S. He, and Y. Jin, *Phys. Rev. B*, Vol. 75, 045103 (1–7), 2007.
6. Xiong, Y., Z. Liu, and X. Zhang, *Appl. Phys. Lett.*, Vol. 93, 111116 (1–3), 2008.
7. Zhang, J., H. Jiang, B. Gralak, S. Enoch, G. Tayeb, and M. Lequime, *Optics Express*, Vol. 15, 7720–7729, 2007.
8. Belov, P. A. and C. R. Simovski, *Phys. Rev. E*, Vol. 72, 026615 (1–15), 2005.
9. Silveirinha, M. G. and P. A. Belov, *Phys. Rev. B*, Vol. 77, 233104 (1–4), 2008.

Optimal Parameters of Metallic Nanorods Arrays for Subwavelength Imaging

Pavel A. Belov[1, 2], **Atiqur Rahman**[1], **and Sergei Yu. Kosulnikov**[2]

[1]Queen Mary University of London, UK
[2]St. Petersburg State University of Information Technologies, Mechanics and Optics, Russia

Abstract— Arrays of metallic nanorods are capable of transmitting images with subwavelength resolution [1, 2]. There are two typical geometries of such arrays, suggested by A. Ono, J. Kato, S. Kawata [1] and M. Silveirinha, P. Belov, C. Simovski [2] for different frequency ranges of optical spectrum. In this work we examine these geometries in order to identify optimal parameters of the structures which enable best imaging performance.

In the case of A. Ono et al. the length of rods can be tuned so that imaging of cophasal sources is possible. This tuning provides much better range of applications of the nanorods arrays by providing possibility of imaging arbitrarily shaped sources. These improvements may dramatically change operation of cascaded geometries suggested in [3] for colour subwavelength imaging.

In the case of M. Silveirinha et al. the tuning of the rods diameter provides wider operation bandwidth. The optimum diameter is approximately equal to half of the square lattice period. Astonishingly, the arrays of thicker rods are capable of operating with sources located at significant distances away from the front interface. The arrays in such regime operate very similarly to perfect lens [4], but the distance through which the sources can be detected is limited by the periodicity of the structure rather than the thickness of the slab as in the case of the perfect lens.

REFERENCES

1. Ono, A., J. Kato, and S. Kawata, *Phys. Rev. Lett.*, Vol. 95, 267407, 2005.
2. Silveirinha, M., P. Belov, and C. Simovski, *Phys. Rev. B*, Vol. 75, 035108, 2007.
3. Kawata, S., A. Ono, and P. Verma, *Nature Photonics*, Vol. 2, 438, 2008.
4. Pendry, J., *Phys. Rev. Lett.*, Vol. 85, 3966, 2000.

Strong Coupling of Plasmons with Confined Waveguide Modes

A. Castanié[1], **D. Felbacq**[1], **B. Guizal**[1], **and J. Bellessa**[2]

[1]Charles Coulomb Laboratory, University of Montpellier 2, France
[2]University Claude Bernard Lyon 1, France

Abstract— Plasmonics is a new and rapidly growing field at the intersection of fundamental physics and technological applications. While the physical phenomenon of a localized surface mode on metal is quite well understood, the fine properties of rather simple structures are not so easily obtained. It is especially true when considering the introduction of complex medium such as in the so-called spaser effect or when the quantum electrodynamics of plasmons is at stake.

In view of these applications, wave propagation in a planar metal plasmon waveguide is studied. More specifically, the dispersion curve of a metal-insulator-metal waveguide is investigated. Such structures have been investigated in the past in the situation of a thin insulator film [1]. In this work, the situation when the insulator layer supports guided modes is considered. It is shown that, in that case, it is possible to realize the strong coupling of photon modes with plasmons. By means of complex plane analysis, the influence of this coupling on the losses is studied and, for the hybrid plasmon/waveguide photon mode, spatial Rabi oscillations are observed [2]. Finally the introduction of gain is considered as well as some more complicated geometries in view of the practical realization of devices.

ACKNOWLEDGMENT

This work was realized in the framework of the ANR contract SCOP ANR-07-NANO-053-01. Support from the Institut Universitaire de France is gratefully acknowledged.

REFERENCES

1. Dionne, J. A., L. A. Sweatlock, and H. A. Atwater, "Planar metal plasmon waveguides: Frequency-dependent dispersion, propagation, localization, and loss beyond the free electron model," *Phys. Rev. B*, Vol. 72, 075405, 2005.
2. Symonds, C., J. Bellessa, J. C. Plenet, E. Cambril, A. Miard, L. Ferlazzo, and A. Lematre, "Planar metal plasmon waveguides: Frequency-dependent dispersion, propagation, localization, and loss beyond the free electron model," *Superlattices and Microstructures*, Vol. 47, 50–54, 2010.

Session 2P4a
Electromagnetic Nondestructive Evaluation (NDE) 2

Development of Microwave Interferometry Nondestructive Testing Solution

Karl Schmidt and Jack Little
Evisive, Inc., Baton Rouge, Louisiana 70808, USA

Abstract— Application of engineered ceramic materials in high temperature environments of advanced propulsion systems in high performance aircraft; structural demands in ceramic-composite armor; application of high density polyethylene in piping, and reinforced rubber in nuclear power service; and fiber reinforced resin overwraps for piping, all present demanding nondestructive testing challenges. A new technology, Evisive Scan^{TM}, has been recently developed that allows condition monitoring in these challenging materials. The internationally patented Evisive Scan^{TM} method is based on microwave interferometry. It utilizes microwaves to interrogate dielectric materials, including material with complex internal structure. The microwaves are reflected at areas of changing dielectric constant. The reflected energy and the interrogating beam are combined to form an interference pattern which is measured in the transceiver as a signal voltage. The method requires access to only one surface, does not require contact or a coupling medium. The signal voltage is sampled at many positions in the inspection area. This point cloud is displayed as an Evisive Scan^{TM} image, which presents volumetric detail of the inspected part. This data is rich with information which is processed in near real time for advanced analysis.

Over the past year, the technology has been successfully applied to Ceramic Matrix Composites where it is used to measure density and porosity and identify manufacturing defects. The method has been demonstrated to be applicable to ceramic composite armor made of monolithic ceramic tiles in complex, multilayer structures. It has also been demonstrated to detect irregularities in thermally welded high density polyethylene (HDPE) pipe, including "cold fusion". The technology has been successfully demonstrated on fiber reinforced resin pipe overwraps, and the technology has been used for condition monitoring of reinforced rubber flexible couplings in nuclear power plants. The nuclear power plant application is performed under a fully qualified, US nuclear quality assurance 10CFR50 App B and NQA-1 compliant program.

Examples of these applications are presented, with explanation of the operating principles of the technology and illustrations of the individual applications. Work included in the report is supported by the US Air Force Research Laboratory, US Army *Tank-Automotive Research, Development and Engineering Center (TARDEC), US Army Research Laboratory and US Air Force Research Laboratory.* Evisive would like to acknowledge project participation and support by Argonne National Laboratory, Exova and Saudi Aramco.

Design and Fabrication of a Modular Eddy Current Micro Sensor

T. Griesbach, **M. C. Wurz**, **and L. Rissing**
Institute for Micro Production Technology, Center for Production Technology
Leibniz Universitaet Hannover, Garbsen, Germany

Abstract— Modern production technology requires the acquisition of manifold process data. First of all, having basic information on the production process guarantees the reliability during the whole fabrication run. Second, the acquired process data are used to verify the quality of a product at the end of the production. A novel approach is proposed within the Collaborative Research Center 653 which is funded by the DFG (German Research Foundation). In order to come up with "genetically intelligent" (gentelligent) machine tools or components, various sensors were developed to gather process data not only during the production, but also later on during the entire life cycle [1]. So far, a family of modular magnetic micro sensors covering both, force and strain measurements was developed [2].

Eddy current testing is a reliable method to provide a contactless measurement technique for the detection of surface damages. In order to provide such a contactless measurement technique, a modular design of an eddy current micro sensor was developed. The sensor was fabricated in thin-film technology. To be able to enhance the output signal, reliable data on the intensity and distribution of the eddy currents are required. A finite element method (FEM) analysis was conducted by using the ANSYS® simulation software to model the eddy currents to be expected. The micro sensor was fabricated on a Si wafer and consists of two parts, a single-turn excitation coil and an anisotropic magneto-resistance (AMR) sensor. The AMR sensor detects the change of the magnetic field induced in the sample by the excitation coil. For the fabrication of micro molds used as a masking for the electrodeposition of the sensor elements, UV depth photolithography was applied. For depositing both, the contact pads and the excitation coil, Cu electroplating was used. Photosensitive epoxy (SU-8™) served as embedding material. The seed layer required for the electroplating was fabricated by sputter deposition before the photomask was created. After the electroplating process, the respective seed layer was removed by ion beam etching (IBE). The thin-film fabrication of the eddy current sensor was already completed. Next, the electrical and magnetic properties will be evaluated.

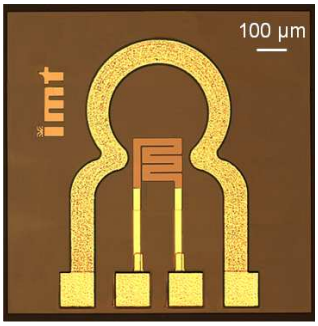

Figure 1: Micrograph of a completed eddy current micro sensor (top view).

REFERENCES

1. Denkena, B., K. Hasenfuß, and C. Liedtke, "Genetik und intelligenz in der produktionstechnik," *ZWF Zeitschrift für Wirtschaftlichen Fabrikbetrieb, Spur, G. (Hrsg.)*, Vol. 100, No. 10, 569–572, 2005.
2. Hansen, S., L. Rissing, and H. H. Gatzen, "A concept for a toolbox of components for modular magnetic microsensors," *Symposium on Magnetic Materials, Processes and Devices, 210th Meetting of the Electrochemical Society*, Vol. 3, No. 25, 235–246, Cancun, Mexico, 2006.

Effect of Nonperfect Contact between the Material under Test and an Open-ended Coaxial Probe on Complex Permittivity Measurement

M. D. Perèz, U. Reggiani, and L. Sandrolini
Department of Electrical Engineering, University of Bologna
Viale del Risorgimento 2, Bologna I-40136, Italy

Abstract— The electrical characterization of dispersive materials can be conveniently carried out through the widespread open-ended coaxial probe technique. The complex permittivity of the material is related to the coaxial probe aperture admittance which, in turn, can be obtained from the complex reflection coefficient measured with a vector network analyzer [1]. The complex permittivity can then be determined from the measurement by means of a numerical extraction procedure [2]. To take the frequency dependence of the complex permittivity into account, dielectric relaxation models such as Havriliak-Negami, Cole-Cole or Debye can be used. In order to limit the uncertainty in the measurement, the open end of the probe must be in good contact with a specimen of the material under test (MUT), addressing this technique in particular to liquids or malleable solids. For solid materials, the prediction of the permittivity can be affected by air gaps between sample and probe, or by sample surface roughness [3].

This paper aims to investigate the effect of nonperfect contact between the MUT and an openended coaxial probe on the complex permittivity measurement. The contact between a material with a surface roughness R_0 (root mean square average of the roughness profile) and the coaxial probe is represented with two layers of permittivity ε_0 and $\hat{\varepsilon}_{\mathrm{MUT}}$. where ε_0 is the permittivity of vacuum and $\hat{\varepsilon}_{\mathrm{MUT}}$ is the complex permittivity of the MUT, respectively. The effective permittivity $\hat{\varepsilon}_{eff}$ of the resulting two-layered material can then be calculated from a series-capacitance model

$$\hat{\varepsilon}_{eff} = \frac{t_1 + t_2}{t_1 + t_2/\hat{\varepsilon}_{\mathrm{MUT}}} \tag{1}$$

where $t_1 = R_0$ and t_2 are the thickness of the air gap and the MUT sample, respectively. In order to estimate the uncertainty on the complex permittivity introduced by the sample roughness, the aperture admittance of the coaxial probe is calculated for different values of R_0 and compared to that corresponding to the ideal case of perfect contact. The calculations are carried out analytically with Marcuvitz's formula for the aperture admittance using (1) and numerically with two different full-wave electromagnetic simulator (CST Microwave Studio) models to represent the contact: The former between the probe and an homogeneous layer of permittivity $\hat{\varepsilon}_{eff}$, the latter between the probe and the MUT with a roughness profile closer to the real one. A complete series of results will be presented and discussed in the final paper.

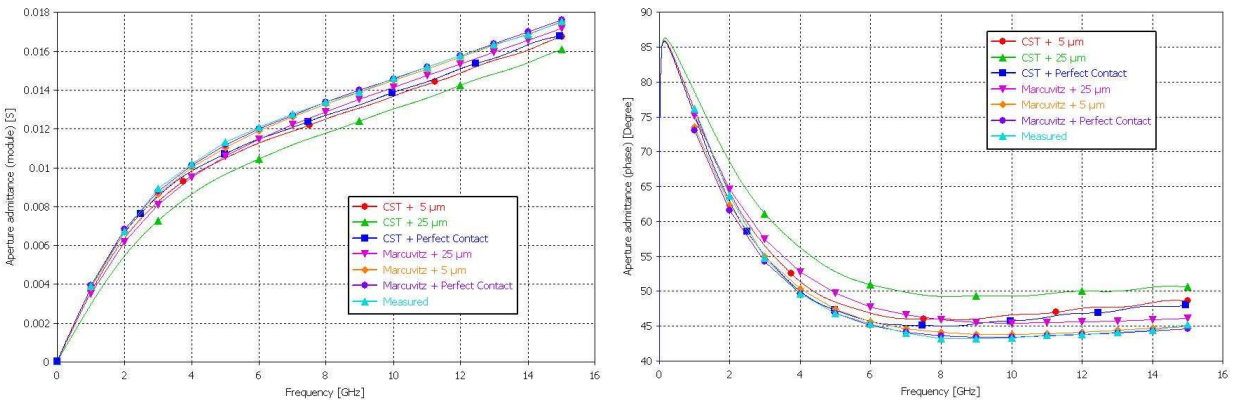

Figure 1: Magnitude and phase of the aperture admittance of a coaxial probe as a function of surface roughness.

REFERENCES

1. Misra, D., M. Chabbra, B. Epstein, M. Microtznik, and K. Foster, "Noninvasive electrical characterization of materials at microwave frequencies using an open-ended coaxial line: Test of an improved calibration technique," *IEEE Trans. Microwave Theory and Tech.*, Vol. 38, 8–14, Jan. 1990.
2. Artioli, M., M. D. Perez, U. Reggiani, and L. Sandrolini, "Extraction of the complex permittivity of dispersive materials with a stochastic optimization technique," *Proc. of the 26th Annual Review of Progress in Applied Computational Electromagnetics*, 18–23, Tampere, Finland, Apr. 25–29, 2010.
3. Baker-Jarvis, J., M. Janezic, P. Domich, and R. Geyer, "Analysis of an open-ended coaxial probe with lift-off for nondestructive testing," *IEEE Transactions on Instrumentation and Measurement*, Vol. 43, 711–718, Oct. 1994.

Session 2P4b
Sensor-based Structural Damage Detection: Concrete Applications

Wireless Electronic Structural Surveillance Sensors Using Inductively Coupled Sacrificial Transducers

P. Pasupathy[1], **A. Abu Yousef**[2], **D. P. Neikirk**[1], **and S. L. Wood**[2]

[1]Department of Electrical and Computer Engineering
The University of Texas at Austin, USA
[2]Department of Civil Architectural and Environmental Engineering
The University of Texas at Austin, USA

Abstract— Monitoring corrosion of the steel reinforcement in concrete continues to be a challenging problem. Our efforts to address this problem have led to the development of low cost, wireless, battery free, Electronic Structural Surveillance (ESS) corrosion sensors. Results from our efforts to improve the performance of such electronic structural surveillance tags will be presented. The ESS tags use an unpowered embedded resonant L-C sensor read by an external reader using an inductively coupled impedance measurement. Read range of coupled tags is largely dependent on the strength of inductive coupling which is influenced by the relative shape and size of the coils used in both the reader and the sensor. Reader coil geometries can be optimized to increase read range. Our previous embedded sensors use a steel wire which corrodes when the conditions in the concrete promote corrosion. Such a sacrificial transducer in its native environment is the most direct method of monitoring corrosion. In the previous generation design, this transducer was connected directly to the sensor, hence breaching the hermetic seal protecting the sensor circuit. A new transduction scheme will be discussed which incorporates a fully exposed sacrificial transducer element that is inductively coupled to the sensor resonant circuitry, hence providing a non-contact interaction. The strength of the interaction of the fully exposed, sacrificial transduction layer is set by flux screening and mutual inductance effects. This design also allows the transducer to make use of a variety of materials and morphologies. We present various designs and experimentally demonstrate the behavior of our prototype sensor, illustrating a new paradigm for transduction in passive wireless sensors.

A Meta Model for Damage Prognosis of Concrete Structure

Othman Sidek, **S. A. Quadri**, **and Shahid Kabir**
Collaborative Microelectronic Design Excellence Centre (CEDEC)
Universiti Sains Malaysia, Engineering Campus, Malaysia

Abstract— Deterioration of concrete structures is a big problem; premature or unexpected failures of these structures are often catastrophic. Damage prognosis has become a new research focus that tries to use damage diagnosis knowledge to inform the responsible authorities on the expected remaining service life of the structure. The purpose of prognosis is to extract damage features from input-output or output-only data and model damage evolution to predict the remaining life of the structure. In this paper, we are presenting a reduced order model (Meta model) prototype for damage prognosis of concrete structure, which captures the relationship between inputs and outputs without providing a detailed description of the physics and geometry.

Multi Agent System for Agile Wireless Sensor Network to Monitor Structures

Othman Sidek, **S. A. Quadri**, **and Shahid Kabir**
Collaborative Microelectronic Design Excellence Centre (CEDEC)
Universiti Sains Malaysia, Engineering Campus, Malaysia

Abstract— The rapid and enormous construction of structures call for rigorous SHM programme during construction, operation and maintenance. Thus much of the structures success or failure depends upon efficient SHM programs. The basic technology underlying SHM to detect cracks and failures is incorporated by Wireless Sensor Network technology. Thus the agility of WSN is a prominent factor for successful SHM programme. Unpredictable external events such as earth quake or high impact are an inevitable fact of life. For such an event WSN should be active and efficient enough to perform the assigned task without failure. The NMAOS (Never miss an opportunity scheme) a prototype based on Multi agent technology is proposed in this paper to provide agility to Wireless Sensor Network.

Optical Image Analysis Based Concrete Damage Detection

Akram Salem[1], **Shahid Kabir**[2], **and Atif Musbah**[1]

[1]School of Civil Engineering, Engineering Campus, Universiti Sains Malaysia (USM), Malaysia
[2]Sustainable Materials and Infrastructure (SMI) Cluster
Collaborative μ-electronic Design Excellence Centre (CEDEC)
Engineering Campus, Universiti Sains Malaysia (USM), Malaysia

Abstract— The deteriorating condition of concrete infrastructure and the prohibitive costs required for upgrading them require the development of innovative and effective decision support tools. Such tools will enable predictions about the condition and future performance of concrete structures and the allocation of limited funds for optimized maintenance that yields improved reliability and minimum life cycle costs. Furthermore, improved control on the variability between predicted and actual repair quantities would tend to reduce the long-term unit price of repair work, as contractors adapt to less instances of work shortfalls. There is a growing need for precise and reliable methods that use non-destructive testing (NDT) techniques to assess the deterioration in concrete structures and the extent of associated damage. Current use and development of monitoring methods and imaging techniques employing NDT is limited due to the unavailability of enough experimental data and field applications. This research aims to enhance image processing methods for application to imagery of concrete blocks that were exposed outdoors to the elements, and concrete slabs that were kept in the laboratory in controlled environments, in order to extract quantitative deterioration information from the concrete images obtained using various NDT imaging methods. Evaluations are done on the efficiency of the various types of NDT imaging methods of colour and greyscale imagery, in detecting different types of concrete deterioration and correlation between damage quantities obtained from processing of the concrete imagery and test measurements recorded for the laboratory specimens is established.

Sensors-based Noise Removal Method from Pile Integrity Test (PIT) for Concrete Marine Piles

S. Mohsen[1], **S. Asaei**[2], **Shahid Kabir**[1], **and Atif Musbah**[1]

[1]School of Civil Engineering, University Sains of Malaysia (USM), Engineering Campus P. Pinang, Malaysia
[2]Collaborative Micro Electronic Design Excellence Centre (CEDEC) Universiti Sains, Engineering Campus, Nibong Tebal, Penang, Malaysia

Abstract— Marine piling is the most commonly used method for offshore construction. Cast-in-situ piles are the most helpful columns substantially used in marine structures. Considering the aggressive condition of the marine environment within the vicinity of piles, these columns are susceptible to corrosion. The piles must be tested to address their deficiencies, and the pile integrity test (PIT) method is widely used. This method is based on waves made by some special hammers that beat the piles, and the response waves are recorded. However in this case, the noise produced by marine waves must be taken into account. This paper describes the method adopted for measuring marine pile noise, which is designed based on wave force and the beating period of marine waves. In this method, a system of sensors is simultaneously deployed at the front side of piles through wave vectors. This system allows the measurement of the beating intensity sequence of wave collisions with piles, which may interrupt the response waves recorded by the PIT system. This enables the prompt determination of the effects of any wave collision. Relevant formulas are used to measure force and time, and to generate the most accurate graphs.

Sub-surface Concrete Structure Damage Quantification Using TIR and Visual Inspection

Atif Musbah[1], **Shahid Kabir**[2], **and Akram Salem**[1]

[1]School of Civil Engineering, Engineering Campus, Universiti Sains Malaysia (USM), Malaysia
[2]Sustainable Materials and Infrastructure (SMI) Cluster
Collaborative μ-electronic Design Excellence Centre (CEDEC), Engineering Campus
Universiti Sains Malaysia (USM), Malaysia

Abstract— Infrared (IR) thermography has become a common technique for non-destructive inspections in various engineering fields. The IR thermography technique identifies and measures near surface defects by detecting the temperature gradient on the surface of a target object (e.g., a concrete wall). This study concerns the evaluation of the efficiency of the different types of NDT imaging methods of thermographic, colour, and greyscale imagery, in detecting various types of concrete damage. Data from the NDT imaging techniques are used to quantify near-surface structural damage by using image processing techniques, and validation of damage quantities is done with data from visual inspection. In terms of imagery, the thermographic classifications produced higher accuracies than the greyscale classifications. This is partly due to the fact that thermographic images contain less variability within the concrete imagery, and at the same time increase the visibility of cracks that may be otherwise imperceptible. The results show good correlation between damage quantities obtained through the image processing techniques applied to the IR thermography and optical imaging and the results obtained through visual inspection using the Feeler gauge and crack detection microscope.

Infrared Thermography for Assessing and Monitoring Electrical Components within Concrete Structures

Mohd Shawal Jadin[1], **Soib Taib**[1], **and Shahid Kabir**[2]

[1]School of Electrical and Electronic Engineering, Universiti Sains Malaysia
Nibong Tebal 14300, P. Pinang, Malaysia
[2]Collaborative Micro-electronic Design Excellence Centre (CEDEC)
Universiti Sains Malaysia, Nibong Tebal 14300, P. Pinang, Malaysia

Abstract— The paper presents the application of infrared thermography (IRT) for assessing and monitoring electrical components within concrete structures. It is well known that the integrity of a power system is of paramount importance when it supplies electricity throughout a facility, especially during peak time. Overloading, load imbalance, corrosion and loose connection of electrical components can produce a thermal anomaly or hot spot. The abnormality of the components will occur when its internal temperature reached beyond its limits. Consequently, the overheating can lead to subsequent failure of the components that can potentially result in unplanned power outages, possible injury and fire hazard. In addition, the efficiency of an electrical system becomes low prior to failure, thus energy is spent generating heat, causing unnecessary loses. Therefore, early prevention is required to avoid future faults and increase the reliability of the electrical components. Conventionally, for a large building and wide area of power distribution systems, the inspection of electrical power components requires many workers to conduct the inspection and take a lot of time as well as cost. Furthermore, only certified and experienced personnel can justify the severity of the problematic components. This is due to the complex analysis and various factors that need to consider during the inspection. Therefore, this research proposed a new method of an intelligent monitoring system for electrical components by diagnosing its thermal profiles. The system uses infrared thermographic camera or thermal imager in order to capture the thermal behavior of electrical components. The main feature of the proposed system is to automatically identify the thermal anomaly in electrical components and classify its level of severity if the anomaly is detected. A new method of inspection is introduced by implementing the combination of an advanced image processing technique and artificial intelligence system. Finally, the system will give a complete analysis report, including the most suitable action to be taken for the problem that was detected.

Detection and Quantification of Corrosion Damage Using Ground Penetrating Radar (GPR)

Shahid Kabir[1] and Ahmad Zaki[2]

[1]Sustainable Materials and Infrastructure (SMI) Cluster
Collaborative μ-electronic Design Excellence Centre (CEDEC), Engineering Campus
Universiti Sains Malaysia (USM), Malaysia
[2]School of Civil Engineering, Engineering Campus, Universiti Sains Malaysia (USM), Malaysia

Abstract— Corrosion of steel reinforcement in concrete structures is a main cause of structural damage that needs improved methods for detection and quantification. Non-destructive testing (NDT) methods show great potential to be used to determine the location and extent of corrosion damage. One such NDT method, the Ground Penetrating Radar (GPR), can be used for evaluating existing reinforced concrete structures in order to determine their structural health. This research aims to detect the damage due to corrosion of reinforcing steel in concrete structures using GPR and conventional NDT methods such as half-cell potential (HCP). A method to accelerate corrosion of the steel rebar in concrete samples to different degrees is employed, which consists of introducing a direct current power supply and 5% sodium chloride (NaCl) solution as an electrolyte to the rebar to induce significant corrosion within a short period of time. The 2 GHz GPR and half-cell potential (HCP) are used to detect the corrosion in the reinforced concrete slabs after 28 days of standard moist preservation. Results are compared with those obtained using GPR and the half-cell potential (HCP) method. Results show good performance in determining the degree of corrosion damage with high accuracy through the methods employed, as well as good correlation between results obtained through GPR and HCP methods.

Radar-based Quantification of Corrosion Damage in Concrete Structures

Ahmad Zaki[1] **and Shahid Kabir**[2]

[1]School of Civil Engineering, Engineering Campus, Universiti Sains Malaysia, Malaysia
[2]Sustainable Materials and Infrastructure (SMI) Cluster
Collaborative μ-Electronic Design Excellence Centre (CEDEC), Engineering Campus
Universiti Sains Malaysia, Malaysia

Abstract— The NDT of ground penetrating radar (GPR) methods has been found to be useful in evaluating the corrosion damage in the concrete structures. However, the GPR image is very difficult to be interpreted because it requires processing technique. This paper studies the GPR to detect the corrosion of concrete structure using image processing technique. The C30 reinforced concrete $1 \times 1 \times 0.3$ m slabs, are corroded as results of galvanostatic method. The galvanostatic method is used to accelerated the corrosion. The method is a current technique using direct current (DC) power supply with 5% sodium chloride (NaCl) solution. The 2 GHz of GPR, are used for detection the corrosion damage in the concrete slabs. The GPR data showed that the corrosion can be detected, however need to analyzed and interpretation by using image processing and artificial neural network (ANN). Image processing technique is applied for quantification of corrosion data while ANN is applied to classify the data.

Determining the Effect of Faraday-rotation and Optimum Rotation Angle in Different Types of Magneto-optical PBG Structures

Othman Sidek, **Muhammad Hassan Bin Afzal**, **and Shahid Kabir**
Collaborative Micro-Electronic Design Excellence Centre (CEDEC)
Universiti Sains Malaysia, Malaysia

Abstract— MO-PBG structures have been used in industrial arena with wide popularity and greater authority. Basically, the unique characteristics such as trapping light and transmitting the signal without allowing them to reflect back has made this structural concept widely acceptable and user friendly. Although, these properties can be significantly improved by introduced defect on the lattice structure. In recent studies and findings, it has been revealed that, periodic multi-layered Magneto-Optical (MO) structure consisted of magneto-optical and dielectric layers including defects can boost the Faraday rotation of polarized light when weigh against bulk magneto-optical material. The defining characteristics of a MO-PBG structure are the periodicity of dielectric materials along with one or more axis. In case of MO-PBG structures, when the light is transmitted pass through the magnetized substance and reflected from Magneto-Optical substance known as Faraday Effect. Two very essential effects are required special attention while designing the Magneto-Optical PBG structure such as oblique incidence of the incoming signal and the beam size. To achieve a better transmission it is needed to attain the ideal 45° of Faraday rotation and the ideal beam size. Usually there are two types of problems occurred while designing these types of MO-PBG structures. Firstly the overall transmission is being reduced for 45o of Faraday rotation. Three to four defects can be introduced in these structures to improve the overall transmission quality. Now the second problem arises as the thickness of these structures increases notably and goes over 40 μm. Because of these two effects, the overall performance of MO-PBG structures decreased significantly. But by using certain amount of defects and a well constructed structure could help to overcome these problems and achieve the 45° of Faraday rotation and much improved transmission properties. A front-end programme was designed to evaluate the different properties and performances of MO-PBG structures under different circumstances. It also notifies the users about different layers of MO-PBG structures and their properties such as variation in rotation degree, in transmittance and also in thickness. The present paper deals with different types of MO-PBG structures and properties, the Faraday rotation effect, bulk thickness and probable solution to overcome these problems. The output results attained such as the best possible rotation degree for each MO-PBG structure and thickness are consistent with reference data.

Underwater Communication Systems: A Review

Mohd Ansor Bin Yusof[1] **and Shahid Kabir**[2]

[1]School of Electrical and Electronic Engineering
Universiti Sains Malaysia, Engineering Campus, Nibong Tebal, P. Pinang, Malaysia
[2]Sustainable Materials and Infrastructure (SMI) Cluster
Collaborative μ-electronic Design Excellence Centre (CEDEC)
Engineering Campus, Universiti Sains Malaysia (USM), Malaysia

Abstract— There is a high demand for underwater communication systems due to the increase in current human underwater activities. Underwater communication systems employ either sonar or electromagnetic waves as a means of transferring signals. These waves are different physically and electrically, and thus the systems that employ them also differ in their design architecture, wave propagation and devices used for emission and reception. As a result, the two systems have varying advantages and limitations. This paper presents an in-depth review of underwater communication based on sonar and electromagnetic waves, a comparison of the two systems and a discussion of the environmental impacts of using these waves for underwater communication. In the tradeoff between preserving the underwater environment and the need for underwater communication, it appears that underwater electromagnetic wave communication has the most potential to be the environmentally-friendly system of the future.

Session 2P5
Emerging Strategies and Innovative Algorithms for the Solution of Inverse Scattering Problems 2

Novel Techniques for UWB Microwave Imaging of Objects with Canonical Shape

Gianluigi Tiberi[1], **Navid Ghavami**[2], **David J. Edwards**[2], **and Agostino Monorchio**[1]

[1]Department of Information Engineering, University of Pisa, Via G. Caruso 16, Pisa I-56122, Italy
[2]Department of Engineering Science, University of Oxford, Parks Road, Oxford, UK

Abstract— Microwave imaging has attracted growing attention in the last decade, especially for its applicability to breast cancer detection, motivated by the significant contrast in the dielectric properties at microwave frequencies of normal and malignant tissues. Current research can be divided mainly into microwave tomography and ultrawideband (UWB) radar techniques. In tomographic image reconstruction, a nonlinear inverse scattering problem is solved to recover an image of the dielectric properties. In contrast to tomography, the UWB radar approach solves a simpler computational problem by seeking only to identify the significant scatterers. In order to reconstruct the image, beamforming techniques are required. Current beamforming techniques use time domain processing algorithms; however, these present major problems in three dimensional imaging spaces which possess volumes of varying dielectric constant. In fact, internal refraction cannot be easily removed and would render the image highly inaccurate. Thus, further research and novel approaches need to be exploited to open new horizons in microwave imaging.

In this context, the aim of this paper is to develop novel, fast and accurate UWB microwave imaging methods. First, we introduce a procedure based on the Mode Matching (MM) of Bessel functions, which permits to identify the presence and location of significant scatterers inside cylindrically-shaped objects. Next, with the aim of investigating more general 3D problems, a method based on Huygens Principle (HP) is presented. Using the MM Bessel function procedure leads to the generation/inversion of a rather small matrix, whose dimensions are not related to the discretization of the volume where the image is required. Conversely, using the HP procedure to forward propagate the wave removes the need to solve inverse problems and, consequently, no matrix generation/inversion is required. Together with their simplicity, the two methodologies permit the capturing of the contrast (dielectric variation), i.e., the extent to which different tissues, or differing conditions of tissues, can be discriminated, and hence render contrast in the final image. Moreover, UWB allows all the information in the frequency domain to be utilized by combining the information from the individual frequencies to construct a consistent image. Validation of the techniques through both simulations and measurements on cylinders and spheres with inclusions has been performed and results are presented, illustrating the effectiveness of the methods. In particular, an agar-agar gel cylinder with different kind of inclusions has been considered in order to mimic high-water-content human tissues imaging.

High Resolution Optical Profilometry Using Diffractive Tomographic Microscopy

S. Arhab, **G. Soriano**, **K. Belkebir**, **A. Sentenac**, **and H. Giovannini**
Institut Fresnel (CNRS UMR 6133), Aix-Marseille Université
Campus de St Jérôme, Marseille 13013, France

Abstract— Far-field optical profilometry is a noncontact surface metrology technique that is used to determine the topography of surfaces at a submicrometer scale. It has important applications in the industrial domain and many systems are commercially available. Interferometric techniques, confocal scanning or chromatic arrangements can give nanometric vertical resolutions provided the surface slopes are small enough so that, locally, the incident beam is considered to be reflected by a horizontal plane at a given height. Hence, the lateral resolution of such techniques is generally greater then the incident wavelength. Now, with the improvements of nanofabrication especially in the micro-electronic domain, there is a strong need for optical instruments able to retrieve the roughness of surfaces with typical transverse dimension about 100 nm.

Recently, it was shown that tomographic diffractive microscopy could be a powerful technique for determining the reflectance of rough surfaces with high resolution [1]. This approach consists in recording many holograms of the sample under various incident angles. The reflectance of the surface is retrieved by Fourier transforming the set of holograms. Using Fraunhofer approximation, it is possible is some cases to estimate the height of the profile from the reflectance with nanometer accuracy. This simple numerical reconstruction procedure relies on two restrictive hypothesis, paraxial approximation and single scattering regime.

The Fraunhofer hypothesis cannot be assumed when high transverse resolution is sought. Indeed, the paraxial approximation does not hold when high numerical aperture objectives are used and surfaces presenting small transverse dimensions often support multiple scattering. The direct scattering problem can be rigorously modelized by boundary integral equations, but these relations between the profile and the scattered field are nonlinear. The inversion problem is then recasted as an optimization problem. In this work, the Newton-Kantorovitch (NK) method [2] is used to iteratively build up the solution by successively solving the forward problem and a local linear inverse problem. The derivation is notably based on the reciprocity theorem [3].

We present in this talk the performances of tomographic diffractive microscopy on synthetic data for profilometry application. For simplicity, we consider one-dimensional surfaces. As in a tomographic diffractive microscopy experiment, the surface is illuminated successively by a collimated beam under different angles of incidence. For each illumination, the complex amplitude of the far-field diffracted by the surface is computed along various directions. The Fraunhofer approximation as well as the rigorous modeling NK are compared on rough surfaces with different correlation lengths larger or smaller than the Rayleigh criterion. The numerical experiment clearly shows that the occurence of multiple scattering, which usually plagues most optical imaging instruments, can be an advantage for a nonlinear reconstruction procedure.

REFERENCES

1. Maire, G., F. Drsek, J. Girard, H. Giovannini, A. Talneau, D. Konan, K. Belkebir, P. C. Chaumet, and A. Sentenac, "Experimental demonstration of quantitative imaging beyond Abbe's limit with optical diffraction tomography," *Phys. Rev. Lett.*, Vol. 102, 213905–4, 2009.
2. Roger, A., "Newton-Kantorovitch algorithm applied to an electromagnetic inverse problem," *IEEE Transactions on Antennas and Propagation*, Vol. 29, No. 2, 232–238, 1981.
3. Roger, A., "Reciprocity theorem applied to the computation of functional derivatives of the scattering matrix," *Electromagnetics*, Vol. 2, No. 1, 69–83, 1982.

An Inversion Strategy for Fast Multi-frame Microwave Tomography

S. Semenov[1], **B. Nair**[1], **J. Kellam**[2], **T. Williams**[2], **and M. Quinn**[2]

[1]Keele University, School of Medicine, ISTM, Stoke-on-Trent, ST4 7QB, UK
[2]Carolinas Medical Center, Charlotte, NC 28203, USA

Abstract— Microwave tomography (MWT) is a novel, emerging imaging modality. Noninvasive assessment of functional and pathological conditions of biological tissues in fast, multi-frame manner is one of potential competitive advantages of MWT. To explore the potential we used our recently developed 2D MWT system capable for fast, multiframe imaging. The 2D MWT system with full electronic scanning and control allows for a multi-frames data acquisition (up to 150 frames) with as minimal as 10 msec data acquisition per each frame. We vary operation frequency from 1.05 to 1.5 GHz. The imaging chamber of the system is a metallic cylinder with inner radius 10.75 cm with 24 ceramic waveguide antennas equidistantly located at the perimeter of the central crosssection of the imaging chamber. During an imaging procedure the chamber is filled in with matching solution.

Three Yorkshire domestic cross/farm pigs, males and females, were used in this study. Animals were cared for under an Institutional Animal Care and Use Committee approved research protocol and the NIH guidelines for laboratory research. Top left portion of animal extremity was position inside of an imaging chamber and a multi-frame data acquisition procedure was performed during baseline period. Further on, different interventions were modeled, such as short blood flow reductions with hypoxia or a short hypoxic period and multi-frame data acquisition was repeated multiple times.

In our experiments we acquired more than 100 frames per each 13 sec measurement cycle. Further on, we repeated the 13 sec measurement cycle multiple times during baseline period and various interventions. The inversion of such large number of sets of raw data possesses a challenging problem. The decrease of data inversion time per each frame and per each cycle is the major goal here. We've explored different inversion strategies using iterative Newton and Born approaches and their combinations.

An Innovative Inversion Approach Based on Contrast Source-extended Born Model and Markov Random Fields

R. Autieri[1, 3], **M. D'Urso**[2], **C. Eyraud**[3], **A. Litman**[3], **V. Pascazio**[1], **and T. Isernia**[4]

[1]Dipartimento per le Tecnologie, Università di Napoli Parthenope, Italy
[2]SELEX Sistemi Integrati SpA, a Finmeccanica Company, Giugliano in Campania, Napoli, Italy
[3]Institut Fresnel UMR CNRS 6133, Université Paul Cézanne Aix-Marseille III
Ecole Centrale de Marseille, Université de Provence Aix-Marseille I, Marseille, France
[4]DIMET, Università Mediterranea di Reggio Calabria, Italy

Abstract— Microwave tomography is a non invasive technique able to achieve quantitative image of the internal properties of not accessible targets by solving a non-linear and ill-posed inverse problem [1–5]. The actual capability to solve such a problem in an accurate and possibly fast fashion affects the feasibility and performances of many diagnostic techniques, as the ones adopted in medical imaging, in detection of internal defeats in nuclear plants, or in ground penetrating radar imaging. The applicability of the technique is limited from both the inherent non linearity, which may induce "false solutions" of the problem, as well as from ill-posedness, which implies the need of some form of regularization generally resulting in a low-pass version of the original image.

Although introducing limitations on the applicability of the inherent equations, linearized approximations of the scattering phenomena are of interest, as witnessed from as very large body of literature. Also, it has to be taken into account that some form of regularization of the ill posed problem allows some extension of the applicability of the linearized models. As a consequence, a smart choice of the kind of linearization and of the regularization to be used can allow satisfactory reconstructions in cases wherein more usual linearized techniques fail, or are not accurate.

In this communication, we propose a new inversion approach which takes definite advantage from the joint use of the linearized Contrast Source-Extended Born (CS-EB) model [4], and of a Bayesian estimation procedure [2, 3] based on a Markov Random Field (MRF) regularization scheme [3]. The inversion strategy takes advantage both from the reduced degree of nonlinearity of the CS-EB scattering model with respect to parameters embedding the unknowns of the problem, and from the chosen regularization procedure. As matter of fact, Bayesian approaches [2, 3] have recently been adopted to obtain unsupervised inversion procedures, where the unknowns are modelled by means of random process and the regularization parameters are estimated starting from the (corrupted) scattered fields data without using any a priori information on the unknown targets to reconstruct. To define the a priori function, we have to estimate two hyper-parameter maps (for the real and imaginary part of the overall unknowns of the imaging problem) before actually performing the inversion. Once these parameters have been estimated, they are exploited in the inversion procedure to retrieve the unknown contrast profile, i.e., the permittivity and conductivity profiles of the system of obstacles located in the region under test.

In order to take into account the random noise which is present in the experiment, we also considered an adequate cost functional appropriately weighted by coefficients which change with the frequency, the incident angle and the receiving angle [5]. In particular, each scattered field measurement is balanced with the noise disturbing the data.

Experimental results will be presented and discussed during the conference to highlight the effectiveness and usefulness of the method.

REFERENCES

1. Bucci, O. M., L. Crocco, T. Isernia, and V. Pascazio, "Inverse scattering problems with multi-frequency data: Reconstruction capabilities and solution strategies," *IEEE Transaction Geoscience and Remote Sensing*, Vol. 38, 1749–1756, 2000.
2. Autieri, R., M. D'Urso, V. Pascazio, and T. Isernia, "Exploiting markov random field and an extended range linear approximation for 2D inverse scattering problems," *3rd European Conference on Antennas and Propagation*, 757–760, Berlin, Germany, Mars 2009.
3. Autieri, R., G. Ferraiuolo, and V. Pascazio, "Bayesian regularization in non-linear imaging: Reconstructionfrom experimental data in microwave tomography," *IEEE Transaction Geoscience and Remote Sensing*, in print.

4. Crocco, L., M. D'Urso, and T. Isernia, "New tools and series for forward and inverse scattering problems in lossy media," *IEEE Geoscience and Remote Sensing Letters*, Vol. 1, 327–331, 2004.
5. Eyraud, C., A. Litman, A. Hérique, and W. Kofman, "Microwave imaging from experimental data within a Bayesian framework with realistic random noise," *Inverse Problems*, Vol. 25, 024001, 2009.

Inversion of Subcanopy Soil Moisture Profile Using Radar Data

A. Tabatabaeenejad and M. Moghaddam
Radiation Laboratory, Department of Electrical Engineering and Computer Science
University of Michigan, Ann Arbor, MI 48109, USA

Abstract— Inverse problems in radar remote sensing are of special interest in science and engineering. These problems are translated as determining ecosystem properties such as surface and root-zone soil moisture from radar data. Soil moisture, which determines electromagnetic wave speed profile in the ground, is of particular interest due to its important role in many hydrological and biological processes. Soil moisture information is vital to understanding the cycling of water, energy, and carbon in the Earth system. Knowledge of soil moisture is also critical to agencies concerned with weather and climate prediction, runoff potential and flood control, soil erosion, agricultural productivity, drought monitoring, and human health. The need to monitor soil moisture on a global scale has motivated satellite Earth observation missions such as NASA's Soil Moisture Active and Passive (SMAP). As an airborne complement, the Airborne Microwave Observatory of Subcanopy and Subsurface (AirMOSS) has recently been selected by NASA to provide estimates of root-zone soil moisture as a parameter to reduce the uncertainty in quantifying carbon exchanges between the North American ecosystem and the atmosphere.

Due to the challenging inverse problem associated with estimation of soil wave speed profile, the previous works on subcanopy soil moisture retrieval have mostly modeled the vegetation cover with only one parameter such as an effective dielectric constant, vegetation water content, or vegetation biomass, assuming other parameters of the vegetation are known a-priori. Previous methods have also assumed that the soil medium is a homogeneous half space. This approach neglects the fact that radar response to vegetation is sensitive to several parameters such as vegetation height and other geometrical properties, density, and component dielectric constants, and not simply a function of a single equivalent parameter. Therefore, the geometric arrangement of scatterers has to be taken into account. Moreover, since most of these model parameters such as the branch orientation and soil roughness parameters are characterized with distribution functions, the forward scattering model should incorporate the random nature of these parameters. The other challenge in radar remote sensing problems is that due to the limited number of frequency points and observation angles in the measurements, there are usually fewer number of data points than unknown parameters, making the inverse problem highly ill-posed and under-determined.

We will use a numerical forest scattering model combined with a forward solution for scattering from a rough surface structure to develop a subcanopy soil moisture estimation method with synthesized radar data. We have previously shown that a global optimization scheme such as simulated annealing can retrieve several model parameters in a similar inverse problem with bare soil. We examine the performance of this technique in retrieving subcanopy soil moisture where the vegetation cover is modeled with more than one model parameter. This approach increases retrieval accuracy by eliminating the need to assume several parameters of the vegetation are known a-priori. We also examine the capability of our inversion algorithm in retrieving root-zone soil moisture by modeling the soil with a profile containing more than one layer instead of a single homogeneous half space. The ability to extract additional information comes at the expense of including more measurements, especially at frequencies lower than L-band. This approach therefore assumes availability of two or more frequencies and two or three polarizations, from either airborne or spaceborne instruments. We present inversion results for noise-free data, but the noise response of the inversion for some cases will also be presented.

The Solution of Thick Region Inverse Source Problems with Time Domain TLM

Mohamed H. Bakr, **Yu Zhang**, **and Natalia K. Nikolova**
Department of Electrical and Computer Engineering, McMaster University
Hamilton, Ontario L8S 4K1, Canada

Abstract— The Inverse Source Problem (ISP) aims at solving for the unknown source distribution within a certain source region using available field information. This problem is usually an intermediate step towards solving for the unknown dielectric distribution. This problem is usually non unique and some regularization is required. The vast majority of techniques that aim at solving this problem are frequency domain techniques. With the shift towards utilizing wideband excitations, there is more interest in time domain inversion problems.

In this work, the electromagnetic inverse source problem is solved numerically using the Transmission-Line Modeling (TLM) method. By transforming the fields into the equivalent transmission line (link) voltage impulses, a linear inversion formulation for this vector inverse source problem is developed. We utilize a novel approach for recovering the temporal values of sources in a thick source region using available temporal near field measurements. By back propagating the TLM voltage impulses and imposing both spatial and temporal continuity conditions on the recovered source values, the source temporal values are recovered for the general thick source region case. The computational cost of our approach involves the solution of a small size system of linear equations at each time step. The utilized matrix has constant coefficients and can be LU decomposed only once at the first time step of the inversion process.

Our approach has been successfully illustrated for a number of problems using 2D and 3D TLM examples. In all these examples, we are able to recover the source distributions with good accuracy. Our approach is also shown to be robust against noise in the measured data.

On the Use of Eigenfunction Expansions in Microwave Tomography

J. LoVetri and P. Mojabi
Department of Electrical and Computer Engineering, University of Manitoba
Winnipeg, Manitoba R3T 5V6, Canada

Abstract— During the past few years we have investigated Microwave Tomography (MWT) for biomedical imaging applications. One prototype MWT system that has been constructed consists of a Plexiglas enclosure with 24 co-resident vivaldi antennas being used to acquire scattered-field data in the microwave frequency range of 1 to 6 GHz [1]. Although this configuration has provided good results for imaging in air, redesign of the system such that a lossy matching fluid having a high dielectric constant can be used is still ongoing. At the same time, we've been investigating the use of PEC enclosures within which to perform the scattered-field data collection [2], and several prototypes have been developed where the PEC enclosure is a circular cylinder. We have developed several inversion algorithms based on the Contrast Source Inversion [3] and the Gauss-Newton Inversion [4] algorithms which invert data collected within PEC enclosures of arbitrary shape [5]. These use the finite-element method to discretize the electromagnetic field problem, but we've recently shown how the eigenfunctions of the chamber can be used to expand the unknown contrast function which is to be determined [6]. In this way, the eigenfunction expansion discretizes the problem and the coefficients of the expansion become the unknowns to be determined.

The use of the eigenfunctions to effectively discretize the unknown contrast provides some interesting regularization effects of the inverse problem. It is found that the number of eigenfunctions used acts as a regularization parameter. In [6] the eigenfunctions for a circular PEC enclosure were used. Here we investigate eigenfunction expansions for differently shaped enclosures. In particular, the right-angle isosceles triangle is a shape where the eigenfunctions come in closed-form. We show how these can be used to perform MWT imaging inside a triangular enclosure which is rotated while keeping the antennas fixed with respect to the target being imaged. The rotation of the triangular enclosure in this way provides different boundary conditions for the electromagnetic field problem, and thus diverse information is obtained from the collected scattered-field data. In addition, we investigate the projection of the collected scattered-field data onto the eigenfunction space and discuss how such a procedure may effectively remove some of the measurement noise in the data. Finally, we investigate the use of the orthogonality properties of the eigenfunctions to accurately and efficiently compute the inverse problem functionals.

REFERENCES

1. Gilmore, C., P. Mojabi, A. Zakaria, M. Ostadrahimi, C. Kaye, S. Noghanian, L. Shafai, S. Pistorius, and J. LoVetri, "A wideband microwave tomography system with a novel frequency selection procedure," *IEEE Trans. Biomed. Eng.*, Vol. 57, 894–904, Apr. 2010.
2. Gilmore, C. and J. LoVetri, "Enhancement of microwave tomography through the use of electrically conducting enclosures," *Inverse Problems*, Vol. 24, No. 3, 035008.1–035008.21, 2008.
3. Abubakar, A., P. M. van den Berg, and J. J. Mallorqui, "Imaging of biomedical data using a multiplicative regularized contrast source inversion method," *IEEE Trans. Microwave Theory Tech.*, Vol. 50, 1761–1777, Jul. 2002.
4. Mojabi, P. and J. LoVetri, "Microwave biomedical imaging using the multiplicative regularized Gauss-Newton inversion," *IEEE Antennas and Wireless Propagation Letters*, Vol. 8, 645–648, 2009.
5. Mojabi, P., C. Gilmore, A. Zakaria, and J. LoVetri, "Biomedical microwave inversion in conducting cylinders of arbitrary shapes," *13th International Symposium on Antenna Technology and Applied Electromagnetics and the Canadian Radio Science Meeting (ANTEM/URSI)*, 1–4, Feb. 2009.
6. Mojabi, P. and J. LoVetri, "Eigenfunction contrast source inversion for circular metallic enclosures," *Inverse Problems*, Vol. 26, No. 2, 025010, 2010.

Combination of Contrast Source Extended Born Model and Subspace Based Optimization Method for Reconstruction of Lossy High Dielectric Scatterers

Krishna Agarwal[1], **Michele D'Urso**[2], **and Xudong Chen**[1]

[1]National University of Singapore, #E4-05-45, 4 Engineering Drive 3, 117576, Singapore
[2]SELEX Sistemi Integrati, Via Circumvallazione Esterna di Napoli
zona ASI, I-80014 Giugliano, Napoli, Italy

Abstract— The current work applies subspace based optimization method in the framework of contrast source extended Born model for reconstruction of lossy and high dielectric scatterers. The problem of reconstructing the high dielectric extended scatterers is difficult due to the increase in the mathematical non-linearity of the physical scattering model.

Contrast Source Extended Born model (CSEB) was presented in [1, 2] for reducing the degree of non-linearity of the reconstruction problem of lossy and high dielectric scatterers. It considers the contrast source model (also called the coupled dipole model) and proposes a mathematically equivalent model that has lesser non-linearity than the original problem. It achieves this aim by modifying the contrast function and the internal field mapping operator. The original proposition of CSEB was for the case where the background medium is lossy. Recently, its applicability has been studied for lossless background medium too.

Subspace-based Optimization Method (SOM) [3, 4] was proposed recently for two-dimensional scalar electromagnetic inverse problems. SOM utilizes information of physical import for optimization by splitting the induced currents into mathematically deterministic and ambiguous portions and using optimization for the ambiguous portion only. The deterministic portion provides a good initial guess for the optimization problem. Due to this, SOM is robust to noise and converges fast. The original work on SOM considered the coupled dipole model (CDM) as the physical scattering model.

In this paper, we combine CSEB and SOM (and call it CSEB-SOM). We test the effectiveness of the combination in two ways:

1. We perform a comparison of the convergence characteristics of CSEB, SOM, and CSEB-SOM.
2. We compare the reconstruction results obtained by CSEB, SOM, and CSEB-SOM.

Our results show that:

1. CSEB-SOM not only converges faster than both CSEB and SOM, it also provides better reconstruction results as compared to both the techniques.
2. SOM-CSEB is benefitted by the decrease in the non-linearity due to the CSEB model.
3. SOM-CSEB is benefitted by the fast convergence characteristics of SOM.
4. SOM-CSEB is benefitted by a good initial guess used in SOM. Both SOM and CSEB-SOM begin at a lower value of the cost function as compared with the CSEB.

REFERENCES

1. Catapano, I., et al., "A novel effective model for solving 3-D nonlinear inverse scattering problems in lossy scenarios," *IEEE Geoscience and Remote Sensing Letters*, Vol. 3, 302–306, 2006.
2. Isernia, T., et al., "New tools and series for forward and inverse scattering problems in lossy media," *IEEE Geoscience and Remote Sensing Letters*, Vol. 1, 327–331, 2004.
3. Chen, X., "Application of signal-subspace and optimization methods in reconstructing extended scatterers," *Journal of the Optical Society of America A*, Vol. 26, 1022–1026, 2009.
4. Chen, X., "Subspace-based optimization method for solving inverse scattering problems," *IEEE Transactions on Geoscience and Remote Sensing*, Vol. 48, 42–49, 2009.

Elastodynamic Wave Field Inversion for Applications in Non-destructive Testing

K. J. Langenberg
University of Kassel, Germany

Abstract— In contrast to acoustic and electromagnetic waves elastic waves in solids exhibit two different wave modes, i.e., pressure waves with longitudinal and shear waves with transverse polarization. Since the two wave modes have different phase velocities, they can be time gated in an ultrasonic experiment for defect detection in specimens. Within a further approximation the remaining one mode data can be additionally simplified assuming them as scalar quantities. Appropriate inversion schemes can then rely on scalar diffraction tomography in the time domain. Yet, unfortunately, important information about scatterers is thrown away applying this procedure. Therefore, the paper proposes a (linear) elastodynamic inversion scheme based on the simultaneous utilization of directly scattered and mode converted contributions to the data. It essentially relies on the polarization properties of the different wave modes to be directly exploited in the K-space of diffraction tomography. Applications to synthetic data validate the algorithm that is subsequently applied to experimental data obtained from ultrasonic non-destructive testing of concrete to show its superiority with regard to previous scalar algorithms.

Experimental Study on Imaging Algorithm with Simple UWB Radar for a Target with Translation and Rotation

T. Sakamoto and T. Sato
Graduate School of Informatics, Kyoto University, Yoshida-Honmachi, Sakyo-ku, Kyoto 606-8501, Japan

Abstract— Ultra Wide-Band (UWB) radar has been considered a promising technology for the development of a reliable security system. To develop a cost-effective high-resolution radar imaging system, one important factor is the number of antennas required in the system. Most conventional imaging methods [1, 2] employ systems with large-scale antenna arrays. Matsuki et al. [3] proposed a method using only three antennas which estimates the translation motion of the target. However, this method cannot be applied to a target with rotation. This paper presents a new algorithm that can obtain an image of a target with arbitrary motion including rotation.

A 2-dimensional model is assumed for simplicity. A 5-element linear antenna array is installed at fixed intervals. Each antenna is operated as a mono-static radar system. $R_i(t)$ is defined as a measured range to the target from the i-th antenna. The proposed method estimates a local target shape for each time step using an elliptical model with five parameters; the long and short axes a and b, the center of the ellipse (x_0, y_0), and the rotation angle θ. The distance between the i-th antenna and this elliptic model is denoted as $r_i(a, b, x_0, y_0, \theta)$. The parameters (a, b, x_0, y_0, θ) are estimated by an optimization process. The optimization process is divided into two phases; optimization of the shape parameters (a, b) and the motion parameters (x_0, y_0, θ).

The parameters (a, b) are estimated by minimizing the following function using a linear search algorithm

$$(\hat{a}, \hat{b}) = \arg\min_{a,\,b} \sum_{t=T_1}^{T_2} \min_{x_0, y_0, \theta} \sum_{i=1}^{N_a} |r_i(a, b, x_0, y_0, \theta) - R_i(t)|^2, \tag{1}$$

where $N_a = 5$ is the number of antennas. For each (a, b), the rest of the parameters (x_0, y_0, θ) are optimized using the Levenberg-Marquardt algorithm. In the optimized parameter set, (x_0, y_0) and θ correspond to the translation and rotation of the target. The target image at $t = 0$ is estimated from the scattering center points by compensating for these motion parameters. The proposed method is applied to experimental data measured with the UWB experimental system shown in Fig. 1. Solid lines in Fig. 2 show the actual target shapes moving to the right-hand side while rotating counter-clockwise. Here, triangle symbols on the x-axis show 5 antenna positions. An estimated image is shown with black dots in Fig. 2 along with the estimated translation (x_0, y_0), which shows the proposed method can accurately estimate a target shape with actual measurement data.

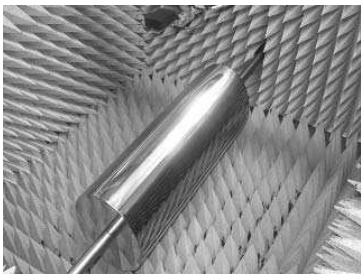

Figure 1: Experimental site for UWB radar imaging.

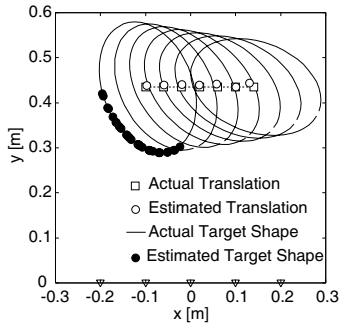

Figure 2: Target shape estimated by proposed method.

REFERENCES

1. Yarovoy, A. G., et al., *IEEE Trans. on Microwave Theory & Tech.*, Vol. 55, No. 6, Part 2, 1288–1295, Jun. 2007.
2. Jofre, L., et al., *Proceedings of the IEEE*, Vol. 97, No. 2, 451–464, 2009.
3. Matsuki, Y., et al., *Proc. 20th International Conf. on Applied Electromagnetics and Commun.*, Sep. 2010.

Re-arranging Scattering Equations to Counteract Non Linearity of the Inverse Problem: Rationale and Comparisons

L. Crocco[1], **M. D'Urso**[2], **T. Isernia**[3], **and A. F. Morabito**[3]

[1]Istituto per il Rilevamento Elettromagnetico dell'Ambiente, CNR
Via Diocleziano 328, I-80324 Napoli, Italy
[2]Innovation Team, Intangible Capital Directorate Managment, SELEX Sistemi Integrati S.p.A.
Via Circumvallazione Esterna di Napoli, Loc. Pontericci zona ASI
I-80014 Giugliano di Napoli, Napoli, Italy
[3]Dipartimento di Informatica, Matematica, Elettronica e Trasporti
Università 'Mediterranea' di Reggio Calabria, I-89124 Reggio Calabria, Italy

Abstract— In the electromagnetic community, the development of convenient equation models for describing electromagnetic scattering phenomena and/or solving the corresponding forward and inverse problems is a crucial, open issue. The adopted formulations strongly affect the feasibility, effectiveness, and computational complexity of the corresponding solution procedures and play a key role in a large number of applications adopting noninvasive diagnostic techniques, among which ground-penetrating radar and medical imaging.

This contribution is aimed at reviewing and properly comparing a number of approaches proposed for the quantitative solution of inverse scattering problems, from one side, and at presenting possible new ideas to enlarge feasibility and performances of the corresponding techniques, from the other. In particular, while a general overview of all the available solution strategies is outside of the scope of this letter, we will focus on some models which try to solve the problem in terms of both the constitutive characteristics of the targets and a field in the domain of interest.

In particular, the approaches based on the so-called modified gradient technique by Kleinman and Van den Berg [1], the subsequent approach by the same authors based on *Source-Type Integral Equation* (see f.i. [2]), as well as the more recent approach by Isernia et al. [3], and possible approaches based (when applicable) to the so called 'Strong permittivity fluctuation theory' [4] will be reviewed and compared on the basis of the concept of the *degree of non linearity* [5, 6] of the problem with respect to constitutive parameters.

Finally, some suggestions for further improving robustness with respect to false solutions (arising from non linearity) will be given.

REFERENCES

1. Kleinman, R. E. and P. M. Van Den Berg, "An extended modified gradient technique for profile inversion," *Radio Sci.*, Vol. 28, 877–884, 1993.
2. Van Den Berg, P. M. and R. E. Kleinman, "A contrast source inversion method," *Inv. Probl.*, Vol. 13, No. 6, 1607–1620, Dec. 1997.
3. Isernia, T., L. Crocco, and M. D'Urso, "New tools and series for forward and inverse scattering problems in lossy media," *IEEE Geosci. Remote Sens. Lett.*, Vol. 1, No. 4, 327–331, Oct. 2004.
4. Ma, J. L., W. C. Chew, C. C. Lu, and J. M. Song, "Image reconstruction from TE scattering data using strong permittivity fluctuation theory," *IEEE Antennas and Propagation Society International Symposium*, Vol. 2, 702–705, 1998.
5. Isernia, T., V. Pascazio, and R. Pierri, "On the local minima in a tomographic imaging technique," *IEEE Trans. Geosci. Remote Sens.*, Vol. 39, No. 7, 1596–1607, Jul. 2001.

Solving 2-D Inverse Scattering Problems Using Truncated Cosine Fourier and Cubic B-spline Expansions

Abbas Semnani[1], **Ioannis T. Rekanos**[2], **Manoochehr Kamyab**[1], **and C. S. Antonopoulos**[2]

[1]K. N. Toosi University of Technology, Tehran, Iran
[2]Aristotle University of Thessaloniki, Thessaloniki, Greece

Abstract— From the mathematical point of view, an inverse problem is governed by two main difficulties [1]. First, it is a nonlinear problem, which is usually solved by iteratively minimizing a cost function describing the discrepancy between measured and estimated field data. The second difficulty is the ill-posedness introduced by the compactness of the direct scattering operator which is usually suppressed by means of regularization techniques [2], by imposing any a priori information in the scatterer description [3], and by applying frequency-hopping techniques [4].

Usually in solving inverse scattering problems, the properties inside the scatterer region are expressed as a sum of weighted pulse functions of rectangular support which is referred as the pulse function expansion (PFE) [5]. The PFE results in fine resolution of the reconstructed scatterer profile, but it requires the determination of huge number of unknown parameters. Furthermore, the PFE is very sensitive to the ill-posedness effects, especially when noisy field measurements are involved. In an alternative approach, the number of problem unknowns and consequently the ill-posedness can be suppressed by reducing the dimensions of the functional space of the spatial distributions of the scatterer properties. For example, it is possible to represent the unknown scatterer profile in an expansion and optimize the expansion coefficients in an optimization routine [6].

In this paper, we consider solving two-dimensional (2-D) inverse scattering problems by using truncated cosine Fourier expansion (TCFE) and cubic B-spline expansion (CBSE). Both expansion techniques are examined in reconstruction of some unknown scatterers and the results are compared in terms of reconstruction accuracy and convergence speed. Also, the effect of number of expansion terms in the quality of reconstruction is investigated for each expansion techniques. Fig. 1 shows the results of a sample permittivity profile reconstruction.

It is shown that both expansion methods are powerful tools in solving inverse scattering problems with the main features of reduction the number of unknowns and removal the need to regularization term in comparison with conventional pulse function expansion (PFE) method. Although CBSE has the winning factors of controllable coefficients and consequently faster convergence rate, TCFE has the better ability of reconstruction the sharp edges especially with the number of expansion terms larger than four if the routine let to completely converge by increasing the number of optimization iterations.

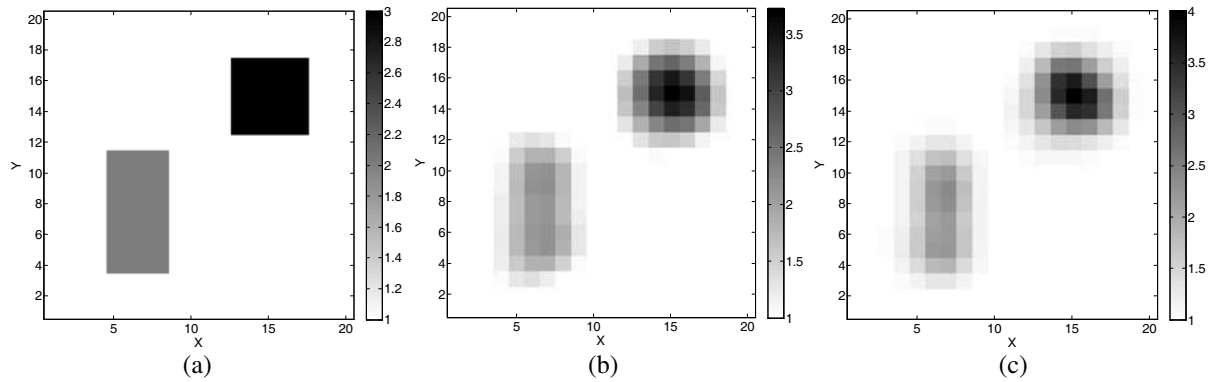

Figure 1: Permittivity profile reconstruction. (a) Original profile, (b) by TCFE method, (c) by CBSE method, both with $7 * 7$ expansion terms after 800 iterations.

REFERENCES

1. Colton, D. and R. Kress, *Inverse Acoustic and Electromagnetic Scattering Theory*, Springer-Verlag, Berlin, 1992.
2. Tikhonov, A. N. and V. Y. Arsenin, *Solutions of Ill-Posed Problems*, Winston, Washington, DC, 1977.
3. Fhager, A. and M. Persson, "Using a priori data to improve the reconstruction of small objects in microwave tomography," *IEEE Trans. Microwave Theory Tech.*, Vol. 55, No. 11, 2454–2462, Nov. 2007.
4. Rekanos, I. T. and T. D. Tsiboukis, "A finite element based technique for microwave imaging of two-dimensional objects," *IEEE Trans. Instrum. Meas.*, Vol. 49, No. 2, 234–239, Apr. 2000.
5. Rekanos, I. T., T. V. Yioultsis, and C. S. Hilas, "An inverse scattering approach based on the differential E-formulation," *IEEE Trans. Geosci. Remote Sensing*, Vol. 42, No. 7, 1456–1461, Jul. 2004.
6. Semnani, A. and M. Kamyab, "Truncated cosine Fourier series expansion method for solving 2-D inverse scattering problems," *Progress In Electromagnetics Research*, Vol. 81, 73–97, 2008.

Session 2P6a
Antenna and Array 2

New Reconfigurable PIFA Antenna Based on the Transform of Geometry in Space

Trong Duc Nguyen[1], **Ngoc Hien Doan Thi**[1], **Yvan Duroc**[2], **Van Yem Vu**[3], **and Tan Phu Vuong**[1]

[1]Laboratory LAHC, Institute Microelectronic Electromagnetic and Photonic, Grenoble INP-Minatec
3 Parvis Louis Neél, BP 257, 38016 Grenoble Cedex 1, France
[2]Laboratory LCIS, Grenoble INP, 50 Barthélémy de Laffemas BP 54, 26902 Valence Cedex 9, France
[3]Faculty of Electronics and Telecommunications, Hanoi University of Science and Technology
1Dai Co Viet Road, Hanoi, Vietnam

Abstract— The development of new wireless communication systems such as cognitive radio, wireless sensor network, ad-hoc network is experiencing an exponential growth. As a result, new antennas have to be developed to provide a large bandwidth, a compact size and especially the possibility of their adaptive parameters for environment changing. The reconfigurable PIFA antenna is an interesting model one. Reconfigurable antenna is used common in the broadband wireless communication systems and it can change the configuration itself. The change of antenna configuration is made by a modification of frequency, radiation pattern, the polarization or a combination of all factors. Reconfiguring an antenna may be achieved by many techniques. Some designers have used circuit elements, while others rely on the mechanical alteration of the structure such as rotation or bending of one or more of parties. Other approaches use different antennas parties at different times, the supply networks or reconfigure appropriately exciting the antenna arrays. More recently, designers have used antennas switches actuated variable capacitors electric to achieve a reconfiguration diode PIN, MEMs some of the most widely used electrical devices operated. All these approaches have significantly contributed to the development of reconfigurable antennas during the last decade. With a Reconfigurable Planar Invert F Antenna (RPIFA) antenna, changing the frequency or polarization is quite simple by varying the shape of the radiation patch or by adding some slots on the patch. In this paper, we propose a new reconfigurable PIFA antenna that can be tuned in a wide frequency band of 5 GHz from 2 GHz to 7 GHz by changing the geometry of the radiation patch. Starting from an initial antenna with a triangular patch that is combined from the smaller triangles and when converting this section to the center or the axis of rotation we can obtain different structures corresponding to the different geometries such as rectangular, square etc. With each patch obtained from different geometries, we collect the corresponding antenna with the operating frequency band from 2 GHz to 7 GHz. We also develop an automatic embedded Genetic Algorithm in Computer Simulation Technology tool for multiple antenna parameters optimization. The novel RPIFA antenna is designed optimized and implemented using the developed GA model. The simulation and measurement results of antenna parameters are compared to show the performance of the developed antenna.

Miniaturized Printed Yagi Antenna for 2.45 GHz RFID Readers

G. Bulla[1, 2], M. T. Le[1], A. A. A. de Salles[2], and T. P. Vuong[1]

[1]Institut de Microélectronique Electromagnétisme et Photonique
Laboratoire d'Hyperfréquences et de Caractérisation, Grenoble Institute of Technology (GINP), France
[2]Electrical Engineering Department, Federal University of Rio Grande do Sul (UFRGS), France

Abstract— In this paper, a miniaturized printed Yagi antenna with bent arms is proposed for radio frequency identification (RFID) readers operating at the frequency of 2.45 GHz. The proposed antenna design, analysis and characterization has been performed using CST electromagnetic simulation software. The antenna was fabricated with ROGERS4003 substrate. Reflection coefficient and directivity results were simulated and measured.

In recent years, RFID has been widely used in service industries as an automatic identification tool. Several frequency bands have been standardized for this technology, low frequency (LF, 125–134 kHz), high frequency (HF, 13.56 MHz), ultra-high frequency (UHF, 860–960 MHz) and microwave (2.4 GHz and 5.8 GHz). The systems using the UHF band and 2.45 GHz band are believed suitable for long-distance communication utilizing a passive type RFID. However, because the UHF band overlaps with the frequency of a cellular phone, the UHF band is not preferable. Therefore, the 2.45 GHz band is preferred.

Printed Yagi antennas are attractive alternatives to conventional wire Yagi antennas since they can be manufactured using printed circuit techniques and are thus readily amenable to large scale integration with microstrip technology. In this paper, a new microstrip-fed printed Yagi antenna working at 2.45 GHz for RFID reader application is presented. By bending the arms of the Yagi antenna a new miniaturized antenna designed.

The initial configuration is a printed Yagi antenna with arm with length L and a distance D from the ground plane, one radiator with length Lr is also present. ROGERS4003 substrate with height 0.8 mm was used. The two arms of the Yagi antenna are printed on opposite sides of the substrate to maintain the correct phasing between the arms. In order to maximize end-fire radiation, the printed dipole is designed so that it is approximately a quarter wavelength ($D = \lambda/4$) from the ground plane. The length L was chosen in order to obtain the antenna resonance at 2.45 GH and Ld was chosen in order to maximize the directivity. The final length L is 25 mm. The miniaturization is achieved by bending both arms of the Yagi antenna at a position Lm. The final geometry has $Lm = 15.5$ mm. The total size of the arm is the same as the initial design. The total width of the miniaturized Yagi antenna is about 30% smaller than the initial design. An array with 2 miniaturized antennas elements was also designed and analyzed.

The antennas were prototyped. Reflection coefficient and directivity were measured. Good agreement between simulated and measured results is observed. The relative bandwidth is about 14% for both antennas (miniaturized and non-miniaturized antenna). The central frequency of the initial antenna is close to 2.45 GHz. A small increase in the central frequency is observed when the dipole arms are bent.

The initial antenna shows 6.41 dBi directivity, 70.4° for the angular width at the xy plane, and 133° for the angular width at the zx plane. The miniaturized antenna shows 4.9 dBi directivity, 80° for the angular width at the xy plane, and 165° for the angular width at the zx plane. The array of antennas with 2 miniaturized elements shows 7.4 dBi directivity, 43° for the angular width at the xy plane, and 161° for the angular width at the zx plane.

A Matrix-vector-potential Analysis of the Bi-elliptical Toroidal Helical Antenna

S. A. Adekola[1, 2], **A. Ike Mowete**[1], **and H. A. Muhammed**[1]

[1]Department of Electrical and Electronics Engineering, Faculty of Engineering
University of Lagos, Lagos, Nigeria
[2]Department of Electrical and Electronics Engineering, Niger Delta University
Wilberforce Island, Yenegoa, Nigeria

Abstract— This paper develops exact expressions for the radiation fields of a single-wound bi-elliptical toroidal helical antenna, based on the vector magnetic potential approach. Using the conventional thin-wire approximation in which current flow is constrained along the wire's axis, a vector-potential-matrix is developed for the problem in terms of the unknown current distribution and physical attributes of the wire antenna. Entries into this vector-potential-matrix lend themselves into certain physical interpretations, which facilitate a number of conclusions concerning the physics of the problem. For example, it becomes readily discernible that the antenna's radiation field admits description as a sum of two expressions; one deriving from the main loop, and the other associated with the poloidal loops of the antenna. This same conclusions were arrived at from the results of the empirical investigations reported in the open literature by Wanamassa et al. [1], and Corum [2].

Analytical results obtained in the paper also clearly indicate that the radiation fields may also be attributed to contributions associated with electric and magnetic currents excited in the antenna's main loop and poloidal loops, respectively. It is shown in the paper that the field expressions developed by the analytical approach reported, also serve as corresponding expressions for certain other configurations of the toroidal antenna as special cases.

REFERENCES

1. Wanamassa, M. A., K. I. Elberon, and W. A. S. Fair Haven, "Helical coil coupled to a live tree to provide a radiating antenna," U. S. Patent Number 3, 646, 562, February 29, 1972.
2. Corum, J. F., "Toroidal antenna," U. S. Patent Number 4, 622, 558, November 11, 1986.

Applications and Properties of Array Lenses for Circular Polarization

M. Okoniewski and R. H. Phillion
Department of Electrical and Computer Engineering, University of Calgary, Canada

Abstract— Array lens antennas can be phased using several techniques, including element rotation. Any of the techniques can be used to collimate radiation from a feed antenna into a narrow beam; however, the element rotation technique can be used for some additional applications, as it possesses unique properties.

For this technique, which applies exclusively to circular polarization (CP), the elemental antennas of the array are all identical, but they have different rotational orientations in the plane of the array. The interaction between the rotational nature of CP and the physical element rotation creates a phase shift if the element is designed to meet certain criteria. Specifically, the element must change the handedness of CP as the incident wave passes through the lens. If this is achieved, rotation of an element will shift the phase of the transmitted wave by twice the rotation angle. Importantly, the sign of the phase shift is determined by the handedness of the incident wave, i.e., the phase shift is polarization dependent.

This property can be used to create array lenses with interesting cross-polarization properties. The applications of these lenses include high-gain antennas, beam-splitters and polarization purifiers. When used as part of a high-gain antenna, the lens converges radiation from a feed antenna. By using element rotation to phase the array, only one handedness of CP will be converged. In fact, the lens will diverge the radiation component in the cross-polarized handedness. For a large array, this will result in an antenna system with a good cross-polarization discrimination ratio. Other applications and measurement results will also be presented.

Dual Band 3×3 Polarised Mimo Antenna System

Muhammad Usman, **Mohamad Rahal**, **and Ibrahim Rida**
Department of Electrical Engineering, University of Hail, P. O. Box 2440, Hail, Saudi Arabia

Abstract— A triple, dual-band inverted F antenna system is presented, intended for MIMO applications in mobile handsets accessing high-speed wireless local area networks (IEEE 802.11a/b/g /n standards). A comprehensive study was carried out in order to understand the enhancement of channel capacity and the effect of polarisation diversity. Means of achieving minimum coupling between the three antennas were investigated over the 2.45 GHz and 5.2 GHz bands. The antennas are placed in a geometrical configuration appropriate to implement the desired field and polarisation. All of the three polarised antennas in the system are resonant at 2.4 GHz and 5.2 GHz, with the return loss and coupling less than −12 dB. The overall volumetric dimensions of each antenna were $30 \times 15 \times 8$ mm. Each antenna contains two parts: a PIFA resonant at 2.4 GHz and an inverted-L behaving as a capacitive load and responsible for the resonance at 5.2 GHz. Furthermore, the results has been simulated and measured for the 3×3 MIMO system without and with human hand around it.

Session 2P6b
Reconfigurable Antennas

Design of an Antenna with Reconfigurable Band Rejection for UWB Cognitive Radio

M. Al-Husseini[1], Y. Tawk[2], C. G. Christodoulou[2], K. Y. Kabalan[1], and A. El-Hajj[1]

[1]ECE Department, American University of Beirut, Beirut 1107 2020, Lebanon
[2]ECE Department, University of New Mexico, Albuquerque, NM 87131, USA

Abstract— Ultrawideband (UWB) communication is commonly achieved using the impulse radio based UWB technology (IR-UWB), or the Orthogonal Frequency Division Multiplexing based UWB (UWB-OFDM). IR-UWB is carried out by transmitting extremely short pulses, whereas in OFDM-based UWB, orthogonal subcarriers are employed to modulate the transmitted data. As per FCC regulations, UWB systems are allowed to operate in the 3.1–10.6 GHz band without a license requirement, but under very strict transmission power limits. This property of UWB, in addition to its other advantages, makes it very suitable as the enabling technology for underlay Cognitive Radio [1].

Though usually associated with the underlay mode, UWB can also be used in the overlay Cognitive Radio mode (also called opportunistic spectrum access or OSA). In the overlay mode, the transmitted power can be increased to a level that is comparable to the power of licensed systems (an advantage would be long-distance communication as compared to short- and medium-range communication in the underlay case), but this requires the UWB transmitter to avoid spectrum bands that are used by other systems. This can be achieved in UWB-OFDM by turning off the subcarriers in the bands used by primary services, and in IR-UWB by using adaptive UWB pulses characterized by the ability to form, in their spectral masks, notches in the bands used by existing narrow-band wireless services operated in the 3.1–10.6 GHz UWB range [2].

In the overlay UWB scenario, the antenna at the front-end of the Cognitive Radio device should be capable of operating over the whole UWB range, for sensing and determining the bands that are being used by primary users, but should also be able to induce band notches in its frequency response to prevent interference to these users. In this paper, we propose such an antenna. Depicted in Fig. 1, the antenna is a monopole printed on a 1.3-mm-thick Rogers RO3006 substrate with $\varepsilon_r = 6.15$, and features a partial ground plane. A ring slot is etched on the patch, and three electronic switches, S1, S2 and S2', are mounted across it, as shown in Fig. 1. When any of the

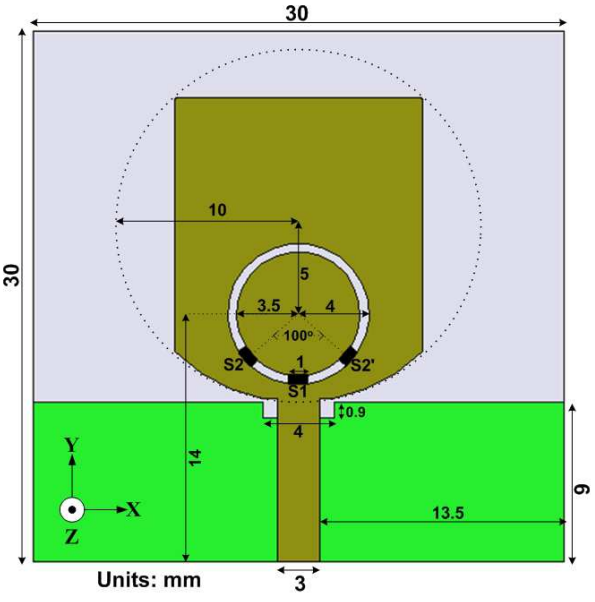

Figure 1: Antenna configuration.

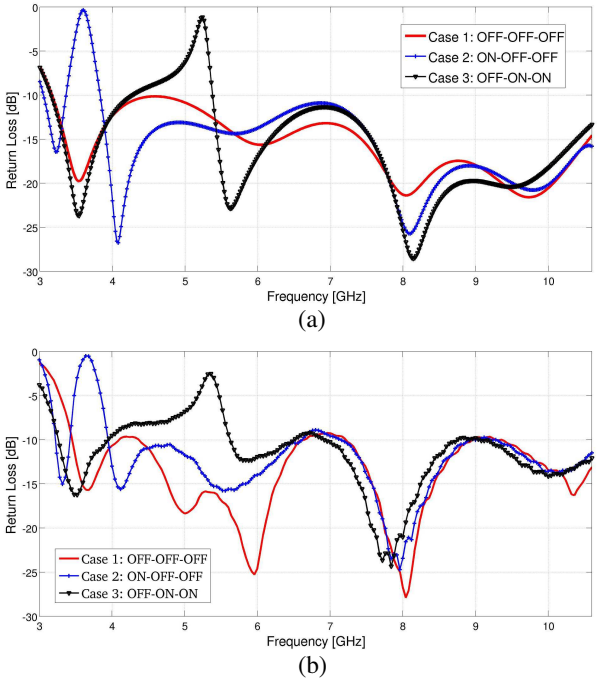

Figure 2: (a) Simulation S_{11}. (b) Measured S_{11}.

switches is ON, the slot will behave as a complementary split-ring resonator (CSRR). CSRRs and their dual-counterparts, the split-ring resonators, are employed in [3] in the design of UWB antennas with fixed notched bands. When all three switches are OFF, the antenna has a UWB response (required for sensing). When only S1 is ON, the antenna has a band rejection in the frequency range used by fixed satellites. When S2 and S2' are ON, a notch appears in the U-NII band. The notches are strong, with values better than -2 dB. The antenna has omnidirectional patterns and good gain values in the band(s) of operation.

REFERENCES

1. Arslan, H. and M. Sahin, "UWB-based cognitive radio networks," *Cognitive Wireless Communication Networks*, E. Hossain and V. Bhargava, (Ed.), 213–230, Springer, US, 2007.
2. Zhang, H., X. Zhou, and T. Chen, "Ultra-wideband cognitive radio for dynamic spectrum accessing networks," *Cognitive Radio Networks*, Y. Xiao and F. Hu, (Ed.), 353–382, CRC Press, Boca Raton, Florida, 2009.
3. Zhang, Y., et al., "Planar ultrawideband antennas with multiple notched bands based on etched slots on the patch and/or split ring resonators on the feed line," *IEEE Trans. Antennas Propagat.*, Vol. 56, No. 9, 3063–3068, Sept. 2008.

Overview of Reconfigurable and Compact Antennas Using a Magneto-dielectric Material

L. Huitema[1], **M. Hajj**[1], **T. Monédière**[1], **D. Souriou**[2], **A. Chevalier**[2], **J.-L. Mattei**[2], **and P. Queffelec**[2]

[1]Xlim Laboratory, 123 av. Albert Thomas, Limoges 87060, France
[2]Labsticc Laboratory, UMR CNRS 3192, 6 av. Le Gorgeu 29238, Brest cedex 3, France

Abstract—

Introduction: An overview of the challenges to design reconfigurable and compact antennas, developed in the framework of a project called NAOMI is presented. Two novel designs dedicated to low frequencies handheld applications are explained. Since reconfigurable radiation patterns allow improving the quality and reliability of wireless links, the first design exhibits a wideband compact antenna with pattern diversity. The second one explains a tunable frequency antenna thanks to a varactor component. Both designs are suitable for mobile devices. Good performances, compactness and low frequencies are obtained thanks to a magneto-dielectric material elaborated with nanoferrites particles.

Overview of The Two Designs:

First design: The antenna structure presented Fig. 1 in this subsection is based on the IFA design [1, 2]. In order to decrease the global antenna dimensions, the monopole has been folded on a magneto-dielectric material. The antenna is studied on a 230 mm×130 mm ground plane, defined by the project specifications to correspond to a standard DVB-H handheld receiver. To obtain pattern diversity, two radiating elements are orthogonally integrated. This antenna covers nine channels of the DVB-H band going from 790 MHz to 862 MHz with a realized gain higher than the one required by the DVB-H application as shown Fig. 2.

Second design: The value added by this new design presented Fig. 3, based on the first one, is to integrate a varactor component allowing the frequency tunability of the antenna on the entire DVB-H band as shown Fig. 4.

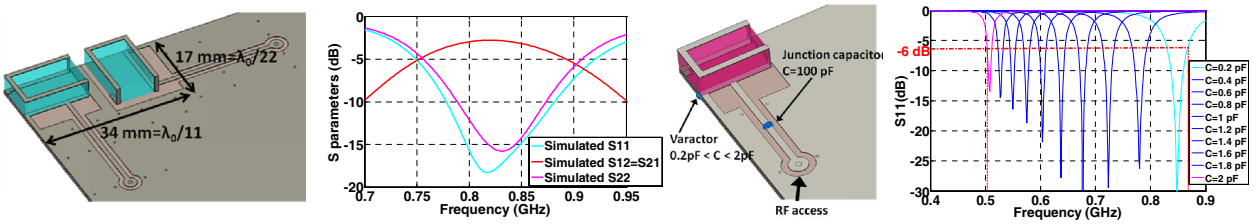

(a) (b) (c) (d)

Figure 1: (a) Design of the first antenna. (b) S parameters of the first antenna. (c) Design of the second antenna. (d) S_{11} parameters for each capacity value.

Conclusions: Two antenna designs have been presented. They both have reconfigurable radiation patterns. Moreover, one of the two designs integrates a varactor component allowing the frequency tunability of the antenna on the entire DVB-H band. The first design has been realized and it presents the same performances in measurement as in simulations. The second one is in process to be manufactured.

REFERENCES

1. Ling, C.-W., C.-Y. Lee, C.-L. Tang, and S.-J. Chung, "Analysis and application of an on-package planar inverted-F antenna," *IEEE Transactions on Antennas and Propagation*, Vol. 55, No. 6, 1774–1780, June 2007.
2. Ammann, M. J. and L. E. Doyle, "A loaded inverted-F antenna for mobile handset," *Microwave and Optical Technology Letters*, Vol. 28, 226–228, 2001.

An Ultra-miniature Tunable Antenna Using a Magneto-dielectric Material for DVB-H/DVB-T Applications

C. M. A. Niamien, S. Collardey, A. Sharaiha, and K. Mahdjoubi
Institut d'Electronique et des Télécommunications de Rennes
Groupe Antennes & Hyperfréquences, Université Européenne de Bretagne (UEB), UR1
263, Avenue du Général Leclerc CS 74205, 35042 Rennes cedex, France

Abstract— In the concept of the mobile TV reception, building microwave modules such as antennas that exhibit small sizes and good performances is still a challenge. Because a mobile TV receiver is of a few centimeter-sized (typically $23 \times 13\,\mathrm{cm}^2$), classical antennas such as monopoles are inconvenient. With folded radiating elements (meanders, fractals, etc.) small sizes can be achieved but such antennas are rather low-efficiency and short-bandwidth antennas [1]. The use of high-permittivity dielectric materials offer an interesting size reduction but the bandwidth is significantly reduced [2]. However, this limitation is overcome by magneto-dielectric materials which give a larger bandwidth than dielectric ones [3–5].

Therefore, a promising technique to obtain an efficient small antenna could be achieved by combining both a folded radiating element with the use of a magneto-dielectric material as a superstrate (MF114 [6]). In this paper, the effectiveness of such a miniaturization technique is investigated and validated experimentally by the design of an ultra-miniature planar meander antenna (of size $\lambda_0/41$) which is designated for DVB-H/DVB-T applications around 470MHz (Figure 1). In order to cover the entire DVB-H frequency band (470–862 MHz) without enlarging the antenna size, the frequency agility is achieved by using only some lumped variable capacitors without adding an external impedance matching circuit.

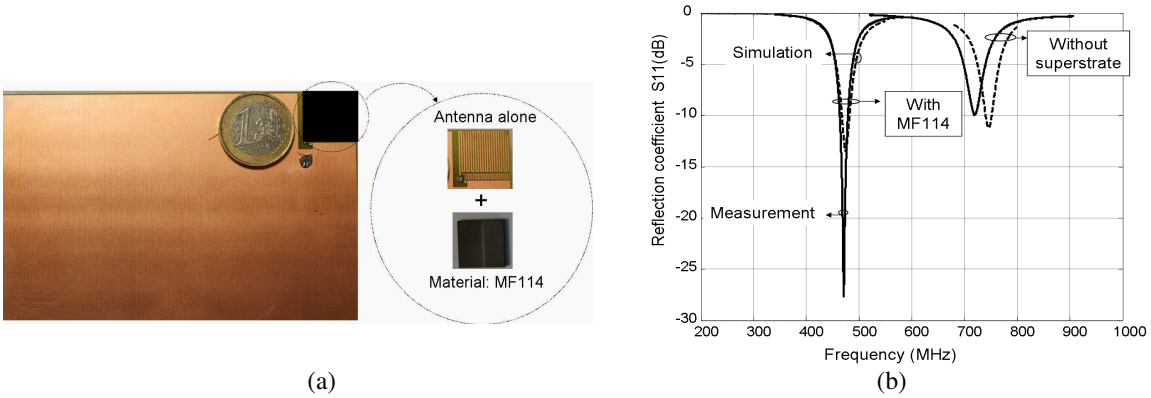

(a) (b)

Figure 1: Prototype of the realized antenna. (a) Photograph. (b) Simulated and measured reflection coefficient S_{11}.

REFERENCES

1. Best, S. R., "A comparison of the performance properties of the Hilbert curve fractal and meander line monopole antennas," *Microwave Opt. Technol. Lett.*, Vol. 35, 258–262, 2002.
2. Hwang, Y., Y. P. Zhang, G. X. Zheng, and T. K. C. Lo, "Planar inverted-F antenna loaded with high permittivity material," *Electron. Lett.*, Vol. 20, 1710–1712, 1995.
3. Hansen, R. C. and M. Burke, "Antennas with magneto-dielectrics," *Microwave Opt. Technol. Lett.*, Vol. 2, 75–78, 2000.
4. Mosallaei, H. and K. Sarabandi, "Magneto-dielectrics in electromagnetic: Concept and applications," *IEEE Trans. Antennas and Propagat.*, Vol. 52, 1558–1567, 2004.
5. Ikonen, P., et al., "Magneto-dielectric substrates in antenna miniaturization: Potential and limitations," *IEEE Trans. Antennas and Propagat.*, Vol. 54, 3391–3399, 2006.
6. ECCOSORB®MF, Emersion & Cuming Microwave products website. [Online]. Available: http://www.eccosorb.com/products.

Small Reconfigurable PIFA for DVB-H Applications

F. Canneva, F. Ferrero, J. M. Ribero, and R. Staraj
Laboratoire d'Electronique Antennes et Télécommunications, Université de Nice Sophia-Antipolis
bât. 4, 250 rue Albert Einstein, Valbonne 06540, France

Abstract— This paper presents a new miniature reconfigurable DVB-H antenna for a portable TV or tablet PC device. The antenna consists in a Printed-Inverted-F-Antenna (PIFA) loaded by a varactor diode. The antenna has a size of $30*30*5\,\mathrm{mm}^3$ and is mounted on a $230*130\,\mathrm{mm}^2$ PCB. The antenna is loaded by a varactor diode, connected to the antenna by a 3 mm-thick metallic strap, which will allow to choose the desired channel in the DVB-H band. Indeed, as the frequency behavior of the PIFA can be modeled by a RLC shunt resonator, the system is then able to select the desired resonance frequency by changing the capacitance C of the varactor diode. The RF/DC decoupling is done by a slot etched in the ground plane. A 100 pF CSM capacitor is placed across the slot to increase its capacitance and keep the antenna matched. The ground plane is design on a 0.8 mm-thick FR4 substrate with a dielectric permittivity $\varepsilon_r = 4.7$. Dimensions and position of the decoupling slot are shown on Figure 1. A prototype has been realized using a surface-mount GaAs hyperabrupt varactor from MACOM (MA46416). We observe a good agreement between simulation (with HFSS) and measurement.

Despite its reduced size (about $\lambda/30*\lambda/30\lambda/180$ at 470 MHz), the antenna can cover dynamically the whole DVB-H band with a bandwidth wider than 8 MHz by biasing the diode by a reverse voltage from 1.55 to 8.06 V.

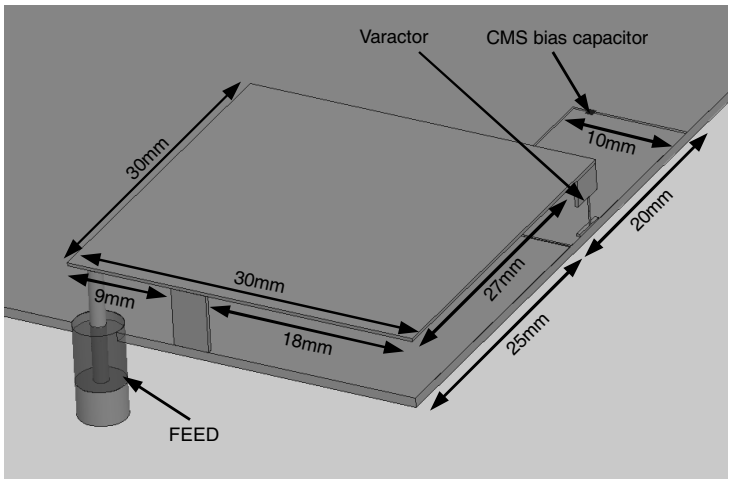

Figure 1: Dimensions of the antenna.

A Frequency Reconfigurable Microstrip Rectangular Patch Antenna Using Stubs

Lama Mokalled, Mohammed Al-Husseini, Ali Ramadan, Karim Y. Kabalan, and Ali El-Hajj
ECE Department, American University of Beirut, Beirut 1107 2020, Lebanon

Abstract— This paper presents a frequency reconfigurable microstrip antenna based on matching stubs connected to the feed line via electronic switches [1]. The antenna, which is printed on a 1.6-mm-thick FR4 epoxy substrate, is depicted in Fig. 1. It originally resonates at 2.4 GHz (ISM band), where it has good omnidirectional patterns. To achieve resonances at 3.5 GHz (WiMAX), and 5.5 GHz (U-NII), matching stubs are connecting to the feed line via two switches, S_1 and S_2 [2]. The matching stubs have little effect when the two switches are OFF, thus the antenna resonates at 2.4 GHz.

Three types of stubs are considered: open stubs, shorted stubs, and balanced stubs. These are designed such that when S_1 is ON and S_2 is OFF, a 3.5 GHz resonance frequency is achieved. On the other hand, when S_1 is OFF and S_2 is ON, a resonance at 5.5 GHz is obtained.

The designs are compared for each stub type: The open-stub case is the easiest to implement, however the resulting radiation patterns are not fully omnidirectional at 3.5 and 5.5 GHz. This is because the stubs radiate when S_1 or S_2 is ON. Increasing the characteristic impedance of the open stub lines does not fully solve the problem. Shorted stubs improve the radiation omnidirectionality at 3.5 GHz, but not fully at 5.5 GHz. Balanced stubs finally prove their ability to offer better omnidirectional patterns in the high operation band.

The antenna has been simulated using Ansoft HFSS and Agilent ADS. Complete simulation and measurements results, for the three stub types and all switching cases, will appear in the full paper. Figs. 2 and 3 respectively show the return loss of the open stub case when S_1 and S_2 are OFF, and when S_1 is ON and S_2 is OFF.

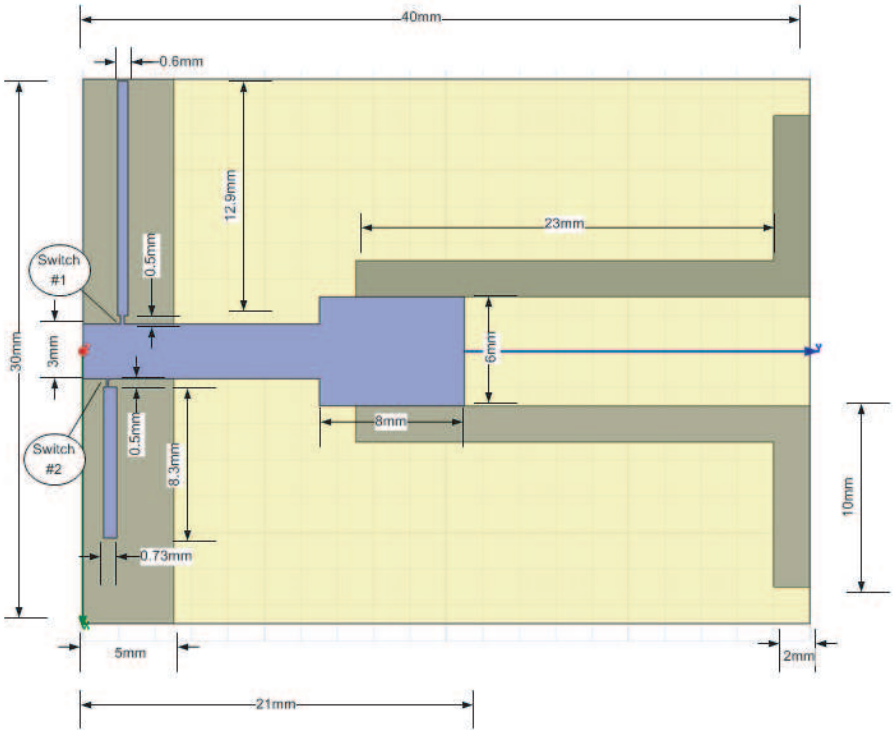

Figure 1: Antenna shape for the open end stub.

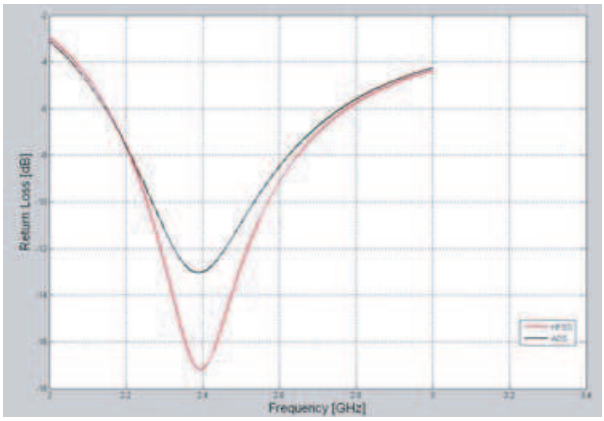

Figure 2: S_{11} parameter at 2.4 GHz.

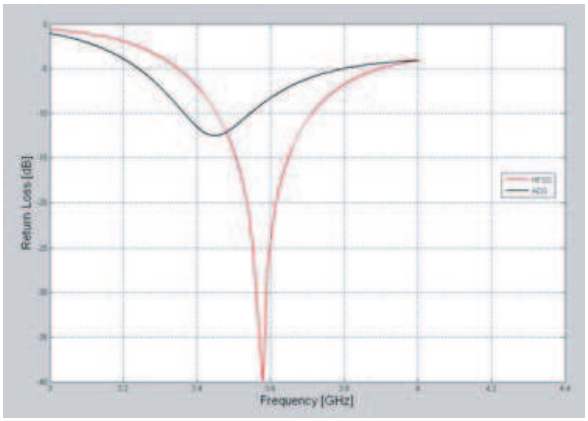

Figure 3: S_{11} parameter at 3.5 GHz.

REFERENCES

1. Demestichas, P., G. Vivier, K. El-Khazen, and M. Theologou, "Evolution in wireless systems man-agement concepts: From composite radio environments to reconfigurability," *IEEE Communications Magazine*, Vol. 42, 90–98, 2004.
2. Zhang, M.-T., Z.-B. Weng, Y.-C. Jiao, and F.-S. Zhang, "A reconfigurable space-filling-based slot antenna for 2.4/5.2 GHz band applications," *IEEE 7th International Symposium on Antennas, Propagation & EM Theory, 2006*, 1–4, 2006.

A DVB-H Antenna Using a Magneto-dielectric Superstrate

Fabien Ferrero[1], **Jean-Marc Ribero**[1], **Robert Staraj**[1], **Jean-Luc Mattei**[2], **and Patrick Queffelec**[2]

[1]LEAT, CNRS, University of Nice Sophia Antipolis, Valbonne, France
[2]Lab-STICC, CNRS, University of Brest, France

Abstract— Digital video broadcasting for handheld terminal (DVB-H) is emerging as a new service for mobile multimedia device. The operating frequency is ranging from 470 to 862 MHz. The large free-space wavelength at the lower end of the frequency band ($\lambda_0 = 64$ cm) compared to the typical size of handheld devices generally implies to miniaturize the radiating element. However, miniaturization of antennas is well known to reduce both bandwidth and efficiency. Fortunately, DVB-H standard is based on the use of 8 MHz tunable narrow channels selected over the whole DVB-H bandwidth. Narrow band tunable antennas have the potential to exhibit higher efficiency, smaller size and lower return losses than wideband coverage solutions.

These last years, LabSTICC researchers developed a new type of magneto-dielectric material composed by a $Ni_{0.5}Zn_{0.3}Co_{0.2}In_{0.02}Fe_{1.98}O_4$ nanopowder. Measurements show for this material a magnetic permeability of 5.5 and a dielectric permittivity of 3.5. Losses were found to be in the 10^{-3} and 10^{-2} ranges for dielectric and magnetic losses respectively. After shaping and appropriate thermal treatments, a porous ceramic is obtained.

The purpose of this study was to develop a small antenna placed on a $230 * 130\,mm^2$ PCB ground plane for tablet PC or portable TV handsets. A folded monopole structure was chosen for its good tradeoff between bandwidth, size and efficiency, and was incorporated on a small aperture realized in the corner of the metallization of the PCB ($18 * 5\,mm^2$). The monopole (total length 7 cm) is folded around the magneto-dielectric superstrate in a $0.9\,cm^3$ volume ($18 * 5 * 10\,mm^3$). A view of the antenna, designed on a 0.8 mm-thick FR4 substrate with $\varepsilon_r = 4.7$, is given on Fig. 1(a). A varactor diode is then positioned between the top of the monopole and its basis. Return loss measurements of the antenna versus frequency for varactor reverse bias voltages between 1.5 V and 13 V are presented in Fig. 1(b). The operating frequency can be continuously tuned over the DVB-H band. Concerning the bandwidth, the narrowest −6 dB return loss bandwidth (9 MHz) was measured at 474 MHz. Thus, the antenna fulfils the DVB-H specifications.

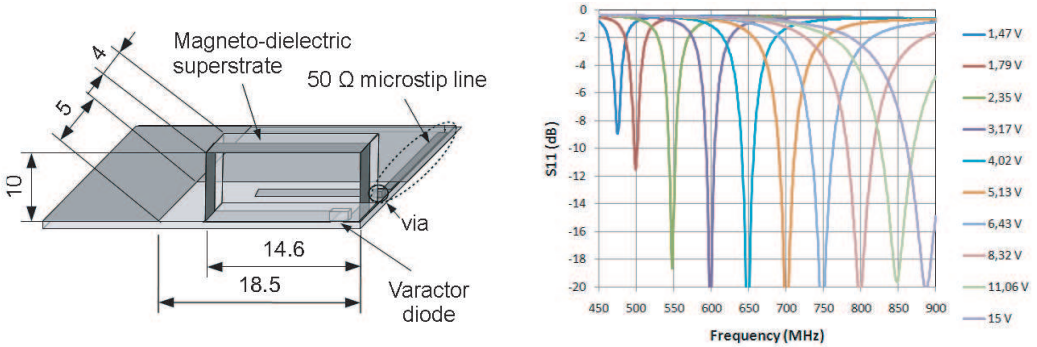

(a) (b)

Figure 1: (a) View of the antenna. (b) Return loss for several reverse voltages of the varactor diode.

Reconfigurable Directivity Antenna Array Integrated into the Substrate

Gilma Inés Angel Castillo, **Juan Carlos Bohórquez Reyes**,
Omar Ariel Nova Manosalva, **and Néstor Misael Peña Traslaviña**
Los Andes University, Colombia

Abstract— The work presents the design and experimental results of a reconfigurable directivity antenna array integrated into the substrate. The proposed arrays have 2 and 4 elements, at two different frequency ranges each one. An explanation of the overall system and of each constitutive block is presented. The constitutive blocks are: the input transition coupling between the microstrip and the substrate integrated waveguide, the power divider and the transition between the waveguide and the cavity-backed antennas. The relevance of this work relies on the integration of the antenna excitation into the substrate which leads to accommodate the whole system into it. Each of the blocks of the topology was individually designed and simulated with Ansoft High Frequency Structure Simulator (HFSS) and then integrated into the arrays. The system was built using the Rogers RT/duroid 5880 substrate with a thickness of 62 mils, relative permittivity, $\varepsilon_r = 2.2$, and dielectric loss tangent, $\tan\delta = 0.0009$. The prototypes were measured in the anechoic chamber of Los Andes University, which meets the ANSI/IEEE 149–1979 standard. Good agreement between simulations and measurements was obtained. The measurement of the two arrays with 2 antennas showed central frequency, f_0, of 4.62 GHz and 9.59 GHz, bandwidth, BW, of 0.65% and 0.52%, front to back ratio, $FTBR$, of 17.24 dB and 12.71 dB and gain, G, of 7.4 dBi and 6.4 dBi, respectively. The measurement of the two arrays with 4 antennas exhibited f_0 of 4.6 GHz and 9.7 GHz, BW of 0.86% and 1.03%, $FTBR$ of 22.06 dB and 15.00 dB and G of 6.2 dBi and 7.4 dBi, respectively.

Ultra Miniature CPW Reconfigurable Slot Antenna in the UHF Band

B. Jannier and A. Sharaiha
IETR, Universite de Rennes 1, France

Abstract— In the recent years, the number of services available for handheld devices has increased and with the development of mobile television broadcasting, the need for space saving antennas in the UHF bands with the ability of reconfiguration has arisen.

In order to face the challenge of building an ultra miniature antenna working in the UHF IV-V bands we combined known miniaturisation techniques like short-circuiting and meandering the radiating elements [1] and also the use of a magneto-dielectric material. The reference antenna, studied by S. Boucher in [1], is a coplanar slot printed on a epoxy FR4 substrate which thickness is $H_{sub} = 0.835\,\text{mm}$ and relative permittivity is $\epsilon_r = 4.4$. The size of the substrate is $230 \times 130\,\text{mm}$ to simulate the circuit board of a handheld device.

To reduce the size of the antenna, one of the two slots is short circuited and the other slot is meandered to be given a spiral shape so that the overall surface occupied by the antenna is $17 \times 16\,\text{mm}$. A $15 \times 15\text{mm}$ 3 mm-thick piece of magneto-dielectric material is placed over the meandered slot to decrease the resonant frequency of such a small antenna. The relative permittivity and permability of the material are $\epsilon_r = 4.5$ and $\mu_r = 5.5$ with loss tangents: $\tan\delta_e = \tan\delta_m = 0.01$.

The resonant frequency of the antenna can be tuned by adjusting the total length of the meandered slot. For a given slot length the impedance matching is performed by adjusting the distance of the short-circuit on the slot from the feed line. However our goal was to make a frequency-agile antenna. We achieved this by adding a variable capacitor on the meandered slot. The varicap is polarized by a continuous voltage from 0 V to 28 V. A 56 pF capacitor is also used to ensure the DC decoupling of the varicap pins.

We will present both finite element simulation and measurement results. The voltage sweep allow a change in the varicap value from 18 pF to 2 pF and frequency change from 680 MHz to 470 MHz. Despite the wide frequency range covered by the antenna, it has a very good impedance match on the whole required frequency band. The radiation pattern is slightly different at the lower limit of the band from the higher limit but is overall very similar to an omnidirectionnal one.

REFERENCES

1. Boucher, S. and A. Sharaiha, "Small-meandered coplanar antenna in UHF bands," *MOTL*, accepted, will be published in December 2010.

Session 2P7
Computational Electromagnetics, Hybrid Methods

Numerical Models, Based on the Finite Element Method, for Asymmetric High Impedance Surfaces

Y. Zhu[1], **A. Bossavit**[1], **Y. Duval**[2], **and S. Zouhdi**[1]

[1]Laboratoire de Genie Electronique de Paris
11, rue Joliot-Curie, Plateau du Moulon, Gif-suf-Yvette 91192, France
[2]EADS Innovation Works, 12, rue Pasteur, BP 76, Suresnes 92150, France

Abstract— A High Impedance Surface (HIS) generally consist sofa frequency selective surface (FSS) on the top of a grounded substrate with embedded vertical metal vias. Within a certain frequency band, the HIS can enhance the gain of antennas while simultaneously suppressing the unwanted surface waves [1]. Thanks to these two properties,abetter coupling to the surrounding circuits and more desirable antennas radiation patterns can be achieved [2].

Various kinds of HIS structures have been proposed and explored. A few analytical models, such as the effective model [1] and the transmission-line model [3] are first studied, which helps us to get a good knowledge of HIS characteristics, but are frustrating when one has to model complicated and asymmetric structures.

With the development of computing capability, many numerical methods have been used to resolve this problem. In [4], we proposed two new numerical methods of calculating the surface impedance for general HIS structures, based on the 3D Finite Element Method (FEM). These methods were validated by comparing analytical, numerical and measurement results for symmetric HIS structures.

In this paper, we focus on applications of these methods to calculation of surface impedance for asymmetric HIS structures. Besides, more structures were fabricated and tested to verify the accuracy of the numerical models. Through these simulations and experimental tests, the trade-os of our numerical models and the measurements are more thoroughly investigated and discussed.

REFERENCES

1. Sievenpier, D., L. Zhang, R. F. J. Broas, N. G. Alexopoulos, and E. Yablonovitch, "High impedance electromagnetic surfaces withaforbiddenfrequency band," *IEEE Trans. Microw. Theory Tech.*, Vol. 47, No. 11, 2059–2074, 1999.
2. Youse, L., B. Mohajer-Iravani, and O. M. Ramahi, "Enhanced bandwidth articial magnetic ground plane for low-prole antennas," *IEEE Antennas Wireless Propag. Lett.*, Vol. 6, No. 11, 289–292, 2007.
3. Simovski, C. R., P. De Maagt, and I. V. Melchakova, "High-impedance surface having stable resonance with respect to polarization and incidence angle," *IEEE Trans. Antennas Propagat.*, Vol. 53, No. 3, 908–914, 2005.
4. Zhu, Y. and S. Zouhdi, "Calculation of surface impedance for high impedance surface," *META10, 2nd international Conference on Metamaterial, Photonic Crystals and Plasmonics*, Cario, Egypt, Feb. 2010.

Modeling and Simulation of Temperature Distribution in Laser-tissue Interaction

A. Yasin Citkaya and S. Selim Seker
Department of Electrical & Electronics Engineering, Bogazici University
Istanbul 34342, Turkey

Abstract— In this paper, modeling and simulation of interaction between light sources and living biological tissue is studied. One of the most important results of physical interactions of light with biological tissue is thermal changes which is a consequence of absorption of light. The severity of the effects are dependent upon several factors, including exposure duration, wavelength of the beam, energy of the beam, the area and type of tissue exposed to the beam. The temperature response of tissue irradiation is governed by extensively used Pennes bio-heat equation in a 3-dimensional space with boundary conditions. The Pennes equation is solved for a single layer model of the human skin to predict the temperature distribution using CO_2 laser light source radiation burn at a steady state. The numerical solutions are obtained by the Finite Element Method (FEM), in which the geometry studied is divided into a finite element mesh. This method gives better description of the geometry with smaller number of nodes. Less memory space and disk space with shorter run times make this method more advantageous to other numerical solution techniques. Temperature contours and penetration depths are plotted in three dimensional spaces. Additional numerical solutions of model with different tissue properties are also examined. These results are compared with finite volume approach which is existed in literature. Boundary effects are also analyzed and illustrated with the figures. In this work, it is demonstrated that by adjusting exposure duration, wavelength of the beam, energy of the beam, and the area and type of tissue, temperature effects on tissue can be altered. The study is expected to be useful in biomedical applications for different laser sources, especially in laser surgery. Furthermore, this modeling technique is also applicable to conventional light sources.

Using Bioheat Equation 3D WEB-spline Prediction of Ocular Surface Temperature

F. C. Kunter and S. S. Seker
Department of Electrical and Electronics Engineering, Bogazici University, Turkey

Abstract— A bioheat transfer model of the human eye is constructed using weighted extended b-splines (web-spline) as shape functions for the finite element method. This newly developed computational approach is employed to calculate the steady-state temperature distribution in a normal human eye using Pennes bioheat equation. For a more precise representation of the actual human eye, three dimensional modeling is simulated using these new finite elements in conjunction with linear, quadratic and cubic b-splines. Error analysis indicates that our web-spline based method is successful in determining the temperature distribution in the eye. The errors decrease with increasing basis spline degrees. Besides diminishing the number of nodes, low computational time is also achieved by the web-spline method. In this study, grid convergence for the 3D web-spline model and thermal pattern of the 3D human eye model are plotted. Additional numerical solutions of model with the standard finite element method (FEM) approach which is existed in literature are also given. The results indicate that FEM with web-spline method is observed to offer a much better performance than the standard FEM. Grid convergence number estimates are derived for the sets of simulations. It is shown that this method reaches higher precision in a shorter period of time with fewer nodes. Our findings indicate that weighted extended b-spline solutions improve the computational method of the standard FEM.

FDTD Method on a FCC Grid for the Wave and Maxwell Equations

M. E. Potter
University of Calgary, Canada

Abstract— Cartesian (Yee) grids in FDTD methods exhibit a strongly anistropic numerical dispersion relation, causing non-physical distortions of the wavefront, which can be compensated with i) optimization of finite difference stencil coefficients; ii) higher order stencils; and iii) utilizing a different grid. As an alternative way to deal with the anistropy, a face centred cubic (FCC) 3D grid is proposed for utilizization in the FDTD method for the wave equation, and the Maxwell equations. FCC grids are the logical extension of hexagonal grids in 2D, and have been shown previously to provide optimal sampling of space based on close packing of spheres (highest density). The difference equations are developed for the wave equation and Maxwell equations on this alternative grid, and the dispersion relationship and stability for grids of equal and nonequal aspect ratios are derived. A comparison is made between the FCC formulation and a Cartesian formulation, based upon having an equal volume density of gridpoints in each method (i.e., the computational storage requirements of each method would be the same for the same simulated space). The comparison shows that the FCC grid exhibits a much more isotropic dispersion relation than the Cartesian grid of equivalent density. Furthermore, for an equivalent density, the FCC method has a more relaxed stability criterion by a factor of approximately 1.35, resulting in a further reduction in computational resources.

On the Integration of Behavioral Component Descriptions in the Full-wave Transmission-line Modeling Method

I. Scott[1], **G. Kergonou**[1], **C. Christopoulos**[1], **F. Canavero**[2], **S. Greedy**[1], **Dave W. P. Thomas**[1], **and P. Sewell**[1]

[1]George Green Institute for Electromagnetics Research, University of Nottingham
University Park, Nottingham NG7 2RD, UK
[2]Dipartimento di Elettronica, Politecnico di Torino
Corso Duca degli Abruzzi, 24, Torino 10129, Italy

Abstract— IBIS (input/output buffer information specification) [1] and macromodels [2] are behavioral models that reproduce the input/output port nonlinear behavior of digital integrated circuits (ICs). IBIS describes a component by using a collection of lookup tables of voltages and currents. Macromodels rely on a local linear state-space parametric representation of the current function of the voltage. Both descriptions enable the insertion of active components as sub-structures under a full-wave solver, which is an essential tool for accurate analysis of electromagnetic compatibility and signal integrity of high-speed electronic applications.

The Transmission-Line Modeling (TLM) [3] method offers a suitable environment for incorporating active models. The method exploits the analogy between field propagation in space and voltage/current propagation in a spatial transmission-line network. It has the advantage, compared to the finite-difference time-domain method (FDTD), of calculating field components at the same time and at the same location, with guaranteed stability due to the underlying electrical circuit formulation [3]. Embedding of the behavioural models can be realised in two ways: either through an external link to a circuit simulator such as SPICE, or by direct embedding as in [4] with digital IC macromodels. The first approach gives access to a wide range of models via the SPICE libraries. Unfortunately, it slows the calculation speed as the TLM solver must call SPICE at each time step. The second option avoids the slow speed problem. It forms the subject of this paper by completing the previous works to include an IBIS description of a component, thus incorporating the advantage of a wide selection of devices that can be embedded without the need to use the SPICE libraries. In addition, the study provides a comparison of the IBIS and macromodel implementations, each one being based on a different TLM formulation.

REFERENCES

1. Leventhal, R. and L. Green, *Semiconductor Modeling: For Simulating Signal, Power, and Electromagnetic Integrity*, Springer, New York, 2006.
2. Steviano, I. S., C. Siviero, F. G. Canavero, and I. A. Maio, "Behavioral modeling of digital devices via composite Local-Linear State-Space relations," *IEEE Trans. on Inst. and Meas.*, Vol. 57, No. 8, 1757–1765, 2008.
3. Christopoulos, C., *The Transmission-line Modeling Method: TLM*, Wiley-IEEE Press, New York, 1995.
4. Kergonou, G. and F. G. Canavero, "Implémentation de modèles de circuits non-linéaires sous la TLM," *CEM 2010*, Limoges, France, 2010.

On the Use of Fast Iterative PO to Model SAR Signal from Complex Structures

Alessandro Mori, **Mario Calamia**, **and Angelo Freni**
Department of Electronics and Telecommunications, University of Florence
Via di Santa Mara, 3, Firenze 50139, Italy

Abstract— Electromagnetic models of the backscattered signal from natural and artificial targets are widely used in remote sensing, for both validation and development of data processing algorithms. Numerical models exhibit a better accuracy and a larger range of application with respect to the analytical ones. Among these, Physical Optics (PO) is often adopted. Its computational complexity is related to the number of points N on the object's surface employed in the evaluation of the PO integral. Such number N is proportional to the illuminated area (normalized to the wavelength squared) of the object. In the case of complex objects (like a ship), the multiple-bounces contribution can dominate and it should be included in the model (leading to a Iterative PO algorithm), to obtain a reliable solution.

The evaluation of each bounce contribution is a $O(N_2)$ process. In case of complex and very large objects the total computational cost can be too high. However, acceleration techniques, for instance based on the Multilevel Fast Multipole Approach or the Adaptive Integral Method (widely used in full wave electromagnetic analysis), can be applied to evaluate the bounces PO contribution, reducing the computational complexity from $O(N_2)$ to $O(N \log_2 N)$, and obtaining an efficient algorithm able to analyze very large objects (Fast Iterative PO). This approach has been firstly used in evaluation of the RCS of cavities (jet engine inlets [1]), and recently has been employed to general objects [2].

In this paper, a Fast Iterative PO that exploits the Multilevel Fast Multipole Approach (MLFMA) is employed to evaluate the RCS of ships. The problem of the inclusion of shadowing rules has been also addressed. In particular, two shadowing rules are considered: the back-face culling, that can be easily introduced in the MLFMA group's radiating function; and an approximated shadowing condition based on the geometrical position of MLFMA groups.

Some comparison with a complete full wave solution of electrically large ships will show the accuracy of the model.

ACKNOWLEDGMENT

This work was supported by Italian Space Agency — COSMO/SkyMed activity (contract I/046/-09/0).

REFERENCES

1. Obelleiro, F., J. L. Rodriguez, and R. J. Burkholder, "An iterative physical optics approach for analyzing the electromagnetic scattering by large open-ended cavities," *IEEE Trans. Antennas and Propagation*, Vol. 43, No. 4, 356–361, April 1995.
2. Burkholder, R. J., C. Tokgoz, C. J. Reddy, and P. H. Pathak, "Iterative physical optics: Its not just for cavities anymore [EM wave propagation]," *2005 IEEE Antennas and Propagation Society International Symposium*, Vol. 1A, 18–21, July 3–8, 2005.

3D FEA of SMPM Accounting for Skew and End Windings

M. Hédi Gmiden and H. Trabelsi
Sfax Engineering School, University of Sfax, Tunisia

Abstract— This paper presents the use of the three dimensions finite element method for analyzing the surface mounted permanent magnet motor. The saturation of the motor is taken into account in determination of the flux distribution and the inductances. Skew and end windings are also taken into account. The results are presented and compared to demonstrate the effect of skew and end windings.

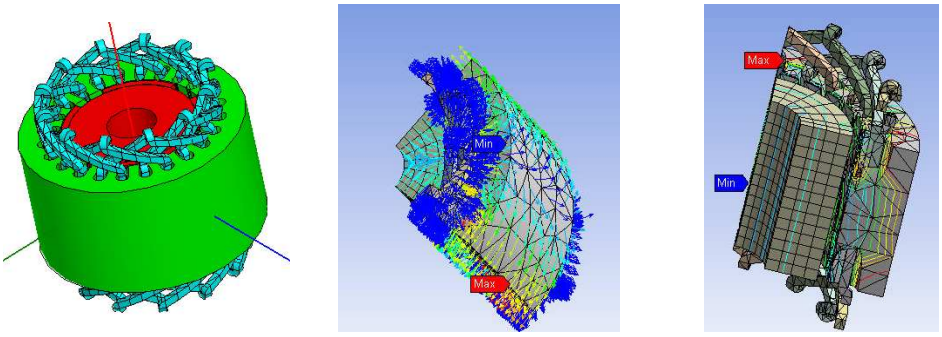

(a) (b) (c)

Figure 1: (a) Motor model. (b) The flux distribution by the magnet. (c) The flux distribution by the magnet and the stator current.

REFERENCES

1. Geuzaine, C. and J.-F. Remacle, "Gmsh: A 3-D finite element mesh generator with built-in pre- and post-processing facilities," *International Journal for Numerical Methods in Engineering*, Vol. 79, No. 11, 1309–1331, September 10, 2009.
2. Chen, S., Z. Q. Zhu, and D. Howe, "Calculation of d- and q-axis inductances of PM brushless ac machines accounting for skew," *IEEE Transactions on Magnetic*, Vol. 41, No. 10, October 2005.

Performance Improvement of Different Topologies of Claw Pole TFPM Based on a 3D FEA

Anis Njeh and Hafedh Trabelsi
CES, Sfax Engineering School, University of Sfax, BP 1173, 3038 Sfax, Tunisia

Abstract— The transverse flux permanent magnet machine (TFPM) is currently given an increasing attention, especially in electric and hybrid propulsion applications because of the highest output torque per unit volume ratio compared to the conventional electric machines. Although significant improvements have been carried out on the earlier topologies, much work is still required before the TFPM can be regarded as a mature concept. Of particular interest are the output torque maximization, the cost minimization and the cogging torque reduction which is a vital requirement in propulsion applications, as far as passenger comfort is concerned.

The present paper deals with, in a first step, a description and comparison between tow topologies of claw pole TFPM. The first one is the surface mounted magnets claw pole witch present the non flux concentrated topology. The second one is the buried mounted magnet claw pole topology with flux concentrated design. This done, the used materials are described to highlight the necessity of the use of the soft magnetic composite in the magnetic circuit since we have a three dimensional magnetic field distributions and variations through the magnetic circuit.

In a second step, a 3D Finite Element Analysis (FEA) based investigation of the output torque and the cogging torque of the proposed claw pole TFPM for Performance improvement by reducing the cogging torque and increasing the output torque.

On the Iron Losses Computation of a Three Phase PWM Inverter-fed SMPM by Using VPM and Transient FEA

Ali Mansouri and Hafedh Trabelsi
Laboratory of Computer, Electronics & Smart Engineering Systems Design
Engineering School of Sfax, ENIS, Route de Soukra, Km 3.5-BP W, 3038, Tunisia

Abstract— This paper deals with the iron losses computation in a pulse-width-modulation (PWM) inverter fed surface mounted permanent magnet motor (SMPM). The used iron loss model has been developed in an earlier works and validated for the evaluation of both no-load and sinusoidal load iron losses of the considered SMPM. This model requires the separation of the iron losses into hysteresis, classical eddy currents and excess losses components. The use of such model needs the knowledge of the magnetic field distributions and variations thought the magnetic circuit. This has been obtained by using a 2D transient finite element analysis (FEA). In order to estimate accurately the hysteresis losses component the hysteresis phenomenon must be incorporated into FEA field equations. In this work, the inversed vector Preisach hysteresis model (VPM) is used for the modeling of the ferromagnetic materials, which is limited to the stator regions. This is due to the low hysteresis losses and time magnetic field variations in the rotor running at synchronous speed. Therefore the computational method of the PWM fed inverter SMPM iron losses consists of the VPM incorporated into transient FEA and coupled with iron loss analytical model. In a first step, the machine features, such as the air gap induction and the output torque are investigated, and in a second step the iron losses are computed. A special attention is paid to the B-H relationship in the ferromagnetic parts and to the iron losses values.

Efficient FEM/BEM Procedures for Time-dependent Electromagnetic Scattering Problems

E. P. Stephan, **A. Issaoui**, **and Z. Nezhi**
Institute for Applied Mathematics, Leibniz University Hannover, Germany

Abstract— The main objective of this work is the implementation and analysis of the FEM/BEM coupling method to solve time-dependent electromagnetic scattering problems. This analysis is based on a discoutinuous time stepping Galerkin scheme together with the use of retarded potentials. We give here a space time variational formulation and we prove stability and convergence of such numerical method. Our numerical experiments underline our theoretical results.

Scattering of Electromagnetic Waves by Inhomogeneous Dielectric Gratings Loaded with Parallel Perfectly Conducting Strips — Matrix Formulation of Point Matching Method —

Tsuneki Yamasaki, **Keizo Doi**, **Ryosuke Ozaki**, **and Takashi Hinata**
Department of Electrical Engineering, College of Science and Technology
Nihon University, Japan

Abstract— The scattering of electromagnetic waves by inhomogeneous dielectric gratings is of both theoretical and practical interest for integrated optics acousto-optics, optical filters, and holography. Because of recent advances, the refractive index can easily be controlled in the manufacture of periodic structures to serve as fiber gratings, frequency-selective or polarization-selective devices, and photonic crystals. Thus, many analytical and numerical methods have been proposed that are applicable to dielectric gratings having arbitrary structures. To deal with multilayered dielectric gratings such as photonic crystals, it is necessary to analyze the periodic circular arrays. We have also analyzed the scattering problem with multilayered columnar dielectric gratings loaded with rectangular dielectric constant for the case of permittivity variation in rectangular cylinders and elliptical cylinders, by utilizing an improved Fourier series expansion method, multilayer method, and Eigen value matrix method. However, most theoretical and numerical studies have considered the periodic structures in which the material forming grating was either metallic or dielectric in homogeneous media.

In this paper, we have proposed a new method for the scattering of electromagnetic waves by inhomogeneous dielectric gratings loaded with parallel perfectly conducting strips as shown in Fig.1(a) using the combination of improved Fourier series expansion method and point matching method for TE wave. This approach can treat periodic configurations having arbitrary combinations of dielectric, metallic, and perfectly conducting components.

In the inhomogeneous dielectric region S_2 $(0 < x < D)$, the permittivity profile $\varepsilon_2(x, z)$ is generally not separable with respect to the x and z variables. Main process of our methods are as follows: (1) The inhomogeneous layer is assembly of M stratified layers of modulated index profile $\varepsilon^{(l)}(z)$ with step size $d_\Delta (= D/M)$ as shown in Fig. 1(b). (2) Taking each layer as a modulated dielectric grating, the electromagnetic fields are expanded appropriately by a finite Fourier series. (3) In the perfectly conducting cylinder with the arbitrary shape is composed of the conducting strip and it consists of two boundary at C_j (or $\bar{C}_j$); $j = 1 \sim 3$. (4) the electromagnetic fields are matched using an orthogonality relation which makes the matrix relation on both sides using point matching method. (5) Finally, all stratified layers include the metallic regions are matched at appropriate boundary conditions to get the inhomogeneous dielectric gratings loaded with parallel perfectly conducting Strips using matrix formulation of Point Matching Method.

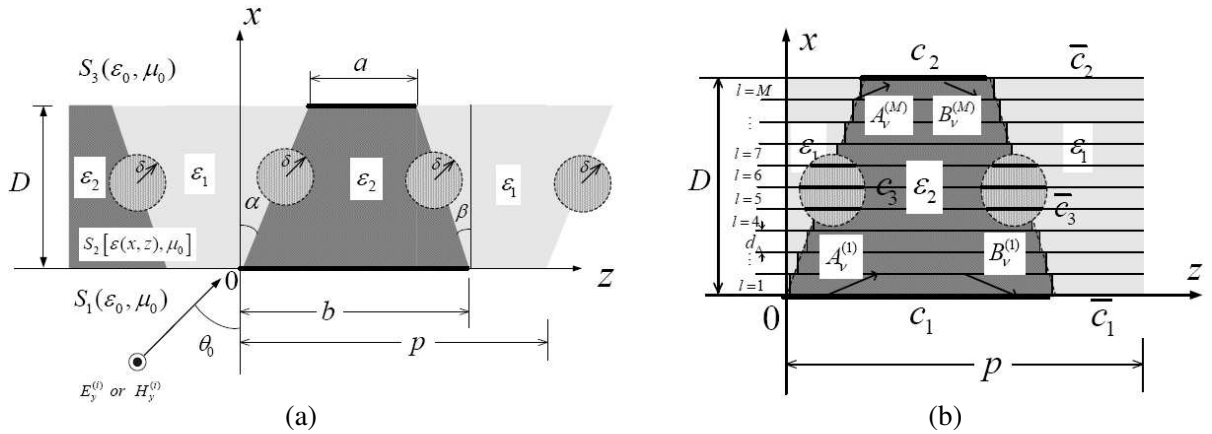

Figure 1: Structure of inhomogeneous dielectric gratings loaded with Parallel Perfectly Conducting Strips.

A Combined Field Integral Equation for Higher-order Generalized Impedance Conditions

A. Bendali[1, 2], M'B. Fares[2], K. Lemrabet[3], F. Millot[2], and S. Pernet[2]

[1]University of Toulouse, IMT UMR CNRS 5219, INSA, Toulouse, France
[2]CERFACS, EMA Team, Toulouse, France
[3]Faculté de Mathématiques, USTHB, Algiers, Algeria

Abstract— The modeling of the effect of a thin dielectric layer located on a perfectly conducting object remains a challenge. A direct approximation of this layer is often difficult and stays expensive. Thefore the use of approximate models is preferred. These models usually take the form of generalized impedance conditions. The methodology used to construct them fully determines their effectiveness: accuracy, stability and easy to implement. In particular, the higher-order impedance conditions are often difficult to implement in the classical numerical schemes due to the presence of higher-order differential operators (whose the order is strictly greater to two). Recently, A. Bendali and K. Lemrabet have proposed a new family of impedance conditions [1] which is only composed of second-order differential operators for approximations up to third order (in the sense of the truncation of the asymptotic calculus which is made according to the thickness of the layer). For exemple, the third order condition can be written:

$$\mathbf{n}\times(\mathbf{E}_{|\Gamma}\times\mathbf{n}) = -ik\mu\delta\left(\Phi+\frac{1}{k_c^2}\nabla_\Gamma\theta\right)$$

where Φ and θ is solution of:

$$\left(1-\frac{\delta^3}{3}\nabla_\Gamma\nabla_\Gamma\cdot+\frac{\delta^2}{3}\nabla_\Gamma\times\mathrm{curl}_\Gamma\right)\Phi = \left(1-\delta(\mathcal{C}-\mathcal{H})+\frac{\delta^2}{3}(k_c^2+2(\mathcal{C}-\mathcal{H})(\mathcal{C}-2\mathcal{H}))\right)(\mathbf{n}\times\mathbf{H}_{|\Gamma})$$

$$\left(1-\frac{\delta^2}{3}\Delta_\Gamma\right)\theta = \left(1+\delta\mathcal{H}+\frac{\delta^2}{3}(k_c^2+4\mathcal{H}^2-G)\right)\nabla_\Gamma\cdot(\mathbf{n}\times\mathbf{H}_{|\Gamma})$$

with $\mathcal{C}$ is the surface curvature operator, $\mathcal{H}$ is the mean curvature, δ is the thickness of the layer, $\mathbf{n}$ the unit outward normal, G is the geometrical curvature, k is the wavenumber and $k_c = k\sqrt{\varepsilon\mu}$.

We propose to present a numerical method based on a Combined Field Integral Equation which uses these new impedance conditions up to third order. The main difficulties remain the presence of quantities of different functional nature which are difficult to take account numerically, the evaluation of the curvature tensor from the mesh and an unobvious direct assembling of the problem. The proposed method is based on an iterative process to synthesize the problem, an augmented formulation for the third order condition in order to obtain a straightforward discretisation and a consistent computation of the curvature tensor by using the variation of the normal at each node of the mesh.

REFERENCES

1. Bendali, A. and K. Lemrabet, "Asymptotic analysis of the scattering of a time-harmonic wave by a perfectly conducting metal coated with a thin dielectric shell," *Asymptotic Analysis*, Vol. 57, 199–227, 2008.

Session 2P8
Signals, Waves and Shielding

The Methods of Measuring Attenuation of Thin Absorbent Materials Used for Electromagnetic Shielding

L. Nowosielski, **R. Przesmycki**, **M. Wnuk**, **and J. Rychlica**
Faculty of Electronics, Military University of Technology
Gen. S. Kaliskiego 2 str., Warsaw 00-908, Poland

Abstract— Along with an increasing number of devices producing electromagnetic radiation there is a need of protecting devices and people against undesirable electromagnetic radiation. The problem of protection against undesirable radiation is particularly important in the issues of electromagnetic compatibility. One of the methods of protection against undesirable radiation are electromagnetic shielding. Generally we can distinguish two ways of functioning of electromagnetic shield — through reflection of incident electromagnetic wave or absorption of electromagnetic energy.

The article concerns the problems connected with electromagnetic compatibility. Two methods of measuring attenuation of thin absorbent materials used for electromagnetic shielding are described here. The measurements have been conducted in a coaxial measuring line, which provides a large broad band of realized measurements. The first method is based on measuring the signal level with a measuring receiver at the output of the coaxial measuring line. The second method is based on measuring parameters of S matrix with the use of a network analyzer, which allows to determine the amount of absorbed energy and reflected by a sample. Exemplary measurements of attenuation have been conducted for two samples in the frequency range from 200 MHz to 5200 MHz.

Small Chambers Shielding Efficiency Measurements

Rafal Przesmycki, **Marian Wnuk**, **Leszek Nowosielski**, **and Kazimierz Piwowarczyk**
Faculty of Electronics, Military University of Technology
Gen. S. Kaliskiego 2 Str., Warsaw 00-908, Poland

Abstract— The problem of protection against undesirable electromagnetic radiation is particularly important in the issues of electromagnetic compatibility. One of the protection methods against interaction of undesirable radiation are electromagnetic shielding. Valid standardization documents concerning the methodology of measuring attenuation of shielded objects have applications only in efficiency measurements of shielded chambers of internal dimensions not smaller than 1.5 m × 1.5 m × 1.5 m. For that reason there occurred the need of drawing up the methodology of measuring shielded chambers of smaller dimensions.

The article concerns the problems connected with electromagnetic compatibility. The methodology of shielding efficiency measurements of small chambers (e.g., casing of the central processing units (CPU) and the 'racks') assigned for installing devices or electronic components in the frequency range from 80 MHz to 1000 MHz as well as the description of measuring position have been presented in it. The designed method of shielding efficiency measurement of small chambers comes down to making two measurements of the level of electromagnetic field strength for a particular probing frequency. The first measurement is performed as so-called reference measurement, whereas the second is principal measurement.

The results of the research conducted in accordance with the designed measuring methodology concerning attenuation measurements contributed by the central processing unit casing from four sides of the object and their analysis from the perspective of using casing as an protection element against undesirable electromagnetic emission have been presented in the article.

Procedure for Absorption Measurements of Absorbing Materials

K. Piwowarczyk, M. Bugaj, L. Nowosielski, and R. Przesmycki
Faculty of Electronics, Military University of Technology
2, Gen. S. Kaliskiego Str., Warsaw 00-908, Poland

Abstract— The aim of this work is to present the procedure for absorption measurements of absorbing materials. In presented procedure as the electromagnetic wave absorption measure was used the signal levels difference between probe signal level reflected from the reflector material not covered and covered by the absorbing material. It is a measure of strength of the electromagnetic wave absorbed by a absorbing material for a given incident power. The presented measurement procedure requires two flat aluminium panels, where one is used as reflector material (reference) and the other is coated with absorbing material. The panel is fixed on a support, which is positioned in front of the receiving and transmitting antennas. With this method is necessary to make two separate measurements of the signal level reflected by the plate with and without absorbing material. In the paper the methodology, detailed description of laboratory stand and laboratory stand calibrating procedure were presented.

The absorption of broadband absorber constructed as flat and impregnated with a magnetic material was successfully evaluated using described method in the frequency range of (1–10) GHz. The measurements were carried out in the anechoic chamber located at Laboratory of Electromagnetic Compatibility, Faculty of Electronics, Military University of Technology in Poland. In this paper the measurements results and discussion on the results are presented too.

Multilayer Microstrip Antenna on Flat Base in the X Band (8.5 GHz–12 GHz)

M. Wnuk, R. Przesmycki, L. Nowosielski, and M. Bugaj
Faculty of Electronics, Military University of Technology
Gen. S. Kaliskiego 2 Str., Warsaw 00-908, Poland

Abstract— Microstrip structures in aerial technique occurred relatively late. However recently there has been noticed an unusual development of constructing these antennas and enormous interest in their abilities as far as modern technology is concerned. Nowadays microstrip antennas are widely used in all radio-communication fields. It is due to simplicity of their construction, making facility and relatively low production costs.

This report concerns problems connected with aerial techniques. A structure of microstrip antennas on dielectric base operating in the X band (8.5 GHz–12 GHz) has been described here. The mentioned antennas have been made as multilayer microstrip antennas slotted-supplied on flat base. In this article there have been discussed antennas in form of antenna with a single radiator and array consisting of four radiators linearly-located and supplied in phase. In the article there has also been presented the measurement methodology of antenna parameters such as: antenna pattern, standing wave-ratio and antenna gain. For made models of antennas there have been conducted measurements of antenna electrical parameters in non-reflection chamber and placed in the article the results of the conducted measurements of the above mentioned antennas & comparison of them.

Active Microstrip Antennas Operating in X Band

Marek Bugaj, **Rafal Przesmycki**, **Leszek Nowosielski**, **and Kazimierz Piwowarczyk**
Faculty of Electronics, Military University of Technology, Gen. S. Kaliskiego 2 Str., Warsaw 00-908, Poland

Abstract— The paper describes problems related to antenna technology. The paper shows the construction of active microstrip antennas on a dielectric substrate operating in X band (8.5 GHz–12 GHz). Microstrip antennas in antenna technology appeared relatively late, but in recent years has been a very large development of the design of these antennas and the huge interest in their capabilities. Microstrip antennas are often used in all areas of radio communications. This is due to the simplicity of their design, ease of implementation and relatively low production costs. An important advantage of these antennas is their shape, small size, low weight and aesthetic appearance. Microstrip antennas also provide high repeatability parameters and high resistance to weather conditions.

The article presents two active antennas have been designed as a multilayer structure of microstrip antennas performed on two different shapes of the substrate. The microstrip patch is feed by microstrip line trough slot in the common ground plane. The first of these antennas is the four elements array on flat substrate consisting of four dielectric layers. The second antenna is the four elements array located on the conformal substrate consists of two dielectric layers. For so performed antenna models were made measurements in the anechoic chamber of typical electrical parameters, such as standing wave ratio, input impedance, radiation pattern, gain. The article also analyzes the results of computer simulations and measurements, thereby demonstrating the advantages and disadvantages of microstrip antennas placed on different surfaces.

Efficient Method of 3G Signal Detection

Paweł Skokowski and Jerzy Łopatka
Faculty of Electronics, Military University of Technology, Gen. S. Kaliskiego 2 Str., Warsaw 00-908, Poland

Abstract— This paper concerns the problems of efficient methods enabling detection of the 3G signals. There is a lot of standards used for the wireless transmission using different techniques of modulation and exploit channels with various bandwidths. Systems are expected to be faster, safer, interferences resistant and should effectively use available frequency band. Some of them use the shareable sets of frequency channels that require an effective recognition of the working system. Monitoring of their work and whole electromagnetic situation is important in government reconnaissance systems and in cognitive radios. Narrowband emissions, with large SNR can be easily detected, using simple level detectors. More sophisticated is detection of wideband DSSS signals, hidden below the background noise level. Universal Mobile Telecommunications System (UMTS) uplink signal, transmitted with relatively low level by mobile terminal additional spreaded and scrambled before transmission is one of the most interesting cases.

For analysis of DSSS signals specialized devices like spectrum analysers or dedicated software can be used. They enable monitoring of UMTS Uu interface and require cooperation with system operator. Currently available solutions are mainly devoted to analysis only the IuB interface what means they are able to analyse only the communication protocol. Analysis using non-cooperative (means that analysis is performed without logging into the system and knowledge about transmitted signal parameters what is very difficult) systems are limited. It seems that the most important thing is to detect radio transmission especially in case of electromagnetic warfare, signal detection (for example to prevent RC-IED) and recognition to prevent terrorist attacks, crimes etc.

Proposed method is realized using software application, which means that additional devices are not required.Worked out procedures enable detection of the 3G signal in uplink and downlink transmission using spectrum and autocorrelation function analysis method. Efficiency tests of proposed detection method are also introduced in the work. Authors decided to accept the probability of detection as the basic merit of the proposed method efficiency.

The elaborated method of detection can be used for monitoring of UMTS signals and also used to design device enabling the detection of UMTS signals for government reconnaissance, to prevent RC-IED attacks or as a signal sensing part of monitoring manager in cognitive radios.

Power Amplifier Linearization for Software Defined Radio Using Look-up Table

Piotr Marszalek, **Pawel Skokowski**, **and Jerzy Lopatka**
Faculty of Electronics, Military University of Technology
Gen. S. Kaliskiego 2 str., Warsaw 00-908, Poland

Abstract— In this paper we present simple method for reducing transmitter's power amplifier nonlinearities in a real RF frontend. The linearization is performed by digital predistortion technique using Look-up-Table (LUT). This method is simple and cost-effective, due to implementation over raw IQ samples, and does not require any hardware modifications.

The LUT could be easily used in every software enviroment as a additional processing block in developed communications chain, after modulation and before analog part of a transmitter.

For measurments we have choosen generic OFDM signal, beacuse of two reasons: OFDM modulation is perspective and used by many modern radio systems (e.g., WiMAX, WLAN, LTE, DVB, DAB); and OFDM modulation is sensitve to nonlinear distortions beacuse of its high PAPR value and required phase linearity.

The device under test is the WBX's transmitter placed on USRP2 motherboard. The WBX doughterboard is a full-duplex transceiver, which covers 50 MHz–2.2 GHz frequency range and transmits up to 100 mW with 25 dB software power control range.

In this paper we propose digital predistortion technique using Look-up-Table and WBX transmitter measurments as a AM/AM and AM/PM curves. The iterative calculations are performed to obtain optimal LUT values. The performace of proposed technique is shown and discussed at the end.

MIMO Implementation with Alamouti Coding Using USRP2

Anna Kaszuba, **Radoslaw Checinski**, **and Jerzy Lopatka**
Faculty of Electronics, Military University of Technology, Warsaw 00-908, Poland

Abstract— Fast evolution of mobile communication facesgrowing users' demands for throughput, quality of service and coverage. The most promising data transmission technology, which is able to fulfill these requirements, is Multiple Input Multiple Output (MIMO). This technique is an active area of research. More and more standardization documents and recommendations describe how to implement MIMO in specific system solutions. MIMO in comparison with SISO allows to increase radio channel capacity and the quality of service, exploiting the spatial diversity, overcoming the effects of multipath fading.

In this paper authors present novel implementation of 2×2 MIMO system with Orthogonal Frequency-Division Multiplexing (OFDM) modulation using GNU Radio with USRP2. GNU Radio is a library designed for signal processing, which allows users to create streams of the signal processing by combining ready components. In addition with software defined radio it offers testing of theoretical models under real-world conditions. Model of transmitter was created by using algorithm and methods which are implemented in GNU Radio SISO OFDM modulator. Authors extend them by Alamouti STBC/SFBC coder, because it is very effective and also simple in implementation. The Alamouti STBC/SFBC is a rate-1 code. It takes two time-slots to transmit two symbols. The receiver decoding is provided by determining channel estimation matrix and maximum-likelihood detector.

Experimental results of MIMO link performance are also presented.

Session 2P9
Poster Session 4

Optoelectronic Phase Noise System Designed for X-band Sources Measurements in Metrology Applications

A. Hmima[1], **N. Cholley**[1, 2], **E. Pavlyuchenko**[1], **M. Zarubin**[1], **Y. K. Chembo**[1], **and P. Salzenstein**[1, 2]

[1]Franche-Comté Électronique Mécanique Thermique Optique Sciences et Technologies (FEMTO-ST)
Centre National de la Recherche Scientifique (CNRS), UMR 6174
ENSMM, 26 Chemin de l'Épitaphe, 25030 Besançon, France
[2]LNE-LTFB, Laboratoire Temps Fréquence de Besançon Associated to Laboratoire National de Métrologie et d'Essais (LNE), Besançon, France

Abstract— The performance advances in communication systems as well as Radar system, precision navigation, space application and time and frequency metrology require more stable frequency and low phase noise system. In this paper we present a configuration of phase noise measurement system operating in X-band using a photonic delay line as a frequency discriminator. The main advantage of this system is that it does not require an excellent frequency reference and works in any range of microave frequencies between 8.2 and 12.4 GHz [1, 2]. At 10 GHz, the noise floor for a 2 km delay line is respectively −145 and −163 dB rad^2/Hz at 100 Hz and 100 kHz with 200 averages using cross correlation method. The sensitivity of our system allows characterizing sources on a larger Fourier frequency interval around the carrier by commuting two lines with diffrent length. Developed in the context of association with the national french metrology institute (laboratoire national de métrologie et d'essais, LNE), this calibration system is to be integrated in measurements means of the accredited laboratory to improve the Calibration Metrlogy Capabilities (CMC) of the LNE.

REFERENCES

1. Salzenstein, P., J. Cussey, X. Jouvenceau, H. Tavernier, L. Larger, E. Rubiola, and G. Sauvage, "Realization of a phase noise measurement bench using cross correlation and double optical delay line," *Acta Physica Polonica A*, Vol. 112, No. 5, 1107–1111, 2007.
2. Volyanskiy, K., J. Cussey, H. Tavernier, P. Salzenstein, G. Sauvage, L. Larger, and E. Rubiola, "Applications of the optical fiber to the generation and to the measurement of low-phase-noise microwave signals," *Journal of the Optical Society of America B*, Vol. 25, No. 12, 2140–2150, 2008.

Application of EH4 in the I Forecast Area in Yushiwa Iron Deposit of Hanxing Area, China

Zhaohui Ke, **Songling Chen**, **Tagen Dai**, **and Gaofeng Du**
School of Geosciences and Environmental Engineering, Central South University
Changsha, Hunan 410083, China

Abstract— Yushiwa area in north western of the Wuan depression depression, and west of the Taihang concave arch, China. The authors have reached the conclusion that the iron ore bearing horizon is middle Ordovician, the magmatic rock mass is Late in the Yanshan-mafic intrusions. EH4 is widely used in solid minerals, especially in finding concealed ore deposit. In this paper, the author adopted EH4 method to make a synthetic study on I forecast area in Yushiwa iron Deposit of Hanxing area. The result showed that the geophysical method was quite useful in the exploration of concealed ore deposit.

Determination of Thermal Model Parameters for Stator Slot Using Numerical Methods

L. Idoughi, X. Mininger, L. Bernard, and F. Bouillault
LGEP, CNRS UMR 8507, Supélec, Université Paris-Sud, UPMC Paris 6
Plateau de Moulon, 11 Rue Joliot Curie, F 91192 Gif sur Yvette Cedex, France

Abstract— In the thermal modeling of electrical machines, one of the main problems concerns their winding where the temperature often rises to its maximum value. Indeed, appropriate models for the windings are necessary to find the hot spot of the machine. The objective of the present study is then to describe an accurate thermal model with low calculation cost for stators with complex slot geometries, allowing the estimation of maximum and mean temperatures in the winding. The method proposed here is based on the discretization of the geometry using a Finite Integration Technique (FIT) in order to obtain a first order equivalent thermal model for the transient analysis of one desired temperature Ti in the slot:

Thermal equations:

$$\begin{cases} \mathrm{div}(\vec{\varphi}) + p = \rho C_p \dfrac{\partial T}{\partial t} \\ \vec{\varphi} = -\lambda \cdot \vec{grad}(T) \end{cases}$$

FIT

Matrix equations:

$$\begin{cases} -\tilde{S}\hat{\varphi} + P = C \cdot \dfrac{dT}{dt} \\ \hat{\varphi} = M_\lambda \hat{h} = M_\lambda \hat{S}^T T \end{cases}$$

Thermal resistances

$$\begin{pmatrix} T_1 \\ \vdots \\ T_n \end{pmatrix} + (\tau_{RC}) \frac{d}{dt} \begin{pmatrix} T_1 \\ \vdots \\ T_n \end{pmatrix} = \begin{pmatrix} R_1 \\ \vdots \\ R_n \end{pmatrix} P_0 + \begin{pmatrix} 1 \\ \vdots \\ 1 \end{pmatrix} T_f$$

R_i represents directly the equivalent thermal resistances between the considered point i and the slot/iron boundary, T_f is the iron temperature. Thermal capacities are deduced by the evaluation of the eigen values of the time-constant matrix (τ_{RC}), the highest eigen value $\tau_{\max}$ being chosen as time constant of the first order system. Determinations of the equivalent thermal resistances and capacitors associated with each node are detailed in the full paper.

A stator slot of flux-switching machine is considered to validate the proposed equivalent thermal model (Figure 1). Two cases are assumed: Isothermal slot border at temperature T_f or a slot border divided into several isothermal parts. Figure 2 presents the simulation results obtained for the hot spot, including the comparison with the finite element method (FEM) implemented in the ANSYS software.

Considering the presence of the iron, the results obtained with the equivalent model in the static and transient analysis present a good accuracy in the case of the non-isothermal border (here 3 isothermal parts are considered). The isothermal-border hypothesis, giving the smallest thermal model, seems here to be inadequate, leading to a too low hot spot temperature. In the full paper, more details will be presented on the methodology to obtain the model parameters. Moreover, the model of the iron part of the stator will be detailed to obtain the overall thermal model of the stator.

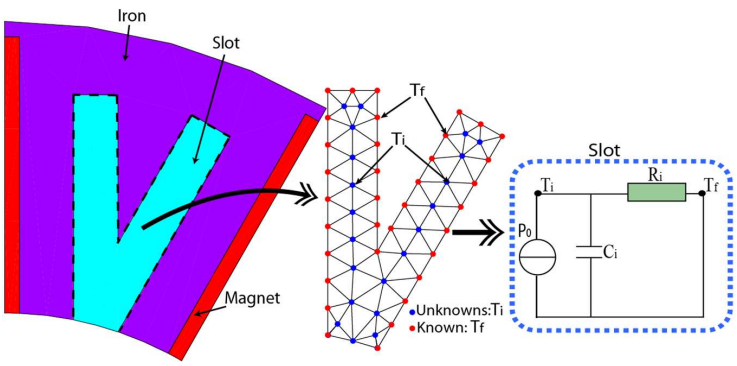

Figure 1. Equivalent thermal model of the slot.

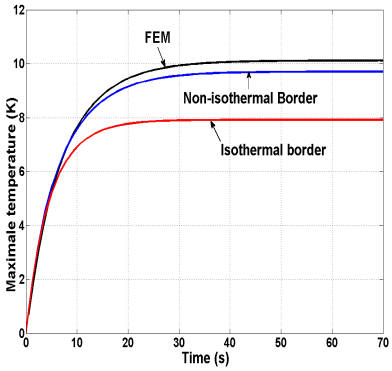

Figure 2. Simulation results.

Effect of High-order Modes on Tunneling Characteristics

H.-Y. Yao and T.-H. Chang
National Tsing Hua University, 101, Section 2, Kuang Fu Road, Hsinchu 300, Taiwan, R.O.C.

Abstract— Most tunneling effects are investigated using a one-dimensional model, but such an approach fails to explain the phenomena of the propagation of wave in a system with geometric discontinuities. This work studies the tunneling characteristics in a waveguide system that consists of a middle section with a distinct cutoff frequency, which is controlled by the cross-sectional geometry. Unlike in the one-dimensional case, in which only the fundamental mode is considered, in a virtually three-dimensional system, multiple modes have to be taken into consideration. High-order modes (HOMs) modify the amplitude and the phase of the fundamental mode (TE_{10}), thus subsequently affecting the transmission and group delay of a wave. The effect of the high-order evanescent modes is calculated, and the results are compared with the simulated ones using a full-wave solver. Both oversized and undersized waveguides reveal the necessity of considering the HOMs. The underlying physics is manifested using a multiple-reflection model. This study indicates that the high-order evanescent modes are essential to the explanation of the phenomena in a tunneling system with geometrical discontinuities.

Physical Regularization of Incorrect Electrodynamic Problems

V. A. Neganov, **D. P. Tabakov**, **and D. S. Klujev**
Povolzhskiy State University of Telecommunications and Informatics, Russia

Abstract— Integral equations (IEs) of Pocklington and Hallen are usually used for the calculation of radiating current's distribution and input impedance of oscillating antennas. Actually, the physical model that corresponds these IEs isn't correct, because radiating points and a surface of the observation have space between them. Besides, they use usually an approach of thin wire neglecting the wide of the antenna [1]. In this case the relation between the surface density η_Z (z-a coordinates along the oscillating antenna) and magnetic intensity H_φ is disturbed, thus the cause of the emergance of electromagnetic field in the theory of antennas is eliminated as well [2].

Using Hallen's equations it is necessary to take into account that the generator of outer EMF is situated in an infinitely thin slot. It leads to an unstable and physically not adequate solution [2]. Nevertheless, these IEs have an advantage — in the simplicity of their expressions.

One of the alternatives of Pocklington IEs is a singular integral equation (SIE) with singularity of Cauchy obtained for tubular model of the oscillator [2, 3]. The tubular model is physically correct and the solution of SIE has no problem with instability. Its disadvantage is the relative complexity of kernel's expression. This model can be considered as one of regularization's method of electrodynamic problem, but IEs of Pocklington or Hallen are actually regularized mathematicaly by Tokhonov [4].

The first and the most easily implemented step of physical regularization is used directly to incorrect IEs. It is about taking into account of a gap with finit wide where the outer EMF is placed. This approach is considered in [3]. The results show that this method allows to increase a radius of the oscillator with a saving of the results' stability. The second and the most effective step is a receiving correspondent SIE with logarithmic singularities and hypersingularities. Finally, the third step of physical regularisation is taking into account of metal's finite conductivity.

REFERENCES

1. *Computer Techniques for Electromagnetics*, edited by R. Mittra, 486, Perganon Press, Oxford, New York, Noronto Sydney, Braunsch Weig, 1973.
2. Neganov, V. A., *Physical Regularization of Some Incorrect Problems of the Electrodynamic*, 450, Sains Press, Moscow, 2008.
3. Neganov, V. A., E. A. Pavlovskaya, and G. P. Yarovoy, "Radiation and diffraction of electromagnetic waves," *Radio I Svyaz*, 264, Moscow, 2004.
4. Tikhonov, A. N. and V. Y. Arsenin, "Solution's methods of incorrect problems," *Nauka*, 288, Moscow, 1979.

The Physical Regularization of Incorrect Electrodynamic Problems

V. A. Neganov and D. P. Tabakov
Povolzhskiy State University of Telecommunications and Informatics, Samara, Russia

Abstract— In modern computer-aided design (CAD) in the solution of the boundary electrodynamic problems are used direct and indirect mathematical methods. The first part include such methods as the finite elements method and the method of Finite Difference Time Domen (FDTD).

Indirect methods are based on receiving of analytic solution of auxiliary problem that is about a structure's excitation with elementary current source that is called Green's function. If this function can be defined analytically, then the solution's efficiency cardinally increases and the dimension decreases, because calculations are performed only on radiating surface.

A significant advantage of indirect mathematical methods to direct is the fact, that they allow to eliminate various kinds of improperty in antennas' computing [1]: The gap between the surface density of electric current on the antenna and the magnetic field, the emergence of unstable solutions, etc.

Despite the fact that the Green's function can be determined analytically only for a limited number of structures, indirect methods can solve a wide range of electrodynamic problems. The report focuses on a variety of integral equations (IE), obtained for some types of spiral antennas. Both the correct and incorrect physical models are considered. Incorrect model based on the use of thin wire approximation and leads to Fredholm's IE of first kind (it includes Hallen's and Pocklington's IE), which have a known problem — The possible instability of the solution. Correct models lead to IE containing hypersingularities, logarithmic and. These IE have a stable solution, but requires a lot of computing time. Earlier, singular IE were successful used by authors to analyze a tubular electric oscillator [2], loop antenna [3], linear and curved microstrip antennas.

REFERENCES

1. Neganov, V. A., *Physical Regularization of Some Incorrect Problems of the Electrodynamic*, 432, Sains Press, Moscow, 2008.
2. Neganov, V. A., E. I. Nefyodov, and G. P. Yarovoy, "Electrodynamic methids of design of microwave devices and antennas," *Radio I Svyaz*, 415, Moscow, 2002.
3. Neganov, V. A. and D. P. Tabakov, "An applying of singular integral equations to electrodynamic analysis of flat ring antenna," *A Physic of Wave Processes and Radiotechnical Systems*, 4–6, 2008.

Circularly Polarized RFID Reader Antennas for Robotic Application

S. Hebib[1, 2], **S. Bouaziz**[1, 2], **H. Aubert**[1, 2], **and F. Lerasle**[1, 2]

[1]CNRS, LAAS, 7 Avenue du Colonel Roche, Toulouse F-31077, France
[2]Université de Toulouse, UPS, INSA, INP, ISAE, LAAS, Toulouse F-31077, France

Abstract— This work deals with the design of compact circularly polarized RFID reader antennas which are compatible with the unusual embeddability imposed by the autonomous robotics context. These antennas would be part of a radiolocation system implemented on an interactive robot-guide called *Rackham* [1] and should be adapted to an existing RFID tags operating between 860–960 MHz. The challenge was to integrate the designed antennas directly on the cylindrical surface of *Rackham* which is a 4-feet (118 cm) tall and 20-inches (52 cm) wide cylinder. A set of 8 RFID reader antennas is required to provide an optimum RFID coverage of the robot's surroundings. To fulfil such requirements, a compact antenna composed of 4 inverted L radiating elements arranged as a cross is proposed (Figure 1(a)). The circular polarization of this antenna is obtained by the means of a feeding circuit providing a quadrature phase excitation. This feeding circuit consists of three miniaturized power dividers. The antenna is printed on a flexible substrate of 635 µm thick that will be mounted on *Rackham* cylindrical body. The designed antenna radiates quasi-omnidirectional radiation patterns with a gain of 4 dBi and a bandwidth of 13% (centred at 900 MHz). It occupies an area of 20 cm × 20 cm with a height of 4 cm.

Several tests have been conducted in order to estimate the performance of the designed antennas and, in particular, their RFID read range. Figure 1(b) depicts one of these tests, which is based on probabilistic analysis of tag detection using only two of the designed antennas. The obtained results confirm the good performance of the designed RFID reader antennas with a reliable read range of 3 meters. Complementary studies are underway to evaluate the possibilities of: (1) increasing the RFID read range and (2) using only 6 antennas instead of 8.

(a) (b)

Figure 1: (a) Photograph of the designed RFID reader antenna. (b) Two designed antennas mounted on *Rackham*.

REFERENCES

1. Clodic, A., et al., "Rackham: An interactive robot-guide," *The 15th IEEE International Workshop on Robots and Human Interactive Communication (ROMAN)*, 502–509, 2006.

Novel Concept of ENG Metamaterial in Rectangular Microstrip Patch Antenna (Partially Loaded Case) for Dual Band Application

Mahdy Rahman Chowdhury Mahdy, **Md. Rashedul Alam Zuboraj**, **Abdullah Al Noman Ovi**, **and Md. Abdul Matin**
Department of Electrical and Electronic Engineering
Bangladesh University of Engineering and Technology, Dhaka, Bangladesh

Abstract— In this paper, the 'General Idea' of radiation pattern modification of a slot-less rectangular microstrip patch antenna, partially loaded with SNG (ENG or MNG) metamaterial has been proposed. Previously, radiation pattern of conventional TM_{020} mode of rectangular patch antenna was modified using MNG metamaterial. But the idea of using ENG metamaterial to modify such mode is different and a novel concept. Using this idea novel design of dual band rectangular patch antenna partially loaded with ENG metamaterial has been introduced successfully. Actually, this mode modification has been possible by ENG metamaterial with the help of proposed better radiation conditions, relevant theory of dispersive metamaterial and 'CST MICROWAVE STUDIO' based realistic simulated results. In case of using ENG metamaterial (partially loading case), 'Zero radiation problem' appears in sub-wavelength rectangular patch antennas. But in this paper, potential application of ENG metamaterial (mode modification) for conventional rectangular patch antennas has been shown in higher frequency range with the help of proposed novel idea. This ENG based partially loaded rectangular patch antenna is not only a good resonator, but also a good radiator (dual band application). The 'General Idea' proposed here has also explained the impossibility of sub-wavelength rectangular microstrip patch antenna as a good radiator. Moreover, this idea also explains the TM_{020} mode modification using MNG metamaterial successfully. But obviously the most interesting fact is that it creates the new way to use ENG metamaterial to load partially the rectangular microstrip antenna for TM_{020} or $TM_{0\partial 0}$ $(2 < \partial < 3)$ mode modification. The mechanism of improving radiation of conventional TM_{020} mode of a rectangular microstrip patch antenna using MNG metamaterial is not same as using ENG metamaterial (partially loaded case). If the conventional idea of mode modification using MNG metamaterial has been applied in case of ENG metamaterial (partially loaded case), serious degradation of patch antenna performance of the conventional rectangular microstrip patch antenna will be observed in 'CST MICROWAVE STUDIO' based realistic simulated results. This problem has been overcome using the 'General Idea' proposed here. In short, realistic numerical simulations; considering material dispersion, losses and the presence of the antenna feed are presented, showing how a practical realization is foreseeable.

Input Impedance Calculation for Coax-fed Rectangular Microstrip Antenna with and without Airgaps Using Various Algorithms

K. Chemachema and A. Benghalia
Department of Electronics, University of Constantine, Algeria

Abstract— Multilayered-perceptron-based neural models for calculating the input impedance of coaxfed rectangular microstrip antenna with and without airgaps are presented. eight learning algorithms: LM Trainlm — Levenberg-Marquardt, BFG trainbfg — quasi-Newton backpropagation, RP trainrp — Resilient Backpropagation, SCG trainscg — Scaled Conjugate Gradient, CGF traincgf — Fletcher-Powell Conjugate Gradient, OSS trainoss — One-Step Secant, GDX traingdx — Variable Learning Rate Backpropagation, GDM Traingdm — Gradient descent with momentum are used to train the multilayered perceptrons. The input impedance results obtained by the neural models are in very good agreement with the results of Aboud. The LM algorithm converges rapidly after some point, but only after the other algorithms have already converged.

Helically Corrugated Feed Antenna with Far out Sidelobes Reduction

S. H. Mohseni Armaki[1], **F. Hojat Kashani**[2], **J. Rashed-Mohassel**[1], **and M. Fallah**[1]

[1]Iran University of Science and Technology (IUST), Tehran, Iran
[2]University of Tehran, Tehran, Iran

Abstract— This paper presents experimental studies of a helically corrugated circular waveguide (HCCW) antenna feed. The experimental results agree with the simulated results and demonstrate a moderate influence on suppression far out sidelobes of open ended HCCW.

Introduction: The helically corrugated waveguide (HCCW) in its many applications has attracted considerable interest as device for the propagation of electromagnetic energy [1–4]. In usual way open ended circular cylindrical waveguide (CCW) was being used as feed antenna. In an open ended CCW, there is spillover of radiated power through far-out side lobes, and this become more predominant in the E-plane. The reason for this is that fields diffracted by the open end of waveguide induced conduction currents on the outer wall of the waveguide, which in turn radiate and contribute to increases spillover. With a view to reducing spillover a suggestion was presented by Narasimhan [5]. Another way is using helically corrugation in inner surface of CWW as shown in Fig. 1.

In this paper, we have presented the experimental study on reduction far out spillover radiation pattern of feed antennas. Measurements reveal that helically corrugations do help reduction of far out sidelobes and cross polarization levels. Moreover, only with helically corrugation it is possible to realize reduction in far out sidelobes over a broad band (about 28 percent) without any significant deterioration of the other radiation characteristics.

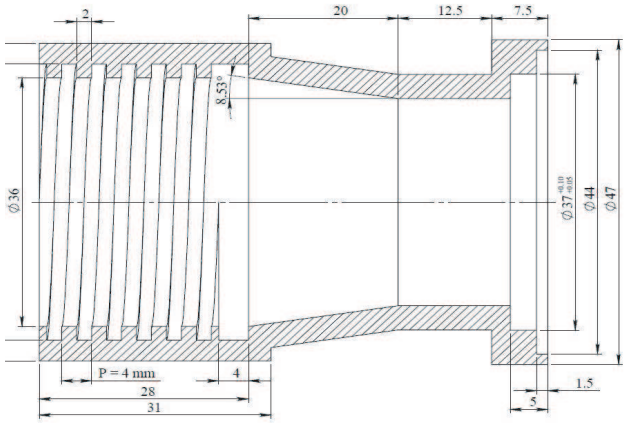

Figure 1: Dimensions of HCCW. All dimensions in mm.

REFERENCES

1. Foulds, K. W. H., et al., "Propagation of an electromagnetic wave through a helical waveguide," *IEE Proc.*, Vol. 11, No. 11, 1789–1798, Nov. 1964.
2. Tang, C. C. H., "On the wave propagation and mode conversion in a helically corrugated multimode circular waveguide," *IEEE Trans. on Microwave Theory and Techniques*, Vol. 14, No. 6, 275–284, Jun. 1966.
3. Ghosh, S. and G. P. Srivastava, "Corrugated waveguide with helically continues corrugation," *IEEE Trans. on Antennas and Propagation*, Vol. 27, No. 4, 564–567, Jul. 1979.
4. Wei, Y., et al., "Experimental demonstration of the effect of groove shape on the wave properties of the helical groove waveguide," *IEEE Microwave and Wireless Components Letter*, Vol. 13, No. 11, 484–486, Nov. 2003.
5. Narasimhan, M. S. and K. R. Govind, "Radiation characteristics of a corrugated circular cylindrical waveguide horn exited in the TE11 mode," *IEEE Trans. on Antennas and Propagation*, Vol. 36, No. 8, 1147–1152, Aug. 1988.

Design and Development of Monopulse Dual Mode Corrugated Horn

S. H. Mohseni Armaki[1], **F. Hojat Kashani**[1], **J. Rashed-Mohassel**[2], **and M. Fallah**[1]

[1]Iran University of Science and Technology (IUST), Iran
[2]University of Tehran, Iran

Abstract— This paper describes the design and test of a corrugated feed horn antenna which can propagate sum and difference patterns suitable for monopulse tracking in remote sensing earth stations. The prototyped horn designed here operates in the frequency range 7–9 GHz for sum mode and 7.5–9 GHz for difference mode. The gain of sum pattern is 22 dB with at least 32 dB cross-polarization. The measured results validate that the feed operation is satisfactory for 20% bandwidth.

Miniaturized Planar UWB Antenna with a Trapezoid Shape Ground

Yangjun Zhang, Yusuke Takeuchi, and Toyokatsu Miyashita
Department of Electronics & Informatics, Ryukoku University, Seta, Ohtsu 520-2194, Japan

Abstract— A circular disc monopole UWB antenna fed with a tapered microstrip line on an arched shape ground has been proposed [1]. This paper presents a miniaturized planar UWB antenna using a trapezoid ground. The presented antenna shows a simple configuration, and suggests that a much smaller planar UWB could be obtained.

The top view of the presented antenna is shown in Fig. 1(a). The diameter of radiation disc is 12.4 mm, and it is fed with a tapered microstrip line. The antenna is implemented on a FR-4 substrate ($\varepsilon_r = 4.4$), and the total size is $40 \times 30\,\text{mm}^2$. Two kinds of ground pattern, 1-stage trapezoid and 2-stage trapezoid ground shape as shown in Figs. 1(b) and 1(c) respectively, have been studied. It was found that a trapezoid shape ground could improve impedance matching over UWB frequency band. The measured results of return loss are shown in Fig. 2 with a comparison with simulation results. For the antenna with 1-stage trapezoid ground, the simulation result for 10-dB return loss bandwidth is 3.4–10.2 GHz, while the measurement result is 2.5–9.7 GHz with a mismatching around 4.6 GHz. For the antenna with 2-stage trapezoid ground, the simulation result for 10-dB return loss bandwidth is 3.1–10.6 GHz, while the measurement result is 2.85–10.5 GHz. The radiation patterns of the antenna with 2-stage trapezoid ground at 8 GHz are shown in Fig. 3. The measured and simulated radiation patterns agree well, and an omnidirectional radiation pattern in xy-plane is obtained.

The simulated current distribution at the first and the second resonant frequency are shown in Figs. 4(a) and 4(b), respectively. It is clear that the overlap of the two resonant modes leads to impedance matching over wide frequency range. The current distribution on the ground indicates that the trapezoid ground can be miniaturized as the shape shown in Fig. 4(c) with little change

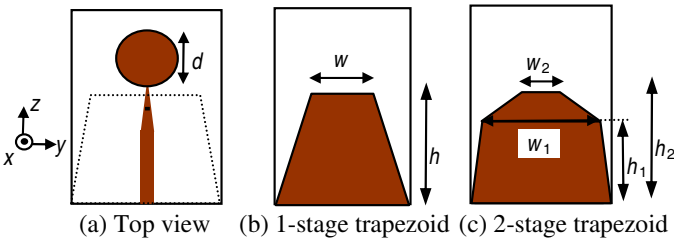

Figure 1: The UWB antenna configuration.

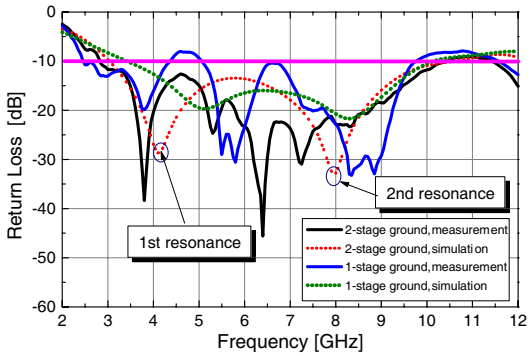

Figure 2: Measured and simulated return loss.

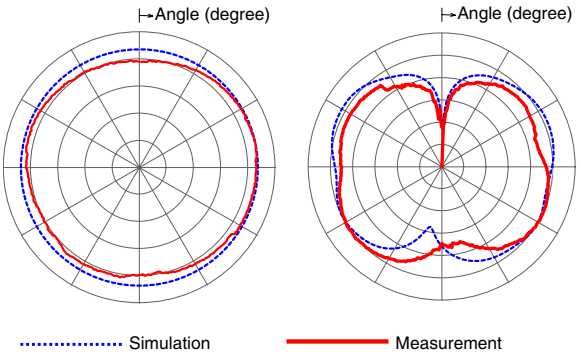

Figure 3: Measured and simulated radiation patterns at 8 GHz.

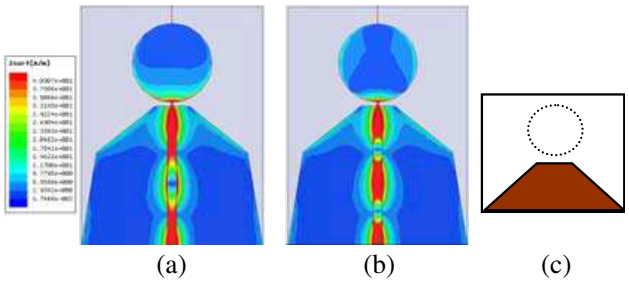

Figure 4: Simulated current distribution at (a) first resonance 4.2 GHz, (b) second resonance 7.9 GHz, and (c) a much smaller antenna with a trapezoid ground

on the resonant current distribution. The antenna with Fig. 4(c) ground shape is now being studied, and a good initial result has been obtained.

REFERENCES

1. Zhang, Y., M. Shimasaki, and T. Miyashita, "A circular disc monopole UWB antenna fed with a tapered microstrip line on a circular ground," *Progress In Electromagnetics Research Symposium Abstracts*, 105, Moscow, Russia, August 18–21, 2009.

Novel Application of MNG Metamaterial in Rectangular Microstrip Patch Antenna (Partially Loaded Case) for Dual Band Application

Mahdy Rahman Chowdhury Mahdy, **Md. Rashedul Alam Zuboraj**,
Abdullah Al Noman Ovi, **and Md. Abdul Matin**
Department of Electrical and Electronic Engineering
Bangladesh University of Engineering and Technology, Dhaka, Bangladesh

Abstract— Previously, it has been shown that sub-wavelength rectangular microstrip patch antennas partially loaded with ENG metamaterial are good resonators but not good radiators. Such patches, even if working at resonances in the sub-wavelength regime do not radiate energy efficiently in free space. These antennas give broadside null radiation pattern. This phenomenon is referred as 'Zero Radiation Problem'. In this paper, we have reported a 'Partial Solution' of 'Zero Radiation Problem' for sub-wavelength resonance using MNG metamaterials. A general idea for better radiation has been introduced first. Due to the use of that novel idea, the proposed rectangular patch antenna serves not only as a good resonator, but also a good radiator. This unslotted antenna will be used for dual band applications (Figs. 1, 2, 3, 4). Resonance of this $TM_{0\delta 0}$ mode ($0 < \delta < 1$) with good radiating property (above 5 dB at broadside) has been possible due to the use of our proposed 'General Idea' of mode modification for better radiation. All the ideas regarding this metamaterial based rectangular microstrip patch antenna have been verified with analytical calculations, 'MATLAB' based simulated results and 'CST MICROWAVE STUDIO' based realistic simulations. If our proposed 'General Idea' of 'Better Radiation Conditions' and

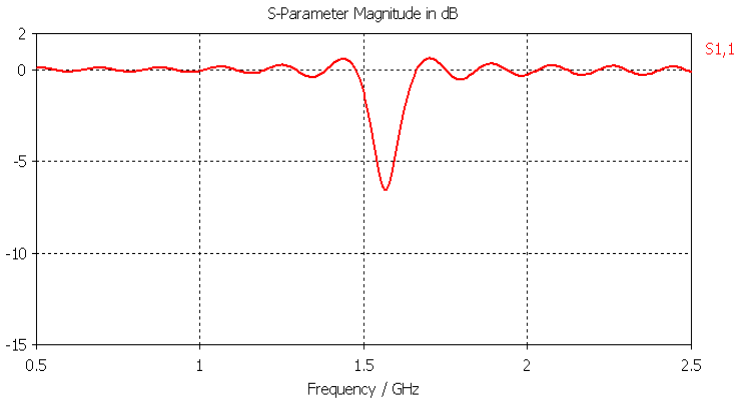

Figure 1: A 50 mm × 40 mm rectangular patch antenna using DPS only, S-parameter performance.

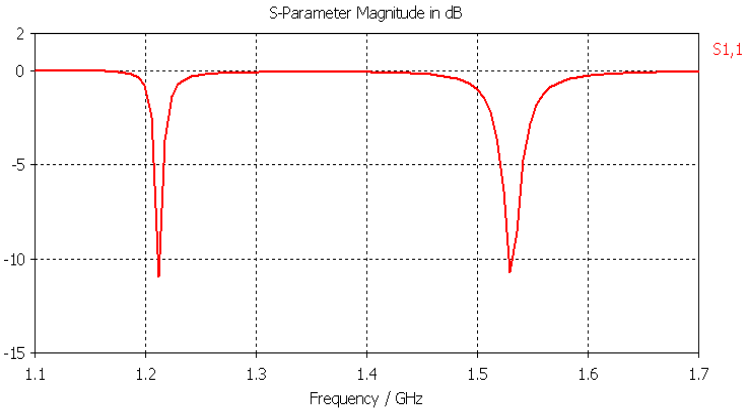

Figure 2: Proposed 50 mm × 40 mm rectangular patch antenna using DPS and MNG metamaterial, S-parameter performance. Plasmonic resonance at 1.212 GHz with quite satisfactory radiation pattern (Fig. 3).

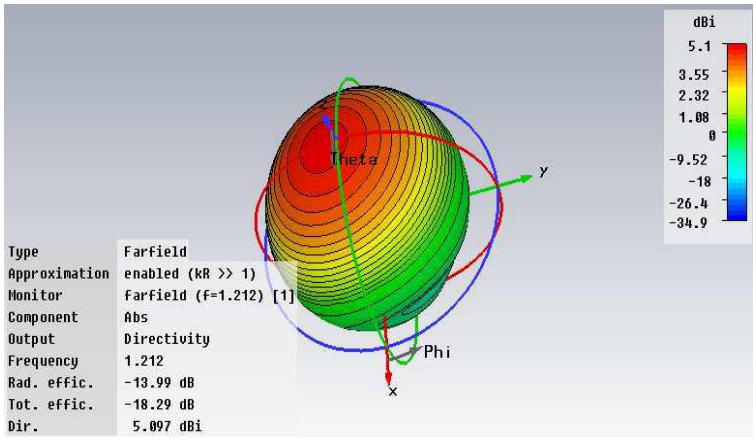

Figure 3: Radiation Pattern at 1.212 GHz ($TM_{0\delta0}$ mode $(0 < \delta < 1)$).

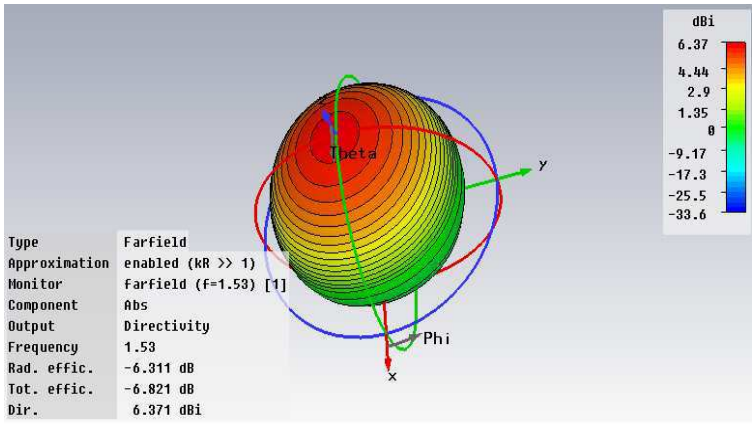

Figure 4: Conventional TM_{010} mode radiation pattern at 1.53 GHz.

relevant theory of dispersive metamaterial are not maintained properly, this type of atypical performance of rectangular patch is quite impossible. In case of such rectangular patch antenna, arbitrary low value of resonance along with arbitrary small length of the antenna is impossible. But yet low value of fundamental resonance ($TM_{0\delta0}$ mode $(0 < \delta < 1)$) using plasmonic resonance has been reported here. Thus, the term 'Partial Solution' is used. Moreover, almost 50% size reduction of rectangular patch antennas has been possible with this type of novel design along with its dual band applications.

Novel Design of Dual Band Rectangular Microstrip Patch Antenna Partially Loaded with MNG Metamaterial for S-band Application

Mahdy Rahman Chowdhury, **Md. Rashedul Alam Zuboraj**,
Abdullah Al Noman Ovi, **and Md. Abdul Matin**
Department of Electrical and Electronic Engineering
Bangladesh University of Engineering and Technology, Dhaka, Bangladesh

Abstract— Miniaturized size and high directivity performance of an antenna are primary requirements for modern satellite based communication systems. Prior to our work, it has been shown that the size of rectangular microstrip patch antenna cannot be made arbitrarily small. But almost 50% size reduction of such an antenna has been possible using our proposed 'General Idea' and 'Better Radiation Conditions'. In this paper, two novel designs of such antennas partially loaded with MNG metamaterial has been proposed for S-band applications. In case of first design, using plasmonic resonance, $TM_{0\delta 0}$ mode ($0 < \delta < 1$) has been excited at 2.47 GHz with only a 25 mm × 15 mm rectangular patch. At both bands (2.47 GHz and 3.01 GHz), this antenna shows quite satisfactory radiation performance (directivity above 5.5 dB at broadside for both bands, Figures 1, 2, 3, 4). Again, almost 50% size reduction has been possible here with respect to conventional rectangular patch antenna. In our second design, using MNG metamaterial, again plasmonic resonance has been used to excite $TM_{0\delta 0}$ mode but now $1 < \delta < 2$. Previously, applying MNG metamaterial, TM_{020} mode of conventional rectangular microstrip antenna has been modified using 72.8 mm × 50 mm patch. But here, using our 'General Idea' and 'Better

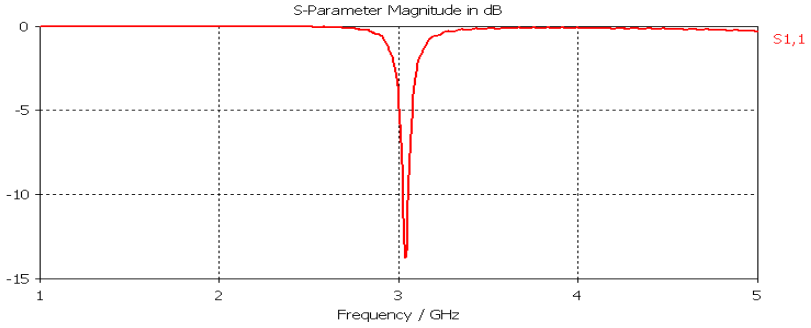

Figure 1: A 25 mm × 15 mm rectangular patch antenna using DPS only, S-parameter performance.

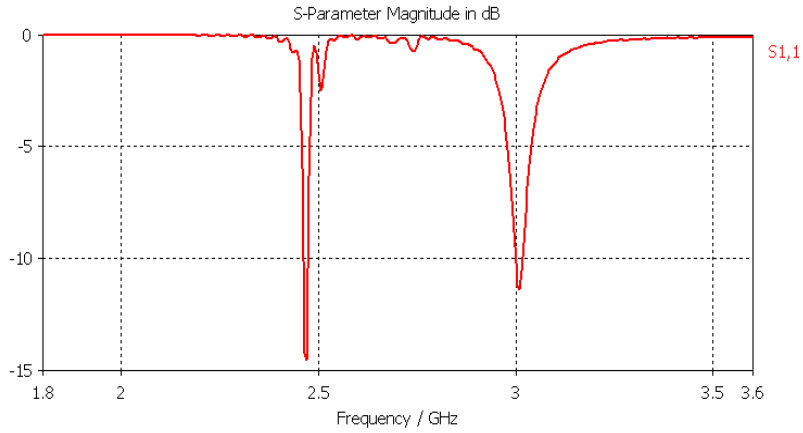

Figure 2: Proposed 25 mm × 15 mm rectangular patch antenna using DPS and MNG metamaterial, S-parameter performance. Plasmonic resonance at 2.47 GHz with quite satisfactory radiation pattern (Figure 3).

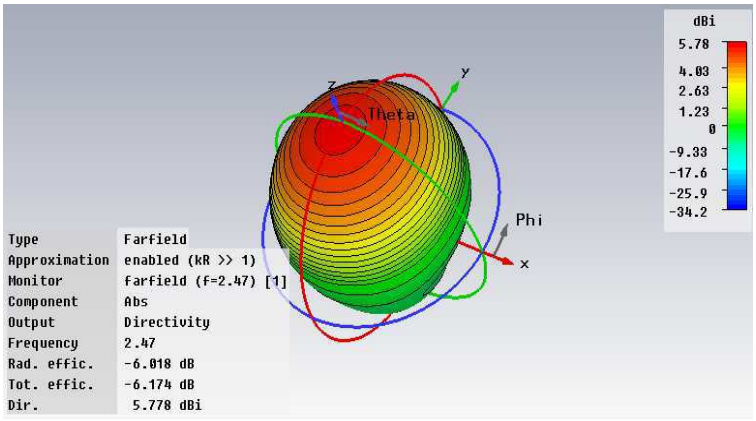

Figure 3: Radiation Pattern at 2.47 GHz ($TM_{0\delta0}$ mode, $0 < \delta < 1$).

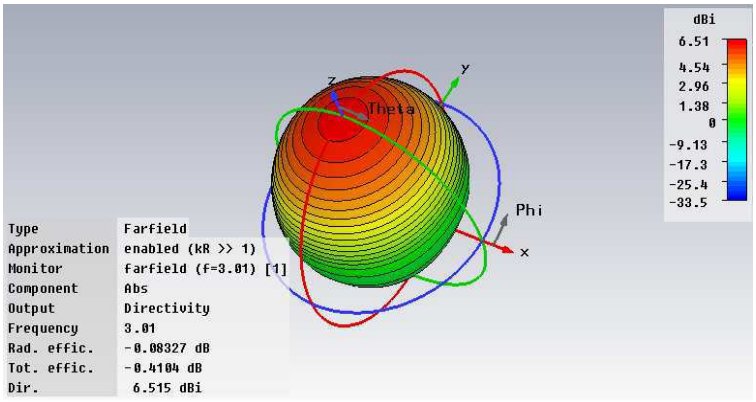

Figure 4: Conventional TM_{010} mode radiation pattern at 3.01 GHz.

Radiation Conditions', with a conventional size, this unconventional $TM_{0\delta0}$ mode ($1 < \delta < 2$) has been produced for S-band application. All our analytical results have been verified using 'MATLAB' based codes and 'CST MICROWAVE STUDIO' based realistic simulated results.

New Formulation of the Method F.W.C.I.P. for the Modelling of a Planar Circuit Integrating a via-hole

Sameh Toumi, **Fethi Mejri**, **and Taoufik Aguili**
Laboratoire des Systèmes de Communication, École Nationale d'Ingénieurs de Tunis (ENIT), Tunisia

Abstract— In our work the structure microstrip is a planar circuit, single layer, consisting of a metallic conductor connected to ground through a via-hole deposited on the upper surface of a dielectric substrate and fed by a localised auxiliary source. The fundamental mode of propagation of such support is not spread TEM (transverse electromagnetic) because the transverse section is not homogeneous. However, since the amplitudes of the longitudinal components of electric and magnetic fields are sufficiently low to be neglected, therefore we speak of quasi-TEM mode. Then is possible to make the modeling of the structure as a transmission line of characteristic impedance Zc immersed in an equivalent homogeneous area characterized by a relative permittivity $\varepsilon_{r_{eff}}$. We are interested in this work for via-holes in planar technology that allow better use of both sides of a printed circuit substrate. To model the structure of such iterative method we must take into account the presence of the via-hole in the circuit. In this formulation the TE (transverse electric), TM (transverse magnetic) and TEM modes are used as the basis of numerical spectral domain in which the FFT (Fast Fourier Transform) is projected. Subsequently, the concept of fast wave is introduced to translate the boundary conditions and continuity of relation on different parts of the interface in terms of waves. The method consists in determining an effective relation to link the incident and the reflected waves in the different dielectric layers by expressing the reflexions in the modal domain and the boundary conditions and continuity, expressed in terms of waves in space domain. We use the iterative process to pass from an area to another by means of the FMT (Fast Modal Transform) thus making it possible to accelerate the iterative process and then the convergence of the method. This formulation keeps the advantages of the iterative method in particular the simplicity of implementation and speed of execution compared to other methods. The structure study gives us the convergence of the impedance input Ze and the same results obtained by the analytical formula.

Fine Synchronization with UWB TH-PAM Signals in Ad-Hoc Multi-user Environments

M. Hizem and R. Bouallegue
6'Tel Research Unit, Higher School of Communications of Tunis, Sup'Com, Tunisia

Abstract— Currently, the most important discussion subject in ultra wideband (UWB) ad-hoc impulse radios is how to obtain the best possible synchronization and more specifically an efficient timing offset estimation. The synchronization complexity is accentuated in UWB systems compared to others due to the fact that waveforms are impulse-like and have low amplitude. Furthermore, the difficulty of timing UWB signals is provoked by the dense multipath channel unknown at the synchronization step. These reasons explain why synchronization has taken so much importance in UWB literature. An algorithm has grown substantially in recent years is timing with dirty templates (TDT) introduced and developed for UWB signals.

The UWB time hopping impulse radio signal considered in this paper is a stream of narrow pulses, which are shifted in amplitude modulated (PAM). The transmitted signal propagates through the UWB multipath channel corresponding to each user.

In the present work, we develop a novel fine synchronization algorithm for UWB TH-PAM signals in ad-hoc multi-user environments. To ameliorate the synchronization performance, our contribution is to realize a fine synchronization floor and insert it after the coarse one (which is TDT). The principle is to make a fine search for the exact moment of pulse beginning (timing offset) by correlating two consecutive symbol-long segments of the received waveform in an interval that corresponds to the frames number included in one data symbol.

With the fine synchronization algorithm introduced in second floor after the TDT (first floor), we can achieve a fine estimation of the frame beginning. The simulation results show that even without training symbols, our new synchronizer can enable a better performance than the original TDT in non-data-aided (NDA) mode and offers a slight improvement in data-aided (DA) mode.

Performance Parameter of Hybrid Wireless-optical Broadband-access Network (WOBAN): A Study on the Physical Layer of Optical Backhaul and Wireless Front-end

Redhwan Q. Shaddad, **Abu Bakar Mohammad**, **and Abdulaziz M. Al-Hetar**

Photonic Technology Center, InfoComm Research Alliance
Universiti Teknologi Malaysia, Johor 81310, Malaysia

Abstract— The hybrid wireless-optical broadband-access network (WOBAN) is a promising broadband access network. It provides blanket coverage of broadband and flexible connection for wireless end-users. In this paper, the architecture of the WOBAN is proposed and designed based on both a wavelengths division multiplexing/time division multiplexing passive optical network (WDM/TDM PON) at the optical backhaul and wireless fidelity/worldwide interoperability for microwave access (WiFi/WiMAX) technologies at the wireless front-end. The power budget of the optical backhaul based on maximum split ratio of 1/32 for each wavelength channel and a fiber length of 23 km from the central office (CO) to the access point (AP) is analyzed with bit error rate (BER) of 10^{-9}. Most of the existing works, based on performance evaluation are concerned on network layer aspects. We report the performance analysis in terms of BER, eye diagram, error vector magnitude (EVM), and signal-to-noise ratio (SNR) of the WOBAN physical layer. It is demonstrated 2 Gb/s for downstream/upstream can be achieved at optical backhaul for each wavelength channel, at data rates of 54 Mb/s (WiFi) and 30 Mb/s (WiMAX) per AP along a 50 m and 5 km wireless links respectively.

Properties of Spread-F in High and Low Latitude Ionospheres

J. K. Shi[1], **W. Tao**[1], **G. J. Wang**[1], **G. Zherebotsov**[2], **O. Pirog**[2], **and A. Stepanov**[3]

[1]State Key Laboratory for Space Weather, CSSAR/CAS, Beijing, China
[2]Institute of Solar-Terrestrial Physics, RAS, Irkutsk, Russia
[3]Institute of Cosmophysical Research and Aeronomy, RAS, Yakutsk, Russia

Abstract— The ionospheric spread-F has many significant effects on the radio waves that propagation through the Earth's atmosphere, such as refraction, reflection, absorption, time delay, phase change, amplitude change, frequency change, and so on. In this paper, we used the data from the DPS-4 digisonde at the low latitude station in Hainan (19.4°N, 109.0°E), China, and Yakutsk (62°N, 129°E) and Zhigansk (66°N, 123°E), Russia to study ionospheric Spread-F (SF) properties during the magnetic storm time. Some new results are obtained by the data analysis. In general, the SF takes place in period from 20 : 00 LT to midnight, but at high latitude station Zhigansk, the SF can take place in the afternoon and morning. During the storm time, SF at Yakutsk station was more activity. The SSF concerned with the equatorial plasma bubble in the ionosphere is observed only at low latitude station Hainan, but not at high latitude stations Yakutsk and Zhigansk. The branch SF is never observed at Hainan station. In most time, the start time of the SF is later if the latitude is lower. We also make a discussion on the properties of the SF for different stations.

Monitoring of Thermal Dome as an Iridescent Sphere above the Atmosphere

Shigehisa Nakamura
Kyoto University, Japan

Abstract— The author is intending to have a physics of a thermal dome appeared in a form of an light sphere or an iridescent sphere above the atmosphere. One example of the iridescent spheres was introduced. This was introduced by a scientist in a physical periodical publishing, for example, in the Physics Today. This publication says that the problem of the iridescent dome as a part of a digestive article in a form of one example of the photographic illustrations after courtesy by Danny Stillman. It is noted that what is introduced as one example of the iridescent sphere illustrations appeared off Scandinavia or northern China. The dome expanded very rapidly, at around 3 km/s, with the center remaining quite transparent. This dome must be formed an explosive thermal energy release. A model is constructed in a scope of fluid dynamics. A simple formulation helps us a key to realize what mechanism is possible to produce such a light sphere.

Monitoring of Thermal Dome in the Earth Surface Layer

Shigehisa Nakamura
Kyoto University, Japan

Abstract— The author introduces a model of thermal dome formed in the atmospheric layer on the earth. First, it is introduced a formulation of equation of motion in order to analyze in a mathematical technique for the author's convenience. An approximated linear solution for the equation is reduced under several conditions. In order to concentrate our interest to a thermal dome in the atmospheric layer on the earth, a system of cylindrical coordinates with the origin on the earth surface is assumed. For a convenience, no circular motion of the atmospheric particles is considered in as a horizontal motion at any altitude above the earth surface. This gives us a condition of no thermal problem along any horizontal orbital motion of the air particle. The author may now consider a two dimensional problem in a vertical cross section with the vertical axis passing the origin in the coordinates. Obtained solution tells us that a form of the interested thermal dome is determined by the heat source pattern on the earth surface. An assumption makes it possible to describe the heat source pattern by a mathematical function. The author noted some specific pattern of the thermal dome as a solution in relation to a possible pattern of the thermal dome in the actual atmospheric layer. Some remarks are given for application of the thermal dome model.

Monitoring of Thermal Dome Shock Front Pattern on the Earth

Shigehisa Nakamura
Kyoto University, Japan

Abstract— This is an introduction to a model of thermal dome formed in the ocean surface layer on the Earth. First, it is introduced a formulation of an equation of motion in order to analyze in a mathematical technique for the author's convenience. A solution of an approximated equation expressed in a linear form is reduced for obtaining an approximated solution in the author's purpose. For a convenience, no assumption is considered about any circular motion around the source point of the thermal dome. This make us to see a two dimensional problem of the thermal dome which is axi-symmetric about the vertical line passing the source point of the thermal dome. The obtained solution shows a specific thermal pattern around the source point. With consideration of the water surface layer on a thin sheet of coral lagoon covering the crust layer on the Earth, the thermal dome problem can be taken as a two dimensional problem. An expected pattern of the thermal dome is semi-spherical in the atmospheric layer above the ocean surface. The author notices about several points to be effective for the successive work related on physics of thermal dome formation. A remark might be a key to an application of this work.

Circuit Simulation of Varactor Loaded Line Phase Shifter

M. Ould-Elhassen[1], **M. Mabrouk**[1], **A. Ghazel**[1], **and P. Benech**[2]

[1]CIRTACOM, SUPCOM, ISETCOM de Tunis, Tunisia
[2]IMEP-LAHC (CNRS-INPG-UJF), France

Abstract— With the explosion during recent years of wireless communications, multi-path and phased array systems technologies, the need for a robust, simple, cheap, digital or analogue solutions, is becoming very important for several applications such radars, phased arrays and instrumentation. Phase shifter has been used for a variety of applications, both nonlinear and linear.

The present studied phase shifter is comprised of high-impedance (Z_i) transmission lines periodically loaded with voltage variable capacitors (Varactor). We defined a unit cell for this periodic structure; which consists of serial transmission line section with a length (L_{sec}) and parallel variable capacitor connected to the ground. The transmission line can be approximated as a lumped inductance (L) and capacitance (C).

This paper describes circuit simulation of phase shifter based on distributed CPW transmission lines combined with Varactors diode components. The expression of phase shifting is obtained through the global (S_{ij}) matrix of 9 units of proposed phase shifter. The simulations are carried out on ADS simulator. Comparison between our simulated results and published measurements of the studied phase shifter is made and a good agreement is obtained.

In our simulation, we used the same parameters mentioned below. The length of input section is 17 mm and the one of central section length is 10 mm. We also used the Rogers RO4003 substrate with $\varepsilon_r = 3.36$, $H = 813\,\mu\text{m}$ and $\text{tg}(\delta) = 1.5 * 10^{-3}$. The phase shift obtained was linear from 100 MHz up to 800 MHz. Then the phase shift has a quadratic variation from 800 MHz up to 1.2 GHz. In the final paper, we will also present the insertion loss and return loss versus frequency of our studied phase shifter.

60 GHz Rectangular Patch Antennas on Flexible Substrate: Design and Experiment

Ahmed Ali[1, 2], **Mohamed M. Jatlaoui**[1, 2], **Sami Hebib**[1, 2], **Hervé Aubert**[1, 2], **and Daniela Dragomirescu**[1, 2]

[1]CNRS, LAAS, 7 Avenue du Colonel Roche, F-31077 Toulouse, France
[2]Université de Toulouse, UPS, INSA, INP, ISAE, LAAS, F-31077 Toulouse, France

Abstract— The rapid development of nowadays wireless applications implies an increasing demand on high speed wireless communication systems. As a matter of fact, a particular attention has been devoted recently for the mm-wave band around 60 GHz for short-range communication applications offering a high level of frequency reuse such as wireless fiber extension links, Radio Local Area Networks (RLAN) [1], etc..

Millimeter-wave antennas are naturally an essential component of such applications. To offer more flexibility of such communication systems at such high frequencies while ensuring low-cost fabrication processes and reliable components, the use of low-loss flexible substrates has become a natural challenge seeking low-loss, light-weight conformal antennas and short-range front-end modules. Promising simulation-based study has been recently reported in [2] for such antenna on flexible liquid crystal polymer.

In this work, 60 GHz rectangular patch antennas are designed fabricated and measured on a flexible 127 µm thick polyimide substrate. The chosen substrate (Kapton 500 VN) has a permittivity of 3.5 and loss tangent $\tan\delta = 0.002$. A well matured fabrication process is used where first a polymer spin coating is performed for the adhesion of the polyimide on the holding wafer. The Kapton polyimide is then patterned on the substrates by lamination. A resin lift spin coating is then realized followed by a photolithography for the TA/Cu metallization layer. Different components have been designed and realized at 60 GHz. A classical rectangular patch antenna is first designed (see the inset in Fig. 1(a)). Then, to increase the antenna directivity, the antenna width is doubled and a simple microstrip corporate feed network is used (see the inset in Fig. 1(b)). A simple gap coupled resonator is also designed to characterize precisely the dielectric permittivity and loss tangent at the design center frequency. Preliminary results for the simulated and measured reflection coefficient of the latter antenna are shown in Fig. 1(b) and show quite good agreement. The observed frequency shift is due to the use of the communicated permittivity value in the simulations. Further results will be presented in the conference with more focus on the measurements conditions and the integration techniques that will be used.

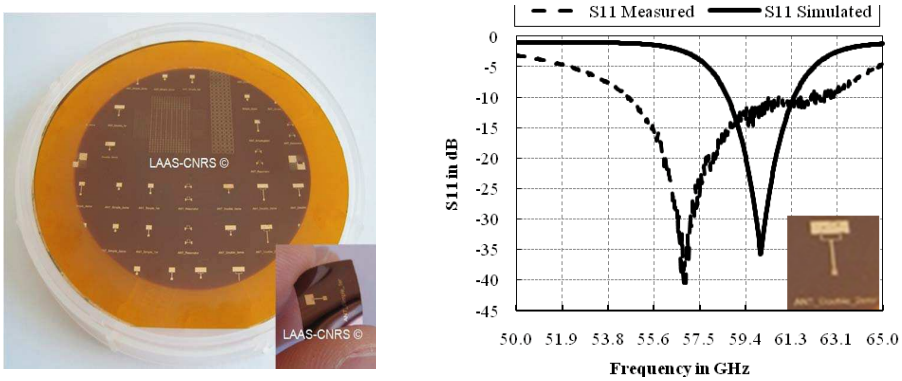

(a) (b)

Figure 1: (a) Photograph of different fabricated components (60 GHz resonator and path antennas). (b) Simulated and measured reflection coefficients of the developed antenna with microstrip corporate feed network.

ACKNOWLEDGMENT

This work was supported by the NanoComm project as part of the Nano-Innov French program.

REFERENCES

1. Sestini, F., J. Fernandez, and J. Schwarz, "Expanding the wireless universe: EU research on the move," *IEEE Communications Magazine*, Oct. 2002.
2. Amadjikpe, A., A. Vera, D. Choudhury, and J. Papapolymerou, "Study of a 60 GHz rectangular patch antenna on a flexible LCP substrate for mobile applications," *IEEE Antenna Propagat. Symp.*, Jul. 2008.

Characterization of Ferromagnetic Materials Used in Inkjet Technology

K. Haj Khlifa, **F. Ndagijimana**, **and T. P. Vuong**
IMEP-LAHC, 3, Parvis Louis Néel, Grenoble 38016, France

Abstract— The development of wireless applications leads to an increasing demand of electronic broadband components. Inductances and transformers are key components for power management and communication stages. The knowledge of the electric behaviour of the magnetic materials is critical especially when broadband applications are concerned. The main materials used for designing inductances and transformers are ferromagnetic ones of types MnZn and NiZn with relative permeability up to 20000 at low frequencies.

To characterize a toroidal ferromagnetic material, there are two very common methods (Figs. 1, 2):

- The first method consists in winding up a conducting wire on a toroid core, in order to realize an inductance. The permeability is extracted easily from the measured inductance.
- The second method is to use a coaxial transmission line to determine both permittivity and permeability. A factor that greatly influences the accuracy of the results is the air gaps between the material under test and the coaxial transmission line test fixture.

The novel approach we are proposing is to adapt these techniques to characterizing ferromagnetic materials deposed by inkjet process. The material transformations from solid to liquid state and also from liquid to solid is accompanied by changes of electrical parameters. Therefore we need to characterize this ferromagnetic material in different process steps, taking into account the dimensional constraints imposed by inkjet technology. Electromagnetic simulations show the advantages and disadvantages of the characterization methods mentioned above by using this technology.

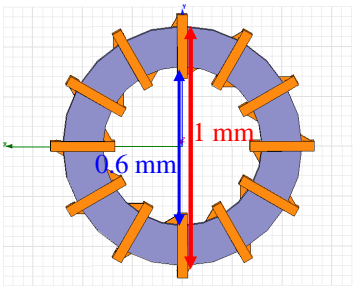

Figure 1: Toroïdal inductor.

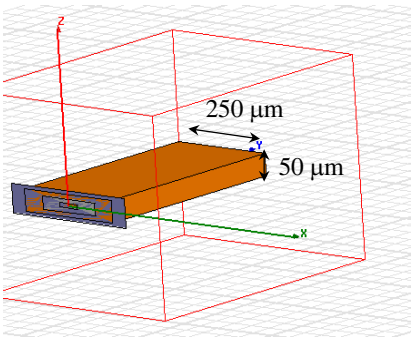

Figure 2: Coaxial transmission line test fixture.

Design and Optimization of RF Square Spiral Inductors Realized by Inkjet Technology

L. Mutwewingabo[1, 2], **B. Krafft**[2], **and F. Ndagijimana**[1]

[1]IMEP-LAHC, Grenoble, France
[2]MICROSPIRE, Illange, France

Abstract— The miniaturization of radio frequency (RF) devices has enabled the development of increasingly complex products in radio communications. In a mobile phone, the elements most difficult to integrate are inductors and micro-transformers (front-end RF).

In this paper, we proposed a novel design of RF square spiral inductors based on a new process called inkjet technology. This technology allows successive deposits of micro-droplets (of some picoliters) layer by layer of different materials (conductor, dielectric and magnetic ink which is new in this process), ejected from a printing head, from files trajectories of an RF square spiral inductor defined by computer-aided-design (CAD). The proposed inductor is shown in figure1. The inductors are simulated by using the ANSYS simulation software High Frequency Structure Simulator (HFSS). We demonstrate that by using inkjet technology we obtain a high performance, flexibility in the design of square spiral inductors and low cost in process technology. The effect of inkjet technology has been investigated by designing several inductors with varying geometries to realize the property of the novel square spiral inductors compared with the MICROSPIRE miniature chip inductors (MPCI).The simulation shows good agreement between models and experiments.

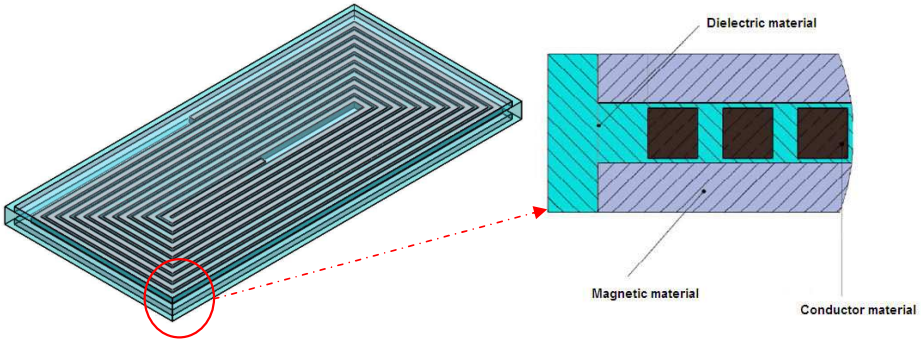

Figure 1: Square spiral inductor realized by inkjet technology.

Above Threshold Analysis of Photonic Crystal Laser

M. Koba[1,2], **T. Osuch**[2], **R. Piramidowicz**[1], **and P. Szczepanski**[1,2]

[1]Warsaw University of Technology, Poland
[2]National Institute of Telecommunications, Poland

Abstract— We present the model of 2D photonic crystal (PhC) laser operation. It describes the laser with the active medium that is confined in the square region with circular holes arranged in square or triangular Bravais' lattices. The analysis is based on the two dimensional coupled wave equations taking into account surface emission losses [1–4], and energy theorem [4, 5]. The model includes the gain saturation and spatial hole burning effects.

Starting from nonlinear coupled mode equations (suitable for rectangular or triangular lattices and TE or TM modes) and employing the energy theorem we obtained formulas for TE and TM modes in PhC laser structures. Obtained equations relate the small signal gain coefficients (α_0) required to obtain a given output power level and the system parameters, such as structure geometry and properties (lattice constant a, filling factor f, and dielectric permittivity ε), linear losses (α_L) and spatial hole burning strength (η).

The simulation part consists of continuous wave operation characteristics made for developed model. For the purpose of numerical calculations we used finite difference method. We analyzed the structure for the coupling constant values range which correspond to the possible real structures, and for different filling factors. Thus shown characteristics include dependences of normalized small signal gain coefficient as a function of coupling constant and filling factor. They reveal regions of coupling which should provide optimum power efficiency of laser structure.

We showed, by the laser characteristics, that using derived formulas, it is possible to design laser structure, which provides maximal power efficiency.

REFERENCES

1. Sakai, K., E. Miyai, and S. Noda, "Two-dimensional coupled wave theory for square-lattice photonic-crystal lasers with TM-polarization," *Opt. Express*, Vol. 15, No. 7, 3981–3990, 2007.
2. Sakai, K., J. Yue, and S. Noda, "Coupled-wave model for triangular-lattice photonic crystal with transverse electric polarization," *Opt. Express*, Vol. 16, No. 9, 6033–6040, 2008.
3. Sakai, K., E. Miyai, and S. Noda, "Coupled-wave theory for square-lattice photonic crystal lasers with TE polarization," *IEEE Journal of Quantum Electronics*, Vol. 46, No. 5, 788–795, 2010.
4. Koba, M. and P. Szczepanski, "Approximate analysis of nonlinear operation of square lattice photonic crystal laser," *IEEE Journal of Quantum Electronics*, Vol. 46, No. 6, 1003–1008, 2010.
5. Koba, M. and P. Szczepanski, "Nonlinear operation of a 2D triangular lattice photonic crystal laser," *IEEE Journal of Quantum Electronics*, in press.

A Threshold Mode Structure Analysis of Photonic Crystal Laser

M. Koba[1,2], **T. Osuch**[2], **R. Piramidowicz**[1], **and P. Szczepanski**[1,2]

[1]Warsaw University of Technology, Poland
[2]National Institute of Telecommunications, Poland

Abstract— In this work, the threshold analysis of a 2D photonic crystal (PhC) laser operation is presented. An active region of considered structure has circular holes arranged either in square or triangular symmetry. The lasing action is assumed at the band edge (Γ point). The analysis is based on the two dimensional coupled wave equations, derived in [1–4]. These equations describe laser structure operation at the threshold for TM and TE modes in the case of square and triangular lattices.

Articles [1, 3] describe threshold analysis for some specific values of coupling coefficient in a square lattice photonic crystal laser. In contrast to that, we conduct numerical analysis for a wide range of coupling coefficients to encompass real values of permittivities. Furthermore, we take under consideration a threshold mode structure of a 2D triangular lattice photonic crystal laser. For both investigated structures (square and triangular) and in each case for both possible polarizations (TE and TM) we provide the threshold mode structure analysis.

We show analytical and numerical calculations describing the dependence of the deviation from Bragg frequency on the coupling coefficients. This allows us to attribute the field distributions to its threshold gain and Bragg frequency deviation. Moreover, we present the threshold field distributions corresponding to each of the basic modes at the Γ point, i.e., in the case of the square lattice for four basic modes, and in the case of the triangular lattice for six basic modes. We conclude showing the trend of the threshold gain by plotting it as a function of the deviation from Bragg frequency for wide range of coupling coefficients.

REFERENCES

1. Sakai, K., E. Miyai, and S. Noda, "Two-dimensional coupled wave theory for square-lattice photonic-crystal lasers with TM-polarization," *Opt. Express*, Vol. 15, No. 7, 3981–3990, 2007.
2. Sakai, K., J. Yue, and S. Noda, "Coupled-wave model for triangular-lattice photonic crystal with transverse electric polarization," *Opt. Express*, Vol. 16, No. 9, 6033–6040, 2008.
3. Sakai, K., E. Miyai, and S. Noda, "Coupled-wave theory for square-lattice photonic crystal lasers with TE polarization," *IEEE Journal of Quantum Electronics*, Vol. 46, No. 5, 788–795, 2010.
4. Koba, M. and P. Szczepanski, "Nonlinear operation of a 2D triangular lattice photonic crystal laser," *IEEE Journal of Quantum Electronics*, in press.

Transfer Matrix Method for Threshold Analysis of One-dimensional Photonic Crystal Defect Mode Raman Laser

T. Osuch[1], **M. Koba**[1, 2], **P. Szczepański**[1, 2], **and T. Kossek**[1]

[1]National Institute of Telecommunications, Szachowa 1, Warsaw 04-894, Poland
[2]Warsaw University of Technology, Koszykowa 75, Warsaw 00-662, Poland

Abstract— The transfer matrix in its classical form with size of 2×2 is usually used for description of light propagation in isotropic stratified media. However, in optics we often deal with a case of interaction of more than one wavelength with the matter.

In this communicate we present generalized transfer matrix approach for multi-wavelength case. By an appropriate notation of the refractive indices as a function of intensities of propagating wavelengths it is possible to analyze amplification and lasing in optically pumped system.

We also propose using multi-wavelength matrix method to determine the threshold operation conditions of the one-dimensional (1D) photonic crystal (PC) defect mode Raman laser. For isotropic active medium of the laser, transfer matrix has 4×4 elements, and interaction between Raman and pump signals are realized by dependence of refractive index of PC active layer on electromagnetic waves intensities.

When a nondepleted pump is assumed, the intensity of the pump is constant in the entire length of the photonic crystal structure and the 4×4 matrix is reduced to a standard 2×2 one (describing only Raman signal). In this case, one can derive the equation for threshold gain operation, which contains stratified medium parameters and complex coefficients of end-reflection mirrors of the laser.

As an example, the threshold operation of one-dimensional photonic crystal defect mode Raman laser was analyzed. In particular, the threshold gain and corresponding wavelength was examined as a function of photonic crystal and defect parameters as well as reflectivity of end-reflection mirrors. The simulations were based on real material parameters, i.e., Si/SiO_2 PC layers and complex reflectance of laser mirrors.

The results of numerical calculations show that by proper choice of geometric parameters of the active medium and complex reflection coefficients of the laser mirrors it is possible to obtain optimal threshold operation conditions (with minimum achievable threshold gain and wavelength of Raman signal in third telecommunications window region).

Development of a Double-clad Fiber Laser Simulator for the Design of Laser Cavities with Specific Applications

D. Mgharaz[1], **A. Boulezhar**[2], **and M. Brunel**[1]

[1]UMR 6614 CORIA CNRS, Université de Rouen, France
[2]Université Hassan II Ain Chock, Casablanca, Morocco

Abstract— In the last decade, double-clad (DC) fibers have shown their potentiality for the development of low cost, compact, high power fiber lasers. A wide range of operating regimes have been demonstrated from Continuous Wave operation to Q-switched, or mode-locked regimes. In the same time, much attention has been devoted to the development of numerical simulations which have proven their ability to describe quantitatively the behaviors observed experimentally. It is now possible to simulate precisely DC fiber laser cavities and to design specific cavities for specific applications. Of main interest is the development of Q-switched DC fiber lasers that are able to emit a pair of nanosecond pulses separated by more than 500 ns. The main application of such laser systems is the Particle Image Velocimetry (PIV) technique. PIV is commonly involved in flow measurements (fluid mechanics and turbulent flow characterizations, combustion. A second domain of application concerns the emission of long nanosecond pulses in such a way that their peak power remains relatively low while their energy is important. Scientific and industrial applications are coherent anti-Stokes Raman spectroscopy, emission spectroscopy of laser ablation, texturing and coloring surface in the domain of metal surface treatments.

We have developed a numerical simulator to design actively Q-switched Yb-doped Double Clad fiber lasers [1]. Based on our simulator, we can design specific fiber laser cavities for various applications: the first example that will be presented is a cavity able to emit a pair of sub-nanosecond pulses separated by more than 500 ns for Particle Imagery Velocimetry applications. The time delay between the pulses can be adjusted by proper choice of the length of an un-doped fiber inserted in the cavity. The second cavity designed allows to emit long 150 ns pulses exceeding a few millijoules per pulse. Applications concern in this case materials science and combustion. In both cases, the rise time of the Q-switch modulator is an essential parameter.

In a second part, we show that our simulator can be used to describe laser combining. High efficiency coherent combining of CW fiber lasers has been demonstrated in the last years. The combining method can be based on the use of a multi-arm resonator in an interferometric configuration. Michelson and Mach-Zehnder type resonators have been successfully used to reach nearly 100% combining efficiency with two fiber lasers. This concept, which is adapted to the use of double clad doped fibers, has brought some novel perspectives for scaling the output power of the CW monomode fiber lasers. In a similar way, the power rising of an actively Q-switched erbium-doped fiber laser by using two coupled cavities with amplifying fibers could be demonstrated. The pulse peak power obtained could be 1.7 higher than in the case of a unique laser. This concept brings some novel perspectives for scaling the output peak power of single mode Q-switched fiber lasers, where the number of industrial applications is particularly important. In this paper, we present the development of a numerical simulator that can predict precisely the output pulses emitted by a laser system composed of two coupled Q-switched fiber laser cavities.

REFERENCES

1. Mgharaz, D., N. Rouchdi, A. Boulezhar, and M. Brunel, *Optics and Lasers in Engineering*, 2010, to appear.

Maize Crop Yield Map Production and Update Using Remote Sensing

Jesus Soria-Ruiz[1] and Yolanda Fernandez-Ordonez[2]

[1]National Institute of Research for Forestry, Agriculture and Livestock (INIFAP), Mexico
[2]Colegio de Postgraduados, Montecillo, México

Abstract— Crop yield mapping is an important endeavor for agricultural policy making in Mexico where it is a main staple crop. In central Mexico, maize is cultivated under different technological regimes ranging from traditional rain water dependency and using native seeds up to irrigation and improved seeds regimes. Yield variation is in the range of 1.0 ton/ha to over 12.0 ton/ha under the different regimes. It is necessary to explain the increase in average state yield for this crop in the past 10 years in view of a notorious decline tendency in cultivated and harvested area. Precision farming is a system of advanced technologies and procedures which merge spatial mapping variables of the terrain and surrounding conditions with specific management actions for crops. PF requires the integration of several basic component systems such as global positioning system (GPS), data collection and processing devices based on remote sensing and geographical information management systems. Measurements provided by these systems are oriented towards assessing terrain characteristics and spatial variability and can help to locate the better areas to orient management actions to best practices. In order to determine maize cultivated areas in the State of Mexico, SPOT panchromatic and multispectral satellite images are processed on a yearly basis over the growth and development stages of the plants. From this crop yield is estimated within a geographic area and maps are produced depicting with color tones and annotations the expected yield ranges of different areas. The results are then subjected to post-harvest accuracy assessment to produce the maps that are distributed to government agencies, producer associations and research institutions. This is the essence of crop monitoring and evaluation towards PF policies, involving continuous acquisition, analysis and synthesis of crop yield data and their precise remotely sensed location and other terrain, climate and geographic characteristics. Remote sensing contributes to improved credibility of cultivated areas, yield and production volumes over traditional agricultural statistics gathering methods, which are based solely on field sampling and producer surveys. The map production and update described in this work is introducing advances in geo-science and associated technologies to crop monitoring. The six year study carried out over the period 2004–2010 has shown the economic and technological advantages over traditional methods. Other State governments in the country are interested in using remote sensing for maize and for other crops.

Session 3A1
Rogue Waves in Nature and Extreme Events

Rogue Waves in Superfluid ^{4}He

V. B. Efimov[1], **A. N. Ganshin**[2], **G. V. Kolmakov**[3], **P. V. E. McClintock**[4], **and L. P. Mezhov-Deglin**[1]

[1]Institute of Solid State Physics RAS, Chernogolovka, Moscow region, 142432, Russia
[2]Laboratory for Elementary-Particle Physics, Cornell University, Ithaca, NY 14853-5001, USA
[3]Department of Chemical and Petroleum Engineering, Pittsburgh University, Pittsburgh, PA 15261, USA
[4]Department of Physics, Lancaster University, Lancaster LA1 4YB, UK

Abstract— We discuss recent experiments on nonlinear wave interactions in superfluid ^{4}He leading to the observation [1] of rogue waves. The equivalent phenomenon on the ocean [2] involves waves that are rare, and much higher (and steeper) than all the other waves around them. For obvious reasons, they are a menace to shipping. There have been several suggestions about possible mechanisms for the creation of rogue waves. These include the combined effects of wind and currents, and the focusing effects associated with the profile of the ocean floor and nearby shorelines. Where rogue waves appear in deep water far from any shore, which they sometimes do, it seems likely that they must evolve through nonlinear interactions within the "noisy background" of smaller wind-blown waves [3]. Rogue waves have been sought experimentally and/or studied in, e.g., large wave tanks, optical systems, and superfluid ^{4}He.

In the present experiments, we investigate high-intensity second sound (temperature-entropy) waves within a resonant cavity filled with superfluid ^{4}He at 2.1 K. Under steady state conditions, with a constant oscillatory driving force at the resonant frequency, the second sound waves are turbulent and fluxes of energy flow towards both high and low frequencies [4]. It is found [1] that rogue waves appear under the nonequilibrium conditions that prevail shortly after the drive has been switched on, prior to establishment of the steady state. These observations are consistent withe the ideas of Dyachenko and Zakharov [3]. We conclude that second sound in superfluid ^{4}He constitutes a convenient laboratory scale experimental system for studies of rogue waves. Our experimental observations and numerical simulation show that it is the nonlinear wave interaction that are responsible for generation of the direct and inverse energy cascades in the turbulent wave system. Rogue waves are created in profusion during the transient process towards the state where the inverse cascade exists in steady state. We suggest that the underlying mechanism for the development of the rogue waves in superfluid helium, i.e., the decay instability of large-amplitude waves, is analogous to that responsible for the generation of rogue waves on the ocean surface.

REFERENCES

1. Efimov, V. B., A. N. Ganshin, G. V. Kolmakov, P. V. E. McClintock, and L. P. Mezhov-Deglin, *Eur. Phys. J. Special Topics*, Vol. 185, 181–193, 2010.
2. Kharif, C., E. Pelinovsky, and A. Slunyaev, *Rogue Waves in the Ocean*, Springer-Verlag, Berlin, 2009.
3. Dyachenko, A. I. and V. E. Zakharov, *JETP Lett.*, Vol. 81, 255, 2005.
4. Ganshin, A. N., V. B. Efimov, G. V. Kolmakov, L. P. Mezhov-Deglin, and P. V. E. McClintock, *Phys. Rev. Lett.*, Vol. 101, No. 6, 065303, 2008.

Emergence of Rogue Waves from Optical Wave Turbulence

K. Hammani, **B. Kibler**, **C. Michel**, **C. Finot**, **G. Millot**, **and A. Picozzi**
Laboratoire Interdisciplinaire Carnot de Bourgogne, UMR 5209 CNRS, Université de Bourgogne
9 Avenue Alain Savary, Dijon 21078, France

Abstract— The understanding of the mechanisms underlying the process of rogue wave generation in the context of nonlinear optics is a subject of growing interest. The recent studies have confirmed the major role of the interplay between linear and nonlinear effects in the formation of L-shaped distributions of the optical intensities, such as, e.g., the convective effect due to third order dispersion, the modulation instability, or the collision of solitons or breathers structures. These previous works have been focused on the study of two well-known classes of solutions of the nonlinear Schrödinger equation: (i) soliton or quasi-soliton solutions, (ii) the Peregrine solution and its generalizations, namely the Akhmediev breathers solutions. It turns out that, under certain conditions, the collision of (quasi-) solitons or the collision of Akhmediev breathers, have been recognized as the essential mechanisms responsible for the generation of optical rogue waves. Here we provide some general physical insights into the emergence of rogue wave events from optical turbulence by analyzing the long term evolution of the field. Depending on the amount of incoherence in the system, we identify three turbulent regimes that lead to the emergence of specific rogue wave events: (i) persistent and coherent rogue quasi-solitons, (ii) intermittent-like rogue quasi-solitons that appear and disappear erratically, and (iii) sporadic rogue waves events that emerge from turbulent fluctuations as bursts of light or intense flashes.

This last regime (iii) refers to the genuine turbulent regime, which can be described in detail by the wave turbulence theory. This kinetic approach provides an analytical description of the evolution of the wave spectrum, which has been found in quantitative agreement with the numerical simulations, without using adjustable parameters. Recent numerical investigations reveal that the sporadic rogue wave events identified in the turbulent regime (iii) exhibit properties reminiscent of Peregrine solitons and high-orders Akhmediev breathers.

Rogue Waves in a Multistable Fiber Laser

Alexander N. Pisarchik[1] and Majid Taki[2]

[1]Centro de Investigaciones en Optica
Loma del Bosque 115, Lomas del Campestre, Leon 37150, Gto., Mexico
[2]Université des Sciences et Technologies de Lille
CNRS UMR 8523, UFR de Physique, Bâtiment P5, 59655 Villeneuve d'Ascq Cedex, France

Abstract— Multistability or the coexistence of multiple attractors is a widespread phenomenon in real dynamical systems. Moderate strong noise in such systems destabilizes the coexisting states and converts the multistable system into a metastable one. This leads to a competition between different attracting states resulting in irregular jumps among different periodic or chaotic regimes. This phenomenon known as attractor hopping was first experimentally observed in a diode-pumped erbium-doped fiber laser. When the pump laser current is subject to an external harmonic modulation, the laser exhibits the coexistence of as much as four periodic or chaotic attractors with different laser pulses intensities. Periodic regimes with lager periods and higher amplitudes are seldom observed and when they do, they last for only few modulation periods, the laser waveform is then perceived as a rogue wave. The probability that such event occurs is very low and decreases as the noise amplitude increases. It can be seen that at 90-kHz pump modulation the amplitude of the laser response in period-5 regime is 6–8 times higher than that in period-1 regime, while the average time between consecutive jumps for period 5 is about 1 min. Depending on the noise amplitude, the probability distribution of the laser peak intensity has a similar shape to that observed in the absolute quantum system without Raman effect and with zero third-order nonlinearity. This work demonstrates the similarity of the rogue wave produced by the laser stochastic dissipative system with the rogue wave in the stochastic conservative system modeled by nonlinear Schrödinger equations.

From Supercontinuum to Optical Rogue Waves and Localized Structures

Goëry Genty[1], **Miro Erkintalo**[1], **and John M. Dudley**[2]

[1]Optics Laboratory, Tampere University of Technology, P. O. Box 692, FI-33101, Finland
[2]CNRS, Institut FEMTO-ST, University of Franche-Comte, 16 Route de Gray 25000, France

Abstract— A central challenge in understanding extreme events in science is to develop rigorous models linking the complex (often nonlinear) generation dynamics and the associated statistical behavior. Quantitative studies of extreme phenomena, however, can be frequently hampered in two ways: (i) the scarcity of the events under study and (ii) the fact that such events often appear in environments where measurements are difficult. A case of interest concerns the infamous oceanic rogue waves associated with many catastrophic maritime disasters. Studying rogue waves under controlled conditions is problematic, and the phenomenon remains a subject of intensive research. On the other hand, there are many qualitative and quantitative links between wave propagation in optics and in hydrodynamics, and it is thus natural to consider how insights from studying instability phenomena in optics can be applied to other systems.

Significant recent experiments on the shot-to-shot instabilities in the extreme nonlinear optical spectral broadening process of supercontinuum generation have shown that these fluctuations contain a small number of statistically-rare "rogue" events associated with a greatly enhanced spectral bandwidth and the generation of localized temporal solitons with greatly increased intensity. Crucially, because these experiments were performed in a regime where modulation instability plays a key role in the dynamics, an analogy was drawn with hydrodynamic rogue waves, whose origin and dynamics has also been discussed in terms of modulation or, as it often referred to in hydrodynamics, the Benjamin-Feir instability. The analogy between the appearance of localized structures in optics and the rogue waves on the ocean's surface is both intriguing and attractive, as it opens up possibilities to explore the extreme value dynamics in a convenient benchtop optical environment. In addition to the proposed links with solitons, other recent studies motivated from an optical context have experimentally demonstrated inks with nonlinear breather propagation.

The purpose of this paper is to review our recent work in the field of optical rogue wave physics and applications.

Granularity and Nonlocality Are the Joint Generators of Rogue Wave Phenomena

F. T. Arecchi[1, 2], U. Bortolozzo[3], A. Montina[4], and S. Residori[3]

[1]Dipartimento di Fisica, Università di Firenze, Italy
[2]CNR-INO, largo E. Fermi 6, Firenze 50125, Italy
[3]INLN, Université de Nice Sophia-Antipolis, CNRS, 1361 route des Lucioles, Valbonne 06560, France
[4]Perimeter Institute for Theoretical Physics, Waterloo, Ontario, N2L 2Y5, Canada

Abstract— Giant events may occur in systems characterized by the presence of many waves, with a frequency much higher than that expected for a random dynamics. Thus far, the origin of the phenomenon, called "rogue waves", has not been completely characterized. Here, we identify the two key ingredients for the appearance of giant waves, namely, granularity, that is, fragmentation of the wave pattern into a large number of clusters of minimal size, and nonlocality, that is, coupling of distinct clusters. We present experimental evidence for these claims, based on a nonlinear optical cavity as well as on linear light propagation in an optical fiber.

In the first case, the experiment consists of a nonlinear optical cavity, formed by a ring oscillator with a liquid crystal photo refractive layer acting as the gain medium. Photons are injected in the cavity through a two-wave-mixing process, pumped by a laser. While for low pump intensity the amplitude of the cavity field follows a Gaussian statistics, for high pump we observe large deviations from Gaussianity, corresponding to the emission of extreme waves. Rogue waves on the transverse profile of the optical beam develop erratically in time and in space. The observations are confirmed by numerical simulation and fitted by a stretched exponential for the PDF of the light intensity. The generation of rogue waves requires furthermore a nonlocality or symmetry breaking, provided by the geometry of the cavity. It consists of a transverse shift of the return light after one cavity round trip. A crucial parameter is the nonlocality size, measured in units od the fundamental grain size, that in our case is the tranverse beam size limited by the nonlinear dynamics to the value $\sqrt{\lambda L}$ (λ being the light wavelength and L the mirror size). A relevant question is: what are the duration of an extreme event and the time separation for two successive extreme events occurring on the same grain? The duration is given by the relaxation time τ of the photorefractive excitations, while the time separation has a log-Poisson statistics.

In conclusion,the two key elements for rogue waves are granularity and some nonlocality of the dynamics, the resulting evidences are a stretched exponential distribution of intensities and a log-Poisson distribution of time occurrences.

The key elements do not necessarily imply a nonlinear dynamics,as hypothesized so far in theoretical approaches to rogue waves.Indeed we have performed a linear experiment whereby we feed a linear optical fiber with light focused on the fiber entrance by a large numerical aperture lens.The grain size is due to the diffraction limit of the input beam,the nonlocality is provided by an asymmetric mask immediately behind the focusing lens, and the limited duration time τ is provided by a time dependent mechanical perturbation applied to the fiber.We again obtain a stretched intensity statistics and a log-Poisson time statistics.The amount of stretching, that measures the deviation from an exponential speckle statistics, is here provided by the geometry of the asymmetric mask.

We compare our linear experiment with a recent one performed in the microwave domain, and explain all reported cases in terms of our key elements.

Energy Concentration in Arrays of Nonlinear Waveguides by Exciting Rogue Waves

Yuliy V. Bludov[1], **Vladimir V. Konotop**[2, 3], **and Nail Akhmediev**[4]

[1]Centro de Fisica, Universiade do Minho, Campus de Gualtar, Braga 4710-057, Portugal
[2]Centro de Fisica Teorica e Computacional, Universidade de Lisboa
Complexo Interdisciplinar, Avenida Professor Gama Pinto 2, Lisboa 1649-003, Portugal
[3]Departamento de Fisica, Faculdade de Ciencias, Universidade de Lisboa, Campo Grande
Edificio C8, Piso 6, Lisboa 1749-016, Portugal
[4]Optical Sciences Group, Research School of Physics and Engineering
Institute of Advanced Studies, The Australian National University
Canberra ACT 0200, Australia

Abstract— Rogue waves can be defined as strongly compressed wave packets with high energy content that appear on the otherwise chaotic average wave field. Although the term "rogue waves" comes from oceanography [1], they can be useful in optics [2], opening ways for generating powerful ultrashort pulses with high concentration of energy in the peaks. One of the main features of the rogue waves until now was their chaotic nature; their appearance in the open ocean is defined by the chaotic nature of the waves in general. Even in optics, their experimental observation is based on detection of random events [2], despite the fact that when we know rogue wave exact solution [3], laboratory conditions would allow us to make experiments more deterministically. Namely, we study theoretically an array of coupled nonlinear waveguides, described by the discrete nonlinear Schrodinger equation. Despite that it does not possess exact analytical solution in the form of rogue wave, in the low-amplitude limit smooth solutions can be approximated by the respective solutions of the continuous nonlinear Schrodinger equation [3]. Unlike the conventional ocean and optical rogue waves evolve in space, our solutions represent rogue waves "frozen" in time. As a result, if proper amplitude and phase distribution at input of the array is achieved and rogue wave is excited, despite the fact that the input energy has nearly homogeneous distribution over hundreds of waveguides, at the output plane of the structure practically all the energy concentrates into a single waveguide. Although this approximation is valid for small enough amplitudes only, the rogue wave can be excited in high amplitude case as well, creating special initial conditions. We determine (from numerical simulations) the required input profile of the electric field to achieve this. In this case the giant energy concentration at the output of the array is achieved when initial conditions are properly adjusted to the length of the system and to the number of waveguides.

REFERENCES

1. Muller, P., C. Garrett, and A. Osborne, *Oceanogr*, Vol. 18, 185, 2005.
2. Solli, D. R., C. Ropers, P. Koonath, and B. Jalali, *Nature*, Vol. 450, 1054, 2007.
3. Akhmediev, N., A. Ankiewicz, and M. Taki, *Phys. Lett. A*, Vol. 373, 675, 2009.

Rogue Waves in Crossing Seas

Miguel Onorato
Dipartimento di Fisica Generale, Università di Torino, Italy

Abstract— Nowadays there are a number of mechanisms that are recognized to be responsible for the formation of rogue waves in the ocean. The first mechanism is the classical linear superposition of waves; for random phases and narrow spectra it is straightforward to calculate the probability of occurrence of such large waves. It turns out that 1 wave out of 2980 is larger than 2 times the significant wave height or 8 times the standard deviation of the distribution of the wave amplitudes. In the absence of an ambient current, waves larger than 2 times the significant wave height can be the result of the Benjamin-Feir or modulational instability. Such instability is described, at the leading order, by the nonlinear Schroedinger equation assuming potential flow, weakly nonlinearity and quasi-monochromatic waves. In a random wave field, theoretical, numerical and experimental it has been demonstrated that the modulational instability is responsible for a substantial increase of the probability of occurrence of freak waves, provided the wave field is sufficiently steep and narrow banded, i.e., the spectral energy is concentrated over a restricted range of frequencies and directions.

In the present paper I consider a third mechanisms of formation of extreme waves that is related to the presence of two sea states propagating in different directions. The problem is discussed in terms of a system of two coupled Nonlinear Schroedinger equations. The asymptotic validity of such system is discussed. We show that for some specific angles between the two wave trains, the equations reduce to an integrable system. Besides studying the standard stability analysis, we also consider analytically the maximum amplification factor for an unstable plane wave solution. I find that angles between 20° and 30° are potentially the most probable for establishing a freak wave sea. I also show that theoretical expectations are consistent with numerical simulations of the Euler equations and experimental work performed in one of the large wave tank in Marintek (Norway).

Optical Rogue Waves: New Developments

M. Taki[1], **A. Mussot**[1], **A. Kudlinski**[1], **M. I. Kolobov**[1], **E. Louvergneaux**[1], **and N. Akhmediev**[2]

[1]Laboratoire PhLAM, UMR CNRS 8523, Université des Sciences et Technologies de Lille 1
59655 Villeneuve d'Ascq Cedex, France
[2]Optical Sciences Group, Research School of Physical Sciences and Engineering
The Australian National University, Canberra, Australia

Abstract— In the ocean, giant waves (also called killer waves, freak or rogue waves) are extremely rare and strong events. They are not well understood yet and the conditions which favour their emergence are unclear. Very recently, it was shown that the governing equations [1] as well as the statistical properties of an optical pulse propagating inside an optical fibre [2] mimic very well these gigantic surface waves in the ocean. Here we generate both *experimentally* and *numerically* optical rogue waves in a photonic crystal fiber (microstructured fiber) with continuous wave (CW) pumps. This is relevant for establishing an analogy with rogue waves in an open ocean. After recalling fundamental rogue waves [3] known as Akhmediev breathers that are solutions of pure nonlinear Schrödinger (NLS) equation, we analytically demonstrate that a *generalized* NLS equation, which governs the propagation of light in the fiber, exhibits *convective instability* [4]. The latter provides one of the main explanations of the optical rogue wave extreme sensitivity to noisy initial conditions at the linear stage of their formation. In the highly nonlinear regime, we provide the evidence that optical rogue waves result from soliton collisions leading to the rapid appearance/disappearance of a powerful optical pulse [5].

REFERENCES

1. Voronovich, V. V., V. I. Shrira, and G. Thomas, *J. Fluids Mech.*, Vol. 604, 263–296, 2008.
2. Solli, D. R., C. Ropers, P. Koonath, and B. Jalali, "Optical rogue waves," *Nature*, Vol. 450, 1054–1058, 2008.
3. Akhmediev, N., A. Ankiewicz, and M. Taki, "Waves that appear from nowhere and disappear without a trace," *Phys. Lett. A*, Vol. 373, 675, 2009.
4. Mussot, A., E. Louvergneaux, N. Akhmediev, F. Reynaud, L. Delage, and M. Taki, "Optical fiber systems are convectively unstable," *Phys. Rev. Lett.*, Vol. 101, 113904, 2008.
5. Mussot, A., A. Kudlinski, E. Louvergneaux, M. Kolobov, M. Douay, and M. Taki, "Observation of extreme temporal events in CW-pumped supercontinuum," *Optics Express*, Vol. 17, 17010, 2009.

Supercontinuum Seeding and Optical Rogue Waves

D. R. Solli[1,2], **B. Jalali**[1], **and C. Ropers**[2]

[1]Department of Electrical Engineering, University of California at Los Angeles, USA
[2]Courant Research Center Nano-Spectroscopy and X-Ray Imaging, University of Göttingen, Germany

Abstract— The generation of supercontinuum radiation in optical fiber has enabled numerous innovations in diverse areas in physics and biology. One of the main challenges in improving supercontinuum sources is the control and minimization of noise and fluctuations, which arise from the highly nonlinear nature of the process [1]. In optical fibre, especially large broadening factors between incident and outgoing optical spectra can be obtained, which in turn results in a particularly high sensitivity to input noise, e.g., in the form of non-gaussian pulse statistics and optical rogue waves [2]. In the long pulse regime with incident picosecond or nanosecond pulses, supercontinuum generation typically involves a number of processes, including (noise-sensitive) spontaneous modulation instability (MI), soliton fission and Raman scattering.

It was recently shown that seeding at the MI wavelength can greatly enhance and stabilize supercontinuum generation [3–5]. Here, we use the signal and idler waves of an optical parametric oscillator to observe both MI gain and MI-induced soliton fission in a highly nonlinear fiber (HNLF) [5]. A strongly chirped broadband seed pulse is temporally scanned across a narrowband pump pulse, and the output spectrum is recorded as a function of relative pump-seed delay (see Fig. 1). The data illustrate a transition between pure MI gain (at the spectral component of the seed overlapping with the pump) and supercontinuum generation induced by seeding in the center of the MI gain bandwidth. The achieved broadening scales about linearly with the pump power and exponentially with the seed power. RF characterization indicates a strong seed-induced noise suppression, and improved coherence properties are evident from persistent spectral fine structure.

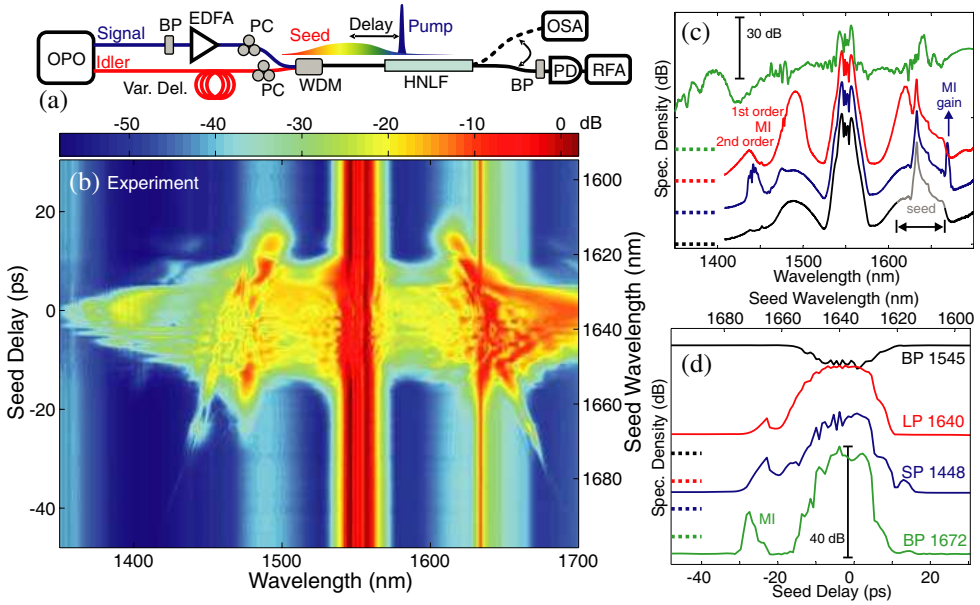

Figure 1: (a) Experimental setup. (b) Output spectral density from the HNLF as a function of seed time delay. (c) Spectral density vs. wavelength at seed delays of −48 ps (black), −26 ps (blue), −1 ps (green), and 12 ps (red). Curves offset by 15 dB, dashed lines label −60 dB levels. Seed spectrum (gray trace) is superimposed on noise-induced MI lobe taken at −48 ps delay (black trace). (d) Spectral density vs. seed delay at selected spectral regions: BP 1545 (bandpass, $\Delta\lambda \sim 3$ nm), LP 1640 (longpass), SP 1448 (shortpass), BP 1672 (bandpass, $\Delta\lambda \sim 1$ nm). (See Ref. [5] for more details.).

REFERENCES

1. Dudley, J. M., G. Genty, and S. Coen, "Supercontinuum generation in photonic crystal fiber," *Rev. Mod. Phys.*, Vol. 78, 1135–1184, 2006.

2. Solli, D. R., C. Ropers, P. Koonath, and B. Jalali, "Optical rogue waves," *Nature*, Vol. 450, 1054, 2007.
3. Solli, D. R., C. Ropers, and B. Jalali, "Active control of rogue waves for stimulated supercontinuum generation," *Phys. Rev. Lett.*, Vol. 101, 233902, 2008.
4. Moselund, P. M., M. H. Frosz, C. L. Thomsen, and O. Bang, "Back-seeding of higher order gain processes in picosecond supercontinuum generation," *Opt. Express*, Vol. 16, 11954, 2008.
5. Solli, D. R., B. Jalali, and C. Ropers, "Seeded supercontinuum generation with optical parametric down-conversion," *Phys. Rev. Lett.*, Vol. 105, 233902, 2010.

Session 3A2
Microwave and Millimeter Wave Circuits and Devices, CAD

Adaptive RF Power Amplifier Tuned with Ferroelectric BST Varactor

Yulan Zhang and T. S. Kalkur
Microelectronics Research Laboratories
Department of Electrical and Computer Engineering
University of Colorado at Colorado Springs
CO 80933-7150, USA

Abstract— Recent advancements in wireless communication systems necessitate improvements in system functionality and performance with reduced cost and size. Present communication systems use fixed band width amplifiers, antennas and filters which increases the need for large RF components. The development of tunable capacitors using ferroelectrics gives us the opportunity to develop tunable RF blacks. By changing the applied voltage to these capacitors the band width of the components can be changed significantly. In this paper, we will discuss the fabrication and characterization of ferroelectric thin film BST (Barium Strontium Titanate) capacitor for RF applications. BST capacitors operating in the paraelectric region offer a tenability above 50% within an applied voltage of ±5 Volts up to 10 GHz. We have measured the distortion in these tunable capacitors using parallel resonant circuit approach. We will also present the design and characterization of an adaptive matching network which is made of thin-film Barium-Strontium-Titanate ($Ba_{0.7}Sr_{0.3}TiO_3$ (BST)) for a class A RF amplifier. A gain of 14.479 dB has been achieved. The maximum output power load performance with both input and output matching networks of tunable amplifier is improved compared to fixed-impedance amplifier. Control bias variation of 4 V results in about 5.8 dB gain difference at 900 MHz. It provides the adaptation for frequency bands of 600, 700, 800 and 900 MHz and different power levels.

REFERENCES

1. Zhang, Y. and T. S. Kalkur, "Analysis of distortion in ferroelectric varactors," *Journal IEEE Transactions on Ultrasonics and Ferroelectrics*, Vol. 57, No. 6, 2010.
2. Boeck, G., D. Pienkowski, R. Circa, M. Otte, B. Heyne, P. Rykaczwski, R. Wittman, and R. Kakerow, "RF front end technology for reconfigurable mobile systems," *IEEE MTT-S International*, Vol. 2, 863, 2003.

Practical Use of the Kramers-Kronig Relation at Microwave Frequencies. Application to Photonic Like Lines and Left Handed Materials

J. Lucas[1], **E. Géron**[1], **T. Ditchi**[2], **and S. Holé**[2]

[1]Laboratoire d'Electricité Général, ESPCI-Paris Tech, France
[2]Laboratoire de Physique et d'Etude des Matériaux, UPMC Univ Paris 06, ESPCI-Paris Tech CNRS UMR8213, France

Abstract— As early as 1914 Arnold Sommerfeld published two papers in *Annalen der Physik* discussing the question of signal velocity in dispersive media. This work was at this time of pure academic interest. Nowadays photonic crystals, and left handed materials are common objects at microwave frequencies, and the questions raised by Arnold Sommerfeld, and addressed by Léon Brillouin in his famous book of 1960[1] are practically encountered in everyday physics at the laboratory. The famous well known second order differential equation known as the wave equation is indeed not satisfied in dispersive medium such as photonic crystals and left handed materials. Group velocities greater than the speed of light in vacuum and negative phase velocities are encountered respectively in photonic crystals and left handed materials. These phenomenons arise many questions especially insofar the theory of relativity is concerned and promise many applications. A. Sommerfeld stated the problem considering the propagation of a signal terminated on one side, and L. Brillouin carried out the calculus trying to find out a general signal velocity. The results that can be obtained using this methodology which is equivalent to considering the causality of a signal is more widely known particularly in optics through the Kramers-Kronig relation. This relation has many applications and allows to link for instance the imaginary part to the real part of the dielectrical constant of materials for instance. It is also often used to explain the so-called anomalous dispersion phenomenon of light encountered in some materials.

In this work, after a brief presentation of the implication of attenuation on the interpretation of the group velocity, we demonstrate the use of the Kramers-Kronig relation for instance to obtain the dispersion from an attenuation measurement at microwave frequencies in microstrip lines. The measurements obtained using a Vector Network Analyser are compared to those calculated from a single spectrum analyzer measurement on a photonic microwave crystal. We discuss at this point the different nature of the attenuation required by causality, and the one due to the losses in the media and how they interfere with each other. The method is also successfully applied to periodical structures presenting evanescent waves as well as to left handed materials. Finally we emphasize on the efficiency of the method to deal with causality and related pulse reshaping considerations in a far more efficient way than transient or pulsed measurements or considerations.

[1]Wave Propagation and group velocity, ACADEMIC PRESS INC.

Coaxial Quasi-elliptic Filter Using a Suspended Resonator and Vertically Stacked Coaxial Lines

Aline Jaimes-Vera[1], **Ignacio Llamas-Garro**[2], **and Alonso Corona-Chavez**[3]

[1]Signal Theory and Communications Department, Technical University of Catalonia
Barcelona 08034, Spain
[2]Centre Tecnologic de Telecomunicacions de Catalunya, CTTC
Barcelona 08860, Spain
[3]National Institute for Astrophysics, Optics and Electronics
Puebla 72840, México

Abstract— In this paper, pairs of air suspended coaxial resonators have been used to obtain electric, magnetic and mixed couplings to produce a four pole quasi-elliptic, narrowband filter at X-band. The filter is composed of two vertically stacked rectangular coaxial lines. One pair of resonators is placed on the lower coaxial line and another pair is located on the upper line, coupling between coaxial lines is achieved through an iris in the common coaxial ground plane. The resonator is suspended by short circuited stubs, and can be used to produce quasi-elliptic function or linear phase responses.

The proposed structure is smaller in size compared to conventional coaxial-combline cavity filters [1], which are commonly used for mobile communication applications. The unloaded quality factor of a single resonator was measured and has been found to fall in-between the high Q obtained through optimized conventional coaxial-combline cavities and interdigital or microstrip-combline filters. This structure avoids the use of coupling probes [2], and also avoids the use of extra cavities or small metal plates among the resonators to design quasi-elliptic filters [1, 3].

The filter has been designed with a center frequency of 9.1 GHz with a 4% fractional bandwidth and presents a transmission zero at each side of the pass-band. The device is made of nine planar copper layers which are machined, stacked and compressed together to form the two rectangular coaxial lines that form the quasi-elliptic filter. The planar implementation allows scaling the designs to the millimeter-wave frequency range, using micromachining [4]. Design methodology, simulated and measured results for the proposed device will be presented.

REFERENCES

1. Wang, Y. and M. Yu, "True inline cross-coupled coaxial cavity filters," *IEEE Transactions on Microwave Theory and Techniques*, Vol. 57, No. 12, 2958–2965, Dec. 2009.
2. Wang, C. and K. A. Zaki, "Full-wave modeling of electric coupling probes in comb-line resonators and filters," *IEEE Transactions on Microwave Theory and Techniques*, Vol. 48, No. 12, 2459–2464, Dec. 2000.
3. Cogollos, S., R. J. Cameron, R. R. Mansour, M. Yu, and V. E. Boria, "Synthesis and design procedure for high performance waveguide filters based on nonresonanting nodes," *IEEE MTT-S International Microwave Symposium Digest*, 1297–1300, Honololu, Jun. 2007.
4. Lancaster, M. J., J. Zhou, M. Ke, Y. Wang, and K. Jiang, "Design and high performance of a micromachined k-band rectangular coaxial cable," *IEEE Transactions on Microwave Theory and Techniques*, Vol. 55, No. 7, 1548–1553, Jul. 2007.

Asymmetric Microstrip Right/Left-handed Line Coupler with Variable Coupling Ratio

E. Géron[1], **T. Ditchi**[2], **J. Lucas**[1], **and S. Holé**[2]

[1]Laboratoire d'Electricité Général, ESPCI-ParisTech, France
[2]Laboratoire de Physique et d'Etude des Matériaux, UPMC Univ Paris 06, ESPCI-ParisTech
CNRS UMR 8213, 10, rue Vauquelin, Paris 75005, France

Abstract— Since the nineties, the feasibility of materials presenting simultaneously a negative permeability and permittivity are demonstrated in built up macro-structures named metamaterials. A negative phase velocity for the electromagnetic waves is observed in such structures. Consequently, the propagation vector, the electrical field vector and the magnetic field vector constitute an indirect trihedron. Thus such metamaterials are called Left Handed materials (LH) in opposition to the standard Right Handed propagation (RH). The singularity of this negative phase velocity has triggered a great interest and a lot of works have been carried out lately to develop these metamaterials in 1D, 2D and 3D structures. 1D structures such as hybrid transmission lines are potentiality relevant for microwave circuit applications. Symmetrical coupling structures using two LH coupled lines or asymmetrical structures using one LH line and one RH line coupled together are excellent candidates to develop new circuits for telecommunications such as coupler to be used in frequency synthesizers for instance. In a great number of applications both a large coupling bandwidth and a high coupling ratio are required. At high frequencies these electromagnetic couplers are often designed by closing up two RH lines. The frequency range of such couplers is limited since it is directly dependent on the length of the two lines in regard. In this case, the ratio between the coupled output and the transmit output can only be adjusted by the gap between the two lines. In some applications, a variable coupling ratio is necessary.

This work presents a microstrip coupler with a variable ratio. After some considerations on the LH line theory, the asymmetric RH/LH coupler is presented focusing on the parameters yielding the coupling ratio and the frequency range. This type of couplers exhibits a high coupling ratio though the gap between the two coupled lines is relatively large compared to the one of the classical RH couplers which makes it easier to build. Furthermore, the frequency range of this kind of couplers does not depend on its length. Both simulations and measurements of the coupling ratio versus the number of cells constituting the coupler are presented. From these results, we explain why such a structure is a good way to realize a coupler presenting a variable ratio. Finally the feasibility of electronically controlled ratio couplers presenting a large bandwidth is discussed.

A Directional Coupler Using Back-to-back Microstrip Lines and Common Defected Ground Window Structures

Jongsik Lim[1], **Jaehoon Lee**[1], **Jun Lee**[1], **Bokyun Kim**[1], **Yongchae Jeong**[2], **Sang-Min Han**[1], **and Dal Ahn**[1]

[1]Soonchunhyang University, Republic of Korea
[2]Chonbuk National University, Republic of Korea

Abstract— A new directional coupler structure using defected ground window structures between back-to-back microstrip lines is described in this paper. Directional couplers have been designed and fabricated conventionally with planar substrate structures such as microstrip line (Fig. 1) and striplines. Even though a few three-dimensional (3-D) directional couplers have been proposed previously as extremely exceptional cases, but the required costs are too expensive because semiconductor fabrication processes should be provided for fabrication. In order to overcome the cost problem and propose a new solution for 3-D directional couplers with cheap microstrip lines, the authors propose a directional coupler, which consists of back-to-back microstrip lines and a defected ground window structure on the common ground plane. The side view of Fig. 2 shows the structure of back-to-back microstrip lines with the common ground plane. If the line from port1 to port 2 is placed on the top plane, while the other one from port 3 to port 4 bottom plane, and if the long rectangular area called defected ground window structure (DGWS) is removed on the ground plane with a good alignment for the coupling section, a 3-D directional coupler is designed with cheap microstrip structure as shown in Fig. 3. It is noted that the coupling coefficient depends on not only the line width and dielectric media as general cases, but also the dimensions of DGWS strongly. Fig. 4 shows the S-parameters of the proposed directional coupler when the dielectric constant and thickness of the microstrip substrate are 2.2 and 31 mils, respectively. In Fig. 4, the coupling coefficient (S_{41}) in this case is 15 dB with an excellent isolation property (S_{31}). The advantages of the proposed coupler structures are; 1) reduced size 2) improved directivity than conventional design, 3) coupling coefficients are also controlled by the dimensions of DGWS, 4) more flexible design, 5) possibility for providing better density of integration because additional high frequency circuits can be realized on both sides of microstrip line, and so on.

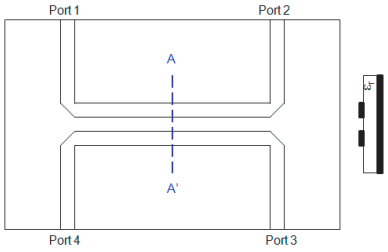

Figure 1.

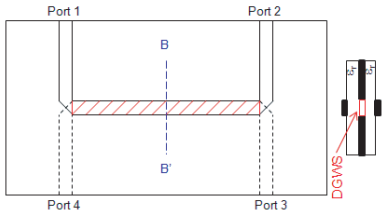

Figure 2.

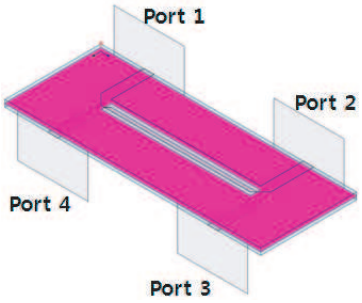

Figure 3.

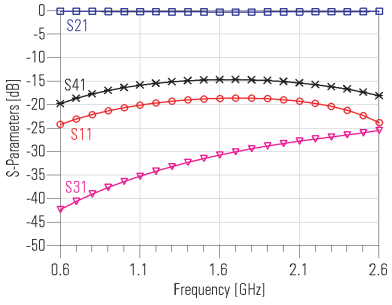

Figure 4.

ACKNOWLEDGMENT

This work was supported by the National Research Foundation of Korea Grant funded by the Korean Government (MEST) (KRF-2009-220-D00074).

Multi-mode Cavities for a High-gradient Two-beam Particle Accelerator Structure

Y. Jiang[1], **S. V. Kuzikov**[2, 3], **S. Yu. Kazakov**[2, 4], **and J. L. Hirshfield**[1, 2]

[1]Department of Physics, Yale University, New Haven, CT 06520, USA
[2]Omega-P, Inc., New Haven, CT 06510, USA
[3]Institute of Applied Physics, RAS, Nizhny Novgorod 603950, Russia
[4]Fermi National Accelerator Laboratory, Batavio, IL 60510, USA

Abstract— A novel class of microwave cavities is described that have eigenmode spectra that are harmonically related. A structure embodying a chain of such cavities could be the basis for a two-beam, high-gradient, particle accelerator [1]. Versions of the structure could be used for acceleration of beams of electrons, positrons, muons, protons, or heavier ions; with either electron or proton drive beams. Excitation of the cavities in several harmonically-related eigenmodes can be such that RF fields reach their peak values only during small portions of each basic RF period. This feature could help raise breakdown and pulse heating thresholds. In this configuration, no transfer elements are needed to couple RF energy from the drive beam to the accelerated beam, since both beams traverse the same cavities. Purposeful cavity de-tuning is used to provide much smaller deceleration for a high-current drive beam, than acceleration for a low-current accelerated beam, i.e., to provide a high transformer ratio. A self-consistent theory based on elementary circuit concepts is presented to calculate idealized acceleration gradient, transformer ratio, and efficiency for energy transfer from the drive beam to the accelerated beam, for either parallel or anti-parallel motion of the beams. The theory has been cast in dimensionless quantities so as to facilitate optimization with respect to efficiency, acceleration gradient, or transformer ratio; and to illuminate the interdependence of these parameters. Means for dramatically shortening the structure fill time for the cavities are also described.

ACKNOWLEDGMENT

Research sponsored by Office of High Energy Physics, US Department of Energy.

REFERENCES

1. Kazakov, S. Y., S. V. Kuzikov, Y. Jiang, and J. L. Hirshfield, *Phys. Rev. ST Accel. Beams*, Vol. 13, 071303, 2010.
2. Kuzikov, S. V., S. Y. Kazakov, Y. Jiang, and J. L. Hirshfield, *Phys. Rev. Lett.*, Vol. 104, 214801, 2010.

A Dual-band Wilkinson Power Divider Utilizing EBG Structure

Hsin-Hao Chen and Yi-Hsin Pang
Department of Electrical Engineering, National University of Kaohsiung, Taiwan, R.O.C.

Abstract— This paper presents a novel dual-band Wilkinson power divider which utilizes the electromagnetic band-gap (EBG) structure. The conventional Wilkinson power divider is composed of two transmission lines, each of which the characteristic impedance is $70.7\,\Omega$. A lump resistor of resistance $= 100\,\Omega$ is connected between the output ports for good isolation. In addition, the electrical length of each transmission line could be $\theta = n\pi/2,\ n = 1, 3, 5, \ldots$. The Wilkinson power divider inherently possesses the multiband characteristics. However, odd harmonics of the fundamental frequency are required. Utilizing the EBG structure, a lower operated frequency could be acquired. Fig. 1 shows the relationships between frequency and phase constant β for a microstrip line with and without the EBG structure, respectively. For the microstrip line with the EBG structure, a band-gap is presented and the phase constant β increases nonlinearly with frequency. At a lower frequency f_1, the electrical length of the microstrip line with the EBG structure is designed to be $\theta = \pi/2$. By adjusting the size of the EBG structure, the electrical length of the microstrip line would be $\theta = 3\pi/2$ at the desired second frequency f_2 which is less than $3f_1$ due to the rapid change of β near the band-gap. The required dual-band operation is then achieved. In this work, a dual-band Wilkinson power divider was designed and simulated using the full-wave simulator Agilent Momentum. The power divider has been fabricated on an FR4 printed circuit board (PCB) of thickness $h = 1.6\,\text{mm}$, relative permittivity $\varepsilon_r = 4.33$ and loss tangent $\tan\delta = 0.022$, and would be measured for verification.

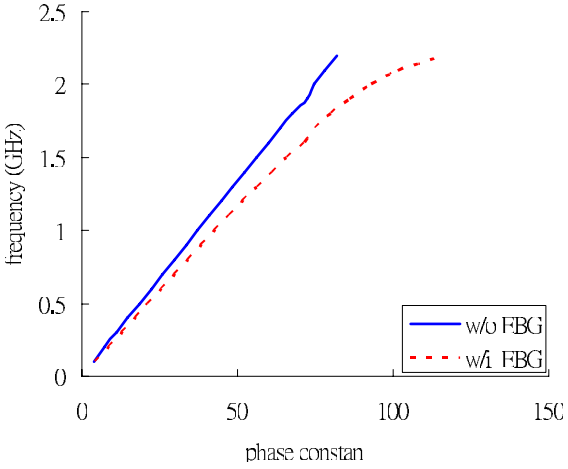

Figure 1: Dispersion diagrams of a microstrip line with and without the EBG structure, respectively.

Large Scale Measurement of Microwave Electric Field Using Infrared Thermography and Electromagnetic Simulation

D. Prost, **F. Issac**, **and P. Reulet**
ONERA — The French Aerospace Lab, 2 avenue E. Belin, Toulouse, France

Abstract— We present an original method for measuring the microwave electric field and achieving large scale field cartography. This is based on the use of a conductive and thermoemissive thin film of large dimensions, where induced currents due to incident field are responsible for ohmic losses and therefore create thermal heating. This heating is recorded by an infrared camera. The obtained thermal frame is obviously directly linked to the electromagnetic energy dissipated inside the film. This frame can be used qualitatively, for example to detect field leakage near electromagnetic junctions or to get antenna near field patterns, as it has been used for many years at French Aerospace Lab ONERA. To get a quantitative field evaluation, a calibration is necessary and needs a field sensor.

However, with the help of simulation we are able to get quantitative information, like field amplitude or even component values of the field, making the film become an electric field sensor. The simulation work addresses both electromagnetism, through EFIE computation of the electric field, and thermal finite elements simulation, to get the temperature frame on the film. The computed frame is compared to the recorded image and an iterative process is launched to get acceptable matching of the two temperature cartographies. The correct electric field is assumed to be the heating source whose thermal simulation gives compatible with measurement results, taking into account the perturbation on the field due to the film itself. Moreover, through the use of anisotropic films, components of the field can be obtained using the same method, providing a complete picture of the microwave incident field.

Numerical Study of a Coplanar Zeroth-order Resonator on YIG Thin Film

Aziza Zermane[1, 2, 3], **Bruno Sauviac**[1, 2], **Bernard Bayard**[1, 2], **and Abdelmadjid Benghalia**[3]

[1]Université de Saint-Etienne, F42023, France
[2]TELECOM Saint-Etienne, école associée de l'Institut TELECOM, DIOM
EA 3523, F-42023, 25 rue Dr. Rémy Annino, Saint-Etienne 42000, France
[3]Laboratoire LHS, Université Mentouri de Constantine
Route d'Ain EL Bey 25000 Constantine, Algérie

Abstract— The objective of this work is to study numerically the behaviour of a coplanar composite right-left handed zeroth order resonator (CRLH ZOR) realized on a YIG (Yttrium Iron Garnet) thin film. We are focusing on the effects on the resonant frequency when changing the magnetic bias and the thickness of the YIG. This study presents for the first time a tunable CRLH ZOR with a coplanar structure on YIG thin film. The length of the proposed design (device) is 5.2 mm, which is very small compared to a traditional half wave resonator. The proposed resonator is designed to be tuned over the 5–6 GHz frequency band; insertion loss is lower than 1 dB and return loss is better than 10 dB.

The concept of the Composite Right-Handed Transmission Line (line with traditional propagation) and Left-Handed Transmission Line (line having a negative phase velocity) was proposed by UCLA group [1]. Recently, ferrite materials have been used in metamaterials and in meta-line too. Tsutsumi and Abdalla proposed a nonreciprocal left-handed transmission line in microstrip and in coplanar waveguide configurations respectively over the ferrite substrate (thick layer) [2, 3].

Zeroth order resonator (ZOR) is one of the novel applications of LHMs (Left-handed materials). The interest lies in the fact that the resonant frequency is independent from the physical length of the resonator. Due to metamaterials properties, negative and zero resonances are possible. The zeroth-order CRLH resonance ($\ell/\lambda_g = 0$, $m = 0$) is particularly unique and interesting [4], since it has infinite guided wave-length at a specific frequency. The proposed resonator is realised in coplanar waveguide configuration constructed using an interdigital capacitor (IDC) and a short-circuited stub inductor (SSI).

Our objective is to prove that it is possible to make a tunable CRLH ZOR with a 15 µm ferrite film only. The ferrite substrate has a relative dielectric permittivity close to 15, a saturation magnetization equal to $M_s = 1780$ Gauss and a ferromagnetic resonance (FMR) line width $\Delta H = 20$ Oe. It is supposed to be saturated and the internal bias field is supposed to be uniform. In this work our magnetic layer is magnetized in a direction perpendicular to the propagation direction.

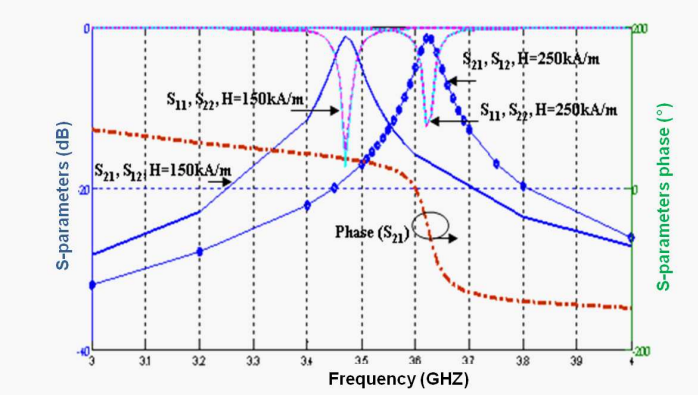

Figure 1: Example of Tuned response of the ZOR with ferrite.

REFERENCES

1. Caloz, C., A. Sanada, and T. Itoh, "Microwave circuits based on negative refraction index material structures," *33rd European Microwave Conference*, Munich 2003.

2. Tsutsumi, M. and T. Ueda, "Nonreciprocal left-handed microstrip lines using ferrite substrate," *IEEE MTT-S Int. Microwave Sym. Dig.*, Vol. 1, 249–252, 2004,
3. Abdalla, M. and Z. Hu, "A nonreciprocal left handed coplanar waveguide on ferrite substrate with only shunt inductive load," *Proceeding of Metamaterials*, October 2007.
4. Sanada, A., C. Caloz, and T. Itoh, "Novel zeroth-order resonance in composite right/left-handed transmission line resonators," *Asia Pacific Microwave Conference*, 2003.

Session 3A3
Electromagnetic Wave Propagation in Dissipative Media

Transfer Matrix Method for Electromagnetic Waves in 1D Inhomogeneous Media with Dissipation

G. V. Morozov[1], **F. Placido**[1], **and D. W. L. Sprung**[2]

[1]Thin Film Centre, University of the West of Scotland, Paisley PA1 2BE, Scotland, UK
[2]Department of Physics and Astronomy, McMaster University, Hamilton, Ontario L8S 4M1, Canada

Abstract— Electromagnetic wave propagation in one-dimensional (1D) inhomogeneous media with dissipation (including metal slabs) is studied analytically, using two different forms of the transfer matrix. A general case of oblique propagation is considered, i.e., both TE (s) and TM (p) waves are treated. The proper effective refractive indices and extinctions of dissipative media in case of oblique propagation are used. Propagation in a bilayer dielectric-metallic photonic crystal and in a rugate filter with low absorption are computed as examples.

Metallic Absorptivity at Normal Incidence above Far-infrared

F. E. M. Silveira
Centro de Ciências Naturais e Humanas, Universidade Federal do ABC, Santo André, Brazil

Abstract— The absorptivity of monochromatic radiation at normal incidence on metals is described by the Hagen-Rubens (H-R) relation, provided the wave energy is not higher than $\sim 100\,\mathrm{meV}$ (wavelength not shorter than $\sim 10\,\mu\mathrm{m}$), that is, it is restricted to the far-infrared and downwards. The H-R relation is a consequence of Maxwell's equations together with Ohm's law. This work proposes an extension of the H-R relation above the far-infrared by taking into account inertial effects due to charge carriers. The influence of inertia is described by introducing a relaxation time for the current density in the framework of a generalized Ohm's law. In the extended approach, it is found that the unique characteristic length scale of the problem, the penetration depth of the wave into the conductor, splits in two such that two distinct regimes for the skin effect can be identified: at low frequencies, the fields exhibit the usual attenuated oscillations; at high frequencies, they become purely attenuated in space. A transition frequency between the regimes is also identified. It is shown as well that the relaxation time can be fully determined from the metallic permittivity and angular frequency. The extended formulation is applied to aluminum and it is found that its relaxation time $\sim 6.91\,\mathrm{fs}$ at room temperature. It is also shown that the absorptivity by aluminum is in excellent agreement with the extended theory up to the near-infrared ($\sim 200\,\mathrm{meV}$).

REFERENCES

1. Silveira, F. E. M. and J. A. S. Lima, "Attenuation and damping of electromagnetic fields: Influence of inertia and displacement current," *J. Phys. A: Math. Theor.*, Vol. 42, 095402, 2009.
2. Silveira, F. E. M. and J. A. S. Lima, "Skin effect from extended irreversible thermodynamics perspective," *Journal of Electromagnetic Waves and Applications*, Vol. 24, No. 2–3, 151–160, 2010.
3. Silveira, F. E. M. and S. M. Kurcbart, "Hagen-rubens relation beyond far-infrared region," *EPL*, Vol. 90, 44004, 2010.

Enhanced SBS Instability Growth Rate of Extraordinary Electromagnetic Waves in Strongly Coupled, Magnetized Plasma

M. S. Bawa'aneh[1, 2], **Ibrahim Y. Abualhaol**[1], **and Feras Al-Dweri**[2]

[1]Khalifa University of Science, Technology and Research, Sharjah, P. O. Box 573, United Arab Emirates
[2]Department of Physics, The Hashemite University, Zarqa, Jordan

Abstract— Stimulated Brillouin Backscattering (SBBS) of a large amplitude, extraordinary electromagnetic wave travelling across an ambient *dc*-magnetic field in a strongly coupled plasma is investigated. In this study, we consider a static magnetic field perpendicular to the direction of the electrostatic density fluctuation and to the direction of polarization of the incident laser field. For the geometry where electrostatic fluctuations are along the x-axis, the incident laser beam polarized along the y-direction and the static *dc*-magnetic field along the z-direction, perpendicular to both the pump field and the direction of propagation, both longitudinal and transverse components of the electron perturbation velocity take high and low frequency components; High frequency components are due to the highly oscillating electric field of the electromagnetic wave and low components are due to electrostatic fluctuations and to the low frequency gyration of electrons in the plane perpendicular to the *dc*-field [1].

Using a magnetohydrodynamic model, a system of coupled equations that describes the problem is derived [2]. This system of equations is then solved for a strongly coupled regime to obtain a modified expression for the maximum growth rate in magnetized plasmas, where the maximum growth rate is found to be the solution of a cubic equation. In the absence of the magnetic feld, both the system of coupled equations and the modifed expression for the maximum growth rate reduce to the corresponding expressions known in the literature for Stimulated Brillouin Backscattering in non-magnetized plasmas [3].

The numerical solution of the cubic equation shows a real solution and two complex conjugates. For the unstable mode, the static magnetic field is found to increase the instability growth rate. Ignoring the magnetic field, the instability growth rate values, again, reduce to a value that is consistent with the result known in literature for non magnetized plasma.

REFERENCES

1. Bawa'aneh, M. S., *Contrib. Plasma Phys.*, Vol. 43, No. 7, 447–455, 2003.
2. Bawa'aneh, M. S., et. al., *IEEE Transactions on Plasma Science*, Vol. 38, No. 5, 1066–1072, 2010.
3. Kruer, W. L., *The Physics of Laser Plasma Interactions*, Westview Press, 2003.

Thin Films and Multilayers Grown on Insulating Bulk Substrates as Nanoelectromecanical Resonators

F. G. Aliev[1] and V. V. Pryadun[2]

[1]Departamento de Fisica de la Materia Condensada, C-III
Universidad Autonoma de Madrid, Madrid 28049, Spain
[2]Low Temperature Physics Laboratory, Faculty of Physics
Moscow State University, Moscow 11899, Russia

Abstract— Dynamic properties of thin films and multilayers have been recently subject of intensive investigation. The high density alternating current (*ac*) flowing through a conducting film situated in a *dc* magnetic field creates the longitudinal voltage drop. In addition, electromotive resonances excited by a time dependent Lorentz force might be observed. These resonances down to kHz frequencies could be either due to time dependent current re-distribution in semiconducting films or mechanical vibrations in suspended films. Here we report on unexpected resonant response in $[Fe/Cr]_{10}$ multilayers (MLs) epitaxially grown on MgO(100) substrates and in thin Nb films grown by sputtering on Si(100) substrates [1]. This response exists only when both *ac* current and *dc* magnetic field are simultaneously applied and electromotive response is measured in 5-probe or Hall geometries [1]. We demonstrate that the magnitude of the resonances is determined by the multilayer magnetization proving their intrinsic character. For Fe/Cr multilayers it is found that the reduction of interface epitaxy leads to non-linear dependence of the magnitude of resonances on the alternating current density. We suggest that the existence of the interface transition zone could facilitate the subatomic vibrations in thin metallic films and multilayers grown on bulk insulating substrates. Although this possibility is supported by simple estimations [1], exact physical mechanism behind still remains to be fully clarified.

REFERENCES

1. Aliev, F. G., V. V. Pryadun, and E. Snoeck, *Phys. Rev. Lett.*, Vol. 102, 035503, 2009.

Strange Solutions of Maxwell Equations: Loop Modes Induced by Thermal Tuning

D. Stuerga[1, 2], **C. Lohr**[2], **and P. Pribetich**[1]

[1]GERM (Groupe d'Etudes et de Recherches sur les Microondes)
LICB (Laboratoire Interdisciplinaire Carnot de Bourgogne)
UMR 5209 CNRS, Université de Bourgogne, France
[2]NAXAGORAS Technology SAS, France

Abstract— Study of high power industrial applicators implies full wave analysis of loaded device as waveguides and especially cylindrical waveguides. In case of lossy media, due to high level of dielectric losses, limits of classical perturbations approaches and modes established for lossless structures can be completely avoided.

The authors have made full-wave analysis of microwave applicator which was constituted by two coaxial rods. The central lossy rod is constituted by water and the other medium is air (lossless dielectric). The tuning due to thermal dependency of dielectric properties of water induces consequent change of the phase (β) and attenuation (α) constants of the propagation constant ($\gamma = \alpha + j$) within the temperature range 10°C–140°C at 2.45 GHz.

TE and TM modes have been studied and all these modes obtained have been classified according to four classes: the propagative ($\beta > \alpha \approx 0$), the quasi-propagative ($\beta \approx \alpha$), the attenuated ($\alpha > \beta$), and the evanescent ($\alpha > \beta \approx 0$). The authors have obtained original modes which exhibit loop within (α, β) complex plane. Despite the strong tuning due to thermal dependency of dielectric properties of water, the mode guided wavelength has variation close to few millimetres within the temperature range 10°C until 140°C. According to these results; predictive control and design of optimized travelling wave applicators could be obtained. According to authors, a viable alternative to the trial and error methods currently used for designing microwave applicator for industrial heating applications has been set up.

Loss Effects on the Surface Plasmon Resonance in Kretschmann Configuration

Atef Shalabney and I. Abdulhalim
Department of Electro-optic Engineering
The Ilse Katz Institute for Nanoscale Science and Technology
Ben-Gurion University of the Negev, Beer Sheva 84105, Israel

Abstract— Surface plasmon resonance (SPR) in Kretschmann configuration is usually observed using gold and silver metals because these metals are less lossy, hence providing sharp and well defined dip in the TM reflectivity. When the metal is absorptive such as aluminum or chromium, the SPR dip widens. The same happens when the metal is not a closed thin film, but rather has some pores in it so that scattering losses take place. Above a certain value of loss the dip become very wide and almost disappears leaving behind a peak near the onset to the total internal reflection (TIR) angle. Although the SPR dip widens, its minimum location sensitivity to the refractive index of an adjacent dielectric increases. To maintain the same detection limit the use of the TIR peak is proposed which is shown to give the same sensitivity. Experimental and theoretical results will be presented both for absorptive and porous metal films.

On the Electrodinamics of Counter Propagating Transverse-electric and Transverse-magnetic Waves in the Absorbing Plate in a Waveguide

E. A. Gevorkyan
Moscow State University of Economics, Statistics and Informatics
7 Nezhinskaya Str., Moscow 119501, Russia

Abstract— Propagation of two coherent counter propagating transverse-electric (TE) and transverse-magnetic (TM) electromagnetic waves in the absorbing plate placed in a waveguide of arbitrary cross section is considered. It is supposed that the electromagnetic waves of various initial phases incident on the plate from two sides. Fresnel formulas and analytical expressions for the power reflection, transmission and transmission interference coefficients are obtained. Some physical features of tunnel interference effect in the absorbing plate are discussed.

Dissipative Homogeneous Stationary Bianisotropic Medium, Time Dilation and Speed of Light in Vacuum Computation for Different Galilean Reference Systems

Namik Yener
Technical Education Faculty, Umuttepe Campus, Kocaeli University, Izmit, Kocaeli 41380, Turkey

Abstract— Having determined in a series of articles that the principle of constancy of speed of light in vacuum of the Special Relativity Theory is false because it cannot account for the loss in one of the two media which are in uniform rectilinear motion with respect to each other, in the present work we attempt to develop a procedure that will yield the speed of light in vacuum for the most general homogeneous and stationary media that constitutes the system K (medium (I)), and with respect to which a system K', a second system (medium (II)) assumed in this work to be a perfectly conducting medium, is in uniform rectilinear motion. The first medium is naturally a dissipative bianisotropic medium that is homogeneous and stationary. We assume in this work that the incident wave on the infinite plane boundary between media (I) and (II), makes an angle of $\theta = \pi/2$ with the direction of the velocity of K' with respect to K, which direction is perpendicular to the boundary interfacing the two media. This allows use of the time dilation formula in terms of frequencies and hence a simplification of the formulas, making the problem easier to analyze. After determining a general formula for c, the speed of light in vacuum for K, two examples are given in which the formula found is employed. First we consider a simple dissipative medium as medium (I) and as the second example we take up an electrically uniaxially anisotropic medium as medium (I). The second example is worked out for the high conductivity case. It is shown that the expressions found for c ensure a real and positive value in both cases.

Session 3A4
Electromagnetic Modeling and Imaging of Anisotropic Media

Tensorial Mathematic Formulation for the Generalization of Effective Dielectric Concept in Electromagnetism: Superlattices of Any Symmetry with One and Two Directions of Periodicity

B. Bêche[1, 2] and E. Gaviot[3]

[1]Institut de Physique de Rennes, IPR UMR CNRS 6251, Rennes 35042, France
[2]Institut Universitaire de France (IUF), 103 bd Saint-Michel, Paris 75005, France
[3]Laboratoire d'Acoustique, LAUM-UMR CNRS 6613, Le Mans 72000, France

Abstract— I introduce a new theoretical formulation based on a composition method and a statistical discretization approach by matrical block so as to shape analytical expressions of effective dielectric tensors of superlattices (SLs) in electromagnetism by considering anisotropic properties and boundary conditions. Such a general framework describing the effective dielectric tensors of idealized free-standing SLs possessing respectively one and two directions of periodicity (1D-SLs and 2D-SLs), composed of thin alternating layers and bars of any symmetry is derived, as a function of the dielectric tensors of each of the N and $(N \times M)$ constituents [1, 2]. For the case of 1D-SLs of any symmetry, it is possible to unify and to infer from such global formulation the particular relationships on effective dielectric tensors known as the 'Vegard rules' in solid state physics. Moreover, it is worth noting that in the simplified case of a 2D-SL made of only two different isotropic materials showing off the same periodicity in both directions, our general matrix formulation, due to the alternative composition laws, leads to the well-established results called, respectively, 'Wiener's and Lichtenecker's bounds' [3, 4] regarding the dielectric constants. This new formalism refashions the concept of bounds of effective dielectric tensors and the notion of form birefringence [6] applied to 1D- and 2D-SLs, with respectively relevant N multilayers and $(N \times M)$ rectangular anisotropic columns for arbitrary symmetries. The results are applied to SLs with layers of all classes of all symmetries (triclinic, monoclinic, orthorhombic, hexagonal, tetragonal, and cubic).

REFERENCES

1. Bêche, B. and E. Gaviot, "Effective electro-optic constants of free standing superlattices of any symmetry," *Phys. Rev. B*, Vol. 65, No. 3, 033303/1–4, 2002.
2. Bêche, B. and E. Gaviot, "A new formulation to shape the concept of bounds in effective dielectric tensors for two directions periodicity," *J. Phys. A: Math. General.*, Vol. 38, 10057–10067, 2005.
3. Lichtenecker, K., "Uber den widerstand gewisser zusammen-gesetzter köporlicher leiter," *Phys. Zeitschr.*, Vol. 19, 374–377, 1918.
4. Lichtenecker, K., "Der elektrische leitungswiderstand künstlicher and natürlicher aggregate," *Phys. Zeitschr.*, Vol. 25, 225–228, 1924.
5. Born, M. and E. Wolf, *Principles of Optics*, 6th Edition, Pergamon Press, Oxford, 1980.

Harmonic Imaging through Nonlinear Metamaterial Surfaces

Zhiyu Wang[1], **Yu Luo**[1,3], **Tao Jiang**[1], **Zheng Wang**[2], **Jiangtao Huangfu**[1], **and Lixin Ran**[1]

[1]Department of Information and Electronic Engineering, Zhejiang University, Hangzhou 310027, China
[2]Department of Physics, Massachusetts Institute of Technology, Cambridge, MA 02139, USA
[3]Department of Physics, Imperial College, London SW7 2AZ, UK

Abstract— In linear media, the spatial resolution of an EM imaging system has long been considered to be limited by the Rayleigh limit, approximately at one half of the wavelength. Recent studies in left-handed metamaterials and nonlinear microscopy have resulted in several super-resolution schemes that promise sub-wavelength imaging. Using only linear media, artificial left-handed metamaterials have been proposed and experimentally verified to restore the evanescent waves that carry sub-wavelength spatial information in near-field and far-field configurations. Nevertheless linear metamaterials are intrinsically lossy and higher spatial resolution often comes at the price of much reduced signal-to-noise ratio. To apply such subwavelength imaging schemes by nonlinear media, one can conceivably extend the concept of metamaterials to synthesize artificial nonlinearities from active circuit elements. Indeed, enhanced electromagnetic nonlinearities from microwave metamaterials have been proposed by Pendry et al. and have been realized.

In this paper, we experimentally demonstrate a microwave far-field imaging modality with the transverse resolution exceeding the diffraction limit through the use of a single layer of highly nonlinear metamaterial. We show that metamaterial included with active elements can easily behave strong nonlinearity under weak incident EM powers. Microwave diodes are used as the active elements in each unit cell and a direct current (DC) source is used to bias the diodes, choosing a strongly nonlinear region of the volt-ampere characteristic curve of the diodes to obtain a strong nonlinearity. By covering such a thin flat nonlinear metamaterial on the sources, the harmonic fields of the nonlinear metamaterial surface allow the far-field propagation of wavefronts with spatial frequencies several times higher than that of the fundamental field. Near-field images can therefore be recovered by measuring the far-field radiation of the sources at the harmonic frequencies and calculating the corresponding inverse Fourier transformation (IFT). The application of the nonlinear sample proposed in this paper would have important potential in improving the sub-wavelength resolution in the near future.

Generation of Waves by a Neutron Beam in a Quantum Plasma of Nonzero Spin. An Influence of the Spin-orbit Interaction

P. A. Andreev[1] and L. S. Kuz'menkov[2]

[1]Department of General Physics, Physics Faculty, Moscow State University, Russian Federation
[2]Department of Theoretical Physics, Physics Faculty, Moscow State University, Russian Federation

Abstract— In the present paper we model the electromagnetic process in a plasma placed in an external magnetic field. This plasma is an anisotropic medium with strongly expressed electromagnetic properties. For the modeling of the electromagnetic quantum properties, we use the Schrödinger equation.

Based on a Hamiltonian of a charged particle system with an intrinsic magnetic moment in an external electromagnetic field quantum, hydrodynamic equations are derived. The Coulomb, spin-spin, spin-current and spin-orbit in the Hamiltonian are included. The equations for number of particles, momentum and magnetic moment are obtained. The self-consistent field approximations of these equations are considered.

Based on the quantum hydrodynamic equations the process of generation of waves by a neutron beam in a dense quantum plasma of nonzero spin is considered. Existence of new wave solutions of the quantum hydrodynamic equations is shown (with respect to our previous works as described in [1, 2]). One type of such waves propagates perpendicularly to the direction of the external magnetic field. Another type is the spin waves which propagate at arbitrary angle with respect to the direction of the external magnetic field. Dispersion relations for waves in a medium traversed by a beam of neutrons whose velocity has a nonzero constant component are derived. Extreme cases of waves propagation parallel or transverse to the direction of the external magnetic field are considered. Generation of plasma, electromagnetic and self-consistent spin waves is investigated. The analytic formulas for the increments of instability are obtained. The contributions of spin-orbit interaction in the process of generation waves are investigated. The spin-spin, spin-current and spin-orbit interactions are the physical mechanism of instabilities in two-component quantum plasma traversed by a beam of neutrons.

The collective dynamic of the magnetic moment of particles and methods of generation of this process can influence the properties of spintronic devices.

REFERENCES

1. Andreev, P. A. and L. S. Kuz'menkov, "Eigenwaves in a two-component system of particles with nonzero magnetic moments," *Moscow University Physics Bulletin*, Vol. 62, No. 5, 271, 2007.
2. *Physics of Atomic Nuclei*, Vol. 71, No. 10, 1724–1729, 2008.

Reconstruction of Complex Anisotropic Scatterers Using Subspace Based Optimization Method

Krishna Agarwal and Xudong Chen
National University of Singapore, Singapore

Abstract— The current work applies subspace based optimization method for generic transverse electric (TE) inverse scattering problems involving two-dimensional complex anisotropic dielectric scatterers. Subspace-based Optimization Method (SOM) [1, 2] was proposed recently for two-dimensional scalar electromagnetic inverse problems. SOM utilizes information of physical import for optimization by splitting the induced currents into mathematically deterministic and ambiguous portions and using optimization for the ambiguous portion only. The deterministic portion provides a good initial guess for the optimization problem. Due to this, SOM is robust to noise and converges fast.

Reconstruction of complex anisotropic dielectric scatterers is mathematically and numerically more challenging than the reconstruction of isotropic scatterers, because there exist up to five

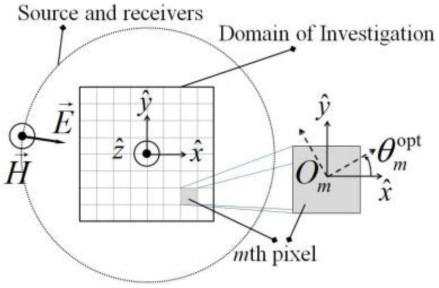

Figure 1: The experimental setup. The entire setup is invariant along the z axis. The sources and receivers are placed along a circular contour which is centered at the origin. The illumination is transverse electric, meaning that the magnetic fields are along the z axis and the electric fields are in the x-y plane. The domain of investigation is discretized into pixels. The optical axes for the mth pixel are characterized by the orientation angle θ_m^{opt}.

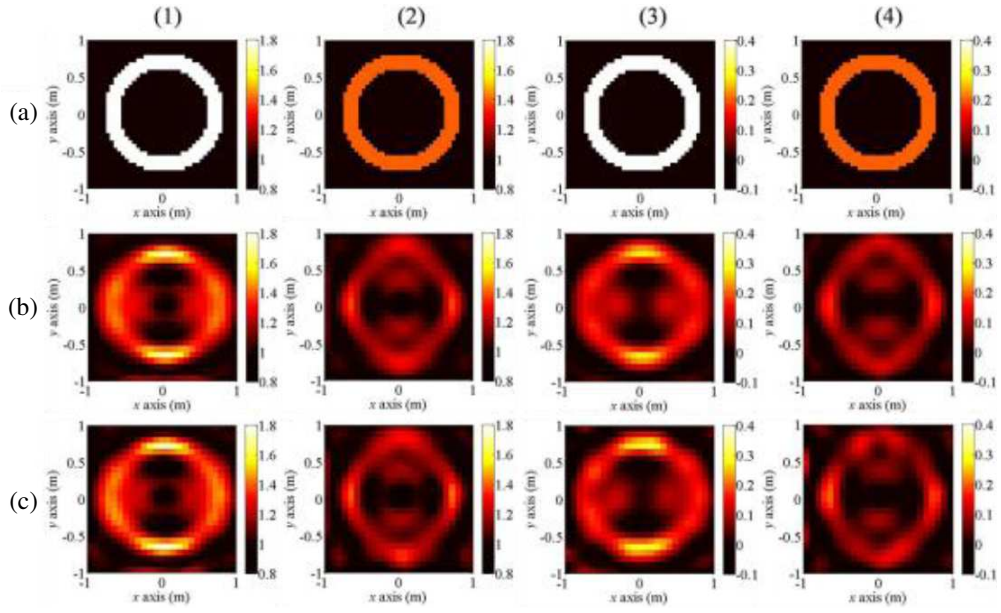

Figure 2: Annulus with complex anisotropic permittivity. Columns (1)–(4) show ε_m^{r1}, ε_m^{r2}, ε_m^{i1}, and ε_m^{i2} respectively where the relative permittivity of the scatterer is given by $\bar{\bar{\varepsilon}}_m^{\text{rel}} = \Xi^{-1}(\theta_m^{\text{opt}}) \cdot \text{diag}(\varepsilon_m^{r1} + i\varepsilon_m^{i1}, \varepsilon_m^{r2} + i\varepsilon_m^{i2}) \cdot \Xi(\theta_m^{\text{opt}})$. Rows: (a) Actual profile of the scatterer. (b) Reconstruction in the absence of noise after 20 iterations. (c) Reconstruction in the presence of 20 dB white Gaussian noise after 20 iterations.

unknowns at any given point in the region of interest. Further, the physics behind the scattering from anisotropic dielectric scatterers is significantly different from the scattering problem involving isotropic scatterers. Due to the anisotropy, the direction of the source induced at a point on an anisotropic scatterer is not necessarily in the same direction as the incident electric field (as opposed to the isotropic scatterers) and its direction depends upon the interaction of the electric field with the permittivity along the individual principal axes at that location. In this work, we present two major contributions:

1. Despite the complicated nature of the problem of reconstruction of two-dimensional complex anisotropic dielectric scatterers, the subspace-based optimization method has been applied successfully for reconstruction (Fig. 2). It is also shown that in the TE case, the computational complexity involved in the reconstruction of complex anisotropic dielectric scatterers using the subspace-based optimization method is not larger than the problem involving isotropic dielectric scatterers having only real permittivities.

2. We also discuss the nature of the induced currents in the anisotropic scatterers and the limitation they impose on the reconstruction. It is shown that the reconstructed profile of the anisotropic scatterers exhibit strong directionality (Fig. 2). This is explained by studying the distribution of currents on the scatterers due to various illumination directions (Fig. 1 and Fig. 3).

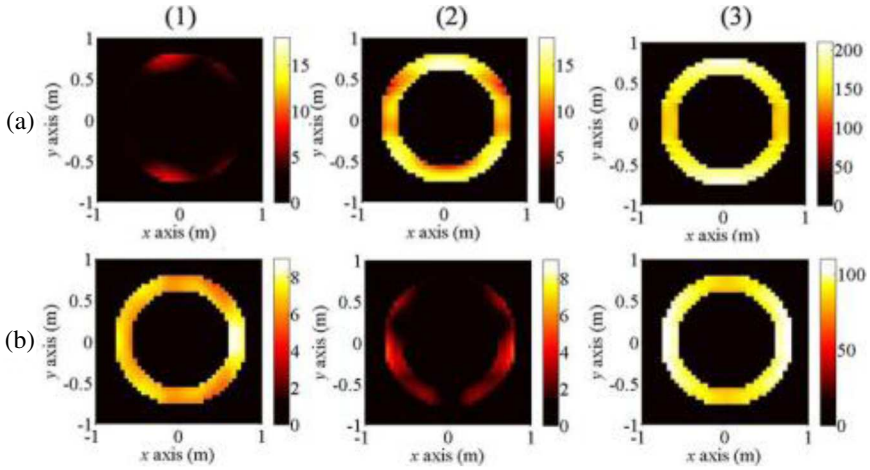

Figure 3: Example 1: Magnitudes of the induced currents along the optical axes. Columns (1)–(2) show the magnitude of induced currents for incidences from two source locations, $(2, 0)$ m and $(0, 2)$ m, respectively. The column (3) shows the sum of magnitudes of the current induced for all the incidences. Rows: (a) Magnitude of induced current along the x axis ($\times 10^{-6}$ A). (b) Magnitude of induced current along the y axis ($\times 10^{-6}$ A).

REFERENCES

1. Chen, X., "Application of signal-subspace and optimization methods in reconstructing extended scatterers," *Journal of the Optical Society of America A*, Vol. 26, 1022–1026, 2009.
2. Chen, X., "Subspace-based optimization method for solving inverse scattering problems," *IEEE Transactions on Geoscience and Remote Sensing*, Vol. 48, 42–49, 2010.

Joint Magnetotelluric and Controlled-source Electromagnetic Inversion Algorithm for Anisotropic Media

Aria Abubakar, **Maokun Li**, **Guangdong Pan**, **and Tarek M. Habashy**
Schlumberger-Doll Research, Cambridge, USA

Abstract— In offshore hydrocarbon (oil and gas) explorations, both the magnetotelluric (MT) method and the controlled-source electromagnetic (CSEM) method have been widely used. The MT method uses the electromagnetic fields due to natural sources that can be modeled by using plane waves. It has a relatively large depth of investigation and can be effectively used to obtain rough resistivity estimate of the Earth's subsurface and mainly sensitive to conductive objects. On the other hand, the CSEM method measures the field generated by a low-frequency electric dipole that is towed by a ship at several tens of meters above the seabed. The CSEM data are mainly sensitive to resistive objects, which makes it capable of providing useful information of the locations and shapes of hydrocarbon reservoirs. It is well known that MT and CSEM data provide complementary information: MT may provide information on the background conductivity structures, while CSEM may identify resistive targets (hydrocarbon reservoirs).

Constable and Weiss [1] also pointed out the practical importance of MT data: The same receivers can collect both CSEM and MT data; hence MT data come at a very low cost since they can be recovered from time series data when the CSEM source is turned off. Usually CSEM and MT data are separately inverted. In a joint interpretation workflow, MT data is first inverted and then the results are used as an initial model for the CSEM data inversion. Mackie et al. [2] showed the improvements that may be obtained by simultaneously inverting these two data sets. However, they also pointed out that in this joint inversion approach one has to carefully choose the relative weighting between MT and CSEM data. Abubakar et al. [3] proposed to use a multiplicative cost function for simultaneous inversion of MT and CSEM data. By using this cost function there is no need to choose the relative weighting between MT and CSEM data. This multiplicative cost function will effectively put equal weighting for both MT and CSEM data. The inversion scheme is based on a regularized Gauss-Newton inversion approach (Habashy and Abubakar [4]), a number of techniques have been used to make this solver robust and efficient (see Abubakar et al. [5]). In this presentation we will review the method of Abubakar et al. [3] and discuss its extension for inverting Transverse Isotropic (TI) anisotropic medium. In this TI-anisotropic medium we simultaneously invert horizontal and vertical resistivity distributions. We will show some inversion results using both synthetic and field data.

REFERENCES

1. Constable, S. and C. Weiss, "Mapping thin resistors and hydrocarbons with marine EM methods: Insights from 1D modeling," *Geophysics*, Vol. 71, No. 2, G43–G51, 2006.
2. Mackie, R., M. D. Watts, and W. Rodi, "Joint 3D inversion of marine CSEM and MT data," *SEG Technical Program Expanded Abstracts*, Vol. 26, 574–578, 2007.
3. Abubakar, A., M. Li, J. Liu, and T. M. Habashy, "Simultaneous joint inversion of MT and CSEM data using a multiplicative cost function," *SEG Technical Program Expanded Abstracts*, Vol. 28, 719–722, 2009.
4. Habashy, T. M. and A. Abubakar, "A general framework for constraint minimization for the inversion of electromagnetic measurements," *Progress In Electromagnetic Research*, Vol. 46, 265–312, 2004.
5. Abubakar, A., T. M. Habashy, V. Druskin, D. Alumbaugh, and L. Knizhnerman, "2.5D forward and inversion modeling for interpreting low-frequency electromagnetic measurements," *Geophysics*, Vol. 73, F165–F177, 2008.

Horn Antennas Loaded with Metamaterial for UWB Applications

M. Lashab[1], **H. I. Hraga**[2], **Read Abd-Alhameed**[2], **C. Zebiri**[1], **F. Benabdelaziz**[1], **and S. M. R. Jones**[2]

[1]Electronics Department, Skikda University, Algeria
[2]Mobile and Satellite Communication Research Centre, University of Bradford, Bradford, UK

Abstract— In this paper, a conical horn antenna has been designed for Ultra-Wideband applications by loading its section with a metamaterial. The work aims first to compare results obtained by the wavelet-moment method to a simulation performed using HFSS. Secondly the conical horn is loaded with a very thin layer of metamaterial to enhance the radiation pattern and the bandwidth performance of the conical horn antenna and reduce the size of the antenna. The operating bandwidth of the proposed antenna is in the range of 10–13 GHz. The results obtained from HFSS and moment method are in good agreement.

Introduction: Artificial materials such as metameterials and chiral have been, recently for great interest of study both theoretical [1, 2], and experimental [3, 4], the metamaterial for instance exhibit either negative permittivity or negative permeability, if both of them are negative at given frequency, the material is this case is characterised by an effective negative index of refraction, so often referred to a left handed metamaterial (LHMs), this type has interested many research work [5, 6]. The main objective attained in all these research work done on (LHMs) is the improvement of the radiation pattern, directivity, bandwidth and antenna size reduction.

Horn antennas loaded dielectrics or materials [7], are well known for having desirable properties such as increased directivity, reduced side lobe level, wide bandwidth, low loss, and ease of fabrication [8, 11]. These properties are particularly attractive for applications such as in ultra-wideband (UWB) ground penetrating radars (GPR) [12, 13]. However, the characterization of such antennas with increasingly complex designs using analytical techniques is often not possible. On the other hand, a numerical model can provide a virtual test bench to explore different design possibilities before any costly prototyping. Although many numerical techniques can be used to model and study the characteristics of such antennas, the moment method is well known to be very accurate method [14, 15], here in this paper an improvement has been made by the introduction of wavelets.

This paper is dealing with a comparison between improved moment method and Ansoft's HFSS in first step, then an observation of the effect of loaded horn antenna.

Anisotropy in Seemingly Isotropic Media

Henrik Kettunen, **Jiaran Qi**, **Henrik Wallén**, **and Ari Sihvola**
Department of Radio Science and Engineering
Aalto University School of Science and Technology, Finland

Abstract— Composites with sufficiently symmetric unit cells are inherently isotropic. This seemingly obvious property is, however, strictly true only for an infinite lattice of unit cells in the quasi-static limit. Unless the size of the unit cells remains extremely small compared with the wavelength, the effective material parameters of a finite-thickness composite slab may become surprisingly complicated.

In this presentation, we study the homogenization of a composite medium slab by computational methods. The considered slab consists of a periodical array of infinitely long circular cylinders embedded in vacuum. The slab is infinite in the transverse plane, but its thickness is measured in only a couple of layers of unit cells. The slab is illuminated by a plane wave with varying angle of incidence. The polarization of the **E** field is chosen perpendicular to the axes of the cylinders and the geometry is modeled in 2D using Comsol Multiphysics software, which is based on the finite element method (FEM).

The effective permittivity of the dielectric non-magnetic composite slab is retrieved based on a straightforward method of field averaging [1]. Due to the symmetry of the unit cells, the material could be assumed effectively isotropic. However, under oblique incidence, due to its finite thickness, the slab shows anisotropic behavior. Moreover, the field averaging technique allows us to study each unit cell separately. It is found that the cells on the outermost boundary layers have effective permittivity different from all other cells inside the slab. The boundary layers are clearly anisotropic, whereas the inner layers can be considered isotropic, which is theoretically predicted in [2]. The permittivity of the inner layers agrees with the bulk material predictions given by electrostatic mixing rules [3]. Also, the obtained permittivities of the individual boundary cells and inner cells do not depend on the slab thickness.

However, as mentioned, these observations apply only in the quasi-static limit where the unit cells are extremely small compared with the wavelength of the impinging field. Moreover, this comparison must be made with the effective wavelength of the composite, which is usually reduced from the free-space value. Increasing frequency, i.e., increasing electrical size of the unit cells, eventually causes spatial dispersion, which can further give rise to bianisotropic effects [4, 5]. In this region, more sophicticated homogenization procedures are required.

REFERENCES

1. Kettunen, H., J. Qi, H. Wallén, and A. Sihvola, "Homogenization of thin dielectric composite slabs: Techniques and limitations," submitted to *ACES Journal*.
2. Simovski, C. R., S. A. Tretyakov, A. H. Sihvola, and M. M. Popov, "On the surface effect in thin molecular or composite layers," *Eur. Phys. J. AP*, Vol. 9, 195–204, 2000.
3. Sihvola, A., *Electromagnetic Mixing Formulas and Applications*, IEE, London, 1999.
4. Serduykov, A., I. Semchenko, S. Tretyakov, and A. Sihvola, *Electromagnetics of Bi-anisotropic Materials: Theory and Applications*, Gordon and Breach Science Publ., Amsterdam, 2001.
5. Fietz, C. and G. Shvets, "Current-driven metamaterial homogenization," *Physica B*, Vol. 405, No. 14, 2930–2934, 2010.

Computation of Electromagnetic Transmission Eigenvalues Using Integral Equations and Far Field Data

Francis Collino[1], **Anne Cossonnière**[1], **MBarek Fares**[1], **and Houssem Haddar**[2]

[1]CERFACS, Toulouse, France
[2]INRIA, Saclay-Ile, France

Abstract— We consider the scattering of time-harmonic electromagnetic waves by an anisotropic medium D in $\mathbb{R}^3$. We propose a method to compute transmission eigenvalues using integral equations and finite elements method. This leads to an eigenvalue problem for a compact operator. Since the problem consists in finding "compact" operators with 0 as an eigenvalue, we will use a preconditioner in order to shift the accumulation point out of 0. To validate this method, we compare the results with values computed from far field data.

The study of transmission eigenvalues is closely linked to the study of the interior transmission problem which has been a subject of great interest in scattering theory for the past few years. This is due to the fact that transmission eigenvalues can give information on the properties of an obstacle, for instance on the index of refraction or if it contains a cavity or a crack. The interior transmission problem is defined by:

$$\operatorname{curl}\operatorname{curl}\mathbf{E} - k^2 N\mathbf{E} = 0 \text{ in } D \tag{1}$$

$$\operatorname{curl}\operatorname{curl}\mathbf{E}_0 - k^2\mathbf{E}_0 = 0 \text{ in } D \tag{2}$$

$$\nu\times\mathbf{E} - \nu\times\mathbf{E}_0 = 0 \text{ on } \partial D \tag{3}$$

$$\nu\times\operatorname{curl}\mathbf{E} - \nu\times\operatorname{curl}\mathbf{E}_0 = 0 \text{ on } \partial D \tag{4}$$

and transmission eigenvalues are values of k for which the interior transmission problem has a nontrivial solution. Although theoretical results about existence of transmission eigenvalues and the fact that they form a discrete set has been proven in many articles, a few papers consider the computation of transmission eigenvalues for general geometry and even less in electromagnetics.

The method we shall use here is based on the CESC code developped by the CERFACS which combines integral equations and finite elements. It first consists in expressing the solutions $(\mathbf{E}, \mathbf{E}_0)$ of the previous interior transmission problem with integral equations. Then the boundary conditions (3) and (4) lead to solve a system of the form $Z_k X = 0$ where $X = \begin{pmatrix} J \\ M \end{pmatrix}$ with $J = -\nu\times\operatorname{curl}\mathbf{E}$ and $M = \nu\times\mathbf{E}$. Transmission eigenvalues are values of k for which 0 is an engenvalue of Z_k. The main difficulty is that the operator Z_k is compact and therefore 0 is an accumulation point of its eigenvalues. As a consequence, the real eigenvalue 0 is "lost" numerically in the accumulation region. To get around this difficulty, we use a preconditioner B_k to shift the accumulation to 1 and we solve the generalized eigenvalue problem $Z_k X = \lambda B_k X$. We shall discuss proper choices of the operator B_k.

Another way to compute the transmission eigenvalues is to use far field data and the Linear Sampling Method. The Linear Sampling Method is based on solving an ill-posed far field equation using Tikhonov regularization. This method is usually used to determinate the shape of an obstacle. However, it can be shown that when k is a transmission eigenvalue for a sampling point $z \in D$ the norm of the regularized solution to the far field equation cannot be bounded as the parameter tends to zero. Thus this property provides us another method to find transmission eigenvalues as the location of the peaks on the plot of the regularized solution's norm against k. We shall numerically demonstrate the concordance of the results provided by both methods.

Transmission Eigenfrequencies for Dielectrics and Their Use in the Identification Problem

H. Haddar[1] and F. Cakoni[2]

[1]INRIA Saclay Ile de France and Ecole Polytechnique, France
[2]University of Delaware, USA

Abstract— We shall address in this talk recent progress in the analysis of so called transmission eigenfrequencies for dielectric (anisotropic) inclusions and their use in the identification problem, where one is interested in getting qualitative information on the inclusion physical parameters from measurements of electromagnetic scattered waves. We shall also outline possible applications in non-destructive testing of complex media, where no a priori knowledge on the structure of the media is available. Exploiting these special frequencies in the identification problem is a quite recent idea that seems promising and that also arises many numerical and theoretical questions that will be discussed in the talk.

The interior transmission problem is a new class of boundary value problems for elliptic equations which was first discussed by Colton, Kirsch and Monk in the mid nineteen eighties in connection with the inverse scattering problem for acoustic waves in an inhomogeneous medium. Since that time the interior transmission problem has come to play a basic role in inverse scattering for both acoustic and electromagnetic waves.

Although simply stated, this problem is not covered by the standard theory of elliptic partial differential equation, since as it stands, it is neither elliptic nor self-adjoint. Till recently, most of the known results on the interior transmission problem were concerned with well-posedness questions. Roughly speaking, two main approaches are available in this direction, namely integral equation and projection methods, and variational methods typically applied to a fourth order equivalent boundary value problem. Applications of those results are essentially linked with uniqueness and reconstruction of the support of the inhomogeneous inclusion from multi-static data at a fixed frequency. In particular they provide the basic ingredient in the theoretical justification of so-called Linear Sampling Method.

In that perspective, of particular interest is understanding of the spectrum associated with this boundary value problem, i.e., the set of eigenfrequencies, called transmission eigenvalues, for which uniqueness results fail. The occurrence of a transmission eigenvalue corresponds to the far field operator having non trivial kernel, or equivalently the scattering matrix having an eigenvalue equal to one. It is well known for instance that at those frequencies the Linear Sampling algorithm fails in reconstructing the shape of the inclusion.

More recently came the idea of exploiting the failure of sampling methods to locate these special frequencies from time-dependent multi-static data. These (being observable) values can then be practically used to obtain information about the index of refraction but also to inspect the presence of cavities inside the media. The latter qualitative information can be obtained from relating the eigenvalues to the material properties.

The talk will be dedicated to providing a survey of all these aspects of the use of transmission eigenfrequencies in inverse scattering theory. A special focus will be given on the recent theoretical result related to existence of transmission eigenvalues, their observability from far field measurements and their use in non-destructive testing of complex media.

Comprehensive Model of Charge Transport in Alumina Composites Containing Semiconductive Silicon Carbide Whiskers: Effects of Frequency, Temperature, Bias, Percolation, and Anisotropic Microstructure

Brian D. Bertram, **Rosario A. Gerhardt**, **and John W. Schultz**
School of Materials Science and Engineering, Georgia Institute of Technology
Atlanta, Georgia 30332-0245, USA

Abstract— Ceramic composites of alumina containing axisymmetric spatial dispersions of silicon carbide whiskers were fabricated by hot pressing. Several parameters were varied over wide ranges (concurrently, to some extent) during electrical measurements. These include frequency (0.1 Hz–1.8 GHz), temperature (20–70°C), bias (0–40 V), whisker volume fraction (0–30 vol%), and measurement direction (relative to material anisotropy). The electrical results were correlated to stereological measurements of the anisotropic interwhisker distance distributions in the development of an original model which incorporates as many issues as possible and is consistent with the experimental data. The new model employs new concepts, takes into account the semiconductive behavior of the SiC whiskers, and includes various elements from existing models. These include treatments of charge transport and polarization processes, percolation, and material microstructure based on equivalent circuits and symmetry concepts. Some theoretical work concerning the insulator-conductor transition (i.e., percolation) in general media may also be presented. The combined work represents an advancement in the science of composite dielectric materials and might lead to engineered dielectrics with tailored properties. I am uploading some papers previously accepted to high-quality journals which are related to the abstract above. This is to show the quality of my work in this field.

Session 3A5
Electromagnetics in Remote Sensing

Dimensions of Microwave Remote Sensing and of a Radar Designer: A Tribute to Dr. William T. K. Johnson

Stephen D. Wall
Jet Propulsion Laboratory, California Institute of Technology, USA

Abstract— Microwave remote sensing has matured in the last few decades from an experimental technique to a valuable tool in the stable of remote sensing instruments. The breadth of this maturation comes largely from the multiple dimensions that this wavelength offers: wavelength, polarization, geometry and others. We will explore the relationships between these dimensions and the surface phenomena that they address, and show how these have evolved since the 1970's.

Paralleling this growth, and largely responsible for it, has been the career of Dr. William T. K. Johnson, a physicist and instrument design engineer well known to the PIERS community whose life was ended prematurely, in September of 2010, by Amyotrophic Lateral Sclerosis, or ALS. Bill fulfilled the badly-needed role of an instrument architect, following both increasing scientific needs and engineering capabilities — and creating innovative methods of using the latter to satisfy the former. The history and engineering challenges of the instrumentation closely follow the work of Dr. Johnson, so this talk will serve as an intertwined review of both.

Also in parallel with the growth of microwave instrumentation and research has been the analysis techniques that are used to extract surface and subsurface phenomenology from the remotely-sensed data. With each increase is has seemed that every "ounce" of information had been squeezed out the data provided, but clever extraction techniques have continued to arise. It is this advance, fueled by those listed above, that has resulted in the use of microwave sensors on Earth, Venus, Mars, Titan, and other planetary objects. Examples of both data and interpretation from several of these will be used to illustrate the diverse dimensions that now exist in the microwave segment of the electromagnetic spectrum.

ACKNOWLEDGMENT

The research described in this paper was carried out at the Jet Propulsion Laboratory, California Institute of Technology, under a contract with the National Aeronautics and Space Administration.

Radar Studies of the Plains of Titan

E. R. Stofan[1], **S. W. Wall**[2], **T. Farr**[2], **A. Hayes**[3], **M. A. Janssen**[2], **R. L. Kirk**[4], **A. Le Gall**[2], **R. M. Lopes**[2], **R. D. Lorenz**[5], **J. I. Lunine**[6], **K. Mitchell**[2], **J. Radebaugh**[7], **L. A. Soderblom**[4], **C. A.Wood**[8], **and The Cassini Radar Team**

[1]Proxemy Research, P. O. Box 338 Rectortown, VA 20140, USA
[2]Jet Propulsion Laboratory, California Institute of Technology, Pasadena, CA, USA
[3]Div. Geol. Planet. Sci., California Institute of Technology, Pasadena, CA, USA
[4]USGS Astrogeology Div., Flagstaff, AZ, USA
[5]Applied Physics Laboratory, Laurel, MD, USA
[6]Univ. Rome Tor Vergata, Rome, Italy
[7]Dept. Geol. Sciences, Brigham Young University, Provo, UT, USA
[8]Wheeling Jesuit University, Wheeling, WV, USA

Abstract— Much of the surface of Saturn's moon Titan is characterized by relatively low-lying, flat plains, typical of other planetary bodies such as Venus and Mars. Cassini SAR images reveal generally featureless dark to mottled regions, in places covered by dunes and infrequently interrupted by apparently older hill terrains. Understanding the origin of these plains is critical to understanding the geologic evolution of Titan, and we rely on SAR, scatterometry, radiometry and limited altimetry from the Cassini Radar, as well as data from the Cassini Visual and Infrared Mapping Spectrometer (VIMS) to characterize these extensive but enigmatic regions.

Cassini SAR images have backscatter variations that can be interpreted in terms of variations in surface slope, surface roughness, and variations in dielectric properties of the surface, although volume scattering has also been found to be significant in some areas (e.g., [1]). Likely surface materials on Titan (water ice, possibly with ammonia in places, dry ice, hydrocarbons, tholins) are significantly different from planetary surfaces previously studied with planetary radars. A critical question is the extent to which the plains are volcanic in origin: extensive resurfacing by volcanic activity has implications for Titan's interior evolution, as well as that of its atmosphere. Outgassing from volcanism is a likely source of atmospheric methane, which must be resupplied from the interior to feed Titan's active methane cycle as it is destroyed over time by photodissociation in the atmosphere. Putative cryovolcanic terrains have been identified on the surface (e.g., [2, 4]), but their origin has been debated ([3]). Possible cryovolcanic flows have significant variations in radar brightness, as do other plains deposits that are more clearly sedimentary in origin. We review the radar properties, as well as other available Cassini data, over some of these terrains to understand better the materials that make up these surfaces, to provide some insights into the overall origin and evolution of Titan's plains regions.

REFERENCES

1. Elachi, C., et al., "Cassini radar views the surface of titan," *Science*, Vol. 308, 970–974, 2005, doi:10.1126/science.1109919.
2. Lopes, R. M. C., et al., "Cryovolcanic features on Titan's surface as revealed by the cassini titan radar mapper," *Icarus*, Vol. 186, 395–412, 2007.
3. Moore, J. M. and R. T. Pappalardo, *Icarus*, Submitted, 2010.
4. Wall, S. W., et al., "Cassini RADAR images at Hotei Arcus and western Xanadu, Titan: Evidence for geologically recent cryovolcanic activity," *Geophys. Res. Lett.*, Vol. 36, L04203, 2009, doi:10.1029/2008GL036415.

Interpreting the Geology of Titan Using RADAR Data from Cassini

R. M. Lopes[1], **A. Le Gall**[1], **L. Wye**[2], **E. R. Stofan**[3], **R. Peckyno**[4], **J. Radebaugh**[5], **R. Kirk**[6], **A. Hayes**[7], **O. Aharonson**[7], **K. Mitchell**[1], **B. Stiles**[1], **S. Wall**[1], **M. Janssen**[1], **and The Cassini RADAR Team**

[1]Jet Propulsion Laboratory, California Institute of Technology, Pasadena, USA
[2]Stanford University, Stanford, USA
[3]Proxemy Research, Bowie, Maryland, USA
[4]Oregon State University, Corvallis, USA
[5]Brigham Young University, Provo, USA
[6]US Geological Survey, Flagstaff, USA
[7]California Institute of Technology, Pasadena, USA

Abstract— Interpreting geology from RADAR data presents some unique challenges. The Cassini RADAR acquires data in several modes including SAR, radiometry, and scatterometry. Geologic units are generally identified in the SAR data, but they will only be apparent if their backscatter characteristics are sufficiently different from those of surrounding terrains. Structures are more easily recognized when oriented perpendicular to the radar's look direction. At Titan, the SAR mode of the RADAR instrument is used at altitudes under $\sim 4,000$ km, resulting in resolution cell size ranging from ~ 350 m to > 2 km, which is in some places insufficient to identify different geologic units on the surface. On Titan, the candidate surface materials (water ice, water-ammonia ice and other ice mixtures, hydrocarbons, tholins) are different from the rocky surfaces more usually imaged with radars; in particular, volume scattering at Titan is thought to be significant. We have, however, been able to identify a wide variety of geologic features on Titan's surface using SAR swaths, which now cover $\sim 45\%$ of the surface. The data are distributed over a wide latitudinal and longitudinal range, enabling some conclusions to be drawn about the global distribution and significance of processes. They reveal a geologically complex surface that has been modified by all the major geologic processes seen on Earth. We have updated the geologic unit map that used flybys up to T30 (Lopes et al., 2010, Icarus, 205, 540–558), representing $\sim 20\%$ of the surface. We find that the overall correlations found previously still hold given more than double the areal coverage. In terms of global areal distribution, both dunes and mountainous terrains (including Xanadu) cover more area (respectively 9.2% and 14.6% of the observed area) than other identified geologic units. In terms of latitudinal distribution, dunes and mountainous terrains are located mostly at low latitudes (less than 30 degrees), with no dunes being present above 60 degrees. Channels formed by fluvial activity are present at all latitudes, but lakes filled with liquid are found at high latitudes only (above 60 degrees). Impact structures are mostly located at low latitudes, with no confidently identified craters above 60 degrees latitude, possibly indicating that more resurfacing has occurred at higher latitudes. Putative cryovolcanic features, consisting mostly of flows, are not ubiquitous and are mostly located in the areas surrounding Xanadu. We examine temporal relationships between units and conclude that aeolian and fluvial/pluvial/lacustrine processes are the most recent, while tectonic processes that led to the formation of mountainous terrains and Xanadu are likely the most ancient. Mountainous terrains, which along with Xanadu may have at least in part a tectonic origin, are radar-bright and radiometrically distinct from most other areas. They may have been washed clean of organic particulates by methane rains. Radiometric data from the Sinlap ejecta blanket reveals fresh water ice, indicating that the crater is relatively young. Preliminary correlations between geologic units and surface properties derived from the radiometry measurements (brightness temperature, effective dielectric constant, and degree of volume scattering) will also be presented.

Titan's Hydrocarbon Seas: Physical Properties and Measurement Prospects

Ralph D. Lorenz
Applied Physics Laboratory, Johns Hopkins University
11100 Johns Hopkins Road, Laurel, MD 20723, USA

Abstract— The Cassini mission has discovered extensive lakes and seas of liquid hydrocarbons on Saturn's moon Titan. These seas, most notably Kraken Mare and Ligeia Mare, about 1000 km and 500 km across, respectively, are found in Titan's northern polar regions, a distribution that may reflect the astronomical forcing of Titan's climate. Geometric similarity with terrestrial lakes suggests the liquid may be hundreds of meters deep.

Several means of probing the properties of these seas are available to Cassini. First is 'optical' remote sensing (actually near-IR), which has only recently become possible with the emergence of Titan's north polar regions from winter darkness (northern spring equinox was in 2009). Spectroscopic constraints on composition and suspended materials may be possible to derive, and imaging of the specular solar reflection on the sea surface constrains surface roughness.

Second is by radar backscatter in SAR imaging (the means by which the northern lakes were first discovered). So far, most large lakes appear very dark (typical sigma-0 of < -25 dB), suggesting a very smooth surface. Microwave radiometry additionally introduces important constraints on the characteristics of the sea, including their physical temperature (which, due to evaporative cooling, may not be the same as the air immediately above the sea surface). The data together are consistent with a low-dielectric constant composition, with no significant suspended scatterers and with sufficient depth to attenuate a bottom echo.

Finally, Cassini is expected to conduct bistatic scattering experiments at two wavelengths (X and S-band), directing a radio beam onto Titan's surface from where the forward-reflected radiation can be detected by large radio telescopes. In addition to roughness, polarimetric detection of the scattered radiation can be used to determine the liquid dielectric constant via the Brewster angle.

The relative contributions of these techniques, previous observations and upcoming observing opportunities and the prospects for evaluating the liquid's dielectric constant and surface roughness will be discussed. Near-shore depth estimations have been made in a shallow southern lake, Ontario Lacus, using the attenuation of the bottom echo, but the large northern seas are likely deep enough to be considered uniform 'semi-infinite' dielectric targets, simplifying analysis. Roughness, due to wind-driven waves, is of particular interest as numerical models of Titan's winds over the Titan year suggest that although previous observations have been made in a quiescent epoch, an increase in surface windspeed is imminent. The empirical wind-wave relationships used in Earth science are of course not directly applicable to Titan where the atmospheric and fluid density, the gravity, surface tension and viscosity are all different : experimental and theoretical results on waves will be presented.

Ultimately it would be desirable to investigate the seas directly with in-situ methods. A spacecraft mission (TiME — Titan Mare Explorer) has been proposed to NASA which would use a sonar for depth measurement, a camera and inertial measurements to characterize waves and an immersed capacitor to measure dielectric constant directly.

Monostatic Statistical Shadowing Function with Reflection of Random Rough Surfaces

H. Li, **N. Pinel**, **and C. Bourlier**
IREENA Laboratory, Université de Nantes, France

Abstract— Shadowing function is an important parameter in ocean remote sensing. It is reported that an error of 0.5% in the sea surface infrared emissivity results in an error of 0.3 K when estimating the sea surface temperature [1]. As a result, it is essential to obtain a shadowing function with high accuracy. Geometric optics approximation is usually assumed to be valid when deriving sea infrared emissivity, so it is also true for the corresponding shadowing function. Direct sea surface infrared emissivity (Fig. 1(a)) was studied by several authors [2, 3]. However, infrared emissivity with surface reflection (Fig. 1(b)) is seldom considered, although it is too significant to ignore, especially at large emission angles for sea surfaces with large RMS slopes σ_s [4]. Bourlier derived a shadowing function with surface reflections to calculate the sea infrared emissivity, but large underestimation is observed [5].

This paper derives a monostatic statistical shadowing function considering one surface reflection, basing on the shadowing model of Smith [6]. The correlation between slopes and heights is ignored to obtain an uncorrelated statistical shadowing function with single surface reflection. The marginal slope and height probability densities of the shadowing function are shown, which are related to the slope and height distributions of the illuminated points. The average shadowing function is also performed, which indicates the proportion of the area to the whole surface where surface reflections occur. It is shown that the surface reflections are weak for surfaces with small σ_s. As expected, this phenomenon becomes significant when σ_s increases.

To evaluate the accuracy of the model, a ray-tracing Monte Carlo algorithm is employed as a reference. It is shown that the Monte Carlo result agrees quite well with that of the uncorrelated model. The comparison shows better agreement by taking the correlation between slopes and heights into account. However, a much longer computation time is required. To reduce the computation time while maintaining high performance, an empirical factor is introduced to improve the uncorrelated model. Thus, the empirical uncorrelated model matches well the performance of the correlated one, while no extra computation time is needed.

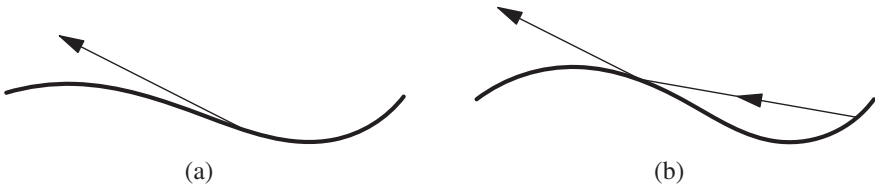

Figure 1: (a) Direct emissivity and (b) emissivity with one reflection.

REFERENCES

1. Wu, X. and W. L. Smith, "Emissivity of rough sea surface for 8–13 μm: Modeling and verification," *Appl. Opt.*, Vol. 36, No. 12, 2609–2619, 1997.
2. Masuda, K., T. Takashima, and Y. Takayama, "Emissivity of pure and sea waters for the model sea surface in the infrared window regions," *Remo. Sensing Environ.*, Vol. 24, 313–329, 1988.
3. Bourlier, C., "Unpolarized infrared emissivity with shadow from anisotropic rough sea surfaces with non-Gaussian statistics," *Appl. Opt.*, Vol. 44, No. 20, 4335–4349, 2005.
4. Henderson, B. G., J. Theiler, and P. Villeneuve, "The polarized emissivity of a wind-roughened sea surface: A Monte Carlo model," *Remo. Sensing Environ.*, Vol. 88, 453–467, 2003.
5. Bourlier, C., "Unpolarized emissivity with shadow and multiple reflections from random rough surfaces with the geometric optics approximation: Application to Gaussian sea surfaces in the infrared band," *Appl. Opt.*, Vol. 45, No. 24, 6241–6254, 2006.
6. Smith, B., "Geometrical shadowing of a random rough surface," *IEEE Trans. Ante. Propa.*, Vol. 15, 668–671, 1967.

A Combined Active/passive Model for the Radar-bright Terrains on Titan

Michael A. Janssen[1], **Alice Le Gall**[1], **and Lauren Wye**[2]

[1]Jet Propulsion Laboratory, California Institute of Technology, Pasadena, CA, USA
[2]Electrical Engineering Department, Stanford University, Stanford, CA, USA

Abstract— Since Cassini arrived at Saturn in 2004, its moon Titan has been thoroughly mapped by the RADAR instrument at 2-cm wavelength, in both active and passive modes. Some regions on Titan, including Xanadu and various bright hummocky bright terrains, contain surfaces that are among the most radar-bright surfaces encountered in the Solar System. The high brightnesses observed on some outer-planet satellites have been generally attributed to volume scattering processes in the kind of inhomogeneous, low-loss medium expected for cold, icy satellite surfaces. Using Kirchhoff's law of thermal radiation that relates radar and radiometric properties, we have developed a model that tests this assumption for Titan's bright terrains, using comprehensive radiometric measurements that have now been obtained with unprecedented accuracy (Janssen et al., 2009). We compare the predictions of our model to the observational data, and conclude that either the reflective characteristics of the putative volume scattering subsurface must be highly constrained, or, more likely, organized structure on or in the surface is present that enhances the backscatter.

Use of the Neural Net for Road Extraction from Satellite Images, Application in the City of Laghouat (Algria)

F. Benkouider[1], **L. Hamami**[2], **and A. Abdellaoui**[3]

[1]Electrical Engineering Department, Amar Telidji University of Laghouat, Algeria
[2]Electrical and Computer Engineering Department, National Polytechnic School, Algeria
[3]Department of Geography, URF Letters and Human Sciences, Paris XII, France

Abstract— Road extraction in urban areas has been an important task for generating Geographic Information Systems (GIS). In recent years, mainly, the rapid development of urban areas makes it urgent to provide up-to-date road maps. The timely road information is very useful for the decision-makers in urban planning, traffic management and car navigation fields, etc. The satellite image is characterized by its big quantity of rich and varied information constitutes a source of data for generating the roads maps by automatic seen techniques according to their importance. The interpretation of this one requires mostly, a treatment based on a set of techniques: shaping of the information, the filtering, the segmentation and the classification, etc. We present in this work a method based on neuronal net strategy for extracting road net based on spectral characteristics of the pixel from satellite image. Normalized spectral information in a window (3×3) around each pixel is extracted, as 9 red, 9 green and 9 blue (corresponding respectively to red, green and near infra red channels) constitute the input vector of 27 neurons. The origin of the motivation is the homogeneity of roads in high-resolution satellite images, since homogeneity is a characteristic that can be recognized with respect to neighbor pixels, and their spectral information. The system output is represented by one neuron normalized representing the road or not-road characteristics. As the neuronal net require a large coded data bases in their training stage, we have used a set of road net manually drown using special software. The image used in this application concerns a Spot HVR image acquired on March 26 (2007) over Laghouat (Algeria), an oasis city located at 400 km south Algiers (Algeria) (10 m of resolution). We have obtained a very accuracy results with less than 0.022 for the MSE. A set of various applications are presented.

Titan Exploration New Research Lines

Giorgio Franceschetti[1], **Antonio Iodice**[2], **and Daniele Riccio**[2]

[1]JPL, Pasadena, USA
[2]University of Naples Federico II, Napoli, Italy

Abstract— The Cassini mission is providing an unexpected amount of radar data relevant to Titan. At the mission kick-off, Cassini was expected to acquire data from year 2004 through year 2008. But the Extended-Extended Mission (XXM), with flybys over Titan planned up to the year 2017, is taking place and providing a very large amount of additional data, thus calling for new processing of the acquired information. In particular, the longer radar data acquisition phase is worth to be deeper analyzed, to uncover new parameters relevant to the Titan environment. A list of new research activities that are worth to be explored, and also we intend to explore is in order.

1. *Local estimate of Titan surface parameters.* "Global" fractal parameters of any acquired Titan surface profile has been demonstrated, by using Cassini altimeter data [1], thus providing just two numbers, i.e., the fractal dimension and the incremental standard deviation, for each track. The possibility to estimate "local" fractal parameters, relevant to limited portions of the profile, should be explored for any single track.
2. *Data comparison from different intersecting passes.* Altimeter data from different intersecting passes should be compared, from the fractal analysis viewpoint. As far as the intersecting region is concerned, this would lead, for the altimeter data, to move from the obtained two-dimensional fractal maps (along Titan profiles), towards a three-dimensional fractal representation (Titan surface).
3. *Scattering models for layered surfaces.* Advanced scattering models applied to altimeter and SAR data are worth to be explored. Models of multi-layered surfaces with fractal interfaces should be formalized, including volume scattering from prescribed layers. This kind of model is particularly appropriate to arid surfaces over a solid background, where the arid layer responsible of the volume scattering may be modeled as Cantor dust.
4. *Scattering models for unconventional surfaces.* Scattering models with multiple reflections features have been postulated to account for the unusual values of radar cross sections measured on Titan by the Cassini SAR. Electromagnetic models consistent with geological expectations are worth to be developed, implemented, and compared with experimental SAR data.
5. *Data comparison between different sensors.* XXM increases the number of Titan areas covered by both altimeter and SAR sensors. Then a comparative analysis of altimeter and SAR data should be addressed. A first but not unique possibility is to use the altimeter to evaluate the Titan surface fractal parameters, design a SAR simulator code, and compare simulated with actual SAR images. Accordingly, the backscattering models (see activities #3 and 4, among others), postulated in the simulation code can be validated.

Above points detail valuable research lines, of interest to the Cassini Radar Team. At the Conference, these lines of research are briefly presented, indicating their appropriate development. In addition, preliminary interesting results relative to activity #1 are illustrated and discussed.

REFERENCES

1. Franceschetti, G., P. Callahan, A. Iodice, D. Riccio, and S. Wall, "Titan, fractals and filtering of cassini altimeter data," *IEEE Transactions on Geoscience and Remote Sensing*, Vol. 44, 2055–2062, 2006.

SAR Monopulse Amplitude Comparison Method applied to Cassini RADAR SAR Imagery of Titan's North Polar Lake District

Karl L. Mitchell, **Bryan W. Stiles**, **Chandini Veeramachaneni**,
Philip Callahan, **and the Cassini RADAR Team**
Jet Propulsion Laboratory, California Institute of Technology, USA

Abstract— The multi-beam nature of the Cassini RADAR instrument makes possible the application of the SAR Monopulse Amplitude Comparison method [1]. This technique estimates surface heights by comparing the calibration of overlapping Titan SAR imagery obtained from different antenna feeds (beams) of the RADAR instrument onboard the Cassini spacecraft. In implementation, we vary the estimate of the local Titan radius used to process the images and select the local radius that minimizes the amplitude mismatch between the two beams. The result has been the development of the SARTopo product [2], which supplements the scant altimetric coverage of Titan with data that are conveniently located with SAR footprints. These data have been bundle adjusted simultaneously over the entire planet, using topographic data gathered by the same instrument in nadir-pointing altimetric mode as "truth", and used successfully to determine the size and shape of Titan [3], which differs from the measured geoid, suggesting that the polar regions are topographically depressed relative to lower latitudes.

The original incarnation of the SARTopo algorithms [2] was designed for global shape modeling, and smooth the noisy data by 51 pixels, giving topography of ~ 9 km in horizontal resolution with a height uncertainty of ~ 75 m. However, this arbitrary degree of smoothing did not consider the actual signal strength, and so is excessive in areas of good radar return where topography varies within the measurement width, and insufficient in areas of low radar backscatter (e.g., the polar lakes and seas). This is particularly problematic around the lakes, the rims of which appear to exhibit considerable slopes.

In an attempt to derive more value from the product, particularly in the topographically-variable terrain around Titan's high latitude lakes and seas, we pursue a less aggressive horizontal smoothing strategy. Height uncertainties due to random signal error are reported in the SARTopo product, with unsmoothed median height uncertainties typically ~ 300 m, but are strongly dependent on the magnitude of the radar backscatter, σ_0 and so may vary greatly. Uncertainty in height in the SARTopo method approximates normal noise characteristics unless number of looks is very low. Our strategy was to takes unsmoothed SARTopo, and then box-filter it using an adaptive algorithm which increases in size until vertical precision is finer than a user-defined threshold. This allows for much smaller observation widths at the expense of vertical precision.

SARTopo data were re-derived for Titan's topographically-variable North Polar lake district, using a target vertical precision of ~ 100 m, resulting in finer topographic details at in the km-scale. Along-track observation widths average 1.4 km for the area shown, compared with a fixed 8.9 km for the 51-pixel version. Our results reveal details in the morphology around polar lakes that were only previously possible to determine using radarclinometry, which is strongly backscatter model dependent and error-prone, and stereo techniques, which require SAR image overlap and so are limited in coverage. Strategies for noise reduction in future local studies should be developed with careful consideration of the nature of the terrain, and will require unsmoothed input data.

ACKNOWLEDGMENT

This work was carried out at the California Institute of Technology Jet Propulsion Laboratory under a contract with NASA. We acknowledge support of the Cassini RADAR team and a Cassini Data Analysis Program grant.

REFERENCES

1. Chen, C. W. and S. Hensley, *J. Opt. Soc. Am. A*, Vol. 22, 529, 2005.
2. Stiles, B. W., et al., *Icarus*, Vol. 202, 584, 2009.
3. Zebker, H. A., et al., *Science*, Vol. 324, 921, 2009.

Global Ionospheric Maps Analysis with Radio Tomography, Satellite Altimetry and UV Data

E. S. Andreeva, **S. A. Kalashnikova**, **V. E. Kunitsyn**, **and I. A. Nesterov**
M. V. Lomonosov Moscow State University, Russia

Abstract— Global Ionospheric Maps (GIMs) provide an opportunity of regular and worldwide studies of ionospheric vertical total electron content (TEC) since 1998. The methods applied in the GIMs construction at several data processing centers are different although all based on the common idea of finding the appropriate model parameters to fit the selected model of the vertical distribution of electron density to the observed GPS data. Being widely used in geophysical applications, GIMs are interesting to be compared with other well-developed methods, such as low-orbital (LORT) and high-orbital (HORT) ionospheric radiotomography, satellite altimetry and UV-imaging.

The purpose of the present work is to compare vertical TEC estimations based on GIMs from different processing centers, with HORT and LORT reconstructions for periods of various geomagnetic activity during 2003–2007 years. The direct observations of vertical TEC provided by the TOPEX dual-frequency altimeter above oceans and seas, where very few GPS measurements are available, were also taken into comparison to test GIMs in that areas. In this work we also consider the night-time measurements of 135.6 nm line from GUVI far-ultraviolet scanning imaging spectrograph as far as, in a first approximation, this radiance is proportional to the integral of squared electron density, and provides additional information about nighttime ionosphere.

The results of such comparison showed that the resolution of GIMs, declared to be 5° of longitude and 2.5° of latitude is, in fact, not so good. Large structures reaching the size of about 10° distinctly reconstructed by HORT, LORT, GUVI and TOPEX are often not observed in GIMs or have larger scales, especially during the periods of strong geomagnetic activity. GIM vertical TEC is often much more smoothed, compared to LORT, HORT and TOPEX data, and can't represent all fast processes taking place in the ionosphere. The reconstructions for quiet periods are basically similar, although higher GIM and HORT vertical TEC values compared to LORT vertical TEC, which might be due to the plasmaspheric contribution, are still noteworthy.

ACKNOWLEDGMENT

The work was supported by Russian Foundation for Basic Research (RFBR), grants No. 10-05-01126, 11-05-01157 and grant of Russian Ministry of Education, project NK-56P-24.

Session 3A6
RFID and RFID-enabled Sensors

UHF RFID Chip Impedance Measurement without Vector Network Analyzer

Rainer Kronberger[1], **Volker Wienstroer**[1], **and Barbara Friedmann**[2]

[1]High Frequency Laboratory, Cologne University of Applied Sciences, Germany
[2]Noretec GmbH & Co., Koeln, Germany

Abstract— To achieve optimum performance with UHF RFID tags a careful adaptation of the antenna to the chip impedance is mandatory. Otherwise, mismatch losses result, which reduce the read range of the tag significantly. This issue has been outlined in several papers before (e.g., [1–3]). In general, the chip impedance can be found in the data sheet of the chip manufacturer but it often depends on the mounting technique of the chip. For optimum matching condition the exact reference plane of the impedance has to be known. Therefore, impedance measurements have to be done to find out the correct impedance value of the chip-antenna interface. Those measurements are performed with a vector network analyzer (VNA) and in addition to achieve a higher accuracy with a signal generator [1, 2]. In most cases this is very cost-intensive.

This paper proposes a new method that allows the determination of the chip impedance of an UHF RFID chip in different way. It is based on the extremely narrow wake up threshold of an RFID chip and the power mismatch between chip and source. By using a set of different and known source impedances also different wake up power signals will result. This allows the accurate calculation of the chip impedance exactly at the wake up threshold. In the simplest form a low cost impedance measurement system could be realized with a standard RFID reader system and few external rf components.

The method is based on the fact, that maximum power transfer results for the case that the antenna impedance $\underline{Z}_{Ant}$ is conjugate complex to the chip impedance $\underline{Z}_C$. Otherwise mismatch between the antenna and the chip results, which reduces the available power P_C into the chip. In addition, the RFID chips react very sensitive to the applied power and provide a very sharp wake up threshold. Mathematically, constant mismatch in the complex impedance plane is described by a circle around the chip impedance. Such a mismatch circle is be defined by two points and the radius. Applying this to our case such a circle gets defined by the chip impedance $\underline{Z}_C = R_{Chip} + jX_{Chip}$, the source impedance $\underline{Z}_i = R_i + jX_i$ and the mismatch between both. This means vice versus, that from a set of test impedances $\underline{Z}_i$ with corresponding mismatch values, the radius of the circle could be calculated. Having this twice for two different mismatch values the center point, which represents the so far unknown chip impedance $\underline{Z}_c$ can be calculated. To apply this method the RFID chip with unknown impedance has to be connected to generator with 3 known but different source impedances and the wakeup power level has to be detected.

The paper describes the mathematical way to set up the equation system and how to find the correct chip impedance, it presents the measurement system that has been created and used for the measurements and in addition results are shown and compared to conventional RFID chip measurements. Main advantage of this method is that precise impedance measurements can be performed even with slightly modified RFID interrogators. Especially at the wake up threshold this is very helpful to determine the chip impedance under realistic operating conditions.

REFERENCES

1. Nikitin, P., V. Rao, R. Martinez, and S. Lam, "Sensitivity and impedance measurements of UHF RFID chips," *IEEE Transactions on Microwave Theory and Techniques*, Vol. 57, No. 5, 1297–1302, May 2009.
2. Mayer, L. W. and A. L. Scholtz, "Sensitivity and impedance measurements on UHF RFID transponder chips," *The 2nd Int. EURASIP Workshop on RFID Technology*, Budapest, Hungary, 2008.
3. Dobkin, D., *The RF in RFID: Passive UHF RFID in Practice*, Elsevier, New York, 2007.

RFID Chip Impedance Measurement for UHF Tag Design

M. Daiki[2], **H. Chaabane**[1], **E. Perret**[1], **S. Tedjini**[1], **and T. Aguili**[2]

[1]Grenoble-INP/LCIS, 54 Rue Barthélémy Laffemas, Valence 26902, France
[2]Sys'Com, ENIT, BP 37 Le Belvedere, Tunis 1002, Tunisia

Abstract— **Introduction:** RFID systems are heavily used in many different areas such as traceability, access control [1] and tomorrow as low cost captors [2]. A RFID tag consists of an RFID chip attached to a surrounded antenna. The communication principle of RFID is relatively simple; indeed the response of the RFID tag is formed by the retro-modulation of the emitted signal by the RFID reader [3]. To modulate the signal the tag IC must present two different impedance states Z_1 and Z_2. The RFID chip can easily be modeled as lump impedance connected to the edge of the antenna with a variable value depending on the state of the tag. These impedance values are assumed to be frequency and power dependant $Z_i(f,p)$, $i = 1, 2$. In order to use such tags for non ordinary use such as captors, it is fundamental to be able to characterize precisely the IC impedance in term of frequency and power. It is all the more true since the manufacturer's data is generally limited to a single impedance state (the tag antenna is generally matched to Z_1) for a single power. The frequency dependence is generally available at one power (the threshold power, i.e., the minimum transmission power required to activate the tag) by the equivalent electric circuit provided in datasheet (the equivalent resistance R and the capacity C). So the only way to access to these values is by measurement. In this field, some measurement beds have been developed [4, 5]. In current UHF applications, the performances of the system are limited by the forward link (reader to tag). It is the reason why the mismatch IC impedance state Z_2 is rarely investigated. In these configurations, once the tag is sufficiently powered (which is a function of the matching between Z_1 and the antenna impedance), the reader sensibility is generally enough to catch the information form the tag. For semi-active UHF tags or even for captor applications, the reverse link (tag to reader) must be taken into account, and so, the second state Z_2 has also to be characterized as a function of frequency and power.

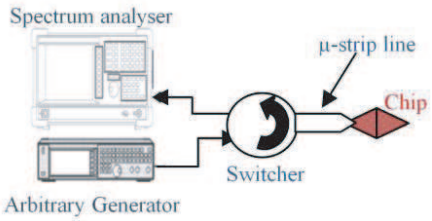

Figure 1: Measurement bed description.

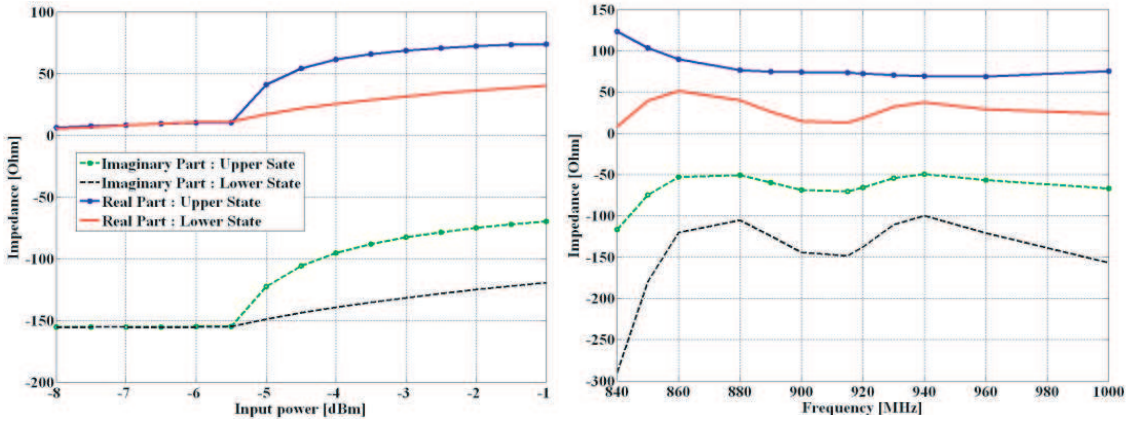

Figure 2: NXP Chip input impedance real (solid line) and imaginary part (dashed line) in upper (o) and lower (no marker) state versus input power at 915 MHz (a) and operating frequency (b) for −2.6 dBm.

Chip Impedance Measurement Methodology: The method we propose in this paper is based on the measurement bed presented Fig. 1. The recording and processing of the chip response of the chip led us to access to the two chip impedances steps according to the input signal frequency and power.

The measurement bed is constituted of an arbitrary wave generator in order to send a reader request, a spectrum analyzer to detect tag response and a circulator to switch between transmitting request and receiving as shown in the Fig. 1. Because of the impossibility to connect the RFID chips directly to measurement bed, a micro strip line at the chip pins has been added. A SOL calibration procedure is then used to extract chip impedance values.

In the Fig. 2, we present the real and imaginary part of the NXP GX2L chip input impedance versus power for a fix frequency of 915 MHz (Fig. 2(a)) and versus frequency for fixed power of -2.6 dBm (Fig. 2(b)). These two measurement results show much more information about chip behavior than information given by datasheet ($R = 16\,\Omega$, $C = 1.16$ pF, $Pth = -15$ dBm.). Besides, it's clear in Fig. 2 that the chip impedance is a function of frequency and power and could be considered as $Z_i(f, p)$.

Conclusion: The information obtained by the measurement methodology proposed here would be used to optimize the antenna-chip impedance mismatch for the both states in the whole RFID UHF frequency band. Delta RCS considerations would be investigated in order to developed effective semi-active tags or new UHF RFID based captors.

REFERENCES

1. Chakra, S. A., U. O. Farrukh, E. Colin, and A. Moretto, "Ultra high frequency-radio frequency identification tags modeling," *ACTEA*, Lebanon, 2009.
2. Marrocco, G., C. Occhiuzzi, and F. Amato, "Sensor-oriented passive RFID," Book Chapter, "The Internet of Things," Part 4, 273–282, 2010.
3. Nikitin, P. V. and K. V. S. Rao, "Theory and measurement of backscattering from RFID tags," *IEEE Ant. and Prop. Mag.*, Vol. 48, 212–218, 2006.
4. Chen, S. and K. Lin, "Characterization of RFID strap using single-ended probe," *IEEE Trans. on Instru. and Meas.*, Vol. 58, 3619–3626, 2009.
5. Mayer, L. W. and A. L. Scholtz, "Sensitivity and impedance measurements on UHF RFID transponder chips," *2nd International EURASIP Workshop on RFID Technology*, Hungary, 2008.

A 2.45 GHz Rectenna with Optimized RF-to-DC Conversion Efficiency

O. A. Campana Escala, **G. A. Sotelo Bazan**, **A. Georgiadis**, **and A. Collado**
Centre Tecnologic de Telecomunicacions de Catalunya (CTTC), Castelldefels 08860, Barcelona, Spain

Abstract— RFIDs and RFID enabled sensors call for energy harvesting technologies in order to achieve autonomous operation [1]. A 2.45 GHz rectenna is presented, consisting of a circularly polarized antenna and a rectifier circuit optimized for low power incident electromagnetic signals. The radiator is designed following the topology proposed in [2]. The patch and feed network are etched on two 20 mil Arlon A25N layers separated by a 9 mm foam layer (Fig. 1(a)). Circular polarization is achieved by a coupling slot with 45° inclination relative to the feed line, in addition to perturbing the circular surface of the patch [2]. The S-parameters and axial ratio of the antenna are shown in Fig. 1(b) and Fig. 1(c). The Skyworks SMS7630 Schottky diode was used for the rectifier circuit. Several charge pump circuits were considered with a varying order from 1 to 4 (Fig. 1(d)). Harmonic balance was used to optimize the RF-to-DC conversion efficiency, by optimizing the capacitors and load resistor of the charge pumps in addition to an L-section input matching network [3]. Fig. 1(d) shows the obtained simulated efficiency versus the available input power when the rectifier components were optimized for an input power of −20 dBm. It is verified that for the given diode the detector of order 1 using a series diode leads to maximum efficiency.

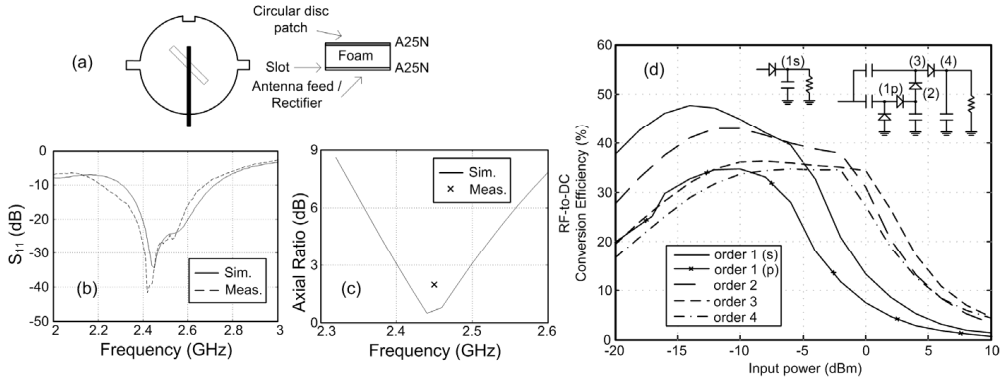

Figure 1: Rectenna circuit design. (a) Circularly polarized antenna topology. (b) S-parameters. (c) Axial ratio. (d) Simulated RF-to-DC conversion efficiency of voltage multiplier circuits of various orders (f = 2.45 GHz).

ACKNOWLEDGMENT

The authors acknowledge Selva Via for helping with the fabrication of the prototypes. This work was supported by European COST Action IC0803, by PTQ-06-02-0555, PTQ-08-01-06432, TEC2008-02685/TEC from the Ministry of Science and Innovation Spain, and Marie Curie project FP7-PEOPLE-2009-IAPP 251557 (SWAP).

REFERENCES

1. Rida, A., L. Yang, and M. Tentzeris, *RFID-enabled Sensor Design and Applications*, Artech House, 2010.
2. Wang, C. and K. Chang, "A novel CP patch antenna with a simple feed structure," *Proceedings of the IEEE International Symposium on Antennas and Propagation (AP-S)*, 1000–1003, Salt Lake City, USA, July 2000.
3. Georgiadis, A., G. Andia-Vera, and A. Collado, "Rectenna design and optimization using reciprocity theory and harmonic balance analysis for electromagnetic (EM) energy harvesting," *IEEE Antennas and Wireless Propagation Letters*, Vol. 9, 444–446, 2010.

Novel Compact RFID Chipless Tag

A. Vena, E. Perret, and S. Tedjni
Laboratoire de Conception et d'Intégration des Systèmes (LCIS), Grenoble Institute of Technology, France

Abstract— Chipless technology is dedicated to enter market of item tracking, representing every year 10 trillion items sold [1], and still addressed today by optical barcode. In this communication a new RFID chipless tag is presented. The density of coding per surface of this novel tag is important and reaches 3 bits/cm^2. For a surface of $1.5 \times 2\,\text{cm}^2$, it is possible to encode 9 bits. The design presented in this paper Fig. 1, based on multiband coplanar strip, brings enhancement in term of miniaturization, configurability and cost of fabrication. Unlike previous solution [2, 3], only one layer of metal is necessary. Of course conductive ink could be considered to produce the tag.

The proposed design uses 4 resonators as represented on Fig. 1 by the numbers 1 to 4. Even if the device is quite compact, each resonator have a resonant frequency that can be tuned independently. Moreover, the methodology used here for the information coding allows a significant decrease of tag size compared to previous technique [2, 3]. It consists in varying the resonant frequency of each resonator around a reference by changing short-circuit lengths denoted by L_1, L_2, L_4 (see Fig. 1). Three tags having different short-circuit configurations, have been designed, realized and tested. For Tag 1, $L_1 = 0\,\text{mm}$, $L_2 = 1\,\text{mm}$, $L_3 = 0\,\text{mm}$, for Tag 2, $L_1 = 3.5\,\text{mm}$, $L_2 = 0\,\text{mm}$ and $L_3 = 0\,\text{mm}$ and for Tag 3, $L_1 = 0\,\text{mm}$, $L_2 = 0\,\text{mm}$ and $L_3 = 3.5\,\text{mm}$.

Figures 2(a), 2(b), 2(c) show the corresponding frequency signature obtained using a VNA in a radar bi-static configuration. A very good agreement is observed between results obtained from CST and measurements in the whole frequency band. As a first result, it can be noticed that resonant frequency F_1, F_2 and F_4 linked to respectively, short-circuit length L_1, L_2, L_4 are fully independents. It is the reason why this device can be used to encode information. In the full version of the paper, coding technique and measurement setup will be discussed and additional results obtained from time domain approach will be presented.

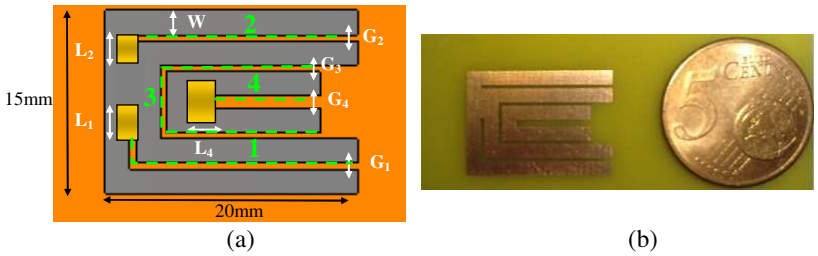

Figure 1: (a) Geometry of the chipless RFID tag. (b) Photography of designed tag 1 (15 mm × 20 mm). Substrate is FR4, and thickness is 0.8 mm.

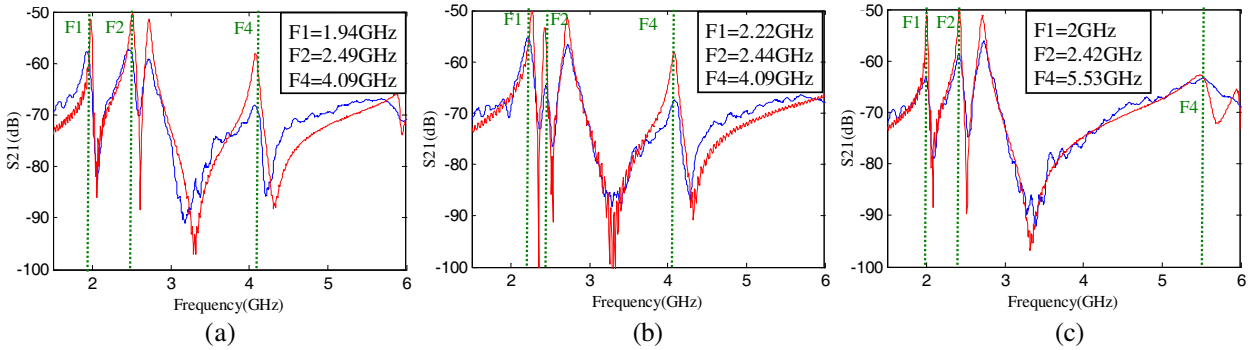

Figure 2: Measurement results in frequency domain (blue solid curve) and simulation results (red dotted curve) for (a) Tag 1, (b) Tag 2, (c) Tag 3.

REFERENCES

1. IDTechEx, "Printed and chipless RFID forecasts, technologies & players 2009–2019," www.IdtechEx.com.
2. Preradovic, S. and N. C. Karmakar, "Design of fully printable planar chipless RFID transponder with 35-bit data capacity," *Proceedings of the 39th European Microwave Conference*, Rome, Italy, 2009
3. Jalaly, I. and D. Robertson, "RF barcodes using multiple frequency bands," *IEEE MTT-S Digest*, June 2005.

RFID Tag Antenna Design on Metallic Surface by Using Rectangular Micro-strip Feed

Ding-Bing Lin[1], **Chao-Chieh Wang**[1], **I-Tseng Tang**[2], **and Mau-Phon Houng**[3]

[1]Institute of Computer and Communication Engineering
National Taipei University of Technology, Taipei, Taiwan
[2]Department of Environment and Energy, National University of Tainan, Tainan, Taiwan
[3]Institute of Microelectronics, National Cheng Kung University, Tainan, Taiwan

Abstract— In recent years, radio-frequency identification (RFID) technology has become a popular application since it provides a convenient identification information, small size, long reading range and fast reading speed. The operating band of RFID in UHF is mainly from 860 to 960 MHz. When the operating frequency of RFID rises to microwave region, the antenna design including the impedance matching becomes more important to enhance the system performance. To provide a better impedance matching network between an antenna and a tag chip is the way to improve the chip power and maximize the reading range. As the cost and fabrication requirements, the antenna must directly match to large capacitive reactance and small resistance of tag chip that different from 50 ohm. Because of chip impedance with high Q, the design of a matched antenna is difficult. T-matching networks or inductively coupled [1–3] feed that are commonly used for the efficient matching of UHF tags. Most RFID antennas are currently used to stick on nonmetal material or easy card. We introduced a new RFID antenna structure that can stick on metallic surface. A printed rectangular antenna by using microstrip feed structure on system ground which has the same size as antenna. By using the inductive property of the microstrip line with short end to match the capacitive reactance of tag chip, and the performance in free space on metallic surface was measured. The half-power matching bandwidth (VSWR < 3) of the antenna in free space was measured to be in the frequency range 914–934 MHz. The measured reading range in free-space is 2–3 m.

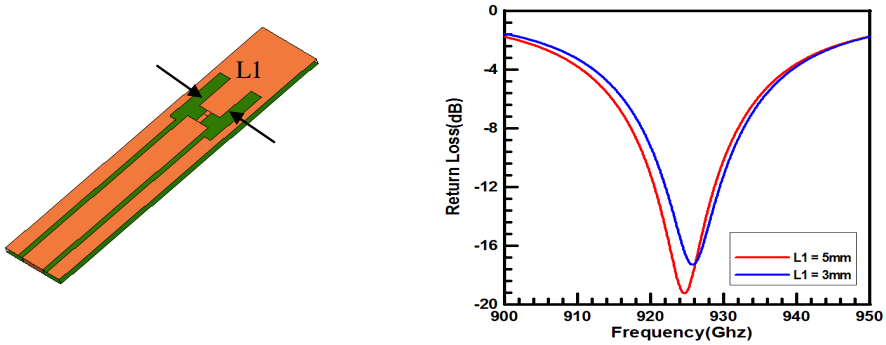

(a) (b)

Figure 1: Printed rectangular RFID antenna. (a) Antenna structure. (b) Return loss against f for different values of L1.

REFERENCES

1. Choi, Y., U. Kim, and Jaehoon Choi, "Design of a dipole tag antenna enclosed by a short-stub for UHF RFID application," *Antennas and Propagation Society International Symposium*, 1–4, Jul. 2008.
2. Son, H. W. and C. S. Tyo, "Design of RFID tag antennas using an inductively coupled feed," *Electronics Letters*, Vol. 41, 994–996, Sep. 2005.
3. Deavours, D. D., "Analysis and design of wideband passive UHF RFID tags using a circuit model," *IEEE International Conference*, 283–290, Apr. 2009.

Simplified Design Approach of Rectangular Spiral Antenna for UHF RFID Tag

Khalil El Khamlichi Drissi[1], **El Mostafa Makroum**[2, 3], **Mounir Rifi**[2], **Mohamed Latrach**[4], **and Ali Benbassou**[5]

[1]Laboratoire LASMEA, Université Blaise Pascal, Clermont Ferrand, France
[2]Networks Laboratory, Computer, Telecom & Multimedia, EST, Morocco
[3]CED sciences de l'ingénieurs, ENSEM
Km 7, Route El Jadida, B.P. 8012 Oasis Casablanca Oasis Casablanca, Morocco
[4]Radio & Microwave Group, ESEO, Graduate School of Engineering
4 Rue Merlet de la Boulaye, P. O. 30926, Angers 49009, France
[5]Laboratory of Transmission and Processing of Information EMC/Telecom
School of Technology (TSE), P. O. 2427 FES, Morocco

Abstract— During these last decades, the technologies of information and communications (ICT) have known unprecedented development. The identification technologies are part of these information technologies. Due to the recent development of microelectronics and wireless systems, new contactless identification technology has emerged: the radio identification technology (or RFID for Radio-Frequency IDentification). These new technologies, by their greater flexibility, make the exchange of information much faster and efficient.

The first RFID systems which have emerged operate in low frequency bands and are now widely used. They have paved the way toward the development of a new technology RFID, more efficient and low-cost operating at higher frequencies: passive UHF RFID. The latter has a very specific mode of operation. The identification is carried out by some tags (also called "smart tags") that are composed of an electronic chip and an antenna. Unlike conventional communication systems, they are powered remotely and have no own RF emission source.

The development of passive UHF RFID tags is the subject of our work. We are particularly interested in their antennae.

In this paper we present a method to simplify the calculation of spiral antennas for RFID tag settings without resorting to numerical analysis methods. It saves up to 99% of the time required by the simulation based on the method of moments. Thus we present a theoretical and experimental study for the design of the spiral antennas for RFID label in the UHF band. We present in this study the S_{11} parameter that enables us to evaluate the evolution of current distribution and therefore the resonance frequency of the spiral antennas. This parameter is calculated theoretically by applying the method of moments to wired antenna formed by the rectangular copper spiral printed on a dielectric substrate. The experimental validation of our theoretical models is performed using a network analyzer. The confrontation theory-experience allows us to draw some interesting conclusions concerning the number of loops of the spiral and the choice of dielectric substrate.

Electromagnetic Analysis of the Near Field Coupling between a RFID Tag and Harness for Aeronautic Applications

Alexandru Takacs[1,2], **Anthony Coustou**[1,2], **Herve Aubert**[1,2], **and Manos M. Tentzeris**[3]

[1]CNRS, LAAS, 7 avenue du Colonel Roche, Toulouse F-31077, France
[2]UPS, INSA, INP, ISAE, LAAS, University of Toulouse, Toulouse F-31077, France
[3]The School of Electrical and Computer Engineering, Georgia Institute of Technology
Atlanta, GA 30332-250, USA

Abstract— During the past decade, Radio Frequency IDentification (RFID) technologies have been widely used in aeronautic industry. Typical applications include, but are not limited to: control of the cargo traffic in large international airports, real-time localization of systems for large assembling plans, and efficient management of the stock of spare parts. Another very promising application consists of the identification of electrical cables bundles (harnesses) by using RFID tags in order to maximize time and cost efficiency during aircraft manufacturing or maintenance. Up to now, the harnesses have been identified using visual methods based on letter/numerical codes. RFID systems can be used as a very effective alternative means to identify harnesses. From an engineering point of view, few technical issues need to be resolved before implementing this approach widely. The major challenge is to minimize the impact of the harness and its close environment on RFID tags' performance. This paper addresses the electromagnetic analysis of the coupling between the tag and the harness. A commercially available tag from Alien working in the range of 902.1–927.7 MHz band has been chosen as reference for our study. This frequency band offers a good trade-off in terms of range, global performance, and miniaturization for our selected application. Note that this tag has been chosen mainly for availability reasons, but also for its free-space quasiomnidirectional radiation pattern. The electromagnetic coupling between the tag and the harness is basically magnetic in the near-field region. Consequently, only the metallic parts of the electrical harness have been taken into account. Fig. 1 shows the simulation models developed by using FEKO, a full-wave electromagnetic software based on the method of moments. A worst-case scenario has been chosen for the harness (multi-wire harness with exterior electric outer diameter of 35 mm). The performance of the tag alone (Fig. 1(a)) has been taken as the reference to evaluate the impact of the harness on the link performance between

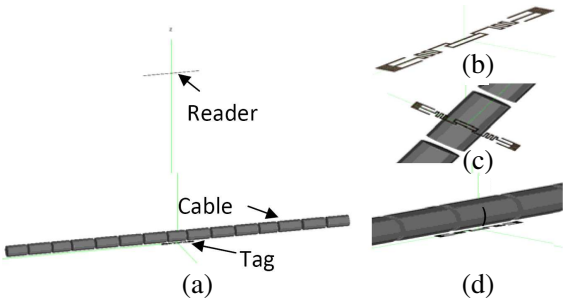

Figure 1: (a) Simulation model for the link between the reader and the tag positioned in the vicinity of the harness; (b) The tag model; (c) The tag is perpendicular on the harness axis.

Table 1: Transmission coefficients of the link between tag and reader for various configurations.

Simulated setup	D (mm)	g(mm)	α (°)	$\lvert S_{21}\rvert$ dB
Tag-Reader	55	-	-	−35
Tag-Harness-Reader	55	5	0	−39
	55	−5	0	−45
	55	5	90	−35
	55	5	90	−35

the tag end the reader. The maximum distance D between the tag and the reader without any obstruction has been measured to be 55 mm.This distance is quite reasonable for the intended application and can be increased with a more sensitive reader. The simulated magnitude of the transmission coefficient corresponding to range $D = 55$ mm has been taken as reference. Some of the ensuing results are summarized in Table 1, where g is the distance between the tag and the harness (positive if the tag is between the harness and the reader and negative if the harness is placed between the tag and the reader) and α is the angle between the tag and the harness. We found that the link between the tag and the reader is affected by mainly by two factors: (i) the near field coupling between the tag and the harness, and, (ii) the masking effect introduced by the harness itself. These effects depend on the distance between the tag and the reader, their relative orientation, and the harness diameter. As shown in Table 1, the link budget is strongly affected by the relative tag position and the optimal tag position can be found if the tag is located at least at 5 mm away from the harness.

This work shows that an electromagnetic analysis based on appropriate simulation models can be very useful. We conclude that for a given tag we can minimize the impact of the harness on its performance, identifying an optimal position for the tag. Moreover, based on this electromagnetic analysis performed in the near field region, we are able to choose the most appropriate tag among all commercially available versions, or even design a more specific tag less sensitive to the impact of the harness. We are currently analyzing the tag Alien positioned in conformal arrangement, as well as other commercially available tags. Future work will also take into account the close environment where the tag and the harness are mounted (i.e., metallic parts of the aircraft body).

Inkjet-printed Paper/Polymer-based "Green" RFID and Wireless Sensor Nodes: The Final Step to Bridge Cognitive Intelligence, Nanotechnology, Biomonitoring and RF?

M. M. Tentzeris, **A. Traille**, **H. Lee**, **R. Vyas**, **V. Lakafosis**, **and A. Rida**
School of ECE, Georgia Institute of Technology, GA 30332-250, Atlanta, USA

Abstract— In this talk, inkjet-printed flexible antennas, RF electronics and sensors fabricated on paper and other polymer (e.g., LCP)substrates are introduced as a system-level solution for ultra-low-cost mass production of UHF Radio Frequency Identification (RFID) Tags and Wireless Sensor Nodes (WSN) in an approach that could be easily extended to other microwave and wireless applications. The talk will cover examples from UHF up to the millimeter-wave frequency ranges. A compact inkjet-printed UHF "passive-RFID" antenna using the classic T-match approach and designed to match IC's complex impedance, is presented as a the first demonstrating prototype for this technology. Then, we will briefly touch up the state-of-the-art area of fully-integrated wireless sensor modules on paper or flexible LCP and show the first ever 2D sensor integration with an RFID tag module on paper, as well as numerous 3D multilayer paper-based and LCP-based RF/microwave structures, that could potentially set the foundation for the truly convergent wireless sensor ad-hoc networks of the future with enhanced cognitive intelligence and "rugged" packaging.

The talk will cover also cover issues concerning the power sources of "near-perpetual" RF modules, including flexible minaturized batteries as well as power-scavenging approaches involving thermal, EM, vibration and solar energy forms. The final step of the presentation will involve examples from wearable (e.g., biomonitoring) antennas and RF modules, as well as the first examples of the integration of inkjet-printed nanotechnology-based (e.g., CNT) sensors on paper and organic substrates. It has to be noted that the talk will review and present challenges for inkjet-printed organic active and nonlinear devices as well as future directions in the area of environmentally-friendly ("green") RF electronics and "smart-skin" conformal sensors.

Design of Autonomous Sensing Tag Based on Energy Harvesting

Naoya Nakashima, **Hiroshi Nishimoto**, **Yoshihiro Kawahara**, **and Tohru Asami**
Graduate School of Information Science and Technology, The University of Tokyo, Japan

Abstract— Wireless sensing system is vital for the realization of ubiquitous computing society as an information acquisition media. Such wireless sensing systems must be composed of low cost hardware components and must be operated without battery replacement. However, traditional wireless sensing systems require a primary battery and a high-end microcontroller for data calculation. Wireless sensing system with energy harvesting is another approach. Though, existing methods require a high-end microcontroller as well as a harvester with a complicated energy management. Thus, the high-cost problem cannot be solved.

This paper proposes "Sensing through Harvesting" concept [1], which is a new paradigm of a wireless sensing system to achieve low-cost implementation. The main idea of our proposal is this fact that sensor often generates energy and its sensing is a measurement of this energy as an observed value. "Sensing through Harvesting" concept integrates sensor and harvester, exploiting this feature. The goal of our proposal is to build a low-cost wireless sensing system by measuring the interval of beacon transmissions to estimate the quantity of electrical power harvested at sensor nodes. The major technical challenge to this concept is to find a method for data extraction from the beacon interval. To solve this problem, each beacon transmission is designed to occur at a certain amount of charged energy. With this energy management, an AP can estimate the electrical power harvested at the node dividing the energy per one beacon by the interval of beacon. After that, the data can be extracted with a proper calibration. For an implementation, we design the sensor node as shown in Fig. 1. The energy management function is realized using a reset IC and a thyristor. When the voltage across the capacitor C exceeds the detection voltage of the reset IC, the energy management circuit starts to supply energy. The energy supply automatically stops at a certain voltage across the capacitor C caused by a shortage of the current at the thyristor. To confirm the feasibility of the proposal, we evaluate the accuracy of sensing based on the variance of data at the same illumination intensity. Illumination intensity sensor nodes were implemented using both a traditional and the proposed method. The data was smoothed at an AP by calculating the moving average of the last 10 seconds of data at each beacon arrival to lessen variability. As a result, the accuracy of the proposed method was rarely different from the traditional one.

As an implementation of the whole system, we made a demo system [1] of the proposed method. Fig. 2 shows the Graphical User Interface (GUI) of the demonstration. The value at the lower left indicates the interval of beacons. From this value, an AP estimates the electrical power harvested at the sensor node based on the value and the voltage decrement of the capacitor C. The estimation result is shown at the lower right of Fig. 2. Finally, the AP decides the state of the sky by the estimated electrical power and shows it on the GUI. The state is divided into following four levels; sunny, cloudy, sunset, and night. The case of Fig. 2, the GUI says the state is sunset. Experiment results proved that the system works correctly, and this fact confirms the feasibility of our proposal. Another implementation was made for human density sensing using the same method. Therefore, our method has broad utilities.

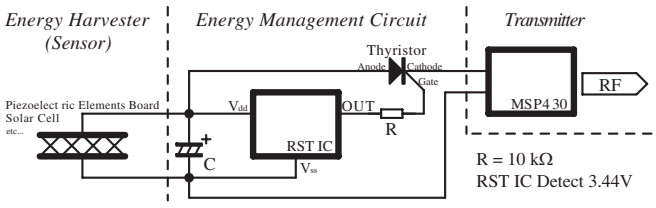

Figure 1: Design of sensing tag.

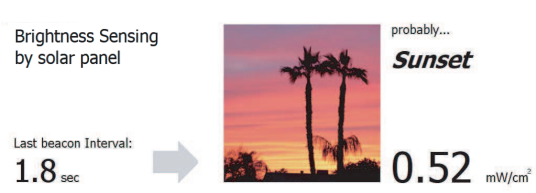

Figure 2: Screenshot of demo GUI

ACKNOWLEDGMENT

This work is supported by Ministry of Internal Affairs and Communications, Japan (Ubiquitous ServicePlatform) and the New Energy and Industrial Technology Development Organization (NEDO).

REFERENCES

1. Nakashima, N., H. Nishimoto, Y. Kawahara, and T. Asami, "Human detection system based on sensing through harvesting concept," *Proceedings of Internet of Things 2010 Conference*, Tokyo, Japan, November 2010.

Development of a Localization System by the Passive RFID UHF Technology in the Indoor Environment

Thi Ngoc Hien Doan[1, 3], **Tan Phu Vuong**[1], **Smail Tedjini**[2], **and Thi Ngoc Yen Pham**[3]

[1]Laboratory LAHC, Institute Microelectronic Electromagnetic and Photonic
Grenoble INP-Minatec, 3 Parvis Louis Neél, BP 257.38016 Grenoble Cedex 1, France
[2]Laboratory LCIS, Grenoble INP
50 Barthélémy de Laffemas, BP 54 26902 Valence Cedex 9, France
[3]International Research Center MICA (Mutilmedia Information Communication Application)
Hanoi University of Science and Technology, 1Dai Co Viet Road, Hanoi, Vietnam

Abstract— Today the technology of radio frequency identification, RFID, is applied in many areas, especially in the access control and tracking. This technique is appeared in the 1950s but has experienced in the real since the 2000s, with its implementation more and more widely. The most advantage of this technology is the low cost of RFID transponders. It has shown many interests in various fields and allowed return on investment in the industry. One of applications of RFID technology is the localization. The localization and positioning of radio frequency identification will bring many new ideas and new possibilities for radio systems. The famous localization system is the GPS but it is not operational in the environment indoor. A key element for wide deployment of a localization solution in the environment is its cost. A system based on the technology radio frequency identification is a good candidate. Indeed, an RFID tag can be equipped with one or more sensors (temperature, acceleration, pressure...) to perform distance measurement operations. It allows both to locate the subject and gets information concerning it. In this paper, we develop an antenna for the reader RFID and an algorithm for locating objects of people in an indoor environment by using passive RFID UHF technology. The research of mapping and localization systems has opened the opportunity to various areas of application of RFID technology as the people tracking, objects tracking and healthcare. The location study to be presented is focused in a typical case of a fixed object. The localization technique is based on the use of tags on the reference map, called here by landmarks. The triangular pattern distribution was chose for mapping of the RFID tags in the environment indoor. An antenna Yagi-Uda UHF antenna of three elements which offers a gain of 11.2 dBi at 868 MHz is developed for the RFID reader of localization system. The experiments and the results of the precision of the localization system are presented and we propose how to get the system more exact.

Session 3A7
Validation of Computational Electromagnetics and Quantitative Comparisons

Experimental Verification of Snell's Law at Sub-optical Frequencies

Jason Ramage[1], **Paul G. Huray**[1], **Kevin Slattery**[2], **Xiaopeng Dong**[2], **and Mike Resso**[3]

[1]Electrical Engineering, University of South Carolina, Columbia, SC 29208, USA
[2]Intel Corporation, 2111 NE 25th Ave., Hillsboro, OR 97124, USA
[3]Signal Integrity Applications, Agilent Technologies, Inc.
1400 Fountaingrove, Parkway, Santa Rosa, CA 95403, USA

Abstract— In 1621, Willebrord Snellius observed that light in the visible spectrum, incident at angle, θ_i, on a boundary between an isotropic material and Air was refracted by an angle, θ_r, according to the relationship, $n \sin\theta_i = \sin\theta_r$ (called Snell's Law) where n was a dimensionless constant ($n > 1$) he called the index of refraction. With the publication of Maxwell's equations in 1865, it was found that light was a special case of electromagnetic propagation at optical frequencies and that the more general relationship for the angle of refraction could be more generally expressed as $n \sin\theta_i = n_{Air} \sin\theta_r$; where n and n_{Air} were the indices of refraction of the homogeneous material and Air respectively and were related to their relative electric permittivity, ε_r, and permeability, μ_r, by $n = c/u_p = \sqrt{\varepsilon_r \mu_r}$ where $c = 1/\sqrt{\varepsilon_0 \mu_0}$ is the speed of light in a vacuum (or in Air) and u_p is the speed of light in the isotropic material. For non-magnetic materials ($\mu_r = 1$), Snell's Law can be written $\sqrt{\varepsilon_r(f)} \sin\theta_i = \sin\theta_r$ and is assumed to be valid for electromagnetic applications at all frequencies, f. But has it been experimentally shown that Snell's Law holds at non-optical frequencies? We have used a near field scanner with propagating electromagnetic fields operating at $f = 300\,\text{MHz}$ and $f = 3\,\text{GHz}$ incident on a non-magnetic liquid FC-40 ($n = \sqrt{\varepsilon_r(f)} \approx$ constant 1.89)/Air interface to verify that the critical angle, $\theta_i = \theta_c = 31.9°$, predicted by Snell's Law for $\theta_r = 90°$ applies at sub-optical frequencies.

Backward Wave Modes of Partially Plasma Column Loaded Cylindrical Waveguide

E. Kelebekler and N. Yener
Technical Education Faculty, Kocaeli University, Turkey

Abstract— When two waves traveling in the same or opposite direction are interfered, they can attenuate or increase each other. The backward wave oscillators work with the same principal that interference between two waves traveling in opposite directions increases the amplitude along propagation direction. There are backward wave oscillators which use interaction of plasma-electron beam, in the literature. The method of moment (MoM) is a widely used technique for numerical simulation of propagation and scattering problems. In this study, backward wave modes of the plasma column loaded cylindrical waveguide have been investigated by using Method of Moment (MoM). In previous studies, the authors presented the validation of the method for gyro-resonance region. For the structure, the backward waves appear in the plasma resonance region. Unlike gyro-resonance region modes (called plasma modes), to obtain the plasma resonance modes (called cyclotron modes), it is necessary to use very large dimensions for the linear algebraic equations system used in the MoM. Indeed in the implementation of the MoM in the plasma resonance region for the cyclotron modes, we have found that the method exhibits discrepancies with the exact solution which do not disappear unless very large numbers of expansion functions are used. The objective of this work is to report these discrepancies and suggest a possible numerical technique to overcome them. Also presented are the dispersion curves of the backward wave modes. This technique consists in using additional computer time and memory space. In particular it is demonstrated that the mean relative error is confined to less than 0.001 over the whole frequency band of interest which would be impossible if insufficient computing power was used.

Scattering Analysis of a Submerged Conducting Object in Lossy Media via Low Frequency EM

Amna Ajaz, Jia-Dong Xu, and Wei Yan
School of Electronics and Information, Northwestern Polytechnical University (NPU), Xi'an 710072, China

Abstract— The emerging concerns to sensibly detect presence of objects in hide outs of shallow waters and to follow the activities of identified objects (civilian & military), asks for enhanced surveillance over the related offshore environments. However, due inherent geometrical and background noise limitations for acoustics in shallow sea, pushes the technological shift to non-acoustic means as well. One of the recent trends in monitoring the strategic littoral sites closely has started with the investment in the EM based wireless sensor network (WSN) technologies. Additionally, there is a need for analyzing the scattering scenarios from silent objects. The presence of these objects may remain unnoticed unless radiated by active emitters. This paper is an effort to further study the EM scattering from a conducting object in a lossy layered media as has been investigated previously by King and later Marius. In the current study, MoM based commercial EM prediction software Feko is used to simulate the scattering fields from a conducting submerged cylinder by using low frequency EM. Models for the scattering in half-space and in layered media are defined in Feko. Further, analytic expression for scattering in half-space is computed with Matlab. Also, it is learned that lateral waves propagate along the interface between two media with differing dielectric properties. Considering this wave propagation phenomenon in the presence of bounded media is observed to be useful in obtaining enhanced scattered field response from the submerged object. However, related literature review on incorporation of lateral waves reveals that it is yet to be matured with its tangible realization. In future, the effect of lateral wave for sea environment and in conjunction with the scattering objects will be investigated in more detail.

The Feature Selective Validation (FSV) as a Means of Formal Validation of Electromagnetic Data

A. P. Duffy and H. G. Sasse
De Montfort University, The Gateway, Leicester, UK

Abstract— Custom-and-practice is not always the best way to achieve any goal. However, the evolution of the 'computational' branch of electromagnetics relied on the modellers looking at the results their solvers or model implementations had produced, comparing these against measurements or expected results and asking "is this good enough?" Clearly, a means of providing a quantified version of this comparison is desirable. This paper will review the state-of-the art in quantitative validation for computational electromagnetics as a timely and much needed assessment of current practice. The customary base technology for undertaking those comparisons has been visual inspection informed by experience and expectation. While this is acceptable and does allow the experience of the user to dominate, it does not take into account subjective differences between users. Statistical approaches to quantifying comparison using non-parametric tests such as the Kolmogarov-Smirnov test have found application in some areas, but statistical approaches generally fail for various reasons, such as failing to account for a likely group response of a number of users and failing to show whether that "good enough" is governed by broad agreement across much of the data or detailed agreement over all the data. This led to the development of the Feature Selective Validation (FSV) method in the late 1990s which has since been augmented and recently adopted into the IEEE standard 1597.1. This paper will describe the origin of FSV based on studies in correlation and reliability functions as well as the set of guiding principles in its design, the introduction of categorisation and the use of the Visual Rating Scale to verify FSV and provide a set of natural language descriptors. It will then review a range of FSV developments such as the use of FSV with complex valued signals, the introduction of the offset difference measure, studies into the impact of data density and research to account for the allowances normally made by users when visually assessing the comparisons. It will conclude with a discussion on a number of the key challenges facing further FSV developments.

Comparing EMC-signatures by FSV as a Quality Assessment Tool

J. Knockaert[1], **D. Pissoort**[2], **and F. Vanhee**[2]

[1]University College of West-Flanders, Ghent University
Graaf Karel de Goedelaan 5, Kortrijk 8500, Belgium
[2]Catholic University College Bruges — Ostend, Catholic University Leuven, ESAT-MICAS
Zeedijk 101, Oostende 8400, Belgium

Abstract— Electromagnetic interference radiated by a consumer product is measured on a sample of similar devices under test. It is known that this EMC-signature can drift by several reasons.

Changes through Time: A first reason is thermal and mechanical stress on the device. Thermal stress or an environmental temperature differing from the temperature at measurement time will influence the emitted spectrum. Due to the temperature coefficient of passive components and f.i. due to changing clock frequencies, the initial spectrum can change up to 10 dB or more. A second reason is tolerances on the components. This is again the case for passive components. A third reason is aging. Aging has its influence on passive components and connections. During years, thermal cycles can degrade the used materials. Also mechanical stress and vibrations can influence connections. Especially capacitors are susceptible to mechanic resonances, where the connection to the PCB can suffer. Hard environments for electronics are automotive and agricultural applications.

Differences at Production Time: The EMC-signature of two supposed identical devices can be different. First reason is an anomaly at production or assembly. Examples are a bad grounding connection or a slightly different length of used wires by the assembler. Different lengths results in different self- and mutual inductances, which changes the electromagnetic emission of the device. Second reason is the use of a different component. Components can become obsolete, while the replacing component can cause another EMC-signature.

Role of FSV: From previous parts, it is obvious that the EMC-signature can be used as a quality check tool. In the paper, it is proposed to use FSV (Feature Selective Validation Method) to compare two signatures. FSV is developed to compare two datasets, normally a measurement with a simulation result. Nevertheless, it was proven that FSV can also be used to compare two EMCmeasurements. In this paper, another new application is proposed. FSV will be used to compare the EMC-signature of a reference device, with the signature of the device under test. The results of the comparison gives an idea if both devices are really similar. Besides this, FSV can be used to see if older devices are still as electromagnetic compatible as intended or if they have suffered from stress and aging.

Pitfalls: The following things have to be solved before FSV can be used as a quality check tool. Is it possible to compare two EMC-measurement without suffering from the noise on the data? Is the GDM (global difference measure) sufficient for evaluation or is a point by point comparison more appropriate? At what moment is the quality insufficient? The first point has already been solved in a previous paper. For the second and the third point, this depends on the application. Research will be done for the full paper how FSV reacts on different realistic changes.

On the Psychological Processes of Decision Making in Displays of Electromagnetic Data

M. O. Scase[1], **M. Shafiullah**[1], **and A. P. Duffy**[2]

[1]Division of Psychology, De Montfort University, UK
[2]Faculty of Technology, De Montfort University, UK

Abstract— Feature selective validation (FSV) is an international standard for comparing visually complex 1D data. Initial verification of FSV was performed by presenting a visual rating chart accompanying comparative data. Eye-scanning data was analysed from observers as they compared graphically presented data. However, little is understood about how observers interpret displays of multidimensional datasets. We have been applying psychological principles of judgment and decision making to investigate the processes involved in this task. The goal has been to establish the main factors that influence observers when they make decisions when viewing displays. The interpretation of complex scenes by human observers to recognise or detect particular features is limited by the structure and performance of the visual system. Therefore to devise displays for observers to detect features from n-dimensional data sets one needs to appreciate the functional limitations of our perceptual system. First, observers must be screened for any visual dysfunction. Factors which can limit or affect processing include: attention; cognitive load; and differences between expert and novice observers' data visualisation, interpretation and mental models. The psychological validation of multi-dimensional FSV models demands a range of experimental methods to collect data from human observers. This includes a) users' responses (reaction times and errors) to a range of n-dimensional data with systematic manipulations of observer attributes, perceptual features and cognitive elements, b) real-time observational data collection using a "talk-aloud" protocol and c) eye-fixation data collection of observers. Outcomes of the psychological studies could then be fed into the development of formal validation models.

Numerical Noise Reduction in the Fourier Transform Component of Feature Selective Validation

Hugh G. Sasse and Alistair P. Duffy
De Montfort University, UK

Abstract— Feature Selective Validation (FSV) was developed as a means of making the subjective judgements about the quality of a comparison (a) repeatable, (b) consistent with the experience of a group of engineers and (c) amenable to automation. Over the past decade it has gained acceptance and is now the core technique in an IEEE standard. However, there is still scope for further research and refinements to the technique and its implementation are still possible. FSV, as defined in the standard IEEE Std 1597.1, is built around the Fourier Transform, and the Fast Fourier Transform (FFT) is assumed to be the implementation of choice. When testing an implementation of the FFT it was found that the inverse of the transform differed from the original real signal by a small amount, and this was revealed by small imaginary components of the order of 10^{-15}. This was inferred to be numerical noise. The Standard does not discuss numerical noise, and for most signals such noise is irrelevant. However, when dealing with small signals or transients this becomes important, because there will be significant proportions of the data where the signal will be at or near zero. When the FSV components are calculated in dBs the constituent ratios will depend on two small and potentially pseudo-random numbers which then may lead to a false and potentially large component of FSV. Using the linearity property of the Fourier Transform, an approximation to this numerical error is obtained and this noise is then subtracted to provide a closer approximation to the ideal transform. This paper discusses the use of this approach for various classes of signal and the paper discusses implications for the reliability of the FSV results.

Study of Transient Phenomena with Feature Selective Validation Method

R. Jauregui[1] **J. Rojas-Mora**[2], **and F. Silva**[1]

[1]Universitat Politècnica de Catalunya, Spain
[2]University of Barcelona, Spain

Abstract— The increase in computer simulation and electromagnetic modeling to analyze complex problems has led to more stringent validation requirements [1]. The feature Selective Validation Method (FSV) [2] is currently one of the most widely used and offers significant advantages when computational electro-magnetics results are compared [3].

Despite all the benefits offered by the FSV in the validation processes is has been observed in previous studies that there may be some problems when trying to use it in transient signals [4]. To overcome these drawbacks and to make a correct validation of transient signals was an ingenious solution proposed [5].

The solution is to split the signal to be analyzed in three different sectors and assign a specific weight to each of them. The first stage (pre-transient) is defined from $t = 0$ to the transient event. The second stage (transient) is defined as a transitory event itself, up to the point where the energy has fallen to a predefined limit. Finally, the third stage is defined from the end of the last stage (transient) to the end of the signal. The only problem is that not all transients are equal, so the biggest problem that arises in this new technique is the assignment of weights in each event for different types of transients.

This paper presents an analysis of different configurations on the weight of FSV for nine types of transients (Table 1). Transients were chosen in order to bring the method to the most extreme situation possible. Specifically, the study focuses on analyzing four different FSV configurations:

1- **FSV**. In this configuration, the FSV was used without applying any variation, in other words, the traditional FSV method [11].
2- **FSV-DC**. In this case, an offset was applied to both signals in order to correct the errors caused by the OMD indicator.
3- **FSV-events**. In this case, the transient is divided into three regions or events, "pre-event", "event" and "post-event". Subsequently, the FSV is calculated and assigned a fixed weight for each "event". The main problem with this technique is that the weight is assigned regardless of the type of transient being analyzed.
4- **FSV-events 2**. This case is similar to the "FSV-events", with the only difference that the weights vary depending on the characteristics of the transients. This method seems to be the most appropriate and closest to the expert opinion.

Finally, to consolidate these results we surveyed the expert within the field (Figure 1). This allowed the results to be even closer to the visual perception of the experts. The results showed the importance of defining the proper weight on each transient area for proper analysis.

REFERENCES

1. Drozd, A. L., "Selected methods for validating computational electromagnetic modeling techniques," *2005 International Symposium on Electromagnetic Compatibility, EMC 2005*, Vol. 1, 301–306, 2005.
2. Duffy, A. P., A. J. Martin, A. Orlandi, G. Antonini, T. M. Benson, and M. S. Woolfson, "Feature selective validation (FSV) for validation of computational electromagnetics (CEM). Part I — The FSV method," *IEEE Transactions on Electromagnetic Compatibility*, Vol. 48, 449–459, 2006.
3. Coleby, D. E. and A. P. Duffy, "Analysis of techniques to compare complex data sets," the current issue and full text archive of this journal is available, Vol. 21, 540–553, 2002.
4. Jauregui, R., P. J. Riu, and F. Silva, "Transient FDTD simulation validation," *Signals*, 257–262, 2010.
5. Telleria, R. J., F. Silva, A. Orlandi, H. Sasse, and A. Duffy, "Factors influencing the successful validation of transient phenomenon modelling," *Asia-Pacific Electromagnetic Compatibility Symposium and Technical Exhibition*, 2–5, Beijing, 2010.
6. University of L'Aquila EMC Laboratory (http://ing.univaq.it/uaqemc/FSV_4_0_3L/), "FSV 4.0.".

Performance Improvement of FSV in a Special Situation

Gang Zhang[1], **Lixin Wang**[1], **and Alistair Duffy**[2]

[1]School of Electrical Engineering and Automation, Harbin Institute of Technology, Harbin, China
[2]Department of Engineering, De Montfort University, Leicester, UK

Abstract— As the Feature Selective Validation (FSV) technique is becoming a dominant quantitative validation method of computational electromagnetic simulation results. Some studies have been undertaken, and subsequent enhancements made, to improve its performance. For example, the offset difference measure (ODM), as an important improvement, has been introduced to reflect the level of DC difference between two sets of results. This paper illustrates a situation in which the FSV results do not agree with expectation: data sets consist of high transient event and relative low pre-transient and post-transient regions. This situation has been discussed in several papers, and solutions have been proposed to improve the performance of FSV. For instance, it could be solved by offsetting the original data to one half plane and changing the weight of the transient event in the FSV results. However, further studies are still necessary to reveal the root of these two issues and solve them thoroughly. In this paper, reasons for this discrepancy are discussed in detail through an exemplification. It is shown that the relative difference of DC components between data sets may be significant, although the absolute value of that could be ignored compared with the other components. As a result, the value of the ODM becomes unreasonable, and then ADM and GDM are influenced. The paper then presents a modification to ODM in order to avoid this apparent error without any pre-processing to original data sets. In addition, the influence of the modification on the validation results, when FSV applied to other data sets, is also discussed. It is finally shown that the modified FSV method could avoid the error and has no influence on the comparing of other data sets.

Antenna Siting Sensitivity Analysis Using the Feature Selective Validation

Andrew L. Drozd, **Irina Kasperovich**, **Clifford E. Carroll, Jr.**, **and Adrienne A. Croneiser**
ANDRO Computational Solutions, LLC Beeches Professional Campus, Rome, NY 13440-2067, USA

Abstract— This topic illustrates the use of the Feature Selective Validation (FSV) technique to perform antenna siting for a complex geometry. The FSV is based on the *IEEE 1597.1 Standard for the Validation of CEM Computer Modeling and Simulations*. It is used to analyze various antenna configurations in order to optimize both radiator performance and electromagnetic compatibility (EMC) for complex geometry installations. In this topic the results of a limited sensitivity study are presented to identify the best placement of a simple dipole antenna in the vicinity of a canonical mounting plate structure. The FSV facilitates comparisons between sets of electromagnetic observables to determine the impact of various antenna placements. The results of hybrid moment method and uniform theory of diffraction (MoM/UTD) simulations at high frequencies approaching 1 GHz are compared to the case of a Hertzian half-wave dipole in order to validate results and demonstrate the efficacy of the FSV method. This approach can be used to perform sensitivity analyses for virtually any antenna siting application and for any type of complex system. The method is first illustrated for simple geometries and placements; however, the general FSV method is applicable to any type of problem of geometry of varying complexity.

Session 3A8
Extended/Unconventional Electromagnetic Theory, EHD(Electro-hydrodynamics)/EMHD(Electro-magneto-hydrodynamics), and Electro-biology

Supplement on the Non-constancy of Speed of Light in Vacuum for Different Galilean Reference Systems

Namik Yener
Technical Education Faculty, Kocaeli University
Umuttepe Campus, 41380 Izmit, Kocaeli, Turkey

Abstract— The objective of the paper is to make rigorous a development that was presented in a previous article. In particular we want to justify the steps of that development that led to negation of Special Relativity Theory. In that article, a simple medium with loss (medium (I), to which is attached a frame K) was considered interfaced by a perfect electric conductor filling a half space (medium (II), to which is attached a frame K') that is in uniform rectilinear motion with respect to medium (I). It is noted that the result obtained by taking the difference of dispersion relations for incident and reflected waves is actually a simultaneous solution of the two dispersion relations for frequency ω' and wave number k_1'. It is indicated that because of the loss in the medium, the solution set (ω', k_1') is non-zero and a relation exists to falsify the Special Relativity Theory. When the loss is nullified, the only simultaneous solution of the two dispersion relations becomes the trivial solution $\omega' = k_1' = 0$ and no relation exists to negate the Special Relativity Theory. The relation used to argue against the Special Relativity Theory involves frequency ω' measured from K', v the speed of K' with respect to K, speed of light in vacuum c and the constitutive parameters of medium (I); ε_1, μ_1, σ_1. It is thus shown that c depends on frequency and by rewriting the said relation employing an expression for ω' in terms of v, c and the incident wave parameters, it is shown at c depends on v too. Alternatively the solution for k_1' is used in a similar manner and it is demonstrated that this expression can also be used to falsify the Special Relativity Theory.

Permittivity of Vacuum and Speed of Light in Vacuum which Vary with Relative Speeds of Media in Uniform Rectilinear Motion with Respect to Each Other

Namik Yener
Technical Education Faculty, Umuttepe Campus, Kocaeli University
Izmit 41380, Kocaeli, Turkey

Abstract— Having determined in a series of articles that the principle of constancy of speed of light in vacuum of the Special Relativity Theory is false and has to be put aside because it cannot account for the loss in one of the two media which are in uniform rectilinear motion with respect to each other, it has become necessary to use different speeds of light in vacuum for different Galilean reference systems. In this paper this is demonstrated again by obtaining of a relation that relates the speed of light in vacuum c, constitutive parameters of the medium, frequency and the speeds of two media in uniform rectilinear motion with respect to each other. This in turn necessitates the revision of the concept of the permittivity of vacuum for different Galilean reference systems. Therefore first we determine the speed of light in vacuum for one of the two moving media, and define the permittivity of vacuum for that medium using the speed of light in vacuum found for that medium. We assume the permeability of vacuum is an invariant quantity given as $\mu_0 = 4\pi \times 10^{-7}$ [H/m]. The same procedure is repeated also for the second medium. The two media which are in relative motion with respect to each other and which are taken up in this paper, are a simple medium with loss and a perfectly conducting medium filling a half space. Their interface is an infinite plane perpendicular to the direction of the uniform rectilinear motion of the second medium which is constituted of the perfectly conducting half space. For simplicity we have assumed the incident wave that impinges on the interface has a wave vector that makes an angle of $\theta = \pi/2$ with the direction of the velocity of the moving medium and hence we can make use of the time dilation formula to transform the frequencies between the Galilean reference systems. The permittivity of vacuum and speed of light in vacuum results obtained are particular to this electromagnetic system.

Reconstruction of Tumors in Human Livers by Magnetic Resonance Imaging

J. Mikulka[1], **E. Gescheidtova**[1], **P. Fiala**[1], **and K. Bartusek**[2]

[1]Department of Theoretical and Experimental Electrical Engineering, Brno University of Technology
Kolejni 2906/4, Brno 612 00, Czech Republic
[2]Institute of Scientific Instruments, Academy of Sciences of the Czech Republic
Kralovopolska 147, Brno 612 64, Czech Republic

Abstract— This article deals with three-dimensional reconstruction and visualization of segmented images of human liver with tumors. The source images were observed by standard hospital MR tomography equipment. There were acquired many slices of the liver area in all three planes. There were found the segmentation methods based on level set approach with many advantages. The resultant boundaries found by these methods are closed curves and bounds the whole tumor. The segmentation consists of automated processing of each slice. The found boundaries are consequently used for 3D image creation and the liver tumor is visualized in Matlab environment. The volume of the tumor is calculated and compared with the results of volume evaluation after manual boundary tracing. The algorithms are prepared for implementation to C++ application for medical usage.

REFERENCES

1. Li, C., C. Xu, C. Gui, and M. D. Fox, "Level set evolution without re-initialization: A new variational formulation," *Proceedings of the 2005 IEEE Computer Society Conference on Computer Vision and Pattern Recognition CVPR'05*, 430–436, San Diego, USA, IEEE Computer Society, Washington, DC, USA, 2005, ISBN 0-7695-2372-2.
2. Aubert, G. and P. Kornprobst, *Mathematical Problems in Image Processing: Partial Differential Equations and the Calculus of Variations*, 2nd Edition, 377, Springer Science + Business Media, LLC, New York, 2006, ISBN 0-387-32200-0.
3. Mikulka, J., E. Gescheidtova, and K. Bartusek, "Processing of MR slices of human liver for volumetry," *PIERS Proceedings*, 202–204, Xi'an, China, March 22–26, 2010.

C-ring Metamaterial in Close Field

R. Kubásek, **P. Drexler**, **P. Fiala**, **and K. Bartušek**
Department of Theoretical and Experimental Electrical Engineering
Brno University of Technology, Kolejní 2906/4, Brno 612 00, Czech Republic

Abstract— In the complicated material structure for the micro-wave application (tensor and composite character) is its material properties study by classical single frequency methods connected with a difficulty [1]. In boundary changes with the size close to wave-length can occurs fake information about the examined objects [2]. One possible way to suppress the negative sources of signals is use of wide-band signals, as white noise, and study absorption in the examined material.

The article describe c-ring metamaterial in close electro-magnetic field response in frequency domain. Experiment measurement show its properties around resonator frequency assembled in close field of antennas. The metrology method for metamaterial study in the frequency range about 100 MHz to 10 GHz is present. Also some simulation and time characteristic will be shown.

ACKNOWLEDGMENT

This work was supported within the project of the Grant Agency of the Czech Republic No. 102/09/0314.

REFERENCES

1. Maslovski, S., S. Tretyakov, and P. Alitalo, "Near-field enhancement and imaging in double planar polariton-resonant structures," *J. Appl. Phys.*, Vol. 96, 1293, 2004.
2. Freire, M. and R. Marques, "Near-field imaging in the megahertz range by strongly coupled magnetoinductive surfaces: Experiment and ab initio analysis," *J. Appl. Phys.*, Vol. 100, 063105, 2006.
3. Machac, J., P. Protiva, and J. Zehentner, "Isotropic Epsilon-Negative Particles," *2007 IEEE MTT-S Int. Microwave Symp. Dig.*, TH4D-03, Honolulu, USA, June 2007.

Sensors and Experimental Model Development for PD Localization in HV Transformers

P. Drexler, **P. Fiala**, **M. Friedl**, **P. Marcon**, **M. Steinbauer**, **and Z. Szabo**
Department of Theoretical and Experimental Electrical Engineering
Brno University of Technology, Kolejni 2906/4, Brno 612 00, Czech Republic

Abstract— One of the problematic phenomena in the field of high-voltage technology, is the occurrence of partial discharge. Several other effects have combined with this notion over time [1]. In consequence of these effects there emerge short electromagnetic pulses with a defined and measurable spectre in the characteristic frequency band [2]. The group of end products attributable to the emergence of interfering signals involves, for example, displacement current in a dielectric, pulse current on the interface between dielectrics, or the dielectric/metal interface owing to high electric field intensity and structure of the dielectric.

In HV and VHV transformers the dielectric is mineral or synthetic oil. Due to the increase in partial discharge activity in transformer oil free atoms of carbon, hydrogen and oxygen develop from hydrocarbons, and there also generates a certain percentage of water and other organic compounds. All of these elements decrease the quality of the dielectric. In addition to that, rapid increase in pulse activity may cause the formation of a hazardous explosive compound of oxygen and hydrogen. Then, this situation may result in explosion and damage to the device.

In order to prevent the transformer failure the observation of pulse activity is necessary. The occurrence of discharge with substantial charge transport level can be localized in critical areas of the transformers. Having a possibility to localize the increased discharge activity in some of the critical areas allows us to undertake precautions in order to avoid the critical transformer failure. The discharge activity localization can be determined on the basis of processing of signals from suitable installed sensors. The evaluation of the discharge location utilizes the model of wave propagation inside the transformer, which has been presented in early work [3].

For the experimental verification of localization method a model setup has been built, Fig. 1. The model setup is equipped with antenna sensors, RF amplifiers and data acquisition unit. The model setup is described in the paper as a following step of the research. The result of the measurement which has been performed up to the present are presented also.

ACKNOWLEDGMENT

The research described in the paper was financially supported by FRVS (a fund of university development) by research plan No. MSM 0021630513 ELCOM, No. MSM 0021630516, grant of Czech ministry of industry and trade No. FR-TI1/001, GACR 102/09/0314 and project of the BUT Grant Agency FEKT-S-10-13.

REFERENCES

1. Fiala, P., "Transformer partial discharge modeling, minimal breakdown value set in a critical parts of transformer design," Research Report, Laboratory of Modeling and Optimization Field in Electromagnetic Systems, FEI VUT and ABB EJF a.s. Brno no.2/99, 18.3.1999, Brno, Czech Republic, 1999.
2. Sarathi, R., A. J. Reid, and M. D. Judd, "Partial discharge study in transformer oil due to particle movement under DC voltage using the UHF technique," *Electric Power Systems Research*, Vol. 78, 1819–1825, Elsevier, 2008.
3. Fiala, P., T. Jirku, P. Drexler, and P. Dohnal, "Detection of partial discharge inside of hv transformer, modeling, sensors and measurement," *Progress In Electromagnetics Research Symposium Proceedings*, 1013–1016, Cambridge, USA, July 5–8, 2010.

Comparison of Different Methods for Measurement of Shielding Fabrics Properties

Z. Szabó
Department of Theoretical and Experimental Electrical Engineering
Brno University of Technology, Kolejní 2906/4, Brno 612 00, Czech Republic

Abstract— Shielding is a very popular method of ensuring electromagnetic compatibility and of protecting electronic and electrical equipment and human beings against radiated electromagnetic energy. The suitable alternative to the classical shielding materials can be special shielding-fabrics. The main advantages of these fabrics are their low weight, flexibility and their easy processability The knowledge of shielding effects of different types of material represents a basic prerequisite for further development and implementation of shielding devices. Measuring shielding and absorption qualities of fabrics materials is relatively difficult. There were developed many measuring methods that are used in various laboratories to solve these problems. A lot of producers who develop this type of fabrics are searching for relatively simple, not time-consuming and reliable measuring methods to measure shielding and absorption qualities which operate in a wide frequency range. This paper presents a comparison results from two different methods for measuring shielding and absorption qualities shielding fabrics.

ACKNOWLEDGMENT

The research described in the paper was financially supported by the research program MSM 0021630516 and research plan MSM 0021630513, Ministry of Defence of the CR, Ministry of Industry and Trade of the CR (Diagnostics of Superfast Objects for Safety Testing, FR-TI1/368), Czech Science Foundation (102/09/0314) and project of the BUT Grant Agency FEKT-S-10-13.

REFERENCES

1. Donohoe, J. P., J. Xu, and C. U. Pittman, Jr., "Variability of dual TEM cell shielding effectiveness measurements for vapor grown carbon nanofiber/vinyl ester composites," *International Symposium on Electromagnetic Compatibility 2005, EMC 2005*, 2005.
2. Pocai, M. R. and E. Bottari, "Electromagnetic characterization of protective clothing," *International Symposium on Electromagnetic Compatibility*, Tokyo, May 17–21, 1999.
3. Wilson, P. F. and M. T. Ma, "Techniques for measuring the electromagnetic shielding effectiveness of materials: Part 11 — Near-field source simulation," *IEEE Transactions on Electromagnetic Compatibility*, Vol. 30, No. 3, Part 2, 251–259, Aug. 1988.
4. Wilson, P. F. and M. T. Ma, "Techniques for measuring the electromagnetic shielding effectiveness of materials. I. Far-field source simulation," *IEEE Transactions on Electromagnetic Compatibility*, Vol. 30, No. 3, Part 2, 239–250, Aug. 1988.
5. Szabó, Z. and P. Fiala, "Characterisation and testing shielding fabrics," *PIERS Online*, Vol. 5, No. 7, 609–612, 2009.

Propagation of Electromagnetic Wave in Layered Heterogeneous Medium

R. Kadlec, **E. Kroutilová**, **D. Nespŏr**, **and P. Fiala**
Department of Theoretical and Experimental Electrical Engineering
Brno University of Technology, Kolejní 2906/4, Brno 612 00, Czech Republic

Abstract— The paper presents the problem of numerical modelling of high frequency electromagnetic (EM) waves propagation in inhomogeneous materials. For this method, a numerical model was prepared. The model was created in the MatLab. For a layered heterogeneous medium, an algorithm was prepared for the reflection on several layers in MatLab program environment. Reflection and refraction in many directions on heterogenous material are solved by means of the numerical method. Central in this respect are the refractions and reflections on the boundary of materials with different properties. This method is suitable for the design application of metamaterials. The deduced algorithm was projected for the wide spectrum of EM wave.

ACKNOWLEDGMENT

The research described in the paper was financially supported by the research program MSM 0021630516 and research plan MSM 0021630513, Ministry of Defence of the CR, Ministry of Industry and Trade of the CR (Diagnostics of Superfast Objects for Safety Testing, FR-TI1/368), Czech Science Foundation (102/09/0314) and project of the BUT Grant Agency FEKT-S-10-13.

REFERENCES

1. Stratton, J. A., *Teorie elektromagnetického pole*, STNL, Praha, 1961.
2. Dedek, L. and J. Dedková, *Elektromagnetismus*, Vol. 2, 232, VITIUM, Brno, 2000, ISBN 80-214-1548-7.
3. Orfanidis, S., *Electromagnetic Waves and Antennas*, 1031, 2008. Available: www.ece.rutgers.edu/ orfanidi/ewa.
4. Moss, C., "Numerical metods for electromagnetic wave propagation and scattering in comlex media," 240, 2004. Available: http://portal.acm.org/citation.cfm?id=1023429.
5. Nešpor, D., "Electromagnetic wave propagation study in heterogeneous structures," 20, Supervisor Doc. Ing. Pavel Fiala, Ph.D., 2009.
6. Jin, G. A., "Survey of Radiosity and ray-tracing methods in global illumination," Institute for Computer Graphics [online], 2000. Available: http://www.icg.seas.gwu.edu/cs367/global.pdf.
7. Fiala, P., "Finite element method analysis of a magnetic field inside a microwave pulsed generator," *2nd European Symposium on Non-Lethal Weapons*, Ettlingen, SRN, May 13–15, 2003.

Measurement of Concentration and Water Flow

M. Friedl, **P. Fiala**, **P. Marcon**, **and R. Kubasek**
Department of Theoretical and Experimental Electrical Engineering
Brno University of Technology, Kolejni 2906/4, Brno 612 00, Czech Republic

Abstract— This article deals about non-destructive measuring the water concentration and its movement in the tissues of tree structures. Measurement method is based on changes in impedance sensor monitoring or to monitor changes in the resonant frequency of the sensor in a porous material. Water flow and its concentration affect the sensor permittivity, and thus changing its impedance. Sensor selection was based on experimental measurement in anechoic chamber at DTEE.

The following measurements were aimed at measuring water flow in the tube. The sensor was placed on the outside of the tube and connected with a vector analyzer. The impedance of sensor was measured in the range from 100 Hz to 40 MHz. The measurement was done in outdoor environment. The tube was fixed one location during measurement and impedance value of sensor was recorded during flow water.

The next experimental measurement of water flow was done in dependence on the added magnetic field. The magnetic filed was created by the help of two super magnets. The vertical and horizontal magnetic field to the sensor plane was tested.

Dependence of sensor impedance on the concentration of water in porous materials was measured as a last resort.

ACKNOWLEDGMENT

The research described in the paper was financially supported by FRVS (a fund of university development) by research plan No. MSM 0021630513 ELCOM, No. MSM 0021630516, grant of Czech ministry of industry and trade No. FR-TI1/001, FR-TI1/368, GACR 102/09/0314 and project of the BUT Grant Agency FEKT-S-10-13.

REFERENCES

1. Fluid flow sensors. PRAGUE: CVUT in Prague, 2010 [cit. 2010-05-13]. Available on: <http://measure.feld.cvut.cz/cs/system/files/files/cs/vyuka/predmety/x38ssd/07_Prutok.pdf>.
2. Measuring of fluid concentration by the help of electric conductivity. PRAGUE: VSCHT in Prague, 2010 [cit. 2010-05-13]. Available on <http://www.vscht.cz/ufmt/cs/pomucky/machacj/docs/E3-Elektricka%20vodivost%20kapalin.pdf>.
3. Bode 100 [online]. 2010 [cit. 2010-05-12]. OMICRON-LAB. Available on: <http://www.omicron-lab.com/bode-100/measurement-capabilities.html>.

Using Metamaterials as Electromagnetic Lens for MR Tomograph

D. Nespor, **P. Drexler**, **P. Fiala**, **and K. Bartusek**
Department of Theoretical and Experimental Electrical Engineering
Brno University of Technology, Kolejni 2906/4, Brno 612 00, Czech Republic

Abstract— Electromagnetic field is possible to manipulate by means dielectric materials. Electromagnetic field will be affected due to values of dielectric constant ε_r and permeability μ_r Viktor Veselago has defined theoreticaly the usage material with negative parameters (metamaterial) as an electromagnetic lens. If we put metamaterial between transceiver and receiver we can see increase in detected energy. It appears from this that the metamaterial behaves like electromagnetic lens. The subject of this work is construction and optimization of electromagnetic lens for mid-field MR tomograph. Principles of lens construction are in [1–3]. Paper contains analytic calculations of basic design of the lens and numerical calculations of the optimized lens.

The lens was constructed as periodic structure of single split ring resonators [1, 2]. A negative effective permeability μ_r can be imposed on this structure. If we will put several of this structures side-by-side, we can to obtain a negative effective permittivity ε_r. The main problem is to set up the resonance frequencies of the resonators. The demand for the metamaterial structure is that the resonators size has to be much smaller then length of electromagnetic wave. The intended application of the designed structure is the increasing of the magnetic resonance (MR) system sensitivity. The frequency of the MR system is 198.75 MHz. But single split resonators for that frequency would be too big. That is why the constructed resonators with resonant frequency about 6 GHz has been modified by means of chip capacitors. There ceramic chip capacitors has been assembled over the interspaces [1, 4]. But this solution is inconvenient in many aspects. The main inconveniency is the inaccuracy of capacitors and soldered pads. Next inconveniency is the need of the surface mount. The spiral resonator design is described in the next part of this paper. This design was created with Comsol software. Spiral resonators are possible to manufacture as a planar types without the external component assembly. That is the main advantage of these resonators.

ACKNOWLEDGMENT

The work described in the paper was financially supported by the research project GA102/09/0314, research plan MSM 0021630513 and project of the BUT Grant Agency FEKT-S-10-13.

REFERENCES

1. Manuel, J., L. Jelinek, and R. Marques, "On the application of $\mu = -1$ metamaterial lences for magnetic resonance imaging," Departamento de Electronica y Electromagnetismo, Universidad de Sevilla.
2. Marqués, R., F. Martín, and M. Sorolla, *Metamaterials with Negative Parameters*, John Wiley & Sons, Inc., ISBN 2007017343, Hoboken, New Jersey, Rok, 2007.
3. Caloz, C. and T. Itoh, *Electromagnetic Metamaterials: Transmission Line Theory and Microwave Applications*, John Wiley & Sons, Inc., Hoboken, New Jersey, Rok, 2006, ISBN 2005048976.
4. Bartusek, K., P. Drexler, P. Fiala, R. Kadlec, and R. Kubasek, "Magnetoinductive lens for experimental mid-field MR tomography," *Progress In Electromagnetics Research Symposium Proceedings*, 1047–1050, Cambridge, USA, July 5–8, 2010.

The Design of High-impedance and High-voltage Input Amplifier for Measurement of Electropotentials on Solid-liquid Phase Boundary

Z. Roubal[1], **Z. Szabó**[1], **M. Steinbauer**[1], **D. Heger**[2], **and R. Kubásek**[1]

[1]Department of Theoretical and Experimental Electrical Engineering, Brno University of Technology
Kolejní 2906/4, Brno 612 00, Czech Republic
[2]Department of Chemistry, Faculty of Science, Masaryk University
Kamenice 5/A8, Brno 625 00, Czech Republic

Abstract— On interface of solid-liquid phases of water solutions some electric potential occurs during freezing process, caused by separation of ions from solid phase. Whenever freezing is often used for preservation of biological samples, the influence of electric field induced by this process to biological samples is the subject of investigation. For this purpose, we need some facility and measurement device to measure this potential.

In this paper will be analyze the design of electrometric amplifier for measurement of voltage of order 10^2 Volts. Because the measured source has very high inner resistance and low capacity, the input resistance of amplifier must be greater then $10^{14}\,\Omega$ with negligible parallel capacity. For the same reason, using the input voltage divider is problematic. Such high input impedance can be achieved only when using active shielding and special input amplifier. Standard OA has measurement range about $\pm 10\,\mathrm{V}$. For expansion of this range without using input voltage divider is necessary to use voltage shifting for OA power supply. The circuit with floating supplies is susceptible to oscillation without right frequency corrections. Proposed electrometric amplifier with high voltage input range will be simulated using Spice.

ACKNOWLEDGMENT

The work described in the paper was financially supported by the research project GA102/09/0314, research plan MSM 0021630513 and project of the BUT Grant Agency FEKT-S-10-13.

REFERENCES

1. Robinson, C., C. S. Boxe, M. I. Guzmán, A. J. Colussi, and M. R. Hoffmann, "Acidity of frozen electrolyte solutions," *J. Phys. Chem. B*, Vol. 110, No. 15, 7613–7616, 2006.
2. Parameswaran, V. R. (Sivan), C. R. Burn, A. Profir, and Q. Ngo, "A note on electrical freezing and shorting potentials," *Cold Regions Science and Technology*, Vol. 41, No. 2, 83–89, 2005.
3. *Low Level Measurements Handbook: Precision DC Current, Voltage, and Resistance Measurements*, 6th Edition, Keithley Instruments, Inc., Cleveland, Ohio, 2004.

Session 3A9
Poster Session 5

Analytical Expressions of Diffraction' Free Beams Obtained by Diffraction on an Opaque Disk

Q. Huang[1, 2], **S. Coëtmellec**[1], **A. Louis**[3], **F. Duval**[3], **H. Leblond**[4], **and M. Brunel**[1]

[1]UMR 6614 CORIA CNRS, Université de Rouen, France
[2]Xidian University, Xi'an, China
[3]IRSEEM, ESIGELEC, Saint-Etienne du Rouvray, France
[4]LΦA EA 4464, Université d'Angers, France

Abstract— We establish approached analytical expressions that demonstrate that the beam produced after diffraction of a gaussian beam by an opaque disk and collimation by a lens can be described by a diffraction-free J_0 Bessel function. We further demonstrate that a similar analytical expression can be established in the case of femtosecond incident pulses.

Diffraction-free beams have attracted much attention since pioneer work of Durnin and coworkers [1]. Different beam-shaping techniques exist. Most well-known are based on the use of an annular aperture, a computer generated-hologram or an axicon. Although an annular aperture induces many losses, the technique based on this element has recovered much interest in view of recent studies involving sub-wavelength apertures. They could indeed allow the design of systems in sub-wavelength optics.

We have recently proposed another method based on the occultation of an incident beam. We could indeed demonstrate that diffraction of a Gaussian beam by an opaque disk leads to the generation of a diverging Bessel'like beam, that can then be collimated with a lens into a diffraction-compensated beam [2]. The simplicity of the method allows its application directly at the output of a pigtailed laser diode. Numerical developments associated to comparisons with experimental results could validate these results. They showed that the beam diffracted by the opaque disk can be expressed as a sum of approximately 20 Bessel functions of odd orders. Unfortunately, these expressions are so complex that they do not allow to establish any simple expression of the diffraction-compensated beam after the collimating lens. Numerical integration is required to obtain correct simulations. In this case, collimation by the lens is expressed numerically using a phase factor and a Fresnel transform.

We present in this communcation a simplest formulation that demonstrates theoretically the diffraction' free nature of the beam that is generated. After some simplifications that are detailed expressly, the beam is shown to be correctly described by a zeroth-order Bessel diffraction-free beam. We further show at his expression can then be generalized to the case of 100 fs incident pulses. We first establish a new expression of the field diffracted by an opaque disk, assuming an incident Gaussian beam. Our method uses in this case the traditional definition of a Green function. Results are compared with experimental results and our previous theoretical developments. The domain of validity of this new approach is discussed. Collimation by the lens is then considered and an expression is established that takes into account the phase factor introduced by the lens, the lens and propagation in free space after the lens. Under assumptions that are discussed, this expression can be much simplified and the beam that is finally obtained is shown to be a non-diffracting zeroth-order Bessel function. Based on these previous developments, we establish then an analytical expression of the diffraction-free beam produced when the incident Continuous Wave (CW) laser is replaced by a femtosecond laser. Finally, those simple analytical relations allow the simple design of systems in different wavelength regions, particularly in the microwave regime, while very long computing times were necessary using previous numerical developments.

REFERENCES

1. Durnin, J., J. J. Miceli, Jr., and J. H. Eberly, *Phys. Rev. Lett.*, Vol. 58, 1499–1501, 1987.
2. Brunel, M. and S. Coëtmellec, *J. Opt. Soc. Am. A*, Vol. 24, 3753–3761, 2007.

Magnetic Photonic Crystal against Optimized Magneto-optical Multilayer — What Is the Best Choice for Visible Spectral Region

V. A. Kotov[1], **M. Vasiliev**[2], **K. Alameh**[2], **V. I. Burkov**[3], **and V. G. Shavrov**[1]

[1]V. A. Kotelnikov Institute of Radio Engineering and Electronics, RAS
11 Mohovaya St., Moscow 125009, Russia
[2]Electron Science Research Institute, Edith Cowan University, Joondalup, WA 6027, Australia
[3]Moscow Institute of Physics and Technology, Dolgoprudny 141700, Russia

Abstract— Since the initial proposal of using magnetic photonic crystals (MPC) in magneto-optical (MO) devices reported back in 1998, there were some hundreds of reports devoted to this topic. At the same time, the problem is still current in the sense that MPCs are still far from being introduced into optical integrated circuits. A question arises immediately — what is the reason for this. The first problem is related to the choice of MO material. Since the discovery of the high Faraday rotation of Bi-substituted iron garnet (BiIG) made in 1969, in the visible spectral region this material remains the best transparent MO material for use in practical applications.

There is a large number of publications predicting the excellent MO properties in different MPC structures in comparison with the modelled performance of single-layer MO devices. The BiIG is extremely transparent in the infrared spectral region (from 1300 up to 5000 nm) but unfortunately, for visible light the absorption coefficient exceeds $1000\,\mathrm{cm}^{-1}$ (at the wavelength of 633 nm) thus preventing the introduction of MPC based on BiIG into practical MO devices.

Unfortunately, most of the calculations of the optical and MO parameters of MPC devices were provided using correct data on Faraday rotation but still assuming zero level of optical absorption. As a result, all attempts to create MO modulators or high-speed displays demonstrated the Faraday rotation of different MPC structures of about 5 deg. at 633 nm or 20 deg. at 780 nm and insufficient optical transmittance. The physical nature of the observed results is related to the fact that the high-quality MO resonator of MPC structure provided a linear growth in the value of Faraday rotation after multiple passes of the light rays inside the resonator, but the absorbed optical power demonstrated an exponential increase. As a result, if the several passes of light beam inside an MPC resonator provided close to 99% absorption losses, the MPC structure showed no real benefit compared to single-layer MO devices.

We provided a calculation of a different MPC structure design and a comparison of the results obtained with the multilayer structures in which the thicknesses of MO material were comparable with that of the MPC structure. We have found that in the intermediate case of moderate optical absorption levels, the optimized multilayers provided a better optical and MO performance compared to the MPC structures. Moreover, the optimized multilayer demonstrated a better design flexibility due to more freedom in the choice of the appropriate optical transmission linewidth compared with the typical MPC structure designs.

Experimental investigations of the optical and MO properties of ultrathin films of BiIG intended for use in MPC structures and in optimized multilayers have been performed. It has been shown that transitional layers with practically zero MO activity located between the substrate and BiIG films existed. The typical thicknesses of such transitional layers forming on the boundary between $Gd_3Ga_5O_{12}$ substrates and BiIG films were near 5 nm, and about 30 nm if glass substrates were used.

Linear and Non Linear Dielectric Properties of a Short Pitch Ferroelectric Liquid Crystal Stabilized by an Anisotropic Polymer Network

J. Hemine[1], **Y. Cherfi**[4], **R. Douali**[2, 5], **J. M. Leblond**[2, 5], **N. Beldjoudi**[4], **and A. Daoudi**[2, 3]

[1]Université Hassan II Mohammedia-Casablanca, LPMC-FSTM, Mohammedia, Morocco
[2]Université Lille Nord de France, F-59000 Lille, France
[3]Université du Littoral Côte d'Opale, UDSMM, F-59140 Dunkerque, France
[4]Université des Sciences et de la Technologie Houari Boumediene, Alger, Algérie
[5]Université du Littoral Côte d'Opale, UDSMM, F-62228 Calais, France

Abstract— Composite materials based liquid crystals (LCs) represent an exciting field of functional materials, providing a large range of applications in display devices. In recent years, polymer stabilized ferroelectric liquid crystals (PSFLCs) have been investigated [1, 2] in order to enhance and to improve their electro-optic and mechanical properties. These materials were obtained by a UV-polymerization process of photo-curable mesogenic monomers initially dissolved in a ferroelectric liquid crystal [3] host The resulted morphology consists on an anisotropic and fibrillar structure of the polymer network dispersed in LC media.

We report in this contribution linear and non linear dielectric measurements [4, 5] on PSFLC systems using a FLC material with a short helical pitch and a high spontaneous polarization. These studies were also completed by structural and ferroelectric characterizations. Physical parameters as the ferroelectric polarization; the twist elastic energy and the rotational viscosity were determined The effect of the polymer network density on these physical parameters is also studied and discussed.

REFERENCES

1. Petit, M., A. Daoudi, M. Ismaili, and J. M. Buisine, *Eur. Phys. J. E*, Vol. 20, 327, 2006.
2. Hikmet, R. A. M., H. M. J. Boots, and M. Michielsen, *Liq. Cryst.*, Vol. 19, 65, 1995.
3. Meyer, R. B., L. Liebert, L. Strzelecki, and P. Keller, *J. Phys. Lett.*, Vol. 36, L69, 1975.
4. Leblond, J. M., R. Douali, C. Legrand, and R. Dabrowski, *Eur. Phys. J. Appl. Phys.*, Vol. 36, 157–163, 2006.
5. Kimura, Y., S. Hara, and R. Hayakawa, *Ferroelectrics*, Vol. 245, 61, 2000.

Electroclinic Effect of Ferroelectric Liquid Crystals Near to N*-SmA-SmC* Multicritical Point by Electro-Optical and Dielectric Spectroscopy

J. Hemine[1], **A. Daoudi**[2, 3], **C. Legrand**[2, 4], **A. El kaaouachi**[5], **A. Nafidi**[5], **and H. T. Nguyen**[6]

[1]LPMC-FSTM, Université Hassan II Mohammedia-Casablanca, Mohammedia, Morocco
[2]Université Lille Nord de France, F-59000 Lille, France
[3]ULCO, UDSMM, F-59140 Dunkerque, France
[4]ULCO, UDSMM, F-62228 Calais, France
[5]Laboratoire de Physique de la Matière Condensée, Faculté des Sciences
Ibnou Zohr, BP 28/S 80000 Agadir, Morocco
[6]CRPP, Université de Bordeaux 1, 33600 Pessac, France

Abstract— We present electro-optic and dynamic properties of three homologous of the same series of ferroelectric liquid crystals (FLCs) exhibiting the chiral smectic C phase (SmC*) [1]. From electro-optic investigations, the tilt angle and spontaneous polarization have been determined as a function of temperature. In the dielectric measurements carried out without a DC bias field, we have studied the soft-mode relaxation mechanism in the SmA phase. From experimental data, we have evaluated the soft mode rotational viscosity and the electroclinic coefficient [2, 3]. The main result is that a relaxation process was observed in the cholesteric phase (N*) phase for two homologues [4] and is interpreted as a soft-mode-like mechanism. This mechanism is related to the appearance of smectic order fluctuations within N* phase, whose amplitude is increased when approaching the SmC*-SmA-N* multicritical point.

REFERENCES

1. Meyer, R. B., L. Liebert, L. Strzelecki, and P. Keller, *J. Phys. Lett.*, Vol. 36, L69, 1975.
2. Garoff, S. and R. B. Meyer, *Phys. Rev. Lett.*, Vol. 38, 848, 1977.
3. Garoff, S. and R. B. Meyer, *Phys. Rev. A*, Vol. 19, 338, 1979.
4. Hemine, J., C. Legrand, A. Daoudi, N. Isaert, and H. T. Nguyen, *Liq. Cryst.*, Vol. 34, 241, 2007.

Rescaled Range Analysis of ELF Natural Electromagnetic Noise from Antarctica

A. Salinas[1], **S. Toledo-Redondo**[1], **J. A. Morente**[2], **J. A. Portí**[2], **E. A. Navarro**[3], **A. Méndez**[1], **J. F. Fornieles**[1], **M. Rodríguez-Sola**[2], **N. Novas**[4], **J. A. Gázquez**[4], **and R. García-Salvador**[4]

[1]Department of Electromagnetism and Matter Physics, University of Granada, Granada 18071, Spain
[2]Department of Applied Physics, University of Granada, Granada 18071, Spain
[3]Department of Applied Physics, University of Valencia, Burjassot, Valencia 46100, Spain
[4]Department of Computer Architecture and Electronics, University of Almería
La Cañada de San Urbano 04120, Almería, Spain

Abstract— We present the results of a statistical rescaled range (R/S) analysis of natural electromagnetic noise in the extremely low frequency (ELF) band. The Hurst exponent was derived from the records of two horizontal magnetic antennas taken in Antarctica with a sample frequency of 512 Hz, to guarantee enough resolution with the small number of samples in the analysis. The study shows that ELF radio noise is a persistent random process, maintaining its value between 0.75 and 0.85 for the different series analyzed. A numerical simulation was performed, in which each discharge was modeled by the radiated field of a wire antenna excited by a Gaussian pulse, demonstrating a way of inferring lightning rates from R/S analysis.

Study of Plasma Breakdown Located in Apertures to Shield Electronic Components inside Cavities

R. Klein[1], **A. Hamiaz**[2], **X. Ferrieres**[1], **O. Pascal**[2], **and J. P. Boeuf**[2]

[1]DEMR, ONERA, 2 Avenue Edouard Belin, Toulouse 31055, France
[2]LAPLACE, 118 route de Narbonne, 31062 Toulouse CEDEX 9, France

Abstract— Plasma physics has recently a significant expansion in the electromagnetism domain to define metamaterials, virtual antennas, ... In this paper, we are interested to the use of plasma to shield a system illuminated by a high powered microwave source. More exactly, the system is defined as a metallic cavity having a small aperture and different electronic components inside it. To avoid dammages on the components, we suggest to use a plasma material confined in a dielectric vessel located on the aperture. Indeed, the intense electromagnetic field can induce a breakdown and initiate a plasma. The incident wave is then reflected when the plasma density reaches a critical value for which $\omega_p \sim \omega$ where ω_p is the plasma frequency and ω the incident wave frequency [1].

Our goal is to study how the plasma reacts with the incident wave and evaluate the shielding efficiency. For this purpose, we describe the mathematical model introduced for the plasma dynamics and its coupling with the Maxwell equations. This model is then solved using a FDTD approximation in the 2D case. In this approximation, the unknowns linked to the plasma parameters are introduced in the classical Yee's scheme [2]. The results obtained on different configurations show that it is necessary to use a very sharp spatial mesh ($\sim \lambda/300$) in order to describe accurately the evolution of the plasma density. This spatial sharpness also induces a small time step to satisfy the CFL condition on the Maxwell equations. For example, the size of the computation domain is 900×900 in our simulations, and the number of iterations is about 10^7. To achieve this kind of computation, it is necessary to use a parallel version software. However, even using parallel software, the time of computation stays important. If we want to implement 3D computations of this method, the time computation would be several days. The plasma density being located in space, it is interesting to consider a FVTD method [3] in order to improve the computation efficiency. Indeed, this method allows one to have a local mesh refinement and a local time stepping strategy which reduces the cell number of the mesh and the time iteration number. To evaluate this solution, we have developped a 2D FVTD approach taking into account the physical model.

To illustrate the shielding effect of the plasma, we present results obtained with the FDTD and FVTD methods on a $3\lambda \times 3\lambda$ cavity and for a simulation duration of 50 ns.

This study shows that using a plasma seems to be an efficient way for shielding microwave radiations.

REFERENCES

1. Boeuf, J. P., B. Chaudhury, and G. Q. Zhu, "Theory and modelling of self-organization and propagation of filamentary plasma arrays in microwave breakdown at atmospheric pressure," *Phys. Rev. Lett.*, Vol. 104, 015002, 2010.
2. Yee, K. S., "Numerical solution of initial boundary value problems involving maxwell's equations in isotropic media," *IEEE Transactions on Antennas and Propagation*, Vol. 14, No. 3, 302–307, 1966.
3. Bonnet, P., X. Ferrieres, F. Issac, F. Paladian, J. Grando, J. C. Alliot, and J. Fontaine, "Numerical modeling of scattering problems using a time domain finite volume method," *Journal of Electromagnetic Waves and Applications*, Vol. 11, No. 8, 1165–1189, 1997.

Modelling of the Micro Plasma Discharges to Control the Electromagnetic Wave Propagation in Printed Microwaves Circuits

Mohamad Almustafa, **Jacque David**, **and Thân-Hôa Vuong**
Université de Toulouse; INPT, UPS; LAPLACE; ENSEEIHT
2 rue Charles Camichel, BP 7122 Toulouse cedex 7, France

Abstract— A theoretical and practical study to use micro electric discharges in microwave systems is presented. The interest of the electric discharge creation in microstrip circuit is discussed by introducing a microwave printed circuit with a couple of millimetre discharge [1] as a microwave switch in which plasmas play the role of a conducting material. The electric discharge to create plasma is obtained by planar electrodes which make a party from the circuit itself. The gas used is the Argon under low pressures, about 200 torr. Some physical characteristics of this gas are shown in order to see the impact of the physical conditions accompanying by this gas such as the pressure on the electromagnetic wave propagation. A parameter, very important to specify the behaviour of plasma, is the electron density n_e on which the plasma frequency depends directly. The used plasma was created on the circuit board, and the last one was put inside a bell made of glass. Thus we did not use a discharge tube but plat electrodes.

Micro discharge areas on printed microwave circuits are modelled by two different ways, analogue method that depends on discharge current value and transmission coefficient value to find out the plasma equivalent electrical circuit. By using the experimental data, we find a simple electric model of the micro discharge area. The second method uses Drude Model [2, 6] to model plasmas then we study the interaction between plasmas and electromagnetic waves. Some features of those two methods are mentioned to see the difference between them.

Depending on the 2nd method that allows to model complex plasma structures and to achieve numerical simulations by using various methods such as the finite element method [3], we present the effect of the plasma electron density to control the electromagnetic wave propagation by two ways, using the transmission coefficient and the electromagnetic field. When we lunch an electromagnetic wave from the input of microwave circuit towards its output, we can see that the transmitted signal depends on the signal frequency, in other words, we observe three cases; reflection, absorption and reflection of the waves. Plasma plays a flexible role; it is for that it is exploitable for the design of the smart antennas [4] or in general for the plasma antennas [5]. Plasma can also be used to manufacture RF filters, micro switches and to tune resonant cavity structures.

REFERENCES

1. Sakai, O. and K. Tachibana, "Dynamic control of propagating electromagnetic waves using tailored millimeter plasmas on microstrip structures," *IEEE Transactions on Plasma Science*, Vol. 34, No. 1, February 2006.
2. Eleftheriades, G. V. and K. G. Balmain, *Negative-refraction Metamaterials Fundamental Principles and Applications*, Wiley, USA, 2005.
3. Booton, R. C., *Computational Methods for Electromagnetics and Microwaves*, Wiley, USA, 1992.
4. Chanc, K., *Smart Antennas*, Wiley, USA, 2003.
5. Kumar, R. and D. Bora, "A reconfigurable plasma antenna," *Journal of Applied Physics*, Vol. 107, 053303, 2010.
6. Raizer, Y. P., *Gas Discharge Physics*, Berlin, Germany, Springer, 1987.

Band Structure in One-dimensional Aperiodic Structures with Left-handed Materials

X. I. Saldaña
Instituto de Física, Universidad Autónoma de Puebla, Apartado Postal J-48, Puebla 72570, México

Abstract— Structures with left-handed materials LHM where the dielectric permittivity ε and the magnetic permeability μ are simultaneously negative have been the focus of attention in the past decades. The properties of these materials where first described by V. Veselago [1, 2] in 1968. In particular, the band structures of one-dimensional periodic multilayers including LHM have been recently studied by D. Bria et al. [3]. They show that these structures exhibit new types of electromagnetic modes which do not exist in superlattices composed only with right-handed materials RHM. In this work, it is presented a theoretical study of the photonic band of one-dimensional aperiodic structures constructed considering bilayer units AB with layer A characterized by refractive n_a and thickness d_a and layer B being a left-handed material whose thickness is modulated by an aperiodic sequence following a recurrence relation $P_j = \{P_{j-1}\}\&\{P_{j-1}+1\}$ with $P_0 = 0$. $j = 1, 2, \ldots$ is the generation number of the aperiodic sequence [4]. It is observed that the band structure shows electromagnetic modes below the light line corresponding to materials A y B not found in structures formed only with right-handed materials. If ε and μ are constant and both negative, the band diagram presents autosimilarity. Finally, it is presented a discussion of the band gaps when the average of the refractive index is zero. For this calculation it is used the transfer matrix method and the rational approximation [5, 6]. The possibility to construct multilayer structures including LHM with the available technologies [7], makes these new aperiodic structures potentially useful for new technological applications.

REFERENCES

1. Veselago, V. G., *Usp. Fiz. Nauk*, Vol. 92, 517, 1967.
2. Veselago, V. G., *Sov. Phys. Usp.*, Vol. 10, 509, 1968.
3. Bria, D., B. Djafari-Rouhani, A. Akjouj, L. Dobrzynski, J. P. Vigneron, E. H. El Boudouti, and A. Nougaoui, *Phys. Rev. E*, Vol. 69, 066613, 2004.
4. Saldaña, X. I., E. López-Cruz, and D. A. Contreras-Solorio, *J. Phys.: Condens. Matte.*, Vol. 21, 155403, 2009.
5. Yeh, P., *Optical Waves in Layered Media*, Wiley-Interscience, New York, 1988.
6. Hawrylak, P., G. Eliasson, and J. Quinn, *Phys. Rev. B*, Vol. 36, 6501, 1987.
7. Lugo, J. E., B. de la Mora, R. Roti, R. Nava, J. Tagueña, A. del Río, and J. Faubert, *Optics Express*, Vol. 17, 3043, 2009.

Hybrid Method to Compute the Magnetic Field in Bird Cage Coil for a Magnetic Resonance Imaging System

N. Benyahia[1], **and M. E. Latreche**[2]

[1]Department of Electrical Engineering, University of Biskra, Algeria
[2]Department of Electro technical, University of Constantine, Algeria

Abstract— Radio frequency (RF) coils, are key components in a magnetic resonance imaging (MRI) system. They serve two purposes. The first is to generated RF pulse at the Larmor frequency to excite the nuclei in the object to be imaged. The second is to pick RF signals emitted by the nuclei at the same frequency. To obtain high quality MRI images, RF coils must be able to produce a homogeneous B_1 field in the volume of interest at the Lamor frequency so that the nuclei can be excited uniformly.

Over two decade, ago, bird cage resonators (Fig. 1) are most popular because they generate a very homogeneous field over a large volume within the coils.

To compute the magnetic field generated by the birdcage resonator its expression outside the conductors coils is given by a Biot-Savart formula which are derived in the Cartesian coordinates for the magnetic field consist to develop the different integrals of the formula.

There are many computational methods which have been published for calculating the magnetic field of the birdcage resonator. These cases have been treated by evaluating the magnetic field analytically in terms of functions such as complete or incomplete elliptic integrals of first and second types.

So in this paper we propose a hybrid method to compute the magnetic field ($Bt(x, y, z)$) which the sum of all magnetic fields produced by conductors coils.

The idea of this work consist to meshing the study area and calculate the magnetic fields produced by the high end ring ($Bah(x, y, z)$), law end ring ($Bab(x, y, z)$) and legs ($Bbr(x, y, z)$) of the birdcage resonator at each point ($M(x, y, z)$) of the numerical mesh, where the magnetic fields $Bah(x, y, z), Bab(x, y, z), Bbr(x, y, z)$, are the sum of the magnetic fields created by the infinitesimal element located on the high end ring , law end ring and legs, respectively in the three dimension study area using the analytical formula (Biot-Savart).

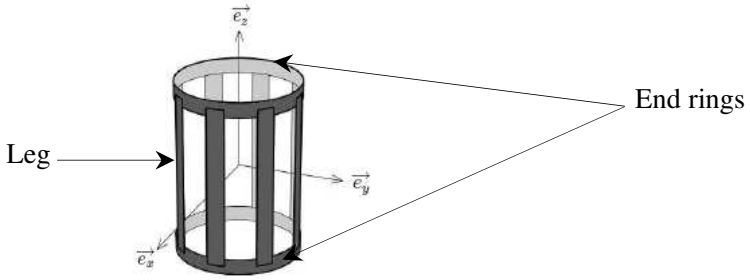

Figure 1: Illustration of Birdcage coil.

Performances of Textile Patch Antennas

Mohamad Mantash, **Anne-Claude Tarot**, **Sylvain Collardey**, **and Kouroch Mahdjoubi**
IETR, University of Rennes 1, France

Abstract— Wearable antennas are meant to be a part of the clothing used for communication purpose, which includes tracking and navigation, mobile computing and public safety. In this scenario, conformal antennas for WIFI applications (2.45 GHz and 5.6 GHz) are becoming an emerging research topic. Wearable antennas need to be hidden and low profile: textile materials (felt, denim ...) are then used to replace the dielectric substrate and the electrotextile (Zelt, Shieldit, Flectron ...) to replace the conductor [1, 2].

The aim of this paper is to compare the performances (return loss, radiation pattern, gain ...) of patch antennas printed on both textiles (denim) and dielectric materials (TACONIC TLX-8).

To realize the radiating element and the ground plane, an electrotextile (Shieldit [3]) was used and compared to the copper tape.

The simulation and measurements results for 2.43 GHz WIFI patch antennas using different textile dielectrics and electrotextiles will be shown in the final paper.

In the first step, a simple patch covering the 2.43 GHz for Wi-Fi application is designed using denim fabric (jeans) as substrate with $\varepsilon_r = 1.7$, tan = 0.05 and thickness = 0.8 mm. Metallic copper tape is used for the patch itself and the ground plane.

	TACONIC TLX-8	Denim Textile
Copper		
Shieldit		

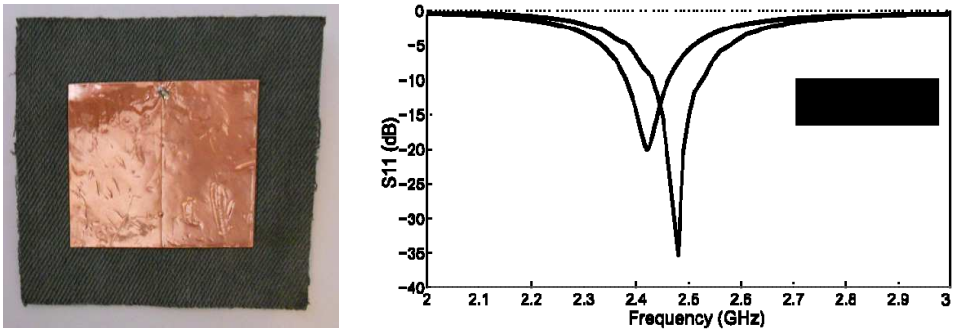

(a) (b)

Figure 1: Patch antenna on denim for 2.43 GHz WIFI band: (a) antenna manufactured prototype and (b) return loss simulation and measurement.

REFERENCES

1. Carla Hertleer.
2. Muhammad Azfar Bin Abdullah.
3. Shieldit.

Polar Decomposition of the Mueller Matrix Applied to Nanoparticle Sizing

J. M. Sanz, **P. Albella**, **J. M. Saiz**, **R. Alcaraz**, **F. Moreno**, **and F. González**
Departamento de Física Aplicada, Univ. De Cantabria
Av. Los Castros s/n, Santander 39005, Spain

Abstract— The Mueller Matrix (MM) contains all information about the scattering properties of a system, for a given wavelength and scattering geometry. Because the MM is a result of the action of a system, its knowledge and characterization constitutes a way for finding out some of such properties. This non-unique procedure is one of the so-called inverse problems in scattering research. Being the MM such a complete result, there has been much work trying to exploit its capabilities, in the line of connecting MM properties to those, either optical or geometrical, of the scattering target. For many systems, however, the elements of the MM are not easily related to the properties of the system, unless some kind of transformation is introduced. Following this idea, MM decomposition, i.e., expressing it as a product -or sum- of several matrices, has become very popular in recent years. Polar Decomposition (PD), in particular, introduces 3 matrices, M_Δ, M_R and M_D, representing independent actions of the system on the polarimetric properties of the scattered light, respectively: depolarization, retardation and diattenuation. If it is proved that a particular feature of the system is related to any of the parameters contained in such matrices, a more direct way of analysis is then opened. The PD method has been used in medicine, to improve results in tissue exploration, and in other applications, like imaging polarimetry or radar detection.

Here PD is applied to a set of MM's obtained either experimentally, on a volume scattering system containing metallic nano-particles, or by numerical simulation based on Discrete Dipole Approximation (DDA), and the behavior of particular parameters has been compared. The mean retardation PD parameter, δ, shows an angular dependence that, when compared with its simulated counterpart, shows itself as a strong indicator of the size. In addition to this, calculations show that the spectral evolution of PD parameters has a potential in sizing metallic nanoparticles.

Coils and Magnets: 3D Analytical Models

R. Ravaud[1], **G. Lemarquand**[1], **and V. Lemarquand**[2]

[1]Universite du Maine, LAUM, UMR CNRS 6613, Le Mans, France
[2]Universite de Toulouse, LAPLACE, UMR CNRS 5213, IUT Figeac, France

Abstract— First, this paper deals with analytical models for computing the magnetic fields created by both kinds of magnetic sources: coils and permanent magnets. Moreover, it shows that the same analytical model can be used for modeling a permanent magnet or a coil and highlights and explains the mathematical difficulties encountered in solving problems with cylindrical properties. As a remark, each type of source, coil or permanent magnet, can be modeled by both approaches too: the coulombian or the amperian one. The presented three-dimensional mathematical model is accurate whatever the magnetic source dimensions, so for the near field and the far field.

Moreover, various electromagnetic applications are composed of two thick coils that form a loosely coupled transformer. Then, the first coil produces a magnetic field which is partly picked up by a secondary coil. A good criterion for evaluating the efficiency of such a device is the mutual inductance of the coupled transformer [1]. The calculation of the mutual inductance between circular coils has been studied by many authors. On one hand, the approaches used are based on the application of Maxwell's formula, Neumann's formula and the Biot Savart law. These approaches lead to expressions based on elliptic integrals of the first, second and third kind, the Heummann's Lambda function or the Bessel functions. On the other hand, authors generally use the finite element method, the boundary element method or numerical algorithms which evaluate the Laplace's equation in all points in space.

Then, this paper presents a method for calculating the mutual inductance between two thick coils which leads to an interesting analytical formulation too. As said previously, both models of a source can be used. Thus, this paper presents general expressions that have been obtained with the coulombian and the amperian models of a permanent magnet. But the point is that some configurations may be modeled indifferently with the two previous models where others should be modeled either with the coulombian model or the amperian current model in order to obtain interesting formulations for the result. For instance, the use of the coulombian model for a thin coil will lead to useful formulations whereas the amperian current model only will give good results in the case of a thick coil.

In this paper, a thick coil is replaced by a toroidal conductor carrying a uniform current volume density for calculating both the force exerted between two thick coils and their mutual inductance. These conductors are assumed to be perfectly circular and radially centered. An equivalent current volume density is defined which is linked to the number of windings and the coil dimensions. The Lorentz Force (which is linked to the amperian current model) is used for calculating the exact axial force exerted between two thick coils. Then, the potential vector and the Stocke's theorem are used for calculating the mutual inductance of two thick coils in air. The obtained and presented formulation is interesting as it is fully based on elliptic functions whose numerical calculation is fast and robust, a quality which is appreciated for optimization purposes.

Eventually, it has to be noted that all the expressions given have been compared with previous ones published in the literature.

REFERENCES

1. Akyel, C., S. I. Babic, and M. M. Mahmoudi, "Mutual inductance calculation for non-coaxial circular air coils with parallel axes," *Progress In Electromagnetics Research*, Vol. 91, 287–301, 2009.

Discussion on the Magnetic Pole Volume Density in Analytical Models of Permanent Magnets

R. Ravaud[1], **G. Lemarquand**[1], **and V. Lemarquand**[2]

[1]Universite du Maine, LAUM, UMR CNRS 6613, Le Mans, France
[2]Universite de Toulouse, LAPLACE, UMR CNRS 5213, IUT Figeac, France

Abstract— Some new analytical formulations have been proposed in the past few years for the expressions of the three components of the magnetic field created by radially polarized ring or tile permanent magnets or for the torque exerted between two such magnets [1, 2]. These formulations have been obtained by the use of the colombian model of the permanent magnets.

Thus, the ring permanent magnet (or the tile magnet) is represented by two curved planes charged with opposite magnetic pole surface densities and a magnetic pole volume density located inside the ring permanent magnet. In the case of the magnetic field calculation, the contributions of the pole surface densities to the magnetic field lead to analytical formulations of the magnetic field components.

The expressions of the contribution of the magnetic pole volume density are determined semi-analytically. The total computational time, though far shorter than finite element calculations, is increased when the volume pole density is taken into account. So, it is interesting to study the influence of this volume density on the result in order to discuss the necessity of its taking into account with regard to the result accuracy. Indeed, taking all the pole densities leads to the exact value of the magnetic field components, but what is the difference if the volume densities are neglected?

To give some answers, different configurations of radially polarized magnets are studied in this paper. The ring permanent magnets dimensions are varied, especially their inner and outer radii, to consider radially thin or thick magnets as well as smoothly curved or not ones.

Furthermore, the asked question is even more relevant when it comes to the force and torque calculations. Indeed, the interaction between two magnets is the sum of the interactions between all the pole densities (nine contributions). And the evaluation of the force between two magnets is often needed to evaluate the resulting torque between two assemblies of magnets, as in permanent magnets couplings.

Thus, the discussion of the influence of the pole volume density on the result accuracy is an issue, as the computational cost is far more increased. On the other hand, in small permanent magnet couplings, the radius of curvature has a great influence on the torque value exerted between the two rotating parts.

REFERENCES

1. Ravaud, R. and G. Lemarquand, "Comparison of the coulombian and amperian current models for calculating the magnetic field produced by arc-shaped permanent magnets radially magnetized," *Progress In Electromagnetics Research*, Vol. 95, 2009.
2. Ravaud, R., G. Lemarquand, V. Lemarquand, and C. Depollier, "The three exact components of the magnetic field created by a radially magnetized tile permanent magnet," *Progress In Electromagnetics Research*, Vol. 88, 307–319, 2008.

A Coupled Simulation of Microwave Heating Effect Accouting for the Radiation Cooling of the Sample

Pawel Kopyt
Institute of Radioelectronics, Warsaw University of Technology
ul. Nowowiejska 15/19, Warsaw 00-665, Poland

Abstract— Microwave heating since its dicovery in the 40's of the last century has gained interests of researchers and practitioners in large number of scientific disciplines and industry sectors. The applications are numerous and range from the food processing, through wood drying and curing processes and sintering processes in the material engineering to high temperature processing of ceramics. While most of the applications based in the food processing applications the temperatures reached are on the level of 100°C [1], the curing processes of rubber [2], adhesives [3] or polymer coatings [4] in the packaging industry does require much higher temperature, effective sintering or ceramics processing may only occur at temperature level of several hunders degrees and often exceed 1000°C (e.g., sintering of diamond-silicon composite [5]). The sources of energy losses from the surface of the processes samples are at low-temperatures often limited to convective cooling in models. As the temperature rises the percentage of the losses due to radiation. This effect plays a decisive role at sintering temperatures, but can ber also pronounced at much lower temperatures [6–8].

Proper use of well-verified numerical models of coupled modeling of electromagnetic-thermal phenomena may to some extent facilitate designing new industrial processes and scientific experiments. A highly accurate multiphysics solver can greatly reduce the number of trial runs of the expeirmental set-up. For this reason accounting for energy losses due to radiation seems an important element in improving the accuracy of coupled numerical models. Some developers of commercially available multiphysics solvers have recognized these requirements and allow defining the radiative boundary condition among others. However, the models employed for numerical treatment of the radiation phenomenon are often limited to simplest surface-to-surface (zonal method) [9] approach ignoring any absorption, emission, or scattering of radiation. This may limit the accuracy of the solution in same cases mainly limited to ceramics and glass processing, where the heated sample cannot be always treated as a non-participating medium.

One way of improving the modeling accuracy in selected problems of high-temperature processes modeling is coupling an electromagnetic solver with a fully-fledged Computational Fluid Dynamics (CFD) analysis tool offering a number of more advanced models of radiation. In this paper a modeling system built of QuickWave-3D [10] electromagnetic solver and Fluent CFD [11] tools described in [12] is extended in order to properly handle radiation effects in microwave heating using the radiation models in-built into the Fluent environment. The article presents also an example problem solved using the developed coupled model.

REFERENCES

1. Ma, L., D.-L. Paul, N. Pothecary, C. Railton, J. Bow, L. Barrat, J. Mullin, and D. Simons, "Experimental validation of a combined electromagnetic and thermal FDTD model of a microwave heating process," *IEEE Trans. Microwave Theory Tech.*, Vol. 43, No. 11, 2565–2572, Nov. 1995.
2. Makula, N. and P. Rattanadecho, "Microwave pre-curing of natural rubber-compounding using a rectangular wave guide," *International Communications in Heat and Mass Transfer*, Vol. 37, No. 7, 914–923, Aug. 2010.
3. Glinski, G. P. and C. Bailey, "Microwave cure of conductive adhesives for flip-chip & microsystems applications," *Conf. on Thermal and Thermomechanical Phenomena in Electronic Systems (ITHERM 2002)*, 848–853, San Diego, USA, May 2002.
4. Tilford, T., K. I. Sinclair, C. Bailey, A. K. Parrott, and A. J. Sangster, "Multiphysics simulation of microwave curing in micro-electronics packaging applications," *Journal of Soldering & Surface Mount Technology*, Vol. 19, No. 3, 26–33, 2007.
5. Leparoux, S., C. Diot, A. Dubach, and S. Vaucher, "Synthesis of silicon carbide coating on diamond by microwave heating of diamond and silicon powder: A heteroepitaxial growth," *Scripta Materialia*, Vol. 57, 595–597, 2007.

6. Guenin, B. M., "Don't underestimate radiation in electronic cooling," *Electronics Cooling*, Feb. 2001, http://www.electronics-cooling.com/2001/02/dont-underestimate-radiation-in-electronic-cooling.
7. Cheng, X., F. J. Erbacher, and H. J. Neitzel, "Passive containment cooling by natural air convection and thermal radiation after severe accidents," *Nuclear Engineering and Design*, Vol. 202, No. 2–3, 219–229, Dec. 2000.
8. Twomey, P., C. O'Sullivan, and J. O'Riordan, "An experimental investigation of the role of radiation in laboratory bench-top experiments in thermal physics," *European Journal of Physics*, Vol. 30, 559–566, 2009.
9. Siegel, R. and J. R. Howell, *Thermal Radiation Heat Transfer*, Hemisphere Publishing Corporation, Washington DC, 1992.
10. QuickWave-3D, 1997–2007, QWED Sp. z o.o., http://www.qwed.com.pl.
11. Fluent 12.1.4 university license, ANSYS, Inc. Southpointe, USA, http://www.ansys.com.
12. Kopyt, P. and M. Celuch-Marcysiak, "Coupled simulation of microwave heating effect with quickwave and fluent simulation tools," *10th Intl. Conference on Microwave and High Frequency Heating*, Modena, Włochy, Sept. 2005.

Resonators with Nonreciprocal Media and Three- and Four-port Integrated Optical Circulators Based on 2D Photonic Crystals

Victor Dmitriev, **F. J. M. de Souza**, **and G. Motta de Moraes**
Electrical Engineering Department, Federal University of Pará, Belém-PA, Brazil

Abstract— Nonreciprocal devices are important elements in integrated optics. They permit to mitigate the influence of parasitic reflections of electromagnetic signals from non-ideally matched components because the reflected light causes instabilities of lasers and amplifiers. However, the traditional optical isolators and circulators have rather large dimensions; for example, the ferrite isolators based on Faraday effect have the length of several millimeters [1]. Besides they do not permit integration with other optical elements. Our aim is a theoretical investigation of new compact circulators based on 2D photonic crystal waveguides. The nonreciprocity of such circulators is defined by Time-reversal asymmetry of gyrotropic media, for example, the tensor of permeability of magnetized ferrites and the tensor of permittivity of semiconductors [1]. It is known that magneto-optic activity of the ferrites and magnetized semiconductors is very small. One of the ways to overcome this difficulty is the use of some resonant effects. The circulators suggested in our work are very compact because the physical principle of their functioning is a combination of different resonances of a nonreciprocal resonator and of corresponding junctions. The linear dimensions of them are of several wavelengths which is much lower than those of the published circulator [2]. Notice also that in paper [2] only three-port circulator is investigated. We present in our work some theoretical results concerning resonators with nonreciprocal media and three- and four-port integrated optical circulators based on the waveguide junctions with such resonators. The proposed three-port circulator is based on the hexagonal lattice and the four-port circulator on the square one. The corresponding Y- and X-junctions of photonic crystal waveguides with a magnetized central regions form the nonreciprocal devices. For theoretical simulations, the commercial software FEMLAB MULTIPHYSICS was employed.

In Fig. 1, preliminary results for a four-port circulator are shown. We can see that for an excitation with wavelength $\lambda = 1.329837\,\mu$m applied in the port 1, the return loss is about $-35\,$dB and the transmission in the port 2 is about $-0.48\,$dB. Also, there is a good isolation of the ports 3 and 4.

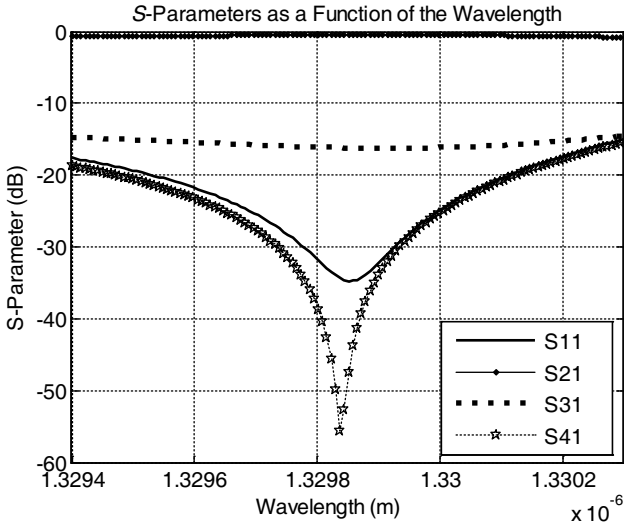

Figure 1: S-parameters of the 4-port circulator.

REFERENCES

1. Zvezdin, A. and V. Kotov, *Modern Magnetooptics and Magnetooptical Materials*, Institute of Physics Publishing, Bristol and Philadelphia, 1997.
2. Wang, Z. and S. Fan, "Optical circulators in two-dimensional magneto-optical photonic crystal," *Optics Letters*, Vol. 30, No. 15, 1989–1991, 2005.

Detection of Micro-cracks on Metal Surfaces Using Near-field Microwave Dual-behaviour Resonators Filters

Julien Kerouedan[1, 2], **Philippe Talbot**[1], **Patrick Queffelec**[1], **Cédric Quendo**[1], **and Alain Le Brun**[2]

[1]Lab-STICC, UMR 3192, Université Européenne de Bretagne
Université de Bretagne Occidentale, France
[2]EDF-R&D / STEP, 6 quai Watier, BP 49, 78401 Chatou Cedex, France

Abstract— This paper demonstrates how micro-cracks at the surface of metals can be detected and imaged by near-field microwave techniques from the crack-induced variations of the resonance frequency and of the resonant circuit quality factor. It deals with two novels resonant sensors: a first-order Dual-Behaviour Resonator (DBR) band-pass filter probe [1] and a first-order DBR band-pass filter probe with an opening in the ground plane. The detection principle was validated theoretically and experimentally, and we showed the good spatial resolution and the high sensitivity of the DBR filter probes and their ability to differentiate between notches of different depths and notches of different widths [2]. Measurements were mainly carried out on a stainless steel and an aluminum mock-up with several Electric Discharge Machining (EDM) rectangular surface notches at the surface of a steel plate used to validate our method presenting widths between 0.1 and 0.3 mm and depths between 0.5 and 3 mm. The experimental data on two different metals presented in this paper show the influence of the width and depth of the notch on the HF stub frequency variations (Δf_{HF}) and the enhancement of the detection sensitivity by using a first-order DBR filter with open-ground plane.

Further investigations will be aimed at studying the dependence of the Δf_{HF} variations on the dimensions of the notch (depth, width and length).

We also plan to evaluate the potential of the DBR probes to detect fatigue cracks and stress corrosion flaws.

REFERENCES

1. Quendo, C., E. Rius, and C. Person, "Narrow bandpass filters using dual-behavior resonators," *IEEE Transactions on Microwave Theory and Techniques*, Vol. 5, 734–743, 2003.
2. Kerouedan, J., P. Queffelec, P. Talbot, C. Quendo, S. De Blasi, and A. Le Brun, "Detection of micro-cracks on metal surfaces using near-field microwave dual-behavior resonator filters," *Measurement Science and Technology*, Vol. 19, 105701 (10 pages), 2008.

A Peak to Average Power Ratio Reduction of Multicarrier CDMA System Using Error Control Selective Mapping

Sajjad A. Memon, **A. W. Umrani**, **F. A. Umrani**, **and A. K. Baloch**
Institute of Information and Communication Technologies
Mehran University of Engineering & Technology
Jamshoro 76062, Pakistan

Abstract— Multicarrier Code Division Multiple Access (MC-CDMA) is one of the most promising techniques for high bit rate and high capacity transmission for future broadband mobile services. One major drawback associated with multicarrier systems that significantly degrades power efficiency and makes it less preferred by the industry is Peak to Average Power Ratio (PAPR). One method for reducing PAPR in multicarrier CDMA systems is to use Selective Mapping. We aim to analyze the system performance of multicarrier CDMA system and reduce PAPR using selective mapping that employs convolutional codes to avoid the need of side information. Simulation results show that the error control selective mapping is more effective than the selective mapping. Results also show that the increasing number of PAPR control bits results in much reduced PAPR value but also increases the system complexity.

Detection of Singularities by Wavelet Technique for Extracting Leaky Waves in Piezoelectric Material

D. Benatia[1], **T. Fortaki**[1], **and M. Benslama**[2]

[1]Département d'Electronique, Faculté des Sciences de l'Ingénieur, Université de Batna, Algeria
[2]Département d'Electronique, Faculté des Sciences de l'Ingénieur, Université de Constantine, Algeria

Abstract— In the present paper, we propose a new efficient numerical method for detection of leaky waves of an acoustic microwave signal during the propagation of acoustic microwaves in a piezoelectric substrate (Niobate of Lithium $LiNbO_3$). For this reason, we have used a wavelet transform as a numerical analysis method. Moreover, we know that the Fourier transform presents a global spectral study of signal, this is not interesting if we want to study a signal locally and know its features in a more precise manner. By the use of wavelet transform, we can reduce this drawback. The originality of the wavelet transform consists of the local analysis of signal singularities where abrupt events appear and hence access to hidden information by using the scale of this transform as up scaling parameters. These singularities inform us of presence of leaky waves in piezoelectric materials.

In this work, we have a very important parameter called acoustic velocity. Its importance is due to the fact that its variation begets the variation of the other parameters such as penetration coefficient. On the other hand, it permits to provoke singularities at the level of the wave. Some results are given; they lead to some interesting conclusions.

Magneto-optical Spectroscopic Scatterometry of 1D Gratings

Martin Veis, **Roman Antos**, **and Stefan Visnovsky**
Institute of Physics, Faculty of Math. & Phys., Charles University, Czech Republic

Abstract— Magneto-optical (MO) spectroscopy is often used as a high sensitive non-destructive technique to probe physical properties of various magnetic materials down to the nanometer scale. In combination with spectroscopic ellipsometry (SE) as a complementary tool it can provide important information about the geometrical and material properties. MO spectroscopic scatterometry combines theoretical and experimental investigation of MO spectral response of patterned periodic magnetic nanostructures. Here we report on analyzing two types of one-dimensional gratings formed by magnetic materials, permalloy ($Ni_{81}Fe_{19}$) and nickel. Periodic lamellar grooves were etched by electron-beam lithography and ion milling on a 32-nm-thick permalloy layer deposited on an Si substrate. The depths of the grooves was nominally chosen between 8 and 32 nm, with a period of 1000 nm and with a top lateral linewidth of 500 nm. Periodic Ni wires were fabricated by the lift-off procedure on an Si substrate with a 500-nm-thick SiO_2 overlayer. For the theoretical calculations fast Fourier factorization rules with complex polarization bases were employed. All samples were characterized by atomic force microscopy (AFM) prior to MO scatterometry measurements. The half-micrometer SiO_2 layer causes significant interference effects, which enable sensitive monitoring of both the thickness and the material properties. The wire linewidth, however, had to be taken from the AFM measurement. By performing this procedure, we found the thickness in reasonable accordance with that determined by AFM. Moreover, the Ni was found partially oxidized with homogenous concentration of NiO in depth, which suggests a strong possibility of a reduced quality of vacuum during the deposition of Ni. The concentration of NiO within the Ni layer was determined equal to 52%. The material constants of the system of Ni+NiO was modeled by the effective-medium approximation.

Adjustable Group Delay Circuits Capable of Switching between Negative and Positive Group Delays

Chia-Chi Lin[1], **Ken-Huang Lin**[1], **and Hsin-Lung Su**[2]

[1]Department of Electrical Engineering, National Sun Yat-Sen University, Taiwan
[2]Department of Computer and Communication, National Pingtung Institute of Commerce, Taiwan

Abstract— In communication systems, a flat group delay over the frequency band is necessary to avoid distortion. When the group delay variations are too large, compensation or equalization is usually required to alleviate the variations. In this paper, an active circuit is proposed to provide adjustable group delays (GD). This GD circuit consists of an operational amplifier and one or more RLC elements and is capable of achieving both negative group delay (NGD) and positive group delay (PGD). Our design is flexible in that the desired PGD or NGD can be obtained by placing the RLC passive element at different positions of the group delay circuit, such as those in a negative feedback loop or between the input port and non-inverting (+) port, or by using different types of RLC passive elements such as a shuntor a series-RLC configuration.

We first study the effect on GD based on zeros and poles of the circuit. Starting with circuits of a single zero or single pole, it is found that the zero introduces NGD and the pole introduces PGD. The investigation then extends to circuits with multiple poles and zeros. The amount of NGD or PGD can be controlled by adjusting suitable parameters of the RLC elements. The operating frequencies can also be adjusted in the same manner. Hence, GD can be easily analyzed and realized based on the concept of the zero and pole.

By applying our design method, the GD circuit can be further made switchable between NGD and PGD easily. Several examples will be shown to demonstrate this property. The GD circuits are simulated with the Agilent's ADS and the results agree with the derivations well. This capability of switching makes the proposed circuit more adaptive and can thus be applied to channels where the group delays are changing.

Analysis of AOA-TOA Signal Distribution in Indoor RF Environments

L. Ali, Y. Ben Shimol, and N. Blaunstein
Department of Communication Systems Engineering
Ben-Gurion University of the Negev, Beer Sheva 84105, Israel

Abstract— Increasing demand for wireless communication systems in the recent decades requires lightweight portable personal communication systems; partly for indoor communication, where fixed base station transmits voice and data to portable units inside buildings. Therefore, detailed knowledge of radio propagation conditions inside buildings is critical for efficient design of indoor communication systems. Current models mostly address the path-loss behavior of indoor channels. Implementations of the 4-G broadband technologies for pico-cell indoor environments, as well as, growing number of subscribers working with portable multi-beam antennas, have motivated the renewed interest for accurate channel modeling not only in the space (along the radio path), but also in the time-of-arrival (TOA) and angle-of-arrival (AOA) domains, mostly for multiple-input-multiple-output (MIMO) multiple access servicing.

In this work, the statistical multi-parametric approach that was originally proposed for the outdoor urban environment and was approbated by numerous experiments carried out for various elevations of base station (BS) and mobile subscriber (MS) antennas with respect to building surrounding, is adopted for modeling the indoor propagation conditions.

The joint AOA-TOA distribution for indoor corridor and crossing corridors accompanied with rooms lining each corridor, which consists various obstructions (furniture, machinery, architecture elements etc.) is derived in this work. The derived stochastic multi-parametric model accounting for obstructions' density surround antennas, the gaps between rooms lining the corridor, heights of both terminal antennas with respect to obstructions' heights (model is valid only when both terminal antennas are below the walls' height), effects of absorption by walls, and many others.

The accuracy of the proposed model is validated using the collected measurements. The separate and the joint AOA-TOA measurements were obtained via a time-domain based data collection method and highly directive parabolic antennas. An accurate agreement between the derived statistical multi-parametric model and the experimental data is demonstrated for single-corridor and crossing-corridors indoor environments.

Electromagnetic Study of Planar Periodic Structures Using a Multi-scale Approach

S. Mili and T. Aguili
Laboratory of the Communication Systems, National Engineering School of Tunis, Tunisia

Abstract— The electromagnetic behavior of structures with periodically arranged elements was widely investigated during this century. Such periodic structures play a key role in many antennas systems since they can offer multi-band and/or broadband characteristics which can be tuned by integrating PIN diodes into the elementary cells.

When the elementary cell contains fine details, the study of the whole structure leads to badly scaled matrices and the convergence of numerical results is hard to reach.

To circumvent such difficulties, a multi-scale (MS) approach combined to the generalized equivalent circuit modeling is used in this paper, for the electromagnetic study of planar periodic structures. Its main idea is to dissociate the elementary cell from the whole structure. Next the elementary cell is enclosed by convenient boundary conditions which respect its real electromagnetic state. In the next step, N modal sources are artificially introduced to excite the considered cell in order to compute its input impedance matrix. The multi-scale method is based on converting this impedance matrix into an impedance operator. Then, the study of the whole structure is done by replacing the unit cell by its impedance operator. When the structure contains PIN diodes, these latter are easily integrated in the MS approach thanks to their impedance model.

The main advantage of the MS method is the significant reduction of the problem's high aspect ratio since fine details are studied separately of the larger structure. Consequently, the manipulated matrices are well conditioned. Moreover, the processing time and the memory storage are significantly reduced compared to the MoM. Values obtained by the MS method are in total agreement with those given by the Moment method when a sufficient number of modal sources are used at the elementary cell.

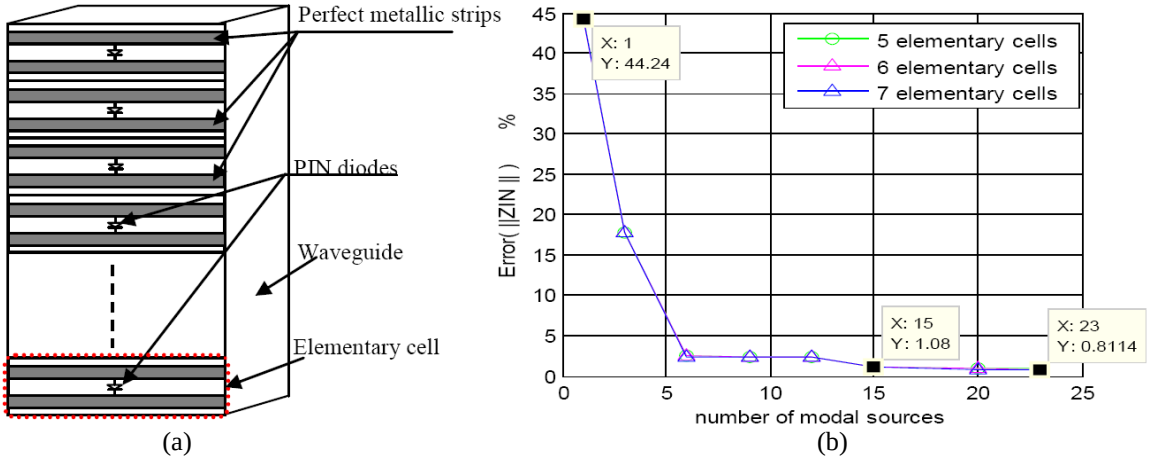

Figure 1: (a) Planar periodic structure with PIN diodes. (b) Variation of the relative error ($\xi(\%)$) on the input impedance with the number of modal sources and the number of unit cells. $\xi = 100\frac{\|Z_{IN\_MOM}\| - \|Z_{IN\_MS}\|}{\|Z_{IN\_MOM}\|}$.

Study of Edge Effect of 4340 Steel Specimen Heated by Induction Process Using Axi-symmetric Simulation

N. Barka, **A. Chebak**, **and J. Brousseau**
Département de mathématiques, d'informatique et de génie
Université du Québec à Rimouski, Rimouski, Québec G5L 3A1, Canada

Abstract— Induction heating is a case hardening process used to improve the performance of machine components by generating a hard martensitic microstructure and high compressive residual stresses at the surface. A typical industrial application of induction hardening consists in heating specific regions of a part above the austenitizing temperature. The hardness profiles have to be controlled to improve wear resistance and enhance contact and bending fatigue life. This paper presents a study of electromagnetic edge effect on cylindrical specimen heated by induction heating process using high frequency generator. This research is performed by 2D finite element simulation and it conducts to develop a uniform hardness profile. The simulation is based on coupling of electromagnetic field and heat transfer. The axisymmetric model is developed using Comsol software based on an adequate formulation and taking into account the material properties and process parameters such as the initial inductor current density (A/m^2), the frequency (kHz) and the heating time (s). The obtained induced currents and temperatures distributions in the part are analyzed versus the inductor dimensions. This paper is original since it introduces a new method to eliminate completely the electromagnetic edge effect in the high frequency heating case and therefore to have a uniform hardness profile. The proposed method consists principally to place two thin cylindrical discs (flux concentrators) such a way the part is taken in sandwich, taking care to leave a small gap that can be optimized by simulation. The obtained results demonstrate that the final hardness profile is quasi-uniform as the temperature and induced currents are almost identical across the part.

REFERENCES

1. Barka, N., P. Bocher, J. Brousseau, M. Galopin, and S. Sundararajan, "Modeling and sensitivity study of the induction hardening process," *Advanced Materials Research*, Vols. 15–17, 525–530, 2007.
2. Rudnev, V., D. Loveless, R. Cook, and M. Black, *Handbook of Induction Heating*, Marcell Dekker Inc., New York, NY, USA, 2003.
3. Magnabosco, I., "Induction heat treatment of a ISO C45 steel bar: Experimental and numerical analysis," *Computational Materials Science*, Vol. 35, 98–106, 2006.
4. Kawagushi, H., M. Enokizono, and T. Todaka, "Thermal and magnetic field analysis of induction heating problems," *Materials Processing Technology*, Vol. 161, 193–198, 2005.
5. Wang, K. F., "Simulation of quenching and induction heat treatment process with experimental verification," Ph.D. Thesis, School of Aeronauts and Astronautics, Perdue University, USA, 1993.
6. U.S. Defense Departement, "Metallic materials and elements for aerospace vehicle structures," *Military Handbook — MIL-HDBK-5H*, 1998.

Optimization of Hardness Profile of Bearing Seating Heated by Induction Process Using Axisymmetric Simulation

N. Barka, **A. Chebak**, **and J. Brousseau**
Département de mathématiques, d'informatique et de génie
Université du Québec à Rimouski, Rimouski, Québec, G5L 3A1, Canada

Abstract— The mechanical components are always expected to be hardened in order to ameliorate their behavior in service. Various surface heat treatment processes are commonly used, such as induction heating process and thermo-chemical processes (carbonizing, intruding, etc.). The induction heating is an efficient and promising process, since it exhibits several industrial advantages as heating is done into superficial layer and during a short time not exceeding 1 second. In addition, the process can be easily implemented in automated manufacturing cells and it not produces greenhouse gas emissions. However, the process is not completely under control since the electromagnetic effects influence greatly the final temperature profile in the part. Consequently, it is difficult to produce uniform hardness profiles that constitute a design requirement. The paper presents an analysis of hardness profile of bearing shoulder made from 4340 steel and heated by induction process. The work is carried out by 2D finite element analysis with Comsol software and by coupling the Maxwell equations and the heat transfer equations. The obtained results show that some useful modifications of the part and the coil form can be used to better control hardness profile and make it uniform. The proposed study is carried out in few steps. First, an axis-symmetrical model representing the bearing shoulder was built using the adequate formulation and taking into account the material properties. This model is used to determine the variation of the temperature and induced currents density in the part with the machine parameters. Second, a new method is proposed to optimize the temperature profile and hence the case depth profile of the shoulder. This method consists to add two flux concentrators near the part and to modify the inductor form. The obtained results are very useful and show that a uniform case depth of the bearing shoulder can be easily obtained.

REFERENCES

1. Barka, N., P. Bocher, J. Brousseau, M. Galopin, and S. Sundararajan, "Modeling and sensitivity study of the induction hardening process," *Advanced Materials Research*, Vols. 15–17, 525–530, 2007.
2. Rudnev, V., D. Loveless, R. Cook, and M. Black, *Handbook of Induction Heating*, Marcell Dekker Inc., New York, NY, USA, 2003.
3. Magnabosco, I., "Induction heat treatment of a ISO C45 steel bar: Experimental and numerical analysis," *Computational Materials Science*, Vol. 35, 98–106, 2006.
4. Kawagushi, H., M. Enokizono, and T. Todaka, "Thermal and magnetic field analysis of induction heating problems," *Materials Processing Technology*, Vol. 161, 193–198, 2005.
5. Wang, K. F., "Simulation of quenching and induction heat treatment process with experimental verification," Ph.D. Thesis, School of Aeronauts and Astronautics, Perdue University, USA, 1993.
6. U.S. Defense Departement, "Metallic materials and elements for aerospace vehicle structures," *Military Handbook — MIL-HDBK-5H*, 1998.

A Time Domain Hybrid Approach to Study Buildings Connected by Cables

N. Muot[1], **E. Bachelier**[2], **X. Ferrieres**[2], **and C. Girard**[1]

[1]AxesSim, Strasbourg, France
[2]ONERA, Toulouse, France

Abstract— In term of application for large and complex systems, some hybridization and multidomain approaches have been studied in many different ways and have shown its capabilities to deal with electromagnetic problems. However, as far as we are interested in applications like lightning electromagnetic induced effects on buildings, interconnected by powerlines or communication networks, the usual multidomain methods need to be improved. For these problems, the challenge is to reduce the computational problem for the area between the buildings. The problem is to take into account the interactions between soil, buildings and cables, without a 3D meshing of the global scene. The paper presents a multidomain strategy based on a hybrid approach in time domain, by coupling 3D methods (FDTD, FVTD...) with a transmision line method, first step of the general problem.

The idea is to define a 3D problem around each building and a 1D problem along the transmission lines. Then, the hybridization strategy consists in making exchanges of some quantities at an interface between the two problems. In our way of coupling, the interface considered is reduced to a dipole on which we propose to exchange data of both domain by the introduction of a local Thevenin equivalent circuit. Through the impedance, the local condition of continuity at the virtual interface of the line is ensured. On the other hand, the generator send the signal relative to the other computational domain.

Considering the applied problem we are interested in, the next step to investigate is the influence of the soil conductivity on the induced effects, between buildings, grounding and networks. The paper will also present the actual fields of investigation for this specific aspect.

The Effect of Metamaterial Patterning to Improve the Septum GTEM Chamber Performance

H. X. Araújo and L. C. Kretly
University of Campinas, Brazil

Abstract— In many cases, integrated circuits and electronic boards are the mainly causes of interference in others electronics equipments. The EMC — Electromagnetic Compatibility of an electrical device is its capability to operate safely in an electromagnetic environment without interfering and be not susceptible by other interference sources. In this context, the EMC work is on increase demand.

Different approaches support the pre-compliance tests (EMC/EMI/EMS) setups which have consolidated standards and regulations. These setups include TEM/GTEM cells, Magnetic Loop, Magnetic probe, Workbench Faraday Cage, OATS — Open Area Test Site and others.

Based on the frequency range, in this work, from 500 MHz–18 GHz, the GTEM — Gigahertz Transverse Electromagnetic chamber has advantages over the others test setups.

A GTEM chamber, used for testing EMI and EMS of electronic devices and systems has a thin metallic baffle, called *septum* to conduct the radiation over the device under test.

In this work, a metamaterial patterning is applied to the *septum* in order to obtain a better coupling between the EM field and the DUT. The basic cells consist of a ring resonator — RR (Ring Resonator) or CLL (Capacitively Loaded Loop) in SRR (Split Ring resonator) or CSRR (Complementary Split Ring Resonator) configuration topologies. They are oriented depending on the wave direction from the device to the measuring port or from the exciter side — APEX to the device under test. Actually, resonant type metamaterial transmission lines are very similar to CLL lines. However, the first one exhibit a transmission zero at a finite frequency (to the left of the left handed band) due to the coupling between the host line and the loading resonators (magnetic coupling in SRR-loaded lines and electric coupling in CSRR-loaded lines).

The simulated results show the direction property of the patterned *septum* in comparison with the useful one. This new and promising technique appears to improve the GTEM chamber performance.

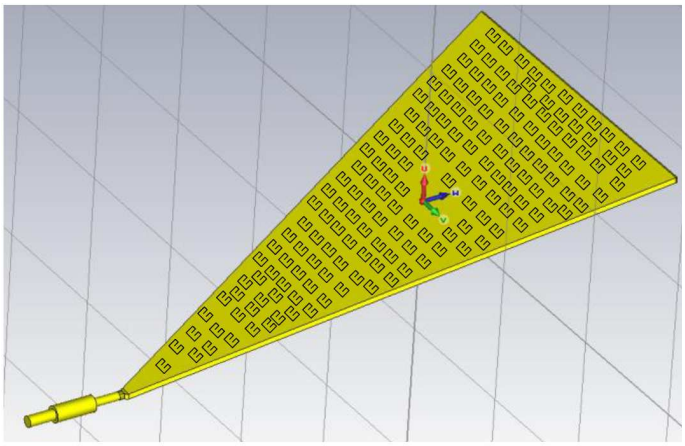

Figure 1: Metamaterial cells applied to the *septum*.

The Integration of the Multihoming Concept in Ad Hoc MANET Mobile Networks

A. Messai, **S. Sadouni**, **S. Aris**, **H. Mokhtari**, **and M. Benslama**
Electromagnetism and Telecommunication Laboratory, University of Constantine, Algeria

Abstract— Today, huge technological advances are taking place in the field of wireless telecommunications. The latter are characterized by the increasing capacities in data processing, as well as miniaturization of equipment. However, mobile networks users who are no more satisfied with cell phone service providers are being very demanding, and are claiming to benefit from continuous and performing multimedia services.

In this light, our task is at its earliest stages to achieve the concept of: "seamless mobility", thanks to which one can easily move from one network to another without fearing to get cut off from the network. This latter perspective represents the objective of heterogeneous networks based on the use of Multihoming which was created and developed for wired networks. It enables a node to simultaneously use several network interfaces; switching therefore from one interface into another without interrupting the current data transmission.

The primary objective of this work is to integrate the Multihoming concept to mobile networks, in order to increase their hardiness, resistance to breakdowns, as well as to share the load carried by several nodes. This, in turn, will consequently lead to a high throughput. For this purpose, we have chosen the BGP protocol which will have the task of introducing the Multihoming concept to Ad Hoc MANET networks. In order to do so, the BGP protocol must be combined with other Ad Hoc routing protocols which fall into three categories: reactive, proactive and hybrid.

The functioning of every protocol category is based on a particular routing technique. This latter has some qualities and certain flaws. Thus, it would be our major concern to define in which protocol category the Multihoming integration will be favourable in terms of: network load, and resistance to the effects of mobility.

In order to reach our goal, our conclusions will be based on a simulation of an Ad Hoc network containing many scenarios: Some combine the BGP to the AODV when it comes to the reactive protocol type; and others will link it to the OLSR for the proactive protocol type.

Electromagnetic Compatibility of CMOS Circuits along the Lifetime

R. Fernández-García[1], **J. M. Ruiz**[2], **I. Gil**[1], **and M. Morata**[2]

[1]Electronic Engineering, UPC Barcelona Tech. 08222 Colom 1, Terrassa, Spain
[2]Escuela Universitaria Salesiana de Sarriá, Barcelona 08017, Spain

Abstract— The continuous scaling of CMOS circuit has set the MOSFET transistor in the nanoelectronic era. In this context, the functionality and complexity of integrated circuits (ICs) are growing up. However, the operation voltage is reduced. The higher complexity of ICs has allowed including electronic systems in a lot of safety critical applications (i.e., automotive, aeronautics and/or medical applications). Therefore, the functionality of these electronic equipments must be assured and the risk of electromagnetic interference (EMI) must be reduced during their lifetime. Nowadays, circuits' robustness to electromagnetic interference is checked in a burn-in component [1], without taking into account the impact of the natural devices' aging. However, shrunk dimensions cause the appearance of several wear out mechanisms, which can limit the functionality of the circuits and modify their electromagnetic performance [2]. Therefore, the time dependence of electromagnetic behaviour, which is known as Electromagnetic Robustness or Electromagnetic Reliability (EMR), should be evaluated. The switching noise is probably one of the main EMC emission problems in CMOS circuits [3]. It is know that wear out mechanism affects the switching behaviour of CMOS circuits. Therefore, some effects on EMC performance of these circuits should be expected. In this work, the switching noise behaviour or CMOS circuits under different wear out conditions are analyzed by means of electrical simulation. In order to do that, a characterization of wear out mechanism on single MOSFET is presented and modelled. The results show a reduction on the switching noise emission in circuits subjected to wear out, due to the reduction of the drain current of MOSFET.

ACKNOWLEDGMENT

This work has been supported by the Spain-MICINN under Project TEC2009-09994 and AGAUR 2009 SGR 1425.

REFERENCES

1. Dhia, S. B., A. C. Ndoye, A. Boyer, L. Guillot, and B. Vrignon, "IC emission spectrum drifts after burn-in cycles," *Asia-Pacific Symposium on Electromagnetic Compatibility and 19th International Zurich Symposium on Electromagnetic Compatibility, APEMC*, 255–258, May 19–23, 2008.
2. Kang, K., H. Kufluoglu, K. Roy, and M. Alam, "Impact of negative-bias temperature instability in nanoscale sram array: Modeling and analysis," *IEEE Transactions on Computer-Aided Design of Integrated Circuits and Systems*, Vol. 26, No. 10, 1770–1781, Oct. 2007.
3. Ben Dhia, S., M. Ramdani, and E. Sicard, *Electromagnetic Compatibility of Integrated Circuits*, Springer, 2005, ISBN 0-387-26600-3.

The Ratio of Models for Fuel and Building Power Plants in Thailand in 2564

Vallop Phupha
Faculty of Engineering, Rajamangala University of Technology Phra Nakhon (RMUTP)
1381 Piboonsongkurm Rd., Bangsue, North Bangkok 10800, Thailand

Abstract— The Current problems in global energy. Because natural energy resources are gone, so every country must find alternate energy sources or alternative production cost per unit the lowest. Therefore, government policies to the Electricity Generating Authority of Thailand (EGAT) conducted a Power Development Plan of Thailand Under the name of PDP 2007 (Power Development Plan) from the committee to support the multiple plans. To operate in a variety of factors, such as survey information. Parameter Value problem affected the growth of the economy. Reserve in the planning of future power generation. Current fuels used to produce electricity, but it is certainly not the same unit cost of natural gas with coal as environmental impact is different. Therefore, in this study must be done. Educational models for decision to create a ratio of power in Thailand in 2564.

Characterization and Modeling of the Electromagnetic Emission of an ADC Converter

N. Berbel, **R. Fernández-García**, **and I. Gil**
Department of Electronic Engineering, Universitat Politècnica de Catalunya
08222 Colom 1, Terrassa, Spain

Abstract— Analog-to-digital converters (ADC) are widely used in consumer electronics, as well as aeronautic, space and automotive development fields. The ADC clock frequency has been increasing in the latest years due to the continuous downscaling in CMOS technology. This constant rising of the operating frequency implies a significant enhancement of the electromagnetic inference (EMI). Therefore, in order to predict the impact of the EMI on the electronic systems performance, electrical circuit models, involving these EMC issues, are required. In this sense, an electromagnetic model of integrated circuits has been internationally standardized (ICEM model) [1]. This model includes a passive distribution network (PDN), which presents the characteristics of propagations paths of electromagnetic noise and the internal activity (IA), which corresponds to the electromagnetic noise source that originates in switching of active devices in the integrated circuit (IC), measured according to [2]. This work addresses the characterization and modeling of a 10-bit Analog-to-Digital Converter in a 8-small outline integrate circuit (SOIC) package, according to the international standard IEC 62433-2. The ADC has a 3.3 V supply voltage, and an operating frequency of 2.8 MHz. The clock (CLK) corresponds to a square signal with a duty cycle of 50% and the chip select (CS) is a square waveform of 100 kHz with a duty cycle of 10%. The input voltage has been chosen to have the worst condition, (i.e., when the ADC output has the maximum number of transitions from 0 to V_{CC} and vice versa). Fig. 1 shows the spectrum of the ADC's IA measured according to EN 61967-4. The spectrum contains several harmonics due to the CLK and CS signals. The first harmonic is located at 1.4 MHz which corresponds to the frequency of the ADC serial output, and then successive harmonics at even and pair frequencies are produced. All the ADC serial output harmonics present sidebands due to the CS signal. Fig. 2 depicts the return losses parameter (S_{11}) in the power supply pin, which has been obtained by means of a vector network analyzer. The information obtained with S_{11} is related with the input impedance of the integrated circuit and the characteristics of propagation paths. From these dates, the ICEM model of the ADC converter has been obtained.

ACKNOWLEDGMENT

This work has been supported by the Spain-MICINN under Project TEC2009-09994 and AGAUR 2009 SGR 1425.

REFERENCES

1. IEC, "EMC IC modelling — Part 2: Models of integrated circuits for EMI behavioural simulation — Conducted emissions modelling (ICEM-CE)," 2008.

Reconfigurable RF-MEMS Metamaterials Filters

I. Gil[1], **M. Morata**[2], **R. Fernández-García**[1], **X. Rottenberg**[3], **and W. De Raedt**[3]

[1]Department of Electronic Engineering, UPC Barcelona Tech., Colom 1, Terrassa 08222, Spain
[2]Escuela Universitaria Salesiana de Sarriá, Barcelona 08017, Spain
[3]IMEC, Leuven B-3001, Belgium

Abstract— In this work, the design procedure, modelling and implementation of reconfigurable filters based on RF microelectromechanical systems (RF-MEMS) metamaterials is presented. Specifically, tunable stop-band and pass-band frequency responses are obtained by combining RF-MEMS [1] with complementary split rings resonators (CSRRs) [2]. CSRRs, which are the dual image of split rings resonators (SRRs), allow for the design of negative effective permittivity transmission lines, providing forbidden propagation frequency bands. Moreover, CSRRs properly combined with metal vias in transmission lines, generate a simultaneously $\varepsilon < 0$ and $\mu < 0$ effective media which involves an allowed frequency band. These two phenomenon have been used in order to implement stop-band and pass-band filters. Since CSRRs present a LC-tank behaviour and are electrically coupled to the host line, the tunability is achieved by means of the RF-MEMS, which modify the electrical characteristics of the CSRRs and the electric coupling (i.e., the effective resonance frequency). Fig. 1(a) shows the layout of one of the proposed prototypes. It consists of a 50 Ω coplanar waveguide structure (CPW) loaded with rectangular shaped CSRRs etched in the metal strip and RF-MEMS bridges over them. The actual RF-MEMS structures implemented in the CSRRs uses an electrostatic floating bridge anchored on the substrate in holes of the CPW ground planes. Under DC bias, bridge is in down-state and contacts only the centre of the CPW strip. Therefore, the effective capacitance of the CSRRs can be modified, and hence, their intrinsic resonance frequency. As a result, a reconfigurable stop-band filter response is achieved, as depicted in Fig. 1(b). In order to obtain a band-pass filter response, the same topology can be reused by adding two metal wires (per stage) connecting the central CPW strip and the ground planes. A full electrical model for the description of the proposed structures is presented. The circuit models take into account the electrical characteristics of the RF-MEMS, CSRRs and transmission lines as well as the involved electromagnetic coupling and are used for accurate prediction of switchable filters response.

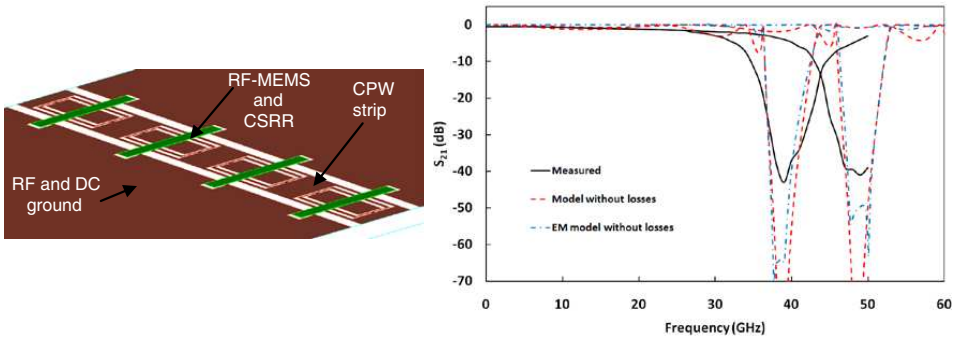

(a) (b)

Figure 1: (a) Layout of a 4-stage CSRR/RF-MEMS switchable filter. (b) Transmission frequency response (insertion losses) corresponding to the RF-MEMS up and down-state. Experimental data, electromagnetic simulations and electrical model are shown.

ACKNOWLEDGMENT

This work has been supported by the Spain-MICINN under Project TEC2009-09994 and AGAUR 2009 SGR 1425.

REFERENCES

1. Rebeiz, G. M., *RF MEMS: Theory, Design and Technology*, John Wiley & Sons, 2003.
2. Falcone, F., T. Lopetegi, J. D. Baena, R. Marqués, F. Martín, and M. Sorolla, "Effective negative-ε stopband microstrip lines based on complementary split ring resonators," *IEEE Microwave Wireless Compon. Lett.*, Vol. 14, 280–282, June 2004.

Critical Behavior and Magnetocaloric Effect Near the Paramagnetic to Ferromagnetic Phase Transition Temperature in $La_{0.7}Pb_{0.05}Na_{0.25}MnO_3$

A. Tozri[1, 2], **E. Dhahri**[1], **E. K. Hlil**[2], **M. Sajieddine**[3], **and M. Valente**[4]

[1]Laboratoire de Physique Appliquée, Faculté des Sciences de Sfax
Université de Sfax, B. P. 1171, Sfax 3000, Tunisie
[2]Institut Néel, CNRS, Université J. Fourier, B. P. 166, Grenoble 38042, France
[3]Laboratoire de Physique et Mécanique des Matériaux, Faculté des Sciences et Techniques
Université Sultan Moulay Sliman, B. P. 523, Béni-Mellal 23000, Morocco
[4]I3N and Physics Department, University of Aveiro, Aveiro 3810-193, Portugal

Abstract— We report a study on the magnetic properties of $(Nd_{1-x}Gd_x)_{0.55}Sr_{0.45}MnO_3$ ceramic material. As the variance σ^2 increases, the paramagnetic-ferromagnetic transition shows a gradual decrease and broadening. However, for $x > 0$ second step magnetic transition has been observed at low temperature. The critical behaviour at the paramagnetic to ferromagnetic phase transition is studied using different techniques. The estimated critical exponents β, γ and δ for the undoped sample are close to the mean-field interaction model. While, for $x > 0$ the critical phenomenon could not be described within the framework of existing universality classes and probably belong to a separate class.

Magneto-impedance Hysteresis in Thin Amorphous Microwires

M. Ipatov, **V. Zhukova**, **J. Gonzalez**, **and A. Zhukov**
Dpto. de Física de Materiales, Fac. Químicas, Universidad del Pais Vasco, San Sebastián 20009, Spain

Abstract— The magneto-impedance effect is understood as the dependence of the impedance on the external axial magnetic field. The high and sensitive magneto-impedance (MI) is related with certain well established magnetic anisotropies and small anisotropy constant. In particularly, these conditions are met in amorphous wires with vanishing magnetostriction constant (CoFe-based microwire) [1]. The outer shell of such wires, where the high frequency current is concentrating due to skin effect, can be treated as a single domain particle with circular magnetization, as the division to domains is unfavorable for short and uniform samples [2]. Therefore, the static magnetization process in the outer shell of such wires runs trough the magnetization rotation and determines the MI dependence. At magnetic field below the anisotropy field H_k, the MI exhibits very high sensitivity to magnetic field $\partial Z/\partial H$ that is of great importance in sensor application. The main drawback, limiting the sensor's resolution is the hysteresis. This hysteresis does not change with the frequency and is attributed to the static magnetization process.

Here we report the novel result in the study of the low-field magneto impedance behavior in amorphous glass-coated microwires with vanishing magnetostriction. The origin of the MI hysteresis and the method of its suppressing are discussed.

REFERENCES

1. Panina, L. V., K. Mohri, T. Uchiyama, M. Noda, and K. Bushida, "Giant magneto-impedance in Co-rich amorphous wires and films," *IEEE Trans. Magn.*, Vol. 31, 1249–1260, 1995.
2. Usov, N., A. Dykhne, A. Antonov, and A. Lagar'kov, "Possible origin for the bamboo domain structure in Co-rich amorphous wire," *J. Magn. Mat.*, Vol. 174, 127–132, 1997.

Femtosecond Laser Focus Determination through Its Perturbation of an Electric Field

Mayo Villagrán-Muniz[1], **Citlali Sanchez-Aké**[1], **and Fausto O. Bredice**[2]

[1]Laboratorio de Fotofísica, Centro de Ciencias Aplicadas y Desarrollo Tecnológico
Universidad Nacional Autónoma de México
Apartado Postal 70-186, México D.F. 04510, México
[2]Centro de Investigaciones Opticas, P. O. Box 124, C. P. 1900 La Plata, Argentina

Abstract— Laser-induced plasmas inside a capacitor cause a redistribution of electric charges between the plates. This effect is measured as a voltage drop through a resistor connected to the ground plate. In previous works we found that the amplitude of the signal was helpful for focusing nanosecond laser pulses onto a target, Ref. [1]. In this work, this procedure was applied in order to determine the best focus of plasmas generated by femtosecond lasers. The result was corroborated by recording the noise amplitude of the shockwave generated by the plasma. The experimental setup used in this work was modified in order to have the maximun signal-noise ratio of the electrical signal. The variation of the intensity of the electrical signal as a function of the number of pulses impinging on the target is another important factor that must be taken into account in order to find the best focus.

REFERENCES

1. Bredice, F., D. Orzi, D. Schinca, M. Sobral, and M. Villagrán-Muniz, "Characterization of pulsed laser generated plasma through its perturbation in an electric field," *IEEE Transactions on Plasma Science*, Vol. 30, No. 6, 2139–2143, Dec. 2002.

A Novel Bandwidth Enhancement Technique for a Compact Right/Left-handed (CRLH) Transmission Line (TL) Based Antenna

Mimi Aminah Wan Nordin, Hany Essam Abd El-Raouf, and A. H. M. Zahirul Alam
ECE Department, Faculty of Engineering, International Islamic University Malaysia (IIUM)
P. O. Box 10, Kuala Lumpur 50728, Malaysia

Abstract— A novel composite right/left-handed (CRLH) transmission line (TL) based metamaterial antenna with wide bandwidth is presented in this paper. The motivation behind the work was the increase in demand for compact metamaterial antennas for applications that require wide bandwidths [1]. Enhancement to the bandwidth of the antenna is achieved by incorporating two additional capacitances, in both, the shunt and series arm of the CRLH TL unit cell equivalent circuit. The additional capacitance in the series arm of the CRLH TL unit cell was added in parallel to the left-handed capacitance, C_L, by which an increase in the total series capacitance is achieved. This was done by means of a cap in the form of the metal-insulator-metal (MIM), which was introduced on a layer below the radiating patches. The additional capacitance in the shunt arm of the CRLH TL unit cell was added in series to the right handed capacitance, C_R, by which a decrease in the total shunt capacitance is achieved. This was done by means of a parallel plate that is being introduced on a layer between the vias and the ground plane of the unit cell. The proposed unit cell consists of the original mushroom structure (which is made up of a patch and a via connecting the patch to the ground plane), a cap and a parallel plate. Analysis of the dispersion characteristic of the proposed unit cell reveals a reduction in dispersion as compared to the unit cell without the two additional capacitances. This factor contributes to the increase in the bandwidth of the structure. The antenna configuration is in the form of a 2×2 patch. A comparison made between the bandwidth of the proposed CRLH TL antennas with the conventional CRLH TL antenna, shows an increase in bandwidth from 9.2% to 18.5%. The proposed antenna is a tri-band and its length, width and height at the first resonant frequency are $\lambda_0/26$, $\lambda_0/26$ and $\lambda_0/27$, respectively; where, λ_0 is the free space wavelength.

REFERENCES

1. Freeman, M., "Rayspan's small antennas save space in wireless world," *Homepage — Rayspan*, Aug. 4, 2010. [Online]. Available: http://www.rayspan.com/news-events/news_20100804.htm. [Accessed]: Sep. 1, 2010.

Performance of GMI Sensors for the Detection of Magnetic Nano-particules and Imaging

Alain Fessant[1], **Philippe Talbot**[2], **Jacek Gieraltowski**[1], **and Emeline Poitevin**[1, 2]

[1]LMB, UEB, Université de Bretagne Occidentale, France
[2]Lab-STICC, UMR 3192, UEB, Université de Bretagne Occidentale
CS 93837, 6 avenue Le Gorgeu, 29238 Brest Cedex 3, France

Abstract— The use of magnetic nanoparticles as a contrast detection agent is interesting in several fields of science and engineering and in particular in those pertaining to biomedical applications [1].

Sensor systems using these nanoparticles are targeted to achieve fast and accurate detection. In many applications it is desirable to have a small device size, low power consumption and high integration capability.

Giant-magnetoimpedance (GMI)-based sensors possess all these properties. The detection device we have developed is based on a network analyzer measurement (S-parameter) of the MagnetoImpedance (MI) spatial profile sensed by a Co-rich amorphous microwire. The sensor transducer is 100 µm in diameter, with a high magnetic permeability and almost zero magnetostriction coefficient. MI measurements are carried out in the [1–500 MHz] frequency range, with an HP 8753C network analyser using a novel broad-band measurement method described elsewhere [2]. The Helmholtz coils used in our apparatus create a static magnetic field Hdc parallel to the microwire axis ranging from 160 Oe to +160 Oe.

In our work, we evaluate and optimize the performance for this type of sensor, particularly in terms of sensitivity and spatial resolution for imaging purpose testing. The automatic measurement process providing a full mapping of a planar test sample is described and analyzed.

We also plan to evaluate the potential of the GMI-based sensors to detect stress corrosion flaws.

REFERENCES

1. Nabily, S., J. Gieraltowski, F. Alves, and B. Kaviraj, "Giant magneto impedance sensors based on microwire and sandwiched structures for non destructive testing applications," *Sensors Letters*, Vol. 7, 278–281, 2009.
2. Fessant, A., J. Gieraltowski, C. Tannous, and R. Valenzuela, "A novel broadband measurement method for the magnetoimpedance of ribbons and thin films," *J. Mag. Mag. Mat.*, Vol. 272–276, Part 3, 1871–1872, 2004.

Effect of Ga-doping on the Magnetic and Magnetocaloric Properties of (LaCaSr)(MnGa)O_3 Compound

A. Omri[1], **M. Bejar**[1], **M. Sajieddine**[2], **E. Dhahri**[1], **E. K. Hlil**[3], **and M. A. Valente**[4]

[1]Laboratoire de Physique Appliquée, Faculté des Sciences de Sfax
Université de Sfax, B. P. 1171, Sfax 3000, Tunisia
[2]Laboratoire de Physique et Mécanique des Matériaux, Faculté des Sciences et Techniques
Université Sultan Moulay Sliman, B. P. 523, Béni-Mellal 23000, Morocco
[3]Institut Néel, CNRS, Université J. Fourier, B. P. 166, Grenoble 38042, France
[4]Physics Department (UA), Campus Universitario, Aveiro 3810-193, Portugal

Abstract— The magnetic and magnetocaloric properties of a series of manganites with the composition $La_{0.76}Ca_{0.08}Sr_{0.17}Mn_{1-x}Ga_xO_3$ ($x = 0$ and $x = 0.2$) have been investigated to explore the influence of Ga doping. The variation of the magnetization M vs. temperature $M(T)$ reveals that all samples exhibit a single transition from a ferromagnetic to a paramagnetic phase at T_C. The magnetoclaoric effect (MCE) was estimated, in terms of isothermal magnetic entropy change ($-\Delta S_m$), using the $M(T, H)$ data and employing the thermodynamic Maxwell equation. The magnetic-entropy value decreases from 2.87 J/kg·K for $x = 0$ to 1.17 J/kg·K for $x = 0.2$ near their respective T_C at 2 T. We have found that our samples present a comparable magnetic-entropy change ($-\Delta S_m$) with those reported for the hole doped-manganites used as competitive material for magnetic refrigeration. These results indicate that these materials are potential candidates for magnetic refrigerants working.

Session 3P1
Anisotropic Media and Liquid Crystals Optics

Industrial Trends in Photo-aligned Liquid Crystals

Mohammed Ibn-Elhaj
Head Liquid Crystal Displays Technology, Rolic Technologies Ltd., Allschwil, Switzerland

Abstract— Anisotropically photo-aligned liquid crystal materials are becoming key components in many optical devices and applications requiring light and polarization control. Especially, optical alignment of monomeric and polymeric liquid crystals enables novel molecular configurations in liquid crystal displays (LCD) as well as a plethora of new thin-film optical elements on single substrates. Besides technological and ecological advance, cost-effective industrial production is a crucial challenge. To illustrate technological and industrial progress and trends, application examples of 2D-, 3D-displays and optical film devices will be presented.

Optical Modeling of Liquid Crystal Biosensors

Dae Kun Hwang[1] and Alejandro D. Rey[2]

[1]Department of Chemical Engineering, University of Saskatchewan
57 Campus Drive, Saskatoon, SK S7N 5A9, Canada
[2]Department of Chemical Engineering, McGill University
3610 University Street, Montreal, Quebec H3A 2B2, Canada

Abstract— Optical simulations of a liquid crystal biosensor device is performed using an integrated optical/textural model based on the equations of nematodynamics and two optical methods: the Berreman optical matrix method and the discretization of the Maxwell equations based on the Finite Difference Time Domain Method (FDTD). Testing the two optical methods with liquid crystal films of different degrees of orientational heterogeneities demonstrates that only the FDTD method is suitable to model this device. Basic substrate-induced texturing process due to protein adsorption gives rise to an orientation correlation function that is nearly linear with the transmitted light intensity, providing a basis to calibrate the device. The sensitivity of transmitted light to film thickness, protein surface coverage, and wavelength is established. A cross-over incident light wave-length close to $\lambda_{co} \approx 500\,\text{nm}$ is found, such that when $\lambda > \lambda_{co}$ thinner films are more sensitive to the amount of protein surface coverage, while for $\lambda < \lambda_{co}$ the reverse holds. In addition it is found that for all wave-lengths the sensitivity increases with the amount of protein coverage. The integrated device model based on FDTD optical simulations in conjunction with the Landau-de Gennes nematodynamics model provides a rational basis for further progress in LC biosensor devices.

Liquid-crystalline Hybrid Nanomaterials with Magnetic Properties

D. Guillon, B. Donnio, S. Bégin, J. L. Gallani, E. Terazzi, and A. Demortière
Institut de Physique et Chimie des Matériaux de Strasbourg
23 rue du Loess, 67034 Strasbourg Cedex 2, France

Abstract— The nanotechnology revolution shall probably not occur without the prior emergence of reliable self-assembling techniques. In that respect, the so-called bottom-up approach is appropriate to build up nanostructures and assemble them from individual atoms, molecules or macromolecules. On one hand, dendritic architectures have been considered, during the last decade, as promising materials for the elaboration and assembly of nanostructures. On the other hand, the possibility to develop large multifunctional macromolecular structures which can further self-assemble into nanosize objects, makes liquid-crystalline dendrimers highly attractive candidates in the field of materials science and may represent an original strategy for the realisation of molecular electronic-based devices.

Using this approach, novel gold nanoparticles protected by a mixture of thiol dendrimer and dodecanethiol chains have been synthesized and characterized. These particles self-organize into a thermotropic body-centered cubic mesophase which is a liquid crystal analogue to the well known nanoparticles superlattices. Moreover, these decorated particles are ferromagnetic at room temperature [1]. We show how the liquid-crystalline order interacts with the magnetic properties, as evidenced by the onset of an unusually slow relaxation of the remnant magnetization as the order develops. Then we suggest that there might be a spin glass-like type of magnetism at the individual particle level and that the observed relaxation is under the influence of the mesophase *via* ligands orientation [2].

We will show also how to control the magnetic anisotropy of Mn_{12} Small Molecular Magnet (SMM) ($[Mn_{12}O_{12}(L_i)_{16}(H_2O)_4]$) by surface hybridization and subsequent supramolecular organisations. In particular, we will focus on pro-mesogenic ligands which can provide a means for finely tuning the molecular geometry of the SMM without deleterious effects on the magnetic behaviour. Such SMM can be rendered mesomorphic by surfacial acetates substitution with gallic derivatives, hence providing self-organized SMM with 3D order [3]. Comparison of the bulk magnetic properties of the series provides evidence of a striking correlation between molecular structure and coercive field. All of these results confirm that the deliberate distortion of the molecular structure can indeed influence the final magnetic properties.

The last example that we describe is the case of mesogen-hybridized monodisperse iron oxide nanocrystals which display magnetic and mesomorphic behavior with a nematic-like order [3]. We show how the magnetic properties are affected after surface-hybridization, suggesting that a modification of the magnetic anisotropy and/or the surface state of the hybrids has taken place.

REFERENCES

1. Donnio, B., P. García-Vázquez, J. L. Gallani, D. Guillon, and E. Terazzi, *Adv. Mater.*, Vol. 19, 3534, 2007.
2. Donnio, B., A. Derory, E. Terazzi, M. Drillon, D. Guillon, and J. L. Gallani, *Soft Matter*, Vol. 6, 965, 2010.
3. Terazzi, E., C. Bourgogne, R. Welter, J. L. Gallani, D. Guillon, G. Rogez, and B. Donnio, *Angew. Chem. Int. Ed.*, Vol. 47, 490–495, 2008.
4. Demortière, A., S. Buathong, B. P. Pichon, P. Panissod, D. Guillon, S. Bégin-Colin, and B. Donnio, *Small*, Vol. 6, 1341, 2010.

Optimization of Coherence Multiplexed Coding for High Density Signal Processing

S. Elwardi[1, 2], **M. Zghal**[1], **and B.-E. Benkelfat**[2]

[1]Cirta'Com Laboratory, Engineering School of Communication of Tunis (Sup'Com)
University of Carthage, Ghazala Technopark, Ariana 2083, Tunisia
[2]Institut Télécom, Télécom SudParis SAMOVAR UMR INT-CNRS 5157
9 rue Charles Fourier 91011 Evry Cedex, France

Abstract— In the context of increased need of optimization and performance in optical multiplexed networks, we study the effect of diffraction in coherence multiplexed systems. Coherence modulation of light is an interesting alternative method among the existing different techniques for optical communication and signal processing. It allows an original simultaneous multiplexing of several signals through a single light beam. Also, the detection of high intensities and frequencies signals using this method has been successfully achieved.

The N-multiplexed coherence system is composed by a cascade of N encoding modules (EM) and a decoding module (DM). Each EM_i is formed by a birefringent electro-optic modulator (EOM_i) and a birefringent slab Q_i set between two polarizers (P) and introducing a static optical path difference (OPD_i), $i = 1, \ldots, N$. To reduce crosstalk between channels, a specific relation between the OPD_is must be used. For a two-channel coherence multiplexing system, OPD_1 must be equal to 3*OPD_2 [1]. Furthermore, it was showed that the optical crosstalk between channels is closely dependent on the spectrum envelope of the source used. It has been shown that the best performance in terms of crosstalk is obtained using a source with a Gaussian emission spectrum.

In this paper, we study the effect of the Gaussian beam diffraction on crosstalk in coherence multiplexed systems. By using a simple Gaussian model, we report that the measurement of the coherence length of the source can lead to an important error [2]. We show that the value of the measured coherence length $L_{c,mes}$ decrease when the angular divergence θ increases and remains smaller than the real value $L_{c,mes} < L_{c,real}$. We also numerically determine the variation of the coherence length as function of the angular divergence. Our results show the variation of the visibility for different wavelength. We finally find out the value of the additional crosstalk introduced in the system as function of the divergence and suggest a solution based on the optical properties of the birefringent elements to reduce the crosstalk.

REFERENCES

1. Geodgebuer, J.-P., A. Hamel, H. Porte, and N. Butterlin, *IEEE J. of Quan. Elec.*, Vol. 26, No. 7, 1217–1226, 1990.
2. Al-Saeed, T. A. and D. A. Khalil, *Applied Optics*, Vol. 49, No. 20, 3960–3966, 2010.

Direct Excitation of Surface Plasmons with TE and TM Waves at Anisotropic Film-metal Interface

I. Abdulhalim
Department of Electro-optic Engineering, Ben-Gurion University of the Negev
Beer Sheva 84105, Israel

Abstract— The two widely used configurations to achieve extended surface plasmon (SP) excitation are either by grating coupling or using the configuration prism-metal-dielectric system called the Kretschmann configuration. The Otto configuration is different in that the dielectric film resides between the prism and the bulk metal surface, and the gap between the prism and the bulk metal has to be less than the wavelength in order for the coupling to take place.

Direct excitation of TE and TM surface plasmon waves at the interface between thin anisotropic film and metal is shown to be possible in the Otto configuration with the anisotropic layer being thicker than the evanescent region. Total absorption occurs at specific wavelengths or incidence angles both for TE and TM waves. Polarization conversion at the resonance is shown to occur when both modes are excited in the anisotropic layer. Tuning the orientation of the dielectric tensor ellipsoid or its principal values allows tuning of the resonance location.

This new configuration can be implemented using liquid crystal or electrooptic polymer thin film, which then allows for building fast switching devices. It is possible to use this configuration as well for sensing of fluids by making the anisotropic film from porous material such as zero order grating structure or sculptured thin films. Detection of the polarization conversion is particularly of interest because it can be measured with modulated polarimetry which allows smaller detection limit.

Highly Birefringent Photonic Crystal Fiber for Coherent Infrared Supercontinuum Generation

A. Ben Salem[1], **R. Cherif**[1], **M. Zghal**[1], **and J. Burger**[2]

[1]Cirta'Com Laboratory, Engineering School of Communication of Tunis (Sup'Com)
University of Carthage, Ghazala Technopark, Ariana 2083, Tunisia
[2]National Metrology Institute of South Africa (NMISA), Pretoria 0001, South Africa

Abstract— We report numerical and experimental studies of supercontinuum (SC) generation in a silicabased nonlinear polarization-maintaining photonic crystal fiber (PM-PCF). A full-vectorial finite element method (FEM), which is highly suited to the analysis of periodic structures, was applied to analyze the propagation properties of the PCF. The optical properties of the fundamental mode of the PM-PCF were numerically determined in terms of birefringence, chromatic dispersion and nonlinear coefficient. The fiber has an air hole diameter of 0.6 µm and a pitch of 1.25 µm exhibiting a nonlinear coefficient of $90\,\mathrm{km^{-1}W^{-1}}$ and a high value of birefringence which we found equal to $4 \cdot 10^{-4}$ at $\lambda = 820\,\mathrm{nm}$. The high birefringence is induced by the asymmetry generated by two big holes alongside the core enlarged during the fabrication process. Thus, the $\frac{\pi}{3}$ symmetry and the degeneracy of the propagation modes are broken. We also determined the positions of the slow and fast axes of the PM-PCF according to the laboratory frame, using two different techniques based on both near and far fields. The generation of over 800 nm bandwidth of visible and infrared light on both axes (slow and fast) was observed in the 2-m-long silica-based nonlinear PM-PCF, in both anomalous and normal dispersion regimes. The SC was generated by coupling ultra-short pulses delivered by a mode-locked femtosecond Ti : Sapphire laser centered at 820 nm. The pulses had been generated with a repetition rate of 202 MHz at the average power of 20 mW and had a duration of 56 fs. We found that the dynamics behind the SC generation was mainly ruled by the effects of self phase modulation, the Raman effects as a responsible for solitonic fissions and the dispersive wave radiation. Finally, the coherence and noise structure of the supercontinua generated in the PM-PCF had been modeled and studied.

Semiclassical Coupled Wave Theory for Bandgap Calculations in Periodically Stratified Dielectric Media

G. V. Morozov[1], **F. Placido**[1], **D. W. L. Sprung**[2], **and Joan Martorell**[3]

[1]Thin Film Centre, University of the West of Scotland, Paisley PA1 2BE, Scotland, UK
[2]Department of Physics and Astronomy, McMaster University, Hamilton, Ontario L8S 4M1, Canada
[3]Facultat Fisica, Departamento d'Estructura i Constituents de la Materia
University of Barcelona, Barcelona 08028, Spain

Abstract— Photonic crystals are artificial low-loss either two-dimensional (2D) or three-dimensional (3D) dielectric structures with a periodic modulation of the refractive index. Due to Bragg reflection, electromagnetic (optical) waves cannot propagate through such structures in certain directions, at certain frequencies. Hence, photonic crystals can exhibit bandgaps (even omnidirectional bandgaps in certain cases) and, as a result, control the propagation of electromagnetic waves in novel ways, with obvious application to dielectric mirrors, dielectric waveguides, and dielectric laser cavities.

A conventional one-dimensional (1D) periodically stratified dielectric structure retains most of useful properties of 2D and 3D photonic crystals for incident light. However, it is much more attractive from a technological point of view. The usual theoretical methods for calculation of bandgaps and reflection/transmission characteristics in periodically stratified media include the Floquet-Bloch formalism, the transfer matrix method, and the coupled wave theory. Among these three, the coupled wave theory offers superior physical insight and gives simple analytical results in limiting cases. Unfortunately, the conventional coupled wave theory of Kogelnik fails in the case of high refractive index contrast, which is essential for a functional 1D crystal.

In this paper, we apply the recently developed semiclassical coupled wave theory to calculate the bandgaps in bilayer, rugate, and exponential rugate periodic stratifications. Comparison with the exact numerical results obtained from the transfer matrix method is given. It turns out that being analytically almost as simple as the conventional coupled wave theory, the semiclassical version is essentially exact for any achievable modulation of the refractive index in those structures.

On the Role of Maxwell Fields in the Resonant Transfer of Energy

A. Salam
Department of Chemistry, Wake Forest University
Winston-Salem, NC 27109-7486, USA

Abstract— A fundamental intermolecular interaction is the resonant transfer of electronic excitation energy between an initially excited donor entity, D, located at $\vec{R}_D$, and an acceptor species, A, in the ground state and positioned at $\vec{R}_A$, with $\vec{R} = \vec{R}_A - \vec{R}_D$. After migration of energy, A becomes excited while D returns to its lowest energy level. This is a much studied process, dating back to Fermi's classic work [1], with subsequent contributions from many others [2–13] seeking to gain insight into the basic mechanism at play using the theory of molecular quantum electrodynamics [12, 13]. Use of this methodology is advantageous in that it allows a unified description to be given for the exchange of energy. According to this theory, resonant energy transfer occurs via the exchange of a single virtual photon between the pair, resulting from emission at one site followed by absorption at the other. Second-order time-dependent perturbation theory within the electric dipole approximation is employed to evaluate the leading contribution to the matrix element, from which the transfer rate may be calculated using the Fermi golden rule. Radiationless (R^{-6} Förster) and radiative (R^{-2} long-range) transfer appear as near- and far-zone asymptotic limits of the result valid for all inter-chromophore separation distances, extending the usual but limited, and obviously unphysical semi-classical derivation [11].

An alternative approach to the matrix element, to be detailed in this talk, is to first calculate the Maxwell fields of the excited donor species followed by the response of an unexcited acceptor moiety which couples to these fields through its electric dipole moment [5]. Expressions for the quantum electrodynamical Maxwell fields in the vicinity of a source are most readily obtained by solving the Heisenberg equations of motion for the second quantized fermionic and bosonic creation and annihilation operators for the electron and photon, respectively. The method is easily extended to account for discriminatory transfer of energy between optically active (chiral) molecules [14] as well as for the modification of the rate by a chiral dielectric medium that can also undergo absorption and dispersion [15]. For this last case it is found that the medium amplifies both the electric dipole and chiral discriminatory transfer rate, with the former contribution enhanced to a greater extent than the latter relative to the rate in a racemic mixture.

REFERENCES

1. Fermi, E., *Rev. Mod. Phys.*, Vol. 4, 87, 1932.
2. Förster, T., *Ann. der Physik*, Vol. 6, 55, 1948.
3. McLone, R. R. and E. A. Power, *Mathematika*, Vol. 11, 91, 1964.
4. Avery, J. S., *Proc. Phys. Soc.*, Vol. 88, 1, 1966.
5. Power, E. A. and T. Thirunamachandran, *Phys. Rev. A*, Vol. 28, 2671, 1983.
6. Andrews, D. L. and B. S. Sherborne, *J. Chem. Phys.*, Vol. 86, 4011, 1987.
7. Andrews, D. L., *Chem. Phys.*, Vol. 135, 195, 1989.
8. Craig, D. P. and T. Thirunamachandran, *Chem. Phys.*, Vol. 167, 229, 1992.
9. Power, E. A. and T. Thirunamachandran, *Phys. Rev. A*, Vol. 56, 3395, 1997.
10. Andrews, D. L. and A. A. Demidov, Eds., *Resonance Energy Transfer*, Wiley, Chichester, 1999.
11. Scholes, G. D., *Ann. Rev. Phys. Chem.*, Vol. 54, 57, 2003.
12. Craig, D. P. and T. Thirunamachandran, *Molecular Quantum Electrodynamics*, Dover, New York, 1998.
13. Salam, A., *Molecular Quantum Electrodynamics*, Wiley, New Jersey, 2010.
14. Salam, A., *J. Chem. Phys.*, Vol. 122, 044113, 2005.
15. Rodriguez, J. J. and A. Salam, *Chem. Phys. Lett.*, In Press.

Raman Response of a Highly Nonlinear As_2Se_3-based Chalcogenide Photonic Crystal Fiber

A. Ben Salem, **R. Cherif**, **and M. Zghal**
Cirta'Com Laboratory, Engineering School of Communication of Tunis (Sup'Com)
University of Carthage, Ghazala Technopark, Ariana 2083, Tunisia

Abstract— We characterize the nonlinear propagation of ultra-short femtosecond pulses in a highly nonlinear As_2Se_3-based chalcogenide photonic crystal fiber (PCF). We propose a design of a highly nonlinear As_2Se_3-based chalcogenide PCF with an air hole diameter of 1.26 µm and a pitch of 1.77 µm, showing a nonlinear coefficient γ of 17.2 $m^{-1}W^{-1}$ at $\lambda = 2.8$ µm. In order to determine the optical properties of the PCF, namely the chromatic dispersion and the nonlinear coefficient, a second order Sellmeier approximaion is proposed to determine the variation of the refractive index of the As_2Se_3 material as a function of the wavelength. We also propose an accurate fit for the Raman response function for the As_2Se_3 chalcogenide fibers in order to evaluate the effect of the stimulated Raman scattering on the supercontinuum generation. The Raman response was extracted from the very recent measurements of the Raman gain spectrum of an As_2Se_3-based chalcogenide fiber [1].

We have investigated the interplay of the nonlinear effects leading to the SC generation as a function of the input power and the fiber length. Less than 1 cm length of the As_2Se_3 PCF was sufficient to numerically obtain over two octaves-spanning supercontinuum (SC) under a low energy femtosecond pumping in the anomalous dispersion regime. The SC spanning from 1.9 µm to 4 µm was generated in few millimeters fiber length with 200 fs pulses at an input average power of 500 µW. The generation of the supercontinua has been mainly attributed to the Raman effect as a responsible for solitonic fissions and dispersive wave radiation. The intrinsic properties of the As_2Se_3 glass and the microstructure provide enhanced optical properties and offer numerous applications in the infrared field including ultrafast all optical switching, Raman fiber lasers, and high resolution spectroscopy.

REFERENCES

1. Hu, J., C. R. Menyuk, L. B. Shaw, J. S. Sanghera, and I. D. Aggarwal, "Maximizing the bandwidth of supercontinuum generation in As_2Se_3 chalcogenide fibers," *Opt. Express*, Vol. 18, 6722–6739, 2010.

Session 3P2
Terahertz Radiation Detection and Emission by Field Effect Transistors

Generation and Detection of Terahertz Radiation by Field Effect Transistors

M. I. Dyakonov
CNRS, Université Montpellier II, Place E. Bataillon, Montpellier 34095, France

Abstract— This is an overview of the main physical ideas for application of Field Effect Transistors (FETs) for generation and detection of THz radiation. Resonant frequencies of the two-dimensional plasma oscillations in FETs increase with the reduction of the channel dimensions and reach the THz range for sub-micron gate lengths. When the mobility is high enough, the dynamics of a short channel FET at THz frequencies is dominated by plasma waves. The possibility of generation is related to the instability of the current-carrying steady state against spontaneous generation of plasma oscillations [1]. The effect is similar to the generation of sound in wind musical instruments. For submicron gate lengths, the characteristic frequencies belong to the THz range.

Detection [2] is based on the nonlinear properties of the electron gas in the FET channel, which lead to the rectification of the ac current induced by the incoming radiation, resulting in a photoresponse in the form of a dc source-drain voltage. Depending on the frequency, electron mobility, and the gate length, the detection can be either resonant (related to the excitation of discrete plasma modes), or non-resonant. In the latter case the FET operates as an efficient room-temperature broad-band detector.

There is now a large body of experimental results on emission, detection, and THz imaging with FETs. After an introduction to the basic ideas, these results will be presented and discussed.

REFERENCES

1. Dyakonov, M. I. and M. S. Shur, *Phys. Rev. Lett.*, Vol. 71, 2465, 1993.
2. Dyakonov, M. I. and M. S. Shur, *IEEE Transactions on Electron Devices*, Vol. 43, 380, 1996.

300-GHz Band Wireless Communications Based on Diode Technologies

Tadao Nagatsuma, **Takuma Takada**, **Masashi Kawamura**, **and Daisuke Asa**
Graduate School of Engineering Science, Osaka University
1-3 Machikaneyama, Toyonaka, Osaka 560-8531, Japan

Abstract— Recently, there has been an increasing interest in the use of electromagnetic waves at frequencies above 275 GHz for wireless communications. This is mainly because that these frequency spectra have not yet been allocated to specific applications and thus we can possibly make use of "extreme bandwidth" for high-speed communications. For example, wireless transmission of OC-768/STM-256 data (43 Gbit/s) requires over 70-GHz DSB bandwidth with ASK/OOK format. As the first step for the exploration of these electromagnetic waves, 300 $\sim$ 400 GHz range is considered to be realistic since enabling semiconductor electronic and photonic devices operating at this frequency range have recently started to be in our hands.

This paper describes recent demonstrations of wireless link using 300 $\sim$ 400 GHz carrier frequencies. For the transmitter, we generate and modulate terahertz waves using photonics technologies. An optical RF signal is generated by heterodyning the two wavelengths of light from the wavelength-tunable light sources. The optical signal is digitally modulated by the optical intensity modulator driven by data signals. Finally, the optical signal is converted to an electrical signal by the terahertz "**photodiode**". The receiver consists of a Schottky barrier "**diode**" and an IF filter followed by a low-noise pre-amplifier and a limiting amplifier. In contrast to the contemporary microwave technologies, where complicated multi-value modulation schemes are introduced to efficiently use limited bandwidths, the diode-based approach is simple and cost-effective. We discuss theoretical performance and limitation of this approach, and show some experimental results of short-distance transmission with a bit rate of over 20 Gbit/s.

Possible Applications of Terahertz FET Devices

Chiko Otani
RIKEN Advanced Science Institute (ASI), Sendai, Japan

Abstract— Diagnosis using terahertz (THz) waves holds a great potential for various applications because of its transparency to many soft materials as well as the good spatial resolution comparable with its wavelength (typically a few hundreds μm). In addition, the specific spectral absorption features due mainly to intermolecular interaction were found in many crystalline materials, and it has been proved that the features can be used to identify these materials. Moreover, THz wave is strongly absorbed by water, and we can make sensitive measurements of water contents by using THz waves. In this presentation, we will introduce possible applications of THz waves and would like to explore the possibility of FET devices related to THz emission or detection. Escpecially, we will introduce THz imaging and spectroscopic applications in security, quality testing and bioscience. We will also introduce the future prospects of THz technology and applications.

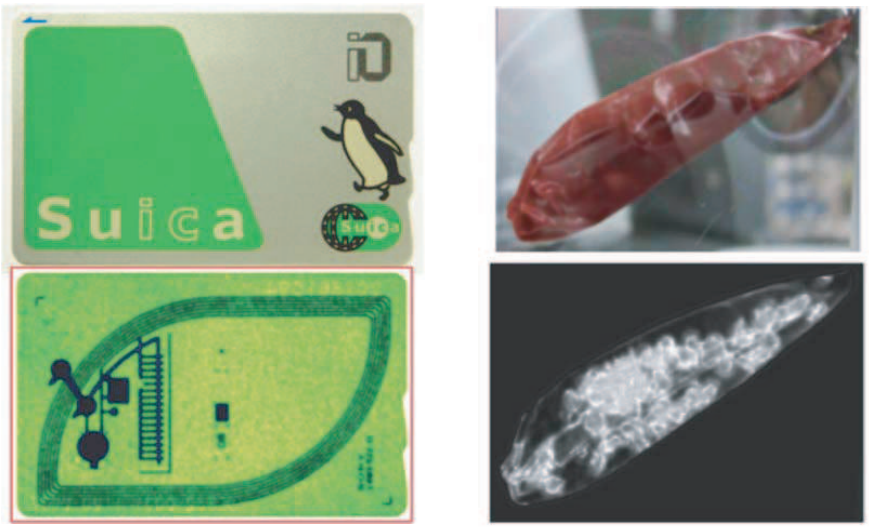

(a) (b)

Figure 1: (a) Terahrtz imaging of Railway's touch-and-go IC card and (b) a red pepper.

Current Driven Terahertz Detection by Plasma Waves in Nano-transistors

F. Teppe[1], **S. Boubanga-Tombet**[1], **J. Torres**[2], **O. Klimenko**[1], **H. Videlier**[1], **S. Nadar**[1], **N. Dyakonova**[1], **D. Coquillat**[1], **A. El Fatimy**[3], **C. Consejo**[1], **B. Chenaud**[1], **C. Chaubet**[1], **and W. Knap**[1]

[1]Groupe d'Etude des Semiconducteurs, CNRS, Université Montpellier 2, Montpellier 34900, France
[2]Institut d'Electronique du Sud, CNRS, Université Montpellier 2, Montpellier 34095, France
[3]School of Physics and Astronomy, Cardiff University, Cardiff CF24 3AA, UK

Abstract— The plasma waves in gated two-dimensional electron gas have a linear dispersion law, similar to the sound waves. The transistor channel is acting as a resonator cavity for the plasma waves, which can reach frequencies in the Terahertz (THz) range for a sufficiently short gate length Field Effect Transistors (FETs) [1, 2]. A variety of possible applications of FET operating as a THz device have been suggested. In particular, it was shown that the nonlinear properties of plasma oscillations can be utilized for terahertz detectors, broadband detectors, mixers and frequency multipliers.

We have demonstrated in various materials that the detection of THz radiations by plasma waves might be strongly modified by the application of a dc drain current [3, 4]. We found that driving a transistor into the saturation region enhances the non-resonant detection and can lead to the resonant detection [5–7]. even if the condition $\omega_0\tau \gg 1$ is not satisfied (ω_0 is the fundamental plasma wave frequency and τ is the momentum relaxation time), since the effective decay time for plasma oscillations is $1/\tau_{eff} = 1/\tau - 2v/L$, where v is the electron drift velocity.

REFERENCES

1. Dyakonov, M. and M. S. Shur, *Phys. Rev. Lett.*, Vol. 71, 2465, 1993.
2. Dyakonov, M. and M. S. Shur, *IEEE Trans. Electron Devices*, Vol. 43, 380, 1996.
3. Veksler, D., F. Teppe, A. P. Dmitriev, V. Y. Kachorovskii, W. Knap, and M. S. Shur, *Phys. Rev. B.*, Vol. 73, No. 12, 125328, 2006.
4. Teppe, F., D. Veksler, V. Y. Kachorovski, A. P. Dmitriev, X. Xie, X.-C. Zhang, S. Rumyantsev, W. Knap, and M. S. Shur, *Applied Physics Letters*, Vol. 87, 022102, 2005.
5. Teppe, F., W. Knap, D. Veksler, V. Y. Kachorovskii, A. P. Dmitriev, S. Rumyantsev, and M. S. Shur, *Applied Physics Letters*, Vol. 87, 052107, 2005.
6. Teppe, F., M. Orlov, A. E. Fatimy, A. Tiberj, W. Knap, J. Torres, V. Gavrilenko, A. Shchepetov, Y. Roelens, and S. Bollaert, *Applied Physics Letters*, Vol. 89, 222109, 2006.
7. Boubanga-Tombet, S., F. Teppe, D. Coquillat, S. Nadar, N. Dyakonova, H. Videlier, W. Knap, A. Shchepetov, C. Gardes, Y. Roelens, S. Bollaert, D. Seliuta, R. Vadoklis, and G. Valusis, *Applied Physics Letters*, Vol. 92, 212101, 2008.

Detection of Terahertz Radiation from Strained Silicon Modulation Field Effect Transistor

Y. M. Meziani[1], **E. Velazquez**[1], **E. Diez**[1], **N. Dyakonova**[2], **W. Knap**[2], **A. Elmoutaouakil**[3], **K. Fobelets**[4], **and T. Otsuji**[3]

[1]Salamanca University, Spain
[2]Groupe d'Etude des Semiconducteurs, Montpellier 2 University, France
[3]Research Institute of Electrical Communication, Tohoku University, Japan
[4]Department of Electrical and Electronic Engineering, Imperial College London, UK

Abstract— We report on detection of terahertz radiation by using submicron size strained silicon modulation FET. A non-resonant response was observed at room temperature. However, when the device was cooled down to 4.2 K a clear resonant response is observed. We also report on photomixing function of the device within terahertz range.

Terahertz rays are located in the spectral region 0.1–10 THz (3 mm–30 μm) between the microwave and the infrared portion of the electromagnetic spectrum. T-rays has the potential to penetrate most common living materials like cloth, papers or plastics. Collective charge density oscillations in two-dimensional electrons systems can be used either for detection and/or emission of terahertz electromagnetic radiations. The resonant frequency of the plasma oscillation is given by the following formulas $f \approx v_p/\lambda = (e^2 n_s d/m\varepsilon)^{1/2} \times l/L$ where v_p the plasma waves velocity, λ the wave length, n_s the electron density and L the gate length. Two important remarks can be deduced: (i) the resonant frequency can reach terahertz range for sub-micron size transistors (ii) the electron density (i.e., gate bias) is the key parameter to tune of the resonant frequency. When the plasma waves excited by an external electromagnetic radiation the induced ac electric fields can be converted into measurable dc signal via nonlinear conversion mechanism.

In the present work, a submicron size strained silicon MODFET was subjected to pulsed terahertz radiation at room temperature. A non resonant resonant detection was observed and explained as due to the excitation of the plasma waves. A maximum of signal was also observed when the polarization of the light was parallel to the channel. The device was cooled down to 4.2 K to increase the mobility and we observed a resonant detction where the signal shift according to Dyakonov-Shur theory. We will also report on photomixing function of the transistor within terahertz range. The device was subjected to two CW laser where the difference frequency was fixed at 4 THz and the photoresponse signal shows a maximum for $V_g = -0.15$ V. This was explained as due to the mode locked regime of the plasma waves in the channel. This type of transistors could be a good room temperature sensor based on mature Silicon technology and which could integrate new compact terahertz imaging/spectroscopy systems.

ACKNOWLEDGMENT

This work was financially supported in part by the aid of the MICINN-Spain under the PPT-120000-2009-4. The authors want to the Ramon y Cajal Program in Spain for the support.

Sub-terahertz Imaging with AlGaN/GaN Based MISFETs and FETs Using Field-plate Technology

F. Teppe[1], **D. Coquillat**[1], **N. Dyakonova**[1], **S. Nadar**[1], **O. Klimenko**[1], **H. Videlier**[1], **K. Madjour**[2], **G. Ducournau**[2], **C. Gaquière**[2], **M. A. Poisson**[3], **S. Delage**[3], **A. Dobroiu**[4], **and W. Knap**[1]

[1]Groupe d'Etude des Semiconducteurs, UMR 5650, CNRS, Université Montpellier 2, France
[2]IEMN, UMR 8520, Villeneuve d'Ascq 59655, France
[3]Thales Research and Technology, Orsay 91404, France
[4]RIKEN, 519-1399 Aramaki-Aoba, Aoba-ku, Sendai, Miyagi 980-0845, Japan

Abstract— As terahertz applications emerge, the need for sensitive detectors capable of fast response is becoming crucial and the room temperature operation is often required. Amongst these detectors, emerging plasma wave electronic devices such as field effect transistors (FETs) [1] offer performance comparable to commercially available devices with the advantages of easy matrix focal plane integration. AlGaN/GaN FETs have great potential because of their material advantages such as high breakdown voltage, high electron mobility, and high saturation velocity. These advantages could be exploited for resonant and non-resonant terahertz detection [2, 3].

We have designed, fabricated, and characterized different AlGaN/GaN FETs as single pixel terahertz detectors. This work focuses on two different structures: a metal-insulator-semiconductor FET (MISFET) and a FET using field-plate technology. To evaluate their optical performance as a non-resonant terahertz detector at room temperature, we measured the responsivity and the noise equivalent power (NEP). The dependence of the photoresponse was analyzed as a function of the voltage applied on the gate and as a function the azimuthal angle between the THz electric field and the source-to-drain direction for the structure. The imaging performance of the detectors was evaluated by scanning objects for different gate voltages.

ACKNOWLEDGMENT

This work was financially supported by the ANR "TeraGaN" and ANR-JST "WITH" projects. The authors from Montpellier University acknowledge the CNRS guiding GDR-I projects "'Semiconductor sources and detectors of THz frequencies", the GIS "TeraLab", and STMicroelectronics through the "NANO 2012" project.

REFERENCES

1. Dyakonov, M. I. and M. S. Shur, *IEEE Transactions on Electron Devices*, Vol. 43, 380, 1996.
2. El Fatimy, A., S. Boubanga Tombet, F. Teppe, W. Knap, D. B. Veksler, S. Rumyantsev, M. S. Shur, N. Pala, R. Gaska, Q. Fareed, X. Hu, D. Seliuta, G. Valusis, C. Gaquiere, D. Theron, and A. Cappy, *Electron. Lett.*, Vol. 42, 1342, 2006.
3. Muravjov, A. V., D. B. Veksler, V. V. Popov, O. V. Polischuk, N. Pala, X. Hu, R. Gaska, H. Saxena, R. E. Peale, and M. S. Shur, *Appl. Phys. Lett.*, Vol. 96, 042105, 2010.
4. El Fatimy, A., N. Dyakonova, Y. Meziani, T. Otsuji, W. Knap, S. Vandenbrouk, K. Madjour, D. Théron, C. Gaquiere, M. A. Poisson, S. Delage, P. Prystawko, and C. Skierbiszewski, *J. Appl. Phys.*, Vol. 107, 024504, 2010.

Terahertz and Infrared Detectors Based on Multiple-graphene Layers with p-i-n Junctions: Device Model and Characteristics

M. Ryzhii[1], **V. Ryzhii**[1], **T. Otsuji**[2], **and V. Mitin**[3]

[1]The University of Aizu, Aizu-Wakamatsu 965-8580, Japan
[2]Research Institute of Electrical Communication, Tohoku University, Sendai 980-8577, Japan
[3]University at Buffalo, The State University of New York, NY 14260, USA

Abstract— Among the carbon-based materials, graphene layer structures promise particularly interesting device applications. Apart from several unique features, graphene layers (GLs) exhibit very specific optical properties associated with the gapless energy spectrum. A rather high coefficient of interband transitions in a single GL makes GLs, as well as graphene bilayers (GBLs) and graphene nanoribbons (GNRs), very attractive for lasers and detectors of terahertz (THz) and infrared (IR) radiation [1–3]. As demonstrated recently (see Ref. [4] and the references therein), the stacks of disoriented (the non-Bernal stacked) GLs exhibit virtually the same electron and optical properties as individual GLs, except, certainly, much higher absorption coefficient. The multiple-GL photodiodes (MGL-PDs), which can operate as THz and IR detectors, with either chemically doped or electrically induced p-i-n junctions were recently proposed [3]. In this communication, we report on the device model for MGL-PDs and the results of their characteristics calculations.

The device structures under consideration are schematically shown in Figs. 1(a) and 1(b). Using the developed model, we obtain analytical formulas for the MGL-PD responsivity and dark-current limited detectivity and compare the MGL-PD characteristics with those of the field-effect phototransistors based on GBLs (GBL-PTs shown in Fig. 1(c)) proposed earlier [5].

We demonstrate that at lower temperatures, GBL-PT can surpass MGL-PDs exhibiting huge values of the responsivity and detectivity. We also show that MGL-PDs can overperform other THz and IR detectors, particularly, at elevated (room) temperatures.

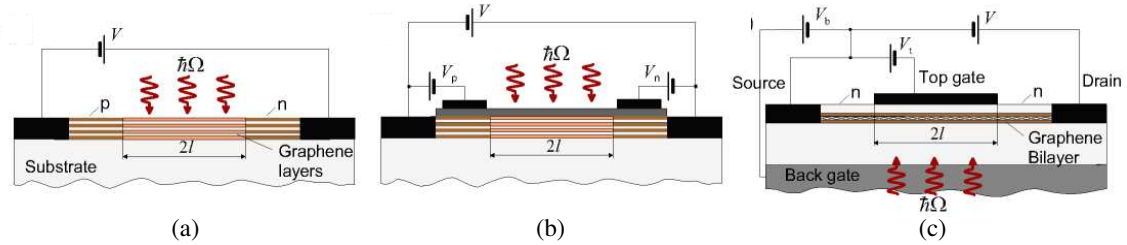

Figure 1: Device structures of MGL-PDs (a) with doped and (b) with electrically induced p-i-n-junctions, and (c) device structure of GBL-PD.

REFERENCES

1. Ryzhii, V., M. Ryzhii, and T. Otsuji, *J. Appl. Phys.*, Vol. 101, 083114-1-4, 2007.
2. Ryzhii, V., M. Ryzhii, A. Satou, T. Otsuji, A. A. Dubinov, and V. Y. Aleshkin, *J. Appl. Phys.*, Vol. 106, 084507-1-5, 2009.
3. Ryzhii, V., M. Ryzhii, V. Mitin, and T. Otsuji, *J. Appl. Phys.*, Vol. 106, 084512, 2009.
4. Orlita, M. and M. Potemski, *Semicond. Sci. Technol.*, Vol. 25, 063001, 2010.
5. Rana, F., P. A. George, J. H. Strait, and S. Shivaraman, *Phys. Rev. B*, Vol. 79, 115447-1-5, 2009.

Photon Helicity Driven Currents in Graphene

S. D. Ganichev
Terahertz Center, University of Regensburg, Regensburg 93040, Germany

Abstract— We report on the observation of photon helicity driven currents in graphene. We demonstrate that by illuminating unbiased monolayer graphene samples with terahertz (THz) laser radiation at room temperature under oblique and normal incidence causes directed electric currents. This includes currents which are solely driven by the light's helicity. In this case we observe a net electric current, whose sign reverses upon switching the radiation helicity from left- to right-handed circularly polarized light. The phenomenological and microscopic theories of the observed photocurrents are developed. We demonstrate that under oblique incidence the helicity driven current is caused by the circular ac Hall effect in the bulk of the graphene sheet driven by the crossed ac E- and B-fields of circularly polarized radiation. Alike the classical dc Hall effect, the voltage is caused by crossed E and B fields which are, however, rotating with the light's frequency. By contrast, the effect observed at normal incidence stems from the sample edges, which reduce the symmetry and result in an asymmetric scattering of carriers driven by the radiation electric field. Observation of the helicity driven photocurrent in graphene demonstrates that this material may be a good candidate for novel type of detectors of terahertz radiation. Besides photon helicity dependent currents we also observe photocurrents driven by linearly polarized radiation. The microscopic mechanisms governing this effect are discussed.

Terahertz Emission, Detection and Modulation Using Two-dimensional Plasmons in High-electron-mobility Transistors Featured by a Dual-grating-gate Structure

Taiichi Otsuji
Research Institute of Electrical Communication, Tohoku University, Sendai, Japan

Abstract— Two-dimensional plasmons (2DPs) in high-electron mobility transistors (HEMT's) have attracted much attention due to their potentiality promoting emission and detection of terahertz (THz) radiation. In this talk recent advances in our original HEMT-based terahertz plasmon-resonant devices will be reviewed.

The 2DP itself has the nature of nonlinearity. If the 2DP is confined in a submicron channel of a HEMT, the 2DP nonlinearity can help rectify the THz radiation so that it can work as a THz detector [1]. When the 2D plasmon cavity (defined in the HEMT channel) has an asymmetric boundary (source-ground and drain-open), the DC current flow can promote the instability leading to self-oscillation so that it can work as a THz source [2]. The 2DPs are non-radiative longitudinal modes of evanescent waves. To couple the 2DPs with radiative photons of the THz waves, an antenna structure is needed. A grating coupler is well known as a broadband antenna [3]. In our original device structure an interdigitated dual grating gate (DGG) is introduced for this purpose [4]. The plasmon resonant frequency can be tuned by the 2D electron density that is controlled by the gate bias. When the frequency of THz incoming radiation is resonant (off-resonant) to the 2DP, it will be well absorbed in (transmitted throught) the HEMT channel. Thus one can control the transmissivity of THz radiation by the gate bias, leading to an intensity modulation function to the THz radiation [5].

We have developed 2DP-resonant DGG-HEMT emitters/detectors using GaAs-based or InP-based material systems [6–8]. Under DC-biased conditions with relatively high drain bias, the device can emit broadband (0.5 to 6.5 THz) radiation even at room temperature, originated from multimode plasmons including coherent type due to DC-current-driven instability and incoherent type due to thermal excitation [6]. Currently maximum available THz output power is estimated to be on the order of 10 μW from a single die active area of $30 \times 75\,\mu m^2$ with an excellent power conversion efficiency of 10^{-4} [7]. To realize coherent monochromatic THz emission laser photomixed injection locking will be a solution [9]. On the other hand, when the device operates under low drain bias conditions, it detects the THz radiation. Presently a high-sensitive (NEP $\sim 10^{-10}\,W/Hz^{0.5}$) non-resonant detection has been confirmed at room temperature [10, 11]. Enhancement on the detection sensitivity will need further structural advancement. Regarding the intensity modulation function of the DGG-HEMTs, we have recently numerically confirmed its feasibility by using finite-difference time-domain (FDTD) method. The extinction ratio of more than 80% will be achievable [5]. In summary, above-mentioned three distinctive functionalities will make the 2DP DGG-HEMTs to be possible transmitter/receiver front-end key devices for THz wireless communication systems.

REFERENCES

1. Dyakonov, M. M. and M. Shur, *IEEE Trans. Electron. Dev.*, Vol. 43, 380, 1996.
2. Dyakonov, M. and M. Shur, *Phys. Rev. Lett.*, Vol. 71, 2465, 1993.
3. Allen, Jr., S. J., D. C. Tsui, and R. A. Logan, *Phys. Rev. Lett.*, Vol. 38, 980, 1977.
4. Otsuji, T., M. Hanabe, T. Nishimura, and E. Sano, *Opt. Express*, Vol. 11, 4815, 2006.
5. Nishimura, T., N. Magome, and T. Otsuji, *Jpn. J. Appl. Phys.*, Vol. 49, 054301, 2010.
6. Otsuji, T., Y. M. Meziani, T. Nishimura, T. Suemitsu, W. Knap, E. Sano, T. Asano, and V. V. Popov, *J. Phys.: Condense Matter*, Vol. 20, 384206, 2008.
7. Tsuda, Y., T. Komori, A. El Fatimy, T. Suemitsu, and T. Otsuji, *J. Opt. Soc. Am. B*, Vol. 26, A57, 2009.
8. El Moutaouakil, A., T. Komori, K. Horiike, T. Suemitsu, and T. Otsuji, *IEICE Trans. Electron.*, Vol. E93C, 1286, 2010.
9. Otsuji, T., T. Nishimura, Y. Tsuda, Y. M. Meziani, T. Suemitsu, and E. Sano, *Int. J. High Speed Electron. Sys.*, Vol. 19, 33, 2009.

10. Coquillat, D., S. Nadar, F. Teppe, N. Dyakonova, S. Boubanga-Tombet, W. Knap, T. Nishimura, T. Otsuji, Y. M. Meziani, G. M. Tsymbalov, and V. V. Popov, *Opt. Express*, Vol. 18, 6024, 2010.
11. El Moutaouakil, A., T. Suemitsu, T. Otsuji, H. Videlier, S.-A. Boubanga-Tombet, D. Coquillat, and W. Knap, *Phys. Stat. Solidi*, in Press.

Gate Fingers and Device Loading Effect on Terhartz Detection from Dual Grating Gate Plasmon-resonant Structure Using InGaP/InGaAs/GaAs Material Systems

A. El Moutaouakil[1], **D. Coquillat**[2], **W. Knap**[2], **T. Suemitsu**[1], **and T. Otsuji**[1]

[1]Research Institute of Electrical Communication, Tohoku University, Japan
[2]Groupe d'Etude des Semiconducteurs, Montpellier 2 University, France

Abstract— We report on highly sensitive nonresonant THz detection in our original InGaP/InGaAs/GaAs plasmon-resonant DGG-HEMTs at room temperature, by introducing a new device model expressing the loading effect. The calibrated responsivity exhibited higher values by one order than ever.

Terahertz (THz) detection by using the rectification mechanism of two-dimensional plasmons in semiconductor quantum wells like electron channels in high-electron mobility transistors (HEMTs) gained a huge interest in the recent years, and potential applications are foreseen to fulfill the need for better THz detectors which can be used in communication, security, and imaging.

In this paper, we report on nonresonant detection of THz radiation using an InGaP/InGaAs/GaAs plasmon-resonant high-electron-mobility transistor having a dual grating gate (DGG) structure and discuss the loading effect on THz photoresponse, as well as the gate number effect. The experiments were performed using a Gunn diode operating at 300 GHz as the THz source. Thanks to the antenna effect of the DGG and slot-line-feed structures, the measured responsivity showed reasonable coupling and polarization dependence to the THz radiation, taking the highest value when the incident THz radiation is lineally polarized to the source-drain direction (Fig. 1). Compared to the traditional single-gate (SG) HEMTs, however, the responsivity of the DGG-HEMTs was relatively low, which is caused by the device loading effect [3]. The loading effect was mainly related to the parallel resistive factors being loaded along the channel, which is originated from the short-channel effect and/or off-the-DGG area in the channel, increasing the background off current, thus, lowering the responsivity. Moreover, while the theory predicts a higher nonresonant responsivity for the larger gates, the DGG showed more dependence on the number of the gate fingers, showing a higher responsivity for transistors with a higher gate bias/gate fingers ratio.

The obtained performances are well comparable to or even higher than those for traditional SG-HEMTs.

ACKNOWLEDGMENT

This work was supported by the JSPS-SAKURA project. The device process for this work was carried out in part at the Laboratory for Nanoelectronics and Spintronics, RIEC at Tohoku University.

Optical Excitations of Plasma Instability in HEMTS — Possibility of Mode Locking for THZ Emission

P. Nouvel[1], **J. Torres**[1], **H. Marinchio**[1], **T. Laurent**[1], **C. Palermo**[1], **L. Varani**[1], **F. Teppe**[2], **E. Starikov**[3], **P. Shiktorov**[3], **and V. Gružinskis**[3]

[1]Institut d'Electronique du Sud (CNRS UMR 5214), University Montpellier II Montpellier 34095, France

[2]Groupe d'Etude des Semiconducteurs (CNRS UMR 5650), University Montpellier II Montpellier 34095, France

[3]Semiconductor Physics Institute, Goshtauto 11, Vilnius 01108, Lithuania

Abstract— At the present time wide hopes and expectations of development of THz range solid-state devices are connected with the use of modern FETs and HEMTs. This is related to three main features of such transistors:

(i) high mobility of carriers in the transistor channel,

(ii) strong nonlinearity of current owing along the channel governed by a gate, and

(iii) possibility of tuning the frequency of 2D plasma waves excited in the channel under the gate by varying the gate potential.

These peculiarities of carrier transport in the channel allow to use such transistors both for detection and generation of THz radiation [1, 2]. Recently, the possibility of both resonant and nonresonant detection of THz radiation based on these transistors was verified experimentally (see, e.g., [2, 3] and references therein). However, the other possibility, that is to use them as sources of such a radiation due to spontaneous excitation of plasma waves in the transistor channel (for example, owing to Dyakonov-Shur instability [1]), up to now is still under investigation [4]. The aim of this report is to present experimental results of direct measurement of stimulated resonant emission optically excited in InGaAs HEMT channels.

The stimulated excitation was performed by photo-generation of electron-hole pairs in the HEMT channel at the frequency of the beating of two IR-commercially-available InGaAs distributed feedback cw-laser sources with photon energy of about 0.8 eV. The presence of resonances of radiation emission in the range $f_0 \pm 10\,\mathrm{GHz}$ (with f_0 from 0.4 up to 0.5 THz) detected by a Si-bolometer is found. The intensity of THz emission exhibits a nearly exponential growth with increase of the pumping power. In the proposed report we will present experimental details as well as analysis and discussion of possible theoretical interpretation of the obtained results.

REFERENCES

1. Dyakonov, M. and M. Shur, *Phys. Rev. Lett.*, Vol. 71, 2465, 1993.
2. Knap, W., et al., *Appl. Phys. Lett.*, Vol. 84, 2331, 2004.
3. Nouvel, P., et al., *J. Appl. Phys.*, Vol. 106, 013717, 2009.
4. Dyakonova, N., et al., *Appl. Phys. Lett.*, Vol. 88, 141906, 2006.

Subharmonic Mixing in Field-effect Transistors Operating above the Threshold Frequency f_T

A. Lisauskas, **S. Boppel**, **and H. G. Roskos**
Physikalisches Institut, Johann Wolfgang Goethe-Universität Frankfurt
Frankfurt am Main, Germany

Abstract— We theoretically show the feasibility for field-effect transistors to operate as subharmonic mixers at frequencies above the threshold frequency f_T. We discuss the enhancement of the conversion efficiency by the control of the phase of the radio (RF) and local-oscillator (LO) signals when these signals are simultaneously applied to the transistor's gate and drain terminals. The mixing efficiency can furthermore be increased drastically by an electric current flowing through the transistor's channel. Finally, we compare the envisaged performance of transistor-based mixers with a standard solution based on Schottky diodes.

Room Temperature Terahertz Detection: Direct Comparison between Field Effect Transistor and Hot Electron Bolometer Based on AlGaAs/GaAs 2DEG

A. El Fatimy[1,2], **P. D. Mauskopf**[1], **D. Morozov**[1], **and K. Wood**[2]

[1]School of Physics and Astronomy, Cardiff University, Cardiff CF24 3AA, UK
[2]QMC Instruments Ltd., School of Physics and Astronomy, Cardiff University, Cardiff CF24 3AA, UK

Abstract— We compare the use of hot electron bolometric detector with a nanometric plasma wave transistor to detect terahertz radiation. For the same average THz power and frequency modulation, both detection schemes have comparable performance. When the operation temperature is decreased to low than 300 K, signal to noise ratio and sensitivity are better with an antenna-coupled hot-electron bolometer. Using p-InAs surface field emitter, we demonstrate the feasibility of a THz imaging system using both detectors.

An example of direct application of the system in terahertz imaging field is presented in Figure 1. We used a fast terahertz pulse imaging system based on femtosecond Ti : Sa laser oscillator. The system is relatively compact and simple since it does not require a pump probe time delay stage. Consequently, the usual complexity of the optics involved can be greatly reduced.

The results clearly illustrate that plasma wave nanometer transistors and hot electron bolometers can be efficient future detectors for terahertz imaging applications based on a femtosecond pulsed terahertz source once integrated in detector arrays. Future work has to show which type of the HEB system is most suitable for sensitive terahertz source detection.

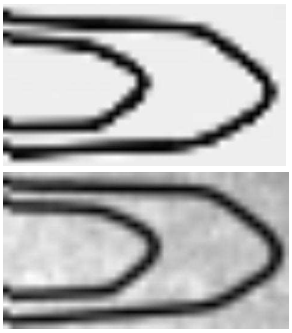

Figure 1: Raster-scan imaging in transmission mode of a metallic paper clip: (Top) without envelope, (Bottom) in envelope. Terahertz image with a numerical aperture of 0.5; 0.3 mm pixel size, 20 mm × 10 mm.

Spin Related Effect in Terahertz Photovoltaic Response of Si-MOSFETs

H. Videlier[1], **N. Dyakonova**[1], **F. Teppe**[1], **C. Consejo**[1], **W. Knap**[1], **J. Lusakowski**[2], **D. Tomaszewski**[3], **J. Marczewski**[3], **and P. Grabiec**[3]

[1]GES-UMR5650, Université Montpellier 2 and CNRS, Montpellier 34095, France
[2]Institute of Experimental Physics, Warsaw University, Warsaw, Poland
[3]Institute of Electron Technology, Al. Lotnikow 32/46, Warsaw 02-668, Poland

Abstract— We report on investigations of photovoltaic response of Si-MOSFETs subjected to Terahertz radiation in high magnetic fields. The MOSFETs develop a dc drain-to-source voltage that shows singularities in magnetic fields corresponding to paramagnetic resonance conditions. These singularities are investigated as a function of incident frequency, temperature and two-dimensional carrier density. We tentatively attribute these resonances to spin transitions of the electrons bounded to Si dopants and discuss the possible physical mechanism of the photovoltaic signal generation.

Photoresponse to sub-Terahertz and Terahertz (THz) radiations in Silicon Metal Oxide Semiconductor Field Effect Transistors (Si-MOSFETs) has been studied previously [1–3]. The obtained values of responsivity and Noise Equivalent Power have shown the potential of Si-MOSFETs as sensitive detectors at room temperature [1]. The photovoltaic response dependences on the gate length and the gate bias were in good agreement with the Dyakonov-Shur plasma wave detection theory [4]. The detection signal results from the rectification of high frequency currents induced by the incident radiation in the transistor channel. The rectification takes place due to a nonlinear response of the gated two dimensional electron gas and a source-drain asymmetry. The main source of nonlinearity is the superposition of two radiation-induced effects: i) the modulation of the carrier density in the channel by variations of the gate potential and ii) drift velocity modulation due to variations of the drain potential. Recently, monolithically integrated THz focal-plane arrays including antennas and amplifiers on a single silicon die has been designed to work at room temperature [5].

In this work, we have studied the effect of high magnetic field on the Si-MOSFETs photovoltaic response subjected to sub-Terahertz radiation.

Si MOSFET structures used in our study had gate length and width respectively, $L_g = 10\,\mu\text{m}$ and $W_g = 5\,\mu\text{m}$. Sub-Terahertz radiation in the range 185–300 GHz was brought from a Backward Wave Oscillator source or a Gunn diode to the transistor through a polished pipe. The photovoltaic signal, ΔU, was measured between source and drain contacts using a standard lock-in technique. The temperature range was from 4 K to 300 K.

The magnetic field affected the photoresponse in two manners: (i) we observed a smooth decreasing of the signal with magnetic field; (ii) we observed a well pronounced structures that shift to higher magnetic fields with increasing light frequency.

The smooth decreasing behavior can be explained by plasma waves damping that takes place at magnetic fields B higher than the cyclotron resonance one $B_c = \omega_c\,\text{m/e}$, where ω_c is the cyclotron frequency, m is the effective mass.

The singularity on the $\Delta U(B)$ curve shift to higher magnetic fields with increasing light frequency and changes with temperature. The position of the structure is qualitatively described by the equation $f = g\mu_B B/h$, where $g = 2$ corresponding to the g factor of typical Silicon dopants. At low temperature (12.5 K) the singularity has a complex structure, composed of several lines. With temperature increase side lines disappear, the structure as a whole narrows and its relative amplitude decreases.

The exact physical mechanism leading to photovoltaic response related to spin resonance transitions is not clear up to now. We can speculate that the signal is related to the change of the free carrier mobility. The change of the mobility can take place at the spin resonance via one of the spin dependent scattering mechanisms. This change of the mobility can lead to the photovoltaic response in a similar way as the change in the carrier density.

However, a full quantitative interpretation of our results requires more complete experimental and theoretical developments.

REFERENCES

1. Tauk, R., F. Teppe, S. Boubanga, et al., "Plasma wave detection of terahertz radiation by silicon field effects transistors: Responsivity and noise equivalent power," *Applied Physics Letters*, Vol. 89, 253511, 2006.
2. Knap, W., F. Teppe, Y. Meziani, et al., "Plasma wave detection of sub-terahertz and terahertz radiation by silicon field-effect transistors," *Applied Physics Letters*, Vol. 85, 675–677, 2004.
3. Stillman, W., M. S. Shur, D. Veksler, S. Rumyantsev, and F. Guarin, "Device loading effects on nonresonant detection of t, erahertz radiation by silicon MOSFETs," *Electronics Letters*, Vol. 43, No. 7, 2007.
4. Dyakonov, M. and M. Shur, "Detection, mixing, and frequency multiplication of terahertz radiation by two-dimensional electronic fluid," *IEEE Transactions on Electron Devices*, Vol. 43, No. 3, 380–387, 1996.
5. Ojefors, E., et al., "A 0.65 THz focal-plane array in a quarter-micron CMOS process technology," *IEEE Journal of Solid-State Circuits*, Vol. 44, No. 7, 1968–1976, 2009.

Session 3P3a
Reduction of the Mutual Coupling and/or Metamaterial Absorbers

Design of 2 x 2 U-shape MIMO slot antennas with EBG material for mobile handset applications

Z. Z. Abidin[1,2], **Y. Ma**[1], **R. A. Abd-Alhameed**[1], **K. N. Ramli**[1,2], **D. Zhou**[3], **M. S. Bin-Melha**[1], **J. M. Noras**[1], **and R. Halliwell**[1]

[1]Mobile and Satellite Communications Research Centre, University of Bradford
Bradford, West Yorkshire, BD7 2DF, UK
[2]Faculty of Electrical and Electronic Engineering, Universiti Tun Hussein Onn Malaysia
Parit Raja, Batu Pahat, Johor, Malaysia
[3]Surrey Space Centre, University of Surrey, Guildford, GU2 7XH, UK

Abstract— Multi-Input Multi-Output (MIMO) antenna systems have attracted considerable interest as an effective way of improving reliability and increasing the channel capacity in wireless mobile communications. MIMO antennas can enable to provide high speed and high quality transmission involving large amount of data transfer in rich multipath environments. MIMO antennas for wireless handset applications require highly efficient antenna design that provides sufficient spatial de-correlation, which challenges for designing in a small handset device. In order to achieve a high isolation, good diversity and multiplexing performance are required.

Primary aim of MIMO antenna design is to reduce correlation between received signals. A significant parameter for the correlation is the mutual coupling since it may marginally change the performance of the system especially at the receiver end. Mutual coupling describes the electromagnetic interactions that exist between antenna elements of an antenna array. One consequence of these interactions is the distortion of the radiation pattern of each element of the multi-element system compared to the radiation pattern of each isolated element. Higher mutual coupling may result in lower antenna efficiencies and higher correlation coefficients. The effect of mutual coupling on capacity of MIMO wirelesschannels is studied in [1]. One of the most critical parameter affecting mutual coupling and correlation is due to spacing between the elements, spatial diversity. Analytical studies have shown that for minimal or no mutual coupling, the distance between typical antenna elements needs to be at least half wavelength [2]. A 2×2 MIMO meander liner planar inverted-F antenna (PIFA) at 2.6 GHz is reported in [3] to obtain the mutual coupling -15 dB. This was obtained with a separation between two antenna elements of 26 mm (0.23λ). The distance between two antenna elements are 20 mm (0.35λ), which is less than half wavelength. In addition, U-shaped slot patch antenna operats at 2.6 GHz for mobile handset application was investigated in which the -20 dB isolation was achieved by pattern diversity. This was obtained with capacity loss of 0.2 bits/s/Hz at 2.6 GHz. Moreover, an H-shaped defected ground structure was applied to reduce the mutual coupling for a two-element array patch antenna. In this paper, a compact dual U-shaped slot PIFA antenna with Electromagnetic Bandgap (EBG) on a relatively low dielectric constant substrate is presented

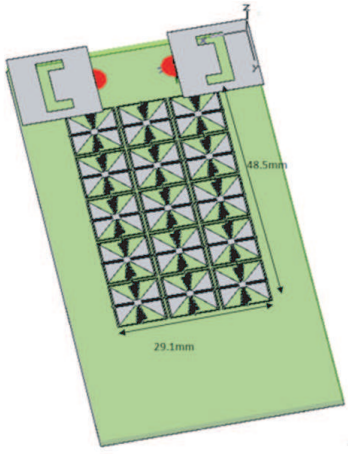

Figure 1: Configuration view the U-shaped slot PIFA antenna with EBG.

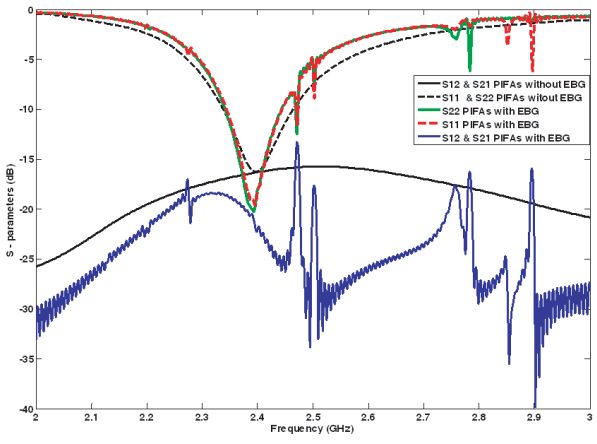

Figure 2: The comparison results for PIFA antenna with/without EBG.

(see Fig. 1). The model shows that the results in EBG stop band frequencies operates at 2.4 GHz for small terminal mobile handset. The scattering parameter is compared for both U-shaped slot PIFA antenna with and without the EBG structures (see Fig. 2). An evaluation of multiple-input-multiple-output (MIMO) antennas is presented by analyzing the mutual coupling, correlation coefficient, total active reflection coefficient (TARC), capacity and total capacity loss.

REFERENCES

1. Chae, S. H., S.-K. Oh, and S.-O. Park, "Analysis of mutual coupling, correlations, and TARC in WiBro MIMO array antenna," *IEEE Antennas and Wireless Propagation Letters*, Vol. 6, 122–125, 2007.
2. Gue, Y., X. Chen, Z. Ying, and C. Parini, "Further investigation of dual-element diversity PIFA for MIMO applications at 2.5 GHz band," *IEEE Antennas and Propagation Society International Symposium*, 2849–2852, 2007.
3. Qiong, W., D. Plettemeier, H. Zhang, K. Wolf, and E. Ohlmer, "Diversity performance of an optimized meander PIFA array for MIMO handsets," *Proceedings of the Fourth European Conference on Antennas and Propagation (EuCAP)*, 1–5, 2010.

Directive Antennas Using Metamaterials

Abdelwaheb Ourir and Julien de Rosny
Institut Langevin, ESPCI ParisTech, UMR 7587, CNRS
Laboratoire Ondes et Acoustique (LOA), 10 rue Vauquelin, Paris 75231, Cedex 05, France

Abstract— The first experimental demonstration of high directive emission with a metallic mesh of thin wires was reported in 2002 [1]. Afterwards, theoretical analysis and simulations of antennas based on metamaterials were also presented [2–4]. In 2006, J. B. Pendry introduced the idea of using metamaterial whose permittivity and permeability values are designed to vary spatially to direct the fields [5]. This idea inspires a new scheme in EM device design, such as cloak, superlens, and directive antennas.

There have been different metamaterial based solutions proposed recently in literature concerning the design of compact directive electromagnetic sources. In this work, several metamaterial designs are proposed for the realization of directive antennas. Here, we present some novel capabilities achieved by the proposed structures. We show that the directivity and the radiation pattern of the whole antenna system can be controlled with these metamaterial based structures.

REFERENCES

1. Enoch, S., G. Tayeb, P. Sabouroux, N. Guerin, and P. Vincent, *Phys. Rev. Lett.*, Vol. 89, 213902, 2002.
2. Ziolkowski, R. W., *Phys. Rev. E*, Vol. 70, 046608, 2004.
3. Zhang, J. J., Y. Luo, S. Xi, H. Chen, L.-X. Ran, B.-I. Wu, and J. A. Kong, "Directive emission obtained by coordinate transformation," *Progress In Electromagnetics Research*, Vol. 81, 437–446, 2008.
4. Ziolkowski, R. W. and A. Erentok, *IEEE Trans. Antennas Propag.*, Vol. 54, 2113, July 2006.
5. Pendry, J. B., D. Schurig, and D. R. Smith, *Science*, Vol. 312, 1780, 2006.

New Directive Planar Antenna for the Next Generation of Point-to-point Communication in E-band Range (71–86 GHz)

M. Gueye[1], **Y. Letestu**[1], **A. Le Bayon**[1], **H. Housilmani**[2], **N. Burokur**[2], **and A. Priou**[2]

[1]Laboratoire R&D, Radio Frequency Systems, Rue J. B. Marcet, Trignac 44570, France
[2]Laboratoire Energétique Mécanique Electromagnétisme (LEME)
Université Paris Ouest Nanterre La Défense, 50 rue de Sèvres, 92410 Ville d'Avray, France

Abstract— The miniaturization and performances of the antennas are essential for their integration with transmitter and receiver. The requirement in terms of gain, polarization, side lobe level, broadband etc are very Severus and must meet standard ETSI (European Telecommunications Standards Institute) and FCC (Federal communication commission) template.

In this paper, a new directive planar antenna array for the next point to point generation in the E-band range from 71 to 86 GHz is proposed. The antenna is characterized by a low profile, high gain and broadband properties. The antenna design has two major parts. The first one is the array radiating Gaussian horn elements. The second part is a mixed rectangular waveguide feed network. It is composed by a vertical feed network for sub arrays of 64 elements. Sub arrays are interconnected to form a planar feed network. The size of the antenna must not exceed $25\,\text{cm} \times 25\,\text{cm} \times 9\,\text{cm}$.

The horn elements are fed in parallel and the waveguides are connected with T-junctions. The matching of the T-junctions is improved by optimization up to 25 dB in the frequency band. The grating lobes in the E and H-plan have been suppressed by optimizing the distance between elements with wavelength. The distance between element is 0.9λ.

The side lobe levels in the E and H-plan are below $-30\,\text{dB}$ using amplitude weighting. The gain higher than 40 dBi and a return loss higher than 14 dB have been obtained in the band 71–86 GHz. The 3D software CST Microwave based on method of moments has been used for modeling the antenna.

ACKNOWLEDGMENT

This work is done under the ELHAN project supported by the Cluster POLE DE COMPETITIVITE SYSTEMTIC, PARIS -REGION.

Study on the Precision of Equivalent Electric Models for Planar Distributed Periodic Structures

Z. Djeffal, H. Talleb, D. Lautru, and V. Fouad Hanna
UPMC Univ. Paris 06, EA 4436, L2E, F-75005, Paris, France

Abstract— Planar distributed periodic structures more commonly known as mushroom structures which present a negative refractive index (NRI) in a very narrow frequency band, are usually studied using equivalent electric models under quasi-static approximation. The dispersion equations for different configurations can be established using Bloch theorem for 2D transmission lines (TL). This paper proposes a critical study concerning the validation of results obtained from these utilised dispersion equations through comparing them to those obtained using a full-wave method. An extraction method has been proposed to simulate the frequency dependent of each distributed element. these results shown a frequency dependence different from that obtained from effective elements calculated using conventional analytical formulas for the effective material parameters of the unit cell.

REFERENCES

1. Sievenpiper, D., et al., "High-impedance electromagnetic surfaces with a forbidden frequency band," *IEEE Trans. on Microwave Theory and Techniques*, Vol. 47, No. 11, 2059–2074, November 1999.
2. Simovski, C. R., P. de Maagt, and I. V. Melchakova, "High-impedance surfaces having stable resonance with respect to polarization and incidence angle," *IEEE Trans. on Antennas and Propagation*, Vol. 53, No. 3, 908–94, March 2005.
3. Caloz, C. and T. Itoh, "Novel microwave devices and structures based on the transmission line approach of meta-materials," *IEEE-MTT Int'l Symp.*, Vol. 1, 195–198, Philadelphia, PA, June 2003.
4. Grbic, A. and G. V. Eleftheriades, "Periodic analysis of a 2-D negative refractive index transmission line structure," *IEEE Trans. on Antennas and Propagation*, Vol. 51, No. 10, 2604–2611, October 2003.
5. Caloz, C. and T. Itoh, *Electromagnetic Metamaterials: Transmission Line Theory and Microwave Applications*, John Wiley & Sons, 2006.
6. Tavallaee, A. and R. Abhari, "2-D characterisation of electromagnetic bandgap structures employed in power distribution networks," *IET Microw. Antennas Propag.*, Vol. 1, 204–211, 2007.
7. German, R. F., H. W. Ott, and C. R. Paul, "Effect of an image plane on printed circuit board radiation," *IEEE International Symposium on Electromagnetic Compatibility*, Washington, D.C., August 1990.
8. Russer, P., *Electromagnetics, Microwave Circuit and Antenna Design for Communications Engineering*, Artech House, 2006.
9. Zedler, M., "Systematic topological design of metamaterials: Scalar and vectorial 3D metamaterials and their realisation," thesis, Lehrstuhl für Hochfrequenztechnik, Technische Universität München, September 2008.

Low Profile Antenna Arrays and Mutual Coupling Reduction

X. Han[1], **H. H. Ouslimani**[1], **A. Priou**[1], **G. Collignon**[2], **and A. Marteau**[2]

[1]Laboratoire énergétique Mécanique et électromagnétisme
University of Paris Ouest Nanterre la Défense, 50 Rue de Sèvres, 92410 Ville d'Avray, France
[2]INEO DEFENSE
Route Militaire Nord, ZA Louis Bréguet, Bat. 8, CS80526 78140 Vélizy-Villacoublay, France

Abstract— Abstract-In this paper, we present the design, the optimization and the characterization of three high impedance surfaces (HIS); the Mushroom-like, the Fork-like and the 2LC elementary cells shapes. All the structures are designed to operate around 10 GHz. The capability of the HIS to suppress the surface waves excited by the microwave arrays is used to reduce the mutual coupling between a compact low profile planar arrays antenna [1–4]. The components are separated, in this case by a short distance 1.5 to $2\lambda_{10\,\mathrm{GHz}}$. In that area, the embedded electromagnetic bandgap HIS is inserted between the antenna components. The coupling between two array antennas is evaluated in the E- and H-plane around the resonance frequency 10.039 GHz. A good mutual coupling reduction ~ 6 dB is achieved for fork-like unit cells, ~ 4 dB for 2LC unit cells and ~ 8 dB for the mushroom EBG unit cells structure.

REFERENCES

1. Yang, F. and Y. Rahmat-Samii, "Microstrip antennas integrated with electromagnetic bandgap (EBG) structures: A low mutual coupling design for array applications," *IEEE Trans. Antennas Propagat.*, Vol. 51, No. 10, 2936–2946, Oct. 2003.
2. Pynttari, V., R. Makinen, J. Heikkinen, and M. Kivikoski, "Microstrip antenna arrays on thin substrates with electromagnetic band-gap structures," *European Conf. on Antennas and Propagation*, 1–5, Nice, France, Nov. 2006.
3. Payandehjoo, K. and R. Abhari, "Employing EBG structures in multiantenna systems for improving isolation and diversity gain," *IEEE Antennas Wireless Propagat. Lett.*, Vol. 8, 1162–1165, 2009.
4. Liang, J. and H. Y. D. Yang, "Analysis of a proximity coupled patch antenna on a metalized substrate," *Proc. IEEE AP-S International Symposium*, 2287–2290, Albuquerque, NM, Jul. 9–14, 2006.

A Wideband 60 GHz CMOS Antenna with UC-PBG and AMC Structure

Ying Peng[1], **Zhirun Hu**[1], **H. Ouslimani**[2], **A. Priou**[2], **and Haiying Zhang**[3]

[1]School of Electrical and Electronic Engineering, University of Manchester, UK
[2]Group Electromagnétisme Appliqué, University Paris X, France
[3]Department of MMICs and Compound Semiconductor Devices
Institute of Microelectronics, Chinese Academy Science, China

Abstract— In this paper, a wideband 60 GHz patch antenna with Uniplanar Compact Photonic Band Gap (UC-PBG) and Artificial Magnetic Conductor (AMC) building on CMOS technique was proposed, as shown in Figure 1. According to the unlicensed frequency band announced for commercial use, this antenna was designed to operate from 54 GHz to 66 GHz that made a full covering of this unlicensed band.

As the IEEE 802.15.3C Task Group was formed to standardize 60 GHz radios, consumer requirements push the millimetre wave developing towards low-cost and high-integrated property. Antenna working around 60 GHz was designed based on CMOS substrate, as shown in [1–3]. However, the low resistivity and high permittivity property of the silicon substrate cause those antennas got very low radiation efficiency.

In this paper, a patch antenna sized 0.4 mm × 0.4 mm with two additional parasitic elements was presented for broadening the bandwidth of this CMOS antenna. In order to minimised the loss induced by the silicon substrate, an AMC plane acting as a reflector was insert between the patch antenna and the silicon substrate. Due to the high impedance formed on the surface of this

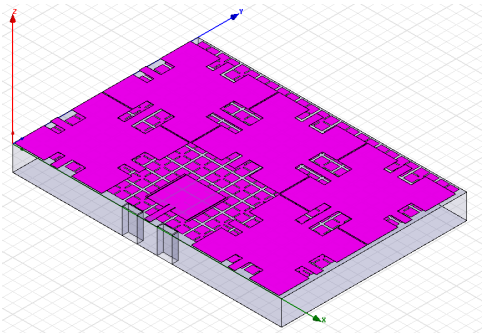

Figure 1: Structure of CMOS antenna with UC-PBG and AMC.

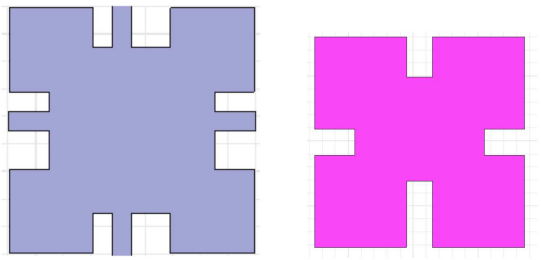

Figure 2: Unit structure of UC-PBG and AMC.

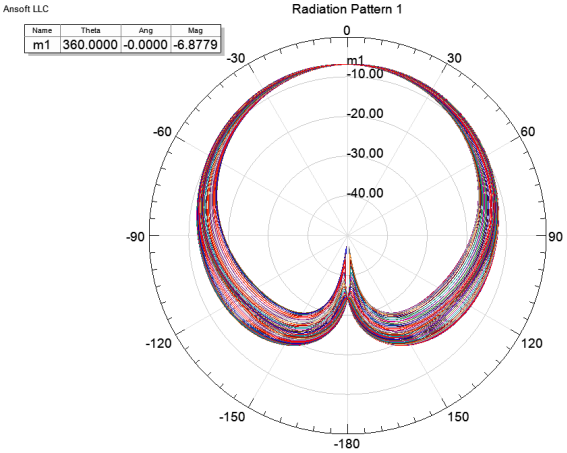

Figure 3: Simulation result of gain at 64 GHz.

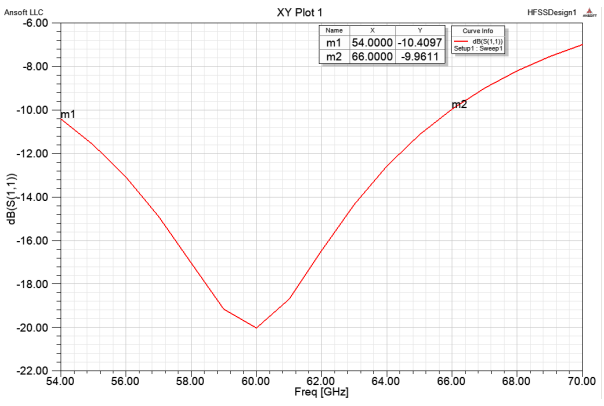

Figure 4: Simulation result of S_{11}.

AMC plane over a certain bandwidth around 60 GHz, reflected wave on the surface becomes in phase with the incident wave, and the high loss effect in the substrate can be partly eliminated. Meanwhile, a UC-PBG plane was built on the same layer surrounding the patch to increase the radiation gain at the operating frequency [4].

Simulation was carried out using full EM wave simulator in Ansoft HFSS v12. Compared with the conventional on-chip antenna having a normal gain of −10 dB, this antenna provides a maximum gain of −6.87 dBi and a wide bandwidth of 12 GHz, as shown in Figures 3 and 4.

REFERENCES

1. Doan, C. H., S. Emami, A. M. Niknejad, and R. W. Brodersen, "Design of CMOS for 60 GHz applications," *Proc. IEEE Solid-state Circuits Conf.*, 440–449, 2004.
2. Zhang, Y. P., M. Sun, and L. H. Guo, "On-chip antennas for 60-GHz radios in silicon technology," *IEEE Trans. Electron Devices*, Vol. 52, No. 7, 1664–4668, Jul. 2005.
3. Kuo, P.-C., S.-S. Hsu, C.-C. Lin, C. Y. Hsu, and H.-R. Chuang, "60-GHz millimeter-wave triangular monopole antenna fabricated using 0.18-μm CMOS technology," *The 3rd International Conference on Innovative Computing Information and Control*, 237, Jun. 2008.
4. Coccioli, R., F.-R. Yang, K.-P. Ma, and T. Itoh, "Aperture-coupled patch antenna on UC-PBG substrate," *IEEE Trans. on Microwave Theory and Tech.*, Vol. 47, No. 11, Nov. 1999.

Session 3P3b
Electromagnetic Research in Photonic Metamaterials

New Concepts in Nanoplasmonics and Plasmonic Metamaterials. Part I: Broadband THz Plasmonic Metamaterials

Stefan A. Maier
Physics Department, Imperial College London, UK

Abstract— New surface geometries such as arrays of annular holes and complementary split ring resonators allow for high-confinement THz surface waveguiding with a significantly wider bandwidth than previously reported with simple square hole or slit arrays. Numerical design and experimental realizations will be presented.

For frequencies close to the intrinsic plasma frequency of the conductor in question, interfaces between a conductor and a dielectric support high-confinement surface plasmon polaritons. A lowering in operating frequency however leads to a breakdown of the confinement, which evolves ultimately to the weakly guiding regime of Sommerfeld-Zenneck waves. However, in this regime a metamaterials approach allows us to engineer spoof surface plasmon polariton modes with effective plasma frequencies controlled mainly by the surface geometry. Numerical results as well as experimental demonstrations of waveguides operating at THz frequencies will be discussed, and their properties assessed. The higher confinement of the guided surface waves also implies a concomitant increase in attenuation, and a large decrease in bandwidth. For example, arrays of blind, unfilled square holes allow for a factor 100 increase in confinement, but only close to the zone boundary [1]. Here, we will outline two new designs that allow us increase the bandwidth of the high-confinement region: firstly, a metamaterial with a unit cell consist of an annular shaped hole leading to two distinct spoof-like plasmon bands, and secondly a metamaterial consisting of complementary split ring resonators for truly broadband spoofing.

In order to increase the bandwidth over which a significant confinement of THz surface waves is achieved, we first study spoof surfaces consisting of holes supporting multiple waveguide modes, such as an array of annular, blind holes. Two plasmon-like modes are supported, originating from the fundamental TEM and a higher order TE modes of each annulus. A comprehensive experimental analysis in term of confinement and dispersion properties [2] will be presented at the conference.

A promising new concept for the creation of surface waveguides supporting spoof surface plasmon polaritons involves arrays of complementary split ring resonators (CSRRs) [3]. The CSSR unit cell exhibits a dispersion curve that departs from the light line already at low frequencies, thus allowing for a high confinement to the surface over a broad frequency regime. In the presentation we will present a comprehensive assessment of the dispersion and waveguiding properties of experimentally realizable geometries.

REFERENCES

1. Williams, C. R., S. R. Andrews, S. A. Maier, A. Fernández-Domínguez, L. Martín-Moreno, and F. J. García-Vidal, "Highly confined guiding of terahertz surface plasmon polaritons on structured metal surfaces," *Nature Photonics*, Vol. 2, No. 3, 175–179, 2008.
2. Williams, C. R., M. Misra, S. R. Andrews, S. A. Maier, S. Carretero-Palacios, S. G. Rodrigo, F. J. García-Vidal, and L. Martín-Moreno, "Dual band terahertz waveguiding on a planar metal surface patterned with annular holes," *APL*, Vol. 96, No. 1, 011101–011101-3, 2010.
3. Navarro-Cía, M., M. Beruete, S. Agrafiotis, F. Falcone, M. Sorolla, and S. A. Maier, "Broadband spoof plasmons and subwavelength electromagnetic energy confinement on ultrathin metafilms," *Optics Express*, Vol. 17, No. 20, 18184–18195, 2009.

New Concepts in Nanoplasmonics and Plasmonic Metamaterials. Part II: Dark Modes and Fano Resonances in Nanoplasmonics

Stefan A. Maier
Physics Department, Imperial College London, UK

Abstract— The design of plasmonic cavities and waveguides will be elucidated, focusing on new developments in nanoplasmonics such as coherent effects for cavity mode shaping, and hybrid structures including active materials for modulation and gain.

This conference presentation will focus on recent results obtained in our programmes on nanoplasmonics and active plasmonics at Imperial College London, aiming at the demonstration of photonic functionalities at the nanoscale. The first part will focus on new principles for the design of plasmonic nanocavities, utilizing coherent effects based on plasmon hybridization. Coupling of bright and dark dipolar modes [1] allows control over the radiative properties of nanoscale plasmonic cavities in concentric disk/ring structures [2], and symmetry-breaking leads to the appearance of Fano-type lineshapes [3]. Such concepts enable not only the design of plasmonic nanocavities with effective mode volumes far below the diffraction limit, but also the optimization of the quality factor for specific applications (Purcell effect, sensing, slow-light applications). Numerical modeling and experimental implementation of such cavities will be discussed.

Nanoscale plasmon waveguides are the second building block of a new photonic infrastructure at the nanoscale. After a brief survey of promising waveguide geometries for nanoscale integration, investigated in our Active Plasmonics programme [4], hybrid nanostructures allowing modulation of localized and propagating surface plasmons will be discussed. Prominent materials systems include ferroelectrics (barium strontium titanate) and the family of highly conductive oxides (ZnO, ITO). Experimental results on plasmon modulation will be presented.

Due to the trade-off between localization and loss in nanoplasmonics, device design of both active and passive structures is constrained by the signal decay length in plasmonic circuits. In order to compensate losses, the incorporation of gain materials into plasmonic systems has hence recently received a great amount of interest. We will present first results for a gain material system with the hallmarks of easy processing in thin film form, based on conjugated polymers.

REFERENCES

1. Koh, A. L., et al., "Electron energy-loss spectroscopy (EELS) of surface plasmons in single silver nanoparticles and dimers: Influence of beam damage and mapping of dark modes," *Acs Nano*, Vol. 3, No. 10, 3015–3022, 2009.
2. Hao, F., et al., "Tunability of subradiant dipolar and fano-type plasmon resonances in metallic ring/disk cavities: Implications for nanoscale optical sensing," *Acs Nano*, Vol. 3, No. 3, 643–652, 2009.
3. Verellen, N., et al., "Fano resonances in individual coherent plasmonic nanocavities," *Nano Lett.*, Vol. 9, No. 4, 1663–1667, 2009.
4. www.activeplasmonics.org.

Synthesis, Fabrication, and Characterization of Optical Metallo-dielectric and All-dielectric Metamaterials

J. A. Bossard, **Z. Jiang**, **F. A. Namin**, **S. Yun**, **D. H. Werner**, **and T. S. Mayer**
Department of Electrical Engineering, The Pennsylvania State University, University Park, PA, USA

Abstract— Metamaterials research has exploded in recent years because of the tantalizing applications enabled by refractive index engineering. While applications such as Pendry's 'perfect' flat lens and the electromagnetic cloak have garnered the most attention and inspired efforts to push metamaterial operating frequencies to THz, infrared (IR), and even visible wavelengths, many other compelling devices have been proposed, including wavelength-selective absorbers, 'perfect' mirrors, emitters, and a general class of transformation optics devices. We have developed synthesis, fabrication, and characterization techniques to produce a variety of metallo-dielectric and all-dielectric optical metamaterials. The metamaterial structure is periodic in two dimensions, and can be comprised of metallic and dielectric or dielectric-only constituent materials. We employ robust optimizers such as a genetic algorithm (GA) to synthesize the unit cell and tailor the metamaterial scattering or effective parameters to application-specific requirements. Using our toolbox, we have successfully demonstrated metallo-dielectric and all-dielectric multi-band wavelength-selective filters for the far- and mid-IR. We have also demonstrated zero- and negative-refractive index metamaterials with extremely low intrinsic and matching losses for the mid-IR and near-IR. Figure 1 shows an example of a dual-band, flexible metamaterial absorber comprised of Au and polyimide and optimized to have a wide field of view. This device was fabricated and measured, demonstrating excellent correspondence with simulation. In this paper we will present an overview of our synthesis and experimental progress towards realizing a variety of optical metamaterials and related devices.

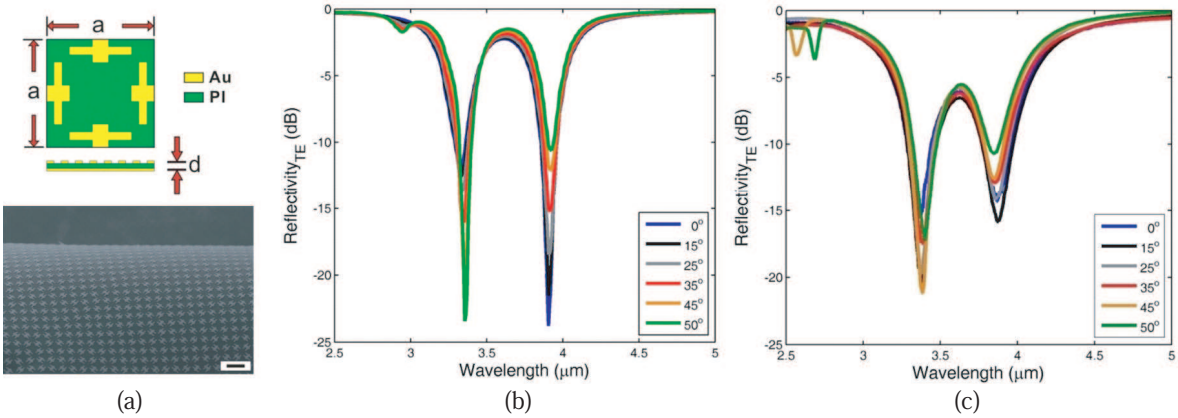

Figure 1: (a) Geometry and FESEM image of a dual-band flexible metallo-dielectric absorber; $a = 1475\,\text{nm}$, $d = 200\,\text{nm}$, and scale bar is 1800 nm. (b) Simulated and (c) measured reflectivities showing two strong dips in the mid-IR over a wide range of incidence angles, corresponding with peaks in the absorption spectrum.

Optimizing Left-handed Metamaterials for the Optical Regime

M. Kafesaki[1,2], **R. Penciu**[1,2], **Th. Koschny**[1,2], **N. H. Shen**[1,2], **E. N. Economou**[1,2], **and C. M. Soukoulis**[1,2]

[1]Institute of Electronic Structure and Laser
Foundation for Research and Technology Hellas (FORTH), Heraklion, Crete, Greece
[2]University of Crete, Greece

Abstract— Left-handed metamaterials (i.e., metamaterials with both negative electrical permittivity and magnetic permeability, resulting to negative index of refraction) have been recently a subject of continuously increasing attention. This is mainly due the novel and unique properties of those materials (like opposite phase and energy velocity, negative refraction, super-resolution, etc) which can result to new capabilities in the manipulation of the electromagnetic waves, and thus to novel approaches in many potential applications, like imaging, information processing, security and safety etc.

The novel and unique properties and capabilities of left-handed metamaterials have motivated strong research efforts to push the operation frequency of those materials from the microwave regime, where left-handed behaviour has been initially demonstrated, to the infrared and optical regime, targeting applications mainly in imaging, lithography and data storage domains. In this talk we will review the current status on the research concerning infrared and optical left-handed metamaterials, and we will present our efforts: (a) to understand the main aspects of the wave propagation in optical left-handed materials, (b) to obtain novel and/or optimized optical left-handed metamaterial designs, and (c) to explore new phenomena and possibilities available with optical left-handed metamaterials.

REFERENCES

1. Penciu, R. S., M. Kafesaki, T. Koschny, E. N. Economou, and C. M. Soukoulis, Magnetic response of nanoscale left-handed metamaterials," *Phys. Rev. B*, Vol. 81, 235111, 2010.
2. Guney, D., T. Koschny, M. Kafesaki, and C. M. Soukoulis, "Connected bulk negative index photonic metamaterials," *Opt. Lett.*, Vol. 34, 506, 2009.
3. Shen, N. H., S. Foteinopoulou, M. Kafesaki, T. Koschny, E. Ozbay, E. N. Economou, and C. M. Soukoulis, "Compact planar far-field superlens based on anisotropic left-handed metamaterials," *Phys. Rev. B*, Vol. 80, 115123, 2009.

Recent Progress in Fishnet Metamaterials at the University of New Mexico

S. R. J. Brueck, Zahyun Ku, and Svyatoslav Smolev
Center for High Technology Materials, Department of Electrical and Computer Engineering
University of New Mexico, 1313 Goddard SE, Albuquerque, NM 87106, USA

Abstract— The fishnet, a metal-dielectric-metal stack perforated with a 2D array of holes, has been the most successful structure for near- to long-wave-infrared metamaterial studies. We discuss two new directions for fishnet structures: 1) high speed (600 fs) all-optical modulation using a semiconductor dielectric and optical excitation of carriers to "short" the metal plates; and 2) hybridization of the magnetic structural resonance of the metamaterial with an electric dipole (absorption) resonance in the dielectric.

The nonlinear optical properties of metamaterials offer exciting possibilities for high speed modulation and frequency-tuning. Recently, we achieved a Tb/s modulator based on a trilayer fishnet structured negative-index metamaterial (NIM) with ~ 600 fs device response and 20% modulation depth in the near-IR. We demonstrate an ultrafast (~ 600 fs), dual-band (1.06 μm/1.58 μm) elliptical NIM (eNIM) with high switching ratio $\sim 70\%$ at telecommunication wavelengths. Ultrafast modulation of the eNIM is pumped using a sub-100-fs, visible pulse to photoexcite carriers above the α-Si bandgap (~ 1.7 eV), and the time-resolved change in transmission is measured with a near IR probe pulse. We measure the pump-induced percentage change in transmission ($\Delta T/T$) — the SR — as a function of pump-probe delay (Δt), pump fluence, pump wavelength, probe wavelength (1.0–2.0 μm), and probe polarization.

For some applications it is interesting to consider the coupling between the metamaterial resonance and an absorbing species located in the metamaterial unit cell. We present modeling and experimental results for a fishnet metamaterial with the dielectric spacer layer containing a simple Lorentzian electric-dipole resonance where a classical anti-crossing behavior is observed. A set of experimental samples with structural resonances spanning 7.4 (0.167 eV) to 10.3 (0.12 eV) μm were fabricated using standard lithographic and cleanroom processing. An Albisbenzocyclobutene (BCB)-Al fishnet structure was used. Transmission data were obtained by FTIR. Plotting positions of the resonance peaks in the transmission response against ω_0 clearly shows coupling between the resonances with classical anti-crossing behavior and is in the good agreement with the modeling. Detailed results will be presented.

Both experiments and modeling were carried out in collaboration with the Sandia/Los Alamos Center for Integrated Nanotechnology (CINT). Antoinette J. Taylor, Keshav M. Dani, Rohit P. Prasankumar and Prashanth C. Upadhya, all of Los Alamos National Laboratory, participated in the ultrafast studies. I. Brener, M. B. Sinclair, G. A. Ten-Eyck, W. L. Langston and L. I. Basilio, all of Sandia National Laboratories, contributed to the hybridization studies.

Imaging Interferometric Microscopy

S. R. J. Brueck, **Alexander Neumann**, **and Yuliya Kuznetsova**
Center for High Technology Materials, Department of Electrical and Computer Engineering
University of New Mexico, 1313 Goddard SE, Albuquerque, NM 87106, USA

Abstract— Imaging interferometric microscopy (IIM) allows the acquisition of high-resolution images using a low NA objective combined with multiple sub-images, off-axis illumination, interferometric reconstruction and digital image processing. We have previously demonstrated a resolution approaching the free-space linear systems limit ($\lambda/4$) with a modest $NA = 0.4$ objective, and described image reconstruction procedures to correct the frequency space distortions resulting from exposures made with a tilted object plane.

Here, we report the use of illumination propagating beyond the total-internal reflection (TIR) angle in the transparent substrate. The evanescent wave associated with the TIR extends beyond the substrate into the sample region where it is scattered by the sub-wavelength sample structure into propagating waves that provide information on the details of the object at spatial frequencies up to $(n_{sub} + NA)/\lambda$ with a normal object plane and $(n_{sub} + 1)/\lambda$ with a tilted optical axis. Further improvements to spatial frequencies of $2n_{sub}/\lambda$ are available by extracting the image information through the substrate with the assistance of gratings on the back surface of the substrate. Stimulated nonlinear processes such as CARS provide an extension to chemically specific imaging. This provides a straightforward route to sub-100 nm resolutions in large field microscopy, that will have impact across a wide range of applications.

The resolvable dimensions for typical source wavelengths are shown in the Table 1. The columns labeled by $n_{\max}$ reflect the largest index transparent material of which we are aware at each wavelength. Other materials may further expand the available resolution. At a 193-nm wavelength, the resolution approaches typical SEM resolutions without requiring vacuum and indeed being fully compatible with water immersion. These resolutions are well beyond the current established perceptions of microscopy capabilities and suggest that advances in optical microscopy will have important impacts across a broad swath of science and technology.

Table 1: Resolution limits (grating half-pitch) for various optical configurations at widely available laser wavelengths. (All dimensions in nm).

λ	IIM (air; $\lambda/4$)	1/2-immersion ($\lambda/2(n+1)$; $n = 1.5$)	full immersion ($\lambda/4n$; $n = 1.5$)	1/2-immersion ($n_{\max}$)	full immersion ($n_{\max}$)
1064	266	213	177	116	74 ($n = 3.6$; Si)
633	158	127	106	74	48 ($n = 3.3$; GaP)
488	122	98	81	71	50 ($n = 2.45$, GaN)
193	48	39	32	34	27 ($n = 1.8$; polymer)

ACKNOWLEDGMENT

This work was partially supported by AFOSR, DARPA and ARO.

The Magical World of Metamaterials

Ekmel Ozbay
Bilkent University, Bilkent, Ankara 06800, Turkey

Abstract— In this talk, we will review experimental and theoretical studies performed on left-handed metamaterials (LHM). The metamaterials exhibit quiet unusual electromagnetic properties such as negative refraction, negative phase velocity, cloaking, subwavelength focusing, subwavelength cavities, chiral structures with giant optical activity and enhanced absorbers for solar cells.

The left-handed metamaterials under investigation are typically composed of periodic arrangement of split-ring resonators (SRRs) and thin wire grids. Periodic thin wire media is responsible for the negative effective permittivity, whereas periodic SRR structure provides negative effective permeability. Although transmission measurements provide some information about the negative phase velocity properties of metamaterial, additional measurements must be done in order to assure that the metamaterial has negative refraction characteristics. For this purpose, we performed experiments to verify the refractive index of the 2D LHM under investigation is indeed negative. Prism-shaped structures can be used to find the sign and the value of the refractive index. We constructed a prism-shaped LHM. Negative refraction angle could only be possible if the measured sample has a negative refractive index. By using Snell's law, the refractive index is calculated as $n_{\text{eff}} = -1.91 \pm 0.05$ when the maximum transmission is observed.

In the subwavelength imaging experiments, we used monopole antennae to imitate the point source. We used two point sources separated by distances smaller than a wavelength to obtain subwavelength resolution. The imaging experiments are performed for two different separation distances between the sources. The measured power distribution of sources, separated by $\lambda/8$, is plotted in Fig. 1. As seen in the figure, the peaks of two sources are resolved. We then increased the separation of the sources to a distance of $\lambda/5$ and the peaks are resolved better. When the sources are $\lambda/3$ apart (green line), we have been able to resolve two peaks entirely.

A uniaxial chiral metamaterial was constructed based on a magnetic dimer that consists of a bilayer of U-shaped metallic resonators mutually twisted at 90 degrees. The chiral metamaterial showed giant optical activity and circular dichroism. Our retrieval works revealed that a negative refractive index was realized for circularly polarized waves due to the large chirality. The experimental results were in good agreement with the numerical results.

We designed, implemented, and experimentally characterized electrically thin absorbers utilizing magnetic resonance of metamaterials at the optical regime. The absorbers consisted of a metal back plate and an artificial magnetic material layer. We investigated absorber performance in terms of absorbance, bandwidth, and electrical thickness, all of which depend on the dimensions of the metamaterial unit cell and the distance between the back plate and metamaterial layer. As a proof of concept, we demonstrated a composite absorber with 185 nm thickness and minimum 90% absorption between the 1078 nm to 2183 nm free space wavelengths.

Other examples of peculiar electromagnetic behavior related to metamaterials will be given during the presentation.

Session 3P4a
Advances in Image Processing

Silhouette Coverage Analysis for Multi-modal Video Surveillance

S. Verstockt[1, 2], **C. Poppe**[1], **P. De Potter**[1], **C. Hollemeersch**[1],
S. Van Hoecke[2], **P. Lambert**[1], **and R. Van de Walle**[1]

[1]ELIS Department Multimedia Lab, Ghent University, IBBT, Belgium
[2]ELIT Lab, University College West Flanders, Ghent University Association, Belgium

Abstract— To improve the accuracy and to reduce the false alarms in video-based object detection, the proposed system takes advantage of the different kinds of information represented by visual, thermal and/or depth imaging sensors. The combination of those types of imagery yields information about the scene that is rich in color, motion, depth and/or thermal detail. Once such information is registered, i.e., aligned with each other, it can be used to improve detection performance and activity analysis in the scene. Since each type of sensor has its own type of detection limitations, misdetections in one sensor can be corrected by the other sensors. As such, the combination of multi-sensor information is considered to be a win-win.

The proposed multi-sensor object detector can be split up in two consecutive parts: the registration and the silhouette coverage analysis. The registration is performed using a three step silhouette-mapping algorithm which detects the rotation, scale and translation between moving objects in the visual, LWIR (long-wave infrared) and/or depth images. First, moving object silhouettes are extracted to separate the calibration objects, i.e., the foreground, from the static background. Key components are dynamic background subtraction, foreground enhancement and automatic thresholding. Then, 1D contour vectors are generated from the resulting multi-modal silhouettes using silhouette boundary extraction, cartesian to polar transform and radial vector analysis. Next, to retrieve the rotation angle (contour alignment) and the scale factor between the multi-sensor image, these contours are mapped on each other using circular cross correlation and contour scaling. Finally, the translation between the images is calculated using maximization of binary correlation. The geometric parameters found at this stage are then further used to coarsely map the silhouette images and coverage between them is calculated.

The silhouette coverage analysis also starts with moving object silhouette extraction. Then, it uses the registration information, i.e., rotation angle, scale factor and translation vector, to map the thermal, depth and visual silhouette images on each other. Finally, the coverage of the resulting multi-modal silhouette map is computed and is analyzed over time to reduce false alarms and to improve object detection.

Prior experiments on real-world multi-sensor video sequences indicate that automated multi-modal video surveillance is promising. This paper shows that merging information from multi-modal video further increases the detection results.

ACKNOWLEDGMENT

The research activities as described in this paper were funded by Ghent University, the Interdisciplinary Institute for Broadband Technology (IBBT), University College West Flanders, Warrington Fire Ghent, the Institute for the Promotion of Innovation by Science and Technology in Flanders (IWT), the Fund for Scientific Research-Flanders, the Belgian Federal Science Policy Office (BFSPO), and the European Union.

Recent Advances in the Design of Hybrid Optical Neural Network-type Filters

Ioannis Kypraios
School of Engineering and Design, University of Sussex, BN1 9QT, UK

Abstract— A robust invariant pattern detection and classification system needs to be able to recognize the object under any usual *a priori* defined distortions such as translation (shift), scaling and in-plane and out-of-plane rotation. Ideally, the system should be able to recognize (detect and classify) any complex scene of objects even within background clutter noise. The general hybrid optical neural network filter combines the digital design of a filter by artificial neural network techniques with an optical correlator-type implementation of the resulting combinatorial correlator-type filter. Previously, we have described in details the three main forms of the filter, called the unconstrained-, constrained-, and modified-hybrid optical neural network filters. All three forms simultaneously achieve translation and out-of-plane rotation invariances, and they are able to successfully recognise a true-class object within cluttered scenes. We combined the complex logarithmic r-θ mapping of a space variant imaging sensor with the general hybrid optical neural network filter for additionally achieving in-plane rotation, and scale and projection invariances. The result was a new filter range called the logarithmic r-θ mapping for hybrid optical neural network filter or briefly logarithmic-hybrid optical neural network filter. Recent advances in the design of the general hybrid optical neural network filter have enabled the recognition of multiple objects of a single or multiple classes. The inherited shift invariance properties of the correlator-type block and, also by augmenting the output layer of the neural network-type block in the design of the general hybrid optical neural network filter enable the recognition of multiple objects of a single or multiple classes. Moreover, the window unit in the design of the logarithmic-hybrid optical neural network filter is modified to accommodate the recognition of multiple objects of a single or multiple classes. Here, for first time, we summarize the design and implementation of all the forms of the general hybrid optical neural network filter and of the logarithmic-hybrid optical neural network-range of filters for multiple objects of a single or multiple classes recognition. Special mention is made to the simultaneously achieved and with a single pass over the input data invariances of all the forms of the general hybrid optical neural network filter and of the logarithmic-hybrid optical neural network-range of filters.

Structural Entropy Based Localization Study of Wavelet Transformed AFM Images for Detecting Background Patterns

Sz. Nagy[1], **A. Fehér**[1], **and L. M. Molnár**[2]

[1]Department of Telecommunications, Széchenyi István University, H-9026 Győr, Egyetem tér 1, Hungary
[2]Department of Electronics Technology, Budapest University of Technology and Economics
H-1111 Budapest, Goldmann Gy. tér 3, Hungary

Abstract— By defining the structural entropy the von Neumann entropy of a charge distribution on a finite grid is divided into two parts. The first one, the extension entropy, is simply the logarithm of the occupation number (i.e., the number of the average grid sites occupied by the charge distribution), while the second part is the structural entropy itself. On a structural entropy versus participation ratio map the different types of localizations follow different, well characterized curves, and every distribution is represented by a vector on the map.

By a structural entropy-filling factor map of any charge distributions on a finite grid (e.g., finite representation of an electron density, or a greyscale atomic force microscope (AFM) image) superstructures of different scale topologies with different decay types can be traced as well. However it is rather hard to distinguish elements of an additive superstructure, especially if the numerical parameters of the different scale patterns are necessary. In the AFM practice the background patterns are sometimes hard to compensate, and by simple structural entropy based calculations it is almost impossible to separate the superstructure of the atomic scale and the image-scale pattern. The reason is the following. Superstructures manifest on the structural entropy map as sum of the sub-structures vector, thus since none of the structures are known, only the sum of their vectors, the sub-vectors are not unique.

Multiresolution or wavelet analysis (MRA) uses a system of basis functions with various time and frequency (space and spatial frequency) parameters for expanding functions. This system makes the time-frequency localization possible. Using some selected MRA resolution levels of the AFM image and carrying out the structural entropy based localization study on each of these levels will determine the decay type of the image at the length scales corresponding to the selected frequencies. This approach is promising for determining the large-scale patterns on AFM pictures.

Integrating Invariant Object Recognition Tools into a Content-based Internet Search Engine

Ioannis Kypraios[1] and Pouwan Lei[2]

[1]School of Engineering and Design, University of Sussex
Falmer, Brighton, East Sussex, BN1 9QT, UK
[2]School of Engineering, Design and Technology, University of Bradford
Bradford, West Yorkshire, BD7 1DP, UK

Abstract— Most available search engines use text to request a piece of information and do not offer any means for explicitly searching through the millions of web pages for visually based information. Recent research has focused in developing reliable visual content search engines to skim through the Internet's vast amount of visual information. We have modified a content-based web search engine to integrate invariant object recognition tools. We have considered both, the combinatorial-type correlator filters and the artificial neural network architectures as our invariant object recognition tools to be integrated. The resulted design of our image-to-image Internet search engine we have called it the Visual Internet Search Engine. The invariant object recognition tools are integrated in the image search and classification module of the engine. We describe in details the design and implementation of the logarithmic-synthetic discriminant function maximum average correlation height filter and the logarithmic-sigmoidal neural network for analogue patterns which will be used as the integrated invariant object recognition tools into the Visual Internet Search engine. We show initial experiments for testing their discrimination abilities and distortion tolerance of the tools for searching e-catalogues' products independent of their background conditions.

A New Spatio-temporal ICA for Multi-temporal Endmembers Extraction and Change Trajectory Analysis

S. Hmissi[1, 2], **K. Saheb Ettabaa**[1, 2], **I. R. Farah**[1, 2], **and B. Soulaiman**[2]

[1]RIADI-GDL, ENSI, Tunis, Tunisia
[2]Téléom Bretagne, Technopôle Brest-Iroise-CS 83818, 29238 BREST CEDEX 3, France

Abstract— Nowadays, earth observation engines produce large time image series over several areas of interest. So far, multitemporal data processing is being actively explored in the remote sensing community for robust land cover recognition and other similar applications [1]. However, the effective use of remotely sensed data for classification case stills remains a difficult task due to some limitations associated with the data resolution, processing, and costs [2]. Indeed, the remote sensing community is facing a serious problem and a significant challenge, it rise a need to develop novel tools enabling efficient extraction of temporal/spectral/spatial patterns contained in intensive collected remotely sensed data.

To address this problem, many works have been done. In [3], authors propose a multi-temporal spectral unmixing model as an extension of mono-temporal one. Thus, information on spatio-temporal change was extracted from multi-date abundance fractions. Freitas et al. present in [4] a new approach for multi-temporal images interpretation. Hence, they perform a fundamental statistical on fractions extracted by linear mixing model. In [5], Martnez and al. proposed a new algorithm based on mathematical morphology and spectral analysis of the hyperspectral spatial-temporal signature and endmemebrs identification. However, several weaknesses are percepted in the presented approaches. First, models are sensitive to data dimensionality, noise and differences in illumination and atmospheric conditions. Second, usually temporal unmixing techniques approach change analysis problem by examining each pixel individually and to determine if it is an endmember. However, hyperspectral images reveal frequently the co-activation of spatially disparate endmembers, which cannot be rigorously investigated with the reviewed techniques since they ignore the spatial relationships between pixels. Then, most works focused on temporal dependence and ignored the fact that endmembers should be extracted by maxing independency over both space and time. Moreover, we noticed a lack of change trajectory analysis at the sub-pixel level. Consequently, the analysis of fractional abundances obtained by multi-temporal hyperspectral images unmixing allows a more refined and sophisticated interpretation [1].

The main objective of this paper is to propose a novel approach for multi-temporal hyperspectral data interpretation based on spatio-temporal ICA. It provides a robust framework for change analysis and multi-temporal endmembers extraction from multifarious datasets taken at different acquisition times and having different spatial/spectral resolutions. As we know, Independent component analysis (ICA) is a statistical technique which attempts to discover hidden sources or features from a set of observed data [6]. Typically, it represents a generative model where the sources are maximally independent, the observations are assumed to be linear mixtures of independent sources. Unlike principal component analysis (PCA) which uncorrelates the data, ICA use higher-order statistics to achieve independence. Chang et al. [7] introduced ICA for hyperspectral images analysis, with the assumption that hyperspectral data is a mixture of spatially independent components. From which, ICA is becoming a very successful tool for endmemebrs identification and it gives very promising results. With the success of ICA in satellite images processing, there is a strong interest in this technique for the analysis of spatio-temporal data.

Hyperspectral data sets contain mixtures of many different sources of variability. Endmembers may overlap spatially and temporally with errors due to atmospheric conditions, spectral distortions and other noise sources. In our research, we propose to extend individual ICA by analyzing time series hyperspectral images. Therefore, the proposed approach is performed by putting the sequence of hyperspectral images in one spatial-temporal multidimensional space. Given the input matrix $X = [X_{ij}] \in \Re^{v \times N}$ matrix containing a sequence of N images $(x_1, \ldots, x_N)$. X_{ij} represents the reflectance of the ith pixel associated with the jth sample (time point), $(i = 1, \ldots, v, j = 1, \ldots, N)$ is modelled as:

$$X = SA \tag{1}$$

where $S \in \Re^{v \times N}$ and $A \in \Re^{k \times N}$ are respectively source and mixing matrix. Thus, separating multi-date hyperspectral data into independent spatio-temporal independent components involves determining three-dimensional maps which are multi-temporal endmemebrs and their associated

time courses of activation (abundance fractions). Therefore, the signal at each pixel can be shown as a mixture of underlying sources signals (Eq. (2)).

$$X_i = a_1 S_1 + a_2 S_2 + \ldots + a_K S_K \tag{2}$$

$$X_i = \begin{bmatrix} a_{11} \\ \ldots \\ a_{1N} \end{bmatrix} S_1 + \begin{bmatrix} a_{21} \\ \ldots \\ a_{2N} \end{bmatrix} S_2 + \ldots + \begin{bmatrix} a_{K1} \\ \ldots \\ a_{KN} \end{bmatrix} S_K$$

Sources (endmembers) are spatially independent and linearly mixed by time courses which are vectors of size $(1 * N)$. The first step in the proposed approach consists to perform a Singular Value Decomposition (SVD). Motivations for this choice are twofold for two reasons. Sense to hyperspectral data dimensionality, SVD is used to provide a reduced rank data set as input to ICA. Moreover, SVD is adopted for ICA methods evaluation. Then, we define: $\tilde{X} \approx X$ by:

$$\tilde{X} \approx X = UDV^T == (UD^{1\backslash 2})(VD^{1\backslash 2})^T = \check{U}\check{V}T^T \tag{3}$$

Given $X = \check{U}\check{V}T^T$, spatio-tempxoral ICA finds the following decomposition:

$$\tilde{X} = S_S \Lambda S_T^{\top} \tag{4}$$

where $S_S \in \Re^{v \times N}$ contains a set of k independent m-dimensional independent images, $S_T \in \Re^{N \times k}$ as a set of k independent temporal sequences of length N, and Λ is a diagonal scaling matrix. There exist two $k \times k$ mixing matrices, W_S and W_T such that $S_S = \check{U}W_S$ and $S_S = \check{V}W_T$.

Spatio-temporal ICA enforces independence constraints over space as well as over time. In a linear decomposition of hyperspectral data, the data matrix can be transformed into a set of spatial independent components by taking linear combinations of multi-temporal endmembers. Moreover, the analysis of the abundance fractions vector has also allowed us to better understand the nature and the trajectory of change.

Results are discussed over both simulated data (Figs. 1 and 2) and a set of multi-temporal Hyperion images. These experiments are based on several steps studying the effect of noise on spatio-temporal ICA. The proposed framework provided very promising recognition performance even in noise presence and small sample size conditions. As we can show, statistical method offers much more robustness and flexibility in terms of handling spatio-temporal variations.

REFERENCES

1. Farah, I. R., S. Hemissi, K. S. Ettabaa, and B. Soulaiman, "Multi-temporal hyperspectral images unmixing and classification based on 3D signature model and matching," *PIERS Online*, Vol. 6, No. 5, 480–484, 2010, doi:10.2529/PIERS091219165514.
2. Jin, H., P. Li, and W. Fan, "Land cover classification using multitemporal CHRIS/PROBA images and multitemporal texture," *IEEE International Geoscience and Remote Sensing Symposium, IGARSS*, Vol. 4, IV-742–IV-745, 2008.
3. Van de Voorde, T., L. Demarchi, and F. Canters, "Multi-temporal spectral unmixing to characterise change in the urban spatial structure of the Greater Dublin area," *28th EARSeL Symposium and Workshops: Remote Sensing for a Changing Europe*, Istanbul, Turkey, June 2–5, 2008.
4. Freitas, R. M., Y. E. Shimabukuro, R. R. Rosa, and A. Huete, "Fraction images derived from EO-1 Hyperion multitemporal data for dry season green up analysis in Tapajós National Forest, Brazilian Amazonia," *IEEE International Geoscience and Remote Sensing Symposium, IGARSS*, Vol. 4, IV-1015–IV-1018, 2009.
5. Martinez, P., R. M. Perez, J. J. Merino, D. Valencia, A. Plaza, and J. Plaza, "New spatial/spectral multitemporal endmember extraction algorithms," *ESA-EUSC Image Information Mining Workshop*, Madrid, Spain, 2006.
6. Hyväinen, A. and E. Oja, "Independent component analysis: Algorithms and applications," *Neural Networks*, Vol. 13, No. 4–5, 411–430, 2000.
7. Chiang, S.-S. and C. I. Chang, "Unsupervised hyperspectral image analysis using independent component analysis," *IEEE International Geoscience and Remote Sensing Symposium, IGARSS*, Vol. 7, 3136–3138, 2000.

Available Seat Counting in Public Rail Transport

P. De Potter[1], **C. Billiet**[1], **C. Poppe**[1], **B. Stubbe**[2], **S. Verstockt**[1,3], **P. Lambert**[1], **and R. Van de Walle**[1]

[1]Multimedia Lab, Department of Electronics and Information Systems, Ghent University-IBBT, Belgium
[2]Televic Group NV, Belgium
[3]ELIT Lab, University College West Flanders, Ghent University Association, Belgium

Abstract— Surveillance cameras are found almost everywhere today. This is feasible due to major advances in video surveillance and corresponding tools, making it possible to increase the number of cameras that can be monitored by a human operator. Surveillance cameras are mostly applied in open places: on the streets, in big public places such as train stations and airport terminals, and in private companies. However, lately they are also used in smaller places, such as vehicles for public transport.

Video analysis on public transport differs from analysis in open places in some aspects. Firstly, due to a limited bandwidth and cheap cameras, the resolution and frame rate of the video feeds are quite low. Secondly, since the vehicles move at a relatively large speed, lighting conditions sometimes change drastically (e.g., when the shadow of an external object is casted in the vehicle or when the vehicle enters a tunnel). Thirdly, a lot of occlusions of passengers take place because of the limited space. In this paper, an elaborate description of these and other conditions is given.

The focus of this paper is on the counting of available seats in real time. We propose an algorithm based on Laplace edge detection, combined with background subtraction. The counting of people is realized using the foreground objects obtained in this step and context information about the transportation vehicle.

This approach was tested on a series of self-directed and self-recorded videos with different diffculty levels. Overall, a precision of 95.24% and a recall of 80.95% were obtained for the detection and localization of seated passengers.

Real-time Insect Detection and Classification in Video Sequences Using Wavelets

M. H. Khan[1], **I. Kypraios**[2], **and N. T. Kypraios**[3]

[1]Computer Vision Research Group (COMVis), Department of Electrical Engineering
COMSATS Institute of Information Technology, M. A. Jinnah Campus
Defense Road Off Raiwind Road, Lahore, Pakistan
[2]School of Engineering and Design, University of Sussex
Falmer, Brighton, East Sussex, BN1 9QT, UK
[3]Department of Production Engineering and Management, Technical University of Crete
Plateia Ag. Titou, Chania, Crete 73132, Greece

Abstract— Previously, we presented initial results of two robust background subtraction algorithms for motion-based segmentation of video sequences. Emphasis was given on the algorithms implementation's real-time performance for digital signal processing embedded hardware platforms. The Six-Frames (6-Frames) algorithm uses the first six video frames for forming the background reference frame whereas the second algorithm the Time Interval with Memory (TIME) uses regular video frames samplings for forming the background reference frame. Both algorithms employ a wavelets-based bandpass video scene filtering for extracting illumination invariant scene features and, then, combine them efficiently into the background reference frame. Hardware efficient image stabilization capability is added to remove the unwanted motion due to the camera movement. Here, we present more results when applying both algorithms for detecting and classifying in real-time bee video sequences with different background conditions. The algorithms are evaluated based on the number of frames in which the flying bee was not recognized correctly in each video sequence. We study now the performance of both algorithms when a bootstrapping method is used for recognizing the flying bee in the video test sequences.

Image Processing Methods for Evaluating Infrared Thermographic Image of Electrical Equipments

Mohd Shawal Jadin[1], **Soib Taib**[1], **Shahid Kabir**[2], **and Mohd Ansor Bin Yusof**[1]

[1]School of Electrical and Electronic Engineering
Universiti Sains Malaysia, Nibong Tebal, P. Pinang 14300, Malaysia
[2]Collaborative Micro-electronic Design Excellence Centre (CEDEC)
Universiti Sains Malaysia, Nibong Tebal, P. Pinang 14300, Malaysia

Abstract— Infrared thermography is well known as one of the effective tools in monitoring the condition of electrical equipments. It has the capability to detect the thermal abnormality in electrical equipments. The recent research in this field has shown the interest on an automatic diagnosis system. This is due to fast analysis and robust compared to manual inspection. Various techniques have been used to identify and classify the thermal anomalies in the infrared thermographic image of electrical equipments. The common method that normally used in analyzing infrared thermogram can be divided into four steps: image preprocessing, segmentation, classification and decision making. The majority of the techniques were implemented in bottom-up order. Conversely, another approach that is more top-down oriented has been introduced recently. This paper presents the review of image processing methods for both approaches in classifying the level of faults in electrical equipments. Some advantages and disadvantages of both approaches are also discussed.

Session 3P4b
Electromagnetic Scattering over Arid Surfaces: Subsurface and Salt Issues

Radar Remote Sensing of the Ancient Rivers of the Sahara

Tom G. Farr[1] and Philippe Paillou[2]

[1]Jet Propulsion Laboratory, California Institute of Technology, USA
[2]Observatoire Aquitain des Sciences de l'Univers, UMR 5804, Floirac, France

Abstract— It has been 30 years since the discovery of buried river valleys in the eastern Sahara with the first Shuttle Imaging Radar. Since then, studies have continued with SIR-B and SIR-C as well as other radar systems operating at L-band and C-band. In addition, old lake shorelines have been found using SRTM topographic data and other satellite images. All of these studies paint a picture of wetter climates in the Sahara's past, a fact known to archaeologists, who have found evidence of human occupation along the shores of the lakes and rivers at various times over the past few hundred thousand years.

As the regional drainage network becomes clearer, additional information on the ages of the rivers and the amount of rainfall they represent can be inferred. The depth of the lakes allows one inference of rainfall, but another is contained in topographic profiles both along and across the river channels. The along-channel profile gives information about the relative efficiencies of tectonic uplift (or baselevel fall) and erosion. The cross-channel profile tells us about the erosive power of the river, a function of the flow and steepness.

Radar sensors can provide the additional information about the channels needed to infer the past climates of the region. Topography from SRTM gives us the along-channel profile, while penetration by long-wavelength radars help define the cross-channel profile. We are using L-band images from SIR-C and Japan's PalSAR to map these channels and ground-penetrating radar to field-check our inferences.

ACKNOWLEDGMENT

Part of this work was performed under contract with NASA.

Use of Multi-temporal C-band Radar Data for the Monitoring of Evaporitic Soils

P.-L. Frison[1], **Ph. Paillou**[2], **and E. Pottier**[3]

[1]University Paris-Est, France
[2]University of Bordeaux, France
[3]University of Rennes, France

Abstract— The presence of water in arid regions is correlated to large evaporitic deposits, with high concentration of salts. Synthetic Aperture Radar observations over such areas show a high variation for both the amplitude and phase of the backscattered signal. This is due to a large dynamic range for both surface roughness and dielectric constant parameters, between the wet and dry season: crystallized salt is rough and presents a low dielectric constant, while salt water surfaces are smooth and conductive. The Chott El Jerid, is a large evaporitic basin located South of Tunisia. Although located within an arid region, environmental conditions show dramatic changes between flooded phases, derived by the main aquifer of the region via springs of the basin floor, and dry conditions, extending from April to September. Past studies have shown that although their rather coarse spatial resolution, spaceborne scatterometers are especially well suited to the monitoring of surface parameters prone to seasonal variations. The temporal dynamic of the radar signal can be related to change in the water content of the surface. Due to its large extent, the Chott El Jerid is especially well suited for observations acquired by ASCAT scatterometer onboard METOP satellite. This sensor allows 25 km spatial resolution observations every 2–3 days over the Chott, allowing the monitoring of sudden flood of the basin. In addition, spatial variations within the Chott are interpreted with ASAR time series. 74 acquisitions made mainly in Wide Swath Medium Resolution mode (i.e., 150 m of spatial resolution) at VV polarization over the 2008–2009 period are analyzed. Results show very large spatio-temporal variations due to change in soil moisture and salinity, as illustrated in the Figure below. The temporal radar polarimetric behavior over the Chott is also analyzed with the help of a Radarsat-2 time series acquisition made in 2009.

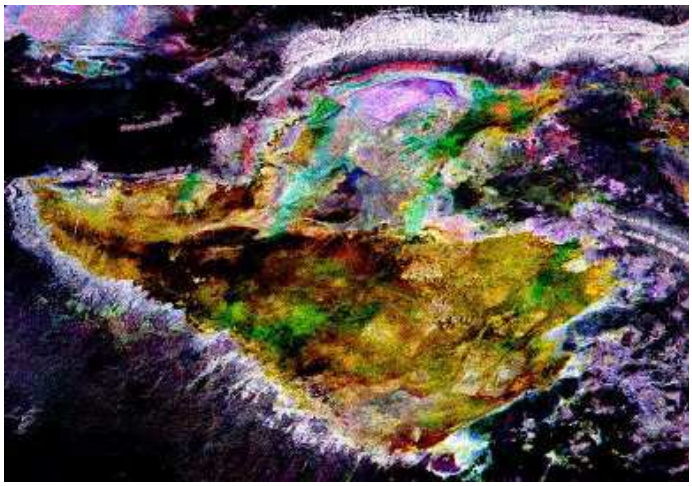

Figure 1: Temporal color composite image of 3 ASAR acquisitions (Wide Swath mode, VV polarization) during the year 2008: Red: October 19, Green: August 29, Blue: May 16.

The TUNISAR Experiment: Flying an Airborne P-band SAR over Southern Tunisia to Map Subsurface Geology and Soil Salinity

Ph. Paillou[1], **O. Ruault Du Plessis**[2], **C. Coulombeix**[2], **P. Dubois-Fernandez**[2], **S. Bacha**[3], **N. Sayah**[3], **and A. Ezzine**[3]

[1]University of Bordeaux, OASU, 2 Rue de l'Observatoire, Floirac 33270, France
[2]ONERA, DEMR, France
[3]CNCT, Tunisia

Abstract— Within the framework of a cooperation project between the University of Bordeaux, the Office National d'Etudes et de Recherches Aérospatiales, and the Centre National de la Cartographie et de la Télédétection de Tunis, and with a financial support of the french space agency CNES, we realized an airborne P-band SAR campaign over southern Tunisia during June 2010. This is the first time a P-band synthetic aperture radar flies over Sahara. The high performance SETHI SAR developed by ONERA acquired several polarimetric radar scenes over three test sites located close to the chott El Jerid and the Ksar Ghilane oasis. The TUNISAR experiment aims at evaluating potentials of low-frequency SAR for three main purposes: Subsurface geology mapping, soil salinity monitoring and archeology. We shall present the airborne P-band data acquired during the TUNISAR campaign with a comparison to higher frequency L-band PALSAR data. We shall also present preliminary results from recent field work investigations over the chott El Jerid and the Ksar Ghilane sites.

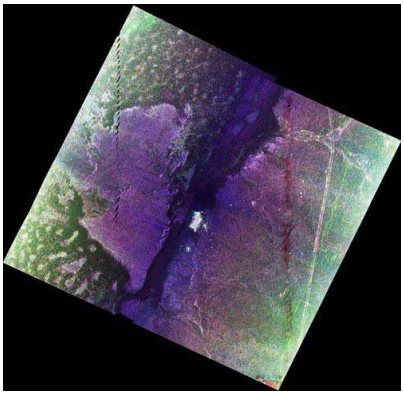

Figure 1: First SETHI P-band SAR image acquired over the Ksar Ghilane oasis.

REFERENCES

1. Paillou, P., T. Farr, A. Rosenqvist, and S. Lopez, "Mapping subsurface geology in sahara using L-band SAR: First results from the ALOS/PALSAR imaging radar," *IEEE J. of Selected Topics in Earth Observations and Remote Sensing*, 2010 (in press).
2. Lasne, Y., P. Paillou, A. Freeman, T. Farr, K. McDonald, G. Ruffié, J.-M. Malézieux, and B. Chapman, "Study of hypersaline deposits and analysis of their signature in airborne and spaceborne SAR data: Example of death valley, California," *IEEE Transactions on Geoscience and Remote Sensing*, Vol. 47, No. 8-1, 2581–2598, 2009.
3. Paillou, P., M. Schuster, S. Tooth, T. Farr, A. Rosenqvist, S. Lopez, and J.-M. Malézieux, "Mapping of a major paleodrainage system in Eastern Libya using orbital imaging radar: The Kufrah River," *Earth and Planetary Science Letters*, Vol. 277, 327–333, 2009, doi: 10.1016/j.epsl.2008.10.029.
4. Lasne, Y., P. Paillou, G. Ruffié, C. Serradilla, J.-M. Malézieux, A. Freeman, T. Farr, and K. McDonald, "Effect of salinity on the dielectric properties of geological materials: Implication on soil moisture detection by means of remote sensing," *IEEE Transactions on Geoscience and Remote Sensing*, Vol. 46, No. 6, 1674–1688, 2008.

Vector Electromagnetic Scattering from Discrete Random Media Embedded in Layered Arbitrary Rough Interfaces for Subsurface Sensing

Xueyang Duan and Mahta Moghaddam
University of Michigan, USA

Abstract— Microwave remote sensing of soil moisture profiles and vegetation structures is one of the current major applications of radar technology. Due to the increased penetration depth, low-frequency radar measurements would include effects of electromagnetic scattering from surfaces and subsurfaces, as well as the volume scattering from buried objects, e.g., vegetation root structures, rocks, sand inclusions, etc. Therefore, modeling electromagnetic scattering from discrete random media with arbitrary rough interfaces is highly desired for quantitatively interpreting the radar measurements and retrieving media properties. A solution to this problem has been previously proposed in 2D, but the 3D vector solution has never been studied before, which is the focus of this work.

We are focusing here on one random medium layer embedded in a layered rough surface structure, representative of vegetation roots or subsurface rocks or other inclusions. Hence, the problem geometry in our analysis is modeled as stacked layers with interfaces of arbitrary roughnesses. The middle layer is viewed as discrete random media consisting of regular- or irregular-shaped scatterers. It is embedded between two homogeneous medium layers with rough interfaces. The scattering matrix of the entire structure can be obtained from cascading of the single-surface scattering matrix of each interface and the scattering matrix of each discrete random medium layer with the propagation matrix in every homogeneous layer. The single-surface scattering matrix of each rough interface is solved using the stabilized extended boundary condition method (SEBCM) we developed in our previous work, which is the only practically applicable and computationally feasible method for solving scattering from multilayer rough surfaces with large roughnesses so far. Scattering from the embedded discrete random medium is modeled by the recursive **T**-matrix method, which is one of the most accurate and computationally ecient methods considering higher order interaction among scatterers, with a numerical plane wave expansion of the spherical harmonics. In our model, the transition matrix (**T**-matrix) of each scatterer is obtained either by its analytical formulation (for spherical scatterers) or by numerically solving the multipole expansion coecients using the method of moments (for irregular-shaped scatterers, e.g., finite-length dielectric cylinders). The aggregate **T**-matrix of the entire medium is obtained through a recursive process utilizing the addition theorem. Thereby, the scattering matrix can be obtained from the aggregate **T**-matrix through the plane wave expansion of spherical harmonics, which can be derived numerically. After solving the scattering matrices of all layers, they are cascaded recursively to reach the total scattering matrix of the overall ground structure. Results of the model simulation will be verified with measurements.

The 3D vector electromagnetic scattering model developed here will provide a more accurate analysis of subsurface and root-zone radar scattering. Together with the above-surface vegetation scattering model, it completes the forward scattering model of vegetated-ground.

Session 3P5a
Lightning Effects to Tall Structures and Wind Turbines

Fair-weather Atmospheric Electric Field Measurements at the Gaisberg Mountain in Austria

Helin Zhou[1], **Gerhard Diendorfer**[2], **Rajeev Thottappillil**[1], **and Hannes Pichler**[2]

[1]Division of Electromagnetic Engineering, School of Electrical Engineering
Royal Institute of Technology (KTH), Stockholm, Sweden
[2]Department of ALDIS (Austrian Lightning Detection & Information System)
Austrian Electrotechnical Association (OVE), Vienna, Austria

Abstract— A field mill (FM) is permanently operated next to the Gaisberg Tower (GBT) in Austria since several years. This radio tower triggers about 60 upward initiated lightning flashes per year and is instrumented in order to measure the lightning current waveforms. The FM is mounted on a 4 m height metal platform at a distance of about 170 m from the tower and hence the E-field measurements suffer from field enhancement. The main purpose of the permanent slow E-field measurements is to determine the background electric field that exists right at the time when lightning is triggered by the 100 m high tower. A special measuring campaign was conducted to determine the fair-weather atmospheric electric field at the Gaisberg Mountain on June 24th, 2010. The main objectives of this campaign were to calibrate the field mill deployed at about 170 m distance from the Gaisberg Tower in order to infer the relation between the electric fields at the tower tip and the ground level measured by the filed mill under thunderstorm conditions. Two Campbell Scientific CS100 Electric Field Meters were used during this campaign, and distances between each other were determined by using the Global Positioning System. Firstly, one CS110 Electric Field Meter was deployed and operated at the surrounding area of the Gaisberg Mountain, the other CS110 was taken to measure the electric field simultaneously at different altitudes along the way up to the Gaisberg Mountain top. Increasing field enhancement factors due to the mountain itself were found with increasing altitudes of the measuring sites. Similarly, at the top of the Gaisberg Mountain, one CS110 was deployed at one place far away from the 100 meter high GBT, the other CS110 was used to measure the electric field simultaneously at different distances from the GBT. The electric field at distances of up to about the height (100 m) of the GBT, was relatively smaller compared to the field measured at larger distance from the Tower. This observation was possibly caused by a shadowing effect of the tower. Overall we determined a field enhancement factor of 7.81 for the permanently installed field mill at the measurement platform next to the Gaisberg Tower with reference to the undisturbed E-field at the top of the mountain. We determined an enhancement factor of 2.75 due to the mountain itself with reference to the mountains surrounding terrain.

New Measurements of Distant Lightning Electric Fields in Florida

Michael A. Haddad and Vladimir A. Rakov
Department of Electrical and Computer Engineering, University of Florida, USA

Abstract— A statistical characterization of electric fields produced by first and subsequent strokes in negative natural lightning at distances ranging from 10 to 330 km is presented. A total of 265 first and 349 subsequent strokes were analyzed. The field waveforms were recorded at the Lightning Observatory in Gainesville (LOG), Florida, in May and June 2009. U.S. National Lightning Detection Network (NLDN) data were used to obtain locations and other information for individual strokes. Typical first-stroke waveforms for different distance intervals, < 50, 50–100, 100–150, 150–200, 200–250, 250–300, and > 300 km, are given. Also given are statistics on the following characteristics of the waveforms: initial peak, opposite polarity overshoot, ratio of the initial peak to opposite polarity overshoot, zero-to-peak rise time, initial half-cycle duration, and opposite polarity overshoot duration. The dependence of each characteristic on distance exhibits a large scatter. The overwhelming majority of both first and subsequent return-stroke field waveforms (96 and 88%, respectively) at 50 to 330 km exhibit an opposite polarity overshoot. This result (for first strokes) is consistent with that of Pavlick et al. [1], who found that only about 4% of 178 first return stroke waveforms at distances ranging from 50 to 250 km did not exhibit a pronounced opposite polarity overshoot within 400 μs of the initial peak and, hence, showed no zero-crossing, which is expected at these distances. On the other hand, in the 10 to 50 km range, only the minority, 20% of the first and 11% of the subsequent strokes examined in this study, show the opposite polarity overshoot. Only 2 of 54 first and 2 of 93 subsequent strokes at 10 to 30 km exhibit this feature. Additionally, return-stroke peak currents, I, reported by the NLDN are compared with those estimated from an empirical formula, $I = 1.5 - 0.037DE$ [2], where I is negative and in kA, E is the electric field peak in V/m and taken as positive, and D is the distance in km, based on rocket-triggered lightning data. The NLDN current is on average about 20% lower than that predicted by the empirical formula for first strokes and about 26% lower for subsequent strokes. The discrepancy is probably associated with poorer upper-frequency response (400 kHz) of the NLDN and stronger propagation effects due to finite ground conductivity in the case of fields recorded by the NLDN (multiple stations at distances up to many hundreds of kilometers from lightning possibly contribute measured fields to the estimation of current) than in the case of fields recorded at the LOG (distances ranging from 10 to 330 km).

ACKNOWLEDGMENT

This research was supported in part by the University Scholars Program at the University of Florida and by the NSF grant ATM-0852869. NLDN data were provided by Vaisala. The authors would like to thank Dimitris Tsalikis and Amitabh Nag for their help with acquisition and processing of the data.

REFERENCES

1. Pavlick, A., D. E. Crawford, and V. A. Rakov, "Characteristics of distant lightning electric fields", *Proc. of the Int. Conf. on Probabilistic Methods Applied to Power Systems (PMAPS)*, 703–707, Naples, Italy, September 22–26, 2002.
2. Rakov, V. A., R. Thottappillil, and M. A. Uman, "On the empirical formula of Willett et al. relating lightning return stroke peak current and peak electric field," *J. Geophys. Res.*, Vol. 97, 11,527–11,533, 1992.

First Direct Lightning Current Measurements on the Newly Instrumented Säntis Telecommunication Tower in Switzerland

Carlos Romero[1], **Abraham Rubinstein**[2], **Mario Paolone**[3], **Farhad Rachidi**[1], **Marcos Rubinstein**[2], **Pierre Zweiacker**[1], **Bertrand Daout**[4], **and Tony Heim**[5]

[1]Swiss Federal Institute of Technology (EPFL), Lausanne, Switzerland
[2]University of Applied Sciences of Western Switzerland, Yverdon, Switzerland
[3]University of Bologna, Bologna, Italy
[4]Montena EMC, Rossens, Switzerland
[5]Swisscom Broadcast, St. Gallen, Switzerland

Abstract— This contribution reports on the first measurements on the newly instrumented Säntis telecommunication tower operated by Swisscom Broadcast on the Saint Gallen region of Switzerland. The 125-m structure, a picture of which can be seen in Figure 1(a), sits on top of the 2505-m mount Säntis. This tower is struck by lightning more often than any other tower in Switzerland [1].

The lightning current is being measured at 20 m and 67 m above the base, using, at each height, two sensors, a Rogowski coil, whose output is processed by an analog integrator to obtain the current waveform, and a specially-designed B-dot sensor for the measurement of the current time derivative.

Maintenance, monitoring and control functions are carried out remotely over the Internet using National Instruments Compact-RIO modules linked via 100Base-FX fiber optics Ethernet to a control room that is connected to the Internet over a standard ADSL link on the Säntis.

Since the installation of the system on 19/05/2010, a total of 42 flashes were recorded: 37 negative and 5 positive (three current measurements at two heights and one B-dot measurement). A plot of the very first return stroke current pulse measured on June 18th 2010 is shown in Figure 1(b).

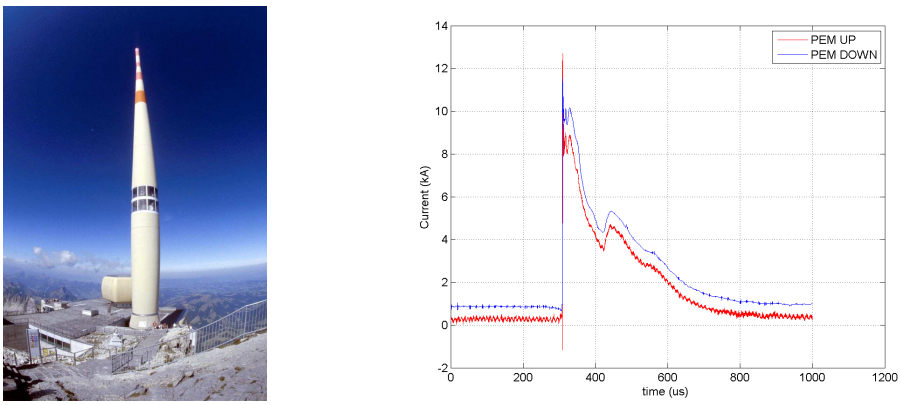

(a) (b)

Figure 1: (a) Säntis Telecommunication Tower near St. Gallen in northeastern Switzerland. (b) Plot of the first return stroke current pulse measured on June 18th 2010.

ACKNOWLEDGMENT

Financial support from the Swiss Office for Education and Research SER (Project No. C07.0037) and the Swiss National Science Foundation (Project No. 200021-122457) are acknowledged.

REFERENCES

1. Rubinstein, A., C. Romero, M. Paolone, F. Rachidi, M. Rubinstein, P. Zweiacker, and B. Daout, "Lightning measurement station on Mount Säntis in Switzerland," *10th International Symposium on Lightning Protection*, Curitiba, Brazil, November 9–13, 2009.

Influence of Ground's Characteristics on the Electromagnetic Fields Radiated by Lightning Strokes to CN Tower

M Khosravi[1], **R. Moini**[1], **S. H. H. Sadeghi**[1], **W. Janischewskyj**[2], **R. Iravani**[2], **and F. Rachidi**[3]

[1]Amirkabir University of Technology, Iran
[2]University of Toronto, Canada
[3]Swiss Federal Institute of Technology Lausanne, Switzerland

Abstract— In this paper, the effects of a lossy ground on the electromagnetic fields radiated by a lightning discharge to the CN Tower (Fig. 1(a)) is investigated. In order to represent the tower, a simple lossless wire model [1] (Fig. 1(b)) is used. The return-stroke channel (RSC) is modeled as a vertical antenna attached to the tower top. distributed inductive elements are used in the modified Antenna Theory (AT) model to control the propagation speed of the upward traveling current wave without using an artificial, higher permittivity dielectric medium, as done in the original AT model [2]. the RSC and the tower are assumed to be fed at their junction point by an appropriate source. The waveform of this source is selected so that the source current resembles a typical lightning current waveform not influenced by the presence of the tall strike object.

A fast and accurate parallel 3D FDTD algorithm is employed to calculate the lightning return stroke current distribution and the related electromagnetic fields.

The effect of ground conductivity and permittivity on the waveshapes of model-predicted electric and magnetic fields at a distance of 2 km from the tower and at a height of 15 m above lossy ground is investigated and compared to results obtained by Petrache et al. [3, 4] and to available experimental data at the CN Tower.

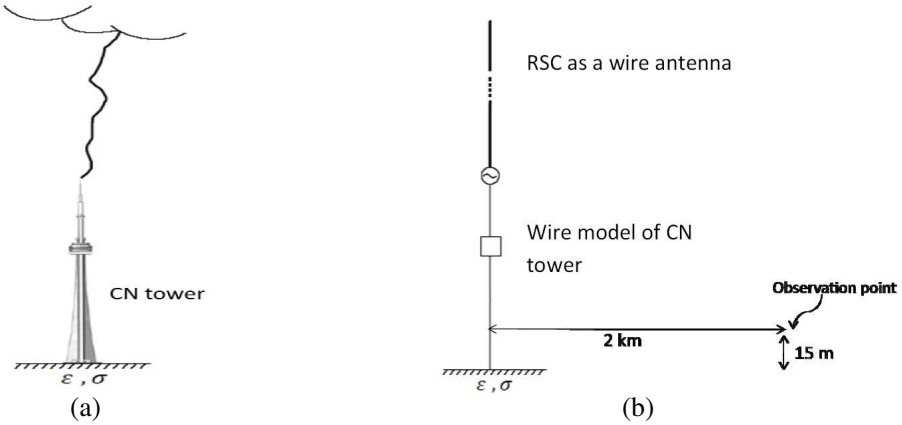

Figure 1: (a) The CN tower. (b) The CN tower's model.

REFERENCES

1. Kordi, B., R. Moini, W. Janischewskyj, A. Hussein, V. Shostak, and V. A. Rakov, "Application of the antenna theory model to a tall tower struck by lightning," *Journal of Geophysical Research*, Vol. 108, 2003.
2. Bonyadi-Ram, S., R. Moini, S. H. H. Sadeghi, and V. A. Rakov, "On representation of lightning return stroke as a lossy monopole antenna with inductive loading," *IEEE Trans. Electromagn. Compat.*, Vol. 50, No. 1, 118–127, Feb. 2008.
3. Petrache, E., F. Rachidi, D. Pavanello, W. Janischewskyj, A. M. Hussein, M. Rubinstein, V. Shostak, W. A. Chisholm, and J. S. Chang, "Lightning strikes to elevated structures: Influence of Gro unding conditions on currents and electromagnetic fields," *IEEE International Symposium on Electromagnetic Compatibility*, Chicago, Aug. 2005.
4. Petrache, E., F. Rachidi, D. Pavanello, W. Janischewskyj, M. Rubinstein, W. A. Chisholm, A. M. Hussein, V. Shostak and J. S. Chang, "Influence of the finite ground conductivity on the transient response to lightning of a tower and its grounding," *28th General Assembly of International Union of Radio Science (URSI)*, New Delhii, India, Oct. 23–29, 2005.

Earth Termination Effects in Tall Metallic Towers: Comparison of Image and Exact Models for Homogeneous and Layered Earth

Vesna Arnautovski-Toševa and Leonid Grcev
Faculty of Electrical Engineering and IT, Ss. Cyril and Methodius University, Skopje, Macedonia

Abstract— In the analysis of the dynamic response of tall towers to fast surge excitation, such as fast front lightning current pulses, the earth is often assumed as ideally conductive and accordingly the effects of the earthing system and imperfect conductivity of the earth are disregarded. Consequently, the image model is often used to account the effects of the earth.

The objective of this paper is twofold: firstly, we investigate the importance of explicit modeling of the earthing system on the dynamic behavior of the tall towers, and, secondly, we compare image and exact models of towers built on homogenous and layered earth to establish the domain of validity of the image models. The earthing system considered is a vertical conductor that penetrate homogeneous or two-layered earth.

In this paper we apply the frequency domain approach and quantity used for comparison is the input harmonic impedance for different positions of voltage source. As it is well known the harmonic impedance does not depend on the excitation but solely on the geometry and electromagnetic characteristics of the tower and the medium.

The "exact" electromagnetic model is based on the Method of Moments (MoM). The mathematical model is formulated in frequency domain by using mixed potential integral equation for vertical electric dipole (VED) in presence of homogeneous or two-layer soil. The corresponding Green's functions are formulated in exact form in terms of Sommerfeld's integrals.

The image approach is based on the quasi-static assumption. The comparison of the computed results is based on the same MoM procedure with alternatively "exact" and image Green's functions due to VED in presence of homogenous or two-layer earth.

Particularly, the paper will focuses on the following aspects:

- The influence of the grounding part of the tower: The tower is considered with or without the grounding part. The first one treats the tower as a vertical thin-wire conductor placed on the soil surface. The second model assumes the grounding part by treating the tower as a vertical thin-wire conductor which penetrates the interface between the air and the earth.
- The influence of the soil parameters: The soil is assumed as homogeneous or as twolayered. The two-layer soil is assumed to be consisted of two horizontal layers — an upper layer of finite height and a bottom layer of infinite height. Two cases are studied: less conductive upper layer, and less conductive bottom layer.
- The influence of the position of the feed point: The excitation is assumed in two distinct feed points on the tower: at the base and on the top of the tower by using a harmonic voltage generator with frequencies in a range from 0.01 to 30 MHz.
- The influence of the model radius: In this work the tower is approximated by a thin-wire cylindrical conductor. The influence of the radius is analyzed by two distinct values.

An Engineering Approach in Modeling Lightning Effects on Megawatt-class Onshore Wind Turbines Using EMTP and Models

Y. Méndez Hernández[1], **G. Drobnjak**[1], **A. Claudi**[2], **and M. Kizilcay**[3]

[1]GE Global Research Europe, Germany
[2]University of Kassel, Germany
[3]University of Siegen, Germany

Abstract— Expected damage of wind turbines caused by lightning strikes has been recently considerably reduced; one of contributing factors for this achievement is coordinated effort of working groups in standardization and testing of wind turbine lightning protection systems coming from the academia, industry and certification organizations around the globe. This paper is addressing the same topic with main focus on utilizing available simulation tools for predicting potential risk of damage due to lightning strikes and evaluation of severity of traveling currents and voltage surges inside the wind park infrastructure. Wind park level simulation models to be used in **E**lectro **M**agnetic **T**ransient **P**rograms like ATP-EMTP are developed and presented; methodology for modeling of individual WT structures and components exposed to a direct lightning strike on WT tower is described. Modern WTs with heights of 60 m and above and rotor diameters above 40 m are exposed to significant over-voltage/current effects caused by high energy surges that propagate along the WT structures. Described methodology can be used to make a fast engineering estimate of lightning effects on different types of WTs and to predict and quantify lightning surge distribution along existing traveling paths in a given wind park.

Session 3P5b
Circuits and Devices, CAD

Consideration on Artificial Neural Network Architecture in Application for Microwave Filter Tuning

J. J. Michalski, **T. Kacmajor**, **J. Gulgowski**, **and M. Mazur**
TeleMobile Electronics, Poland

Abstract— Currently, after assembling a filter on factory lines, there is the necessity of tuning each filter separately. Normally, this process is a manual work done by an operator who checks the appropriate parameters of a filter e.g., the scattering parameters. In order to reach the specification goals, the adjustment of tunable elements has to be executed. Recently, we introduced a novel method of cavity filter tuning with the usage of Artificial Neural Network (ANN) [1]. The method for preparing, learning and testing vectors consisting of sampled scattering characteristics and corresponding tuning screw errors is specified. The ANN is trained on the basis of samples obtained from a properly tuned filters. It has been proved that the usage of multidimensional approximation ability of ANN makes it possible to map the characteristic of a detuned filter reflection in individual screw errors.

This paper considers how the ANN should be designed from the point of view of the number of the input layer neurons according to the given filter topology.

Generally, the transmission and reflection characteristics of a two-port lossless filter network, composed of a series of N intercoupled resonators can be defined as a ratio of two polynomials $S_{11}(\omega) = \frac{F_N(\omega)}{E_N(\omega)}$, $S_{21}(\omega) = \frac{P_N(\omega)}{\varepsilon E_N(\omega)}$, where ω represents angular frequency and ε is a constant normalizing S_{21} to the equiripple level. The degree of a common denominator $E(\omega)$ and $F(\omega)$ is N, and the degree of polynomial $P(\omega)$ corresponds to the number of noninfinite transmission zeros. Based on Cauchy interpolation method a filter characteristic can be represented as $S(\omega) = \frac{A(\omega)}{B(\omega)} = \frac{\Sigma_{i=0}^{M-1} a_i \omega^i}{\Sigma_{j=0}^{N-1} b_j \omega^{j'}}$, and then it can be transformed to $A_{L\times M} a_{M\times 1} - B_{L\times N} b_{N\times 1} = 0$. This equation can be written as the following system of the linear equations $C_{L\times(M+N)} d_{(M+N)\times 1} = 0$. This system can be solved if $L \geq N + M$. Analysing this we can conclude that $L = 2N$ is the minimal number of points of the sampled filter characteristic, which is necessary to describe the entire continuous filter characteristic. In general, we conclude that for $L \geq 2N$ it is possible to have an unambiguous mapping between, filter characteristic S (sampled in L points) and the tuning elements positions. Based on this consideration, for a given filter topology, we can decide on the number of points that we sample the reflection characteristic (fetched from the vector network analyzer). In consequence, we can specify the number of ANN input neurons.

The above theoretical considerations were verified by an experiment. From two filters of different topology, 6 and 11 cavities, the ANN learning vectors were collected. Then, for different number L of samples of the filter reflection characteristic, the ANN learning process has been performed. It has been observed that for $L \geq 2N$ the ANN is able to generalize on efficient level to tune the filter, what is not observed for $L < 2N$. It is a very important remark because minimizing the ANN topology (the number of ANN weights), gives the better performance in the sense of ANN learning and generalization errors and ANN learning time.

REFERENCES

1. Michalski, J. J., "Artificial neural networks approach in microwave filter tuning," *Progress In Electromagnetics Research M*, Vol. 13, 173–188, 2010.

Comparison of the Inverter-based LNA between 180-nm, 90-nm and 65-nm CMOS Process

Mototada Oturu, **Shuhei Amakawa**, **Satoru Tanoi**, **Noboru Ishihara**, **and Kazuya Masu**
Solutions Research Laboratory, Tokyo Institute of Technology, Japan

Abstract— Various wireless IC chips have to be mounted if multi-standard wireless services can be used on one terminal are necessary, but it would consume a high cost. So, the realization of wide-band transceiver chip that supports some frequency bands is necessary. Meanwhile, it has been reported the problem that the input dynamic range will decline because of the lowering power-supply voltage by miniaturization of CMOS process has become a problem. Based on this background, we present a comparison of wide-band and scalable LNA between 180-nm, 90-nm and 65-nm CMOS process.

The architecture of a low-noise amplifier applies two types of technique to widen the frequency band. The first technique is Cherry-Hooper technique, which is a classical technique to decrease parasitic capacitance. The capacitance increase at high frequency limits the frequency band. The second technique applied for the LNA is an active peaking using one-stage inverter, whereby transistor sizes are decided about 1/20 by one of the main inverter amplifier. The added inverter stage shifts the phase and peaks the gain at the high frequency region. Furthermore this technique is not only a technique to widen frequency band but also one to adjust an input matching. These two techniques prevent increase of the chip cost when the process technology is miniaturized because the circuits that applied these techniques are inductor-less and capacitor-less. The LNA shown in Figure 1 was fabricated using CMOS technology with 3 different scales. We evaluated how the wide-band technique would affect the circuit performance. The S-parameter characteristics are shown in Figure 2. It was confirmed that the performance will increase as the process scales down. The bandwidths of S_{21} characteristics are 4.9 GHz, 6.8 GHz and 7.5 GHz, the power consumptions are 30.6 mW, 14.5 mW and 18.2 mW and the areas of the circuit are 0.0067 mm^2, 0.0032 mm^2 and 0.0016 mm^2 in 180-nm, 90-nm and 65-nm technology, respectively.

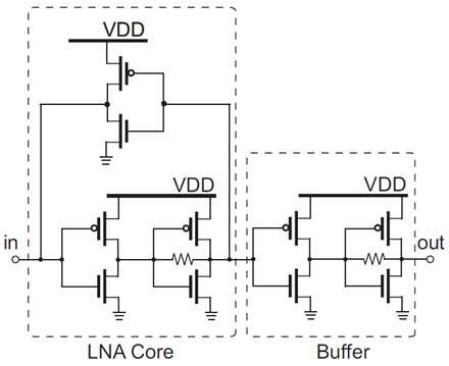

Figure 1: The evaluated circuit.

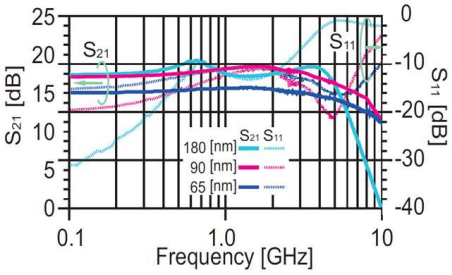

Figure 2: S_{21} and S_{11} characteristics.

Area of Phase Shifter Operation of the Azimuthally Magnetized Coaxial Ferrite Waveguide

Mariana Nikolova Georgieva-Grosse[1] **and Georgi Nikolov Georgiev**[2]
[1]Meterstrasse 4, D-70839 Gerlingen, Germany
[2]Faculty of Mathematics and Informatics
University of Veliko Tirnovo "St. St. Cyril and Methodius"
BG-5000 Veliko Tirnovo, Bulgaria

Abstract— The circular waveguides, containing azimuthally magnetized ferrite, under normal TE_{01} mode excitation possess potentialities of nonreciprocal digital phase shifters [1–5]. It has been established that the frequency range in which the simplest of these configurations — the circular one exhibits such characteristics, is restricted [4]. It might be expected that the same holds for the more complex geometries of the family, as well.

In this study the boundaries of the area in which the coaxial waveguide, completely filled with azimuthally magnetized ferrite produces differential phase shift $\Delta\bar{\beta} = \bar{\beta}_- - \bar{\beta}_+$ for the aforesaid wave are investigated as a function of the relative dimension $\rho = \bar{r}_1/\bar{r}_0\,(0 < \rho < 1)$ of its central switching conductor with respect to the one of the structure. For the purpose, the iterative schemes, suggested lately to trace the limits of region of phase shifter operation of the circular ferrite geometry [4] are extended. Unlike before, the positive purely imaginary roots $\chi^{(c)}_{k,n}(\rho)$ of the characteristic equation of the coaxial transmission line $\Phi(a,c;x_0)/\Psi(a,c;x_0) = \Phi(a,c;\rho x_0)/\Psi(a,c;\rho x_0)$ [3], expressed through the complex Kummer and Tricomi confluent hypergeometric functions $\Phi(a,c;x)$ and $\Psi(a,c;x)$ [6] with $a = c/2 - jk$, $c = 3$, $x_0 = jz_0$, $z_0 = 2\bar{\beta}_2\bar{r}_0$ ($\bar{\beta}_2 = \chi^{(c)}_{k,n}(\rho)/(2\bar{r}_0)$) and $n = 1$, and the $L(c,\rho,n)$ numbers [3], are used. Again, the domain inspected has a left-hand border, connected with the normalized critical guide radii (with the cutoff frequencies) $\bar{r}_{0cr} = \chi^{(c)}_{0,n}(\rho)/(2\sqrt{1-\alpha^2_{cr}})$ and a right-hand one — with the envelope curve in the phase diagram of the configuration of equation $\bar{r}_{0en-} = L(c,\rho,n)/[|\alpha_{en-}|(1-\alpha^2_{en-})]^{1/2}$, $\bar{\beta}_{en-} = (1-\alpha^2_{en-})^{1/2}$ [3]. (The subscripts "cr" and "$en-$" mark the quantities, related to the cutoff and to the envelopes, resp. and the ones "+" and "−" — to the positive ($\alpha_+ > 0$) and negative ($\alpha_- < 0$) magnetization.) Moreover, $\bar{r}_0 = \beta_0 r_0\sqrt{\varepsilon_r}$, $\bar{r}_1 = \beta_0 r_1\sqrt{\varepsilon_r}$, $k = \alpha\bar{\beta}/(2\bar{\beta}_2)$, $\bar{\beta} = \beta/(\beta_0\sqrt{\varepsilon_r})$, $\bar{\beta}_2 = \beta_2/(\beta_0\sqrt{\varepsilon_r})$, $\beta_0 = \omega\sqrt{\varepsilon_0\mu_0}$, α — off-diagonal ferrite permeability tensor element, β — phase constant, $\beta_2 = [\omega^2\varepsilon_0\mu_0\varepsilon_r(1-\alpha^2) - \beta^2]^{1/2}$ — radial wavenumber, r_0 — guide radius, r_1 — central conductor radius, ω — angular frequency of the wave, ε_r — ferrite relative permittivity. The main result of the analysis is that the width of zone examined expands when the parameter ρ grows. Simultaneously, the maximum value $\Delta\bar{\beta}$ might attain, decreases.

REFERENCES

1. Georgiev, G. N. and M. N. Georgieva-Grosse, "An application of the complex Tricomi function," *Proc. Eleventh Int. Conf. Electromagn. Adv. Applicat. ICEAA'09*, 819–822, in CDROM, Turin, Italy, September 14–18, 2009.
2. Georgiev, G. N. and M. N. Georgieva-Grosse, "Iterative method for differential phase shift computation in the azimuthally magnetized circular ferrite waveguide," *PIERS Online*, Vol. 6, No. 4, 365–369, 2010.
3. Georgieva-Grosse, M. N. and G. N. Georgiev, "Differential phase shift characteristics of normal TE_{0n} modes in an azimuthally magnetized coaxial ferrite waveguide," *Proc. 4rd Europ. Conf. Antennas Propagat. EuCAP 2010*, article ID P4-53, 5 pages, Barcelona, Spain, April 12–16, 2010.
4. Georgieva-Grosse, M. N. and G. N. Georgiev, "Advanced studies of the differential phase shift in the azimuthally magnetized circular ferrite waveguide," *PIERS Proceedings*, 841–845, Cambridge, MA, USA, July 5–8, 2010.
5. Georgiev, G. N. and M. N. Georgieva-Grosse, "Analysis of the differential phase shift in the circular ferrite-dielectric waveguide with azimuthal magnetization," *Proc. 2010 IEEE Int. Symp. Antennas Propagat. & CNC-USNC/URSI Radio Science Meeting AP-S 2010*, article ID 330.9, 4 pages, in CDROM, Toronto, ON, Canada, July 11–17, 2010.
6. Tricomi, F. G., *Funzioni Ipergeometriche Confluenti*, Edizioni Cremonese, Rome, Italy, 1954.

Inspection of Passengers Using a Fast Millimetre Wave FMCW Radar

Sebastian Hantscher[1], **Stefan Lang**[1], **Manfred Hägelen**[1], **Helmut Essen**[1], **and Axel Tessmann**[2]

[1]Department of Millimetre Wave Radar and High Frequency Sensors
Fraunhofer Institute for High Frequency Physics and Radar Techniques
Neuenahrer Straβe 20, Wachtberg 53343, Germany
[2]Department of High Frequency Devices and Circuits, Fraunhofer Institute for Applied Solid State Physics
Tullastraβe 72, Freiburg 79108, Germany

Abstract— The event on September 11th in 2001 showed that airports are a potent target for terrorist acts. Up to now, by using the common walk-through metal detectors only enabling the detection of metal, are not suitable for guaranteeing a sufficient high security level. That is why in recent years a lot of new technologies have been developed and now are tested for the practical application on airports. However, a lot of concerns and doubts raised to the new high-tec devices, i.e., concerning the protection of the privacy, possible health hazards and the effectiveness in ratio to the increased costs. A further challenge for new technologies is the handling with steadily growing passenger flows and thus the involved effort of security checks. This leads to completely new approaches in the aviation security. A first step is the EU funded project ATOM combining different technologies and sensors in a sophisticated way to show the feasibility how a reliable but also — from the viewpoint of the passenger — satisfying security check could look like. One of the used sensor type is a millimeter wave radar based scanner giving an indication where suspicious items are located on the body. This preselection which is carried out covert by a very fast scan is an important information for the security staff or further scanners needing just to inspect the selected body areas. During the design process of the millimeter wave radar operating at 94 GHz in the W band, the focus was not only on technical parameters but also on compliance with ethical aspects as well as a minimum influence of the natural passenger flow. The radar is based on a rotating sensor platform enabling a 360 degree scan in just few seconds. The RF front end consists of a monolithic microwave integrated circuit FMCW radar including a varactor tuned VCO, very compact transmit and receive amplifiers and a mixer. To enable bidirectional operation of a single transmit-receive antenna a combination of a Wilkinson divider and a Lange coupler was integrated. The circuit features coplanar technology and cascode HEMTs for compact size and low cost. These techniques result in a particularly small overall chip size of only $2 \times 3\,\mathrm{mm}^2$. For obtaining a sufficient resolution, the principle of the synthetic aperture is applied to simulate a narrow beam antenna by moving a broad beam antenna around the person. Experimental measurements on real persons show that metallic as well as non-metallic forbidden items (such as ceramic knives) could be detected under the clothes of the test persons.

ACKNOWLEDGMENT

The research leading to these results has received funding from the European TRANSPORT (including AERONAUTICS) Community's Seventh Framework Programme AAT.2008.5.2.2. under agreement of No. 234014.

A Dual Linear Polarization Feed Antenna System for Satellite Communications

A. Tribak[1,2], **A. Mediavilla**[1], **Alicia Casanueva**[1], **and K. Cepero**[2]

[1]Department of Communication Engineering, University of Cantabria
Av. Los Castros s/n, Santander 39005, Spain
[2]Dpartment of Physique, University of Abdelmalek Essaadi, Tetouan, Morrocco

Abstract— A dual lineal polarization feed antenna system for satellite communication will be described. It consists of a turnstile-based orthomode transducer (OMT) and two identical duplexers formed by a plane T-junction and of two iris filters. This 4-ports subsystem transmits and receives radio frequency signals in double track in which the transmission Tx is made through two ports having as a access the standard rectangular waveguide WR229 while the reception Rx is made through two ports having as a access the standard rectangular waveguide WR159. The proposed subsystem overcomes the current practical bandwidth limitations by using a very compact octave bandwidth OMT along with two robust duplexers. The subsystem is working in the extended C-band, the 5.8–7.1 GHz range used for the uplink, whereas the 3.6–4.8 GHz range is set to the downlink. The presented architecture exhibits a return loss better than 20 dB in all ports, an isolation between the different rectangular ports better than 80 dB and a transmission loss less than 0.15 dB in both frequency bands (3.6–4.8 GHz and 5.8–7.1 GHz) which represents state-of-the-art achievement in terms of bandwidth.

Our main aim was to increase the quantity of information to be transmitted or received for solving the saturation problems of the available spectral bands. We solved this problem in two different ways: either by the widening of the frequency bands available of the subsystems, or by the use of the double ways for Tx and Rx by using the orthomode polarization operation to increase the traffic capability of the link, or by both of them at the same time. For this reason, we have used a waveguide OMT based in a turnstile junction which provides a good return loss (30 dB) along with an isolation of (60 dB) across a very broadband frequency (2 : 1). The very wide bandwidth is achieved mainly due to the use of double symmetry turnstile junction reduced height waveguide arms along with the use of a reduced height E-plane power combiners/dividers and simple mitered 90° bends. This facilitates the design and the construction of these OMTs. Moreover, two wideband duplexers have been designed and constructed to demonstrate the feasibility of using stepped waveguide junctions for duplexer designs. It consists of two channel filters and a Tee E-plane junction. The relative bandwidth of the whole duplexer is about 64%. The inputs and outputs return losses were better than 25 dB, the isolation is > 80 dB and the transmission loss was 0.1 dB. Furthermore, a manufacturing tolerance has been taken into account during the design step and, therefore, the designed duplexer need not to be tuned after manufacture. Experimental measurements of the whole 4-port subsystem exhibit very good agreement with the simulation results and which represent the better performances in term of the bandwidth reported up to date in the literature.

REFERENCES

1. Tribak, A., J. L. Cano, A. Mediavilla, and M. Boussouis, "Octave bandwidth compact turnstile-based orthomode transducer," *Microwave and Wireless Components Letters, IEEE*, accepted.
2. Uher, J., J. Bohrnemann, and U. Rosenberg, *Waveguide Components for Antenna Feed Systems: Theory and CAD*, Chapter 3, Artech House, Boston, 1993.

Non-integral Sub/superharmonic Injection Locking Technique in Designing CMOS VCO

Sang-Yeop Lee, **Shuhei Amakawa**, **Satoru Tanoi**, **Noboru Ishihara**, **and Kazuya Masu**
Solutions Research Laboratory, Tokyo Institute of Technology, Japan

Abstract— A new direct injection locking technique to achieve non-integral sub/superharmonic locking phenomena is proposed. Conventional direct injection locking techniques have used nMOS switches between differential output nodes. However, the proposed technique used nMOS switches between I/Q output signals in order to make the VCO outputs to be locked to non-integral sub/superharmonics. The proposed ring VCO is shown in Fig. 1(a). It is based on a four-stage differential ring oscillator. To achieve non-integral subharmonic injection locking, 8 nMOS switches are connected at the nodes between which there is a phase difference of 270 deg. To achieve injection locking, rail-to-rail pulses are injected into one of switches. The VCO was fabricated by a 0.18 µm CMOS process. The frequency tuning range in the free-running condition of the VCO was 0.58–1.4 GHz for a 1.8 V power supply. Fig. 2 shows phase noise characteristics of the proposed VCO. The 1-MHz-offset phase noise of the VCO is −120 dBc/Hz at an output frequency of 0.95 GHz with a reference input of 200 MHz (= 4.75 × 0.2 GHz). With a reference input of 1.25 GHz, we achieved a 1-MHz-offset phase noise of −130 dBc/Hz at an output frequency of 1 GHz (= 1/1.25 × 1.25 GHz). Fig. 1(c) shows VCO responses with a reference input of f_{ref} = 0.2 GHz and 1.25 GHz. As the control voltage was swept, the VCO successfully locked to various integral and non-integral sub/superharmonics. Non-integral subharmonic locking enables the use of higher frequency of reference signals with the same frequency resolution. Also, non-integral superharmonic locking makes it possible to use a ring VCO as a frequency divider that has a fractional dividing ratio.

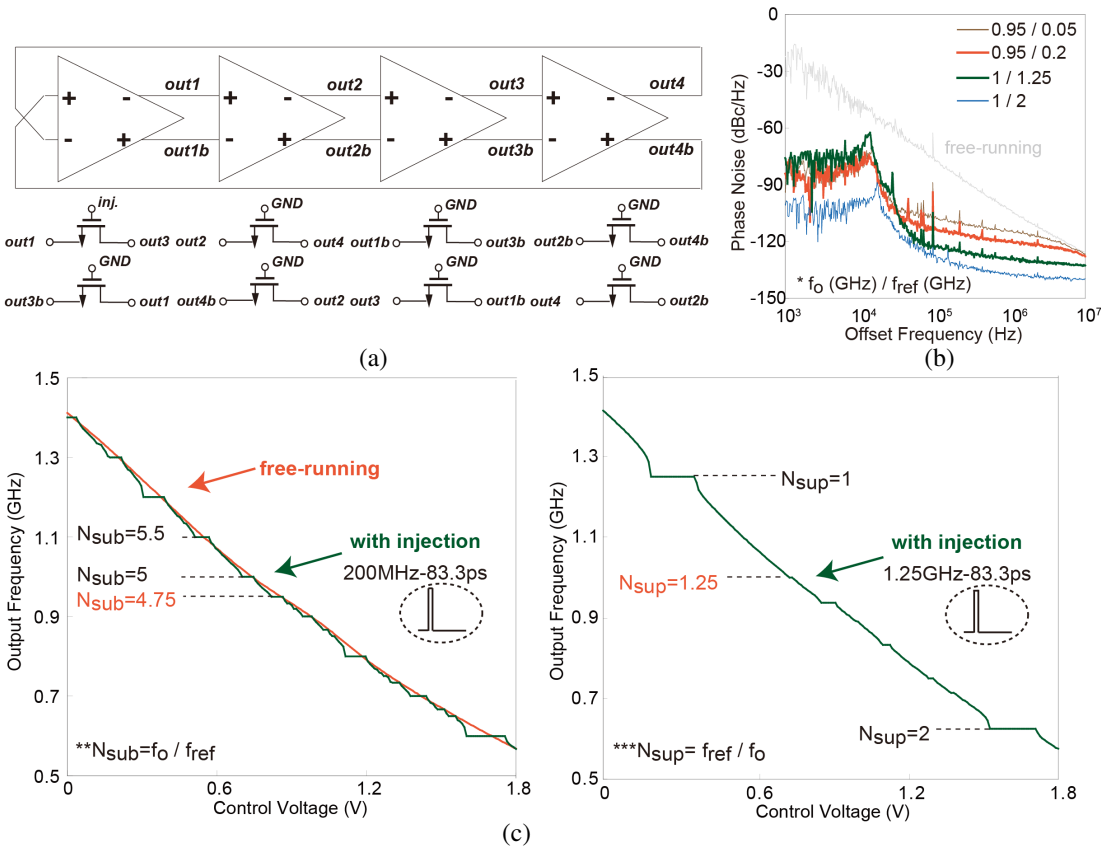

Figure 1: (a) Proposed direct injection locking technique. (b) Measured phase noise characteristics. (c) Measured frequency tuning characteristics.

Study of a Coplanar Circulator Based on a Barium Hexaferrite Nanocomposite

T. Boyajian[1], **D. Vincent**[1], **M. Le Berre**[2], **and S. Neveu**[3]

[1]DIOM Laboratory, Jean-Monnet University, 25 Dr. Rémy Annino Street, Saint Etienne 42000, France
[2]Lyon Institute of Nanotechnology (INL), NSA of Lyon, 7 Jean Chapelle Avenue
Villeurbanne 69621, France
[3]PECSA-CNRS/UPMC/ESPCI Laboratory, 4 Place Jussieu, Paris 75252, France

Abstract— In this paper, we present the design and the analysis of a Y-junction coplanar circulator operating in the frequency range of 40–60 GHz. Circulators belong to a large family of nonreciprocal devices widely used in microwave components and rely on magnetic materials. The magnetic material used in this circulator's study is the Barium Hexaferrite. In fact, it is a hard ferrite (with a high anisotropy [1]) that guarantees the non reciprocity of the circulator by assuring the transit of a maximal signal from the transmitter to the receiver and blocking any signal in reverse direction. It operates without applying any external dc field to polarize the material [2]. In addition to its performance, a circulator should not be bulky assuring size reduction and implementation simplicity in new technology components. For this reason, we chose to replace the conventional bulk ferrite by a magnetic nanocomposite. The final material's structure is made up of barium hexaferrite particles dispersed within a dielectric resin.

A three dimensional finite element method was used to design and evaluate the performance of such a microwave component. The dimensions of the designed circulator are in millimetre scale ($1.65 \times 1.42\,\mathrm{mm}^2$), with a cylindrical magnetic region in the center, with a radius of 465 µm and a thickness of 100 µm. Due to the complexity of representing the magnetic particles in their nanometric dimensions, random orientations and position, we designed the magnetic material by considering it homogeneous, having a magnetization lower than the usual ferrite. This introduces the "volume fraction", which is one of the main issues argued in such nanocomposite materials.

Experimentation wise, we realized several trials on the nanocomposite magnetic material. Barium hexaferrite, synthesized by co-precipitation procedure, is in fine particle form with an average size of 200 nm. The SU-8 resin is the host matrix in which the nanoparticles are dispersed, in order to form the nanocomposite magnetic material. The transmission scattering parameters given by microwave characterization on a coplanar waveguide line [3], verify the non-reciprocity of the magnetic nanocomposite.

REFERENCES

1. Liu, X., L.-M. Gan, and S.-C. Ng, "Improving the magnetic properties of hydrothermally synthesized barium ferrite," *Journal of Magnetism and Magnetic Materials*, Vol. 195, 452–459, May 1999.
2. Ping, S., H. How, Z. Xu, S. D. Yoon, S. A. Oliver, and C. Vittoria, "MMIC circulators using hexaferrites," *IEEE Trans. Magn.*, Vol. 37, 2389–2391, Jul. 2001.
3. Vincent, D., T. Rouiller, C. Simovsky, B. Bayard, and G. Noyel, "A new broad-band method for magnetic thin-film characterization in the microwave range," *IEEE Trans. Microwave Theory Tech.*, Vol. 53, 1174–1180, Apr. 2005.

Session 3P6a
Material, Design and Drive of Functional Devices

New Solutions for Active Radomes Made with Tunable Thin Films Materials

Valerie Vigneras, Guillaume Lunet, Hussein Kassem, and Laurent Oyhenart
IMS Laboratory, University of Bordeaux, 16 Avenue Pey-Berland, Pessac 33607, France

Abstract— One of the possible solutions for the realization of agile antennas, is the use of active radome allowing the antenna to receive or not a signal, following its frequency [1]. The periodic structures present certain interest for the realization of this type of reconfigurable radome; so, photonic crystals including active components (diodes, varactors, MEMs) were developed for that purpose [2]. Another solution, which can be satisfactory in term of time of answer and of manufacturing cost, is to use a frequency selective surface (FSS) combined in a tunable material such a ferroelectric for example [3, 4].

From this idea, several kinds of inductive FSS were studied. The objective is to be able to use the selective surface, at once as band-pass filter and as electrode, allowing by application of a tension, to modify the transmission of the radome by varying the dielectric permittivity of the tunable material. The simulations are realized by using commercial software using respectively the finite elements method and the transmission line matrix (TLM).

A realistic idea of a practical point of view consists in using a single selective surface which includes both electrodes deposited on the ferroelectric material.

We shall present the structure optimized to work in the Q band. Two possible compatible materials were envisaged, a ferroelectric $B_{60}S_{40}T$, the permittivity of which is of the order of 150 and a commercial film terpolymer, P(VDF-TrFE-CFE) whose permittivity is equal to 50 [5, 6]. In both cases, the hypothesis of 30% of tunability was retained. We shall show that this hypothesis leads to a global accordability of the device of about 10%.

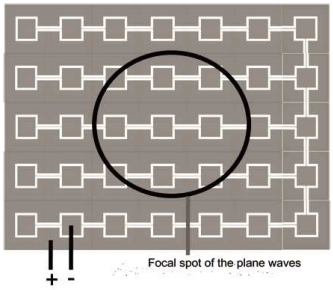

Plan of the selective surface in two electrodes

Figure 1.

REFERENCES

1. McKinzie, W. E., "Electrically thin multi-layer bandpassradome," US Patent, Nov. 2002.
2. Lourtioz, J. M., A. De Lustrac, F. Gadot, S. Rowson, A. Chelnokov, T. Brillat, A. Ammouche, J. Danglot, O. Vanbesien, and D. Lippens, "Toward controllable photonic crystals for centimeter- and millimeter-wave devices," *Journal of Lightwave Technology*, Vol. 17, No. 11, Nov. 1999.
3. Parker, E. A. and S. B. Savia, "Active frequency selective surfaces with ferroelectric substrates," *IEEE Proc. — Microw. Antennas Propag.*, Vol. 148, No. 2, Apr. 2001
4. Munk, B. A., *FSS Theory and Design*, Wiley, 2000.
5. Kassem, H., V. Vigneras, and G. Lunet, "Non destructive dielectric characterization of thin ferroelectric films materials using coplanar line structure," *Integrated Ferroelectrics*, Vol. 94 No. 01, 82–93, Dec. 20, 2007.
6. Bauer, F., E. Fousson, and Q. M. Zhang, "Recent advances in highly electrostrictive P(VDF-TrFE-CFE) terpolymers," *IEEE Transactions on Dielectrics and Electrical Insulation*, Vol. 13, 1149–1154, Oct. 2006.

A Linear Ultrasonic Motor Using a Quadrate Plate Transducer

Jiamei Jin and Chunsheng Zhao
Precision Drive Laboratory, Nanjing University of Aeronautics and Astronautics
Nanjing 210016, China

Abstract— Several linear ultrasonic motors found in literature base on the use of two different vibration modes. Most often flexural and longitudinal modes are combined to achieve an elliptic micro-motion of surface points. This micro-motion is converted to direct linear (or translatory) motion of a slider. To gain high amplitudes of the micro-motion and thus having a powerful motor, the ultrasonic vibrator should be driven near the eigen-frequency of its modes. Additionally, low mechanical and electric losses lead to increased efficiency and large amplitude magnification in resonance. This demands a geometrical design that fits the eigen-frequency of the two different modes. A frequency deviation of only a few percent leads to non-acceptable disturbance of the elliptic motion. Thus, the mechanical design of the vibrator has to be done very carefully. The stator presented in this paper employed a quadrate configuration easy to obtain technologically coincident eigen-frequencies of two same shape modes in two orthogonal directions. Two pair of $Pb(Zr,Ti)O_3$ piezoelectric ceramics are bonded by epoxy glue to a quadrate substrate with four projections made of brass, as illustrated in Fig. 1. Two piezoelectric ceramic plates on the cross were poled in reverse directions with respect to each other. Upon application of drive voltage to the two piezoelectric ceramic plates, a bending vibration is generated in one-direction, one expands, whereas the other contracts. This results in two orthogonal bending vibration modes, as shown in Fig. 2. The four projections were located at the crest and trough of B_{03} in the y-direction, and at the middle point between the crest (or trough) and nodal line of B_{30} in the x-direction, respectively. Upon application of two sine drives to the two pair of the piezoelectric ceramics plates (phase shifted by $\pi/2$), a vibration can be excited at each projection. The tops of the projections move in ellipses, but with different phase in $\pi/2$. Analysis using ANSYS finite element method software illustrates the ellipse movement of the tops, as shown in Fig. 3. The stator's projections were elastically pressed together in order to ensure frictional contact with a slider. The slider was then excited into linear motion, by contact to the projections of the stator. The operating pattern, four projections drive the slider by turn in one vibration cycle of the stator, is promising a large thrust and a high efficiency. The performance characteristics achieved by the prototype are: (i) a maximum linear speed of $> 60\,\text{mm/s}$; (ii) a stroke of $> 150\,\text{mm}$;(iii) a driving force of $> 5.0\,\text{N}$; (iv) a response time of $\sim 0.2\,\text{ms}$.

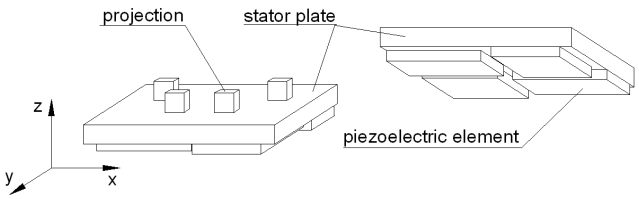

Figure 1: Stator.

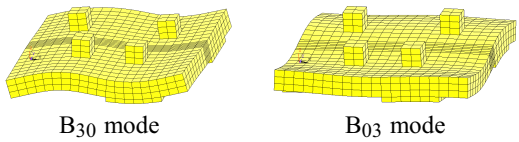

Figure 2: Operating modes.

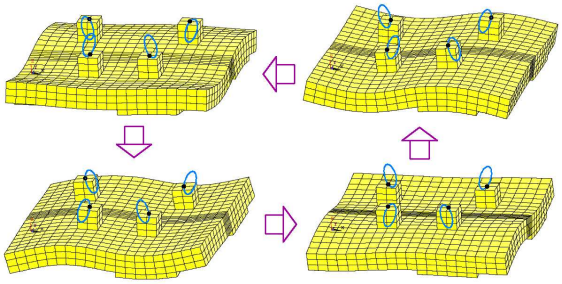

Figure 3: Harmonic analysis.

A Novel LLCC Resonant Network for Ultrasonic Motor

Hua-Feng Li and Wei-Qing Huang
Nanjing University of Aeronautics and Astronautics, Nanjing, Jiangsu 210016, China

Abstract— Ultrasonic motor (USM for short) is a new type of motor developed since the 1970s. The stator of traveling wave USM is constituted by piezoelectric element and the elastic body mounted on it. The rotor of USM is on contact with the elastic body under a moderate static pressure. When two AC voltages, the frequency of which is in ultrasonic range, with $\pi/2$ rad phase difference apply to the piezoelectric element, the traveling wave will be generated on the surface of elastic body, and the rotor will continuously revolve on the stator because of the frictional force between rotor and stator. The advantages of USM, such as high torque/volume ratio, noiseless operation, no electromagnetic induction interference and high holding forces without an energy supply, make it attractive in many applications like space, MEMS, high accuracy system, automatic, and camera and so on.

High driving voltage (peak to peak voltage should be higher than 200 V generally) is required for USM, and the supply voltage of driving circuit is relatively lower, so driving circuit needs transformer to boost voltage. Push-pull circuit is usually used as the driver of USM for its simple configuration. Since the USM is a nonlinear capacitive load which varies with driving frequency, driving voltage, environment temperature, load, and so on, a matching circuit is needed to keep the output voltage and the phase shift of two phases constant. Furthermore, analysis shows that for the switching circuit with push-pull topology, the switching loss is less under inductive load rather than capacitive load, which will increase its efficiency and reliability. To achieve these purposes, a novel LLCC resonant network was proposed and its parameters were given. Theoretical analysis and simulation were presented, which demonstrated that the output voltage and phase shift of the resonant network were independent of driving conditions, such as driving frequency and load. Meanwhile, the load characteristics of the driver can be changed from capacitive to inductive. This novel driver is applied to the TRUM-60 type ultrasonic motor, and the experimental results are presented to verify the effectiveness of the proposed circuit.

Theory and Experiment of the Valveless Piezoelectric Pump with Rotatable Unsymmetrical Slopes

Jianhui Zhang[1], **Qixiao Xia**[2], **Chunsheng Zhao**[1], **and Jiamei Jin**[1]

[1]Precision Driving Laboratory, Nanjing University of Aeronautics and Astronautics, Nanjing 210016, China
[2]College of Mechanical & Electronic Engineering, Beijing Union University, Beijing 100020, China

Abstract— With no relative motion at joint, no internal contamination, low manufacturing cost, and easy to microminiaturization, the valveless piezoelectric pump has unrivaled application in one-time use and miniaturization. However, the microminiaturization of the pump itself cannot microminiaturize the whole system including the pump. Thus, this paper focuses on how to integrate mixing and transport of piezoelectric liquid. Furthermore, the difficult and challenging issues of the ratio of mixing fluid and composition control are also discussed. The valveless piezoelectric pump with rotatable unsymmetrical slopes is put forward under this background. Its major features are setting drive and transfer in one, also setting transfer and mixing in one. Firstly, the design of the valveless piezoelectric pump with rotatable unsymmetrical slopes is proposed and the one-way flow principle is analyzed. Then, the fluid mechanics model of the valveless piezoelectric pump with rotatable unsymmetrical slopes is established. Meanwhile, the flow numerical analysis and calculation of the pump cavity are done. Finally, the experiments on relationship between the rotation angles of the slope and the flow rate and slope angles of rotation and the two inlets flow ratio are conducted. The experimental results show that: the maximum flow reaches 538.56 ml/s. The maximum relative error between the theoretical results and the experimental ones is 14.59%. According to the curve indicating the rotating different angles of rotatable unsymmetrical slopes to the flow ratio of the two inlets, the experimental and theoretical maximum relative error is 3.75%. Thus, the principle feasibility of the valveless piezoelectric pump with rotatable unsymmetrical slopes and the theory reliability are verified and proven.

Microstructure and Electrical Properties of High Power Piezoelectric Ceramics $Pb(Mg_{1/3}Ta_{2/3})O_3$-$Pb(Mn_{1/3}Sb_{2/3})O_3$-$Pb(Zr_{0.52}Ti_{0.48})O_3$

Ying Yang, **Qian Li**, **DandanWan**, **Yu Cheng**, **Meng Zha**, **and Yiping Wang**
Precision Driving Laboratory, Nanjing University of Aeronautics and Astronautics
29 Yudao Street, Nanjing 210016, China

Abstract— The development of ultrasonic motors (USM) puts forward the needs of high power piezoelectric ceramics. Unlike bimorphs, stack actuators and other actuators utilizing static or quasistatic displacements, the ceramics in ultrasonic motors are driven near their resonant frequencies and vibrate continuously to output mechanical energies. Therefore, the vibrating characteristic of the ceramics is crucial to the ultrasonic motors application because it directly reflects their abilities to realize the energy conversion. It is generally accepted that in order to obtain high vibrating velocity, the dielectric constant, electromechanical coupling factor and mechanical quality factor should be increased simultaneously. In this study, PMgT has been introduced into PMnS-PZT ceramics to form a new quaternary system, and the effect of PMgT addition from the structural and electrical properties aspects with the purpose of finding candidates for high power resonance type actuators has been investigated.

The quaternary piezoelectric ceramics of $Pb(Mg_{1/3}Ta_{2/3})O_3$-$Pb(Mn_{1/3}Sb_{2/3})O_3$-$Pb(Zr_{0.52}Ti_{0.48})O_3$ (PMgT-PMnS-PZT) were synthesized with a conventional method. The phase, microstructure, ferroelectric, dielectric and piezoelectric properties were studied in terms of PMgT content. The results indicate that all ceramics have a pure perovskite phase of tetragonal symmetry while the c/a ratio increases with PMgT content. The PMgT substitution also promotes the densification of the ceramics without significant grain growth when no more than 5 mol.%. The spontaneous polarization Ps increases consistently as revealed by the enhanced tetragonality, whereas the coercive field Ec, which is affected by the internal dipolar field, reaches a minimum at 3 mol.%. When no more than 5 mol.% PMgT is introduced, both the soft and hard properties can be improved simultaneously. The 0.05PMgT-0.05PMnS-0.9PZT ceramics have the optimal overall performance: $\varepsilon = 683$, $\tan\delta = 0.3\%$, $d_{33} = 227p\,\mathrm{C/N}$, $k_p = 0.55$, $Q_m = 1830$.

Besides, the effects of Zr/Ti ratio on the structure and electrical properties of the PMgT-PMS-PZT were also investigated in order to obtain the MPB composition of this system. A transition from rhombohedral to tetragonal phase was observed as the Zr/Ti ratio decreased. The P-E loops presented pinched shapes at low electric fields and the distortions disappeared at high electric fields. The dielectric study revealed a diffuse phase transition behavior in the ceramics. Vibration velocity at $\Delta T = 20^{\circ}\mathrm{C}$ was found as high as 0.74 m/s for this composition. The ceramics are promising candidates for high power resonant actuator applications.

EM Wave Based Wireless Drive of Small Piezoelectric Plate and Its Application

Junhui Hu[1] and Satyanarayan Bhuyan[2]

[1]Lab of Precision Drive, Nanjing University of Aeronautics and Astronautics
Nanjing 210026, China
[2]School of Electrical & Electronic Engineering, Nanyang Technological University
Singapore 639798, Singapore

Abstract— In this work, electromagnetic wave is used to wirelessly drive a small piezoelectric plate operating in the thickness vibration mode wirelessly. To enhance the wireless electric energy transmission to the piezoelectric plate, a focused electric field generator in series electric resonance with an inductor is employed. In the focused electric field generator, the ac electric field is focused to the needle ground electrode from plate-shaped live electrode through the piezoelectric plate placed in between them. Experimentally, it has been found that the output power and vibration velocity of the wirelessly driven PZT plate depends on the operating frequency, electrical load, position of the driven plate, and the electric field. A maximum output power of 1.86 W and energy conversion efficiency of 0.81% have been achieved by a small piezoelectric plate with an area of 40 mm^2 operating in the thickness vibration mode at resonance frequency of 782 kHz, an optimum load of 1365 Ω, 4000 Vrms across the live and needle ground electrodes, 4 cm electrodes separation, and a live electrode area of 900 cm^2 of focused electric field structure. The wireless drive method has been used in a small ultrasonic stage for merging micro droplets.

Session 3P6b
Smart Materials

Design of a Multilayer Composite-Antenna-Structure by Spiral Type

D. Kim[1], **J. Kim**[1], **J. Kim**[3], **W.-S. Park**[2], **and W. Hwang**[1]

[1]Department of Mechanical Engineering, POSTECH, Republic of Korea
[2]Department of Electronic and Electrical Engineering, POSTECH, Republic of Korea
[3]Antenna R&D Group, Mobile Comm. Samsung Electronics Co., Ltd., Republic of Korea

Abstract— Communication areas will in the future be expanded by the use of satellite communication and satellite Internet availability in vehicles. To implement these satellite services, especially in vehicles, antenna technology will be central. Antennas located on the surface of a structure take up much space, and suffer from large path-loss and junction-loss. In view of these problems, the Structures Division of the US Air Force's Wright Laboratory is sponsoring the development and demonstration of CLAS.

This program is called "Smart-Skin Structure Technology Demonstration (S3TD)". The program opted for a multi-arm spiral antenna embedded in a CLAS fuselage panel. The final demonstration article was a structurally effective 36×36 inch curved multifunction antenna component panel. It successfully withstood running loads of 4,000 pounds per inch^2 and principal strain levels of 4,700 micro-strain, and featured a broadband (150 MHz to 2.0 GHz), multifunction communication, navigation and identification, and electric warfare (CNI/EW) antenna. The present study aims to design and fabricate the structural and electrical performances of spiral antennas of composite sandwich construction as part of the next generation of structural surface technology.

This is termed a composite-antenna-structure (CAS). The CAS is composed of several composite laminates and nomex honeycombs, and spiral antenna element is located top layer with designed configurations. For the bottom layer, a carbon fiber-reinforced polymer (CFRP) of thickness 3.2 mm was used to provide structural support. The absorber (ECCOSORB MCS) was used for honeycomb part to improve reflective loss and axial characteristic. The antenna has target frequency of $0.5 \sim 2.0$ GHz resonant.

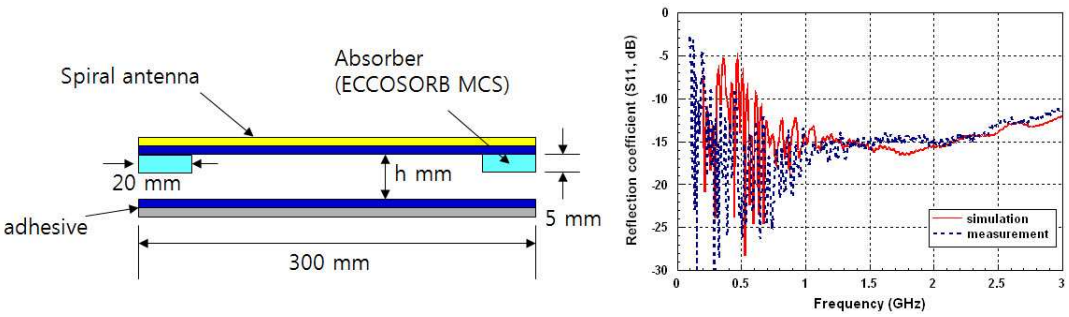

Figure 1: Structure and impedance characteristic of composite-antenna-structure by spiral type.

Impact Behavior of Composite-Surface-Antenna Having Dual Band

J. Kim[1], **D. Kim**[1], **D. Shin**[2], **W.-S. Park**[2], **and W. Hwang**[1]

[1]Department of Mechanical Engineering, POSTECH, Republic of Korea
[2]Department of Electronic and Electrical Engineering, POSTECH, Republic of Korea

Abstract— Nowadays, there are a number of wireless communication systems and broadcasting services which must be integrated into vehicles. Through the innovative integration of antenna elements, amplifiers and ground plane, the reception quality and manufacturability of vehicles is expected to be significantly improved. Even though the articles published to date indicate that the technology has had some spectacular success in its initial stages, little has been published about the problems that remain to be overcome for use in an operational vehicle. The most important outstanding problem that is structurally effective materials cannot be used without reducing antenna efficiency. The present study aims to suggest electrically and structurally effective antenna structures which are termed composite-surface-antenna (CSA), and study mechanical and electrical behavior characteristics of CSA after impact test.

The CSA is composed of two composite laminates, nomex honeycomb, and antenna element. And that is the dual-mode annular ring antenna for both global positioning system (GPS) and satellite digital multimedia broadcasting (DMB), and consists of a coupling feed line and four slots on the annular ring patch. Also, when it is designed, the CAS considered composite materials and adhesive film because of the resonant frequency shift and reduced gain. The GPS antenna patch is designed at the resonant frequency of 1.575 GHz, and the peak gain is 7.6 dBi. The resonant frequency of DMB is 2.635 GHz, and the gain is 5.2 dBi. The CAS was subjected to low-velocity impact by using a drop-weight impact test facility. When 20 J of impact energy is applied to the antenna surface, the maximum contact force was 4 kN and the CAS is resistant to impact The antenna performance of the return loss and radiation pattern was excellent after impact test.

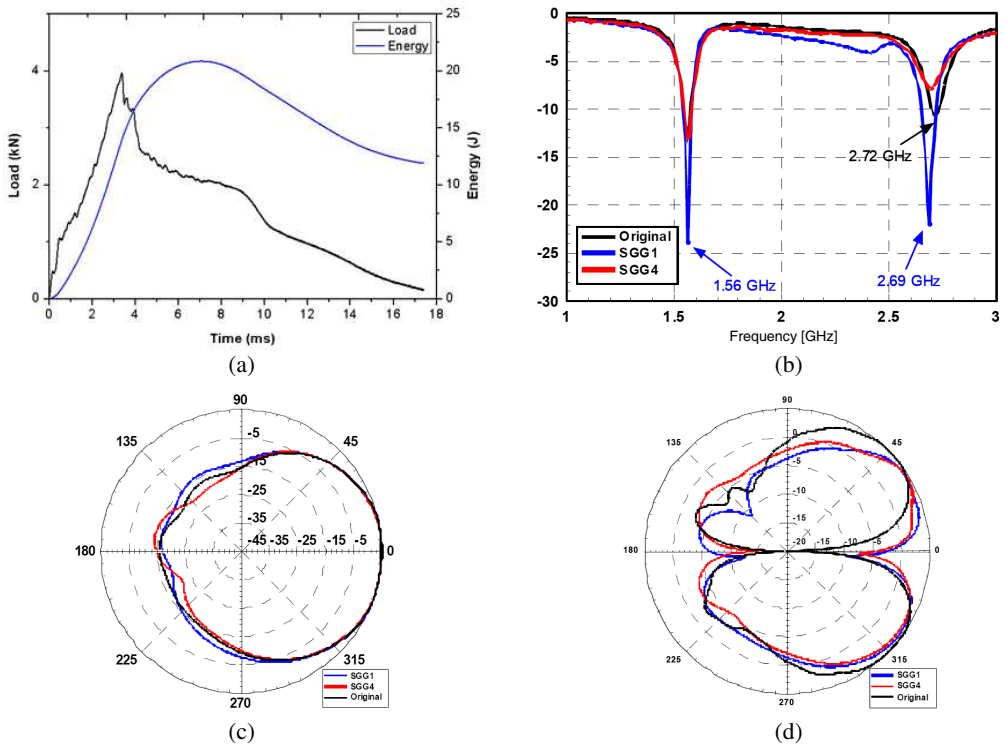

Figure 1: Impact test results of composite-surface-antenna having dual band (GPS/DMB). (a) Contact force history by impact energy of 20 J. (b) Return loss of GPS/DMB. (c) Radiation pattern of GPS at 1.575 GHz. (d) Radiation pattern of DMB at 2.62 GHz.

From Piezoelectric Actuator to Piezomotor

Y. Bernard, J.-L. Christen, C. Hernandez, and A. Razek
Laboratoire de Génie Électrique de Paris (LGEP)
Supelec, Université Paris VI, Université Paris XI, CNRS UMR 8507, France

Abstract— This paper deals with the strategies employed to transform the oscillatory displacements of piezoelectric actuators into either a continuous or a stepping motion. Firstly, the types of actuators likely to be used are taken into consideration (multilayer, bending, Langevin, flextensionnal, bulk, etc) emphasizing on their force-displacement characteristic. Subsequently, the ways to convert a particular type of strain into a sliding motion are studied. The article concludes with an overview of piezoelectric motors in which some of the prototypes built in our laboratory are given as examples.

Actuators: The actuators studied are: 1) the bulks, or a piezoelectric materials sandwiched between two electrodes, 2) the multilayers composed of multiple piezoelectric layers of few micrometers thick, 3) the benders, which suffer a flexural deformation when a piezoelectric material expands 4) the flextensionnal where a passive structure amplifies the displacement, 5) the Langevin where the piezoelectric material is stacked between two masses. For each actuator the advantages and drawbacks are highlighted.

Strategies for Linear Motion Generation: The oscillatory displacement (micrometers to millimetres) has to be converted into a sliding motion. This is effectuated by the use of frictional forces. Here, we study the trajectory of a specific point of the actuator in contact with the slider. This trajectory can be reversible or not. Regardless the case, different well known principles can be employed to obtain the desired motion (stick slip, impact, inchworm, ...).

Examples: As examples, we present some prototypes that have been built and tested in our lab. A stick slip actuator, a linear travelling wave motor and an Inchworm will be exposed in this paper.

REFERENCES

1. Spanner, K. and B. Koc, "An overview of piezoelectric motors," *Actuator*, Vol. 10, 167–176, Bremen, Germany, June 14–16, 2010.

FFT Homogenization Method Applied to Electro-magneto-thermo-elastic Composite Materials

R. Brenner
Laboratoire des Propriétés Mécaniques et Thermodynamiques des Matériaux
CNRS, Université Paris Nord, Villetaneuse 93430, France

Abstract— A numerical homogenization framework based on Fourier transform is applied to investigate the effective response as well as the local fields which take place within smart composite materials which exhibit a multifield coupling behaviour. It consists in the iterative resolution of periodic coupled Lippmann-Schwinger equations. This method is especially attractive because of its computational efficiency and the fact that no meshing of the microstructure is required. A simple scheme relying on the uncoupled Green operators for the corresponding elastic, electrostatics and magnetostatics problems is proposed and assessed, for the cases of piezoelectric and magnetoelectric multiferroic composite materials, by comparison with various analytical and finite element results for different microstructural configurations.

Mean Field Homogenization Methods for Piezoelectric Composites

Romain Corcolle and Laurent Daniel
Laboratoire de Génie Electrique de Paris (LGEP)
CNRS (UMR 8507), SUPELEC, UPMC Paris 6, Univ. Paris-Sud
11 rue Joliot-Curie, Plateau de Moulon, Gif-sur-Yvette 91192, France

Abstract— Homogenization methods based on inclusion problems are a very powerful tool for the determination of the effective behavior of heterogeneous materials. They have been widely used for the prediction of the effective elastic, magnetic or dielectric properties of composite materials. Based on the knowledge of the behavior of the constituents and on a statistical description of the microstructure, they can often provide analytical estimates or bounds on the effective properties. In this paper we apply these homogenization techniques in the case of materials exhibiting a coupled behavior. The example chosen is the case of piezoelectric composites. The results obtained with the proposed method are compared to finite element calculations. It is shown that homogenization techniques provide a very accurate estimate of the effective coupled properties as well as a good description of the mean field (elastic and electric) per phase. The ability of the method to provide information on intraphase fluctuations is then shown.

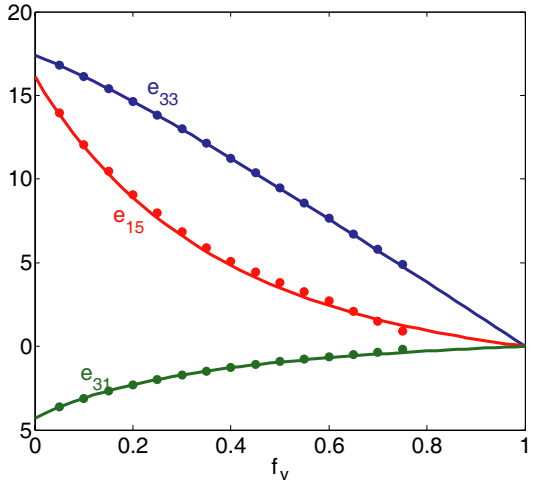

Figure 1: Effective piezoelectric coefficients of a porous piezoelectric material as a function of the porosity: Homogenization (lines) and finite element (dots) results.

Finite Element Modeling of Magnetoelectric Sensors

Thu Trang Nguyen, **Laurent Daniel**, **Xavier Mininger**, **and Frédéric Bouillault**
Laboratoire de Génie Electrique de Paris (LGEP)
CNRS (UMR 8507), SUPELEC, UPMC Paris 6, Univ Paris-Sud
11 rue Joliot-Curie, Plateau de Moulon, Gif-sur-Yvette 91192, France

Abstract— Magnetoelectric (ME) effect in composite materials results from the combination of piezoelectric and magnetostrictive effects. The ME coefficient is defined as the ratio between the measured voltage and the static magnetic field to be measured. A new generation of high sensitivity magnetic sensors takes advantage of this ME effect under dynamic excitation. Indeed it has been observed that when a small amplitude harmonic magnetic field h_{ac} at the resonance frequency of the device is superimposed to the static magnetic field H_{dc} to be measured, the ME coefficient is greatly amplified, resulting in a higher sensitivity for the sensor. This paper proposes a finite element formulation to model this type of sensors under harmonic loadings. It introduces a standard linear piezoelectric constitutive law for the piezoelectric phase and a non linear constitutive law for the behavior of the magnetostrictive phase. The calculation is applied to a trilayer ME sensor. The numerical results reproduce the main trends of the experimental measurements obtained on such sensors. Moreover it is shown that the enhancement of the ME coefficient when a dynamic excitation is applied is directly linked to the non-linearity of magnetic and magnetostrictive behavior.

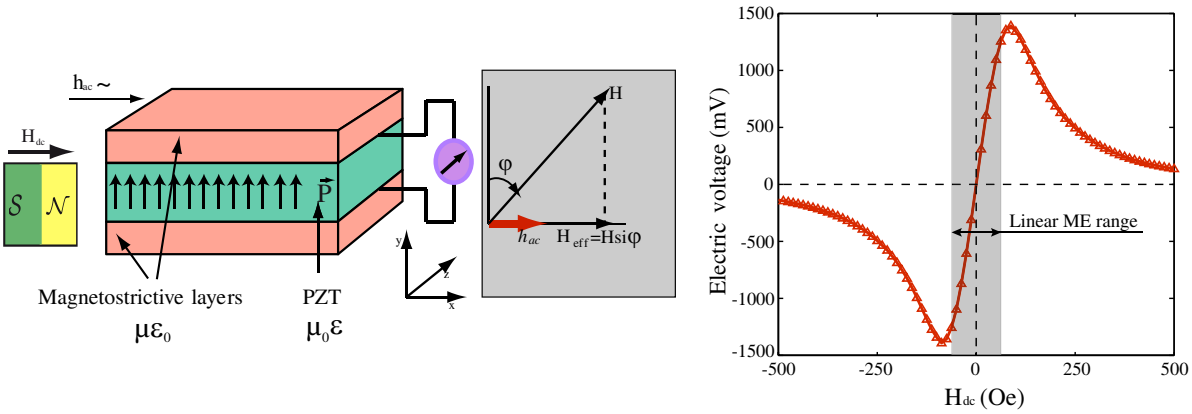

Figure 1: Magnetic sensor based on ME effect — Schematic view and numerical results.

Multiband and Ultrawideband Properties of 2-D Electrochemically-deposited Random Fractal Monopole Antennas

C. Dumond, **M. Khelloufi**, **and L. Allam**
PRISME Institute, IUT of Chartres, Orleans University, France

Abstract— In this study, two 2-D natural fractal monopoles generated by electrodeposition are characterized in term of fractal dimension, measured return loss and efficiencies.

The experimental set-up adapted from [1] consists of an electro-chemical reduction of aqueous metal ions and leads to natural solid metallic thin layer with fractal shapes supported by an insulating substrate. The electrolyte solution is made of copper sulphate prepared with ultra pure water. The current density being the principal drive to obtain fractal morphology, instead of constant voltage used in a first report on this topic [2], a constant DC current is applied between electrodes. An aggregation process by both diffusion and migration of the copper ions allows the growth of thin copper structures after one to five hours.

Due to the random process used, the structures obtained are all different in size and shape but possess common fractal geometry and characteristics. Therefore, depending on the constant DC current used, two main kinds of morphologies can be pointed out: lower currents lead to branched tree-like structures whereas higher currents makes the growth of planar structures with fractal contours possible. Two approximately similar in size samples with both morphologies have been chosen for investigation and will be presented. A 35-mm high branched tree-like structure shown in Fig. 1(a) and a 43-mm high planar structure with fractal contour shown in Fig. 1(b). The fractal dimension of the image of both samples have been computed by the box method and will be reported and discussed.

In order to obtain monopole antenna configurations, structures of Fig. 1 have been mounted vertically above a perpendicular ground plane and connected to a 3.5 mm SMA connector. The input reflection coefficients S_{11} related to 50 Ω have been measured for both antenna up to 12 GHz and will be presented and discussed.

The branched tree-like structure is very interesting from a miniaturization point of vu. In term of return loss, this sample presents a multiband behavior, already pointed out by a previous study [2], with nine apparent matching frequencies (VSWR < 2) within the measured frequency range. By contrast, the planar structure with fractal contour fills more completely the 2-D surface but presents a lower shortening factor. Additionally, its return loss exhibits original and novel UWB capabilities never reported before for natural 2-D fractal antennas. In fact, it appears as a dual band operating system with a second wide band which almost reaches the (3.1–10.6 GHz) band designated by the Federal Communication Commission (FCC) for UWB applications. These broadband characteristics can be linked to higher fractal dimension and attributed to the shape of the opening slot between ground plane and antenna.

Finally, sufficient efficiencies of more than 85% have been measured by the wheeler cap method for both antennas, confirming their possible use as radiating element.

The main advance is to demonstrate the interest of random natural fractal shape with high fractal dimension in actual extensive researches on UWB antennas. In this way, further investigations

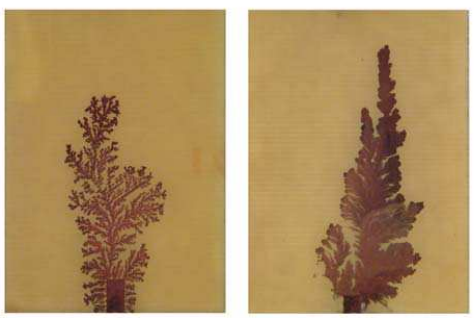

Figure 1.

on samples and image of samples should be done, in particular additional configurations such as feeder of planar slot or as planar monopole could be tested.

REFERENCES

1. Fleury, V., W. A. Watters, L. Allam, and T. Devers, "Rapid galvanic electroplating of insulators," *Nature*, Vol. 416, 716–719, 2002.
2. Puente, C., J. Claret, F. Sagués, J. Romeu, M. Q. Lopez-Salvans, and R. Pous, "Multiband properties of a fractal tree antenna generated by electrochemical deposition," *IEE Electron. Lett.*, Vol. 32, No. 25, 2298–2299, 1996.

Session 3P7
RF and Wireless Communication, Multipath

A Comparison on the Radioelectric Propagation along Grasslands and Scrublands at Wireless Frequency Bands

J. A. Gay-Fernández, I. Cuiñas, and P. Gómez
University of Vigo, Spain

Abstract— This work is part of the research carried out to study the implementation of wireless technologies in rural environments, with the aim of control and management of technical agriculture and extensive cattle farming.

The deployment of these wireless networks could improve, for instance, the quality and quantity of the harvest, since they allow farmers to check, in several points along the plantation, the humidity, temperature, solar radiation, and much more.

Several technologies are involved in this system: WiFi, ZigBee, WiMAX... These technologies usually work at 2.4 GHz, 3.5 GHz or even at 5.8 GHz depending on the standard they use. The rural environments under study usually have the spectrum completely free at these frequency bands and we know there is a lack in the propagation analysis at these frequencies bands in these rural environments. So, several measurement campaigns are required, in order to understand how the radioelectric propagation inside grasslands and scrublands is.

Thus, up to six measurements campaigns were done: one for each frequency and environment. Each set of data has been carefully analyzed and one propagation equation was obtained for each case. Furthermore, a short term analysis was done in order to check the received power variability.

The collected data would allow us to decide the most adequate frequency and technology for each application.

The full paper would describe in detail the measurements campaigns done in grasslands and scrubland as well as the measurement procedure. Furthermore the paper will include all propagation equations, and an extensive comparison between frequencies and environments.

Design and Development of an Electronic Cowbell Based on ZigBee Technology

J. A. Gay-Fernández, I. Cuiñas, and M. G. Sánchez
University of Vigo, Spain

Abstract— Nowadays, the ecologic products consumption is in an exponential growing. People are realizing why the meat of a cow living in an extensive farm is much better and healthier than the meat of a cow fattened up in a static industrial place.

The aim of this contribution is the hardware and software design and test of an electronic cowbell to allow farmers to track the cows that live freely in extensive farms. Some veterinary data, like body temperature, or environmental data, like ambient humidity and temperature, could be gathered with the aid of different sensors plugged into the cowbell. This tailor-made electronic device would be probably ZigBee based because of the mature of this technology in wireless sensor networking and its low power consumption.

Sensor and tracking data would be available in real time at the farm, or even at the veterinary surgery. Thus, the farmers could control and check the health and location of their cattle with only one mouse click.

To get success, the deployment of a wireless sensor network at the grasslands and forests within the farm is needed, too. This network would consist on several ZigBee devices placed at fixed positions. By triangulation, the network provides the location of the cowbell within the exploitation.

The final electronic cowbell will be tested at the laboratory and, if it is possible, it would be run in an outdoor environment to confirm the robustness of the design.

The full paper will describe the complete design of the electronic cowbell system, as well as a detailed description of the data sensors selected for this electronic device. Furthermore some results of the tests done would be included in order to complete the paper.

RFID from Farm to Fork: Traceability along the Complete Food Chain

I. Cuiñas[1], **L. Catarinucci**[2], **and M. Trebar**[3]

[1]Dept. Teoría do Sinal e Comunicacións, Universidade de Vigo, Spain
[2]Dept. of Innovation Engineering, University of Salento, Lecce, Italy
[3]Faculty of Computer and Information Science, University of Ljubljana, Slovenia

Abstract— This paper has the aim to present the works developed along the project "RFID from Farm to Fork", a CIP-Pilot action involved within the 7th Frame Work of the European Union. Our proposal looks for the extension of RFID technologies along the complete food chain: from the farms where cows, fishes, sheep, grapes, etc. grow; to the final consumer at the supermarkets, including all intermediate stages: transports, factory processes, storage.

The main objective is the use of only one system to perform the complete traceability, recording data at each stage. These data could be useful to determine the perfect condition of the final product, but also to control the process during the elaboration. Thus, both final consumers and producers would take advantages of such systems.

The final consumers could obtain different data of the whole process suffered by the product they are buying, just by moving the object in the surroundings of a RFID reader, which can be installed in the supermarket or even as an application at each personal smart phone. The identification of the product allows the software to obtain a complete traceability report from a central database.

Each of the producers along the chain could use the identification by radio frequency to control his production and storage, and to know some previous information of his ingredient matters. Each company could decide which part of the data is just for internal use, which data could be accessible by the other agents involved in the production chain, and also which information is available for the consumer at the shop.

The project involved both the design of the complete system and its tests at different stages of the chain: fishing companies, wine producers, food transporters, and final users, in order to define the actual interest of the system, its performance, and its advantages and disadvantages.

The full paper would show the proposed structure of the system, the technologies involved, and the planned pilot tests.

Recent Evolution of ITU Method for Prediction of Multipath Fading on Terrestrial Microwave Links

Basile L. Agba[1], **Olfa Ben-Sik-Ali**[1], **Robert Morin**[2], **and Germain Bergeron**[2]

[1]Institut de Recherche d'Hydro-Québec, 1800 Lionel-Boulet, Varennes, Québec, Canada
[2]Hydro-Québec, 15000 University, Montreal, Québec, Canada

Abstract— Three methods are commonly used to predict multipath fading on terrestrial line-of-sight (LOS) links namely Barnett-Vigants and Morita methods used respectively in North America and Japan, and the worldwide ITU method. This later method gains in importance even in North America and in Japan due to the regular updates proposed by Study Group 3 of the ITU radiocommunications sector.

The ITU recommendation, ITU-R P.530 provides recommendations based on fading measurements of 251 links in various geoclimatic regions. Since 1978, thirteen revisions were proposed.

The first part of this paper reviews the evolution of the ITU-R P.530 recommendation from 1997 to 2009 with focus on the difference between the last two revisions (Rev. 12 versus Rev. 13).

These differences concern mainly:

- the geoclimatic factor, which depends on the refractivity gradient and the terrain roughness,
- the multipath fade occurrence factor, which is the main parameter affecting worst month outage probability or non-selective and selective outage probabilities when diversity is applied.

The second part of this paper presents parametric studies carried out using our prediction tool, *Microwave link simulator*, to determine the critical parameters affecting link performance. In our studies, 20 links located in Quebec, Canada, are designed based on real-world parameters. The detailed link profiles are known and refractivity gradients are extracted from ITU database according to the ITU-R P.453-9. Climatic conditions are also taken into account using local rain database.

The results of this work show that three climatic parameters (rain intensity, refractivity gradient and annual mean temperature) are critical. Likewise for equipments, radio signature and antenna cross-polarization discrimination highly reduce the overall performance in terms of link availability.

Currently, two year measurements data of five links are analysed. The comparison results with ITU-R P.530-13 show a good agreement. Some statistics such as number of fading events and mean fade duration are also presented.

An Innovative and Reliable Tool for the Electromagnetic Prediction in UMTS Scenarios

Luca Manica[1], **Giacomo Oliveri**[1], **Giovanna Ruscitti**[2], **Lorenzo Gandini**[2], **and A. Massa**[1]

[1]ELEDIA Research Group at DISI, University of Trento, via Sommarive, I-38123, Trento, Italy
[2]Vodafone Omnitel NV, Via Jervis 13, I-10015, Ivrea (TO), Italy

Abstract— The fundamental task of cellular operators is to determine and possibly predict coverage areas, i.e., areas where radio coverage is guaranteed. The computation of coverage areas is usually performed by using a numerical description of the territory and of suitable propagation models to estimate the field strength on a pixel-by-pixel basis [1, 2]. Despite the importance of such tools, coverage area prediction techniques for UMTS systems are usually quite inaccurate. Indeed, standard prediction techniques (developed for GSM systems) neglect co-channel interferences and soft handover mechanisms, which actually play a major role in limiting the coverage of UMTS cells. The aim of this work is to propose an innovative technique for coverage prediction suitable for UMTS systems. Towards this end, the problem of predicting the coverage area in single frequency systems is electromagnetically re-formulated, and an efficient solver is deduced which, taking into account co-channel interferences, not only estimates the coverage area on a pixel-by-pixel basis [Fig. 1(a)], but also provides probabilistic information regarding its reliability [Fig. 1(b)].

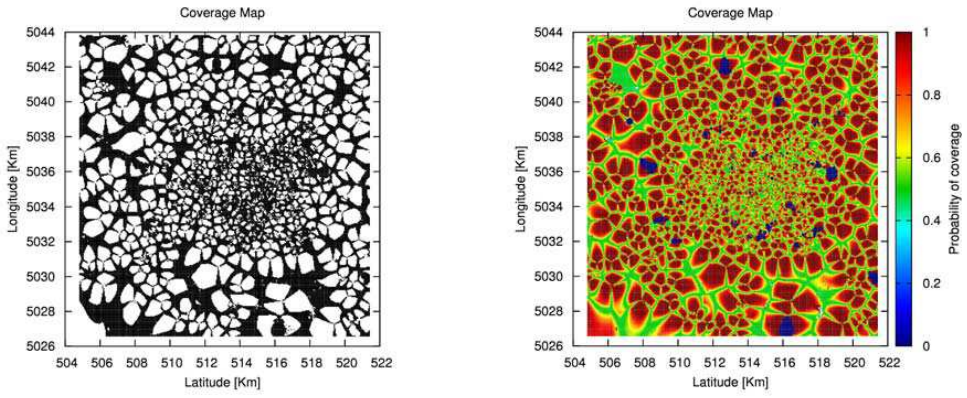

(a) (b)

Figure 1: Example of (a) coverage map and (b) probability map for a large urban scenario.

REFERENCES

1. Davenport, Jr., W. B. and W. L. Root, *An Introduction to the Theory of Random Signals and Noise*, 32–38, IEEE Press, 1987.
2. Holma, H. and A. Toskala, *WCDMA for UMTS — Radio Access for Third Generation Mobile Communications*, John Wiley & Sons, Ltd.

Ultra-wideband Spatio-temporal Channel Sounding with Use of an OFDM Signal in an Indoor Environment

Daisuke Sugizaki, **Naohiko Iwakiri**, **and Takehiko Kobayashi**
Wireless Systems Laboratory, Tokyo Denki University, Japan

Abstract— Microwave vector network analyzers (VNAs) have been widely used as an ultra wideband (UWB) channel sounder. However, channel sounders using VNAs have some limitations: there is only one snapshot; and incoming waves tend to be strongly correlated due to sounding signals of sine waves. To overcome the above issues, a UWB spatiotemporal channel sounder [1], employing an orthogonal frequency division multiplexing (OFDM) signal and virtual array antenna, was developed along with a proposed technique for estimating time-of-arrival (TOA) and angle-ofarrival (AOA) of UWB OFDM signals. In the prototype sounder, the bandwidth of the OFDM signal was 500 MHz (3.25–3.75 GHz). The received collinear virtual array antenna consisted of 8 elements with spacing of 40 mm. The TOAs were calculated by correlating the received waveforms with a transmitting template waveform. The AOAs were derived by extending a multiple signal classification (MUSIC) algorithm and an angular histogram method [2]. Comparison was carried out between the VNA- and the OFDM-based channel sounders in terms of experimental estimation of TOAs and AOAs in an indoor three-path environment. Delay profiles and AOA estimation results, which agreed reasonably well with ray tracing calculation, are shown in Figs. 1 and 2. The proposed design of the OFDM-based channel sounder was validated.

The proposed UWB channel sounder is capable of detecting spectrum and AOA of an in-band (narrowband) interference signal as well as sounding TOA and AOA of the UWB signal itself [3]. A spectral hole can be easily created within an OFDM signal by nulling subcarriers corresponding to the detected spectrum. The proposed sounding technique is therefore applicable to "detect and avoid" cognitive radios.

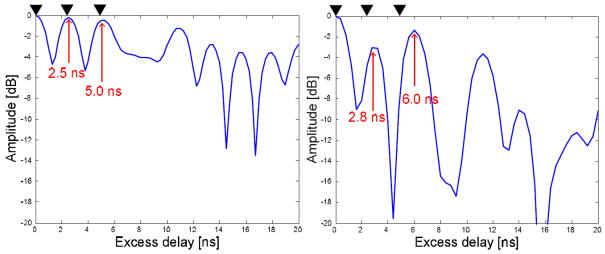

Figure 1: Delay profiles derived from measured data using: (a) VNA- (b) OFDM-based channel sounders. Results of ray tracing calculation are indicated by inverted triangles.

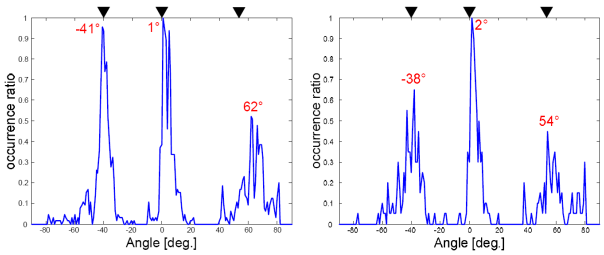

Figure 2: AOA estimation results derived from measured data using: (a) VNA- (b) OFDM-based channel sounders. Results of ray tracing calculation are indicated by inverted triangles.

REFERENCES

1. Iizuka, H., et al., *Progress In Electromagnetics Research Symposium*, Moscow, Russia, August 18–21, 2009.
2. Iwakiri, N., et al., *IEICE Trans. Fundamentals*, Vol. E92-A, 2159, 2009.
3. Iwakiri, N., et al., *4th European Conference on Antennas and Propagation (EuCAP 2010)*, Spain, April 2010.

Densitometry of Electromagnetic Field Exposure Due to Wi-Fi Frequency

A. D. Usman[1], **W. F. Wan Ahmad**[1], **M. Z. A. Ab Kadir**[1], **M. Mokhtar**[2], **and M. A. Zainal Abidin**[1]

[1]Centre of Excellence on Lightning Protection (CELP), Faculty of Engineering
Universiti Putra Malaysia, UPM Serdang, Selangor 43400, Malaysia
[2]Wireless and Photonic Networks (WiPNET), Research Center of Excellence
Faculty of Engineering, Universiti Putra Malaysia, UPM Serdang, Selangor 43400, Malaysia

Abstract— The world is undergoing electromagnetic revolution with many frequencies used for a variety of wireless devices. Recently, the emergence of Wi-Fi technologies deployed in schools, offices and other public places raised a lot of concern by the general pubic on the magnitude and safety of this exposure. To this effect, in situ measurements were conducted at various Wi-Fi access points at both academic and students' residential areas in University Putra Malaysia, Serdang Selangor. An electric field meter with tri-axis probe and a spectrum analyzer were used to carry out measurements at far field distance for 6 minutes average time. Various locations were investigated and it is found that the highest and the lowest readings obtained during the loading and downloading activities were 5.16 V/m and 0.37 V/m, respectively. These readings are far below the ICNIRP reference guidelines for exposure to general public.

Implementation of Channel Estimation and Multi-user Detection Based on Genetic Algorithms

M. Elnamaky, **I. Elshafiey**, **M. Alansi**, **A. Alsanie**, **A. Sheta**,
A. Sulyman, **A. Alsuwailem**, **and H. Alsharari**
Electrical Engineering Department, Prince Sultan Advanced Technologies Research Institute (PSATRI)
King Saud University, Riyadh 11421, P. O. Box 800, Saudi Arabia

Abstract— Multiple Input and Multiple Output (MIMO) systems have been widely used to enhance the performance of modern communication systems. Among their applications, MIMO systems are used to achieve space division multiple access (SDMA) scenarios, where multiple users share the up-link channel for connection to a base station (BS). Orthogonal frequency division multiplexing (OFDM) techniques are typically adopted in implementing such systems. Robust estimation of the MIMO channels is required to detect each user's signal, while reducing the multi-user interference and the multi-path fading. Conventional channel estimation techniques suffer, in general, from either the slow convergence rate or performance degradation and reduction of the effective system throughput.

In this paper, an SDMA OFDM system is considered, in which a group of M users are connected to a BS. Each user is carrying a mobile station that is equipped with a single antenna, while the BS is equipped with N antennas. Multi-user detection (MUD) techniques are invoked for detecting the transmitted signals from various mobile stations. User-specific spatial signatures constituted by the channel impulse responses (CIR) of the MIMO system set the basis of identifying the user signals. MUD optimization techniques do not allow in general an over-loaded scenario, in which M gets higher than N. Development of advanced tools that can overcome this limitation is essential in achieving considerable enhancement of the spectral efficiency, which is a key element for next generation communication systems.

Genetic algorithms (GAs) are investigated in this research to obtain a powerful optimization tool that is implemented in a joint channel estimation and multi-user detection. Optimization is performed to maximize the number of users M for a particular number of antennas N. Genetic algorithms suffer from computational complexity, a fact that inhibits their use in real time implementations. However, the fact that these algorithms are intrinsically parallel allows the introduction of novel realization solutions. Field Programmable Gate Array (FPGA) structures which offer high programming flexibility and parallel architectures are used to expedite the GAs performance and reduce their processing time. Simulation results are presented of the SDMA OFDM system under fading channels, along with hardware validation under Xilinx Virtex-6 environment of the implementation GAs for channel estimation and MUD.

ACKNOWLEDGMENT

This research is funded by *The National Plan for Science & Technology* under project No. 08-ELE262-2.

High Efficiency Power Combining Technique Based on Distributed Amplifier Topology

Steve W. Y. Mung and Wing Shing Chan
Department of Electronic Engineering, City University of Hong Kong
83 Tat Chee Avenue, Kowloon, Hong Kong SAR, China

Abstract— A high efficiency power amplifier (PA) is proposed by using distributed amplifier topology. Different stages of distributed amplifier (DA) have different optimum loadline resistance. This non-uniform load-pull (NLP) power combining technique for distributed amplifier with different stages is proposed. This approach allows efficient distributed combining of field-effect transistors (FETs) output power without the use of multi-way power combiners. The proposed distributed amplifier's topology uses a quarter-wave short-circuit stub or open circuit to replace the drain line lossy dummy load. This topology is able to achieve power equalization among the FETs at microwave frequencies. This design method ensures optimum loadlines are achieved for all FETs and the efficiency obtained is compared with the conventional single-transistor class-A power amplifier using the same FET type.

Distributed amplifier with different stages has different optimum loadline resistance. The optimum characteristic impedance of the drain output transmission line presented here obtains the power-matched condition for all FETs. This NLP power combining technique is demonstrated at 2 GHz with 1-stage, 2-stages, and 3-stages distributed amplifiers. Experimental results show that the power-added efficiency (PAE) of these three different distributed amplifiers is greater than 35% at the 1-dB gain compression point. The maximum efficiency is greater than 35% over a bandwidth of 10%. The 3-stages distributed amplifier demonstrates an output power level of 27.4 dBm at the 1-dB gain compression point with power combining efficiency (PCE) around 90%.

Generalized Two-dimensional Anisotropic Scattering-Doppler Spread and Time Variations in Mobile Wireless Channels

Petros Karadimas and Jie Zhang
Centre for Wireless Network Design (CWIND), Department of Computer Science and Technology
University of Bedfordshire, LU13JU, Luton, UK

Abstract— In mobile wireless channels (downlink case with fixed base station and mobile receiver), when the receiver is far away from the surrounding scatterers, the propagation is considered as that from-the-horizon where multipath power arrives mainly in two dimensions (2-D) [1]. The anisotropic scattering of multipath power, i.e., multipath power arriving at the mobile receiver under a non-uniform regime, is the realistic case in such channels as opposed to the isotropic scattering case considered in the classical paper of Clarke [2]. This is caused when a part of power is blocked by the channel obstacles (shadowing effect) and/or no multipath power arrives from certain directions due to lack of scattering objects in those directions and/or directional receiving antennas are employed. From the angle of arrival (AOA) of the multipath power, we can end up to the temporal autocorrelation function (ACF) and power spectral density (PSD) of the received signal in single-element antenna channels. The time selectivity of such channels is explicitly related to these metrics (ACF and PSD) [3], from which we can further derive the level crossing rate (LCR) and average fades duration (AFD) (i.e., the second order statistics) [4]. Moreover, the directional statistics of the arriving multipath power play a dominant role on the performance of antenna space diversity [5] and antenna angle diversity systems [6].

In this paper, we present a generalized theoretical model for the angle of arrival (AOA) in wireless channels when the scattering is two-dimensional (2-D) anisotropic. This model can constitute a platform for creating new angular distributions for the propagating multipath power and as such, a new distribution accounting for multi-modal arrival will be presented. The latter will represent the case that multipath power arrives into four angular sectors being parametrically defined with respect to the direction of the receiver motion. From the AOA, the power spectral density (PSD) of the received complex signal is analytically derived. Further generalization with multi-modal arrival into an arbitrary number of angular sectors can be treated similarly.

REFERENCES

1. Durgin, G. D. and T. S. Rappaport, "Theory of multipath shape factors for small-scale fading wireless channels," *IEEE Trans. Ant. and Propag.*, Vol. 48, No. 5, 682–693, May 2000.
2. Clarke, R. H., "A statistical theory of mobile-radio reception," *Bell Syst. Tech. J.*, Vol. 47, 957–1000, Jul./Aug. 1968.
3. Bello, P. A., "Characterization of randomly time-variant linear channels," *IEEE Trans. Commun. Syst.*, Vol. 11, 360–393, Dec. 1963.
4. Patzold, M., *Mobile Fading Channels*, Wiley, Chichester, U.K., 2002.
5. Vaughan, R. G. and J. B. Andersen, "Antenna diversity in mobile communications," *IEEE Trans. Veh. Technol.*, Vol. 36, No. 4, 149–172, Nov. 1987.
6. Vaughan, R. G., "Pattern translation and rotation in uncorrelated source distributions for multiple beam antenna design," *IEEE Trans. Ant. and Propag.*, Vol. 46, No. 7, 982–990, Jul. 1998.

Channel Characterization Techniques for Wireless Automotive Embedded Systems

M. Cheikh[1, 2], **J. David**[2], **J. Tartarin**[3], **S. Kessler**[1], **and A. Morin**[1]

[1]Continental Automotive Systems, 1, Av Paul Ourliac, Toulouse 31100, France
[2]LAPLACE, Av Charle Camichel, Toulouse 31000, France
[3]Université de Toulouse — LAAS, 7, Av Colonel Roche, Toulouse 31100, France

Abstract— The number of wireless systems developed for automotive applications increase for security and comfort considerations. Among these applications, the wireless automotive passive entry (Passive Access System Entry: PASE) and the intelligent tire information system (Tire Pressure Monitoring System: TPMS) have expanded considerably.

The radio propagation channel between the transmitters (wheel units for TPMS and badge for PASE) is tricky to model because of the numerous parameters involved. Moreover, the wave propagation in the context of a moving embedded system such as car is penalized by the high wavelength ($\lambda = 69\,\mathrm{cm}$). As the complex design of a vehicle involves metallic modules ranging from less than $\lambda/10$ to some 10. λ, the radiolink budget is thus sensitive to the environment: several mechanisms are involved perturbing the electromagnetic wave propagation such as absorption, reflection, diffraction and scattering by objects (like the body of the car, the passengers, external environment, etc.). The emitted waves thus change in phase and power according to the multi-path propagation and produces both destructive and constructive behaviours all along the channel, and particularly at the receiver side. These environment and operating considerations increase the radio-link budget complexity, and contribute to degrade the global transmission quality of the systems. It is then necessary to develop non disturbing measurement techniques to avoid interaction between the measurement setup and the measured fields. Using such accurate measurements, it is thus possible to find the suitable receiver's position, and antenna's design.

The purpose of this study is to propose an innovating space characterization technique for TPMS and PASE, to characterize the received power distribution inside and around the vehicle. The field variation of the channel is measured versus space and wheel rotation angle for TPMS. The high resolution sounding system allows to track the channel variations and to locate fading effects. Optical components are used to get an accurate non disturbing field measurement technique. The RSSI (Received Signal Strength Indicator) collected at each reception cell is emitted through an optical fiber system which constituted with an optical transmitter, a receiver and a fiber link. The sounded zones are then presented versus a two dimensions diagram inside or around the vehicle close to the expected reception zone. The free radio licence frequency of 434 MHz is chosen for this study.

Performance Comparison of OFDM, MC-CDMA and OFCDM for 4G Wireless Broadband Access and Beyond

Syed M. Zafi S. Shah, **A. W. Umrani**, **and Aftab A. Memon**
Institute of Information and Communication Technologies
Mehran University of Engineering and Technology
Jamshoro 76062, Pakistan

Abstract— This paper compares the error rate performance the three top candidates for access techniques to be used for 4G mobile communication systems, i.e., Orthogonal Frequency & Code Division Multiplexing (OFCDM) with Orthogonal Frequency Division Multiplexing (OFDM) and Multi-Carrier Code Division Multiple Access (MC-CDMA). The objective is to find the most suitable technique for implementation in 4G Communication Systems. The modems of OFDM, MC-CDMA and OFCDM have been redesigned and the performance is tested under a practical 6-tap frequency-selective Rayleigh fading channel. The results reveal that OFCDM, a technique that extracts multiplexing in all three domains of time, frequency and power, provides the lowest bit error rate for a given energy-of-bit-to-noise ratio (E_b/N_0). Furthermore, it was observed that selecting a higher spreading factor for frequency-domain spreading did not lead to any improvement in the bit error rate at small values of E_b/N_0 when the channel is highly frequency-selective, where as time-domain spreading does have a better performance than frequency-domain spreading and therefore former should be prioritized over latter when the E_b/N_0 is small. In retrospect, a higher spreading factor for time-domain spreading leads to an increase in the requirement for the number of subcarriers. This means that when time-domain spreading is prioritized, a greater number of subcarriers will be required for multicarrier transmission.

Session 3P8
Power Electronics

Influence of the Design of Resistance Welding Equipment on the Evaluation of Magnetic Field Exposure of Operators

R. Doebbelin[1], **T. Winkler**[2], **and A. Lindemann**[1]

[1]Institute of Electric Power Systems, Otto-von-Guericke-University, Magdeburg, Germany
[2]Fraunhofer-Institut für Fabrikbetrieb und-automatisierung, Magdeburg, Germany

Abstract— Resistance welding is a widespread joining process in large fields of manufacturing, e.g., in automotive industry. In resistance welding processes welding currents in the kA range are applied resulting in intense magnetic fields in the vicinity of the equipment. Besides welding robots also man-operated welding machines and handheld welding guns are widely used.

Considering the occurring magnetic field exposure, relevant regulations regarding field exposure evaluation have to be taken into account and compliance with given limits has to be ensured to avoid any health hazards to operators of resistance welding equipment.

In addition to the obvious impact of welding current amperage on magnetic field exposure, there is an influence of the dimensions of the welding circuit (as a constructional aspect) on the magnetic flux density distribution which has to be considered in correlation with the position of the operator.

The magnetic field exposure can be evaluated comparing occurring and permissible flux density values. As a special feature, an influence of the electrical design of the respective resistance welding equipment on the magnetic flux density limit values may exist. This results from the characterization of the limit values in the regulations.

In the ICNIRP "Guidelines for limiting exposure to time-varying electric, magnetic, and electromagnetic fields" and related regulations, limit values of the electric current density occurring in the tissues of a human body exposed to an electric or a magnetic field are defined as a basic restriction. Since it is not possible to measure the current density inside the body, a current-density based field exposure assessment requires numerical field calculations by means of an appropriate computer program including a high-resolution model of the human body.

To enable an alternative evaluation, limit values for measurable quantities have been derived from the basic restrictions. In the low frequency range such limits (named reference levels) are given for electric and magnetic field strength and magnetic flux density. Basically, basic restrictions and reference levels represent frequency- dependent limit values for sinusoidal fields. Beyond that, in the guideline BGV B11 "Electromagnetic Fields" also instructions for assessment of exposure to time-varying fields with pulsed waveforms are given.

As a special aspect, it has to be considered that according to BGV B11 in this case the concrete limit values depend on the actual waveform of the field parameters or of the field-generating current and therefore, the respective limit values have to be determined following a procedure which is given in this regulation. In this procedure especially the change rate of the magnetic flux density (which is relevant for resulting current density values inside an exposed human body according to Faraday's law of electromagnetic induction) is regarded. To enable the limit value determination, fundamental waveforms (e.g., triangular, trapezoidal, exponential) of pulsed fields are presented in the guideline together with related calculation formulas.

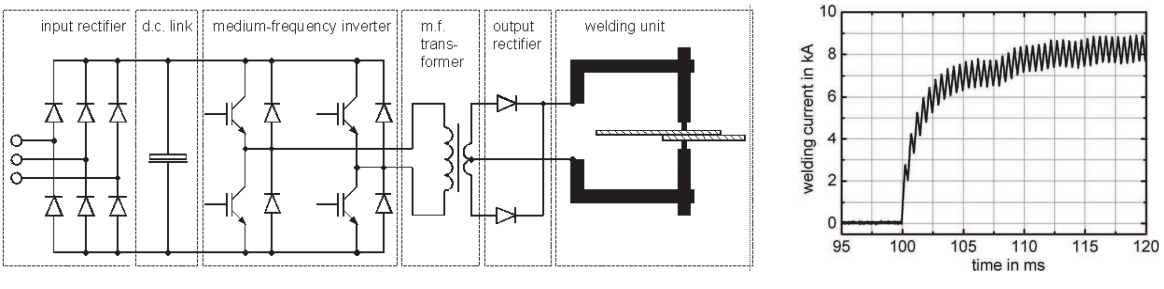

(a) (b)

Figure 1: Resistance welding inverter. (a) block diagram of the power unit. (b) example of a measured welding current.

However, real waveforms of welding current and magnetic field respectively, generated by common resistance welding equipment differ remarkably from these fundamental waveforms. The concrete waveform characteristics depend on the used power electronic topology. In the case of resistance welding inverters (Fig. 1), additionally to the basic shape of the waveform (the d.c. pulse showing exponential slopes), superimposed ripple components occur according to the operation of an inverter power source. So, a 300 Hz component may occur due to imperfect smoothing of the voltage of the d.c. link. In connection with output rectification a ripple component showing the doubled value of the switching frequency appears in the welding current waveform (a 2 kHz component in the case of 1 kHz inverters).

In the paper, a proven approach to adapt the evaluation procedure for pulsed fields to the special characteristics of resistance welding equipment shall be illustrated and the alternative assessment applying an evaluation procedure based on the consideration of basic restrictions shall be discussed.

Matrix Converter Commutation Time Reduction

J. Lettl, L. Linhart, and J. Bauer
Department of Electric Drives and Traction, Faculty of Electrical Engineering
Czech Technical University in Prague, Czech Republic

Abstract— The simulation results, knowledge obtained in the construction of the state machines and comparison of two commutation strategies of a matrix converter are presented in the paper. Used matrix converter is utilizing the FPGA technology for the realization of the modulator. The modulator includes the state machine to ensure the commutation between the input source lines and dead bands of the IGBTs. The FPGA technology is convenient to test different state machines as well as different commutation strategies.

Commutation process is conventionally switch-over of one output phase from one input phase to another one. Commutation strategy resolves the process of transition between two steady switching states. This transition is performed through the sequence of some steps whose number determines the type of commutation strategy. One commutation step involves either the switch-off or switch-on of the IGBT and its duration corresponds to generated dead band period. It is possible to realize the commutation in 1, 2, 3 or 4 steps. The reduction of the number of steps yields decreasing of commutation time and increasing of commutation algorithm complexity.

The important variables for the control of the commutation strategies with odd numbers of the commutation steps are polarities of the input phase-to-phase voltage and output currents. Contrary, the commutation strategies with even numbers of the commutation steps are controlled by either the polarity of the input voltage or the output current.

Best type of switching minimizes the number of steps to the lowest possible value — which is one. For this purpose it is necessary to control both the input line-to-line voltage and the output current. The prearranged state should be changed when any of these control variables is changed. It is the most difficult method of commutation. It is based on the principle that the output phase is always connected with one, two, or three input phases. However, only one transistor is switched-on in the frame of each connected input phase. The polarity of input line-to-line voltages determines the number of input phases (and the number of transistor as well) that are connected. This connection is always realized only through transistors on the same side — either source side, or load side. The direction of the current determines this side. Because this method is the most difficult and requires precise measurement of current we instead choose the two-step method. Presently, two types of two-step commutation method were developed. The older release was oriented to phase-to-phase voltage as a control variable. Second one, two-step current oriented method, is the newest invention. Some limitations of both methods were discovered. The critical region is the control variable zero crossing. In case of the voltage oriented two-step commutation some current peaks may appear closely before (or after) the relevant voltage polarity. It is caused by preliminary diode of non-connected input phase; therefore the current of conductive phase is drained out. For a short time one input phase is connected with two input phases.

A problem of current oriented method appears when the current decreases under the value for which we are uniquely able to determine the current direction. In this case it is necessary to switch on the second IGBT of the plugged phase as well. After the unique determination of the flowing current direction we switch off the IGBT which is not conductive.

Apparently, the best solution may be synergy of both two-step methods. There are two several ways depending on method subordination. The current method can be master and critical region can be bridged by means of voltage method, or it can be contrary. In the first case the number of critical regions is variable, but this number can be in certain circumstances reduced to minimum. Second solution (master method is voltage oriented two-step method) seems to be easier if the better prediction and delay compensation of phase-to-phase voltage are considered.

The Use of Prediction to Improve Direct Torque Control

D. Kuzmanovic and J. Lettl
Faculty of Electrical Engineering, Czech Technical University in Prague, Czech Republic

Abstract— The presented paper shows how it is possible to improve effectively the performance of the Direct Torque Control (DTC) by implementing prediction. The DTC is a modern control technology that uses a simple control algorithm - the estimated torque and flux values are constantly compared to their set points, and if they are out of their tolerance bands, an adequate switching combination is applied to the converter output and as a result the torque and flux are driven to their set values. There are several types of the DTC: Switching Table Based DTC (ST-DTC), Direct Self Control (DSC), DTC using the space vector modulation, DTC using the discrete space vector modulation, neuro-fuzzy DTC, etc. This article deals with the ST-DTC, being the most widely implemented DTC scheme.

The DTC offers many advantages over the Field Oriented Control (FOC): a higher transient response, simple control method without the need for the inner current control loops and the coordinate transformations, etc. However, in order to keep a low torque ripple, it requires a high switching frequency ($\geq 20\,\text{kHz}$). If the switching frequency is not high enough, the only way to increase it, and to improve the DTC performance, is to modify the hardware. This article offers the use of prediction as another solution for the improvement of the DTC when hardware limits are reached. The solution is cost effective, since it doesn't require any hardware modifications.

In the classical DTC algorithm, the selection of the voltage vector for the next cycle is based on the motor state (torque and flux) estimated from the voltage and current measured at the beginning of the current cycle.

The change of the flux magnitude over the switching cycle can in the most cases be neglected, but the torque value can considerably change by the end of the cycle, especially in the case of lower switching frequency. The result is a one cycle delay in the torque control and a higher torque ripple. The proposed scheme predicts the torque and flux values at the end of the cycle, and uses that state to select the voltage vector for the next cycle. The prediction algorithm uses the motor state from the beginning of the cycle and the set voltage vector to predict the torque and flux values at the end of the cycle.

The proposed algorithm was implemented on a test bed containing frequency controlled induction motor drive with switching frequency of 6.67 kHz. The experimental results have shown that the effect of using the prediction is comparable to the effect of increasing the switching rate by 100%.

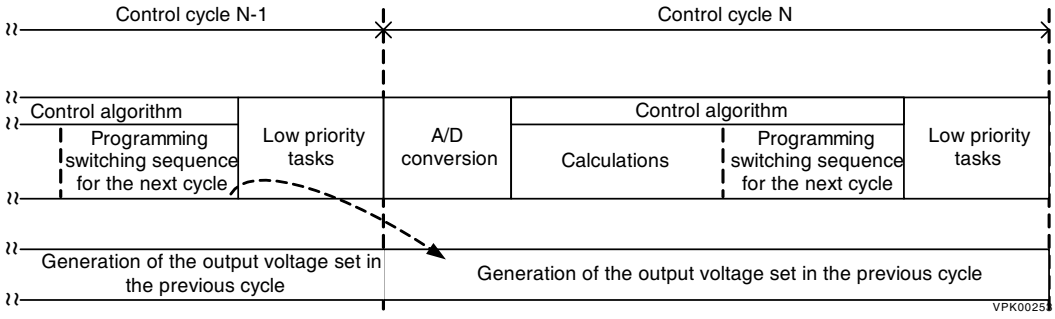

Measurement and Signal Processing for Electric Drive Control System

P. Brandstetter, **P. Bilek**, **J. Szotkowski**, **and P. Vaculik**
Department of Electronics, VSB-Technical University of Ostrava, Czech Republic

Abstract— Paper is focused on presentation of possibilities which come with application of digital signal processing into area of electric drives control. In the paper, description of control system, structures for measurement and signal processing of analog and digital signals are presented. Hardware and software realization of these devices are shown, and also description of control structure which is used for digital signal processing. In conclusion, experimental results of used control system are presented.

Expansion and miniaturization of microprocessor control systems allows significant reduction of cost, dimensions and also simplify usage of microprocessor control systems into wide area of application. Digital signal processing allows to great improvement of control parameters and increases quality of technological processes. It allows simple remote control of the process and communication with superior control system. The application of control system with digital signal processing will be demonstrated on control system of electric drive.

Structure of control system may be divided to three levels. This division is realized according to type of signals which are present at particular level of control system (see Figure 1). The highest level is the digital signal processing (DSP) unit itself. A software signal processing and A/D conversion is realized at this level. To connect DSP unit to the drive, second level called interface is necessary. At this level, input signal level conversion is realized to enable connection of sensors to the DSP unit. Next function of interface level is power boosting of output signals which allows connection of DSP unit to the driver of electric drive. The bottom level of control system is drive level. Acquisition of necessary signals from electric drive is provided by measuring elements.

It is necessary to require measured signals in enough quality to provide good functionality of the whole control structure. To provide this, several demands must be adhered:

1) Enough accuracy: Accuracy of signal measurement is the determinant parameter of accuracy of regulation.

2) High noise resistance: Electric drives usually produce high level of disturbance. It is necessary to reduce influence of this disturbance by selection of proper output signal from sensor.

3) Dynamic range: Some of the measured signals are characterized by steep changes in amplitude. It is necessary to choice sensors with high dynamic range to prevent errors in control.

4) Galvanic insulation between measured signal and sensor output: Galvanic insulation is necessary for safety requirements and is providing simple connectivity between electric drive and interface level of control system.

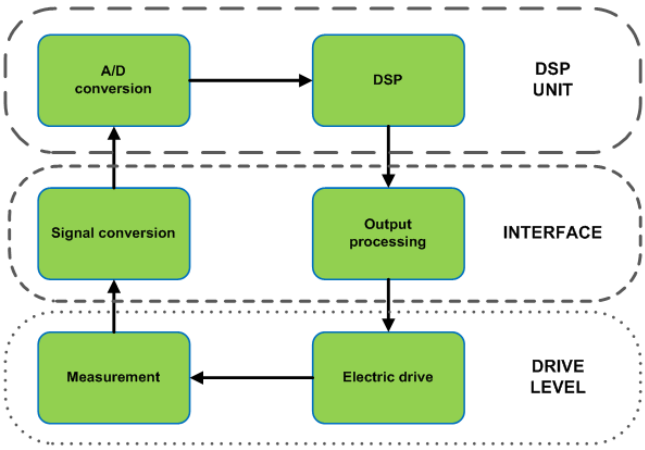

Figure 1: Structure of control system.

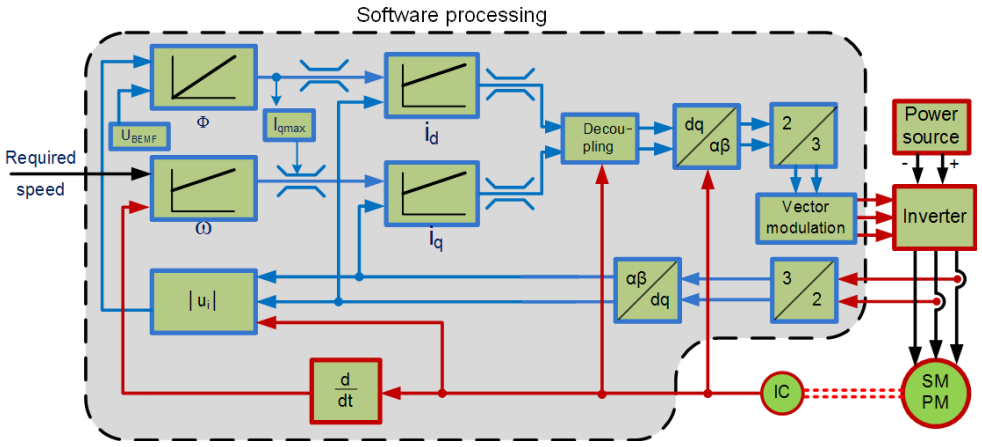

Figure 2: Control structure of AC drive with permanent magnet synchronous motor.

Usually, signals from sensors cannot be directly attached to DSP, because level of voltage output differs with possibilities of input gate of DSP. Signal level conversion is necessary in many cases to allow connection between sensor and DSP. Next important function of interface level is overvoltage protection of DSP input gate.

The software processing gives very interesting possibilities, how quickly, effectively and casual resolve the problems. We know that there is special software for resolving almost all kind of problems. In our case the facility is digital signal controller (DSC) 56F8037 and the software is development environment called Code Warrior.

The signal processing was designed for the vector control of AC machines. The following Figure 2 shows structure such control for permanent magnet synchronous motor. After signal conversion to digital form expressed as integer type we have to convert it to fraction type. It's necessary to measure actual rotor position (for example incremental sensor) for creating the system of coordinates, which always has same direction like rotor. The position sensor is a source of two signals with 90 degrees phase shift. The signals are connected with timer through the differentiating amplifier. There is an actual rotor angle saved in timer register after its correct setting. The Clarke transformation (marked 3/2 on the figure) transfers measured phase currents into orthogonal coordination system. Using Park transformation (marked $\alpha\beta/dq$ on the figure) we obtain rotating orthogonal coordinate system oriented like rotor. The controllers were chosen PI type or I type with limitation their outputs. Furthermore the signals must be decoupled and by inverse progress they are transformed back. The last part is a modulation.

Sensorless Control of Asynchronous Motor Using Voltage Signal Injection

P. Brandstetter, **P. Bilek**, **J. Szotkowski**, **and P. Vaculik**
Department of Electronics, VSB-Technical University of Ostrava, Czech Republic

Abstract— Paper is focused on presentation of possibilities which come with application of voltage signal injection in sensorless control of asynchronous motor. In the paper, description of control system and structure for measurement and signal processing are presented. In conclusion, simulation results of applied control method are presented.

Controlled induction motor drives without mechanical speed sensors at the motor shaft have the attractions of low cost and high reliability. To replace the sensor, the information on the rotor speed is extracted from measured stator voltages and currents at the motor terminals. Vector controlled drives require estimating the magnitude and spatial orientation of the fundamental magnetic flux waves in the stator or in the rotor. Open loop estimators or closed loop observers are used for this purpose. They differ with respect to accuracy, robustness, and sensitivity against model parameter variations. Dynamic performance and steady-state speed accuracy in the low speed range can be achieved by signal injection, exploiting the anisotropic properties of the machine.

Various concepts for controlled high-performance induction motor drives without speed sensor have been developed in the past few years. Eliminating the speed sensor on the motor shaft represents a cost advantage. This combines favorably with increased reliability due to the absence of this mechanical component and its sensor cable. Speed sensorless induction motor drives are well established in those industrial applications in which persistent operation at lower speed is not considered essential.

Just therefore were developed injection method for high dynamic performance in the very low speed range including zero speed and zero stator frequency. Particularly the zero stator frequency problems continue to attract the interest. As of now, a robust solution for general industrial use has yet to be found.

The sensorless techniques were to be developed for synchronous motor, but it is possible used to induction motor too. For asynchronous motor used two injections. One of these is high frequency injection and the other is voltage testing impulses injection. Both method trace motor anisotropy: either saturation for estimation magnetic flux, or asymmetry existent grooved rotor.

Injection accomplish with the help of additional symmetrical three phase sinusoidal voltage signal which is superposed to basic supply voltage (see Fig. 1). Frequency votes within the range 0.5–2 kHz and injection proceeds in system [α, β] composite with stator. In this case have to be carefully select frequency and amplitude. Frequency injected signal must be enough high, to wasn't problem with remove basic frequency in inference current with high frequency, however with regard to the value of switching frequency must be conserved sufficient accuracy. Sinusoidal signal isn't acceptable create with frequency 5 kHz and switching frequency 10 kHz, where would were two closure on one period injection signal, afterwards would it least wasn't sine wave.

Amplitude must be elect so, to injection expressive affect alone activity motor, but at the same time current response on voltage injection must be enough high with the view of next processing. Usually amplitude move at intervals 5–20 V.

Current with high frequency, which will originate injection additional voltage signal, includes two basic components:

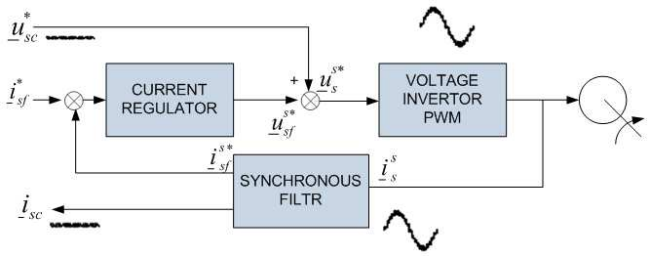

Figure 1: Principle of voltage signal injection.

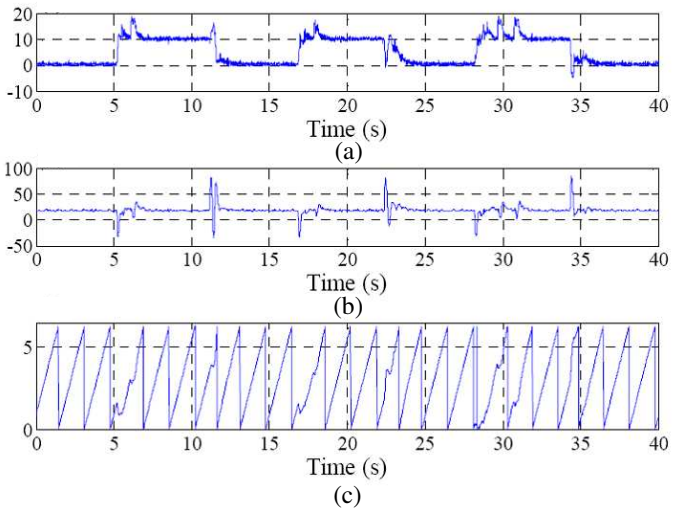

Figure 2: Speed response to step load changes 0–35%. Speed controlled to 18 rpm. (a): Filtered Isq (A). (b): Simulated speed (rpm). (c): Estimated rotor position (rad).

- Positive component, which does not contain information of position. This component is proportional to mean value leakage inductivity.
- Negative component, includes information of position in this phase. This is reflection difference sizes inductivity after perimeter motor.

The simulation results are shown on the Fig. 2 which shows waveforms with simulated speed and rotor position.

Comparison of Different Filter Types for Grid Connected Inverter

Jiri Lettl, **Jan Bauer**, **and Libor Linhart**
Department of Electric Drives and Traction, Faculty of Electrical Engineering
Czech Technical University in Prague, Technicka 2, 166 27 Prague 6, Czech Republic

Abstract— The acquisition of the electrical energy from renewable resources is very trendy in these days. That is also why the applications for renewable energy generation undergo rapid development. In the area of private energy sources, for family houses or as a power supplies in the area where the supply network is not present, the solar energy is the most popular "green source". The water and the wind are not so popular energy sources. The instability and dependence of delivered energy amount can be assumed as the greatest weakness of renewable sources. For example the amount of the energy obtained form the solar panel depends on the surrounding conditions, as intensity of the sun exposure or the temperature of the solar array. In order to stabilize the energy output and to give it some defined waveform and value, the power converter must be connected to the solar panel output. For this purpose, the most suitable choice is the voltage source inverter (VSI) application. The inverter employs mostly the PWM or hysteresis control to generate sinusoidal voltage waveform. This way of control causes that harmonics appear in the output voltage. The content of low order harmonics can be affected by the PWM modulation frequency and the switching frequency of the inverter will always influence the output voltage harmonic spectra. The presence of the harmonics in the grid causes losses on the grid impedances and consequently deformation of the network's voltage waveform.

In order to suppress or reduce these negative effects the filter is connected between the converter and the network. The filter must be designed precisely, because it must have sufficient attenuation at the inverter's switching frequency and it must not bring oscillations to the whole system.

There are several types of filters. The simplest variant is the filter reactor connected to the inverter's output. However, this simple solution is connected with phase shift between the generated voltage and generated current. The reactor also greatly decreases the dynamics of the whole system (converter/filter). That is why combination with capacitor, like LC or LCL, is taken into account, too. The design of the filter is not simple task, because the filter made as a combination of reactor and capacitor forms resonant circuit and is therefore vulnerable to oscillations and it can bring the system into the unstable state. That is the reason why the damping of the filter is considered and some variants of the filter's damping circuits are discussed, too.

This paper deals with design and simulation of such filter types. Simulation models of the inverter-filter systems were made. The simulation results are compared and discussed in the paper. The designed filter will be added to the one-phase low power inverter prototype for photovoltaic application.

Soft-switched Converter for Ultracapacitors

P. Chlebis, **Z. Pfof**, **A. Havel**, **and P. Vaculik**
Department of Electronics, Faculty of Electrical Engineering and Computer Science
VŠB — Technical University of Ostrava, 17. Listopadu 15, Ostrava-Poruba 70833, Czech Republic

Abstract— Paper describes application of zero-voltage soft-switching for converter for ultracapacitor. The main applications of ultracapacitors are notably in energy smoothing and momentary-load devices. The ultracapacitor's efficiency is very high, thus, the converter and ultracapacitor efficiency must be comparable otherwise converter reduce the efficiency of all system. A basic principle of soft-switching using zero-voltage and zero-current switching with power loss comparison between hard and soft switching are shown too.

The idea of using ultracapacitor is offer an alternative source to the batteries and extract higher efficiency from existing power sources. Advantages of ultracapacitor are capable of very fast charges and discharges, large number of cycles without de-gradation (millions or more), extremely low internal resistance or ESR, high efficiency (up to 98%), high capacitance (up to 5 000 farads) and high output power. The ultracapacitor has a many applications, for example for start-up large diesel engines, regenerative breaking in electric/hybrid-electric vehicles or as a back-up power supply for low power systems. For preservation high efficiency is important in order to obtain a high efficiency of converter for ultracapacitor. This can be allowed by soft-switching that also remove a several disadvantages of hard-switching, which can be summarized as switching loss, device stress, EMI problems, etc. Exactly, switching loss is caused by the overlapping of voltage and current waves during each turn-on and turn-off switching. This overlapping creates a large pulse of power loss. Thus, with higher switching frequency, converter loss increases, that is, its efficiency de-crease. Soft-switched converters also provide an effective solution to suppress EMI.

There are two basic types of soft-switching — zero-voltage (ZV) and zero-current (ZC) switching. For achieving zero-voltage or zero-current switching is using a resonant circuit. A resonant circuit is composed from resonant elements L_r and C_r that creates with a semiconductor switch VT so-called a resonant switch. Resonance is allowed to occur for creating zero-voltage or zero-current switching conditions. Both types of soft-switching will be described later in the following subchapter.

Firstly perform a comparison power loss between hard-switching and soft-switching, the individual types of soft-switching will follow. The semiconductor switch voltage and current waveforms for hard-switching RL load is shown in Fig. 1(a). Hard-switching RL load is a very common case for power inverters.

There is designed new concept of the converter for ultracapacitor. It will be a few changes. The first change is about converter on the input side. It will be replaced from buck converter to boost converter. Ultracapacitors will have a less capacitance, but higher voltage value. And especially, converters will be replacing by soft-switched converters. The new concept of converter for ultracapacitor is shown in Fig. 2.

The input converter is a soft-witched boost converter. Resonant components are inductor L_1 and capacitor C_1 that creates zero-voltage switching conditions for transistor VT_1. Inductors L_1,

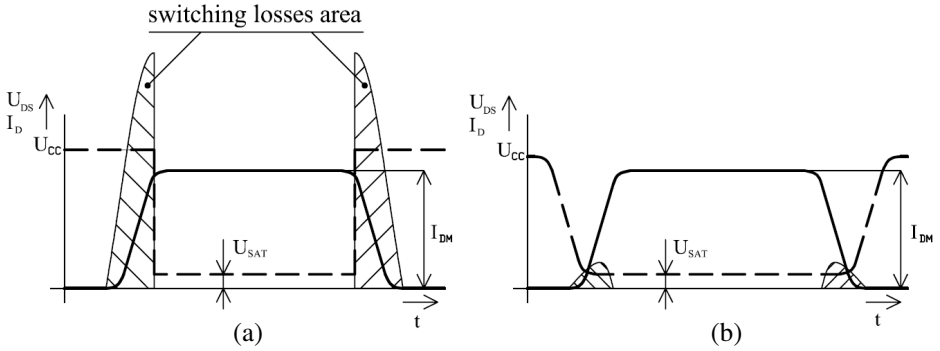

Figure 1: The semiconductor switch voltage and current waveforms: (a) Hard-switching RL load with output diode; (b) Zero-current soft-switching .

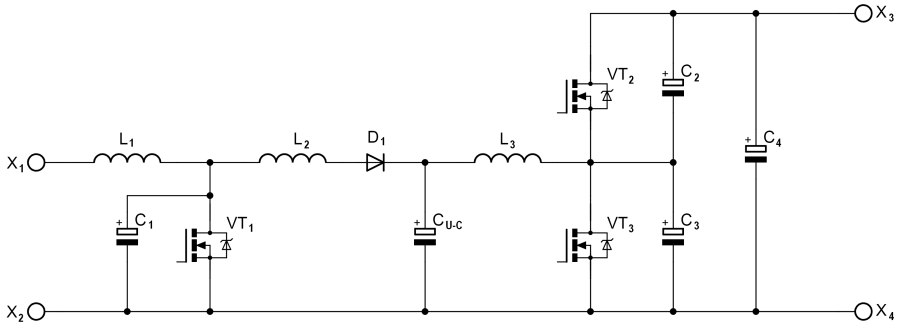

Figure 2: New concept of converter for ultracapacitor.

L_2 are basic components of boost converter. Diode D_1 inhibits the backward power flow from ultracapacitors to the boost converter. C_{U-C} represents the pole of ultracapacitors. The output converter is a soft-witched two-quadrant boost converter. For achieving zero-voltage switching is instrumental inductor L_3 and related capacitor C_2 (or C_3) that is connected in parallel with transistor VT_2 (or VT_3). Both transistors VT_2 and VT_3 must be switched in one period of inductor current. Generation power to the load is controlled by larger pulse ratio for VT_3; VT_2 only sustains the resonant cycle.

For regeneration power from the load, VT_2 has a larger pulse ratio; VT_3 only sustains the resonant cycle. For stabilization output voltage is connected capacitor C_4.

Applications of Resonant and Soft Switching Converters

V. Sladecek, P. Palacky, T. Pavelek, and P. Hudecek
Department of Electronics, Faculty of Electrical Engineering and Computer Science
VŠB-Technical University of Ostrava, 17, listopadu 15, Ostrava-Poruba 70833, Czech Republic

Abstract— High frequency operations of PWM converters allow reduction of the size and weight of their magnetic components. However, at high switching frequency, switching losses and EMI emissions become significant and must be reduced.

Traditional high frequency switch-mode supplies, which rely on generating an AC waveform have used power transistors to "hard-switch" the unregulated input voltage at this rate. This means that a transistor turning on will have the whole raw input voltage, across it as it changes state. During the actual switching interval (less than 50 microseconds) there is a finite period as the transistor begins to conduct where the voltage begins to fall at the same time as current begins to flow. This simultaneous presence of voltage across the transistor and current through it means that, during this period, power is being dissipated within the device. A similar event occurs as the transistor turns off, with the full current flowing through it.

More recently, new power conversion topologies have been developed which dramatically reduce the power dissipated by the main power transistors during the switching interval.

The most common technique employed has been a constant frequency resonant switching scheme, which ensures that the actual energy being dissipated by the active device is reduced to nearly zero.

This method, commonly called is "Zero Voltage Switching" (ZVS), "Zero Current Switching" or "Soft Switching".

These converters use the LC resonance circuit. When using resonant circuits to reduce switching losses, by resonant inductance connected or disconnected from the resonant circuit at zero current passing through this inductance, or that connects or disconnects the resonance capacity at zero voltage.

Leader in this area are quasiresonant converters, which use the properties of resonant LC circuit, only in moments of commutation switches. Reduction in the steepness of the starting and trailing edge of the output voltage when using resonant inverter also has a favorable influence on the electromagnetic interference.

This paper presents the possibility of using soft switching with semiconductor converters for power electronics and electric drives.

Space Vector Control for Quasi-resonant DC Link Inverter

Tomas Pavelek, **Petr Palacky**, **Vaclav Sladecek**, **and Petr Hudecek**
Department of Electronics, Faculty of Electrical Engineering and Computer Science
VŠB-Technical University of Ostrava, 17. Listopadu 15, Ostrava-Poruba 70833, Czech Republic

Abstract— There are summarized results of research of the quasi-resonant voltage type converter in this paper. Results show that the given type of the quasi-resonant converter is a good adept for vector pulse width modulation. The control part is based on the digital signal processor TMS320Cxx line by Texas Instruments, as for direct control of the voltage DC link as for vector pulse width modulation control algorithm too.

A new three-phase voltage source soft switching inverter consists of quasi-resonant DC link with high frequency transformer and conventional three-phase inverter.

High switching frequency of modern power converters leads to increased share of switching losses in total losses of converters. Reduction of the switching losses can be achieved by zero voltage switching or zero current switching. Theses techniques utilize resonant features of LC circuit, which is included in the power part of a converter. Converters, which allow soft switching, are called resonant converters. There exists a special group of converters, so-called quasi-resonant. Resonant circuit of a voltage source inverter with quasi-resonant DC-link is active in the instant of power switches commutation only. For realisation of vector modulation it is needful to use a high performance microcontroller, which provides sufficient computing power. The vector modulation is implemented into digital signal processor TMS320LF2407 powered by Texas Instruments.

To verify correctness of used algorithm it was realized simple measuring workplace, its each component are a quasi-resonant converter, asynchronous motor and control kit with digital signal processor.

It the paper it is presented two experimental results, which show correct operation of the converter and vector modulator.

The work was focused to be the base for realisation of vector control of voltage source inverter with quasi-resonant DC-link and the results to bring some improvement in the field of electrical drives and power electronics. In the future we will deal with measurement on the converter and its optimisation.

Strategy of the Depollution in the Low Voltage Electric Installations Using Artificial Neuron Network

Hosni Bedoui
Laboratory of Electronic and Microelectronic, LR/UR/USCR: LAB IT 06
University of Monastir, Tunisia

Abstract— In this paper we present a strategy of identification and control of a parallel active filter (PAV) used in the electric network depollution. The proposed structure for the filter is achived on the basis of an inverter of which the considered control law permits to inject the harmonic currents that are in opposition of phase with those existing in the electric energy distribution network. In this setting we developed a strategy of control using the neurons networks to estimate references currents from real measures of currents and voltages in term of its good suitability to the fluctuations of the harmonic disturbance of the electric network. It permitted to bring a good improvement in relation to the commonly used in conventional systems. The works of simulation illustrated performances of the adopted method and its suitability to the fluctuations of the harmonic perturbations.

Optimized Dual Randomized PWM Technique for Full Bridge DC-DC Converter

A. Boudouda[1], **N. Boudjerda**[1], **B. Nekhoul**[1], **K. El Khamlichi Drissi**[2], **and K. Kerroum**[2]

[1]LAMEL, University M. S. Ben Yahia Jijel, Algeria
[2]LASMEA, University Blaise Pascal, Clermont Ferrand, France

Abstract— Nowadays, much of the electrical energy is consumed through static converters; they adjust this energy to the desired form. The PWM technique allows the control of the useful component of the output voltage and eliminates some unwanted harmonics [1]. It is required for power converters to provide the desired electrical functionality and to meet international standards of Electro-Magnetic Compatibility (EMC) by reducing conducted and radiated emissions [2]. In order to better meet the EMC standards for conducted disturbances, we can use the filtering technique (passive and/or active power filters). Furthermore, RPWM technique is one of the most effective and least-cost solutions: it allows spreading the power spectrum over a wide frequency range while significantly reducing its amplitude without any additional hardware.

This paper deals with the control of the full bridge dc-dc voltage converter by the RPWM technique. We propose a scheme based on a triangular carrier having two randomized parameters: the period T and the peak position βT (Fig.1). First, we give the modulating principle, and then the voltage analysis based on Power Spectral Density (PSD) shows the advantage from the point of view of Electro-Magnetic Compatibility (EMC) of this scheme compared to conventional RPWM schemes with only one randomized parameter such as the RCFM "Randomized Carrier Frequency Modulation". Moreover, this analysis reveals an optimal value of the variation interval

R_T	Optimal R_β (Trust region)	Optimal R_β (Simplex)
0.2	1.1755	1.1748
0.3	1.1791	1.1782

Table 1: Optimal values of R_β.

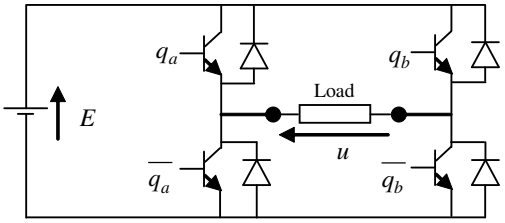

Figure 1: Full bridge DC-DC voltage.

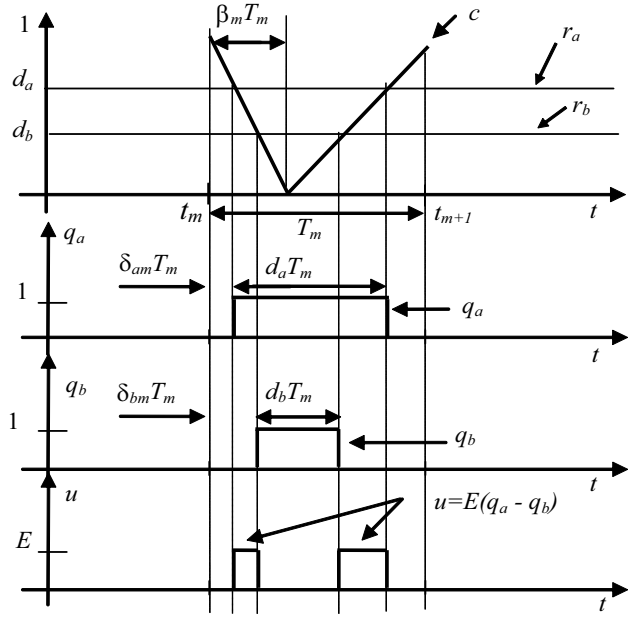

Figure 2: Modulating principle.

of parameter β (randomness level) for a maximum spread of the PSD. Once the optimization problem modeled, the resolution is performed using two powerful methods: trust region method and simplex algorithm. In Fig.1 and Fig.2, we present the converter and the modulating principle. The PSD shape of Fig.3 shows that the dual randomized scheme (RCFM-RPPM) adds a significant spread to the PSD compared to the simple scheme (RCFM). This spread is also accompanied by a decrease in peaks. Nevertheless, a significant increase of the randomness level R_β (Fig. 3) causes an increase in the peak around F_s ($F_s = 3\,\text{kHz}$: Average frequency modulation) and a decrease in the peak around $2F_s$. Our purpose is to spread best the PSD and to reduce its peaks (in order to meet EMC standards), a compromise between the two peaks of the PSD (at F_s and $2F_s$) is achieved with an optimal value of R_β using two nonlinear methods: Trust Region method and Simplex algorithm.

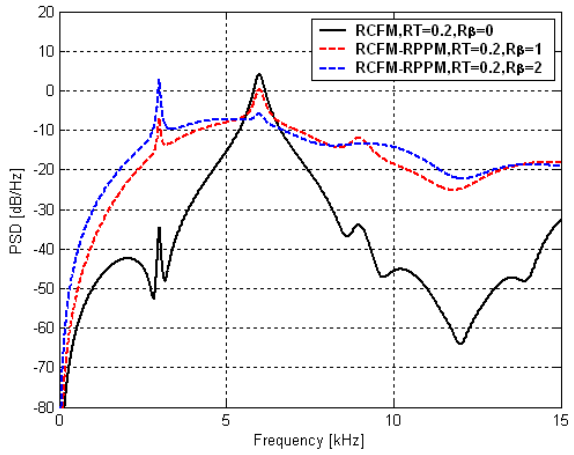

Figure 3: PSD for $R_T = 0.2$ and ($R_\beta = 0$, 1 and 2).

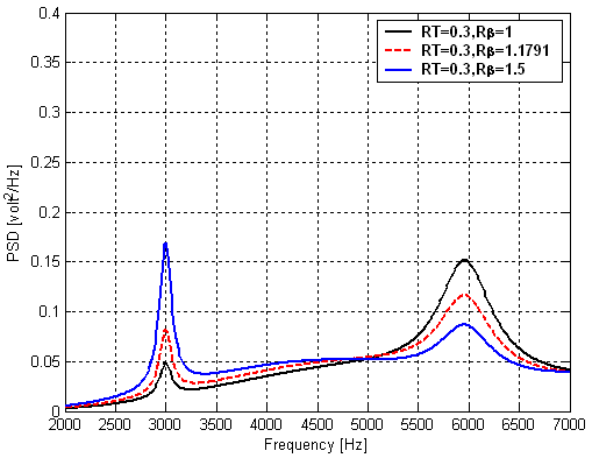

Figure 4: PSD in v^2/Hz.

REFERENCES

1. Kirlin, R. L., M. M. Bech, and A. M. Trzynadlowski, "Analysis of power and power spectral density in PWM inverters with randomized switching frequency," *IEEE Trans. on Industrial Electron.*, Vol. 49, No. 2, 486–499, April 2002.
2. Boudjerda, N., M. Melit, B. Nekhoul, K. El Khamlichi Drissi, and K. Kerroum, "Reduction of conducted perturbations in DC-DC voltage converters by a dual randomized PWM scheme," *Journal of Communications Software and Systems*, Vol. 5, No. 1, March 2009.

Skin Effect in Squirrel Cage Rotor Bars and Its Consideration in Simulation of Non-steady-state Operation of Induction Machines

Marcel Benecke[1], **Reinhard Doebbelin**[1], **Gerd Griepentrog**[2], **and Andreas Lindemann**[1]

[1]Institute of Electric Power Systems, Otto-von-Guericke-University, Magdeburg, Germany
[2]Siemens AG, Corporate Technology CT T DE, Germany

Abstract— The start-up of three-phase induction machines is often controlled by three-phase AC controllers to achieve a soft start-up avoiding high torque and current values. Especially squirrel-cage motors are affected by high start-up torque values caused by skin effect in the rotor bars. To analyze the characteristics of these machines in non-steady-state operations (e.g., start-up) and in the case of feeding by frequency inverters the consideration of skin effect (deep bar effect) is necessary.

The rotor of such machines is a squirrel cage consisting of a number of bars (N_2) arranged all-over the rotor perimeter and grouted with short circuit rings. The energized three-phase stator windings generate a rotary field to which the squirrel cage is exposed. This magnetic flux of the stator rotary field induces voltages which excite mesh currents in the adjacent rotor bars. Their values and phase angles are determined by the resistance and the leakage inductance of rotor bars and ring segments and also by the rotor slip s. The N_2 "windings" constitute a N_2-phase system which generates a rotor field acting like the field of a three-phase slip-ring rotor. So it is possible to model the rotor as three-phase equivalent winding and to model the whole motor using the well-known T-equivalent circuit.

Resulting from a decrease of rotational speed which is connected with an increase of rotor current frequency the current in rotor bars is cumulatively displaced in radial direction to the air gap. This effect is caused by the slot leakage field in the environment of the bars. Under nominal rating conditions the current in the rotor bar cross-section is homogeneously distributed and the leakage flux lines are shaped like illustrated in Figure 1 (left). It is assumed that the rotor bar is divided into several elements. Combined with the adjacent rotor bars they form connected partial coils. Thus, the in radial direction internally located coil is more closely linked with the leakage field and shows the largest leakage inductance ($L_{\sigma i}$) value compared to the leakage inductance values of the upper coils near the air gap. At increased frequency f_2 of the rotor current i_2 (decreased rotational speed n) the leakage reactance predominates compared to the resistivity and the current concentrates in the upper coils (Figure 1, right). Therefore, the effective conducting cross-section decreases and with it the resistance increases. As a consequence, leakage reactance and resistance values of the rotor depend on the slip.

The analytical method to model this slip-dependent effect is the determination of correction factors for sinusoidal supply and fundamental slot geometry characteristics. Another option

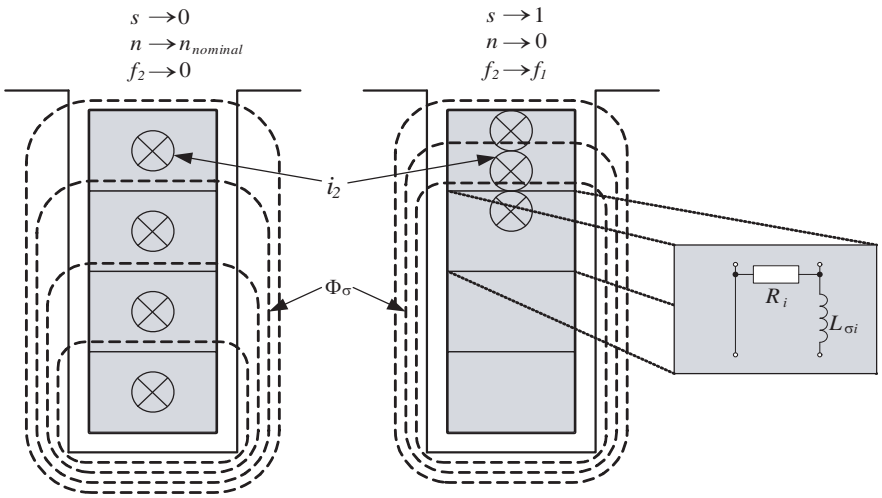

Figure 1: Principle of leakage field distribution in slots of a bar-wound rotor, with s — slip, n — rotational speed, f — electrical frequency (index: 1 — stator, 2 — rotor), i_2 rotor current, Φ_σ — leakage flux.

is modeling of the above defined partial coils as RL-ladder network consisting of a number of elements, each with a resistance R_i and a leakage inductance $L_{\sigma i}$ (see Figure 1, right) and replacing the right side of the T-equivalent circuit by this network. This approach offers the numerical calculation of slip-dependent rotor parameters for more complex rotor bar geometries (e.g., double cage induction machines) and non-sinusoidal feeding of the machine.

The paper presents a method to calculate the slip-dependent rotor current based on the enhanced T-equivalent circuit, wherein the mesh equations are expressed as state-space equations with the state vector representing the partial currents of the ladder elements calculated by means of coefficient matrices consisting of R/L terms. This shall be described in more detail in the full paper. With this state-space model the relevant partial current and with it the entire rotor current can be calculated for known rotor bar parameters. For complex rotor geometries such as double cage rotor profile these parameters can be obtained by approximation of the rotor bar cross-section using rectangle elements and deriving the R_i and $L_{\sigma i}$ values for each element.

The calculation algorithm has been realized in MATLAB-Simulink® by implementation of a specific motor model. An application example for a double cage induction machine shall be given in the full paper. The simulation results demonstrate the advantages of the proposed model in comparison to existing machine models.

Economical Feasibility Study of Large-scale Superconducting Wind Power Generator

Osami Tsukamoto[1] **and Satoshi Fukui**[2]

[1]Office of Industry and Community Liaison Engineering, Yokohama National University, Yokohama, Japan
[2]Graduate School of Science and Technology, Niigata University, Japan

Abstract— Wind power generation is the most practical renewable new energy technologies, such as solar energy, wave energy, and biomass, and is one of the main technologies to reduce CO_2 emission. Reduction of CO_2 emissions recommended by ICPP is in the order of 50–80% by the year of 2050 for environmental sustainability. According to the blue map scenario in the Energy Technology Perspective 2008 of IEA, it is necessary to introduce wind power generation of total capacity 70 GW annually to cut CO_2 emissions by 50% of the present level.

Technology trends of wind power generation show that power generation cost is decreased as the generation capacity increases. Therefore, R&D for scaling-up of a wind power turbine generator is continued. The largest wind turbine generators which ever have been developed using conventional technology with copper coils and iron cores is $5 \sim 6$ MW and it is considered this capacity is reaching limit of the conventional technology, because the head mass (including masses of nacelle, generation system and blades) of wind turbine generators of $5 \sim 6$ MW is as much as ~ 500 t. For scaling-up beyond the capacity limit of the conventional technology, innovation and break-through technologies are necessary. Superconducting technology is one of the most important break-through technologies.

Superconducting coils can produce much higher magnetic fields than conventional copper/iron cores coils and permanent magnets and provide compact and light weight generators. Therefore, superconducting technology can realize large scale, high torque and low rotating generators directly driven by turbine blades without gearboxes. Gearboxes are a dominant drawback of the reliability of conventional wind power generators.

In this study, economical feasibility of 10 MW wind turbine generators using high temperature superconductor (HTS) is investigated by conducting a conceptual design of a 10 MW generator (The key parameters of are listed in Table 1). It was found by the conceptual design that head mass of HTS 10 MW wind power generation system can be comparable with that of conventional 5 MW one. Cost of HTS 10 MW wind power generation system is estimated and found to be much dependent on cost of HTS wire. According to our estimation, an HTS 10 MW wind power generation system can be cost-competitive if the cost of HTS wire of critical current 600 A/cm-width at 10 T and 20 K is \$25/m assuming the cost/capacity scaling of a conventional wind power generator system is \$20 k/kW.

Table 1: Key parameters of the conceptual 10 MW wind power generator.

Type	3-phase synchronous generator
Pole number	8-pole, 12-pole
Output power	10 MW
Rated voltage	3.3 kV (phase-to-phase)
Rated current	1.75 kA (line current)
Rated revolution	10 rpm
Approx. diameter	< 4 m
Effective length	1500 mm

Direct Electromagnetic Torque Control of Induction Motors Powered by High Power PWM Inverters for Two Levels or Three Levels

M. R. Douiri[1], **M. Cherkaoui**[1], **T. Nasser**[2], **and A. Essadki**[3]

[1]Mohammadia School of Engineers (EMI), Morocco
[2]National School of Computer Science and System Analysis (ENSIAS), Morocco
[3]Superior School of Technical Education (ENSET), Morocco

Abstract— This study aims to develop a control strategy for high power induction motor capable of providing, in solicitations binding load torque, electromagnetic torque responses in wide dynamic. Direct torque control will achieve those goals. Indeed, by selecting from a table of switching vectors of the inverter output voltage, it imposes directly the states of power switches based on the electromagnetic state of the motor. Two applications are processed as part of this work. The first concerns the control of an induction motor fed by an inverter 2-voltage levels. The second develops new switching tables for direct torque control of induction motor fed by an inverter 3-voltage levels and structure of NPC. The characteristics of these tables justify the use of such a control strategy for systems implementing high power components such as GTOs. Particular attention is paid to maintaining the balance of the midpoint of the final structure of inverter.

Session 3P9
Poster Session 6

Broad Antireflection Grating by Apodization of One Dimensional Photonic Crystal

A. Mouldi, M. Kanzari, and B. Rezig
Laboratoire de Photovoltaïque et Matériaux Semi-conducteurs, ENIT
BP 37, Le Belvédère, Tunis 1002, Tunisie

Abstract— Dielectric multilayers can usually serve as perfect reflectors, so most researches are performed to broaden the optical band of the total reflexion. In this work, a new examination had been carried out to create a multilayer which acts as an antireflection system. It has been shown that applying an apodization to a one dimensional photonic crystal can significantly enhance the total optical transmission in the structure. The transmission characteristics of the apodized grating are analysed. So, in order to achieve a wideband of total transmission the number of layers, apodization profile and the reference wavelength should be optimized. Apodization was performed to refractive index profile by applying the rule $n(j) = 1 + \exp(\frac{(j-a)^2}{b})$ with j is the layer order, a and b are the parameters defining the apodization profile. The optical thicknesses of layers were taken quarter wavelengths. The spectral range considered in this study is the visible and the near infra-red. From the numerical results performed by the transfer matrix method, it is found that with a dielectric multilayer system of 13 layers we can obtain a large total transmission band (more than 99.95% of the incident light) which covers almost all the visible range (the bandwidth is more than 0.43 µm). In the near infra-red, we can have from this apodized structure a total transmission bandwidth of 1.33 µm with more than 99.95% of the incident light. This result is interesting since we can have with one dimensional photonic crystal with dielectric layers a band structure not only for total reflexion but also for total transmission. The enhancement of optical transmission in this structure is very important since the performance of a number of optical devices could be improved.

Combining Multi-frequency GPR Images and New Algorithm to Determine the Location of Non-linear Objects with Civil Engineering Applications

M. B. Alhasanat[1], W. M. A. Wan Hussin[1], and A. B. A. Hassanat[2]

[1]School of Civil Engineering, University Science Malaysia, P. Pinang, Malaysia
[2]IT Department, Mu'tah University, Mu'tah, Karak, Jordan

Abstract— Recently many researches with the intention to improve GPR images quality that portray best extraction for buried objects representing the real word were carried out. However, it is a well known fact that higher antenna frequencies produce better resolution and quality of GPR images; unfortunately higher antenna frequencies will lead to a lesser penetrating depth of radar wave in the host medium. In the contrary, lower antenna frequencies correspond to higher penetrating depth and lower resolution. Therefore, GPR operators have to use deferent frequencies to ensure getting best results. Thus, interpreters will encounter multiple radar images for the same object. Each radar image resulted from a different frequencies will need separate interpretation. As radar image interpretations were done manually, data redundancy as a result of huge amount of data normally lead to confusion, difficulties and/or perhaps wrong interpretation. This paper proposes a new method of combining all radar images resulted from different frequencies of the same image. The method uses MATLAB software to automatically combine the images. Basic image combination depends on the radar wave depth penetration and resolution. Therefore, each image will be subdivided into horizontal slices 25–100 cm in depth along all image length (depending on the host material, number of images and number of frequency used). Best slices (bands) will then be combined in one image. Bands resulted from high frequencies will automatically be at the top of the final image, and bands resulted from low frequencies will automatically be at the bottom of the image, while remaining bands with medium frequencies in between. Usually 3D model is generated by using only one set of radar images (same frequency). Building 3D models using high frequencies definitely will not show deep buried pipes or cables. The new method will contribute towards getting optimum 3D model, through the use of only one set of radar image of objects under investigation using all frequencies.

A New Algorithm to Estimate the Size of an Underground Utility via Specific Antenna

M. B. Alhasanat and W. M. A. Wan Hussin
School of Civil Engineering, Universiti Sains Malaysia, Engineering Campus, Pulau Pinang, Malaysia

Abstract— Ground penetrating radar is currently one of the most efficient locating tools used for the locating underground utility. Though its ability is to detect metal and non metal buried objects, underground utility sizing is more difficult and there is very little evidence of industrial practice. Images obtained from reflected signals are not photographs of the objects beneath the surface being investigated. GPR cannot determine the exact shape or utility material; consequently the type and purpose of utility is unknown. To know the exact size of buried utility would be a great achievement as size can sometime indicates the type and purpose of utility. In the literatures there are just few studies tried to estimate underground utility size. This paper presents a new algorithm to extract the diameter of buried utility from radar image depending on its hyperbolic shapes. While antenna drag and cross linear object, hyperbola is automatically shaped on the radar image based on travel time of return signal between a buried object and dynamic antenna. Shielded dipole 700 MH and 250 MH antennas with cone has an opening of 90 degree is used in this paper. The pulse transmitted from the antenna has elliptical footprint area underneath; the long axis of elliptical footprint is with the direction of the dragging antenna. However, the algorithm is proved mathematically and the result is an equation with a constant equals to 1.4142136. The algorithm will be applied in an experiment using artificial site filled with dry sand covering known pipes and cables sizes.

The Design of a GPR Test Site for Underground Utilities

W. M. A. Wan Hussin and Mahmoud Bashir Alhasanat
School of Civil Engineering, University Science Malaysia (USM), Engineering Campus
14300 Nibong Tebal, Penang, Malaysia

Abstract— Field-based physical model or laboratory is the best way to improve and better understand data interpretation. In ground penetrating radar, closed laboratory is not suitable due to high clutter that occurs from walls and ceiling. A field model (test site) is therefore the most suitable strategy for actual GPR experiments. Although test site is often costly and not easy to build, it provides significant advantages in GPR data interpretation through the homogeny of host materials, clear interface contrast between buried objects and the host materials, absence of moisture, absence of any potential bodies may reflects unneeded radar waves which lead to clutter, and known sizes and materials of buried objects. To determine the best approach for GPR image reconstruction in the real environment and to compare different inversion techniques, simulation can be applied in a simple and distinct environment (Elena et al., 2009). This paper proposes the design of a test site calibration for GPR The test site of 6 meters in width, 16 meters in length and 4 meters deep is designed to be constructed at Universiti Sains Malaysia Engineering Campus, Pulau Pinang. Different samples of underground utilities are represented as varying buried objects. This paper as well proposes a new algorithm to determine the exact location of small and non-linier objects. Grid method is used to construct a 3D model, but for two scans (line1 and line2) conducted closed enough to non-linear small buried objects, a new algorithm is developed to help locate its exact location and depth.

High Frequency Back Scattering from a Real-scale Aircraft Using SBR and PTD-EEC Method

N. Altın[1] and E. Yazgan[2]

[1]Turkish Aerospace Industries, Inc.
Fethiye Mah., Havacılık Bulvarı No. 17, Kazan Ankara 06980, Türkiye
[2]Electrical & Electronics Engineering Department, Hacettepe University
Beytepe, Ankara 06532, Türkiye

Abstract— Monostatic Radar Cross Section (RCS) of a three dimensional target is calculated Shooting and Bouncing Ray (SBR) method and Physical Theory of Diffraction-Equivalent Edge Current (PTD-EEC) method. The aim of the presented algorithm is modeling of a real-scale aircraft, so the SBR ray tracing method is combined with PTD-EEC method, thus providing fast intersection routines as well as an accurate calculation of the resulting scattered field strengths. The size and complexity of the object is virtually unlimited. Calculated results with SBR and PTD-EEC methods are compared to Physical Optics Method.

Different Scenarios of Uni-layer CPW Bandstop Filters

I. A. I. Al-Naib[1] and O. El Mrabet[2]

[1]Physics Department, Philipps-Universität Marburg, Renthof 5, Marburg 35032, Germany
[2]Electronics and Microwave Group, Faculty of Sciences, Abdelmalek Essaadi University, Morocco

Abstract— Metamaterials have attracted a lot of attention during the last decade owing to theirs exotic properties not found in nature. Different bi-layer metamaterials based on engaging split-ring resonators (SRRs) or its complementary (CSRRs) with coplanar waveguide (CPW) or microstip line have been proposed [1, 2]. CPW technology has many conceptual advantages over the conventional microstrip design such as lower dispersion, easy mounting of lumped elements, as well as insensitivity to substrate thickness. CSRRs have been integrated into the uni-layer CPW to further improve the excitation of the CSRRs [3]. In this conference paper, different scenarios of integrating complementary split ring resonators with coplanar waveguides have been studied. It is shown that there is a best arrangement of etching the resonators where maximum excitation is expected with minimal destructive interference. Fig. 1 shows four different scenarios of CSRRs integrated into a CPW. The CSRRs etched in the grounds and the center conductor for the first and second structure, respectively. However, the CSRRs in the third and fourth structure are moved in y-direction till their centers reach the center of the gaps ($d_y = 4\,\text{mm}$, $d_x = 4\,\text{mm}$) of the CPW and then and in x-direction towards each other ($d_y = 4\,\text{mm}$, $d_x = 0\,\text{mm}$).

As the CSRRs excited better in the second structure compared with the first one, apparent improvement is noticed. However, a tremendous enhancement in the resonance is achieved in the third structure where each resonator is centered along each gap of the CPW. Surprisingly, the fourth structure shows less prominent resonance compared with the third one, but it is still quite good. This is interpreted to a kind of destructive interference between the resonators.

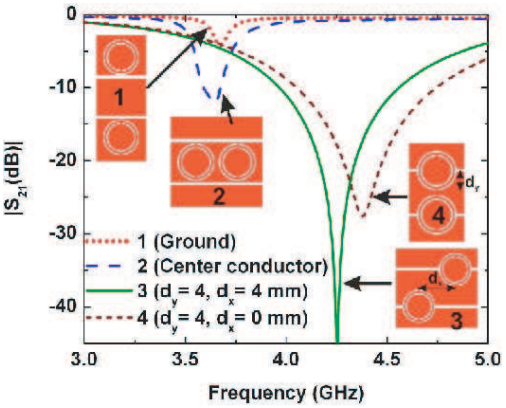

Figure 1: Transmission amplitude of different scenarios of CPW-CSRRs. The substrate of all structures is a lossy FR4 with $\varepsilon_r = 4.4$.

REFERENCES

1. Martin, F., F. Falcone, J. Bonache, R. Marques, and M. Sorolla, "Miniaturized coplanar waveguide stop band filters based on multiple tuned split ring resonators," *IEEE Microwave and Wireless Components Letters*, Vol. 13, 511–513, Dec. 2003.
2. Falcone, F., T. Lopetegi, M. A. G. Laso, J. D. Baena, J. Bonache, M. Beruete, R. Marqués, F. Martín, and M. Sorolla, "Babinet principle applied to the design of metasurfaces and metamaterials," *Phys. Rev. Lett.*, Vol. 93, 197401, Nov. 2004.
3. Ibraheem, I. A. and M. Koch, "Coplanar waveguide metamaterials: The role of bandwidth modifying slots," *Applied Physics Letters*, Vol. 91, 113517, 2007.

Thin Wires Structure for Decoupling of Multiple-antenna Terminals

I. B. Bonev, **O. Franek**, **and G. F. Pedersen**
Antennas, Propagation and Radio Networking Section
Department of Electronic Systems, Faculty of Engineering and Science
Aalborg University, Denmark

Abstract— When having two or more antennas in close proximity some of the electromagnetic energy fed to one of the antenna will be transferred to the other antenna. The latter is unwanted and has to be below a certain level. The effect is called mutual (electromagnetic) coupling and usually for two antennas case it is estimated by the s_{21} of the antenna. In compact devices such as mobile phones, the volume allocated for the antennas is limited and to propose a practically applicable solution to increase the isolation between the antennas is still a challenging task for the antenna designers. The investigation has been carried out through finite difference time domain (FDTD) numerical simulations. The numerical calculations have been performed on the supercomputer Fyrkat at Aalborg University. The use of wire structures close to the antenna radiating elements has been demonstrated to reduce the s_{21} between two PIFAs on a common ground-plane. The PIFAs have been designed to be dual-band covering the LTE 746–786 MHz (low) and the UMTS 1920–2170 MHz (high) bands. The radiating elements have been located closed to each other on the top (or bottom) of the mobile phone. The edge to edge distance between the antennas has been $\lambda/65$ for the low band. Of great interest is to improve the isolation for the low band. Our initial dual band two elements antenna has values for the isolation -3 and -11 dB for the low and high band respectively. A parametric study on the location of the wire structure has been performed in order to get an optimized solution. Further, the radius of the wires and lattice period of the structure has been optimized. For the final solution and the low band, the best achieved isolation has reached a value of -18 dB. A slight improvement in the isolation for the high band has been observed.

Parametric Study of Antenna with Parasitic Element for Improving the Hearing Aids Compatibility of Mobile Phones and the Specific Absorption Rate in the Head

I. B. Bonev, **O. Franek**, **and G. F. Pedersen**
Antennas, Propagation and Radio Networking Section
Department of Electronic Systems, Faculty of Engineering and Science
Aalborg University, Denmark

Abstract— The **R**eactive **N**ear **F**ields (RNF) of the mobile antennas have been an interesting topic among the academia and the industry as their understanding and correct evaluation are of great importance to improve the **H**earing **A**ids **C**ompatibility (HAC) of mobile phone and **S**pecific **A**bsorption **R**ate (SAR) in the head. The current HAC standard suggests the estimation of the RNF to be done in free space. The latter gives some information about the RNF which in many cases can be significantly different than if we have the impact of the user taken into an account. The SAR is evaluated using the **S**pecific **A**nthropometric **M**annequin (SAM) head as the mobile phone is in predefined right cheek position. However, using the **V**isible **H**uman **P**roject (VHP) head phantom, the HAC and SAR has been evaluated for PIFA with a parasitic element attached to the ground-plane. The length, position and orientation of the element on the ground-plane have been optimized in order to get the lowest possible RNF. The investigation has been carried out through finite difference time domain (FDTD) numerical simulations. The numerical calculations have been performed on the supercomputer Fyrkat at Aalborg University. The most important outcome is that the RNF can be significantly reduced when the length of the parasitic element is chosen as it is quarter-length radiator for a frequency which is average of both working frequency bands. Further, the similarity between the HAC and SAR has been discussed as significant guidelines for the antenna design in order to get an optimized HAC and SAR performance have been introduced and developed.

Impact of the Size of the Hearing Aid on the Mobile Phone Near Fields

I. B. Bonev, O. Franek, and G. F. Pedersen
Antennas, Propagation and Radio Networking Section
Department of Electronic Systems, Faculty of Engineering and Science
Aalborg University, Denmark

Abstract— In this paper, we have investigated the influence of the size of the hearing aid on the electric Reactive Near Fields (RNF) for Inverted F Antenna (IFA) and Planar Inverted F Antenna (PIFA) fitting into a mobile phone with candy bar form factor. The RNF are the main factor defining the level of interaction between the mobile phones and the hearing aids which up to now has been evaluated through the Hearing Aids Compatibility (HAC) standard in free space. However, in real life situation both the user and the hearing device will change the fields significantly. Different locations of the radiating elements and dimensions of the antennas have been investigated. Behind the ear and in the canal hearing aids have been analyzed. The user's influence has been represented with the use of six different hand phantoms and the Visible Human Project (VHP) phantom head. In the case of in the canal hearing aid, both peak and average electric fields are much higher than when the hearing aid is not present. However, both the hand and the head attenuate the peak electric fields. The opposite trend has been observed for the magnetic fields as the user increases the peak and average values. For both types of hearing aids under investigation, the most important dimension is the thickness of the hearing aid.

Localized EBG Structure with DeCaps for Ultra-wide Suppression of Power Plane Noise

Jong-Hwa Kwon, Sang-Il Kwak, and Dong-Uk Sim
Radio Technology Research Group, Electronics and Telecommunication Research Institute (ETRI)
138 Gajeongno, Yuseong-gu, Daejeon 305-700, Korea

Abstract—

Introduction: The uni-planar electromagnetic bandgap (UC-EBG) structure is well known as a promising solution for suppressing power noise up to the GHz frequency range in high-speed digital systems. However, if a typical UC-EBG were adopted for the power and ground planes, the discontinuous reference plane would most likely degrade the high-speed signals passing over the EBG patterns because of the discontinuities of the etched reference plane. Also, EBG structures have a limitation in terms of the expansion of the lower bandgap frequency due to their physical size. In this study, a localized EBG-patterned board with decoupling capacitors is proposed as a means of both suppressing noise propagation from extremely low frequencies and of minimizing the effects of the discontinuous reference plane. SSN suppression performance of the proposed structure was validated and investigated by measurement.

Test Board Description: Figure 1 shows the proposed PCB board, which had the localized EBG unit cells and DeCaps on the power plane. The unit cells were etched onto the power plane with their corresponding geometrical parameters, $d = 30\,\text{mm}$, $a = 28.5\,\text{mm}$, $g = 1\,\text{mm}$, $l_1 = 6.5\,\text{mm}$, $l_2 = 7.5\,\text{mm}$, $w_1 = 1.5\,\text{mm}$, and $w_2 = 1.5\,\text{mm}$, respectively. The dimensions of the two-layer PCB were $180\,\text{mm}\times180\,\text{mm}$, with a 1.0 mm FR4 ($\varepsilon_r = 4.5$) substrate. The real decoupling capacitor behaves as a series RLC resonant circuit. To suppress SSN at an extremely low frequency, 8 SMT-type DeCaps were positioned around the noise source, Port 1. The values of the parameters of the used DeCap are $C = 100\,\text{nF}$, $L_{ESL} = 0.55\,\text{nH}$, and $R_{ESR} = 0.02\,\Omega$. The three types of test PCBs used to verify the proposed structure's performance were designed and fabricated as follows: (a) reference plane, (b) localized EBG plane, and (c) localized EBG plane with 8 decoupling capacitors around port 1. The four ports were located as follows: P1 (45, 135, 0 mm); P2 (135, 45, 0 mm); P3 (45, 45, 0 mm); and P4 (135, 135, 0 mm). The point of origin was situated in the lower left-hand corner of the PCB, as shown in Fig. 1. These ports were used to evaluate the insertion loss between the ports by measurement.

Results: The SSN suppression property can be confirmed with the insertion loss between the ports in the frequency domain. A vector network analyzer (Agilent 8236B) was used to obtain the measured insertion losses between the ports. Fig. 2 shows the measured insertion loss, i.e., S_{21} for the proposed localized EBG-patterned power planes with DeCaps located near the noise source, Port 1. The insertion losses of the reference board and the localized EBG board without DeCaps are also presented in the figure for comparison.

The stop bandwidth was defined by 'S_{21} lower than $-30\,\text{dB}$' in this study. As shown in Fig. 2, the suppression property of the proposed structure superposes the properties of the EBG planes

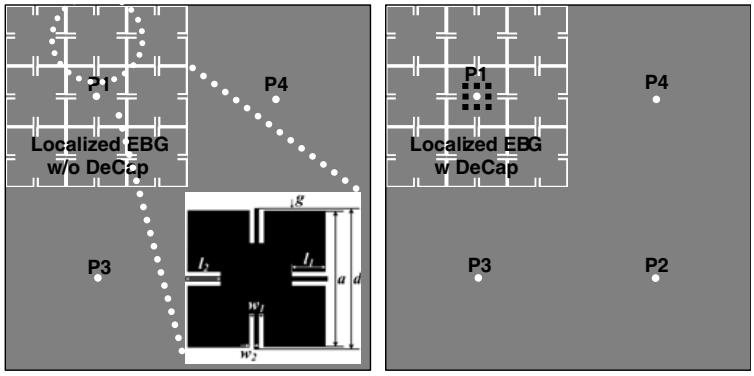

(a) (b)

Figure 1: Test boards: (a) Localized EBG board, (b) Localized EBG with DeCaps on the power plane.

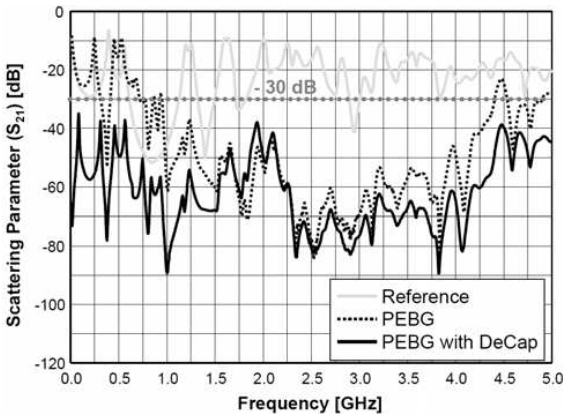

Figure 2: Measured S_{21} of the fabricated test PCB boards.

and DeCaps. That is, the stop bandwidth of the proposed structure is the sum of the stop bands due to both the DeCaps at the lower frequency range and the EBG cells at the higher frequency range; and the average level of suppression within the forbidden bandgap is higher than that of power plane with only the localized EBG unit cells.

In this study, only a portion (25%) of the power plane is used to adopt the EBG unit cells. So, if the solid part of the proposed power plane were used as the return current path for a high-speed signal, the SSN could be sufficiently suppressed and the signal quality improved to a greater extent than the conventional EBG-patterned PDN with fully located unit cells.

Conclusion: In this letter, the localized EBG patterned power plane with decoupling capacitors (DeCaps) located only near the noise source is proposed as a means of both suppressing the noise propagation from DC to several GHz and of minimizing the effect of the discontinuous reference plane. It is seen clearly from measured results that the proposed localized EBG board with DeCaps suppresses sufficiently the propagation of power noise across the entire frequency range from DC to 5 GHz. Furthermore, the remaining solid part of the localized EBG PDN can be used as a stable return current path for high speed signals to minimize the effect of discontinuous EBG-patterned PDN.

Electro-optic and Dielectric Properties of Polymer Stabilized Short Pitch Ferroelectric Liquid Crystal (PSFLC)

A. Daoudi[1,2], **J. Hemine**[3], **R. Douali**[1,4], **M. Petit**[1,2], **and M. Ismaili**[1,5]

[1]Université Lille Nord de France, F-59000 Lille, France
[2]Université du Littoral Côte d'Opale, UDSMM, F-59140 Dunkerque, France
[3]Université Hassan II Mohammedia-Casablanca, LPMC-FSTM, Mohammedia, Morocco
[4]Université du Littoral Côte d'Opale, UDSMM, F-62228 Calais, France
[5]USTL, UDSMM, F-59655 Villeneuve d'Ascq, France

Abstract— We present in this work the effect of the anisotropic polymer network on electric properties of a ferroelectric liquid crystal (FLC) exhibiting a short helical pitch, a large tilt angle and a high spontaneous polarization [1, 2]. The anisotropic polymer network (Figure 1) was elaborated at room temperature within the ferroelectric smectic C phase (SmC*) [3]. Electro-optical and dielectric measurements were performed on a pure FLC material and PSFLC films containing various polymer concentrations. The critical field for unwinding the helical structure of the SmC* phase was measured as a function of polymer concentration. A slight increase of the critical field versus polymer concentration was observed. Dielectric spectroscopy measurements reveal a decrease of the Goldstone-mode dielectric strength with the polymer network density (Figure 2), whereas the relaxation frequency is still not affected by the network. These results demonstrate that the electric properties of the PSFLC studied here are fully controlled by their ferroelectric properties rather than by their twist elastic energy.

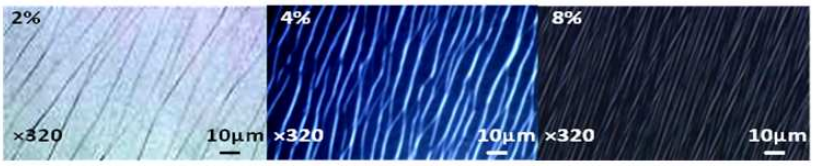

Figure 1: Optical micrographs of PSFLC samples obtained in the isotropic phase ($T = 90°C$) showing the anisotropic structure of the dispersed network with 2%, 4% and 8% polymer concentrations.

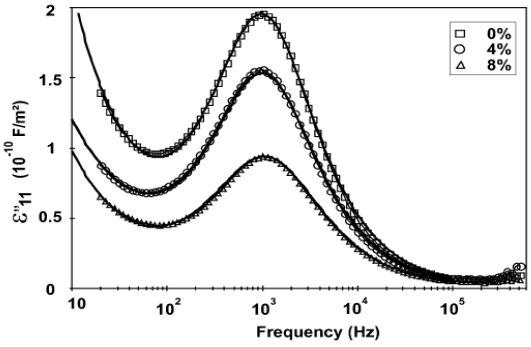

Figure 2: Imaginary part of the dielectric response showing the Goldstone relaxation mechanism obtained on the pure FLC compound and for PSFLCs with two polymer concentrations.

REFERENCES

1. Petit, M., A. Daoudi, M. Ismaili, and J. M. Buisine, *Eur. Phys. J. E*, Vol. 20, 327, 2006.
2. Hikmet, R. A. M., H. M. J. Boots, and M. Michielsen, *Liq. Cryst.*, Vol. 19, 65, 1995.
3. Meyer, R. B., L. Liebert, L. Strzelecki, and P. Keller, *J. Phys. Lett.*, Vol. 36, L69, 1975.

Electromagnetic Field Interaction between Overhead High Voltage Power Transmission Line and Buried Utility Pipeline

K. N. Ramli[1,2], **Raed A. Abd-Alhameed**[1], **H. I. Hraga**[1], **D. T. W. Liang**[1], **and P. S. Excell**[3]

[1]Mobile and Satellite Communications Research Centre, University of Bradford, Bradford BD7 1DP, UK
[2]Faculty of Electrical and Electronic Engineering, Universiti Tun Hussein Onn Malaysia (UTHM)
Parit Raja 86400, Batu Pahat, Johor, Malaysia
[3]Centre for Applied Internet Research, Glyndwr University, Wrexham LL11 2AW, Wales, UK

Abstract— This work presents the development of a new approach of modelling the source excitation and the penetration of structures by continuous propagating electromagnetic (EM) plane waves. The technique incorporates the solution of time-dependent Maxwell's equations and the initial value problem as the structures are illuminated by the plane waves. The propagation of waves from source excitation is simulated by solving a finite-difference Maxwell's equation in the time domain. Finite-difference based on integral formulation [1, 2] has been used in the published literature to improve the accuracy of the finite-difference formulation near the surfaces that does not fit in the lattice or small objects such as thin wires which alter the electromagnetic field distribution significantly. In this case, analytical expressions have been established to express the field near a particular object for precise evaluation of the integrals. Many researchers in the past have been prompted to investigate the subgridding technique as an approach to circumventing the problem [3, 4]. The first advantage of using this method is simple to implement for complicated dielectric or metal structures due to arbitrary electrical parameters can be assigned to each cell on the grid. Second, the entire computational spaces need not to be discretised with a fine grid as it puts unreasonable burden on the computer processing time. The ultimate objective of research in this area is to access the appropriateness of the method in determining the amount of EM penetrating fields between OHTL and underground utility pipeline. The aim of the present work is to develop the general code for solving the electric and magnetic fields within arbitrary metal or dielectric structures, while maintaining a boundary of uncertainty low reflection level in two-dimensional approach.

Figure 1 depicts the cross section and the dimension of a common corridor in which a buried utility pipeline runs parallel to a 132 kV overhead power transmission line. The simulation was carried out using the quasi-static FDTD at the transformed intermediate frequency of 460 kHz and the overall model was then transformed back to the proposed lower frequency of 50 Hz. Sinusoidal wave excitation of 460 kHz ($\lambda = 652.17$ m) was applied at each of the power transmission line cables. The pipeline was separated at a distance of 100 m from the steel lattice suspension towers and buried 2 m beneath the surface of the earth. The soil in the common corridor was designed to be inhomogeneous. The computational region at the coarse grids was discretised at a spatial

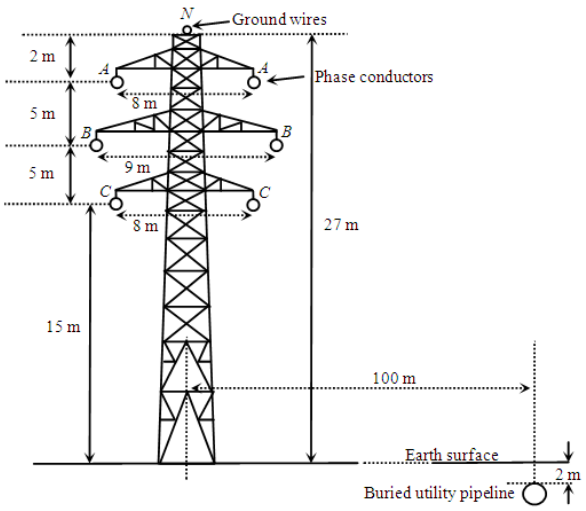

Figure 1: Outline of standard circuit 132 kV steel lattice transmission high voltage suspension towers.

resolution of 2,609 cells per wavelength ($\Delta y = \Delta z = 25\,\text{cm}$). Subgridding involves local mesh refinement in the pipeline and some part of the ground in order to determine the propagation of the waves inside that area while observing the change in the fields. The computational space for the main region was 521 cells × 145 cells (130.25 m × 36.25 m). The computational space for subgrid area was 10 cells × 10 cells. The ratio of the coarse to the fine grids was 4 : 1. Fig. 2 illustrates the electric field distribution in the main FDTD grid. The fields inside the metallic pipeline were found to be zero due to the excess electrons at the surface of the metal preventing any incoming propagating waves from penetrating the pipeline. Some of the waves were reflected back to the surface of the ground thus producing induced EM fields as shown in Fig. 3.

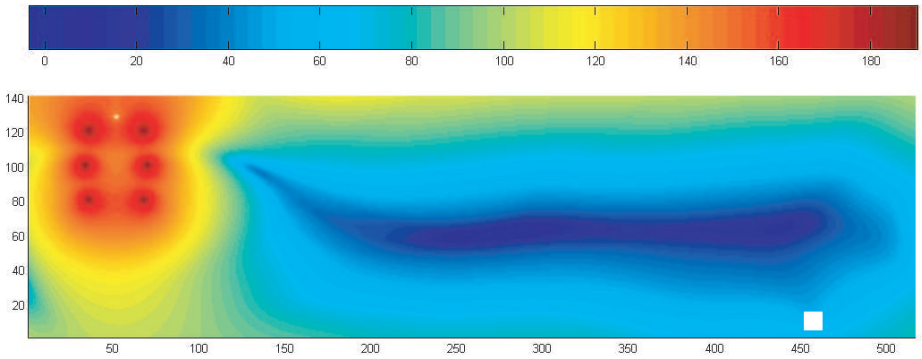

Figure 2: The electric field E_z distribution in the main FDTD grid.

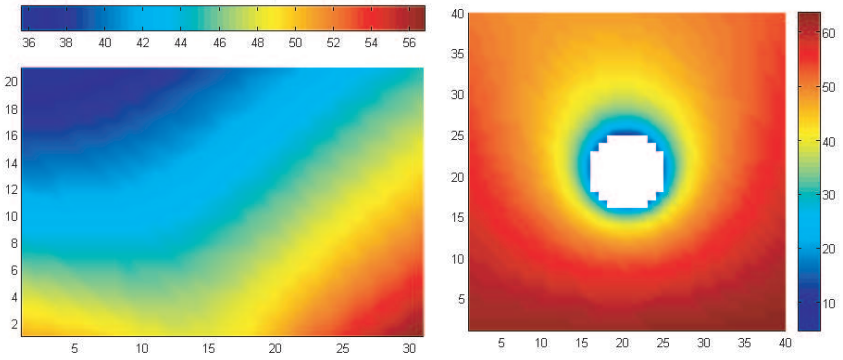

(a) (b)

Figure 3: (a) The induced electric field E_z at 1.75 m above pipeline. (b) The electric field E_{zg} distribution in the subgrid section.

REFERENCES

1. Taflove, A. and S. C. Hagness, *Computational Electrodynamics: The Finite-Difference Time-Domain Method*, 3rd Edition, Artech House, Boston, MA, 2005.
2. Shreim, A. M. and M. F. Hadi, "Integral PML absorbing boundary conditions for the high-order M24 FDTD algorithm," *Progress In Electromagnetics Research*, Vol. 76, 141–152, 2007.
3. Ramli, K. N. and R. A. Abd-Alhameed, "Modelling of complex electromagnetic problems using FDTD subgridding methods," *9th Informatics Workshop for Research Students, University of Bradford, UK*, 200–201, 2008.
4. Wang, S. M., F. L. Teixeira, R. Lee, and J. F. Lee, "Optimization of subgridding schemes for FDTD," *IEEE Microwave and Wireless Components Letters*, Vol. 12, 223–225, 2002.

Optical Properties of Thin Ternary Semiconductor Alloys CdZnTe Prepared by Hot Wall Evaporation Technique

G. E. Hallani[1, 4], **A. Ryah**[1], **N. Hassanain**[1], **M. Loghmarti**[1], **A. Mzerd**[1], **A. Arbaoui**[1], **N. Achargui**[2], **Y. Laaziz**[3], **N. Chahboun**[3], **and E. K. Hlil**[4]

[1]Laboratoire de Physique des Matériaux, Faculté des Sciences, Université Mohammed V-Agdal
4 Av Ibn Battouta, BP 1014, Rabat, Maroc
[2]Département de Physique, Faculté des Sciences et Techniques, Université Cadi Ayyad
Av Abdelkrim ElKhattabi, BP 549, Guéliz, Marrakech, Maroc
[3]Département Systèmes d'Information et de la Communication, ENSA Tanger, Université Abdelmalek ESSAADI, BP 1818, Tanger Principale, Tanger
[4]Institut Néel, CNRS, BP 166, 38062, Grenoble Cedex 9, France

Abstract— $Cd_{1-x}Zn_xTe$ (CZT) thin film fabrication is necessary for its photovoltaic and imaging applications in large scale. In this work, we study polycrystalline CZT witch are prepared on glass substrates by Hot-Wall Evaporation and RF sputtering techniques with different compositions. Optical transmittance, Photoluminescence spectroscopy (PL) and interference fringes are used to investigate optical properties in 320–3500 nm wavelength range at room temperature. As results, high transmittance in higher wavelength region, sharp absorption edge, direct optical transition and homogeneous deposition are highlighted. Refractive index exhibits normal dispersion following Sell Meier formula as well. In addition, electronic structure calculations based on FPLO method are performed and computed energy gap is compared to experimental data.

Session 4A1
Universal Soliton Traits across Different Physical Systems: The Case of Conservative and Dissipative Mechanisms

Synchronization of Weakly Interacting Optical Oscillons

Andrei G. Vladimirov[1], **Dmitry Turaev**[2], **and Sergey Zelik**[3]

[1]Weierstrass Institute for Applied Analysis and Stochastics
Mohrenstr. 39, Berlin 10117, Germany
[2]Imperial College, London, UK
[3]University of Surrey, Guildford, UK

Abstract— Short optical pulses have numerous practical applications including high bit rate communications, optical tomography, spectroscopic measurements, material processing, frequency standards, etc. In relation to their applications for all-optical transmission, storage and processing of information, the problem of interaction of temporal and spatial localized structures of light is of particular importance. Being well separated from one another those structures known also as optical dissipative solitons interact via their exponentially decaying tails. Interference of these tails can produce an oscillating pattern responsible for the formation of soliton bound states. Most of the previous studies on soliton interaction were focused on the case of stationary solitons. On the other hand, it is becoming clear that the soliton itself can exhibit instabilities leading to various dynamical regimes. One of the most important and frequently encountered between them is the Andronov-Hopf bifurcation which leads to undamped pulsations of the soliton's parameters, such as amplitude, width, etc. Such kind of oscillating localized solutions are usually called oscillons. In this presentation we develop a general theory of a weak interaction of two well separated optical oscillons. We derive a set of interaction equations governing slow time evolution of the coordinates and oscillation phases of two interacting oscillons and present the results of numerical simulations of periodically pulsating temporal cavity solitons in the Lugiato-Lefever model. We show that a transition from stationary to oscillation solitons via an Andronov-Hopf bifurcation can lead to a drastic enhancement of their interaction and formation of new types of soliton bound states. Different bound states of oscillons are characterized by different distances between them and oscillation phase difference, i.e., correspond to different oscillon synchronization regimes. An interpretation of the results of numerical simulations based on the analytical analysis of the interaction equations is provided. We have found that a phenomenon of subharmonic synchronization is typically observed in this situation. Furthermore, the effect of a weak periodic external modulation on the interaction of dissipative solitons of the quintic complex Ginzburg-Landau equation has been studied analytically and numerically.

Lightwave Neuromorphic Based Terahertz Pulse Processor

Paul R. Prucnal[1], **Mable P. Fok**[1], **David Rosenbluth**[2], **and Konstantin Kravtsov**[1]

[1]Princeton University, Princeton, New Jersey 08544, USA
[2]Lockheed Martin Advanced Technologies Laboratory, Cherry Hill, New Jersey 08002, USA

Abstract— We proposed and demonstrated a Terahertz pulse processing device using hybrid analog/digital technique based on the combined knowledge of nonlinear optics and biological neurons. This optical device elegantly implements the functionality of an integrate-and-fire neuron using a Ge-doped nonlinear optical fiber and off-the-shelf semiconductor devices. Lightwave neuromorphic technique opens up a wide range of optical processing applications that are scalable, computationally powerful, and have high operation bandwidth. The pulse processing device is built from a small set of basic operations, including delay, weighting, spatial summation, temporal integration, and thresholding. It is configured to perform different functions by adjusting the parameters. (e.g., delays, weights, integration time constant, threshold).

The two key elements in our device are the semiconductor optical amplifier (SOA) based integrator and a Ge-doped nonlinear fiber based thresholder. The exponential recovery behavior of the SOA provides the integration characteristic that a neuron requires. We found an exact correspondence between the equations governing SOA carrier density and the equations governing leaky integration in LIF neuron models. The change in SOA carrier density is converted into pulse intensity through gain sampling. A loop mirror incorporating a short piece of Ge-doped nonlinear fiber is used as the thresholder. It has a cubic transfer function which saturates at high powers, therefore amplitude-discriminates the integrated signal. The optical thresholder removes the undesired weak spikes while equalizing the strong spikes that can be used as a control for a second-stage device.

We demonstrated various important neuronal behaviors based on small-scale lightwave neuromorphic circuits, including the auditory localization algorithm of the barn owl, useful for LIDAR localization. As shown in the illustration in Figure 1(a), the time difference between the signals arriving the owl's left sensor and right sensor is different for object 1 ($t_{1a} - t_{1b}$) and object 2 ($t_{2a} - t_{2b}$), governed by the position of the object. Therefore, by adjusting the weight and delay of the neuron input, it can be configured to respond to a certain object. Figure 1(b) shows the response of the SOA integrator when the two weighted and delayed signals are too far apart. The integrated signal is not strong enough to pass through the thresholder, thus no spike is obtained. As the two inputs are close enough, the threshold is triggered and leads to a spike, as shown in Figure 1(c). This algorithm is useful for LIDAR localization.

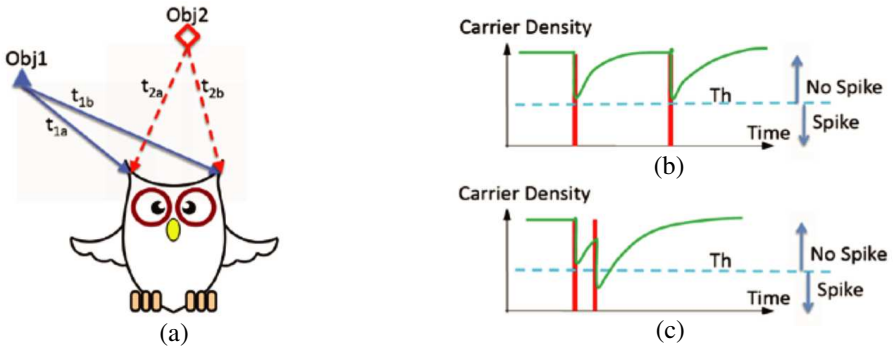

Figure 1: (a) Schematic illustration of the auditory localization algorithm of the barn owl. (b) SOA carrier density — when two signals are far apart (no spike). (c) SOA carrier density — when two signals are close (spike).

Reconstruction of Diffused Images via Seeded Instability

Dmitry V. Dylov[1], **Laura Waller**[2], **and Jason W. Fleischer**[2]

[1]General Electric Global Research Center, USA
[2]Princeton University, USA

Abstract— Pattern-forming instabilities occur in every nonlinear, spatially-extended system [1], including and especially optical ones. Typically, the patterns which result arise from noise. They are therefore random, though boundary conditions and/or other physical processes may determine a characteristic scale size. This scale appears even for a white noise drive, as there is usually a preferred perturbation mode which grows the fastest. For example, in modulation instability, a uniform intensity pattern will break up into an array of solitons, for these are the structures which balance nonlinearity and dispersion/diffraction. On the other hand, an instability which is preferentially seeded can result in an output pattern that is decidedly not random [2]. Here, we take advantage of this fact and use modulation instability to recover images that are diffused beyond recognition.

The experimental setup is show in Fig. 1(a). Light from a 532 nm laser is incident on resolution chart followed by a ground-glass diffuser. A lens then images the resolution chart onto a photorefractive SBN:60 ($Sr_{0.6}Ba_{0.4}Nb_2O_6$) crystal. In this case, the role of the diffuser is to scatter light from the object, so that the chart features are diffused and unrecognizable. The geometry is typical of imaging through a turbid medium, such as clouds or tissue. To give a uniform, rather than speckled, input pattern, the diffuser is rotated a rate (~ 200 Hz) that is much faster than the response time of the crystal (~ 1 s). Fig. 1(b) shows the input image of the resolution chart, without the diffuser in place, while Fig. 1(c) shows the input face with the diffuser added. For the experiments, the intensity is kept constant and the nonlinearity (strength of wave coupling) is controlled by varying an applied voltage bias across the crystalline c-axis of the SBN. Light exiting the nonlinear crystal is then imaged into a CCD camera.

After linear propagation through the crystal (no applied voltage), the output has the same diffuse pattern as the input. As the nonlinearity is increased (Figs. 2(d)–(g)) above a threshold [3–5], a pattern emerges at the exit face. Clearly, nonlinearity can improve the visibility of the signal, reaching an optimal value before too much wave mixing destroys the image. While we have focused on tuning with nonlinearity here, the optimal recovery of the noisy image will depend on many other parameters, such as the modal content of the signal and a matching of feature spatial scales with the correlation length [2]. Digital post-processing techniques will be helpful as well and will be discussed.

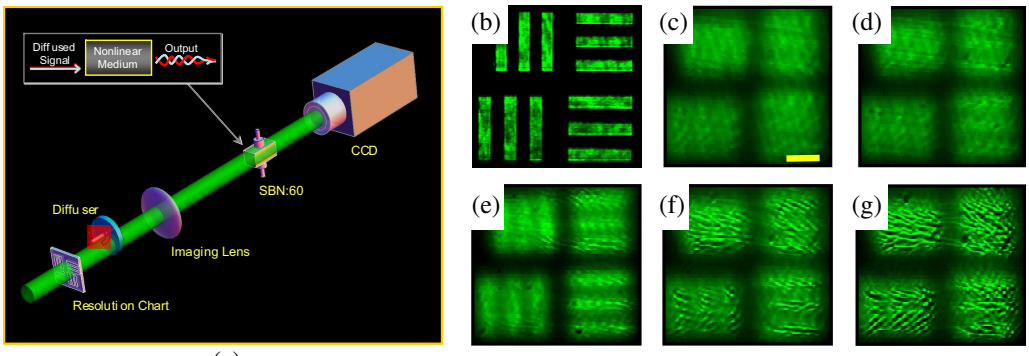

(a)

Figure 1: Reconstruction imaging through seeded instability. (a) Experimental setup. (b) Resolution chart input, without the diffuser in place. (c) Diffused chart input. (d)–(g) Output pictures as nonlinear coupling is increased. Below the nonlinear threshold, the output is the same as (c). Above the nonlinear threshold. ((d): $\delta n = 1.3\times10^{-4}$), intensity modulations form and expose the main features of the chart ((e): $\delta n = 1.7\times10^{-4}$, (f): $\delta n = 2.0\times10^{-4}$, (g): $\delta n = 2.3\times10^{-4}$). Scale bar in (c) is 50 µm.

REFERENCES

1. Cross, M. C. and P. C. Hohenberg, "Pattern formation outside of equilibrium," *Rev. Mod. Phys.*, Vol. 65, 851, 1993.
2. Dylov, D. V. and J. W. Fleischer, "Nonlinear self-filtering of noisy images," *Nature Photonics*, Vol. 4, 323, 2010.
3. Soljacic, M., et al., "Modulation instability of incoherent beams in noninstantaneous nonlinear media," *PRL*, Vol. 84, 467, 2000.
4. Kip, D., et al., "Modulation instability and pattern formation in spatially incoherent light beams," *Science*, Vol. 290, 495, 2000.
5. Chen, Z., J. Klinger, and D. N. Christodoulides, "Induced modulation instability of partially spatially incoherent light with varying perturbation periods," *PRE*, Vol. 66, 066601, 2002.

Cavity Solitons in a Monolithic Vertical-cavity Laser with Saturable Absorber

S. Barbay, **T. Elsass**, **K. Gauthron**, **G. Beaudoin**, **I. Sagnes**, **and R. Kuszelewicz**
Laboratoire de Photonique et de Nanostructures, CNRS-UPR20
Rte de Nozay, Marcoussis 91460, France

Abstract— Cavity solitons are self-localized, dissipative nonlinear optical structures that generally form in a cavity. In laser systems, cavity solitons appear as controllable, self-localized microlasers whose typical size is fixed by the system parameters. They are bistable optical structures that can be switched on and off independently at any transverse location of the cavity. They are interesting for all-optical processing of information since they are robust, manipulable optical structures that can be identified to optical bits of information.

We present recent results on the manipulation and dynamics of cavity solitons in a monolithic, vertical-cavity laser with an intracavity saturable absorber. This is made possible thanks to an original cavity design based on cavity optimization procedures.

In our experiment, the VCSEL is optically pumped over an area of the order of 100 µm. We evidence the presence of bistable, self-localized spots that appear alone or in clusters. These spots can also be switched on and off independently and in sequence by an external perturbation (a pulsed beam) and at a fast rate, up to 80 MHz, thus qualifying them as cavity solitons. Moreover, we have also observed a self-pulsing, self-localized laser structure at different working parameters that we were however not able to control. We also demonstrate the control of the pulsing behavior of a cluster of localized states, showing how irregular, but short, pulses can be triggered on and off by the external optical perturbation. The manipulation of dynamical states pave the way to the observation of pulsed cavity solitons.

Multistability Properties of Localized States in Semiconductor Systems: The Role of Phase Symmetry

S. Barland, **P. Genevet**, **M. Giudici**, **and J. R. Tredicce**
INLN, Universite de Nice Sophia Antipolis
1361 route des lucioles, Valbonne 06560, France

Abstract— Localized structures in dissipative optical systems, also often called cavity solitons, have been observed in several experimental configurations based on semiconductor devices. A commonly expected feature of these systems is the coexistence (for a single parameter set) of multiple states consisting of zero, one, two or more localized structures simultaneously present in the transverse section of the device.

We have explored this phenomenon in two different systems. The first one consists of a semiconductor laser biased below its emission threshold under the injection of a spatially homogeneous (ideally, a plane wave) coherent field. Stationary localized structures appear in this case as bistable and independently addressable light bubbles that form in the vicinity of a modulational instability. Since in this configuration the semiconductor laser acts as a nonlinear optical amplifier, the phase of the field emitted by the device is determined by the phase of the injected field. Therefore, the phase of each localized structure is fixed and this translates into a well defined theoretical framework for the analysis of the stability of each state.

In contrast, the second experimental configuration which we will discuss does have phase symmetry. It consists of two broad area semiconductor lasers coupled in an amplifier/absorber configuration, forming a high Fresnel number optical cavity. Energy is brought into this dissipative system by electrical means only. Under suitable conditions, dissipation of this energy can organize into bistable localized lasing emission. Due to the absence of any phase reference, each of the resulting self-localized microlasers can break the phase symmetry by coherently emitting with a randomly chosen (but fixed) phase.

We discuss the differences between both experimental configurations in terms of the stability properties of solutions consisting of either a single localized structure or a superposition of several of them.

Electromorphing: A Method to Achieve Fast Electro-optical Control of Light Beams through Volume Index of Refraction Patterns

Eugenio DelRe[1, 2], **Jacopo Parravicini**[1, 2], **and Aharon J. Agranat**[3]

[1]Department of Electrical and Information Engineering, University of L'Aquila, L'Aquila 67100, Italy
[2]IPCF-CNR, University of Rome "La Sapienza", Rome 00185, Italy
[3]Applied Physics Department, Hebrew University of Jerusalem, Israel

Abstract— One of the basic goals of photonics is to control light in ever more complex scenarios and at faster speeds. Among the various solutions, the use of three-dimensional optical control systems, that is, optical circuitry integrated in the volume of a solid-state material, truly harnesses the full potential of optical channels. In particular, the miniaturization of an optical network can open the way to the design of devices that expand out from the planar geometry typical of electronics and of traditional integrated optics. The problem with working in the volume is how to fabricate the optical control components in a highly miniaturized design. One basic solution is to use light-induced components. The principal example is self-written waveguides, where a spatial soliton drives itself into the material, guided by the waveguide it is writing. Self-writing, however, serves the sole purpose of forming waveguides. How can other components, such as lenses, splitters, and mode couplers, be formed through spatial solitons? We here discuss how optically induced index-of-refraction patterns based on light-funnels, i.e., patterns that have a three-dimensional footprint typical of a strongly diffracting laser beam, combined with spatial solitons, allows the control of light beams through a large variety of effective components. Furthermore, making use of the quadratic electro-optic effect, we are able to control these components rapidly and morph one component into another simply by changing the bias electric field. Experiments are carried out in photorefractive potassium-lithium-tantalate-niobate (KLTN) where we are able to transform waveguides into lenses, mode-couplers, beam-splitters, and different waveguide arrays, simply by changing an applied electric field. Results indicate a method to spatially control beams with electro-optic speeds for applications that range from imaging and routing, to more pioneering techniques to optically control other physical systems.

From Kerr-cavity to Townes Solitons

D. Gomila[1], **A. Jacobo**[1], **M. A. García-March**[2], **M. A. Matías**[1], **and P. Colet**[1]

[1]IFISC (CSIC-UIB), Campus Universitat Illes Balears, Palma de Mallorca 07122, Spain
[2]Colorado School of Mines, Illinois, USA

Abstract— Conservative and dissipative solitons are in some ways very different: the former are exact solutions of integrable systems, the latter no; conservative solitons appear as one parameter families, dissipative solitons are unique once parameters are fixed, and so on. In some optical systems, however, dissipative solitons are intimately linked to their conservative counterparts. This is the case, for instance, of dissipative solitons in a self-focusing Kerr cavity, also known as Kerr cavity solitons (KCS). A Kerr cavity can be modeled by the Lugiato-Lefever equation (LLE), describing the dynamics of the electric field inside the cavity in the paraxial and mean field approximation. This equation is a prototypical model displaying spontaneous pattern formation. In the limit of large detunings the LLE can be reduced, however, to the conservative nonlinear Schroedinger equation (NLSE). In the LLE, KCS can be formed both in cavities with one and two transverse dimensions. In the 2D case, KCS exhibit a rich variety of dynamical regimes only possible in driven dissipative systems, including oscillations and excitability. In this paper we will show that, as a matter of fact, all this behavior emerge from the properties of the Townes soliton of the conservative 2D NLSE. In particular, in the 2D case, we demonstrate by continuation methods that KCS emerge from the Townes soliton, and that this one sits exactly at a codimension-2 Takens-Bogdanov point. When considering dissipation and driving as unfolding parameters, one can explain the different dynamical regimes observed in the dissipative case, namely, stationary, oscillatory, and excitable cavity solitons, as a consequence of the properties of the cavity solitons in the conservative limit.

Self-lensing and Laser Cavity Solitons

T. Ackemann
SUPA and Department of Physics, University of Strathclyde, Glasgow, Scotland, UK

Abstract— Solitons propagating in conservative systems are stabilized by a compensation of self-lensing and diffraction. In contrast, localized states in dissipative systems are usually understood to result from locking of fronts between coexisting states, being it either the constituent of a hexagonal pattern [1, 2] or island of one homogeneous state emerged in another [3, 4]. A direct connections between the conservative and dissipative case was made apparently only in a few systems [5, 6]. In optics, the archetypical example is a driven nonlinear cavity filed with a Kerr medium, where one can envisage the cavity system to be a folded version of the propagative scheme, leading to the 'soliton-in-a-box' interpretation of the dissipative Kerr soliton [5]. A early treatment in that direction was given in [7], without using the concept of a dissipative soliton explicitly.

Motivated partially by [7], we are studying the suitability and relevance of a 'self-lensing'-picture for solitons in systems with feedback in which a *saturable* nonlinear medium is not filling the cavity. This might be a single-mirror feedback system, in which a thin medium is driven by a laser beam and the retroreflection of the transmitted beam from a plane mirror at a distance d [8], or a vertical-cavity surface-emitting laser (VCSEL), consisting of a few nanometer thin quantum wells as gain medium in a micron long cavity (length L)) [9].

In both cases the size of the emerging soliton can be obtained from a consistency condition between a beam propagation condition and self-lensing. First, the soliton needs to induce a lens with a focal power f such that it is replicated at a size w_0 after propagation through the half cavity $d = L/2$ and back. From Gaussian beam theory, this gives the condition

$$w_0^2 = \frac{d\lambda}{\pi}\sqrt{\frac{1}{g(1-g)}}, \quad \text{with} \quad g := 1 - \frac{d}{2f}. \tag{1}$$

Second, from a Taylor-expansion of the driving field as well as of the resulting refractive index profile [10], the focal lens scales like the square of the size of the driving beam,

$$f \sim w_0^2. \tag{2}$$

The self-consistent size of the soliton is then given by the intersection of Eqs. (1) and (2). The results are in qualitative agreement with experimental observation.

The lensing effect has a local maximum for an intensity in beam center around saturation intensity and is hence only weakly varying with power. Hence, the size of the soliton is mainly determined by the geometrical constraints of the feedback (cavity) setup. It should be noted that the feedback is also responsible for converting the convective instabilities typical for propagative systems to an absolute instability, enabling features like bistability. The driving and dissipative parameters are still responsible for fixing the amplitude and hence the exact width of the soliton, of course. Nevertheless, it is interesting to note that patterns and solitons with a phenomenology very similar to dissipative structures exist in ferrofluids which are not considered to have energy throughput in the stationary state [11].

REFERENCES

1. Firth, W. J. and A. J. Scroggie, *Phys. Rev. Lett.*, Vol. 76, 1623, 1996.
2. Coullet, P., C. Riera, and C. Tresser, *Phys. Rev. Lett.*, Vol. 84, 3069, 2000.
3. Thual, O. and S. Fauve, *J. Phys. France*, Vol. 49, 1829, 1988.
4. Rosanov, N. N., *Spatial Hysteresis and Optical Patterns, Springer Series in Synergetics*, Springer, Berlin, 2002.
5. Firth, W. J. and G. K. Harkness, *Asian J. Phys.*, Vol. 7, 665, 1998.
6. Barashenkov, I. V., N. V. Alexeeva, and E. V. Zemlyanaya, *Phys. Rev. Lett.*, Vol. 89, 104101, 2002.
7. Neubecker, R. and T. Tschudi, *J. Mod. Opt.*, Vol. 41, 885, 1994.
8. B. Schäpers, M. Feldmann, T. Ackemann, and W. Lange, *Phys. Rev. Lett.*, Vol. 85, 748, 2000.
9. Tanguy, Y., T. Ackemann, W. J. Firth, and R. Jäger, *Phys. Rev. Lett.*, Vol. 100, 013907, 2008.
10. Ackemann, T., et al., *Opt. Commun.*, Vol. 147, 411, 1998.
11. Richter, R. and I. V. Barashenkov, *Phys. Rev. Lett.*, Vol. 94, 184503, 2005.

Pyrolitons as a Tool to Induce Waveguides Inside $LiNbO_3$

J. Safioui, **J. Parravicini**, **K. Phan Huy**, **H. Maillotte**, **F. Devaux**, **and M. Chauvet**
Universite de Franche-Comte, France

Abstract— Photorefractive (PR) spatial solitons have been extensively studied during the last twenty years. The most effective way to form such self-trapped beams in PR media consisted in applying a high voltage but our team recently revealed that efficient beam self-trapping can occur in some PR crystals by slightly raising the nonlinear media temperature. This technique relies on a modification of the spontaneous polarization of ferroelectric crystal by pyroelectric effect. Based on this versatile configuration spatial solitons, so-called pyrolitons, have been demonstrated in $LiNbO_3$ crystals [1] using low amplitude uniform temperature increase of crystal as shown in Fig. 1.

This very simple procedure considerably simplifies the formation of self-trapped beams in PR crystals and, as a consequence, offers a straightforward solution to photo-induce low loss waveguide inside bulk ferroelectric crystals such as $LiNbO_3$. In the present work we experimentally study the influence of parameters such as beam polarization, beam power or crystal temperature on beam self-trapping in both congruent and stoechiometric $LiNbO_3$. This experimental work is analyzed with the help of a 3-D numerical model. Optimum conditions to produce useful guiding structures inside $LiNbO_3$ samples are determined.

The technique allows easy formation of multiple waveguides in 3-D memorized inside $LiNbO_3$ which is a key material for photonic applications. Original devices exploiting pyroliton induced structures can thus be foreseen.

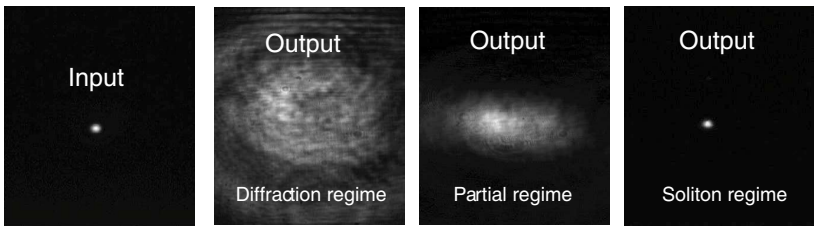

Figure 1: Self-trapping of a 10 µm diameter beam light beam inside a 20 mm long $LiNbO_3$ crystal controlled by a temperature raise of 20°C.

REFERENCES

1. Safioui, J., F. Devaux, and M. Chauvet, "Pyroliton: Pyroelectric spatial soliton," *Opt. Express*, Vol. 17, 2209, 2009.

Spontaneous Motion of Cavity Solitons in Vertical-cavity Lasers with Saturable Absorbers and Their Applications

F. Prati[1], **G. Tissoni**[1], **M. Brambilla**[2], **and K. M. Aghdami**[3]

[1]Dipartimento di Fisica e Matematica, Università dell'Insubria, Via Valleggio 11, Como 22100, Italy
[2]Dipartimento Interateneo di Fisica, Politecnico di Bari, Via Amendola 173, Bari 70123, Italy
[3]Physics Department, Payame Noor University, Mini City, 19569 Tehran, Iran

Abstract— In a vertical cavity semiconductor laser with an intracavity saturable absorber, cavity solitons (CS) behave as localized micro-lasers freely accommodated in the transverse plane, over a zero-intensity, non-lasing background, thus realizing a cavity soliton laser (CSL) [1]. We show that in this system there are parametric conditions for which the CS moves spontaneously in the transverse plane, with a velocity of the order of some μm/ns, depending on the parameters of the system. Key parameters ruling the dynamical instability causing CS motion are the pump and the ratio between the non-radiative decay rates of carriers belonging to the active and passive media.

Interesting effects arise when the pump profile is finite and inhomogeneous and the translational symmetry of the system is broken. For example, for a square pump profile the CS bounces against the boundaries, with a non-Newtonian reflection law. Similarities are found with self-propelled, solitonic structures in hydrodynamics [2]. If the pump has a circular profile, the CS moves along the boundary realizing an optical clock.

We show that a modulation of the pump induce a modulation of the velocity and amplitude of the moving CS and that local injection of suitable pulses can deviate, invert, slow down or trap the CS in its motion, thus exhibiting interesting application-oriented perspectives such as signal delay, reconfiguration, clocking and channeling.

If more than one moving CS are present, repulsive or destructive collisions are observed. Interactions with material defects are also under investigation, giving rise to different dynamical behaviors: depending on the parameters of the system, both attracting and repulsive interactions are found.

REFERENCES

1. Prati, F., G. Tissoni, L. A. Lugiato, K. M. Aghdami, and M. Brambilla, "Spontaneously moving solitons in a cavity soliton laser with circular section," *Eur. Phys. J.*, Vol. 59, 73–79, 2010.
2. Eddi, A., E. Fort, F. Moisy, and Y. Couder, "Unpredictable tunneling of a classical wave-particle association," *Phys. Rev. Lett.*, Vol. 102, 240401, 2009.

Control of Semiconductor Lasers by Optically Induced Photonic Structures in Photorefractives

T. Ackemann[1], **B. Terhalle**[2], **N. Radwell**[1], **P. Rose**[2], **and C. Denz**[2]

[1]SUPA and Department of Physics, University of Strathclyde, Glasgow, Scotland, UK
[2]Institute für Angewandte Physik and Center for Nonlinear Science (CeNoS)
Westfälische Wilhelms-Universität Münster, Münster, Germany

Abstract— Broad-area semiconductor lasers in general and vertical-cavity surface emitting lasers (VCSELs) in particular suffer from poor beam quality and hence a low brightness under high power operation [1, 2]. Although this makes broad-area VCSELs attractive for studies of spontaneous pattern formation, it is of course undesirable for many applications. It was suggested that the existence of photonic band gaps in the linear transmission spectrum of a photonic crystal inserted in an optical cavity can affect the spatial mode pattern and even allow for complete inhibition of the off-axis emission [3]. [3] assumes that the whole transverse plane (i.e., the plane orthogonal to the cavity axis) is filled with a homogeneous photonic crystal creating a stop-band for undesired transverse wavevectors. However, the integration of photonic crystal and gain structures in a monolithic semiconductor device is difficult, not the least because the photonic crystal induces optical and recombination losses. As a consequence, demonstrated photonic crystal VCSELs lase only in defects of the lattice.

In this contribution, we review a realization of this principle based on *combining* a standard VCSEL as gain medium with an optically induced photonic structure in a p*hotorefractive* crystal [4]. Due to their features of wavelength-sensitive, highly reconfigurable refractive index patterns which can be induced at very low power levels, photorefractive photonic lattices [5] provide an ideal tool for experimental studies of such effects.

In our experiments, we use VCSEL devices which are similar to the ones described in [2] and add an external cavity containing a 20 mm long photorefractive SBN crystal in which a two-dimensional photonic lattice is induced by interference of two ordinary polarized plane waves. The cavity configuration corresponds to a telescope providing self-imaging feedback and thus preserving the high Fresnel number of the VCSEL. The focal lengths of the lenses are chosen such that the the length scale of the structure in the VCSEL to be controlled (2–3 µm) is mapped to a scale of the order of some tens of µm, which can be conveniently written within the photorefractive crystal. The resulting periodic modulation of the refractive index leads to a photonic bandgap at a tunable transverse wavenumber.

The VCSEL is brought into a biasing condition in which it emits on-axis and off-axis waves (a stripe pattern) simultaneously, if the photorefractive crystal is homogeneous. The on-axis emission can be suppressed by switching on the light-induced photonic structure with the on-axis emission remaining on.

Thus the experiment demonstrates the feasibility of controlling dissipative structures by photonic band-gaps in general, and the benefit of combining semiconductor devices with optically controlled photorefractive structures in particular. Because of the reconfigurability of photorefractive photonic lattices, the suppression can be dynamically controlled by subsequently erasing the lattice using homogeneous white light illumination or by switching to another controlling structure. Further flexibility and control opportunities arise from the polarization anisotropy of the photorefractive nonlinearity [6].

REFERENCES

1. Grabherr, M., et al., *IEEE Photon. Technol. Lett.*, Vol. 10, 1061, 1998.
2. Babushkin, I., et al., *Phys. Rev. Lett.*, Vol. 100, 213901, 2008.
3. Gomila, D., R. Zambrini, and G.-L. Oppo, *Phys. Rev. Lett.*, Vol. 92, 253904, 2004.
4. Terhalle, B., et al., *Appl. Phys. Lett.*, Vol. 93, 151114, 2008.
5. Efremidis, N. K., et al., *Phys. Rev. E*, Vol. 66, 046602, 2002.
6. Terhalle, B., et al., *Appl. Phys. B*, Vol. 86, 399, 2007.

Session 4A2
Optics, Photonic, Nanophotonic and Plasmonics

Multimode Asymmetrical Optical Power Splitter Utilizing Hollow Structured-waveguide

M. Kamil Abd-Rahman[1], **N. Syafiqah Mohamed-Kassim**[1], **A. Annuar Ehsan**[2], **and M. H. M. Yusoff**[1]

[1]Faculty of Applied Sciences, Universiti Teknologi MARA, Shah Alam 40450, Malaysia
[2]Institute of Microengineering and Nanoelectronics, Universiti Kebangsaan Malaysia Bangi, Selangor, Malaysia

Abstract— We report on a multimode asymmetrical Y-junction optical coupler which splits optical power asymmetrically by shifting the output arm from the propagating-axis of the output port. The design of the 1×2 asymmetric coupler utilizes the technique of shifting the axis of the arm of the output port to allow certain portion of the optical power to propagate to the output port. The hollow-structured waveguide can be designed to achieve predetermined splitting ratios at the two output ports for applications in local area networks (LANs), CATV systems, subscriber-network system, optical instrumentations and optical sensors. The device modeling was performed using non-sequential ray tracing technique employing a metal-based hollow waveguide structure. The 3-dimensional optical coupler devices were designed using Auto-CAD software and were then fabricated on (20×20)-mm^2 surface, 5 mm-thick transparent acrylic substrates, where the designs were engraved onto the mold inserts using CNC machine. It was then followed by coating it with 45-nm-thick layer of gold using sputtering technique into the waveguide to enhance the reflectivity of the waveguide. The Y-junction coupler device, without the shift-port resulted symmetrical optical power splitting of 50 : 50 at the two output ports. Three sets of the devices were fabricated with each set having 10 different output splitting ratios. The fabricated waveguide-devices split the output power asymmetrically in the range of 93 to 7% with ± 3% splitting-ratio accuracy at 630 nm-wavelength. The insertion loss at the shift-port has a minimum value of 5.5 to a maximum of 16.38 dB for 0.00 to 0.90-mm shifting of the axis respectively. While the optical excess loss at the shift-port varies from 1.58 to 4.34 dB. The optical loss in the devices might have been contributed from the coupling loss of the input light source and detectors at the input and output ports respectively. Whilst the surface roughness in the waveguide structures would have caused back-scattered loss.

Localized Optical Modes and Enhancement of Some Optical Phenomena in Spiral Media

V. A. Belyakov
Landau Institute for Theoretical Physics, Russian Academy of Sciences
Chernogolovka, Moscow 142432, Russia

Abstract— Common for all spiral media properties of the localized optical modes are presented here using as an example the case of chiral liquid crystals. A brief survey of the recent experimental and theoretical results on the low threshold distributed feedback (DFB) lasing in chiral liquid crystals (CLC) and new original theoretical results on the localized optical modes [1] (edge (EM) [2] and defect (DM) modes [3]) are presented. It is shown that EM and DM not only ensure a low DFB lasing threshold in the photonic LCs but efficiently reveal themselves also in some other optical phenomena. An analytic theory of EM and DM is developed and applied to the DFB lasing in CLC. The properties of the EM and DM are investigated. The dispersion equations for EM and DM are found, analysed, solved analytically for some limiting cases, and solved numerically for the typical values of the related parameters. The expressions determining the decay rate for these modes are presented. Lasing thresholds at the frequencies corresponding to the spatially localized EM and DM in a CLC layer occur to be much lower than the ones for conventional lasing. The options for a further reduction of the lasing thresholds connected with the pumping at the EM and DM frequencies are predicted (and partially experimentally observed [4]). It is demonstrated that the analytic approach applied to the DFB lasing allows to reveal some qualitative effects escaped from the researchers employing the numerical methods and to predict new options for a low threshold lasing. Namely, the effect of anomalously strong absorption at the DM frequency, a direct analogue of the corresponding effect at the EM frequency [5, 6], is predicted [3]. It is shown also that the localized EM and DM reveal themselves in an enhancement of some inelastic and nonlinear optical processes in photonic LCs. As examples the corresponding experimentally observed effects for the enhancement of nonlinear optical second harmonic generation [7] and lowering of the lasing threshold [4] in photonic LCs are presented. New options for the EM and DM application to the lasing in CLCs and other spiral media are discussed.

ACKNOWLEDGMENT

This work is supported by the RFBR grants 09-02-90417-Ukr_f_a and 10-02-92103-Jpf_a.

REFERENCES

1. Kopp, I., Z.-Q. Zhang, and A. Z. Genack, *Prog. Quant. Electron.*, Vol. 27, No. 6, 369, 2003.
2. Belyakov, V. A. and S. V. Semenov, *JETP*, Vol. 109, 687, 2009.
3. Belyakov, V. A., *MCLC*, Vol. 494, 127, 2008.
4. Matsuhisa, Y., Y. Huang, Y. Zhou, et al., *Appl. Phys. Lett.*, Vol. 90, 091114, 2007.
5. Belyakov, V. A., A. A. Gevorgian, O. S. Eritsian, and N. V. Shipov, *Zhurn. Tekhn. Fiz.*, Vol. 57, 1418, 1987.
6. Belyakov, V. A., A. A. Gevorgian, O. S. Eritsian, and N. V. Shipov, *Sov. Phys. Technical Physics*, Vol. 32, No. 7, 843–845, 1987 (English Translation).
7. Shin, K., H. Hoshi, D. Chang, K. Ishikawa, and H. Takezoe, *Optics Lett.*, Vol. 27, 128, 2002.

Photonic Crystal Based on CdSe Nanoparticles Embedded in a Glass Matrix

A. Labbani and A. Benghalia
Laboratoire Hyperfréquences et Semi-conducteurs, Faculté des Sciences de l'ingénieur
Université Mentouri Constantine, Route d'Ain El Bey Constantine 25000, Algérie

Abstract— We present the evolution of the permittivity of glass containing CdSe nanoparticles with various volume fractions f. The presence of the nano-objets in the host matrix permits to obtain a new composite material with tunable optical properties which can be described by Maxwell-Garnett theory. We have demonstrated the appearance of photonic band gaps in one dimensional photonic crystal based on nanocomposite of CdSe and glass (Figures 1 and 2). The hexagonal and square lattices in 2D photonic structures of circular air rods covered with CdSe shell layer in silica matrix are investigated. Changes in different structure parameters, such as the volume fraction and the cross sectional radius of the air rods, can affect photonic band gap properties as location, number and with. Considered effects provide new possibilities for manufacturing photonic crystals with desired optical properties.

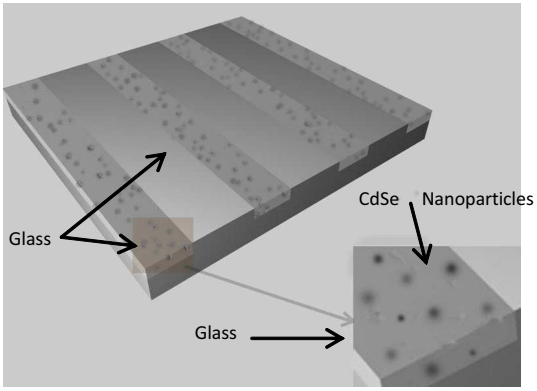

Figure 1: Bragg Mirror (CdSe+glass)/glass.

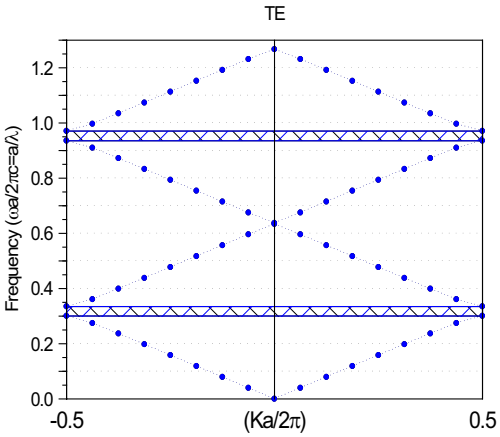

Figure 2: Photonic band structure of the 1D Bragg mirror (CdSe+glass)/glass for $f = 0.25$.

Kinetic Trapping of a Single Particle, Multiple Particles and Particle Aggregations in an Optical Vortex

Baile Zhang[1, 2] **and George Barbastathis**[1, 2]

[1]Singapore-MIT Alliance for Research and Technology (SMART) Centre, Singapore 117543, Singapore
[2]Department of Mechanical Engineering, Massachusetts Institute of Technology
Cambridge, MA 02139, USA

Abstract— Optical forces from laser beams might be the most suitable tools for manipulating, analyzing and organizing mesoscopic objects. For example, optical tweezers have already been widely used in cooling and trapping of atoms and operating DNA molecules. Optical vortices with helical phase front have recently attracted a lot of attention because they can not only attract particles but also transfer orbital angular momentum, which might provide the potential solution to the actuators for microelectromechanical systems and mesoscopic pumps for microfluidic systems. The realistic applications require deep understanding of the mechanism behind the interaction between mesoscopic objects and optical vortices. Although there have been a lot of experiments observing and studying the characteristics of an optical vortex, theoretical predictions are much fewer in the literature, especially for the objects with diameters roughly equal to one wavelength — a size range where many useful applications will fall in.

In this paper, we calculate rigorously the optical forces on particles trapped in an optical vortex with helical phase front and demonstrate the kinetics of these particles in three cases. We first consider a single particle in an optical vortex, whose kinetic properties are mainly determined by the optical vortex itself. The influence of the polarization of the optical vortex is discussed. Secondly, the scenario of interacting multiple particles is studied. The interaction among particles disturbs the motion of individual particles, and may even release a particle that was trapped in an optical vortex. Finally, by imposing constrains of fixed distances or elastically deformable distances among multiple particles, we are able to study the kinetics of particle aggregations in an optical vortex. The aggregation's motion and each particle's motion are discussed respectively. This can be used to model a realistic optical motor or a biological cell aggregation.

Evaluating RF Signal Transmission over Radio-on FSO Links Using Aperture Averaging

Chedlia Ben Naila, **Abdelmoula Bekkali**, **Kazuhiko Wakamori**, **and Mitsuji Matsumoto**
Global Information and Telecommunication Studies (GITS/GITI), Waseda University, Tokyo, Japan

Abstract— Atmospheric turbulence-induced intensity fluctuations severely impair Free-Space Optical (FSO) communication systems, affecting the quality of the propagated laser beam. This leads to significant performance degradation. In this paper, to mitigate the turbulence-induced fading, we consider the aperture averaging technique that consists in adopting a receiver lens whose aperture is larger than the correlation length of the intensity fluctuations. Besides, we propose a model based on the multiple subcarrier modulation (MSM) over Intensity Modulation Direct Detection optical link. Being a sum of narrowband signals, the MSM provides greater immunity to intersymbol distortion and higher bandwidth efficiency than the single carrier modulation schemes. In our model, each subcarrier is modulated using M-ary Phase Shift Keying (PSK) scheme that effectively mitigate the signal scintillation and avoid the need for adaptive threshold normally required by optimum On-Off-keying (OOK). We investigate the impact of aperture averaging on the FSO system based on M-ary PSK-MSM scheme across weak-to-strong turbulence regimes taking into consideration the intermodulation distortion term due to the laser diode non-linearity. By using a modified model for the aperture averaging technique, we analytically evaluate the system performance improvement in terms of the average Carrier-to-Noise and Distortion Ratio (CNDR) as well as the average bit error rate (BER). We also show that there is a design tradeoff between the receiver lens aperture and the required CNDR to achieve a given BER. As expected, especially in the strong turbulence regime, the use of the aperture averaging has shown substantial scintillation fade reduction.

Surface Phonon Polariton Wave Excitation in the Polar Crystal: Boundary Conditions

Dmitry Kazantsev[1, 2] **and Elena Kazantseva**[3]

[1]LEB, Friedrich-Alexander-Universität Erlangen-Nürnberg, Erlangen 91058, Germany
[2]Institute for Theoretical and Experimental Physics, 117218, Moscow
[3]Moscow State University of Instrument Engineering and Computer Sciences, Moscow 107996, Russia

Abstract— The excitation of the surface phonon polariton wave by the resonant coherent external radiation on the surface of the polar crystal was considered for 2-dimensional "micro-particles" of arbitrary shape. These "particles" of subwavelength size were formed on the surface of the polar crystal by the openings in the opaque metal mask. In principle, the surface response to the external radiation, and therefore configuration of the electromagnetic field (with its amplitude and phase) over the surface can be satisfactory simulated by integrating of the Green's function from all open points of the crystal surface. The approach is similar to one used for Lippmann-Schwinger integral equation, with the following difference: the surface polariton wave (known to be an eigenfunction for the infinite open surface), with its dispersion law

$$k_{xy}(\omega) = \omega/c\sqrt{\frac{\varepsilon_{lat}(\omega)\varepsilon_{vac}}{\varepsilon_{lat}(\omega)+\varepsilon_{vac}}}$$

is implemented as Green's function instead of spherical wave with its vacuum dispersion law

$$k(\omega) = \omega/c$$

In some lucky cases, the fit of the simulations to the experimental data (surface polariton wave field distribution map) is perfect, with a precision better than a few percent over whole area. The precision of the method depends, in particular, on the boundary conditions in this 2-dimensional task of the surface wave excitation/propagation. The edge of the metal mask acts in this 2D problem as an interface between two electromagnetically heterogeneous media. Contrary to the conventional optics, in which the tailoring of the waves leads to Fresnel-like formulae, the edge of the metal mask is spatially "soft" compared to the wavelength, in the lateral direction, so that amplitude of the reflected wave can often be neglected. Nevertheless, the boundary conditions, as well as the analytical expressions for the Green's function being used must be taken into account in the rigorous solution of the problem.

Numerical Analysis of Novel Asymmetric SNOM Tips

Valeria Lotito[1, 2], **Urs Sennhauser**[1], **and Christian Hafner**[2]

[1]Electronics/Metrology Laboratory, EMPA, Swiss Federal Laboratories for Materials Testing and Research
Ueberlandstrasse 129, CH-8600 Dübendorf, Switzerland
[2]Department of Information Technology and Electrical Engineering, ETH Zurich
Gloriastrasse 35, Zurich 8092, Switzerland

Abstract— Scanning near field optical microscopy (SNOM) is a valuable tool for the investigation of nanostructures today because it combines the potential of scanning probe technology with the power of optical microscopy. The technique is based on the near field interactions between the sample and a probe, which plays a key role in the overall performance of the system.

In the search for optimized tip structures, fully metal-coated probes appear particularly attractive because of their high-volume manufacturability, the greater manufacturing reproducibility and the easier control over their shape. However, the behaviour of such probes is strongly dependent on the input polarization. If the structure is excited with a radially polarized mode, a localized ultrasmall hot spot with peak field amplitude much higher than the one of linearly polarized modes is generated, as opposed to a broad weak two-lobed distribution under a linearly polarized excitation. These properties can be explained in the light of the characteristics of the surface plasmon polaritons (SPPs) excited on the metal surface and converging towards the tip apex, which interfere constructively in case of radial polarization and cancel out due to the opposite charges on the opposite sides of the tip under linearly polarized excitation [1].

Hence, for high resolution applications, a radially polarized excitation is required, which unfortunately imposes the need for a cumbersome procedure, extremely sensitive to misalignments [2]. In order to circumvent this problem, we propose the introduction of intentional asymmetries, properly tailored to get superfocusing effects similar to those observed under radial polarization by using a more easily excitable linearly polarized mode. More specifically, we have carried out a finite element analysis of two different configurations, one consisting of asymmetric corrugations in the metal coating and the other based on an oblique cut close to the tip apex stripping off both the metal coating and the inner core [3]. Strong field localization is observed for the mode linearly polarized along the direction of the asymmetry. This effect results from the interplay of improved coupling mechanisms between the linearly polarized mode and the radially polarized one and between the inner SPP confined at the silica/metal interface and the outer SPP at the metal/air interface. A thorough analysis of the effects of geometric and material parameters has been undertaken, in order to optimize the probe structure in terms of full width at half maximum and peak value of the resulting distribution.

The use of these promising asymmetric structures could entail an impressive simplification in mode injection procedures for high resolution SNOM applications.

REFERENCES

1. Bouhelier, A., J. Renger, M. R. Beversluis, and L. Novotny, *J. Microsc.*, Vol. 210, 220–224, 2003.
2. Tortora, P., E. Descrovi, L. Aeschimann, L. Vaccaro, H. P. Herzig, and R. Dändliker, *Ultramicroscopy*, Vol. 107, 158–165, 2007.
3. Lotito, V., U. Sennhauser, and C. Hafner, *J. Comput. Theor. Nanosci.*, Vol. 7, No. 8, 1596–1609, 2010.

Electromagnetic Design of Solar Collectors

Anthony Centeno, **Fang Xie**, **Jonathan D. Breeze**, **and Neil Alford**
Department of Materials, Imperial College London, London SW7 2AZ, United Kingdom

Abstract— The energy harvesting efficiency of the solar spectrum using conventional semiconductor solar cells is limited to around 30%. This is primarily due to the fact that they function by the generation of free hole-electron pairs and only photons with energy equal to the band gap can be efficiently harvested. If an optical rectenna device was to harvest incident photons by rectification rather than by free carrier generation then there is the possibility of much higher conversion efficiency. To enable this effective solar collection is required where energy is most available in the spectrum. This happens to be in the visible part of the spectrum, which is around 500nm. Noble metals, such as gold and silver, have negative dielectric constants at these frequencies and plasmonic effects dominate. This means that the simple scaling of metal antenna from longer wavelengths is not possible and computational electromagnetic tools need to be employed. A proposed design for a solar rectennar is shown in Fig. 1. The solar collection is accomplished by a planar array consisting of plasmonic nonoparticles whose localised surface plasmon resonance (LSPR) is at the required wavelengths. The nanoparticles are closely coupled to produce a high electric field in the gaps between the resonant elements. Current is induced into silver nanorods placed within the regions of high field. These Nanorods can then act as top electrode in a MIM device. This paper reports on the use of FDTD to prove the principle of our solar collection design. The main difficulty is obtaining an accurate material model for the metal which is accomplished by using a Drude model within the Finite Difference Time Domain algorithm. The effect of nanoparticle shape on the LSPR and the localised electric field is reported. The induced current in the nanowires is also analysed and discussed.

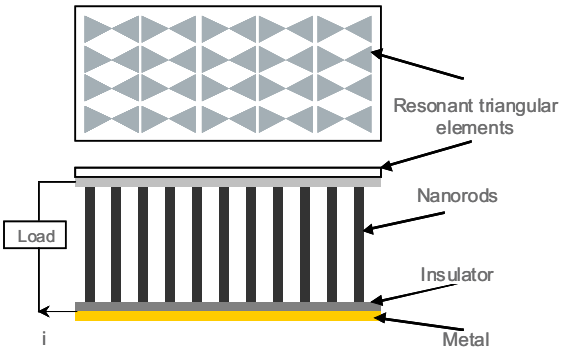

Figure 1: Solar rectenna structure.

Optimizing Geometrically-induced Plasmon-like Waves by Equivalent Circuits

M. Navarro-Cía[1, 2], M. Beruete[1], F. Falcone[1], M. Sorolla[1], and S. A. Maier[2]

[1]Millimeter and Terahertz Waves Laboratory, Universidad Pública de Navarra, Spain
[2]Experimental Solid State Group, Physics Department, Imperial College London, UK

Abstract— The development of surface-plasmon-polariton-based photonics (plasmonics) [1] has allowed overcoming some of the main constraints of classical optics: surface plasmon polaritons have the unique ability of concentrating EM energy in sub-wavelength volumes and propagating EM fields along planar geometries. Thus, it would be desirable to be able to extend the range of plasmonics to those regimes where SPPs do not exist and where the conventional microwaves planar technologies are unavailable, such as THz regime. This has been explored with the so-called spoof-plasmons [2]. However, this approach is still at its infancy and can be benefited by the well-established microwave machinery based on equivalent circuit models and transmission lines concepts.

Under this framework, not only do we revisit the already proposed spoof plasmon geometries [2–4] from the perspective of equivalent circuits and transmission lines [6] but we also take advantage of these powerful tools to optimize them and suggest design parameters to enhance confinement, enlarge the frequency bandwidth of operation [6] and allow truly dual band response [7].

In summary, we apply the formalism of equivalent circuit models and transmission lines to optimize spoof surface plasmon polaritons with enhanced performance such as extreme confinement, broadband behavior and multiband responses.

REFERENCES

1. Maier, S. A., *Plasmonics — Fundamentals and Applications*, Springer, New York, 2007.
2. Pendry, J. B., L. Martín-Moreno, and F. J. García-Vidal, "Mimicking surface plasmons with structured surfaces," *Science*, Vol. 305, 847–848, 2004.
3. García-Vidal, F. J., L. Martín-Moreno, and J. B. Pendry, "Surfaces with holes in them: New plasmonic metamaterials," *J. Opt. A: Pure Appl. Opt.*, Vol. 7, S97–S101, 2005.
4. Lockyear, M. J., A. P. Hibbins, and J. R. Sambles, "Microwave surface-plasmon-like modes on thin metamaterials," *Phys. Rev. Lett.*, Vol. 102, 1–4, 2009.
5. Williams, C. R., S. R. Andrews, S. A. Maier, A. I. Fernández-Domínguez, L. Martín-Moreno, and F. J. Garca-Vidal, "Highly confined guiding of terahertz surface plasmon polaritons on structured metal surfaces," *Nature Photonics*, Vol. 2, 175–179, 2008.
6. Navarro-Cía, M., M. Beruete, S. Agrafiotis, F. Falcone, M. Sorolla, and S. A. Maier, "Broadband spoof plasmons and subwavelength electromagnetic energy confinement on ultrathin metafilms," *Opt. Express*, Vol. 17, 18184–18195, 2009.
7. Navarro-Cía, M., M. Beruete, M. Sorolla and S. A. Maier, "Enhancing the dual band guiding capabilities of coaxial spoof plasmons via use of transmission line concepts," Submitted.

Optical Soliton Perturbation with Time-dependent Coefficients in a Log Law Media

Anjan Biswas
Department of Mathematical Sciences, Delaware State University
1200 N. DuPont Highway, Dover, DE 19901-2277, USA

Abstract— The exact 1-soliton solution to the nonlinear Schrödinger's equation with log law nonlinearity in presence of time-dependent perturbations is obtained. The dispersion and nonlinearity are also taken to be time-dependent. The perturbation terms that are considered are linear attenuation and inter-modal dispersion. The constraint condition between the time-dependent coefficients also fall out as a necessary condition for the solitons to exist.

Session 4A3
Advanced Electromagnetics for Communications in Dissipative Media and Difficult Environments

Channel Estimation in Through-The-Earth Communications with Electrodes

V. Bataller[1], **A. Muñoz**[1], **N. Ayuso**[2], **and J. L. Villarroel**[2]

[1]Advanced Research Laboratories of I3A, Walqa Technological Park, Cuarte, Huesca, Spain
[2]Aragón Institute for Engineering Research (I3A), University of Zaragoza, Zaragoza, Spain

Abstract— Through-The-Earth (TTE) communications has been developed for establishing communication in confined areas as tunnels, mines or caves. Due to the rock conductivity, electromagnetic waves suffer from skin effect attenuation. Because of that, TTE communications works in VLF-LF range. There are two possible medium access solutions: current injection by means of ground electrodes and magnetic induction by means of inductive loops. In current injection a pair of electrodes injects a current into the earth and the receiver electrodes detect a voltage.

One of the main points in the design of a communication system is to know the channel response for a given frequency band. Free space communication channels have been thoroughly characterized for a large range of frequencies. But in the field of TTE communications the work in channel characterization is scant and focused in inductive antennas. In the electrodes case, several studies in the literature offer theoretical formulae that model the communication channel with electrodes. However, they are valid for big electrodes with a large separation between them. This situation is not suitable for TTE communication system where electrode separation is relative small, also its size. Therefore, a method of channel characterization for TTE communications with electrodes has been developed.

A frequency domain method has been selected amongst the different channel characterization techniques found in the literature. A frequency sweep of 40 points between 3 kHz and 150 kHz is applied to the emitter electrodes. Moreover, a reference tone is send together with the corresponding frequency. The sweep tones frequencies are generated applying an IDFT (Inverse Discrete Fourier Transform) in order to assure the orthogonality between the frequencies. The emitter continuously transmits the sweep until the user stop the application, in a circular way. The receptor samples the voltage signal detected by the electrodes and applies the DFT (Discrete Fourier Transform) to the signal captured to recover the frequencies swept. The calculation of the channel is evaluated offline applying the Least Squares algorithm with the frequential samples measured. Furthermore, several solutions have been applied in order to reduce the error in the measurements.

This method has been proved in various experiments for TTE communication with electrodes in surface presenting the results of one of them. The channel response has been obtained for different separation of receiver electrodes and for several distances between emitter and receiver electrodes. As a conclusion of the study, it can be seen that the channel response obtained is nearly flat in amplitude.

Noise Characterization in Through-The-Earth Communications with Electrodes

A. Muñoz[1], **V. Bataller**[1], **N. Ayuso**[2], **P. Molina**[2], **A. Mediano**[2], **J. A. Cuchí**[2], **and J. L. Villarroel**[2]

[1]Advanced Research Laboratories of I3A, Walqa Technological Park, Cuarte, Huesca, Spain
[2]Aragón Institute for Engineering Research (I3A), University of Zaragoza, Zaragoza, Spain

Abstract— Through-The-Earth (TTE) communication systems have been developed in order to allow voice/data communication in confined areas as tunnels, mines or caves. In the design of these systems a correct frequency band selection is of paramount importance, due to the high level of electromagnetic noise found by the receiver. The noise profile depends strongly on the environment. In industrial areas there are a lot of unintentionally generated interferences and, in natural environments, some weak electrical noise can be appreciated caused by nearby electrical farm fences, inverters of broadcast towers, etc. Moreover, several powerful communication systems work in these frequency ranges such as beacons of navigation radio and time synchronization signals. Therefore, noise measurements with electrodes are needed in different situations in order to obtain a good characterization of human generated noise. In this paper the human-generated signals in the VLF-LF band captured with electrodes will be measured. A method of noise measurement captured with ground electrodes is presented in the paper. An analysis both in the frequency and time domains is applied to the data. The Power Spectral Density is calculated for the noise data. Two examples of this process are included in the paper where a noise record is captured for two different locations, at open field an inside a cave, finding the optimal frequency bands for TTE communications in each of them.

Detection of Movement and Impedance Changes behind Surfaces Using Ground Penetrating Radar

Şevket Demirci[1], **Enes Yiğit**[2], **and Caner Özdemir**[1]

[1]Department of Electrical-Electronics Engineering, Mersin University, Mersin, Turkey
[2]Vocational School of Technical Sciences, Mersin University, Mersin, Turkey

Abstract— A common practice for the detection and localization of objects or interfaces beneath the surfaces is the Ground Penetrating Radar (GPR) imaging. Most of the GPR surveys generally concern with the imaging of stationary subsurfaces in which the ultimate goal is to obtain valuable information about the location and the size of the object from the resultant images. On the other hand, recent developments [1] have shown that GPR systems can also successfully detect and image the movement and impedance changes underneath the surface by applying real-time imaging processes and taking different images of the subsurface environment at different time instants.

Thus, to illustrate and further evaluate this capability of GPR, we describe an application of GPR in movement and impedance detection behind surfaces. More specifically, the aim of our ongoing research is to assess whether GPR techniques can be efficiently used to detect the water leaks in buried pipes and the movement or life signs of human being behind walls. For this purpose, a series of GPR experiments have conducted for both A and B-scan configurations:

In the first attempt, the goal was to detect the water leakage of a buried plastic pipe and its location in an outdoor real soil environment. In our recent study [2], it was shown that this task can be accomplished in an ideal case of laboratory sand pool. In this effort, the leak location of a water carrying pipe was found from B-scan GPR images obtained at different time instants for a more realistic situation. A back-projection imaging procedure [3] was applied and reconstructed images for different times were obtained as shown in Fig. 1. The information about the location region of leakage can be deduced from the voids in the images which can be clearly seen as the time evolves.

In the second attempt, it was aimed to find the movement of a person behind the wall with a continuous monitoring of range profiles from consecutive A-scans. A horn antenna, a stepped-frequency continuous wave (SFCW) radar operating at the 3–5 GHz bandwidth and a wall with a thickness of about 30 cm were utilized during the measurements. The "difference signals" between consecutive range profiles were displayed by real-time processing. The resultant radar image is depicted in Fig. 2 which clearly indicates the detection of human movement behind the wall. The results of our efforts to detect heartbeats and life signs will be also be presented.

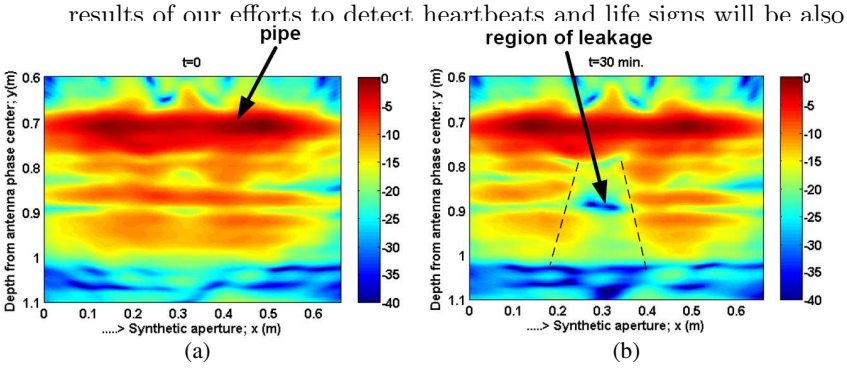

Figure 1: GPR images of water-leak experiment for different times, (a) at $t = 0$, (b) at $t = 30$ min after starting of water leakage.

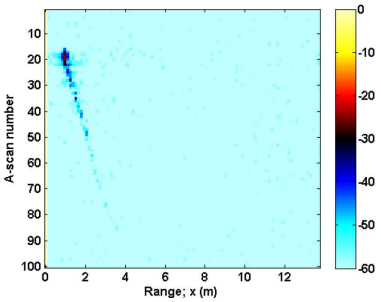

Figure 2: GPR image of a moving person.

REFERENCES

1. Soldovieri, F., R. Solimene, and R. Pierri, "A simple strategy to detect changes in through the wall imaging," *Progress In Electromagnetics Research M*, Vol. 7, 1–13, 2009.
2. Yiğit, E., Ş. Demirci, and C. Özdemir, "On the imaging applications of ground penetrating radar," *URSI Intern. Symp. on Electromagn. Theory*, Berlin, Germany, 2010.
3. Munson, Jr., D. C. and R. L. Visentin, "A signal processing view of strip-mapping synthetic aperture radar," *IEEE Trans. Acoust. Speech Signal Processing*, Vol. 37, No. 12, 2131–2147, Dec. 1989.

Propagation of Random Electromagnetic Beams in Non-Kolmogorov Atmospheric Turbulence

Olga Korotkova[1] **and Elena Shchepakina**[2]

[1]Department of Physics, University of Miami, Florida, USA
[2]Department of Technical Cybernetics, Samara State Aerospace University, Samara, Russia

Abstract— Changes in spectral, coherence and polarization properties in random electromagnetic beams propagating in non-Kolmogorov atmospheric turbulence are predicted on the basis of the unified theory of coherence and polarization of light and the extended Huygens-Fresnel principle. For description of non-Kolmogorov atmosphere we employ a recently developed fractal model for the power spectrum of atmospheric refractive index fluctuations which allows for variation of the fractal dimension and, hence the analysis of various regimes of non-classic atmosphere. The results for classic (Kolmogorov) turbulence can be deduced from our calculations in the special case if the fractal dimension is equal to 11/3. Among the main results that we report are the following: behavior of all the statistical properties of the electromagnetic beams is very sensitive to the fractal dimension of the atmospheric spectrum; the most drastic changes in the statistical properties are found to occur in the case when the fractal dimension takes value of about 3.1, corresponding to altitudes in the interval from 2 to 8 km above the ground; irrespectively of the fractal dimension the spectral and polarization properties of beams reconstruct on propagation at sufficiently large distances from the source, more so along the beam axis, while the coherence gradually degrades, in agreement with results for Kolmogorov atmosphere. Our results are likely to find applications in all areas including electromagnetic beams propagation through the Earth's atmosphere, like lasercom, remote sensing and imaging.

Design and Realization of Mobile Wireless Sensors in Running Water

Daniele Trinchero[1], **Riccardo Stefanelli**[1], **Luca Cisoni**[1], **Mazen Hasna**[2], **Tamer Khattab**[2], **Adnan Abu-Dayya**[3], **and Abdhullah Kadri**[3]

[1]iXem Labs, DELEN, Politecnico di Torino, Italy
[2]Electrical Department, Qatar University, Qatar
[3]Qatar University Wireless and Innovation Center, QUWIC, Qatar

Abstract— In the last years, the chances offered by Wireless Sensor Networks (WSNs) have been widely explored. WSNs have been successfully deployed for numerous applications involving monitoring or assessment of various environmental factors, industrial processes, commercial applications, transport management and service assistance. Wireless sensors are constructed by means of small, integrated, low power devices. Traditionally, they are mainly applied to situations where the wireless channel is not affected by excessive path loss attenuations. Nevertheless, the application of WSNs in dissipative media (mainly, underground) has been recently considered by several authors [1].

In this context, one major field of interest has emerged in the last years, thanks to the application of mobile WSNs (MWSNs) to the monitoring of conduits used to distribute fluids: water, gas or oil. For different purposes: the preservation of the liquid, the identification of possible faults or leakages, the analysis of the quality of the liquid itself. The technology is based on the use of mobile wireless sensors [2], the architecture is typically applied within pipes deployed either underground or under the sea, and the sensors float within the pipelines, transported by the fluid itself.

The architecture is composed by three main tiers: 1) the transmitter, or the detection module, 2) the gateway, and 3) the backend server. The main components of tier 1 are: the acoustic sensor, also known as hydrophone, the microcontroller, the radio frequency part, the antenna, the power supply and the casing. Tier 2 is a gateway that could be used as a relay between tiers 1 and 3 or it can be used to show some basic results. Finally, tier 3 is the main source of information. Also, tier 3 may be used as a historical data server.

This paper shows an efficient and performing configuration for Tier 1, which takes into account all the specifications and the limitations induced by the need to introduce the sensor within the water. Some preliminary results are discussed and performances are consequently analyzed.

REFERENCES

1. Akyildiz, I. F. and E. P. Stuntebeck, "Wireless underground sensor networks: Research challenges," *Ad Hoc Networks*, Vol. 4, 669–686, 2006.
2. Trinchero, D. and R. Stefanelli, "Microwave architectures for wireless mobile monitoring networks inside water distribution conduits," *IEEE Transactions on Microwave Theory and Techniques*, 3298–3306, 2009.

Design and Optimization of Micro-magnetic Antennas for in-Media Transmissions

Luca Cisoni, **Riccardo Stefanelli**, **and Daniele Trinchero**
iXem Labs — DELEN, Politecnico di Torino, Italy

Abstract— The wireless communication channel allows the interconnection of a large number of sensors over huge monitoring areas, without the need of preexisting infrastructures. Consequently, Wireless Sensor Networks (WSNs) offer the possibility to investigate new and distributed fields of application, if compared to isolate sensors or wired sensor networks. WSNs are applied in many technological areas, including environment and habitat monitoring, healthcare applications, home automation, traffic control, industrial automation, industrial production management, logistics, etc [1]. Many researchers are developing studies to analyze the use of WSNs for an increasing number of applications, looking for optimized solutions in terms of power consumption, available bandwidth, sensor dimensions, computational speed, realization costs.

Recently, novel wireless sensor network architectures, suitable to monitor fluids characteristics from inside a conduit, have been proposed in the literature [2]. These techniques require the implementation of a sensor equipped with an electromagnetic front-end able to transmit through a dissipative medium. The sensor itself requires antennas with high transmission efficiency, even if inserted in liquids, in confined spaces, hence with high attention to the reduction of the dimensions.

Due to the physical constraints related to the insertion of the sensor within the pipe, the antenna mounted on board must be as small as possible and should exhibit a low radiation impedance in its near field. Moreover, it has to be omni-directional in its transversal plane. Electromagnetically speaking, it is equivalent to a small magnetic dipole. Electrically small magnetic dipoles exhibit very short dimensions with respect to the wavelength: their perimeter C has to be less than two fifth of the wavelength. The present paper introduces an efficient design procedure that allows an easy and fast definition of the microwave circuit. The procedure is particularly suitable when the antenna is inserted in a complex scenario, with several media in the near field of the radiator.

REFERENCES

1. Raghavendra, C. S., K. M. Sivalingam, and T. Znati, *Wireless Sensor Networks*, Kluwr Academic Press, 2004.
2. Trinchero, D. and R. Stefanelli, "Microwave architectures for wireless mobile monitoring networks inside water distribution conduits," *IEEE Transactions on Microwave Theory and Techniques*, Vol. 57, No. 12, 3298–3306, 2009.

NLOS UWB Undermining Experimental Characterization & Performance Evaluation Using MB-OFDM

M. Ghaddar[1, 2] **and L. Talbi**[1, 2]

[1]University of Quebec in Outaouais, Gatineau, Canada
[2]Underground Communication Research Laboratory (LRCS), Val d'Or, Canada

Abstract— The Federal communications commission (FCC) allocated a large spectral mask from 3.1 GHz to 10.6 GHz for unlicensed use of commercial UWB communication devices. Hence, Ultra-wideband (UWB) technology has shown to be attractive in high-speed data transmissions, and low power communications compared to other wideband wireless systems. Although UWB communications theory has been well documented in the literature; in underground environments UWB propagation is still a relatively new research challenge. To date, only a limited amount of work has been done in confined environments with rough surfaces. Hence, the aim of this paper is to report on the statistical characterization and modeling of UWB propagation channel in an underground mine environment over the frequency range from 3 GHz to 10 GHz. Two kinds of transmission antennas, directional and Omni-directional, were used to investigate the effect of the antenna directivity on the path loss propagation and on the time dispersion parameters in non line-of-sight (NLOS) underground galleries. The measurement and simulation results show that the directional-directional antenna combination yields better radiation efficiency for reducing the time dispersion parameters. Based on channel time domain parameters, and IEEE 802.15.3a working group specifications, an evaluation of Multi-band OFDM (MB-OFDM) based physical (PHY) layer for short-range high data-rate UWB communications is carried out. In this case, results of experimental investigations indicate that the use of Omni-directional antenna configuration renders to be unpractical. In contrast, directional antennas have an efficiency effect to reduce the time dispersion parameters and lead to a better channel capacity.

The Effects of Defects on Magneto-inductive Waveguide

Ye Chen, Praveen Pasupathy, and Dean P. Neikirk
Department of Electrical and Computer Engineering, University of Texas, Austin, TX 78712, USA

Abstract— It has been previously demonstrated that a linear chain (1D array) of inductively coupled L-C resonators behaves as a magneto-inductive (MI) waveguide with a pass-band around the resonance frequency of the individual resonator. We have also examined how such an MI can be used as a distributed sensor in material such as concrete based on changes in the Q of the L-C resonator sub-elements that make up the MI waveguide. In this talk we will summarize ongoing work to understand the behavior of "point" defects in magneto-inductive waveguide. When a defect is present the impedance discontinuity due to a single defect leads to MI wave reflection which introduces small ripples in the pass band. For moderately coupled resonators, the insertion loss in the pass band increases as the defect moves closer to the end of the MI. If a second defect is introduced, we observe the two discontinuities act as a resonant cavity producing much larger ripples in the pass band. Hence, a chain with one intentional defect shows an increase in sensitivity to a second defect compared to a defect-free chain. The peaks appear when the distance between two defects equals an integral multiple of one half a MI-wavelength and the troughs are spaced a quarter MI-wavelength from the peaks. Due to the slow wave nature of propagation in MI waveguides made using L-C resonators the guide wavelength is much less than the free space wavelength, typically roughly a factor of 100 smaller. Based on the relationship between the relative positions of two defects and pass-band ripples, a technique to determine the location of defects has been developed.

Characterization of the Snow Cover Wireless Channel

N. Ayuso[1,2], **A. Muñoz**[1,3], **V. Bataller**[1,3], **J. A. Cuchí**[1,2], **F. Lera**[1,4], **and J. L. Villarroel**[1,2]

[1]Grupo de Tecnologías en Entornos Hostiles (GTE), University of Zaragoza, Zaragoza, Spain
[2]Aragón Institute for Engineering Research (I3A), University of Zaragoza, Zaragoza, Spain
[3]Advanced Research Laboratories of I3A, Walqa Technological Park, Huesca, Spain
[4]Institute of Material Science of Aragón, CSIC-Universidad de Zaragoza, Zaragoza, Spain

Abstract— Snow avalanches claim every year more than 150 lives worldwide, a number that has been increasing over the past few decades. Studies over avalanche reports show that burial time is the main factor which decide if a victim is recovered alive or dead. During the first 15 minutes of burial, the probability of survival is more than 90%, falling to 25% after 45 minutes because of suffocation [1].

Nowadays, there are two devices that allow to recover fully buried victims: the Recco system based on harmonic radar and the avalanche beacons based on a standardized signal at 457 kHz. The latter offers the greatest chance of survival due to members of the affected party can start the search immediately after the accident has occurred. However, current devices are technically limited in range and accuracy, especially at great burial depths. In addition, their usage is complex, particularly in the case of several victims, and intense training is required. Consequently, the search is difficult affecting the chances of a successful rescue.

In recent years, the potential usefulness of GPS based systems in the location of snow avalanche victims has been shown [2, 3]. This type of devices simplifies the search as the GPS receiver of the victim could transmit its position to the rescuer to be used for navigation. Therefore, in the current framework and expected evolution of satellite navigation, GPS positioning and tracking appears promising in avalanche rescue. However further research on GPS based positioning accuracies and data link for ecient communications in this environment is still necessary.

In the present work, the snow cover wireless channel is characterized through COMSOL Multiphysics simulations. The proposed models consider the effects of the water content of the snow, snow layer width, burial depth and composition of the underlying soil in the ISM band. The simulation results show the path loss between an emitter and a receiver within the snow and a receiver on the surface. These outcomes can be applied to the deployment of wireless communications in avalanche rescue operations using current technologies.

REFERENCES

1. Falk, M., M. Brugger, and L. Adler-Kastner, "Avalanche survival chances," *Nature*, Vol. 368, No. 1, 21, 1994.
2. Stepanek, J. and D. W. Claypool, "GPS signal reception under snow cover: A pilot study establishing the potential usefulness of GPS in avalanche search and rescue operations," *Wilderness and Environmental Medicine*, Vol. 8, No. 2, 101–104, 1997.
3. Schleppe, J. B. and G. Lachapelle, "Tracking performance of a HSGPS receiver under avalanche deposited snow," *GPS Solutions*, Vol. 12, No. 1, 1521–1886 (online), January 2008.

Peak to Average Power Ration Reduction in OFDM System Using Constant Envelope for Transmission via PLC Channel

El Ghzaoui Mohammed, **Belkadid Jamal**, **and Ali Benbassou**
Laboratory of Transmission and Data processing, University Sidi Mohammed Ben Abdellah, Fez, Morocco

Abstract— Power line communication (PLC) is a wire line method of communication using the existing electric power transmission and electricity distribution lines. In recent years, in particular since the liberalization of the power and telecommunication markets, Power Line Communications have been the subject of an important research work. At the same time, the growing demand for multimedia communications provides a good prospect for PLC as a promising transmission technique for the "last mile" access network. Orthogonal Frequency Division Multiplexing (OFDM) is a spectrally efficient multicarrier modulation technique for high speed data transmission over multipath fading channels. High Peak-to-Average Power Ratio (PAPR), which leads to power inefficiency in the RF portion of the transmitter, is a major drawback of OFDM. The high PAR of the OFDM signal has to be considered when setting the range of the digital-to-analog converter (DAC) and dimensioning the line-driver. Lots of PAPR reduction techniques are proposed in literatures in last two decades. For instance, amplitude clipping, companding, coding, partial transmit sequence, selected mapping (SLM), interleaving, etc. This paper introduced an improved PAPR reduction scheme using constant envelope modulation. Furthermore, by utilizing continuous phase modulation (CPM) in a CE-OFDM system, the PAPR can be effectively reduced to 0 dB. The CE-OFDM-CPM approach described in this paper is based on the phase modulator transform technique. In essence, the OFDM waveform is used to phase modulate the carrier. The OFDM-PM signal can be viewed as a type of digital FM, whereby the modulating phase signal is a real-valued OFDM baseband waveform. This work is going to open a window to use CE-OFDM-CPM in PLC channel. In this paper, the application of CE-OFDM-CPM in PLC channel is studied. The impact of the electrical appliances and load impedance on the signal transmission is investigated. The paper describes a CE-OFDM based modem for Power Line Communications (PLC) over the low voltage distribution network. Relying on a preliminary characterization of a PLC network, a complete description of the modem is given.

Session 4A4a
Fault Detection, Diagnosis and Tolerant Control

Study of the Impact of Soft Faults on Multiconductor Transmission Lines

Maud Franchet[1], **Nicolas Ravot**[1], **and Odile Picon**[2]

[1]CEA, LIST, Embedded Systems Reliability Laboratory
Point courrier 94, Gif-sur-Yvette cedex 91191, France
[2]Université Paris-Est, ESYCOM, EA2552, 77454 Marne-La-Vallée, France

Abstract— As electronic devices are more and more present and complex, attention has been raised on monitoring the health of their wiring networks. Consider this simple fact: there is a probability of 66% that a wiring defect appears in a plane of more than 20 years [1]. This makes more obvious the need of developing efficient methods of detection, all the more than their consequences can be costly and even tragic.

One method commonly used is called Reflectometry [1]. It is based on the injection of a probe signal into the wiring network and the analysis of the reflected ones measured at the injection point. This works well for severe faults (open or short circuits). However industrials are more and more interested in detecting degradations as soon as possible (soft faults) in order to limit costs and make some prognostic.Unfortunately, no method seems to be efficient enough for detecting faults at their early age in bundles [2]. Although the use of time frequency tools in the case of one single coaxial line (Wavelet transform in [3], Wigner Ville transform in [4]) show some improvement, a better understanding of the effects of soft faults (such a necessity has also been raised in [5]) on the electrical parameters (RLCG) of multiconductor transmission lines (MTL) and on Reflectometry signals is of crucial need in order to develop systematic and efficient methods. This is the purpose of our article.

An analytical study is feasible only in simple cases (e.g., under the weak coupling assumption [6]). In order to study more intricate and realistic structures (such as bundles), simulation tools and experimental data are needed. Here CST MWs and a Laplace code are used. Two kinds of soft faults are considered (when only the dielectric coating is damaged, when the dielectric and the conductor are both degraded). Their consequences on RLCG parameters and on all the voltages measured at the entrance of a bundle of coated wires are examined (2 structures are considered: MTL_2 and MTL_6 where 2 and 6 are the number of wires in the bundle which is over a ground plane).

REFERENCES

1. Furse, C. and R. Haupt, "Down to the wire: The hidden hazard of aging aircraft wiring," *IEEE Spectrum*, Vol. 38, No. 2, 35–39, February 2001.
2. Griffiths, L. A., R. Parakh, C. Furse, and B. Baker, "The invisible fray: A critical analysis of the use of reflectometry for fray location," *IEEE Sensors Journal*, Vol. 6, No. 3, 697–706, June 2006.
3. Buccella, C., M. Feliziani, and G. Manzi, "Accurate detection of low entity cable faults by wavelet transform," *International Symposium on Electromagnetic Compatibility: EMC*, 936–941, Santa Clara, Cuba, August 9–13, 2004.
4. Kwak, K. S., T. S. Yoon, and J. B. Park, "Load impedance measurement on a coaxial cable via time-frequency domain reflectometry," *SICE-ICASE, 2006, International Joint Conference*, 2006.
5. Wheeler, K. R., D. A. Timucin, I. X. Twombly, K. F. Goebel, K. F. Wysocki, and P. F. Wysocki, "Aging aircraft wiring fault detection survey," NASA Ames Research Center, 2007.
6. Franchet, M., M. Olivas, N. Ravot, and L. Sommervogel, "Modelling the effect of a defect on crosstalk signals under the weak coupling assumption," *PIERS Proceedings*, 119–123, Xi'an, China, March 22–26, 2010.

The Influence of Laminate DK Tolerances on Microstrip Butler Matrix Performance

Mateusz Mazur[1, 2]

[1]Telemobile Electronics Ltd., Gdańsk, Poland
[2]Przemysłowy Instytut Telekomunikacji S.A., Hallera 233A, Gdańsk 80-502, Poland

Abstract— In this paper the Butler Matrix (BM) 32×32 working in L band designed and implemented on high permittivity dielectric ($DK = 10$) substrate is presented. The procedures to create BM $N \times N$ schematic circuit consisting of five layers of couplers is widely and well described in literature. The electrical structure is based on $3\,\mathrm{dB}/90^\circ$ couplers and narrowband phase shifters realized as delay microstrip lines. That structure was decomposed to 12 parts. Such decomposition allowed to omit crosses between microstrip lines and reduce size of the device. Physically first group of 4 parts is oriented horizontally and contains three layers of BM, next 8 parts are oriented vertically and contain two last layers of BM. It allows to connect them all together by snap connectors. The disadvantage of that solution is a poor ability to introduce any corrections inside parts of Butler Matrix and between them. Because of that the performance of BM depends mainly on DK parameters deviations. In that papers that influence is presented and possible methods of preventings and corrections are presented. To ensure quality and reduce errors introduced by laminate parameters tolerances, the sheets from that same production batch should be utilized. In that case even if parameters vary from nominal value there is a great probability that deviation of DK is in this same direction in every laminate sheet so it will result in limited differential phase shift error at BM transition parameters. In case when laminate parameters vary from sheet to sheet in different directions, (once DK is higher from nominal, next sheet of laminate has lower DK comparing to nominal) differential phase shift errors are more significant. To reduce errors in manufactured BM different activities may be undertaken like rising DK with dielectric covers or lowing DK with drilling laminate or selecting best fitting components (parts) from bigger lot The efficiency of these methods is validated with measurements of BM or BM's elements and also presented in that paper.

The Effects of Electromagnetic Field Stress on SiGe HBT's

Ali Alaeddine[1, 2], **Kadi Moncef**[2], **and Daoud Kaouther**[1]

[1]GPM, UMR 6634 CNRS, University of Rouen, Saint Etienne du Rouvray, France
[2]IRSEEM, ESIGELEC, Saint Etienne du Rouvray, France

Abstract— A new reliability study in SiGe HBT is investigated resulting from electromagnetic field disturbance. The stress effects have been related to a base current degradation in forward and reverse Gummel plots with a large deviation of capacitance characteristics. As a consequence, Cut-off frequency degradation at low and high injection levels is discussed.

Introduction: This paper is organized as follows: Firstly, the operating conditions of the DUT and the stress effects on the DC characteristics are discussed comparatively with the other stresses. The stress induced effects in the capacitive measurements are presented and discussed, secondly. Finally, the stress effect on the cut-off frequency at low and high injection levels is studied.

DC Degradation: The near-field disturbance method is based on the use of a miniature near-field probe localized above the device under test (DUT) at a given height "H" to produce a strong localized electromagnetic field. It includes automatic near-field mapping system developed by the Research Institute for Electronic Embedded Systems (IRSEEM) [1]. The tested devices used in this study are SiGe HBTs packaged in SOT-343 with a DC current gain of 300 and a usable cut-off frequency up to 10 GHz. These transistors are mounted on a custom Printed Circuit Board (PCB) like a common emitter amplifier. On the typical forward Gummel plots of the HBT measured after 2h30 of stress, we can observe that the collector current remains unchanged during the stress while a large degradation of the base current is occurring. The commonly associated mechanism responsible for this shift in base current is the generation of a damage region between the base and the emitter at the (Si-SiO_2) interface [2]. In addition, the value of the leakage base current (I_B) increases after stress in the reverse Gummel plots while the emitter current remains unchanged. This observed inverse-mode IB degradation can be created by traps induced at the shallow trench oxide edge between the base and the collector [3]. The reverse current gain degrades with an increase of base current after stress. This is probably due to the hot carriers inducing Generation/Recombination trap centers in the defect areas.

Capacitance Measurements: We have measured the Base-Emitter capacitance before and after electromagnetic field stress when the Collector is left open during this measurement. There is a considerable increase in the B-E capacitance characteristics after stress. This could be attributed to an increased of the carrier concentration in the B-E junction [4] which is in agreement with the increase of the non-ideal base current in forward Gummel plots. Concerning the Base-Collector capacitance, and in agreement with the increase after stress of the non-ideal base current as indicated in the reverse Gummel plots, the large number of carriers present in the B-C junction after stress modifies the B-C capacitance causing it to increase. Forward and reverse Gummel plots with capacitance characterizations indicate that the electromagnetic field stress induces traps not only at the Emitter-Base spacer's oxide, but also at the Collector-Base spacer's oxide.

AC Degradation: As well as the DC characteristics, the high-frequency characteristics were also affected by electromagnetic field stress. It was found that the amplitude of the transmission parameter (S_{21}) and the input parameter (S_{11}) were degraded after stress. Hence this indicates significant degradation in forward power gain and changes of the input impedance, respectively. This is consistent with the decrease of the output power versus the small and high input power regime. The cutoff frequency which is the most common AC figures-of-merit for RF transistors was extracted using the measured S-parameters. It is worth noting that, the stress-induced degradation of (f_T) is significant at low and high currents. As expressed in the well-known equation of (f_T), the cut-off frequency is approximately proportional to the base-emitter and the base-collector capacitances at low injection levels. At high injection levels the forward transit time is dominant in this expression, which represents the minority carrier transit time in the base and the emitter [5]. The transition frequency degradation after stress at high injection levels is due to the increase of the transit time induced by the generation/recombination mechanisms. The deviation of this frequency at low current is in consistent with the increase of the both capacitances after stress. Further experiments are under investigations using Emission Microscopy (EMMI) technique and Transmission Electron Microscopy (TEM) cross section specimens, in order to

analyse the failure mechanisms and to qualify the SiGe HBT vulnerability under electromagnetic field stress.

Conclusion: In the present abstract the electromagnetic field stress effects have been reported. We discussed the rise up of the base current component in the forward and reverse Gummel plots which is due to the generation/recombination mechanisms. A large increase of the Base-Emitter and Base- Collector capacitances has been found. Consequently, the cutoff frequency at low and high injection levels is suffered by stress.

REFERENCES

1. Baudry, D., C. Arcambal, A. Louis, et al., *IEEE Transaction on EMC*, Vol. 49, 485–493, 2007.
2. Zhang, S., G. Niu, J. D. Cressler, et al., *IEEE Transactions on Nuclear Science*, Vol. 48, 2233–2237, 2001.
3. Huang, S.-Y., K-M. Chen, G-W. Huang, et al., *Microelectronics Reliability*, Vol. 48, 193–199, 2008.
4. Madhu, K. V., R. Kumar, M. Ravindra, et al., *Solid-State Electronics*, Vol. 52, 1237–1243, 2008.
5. Liu, R., W. Qian, and T. Wei, *Microelectronics Journal*, Vol. 30, 1195–1206, 1999.

Modeling and Diagnostic of Stator Faults in Induction Machines Using Permeance Network Method

Y. Amara and G. Barakat
GREAH, University of Le Havre, 25 rue Philippe Lebon, BP 540, 76058 LE HAVRE Cedex, France

Abstract— This paper presents an accurate and reasonably complicated model to simulate the faulty induction machines. The proposed model is based on a Permeance Network Method (PNM) coupled to the differential equation system governing the induction machine behavior in presence of stator faults. The proposed model allows taking into account the local magnetic saturation due to the relatively high fault current with moderate simulation time compared to the finite element method (FEM). Simulation results illustrating the impact of saturation in the case of some common stator faults such as stator inter-turn short circuits, shorted phase and open phase faults are presented and their comparison with those issued from coupled magnetic circuit based model proof the pertinence of the proposed approach. Experimental results validate the PNM approach in modeling saturated machines. The presented simulation results demonstrate the necessity to survey multiple quantities in order to distinguish between different fault signatures and in so doing to diagnose the type of a stator fault.

A Backstepping-based Fault-tolerant Control Approach for Induction Motor Drives

Omar Benzineb[1], **Mohamed Tadjine**[2], **Mohamed Benbouzid**[1], **and Demba Diallo**[3]

[1]Université of Brest, EA 4325 LBMS, Rue de Kergoat, CS 93837, 29238 Brest Cedex 03, France
[2]Ecole Nationale Polytechnique, Algiers, Algeria
[3]LGEP, Université of Paris Sud P11, CNRS UMR 8507 SUPELEC, 91192 Gif-Sur-Yvette, France

Abstract— This paper deals with the application of implicit fault-tolerant control techniques to induction motor drives based on the Backstepping approach. For that purpose, the induction motor, the disturbances as well as the faults signals have been modeled. A Backstepping control strategy (nominal control) is then synthesized and applied to the induction motor drive for robust control purposes. For fault-tolerant control purposes, an additive control term is generated from an internal state model in order to compensate for the fault effects.

Simulations carried-out on a 1.1-kW induction motor drive clearly show the effectiveness of the proposed approaches.

REFERENCES

1. Zhang, Y., et al., "Bibliographical review on reconfigurable fault-tolerant control systems," *Annual Reviews in Control*, Vol. 32, 229–252, 2008.
2. Campos-Delgado, D. U., et al., "Fault-tolerant control in variable speed drives: A survey," *IET Electric Power Applications*, Vol. 2, No. 2, 121–134, March 2008.
3. Wu, E. N., "Coverage in fault-tolerant control," *Automatica*, Vol. 40, 537–548, 2004.
4. Benbouzid, M. E. H., et al., "Advanced fault-tolerant control of induction-motor drives for EV/HEV traction applications: From conventional to modern and intelligent control techniques," *IEEE Trans. Vehicular Technology*, Vol. 56, No. 2, 519–528, March 2007.
5. Bonivento, C., et al., "Implicit fault-tolerant control: Application to induction motors," *Automatica*, Vol. 40, 355–371, 2004.
6. Tadjine, M., et al., "Robust backstepping vector control for the doubly fed induction motor," *IET Control Theory & Applications*, Vol. 1, No. 4, 861–868, July 2007.

Session 4A4b
Electromagnetic Methods and Instruments for Non Destructive Testing Applications of Ground Penetrating Radar

Interference from the Second Layer in Holographic Radar

M. Inagaki[1], **T. Bechtel**[2], **and V. Razevig**[3]

[1]Walnut Ltd., 1-19-13 Saiwaicho, Tachikawa, Tokyo, Japan
[2]Department of Earth and Environment, Franklin & Marshall College, Lancaster, PA, USA
[3]Remote Sensing Laboratory, Bauman Moscow State Technical University, Russia

Abstract— Holographic radar produces a plan view in a grey scale. It operates at 5 discrete frequencies from 3.6 to 4.0 GHz with two receiving antennae in parallel and cross polarizations relative to the transmitter. As a result, we obtain 2 sets of 5 images. Parallel polarization images among them are used more often for interpretation. The incident wave is not a pulse but a continuous wave. The phase of the reflected wave is dependent upon the distance to a target. If the distance corresponds close to positive max or negative max of the continuous wave, a very strong signal can be obtained. And, if the distance corresponds close to zero point, the signal will be very weak. As holographic radar employs 5 different frequencies, zero gain should not occur in all the images with 5 different frequencies. Experienced facts show that three or four among five images have sufficient gains.

There is no obstacle if the target has only one reflection. However, sometimes the target has more than one reflection that originate at different depths. For instance, an underground void has two reflections, one is the top of the void and the other is the bottom of the void. Reflections occur at both boundaries. There is a possibility these two reflections interfere with each other to disturb the clear image.

Interference phenomena have been experimentally investigated using Rascan holographic radar. Plastic plates (electric permittivity = 2.7) were prepared. Thickness is 3 mm each. Three-layered structure is formed. The first and the third layers are formed of plastic plates. The second layer between both plastic layers is void. This three-layered model was put together with all-plastic layered structure and scanned simultaneously as a control. Holographic images have been produced with the thickness of the void variable. Another experiment has been also carried out by altering the material to rubber sheets (electric permittivity = 8.3) instead of plastic plates at the bottom of void.

When the void thickness is comparatively thin (not too thin), clear reflections are observed at all frequencies. The second reflection disturbs image in some thickness of void first at the highest frequency (4 GHz). The images at lower frequencies are accordingly disturbed at deeper parts. This is the effect of interference. This effect is stronger in the case of a rubber-bottom void. This is because the contrast becomes larger at the rubber boundary. This is an unwelcome effect for interpreting a GPR image properly.

In contrast there is also a useful case. A GPR is routinely used for detecting underground voids. A GPR locates the voids well, however, the thickness of a void is not precisely clarified by a GPR. A boring is needed to do so. Recently nondestructive methods to determine the thickness of voids are much desired. To eliminate thin voids, which give little harm to road safety, a method is needed to avoid the time-consuming and destructive work of checking by boring. Looking through the images over 5 frequencies it may be able to tell the thickness of void by a series of the location of interference. Currently the frequencies are too high to apply for underground void detection. But it might be useful when introducing the lower frequencies with the same concept.

Detection of Latent Damage from Insect Activity in Wooden Structures through the Use of Holographic Subsurface Radar

T. Bechtel[1], **L. Capineri**[2], **P. Falorni**[2], **M. Inagaki**[3], **A. Zhuravlev**[4], **V. Razevig**[4], **S. Ivashov**[4], **and C. Windsor**[5]

[1]Department of Earth and Environment, Franklin & Marshall College, Lancaster, PA 17604, USA
[2]Dipartimento Elettronica e Telecomunicazioni, Università di Firenze, Firenze 50139, Italy
[3]Walnut Ltd., 1-19-13, Saiwaicho, Tachikawa, Tokyo 190-0002, Japan
[4]Remote Sensing Laboratory, Bauman Moscow State Technical University, Russia
[5]116, New Road, East Hagbourne, OX11 9LD, UK

Abstract— Worldwide, termites, other insects, and fungi cause damages totaling billions of dollars per year. The common way to detect hidden infestation is by visual inspection, or destructive probing. Acoustics, trained dogs, CO_2 sensors, and infrared have also been used for active colonies. In this study, RASCAN-type holographic radar was used to scan boards with mock-termite-tunnel drill holes, planks with termite damage, and beams with destructively-detected known damage hidden behind plasterboard wall covering. The results were used to interpret scans of structural elements with former infestation. Scanning revealed locations with latent subsurface damage that was missed by prior inspection and remediation.

Distinguishing Buried Mines from Battlefield Clutter Using Holographic Radar

C. G. Windsor[1] and L. Capineri[2]

[1]United Kingdom Atomic Energy Authority (UKAEA), 116 New Road, East Hagbourne, OX11 9LD, UK
[2]Dipartimento Elettronica e Telecomunicazioni, Università di Firenze, Firenze, Italy

Abstract— It is said that 90% of a deminer's time is spent locating and removing harmless clutter objects. In order to address whether this situation can be improved, a series of holographic radar scans have been made using the Rascan holographic radar system of a simulated mine (a cylindrical plastic sweet container filled with sugar) and several common battlefield clutter objects: a short length of barbed wire, a small unexploded bullet, a coke tin and a large flint stone.

The raw Rascan images which consist of 5 frequencies at parallel and cross polarisations have been combined together by taking the modulus of the image amplitude less the mean background and summing over all the frequencies and two polarisations. The series consists of the same objects placed on a 400 mm × 470 mm area measured at10 mm resolution in a sand box filled with fine dry sand at about 60 mm depth. Some 15 similar images were taken with the same objects placed at different positions over the area and at different depths and orientations.

The above figure shows that the eye, armed with the knowledge of what the Rascan images represent, is readily able to identify them from a combination of their shape, their amplitude, and their "texture" or degree of un-evenness of amplitude. The question is, "Can the skills of the human eye be reproduced by an automated system?".

The image is scanned by a receptive field of a size large enough to contain the objects to be discriminated. If the amplitude above background over the receptive field exceeds some defined threshold, the position of maximum integrated amplitude is located. The part of the image within the receptive field placed optimally over the located object is saved by the system, as an example representation of that object, to be used in subsequent training. The coloured boxes in the figure show such automatically generated object images.

The series of "training" images of known objects is presented to a neural network which is able to adjust its complexity so that other "test" images are optimally classified. Finally quite new "validation" images which have not been previously presented to the network can be used to identify the classification accuracy in terms of the percentage of correctly classified objects and the percentage of false alarms.

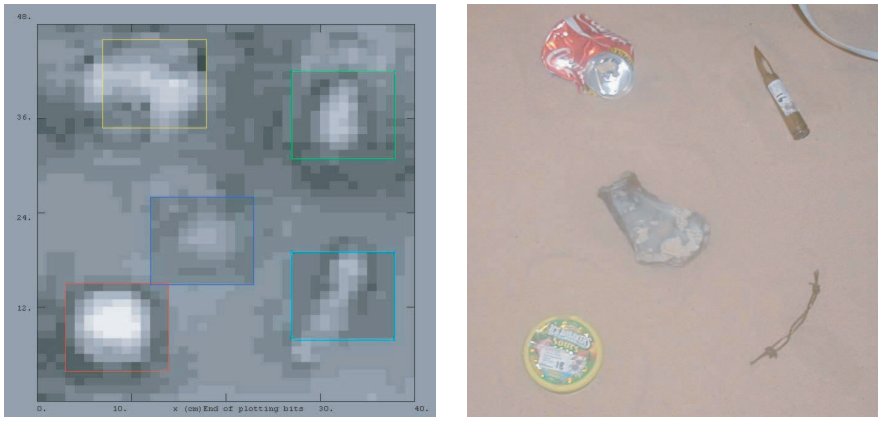

(a) (b)

Figure 1: (a) The Rascan composite image and (b) a photograph of the corresponding objects before being buried under the sand. The coloured boxes show the areas of the image picked out by a scanned receptive field, which can be used for training a neural network.

A Quasi Linear Sampling Method in Electromagnetic Inverse Scattering

G. H. Li, **X. Zhao**, **and K. M. Huang**
School of Electronics and Information Engineering, Sichuan University, Chengdu 610065, China

Abstract— We consider the electromagnetic inverse scattering problem of recovering the shape of perfect conducting scatterers, from knowledge of incident plane waves and the far-field patterns of scattered fields. Traditional Linear Sampling Method identifies the edge based on information from a large number of points, sampled from reconstruction region. In this case, not all the sampled points locate at the edge of scatterer. Avoiding sampling unnecessary points, Quasi Linear Sampling Method is proposed. This new adaptive method determines an approximate initial point 'on' the edge of scatterer through a pre-defined threshold value. From this initial point, other points on the edge are adaptively traced, under the assumption that the edge of scatterer is along continuous curve. Comparison of this newly proposed method with the old one shows that, improvement is achieved in decreasing computational effort while maintaining the same reconstruction resolution.

Session 4A5
Radar Signal Processing, Target Recognition and Identification

Bistatic Radar Target Classification Using Time-frequency Analysis and Multilayered Perceptron Neural Network

Sung-Jun Lee and In-Sik Choi
Department of Electronic Engineering, Hannam University, Daejeon, Korea

Abstract— This paper analyzes the performance of target classification using a bistatic radar cross section (RCS) of four different wire targets. The short time Fourier transform (STFT) and the continuous wavelet transform (CWT) are used for feature vector extraction from the monostatic and bistatic RCS of each target, and the multilayered perceptron (MLP) neural network is used as a classifier. To compare the performance, we also did a simulation using a monostatic RCS data. Simulation result (Figure 1) shows that CWT has a better performance than STFT. In the CWT, the monostatic RCS has a better performance than the bistatic RCS. However, in the STFT, the bistatic RCS is better than the monostatic RCS. The comparison of the classification performance between the monostatic RCS and the bistatic RCS proved that the bistatic RCS also has a relatively good performance. Therefore, the bistatic RCS is a good candidate for application to radar target classification in combination with a monostatic RCS.

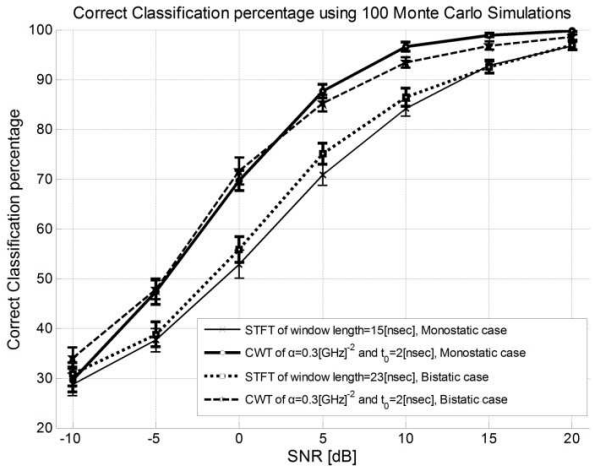

Figure 1: Comparison of correct classification percentage between monostatic and bistatic RCS as a function of SNR [dB].

ACKNOWLEDGMENT

This work was supported by Basic Science Research Program through the National Research Foundation of Korea (NRF) funded by the Ministry of Education, Science and Technology (No. 2010-0016513).

New Models for Radar Targets and Background Coupling

H. J. Mametsa[1], **A. Bergès**[1], **J. Rahm**[2], **E. Zdansky**[2], **Anders Örbom**[2], **C. Cochin**[3], **and B. Maréchal**[3]

[1]ONERA DEMR, 2, Av. E. Belin, 31055 Toulouse Cedex 4, France
[2]FOI Information Systems, Box 1165, 581 11 Linköping, Sweden
[3]DGA Information Superiority, La Roche Marguerite, BP 57419, 35174 Bruz Cedex, France

Abstract— The project is a collaboration between Sweden (FOI) and France (ONERA, DGA Information Superiority) since during earlier common activities, both sides, have realised that they are investigating similar phenomena within the field of radar: improvements in electromagnetic modelling of wave interactions with environment and objects. This involves the development of a new phenomenological and physical approach of radar simulation. Tools for electromagnetic simulation make RCS and ISAR image computations up to millimetre wavelength possible from the CAD file of targets. Nevertheless, the environment of the objects has to be taken into account for a realistic prediction of RCS.

The radar signature of an object on ground/sea can be modelled by dividing the problem into three separate parts, namely the free space RCS of the object, the background clutter and the object-ground (ground-object) interaction contributions. The most common method to calculate the signature of ground vehicles is to make free space calculations of the object and incoherently, to add a clutter background. Thus, the object-ground interactions are not taken into account. This approach is probably valid for many scenarios but certainly not for all. The interaction contributions have in some cases significant impact on the radar signature and it is therefore of great interest to find methods and tools that take these effects into account.

The main objectives of this radar signature of ground based targets investigation are:

- To get a better theoretical understanding of complicated scattering phenomena such as target-background interaction.
- To develop, from different target backgrounds, a bistatic scattering model such as IEM (Integral Equation Model) in order to have a reference rigorously validated electromagnetic software.
- To create a set of reference measurements covering essential aspects of the theories.

Bistatic measurements of different kinds of ground surfaces are performed in order to improve the target-environment scattering understanding and modelling. Then, monostatic SAR and ISAR measurements are made for different elevation angles and different polarisations in X and Ku frequency bands. Scenarios such as military target over sand, grass and asphalt are measured.

The project results in validated methods for calculating radar signatures of targets, backgrounds and target-background interactions under conditions relevant to high-resolution radars. The emphasis is on the target and its immediate surroundings. In particular, the theoretical results may be incorporated in existing software, thus enabling more realistic and reliable RCS calculations of complex scenes. Moreover, the results may be used to investigate resolution effects on radar applications such as target detection, imaging, classification or identification as well as adaptation of the target signature to the background.

Spatially Variant Apodization for Polarimetric SAR Images

Ping Zhang and Zhen Li
Center for Earth Observation and Digital Earth, Chinese Academy of Sciences
Kedian Tower F14, No. 9 Beiyitiao Road, Zhongguancun Haidian District, Beijing 100190, China

Abstract— Synthetic Aperture Radar (SAR) imagery based on conventional Fourier transform (FT) techniques often requires sidelobe control for the high sidelobes. It has traditionally been accomplished by using window functions such as Taylor, Hanning, Hamming, etc. However, the lower sidelobes have been achieved at the expense of broadening the mainlobe width, i.e., it degrades the image resolution.

Spatially Variant Apodization (SVA) is a nonlinear sidelobe reduction method, providing more effective suppression of sidelobes without loss the resolution of mainlobe. This property of SVA is achieved through the selection of a particular frequency domain aperture amplitude weighting function for each pixel in SAR image. SVA is a nonlinear operator based on cosine-on-pedestal frequency domain weighting functions, accomplished on a pixel-by-pixel basis which allows each pixel in an image to receive its own frequency domain aperture amplitude weighting function from a continuum of possible weighting functions. SVA can effectively suppress sidelobes induced by finite-aperture without broadening the mainlobe of the impulse response. SVA takes advantage on the fact that cosine-on-pedestal weighting functions can be implemented as a three-point convolution on a Nyquist sampled image. SVA method has been used in SAR and INSAR image processing. The paper proposes a polarimetric SAR image processing method based on SVA.

The standard imaging process is applied to polarimetric SAR raw data to obtain the single look complex polarimetric SAR image. SVA processing is applied to HH channel SAR image line-by-line first in azimuth, then in range direction on two-dimensional complex data. SVA requires the attention to three pre-conditions which must be fulfilled before it can be applied successfully to the data: 1. The data spectrum should be ideally rectangle shaped; 2. The data should be integer-oversampled or exactly Nyquist-sampled; 3. Any shifts in the data spectrum (e.g., due to squint) must be removed. For SAR image, the condition 1 is apparently satisfied. We choose the standard strip mode polarimetric SAR data to meet condition 3. If the SAR image is integer Nyquist sampled, SVA is then applied to the image domain samples to remove the sidelobes directly. However, most SAR data is not the integer Nyquist sampled, which is not satisfied condition 2. A noninteger Nyquist sampled SVA method is used here to solve the problem. Then the SVA can be carried out on HH channel SAR image and the weights in processing are also computed. The other three channel SAR images can be deal with the same method. We obtain the new polarimetric SAR image after SVA. The new polarimetric SAR image is classified by support vector machine (SVM) method to validate the polarimetric SVA method. The characteristics and accuracy will be analyzed to give the quantitative results of improved classification precision after SVA processing.

Measurement of UWB Radar Signals Using Time-domain and Frequency-domain Measurement System

In-Sik Choi[1] **and Edward J. Rothwell**[2]

[1]Department of Electronic Engineering, Hannam University, Daejeon, Korea
[2]Department of Electrical Engineering, Michigan State University, East Lansing, MI, USA

Abstract— Ultra-wide band (UWB) radar signal has many advantages in the area of NCTR (Non-Cooperative Target Recognition), because it contains both the early-time and the late-time response which are used for extracting target features such as a scattering centers and natural resonance frequencies. In this paper, we introduce the time-domain and frequency-domain UWB measurement system and their calibration procedures. We did the time-domain measurements at Michigan State University (MSU) arch range and frequency-domain measurements at POSTECH compact range. Target used is a 1 : 72 B-52 scale model. From the result (Figure 1), we showed that the early-time and late-time response can be observed both in the time-domain (1–7 GHz frequency band) and the frequency-domain (2–8 GHz) UWB measured signals.

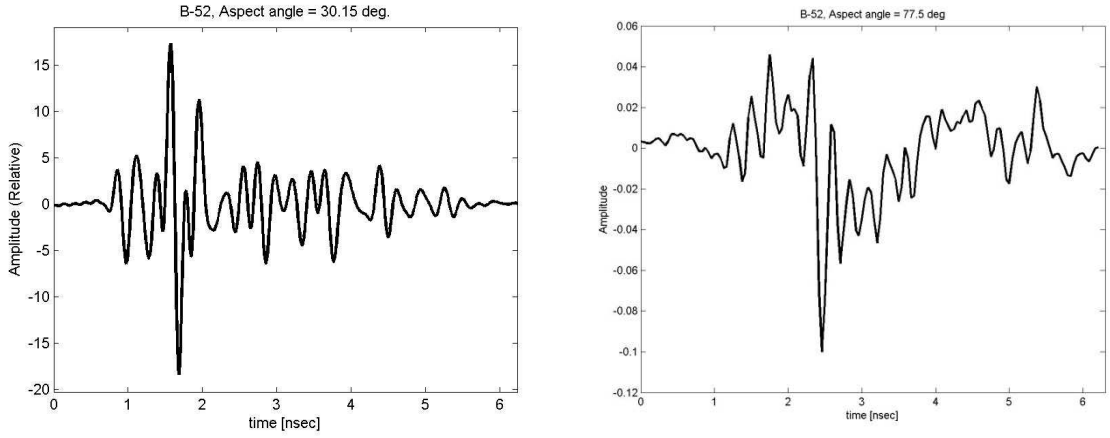

(a) (b)

Figure 1: (a) B-52 transient response measured at time-domain. (b) B-52 transient response measured at frequency-domain.

ACKNOWLEDGMENT

This work was supported by Basic Science Research Program through the National Research Foundation of Korea (NRF) funded by the Ministry of Education, Science and Technology (No. 2010-0016513).

Low Frequency Radar Target Imaging Using Ramp Response Signatures in Arbitrary Directions

J. Chauveau, Y.-H. Wen, and N. de Beaucoudrey
IREENA, Fédération CNRS Atlanstic, Université de Nantes
La Chantrerie, Rue C. Pauc, BP 50609, 44306 Nantes Cedex 3, France

Abstract— Low frequency imaging is useful to characterize stealthy or buried radar targets. Indeed, lower frequency bands permit to counter the stealthiness obtained with composite materials absorbing electromagnetic waves in usual radar frequency bands. In the same way, Ground Penetrating Radar (GPR) systems operate in low frequency bands, since the wave attenuation in most soil increases with the frequency. These low frequency bands correspond to the Rayleigh region and the resonance region for object dimensions respectively small and of the same order compared to electromagnetic wavelengths. Unlike high frequency imaging, low frequency methods cannot bring high resolution, i.e., details on the target, but they provide information on the overall dimension and the approximate shape of the target. Threedimensional (3D) microwave imaging by high frequency inverse scattering methods (diffraction tomography) requires a considerable number of look angles for image reconstruction. On the contrary, a low frequency method proposed by Young [1] and known as "the ramp response technique", needs no more than three viewing angles to generate an image. The ramp response, $h_r(t)$, first suggested by Kennaugh and Moffatt [2] for radar identification, is simply the second integral of the impulse response, $h_i(t)$. In monostatic configuration, $h_r(t)$ is directly related to the "profile function" of the target, which is the transverse cross-sectional area of the target as a function of the distance along the line-of-sight [2]. Former 3D image generation from such ramp profile functions uses approximate limiting surfaces and is therefore limited to single convex objects [1]. That is why, we have developed a new algorithm able to reconstruct non-convex and/or separated objects using their ramp response signatures [3]. For mutually orthogonal observing directions, this algorithm gives satisfactory target images, while its performance decreases in non-orthogonal cases. However, radar equipments often have a limited observing view range for remote and/or large-scale targets. Therefore, the main objective of this study is to improve the performance of our algorithm for arbitrary observing directions. For that, we have first developed an algorithm for calculating profile functions from a 3D object in arbitrary directions. Such reconstructed profile functions can be used as well for verifying the accuracy of a reconstructed image, as a new input for optimizing the reconstruction process.

REFERENCES

1. Young, J. D., "Radar imaging from ramp response signatures," *IEEE Trans. Antennas Propagat.*, Vol. 24, 276–282, May 1976.
2. Kennaugh, E. M. and D. L. Moffat, "Transient and impulse response approximations," *Proc. IEEE*, Vol. 53, 893–901, Aug. 1965.
3. Chauveau, J., N. de Beaucoudrey, and J. Saillard, "Low frequency radar targets 3-dimensional imaging using ramp response signatures," *International Radar Conference*, Bordeaux, Oct. 12–16, 2009.

A Wigner Ville Distribution Based Method for Detection of Gaussian Contaminated Sinusoidal Signal in Frequency Domain

Shahida G. Qadir[1], **Yangyu Fan**[1], **and Fathy M. Ahmed**[1, 2]

[1]School of Electronics and Information Processing, Northwestern Polytechnical University
Xi'an, Shaanxi, China
[2]Military Technical College, Cairo, Egypt

Abstract— Detection and frequency estimation of sinusoidal signals from a finite number of noisy discrete-time measurements have applications in several fields. It has been widely used in sonar and Radar for moving target detection. In, Pulsed Doppler radar, a bunch of Coherent Pulse Interval (CPI) is processed to detect and estimate the frequency of sinusoidal signal corresponding to the speed of target. With the advent of Fast Fourier Transform (FFT) algorithm, the periodogram and its variants such as Bartlett's procedure and Welch method, have been extensively in use for spectral analysis.

In this paper, a Wigner Ville Distribution (WVD) based new method is proposed for the detection and estimation of noisy sinusoidal signals in frequency domain. Cross terms produced due to bilinear nature of WVD are eliminated. The proposed method outperforms the Periodogram and its variants Bartlett and Bartlett-based proposed method by reference [1] in case of off-bin frequencies. The performance is found to be comparable in case of in-bin frequencies. Due to Low-sidelobes reported by WVD, no additional window operation is used, consequently the proposed method outperforms the windowed version of Periodogram and its variants for all 'in' and 'off' bin frequencies. Also, frequency resolution remains intact. However, the issue of increased computation of proposed method can be tackled by using high speed devices and many proposed real time WVD implementation algorithms. Performances of the proposed WVD based method and the other mentioned methods are evaluated through computer simulations by generating Receiver Operating Characteristics (ROCs) via Monte Carlo trials.

REFERENCES

1. Ahmed, F. M., K. A. Elbarbary, and A. R. H. Elbardawiny, "Anaytical performance evaluation of an enhanced frequency domain radar detector," *IEEE Radar Conference, RADAR'08*, 1–5, May 2008.

The Extraction and Analysis of Spatial Information for SAR Image Using Binary Cliques Iterative Decomposition Method with Multifractal Dimensions

Hse Tzia Teng[1], **Hong Tat Ewe**[2], **and Sin Leng Tan**[2]

[1]Faculty of Engineering, Multimedia University, Malaysia
[2]Faculty of Engineering and Science, Universiti Tunku Abdul Rahman, Malaysia

Abstract— Multifractal dimensions have been suggested to be used as parameters to extract textural properties and have obtained good classification results on Airborne Synthetic Aperture Radar (AIRSAR) image for homogeneous regions. Further analysis showed that the multifractal dimensions D_q ($q = -1,\ 0,\ 1,\ 2$), when applying on SAR images for land use classification, provide better surface roughness information when D_q ($q = -1,\ 0,\ 1,\ 2$) were combined in classifying image as different spatial information can be extracted and further enhanced. However, this classification method using multifractal dimensions is not robust as it does not distinguish regions with similar textural information. It is not able to classify these regions efficiently due to insignificant separability for individual D_q ($q = -1,\ 0,\ 1,\ 2$) on these regions.

In this paper, we proposed a binary cliques decomposition method with multifractal dimensions for recognition of similar textural information in SAR images. Texture information being considered are surface roughness, homogeneity, entropy and correlation with neighboring pixels, which are measured using multifractal dimensions D_q ($q = -1,\ 0,\ 1,\ 2$). The potential of the binary cliques in the recognition of patterns and the related optimum size for the cliques are investigated thoroughly. The spatial relation information in a training class is represented using binary cliques:

$$I_k = \sum_{i=1}^{16} C_i \oplus P_i$$

where I_k is the k-th training class, C_i the i-th clique and P_i the corresponding normalized frequency of the i-th clique in the region. The clique having highest normalized frequency, say C_j, is further decomposed into binary cliques for determination of more refined textures in the region:

$$I_k = C_j \oplus P_j + \sum_{\substack{i=1 \\ i \neq j}}^{16} C_i \oplus P_i$$

where

$$C_j \oplus P_j = \sum_{n=1}^{16} C_{j_n} \oplus P_{j_n}.$$

The process continues till the normalized frequencies for all cliques and their sub-cliques are stabilized. The variation of the normalized frequencies of cliques in respective training classes enables us to separate the classes.

The proposed method is tested on an L-band HH-polarized Jet Propulsion Laboratory (JPL) AIRSAR image of Muda Merbok area, Kedah, Malaysia, with 4 training classes and 14 testing areas, and on the L-band HH-polarized JPL AIRSAR image of Flevoland with 11 landuse classes and testing areas. These two images are chosen to investigate on the robustness of the method as the land use classes of the AIRSAR image of Muda Merbok are having vast difference in the textural information whereas land use classes of the AIRSAR image of Flevoland are of similar information. It is noted that for training regions of vast difference in textures, pre-grouping into more coarse classes is also needed for better accuracy; on the other hand for regions of similar textural information, pre-grouping is essential. The classification result shows that this method has potential in classifying regions of similar textural information in SAR image.

Session 4A6
Medical Electromagnetics, RF Biological Effect, MRI

Effects of Millimeter Wave Exposure on Termite Behavior

A. Z. Tirkel[1], **J. C. S. Lai**[2], **T. A. Evans**[3], **and G. A. Rankin**[4]

[1]Scientific Technology, Australia
[2]University of New South Wales at the Australian Defence Force Academy, Australia
[3]CSIRO Entomology, Australia
[4]The University of Adelaide, Australia

Abstract— It has been known that termites are affected by thermal and light gradients [1]. This paper demonstrates that individual and collective behavior of termites can be influenced by thermal effects induced by millimeter wave exposure. This offers the possibility of termite control. Three types of experiments were performed. First, termites in a Petri dish were exposed to 1.0 W of power at 24 GHz out of a pyramidal horn antenna (55 × 45 mm aperture) directly above the dish. The outlines of the dish and horn are visible in the thermal images taken by Micron MikroScan 7200 V thermal camera, as shown in Fig. 1. The termites (Mastotermes darwiniensis: this species was used in all three experiments) moved freely into and out of the beam and took turns in "basking" under the horn, achieving a maximum temperature of 31°C, which is within their thermal comfort zone and preferable to the ambient temperature of 22°C. The second experiment was also carried out in a Petri dish. Termites were exposed to 1.3 W at 28.24 GHz from a 30 × 30 mm pyramidal horn. Termites 12 mm long exhibit resonant absorption near 25 GHz [2]. Individual termites exposed to the increased power density heated to 42°C. This was clearly uncomfortable for them, as evidenced by avoidance of the beam, and evasive behavior, such as reorienting their body to reduce the heating. Absorption is dependent on aspect angle and polarization [2]. In order to entice termites into the beam, a dead termite was placed in the center. This resulted in some termites venturing into the beam to investigate. These termites became distressed, and presumably sent distress signals to others, who followed, resulting in a huddle. This huddle proved suicidal, as shown in Fig. 2, where the peak temperature exceeded 55°C. Termites lack internal thermal regulation, and under the conditions in Fig. 2. lose most of their heat by radiation. The latter is proportional to ST^4, where S is the surface area and T is temperature in °K. By huddling, termites reduce their effective radiating surface area and increase the heat exchange between neighbors by radiation. This accounts for the extra 13°C rise in the huddle. Suicidal huddling behavior was also observed in termites "trying" to cross a water barrier, and it was also speculated that such huddles were also due to individuals in distress (who fell into the water) attracting a crowd of other victims.

The setup involved in the third experiment is shown in Fig. 3. This simulates termites travelling to and from their nest via mud tubes. The "nest" with or without vermiculite is on the left, whilst the food (timber block) is on the right. In this case, no huddling was observed. However, after exposure, three soldier termites were observed in the beam, close to death, and unable to move. The soldiers did not attract the other caste termites, unlike what happened in Fig. 2. It is still not known why the soldiers did not save themselves.

It appears that resonant absorption of millimeter wave radiation has the potential to kill, or to alter the social behavior of termites. Full results of these experiments as well as those obtained with a lens antenna to increase the power density to compensate for the transmission losses through building materials will be presented.

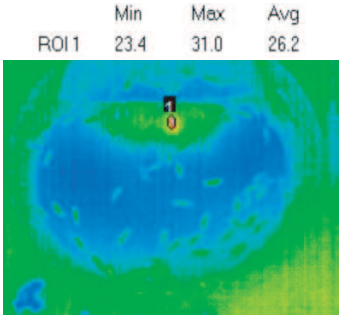

Figure 1: Individual termite "basking" under the horn.

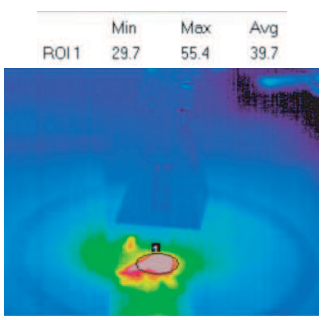

Figure 2: "Death Huddle".

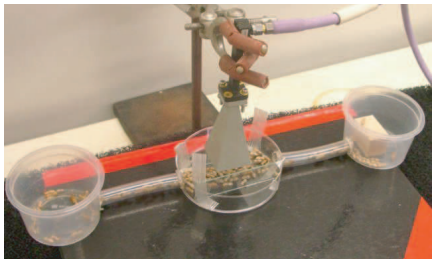

Figure 3: "Mud Tube Simulation".

REFERENCES

1. Cabrera, B. J. and M. K. Rust, "Behavioral responses to light and thermal gradients by the western drywood termite (Isoptera: Kalotermitidae)," *Physiological and Chemical Ecology*, 436–445, Entomological Society of America, 1996.
2. Tirkel, A. Z., J. C. S. Lai, T. A. Evans and G. A. Rankin, "Heating and provocation of termites using millimeter waves," submitted to *Progress In Electromagnetics Research Symposium*, Marrakesh, Morocco, 20–23 March, 2011.

Heating and Provocation of Termites Using Millimeter Waves

A. Z. Tirkel[1], **J. C. S. Lai**[2], **T. A. Evans**[3], **and G. A. Rankin**[4]

[1]Scientific Technology, Australia
[2]University of New South Wales at Australian Defence Force Academy, Australia
[3]CSIRO Entomology, Australia
[4]The University of Adelaide, Australia

Abstract— This paper presents thermal and non-thermal effects of millimeter wave exposure of various species of termites. Conventional eradication uses an array of microwave horns powered by 2.45 GHz magnetrons generating many kW's of power [1, 2], Fig. 1(a). Mortality is indirect. The microwaves heat the surrounding building materials to a lethal temperature, (above 55°C), which then causes mortality by conduction. Direct absorption at 2.45 GHz is negligible, as termite dimensions are a small fraction of a wavelength, and so are well into the Rayleigh region. This indirect mortality is energetically demanding because there is more mass of building material than of termites; considerably lower energy expenditure is theoretically possible by targeting the termites directly. Termites exhibit resonant absorption in the millimeter wave region commensurate with their body dimensions, which is where Mie scattering dominates, Fig. 1(b). Therefore direct heating of termites with minimal background heating is possible with millimeter waves in the 20–80 GHz range.

Our experiments show that simulations performed with Mieschka [3], Fig. 1(b), are confirmed at 24 GHz. Fig. 2(a) shows thermal signatures of various termites exposed to 24 GHz. The temperature rise is directly related to size. The transmitter power was 1.0 W. Termites in a petri dish were exposed to a pyramidal horn antenna (55 × 45 mm aperture) directly above the dish. The outlines of the dish and horn are visible in the thermal images. Fig. 2(b) shows the polarization dependence of the temperature rise. The termite oriented with its long axis parallel to the electric field shows much greater heating, indicating that absorption is greater. This is in

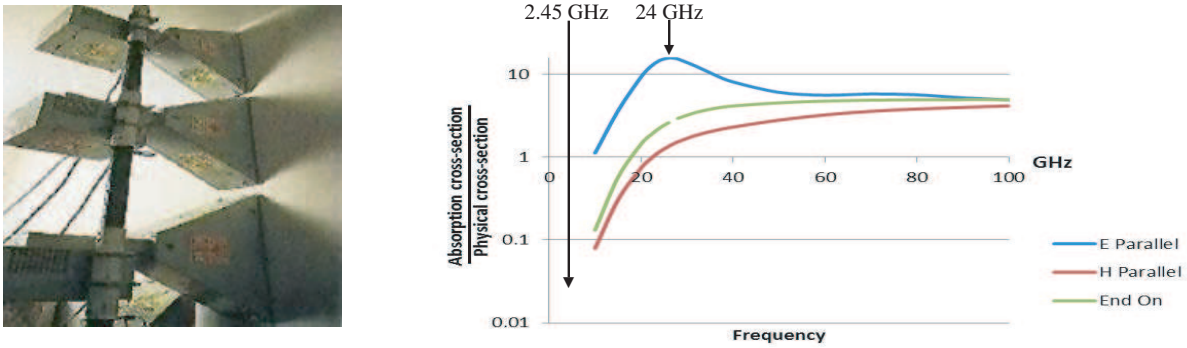

(a) (b)

Figure 1: (a) Conventional eradication using horn array powered by domestic magnetrons generating several kilowatts. (b) Absorption of termites versus frequency in the millimeter wave region showing typical Mie characteristic.

Figure 2: (a) Thermal Image from Micron MikroScan 7200 V demonstrating the size dependence of temperature rise. (b) Thermal Image from MikroScan 7200 V showing polarization dependence of temperature rise.

agreement with theory [4] and simulations. Full results of simulation and experiments, including the behaviour of termites exposed to millimeter waves, will be presented.

REFERENCES

1. Martin, R. S., et al., "In situ microwave insect eradication device with safety system," US Patent, No. 5,575,106, 1996.
2. Lewis, V. R., A. B. Power, and M. I. Haverty, "Laboratory evaluation of microwaves for control of the western drywood termite," *Forest Products Journal*, Vol. 50, No. 5, 79–87, 2004.
3. Wauer, J., et al., "Two software tools for plane-wave scattering on nonspherical particles in the german aerospace center's virtual laboratory," *Applied Optics*, Vol. 43, 6371–6379, 2004.
4. Barber, P. W., "Resonance electromagnetic absorption by nonspherical dielectric objects," *IEEE Transactions on Microwave Theory and Techniques*, Vol. 25, No. 5, 373–381, May 1977.

Electromagnetic Information Transfer of Specific Molecular Signals Mediated through Aqueous Systems: Experimental Findings on Two Human Cellular Models

Alberto Foletti[1], **Settimio Grimaldi**[2], **Mario Ledda**[2], **and Antonella Lisi**[2]

[1]Independent Researcher, Lugano, Switzerland
[2]Institute of Neurobiology and Molecular Medicine, CNR, Rome, Italy

Abstract— Electromagnetic Information Transfer (EMIT) of Specific Molecular Signals according to previous report [3, 5] and ours [1] is having his serious experimental evidence.

The aim of the present work is to understand the possible role of water in mediating the electromagnetic information transfer of biological active molecules [5] such as retinoic acid (RA).

The electromagnetic information signals from the retinoic acid solution (RA-EMIT) was captured and transferred to the target as previously described by a commercially available oscillator (Vegaselect 719). In the present study the retinoic acid signals was first transferred to the cell's culture medium (RA-EMIT conditioned medium) then cells (LAN-5 neuroblatoma and NT2/D1 human teratocarcinoma) cells seeded with RA-EMIT off.

The same experiment was repeated culturing cells under continuous RA-EMIT conditions. As an overall control the direct differentiating effect of RA solution on cell's culture was reported. These experimental findings demonstrated that the RA-EMIT conditioned medium behave like retinoic acid thus inducing cell differentiation in both cell's lines.

As expected the differentiation behaviour of RA-EMIT conditioned medium was less that the differentiation power of RA but surprisingly higher than what found with direct cell exposure to RA- EMIT signals.

REFERENCES

1. Foletti, A. and S. Grimaldi, "Differentiation of human lan-5 neuroblastoma cells by electronically trasmitted retinoic acid (RA)," *PIERS Online*, Vol. 6, No. 6, 518–522, 2010.
2. Lo, S. Y., X. Geng, and D. Gann, "Evidence for the existence of stable-water-cluster at room temperature and normal pressure," *Physics Letters A*, Vol. 373, 3872–3876, 2009.
3. Montagnier, L., J. Aissa, S. Ferris, J.-L. Montagnier, and C. Lavallée, "Electromagnetic signals are produced by aqueous nanostructures derived from bacterial DNA sequences," *Interdisciplinary Sciences Computational Life Sciences*, Vol. 1, 245–253, 2009.
4. Preparata, G., "QED and medicine," *Rivista di Biologia*, Vol. 93, 467–512, 2000.
5. Thomas, Y., M. Schiff, L. Belkadi, P. Jurgens, L. Kahhak, and J. Benveniste, "Activation of human neutrophils by electronically transmitted phorbol-myristate acetate," *Medical Hypotheses*, Vol. 54, 33–39, 2000.

Vectorial Electro-optic Sensors for Microwave Dosimetric Applications

P. Jarrige[1, 2], **S. Kohler**[3], **N. Ticaud**[3], **L. Duvillaret**[1], **G. Gaborit**[1, 2], **P. Leveque**[3], **and D. Arnaud-Cormos**[3]

[1]Kapteos SAS, rue Lac de la Thuile, F-73376 Le Bourget-du-Lac Cedex, France
[2]IMEP-LAHC, CNRS, University of Savoie, F-73376 Le Bourget-du-Lac Cedex, France
[3]XLIM Research Institute, CNRS, University of Limoges, F-87060 Limoges, France

Abstract— Fully dielectric pigtailed electro-optic (EO) sensors have been developed to quantify the energy absorbed by biological tissues exposed to radiofrequency (RF) telecommunication signals (GSM, UMTS, Wifi, WIMAX). These sensors are based on the Pockels' effect that leads, in EO crystals, to an electric(E)-field induced variation of their refractive indices [1]. When a laser probe beam crosses an EO crystal, its polarization state is slightly modified by the applied E field [2]. As the refractive indices of a crystal depends also on its temperature, both applied E field and temperature can be simultaneously measured [3]. The distinction between E field and temperature contributions is simply obtained by frequency filtering. Each of these two physical quantities leads to the Specific Absorption Rate (SAR) which consitutes the reference parameter for microwave dosimetric studies.

The guide line for the design of the EO probes has been defined by the measurement requirements of biological environment. The probes are miniature (3-mm diameter), fully dielectric and the EO crystals (congruent $LiTaO_3$) present a relative permittivity of 42, close to the one of biological tissues in the microwave range of interest (1–10 GHz) [4]. Hence, both invasiveness and induced perturbation on the SAR to be measured are minimized. The EO crystal presents also a strong dispersion of its refractive indices with the temperature, leading to a high temperature probe sensitivity: a resolution of 3 mK has been obtained. Measurements results have been carried out in biological media placed in Petri dishes. We will present during the conference some first results together with a comparison, in the frequency domain, with commonly used probes for SAR measurements. Spatial and temporal resolutions, bandwidth, dynamic range, and sensitivity in temperature and E-field will also be addressed.

Finally, EO probes can also be used in the time domain. Indeed, contrary to antennas that present limited bandwidths neither exceeding 3–4 decades, EO probes present an intrinsically flat response from quasi DC up to 20 GHz. This property has been exploited to perform first *in situ* measurements of ultrashort electrical pulses in electroporation cuvettes. In conclusion, EO sensors constitute a versatile and very competitive technique for studies in bioelectromagnetism.

The authors acknowledge the DGA (French Military Programs Management and Procurement Agency) and the "Fondation Santé et Radiofréquences" for their support.

REFERENCES

1. Yariv, A., *Optical Electronics*, Saunders College Publishing Ed., 1991.
2. Duvillaret, L., S. Rialland, and J. L. Coutaz, "Electro-optic sensors for electric field measurements. I. Theoretical comparison among modulation techniques," *J. Opt. Soc. Am. B*, Vol. 19, 2692–2703, 2002.
3. Bernier, M., G. Gaborit, L. Duvillaret, A. Paupert, and J.-L. Lasserre, "Electric field and temperature measurement using ultra wide bandwidth pigtailed electro-optic probes," *Appl. Opt.*, Vol. 47, 2470–2476, 2008.
4. Gabriel, C., S. Gabriel, and E. Corthout, "The dielectric properties of biological tissues: I. Litterature survey," *Phys. in Med. and Biol.*, Vol. 41, 2231–2250, 1996.

New Techniques to Reduce the Common-mode Signal in Multi-frequency EIT Applications

Mohamad Rahal[1], **Ibrahim Rida**[1], **Muhammad Usman**[1], **and Andreas Demosthenous**[2]

[1]Department of Electrical Engineering, University of Hail
P. O. Box 2440, Hail, Saudi Arabia
[2]Department of Electronic and Electrical Engineering, University College London
London, WC1E 7JE, UK

Abstract— Bio-impedance voltage measurements suffer from many potential errors. One of the key errors that affect the accuracy in medical impedance imaging and bio-impedance measurements is the common-mode error. In electrical impedance tomography (EIT) applications, where current is injected into the subject to make the measurements, the major problem is that the interference does not occur at the power supply frequency (50 or 60 Hz) but at the working frequency. Traditional techniques such as filtering or screening have little effect in reducing this common-mode interference. In this paper, we present a common-mode feedback topology which reduces these errors for use in EIT systems for in-vivo monitoring of neonate lung function (10–200 kHz current injection frequency). A frequency-selective feedback network is described which reduces the common-mode voltage due to electrode impedance mismatch at the input of the differential amplifier. The theory and key design blocks are presented.

The circuit was designed and implemented in a 5-V 0.35-µm CMOS technology, occupying an area of 0.75 mm^2 and dissipating about 20 mW. To verify the design various experiments were conducted using, an RC model of the electrodes, saline tank and ECG electrodes on the forearm to demonstrate the working of the integrated circuit. Measured results show that the common-mode signal is reduced by 85%, 75%, 70% and 65% at 10 kHz, 50 kHz, 100 kHz and 200 kHz, respectively.

Meta-analysis of Occupational and Residential Extremely Low Frequency Magnetic Fields Exposures and Neurodegenerative Disease

Gabor Mezei[1], **Yong-Sung Cho**[2], **Ximena Vergara**[1, 2], **and Leeka Kheifets**[2]

[1]Electric Power Research Institute, Palo Alto, CA, USA
[2]Department of Epidemiology, School of Public Health, UCLA, Los Angeles, CA, USA

Abstract— **Objective:** We will provide a comprehensive evaluation of occupational and residential exposure to extremely low frequency magnetic fields (ELF-MF) and neurodegenerative diseases (NDD) epidemiologic literature.

Introduction: Aging populations may increasingly lead to a high prevalence of age-related diseases such as NDD, a common cause of death. The focus of ELF-MF epidemiologic research has historically been on Alzheimer's (AD) and motor neuron diseases (MND), fewer studies focused on Parkinson's (PD). Early occupational AD studies provide weak evidence for an association with EMF with the strongest evidence among clinic-based studies. For MND, the association between "electric occupations" and amyotrophic lateral sclerosis appears to be consistent; EMF being only one aspect of the job. No consistent association between ELF-MF and PD has emerged. More recently, the ELF-MF and AD literature has been reviewed systematically with results suggestive of an association. Since then, additional studies have been published on neurodegenerative diseases and ELF-MF.

Methods: We identified peer-reviewed publications in PubMed using keyword searches on motor neuron, Parkinson's and Alzheimer's diseases, and dementias. Coders extracted study characteristics such as publication date, type of occupational and residential exposure assessment, number of potential confounders, and summary estimates. We explored studies for heterogeneity, sensitivity to various weighting schemes, differences between subgroups, publication bias and influence of individual studies.

Results: Of 223 articles, 29 separate studies were included in the final analysis. We will present results from our analyses and compare and contrast specific outcomes.

Conclusions: Our findings will provide a critical picture of the available epidemiologic evidence on ELF-MF and NDD. We anticipate our results will help identify methodological gaps in the current epidemiologic literature and aid in defining future ELF-EMF and NDD epidemiology.

Human Exposure to Outdoor PLC System

Vicko Doric[1], **Dragan Poljak**[1], **and Khalil El Khamlichi Drissi**[2]

[1]University of Split, Croatia
[2]Blaise Pascal University, France

Abstract— The purpose of Power Line Communications (PLC) system is ensure necessary communication means via existed power line network and electrical installations in houses and buildings. A serious shortcoming of this new technology is related to electromagnetic interference (EMI) problems, as overhead power lines at the PLC frequency range (1 MHz to 30 MHz) act as transmitting or receiving antennas, respectively. Also, in this frequency region the human body, when exposed to electromagnetic radiation, acts a receiving antenna.

In this paper, human exposure to a simple outdoor PLC system is assessed. An electric field irradiated by the PLC configuration is calculated, Fig. 1, using the wire antenna model. For the frequency range from 1 to 10 MHz the human body is represented by the equivalent thick cylindrical antenna Fig. 3, while in the range from 10–30 MHz a parallelepiped body model is used Fig. 3. Fig. 4 shows the axial current density distribution induced along the body. Table 1 shows the calculated value of surface and whole body averaged SAR, respectively. The obtained values of both the current density and SAR stay well below the exposure limits proposed by ICNIRP.

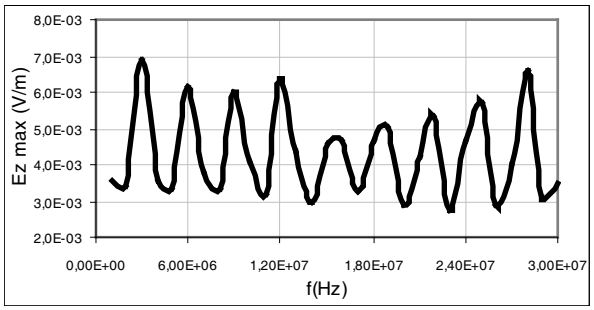

Figure 1: Maximal value of E_z component below the conductor ($x = 0\,\text{m}$, $z = 1.75\,\text{m}$).

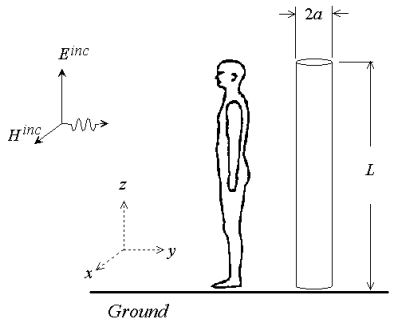

Figure 2: Cylindrical body model.

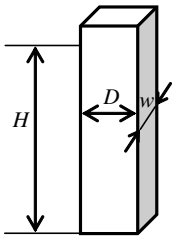

Figure 3: Parallelepiped body model.

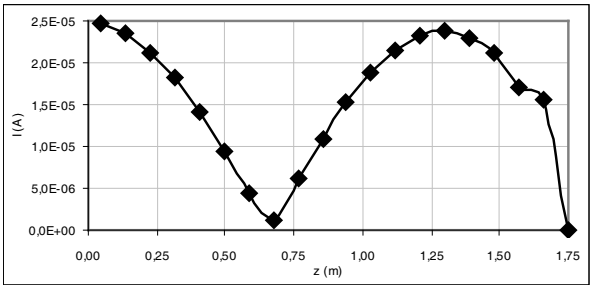

Figure 4: Current density induced along the body ($f = 10\,\text{MHz}$).

Table 1: Induced values of SAR inside the body.

F (MHz)	SAR_{surf} (nW/kg)	SAR_{WB} (nW/kg)
10	0.0347	0.0162
30	0.0727	0.0225

Analysis of Transmit Magnetic Field Homogeneity for a 7 T Multi-channel MRI Loop Array

M. Kozlov and R. Turner
Max Planck Institute for Human Cognitive and Brain Sciences
Stephanstrasse 1A , Leipzig D-04103, Germany

Abstract—

Purpose: Most MRI studies benefit from good homogeneity of the transmit magnetic field. Due to the complexity of the problem at 300 MHz, where the wavelength in human tissue is comparable with the size of most human organs, experimental optimization alone is extremely time consuming and costly. Numerical simulation becomes an important tool for analysis and optimization of transmit magnetic field homogeneity. Our goal was to clarify how shape of load, distance between array and load, Z direction length of array, and loop coil angularity affect transmit field homogeneity, for a set of coil/load geometries. We extended our research to two MRI experimental situations: either the load is much longer than, or it is comparable to, the MRI array length. The latter is typical for MRI scanning of ex-vivo samples and most animal experiments.

Method: We investigated 8 channel loop-type array coils with different diameters (ranging from 85 mm to 280 mm) and lengths (60, 80, 100 and 120 mm). Loop coil angular distribution was varied from 40 degree (the closest coil spacing) to 22.5 degree (the largest gap between coils). To eliminate the influence of RF shimming (adjustment of amplitude and phase for excitation signals) on coil performance, we studied only cylindrical load phantoms (diameters 80, 120, 155 and 190 mm), and spherical phantoms (diameters 80 and 120) mm. Cylindrical loads were as long as 375 mm, to exclude the influence of load length on transverse slice homogeneity for arrays with different lengths. For all loads, electrical properties were close to those of average human tissue at 300 MHz — permittivity 52 and conductivity 0.55 S/m.

Our investigation was performed using RF circuit and 3-D EM co-simulation [1]. The RF circuit simulator was Agilent ADS software, and Ansoft HFSS was chosen as the 3-D EM tool for its robustness in handling complex coil geometry. For all geometries array was tune/match/decoupled using capacitor and inductor based decoupling networks or only tuned by minimization of power reflected by entire array. Transmit magnetic field homogeneity was analyzed at three transversal slices (center and $+/-25$ mm from the array/load center). The array was excited in circular polarization mode, applying the same power to each port, with a sequential 45 degree phase increment.

The scanner gradient shield (with diameter of 683 mm and length 1200 mm) was always included in the numerical domain for simulation of unshielded and shielded arrays. The distance between the array and a 300 mm long local shield was varied between 50 mm and 100 mm, to understand the effect of this distance on transmit field homogeneity.

Results: Array transmit field homogeneity strongly depends on the distance between array and load, as well as on the load diameter and shape. Inhomogeneity increases with load diameter. For cylindrical and spherical loads with the same diameter inhomogeneity can vary by more than 100%. There is an optimal distance between load and array giving best homogeneity. The optimal distance, and the slope of the inhomogeneity curve versus distance, both vary with load geometry. For all cases optimization of homogeneity always entails a trade off of the average value of transmit field for a given slice. Increasing array length does affect within-slice homogeneity. It can reduce the variation of average magnetic field within the slice, while simultaneously decreasing the mean value of this field for transversal slices $+/-25$ mm from the array/load center.

When angular separation of the coils below 30 degrees can rather significantly degrade homogeneity, for most coil/load geometries, changing this separation from 40 degrees to 32.5 degrees has little effect on slice homogeneity. As a result there is some design freedom for an entire transmit array if closely placed loop coils cannot be properly detuned for a set of loads.

The array tuning/decoupling conditions have little effect on homogeneity in most cases, but there are some array/load configurations where use of capacitor based decoupling can increase homogeneity as mach as 50% at the expense of reduced average value over the slices $+/-25$ mm from the array/load center.

For the configurations investigated, the effect of the local shield on transmit field homogeneity was less than 15%.

Conclusion: The strong influence of load shape on field homogeneity eliminates any opportunity for calculation homogeneity using any 2D numerical approaches. The possibility to adjust scanner transmit power for a given slice in real time may have a great effect on homogeneity optimization procedure, because the current transmit power adjustment excludes the minimization of the difference between slice average values from the optimization goal. The optimization of transmit field homogeneity is mostly at the cost of reduced average transmit field for slices $+/-25$ mm from the array/load center.

REFERENCES

1. Kozlov, M. and R. Turner, *Journal of Magnetic Resonance*, Vol. 200, 147–152, 2009.

Session 4A7
Electromagnetic Simulations and Applications 1

Using Rectangular-shape Resonators to Improve the Far-end Crosstalk of the Coupled Microstrip Lines

Ding-Bing Lin[1], **Chen-Kuang Wang**[1], **Chi-Hao Lu**[1], **and Wen-Tzeng Huang**[2]

[1]Graduate Institute of Computer and Communication Engineering
National Taipei University of Technology, Taipei, Taiwan
[2]Department of Computer Science and Information Engineering
Minghsin University of Science and Technology, Hsinchu, Taiwan

Abstract— Modern electronic products must have high-speed, high-density layout, small size, faster rising time and lower voltages supply. With such design, signal integrity (SI) becomes a very important factor because sensitive equipment is affected by electromagnetic interference (EMI) and noise interference. Crosstalk is a major factor in SI from printed circuit boards (PCBs). Crosstalk noise is usually represented in terms of near-end crosstalk (NEXT) and far-end crosstalk (FEXT). In order to cost concerns, microstrip line is widely used for PCBs because it's easy to manufacture. In microstrip line structure, FEXT is induced by the difference between the capacitive coupling ratio (C_m/C_T) and inductive coupling ratio (L_m/L_S). In earlier research, however, many researchers had proposed solutions that are guard trace which are used to reduce NEXT and FEXT [1]. Since a large number of shorting-via degrades the SI and reduces the flexibility of the circuit routing [2]. Another technique to reduce the FEXT noise is serpentine guard trace [3], but this kind of guard trace requires to be terminated with matched resistances at both ends of guard trace. In this paper, we propose a method to reduce the far-end crosstalk by using rectangular-shape resonators (RSR) structure. The RSR structure is used to reduce the FEXT, which needn't use shorting-via and resistance to enhance the FEXT. Figs. 1(a) and (b) show the frequency-domain and time-domain simulation results. The frequency-domain simulation of HFSS shows that the S_{41} of RSR structure is decreased more than 7 dB compared to the 3-W rule. The time-domain simulation of ADS shows that the peak of far-end crosstalk voltage of RSR structure is improved to 54% compared to the 3-W rule.

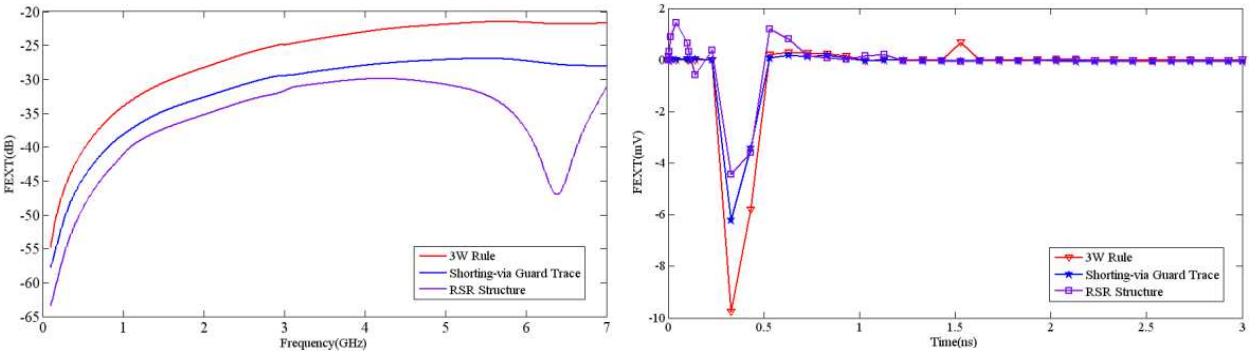

Figure 1: Comparison of simulation results among our proposed approach, 3-W rule, and shorting-via guard trace. (a) Frequency-domain. (b) Time-domain.

REFERENCES

1. Huang, W. T., C. H. Lu, and D. B. Lin, "The optimal number and location of grounded vias to reduce crosstalk," *Progress In Electromagnetics Research*, Vol. 95, 241–266, 2009.
2. Cheng, Y. S., W. D. Guo, G. H. Shiue, H. H. Cheng, C. C. Wang, and R. B. Wu, "Fewest vias design for microstrip guard trace by using overlying dielectric," *IEEE-EPEP*, 321–324, San Jose, CA, Oct. 27–29, 2008.
3. Lee, K., H. B. Lee, H. K. Jung, J. Y. Sim, and H. J. Park, "A serpentine guard trace to reduce the far-end crosstalk voltage and the crosstalk induced timing jitter of parallel microstrip lines," *IEEE Transactions on Advanced Packaging*, Vol. 31, No. 4, 809–817, Nov. 2008.

Electromagnetic Model of In-wall Wiring of Indoor Powerline Communications

V. Arnautovski-Toševa[1, 2], **K. El Khamlichi Drissi**[1], **and K. Kerroum**[1]

[1]LASMEA Laboratory, University Blaise Pascal, Aubiere, France
[2]Electrical Engineering and IT, University Ss. Cyril and Methodius, Skopje, Macedonia

Abstract— Powerline Communications (PLC) represent technology that enables data transfer at narrow or broad band speeds through power lines by using advanced modulation technology. Although the PLC technology in the beginning was promising and was potentially easy to install and inexpensive, it is still not fully developed and standardized. One major concern related to these systems is the electromagnetic field radiation. This paper is aimed to present one approach within the EMC issue related to indoor PLC.

To transmit signal between the transmitter and receiver, PLC technology works by coupling to the existing electrical wiring a modulated signal of the frequency band from 1–30 MHz. The inwall PLC signals are coupled onto the electrical wiring, between phase and neutral line or between different phase wires, using inductive or capacitive couplers, specifically designed for this purpose. However, power lines originally designed for 50 Hz power signals are neither ideal transmitting channel for data transmission at frequencies up to few tens of MHz, nor are well suited from the point of view of EMC. This refers to emissions and immunity of different systems that use the same frequency band. EMC problems arise since between the transmitter and the receiver various forms of electromagnetic coupling are possible, radiated (field) and conducted coupling. These radiated emissions appear in the form of electromagnetic waves that radiate into the immediate surrounding directly from the circuitry and its interface leads.

The proposed model analyses the radiated electromagnetic field due to indoor low voltage circuitry by using the rigorous electromagnetic model. The cabling layout in a wall of a room is modeled by a thin-wire circuit closed by 200 Ω resistor. A high frequency generator is used to inject a harmonic signal of 1 V amplitude with frequencies sweeping from 1 to 30 MHz.

The mathematical model is based on mixed potential integral equation (MPIE), which is solved by the method of moments. The computation of the vector and scalar potentials involves appropriate Green's functions through the following integral form:

$$A = \int_{l_{wire}} \underline{G}_A \cdot I dl \quad \text{and} \quad \phi = \int_{l_{wire}} G_\phi q dl$$

where $\underline{G}_A$ is the dyadic Green's function of the magnetic vector potential, and G_ϕ is the scalar potential Green's function, both for three-layered stratification and ℓ_{wire} is the length of the circuitry. The results will present current distribution and the radiated electric and magnetic field in the surrounding with respect to frequency. The method involves the dynamic choice of calculation points and efficient modeling of the circuit and the wall dimensions and parameters. The software is developed from the principle of open source code, which readily lends itself to a number of parametric optimizations; these include the circuitry and frequency among others.

Analysis of Transmit Performance Optimization Strategies for Multi Channel MRI Array

M. Kozlov and R. Turner
Planck Institute for Human Cognitive and Brain Sciences, Leipzig, Germany

Abstract—

Purpose: MRI multi channel arrays enable several novel applications. Due to the complexity of the problem, experimental optimization alone is extremely time consuming and costly. Numerical simulation may be an important tool for array optimization. However, the published simulation approaches, mainly based on finite difference time domain solvers, are insufficiently flexible for the analysis of multi-channel array decoupling, and cannot be applied for most tune/match/decoupling problems without many time-consuming 3D EM simulations. Our goal was to develop an approach for obtaining coil performance data over a range of tune/match/decoupling strategies, with only one 3D EM computation, and to quantify coil performance realistically as B1+ (in Tesla) versus the square root of the transmit power, for several coil and load geometries.

Method: We investigated 8 channel loop-type array coils with different diameters and length. Our investigation was performed using RF circuit and 3-D EM co-simulation [1]. The RF circuit simulator was Agilent ADS software, and Ansoft HFSS was chosen as the 3-D EM tool for its robustness in handling complex coil geometry. To eliminate the influence of RF shimming (adjustment of amplitude and phase for excitation signals) on coil performance, only cylindrical loads with different diameters and an 80 mm diameter spherical phantom were used in this investigation. Circular mode excitation was used.

We investigated capacitor and inductor based decoupling networks and compared their array performance obtained when the power reflected by the entire coil was minimized. Because the decoupling network influences the value of distributed capacitors, for maximal flexibility, all distributed capacitors were also substituted by lumped ports. The values of distributed capacitors were then obtained by RF circuit optimization. The total number of ports amounts to 80, for an 8 element coil with 8 capacitors in the radiative loop and two connections for decoupling circuits.

After making an initial guess of the values for distributed capacitors, RF circuit optimization for tune/match/decoupling elements was performed in two steps: 1000 random tries, followed by gradient optimization for ensuring the global minimum condition. By monitoring the power reflected by the entire coil, the values of distributed capacitors were adjusted to minimize this power for the given geometry and tune/match/decoupling conditions.

Results: For most cases analyzed, the array performance depends nearly linearly on the square root of the power delivered to the load. The ratio of power delivered to load to the power delivered to the entire coil (a difference between transmit and reflected powers) is stable for a given coil/load geometry. Therefore minimization of the power reflected by the entire coil, which S_{xx} and S_{xy} data alone do not reveal, becomes the major target for array performance optimization. AC simulation allows the evaluation and tuning of the frequency dependence of the power reflected by the entire coil. This eliminates the need to calculate combined 3-D EM fields for each step during coil performance investigation, a feature that additionally reduces the investigation time.

There are two very different behaviors for array performance optimization: large loading, where the power delivered to the load is more than 90% of power delivered to the entire coil; and small loading, where the latter quantity is less than 50%. For the first case the distributed capacitor value and decoupling strategy have minimal influence on array performance, and neither does the type of decoupling. For the second case, only tuning based on the minimization of the power reflected by the entire coil provides array performance that is independent of the values of distributed capacitors. For both inductive and capacitor decoupling approaches, adjustment of the distributed capacitor values mainly allows minimization of the power reflected by entire coil, and thus improvement of the array performance. However, in some array/load configurations, it is impossible to minimize the power reflected by entire coil when decoupling is inductive.

For any geometry/load investigated both capacitor and inductive based decoupling provide greater decoupling for the first neighbour than for the second neighbour coil element.

Conclusion: RF circuit and frequency domain 3-D EM co-simulation is a very powerful and fast approach for array coil investigation, since one multi-port 3-D EM simulation, which can be

calculated in a reasonable time, is sufficient for investigation of the array behavior with different tuning/feeding/decoupling conditions. The necessary inclusion of all tuning/feeding/decoupling circuits enables accurate array performance data to be obtained. For small coil loading, S_{xx} and S_{xy} provide insufficient guidance in regard to the decoupling required to optimize array performance. The power reflected by the entire coil must also be minimized.

REFERENCES

1. Kozlov, M. and R. Turner, *Journal of Magnetic Resonance*, Vol. 200, 147–152, 2009.

Harmonic-suppression Using Adaptive Surface Meshing and Genetic Algorithms

M. S. Bin-Melha[1], R. A. Abd-Alhameed[1], D. Zhou[1], Z. B. Zainal-Abdin[1], C. H. See[1], I. T. E. Elfergani[1], and P. S. Excell[2]

[1]Mobile and Satellite Communications Research Centre, University of Bradford, Bradford, UK
[2]Centre for Applied Internet Research, Glyndwr University, Wrexham, UK

Abstract— Active transmitting antennas often suffer from significant non-linearity; the driving transistor drain (or collector) produces time-harmonic currents which feed directly into the radiator, resulting in unwanted radiated power [1]. In active antenna design these unwanted harmonic currents can be terminated (or substantially eliminated) using the radiator itself, in which case the active circuit does not require any additional complexity for harmonic tuning, thus contributing to the desired compactness of the design. Harmonic suppression antennas (HSAs) are used to suppress power radiation at harmonic frequencies from active integrated antennas. An antenna that presents a good impedance match at the fundamental design frequency (f_o) and maximised reflection at harmonic frequencies is said to be a harmonic suppression antenna. In addition, the input impedance of any HSA design has to have minimised resistance at the harmonic frequencies and hence will be largely reactive [2]. Several techniques have been proposed to control such harmonics, such as shorting pins, slots or photonic bandgap structures [3, 4].

Generally, most of the published designs for modified patch HSA have been based on a specific reference antenna, suggesting that the proposed techniques for rejecting harmonic radiation have specific constraints imposed onto them. For example, in [5, 6] a microstrip-line fed slot antenna was developed for harmonic suppression without using a reference antenna. This was achieved with a rather complex geometry for 5 GHz operation. This process does not usefully generalise, so that if a new operating frequency is required, then the whole structure must be redesigned. Thus there exists a clear motivation to develop a coherent design strategy for microstrip HSA in active integrated applications. In this paper we adopt a computational technique using adaptive surface meshing driven by a genetic algorithm (GA).

Hereafter, a novel design strategy for microstrip harmonic-suppression antennas is presented. The computational method is based on an integral equation solver using adaptive surface meshing driven by a genetic algorithm. Two examples are illustrated; both involving design of coaxially-fed air-dielectric patch antennas implanted with shorting and folded walls (see for example Fig. 1). The characteristics of the antennas in terms of the impedance responses (see Fig. 2) and far field radiation patterns are discussed theoretically and experimentally. The performances of all of the GA-optimised antennas were shown to be excellent and the presented examples show the capability of the proposed method in antenna design using GA.

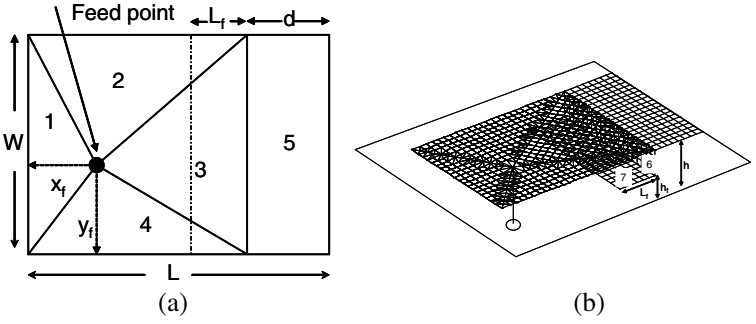

Figure 1: Basic geometry of the folded patch antenna. (a) Top view. (b) 3D surface mesh.

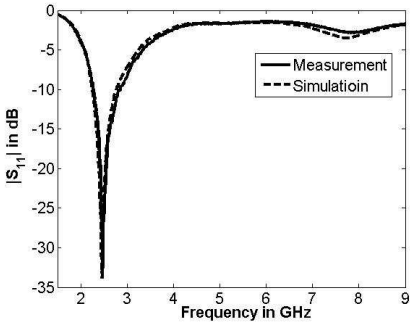

Figure 2: The input return loss of the folded patch.

REFERENCES

1. Elkhazmi, E., N. J. McEwan, and J. Moustafa, "Control of harmonic radiation from an active microstrip patch anrtenna," *Journees Internationale de Nice sur les Antennes*, 313–316, November 1996.

2. Radisic, V., Y. Qian, and T. Itoh, "Class F power amplifier integrated with circular sector microstrip antenna," *IEEE MTT-S Symposium Digest*, 687–690, 1997.
3. Kim, H., K. S. Hwang, K. Chang, and Y. J. Yoon, "Novel slot antennas for harmonic suppression," *IEEE Antennas and Wireless Components Letters*, Vol. 14, No. 6, 286–288, 2004.
4. Sung, Y. J. and Y.-S. Kim, "An improved design of microstrip patch antennas using photonic bandgap structure," *IEEE Transactions on Antennas and Propagation*, Vol. 53, No. 5, 1799–1804, 2005.
5. Chu, Q.-X. and M. Hou, "An H-shaped harmonic suppression active integrated antenna," *International Journal of RF and Microwave Computer-aided Engineering*, Vol. 16, No. 3, 245–249, May 2006.
6. Kim, H. and Y. J. Yoon, "Microstrip-fed slot antennas with suppressed harmonics," *IEEE Transactions on Antennas and Propagation*, Vol. 53, No. 9, 2809–2817, September 2005.

A Reliable Lattice-Boltzmann Solver for Electrodynamics: New Applications in Non-linear Media

M. Mendoza[1] and J. D. Muñoz[2]

[1]ETH Zürich, Computational Physics for Engineering Materials, Institute for Building Materials
Schafmattstrasse 6, HIF, CH-8093 Zürich, Switzerland
[2]Simulation of Physical Systems Group, Ceiba-Complejidad, Departamento de Fisica
Universidad Nacional de Colombia, Crr 30 # 45-03, Ed. 404, Of. 348, Bogotá D.C., Colombia

Abstract— Hereby, we present a recently developed 3D Lattice-Boltzmann solver for the simulation of Maxwell equations in materials. The model allows for both dielectrics and conductors with realistic parameters and simulates the most diverse electromagnetic problems (including microstrips and antennas) all with 2% accuracy. Actually, preliminary tests show that it is one order of magnitude faster than the original FDTD formulation by Yee to reach the same accuracy. To illustrate the power of the new solver, we simulate the propagation of electromagnetic waves through a non-linear and non-dispersive medium. The model constitutes, therefore, a valuable alternative to compute electromagnetic fields in complex systems.

Testing and Finite Element Modeling of Sample Holders for Dielectric and Magnetic Constant Measurements of Nano-scale Powders

Szilvia Nagy[1], **András Fehér**[1], **and C. Rabe**[2]

[1]Department of Telecommunications, Széchenyi István University, H-9026 Gyõr, Egyetem tér 1, Hungary
[2]Department of High Frequency Technique, Hochschule fur Telecommunikation Leipzig
Leipzig, Gustav-Freytag-Strasse, Germany

Abstract— Since more and more nano-scale objects are applied in everyday life, there is a great demand for determining the electromagnetic properties of such materials. The measurement methods for these properties are usually developed for bulk materials or planparallel objects, and mostly not applicable for such small-scale samples like nano films or powders. The amount and the dimension of such materials makes most of the large-scale methods unusable.

For powders a sample holders was built with a press for generating the specimens. The specimen holder is modeled with a finite element package, determining the S-parameters of various setups and various size samples. The calculated results are tested by network analyzer measurements, with samples of various location, dislocation and air-holes between the sample and the sample holder.

Developing Sample Holders for Measuring Shielding Effectiveness of Thin Layers on Compound Semiconductor Substrates

Sz. Nagy and A. Fehér
Department of Telecommunications, Széchenyi István University, H-9026 Győr, Egyetem tér 1., Hungary

Abstract— Wavelet or multiresolution analysis (MRA) is widely applied in advanced data compression algorithms, solving differential equations, and some approaches have already applied this technique in describing electromagnetic fields. The main advantage of the application of MRA is its adaptivity and flexibility. Since the details of the electromagnetic field are not distributed equally over different parts of the system (i.e., the description of some parts need finer details, while others are easily represented at low resolution level), locally different resolution levels can be applied. Wavelet based adaptive solution possibilities of differential equations of electromagnetic field are investigated in the followings. The adaptivity of the method means in this case, that the refinement level of the solution can be increased locally, if the accuracy needs it, during the calculations.

The applicability of the eigenvalue-type differential equation solving method is illustrated by solution of microwave wave-equations of cavity resonators.

Dissipative Losses Evaluation in Magnetic Power Devices with Litz-wire Type Windings

C. Carretero[1], **R. Alonso**[2], **J. Acero**[1], **Ó. Lucía**[1], **and J. M. Burdío**[1]

[1]Departamento de Ingeniería Electrónica y Comunicaciones, Universidad de Zaragoza, Spain
[2]Departamento de Física Aplicada, Universidad de Zaragoza, Spain

Abstract— Power electronics systems usually drive medium to high levels of electrical energy. Presently, Switched-Mode Power Supplies (SMPS) have been extensively used to improve the system performance. Additionally, working frequencies have been gradually increased in order to reduce device sizes. As a consequence, the optimization of different components required to obtain an appropiate efficiency and safety operation conditions has become more difficult.

This work deals with the analysis of the power losses in the magnetic devices, focused on those originated in the windings. The winding power losses can be classified into two different categories: conduction and proximity losses. The first ones are due to currents driven by the windings which are normally made with a low resistivity material, e.g., copper or aluminum, including skin effects. The second ones, proximity losses, are associated with currents induced because the windings are immersed in a magnetic field, and may become more important than the conduction losses at high frequencies, specially, for windings made with a large cross-section area solid wire. The last issue may be partly overcome by using litz wires which consist of multiple small cylindrical strands properly braided to achieve the equivalence among them.

Previous papers evaluates conduction and proximity winding losses by using analytical expressions developed considering an infinite-length cylindrical strand with radius r_0 made of an electrical conductor inside a medium with vacuum properties and exposed to a uniform longitudinal electric field $\mathbf{E}$ and a uniform transversal magnetic field $\mathbf{H_0}$ [1]. In this paper, both expressions are derived from the general solution of the diffusion equation expressed in a cylindrical coordinate frame which describes the magnetic vector potential $\mathbf{A}$. In this solution, radiation has been neglected because the quasi-static approach can be applied. A general solution for the equation is provided in [2] by means of an infinite set of eigenfunctions. Applying correct boundary conditions, both expressions emerged as the zero order solution for the magnetic vector potential longitudinal component A_z and the first order solution for the magnetic vector potential azimuthal component A_φ, respectively. Additionally, a close relationship between the ratio r_0/δ, where r_0 is the strand radius and δ is its penetration depth, and both types of power losses are established, and, as a consequence, the frequency dependence is completely considered by means of the penetration depth δ.

Finally, the expressions derived have been experimentally validated for a ring-type coil composed of several turns of a litz wire by means of a comparison between the frequency dependent resistance associated with the power losses in the winding calculated and experimental measurements.

REFERENCES

1. Acero, J., et al., "Frequency-dependent resistance in litz wire planar windings for domestic induction heating appliances," *IEEE Trans. Power Electron.*, Vol. 21, No. 4, 856–866, 2006.
2. Rothwell, E. J. and M. J. Cloud, *Electromagnetics*, CRC Press, Boca Raton, 2001.

The Minimum Phase Nature of the Transfer Function of the Impulse Radiating Antenna

J. S. McLean[1], **R. Sutton**[1], **and H. Foltz**[2]

[1]TDK R&D Corp., USA
[2]University of Texas — Pan American, USA

Abstract— The Impulse Radiating Antenna, a reflector antenna employing a TEM feed [1, 2], has been shown to provide excellent time-domain pulse reproduction on its principal axis; more specifically as stated in [1, 2], "a step-like signal into the antenna gives an approximate delta-function response in the far field." Such pulse reproduction requires satisfaction of the distortionless transfer function criterion. Distortionless transfer functions are a small subset of a more general group, minimum-phase transfer functions. When a minimum-phase network exhibits a transfer function magnitude which is nearly constant with frequency, its phase function necessarily satisfies the distortionless transfer function criterion; however, many systems exhibiting flat or nearly flat transfer functions are not minimum-phase. A compelling example of a broadband, non-minimum phase antenna is the Log-Periodic Dipole Antenna (LPDA), which exhibits a nominally flat magnitude, but which deviates greatly from minimum phase behavior [3].

The Impulse Radiating Antenna very nearly satisfies the distortionless transfer function criterion and thus is very nearly minimum phase in the frequency domain. However, the miniscule departure of its transfer function from minimum phase is quite interesting. Close examination of the time domain response of the Impulse Radiating Antenna reveals a pre-pulse as well as a long shallow tail following the main pulse [1, 2]. The pre-pulse has been shown to be step-like in the time domain. It radiates from the TEM feed structure and necessarily precedes the main pulse from the reflector. An antenna with a frequency-domain transfer function (as defined in [4]) of unity for all frequency would generate an impulsive electric field in the far field in response to a step input. However, any practical, finite-sized antenna must exhibit at least one zero in its transfer function at DC. Thus, the entire time domain response must average to zero. In [1, 2] some discussion is given concerning how if the area of the pre-pulse could be made to equal that under the main impulse (thus giving zero DC average) then the tail of the response would be small. The area of the pre-pulse is tailored by adjusting the characteristic impedance of the TEM feed of the Impulse Radiating Antenna. Thus, the canonical or ideal response of the Impulse Radiating Antenna is a step followed immediately by an impulse of equal area:

$$h(t) = A\{\Delta t\delta(t) - [u(t) - u(t - \Delta t)]\}.$$

The particular Impulse Radiating Antenna characterized here, the Farr Research IRA-3, exhibits a very good on-axis, time-domain response with a very minimal tail as can be clearly seen in the data in Figure 1 which depicts the on-axis, time-domain response of the IRA-3.

The minimum-phase quality of the transfer function of an antenna is intimately associated with the propagation of energy through the system. A minimum-phase transfer function is obtained when there is equivalently a single path through the network or system. It was shown in [5] that the broadband, double-ridged horn is very nearly minimum phase on its principal axis, but deviates from this condition off-axis. It was surmised that this was due primarily to interference between the direct radiation from the horn's aperture and fields diffracted by the edge of the horn. In [6, 7], it was shown that an asymmetric or half TEM horn such as the Farr Research TEM-1 exhibits a minimum phase response on its principal axis as well as off axis in the E-plane for angles below the ground plane. This is because below the ground plane the radiation is essentially entirely due to diffraction from the edge of the ground plane and hence a single source. In [6, 7] a "thought experiment" was carried out in which the minimum phase function derived from the magnitude of the transfer function via a Hilbert transform was used to generate a time response via an inverse Fourier transform. It was seen that in off-axis directions in the E-plane (where the frequency-domain transfer function was not minimum phase due to interference from diffracted energy from the horn top plate and the ground plane) in the time-domain response associated with the minimum phase function, the precursors to the main pulse were transposed to the opposite side of the main pulse thus providing a clean onset to the main pulse. A similar computation was carried out here. The complex frequency domain transfer function of a the Farr IRA-3 Impulse Radiating Antenna was measured in a fully anechoic chamber using a automatic vector network analyzer and a Farr Research TEM-50 horn, for which the transfer function had previously been

determined. The time-domain response was computed from the measured transfer function. Additionally, the minimum phase function associated with magnitude of the measured transfer function was computed. This minimum phase transfer function was then used to compute a second time-domain response. Both time-domain responses are plotted in Figure 1. It can be seen that in the time-domain response computed from the minimum phase function, the step associated with the radiation from the feed is transposed such that it occurs immediately *following* the main impulse. This behavior can be qualitatively explained in terms of a simple model based on rays representing major sources of radiation. In general, the frequency-domain minimum-phase criterion will be satisfied only if the time-domain field from the strongest radiation source is the first to arrive at the observation point. Enforcing the minimum phase condition in the frequency domain re-orders the time-domain response such that the main impulse is first. In this paper we explore the physical interpretation of the minimum phase transfer function and its application to antennas intended for time-domain pulse reproduction.

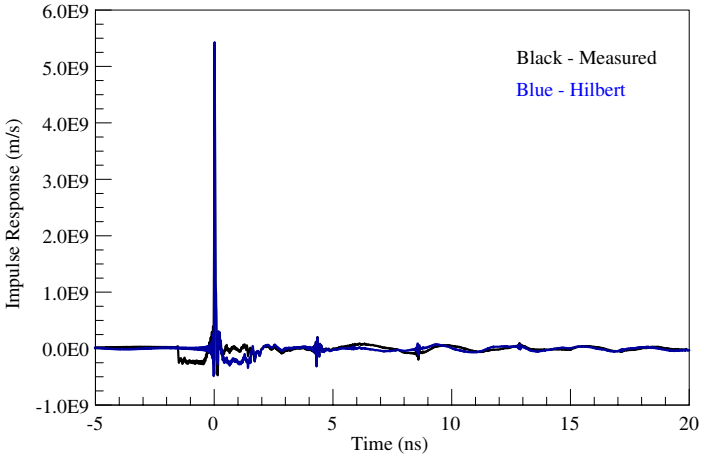

Figure 1: The time domain transfer function of the Impulse Radiating Antenna as derived from frequency-domain data measured in an anechoic chamber (black) and the time domain response derived from the minimum phase transfer function associated with the original measured transfer function (blue). Note that the rectangular pre-pulse the precedes the main pulse in the measured data is transposed such that it follows the main pulse in the response derived from the minimum phase transfer function.

REFERENCES

1. Baum, C. E., E. G. Farr, and D. V. Giri, "Review of impulse-radiating antennas," Chapter 12, *Review of Radio Science 1996–1999*, W. S. Stone, ed., Oxford University Press, 1999.
2. Baum, C. E., E. G. Farr, and D. V. Giri, "Review of impulse-radiating antennas," *URSI General Assembly*, Toronto, Canada, Aug. 1999.
3. McLean, J. S. and H. Foltz, "Minimum-phase/all-pass decomposition of LPDA transfer functions," *Proc. of the IEEE International Conference on Ultra-Wideband (ICUWB)*, Vancouver, Canada, Sep. 2009.
4. McLean, J. S., R. Sutton, A. Medina, H. Foltz, and J. Li, "The experimental characterization of UWB antennas," *IEEE Antennas and Prop. Magazine*, Vol. 49, No. 6, 20–30, Dec. 2007.
5. McLean, J. S., H. Foltz, and R. Sutton, "The directional dependence of the minimum-phase property of the antenna transfer function," *Proc. Loughborough Antenna Conference*, Loughborough, UK, Nov. 2009.
6. McLean, J. S., A. Medina, R. Sutton, and H. Foltz, "Directional dependence of the minimum phase property of the TEM horn transfer function," *AMEREM Conference*, Toronto, Canada, Jul. 2010.
7. McLean, J. S., A. Medina, R. Sutton, and H. Foltz, "Directional dependence of the minimum phase property of the TEM horn transfer function," Submitted to UWB-SP, 2010.

High-power Mesoband Switched Oscillators and Their Integration into Antennas

D. V. Giri
Pro-Tech, 11-C Orchard Court, Alamo, California 94507-1541, USA

Abstract— High-Power Electromagnetic (HPEM) systems can be classified into 4 groups based on their bandwidth, outlined in Table 1.

Note that this terminology is consistent with the formal IEC 61000-2-13 Standard, entitled "EMC, High-power electromagnetic (HPEM) environments — radiated and conducted".

One of these groups is the Mesoband systems with percentage bandwidths (pbw) in the range of 1 to 100%. In this paper, we describe several such mesoband systems (sources and antennas) starting with a system called MATRIX which was integrated into a half-paraboloidal reflector antenna. Based on the switched oscillator design in MATRIX, we outline the problem of designing, fabricating switched oscillators at four different frequencies, 200 MHz, 300 MHz, 400 MHz and 500 MHz. These oscillators are quarter wavelength long coaxial transmission lines with a nitrogen spark gap switch at one end. Two of these oscillators (200 MHz and 500 MHz) have been fabricated with a charge voltage of 30 kV. These two oscillators are modeled using PSpice and their output into a 100 Ω load is estimated and tested by fabricating a 100 Ω transmission line. The switched oscillator has been integrated into a modified commercial helical antenna with a bandwidth of 400 MHz to 600 MHz. Measurements have been made of the S_{11}, voltage into the antenna and also the radiated transient fields. Such mesoband systems are useful in evaluating the susceptibilities of certain electronic equipment.

Table 1: IEME Classification based on bandwidth.

Band type	**Percent bandwidth** $pbw = 200\left(\frac{br-1}{br+1}\right)(\%)$	**Bandratio *br***
Narrow	$< 1\%$	< 1.01
Moderate	$1\% \leq pbw \leq 100\%$	$1.01 \leq br \leq 3$
Ultra-moderate	$100\% < pbw < 163.64\%$	$3 < br < 10$
Hyperband	$163.64\% \leq pbw < 200\%$	$br \geq 10$

Session 4A8
Electromagnetic Theory

The Study on Electromagnetic Force Induced Vibration and Noise from a Normal and an Eccentric Universal Motors

K. Shiohata[1], **R. Kusama**[2], **S. Ohtsu**[3], **and T. Iwatsubo**[4]

[1]Ibaraki University, 4-12-1 Nakanarusawa, Hitachi, Ibaraki, Japan
[2]Toyota Ltd, Japan
[3]Yamagata, Hitachioomiya, Ibaraki 319-3111, Japan
[4]Kansai University, Japan

Abstract— There are many harmonic components in the electromagnetic force caused by electrical motors. The harmonic components induce the structural vibration and noise, frequently. The unbalanced electromagnetic pull force is generated between the rotor and the stator when the rotor is not corresponding to the center of the stator, that is, eccentric in the electrical motor. In the paper, first, the harmonic components of electromagnetic force caused from a normal and an eccentric universal motor are discussed numerically. Then, the effect of the difference of the harmonic components of electromagnetic force caused from a normal and an eccentric motor on the structural vibration are discussed numerically. From the numerical simulation, the spectrum distribution is different in the space region between a normal and an eccentric motor. And the 12th time order components of electromagnetic force and an electromagnetic vibration and noise of eccentric motor are larger than those of a normal motor.

Engineering Students' Conceptual Understanding of Electro- and Magnetostatics

Johanna Leppävirta, Henrik Kettunen, and Ari Sihvola
Department of Radio Science and Engineering
Aalto University School of Science and Technology, Finland

Abstract— At the university level, the teaching of engineering students is easily focused mostly on the development of procedural knowledge, that is, formulating and solving problems mathematically. Another very important factor associated with the enhancement of engineering skills is the conceptual knowledge, the actual comprehension of the physical concepts and the relations between them. Prior research has revealed that academically successful engineering students often lack deep understanding of the basic concepts and principles that underlie their training areas [1]. The aim of the study was to assess undergraduate engineering students' conceptual knowledge of electro-and magnetostatics and examine how this knowledge would change after instruction.

The Conceptual Survey of Electricity and Magnetism (CSEM) [2] multiple-choice test was administered as a pre- and post-test to students (cumulative $N = 233$) enrolled on an elementary course on electromagnetics (Static Field Theory) at Aalto University School of Science and Engineering, Finland. The CSEM was translated into Finnish and only the questions considering static fields were chosen. The CSEM was first applied in autumn 2007 and was administered again in autumn 2010. The latter post-test has not yet been performed at the time this abstract is written.

In 2007, the total pre-test score was 57% (electrostatics 62%, magnetostatics 45%) and the posttest score 67% (electrostatics 72%, magnetostatics 54%) showing a slight increase in the test results after the course. In 2010, the pre-test score was 59% (electrostatics 64%, magnetostatics 45%). The pre-test results indicate that the level of preliminary knowledge of the students was quite equal in both years. Moreover, the concepts of magnetostatics constantly seem to cause more difficulties than those of electrostatics. Surprisingly, it was found in 2007 that the correlation between the students' conceptual and procedural knowledge was quite low [3]. For example, the performance in the homework exercises during the course did not explain the success in the CSEM post-test at all. The findings suggest that more instructional time should be spent on mathematically and conceptually demanding magnetostatics. Furthermore, we need to broaden the view of what type of knowledge is valued and assessed in engineering education. These results encourage us to develop and introduce new instructional practices for enhancing conceptual understanding of students during elementary engineering courses.

REFERENCES

1. Taraban, R., E. E. Anderson, A. DeFinis, A. G. Brown, A. Weigold, and M. P. Sharma, "First steps in understanding engineering students growth of conceptual and procedural knowledge in an interactive learning context," *J. Eng. Educ.*, Vol. 96, No. 1, 57–68, 2007.
2. Maloney, D. P., T. L. O'Kuma, C. J. Hieggelke, and A. Van Heuvelen, "Surveying students' conceptual knowledge of electricity and magnetism," *Phys. Educ. Res., Am. J. Phys. Suppl.*, Vol. 69, No. 7, S12–S23, 2001.
3. Leppävirta, J., H. Kettunen, and A. Sihvola, "Complex problem exercises in developing engineering students' conceptual and procedural knowledge of electromagnetics," *IEEE Trans. Educ.*, 2010, DOI: 10.1109/TE.2010.2043531 (Early access).

A Physical Model of Electro-magnetism for a Theory of Everything

M. J. Underhill
Underhill Research, UK

Abstract— The objective is to link Electro-Magnetism or Electro-Magnetics (EM) to the rest of physics for a Theory of Everything (ToE). Mathematics describes, and does not dictate the physics. Here it is chosen and redefined to agree with the observed physics of the proposed EM transmission line models. Maxwell's Equations are thus significantly revised. An outcome is improved EM simulation requiring no matrix inversion.

The Local Ether Four Transmission Line Model of EM: The chosen physical model is two low-pass and high-pass pairs of co-located transmission lines in a 'local ether'. One LP/HP pair represents conventional and electric displacement current, with electric vector potential. (For this pair E is lamellar and H is solenoidal.) The other pair represents magnetic displacement current and magnetic vector potential. (For this pair H is lamellar and E is solenoidal.) In free space the line pairs have equal velocity but characteristic impedance differing by a few percent. The 'local ether' properties are given by complex, frequency dependent, values of ε and μ along the direction of power flow. E and H are redefined as electric and magnetic vector potentials and are analogues of voltage on the lines. D and B are redefined as electric and magnetic vector charge densities respectively. The electric and magnetic displacement current densities are defined as 'bi-vectors' with one vector component in the D or B field direction, and the other vector component in the direction of current flow. The current magnitudes are obtained by equating the energy of the currents to the energy of the charges (energy conservation). The currents are time domain Hilbert transforms of the charges, and vice versa. For a travelling wave the currents and charges are co-local. For standing waves the currents and charges are a quarter wavelength apart. The local ether acts as a focusing lens for receiving (wire) antennas. Positive quadrature potential of a current indicates radiation. Negative quadrature potential of a current indicates reception. The model also explains the anomalous 'wave-tilt' (reversed at low frequencies) found over real ground.

EM Model Critical Frequency: The low-pass lines are operative predominantly below 47.75 MHz and the high-pass lines above $f_c = 47.75$ MHz. We find that at $f_c = 47.75$ MHz (or $\omega_c = 300$ Mrad/s), $Z_0 = 120\pi = \omega\mu_0 = 1/\omega\varepsilon_0$. For the low-pass electric line, the specific series inductance (per reciprocal unit area and per unit length) is equated to μ and the specific shunt capacitance (per unit area and per reciprocal unit length) is equated to ε. The specific series reactance is $j\omega\mu$ and the specific shunt susceptance is $j\omega\varepsilon$. The high pass electric line has specific series reactance of $1/j\omega\varepsilon$ and specific shunt susceptance of $1/j\omega\mu$. The magnetic transmission lines are duals of the electric lines.

Electro-Magnetic Coupling: In free-space we find that the **co-local electro-magnetic (EM) coupling** between the fields H and D/ε, and between H and B/μ is $\kappa = 1/2\pi$. This means that any field sensors for E, D, H, and B will always also measure respectively D, E, B, and H with reduced sensitivity of -16 dB. This also explains 'dark matter' properties. **Induction** is also a manifestation of **EM coupling**. Potentials (and potential gradients) are induced or created in the local ether surrounding charges and currents by a local induction process. Potentials also induce and create charges and currents. The induction strength is found to be inversely proportional to the square root of frequency. This form of EM coupling defines the profiles of evanescent waves, surface waves, photons, EM strings, and the edges of black holes.

Process Capture: Process capture is an observable fundamental law (originally seen in small tuned loop antennas). Overlapping distributed processes combine at any point according to the RSS (Root-Sum-of-the-Squares) law. The strongest process 'captures' and suppresses the weaker process. Over a short (coupling) distance the suppression is progressive. An outcome is that propagation at or around 47.75 MHz is likely to be initially metastable. Also we find bounded regions in space where one process is almost totally dominant. Analytic Region (AR) modelling is an outcome. It is fast, stable and robust, since no matrix inversion is required. Process capture explains observed 'ether dragging', and this leads to 'Continuous Relativity', which encompasses and joins Special and General Relativity. (Faster-than-light travel is possible.) Process capture reconciles Michelson-Morley results with a real physical ether.

Evanescent Wave Profiles.: EM wave equations are separated into travelling wave and evanescent wave parts. Two prototype evanescent wave profiles are proposed: $(1 - \exp(-\kappa_n/(f^{1/2}\mathrm{r}^n)))$, where $n = 1$ for potential around a source, and $n = 3$ for the profile of the 'substance' of a EM

string or the edge of a black hole. These profiles have finite size and no mathematical or physical singularities. The profile equations can be extended represent complex impedance around antenna surfaces and wires and absorption magnitude and height ($\propto 1/\sqrt{f}$) profile above real ground. EM strings have self-stable evanescent wave profiles. They have a single dominant line spectrum and obey a Schrödinger equation.

Matter and Dark Matter: All charges, currents and potentials have (self-) energy. Energy is 'substance' (charge or current) times potential and *is* gravitational mass. Ordinary matter has point-like atoms and substance dominates over self-potential. The self-potential has a time delay and an offset during acceleration, making inertial and gravitational masses equal. In dark matter the energy of the potential is greater than the substance energy. Dark matter is continuous and diffuse, and has very low inertia. Thermal radiation in space is dark matter. The Goubau single wire (non-radiating) transmission line displays the stable evanescent wave profiles of current filaments and proposed EM 'strings'. Photons are 'dark matter' EM string arrows. Particles are made from EM toroidal string loops of defined size, frequency and dimensionality. String and black hole densities are similar. String loops obey a Schrödinger equation.

Conclusion: The proposed EM transmission line model connects EM to the rest of physics. It allows all forces, all forms of energy, power, gravitational mass, inertial mass, relativity, the Hubble effect etc. to be defined in EM terms.

Space Constants of Auxiliary Waves

T. Koryu Ishii
Marquette University, Milwaukee, Wisconsin, USA

Abstract— Space for propagation of electromagnetic waves defined by permittivity, permeability and conductivity is considered. These constants are termed the space constants for convenience in this work. A space with homogeneous and isotropic space constants for the principal wave is found to be inhomogeneous and anisotropic for auxiliary waves. The principal wave is the electromagnetic wave which is originally launched into space for utilitarian purposes. The auxiliary waves are non-principal waves associated with the principal wave. The auxiliary waves are generated by the principal wave [1, 2]. Principal waves considered in this study are uniform plane waves of both vertical and horizontal polarizations. Various sets of space constants are derived for auxiliary waves based on the propagation constant or wave impedance and polarizations [1, 2].

In this investigation, validity of space constants of auxiliary waves is examined by cross-checking propagation constant, wave impedance, and phase velocity under the same polarization. For example, when space constants based on the propagation constant of vertically polarized auxiliary waves are substituted in a generic equation of wave impedance, a correct wave impedance of vertically polarized auxiliary waves is obtained. When space constants based on wave impedance of horizontally polarized auxiliary waves are substituted in a generic equation of propagation constant, a correct propagation constant of horizontally polarized auxiliary waves is obtained, and this process can be repeated for other cases.

This approach also suggests the existence of a new set of wave impedance for auxiliary waves against wave impedance of the principal wave under a known set of space constants. As a specific numerical example, space constants of free space for auxiliary waves are studied. Space constant pattern of free space for an auxiliary wave is plotted. This plot shows that, although the space constants of free space for the principal wave are homogeneous and isotropic, space constants of free space for auxiliary waves are indeed inhomogeneous and anisotropic.

REFERENCES

1. Ishii, T. K., "Wave impedance of vertically polarized auxiliary waves," *Marquette University Microwave Engineering Seminar*, Milwaukee, Wisconsin, USA, September 7, 2007.
2. Ishii, T. K., "Wave impedance of horizontally polarized auxiliary waves," *Marquette University Microwave Engineering Seminar*, Milwaukee, Wisconsin, USA, January 25, 2008.

Characteristic Equations of Strip-slotted Structures

Seil Sautbekov and Gulnar Alkina
Eurasian National University, Kazakhstan

Abstract— This paper deals with further development of Wiener-Hopf method for obtaining the characteristic equation which follows from the solution of the boundary value problem of electromagnetic waves diffraction on fine strip-slotted structures. The strip or an infinite grating is chosen in return for strip-slotted structures. The boundary value problem is consecutively solved by reducing to the system of singular boundary integral equations, then to the system of the second kind Fredholm equations, which effectively is solved by reducing to a system of the linear algebraic equations with the help of the etalon integral and of saddle point method. Setting the determinant of a system of the algebraic equations equal to zero, we find a characteristic equation, which determines the eigenfrequencies of the structures.

Self-field Theory a Mathematical Description of Physics

A. H. J. Fleming
Biophotonics Research Institute, Melbourne, Australia

Abstract— SFT is a new description of electromagnetic interactions applying across physics. At its heart are bispinorial motions for both the electromagnetic fields and the interacting particles. SFT is intimately related to quantum theory; instead of the single inequality uncertainty relationship, there are two exact equations one applying to electric currents, the other to magnetic currents. SFT is formulated in terms of the E- and H-fields rather than the potentials The mathematics of SFT applies to the 1st order Maxwell Lorentz equations rather than the 2nd order Lagrangian formulation. It has been used to solve a simple Bohr-like model of the hydrogen atom, obtained an analytic estimate for the mass of the photon, and provided the first glimpse of structure within the photon. This may yield an organizational structure for bosons reminiscent of the chemical table first noted by Mendeleev in 1860 via a two-dimensional array of elemental properties. The self-field formulation obtains an analytic expression for Plancks number providing a basis for its understanding as a variable of motion applying equally to the electron, the proton and the photon. SFT appears to apply equally to cosmology as to sub-photonic physics.

REFERENCES

1. Fleming, A. H. J., "Electromagnetic self-field theory and its application to the hydrogen atom," *Physics Essays*, Vol. 18, No. 3, 265–285, 2005
2. Fleming, A. H. J., "Self-field theory, analytic spectroscopy of the ordinary photon," *Proc. 2nd Electromagnetics Health and Environment Intl. Conf.*, Wroclaw, Poland, 18–23, 2007.
3. Fleming, A. H. J., "Self-field theory — Biodiversity may be a resonance process," *PIERS Proceedings*, 828–831, Cambridge, USA, July 5–8, 2010.
4. Fleming, A. H. J., "Self-field theory — A possible gravitational structure for galaxies," *PIERS Proceedings*, 823–827, Cambridge, USA, July 5–8, 2010.
5. Fleming, A. H. J., *Self-Field Theory — A New Mathematical Description of Physics*, Pan Stanford Publishing, to be published 2010.

Self-field Theory: Cosmological and Biological Evolution May Be Linked

A. H. J. Fleming
Biophotonics Research Institute, Melbourne, Australia

Abstract— Recently Self-Field Theory (SFT) was used to propose a link between cycles of biodiversity and galactic gravitational structure. This hypothesis provides a new form of gravitation applicable to galaxies different to solar systems that includes both photons and phonons. According to SFT photons and phonons react to form gluons in regions where the energy density is sufficiently high. The Maxwell-Lorentz equations appear able to be modified to provide a Maxwellian mathematics applicable to strong nuclear regions. Consequently, solidification can occur in galactic structures corresponding to findings of fairly constant galactic orbital speed variation with radial distance known since the 1930's. Universal expansion follows the work of Hubble in the 1920's in identifying a redshift applying to matter within the Universe. Biological evolution may correlate with cosmological evolution. It is known that the first simple forms of life around 4 billions years ago in the case of our own Milky Way Galaxy had single-celled structures. It was around this point in cosmological time that the Solar System is thought to have first formed. The small size of early proto-life forms and their bulk modulus relative to mammals corresponds to the fact that the energy density within the early Milky Way Galaxy would have been relatively higher than during later epochs when mammals of varying size evolved. Life-forms would be expected to grow larger and be more solidified via phonon resonance within the evolving galaxy as the photon energy density fell with inflation. Thus there may be an identifiable correspondence (perhaps similar to dendrochronology) between the phylogenetic tree of life and the inflationary processes of cosmological evolution into gravitational structures able to sustain the various life-forms.

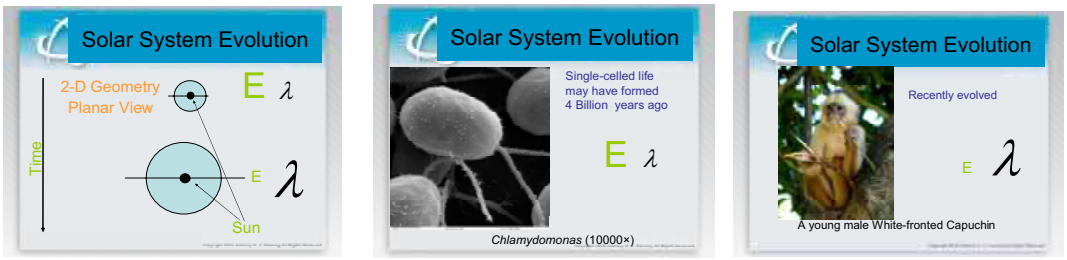

(a) (b) (c)

Figure 1: (a) Solar system grows in size with time. (b) Early life forms are small. (c) While recent species are relatively large.

REFERENCES

1. Fleming, A. H. J., Electromagnetic self-field theory and its application to the hydrogen atom," *Physics Essays*, Vol. 18, No. 3, 265–285, 2005.
2. Fleming, A. H. J., "Self-field theory, analytic spectroscopy of the ordinary photon," *Proc. 2nd Electromagnetics Health and Environment Intl Conf.*, 18–23, Wroclaw, Poland, 2007
3. Fleming, A. H. J., "Self-field theory-biodiversity may be a resonance process," *PIERS Proceedings*, 828–831, Cambridge, USA, July 5–8, 2010.
4. Fleming, A. H. J., "Self-field theory — A possible gravitational structure for galaxies," *PIERS Proceedings*, 823–827, Cambridge, USA, July 5–8, 2010.
5. Fleming, A. H. J., "Self-field theory — A new mathematical description of physics," Pan Stanford Publishing, 2010, to be published.

Self-field Theory and General Physical Uncertainty Relations

A. H. J. Fleming[1], **V. N. Matveev**[2], **and O. V. Matvejev**[2]

[1]Biophotonics Research Institute, Melbourne, Australia
[2]Sinerta Closed Joint-Stock Company, Vilnius, Lithuania

Abstract— The equations of Self-Field Theory (SFT) applying to the hydrogen atom are almost identical to the inequality relationship of Heisenberg's Uncertainty Principle (HUP), the only differences being that the inequality sign of HUP is replaced by an equality relationship and there being two such equations in SFT. The duality is due to both the electric and magnetic currents forming the bispinorial motions of the electron and proton. This relativistic double motion can be compared with the single rotations of the Bohr Theory. In this regard SFT completes the Bohr Theory solution of the hydrogen atom. Although it has revealed a photonic level interaction within and between atoms SFT is seen as a mathematics that applies across physics and not just at the atomic level. Various SFT applications have emerged including a gravitational model for the Galaxy, and a new mathematics applying to the weak and strong nuclear forces. Recently Matveev and Matvejev have uncovered a general macroscopic form of HUP. A macroscopic rod incorporating a pair of synchronized clocks and a macroscopic object performing the function of an ideal physical clock were examined and its motions found to take the form $\Delta p_x \Delta x \geq h$ and $\Delta E \Delta t \geq h$, where h is Planck's constant where the precision and properties of all clocks must be considered. This general form of HUP provides a mathematical basis for the wide application of SFT. UP to the present time quantum theory has stood apart from macroscopic computations. Now quantum theory can be seen to be part of a more general mathematics applying to macroscopic domains.

REFERENCES

1. Hyland, G. J. and P. Rowlands (eds), *Herbert Frohlich FRS: A Physicist Ahead of his Time*, 2nd Edition, University of Liverpool, 2008.
2. Matveev, V. N., *Into the Third Millennium without Physical Relativity*, CheRo Publishing House, Moscow, 2000.
3. Matveev, V. N. and O. V. Matvejev, "General physical uncertainty relations as a consequence of the Lorentz transformation," Submitted to *Progress In Electromagnetics Research Symposium*, Marrakesh, Morocco, March 20–23, 2011.
4. Fleming, A. H. J., "Electromagnetic self-field theory and its application to the hydrogen atom," *Physics Essays*, Vol. 18, No. 3, 265–285, 2005.
5. Fleming, A. H. J., "Self-field theory, analytic spectroscopy of the ordinary photon," *Proc. 2nd Electromagnetics Health and Environment Intl Conf.*, 18–23, Wroclaw, Poland, 2007
6. Fleming, A. H. J., *Self-Field Theory — A New Mathematical Description of Physics*, Pan Stanford Publishing, to be published 2010.

General Physical Uncertainty Relations as a Consequence of the Lorentz Transformation

V. N. Matveev and O. V. Matvejev
Sinerta Closed Joint-Stock Company, Vilnius, Lithuania

Abstract— The uncertainty relations fall into the ranks of the most important quantum relations. It is believed that the uncertainty relation of momentum and coordinates, as well as the uncertainty relation of energy and time in practice are not observed in the macrocosm. The objective of the work at hand was to demonstrate the existence of general physical uncertainty relations that extend to macrobodies. A macroscopic object consisting of a rod equipped with a pair of synchronized clocks and a macroscopic object in and of itself performing the function of an ideal physical clock are examined. General physical relations are directly derived from Lorentz transformations for the case of the object's one-dimensional motion (along the X axis) — The uncertainty relation of the object's x coordinate and the projection of its impulse along the X axis, p_x, and the uncertainty relation of the object's observation time, t, and its energy, E. The relations take the form: $\Delta p_x \Delta x \geq H$ and $\Delta E \Delta t \geq H$. The H value in the relation has action dimensions and is dependent upon the precision of the object's clocks and/or upon the properties of the physical clock. Despite the interpretation of the concept of uncertainty being different from that in quantum mechanics, the relations derived in the limiting case with ideal physical clock take the form of $\Delta p_x \Delta x \geq h$ and $\Delta E \Delta t \geq h$, where h is the Planck constant.

REFERENCES

1. Tarbeyev, Y. V., V. A. Slayev, and A. G. Chunovkina, "Problems with using the international guide to the expression of uncertainty in measurement in Russia," *Izmeritelnaya Tekhnika*, Measurement Techniques, No. 1, 69–72, 1997.
2. European Society for Analytical Chemistry/International Cooperation on Traceability in Analytical Chemistry (EURACHEM/CITAC) Guide Entitled, *A Quantitative Description of Uncertainty in Analytical Measurement*, 2nd Edition, 2000. — Translated from the English, D. I. Mendeleyev, Russian National Metrology Research Institute (RNMRI), St. Petersburg, 2002.
3. Sukhanov, A. D. and O. N. Golubeva, *Lectures on Quantum Physics*, 54, Vysshaya Shkola, Higher School, Publishing House, Moscow, 2006.
4. Okun, L. B., *Advances in the Physical Sciences (APS)*, No. 178, 541–555, 2008.
5. Matveev, V. N., *Into the Third Millennium without Physical Relativity*, CheRo Publishing House, Moscow, 2000.

Complete Imitation of the Special Theory of Relativity by the Means of the Classical Physics

V. N. Matveev and O. V. Matvejev
Sinerta Closed Joint-Stock Company, Vilnius, Lithuania

Abstract— Modern electrodynamics is unthinkable without the special theory of relativity (STR). The relationship of Special Relativity with electrodynamics was reflected in the title of Einstein's revolutionary work in 1905. Since its introduction Einstein's special theory of relativity was not seen as a direct consequence of classical mechanics. For this reason, no serious attempts were undertaken to construct special theory of relativity on the principles of classical mechanics. **However formal manipulations are known, which allow, for instance, to receive Lorentz's transformations in acoustics, but they have no relation to the imitation of special relativity**. In the present work it is shown that a considerable part of relativistic effects can be imitated by means of elementary classical mechanics. On the base of classical mechanics the theoretical model is built describing the behavior in the liquid medium of the objects, which behave according to the formal laws of the special theory of relativity. The model-imitation is based on the consideration of two groups of barges on the surface of flat-bottomed pond. The model reproduces Lorentz length contraction, time dilation, relativity of simultaneity, Doppler effect in his symmetrical relativistic form, effects of the twins paradox. The model makes it possible to obtain the Lorenz transformations and to imitate the four-dimensional Minkowski space-time. All effects imitating the analogous effects of the special theory of relativity prove to be relativistic in form and absolute in substance. The relativity of the physical effects within the framework of the proposed model occurs as a consequence of denial of the existence of the medium, accompanied by the replacement of the fact of the inequality of the signal velocities in opposite directions in the moving medium with the assumption of the equality of these velocities.

REFERENCES

1. Einstein, A., "Zur elektrodynamik bewegter Körper," *Annalen der Physik*, IV. Jg. 17, 891–921, 1905.
2. Boss, B., "Lectures on mathematics," *The Equations of Mathematical Physics*, Vol. 11, Publishing House, Librocom, Moscow, 2008.
3. Matveev, V. N., *Into the Third Millennium without Physical Relativity*, CheRo Publishing House, Moscow, 2000.

Session 4P1
Microwave and Millimeter Wave Integrated Circuits Design

Effects of Hardware Impairments in Six-port Homodyne Receivers for Communication Systems

A. Moscoso-Mártir, **I. Molina-Fernández**, **and A. Ortega-Moñux**
Departamento de Ingeniería de Comunicaciones, ETSI Telecomunicación, Málaga University, Spain

Abstract— Modern wireless microwave receiver design demands increased bandwidth with reduced size and cost. Direct conversion receiver is better suited to monolithic integration than the heterodyne receiver [1]. Since its introduction in 1994 [2] direct conversion six-port receivers have attracted a considerable attention at microwave frequencies as they offer lower hardware complexity, lower LO power, and higher bandwidth as compared with other alternatives that make use of active mixers. Although several papers have studied the performance and features of six-port receiver with analog I/Q generation in multiple situations [3], up to the authors' knowledge, a complete study of the influence of six-port junction hardware impairments on receiver's performance, has not been reported yet. The focus of this paper is to make a detailed study of the performance degradation of analog I/Q generation six-port receiver due to hardware imperfections of the six-port passive junction (ideal square law power detector behaviour is considered throughout this work). Compact expressions are obtained and applied to various architectures comprised of 3 dB hybrids and power splitters (one of them shown in Fig. 1(a)), that give a deeper insight into the mechanisms causing their degradation due to hardware impairments. Furthermore, they allow to easily calculate Error Vector Magnitude and to set hardware specifications to fulfill the design requirements. Specific theoretical formulas are also presented to calculate Bit Error Rate degradation for a QPSK modulation scheme (see Fig. 1(b)). These formulas can be easily extended to other modulation techniques. These developed expressions are applied to compare different six-port receiver architectures and determine the component requirements to accomplish typical receiver specifications.

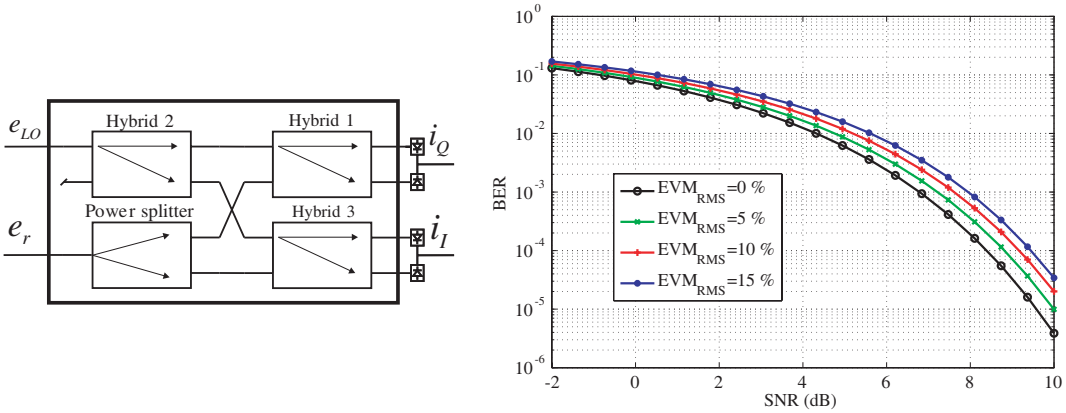

(a) (b)

Figure 1: (a) Typical six-port receiver architecture made by three hybrids and a power splitter. (b) Bit Error Rate in a six-port homodyne receiver for different Error Vector Magnitudes in a QPSK modulation scheme.

REFERENCES

1. Razavi, B., "Design considerations for direct-conversion receivers," *IEEE Transactions on Circuits and Systems II: Analog and Digital Signal Processing*, Vol. 44, No. 6, 428–435, Jun. 1997.
2. Li, R., R. G. Bosisio, and K. Wu, "A six-port digital millimeter wave receiver," *IEEE MTT-S International Microwave Symposium Digest*, 1994.
3. Henstschel, T., "The six-port as a communications receiver," *IEEE Transactions on Microwave Theory and Techniques*, Vol. 53, No. 3, 1039–1047, Mar. 2005.

Investigation on C-loaded Microstrip Line for Very Low Phase Shifting Small Size TL for S-band RF QFN Package

M. Aoutoul[1], **N. Healey**[1], **J. Kiwan**[1], **F. Bourzeix**[1], **B. Lakssir**[1], **and M. Essaaidi**[2]

[1]Moroccan Association for Scientific and Innovation Researches-Microelectronics, Rabat, Morocco
[2]Faculty of Sciences, Tetuan, Morocco

Abstract— RF packaging industry is gaining increasing interest due to extensive consumer's demand on microwave components for civilian RF and wireless industry as well as for military applications. A perfect electronic package is assumed to keep the chip functionalities unchanged. However, packaging processes and operating in microwave frequency range are still suffering because of electromagnetic phenomena such as reflections and signal retardation for high speed circuits.

Packaged microwave phase shifters are critical components in communication systems and phased array antennas. However, the conventional electronic packaging approach involves different interconnection techniques which are responsible of the introduced phase shift because of the inevitable parasitic wire bond inductance, for example, depending on the wire bonding width and length. To remedy this problem some techniques have been used to reduce the wire bonding effect such as multiple wire bond for RF inputs and outputs or the use of ribbon bonding technique. Those techniques can improve significantly the return loss and the insertion loss, but having transmission line with zero degree phase shifting is still a dream.

In this paper, we propose a novel interconnection technique for a flip-chip quad flat no-lead (FC QFN) package which can decrease the amount of the TL phase shift. The die RF I/O are connected to the package lead fingers by a small size, 1000 µm length, microstrip line loaded with a serial capacitor consisting of stacked fingers rather than interdigital fingers, known as C-loaded microstrip line, using a ceramic dielectric material. This technique can reduce the effect of transmission line inductance and, hence, reduces the related amount of the considered TL phase shift caused by the other electrical interconnections (i.e., Wire bonds).

The design approach has been guided by a circuital model using CST Design Studio before considering the equivalent layout distributed elements. The interdigital capacitor technique, which is widely used in RF transmission lines and filters, requires larger TL sizes (few millimetres). This is not the case for small size QFN packages. Therefore, the stacked fingers capacitor design we propose offers controllable capacitance through the fingers length, width and/or fingers number. Consequently, the phase shift can be also controlled.

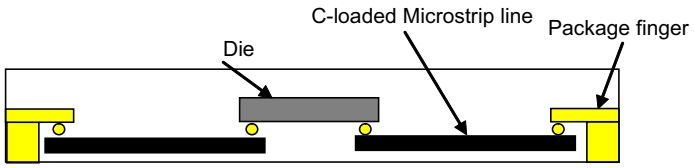

Figure 1: Envisaged FC QFN package with low phase shifting TL inside.

FET-based Frequency Multiplier S-MMICs up to 440 GHz

I. Kallfass[1, 2], **H. Massler**[2], **A. Tessmann**[2], **and A. Leuther**[2]

[1]Karlsruhe Institute of Technology, Institut für Hochfrequenztechnik und Elektronik, Karlsruhe, Germany
[2]Fraunhofer Institute for Solid State Physics, Tullastraße 72, Freiburg, Germany

Abstract— We report on the design and performance of frequency multiplier submillimeter-wave monolithic integrated circuits (S-MMICs) that operate up to 440 GHz. The S-MMICs are based on state-of-the-art metamorphic high electron mobility transistor technology (mHEMT) with gate lengths down to 35 nm and cutoff frequencies f_T and $f_{\max}$ of 550 and 700 GHz, respectively. A class-B FET doubler circuit achieves −14.6 dBm of output power at 400 GHz, when driven with 2.5 dBm input power at 200 GHz. The circuit could be measured in an output frequency range from 380 to 440 GHz, where it shows near constant output power. The circuit is designed in a grounded coplanar (GCPW) environment involving a two metal layer process on thinned 4" GaAs substrates. Ultra-compact transmission lines with a ground-to-ground spacing of 14 µm allow for conventional reactive impedance matching techniques. The S-MMIC's on-wafer characterization involves careful power level normalization taking into account losses in the coplanar measurement probes in WR-2 band (325–500 GHz). While output power is measured using an Erikson calorimeter, S-parameter measurements for probe characterization are carried out using Oleson WR-2 frequency extensions to a standard network analyzer. Further mHEMT-based frequency multiplier MMICs include broadband active multipliers-by-twelve into W-band (75–110 GHz) and frequency doublers to 200 GHz, completing a full MMIC-based multiplier chain for frequency generation up to 400 GHz.

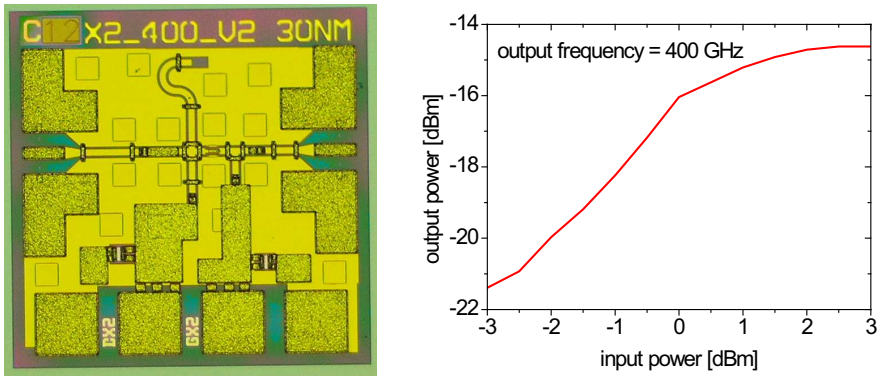

Figure 1: Chip photograph and on-wafer power measurement of a class-B FET frequency doubler to 400 GHz, realized in 35 nm mHEMT technology and achieving −14.6 dBm of output power.

Compact Non-degenerate Dual-mode Filter with Adjustable Transmission Zero

Abdel Fattah Sheta, Majeed Alkanhal, and Zeyad Alhekail
Department of Electrical Engineering and Prince Sultan Advanced Technologies Research Institute (PSATRI), King Saud University, P. O. Box 800, Riyadh 11421, Saudi Arabia

Abstract— Compact, light weight, low cost and high selective filters attract much attention for recent wireless systems. In many applications, sharp cutoff rate filter response is usually required. The conventional way to achieve such response is to use higher order filters which lead to large, complex, and expensive structures. However, sharp cutoff rate can also be achieved using transmission zero concept. In some cases, such as in cellular communications, microwave filters should be more selective on one side of the passband than the other. On other word, a transmit filter should have high attenuation in the receive band and a receive filter should have high attenuation in transmit band. For this case, transmission zero concept would be the best suited.

Non-degenerate dual-mode filter [1] has asymmetric frequency response with the transmission zero located on the upper stopband.

In this paper, two methods to control the filter transmission zero are proposed and investigated. The first is the use of open circuit stubs loading with appropriate stub lengths. The second is to control the position of the trasnmision zero electronically using varactor diode loading. The proposed structure is simply a dual-mode square-patch resonator, with four slots etched in a symmetrical shape loaded at opposite corners by open circuit stubs as shown in Fig. 1. The fields within the conventional square patch resonator can be expanded by the TM^z_{mn0} modes, where z is perpendicular to the ground plane. The two fundamental degenerate modes correspond to TM^z_{100} and TM^z_{010} and the first higher order mode is the TM^z_{110}. These three modes can be excited simultaneously by asymmetrical non-orthogonal feed lines. The resultant modes of the slotted patch can be considered as perturbed types of that of the unslotted square patch. The modes TM^z_{100} and TM^z_{010} have an electric wall along the diagonal between the non-feeding corners. However, the mode M^z_{110} has a magnetic wall along the same diagonal [1]. Therefore loading the patch at magnetic wall will affect only the resonance frequency of the mode TM^z_{110} (f_2) and has almost no effect on the resonance frequency of the modes TM^z_{100} and TM^z_{010} (f_1). The analysis is carried-out for a resonator designed on a Duroid dielectric substrate of 10.3 dielectric constant and 0.635 mm thickness. The dimensions of the simulated patch are $14 \times 14\,\mathrm{mm}^2$. IE3D simulator is used in the analysis. The transmission zero of the filter can be electronically controlled using varactor diodes loading mechanism. Varactor diodes can be connected directly at the patch corners or at the end of the stub. The varactor diode used for this application is the SMTD3001 silicon-based surface mounted structure that can be easily used up to 3 GHz. The diode can operate well in temperature range from $-65°$ to $150°$. The junction capacitance of the diode is approximately changes from 2.2 pF at 0 V reverse bias to about 0.6 pF at 30 V reverse voltage. A filter is designed and implemented and tested. The measured 3 dB bandwidth for the higher capacitance case is 320 MHz; from 2.28 to 2.6 GHz. For the lower capacitance case, the 3 dB bandwidth is 270 MHz; from 2.35 to 2.62 GHz. The midband insertion loss is about 1.8 dB for both cases which is more than the simulated results by about 1 dB. Transmission zeros are very close to the passband in the lower and upper band.

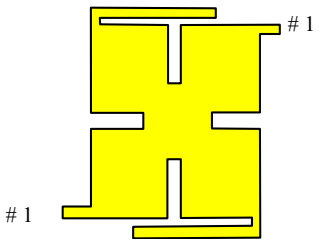

Figure 1.

ACKNOWLEDGMENT

This work is supported by the National Plan for Science and Technology Program- King Saud University, Research Grant: AV. 08-ADV210-2.

REFERENCES

1. Sheta, A. F., N. Dib, and A. Mohra, "Investigation of new nondegenerate dual-mode microstrip patch filter," *IEE Proc. — Microw. Antennas Propag.*, Vol. 153, No. 1, February 2006.

6×3 Microstrip Beam Forming Network for Multibeam Triangular Array

A. Novo-García[1], **M. Vera-Isasa**[1], **Javier García-Gasco Trujillo**[2], **and M. Sierra-Pérez**[2]

[1]Universidad de Vigo, Spain
[2]Universidad Politécnica de Madrid, Spain

Abstract— In satellite communications, large reflector antennas are usually the main element in the ground segment, but other designs with different configurations are also possible. GEODA [1] is a smart dome antenna composed of triangular arrays defined to receive signals from low orbit satellites. It is composed of 60 triangular panels, each of them divided in 15 subarrays of three circular patches referred to as cells. Nowadays, the feeding network for these cells is designed to obtain a phased array structure. Our aim is to design a beam forming network that could provide 6 simultaneous beams with the circular array of 3 elements.

In our paper, two networks based on Butler [2] and Shelton [3, 4] configurations have been designed, using both balanced and unbalanced hybrid couplers, and we have combined them to obtain a 6 inputs and 3 outputs structure which can be used to obtain 6 simultaneous beams. A set of three equations is presented to calculate the lengths of the transmission lines which connect the hybrid couplers of the networks, allowing a flexible design. This way, several structures with different lengths can be calculated, obtaining always the same phase relation at the outputs.

The 6×3 network has been simulated and its performance verified. Phase relations obtained at the outputs of the design can provide, with a triangular array of 3 elements, main beams in the azimuth directions $\phi = 0°$, $60°$, $120°$, $180°$, $240°$ and $300°$. A prototype is also expected to be built, measured and compared with simulations.

REFERENCES

1. Montesinos, I., M. Sierra-Perez, J. L. Fernandez, R. Martinez, and J. L. Masa, "GEODA: Adaptive antenna of multiple planar arrays for satellite communications," *3rd European Conference on Antennas and Propagation, EuCAP 2009*, 773–777, March 23–27, 2009.
2. Butler, J. and R. Lowe, "Beam-forming matrix simplifies design of electronically scanned antennas," *Electronic Design*, Vol. 9, 170–173, 1961.
3. Shelton, J. P. and K. Kelleher, "Multiple beams from linear arrays," *IRE Transactions on Antennas and Propagation*, Vol. 9, No. 2, 154–161, March 1961.
4. Shelton, J. P., "Multibeam, hexagonal, triangular-grid, planar arrays," *Antennas and Propagation Society International Symposium*, Vol. 3, 90–97, August 1965.

Comparative Study of Two Microstrip Beam Forming Networks for Multibeam Triangular Array

A. Novo-García[1], **M. Vera-Isasa**[1], **and M. Sierra-Pérez**[2]

[1]Universidad de Vigo, Spain
[2]Universidad Politécnica de Madrid, Spain

Abstract— In satellite communications ground segment, planar arrays have some advantages with respect to large reflector antennas, regarding their low manufacture and maintenance cost, low complexity and the ability to receive signals from several directions simultaneously. In order to use the last property, a suitable beam forming network is needed.

Butler matrix [1] has been widely used as feeding networks for linear and planar array antennas to obtain simultaneous beams. However, Butler networks are designed to allow only an odd number of inputs and outputs. Nevertheless, Shelton published some papers [2, 3] where a 3 inputs and 3 outputs network is presented. This configuration provides 3 simultaneous beams when it is used with an array of three elements. Some years later, Roederer and Maximo presented a circular structure of a microwave hybrid coupler with 3 inputs and 3 outputs [4]. This design consisted on a simple and concentric arrangement, with one ring inside another, which could provide the same response at the outputs as Shelton's network.

In our paper, we present a comparative study between a 3×3 hybrid coupler based on Roederer's design and a structure with three 2×2 hybrids like Shelton's network, where the lengths of the transmission lines have been calculated with a set of three equations in order to obtain the same phase relation at the outputs. Both circuits have been designed and simulated in microstrip technology. Their performances have been compared, and also design considerations such as size or flexibility have been taken into account. Prototypes of both networks are being constructed and will be measured to verify the results obtained in simulations.

REFERENCES

1. Butler, J. and R. Lowe, "Beam-forming matrix simplifies design of electronically scanned antennas," *Electronic Design*, Vol. 9, 170–173, 1961.
2. Shelton, J. P. and K. Kelleher, "Multiple beams from linear arrays," *IRE Transactions on Antennas and Propagation*, Vol. 9, No. 2, 154–161, March 1961.
3. Shelton, J. P., "Multibeam, hexagonal, triangular-grid, planar arrays," *Antennas and Propagation Society International Symposium*, Vol. 3, 90–97, August 1965.
4. Roeder, A. and M. P. C. Maximo, "Microwave hybrid coupler having $3 \times N$ inputs and $3 \times N$ outputs," United States Patent, Appl. Number 802685, Patent Number 5237294, 1993.

Automatic Design and 3D Electromagnetic Simulation of Sub-nH Spiral Inductors

L. Aluigi, **F. Alimenti**, **and L. Roselli**
Department of Information and Electronic Engineering, University of Perugia, Perugia, Italy

Abstract— Millimeter-wave radiometers are commonly employed in space-based scientific experiments ranging from the observation of the Earth's atmosphere to oceanographic studies, from the measurement of the Cosmic Microwave Background (CMB) to the detection of solar flares. Recently, there is a great interest of several space agencies to the development of miniaturized instruments in such a way as to meet the mission constraints imposed by the adoption of micro- and nano-satellites. From this point of view a great chance is offered by state-of-the-art silicon technologies which, in last years, have been used in millimeter-wave receiver design.

Exploiting these technologies and adopting the System-on-Chip (SoC) approach, highly miniaturized radiometric sensors can be developed. The advantages offered by SoC radiometers over conventional design, however, are not only limited to a significant size and mass saving. Because of the miniaturization, in fact, the power required by the temperature control system can also be significantly reduced. In the mean time, a rapid warm-up as well as the maintenance of highly stable circuit temperature is another strong point in favour of SoC radiometers. Finally, the thermal control system could take advantage from a temperature sensor and a micro-heater integrated in the same silicon chip used by the millimeter-wave front-end. The design of SoC millimeter-wave radiometers for space applications is a low documented research area and, up to now, no silicon circuits have been published. To fill this gap, the study of a two-stage Ka-band LNA (one of the most critical radiometer's building-blocks) has been carried out by our research group. The operating frequency is equal to 31.4 GHz, a channel widely used in the remote sensing of the Earth's atmosphere. The study has been carried-out exploiting a 250 nm SiGe BiCMOS technology.

For simultaneous noise and (input) power matching of the amplifier we used a general LNA design procedure that takes advantage of the scalability of the devices. The designed device has five inductors for input and output matching.

Because of the high input frequency, it was not possible to obtain the required sub-nH inductances from the inductors available in the design-kit library. The mean drawing-time of a custom inductor in a 3D EM simulator, once you have practiced it for several hours, is about half an hour, that means many hours spent in drawing, considering the fact that the designer needs successive optimizations to achieve the desired inductor's behaviour. For this reason, we decided to spend some days in programming. The result is a VbScript that automatically execute a series of simulator's commands. It generates the inductor, with vias and underpasses, in less than one minute. The script asks the user to provide the values he desires of the four parameters: w, s, N and d_{out}. We decided to use planar, octagonal, symmetric, and lying on the topmost metal (which is thicker than the others) inductors. The design flow is composed by the following steps: 1) the designer, using theory and equations for sub-nH inductors, decides on a set of four first-guess values to pass to the script: w, s, N, d_{out}. 2) The script automatically generates and simulates the structures with a custom polysilicon PSG in a full 3D EM simulator environment. Before building the coil, the script reconstructs the technology stack and fills the simulation environment with air. The result is a box with dimension proportional to the desired outer diameter of the coil, with the coil inside ready to be simulated. After the simulation the script presents the resulting graphs for Q, L and R. If there is a match with the expected values, it is possible to go to the final step. In our case, the simulated Q of the planar inductors at 31.4 GHz is 12–20 for 150–450 pH. 3) Automated extraction of the 2pi-model parameters to be used in the schematic editor and generation of the GDSII file to be used in the layout editor.

The tool we developed is very useful as there is currently no such thing in the integrated suites of software more commonly used. The designers then could gain much benefit from the use of this code that potentially can work with every technology. At present in fact, after using it with the 250 nm BiCMOS technology, we are adapting it for use with a 65 nm CMOS technology.

In presenting this procedure in detail, we will explain the scientific rationale and the equations used to underpin the choices made and thus showing the achievements and potentials.

A Novel Dual-mode Dual-band Bandpass Filter with DGS

Chang Chen[1], **Weidong Chen**[1], **and Zhongxiang Zhang**[2]

[1]Department of EEIS, University of Science And Technology of China, Hefei, Anhui 230027, China
[2]Department of PEE, Hefei Normal University, Hefei, Anhui 230061, China

Abstract— Bandpass filter is a key component for modern communication systems. Recently, quick developments in communication systems require the radio frequency (RF) devices operating in multiple separated frequency bands, such as working on 1800 MHz and 1900 MHz for GSM and WCDMA mobile communications. Therefore, there has been growing interest in design of dual-band bandpass filter. Taking advantages of small size, low cost and easy fabrication [1] various microstrip structures are widely applied for realizing dual-band filters. In [2–4], a stepped-impedance resonator (SIR) is used for the design of dual-band bandpass filter as it can easily control the second pass band frequency. In [5], a dual-band bandpass filter is achieved by cascading a broadband filter with a bandstop filter. Meanwhile, due to compact and flexible characteristics, defected ground structure (DGS) is widely used to introduce the bandstop performance by collocating with a transmission line [6] or bandpass performance by coupling with a transmission line [7], respectively in filter design.

As is well known, a dual-mode bandpass filter with elliptic response can be realized by using square loop structure [8]. In [9], dual-mode stacked-loop structure with stacked dielectric layers is designed to achieve dual-band performance and there is a good isolation between two closely adjacent passbands, but two dielectric layers make the design complicated. In this paper, by combining the square loop on top layer and the other loop constructed with DGS on the bottom layer, a novel and simple dual-mode dual-band bandpass filter is thus achieved, and only one dielectric layer is required, so the filter achieves almost 50% volume reduction and then the lower cost. Rather good agreement has been seen between the simulation and experiment results, which validate the design.

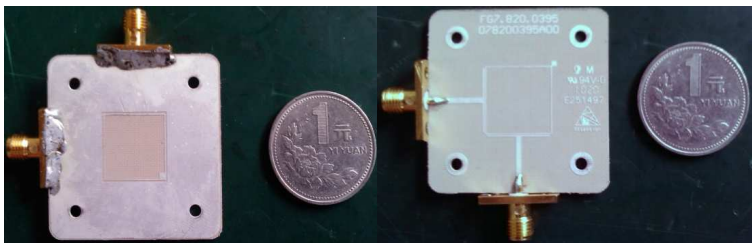

(a) (b)

Figure 1: Photographs of the filter sample.

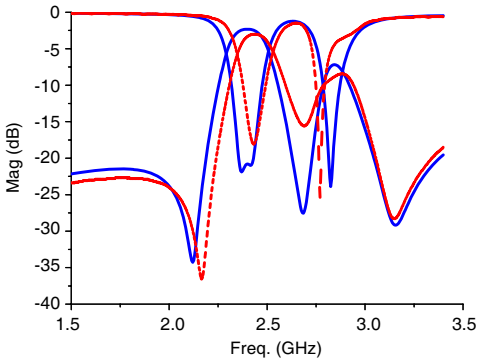

Figure 2: Simulation and experiment results.

Quasi-elliptic Wideband Bandpass Filter Using Grounded Coupled Lines and Chip Capacitor

T. Yasuzumi, M. Kamada, T. Uwano, and O. Hashimoto
Aoyama Gakuin University, Japan

Abstract— Wideband bandpass filters (WBPFs) with sharp attenuation, low insertion loss, and compact size have been paid attention in modern wireless systems. As one of the essential components in ultrawideband communication systems, the BPF with over 100% fractional bandwidth has been required.

This paper presents a novel WBPF composed of grounded coupled lines and a chip capacitor. Figure 1 illustrates a schematic of the proposed BPF. Figure 2 shows transmission characteristics when line separation g changes from 1.0 to 5.0 mm with the constant value of $l_1 = 5.9$ mm, $l_2 = 8.0$ mm, $W_1 = 0.2$ mm, $W_2 = 0.5$ mm and capacitance $C = 1.0$ pF. The results show that the BPF has quasi-elliptic function characteristics and the attenuation poles outspread when g increases. Figure 3 illustrates the flow of matching characteristics when C changes. Note that the filter works as 4-pole BPF by the existence of C. The parameters of the BPF was optimized and measured, and the results are shown in Figure 4. Its measured results have a low insertion loss, 140% fractional bandwidth, and good agreement with calculated ones.

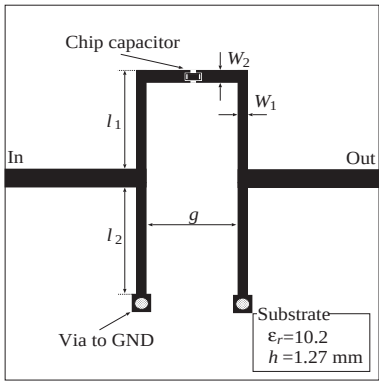

Figure 1: Schematic of the proposed wideband BPF.

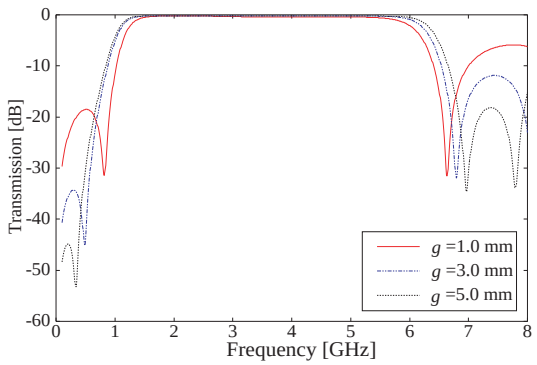

Figure 2: Transmission characteristics when g changes.

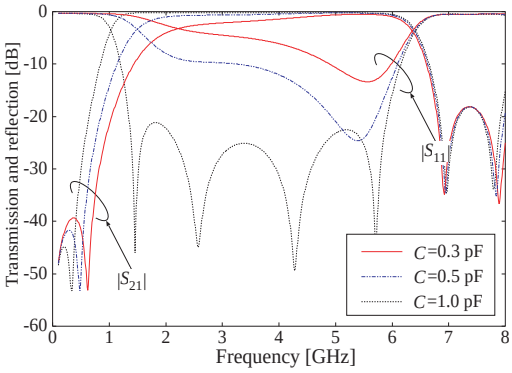

Figure 3: Transmission and reflection characteristics when C changes.

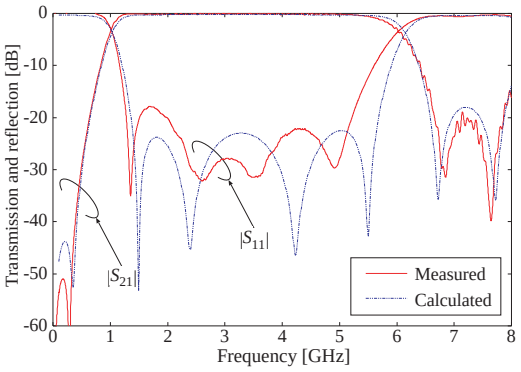

Figure 4: Measured and calculated results of the optimized BPF.

New Compact Dual-band Filter Using Common Resonator Sections and Double-diplexing Structure

Pu-Hua Deng[1], **Jyun-Hao Jheng**[2], **and Wen-Chi Kuo**[1]

[1]Department of Electrical Engineering, National University of Kaohsiung, Taiwan, R.O.C.
[2]Department of Graduate, Institute of Electrical Engineering
National University of Tainan, Taiwan, R.O.C.

Abstract— In this paper, a new compact size dual-band filter based on double-diplexing structure and shared common resonator sections is proposed. The basic configuration is composed of two shared stepped-impedance resonators (SIRs), four separate SIRs, and two T-junction circuits for two passbands. The shared SIRs can adjust fundamental resonant frequency and second harmonic resonant frequency thereof by designing the impedance ratio carefully, and therefore the fundamental resonant frequency and the second harmonic resonant frequency can be used to indicate the required frequencies of the two passbands, respectively. This property will be utilized to design the shared SIRs in the proposed structure. In conventional dual-band filters using single impedance ratio SIRs for dual passbands, the external quality factors of the two passbands cannot be extracted separately due to obstacles such as designing two external quality factors simultaneously with only one feed point. Thus, by adding the SIRs of two different impedance ratios near input port or output port, the fundamental frequencies thereof are designed at the center frequencies of two passbands, respectively, and the two feed points near input port or output port can be utilized to design the external quality factors of two passbands independently. Finally, the double-diplexing structure, i.e., the two T-junction circuits utilized in conventional diplexers, are located near the input and output ports and connected via the SIRs in a back-to-back fashion, and can achieve the required matching conditions at the input and output ports as well as mutual isolation between the two passbands concurrently. Specifically, a fourth-order dual-band filter with a Chebyshev response and 0.1-dB equal ripple is implemented on a substrate with a thickness of 0.508 mm, a relative dielectric constant of 3.55, and a loss tangent of 0.0027. The designed center frequencies of two passbands are 2.4 GHz and 4.1 GHz, respectively. The first and second fractional bandwidths are 11% and 9%, respectively. In conclusion, agreement between measured and simulated results is achieved and the proposed design concept is thereby verified.

Comparative Study of RF Dual-band-pass Filter

L. Bousbia, **M. Mabrouk**, **and A. Ghazel**
CIRTACOM-SUPCOM-ISETCOM de Tunis
Cité Technologique des Communications, Raoued 2088, Tunisia

Abstract— The demand for advanced filtering especially multi-band RF filters has significantly increased with the development of wireless communications standards and telecommunications equipments. Many studies pointed out the major role of this kind of filter. In this work, the performance of RF dual-band-pass filter is analyzed using ADS and HFSS simulators.

The first simulator is based on the method of Moments (momentum) which converts the functional expressions to matrix equations. Momentum is numerical method which solves Maxwell's equation for the design.

The second simulator uses Finite Element Method (FEM) which is mathematically used for finding approximate solution of partial differential equations as well as of integral equations. This method splits surface into sub-regions most often triangular. The structure contains N number of triangle vertices of in the inner limits; we obtain a set of N equations with N variables. Both methods are the most widely used and the most often cited for filters simulation.

Comparison between both (ADS and HFSS) simulators results is made. The major difference between simulation trials is the return loss value at the resonant frequencies. From the reflection parameter magnitude we can deduce that S_{11} result from ADS simulation is of 32.0 dB and is better than the obtained one from HFSS simulation which is of 8.0 dB. The $S21$ obtained result from ADS simulator shows that the proposed filter has an insertion loss of 0.18 dB and 0.3 dB at the first resonant frequency 1.68 GHz, and the second resonant frequency 2.81 GHz respectively. However the insertion losses obtained by HFSS simulation are about 0.4 dB and 0.9 dB respectively therefore are not so impressive compared to those obtained by ADS. The template filter obtained with both methods is not substantially different in general.

Session 4P2
Fiber Optics, Optical Sensors

Vectorial Remote Sensing of Guided Electric Field with Pigtailed Electro-optic Microcavities

A. Warzecha[1], **G. Gaborit**[1, 2], **and L. Duvillaret**[2]

[1]IMEP-LAHC, UMR 5130, Université de Savoie, bât. Chablais, Le Bourget-du-Lac Cedex 73376, France
[2]Kapteos, bât. Chablais, rue Lac de la Thuile, Savoie Technolac, Le Bourget-du-Lac Cedex 73376, France

Abstract— We present the applicability of pigtailed non-linear optical microcavities to perform non invasive vectorial characterization of electric (E) field, especially in guided configuration. Those sensors are based on Pockels' effect, which consists in additional birefringence induced by an applied E field in certain non-centrosymetric crystals [1], called electro-optic (EO) crystals. When a laser probe beam crosses an EO crystal, its phase is slightly modified by the applied E field [2]. By sandwiching the EO crystal between two dielectric mirrors, the E-field induced phase modulation of the laser beam is then enhanced thanks to the resonance of the Fabry-Pérot cavity [3]. Moreover, choosing a working wavelength on the steepest slope of one of the cavity resonance peaks leads to a direct amplitude modulation of the laser, this latter one being directly proportional to the applied E field. Having chosen the inflexion point of one resonance peak as working point, the response of the microcavity presents both highest linearity and sensitivity to the applied E field. The vectorial behavior of the measurement (measurement of a given E field component) is intrinsically linked to the relation that links the crystal refractive index variation to the applied E field through a scalar product with the sensitivity vector of the EO crystal [4].

Developed sensors are based on $LiNbO_3$ optical waveguides obtained by titanium diffusion along to the Y axis of the crystal. The waveguide is finally embedded between two multilayer dielectric mirrors to obtain a Fabry-Pérot microcavity ($\sim 1\,\mathrm{mm}^3$), coupled to a polarization maintaining fiber to perform remote measurements (up to a few 10 meters). We designed and built several sensors with different cavity lengths and quality factors. The whole setup is composed of a 1.5 µm DFB laser, two photodiodes and a half-wave plate used to switch between TE and TM cavity modes.

Those transducers have already been studied in term of sensitivity and a lowest measurable E field of $1\,\mathrm{V{\cdot}m^{-1}{\cdot}Hz^{-1/2}}$ has been achieved. The sensor selectivity to one specific E-field component has been measured by rotating the probe inside a constant E field. A rejection level of the orthogonal components of 30 dB has been obtained. Longitudinal spatial resolution is determinate by the length of the microcavity. Transversal spatial resolution has been estimated to less than 50 µm by measuring fringing E-field above interdigitated coplanar lines. The bandwidth is linked to the inner-cavity photons life time and reaches a few tens of GHz.

Two dimensional E-field mapping of fringing fields have been achieved in frequency domain. Invasiveness of the sensors (influence of the probe on electric signal propagation) is very low and quantitative estimations of this latter one are in progress. They are measured using common microwave differential techniques exploiting the EO-sensor induced variation of phase and amplitude of both transmitted and reflected microwave signals.

ACKNOWLEDGMENT

The authors acknowledge the DGA (French Military Programs Management and Procurement Agency) for its support.

REFERENCES

1. Yariv, A., *Optical Electronics*, Saunders College Publishing Ed., 1991.
2. Duvillaret, L., S. Rialland, and J. L. Coutaz, "Electro-optic sensors for electric field measurements. I. Theoretical comparison among modulation techniques," *J. Opt. Soc. Am. B*, Vol. 19, 2692–2703, 2002.
3. Gaborit, G., G. Martin, J. L. Coutaz, and L. Duvillaret, "High-finesse Fabry-Perot electro-optic sensors with enhanced sensitivity and high spatial resolution," *Appl. Opt.*, Vol. 47, 2001–2009, 2007.
4. Duvillaret, L., S. Rialland, and J. L. Coutaz, "Electro-optic sensors for electric field measurements. II. Choice of the crystals and complete optimization of their orientation," *J. Opt. Soc. Am. B*, Vol. 19, 2704–2715, 2002.

Incorporation of Optical Fiber-loop and FBG as Displacement and Temperature Sensors for Structure Monitoring

M. Kamil Abd-Rahman and N. Jannah Muhd-Satar
Faculty of Applied Science, Universiti Teknologi MARA, Shah Alam 40450, Malaysia

Abstract— Optical fiber sensors have been deployed in structures by embedding them in various host materials or attaching the sensors onto structure surfaces for health monitoring of civil structures, hill-slopes and other geotechnical sites. This paper presents a distributed optical fiber sensor system consisting of single-mode fiber-loop sensor incorporating fiber Bragg grating (FBG) for displacement and temperature detections. The fiber-loop sensor was geometrically designed using SMF-28 to exhibit optical attenuation due to the micro-bending effect in the fiber. The bending effect would develop higher optical loss when the loop diameter is reduced due to the force action of displacement. FBG incorporated in the system not only functions as discrete localized point-to-point detection of minor structural-displacement, it also served as temperature sensor. Temperature-compensating fiber would distinct the temperature sensing effect from the effect of structural displacement. The system is capable to detect faults at several different locations by providing distributed sensing points along a 200-km-length of detection. Optical time-domain reflectometer (OTDR) was used to sense optical attenuation along the length of fiber which acts as the sensing arm of the fiber-loop sensor-heads distributed precisely along the detection-length. Additional sensor heads can be placed conveniently at any locations along the line of detection without incurring additional cost to the system as it uses only the optical fiber as the sensing element. The fiber-loop sensing-head has a sensitivity of 0.0361 dB/mm displacement. The incorporated FBG sensor has a slightly lower sensitivity of 0.0621 dB/mm which was measured using optical spectrum analyzer (OSA). The optical fiber sensor system was used to model the displacement of a hill-slope structure and results show that the diagonal-direction of ground movement gives higher sensitivity to the fiber-loop sensor than linear-, vertical- and sideway-movement of the ground relative to the position of the fiber-loop sensor-head.

Electromagnetic Waves through Fiber Bragg Gratings

P. Pereyra
Departamento de Ciencias Básicas, Universidad Autonoma Metropolitana, Azcapotzalco, CP 02200, México

Abstract— We discuss here some similarities and differences between two theoretical approaches applied to study transmission coefficients of electromagnetic waves through fiber Bragg gratings: The one coupled mode approximation (OCMA) and the theory of finite periodic system (TFPS). A large number of applications, using optical fiber gratings, for optical communications, tunable wavelength filters, sensors, etcetera, were analyzed in the one couple mode approximation [1–14]. As the correct evaluation of the frequency spectra and the fiber Bragg grating transmission coefficients is a rather important issue, it is worth validating these results based on precise calculations. The physical results obtained here (see Figures 1 and 2) help us to contrast the performance of the OCMA and the TFPS describing the Bragg grating fiber of lenght L_o and refractive index

$$r(z) = r_o\left(1 + 2v(z)\cos\frac{2\pi z}{\Lambda}\right), \tag{1}$$

where Λ is the grating period ($\Lambda = \lambda/2n_o$), r_o the effective refractive index, λ the vacuum wave length and $V(z)$ the modulation amplitude. In Figure 1. we have the transmission coefficient and the phase time evaluated using the OCMA while in Figure 2. we have the same quantities, for the same system, using the TFPS. Though the agreement is rather good, some differences will be discussed.

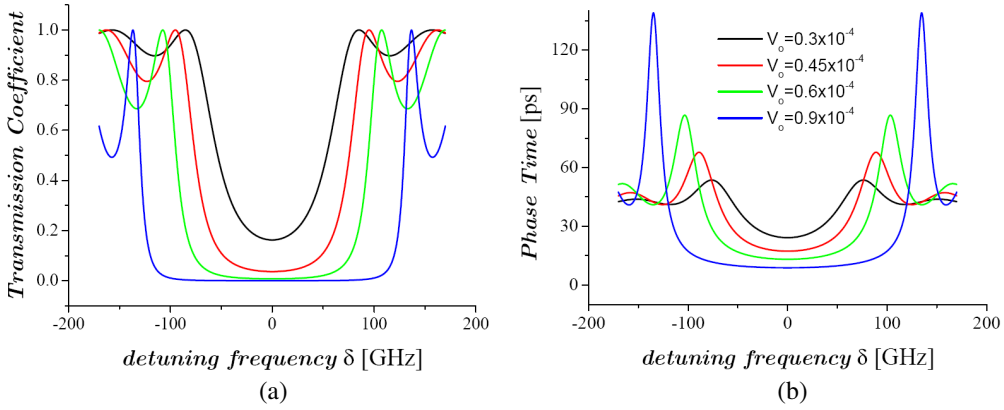

Figure 1: (a) The transmission coefficient and (b) the phase time in the OCMA, as functions of the detuning frequency $\delta = \omega - \omega_B$, for different values of the modulation amplitude V_o with $w_B = 1.261 \times 10^{15}$ Hz, $r_0 = 1.452$, and $L_o = 8.5$ mm.

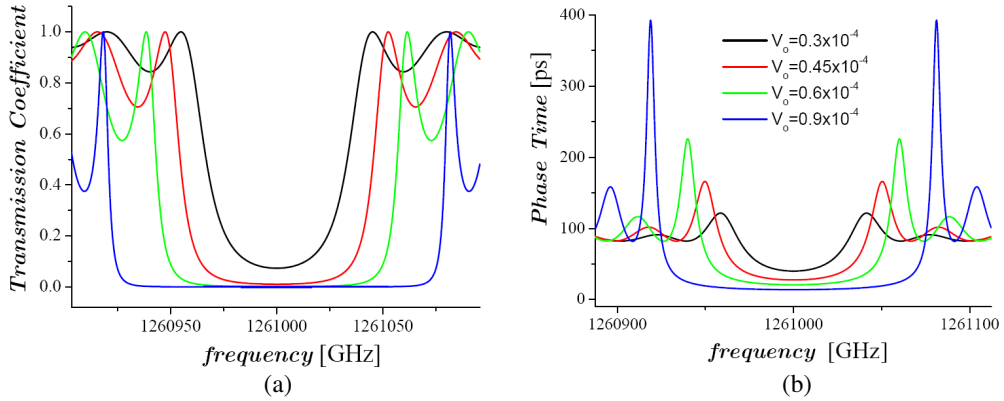

Figure 2: (a) The transmission coefficient and (b) the phase time from the TFPS, as functions of the frequency, for different values of the "modulation amplitude" V_o with $w_B = 1.261 \times 10^{15}$ Hz, $r_0 = 1.452$, and $L_o = 8.5$ mm.

REFERENCES

1. Othonos, A. and K. Kalli, *Fiber Bragg Gratings: Fundamentals and Applications in Telecommunications and Sensing*, Artech House Optoelectronics Library, Artech House, USA, 1999, ISBN 0890063443.
2. Kogelnik, H., "Theory of dielectric waveguides," *Integrated Optics*, T. Tamir, Ed., Chap. 2, Springer-Verlag, New York, 1975.
3. Kogelnik, H., "Switched directional couplers with alternating $\Delta\beta$," *IEEE J. Quantum Electron*, Vol. 12, 396–401, 1976.
4. Kogelnik, H. and C. V. Shank, "Coupled-wave theory of distributed feedback lasers," *J. Appl. Phys.*, Vol. 43, 2327–2335, 1972.
5. Huang, W. P., *J. Opt. Soc. Am. A*, Vol. 11, 963, 1994.
6. Ferraro, P. and G. De Natale, "On the possible use of optical fiber Bragg gratings as strain sensors for geodynamical monitoring," *Optics and Lasers in Engineering*, Vol. 37, 115–130, 2002.
7. Snyder, A. W., "Coupled-mode theory for optical fibers," *J. Opt. Soc. Am.*, Vol. 62, 1267–1277, 1972.
8. Marcuse, D., "Coupled mode theory of round optical fibers," *Bell Syst. Tech. J.*, Vol. 52, 817–842, 1973.
9. Snyder, A. W., Y. Chen, and A. Ankiewicz, "Coupled waves on optical fibers by power conservation," *J. Lightwave Technology*, Vol. 7, 1400–1406, 1989.
10. Streifer, W., "Coupled mode theory," *Electron. Lett.*, Vol. 23, 216–217, 1987.
11. Streifer, W., "Comment on 'fundamental error of recent coupled mode formulations,," *Electron. Lett.*, Vol. 22, 718–719, 1988.
12. Erdogan, T., "Fiber grating spectra," *J. Lightwave Technology*, Vol. 15, 1277–1294, 1997.
13. Guo, T., X. G. Qiao, Z. N. Jia, et al., "Simultaneous measurement of temperature and pressure by a single fiber Bragg grating with a broadened reflection spectrum," *Appl. Optics*, Vol. 45, 2935–2939, 2006.
14. Attygalle, M., C. Lim, G. J. Pendock, et al., "Transmission improvement in fiber wireless links using fiber Bragg gratings," *IEEE Photonics Tech. Letts.*, Vol. 17, 190–192, 2005.

Multi-long-period Gratings for the Optimization of Pump Absorption in Microstructured Optical Fiber Lasers

T. Palmisano[1], **M. Surico**[1], **A. D'Orazio**[2], **M. De Sario**[2], **L. Mescia**[2], **V. Petruzzelli**[2], **and F. Prudenzano**[1]

[1]DIASS Dipartimento di Ingegneria dell'Ambiente e per lo Sviluppo Sostenibile
Politecnico di Bari, Via E. Orabona, Bari 4-70125, Italy
[2]DEE Dipartimento di Elettrotecnica ed Elettronica
Politecnico di Bari, Via E. Orabona, Bari 4-70125, Italy

Abstract— In a number of cases, laser fiber length should be suitably reduced, to avoid non linear effects as stimulated Raman an Brillouin scattering, to minimize the effect of propagation losses (not negligible in some soft glasses employed in near infrared wavelength region) or when the employed fibers must kept straight and cannot be coiled, as it occurs for the rod type ones. In this paper, a novel Long Period Grating (LPG) coupler written into the rare earth doped single-mode core of a Double-Cladding Microstructured Optical Fiber (DCMOF) laser is designed to enhance the coupling of the pump power. It allows the reduction of the total length of the laser and the minimization of the length-dependent nonlinear effects. The design aim is to enhance the power transfer from the inner cladding modes toward the fundamental mode guided in the core at the pump wavelength [1, 2]. The guided modes are investigated via a Finite Element Method (FEM) routine. The coupler spectral characteristics and the laser behavior are modeled by an ad-hoc written computer code integrating the differential equations derived by the multimode coupled-mode theory, the power propagation equations and rare earth population rate equations [3, 4]. More precisely, the developed computer code takes into account the interaction between the two-fold degenerate, x and y polarized, fundamental mode guided in the core (HE_{11}) and the inner cladding modes, at both the signal and pump wavelengths [5–7]. The optical fiber core is ytterbium doped; therefore, the multimode coupled mode theory has been suitably modified and completed, by considering the light-matter interaction phenomena describing the active (rare earth doped) medium. A quasi-two level scheme is employed to describe the ytterbium activated glass-system. The software has been validated by considering the experimental results reported for a similar case (but pertaining to a conventional, not microstructured, fiber laser with a passive LPG coupler) [8]. In our design, an efficient multi-LPG configuration, obtained via a cascade of gratings having suitable periods and lengths, has been identified in the rare earth doped core region of a microstructured optical fiber laser. As preliminary results, the employment of this multi LPG coupler allows to utilize an active fiber about 20%–25% shorter, depending on the laser operation condition, than that used for the laser without LPGs, to parity of performance. Alternatively, the multi LPG coupler allows a laser output higher than 15% with respect the laser without multi LPG coupler, for a laser length close to $L = 1$ m. Further percentage increases are obtained for shorter laser lengths.

ACKNOWLEDGMENT

The work has been partially developed within the COST ACTION MP0702.

REFERENCES

1. Calò, G., A. D'orazio, M. De Sario, L. Mescia, V. Petruzzelli, L. Allegretti, T. Palmisano, and F. Prudenzano, "Improvement of the pump power coupling in double cladding photonic crystal fiber," *2008 IEEE/LEOS Winter Topical Meeting Series*, 146–147, Sorrento, Italy, January 14–16, 2008, ISBN 978-1-4244-1595-3.
2. Mescia, L., "Design of long-period gratings in cladding-pumped microstructured optical fiber," *J. Opt. Soc. Am. B*, Vol. 25, 1883–1839, 2008.
3. Carlone, G., A. D'Orazio, M. De Sario, L. Mescia, V. Petruzzelli, and F. Prudenzano, "Design of double-clad erbium-doped holey fiber amplifier," *J. Non-Cryst. Solids*, Vol. 351, 1840–1845, 2005.
4. Calò, G., A. D'Orazio, M. De Sario, L. Mescia, V. Petruzzelli, and F. Prudenzano, "Design of cladding pumped microstructured fiber amplifier," *Opt. Materials*, Vol. 28, 1243–1246, 2006.
5. Erdogan, T., "Cladding-mode resonances in short-and long-period fiber grating filters," *J. Opt. Soc. Am. A*, Vol. 14, 1760–1773, 1997.

6. Kong, M. and B. Shi, "Field solution and characteristics of cladding modes of optical fibers," *Fiber and Integrated Optics*, Vol. 25, 305–321, 2006.
7. Eggleton, B. J., P. S. Westbrook, C. A. White, C. Kerbage, R. S. Windeler, and G. L. Burdge, "Cladding-mode resonances in air-silica microstructured optical fibers," *J. Lighwave Technol.*, Vol. 18, 1084–1100, 2000.
8. Baek, S., S. Roh, Y. Jeong, and B. Lee, "Experimental demonstration of enhancing pump absorption rate in cladding-pumped ytterbium-doped fiber lasers using pump-coupling long-period fiber gratings," *IEEE Photonics Technology Letters*, Vol. 18, No. 5, 700–702, 2006.

Two-components Electric-field Sensor for Ultra Wide Band Polarimetric Measurements

Y. Gaeremynck[1,2], P. Jarrige[1,2], L. Duvillaret[1], G. Gaborit[1,2] and F. Lecoche[1]

[1]Kapteos SAS, rue Lac de la Thuile, F-73376 Le Bourget-du-Lac Cedex, France
[2]IMEP-LAHC, CNRS, University of Savoie, F-73376 Le Bourget-du-Lac Cedex, France

Abstract— We present a new kind of ultra wide band non invasive pigtailed electric(E)-field sensors which allows to measure simultaneously amplitude and phase of two components of an E field. These sensors are based on the Pockels' effect [1] in isotropic electro-optic (EO) crystals. When such crystals are subjected to an applied E field, they acquire an induced birefringence (directly proportional to the E-field amplitude). This latter one expresses itself as the apparition of only two permitted linear polarization states for any laser probe beam crossing the crystal. As it was theoretically demonstrated [2], when using a <111> cut isotropic EO crystal, the orientation of these two polarization states is directly linked to the orientation of the E-field projection onto the plane normal to the laser probe beam. Consequently, simultaneous measurement of two E-field components becomes possible with a unique laser beam probing a single EO crystal: the first demonstration was done in free space in 2007 [3].

During the conference, we will present first results on a pigtailed version of such 2-components E-field sensor. The access to the 2-components of the E field requires to probe the EO crystal with balanced polarization states, obtained using a circularly polarized laser beam at the crystal entry. For that purpose a polarization maintaining (PM) fiber is used on the outward path up to the crystal, in front of which a quarter-wave plate is placed. A mirror, sticked on the opposite face of the crystal, sends back the laser probe beam in the PM fiber. Due to the E-field induced birefringence of the EO crystal, the polarization state of the laser is no more linear and aligned along one of the eigen dielectric axes of the PM fiber on the return path. This leads to an additional and uncontrolled (strongly temperature dependent) dephasing between the two permitted linear polarization states of the laser, *a priori* leading in turn to a loss of the useful information — the two components of the applied E-field. Indeed, a compensation of the PM-fiber additionnal dephasing is possible [4]. Moreover, a regulation loop compensates in real-time any temperature induced slow variation of this dephasing.

Contrary to classical polarimetric measurements that use crossed polarized antennas, our EO probes measure the two components (both in amplitude and phase) of the E-field rigourously at the same location (inside a few mm^3 crystal) with very minor perturbation on the field to be measured as the probes are fully dielectric. Moreover, such EO probes are perfectly suited to near field measurements and present an ultra wide bandwidth ranging from quasi DC up to a few tens of GHz. EO probes allow also measurements of high power microwave signals (E-field amplitude up to a few MV/m) with a high dynamic range (~ 90 dB in a 1-Hz analysis bandwidth). In the framework of polarimetric measurements, two-components EO sensors constitute a new and very competitive technique as compared to classical ones.

ACKNOWLEDGMENT

The authors acknowledge the DGA (French Military Programs Management and Procurement Agency) for its support.

REFERENCES

1. Yariv, A., *Optical Electronics*, Saunders College Publishing Ed., 1991.
2. Duvillaret, L., S. Rialland, and J. L. Coutaz, "Electro-optic sensors for electric field measurements. II. Choice of the crystals and complete optimization of their orientation," *J. Opt. Soc. Am. B*, Vol. 19, 2704–2715, 2002.
3. Gaborit, G., J. L. Coutaz, and L. Duvillaret, "High-finesse Fabry-Perot electro-optic sensors with enhanced sensitivity and high spatial resolution," *Appl. Opt.*, Vol. 90, 241118-1–3, 2007.
4. Duvillaret, L. and G. Gaborit, "Electrooptic probe for vector measurement of an electromagnetic field," US Patent, US2009262349, 2007.

1-Soliton Solution of the Nonlinear Schrödinger's Equation with Log Law Nonlinearity by Lie Symmetry Analysis

Chaudry Masood Khalique
International Institute for Symmetry Analysis and Mathematical Modelling
Department of Mathematical Sciences, North-West University, Mafikeng Campus
Private Bag X2046, Mmabatho 2735, Republic of South Africa

Abstract— In this talk we obtain the 1-soliton solution of the nonlinear Schrödinger's equation in a log law media. The technique that is used to obtain the solution is the Lie symmetry analysis. A closed form soliton solution is obtained.

Optical Solitons in a Log Law Media by He's Variational Principle

Anjan Biswas
Department of Mathematical Sciences, Delaware State University
1200 N. DuPont Highway, Dover, DE 19901–2277, USA

Abstract— Optical solitons, with log law nonlinearity is studied in presence of perturbation terms, by the aid of He's semi-inverse variational principle. The perturbation terms that are considered are higher order dispersion terms.

A Novel Idea of Quantum Cryptography Coupled with Handover Satellite Constellation for World Cover Communications

Aris Skander[1], **Messai Abderraouf**[1], **Merabtine Nadjim**[2], **Mosleh M. Al-Harthi**[2], **and Benslama Malek**[1]

[1]LET Laboratory, Faculty of Engineering, Mentouri University, Constantine 25000, Algeria
[2]Electrical Engineering Departments, Faculty of Engineering, Taif University, Saudi Arabia

Abstract— Quantum cryptography is a new branch of physics and cryptography which exploit quantum mechanical phenomena to guarantee the secrecy of cryptographic keys. BB 84 proposed the well known protocol that quantum key distribution could also be implemented using polarization photon between quantum systems. In this paper new model of implement BB84 protocol with Handover satellite constellation for possible to couple with quantum communications for more security and free space transmissions. So, the essential work carried in our research paper concerns a new idea development in satellites transmission whit implement of Quantum Key Distribution (QKD) algorithm based on photon encrypted code, including reducing the telecommunication interruption risks and this will provide indeed of a better free space communication quality.

Statistical Modelling of the Polarization Mode Dispersion in the Single Mode Optical Fiber Links

L. Cherbi
Laboratory of Instrumentation
University of Sciences and Technology Houari Boumediene, USTHB, Algeria

Abstract— The PMD is a property of the optical fiber in which the energy of the signal for a given wavelength decomposes to two orthogonal polarization modes possessing two different propagation speeds. The difference between the times of propagation of the two polarization modes is called differential Group delay (DGD). The PMD leads to widening of the pulses propagated in the fiber as well as a limitation of the transmission performances. The main reason of the PMD in the optical fiber is the birefringence. The description of the PMD in a fiber is complicated because the two modes of polarization can exchange the energy between them; this phenomenon is linked to the uncertain modes coupling. The PMD in a fiber varies uncertainly with the wavelength and also with its environmental conditions. There is not exact mathematical model which permits to calculate its value, what leads us to look for the statistical models permitting to value this phenomenon. In this work, we propose a second method of modelling of the PMD in a single mode optical fiber links with strong coupling, based on the formalism of Jones and the model of Dal Farno, while dividing the link in a set of birefringent elements of different lengths, for which their birefringence is calculated with a given method according to used material in the fiber, and which are oriented in an uncertain direction in relation to the other. We compared the results gotten to those of the first method that we already proposed in our previous works while comparing them with measured ones. A very good agreement between theory and experience is reported, confirming the validity of the proposed method.

Session 4P3
Safety and Electromagnetic Compatibility in Ubiquitous Health Environment

New Electromagnetic Environments for Health and Welfare

Victoria Ramos, Jorge García, and Alejandro del Pozo
Telemedicine and eHealth Research Unit, Health Institute Carlos III
C/Monforte de Lemos, 5, Pab. 6, Madrid 28029, Spain

Abstract— There is a growing concern about satisfaction of the increasing needs and economic sustainability for the social system for the provision of appropriate healthcare and for a social service adapted to the personal conditions of an ageing society due to complex transformations in Europe. "Quality of life" is emerging as one of the most critical challenges in Europe. This presents a wide range of opportunities for personalized technologies, mainly wireless communications, to support all areas of ICT. In fact, most national policies are considering these communication and information systems as the basic element for the emerging healthcare and social needs under serious economic constraint.

Nowadays is there an opportunity to develop innovative systems aimed at personal care for elderly and chronically sick in the home and what could be offered in response to the expected needs originated by demographic trend as well as the changing social, cultural and economic context. The rapid evolution of new technologies is one of the factors to consider in conjunction with local demographic changes, the legal and social context, the organization of healthcare and social services and the political framework for sources of variability.

This paper discusses the overall electromagnetic environment created by wireless solutions concerning their application for welfare, independent living and health. There is a large space of needs (opportunities) that could be potentially filled by wireless applications which would allow a variety of healthcare and social services to be provided in a personalized way by the same platform. Even more, a common infrastructure (standards, protocols, tools) which can support different operators while providing personalized services according to the end user profiles and allowing for different business models with public, private and mixed implementation. The convergence can also be observed from operators coming from different business areas such as healthcare, home care, security, tele-alarm, call centre operators, mobile telecom services, and nursing services.

Overall performance and risk analysis of the systems are the basis for any application that must consider first the quality of life of the users. E-Health and e-Care systems are characterized by the complex interaction of a number of entities composed by persons, machines and devices. Such interactions results in more or less risk exposure, vulnerability characteristics and security requirements depending on the target application requirements and the concrete implementation performance.

The growth in mobile data environments, have also posed new challenges. Furthermore, Electromagnetic Compatibility (EMC) issues are emerging as consequence of the proliferation of wireless communication and electronic devices. Telecare systems and devices must operate in non-controlled electromagnetic environments at patient's homes. As a consequence, EMC risk analysis and compatibility measures must be included in the agenda of home care services thus ensuring the safe and secure operation of the system.

Here is presented the electromagnetic evaluation of an architecture of a technologic platform for the diagnostic of the level of dependence of elderly people. The modules were composed of a network of wireless sensors, a 3G router for the communications with the central processer and a household gateway. The devices belonging to the sensor network were motion detectors, magnetic sensors for door opening, pressure sensors for the bed and sofa, a telephone-use sensor and a pill popper sensor.

Electromagnetic Compatibility of Portable RF Emitters in Uniquos Health Environment: Regulatory Issues

F. Censi, **G. Calcagnini**, **E. Mattei**, **M. Triventi**, **and P. Bartolini**
Italian National Institute of Health (ISS), Italy

Abstract— Wireless technology has reached a significant success and diffusion in healthcare: several wireless technology applications (RFID, WiFi, GSM, GPRS) have been developed to improve patient care (medical device and patient tractability, immediate access and exchange of diagnostic and therapeutic information, etc...). Given the potential development of such a technology, care must be paid on the potential risks deriving from the use of wireless device in healthcare, among which one of the most important is the electromagnetic interference with medical devices. In addition, medical devices are also used in other environments such as the home and transport. Also, in this locations, there is less medical supervision to intervene in case of malfunction. The aim of this paper is to review the regulatory issues concerning the electromagnetic compatibility of medical devices, to analyze if and how the application of the current standards allow an effective control of the possible risks associated to the electromagnetic interference on medical devices. Even if medical device regulations differ between Europe and USA, as far as electromagnetic compatibility is concerned both continents consider the standard IEC 60601-1-2 as the one to be met for medical equipment. The most important issues established by the up-to-date revision of the IEC/EN 60601-1-2:2007 concern: 1) the specification of the levels of immunity of medical devices by the manufacturers; 2) the declaration about electromagnetic immunity level to be included in the accompanying documents of the medical device by the manufacturer; 3) the shared responsibility between manufacturers, responsible organizations and operators to ensure that medical devices are used in a compatible electromagnetic environment where the medical devices performs as intended. When mobile RFID readers or WiFi terminals are brought to operate in hospital setting, they must be considered as portable RF communication equipments. Thus, in order to provide the electromagnetic environment where the performance of the medical device would be expected to be normal, a separation distance between the portable system and the medical devices must be assured. In other words, electromagnetic interference caused by RF portable equipment to medical devices can be avoided if the portable RF equipment is far enough from medical devices. How far depends on the level of electromagnetic immunity of the medical device, and on the emitted power and operating frequency of the portable RF equipment, according to the formulas included in the IEC/EN 60601-1-2:2007. Such formulas require the quantitative knowledge of the maximum field generated by the portable RF emitters. The maximum field strength or emitted power of portable RF emitters are subjected to international standards as well as national laws. As far as WiFi equipment are concerned, the IEC/EN 60601-1-2:2007 standard established a safety distance of 73 cm, considering emissions at maximum power (100 mW). For RFID portable equipment, the situation is more complicated: first, some RFID operation frequencies are not considered in the standard, which covers the frequency range from 150 kHz to 2.5 GHz; second, at the frequency of 13.56 MHz there is a misalignment between the standard IEC/EN 60601-1-2 and the RFID regulations concerning the expression of the transmission power of the portable RF equipment: in RFID regulations, the power limit is expressed in terms of the maximum magnetic field generated by the antenna at a distance of 10 m (as Ampere/meter), while in the standard IEC/EN 60601-1-2 the power limit is expressed in terms of antenna's effective radiated power (in Watt). Since the relationship between the magnetic field generated by the antenna and the effective radiated power depends, at these frequencies, from the physical characteristics of the antenna and requires electromagnetic expertise, the computation of the recommended separation distance from a RFID systems operating at 13.56 MHz is neither immediate nor general. However, for a RFID portable equipment working at the maximum emitted power (2 W or 4 W), the separation distance should be greater than 3 meters. In conclusion, from a regulatory point of view, it is desirable that medical devices EMC standards and RF transmitters standards would be updated to remove the current misalignments. In addition, proper policies should be adopted to ensure that the placement/use of RF portable equipment is such that the potential for interference is removed, taking into account the appropriate distance from medical devices as a function of the emitted power. Given the diffusion of medical devices in ubiquos environment, not only medical personnel but also patients and caregivers should be formed to avoid the use of mobile adapters in close proximity to medical devices.

Electromagnetic Evaluation for Personal Communications in Outdoor Environments

Silvia de Miguel[1], **Francisco Falcone**[3], **Miguel Beruete**[3], **Aránzazu Sanchis**[2], **and Victoria Ramos**[1]

[1]Health Institute Carlos III, Telemedicine and eHealth Research Unit, Spain
[2]CNSA, Health Institute Carlos III, Radioprotection Service, Spain
[3]Electric Engineering and Electronic Department, Public University of Navarra, Spain

Abstract— The significant progress in new wireless technologies has involves a great employment of personal communications. There has been a significant impact through the rapid expansion of personal mobile telecommunication and wireless network systems for voice, picture and video communication, internet access and other data transfer applications. Their presence has affected almost every aspect of day-to-day living including the displacements, which has caused the expanding and the increasing interest of the ubiquitous communications.

Due to the increasing types of new wireless communication systems, the fulfilment of exposure level thresholds, and the possible interferences between the different types of signals which share the same transmission way, should be considered to assure a proper, reliable and safe usage of the wireless communication technologies. It is relevant to quantify the risk of the continue exposure that involves the use of this kind of technologies.

This paper analyzes the signals of the different wireless communications systems in an outdoor environment. Taking account of the development of the personal mobile communications and the increasing intention to be connected every time everywhere, the measures have been realized in movement and in a static state to present all the possible conditions.

In the static environment two different techniques of measure have been employed, the electromagnetic fields and the spectral distribution of radiofrecuency (RF) energy have been analyzed using a dosimeter and a spectrum analyzer. The signals have been captured with different types of antennas, polarizations, and directions considering the main sources of signals.

In the dynamic environment values of the electromagnetic fields have been measured with a dosimeter and a GPS to match each value with its accurate position belonged to a predefined path.

The power density obtained with the experimental measures has been estimated with a 3D ray tracing code. This simulation tool lets simulate the real conditions of the different environments considered in this study. The real measures and estimations have been compared and analyzed to gain more reliable results.

Three Dimensional Safety Distance Analysis around a Cellular Base Station

F. Üstüner
TÜBİTAK BİLGEM UEKAE, Turkey

Abstract— The safety distance concept is widely used in the installation of cellular base stations to define a radiation hazard zone around the periphery of the base station. The safety distance around base stations is usually determined using basic antenna gain and RF output power level parameters with the application of free space electromagnetic wave attenuation formulas. However, such an approach gives usually worst case results and sometimes alarms the people in the surrounding area unnecessarily. In order to solve a lawsuit between a local resident and a cellular phone operator, a national court requested the expert view on the safety distance around the base station based on ICNIRP Guidelines. To give the correct answer for this appeal, it is decided to carry out a more realistic calculation of the safety distance around the base station. In this paper, three dimensional safety distance analysis around a specific cellular base station is carried out using ray optic techniques with the diffraction theory included. To carry out this analysis, NEC Basic Scattering Code (NEC BSC) from Ohio State University is chosen as the ray optic calculation tool. The base station antennas are modeled with array antennas giving the same radiation patterns in both elevation and azimuth planes. All details of the antennas such as their $+45°/-45°$ polarization, tilt angles, directions are included in the electromagnetic model. The residential house on which the base station antennas are mounted is modeled with the same geometry and material properties. The geometry of the house with the antennas is given in Fig. 1(a). The RF parameters of the base station's radio equipment are taken into account in the calculations. The electric field is calculated at X-Y grid points around the periphery of the house at every 0.2 m height. The resulting electric field is plotted in a contour line whose level is determined with the ICNIRP Guidelines' maximum permissible exposure limit for general public safety. An example of this plot is given in Fig. 1(b). The contour line actually demonstrates the safety distance around the base station. In the paper, the contour line plots will be given for all heights and the changes in safety distance could be observed at different heights.

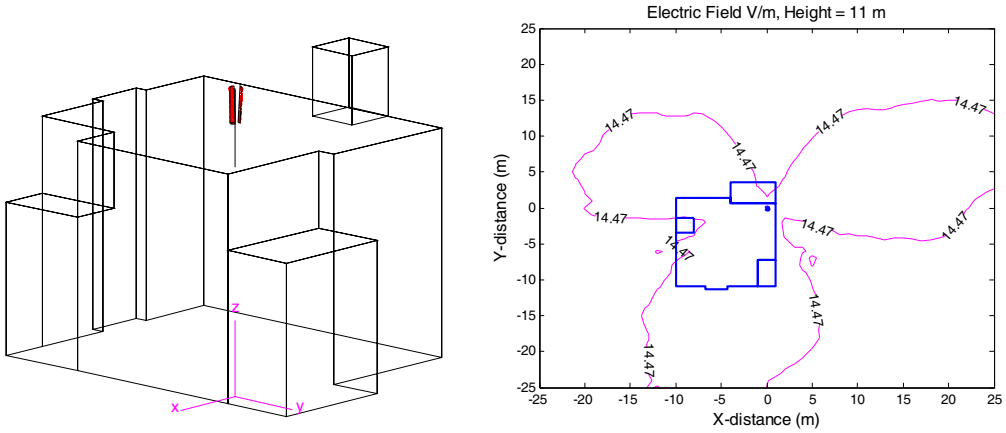

(a) (b)

Figure 1: (a) Ray optic EM model, (b) X-Y plot of E-field results at 11 m height.

Analysis of Electromagnetic Dossimetry of Indoor ZigBee Networks

Victor Torres[1], **Juan Antonio Nazabal**[1], **Miguel Navarro**[1], **Miguel Beruete**[1], **Victoria Ramos**[2], **Carlos Fernández**[1], **and Francisco Falcone**[1]

[1]Universidad Pública de Navarra, Spain
[2]Area de Telemedicina y Sociedad de la Información, Instituto de Salud Carlos III, Spain

Abstract— Wireless sensor networks have become of great use in domestic as well as industrial environments. The popularization of ZigBee (i.e., IEEE 802.15.4 based standard) has lead to many applications such as wireless device control, object location and multiple and diverse sensor deployment, among others.

Due to the fact that ZigBee is able to operate in differente frequency bands, all of them within the RF range, it is necessary to analyze the coverage levels and hence the effective emission that can be achieved within an indoor scenario. In this work, several cases of ZigBee based sensor networks have been analyzed in order to estimate RF emission levels. Full 3D ray launching simulations as well as measurement results are presented, where the topology of the transceivers play a key role in the overall power map that is obtained.

These results can aid in the sensor planning phase prior to integration, in order to minimize overall RF emitted power and obtain the most power efficient configuration.

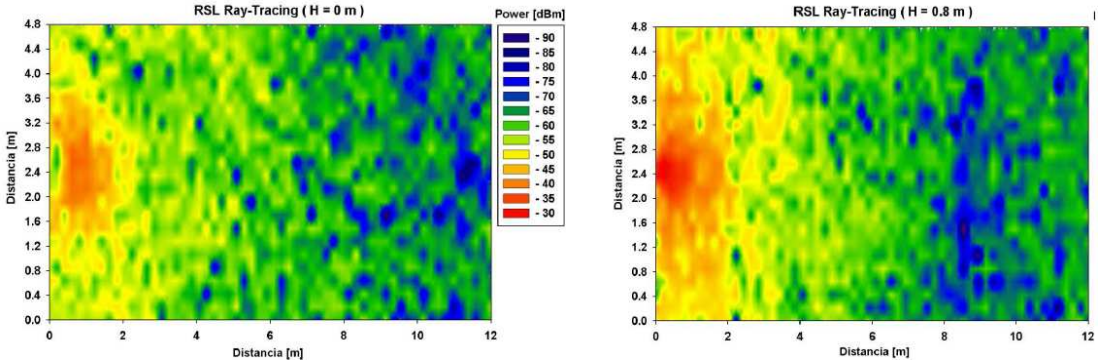

Figure 1: Power emission levels for a ZigBee sensor network within an indoor scenario at two different heights. The topology of the network determines the overall received power within the scenario.

Analysis of High Power Microwave Environments in Common Scenarios

Aránzazu Sanchis[1], **Jose Roldán**[1], **Victoria Ramos**[2], **and Agustín Martín**[3]

[1]National Centre for Environmental Health (ISCIII), Madrid, Spain
[2]Telemedicine and eHealth Research Unit (ISCIII), Madrid, Spain
[3]Applied Physics Institute (CSIC), Madrid, Spain

Abstract— Technological advancements are becoming quickly integrated in present social lifestyle, and our reliance on electromagnetic-based devices is foreseen to get higher since new biomedical devices development within the healthcare domain. These new technologies with high beneficial in either industrial, commercial and social welfare may lead, in some cases, to the reverse effect. Intentional electromagnetic environments (IEME), intentional electromagnetic interference (IEMI) [1], high power electromagnetic (HPEM) environments, are common terms within the electromagnetic compatibility (EMC) framework [2], and are mainly observed as threats regarding to commercial electronic equipments and systems. However, beyond the natural, military or civilian sources producing high field levels disturbing EM environment in close proximity to electronic systems and facilities, some smaller-scale version of powerful sources, can be easily homemade from available components assambled according to instructions that can be found on the Internet [3]. As the URSI Council stated in 1999, the existence of these electromagnetic tools must be taken into consideration as a potential threat [4].

Then, looking for safety in daily places, e.g., at home, we've tackled some threats that could come up from the misuse of already known and accessible devices like microwave ovens. The performance of these low-voltage appliances are governed by national regulations concerning electrical low-voltage devices, according to ICNIRP guidelines for limiting exposure [5]. Hazards associated with incorrect use or radiation leakage is less likely to occur except in closer contact with the appliance [6]. In this work, theroretical and practical analysis of electric field generated by a microwave oven is made, taking into account different operating conditions, in order to get some information about the actual threat to safety in current scenarios due to high power microwave environments.

ACKNOWLEDGMENT

This work has been supported by the Spanish Ministry of Science and Innovation, Projects SPY 1416/09 and TEC2009-13964-C04-02.

REFERENCES

1. Giri, D. V. and F. M. Teche, "Classification of intentional electromagnetic environments (IEME)," *IEEE Trans. EMC*, Vol. 46, No. 3, 322–328, 2004.
2. IEC (International Electrotechnical Commission), "Electromagnetic compatibility (EMC) — Part 2–13: Environment — High-power electromagnetic (HPEM) environments — Radiated and conducted," IEC 61000-2-13, Geneva, Switzerland, 2005.
3. Månsson, D., "Intentional electromagnetic interference (IEMI). Susceptibility investigations and classification of civilian systems and equipment," Ph.D. Thesis, Acta Universitatis Upsaliensis, Digital Comprehensive Summaries of Uppsala, 2008.
4. *Radio Science Bulletin*, No. 290, 62–63, September 1999.
5. ICNIRP, "Guidelines for limiting exposure to time-varying electric, magnetic, and electromagnetic fields (up to 300 GHz)," *Health Phys.*, 494–521, 1998.
6. Bangay, B. and C. Zombolas, "Advanced measurements of microwave oven leakage," *The Journal of the Australian Radiation Protection Society*, Vol. 20, 47–51, 2003.

Risks Communication Strategies in Hospitals to Avoid Electromagnetic Interferences and Healthcare Professionals' Use of Ubiquitous Communication Devices

Maria Dolores Marcos[1] and Victoria Ramos[2]

[1]Agency "Laín Entralgo" for Education and Health Research, Regional Ministry of Health
Autonomous Government of Madrid, Spain
[2]Telemedicine and eHealth Research Unit, Ministry of Science and Innovation
Health Institute Carlos III, Spain

Abstract— The wireless communication industry has experienced tremendous growth in a very few years, digital portable hand-held devices specially. Pretty compact gadgets such as cell-phones, PDAs, Blackberries, iPods... are used by millions of people worldwide.

Developments in wireless technologies have also had a huge influence in the field of medical applications, enabling wireless bio monitoring for medical patient care or workers at risk. Nevertheless, several medical applications use electromagnetic fields in the *radiofrequency* (RF) range whose usual frequencies are those allowed for industrial, scientific, and medical applications similar to most industrial sources. A large healthcare centre currently presents a large variety of wireless telecommunications systems that generate electromagnetic fields (EMF) with different features and intensities.

These radiofrequency devices have been restricted in hospitals in order to avoid interferences with medical technologies or disrupting electromagnetic compatibility. At the same time, the health effects of repeated or long-term exposure to low levels of radiofrequency radiation are not well known. Accordingly, some prevention measures have been developed and disseminated, for instance warning signals or user guides for teaching how to use the devices in a proper and safe way. But all of these methods are based on objective, reliable and comparable information handled by experts in telecommunication technologies.

The aim of this paper is determine what methods and communication strategies used to achieve this goal are being more effective to prevent electromagnetic exposure risks and their capability to modify healthcare professionals' use of ubiquitous communication devices in their job places. There is too much information around for people to keep up to date. On top of this, high quality information is often not easy to find. A systematic review of literature allows inform physicists, patients and healthcare providers about patient security and possible harmful effects in healthcare and hospital environments. We provide an overview of published cases of risks communication strategies in hospitals in order to evaluate the safety and security of job places and the risk perception of the workers involved in these environments.

Session 4P4a
Electromagnetic Property and Measurement

Accuracy of High Temperature Waveguide Measurements

Christer Larsson[1, 2] **and Daniel Sjöberg**[1]

[1]Department of Electrical and Information Technology, Lund University, SE-221 00 Lund, Sweden
[2]Saab Dynamics, SE-581 88 Linköping, Sweden

Abstract— The electromagnetic properties, i.e., the permittivity and permeability, of materials change with temperature. This means that one has to know the electromagnetic properties in the operating temperature range, e.g., when designing radomes that are aerodynamically heated, microwave absorbers operating at elevated temperatures or materials for microwave heating applications.

A single waveguide setup was designed to characterize materials in the temperature range from 22°C to 1000°C for X-band frequencies. The heated parts were manufactured from Inconel 600®. A clamshell oven was used to heat the fixture while using water cooled clamps to thermally separate the hot waveguide parts from the conventional room temperature microwave equipment. This setup makes it possible to use standard size X-band waveguide samples for measurements up to 1000°C. Measurements of the S-parameters are performed and the Nicolson-Ross-Weir inversion procedure is used to determine the permittivity and permeability of the sample.

Thermal expansion of the waveguide and the sample causes reference planes to shift, the waveguide cutoff frequency to change, and the sample thickness to increase. It can also cause a displacement of the sample and an air gap between the sample and the waveguide to form. Correction procedures were developed to mitigate the effects of thermal expansion.

This study focuses on the prediction of the accuracy that can be obtained in the determination of the permittivity and permeability for these high temperature measurements. Recently developed Cramér-Rao bounds are used to theoretically predict the accuracy of the permittivity and permeability using the accuracy of the S-parameters that can be obtained. The predicted accuracy is compared with measurements.

Fast and Accurate Dielectric Characterization Technical to Get Various Electrolytic Parameters

C. Gilbert and O. Meyer
LGEP Supelec, CNRS UMR-8507, UPMC, Paris Sud
11 rue Joliot Curie, Gif-sur-Yvette 91192, France

Abstract— In our current study [1], we have to follow the kinetic of a chemical reaction under a wide broadband frequency spectroscopy. At first, we've hoped that ionic dipolar relaxation will be a marker in the progress of the chemical reaction by discriminating one of the products created as it was in previous studies [2]. However, the actual chemical reaction studied is an hydrolysis and as a direct consequence, the solvent is water which completely shadows any relaxations that can occur in the range of the GHz. We then adapt our measurement system to be compatible with classical electrochemical impedance spectroscopy and found that it is able to characterize a lot of electric parameters in various sort of electrolytes in a very short time and precise way.

Instrumentation: It's composed of 2 impedance analyzers and one network analyzer compatible with our cylindrical discontinuity characterization cell which allows us to get analytical impedance data from 40 Hz to 5 GHz with 350 points within a very short sweep ($<$ 8 sec). Impedance data points are then analytically inverted [3]. The characterization cell is a coaxial cylinder discontinuity with gold plated and submicron polished electrodes which allows us to be free of anodic reaction that could lead to measure faradic current that will shadow electrical parameters of quantified electrolytes.

Results and Strategy of Interpretation: There are a lot of ways to display results in broadband impedance spectroscopy. Since we're looking for some obvious change in electrolytes composition, the best way is then to display each inverted sweep of impedance data in Niquist (Argand) diagram in three different complex electrical parameters, ρ^* (complex resistivity), σ^* (complex conductivity) and ε^* (complex permittivity). Each representation gives us different information as bulk relaxation time, electrolyte permittivity, electrolyte conductivity etc... Models parameters on bulk relaxation or dual capacitance layer could then be correlated among the various sorts of displays. Some results about NaCl solvated into double distilled water are presented here.

Discussion: Broadband dielectric characterization coupled with a suitable measurement cell may lead to very fast and accurate results in electrolytes characterization. More results and discussion about physical interpretation will be presented in the full paper.

REFERENCES

1. Gilbert, C., C. Pareige, A. Fourrier-Lamer, F. Maurel, and O. Meyer, "Characterization of acetylcholine hydrolysis under continuous and pulsed microwaves radiation using broadband dielectric measurement," *PIERS Proceedings*, 1132–1136, Beijing, China, March 23–27, 2009.
2. Meyer, O., et al., "Instrumentation for wide frequency range measurements of epoxy resin during microwave curing," *Rev. Sci. Instrum.*, Vol. 71, No. 4, 1862–1868, 2000.
3. Belladj-Tahar, N. and A. Fourrier-Lamer, "Broad-band analysis of a coaxial discontinuity used for dielectric measurements," *IEEE Transactions on Microwave Theory and Techniques*, Vol. 34, No. 3, 346–350, 1986.

Enzymatic Acetylcholine Hydrolysis Modification by High Voltage and Fast Rise Time Pulsed EMW Using Dielectric Spectroscopy

C. Gilbert and O. Meyer
LGEP Supelec, CNRS UMR-8507, UPMC Univ. Paris 06, Univ. Paris Sud 11
rue Joliot Curie, Gif-sur-Yvette 91192, France

Abstract— In our current study [1], we have to follow the kinetic of a chemical reaction under a wide broadband frequency spectroscopy. At first, we've hoped that ionic dipolar relaxation will be a marker in the progress of the chemical reaction by discriminating one of the products created as it was in previous studies [2]. However, the actual chemical reaction studied is a hydrolysis and as a direct consequence, the solvent is water which completely shadows any relaxations that can occur in the range of the GHz. We then adapt our measurement system to be compatible with classical electrochemical impedance spectroscopy and found a qualitative marker which is located into the dual layer capacitance.

Studied Chemical Reaction & Method: The context of the study is about to approximate threshold effects that electromagnetic pulses could induce to some biochemical reactions. The reaction studied here is the hydrolysis of a major neurotransmitter, Acetylcholine by Acetylcholine Esterase. Purpose of the study is to interpret in which range fast amplitude electrical pulse could affect the reaction. The originality of the measurement lays on a particular technical impedance measurement associated with a full metallic cell which encapsulates the electrolyte into a confined space. Thus, easier modeling of electrical wave into the cell could be made for further biochemical interpretation.

First Results: We have noticed that in the frequency range of measurement [40 Hz–10 GHz]; the only way to discriminate initial substrate from products is located within the dual layer capacitance. Physical interpretation of this phenomenon could be a specific adsorption of acetic acid (one of the product) on the electrode. Results about EMPs effect on the reaction will be discussed in the full paper.

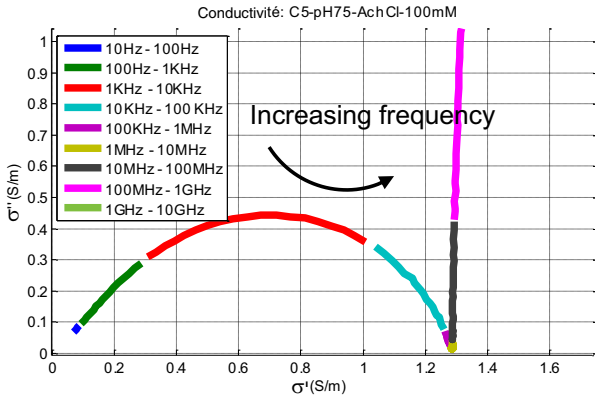

Figure 1: Complex conductivity spectra of AchCl.

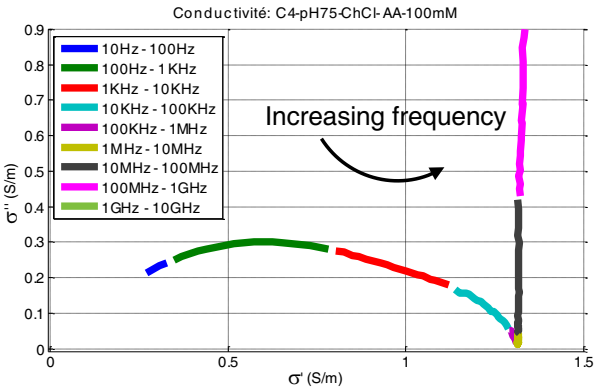

Figure 2: Complex conductivity spectra of ChCl+AA.

REFERENCES

1. Cedric Gilbert, C. Pareige, A. Fourrier-Lamer, F. Maurel, and Olivier Meyer, "Characterization of acetylcholine hydrolysis under continuous and pulsed microwaves radiation using broadband dielectric measurement," *PIERS Proceedings*, 1132–1136, Beijing, China, March 23–27, 2009.
2. Meyer, O., et al., "Instrumentation for wide frequency range measurements of epoxy resin during microwave curing," *Rev. Sci. Instrum.*, Vol. 71, Vol. 4, 1862–1868, 2000.
3. Belladj-Tahar, N. E. and A. Fourrier-Lamer, "Broad-band analysis of a coaxial discontinuity used for dielectric measurements," *IEEE Transactions on Microwave Theory and Techniques*, Vol. 34, No. 3, 346–350, 1986.

Tuneable Metamaterials Containing Arrays of Magnetic Microwires

L. V. Panina[1,2], **M. Ipatov**[1], **V. Zhukova**[1], **J. González**[1], **and A. Zhukov**[1]

[1]Dpto. de Física de Materiales, Fac. Químicas, Universidad del País Vasco
San Sebastián 20018, Spain
[2]On leave from School of Computing and Mathematics, University of Plymouth
Plymouth, PL4 8AA, United Kingdom

Abstract— Composites containing long parallel wires can be characterised by plasma-like dispersion of ε_{ef} [1] with a negative value of the real part of the permittivity below the characteristic plasma frequency, f_p. A number of experimental studies confirmed a negative permittivity in the GHz region for wire media. Surface impedance ζ_{zz} may change under applied magnetic field, H_{ex}, as a result of the MI effect [2]. Then, the permittivity spectra will depend on H_{ex}.

We studied composites containing amorphous ferromagnetic Co-rich microwires exhibiting large MI effect (up to 300% at 500 MHz) by free space methods. Large MI effect makes them very promising for engineering artificial dielectrics with tuneable microwave properties. The S-parameters were measured at 0.9–17 GHz in the presence of external field ranging up to 3000 A/m. The effective permittivity spectra were deduced from S-parameters with the help of Reflection/Transmission Epsilon Fast Model.

We report on magnetic field dependence of the dielectric response in composites with arrays of parallel magnetic wires, continuous and short-cut, in the frequency region of 0.9–17 GHz. Both the real and imaginary parts of ε_{ef} show strong variations with increasing H_{ex} owing to the MI effect which controls the losses in the dielectric response. Long-wire composite has a plasmonic type dispersion of ε_{ef} with negative values of its real part below the plasma frequency (GHz range) for wire spacing of about 1 cm and wire diameter of few microns. The presence of H_{ex} suppresses low-frequency plasmons increasing the value of the real part of the permittivity. For cut-wire composites we confirmed a resonance type of ε_{ef} dispersion due to the dipole resonance in wires at half wavelength condition. Application of H_{ex} broadens the resonance and shifts it towards the higher frequencies. Therefore, both types of wire composites exhibit strong ε_{ef} (H_{ex}) dependence suitable for applications.

ACKNOWLEDGMENT

We acknowledge support under projects MAT2007-66798-CO3-01 (MEC) and Saiotek 08 METAMAT (SPRI).

REFERENCES

1. Pendry, J. B., A. J. Holden, W. J. Stewart, and I. Youngs, "Extremely low frequency plasmons in metallic mesostructures," *Phys. Rev. Lett.*, Vol. 76, No. 25, 4773–4776, 1996.
2. Makhnovskiy, D. P. and L. V. Panina, "Field dependent permittivity of composite materials containing ferromagnetic wires," *J. Appl. Phys.* Vol. 93, 4120, 2003.

Accurate Broadband Electromagnetic Characterization Method for Dielectric and Magnetic Materials

Jorge E. Lezaca[1, 2], **Patrick Quéffélec**[1, 2], **and Alexis Chevalier**[1, 2]

[1]Université Européenne de Bretagne, Brest, France
[2]Lab-STICC UMR-CNRS 3192, Université de Bretagne Occidentale, Brest, France

Abstract— The materials used on microwave applications have to be fully described. This description must have at least the same (better if bigger) bandwidth of operation that the one found in the application considered. To achieve this, broadband measurement techniques are normally based on guided structures like waveguides or transmission lines (coaxial, coplanar, microstrip, etc.) from which wideband properties are easily measured (S-parameters). There are some problems that researchers have to confront when working with these characterization techniques. One of them is the sensitivity. To achieve reliable results in the measurement, a strong interaction between the material (volume) and the wave is needed. The first drawback encountered in these techniques is that the longer the samples under test are, the lower the S-parameters' dimensional resonance frequency is. At these resonances, the S/N relation is too small, so the measured information is not accurate. If thin material samples are used, not enough interaction is accomplished, thus a poor precision is achieved. Another drawback, in the case of planar technology (microstrip or coplanar), is that the measurement becomes destructive. When the sample under test (SUT) makes part of the measurement structure, there is no certainty that the measurement been done for the material is not altered by the mechano-chemical procedure applied in the making of the circuit. Also, differential measurements used in the correction of the intrinsic errors of the measurement cell are not possible in this type of structures. One last drawback is that the broadband techniques are often defined for some specific types of materials: dielectric or magnetic, isotropic or anisotropic, etc.

In our laboratory we are developing a general broadband characterizationmethod in which this drawbacks are overcome. This technique is based on the use of a strip transmission line. This line is well-suited for materials used in planar technologies circuits (coplanar, microstrip, etc.). By doing a broadband optimization procedure, the problems involved with the S-parameters' dimensional resonances are avoided. This allows the use of long samples to achieve a good reliability in the measurements. For the generality of the method, a full-wave analysis of the measurement cell is performed. In this analysis, the calculation for dielectric and anisotropic magnetic magnetized materials is done. The strip transmission line has at the center the SUT and at the sides the possibility to add two different dielectric slabs. This dielectrics are needed in the anisotropic case to create a non-reciprocal effect. The non-reciprocity in the structure assures that the information measured is enough to fully characterize the permeability. Also if needed, this circuit can be allocated between the poles of an electromagnet to produce the external magnetic field that will lead the magnetic material to the desired magnetisation point. From the full-wave analysis of the transmission line, the theoretical S-parameters of the structure are calculated. Then, using the broadband optimization procedure, this theoretical S-parameters are matched to the measured S-parameters. In this optimization procedure, the permittivity and permeability functions (as functions of frequency) are used as optimization variables. Thus, as the result of this procedure, the permittivity and permeability wideband spectrum of the SUT are measured. This method is valid in a frequency range that goes from 0 to 14 GHz.

This is a new broadband characterization method in which by using one S-parameters measurement we will be able to characterize the broadband dynamic behaviour of dielectric or magnetic materials. The use of this method could help manufactures, researchers and engineers to optimize the procedures of fabricating and designing broadband materials and applications. Also, methods to characterize high frequency magnetic parameters like ΔH in a broadband frequency range or very accurate ferromagnetic resonance frequency (FMR) could be developed based on the use of this method. This method could if needed comply with the "in-situ" constraints due to its circuital form, like in the LTCC Technology were ferrite, dielectric and metallic layers are co-fired in the same process.

Session 4P4b
EM Theory: Waves and Media

Metal Nanoshell Characterization by Means of the Linear Polarization Degree at Right-angle Scattering Configuration

P. Albella[2], R. Alcaraz de la Osa[1], F. González[1], J. M. Saiz[1], and F. Moreno[1]

[1]Department of Applied Physics, University of Cantabria
Avda. Los Castros, Santander 39005, Spain
[2]Centro de Física de Materiales CSIC-UPV/EHU and DIPC
Paseo Manuel de Lardizabal 4, Donostia-San Sebastian 20018, Spain

Abstract— The manipulation of purpose-built metallic nanoparticles has achieved a great level of accuracy in the last years [1]. The special case of nanoshells has been widely studied [2], in part due to its numerous applications in biomedicine, ranging from high-resolution tumors imaging (in the case of scattered light), to cancer therapy (this time the absorbed light causes cell death in tumors). In particular, nanoshells can be designed to interact with desired wavelengths of light, making it very useful for detection and treating of cancerous cells [3].

In this contribution, we present a study of different situations involving silver nanoshells. In a first set of results, we let vary both the radius and the refractive index of the core, for a fixed outer radius of 50 nm. As a second step, we will also allow the nanoshells to be embedded in a surrounding medium, controlling its optical properties and the outer radius of the nanoshell itself, thus obtaining a complete study of the subject. We have seen that the linear polarization degree at right angle scattering configuration can be used in the setup of such nanoshells as well as to characterize them [4].

Figure 1(a) shows the linear polarization degree at right angle scattering configuration (PL (90°), varying the internal core radius (with fixed core refractive index $n_{core} = 2$). A big shift can be seen between the case of a pure silver sphere (without core), and the case of a very thin silver shell (more realistic one). Figure 1(b) shows the shifts in the minima of P_L (90°) for a fixed nanoshell of thickness 10 nm and changing core's refractive index.

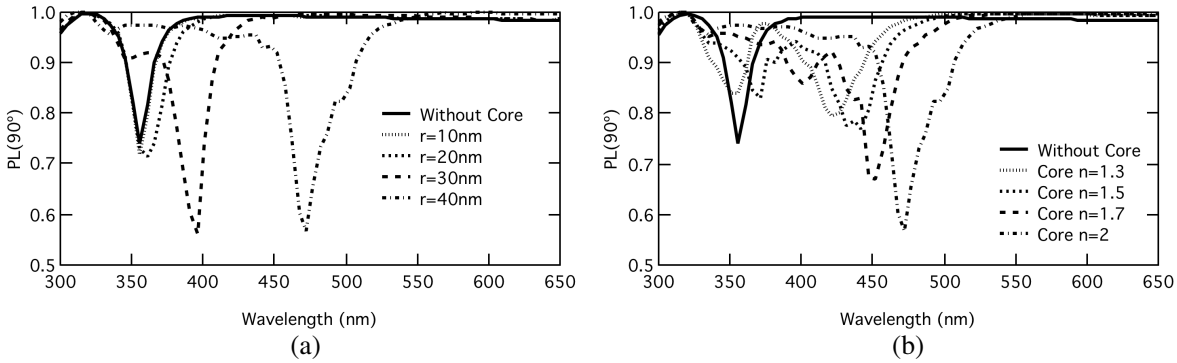

Figure 1: Right angle linear polarization degree spectra for silver nanoshells, (a) varying the internal core radius and (b) modifying core's refractive index between $n_{core} = 1.3$ and $n_{core} = 2$.

REFERENCES

1. Jain, P. K., X. Huang, I. H. El-Sayed, and M. A. El-Sayed, *Accounts of Chemical Research*, Vol. 41, 1578–1586, 2008.
2. Lassiter, J. B., M. W. Knight, N. A. Mirin, and N. J. Halas, *Nano Lett.*, Vol. 9, 4326–4332, 2009.
3. Loo, C., L. Hirsch, M.-H. Lee, E. Chang, J. West, N. Halas, and R. Drezek, *Optics Letters*, Vol. 30, 1012–1014, 2005.
4. Loo, C., L. Hirsch, M.-H. Lee, E. Chang, J. West, N. Halas, and R. Drezek, *Optics Letters*, Vol. 30, 1012–1014, 2005.

Application of the Green's Function to Calculating the Impedance of a Uniform Current Density between Two Multilayered Media

J. Acero[1], **C. Carretero**[1], **R. Alonso**[2], **Ó. Lucía**[1], **and J. M. Burdío**[1]

[1]Dep. Ingeniería Electrónica y Comunicaciones, Universidad de Zaragoza, Spain
[2]Dep. Física Aplicada, Universidad de Zaragoza, Spain

Abstract— The equivalent impedance of a uniform current density placed between two multilayered planar media is derived by using the Green's function. For the system of the Figure 1, the electromagnetic problem is posed in terms of the diffusion equation of the vector potential $\mathbf{A}(\mathbf{r})$ in the frequency domain [1], assuming the quasistatic approach and also considering cylindrical symmetry. The whole set of fields are obtained from the vector potential. In order to solve this equation, the Green's function $\mathbf{g}(\mathbf{r},\mathbf{r}')$ is used, being the solution of the following diffusion equation

$$\nabla^2\mathbf{g}(\mathbf{r},\mathbf{r}') - j\omega\mu\sigma\mathbf{g}(\mathbf{r},\mathbf{r}') = -\delta(\mathbf{r},\mathbf{r}'),$$

where $\delta(\mathbf{r},\mathbf{r}')$ is a current density modelled as a Dirac's delta function. The vector potential $\mathbf{A}(\mathbf{r})$ for a uniform current density $\mathbf{J}_e(\mathbf{r}')$ is obtained by convolution of $\mathbf{J}_e(\mathbf{r}')$ and $\mathbf{g}(\mathbf{r},\mathbf{r}')$. Moreover, taking advantage of the cylindrical symmetry of the system, the convolution operation is reduced to a product of the Fourier-Bessel-transformed versions of functions $\mathbf{J}_e(\mathbf{r}')$ and $\mathbf{g}(\mathbf{r},\mathbf{r}')$.

The vector potential $\mathbf{A}(\mathbf{r})$ for the system shown in the Figure 1 is obtained by adding the vector potential of the current density in the air and the contribution of the media. Considering that the media can be replaced by two equivalent current densities dependent on their properties and geometry, the vector potential representing the contribution of the media can also be obtained by means of a specific Green's function. Analytical expressions of both the Green's function for the coil in air and the contribution of the media are derived.

The impedance of the system is defined as the relationship of the electromotive force (emf) in the domain of the current density and the current. In each turn, the emf is obtained by integration of the electric field, defined as $\mathbf{E}(\mathbf{r}) = -j\omega\mathbf{A}(\mathbf{r})$, along the mean path of the current density. The calculated impedance consists of the series connection of equivalent resistances and inductances. Calculations are verified experimentally by means of measurements of the impedance for different configurations.

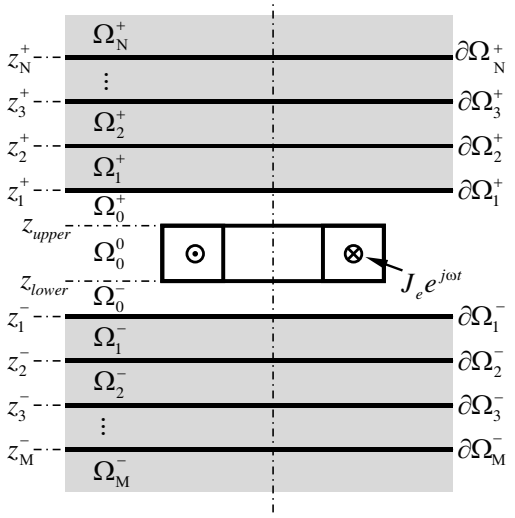

Figure 1: Uniform current density between two multilayered media.

REFERENCES

1. Acero, J., et al., "Electromagnetic induction of planar windings with cylindrical symmetry between two half-spaces," *J. Appl. Phys.*, Vol. 103, 104905(8), 2008.

Heavy Ions Acceleration of Solar Wind in Electromagnetic and Gravitational Fields

Ying Weng[1] and Zi-Hua Weng[2]

[1]College of Chemistry and Chemical Engineering, Xiamen University, Xiamen 361005, China
[2]School of Physics and Mechanical and Electrical Engineering, Xiamen University, Xiamen 361005, China

Abstract— The solar wind plasma mostly consists of the electrons and protons, and about 10% helium ions, and about 0.1% ions of other elements including the carbon, nitrogen, oxygen, and iron etc. The observational facts state that the velocities of helium ions are higher than that of the protons. Similarly the oxygen ions move more rapidly than the helium ions. It activates to suppose there may be one mechanism to accelerate heavy ions preferentially. By means of the octonion field theory the paper attempts to explain why the heavy ions displace faster in the solar wind.

In 1861, J. C. Maxwell first represented the electromagnetic theory with the algebra of quaternions, which was invented by W. R. Hamilton in 1843. Nowadays the gravitational field can be described by the quaternion as well, although the quaternion space for gravitational field is quite different to that for electromagnetic field. Simultaneously the electromagnetic field and gravitational field can be depicted in the octonion space, which comprises the electromagnetic quaternion space and the gravitational quaternion space.

In the octonion space, it is easy to define the field potential, field strength, field source, linear momentum, angular momentum, torque, and force etc of electromagnetic and gravitational fields. The force involves the well-known force terms such as Coulomb electric force, Lorentz force, Newtonian gravity, and inertial force etc. And this force definition encompasses some new force terms. One new force term will cause the charged particles move along the lines of magnetic force, while the other may compel the mass particles shift along the lines of velocity curl.

Due to the existence of magnetic strength and velocity curl, the higher charge ions move quicker, as well as the heavier ions displace more rapidly. Contrastively the electrons transfer slowly even to the contrary direction for their negative charges. These electrons form the resistance medium to slow down positive ions, so that the ions with various charges have different maximum velocity in the solar wind. For the same one ion the acceleration effect may be different in solar surfaces for different magnetic strengths and velocity curls, especially in the Polar Regions of the sun.

ACKNOWLEDGMENT

The author is grateful for the financial support from the National Natural Science Foundation of China under grant number 60677039.

Magneto-optic and Electro-optic Effects in Electromagnetic Fields

Zi-Hua Weng
School of Physics and Mechanical & Electrical Engineering, Xiamen University, Xiamen 361005, China

Abstract— The algebra of quaternions was invented by W. R. Hamilton, and then was first used by J. C. Maxwell to represent field equations of electromagnetic field. At present the gravitational field and electromagnetic field both can be illustrated by the algebra of quaternions. And their quaternion spaces can be combined together to become the octonion space, which was invented by A. Cayley and J. T. Graves independently. In other words, the characteristics of gravitational field and electromagnetic field can be described with the octonion space simultaneously.

In the octonionic field theory for electromagnetism and gravitation, the paper deduces the field equation, wave equation, linear momentum, angular momentum, energy, torque, power, and force etc. The force definition can incorporate various kinds of force terms within one single formula, and then draw out some optic effects, including Zeeman effect, Larmor precession, Faraday effect, Stark effect, Pockels effect, and Kerr effect etc in the electromagnetic field. This method can be considered as one kind of non-quantum theoretical explanation.

The paper studies the impact factors of magneto-optic effects for electromagnetic fields in the presence of gravitational fields. In the description with the algebra of octonions, the deductions of Zeeman effect, Larmor precession, and Faraday effect etc are identical respectively with that in the conventional electromagnetic theory with the vector terminology. Rephrasing the optic effects with the octonions, the inferences are accordant to the existing results from M. E. Verdet, M. Faraday, J. B. Biot, J. MacCullagh, G. B. Airy, H. A. Rowlland, and J. C. Maxwell etc.

In the existing physical theories, it was believed that the description of electro-optic effects had to be dealt with the quantum theory, including that of Stark effect, Pockels effect, and Kerr effect etc. With some new force terms in the octonion space, these electro-optic effects can be deduced from the octonionic field theory of gravitation and electromagnetism. It is easy to think out that the electro-optic effects may be shifted in the unsteady states and some force terms regarding the electric field and gravitational field etc.

ACKNOWLEDGMENT

The author is grateful for the financial support from the National Natural Science Foundation of China under grant number 60677039.

Magnetic Suspension System for Platform Performance

Chin E. Lin and Wei-Cheng Huang
Department of Aeronautics and Astronautics, National Cheng Kung University, Tainan 701, Taiwan

Abstract— Magnetic suspension technology has features of contact-free, friction-free, low contamination and low noise. It is implemented as an important part of mechanical operation system with appropriate control. This paper presents a hybrid mode control implementation on magnetic suspension actuators to demonstrate the ball and plate system operation. A single axis magnetic suspension (MS) actuator is design to offer up and down motion with controllable force. An exquisite platform mechanics is designed supporting from four MS actuators to complete multiple degree-of-freedom performance. The mathematical model of the ball and plate system is derived through the Euler-Lagrange equation. A hybrid mode control law was developed following an enhanced Fuzzy control law and a PID control law. The enhanced Fuzzy control law can reduce overshoot and settling time more than the traditional ones. To implement this ball and plate system, a commercial touch-screen was used to be a position sensor and control circuit is designed and fabricated using a microprocessor as the control kernel. The ball and plate system is tested on both static (toward balance point) and dynamic (rectangular tracking) performances. This paper demonstrates electromagnetic system in industrial applications.

Session 4P5a
Ground Penetrating Radar (GPR) for Civil Engineering Applications

Test Method for Evaluating Asphalt-covered Concrete Bridge Decks Using Ground Penetrating Radar

J. Rhazi
Department of Civil Engineering, Université de Sherbrooke
Sherbrooke (Québec), J1K 2R1, Canada

Abstract— This paper presents the synthesis of an experimental investigation carried out on several reinforced concrete bridge decks concerning concrete deterioration effects on electromagnetic wave propagation. It will demonstrate that the data analysis procedure proposed by the ASTM D6087 "Standard Test Method for Evaluating Asphalt-covered Concrete Bridge Decks Using Ground Penetrating Radar (GPR)" must be revised. A novel methodology of GPR data processing that allows the detection of areas of high probability of rebar corrosion in concrete is presented.

Characterization of the GPR Surface Waves for Civil Engineering Applications

B. Filali[1], **J. Rhazi**[2], **F. Boone**[3], **and G. Ballivy**[2]

[1]Civil Engineering and Electrical Engineering Departments, Sherbrooke University, Qc, Canada
[2]Civil Engineering Department, Sherbrooke University, Qc, Canada
[3]Electrical Engineering Department, Sherbrooke University, Qc, Canada

Abstract— The electromagnetic (EM) surface wave is defined as a part of the volume wave propagating along the interface between two different mediums. This kind of EM waves may be used to assess civil engineering materials. They are especially needed when no echoes are detected from nearly bottom interfaces (ex. Evaluation of water content profile in reinforced concrete). In this purpose, we proceed to the characterization of the surface wave by modeling electromagnetic waves centred at 400 MHz frequency. It is visualised in the time domain as a trace on a radargram, so its travel time and attenuation are obtained from the isolated wave impulse. From different travel times in different mediums, the depth of the propagation layer is deduced approximately and showed to be sufficient for non destructive testing in civil engineering. In addition, we observed that this layer depth increases with the distance from the source. This penetrating depth values are confirmed by the attenuation calculus, where we obtained, for the entire frequency spectrum, values close to those obtained from previous method. The frequency variation of the depth is also observed and explained.

Simulation and Detection Limit of EM Waves in Masonry Structures with Application of an Algorithm for Image Processing

R. Hamrouche[1, 2], G. Klysz[1], J. P. Balayssac[1], J. Rhazi[2], and G. Ballivy[2]

[1]LMDC (Laboratoire Matériaux et Durabilité des Constructions), UPS, INSA, Université de Toulouse
135 avenue de Rangueil, 31 077 Toulouse Cedex 04, France
[2]Department of Civil Engineering, University of Sherbrooke, Sherbrooke, Québec J1K 2R1, Canada

Abstract— The objective of this work is to use Ground Penetrating Radar for the inspection of brick masonry structures and, in particular, to look for deep unfilled joint defects by developing a specific signals processing algorithm that facilitate interpretation of GPR profils and improve it's accuracy. This will help the manager to quantify the volume of mortar to be re-injected in case of reinforcing work.

As a first approach, to better understanding propagation of EM waves in a complex medium as brick masonry structures, a numerical modeling of a GPR antenna with a central frequency of 1.5 GHz is used to simulate the propagation of EM waves in brick masonry structure including different size of deep unfilled joint defects. The simulations are carried out in a separated bistatic configuration. For each transmitter position, several signal acquisitions are implemented using a regularly spaced crescent pattern for the receivers.

The developed signal processing algorithm is based on inverse methods applied in the time domain, it analyzes the travel times of the reflected signals by making the assumption that each point of the modeled space is a reflector. The calculation of the travel time, which helps to identify the signal corresponding to each point of space, is made by using an estimated speed of the direct wave between transmitter and receivers in the material, which is then regarded as representative of the whole of the simulated environment.

Finally, the developed signal processing algorithm is applied on different simulated signals, the goal is to define it's detection limits in terms of size, spacing and depth of the unfilled joint defects. Therefore highlight the improvements that could make the algorithm for the interpretation and the accuracy of GPR signals from brick masonry structures.

GPR Limits for Thin Layers in Concrete Detection: Numerical and Experimental Evaluation

A. Van der Wielen, **L. Courard**, **and F. Nguyen**
University of Liege, Belgium

Abstract— The Ground Penetrating Radar (GPR) is a nondestructive technique increasingly used in civil structures inspection, including bridge decks condition assessment. In such structures, many features that we can intend to detect with GPR have a relatively small thickness compared to their area: the waterproofing layer, degraded or delaminated layers into the slab. For the GPR user, it is thus very important to have a good estimation of the detection limit of the device, as well as of its resolution, defined as the minimum thickness that can be precisely evaluated.

The multiple reflection scheme of the GPR waves on the two interfaces limiting the thin layer is complex, and the theoretical relationships predicting the reflected amplitude are based on multiple simplifying assumptions that are not matched by most commercial GPR machines. Indeed, real GPR impulsions can hardly be approximated by plane and continuous sinusoid waves.

In the first part of this study, we confronted the theoretical curves with numerical finite difference simulations performed with GprMax2D. Then, the influence of every parameter and hypothesis was evaluated. We also tried to draw realistic curves predicting the reflection coefficient, taking into account the actual characteristics of our antenna.

In the second part, we performed experiments on real concrete slabs, separated with an air space of variable thickness. Doing so, we estimated the detection limit and the resolution of our Mala 2.3 GHz antenna, which proved to be relatively close to those predicted by the numerical simulations.

Finally, we studied the possibility to improve the characterization of the detected layers by the use of inversion (with a neighborhood algorithm) of APVO curves obtained with common midpoint measurements.

MARSIS Data Analysis Planning

G. Picardi, **A. Masdea**, **M. Restano**, **and R. Seu**
Infocom Department, University of Rome "La Sapienza", via Eudossiana 18, Rome 00184, Italy

Abstract— MARSIS (Mars Advanced Radar for Subsurface and Ionosphere Sounding) is a low-frequency nadir-looking pulse limited radar sounder and altimeter with ground penetration capabilities, which uses unfocused synthetic aperture technique to highlights subsurface reflections. According to the Mars Express mission, the MARSIS primary scientific objective is to map the distribution of water, both liquid and solid, in the upper portions of the crust of Mars; detection of such reservoirs of water will address key issues in the hydrologic, geologic, climatic and possible biologic evolution of Mars. Three secondary objectives are also defined: subsurface geologic probing, surface characterization and ionosphere sounding.

The principle of operation of MARSIS is based on the transmission of an electromagnetic wave, which will propagate till the top of the Mars surface producing a first reflection echo which propagates backward to the radar. However, due to the long wavelengths employed, a significant fraction of the electromagnetic energy impinging on the surface is transmitted into the crust and propagates downward; in order to maximize the penetration capability of the transmitted pulse, MARSIS operates at 1.3 MHz–5.5 MHz frequency range. Additional reflections, due to the subsurface dielectric discontinuities (due f.i. to water or ice), would occur and the relevant echoes would propagate backward through the first layer medium and then to the radar generating further echo signals, that are typically weaker than the signal from the surface.

The aim of the inversion process is the estimation of the materials, including the impurities, (or at least the compatibilities with a reference list of materials) composing the detected interfaces. The estimation of the inclusions is performed in terms of percentage, dielectric constant of the mixture and reflectivity: in this case there are many solutions and the geologist shall select the proper one taking into account the geological and thermal hypotheses.

The backscattered signal depends by the material features and by the geometric contributions. The last one implies that is necessary to know the scattering behavior of the surface and subsurface, related to their characteristics (flat or rough surface), according with the physical and geometric optics properties. For this task it is necessary the selection of the backscattering models, in order to apply the appropriate one on the surface/subsurface to be investigated for the data inversion.

In addition the analysis of radar sounding data requires the selection of the signals generated by the subsurface interfaces among those coming from the surface topographic features not immediately below the radar so that the time delay between transmission and reception is the same (surface "clutter").

The Martian surface geometric structure has been characterized in terms of a large-scale morphology on which a small-scale geometric structure, due to rocks, is superimposed. The structure of the planet's surface has been described by means of fractals model and, in particular, new Mars surface models have been obtained by processing of MOLA data. Ionosphere models, utilized to recover the correct radar pulse by a closed loop approach, have been analyzed and experimentally verified.

The radar sounder data inversion utilizes a physically based approach and the obtained results, for a particular area in Mars South Pole, are reported.

Insulated Concrete form Void Detection Using Ground Penetrating Radar

Roger Roberts, **Ken Corcoran**, **Michael Arvanitis**, **and Alan Schutz**
Geophysical Survey Systems Inc., Salem, NH, USA

Abstract— Insulated concrete form (ICF) construction consists of interlocking polystyrene forms and poured-inplace concrete. The forms are left in place after the concrete is poured to form an efficient insulation barrier. Consequently, it is difficult to ascertain the presence of flaws in the concrete, such as voids at the boundary between the form and the concrete, using traditional inspection methods without removing, and thus damaging, the polystyrene forms. In a research investigation, it was found that ground penetrating radar (GPR), utilizing a 1.6 GHz center-frequency antenna, is useful for locating voids at the concrete-form boundary and voids buried in the concrete. The highest quality data were obtained from vertical profile lines. The detection of the voids was possible by performing a background-removal process to the data that stripped the direct-coupling between the transmit and receive antennas, which effectively isolated the concrete surface reflection. Mapping the change in arrival time and amplitude of the concrete surface reflection was useful in characterizing, to some extent, the dimensions and depths of the voids. The detection of voids buried 2.5 to 10.8 cm (1.0 to 4.3 in) in the concrete was also achieved after 3 days of curing. Additional data processing was required to enhance the detectability of the buried voids. The generation of a 3-D dataset and subsequently viewing thin depth slices of data was useful in distinguishing the void reflections from the reinforcing reflections.

Session 4P5b
Scattering, Rough Surface Scattering and Remote Sensing

Light Scattering from Surfaces and Multilayers: Measurement and Modeling Using Vector Perturbation Theories

Marcus Trost[1,2], **Sven Schröder**[1], **Angela Duparré**[1], **and Andreas Tünnermann**[1,2]

[1]Fraunhofer Institute for Applied Optics and Precision Engineering
Albert-Einstein-Straβe 7, Jena 07745, Germany
[2]Institute of Applied Physics, Friedrich-Schiller-University, Max-Wien-Platz 1, Jena 07743, Germany

Abstract— Light scattering from interface imperfections and defects is often an unwanted effect in optical systems since it reduces the throughput and image contrast. But, at the same time, scattered radiation carries valuable information about its origins. This can be utilized to characterize the roughness properties of optical surfaces using light scattering measurements and vice versa by applying appropriate light scattering theories [1, 2].

For the case of optically smooth surfaces first-order vector perturbation theories have been developed to link the roughness with the scattering properties of single surfaces as well multilayer coatings. It can be shown that these theories provide a rigorous solution of Maxwell's equations if the interface roughness is sufficiently low compared to the radiant wavelength. While for applications in the infrared spectral region these theories can be assumed to be valid for most optical interfaces, for applications at short wavelengths such as extreme ultraviolet (EUV) lithography or X-Ray optics, this poses tremendous requirements on the interfaces.

The ranges of validity of vector perturbation approaches are discussed. As an example, an EUV multilayer coating for 13.5 nm is chosen. The angle resolved scattering at 13.5 nm is investigated by comparing scatter modeling and at-wavelength measurements using the instrument described in [3]. The relevant substrate and intrinsic thin film roughness properties are analyzed with respect to their impact onto the optical properties.

In addition to the prediction of scattering properties based on roughness data, the rather simple analytic result of vector perturbation theories for a single surface can be inverted and used to retrieve roughness data from light scattering measurements [4]. This is exemplified for large mirror substrates with super-low high-spatial frequency roughness and challenging geometry (ellipsoid, diameter 660 mm). For these surfaces, the presented light scattering method turns out to be superior to conventional characterization methods. The method may also be applied to characterize mirrors for astronomy.

REFERENCES

1. Elson, J. M., "Diffraction and diffuse scattering from dielectric multilayers," *J. Opt. Soc. Am.*, Vol. 69, 48–54, 1979.
2. Bousquet, P., F. Flory, and P. Roche, "Scattering from multilayer thin films: Theory and experiment," *J. Opt. Soc. Am.*, Vol. 71, 1115–1123, 1981.
3. Schröder, S., T. Herffurth, M. Trost, and A. Duparré, "Angle-resolved scattering and reflectance of extreme-ultraviolet multilayer coatings: Measurement and analysis," *Appl. Opt.*, Vol. 49, 1503–1512, 2010.
4. Schröder, S. and A. Duparré, "Finish assessment of complex surfaces by advanced light scattering techniques," *Proc. SPIE*, Vol. 7102, 71020F, 2008.

TE Wave Scattering from a Binary Periodic Random Surface (I) — Bbinary Fluctuation of Zero/One Series

Kazuhiro Hattori[1], **Junichi Nakayama**[2], **and Yasuhiko Tamura**[2]

[1]Mayekawa MFG. Co Ltd., Japan
[2]Kyoto Institute of Technology, Japan

Abstract— This paper deals with the scattering of TE plane waves from a binary periodic random surface, which has binary fluctuation of zero/one series shown in Fig. 1, where 'zero' corresponds to a at part and 'one' to a deformation. We assume that the surface is obtained by superposing a binary periodic random surface on a periodic surface, where both surfaces are composed by the same local profile. The binary periodic random surface is made by displacing the local profile by every integer multiple of the period and modulating their amplitudes by a stochastic binary sequence $\{b_m\}$ taking only ± 1.

For analysis, we employ the stochastic functional approach [1]. Since the binary periodic random surface becomes a periodic stationary process and has shift invariance property in the probabilistic sense, the scattered wave has the stochastic Floquet form, which is a product of an exponential phase factor and an unknown periodic stationary process. Then, such an unknown periodic stationary process is expressed by a harmonic series representation given by mutually correlated stationary process. These stationary processes are represented by a sum of orthogonal binary functional series with band-limited binary kernels. Hierarchical equations to determine such band-limited binary kernels are derived from the Dirichlet boundary condition without approximation. Several statistical properties of the scattering are numerically calculated in terms of such binary kernels.

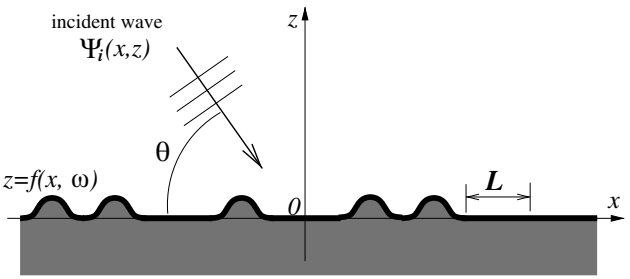

Figure 1: Binary periodic random surface with binary fluctuation of 0/1 series.

REFERENCES

1. Hattori, K., J. Nakayama, and Y. Tamura, "Diffraction and scattering of TM plane waves from a binary periodic random surface," *Waves in Random and Complex Media*, Vol. 18, 585–613, 2008.

Analytically-based Optimization for Load-modulated Scattering Antennas

H. Memarzadeh-Tehran[1], **Jean-Charles Bolomey**[2], **and Jean-Jacques Laurin**[1]

[1]Département of Electrical Engineering, École Polytechnique de Montréal
P. O. Box 6079, Station Centre-Ville, Montreal, Qc, H3C 3A7, Canada
[2]Electromagnetic Research Department, Supélec, France

Abstract— For many decades, load-modulated scattering antennas have been considered for wireless communications and sensing applications. For such applications, using an antenna in its scattering mode allows to avoid any RF front-end resulting in very simple and compact passive or battery-assisted transponders. These advantages are widely exploited in low-cost RFID tags, but also for low-invasive field measurement with MST probes The price to pay is a low sensitivity as compared to standard transmission systems, making the modulated power budget a key issue, more particularly in the case of active or battery-assisted transponders. As well known, for "normal" receiving antennas the power budget can be written as follows:

$$P_{rec}/P_{trans} = |S_{12}|^2 \, LF \tag{1}$$

where S_{12} is the power normalized scattering parameter between the transmitting and receiving antennas, and $LF (0 \leq LF \leq 1)$ the load factor which is maximized by conjugate matching the receiving antenna to the receiver. In practice, both transmit and receive antennas are usually standardized to $50\,\Omega$. In contradistinction, the situation of load-modulated scattering antennas is more complicated. Indeed, such antennas are alternatively switched on two distinct loads which exhibit a high impedance contrast in order to obtain a sufficient modulation depth. Consequently, the backscattered power depends on the probe and load impedances. By using reciprocity theorem, the modulated power budget in arbitrary scenarios (non-free-space, non-far field) can be written in a similar way as (1):

$$P_{rec}^{\mathrm{mod}} /P_{trans} = |S_{12}|^4 \, ME \tag{2}$$

where $ME\,(0 \leq ME \leq 4)$ introduced as the modulation efficiency [1], only depends on antenna and load impedances Equation (2) constitutes the basement of the optimization of the modulated transponder. It can be shown that, for a given load impedance combination, there exists only one antenna impedance providing a maximum modulation efficiency $ME_{\max} \leq 4$. However, this optimal antenna impedance is not necessarily achievable, for instance, due to possible operational constraints. Furthermore, shaping the antenna for obtaining the optimal impedance may also impact some other antenna parameters which are implicitly contained in S_{12}. This paper addresses various antenna optimization strategies taking into account i) the general relationships existing, for any antenna, between parameters impacting both ME and S_{12}, such as input impedance, gain or effective length, and ii) possible dimensional constraints which may become critical in some applications. It is demonstrated that, in many practical cases involving electrically small antennas, the modulation efficiency remains the relevant parameter to consider for maximizing the modulated power budget. With respect to a blind pure numerical optimization approach, the previous analytical formulation provides a valuable support in identifying the key factors as well as in obtaining explicit bounds and sensitivities, and hence paves the way for efficient and physically sounded optimization of global performances. For the sake of illustration, the case of a center-loaded dipole antenna will be discussed with possible application to optically modulated E-field measurement probes [2].

REFERENCES

1. Bolomey, J. C., S. Capdevila, L. Jofre, and J. Romeu, "Electromagnetic modeling of RFID-modulated scattering mechanism," *Proc. IEEE Application to Tag Performance Evaluation*, Vol. 98, No. 9, 1555–1569, Sept. 2010
2. Memarzadeh-Tehran, H., J.-J. Laurin, and R. Kashyap, "Opticaly modulated probe for precision near-field measurements," *IEEE Trans. Instr. Meas.*, to appear.

Localization and Diffusion of Light in Waveguide Systems

Akira Komiyama
Osaka Electro-Communication University, Hatsu-Cho, Neyagawa-Shi 572-8530, Japan

Abstract— A one-dimensional waveguide system composed of a large number of cores is a theoretical model of an image fiber which is used to transmit directly an optical image [1]. The waveguide systems can be classified into three groups: ordered, disordered and random systems. By numerically solving the coupled mode equation for a waveguide system outlines of the propagation properties of light can be known [2, 3]. Light is localized in a disordered system and diffused in a random system. In this paper present states of analytical treatments of their phenomena are described.

The coupled mode equation for an ordered system composed of identical cores can be exactly solved. The solution gives the basis of the description of the light propagation in disordered and random systems.

The coupled mode equation for a disordered system composed of randomly different cores in size has been solved by the perturbation method and the average amplitude in the Laplace transform domain has been derived. It has been shown that the analytical result is in good agreement with the numerical results [4]. The analytical description of the average power is currently under consideration.

In a random system core sizes change randomly along the waveguide axis. From the perturbation solution of the coupled mode equation the differential equations for the average amplitude and the average power can be derived and the equations can be exactly solved [5]. For short correlation length the analytical result is in good agreement with the numerical results.

REFERENCES

1. Komiyama, A. and M. Hashimoto, *Opt. Comm.*, Vol. 107, 49–53, 1994.
2. Komiyama, A., *Proc. 28th GA-URSI*, BP. 13, 2005.
3. Komiyama, A., *IEEJ Technical Report*, EMT-06-46, 2006.
4. Komiyama, A., *IEICE Trans. Electron.*, Vol. E93-C, 46–51, 2010.
5. Komiyama, A., *IEICE Trans. Electron.*, Vol. E92-C, 85–91,2009.

Model Development and Analysis of Multiple Surface Scattering and Surface-Volume Scattering in Snow Layer

Syabeela Syahali[1] and Ewe Hong Tat[2]

[1]Multimedia University, Malaysia
[2]Faculty of Information and Communication Technology, University Tunku Abdul Rahman
46200 Petaling Jaya, Selangor, Malaysia

Abstract— For an electrically dense medium bounded by irregular boundaries such as snow area, multiple surface scattering and second order surface-volume scattering may have significant contribution towards the total backscattering coefficient. To better understand these effects, it is important to develop a reliable theoretical model to study the medium where multiple surface scattering and second order surface-volume scattering may be important. In this study, the backscattering model for electrically dense medium developed in [1] is improved. This is done by considering multiple surface scattering effect together with the single scattering effect in the formulation of the surface scattering on both the top and bottom boundaries. The surface scattering formulation is based on existing Integral Equation Model (IEM) [2]. Improvement is also done by including more surface-volume scattering terms up to second order, in addition to the existing terms considered in [1]. The improved model is applied on a snow layer above ground which is modelled as a volume of ice particles that are closely packed and bounded by irregular boundaries above a homogenous half space. The effect of including multiple surface scattering and additional surface-volume scattering up to second order in calculating the backscattering coefficient of snow layer is studied for both co-polarized and cross-polarized return. Its effect on each scattering mechanism is also investigated to understand the effect of surface multiple scattering and second order surface-volume scattering in more detail. Results show improvement in the total backscattering coefficient especially for cross-polarized return. Comparison with field measurement results is also carried out and promising match is observed.

REFERENCES

1. Ewe, H. T., H. T. Chuah, and A. K. Fung, "A backscatter model for a dense discrete medium: Analysis and numerical results," *Remote Sensing of Environment*, Vol. 65, No. 2, 195–203, 1998.
2. Fung, A. K., *Microwave Scattering and Emission Models and Their Applications*, Artech House, Norwood, MA, 1994.

Session 4P6a
Apparatus for Biological, Medical and Industrial Applications of EM Field

Prospective Applications of EM fields in Medicine

J. Vrba, **L. Oppl**, **D. Vrba**, **J. Vorlíček**, **B. Vrbová**, **and D. Havelka**
Department of EM Field, Czech Technical University, Technická 2, Prague 16627, Czech Rep.

Abstract— Medical applications of microwaves (i.e., a possibility to use microwave energy and/or microwave technique and technology for therapeutical purposes) are a quite new and a very rapidly developing field. Microwave thermotherapy is being used in medicine for the cancer treatment and treatment of some other diseases since early eighties. In this contribution we would like to offer general overview of present activities in the Czech Republic, i.e., clinical applications and results, technical aspects of thermo therapeutic equipment and last but not least, prospective diagnostics based on microwave principals ant technology and instrumentation.

Applicators for Research of Biological Effects of EM Field

Jan Vrba[1], **Lukas Visek**[1], **Ladislav Oppl**[1], **and Luca Vannucci**[2]

[1]Department of EM Field, Czech Technical University in Prague, Prague, Czech Republic
[2]Institute of Microbiology, Czech Academy of Sciences, Prague, Czech Republic

Abstract— Research of interactions between EM Field and biological systems is of growing interests elsewhere. Also here in Czech Republic there are several groups working in this field, often in international co-operations. We will describe here mainly basic technical equipment developed for 5 different research projects in the discussed area of interactions of EM field and biological systems.

Numerical Dosimetry Analysis of Exposure Chamber

Lukas Visek and Jan Vrba
Department of Electromagnetic Field, Czech Technical University
Technicka 2, Prague 166 27, Czech Republic

Abstract— Along with a development and increasing use of sophisticated devices emitting microwave electromagnetic field, mobile phones in particular, public concern has raised about its possible harmful health impacts. Although a lot of researches have been accomplished, no adverse health effects of cellular phones have been confirmed yet. The main aim of this work is to analyze the dosimetry results reached by computer simulations in order to support researches where the influence of electromagnetic field is investigated.

It generally is difficult to measure the SAR directly in a living biological body, and therefore dosimetry efforts are forced to rely on computer simulations. An anatomically based biological model is essential for numerical dosimetry. Therefore the anatomical mouse model was developed. The created model has the resolution 0.1 mm, meaning voxel size $0.1 \times 0.1 \times 0.1$ mm. Each voxel was assigned to one of 11 different tissue types.

The exposure setup operating at 900 MHz was designed with respect to the following points:

- induced uniform field,
- external radiation elimination,
- sufficient space for mice,
- even mice exposure,
- costs.

The setup basic properties such as electromagnetic field distribution and impedance matching were optimized by SEMCAD X.

In order to verify numerical dosimetry results, the simulations were performed in two different electromagnetic field simulators using different numerical methods. As 3D simulators using different numerical methods were chosen SEMCAD X which uses Finite Difference Time Domain (FDTD) method and CST Microwave Studio which uses Finite Integration Technique (FIT) method. The simulations were performed for three positions of mouse in order to verify an even exposure which should be assured by circular polarized wave. The first and the second position of the mouse was chosen perpendicularly to one of the feeding antenna of exposure chamber and the third position was chosen generally.

The simulation results were compared and reached results were in a good agreement. The designed exposure chamber is suitable for researches of effects of electromagnetic field.

Electric Oscillating Field of Microtubule Network

Daniel Havelka[1], **Michal Cifra**[1, 2], **and Jan Vrba**[1]

[1]Department of Electromag. Field, Czech Technical University
Technická 2, Praha 166 27, Czech Republic
[2]Institute of Photonics and Electronics, Academy of Sciences of the Czech Republic, Czech Republic

Abstract— Microtubules, as one of the three types of filaments of cytoskeleton, are composed of very polar structures called tubulin heterodimers. These subunits are situated in medium, which can cause their mechanical oscillations. These mechanical oscillations can generate electromagnetic field in frequency range from kHz to GHz. We approximate electrical properties of tubulin heterodimer by an elementary electric dipole. Oscillations of microtubule are implemented by spatial function. In this paper, we present selected results of calculations of intensity of electric field around microtubule generated by longitudinal axial wave. We also show other selected results such as power generated from microtubular network and intensity of electric field in radial distance from this network.

Contribution of Complex Permittivity Measurement in Hyperthermia Treatment Planning

Jaroslav Vorlíček, **Ladislav Oppl**, **and Jan Vrba**
Department of Electromagnetic Field, Czech Technical University, Czech Republic

Abstract— Relative permittivity, loss factor and conductivity are basic parameters for electromagnetic field modeling and simulations. Although for many materials these parameters could be found in the tables, very often their experimental determination is necessary. Dielectric properties of biological tissues are determining factors for the modeling of the dissipation of electromagnetic energy in the human body and therefore they are useful in hyperthermia cancer treatment. Measurement of the dielectric parameters of biological tissues is also a promising method in the medical diagnostics and imaging. Knowledge of the complex permittivity in treated area, i.e. knowledge of the complex permittivity of healthy and tumor tissue is very important for example in the diagnosing of tumor regions in the human body or in the design of thermo-therapeutic applicators which transform electromagnetic energy into thermal energy in the tissue. The heat dissipation of irradiated tissue needs to be modeled very precisely to give us more accurate view on the heated volume of the tissue in hyperthermia treatment planning.

Microwave thermotherapy or hyperthermia is a method commonly used for cancer treatment in oncology. Together with radiotherapy or chemotherapy it is applied to improve the treatment results. It is based on the principle that cancer cells are more sensitive to higher temperatures. Healthy cells survive temperatures up to 45°C, whereas cancer cells only up to 42°C. Heating biological tissue in temperature interval (42–45°C) results in only cancer cells are being destroyed. In a healthy tissue the blood flow increases together with increasing temperature causing further temperature increase to stop. In tumor tissue, however, this mechanism does not happen because of lack of a sophisticated vascular system.

The work deals with the measurement method for the non invasive and still accurate measurement of complex permittivity of biological tissue. Later the whole process of segmentation of the patients MRI/CT data is described. Created model is inserted into simulator of electromagnetic field and the thermal dissipation of electromagnetic radiation is simulated. The applicators used here are strip TEM wave applicator, lucid horn applicator and TE_{10} applicator. The verification of numeric simulations of Specific Absorption Rate distribution in non-homogenous phantom is accomplished by electromagnetic field simulator SEMCAD 13.4.

ACKNOWLEDGMENT

This research is supported by Grant Agency of the Czech Republic, project: "Non-standard application of physical fields — analogy, modeling, verification and simulation" (102/08/H081).

Applicators for Microwave Thermotherapy: Comparison of SAR Distribution in Homogeneous Phantom and in Anatomical Model

Barbora Vrbova and Jan Vrba
Department of Electromagnetic Field, Faculty of Electrical Engineering
Czech Technical University in Prague, Technicka 2, 166 27 Prague 6, Czech Republic

Abstract—

Background: In this contribution we deal with simulations of SAR distribution obtained by array of microwave stripline TEM mode applicators of the same type radiating at frequency 434 MHz. In this study we compare the SAR distribution in a homogeneous agar phantom (which has similar characteristics to muscle tissue) and in an anatomical based biological model (which has been developed from a computer tomography scan).

Methods: Discussed applicators are made of highly conductible material (copper) and lateral sides of applicator are from acrylic glass. TEM wave is being transferred along a section of microwave stripline transmission line with cross-section dimensions 50×30 mm and length 80 mm. Horn section of applicator has length 80 mm. The horn aperture has dimensions 120×80 mm. Between cylindrical agar phantom and applicator aperture there is a water bolus. The matrix composition of several applicators of the same kind has been studied and will be described in details in full paper. Homogeneous agar phantom represents one of tissues of human body, in our case muscle tissue. This agar phantom is simulated by aid of the SEMCAD X EM Field simulator (SPEAG, Schmid & Partner Engineering AG, Switzerland). Anatomical based biological model is an 3 dimensional model of human body, where several types of tissue is taken into account. This anatomical model is created from 2 dimensional scans (CT scans) by segmentation program — 3D-DOCTOR (vector-based 3d imaging, modeling and measurement software).

Results: The SAR distributions acquire theirs maximum at the same locations both in agar and in anatomical phantom, but the shape of the SAR distribution in the anatomical phantom is influenced by the fat and bone tissue in the studied area.

Conclusions: Simulation of SAR distribution in a homogeneous agar phantom is used for basic evaluation of microwave applicator. But in case of hyperthermic treatment planning it is very useful to create an anatomical model of the treatment area of patient. In future the treatment of tumors can be improved by setting the amplitude and the phase of the single applicators in the matrix.

ACKNOWLEDGMENT

This research is supported by Grant Agency of the Czech Republic, project: "Non-standard application of physical fields — analogy, modeling, verification and simulation" (102/08/H081).

Microwave Applicators for Industrial Purposes

Jan Vrba[1], **Milan Stejskal**[2], **Jan Vrba (Jr.)**[3], **Tomas Vydra**[1], **and Marika Pourova**[1]

[1]Department of Electromagnetic Field, Czech Technical University in Prague
Technická 2, 166 27 Prague 6, Czech Republic
[2]Research Institute of Textile Machines, U jezu 4, Liberec, Czech Republic
[3]Institute of Theoretical Electrotechnic, RWTH Aachen, Aachen, Germany

Abstract— In this paper we describe our new results dealing with microwave industrial applicators used for drying of textile materials. We have designed and evaluated two different types of these applicators: open-resonator-type and waveguide-type one. We describe here basic models of the discussed applicators, results of numerical modelling and experimental evaluation as well. Prototype of microwave drying machine working at frequency 2.45 GHz is reported.

System for Visualization and Evaluation of Microwave Applications

T. Vydra, J. Vrba, and M. Pourová
Department of Electromagnetic Field, Faculty of Electrical Engineering
CVUT in Prague, Czech Republic

Abstract—

Background: As the importance of usage of microwave technologies in many applications is rising it is necessary to develop simple to use, reproducible and exact methods of evaluation of microwave primary (i.e., thermal) effects on biological materials. In medical application we aim not to hurt the patient and we try to enhance efficiency of the treatment to minimize the adverse impact on the healthy tissue. On the other hand in industrial use we need the processing to be economical meaning energy efficient.

It is very difficult to monitor effects of electromagnetic field on biological material in real time but can be crucial for deeper understanding of processes that take place during procedures using microwave energy (i.e., microwave processing of biopolymers, microwave thermotherapy, microwave heating and drying). Using conventional methods of evaluation of temperature, volume and other properties usually effects the distribution of electromagnetic field and interferes with it. It is possible to stop the process at any time and evaluate effects of this partial exposure but it is not very sophisticated way and for example temperature measurements will be affected by this methodology as well. In this paper we are aiming to put contactless and noninvasive methods of measurement of temperature and volume into practical use and we propose methodology and present design of microwave system for visualization.

Methods: Design of the applicator used in the visualization system had to be altered from standard design approach used in conventional applications (i.e., microwave drying, hyperthermia applications etc.). We aimed to design open applicator which could be used safely and would allow sufficient insight for the visualization equipment.

In this paper we chose to visualize microwave processing of constarch beads and evaluate obtained results by processing separate frames of produced film. Standard camera (i.e., recording in visual part of spectrum) and infrared camera served as the visualization equipment.

For processing of obtained images (from the film) we used Matlab and we were able to determine how volume of layer of cornstarch beads and its average temperature are changing. We propose that this method is suitable for many other applications (i.e., evaluation of applicators for medical procedures etc.).

Results: Results of the visualization of the microwave processing and results of evaluation of various single frames in matlab are presented. We propose that we developed suitable and simple to use method for evaluation of trends in microwave processing. In this paper we also designed microwave system for visualization which enables homogenous exposure to electromagnetic field.

Session 4P6b
Nonlinear Dynamics in Magntically Confined Plasmas and Photonic Systems: Part 1

Nonlinear Distribution Functions for Fully Ionized, Collisional, Tokamak-plasmas

Giorgio Sonnino and Philippe Peeters
Department of Theoretical Physics and Mathematics
Université Libre de Bruxelles (U.L.B.), B-1050 Brussels, Belgium

Abstract— Fully ionized L-mode tokamak plasmas in the fully collisional (Pfirsch-Schlüter) and in the low-collisional (banana) nonlinear transport regimes are analyzed. We derive the expressions for particles and heat losses together with the steady-state particle distribution functions in the several collisional transport regimes. The validity of the nonlinear closure equations, previously derived, has been indirectly tested by checking that the obtained particle distribution functions are indeed solutions of the nonlinear, steady state, Vlasov-Landau gyro-kinetic equations. A quite encouraging result is the fact that, for L-mode tokamak plasmas a dissymmetry appears between the ion and electron transport coefficients: the latter submits to a nonlinear correction, which makes the radial electron coefficients much larger than the former. In particular we show that when the L-mode JET plasma is out of the linear region, the Pfirsch-Schlüter electron transport coefficients are corrected by an amplification factor, which may reach values of order 10^2. Such a correction is absent for ions. On the contrary, in the banana regime, the ion transport coefficients are increased by a factor 2 and the nonlinear corrections for electrons are negligible. These results are in line with experiments.

Session 4P7a
Electromagnetic Simulations and Applications 2

Closed-form Green's Functions for Stratified Uniaxial Anisotropic Medium

P. P. Ding[1, 2], **S. Zouhdi**[1], **L. W. Li**[2], **and S. P. Yeo**[2]

[1]Laboratoire de Genie Electrique de Paris, Supelec, France
[2]Department of Electrical and Computer Engineering, National University of Singapore, Singapore

Abstract— The spatial-domain Green's functions for electric and magnetic fields are cast into closed forms with two-level approximation of the spectral-domain Green's functions in the stratified uniaxial anisotropic medium. The spectral-domain Green's functions for general source and observation points are derived by the wave iterative algorithm. The explicit formulations reduced to the isotropic case agrees well with the existing results corresponding to the isotropic medium. By using the discrete complex image method, the closed-form Green's functions are obtained in the spatial domain. Numerical examples show that the closed-form Green's functions in the stratified uniaxial anisotropic medium have good accuracy and efficiency.

Extended Analytical Formulation Based on Marcatili's Approach Coupled to Effective Index Method for Pedestal Waveguides: Convergence with Numerical Methods

B. Bêche[1, 2], T. Begou[1, 3], N. Grossard[4], J. Zyss[5], A. Goullet[3], and E. Gaviot[6]

[1]Institut de Physique de Rennes, IPR UMR CNRS 6251, Rennes 35042, France
[2]Institut Universitaire de France (IUF), 103 bd Saint-Michel, Paris 75005, France
[3]Institut des Matériaux Jean Rouxel, IMN-PCM UMR CNRS 6502, Nantes 44322, France
[4]Photline Technologies S. A., Besançon 25000, France
[5]IFR d'Alembert, ENS Cachan, LPQM-UMR CNRS 8537, Cachan 94235, France
[6]Laboratoire d'Acoustique, LAUM-UMR CNRS 6613, Le Mans 72000, France

Abstract— This study deals with a theoretical study of pedestal waveguides. An extension of the Marcatili method has been developed in order to adapt this analytical method to pedestal structures [1, 2]. Simulations are performed for two different T-pedestal waveguide (T-PW) configurations corresponding respectively to a high and a lower core to pedestal widths ratio. Each configuration is simulated considering two core widths (2 and 4 µm) and a core height ranging from 1 to 2 µm at a 670 nm wavelength. Then, this extended Marcatili method has been compared with methods based on various numerical approaches (finite difference and integral methods) [3, 4]. The simulation of the T-PW structure with these methods shows a good congruence since the relative differences between Marcatili's method and the numerical methods remain below some %. Then, in a second part, such an approach is applied to study the modal birefringence minimization in the case of pedestal structures. Simulations are typically performed for waveguide height and width values ranging, respectively, around (1.6–2.6) µm and (1.8–6) µm, with pedestal widths ranging around (0.4–0.8) µm, at a 670 nm wavelength. The authors stress a specific property of pedestal configurations: by judiciously adjusting the dimensional parameters (core and pedestal width and core height), the birefringence can be completely screened out.

REFERENCES

1. Marcatili, E. A. J., "Dielectric rectangular waveguide and directional coupler for integrated optics," *Bell Syst. Tech. J.*, Vol. 48, 2071–2102, 1969.
2. Begou, T., B. Bêche, N. Grossard, A. Goullet, J. Zyss, G. Jézéquel, and E. Gaviot, "Marcatili's extended approach: comparison to Semi Vectorial methods applied to pedestal waveguides design," *J. Opt. A: Pure Appl.*, Vol. 10, 055310.1–055310.9, 2008.
3. Bêche, B., J. F. Jouin, N. Grossard, E. Gaviot, E. Toussaere, and J. Zyss, "PC software for analysis of versatile integrated optical waveguides by polarized Semi-Vectorial Finite Difference Method," *Sens. Actuators: Phys. A*, Vol. 114, No. 1, 59–64, 2004.
4. Marcuse, D., "Solution of the vector wave equation for general dielectric waveguides by the Galerkin method," *IEEE J. Quantum Electron.*, Vol. 28, 459–465, 1992.

Sidelobe Reduction in Offset Dish Parabolic Antennas Using Metallic Scatters

Ali Harmouch[1], **Walid Kamali**[2], **and Chadi El Moucary**[3]

[1]Computer and Communication Department, American University of Science and Technology, Lebanon
[2]Faculty of Engineering & IT, AL Manar University of Tripoli, Lebanon
[3]Electrical, Computer and Communication Engineering Department, Notre Dame University, Lebanon

Abstract— Offset feed antennas are most commonly used for satellite applications, where very high gain is needed. The benefit of the offset configuration is that it positions the feed horn away from the dish itself so that it does not cast a shadow on the dish. However, this yields to bigger sidelobes which results in a significant interference problem especially between adjacent antennas. Adding metallic scatters (strips) to the antenna at specific positions and with specific dimensions and shapes would significantly minimize the sidelobe level and consequently enhance its directional characteristics. A detailed analysis of the suggested design was performed based on a huge series of electromagnetic simulations and testing experiments, which have clearly demonstrated a sidelobe reduction of about 15 dB.

Influence of Design Parameters on Electromagnetic Field in Coreless Stator Axial Flux Permanent Magnet Synchronous Machines

Peter Virtič
Faculty of Energy Technology, University of Maribor, Hočevarjev trg 1, Krško 8270, Slovenia

Abstract— Axial flux permanent magnet synchronous machines (AFPMSMs) can be designed for higher torque density and higher efficiency than conventional permanent magnet (PM) machines [1]. Considering thermal, mechanical and sizing constraints in the design processes the AFPMSM characteristics which are calculated on the basis of electromagnetic field can be improved by changing the design parameters. In this paper the influence of different design parameters on electromagnetic field of coreless stator AFPMSM with double external rotor has been investigated by analytical method using magnetic vector potential and validated by finite element method (FEM). Within the analytical calculation of electromagnetic field the exact derivation procedure from Maxwell's equations to the final equations in explicit form for electromagnetic field calculation in the AFPMSM application is presented. AFPMSM characteristics which are calculated on the basis of electromagnetic field solution are verified with measurements on prototype AFPMSM.

Authors in [2] proposed the impact of rotor disk thickness on performance characteristics of axial flux PM generator. Alternatively, we investigated the influence on the electromagnetic field static characteristics in AFPMSM of the following design parameters: stator and coil thickness (d_s), coil side width (d_t), angle of PMs (τ_m), inner (r_i) and outer (r_o) radius of PMs, number of turns (N) and copper wire cross-section (S_{wire}) (see Fig. 1(left)). The influence of design parameters on electromagnetic field distribution, back electromotive force and static torque of AFPMSM will be presented in full version of this paper.

Magnetic flux density, which can be calculated separately from electric field, is calculated at the centre of air-gap and centre of permanent magnet radius.

FEM analysis AFPMSM model confirms the validity of analytical method of electromagnetic field calculation according to mechanical angle (see Fig. 1(right)).

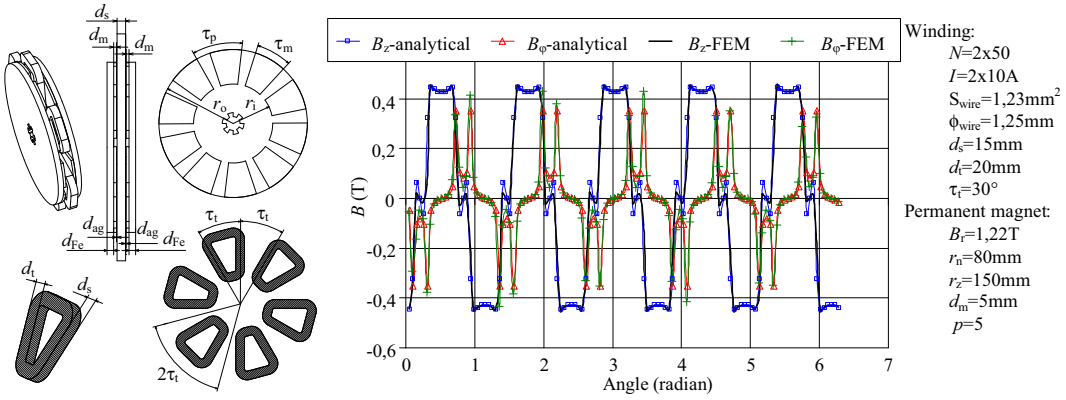

Figure 1: Left: Design parameters of AFPMSM; Right: Axial (B_z) and circumferential (B_φ) component of magnetic flux density distribution by permanent magnets — comparison between analytical and numerical method.

REFERENCES

1. Aydin, M., et al., *IEEE Transactions on Industrial Electronics*, Vol. 53, 822–830, 2006.
2. Sadeghierad, M., et al., *IEEE Transaction on Magnetics*, Vol. 45, 2032–2037, 2009.

Theory of Electromagnetic Field Calculation in Electrical Machines by Using Conformal Mapping

Peter Virtič
Faculty of Energy Technology, University of Maribor, Hočevarjev trg 1, Krško 8270, Slovenia

Abstract— Many mathematical methods exist to calculate electromagnetic field in electrical machines. Mathematical methods for electromagnetic field calculation can be in general divided into two groups, analytical method and numerical method. The most commonly used method from among numerical methods is finite element method (FEM). FEM is often used to calculate electromagnetic field if slots in the machine design have to be modelled if the machine is short with different cross-sections along the machine length. If the machine model is carefully meshed the FEM is very accurate method, but it could be very time consuming, especially when rotating rotor or optimizing the machine design. In contrast, analytical methods are not time consuming, but usually they cannot take into account all details in the machine design. The theory of electromagnetic field offers many approaches for analytical solution of electromagnetic field. Most of those approaches cannot take into account changes in the materials, i.e., slots, along the electrical machine circumference. In this paper the theory of electromagnetic field in electrical machines by using Schwarz-Christoffel Conformal Mapping (SC mapping) is presented. Moreover, this theory is confirmed by using the real example of electrical machine. The SC mapping allows a slotted structure of the machine to be mapped to a geometrically simpler domain for which analytic solutions of electromagnetic field are available. These solutions are mapped back to the original domain and thus solving the original problem.

Electromagnetic Field Analysis of an Axial Flux Synchronous Motor with Ring Permanent Magnets by Using Analytical Method

Peter Virtič and Jurij Avsec
Faculty of Energy Technology, University of Maribor, Hočevarjev trg 1, Krško 8270, Slovenia

Abstract— This paper presents magnetic field analysis of a 10-pole coreless stator axial flux synchronous motor (AFPMSM) with ring NdFeB permanent magnets by using analytical method via magnetic vector potential. For the verification, the numerical calculation (finite element method) of magnetic field is accomplished and the comparison between analytical and numerical solution of static torque and back electromotive force is presented. This article also presents that electric and magnetic field can be calculated separately in AFPMSM. Due to the magnetic linearity of permanent magnets (PM) and air-gap regions the final whole magnetic field can be obtained by the superposition of magnetic fields produced by PMs and armature current. Magnetic flux densities produced by PMs and armature current can therefore also be calculated separately. The back EMF of the AFPMSM at no-load conditions is calculated by using Faraday's law of electromagnetic induction based on the time variation of magnetic flux. The magnetic flux can be obtained through the magnetic flux density B on the cross-section surface inside the coil which has to be perpendicular to the magnetic flux path. The validity of the proposed analytical method is additionally confirmed with measurements on prototype AFPMSM. In order to obtain analytically calculated characteristics the program environment Matlab is used. Considering AFPMSM parameters obtained by analytical solution of electromagnetic field the FEM is accomplished by using Ansys program package. The main advantage of analytical method is several hundred times shorter computational time and more flexible computation in comparison to FEM. For this reason the analytical method is very efficient especially in the early stages of the machine design. FEM and measurements confirm proposed analytical method.

Session 4P7b
Computational Electromagnetics

Computational Electromagnetic Tools for EMC in Aerospace

Jesus Alvarez[1], **Salvador G. Garcia**[2], **L. Diaz Angulo**[2], **and A. Rubio Bretones**[2]

[1]Cassidian Air Systems, EADS-CASA, Spain
[2]University of Granada, Spain

Abstract— The classical Yee FDTD method has become a powerful tool in computational electromagnetics. Its application to EMC certification of aircrafts, under High Intensity Radiated Field (HIRF) conditions, is a current topic of interest in aerospace industry in order to reduce costs at the design stage.

In this work, we present the details of a high performance FDTD-based tool capable of HIRF simulation of large air vehicles, developed under the EU FP7 HIRF-SE project. The objective of this project, which joins 44 industrial and academic partners, is the creation of a synthetic environment where all kind of computational tools (FDTD, MoM, FEM, TDIE, Power Balance, TLM, ...) share a common interfacing language based in HDF Amelet, to be able to simulate totally/partially the behavior of aircrafts and rotorcrafts in a given electromagnetic scenario.

Although the FDTD method is well documented in literature, not all the published ideas are adequate enough for real life problems. The right choice of robust enhancements to deal with the specifical situations found in EMC in aeronautics, is critical to yield stable, fast and accurate simulators. Efficient techniques for the modeling of cables, composites, carbon fibber laminates, arbitrary dispersive materials, slots, etc., will be described in this work.

Parallel computing techniques for distributed memory architectures, will also be described, in the context of the development of a high performance computer FDTD simulator.

Finally, an emerging technique, the Discontinuous Galerkin Time Domain method (DGTD), will be described as a promising alternative to FDTD. The ability of DGTD to use finite element meshes, combined with its quasi-explicit time domain nature, is proven to provide a superior accuracy, at a fraction of the CPU and memory time required by FDTD to achieve the same results.

Development of a Resonant Cavity Multi-line Coupling Model and Validation Using Measurements

R. Orange[1], **P. Eudeline**[1], **S. Louis**[1], **B. Mazari**[2], **and F. Duval**[2]

[1]THALES Air Systems, ZI du Mont Jarret, Ymare 76 520, France
[2]IRSEEM, Technopôle du Madrillet, Avenue Galilée, BP 10 024, Saint-Etienne du Rouvray 76 801, France

Abstract— For several reasons, most electronic systems are set in a metal housing. Such a housing can be assimilated to a cavity and according to its dimensions and to the signal frequencies used, a resonance phenomenon occurs. This phenomenon can cause electromagnetic interferences (EMI) and therefore has to be taken into account in the design of electronic systems, especially high-frequency ones. Nowadays many software programs are able to anticipate most of the conducted or radiated EMI but EMI caused by the resonance phenomenon are not really taken into account. A need from some industries came up to create a user friendly tool able to anticipate EMI caused by the resonance phenomenon. Some methods using Kron formalism have been designed [1]. However, the tensor analysis of networks is not well known enough, so the goal of my work was to create an easy and fast method for technicians or engineers using accessible and common software programs.

The method designed consists of two simulation software programs used together. The first one is a simulation tool for 3D full-wave electromagnetic field that gets the information about the resonance phenomenon and quantifies the inter-line couplings. The second one is a 2D electronic design software for high-frequency systems that takes any components into account. To make the two software programs work together the S-parameters from the 3D software program are imported into the 2D software program. The method enables to quantify the inter-line coupling and to test claddings, substrates, or to place the lines in a different way to know the effects of these parameters on the system functioning. This information helps to find solutions to solve disturbance problems. Since the tool is based on software programs, the results had to be checked by measurements. The simulated system has been recreated to compare the results provided by the simulation to the measurements in order to know in what extent the simulation tool is relevant.

REFERENCES

1. Leman, S., B. Demoulin, O. Maurice, M. Cauterman, and P. Hoffman, "Simulation d'une cavité EM par réduction de circuits électriques couplés formant une super matrice impédance," *14ème Colloque International de Compatibilitè Electromagnètique (CEM'08)*, Paris, May 2008.

Source Identification in Time Domain Electromagnetic — Application to Focusing Problem

J. Benoit[1, 2], **C. Chauvière**[1, 3], **and P. Bonnet**[1, 2]

[1]LASMEA, Clermont University, Blaise Pascal University, Clermont-Ferrand, France
[2]CNRS, UMR 6602, LASMEA, Aubière, France
[3]CNRS, UMR 6620, LM, Aubière, France

Abstract— Time reversal method was first introduced by M. Fink in acoustic [1]. This method consists in saving a signal and resending it in a reverse order in order to obtain a focus at the emission point. This method can also be applied in the electromagnetism domain [2]; the reversed signal has some interesting property, which can be useful for medical and military applications. Time reversal method includes two steps. First, a source emits electromagnetic waves which spread in the entire medium. Saving of this electromagnetic signal after different refractions is made thanks to reception antennas. During the second step, each reception antenna emits the received signal following an inverse chronology. It gives both temporal and spatial focusing at the original source point.

In this study, we propose an original approach which avoids the first step of the time reversal method. This new method consists in solving a linear problem in order to find the required source to obtain a temporal and spatial focusing. The first numerical results, obtained by using a Finite-Difference Time-Domain (FDTD [3]) code, are promising (for example method gives better focusing and signal to noise ratio). The method was validated in one and two dimensions and compared with time reversal method. It appears that this new method can also find a source to obtain any electromagnetic field configuration.

In the final work, a presentation of the new method will be done and construction of the linear problem to be solved will be explained. Resolution method will also be presented and, finally, results of the comparison with time reversal method will be given.

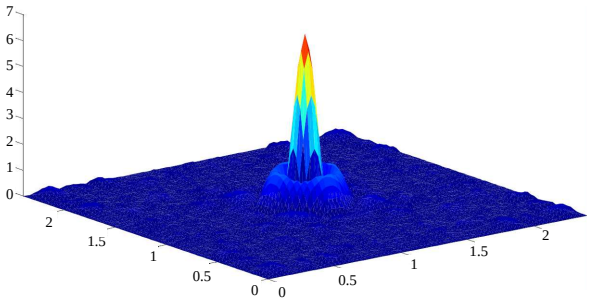

Figure 1: Error between electric target field and electric field obtained with new method.

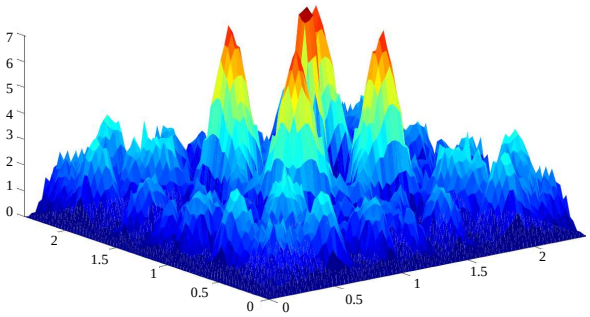

Figure 2: Error between electric target field and electric field obtained with time reversal method.

REFERENCES

1. Fink, M., "Time reversal of ultrasonic fields: Part I. Basic principles," *IEEE Trans. Ultrason. Ferro-elect. Freq. Control*, Vol. 39, No. 5, 555–566, Sept. 1992.
2. El Baba, I., et al., "Electromagnetic time-reversal for reverberation chamber applications using FDTD," *Inter. Conf. on Adv. In Comp. Tools for Eng. App.*, 157–162, Lebanon, July 2009, ISBN 978-1-4244-3833-4.
3. Yee, K. S., "Numerical solution of initial boundary value problems involving Maxwell's equations in isotropic media," *IEEE Trans. Antennas Propagat.*, Vol. 14, 302–307, May 1966.

An Efficient Computational Method Based on Current Measurements for Fields Radiated by a Thin Antenna or a PLC Line

M. Chaaban[1], **K. El khamlichi Drissi**[1], **C. Pasquier**[1], **and A. Ismail**[2]

[1]Blaise Pascal University LASMEA, 24 Avenue des Landais, Aubière 63177, France
[2]Lebanese University, IUT Saida, BP813, Saida, Lebanon

Abstract— Although the PLC system is being improved continuously, there are still concerns regarding emission and immunity level and standardization. These issues are of great importance since PLC operates in an environment already populated by other services at the same frequencies, so that fair co-existence is needed. Simulating the complete PLC network or any significant part of it using numerical techniques, such as the Method of Moments (MoM), is proved to be of limited practical use due to the fact that PLC networks extend over many wavelengths. In this paper we propose an experimental method for the assessment of near and far field respectively radiated by a PLC line.

An integral formulation based on the wire antenna theory is implemented to study the radiation mechanisms of a wire configuration. For a given current distribution; the radiated field is expressed via the vector potential $\vec{A}_M(s) = \frac{\mu}{4\pi}\int_0^L \frac{I(s,z_0)\cdot e^{-\gamma_0(s)\cdot R(z_0)}}{R(z_0)} dz_0\vec{z}$ where $I(z_0,s)$ is the current distribution along the conductor, $s = j\omega$ is the Laplace variable, $R = \sqrt{\rho^2 + (z-z_0)^2}$ the distance between the elementary dipole and the observation point M, $\gamma_0(s) = j\beta_0 = \frac{s}{c}$ is the propagation constant in free space.

In realistic scenarios it is hard to measure the radiated field. We may measure the value of the field at a certain measurement point. The principle of this method is based on the current measurement being much easier than the field measurement. From the measured values, the geometry of the PLC line and the position of observation point, we may evaluate the radiated field at an arbitrary point. Later, the known current distribution is extrapolated with Matrix Pencil (MP) algorithm and replaced by a set of poles and residues.

$$I(z) = \sum_{i=1}^{M} R_i\, Z_i^k \text{ for } k = 1, 2, \ldots, N-1 \text{ and } Z_i = e^{s_i T_s} \text{ for } i = 1, 2, \ldots, M$$

Thus, the current distribution is represented in the form of exponentially damped sinusoids. Their current values are introduced into the Frequency Domain (FD) code based on the antenna model. This may be very useful in order to compute the radiated field in far and near zones with significantly less computational time.

The integral formulation derived from the antenna theory related to a code developed within this work allows the representation of EM field radiation at any observation point in free space. The main contribution we propose in this model is the Integral formulation able to compute the field in the near zone. The survey of the literature shows that it is almost impossible to find analytical formula to calculate the field at close range area.

Therefore, whatever the mode of propagation in the line is, we consider the current in the line to be known and obtained by measurement and extrapolated with MP algorithm. Subsequently the vector potential is expressed by $\vec{A}_M(s) = \frac{\mu}{4\pi}\sum_{i=1}^{M} R_i \int_0^L Z_i \frac{\cdot e^{-\gamma(s)\cdot R(z_0)}}{R(z_0)} dz_0\vec{z}$ using Matrix pencil algorithm.

Multi-GPU Accelerated Finite-difference Time-domain Solver in Open Computing Language

T. P. Stefanski[1, 2], **N. Chavannes**[3], **and N. Kuster**[2]

[1]ETH Zurich, Integrated Systems Laboratory, Gloriastrasse 35, Zurich 8092, Switzerland
[2]IT'IS Foundation, Zeughausstrasse 43, Zurich 8004, Switzerland
[3]SPEAG Software R&D, Zeughausstrasse 43, Zurich 8004, Switzerland

Abstract— Recently, Graphics Processor Units (GPUs) became a source of a cheap computational power for the acceleration of the finite-difference time-domain (FDTD) method [1]. Unfortunately, existing GPU accelerated FDTD codes do not fully utilize the computational power of the multi-core central processing units (CPUs), which are present in most computers today. Recent progress in microprocessor technology shows that both processing technologies, i.e., GPUs and CPUs, will soon be integrated within single-die chips. In general, due to scaling of the processor parallelism according to Moore's law, development of scientific codes being scalable and portable between available and future hardware architectures is a real challenge. These facts motivates our investigations focused on applications of novel parallel programming technologies in computational electromagnetics.

Open Computing Language (OpenCL) [2] seems to be a remedy for overcoming the above mentioned challenges, as it maintains portability between hardware architectures and efficiency of the low-level programming interface. OpenCL is a framework for parallel programming of heterogeneous platforms consisting of multi-core CPUs, GPUs, and other modern processors. This standard opens the way to build heterogeneous computing systems which may simultaneously deploy the computational power of multicore CPUs and GPUs for the tasks best suited to them.

In this contribution we present results of evaluation of the multi-GPU OpenCL FDTD code. Multi-GPU implementations are necessary not only to speed up computations but also to aggregate relatively small GPU memories. In our implementation, the computational domain is decomposed along the slowest direction and electromagnetic field boundary data is shared between neighboring subdomains allocated on different GPUs. The communication overhead between GPUs is proportional to the area of the boundary and represents the rate-limiting step of the method. Portability and efficiency of the developed code were tested on double CPU machine supported by several GPUs. We found that for the utilized hardware devices, communication overhead can be hidden by computations for sufficiently large simulation domains, giving scaling efficiency higher than 90%. Direct porting of the OpenCL code dedicated to GPUs on multi-core CPU does not give satisfactory performance due to the application of architecture specific features in the GPU code. Therefore, OpenCL kernels of the related FDTD code were optimized to improve performance on multi-core CPUs. Despite that, the OpenCL FDTD implementation on CPU was about 1.5 times slower than a commercially available FDTD solver developed in the OpenMP standard. Subsequently, the paper presents applications of the developed multi-GPU OpenCL FDTD code to solve real-life problems of computational electromagnetics in order to demonstrate its performance, accuracy and applicability.

The study concludes that although the OpenCL FDTD simulations perform at a slightly lower speed than native CUDA or OpenMP implementations, it allows the building of multi-GPU code that is portable between devices manufactured by different vendors and executable on modern multi-core CPUs. Therefore, it can be anticipated that the OpenCL framework will increase in popularity in coming years, and might become the standard with respect to parallel programming.

REFERENCES

1. Krakiwsky, S. E., L. E. Turner, and M. M. Okoniewski, "Acceleration of finite-difference time-domain (FDTD) using graphics processor units (GPU)," *2004 IEEE MTT-S Int. Microwave Symp. Dig.*, 1033–1036, 2004.
2. The OpenCL Specification, ver. 1.0, Khronos OpenCL Working Group, electronic file available at: http://www.khronos.org/registry/cl/specs/opencl-1.0.48.pdf, 2009.

Electromagnetic Total Scattering Cross Section from Reverberation Chamber Simulations in Time Domain

I. El Baba[1, 2], **S. Lalléchère**[1, 2], **and P. Bonnet**[1, 2]

[1]LASMEA, Clermont University, Blaise Pascal University, Clermont-Ferrand, France
[2]CNRS, UMR 6602, LASMEA, Aubiere, France

Abstract— The Mode Stirred Reverberation Chamber (MSRC) has become more and more popular since the last fifteen years, mainly for ElectroMagnetic Compatibility (EMC) testing [1]. Under specific conditions, a system placed in the working volume of the MSRC is irradiated by an infinite number of plane waves (random polarization and incidence) [2]. In this study, we adapt the formalism [3] to compute the Total Scattering Cross Section (TSCS) of various objects in MSRC. Theoretically the TSCS measurements need both a free-space environment (for instance anechoic chamber modeled numerically by absorbing boundary conditions) and various plane waves stimulations. The method developed allows predicting the TSCS from few simulations in a MSRC by averaging electric field measurements respectively over various sources/probes and over different target locations. This process enables to define the C ratio with respect to the simulated time t from the MSRC intrinsic damping time τ_s following

$$C(t) = e^{-t/\tau_s} \tag{1}$$

Regarding the relation (1), the TSCS is deduced from τ_s following [3]. The foundations and numerical results presented will demonstrate the ability of the technique to straightforward compute the TSCS with the Finite Difference Time Domain (FDTD) method. The numerical experiments are achieved in a single 2-D MSRC whose walls are designed with Perfect Metallic Conductors (PEC) conditions jointly with lossy materials (conductivity s_v) to model Q-factor (MSRC losses).

Although the decay of the electric field is partially due to the target (diffusion) as depicted by (1), the TSCS appeared relatively independent from MSRC losses (Fig. 1). In the final work, the validity and an illustration of the method will finally be given by comparing results from free-space simulations with ones obtained from FDTD simulations in MSRC.

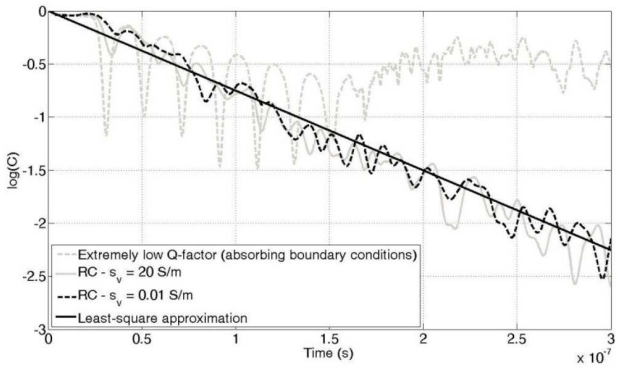

Figure 1: Evaluation of the C ratio (step of the SCS computation).

REFERENCES

1. Corona, P., J. Ladbury, and G. Latmiral, "Reverberation-chamber research — Then and now: A review of early work and comparison with current understanding," *IEEE Trans. Electromagn. Compat.*, Vol. 44, 87–94, 2002.
2. Hill, D., "Plane wave integral representation of fields in reverberation chambers," *IEEE Trans. Electromagn. Compat.*, Vol. 40, No. 3, 209–217, 1998.
3. Lerosey, G. and J. De Rosny, "Scattering cross section measurement in reverberation chamber," *IEEE Trans. Electromagn. Compat.*, Vol. 49, No. 2, 280–284, May 2007.

Artificial Neural Network Modeling of Synchronous Reluctance Motor

Primoz Bajec[1], **Bogomir Zidaric**[1], **and Damijan Miljavec**[2]

[1]Hidria Institute for Materials and Technologies d.o.o., Slovenia
[2]Faculty of Electrical Engineering, University of Ljubljana, Slovenia

Abstract— The work handles with the application of artificial neural networks (ANN) in modeling of the synchronous reluctance motor. Motor geometry, used materials and excitation level dictate the motor performance. Mutual relations between these parameters were investigated due to some simplifications of model multidimensionality. To overcome the model complexity a proper ANN topology and data presentation to ANN were established. Final form of the non-linear model was achieved by joining all trained ANN. Model output results define the magnetic flux density distribution along the air-gap for both d- and q-mode excitations and specific motor geometry. The comparison between ANN model results and finite element calculations confirms the feasibility of use of established non-linear model for further investigation of SRM performance.

Session 4P8
Earth Electromagnetic Environment and Radiowaves Propagation & Scattering: Modelling, Method, Observation and Measurements

HF Ground Wave Propagation over a Randomly Rough Sea Surface

C. Bourlier[1] and G. Kubické[2]

[1]IREENA Laboratory, University of Nantes, France
[2]DGA-MI, CGN1 Division, France

Abstract— For a vertically polarized line source, in the context of HF (3–30 MHz) ground wave propagation over a curved rough sea surface, this paper presents different analytic and rigorous methods to compute the attenuation function related to the ground wave. Then, fast rigorous numerical methods, like the BMIA-CAG (Banded-Matrix-Iterative Approach CAnonical-Grid) and FB-SA (Forward-Backward Spectral-Acceleration) methods, based on the Method of Moments (MoM), are compared and used as benchmark methods to validate analytical asymptotic approaches (works of Bremmer and Wait) by including the surface roughness.

Introduction: There are many problems in communications, navigation, and applied geophysics, in which the system performance is dependent of the electromagnetic ground wave, which has the fundamental property to propagate over a very long distance near the surface. As addressed in the reviews of Wait [1] and Collin [2] (and references therein), in the last century, many asymptotic theories were developed to solve this issue. Recently, for a flat Earth, Bourlier et al. [3] thoroughly studied the ground wave propagation over a one-dimensional rough sea surface from the BMIA-CAG efficient rigorous numerical method, based on the MoM. In addition, the comparison of the closed-form asymptotic expression of Collin [2], valid for a smooth surface and modified by the roughness from the Barrick [6] and Ishimaru [7] works, with the BMIA-CAG showed good agreement for emitter and receiver heights small in comparison to the electromagnetic wavelength. One of the purposes of this paper is to extend the previous works of Bourlier et al. in order to take the Earth curvature into account in the computation of the ground wave propagation. Then, the BMIA-CAG and FB-SA [5] fast numerical rigorous methods are applied to validate different closed-form [1, 8] expressions of the attenuation function obtained from simplifying assumptions. In addition, from a partial fraction expansion of the attenuation function in the Laplace domain, the Bremmer asymptotic expansion [8] is extended to any order and by including the surface roughness. This allows us to express the attenuation function as a sum of flat-Earth attenuation functions.

REFERENCES

1. Wait, J. R., "The ancient and modern history of EM ground-wave propagation," *IEEE Ant. Prop. Mag.*, Vol. 40, No. 5, 7–39, 1998.
2. Collin, R. E., "Hertzian dipole radiating over a lossy earth or sea: Some early and late 20th-century controversies," *IEEE Ant. Prop. Mag.*, Vol. 46, No. 2, 64–79, 2004.
3. Bourlier, C., G. Kubické, and Y. Brelet, "Rigorous prediction of the ground wave above flat and rough highly-conducting one-dimensional sea surfaces in VHF band," *IEEE Trans. Ant. Prop.*, in press.
4. Tsang, L., C. H. Chang, and H. Sangani, "A banded matrix iterative approach to Monte Carlo simulations of scattering of waves by large scale random rough surface problems: TM case," *Electron. Lett.*, Vol. 29, 1666–1667, 1993.
5. Chou, H. T. and J. T. Johnson, "A novel acceleration algorithm for the computation of scattering from rough surfaces with the forward-backward method," *Radio Science*, Vol. 33, 1277–1287, 1998.
6. Barrick, D. E., "Theory of HF and VHF propagation across the rough sea, 1, The effective surface impedance for a slightly rough highly conducting medium at grazing incidence," *Radio Science*, Vol. 6, No. 5, 517–526, 1971.
7. Ishimaru, A., J. D. Rockway, Y. Kuga, and S.-W. Lee, "Sommerfeld and Zenneck wave propagation for a finitely conducting one-dimensional rough surface," *IEEE Trans. Ant. Prop.*, Vol. 48, No. 9, 1475–1484, 2000.
8. Bremmer, H., "Applications of operational calculus to ground-wave propagation, particularly for long waves," *IRE Trans. Ant. Prop.*, Vol. 6, No. 3, 267–272, 1958.

The Physical Mechanism of the Lightning Return Stroke Initiation Point as an Electromagnetic Source

Robert L. Gardner
6152 Manchester Park Circle, Alexandria, VA 22310-4957, USA

Abstract— The lightning return stroke begins when a downward propagating leader (stepped or dart) reaches within a few meters of the ground and connects with an upward propagating leader. This joining of non neutral plasma columns is an extremely energetic and complex event requiring an understanding of the behavior of several charged and charged species at temperatures up to a few electron volts, rapidly changing electric fields of several megavolts/meter and charge transfer of several coulombs in a few microseconds. This region is important in understanding lightning because it is the source of much of the high frequency content of the radio-frequency emission of the return stroke.

Longmire et al. [1], proposed a propagation mechanism for streamer propagation in neutral plasma appropriate to a nuclear lightning environment. The model assumed a conducting streamer that formed when the enhanced fields around the streamer tip reached the air avalanche field. A three species air chemistry model was used along with thermal reservoirs for molecular heating along with neutral and ionized atoms representing oxygen and nitrogen. The model suggested a propagation velocity of 10^5 m/s, consistent with photographs of nuclear lightning, but substantially below that of natural lightning, so work began to understand the initial conditions for a similar model for the natural lightning environment.

Natural lightning leader processes can lower several coulombs of charge into a column that eventually becomes the return-stroke channel. That charge has to wait while the full channel forms and the charges attach to air molecules under those low field conditions forming species like 0^2-. These heavy species are not very mobile and move at velocities much lower than the electron drift velocity of about 10^5 m/s. The like charges repel each other and spread the charge out first as free electrons then as charged molecules as the electric fields get lower than the air avalanche value. Analytic and numerical models were developed to show the charged-species channel expansion. This model showed a column of charge that expanded to about a meter in diameter and consisted of relatively evenly spaced charged species [2].

Work with the Longmire model described above showed that calculation of individual electron dynamics were required near the tip so that the mechanism of this type of model is shown in this paper. A model is shown in which an avalanche field propagates away from the joining point near the speed of light, stripping the electrons from the ions allowing the electrons to move quickly. The dynamics of those electrons form the early part of the return-stroke current and, in particular, the high-frequency fields. The final model is similar to the Longmire model but has a flow of electrons through the avalanche boundary.

REFERENCES

1. Longmire, C. L., et al., *Physics of Fluids*, Vol. 27, 2694, 1984.
2. *Proceedings of the International Conference on Electromagnetics in Advanced Applications*, Sydney, September 2010.

Real-time Correction of Distributed Ionospheric Model by OTHR Coordinate Registration Based on Sea/Land Transition Identification: Method Outline

Luca Facheris, **Fabrizio Cuccoli**, **and Francesco Sermi**
Dipartimento di Elettronica e Telecomunicazioni, U. O. CNIT
Via di Santa Marta, Firenze 3-50139, Italy

Abstract— Knowledge of the ionospheric status is fundamental for a wide range of civil and military applications that employ this medium as part of the transmission channel (e.g., HF communications, Over The Horizon Radar (OTHR) sensors, satellite positioning, navigation systems, etc.).

Typically, such applications make use of seasonal (or climatological) ionospheric models that unfortunately account only for the long-term variations, sometimes periodically updated with real-time data gathered by ionosondes that are able to account for short-term ionospheric phenomena. This approach is mainly limited by the need of considering a wide geographic area, while relying on a small ionosonde network. We propose a method to employ an OTHR sky wave (SW) pulsed, monostatic system as a wide area ionospheric sensor for the real-time correction of the ionospheric model.

Recently we introduced a coordinate registration (CR) method for an OTHR SW sensor based on the identification of Sea/Land transitions (SLTI). The method was outlined, implemented and tested in a simplified scenario and the requirements were highlighted for its applicability, in terms of minimum Clutter-to-Noise Ratio (CNR) and of Sea/Land backscattering coefficients difference. Besides its direct use for the correction of the OTHR antenna footprint position in range, the SLTI method can indeed be adapted to estimate the current ionospheric parameters.

According to the specifications and the long-term model provided by the *International Reference Ionosphere* (IRI-2000) and with the parameterization and correction criteria introduced by the *Real time Simplified Ionospheric regional model updating* (SIRMUP), we identify in f0F2 (Peak Critical frequency for the F-region) and MUF(3000)F2 (Maximum Usable Frequency for a 3000 km single hop refraction off the F2-layer) the parameters to be estimated and then corrected in the adopted model.

By estimating the range error in the OTHR footprint position through the identification of a geographically known reference feature (namely, the sea/land transition), we can identify the actual [f0F2, MUF(3000)F2] couple that characterizes the electron density profile in the specific operating area. The SIRMUP model then gets the corrected profile as a new data input from ionosonde and applies the correction to the distributed model.

In the paper, after having introduced the ionospheric modeling problem, we provide an overview of the OTHR simulated scenario, with particular reference to the OTHR, Ionosphere and clutter models. A brief description follows of the CR method proposed for OTHR-SW system and of its evolution for the estimate of ionospheric parameters. Some simulations in different operative conditions are then described and some result and possible future developments of the method are discussed.

Design of Air Gap and Slotted Microstrip Antenna with Capacitive Feed for Wideband Applications

Malay Ranjan Tripathy[1], **Pawan Kumar**[2, 3], **H. P. Sinha**[3], **and Rachid Talhi**[4]

[1]Department of ECE, JIET, Jind, Haryana, India
[2]Department of ECE, SDITM, ISRANA, Panipat, Haryana, India
[3]Department of ECE, MM University, Mulana, Haryana, India
[4]University of Tours and CNRS, UMR 6115, Orleans 45071, France

Abstract— With the development of wireless communication it is desired to design light weight, low profile, wideband frequency planar configuration antennas. Such antennas would simplify the installation of wideband system. Microstrip antennas have been widely used due to their advantages like low cost, light weight, planner configuration and small in size. However narrow bandwidth and low gain are the main disadvantages of microstrip antennas [1–3]. Several methods for obtaining wideband characteristics have been developed. The wideband frequency operation can be realized by using low dielectric constant substrates, multilayer structures and using slots on the patches. For increasing the impedance bandwidth and gain of the antenna, air gaps have been used between the layers of the antennas [4–7].

The proposed antenna design approach is based on the two types of the rectangular patches. One patch is slotted rectangular patch and other is small rectangular patch which is used for the coaxial probe feed. The separation of rectangular slotted patch and small rectangular feed patch is 0.5 mm. The air gap between the ground plane and the substrate containing patches is 6.0 mm. The dielectric constant, thickness and loss tangent of the substrate are 2.2, 1.5 mm and 0.0004 respectively. The proposed antenna shows the return loss below −10 dB in the frequency range from 4.5 GHz to 6.3 GHz as shown in Figure 1. The maximum directive gain and VSWR are seen to be more than 6.2 dBi and less than 1.5 respectively.

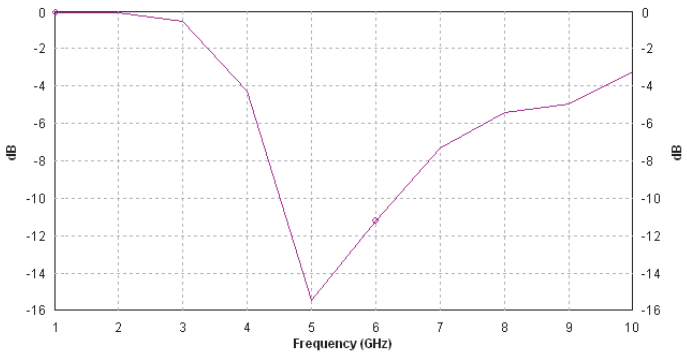

Figure 1: Return loss with frequency.

REFERENCES

1. Balanis, C. A., *Antenna Theory: Analysis and Design*, John Wiley & Sons, Inc., USA, 2005.
2. Wong, K. L., *Compact and Broadband Microstrip Antenna*, John Wiley & Sons, Inc., New York, NY, 2002.
3. Garg, R., P. Bhartia, and A. Ittipiboon, *Microstrip Antenna Design Handbook,* Artech House, Bosten, London, 2001.
4. Ghassemi, N., J. Rashed-Mohassel, S. Mohanna, and G. Moradi, "Aperture coupled microstrip antennas for S and c bands," *Microwave and Optical Technology Letters*, Vol. 51, No. 8, 1807–1809, Aug. 2009.
5. Ray, K. P., V. Sevani, and S. Kakatkar, "Compact broadband gap coupled rectangular microstrip antennas," *Microwave and Optical Technology Letters*, Vol. 48, No. 12, 2385–2388, Aug. 2007.
6. Wi, S.-H., Y.-S. Lee, and J.-G. Yook, "Wideband microstrip patch antenna with U-shaped parasitic element," *IEEE Trans. Antennas and Propagation*, Vol. 55, No. 4, 1196–11999, Apr. 2007.
7. Ghassemi, N., J. Rashed-Mohassel, and M. H. Neshati, "A new ultra wideband aperture coupled microstrip antennas," *Microwave and Optical Technology Letters*, Vol. 51, No. 1, 259–260, Jan. 2009.

Calibration of Earth Atmosphere for Radio Science Experiments

Sami Asmar and Kamal Oudrhiri
Jet Propulsion Laboratory, California Institute of Technology, USA

Abstract— Radio Science experiments utilize radio links on spacecraft in the solar system to investigate changes in the electromagnetic signal characteristics (phase, amplitude, or polarization) to study various geophysical phenomena. Planetary atmospheres are investigated via radio occultations and planetary gravity (and subsequent modeling of planetary mass distribution and interior structure) are investigated via precision Doppler tracking with contribution from ranging. Practically all NASA and ESA deep space missions that have visited planetary systems have conducted Radio Science experiments and all of them have one challenge in common, the proper calibration of the effects of interplanetary plasma and Earth atmosphere from the data. When possible, dual wavelength links (e.g., S-band and X-band, or X-band and Ka-band) are used to differentially isolate the effect of all charged particle effects, including the Earth ionosphere. Advanced Water Vapor Radiometers that co-track the spacecraft with the receiving large antennas of the Deep Space Network provide data to calibrate the Earth troposphere by measuring the path delay. Special Radio Science open-loop receivers capture the incoming RF signal for flexibility in post-processing by the science user, as compared to the closed-loop receiver that creates a real-time Doppler profile. This paper will present an overview of Radio Science experiments to date, recent discoveries in planetary science, as well as the development of the calibration schemes and their typical results on data quality. Examples will be presented from recent missions and concepts for further improvements in the future will be discussed.

Review of Perturbations Induced by Powerful VLF Ground-based Transmitters in the Ionosphere

M. Parrot
LPC2E/CNRS, 3A Avenue de la Recherche Scientifique, 45071 Orléans cedex 2, France

Abstract— This paper is a review of ionospheric observations related to powerful VLF transmitters. Waves and plasma parameters are recorded by the low orbiting satellite DEMETER.

First, the ionospheric perturbations of NWC in Australia will be presented. It is one of the most powerful VLF transmitters in the world. Electrostatic waves from HF to ELF ranges are generated and strong turbulence appears. Fluctuations of electron and ion densities are observed as well as increase of temperature. The perturbations are well located to the geographic North of the transmitter and cover a surface of $\sim 500,000\,\mathrm{km}^2$. This area is centred at the altitude of the satellite (700 km) around the magnetic field line which has a foot at the location of the transmitter. This phenomenon is due to the electron and ion heating of the ionosphere induced by the powerful transmitter VLF wave. A much smaller effect is also observed in the Northern hemisphere at the conjugated location. This ionospheric perturbation observed for the first time is in addition to the already known precipitation of the energetic particles which interact with the VLF wave of the transmitter through a cyclotron resonance mechanism. NAA in US which has the same power as NWC is located at a much higher L value (3.0). Ionospheric perturbations from this transmitter are also detected although intense natural noise is present in this sub-auroral area.

Second, in the MF frequency range, the data of an electric field antenna are recorded up to 3 MHz and global maps of the Earth reveal a persistent wave activity at MF frequencies above the location of ground-based VLF transmitters. It is shown that it is due to the perturbation of the ionosphere by these transmitters which produce ionospheric irregularities. Whistler waves generated by lightning strokes can therefore penetrate trough the ionosphere at MF frequencies at the location of these VLF transmitters.

Third, the paper will show various perturbations of their signals when they cross the ionosphere and are observed by the satellite. It includes spectral broadening, apparition of sidebands, and triggered emissions.

System for Measuring Rain Attenuation in Terahertz Wave Ranges

S. Ishii, T. Kamei, and S. Sayama
National Defense Academy, Japan

Abstract— The recent advances in electronic and electro-optical terahertz devices, and improvements to system technology, have stimulated imaging and sensing applications in the security and non-destructive testing field. Therefore, terahertz technologies that enable imaging and remote-sensing applications in fields that are safe and secure are essential to maintain a comfortable and protected society.

Rain attenuation is one of the most serious obstacles to overcome for imaging and sensing systems to detect hazardous things using microwave and also terahertz waves because of its masking action. Raindrop-size distributions have been found to play an important role in monitoring rainfall and in predicting rain attenuation. Rain attenuation is particularly severe and greatly dependent on various models of raindrop-size distribution in millimeter- and terahertz-wave systems.

Figure 1 outlines the new system for measuring rain attenuation in terahertz wave ranges we designed, which consists of a transmitter, detector, interface, rain-intensity gauge, and ancillary devices such as a thermometer and data-logger/controller. The transmitter and detector use a corrugated conical horn feeding an off-axis elliptical mirror to collimate beams, yielding a directivity of 50 dB. The transmitter has approximately +8 dBm of output power at terahertz wave ranges, and was pulse modulated at 12 kHz using a TTL signal. The terahertz wave transmitter is driven by a phase locked oscillator (PLO) that is oscillated by the dielectric resonant oscillator (DRO) and locked to the 100 MHz of the reference oscillator. The PLO output is then quadrupled and then amplified using a MMIC amplifier to a power level of approximately 1 W. A cascade of three varactor frequency doublers (VFD) are used to convert the amplifier output to the terahertz wave range. The propagated terahertz wave signal is received by a zero-bias Schottky diode detector, and the output voltage is amplified by a low-noise video amplifier followed by a 12-kHz band pass filter (BPF) to reduce the noise bandwidth. The system collects the data on the receiving level, temperature, and rainfall rate, and these are then digitized by an analog-to-digital converter.

Rain attenuation at the terahertz wave range is measured, which is also calculated by using four raindrop-size distributions and the ITU-R specific attenuation model. The calculated results are compared with propagation experiments under a rainfall rate up to approximately 25 mm/hr.

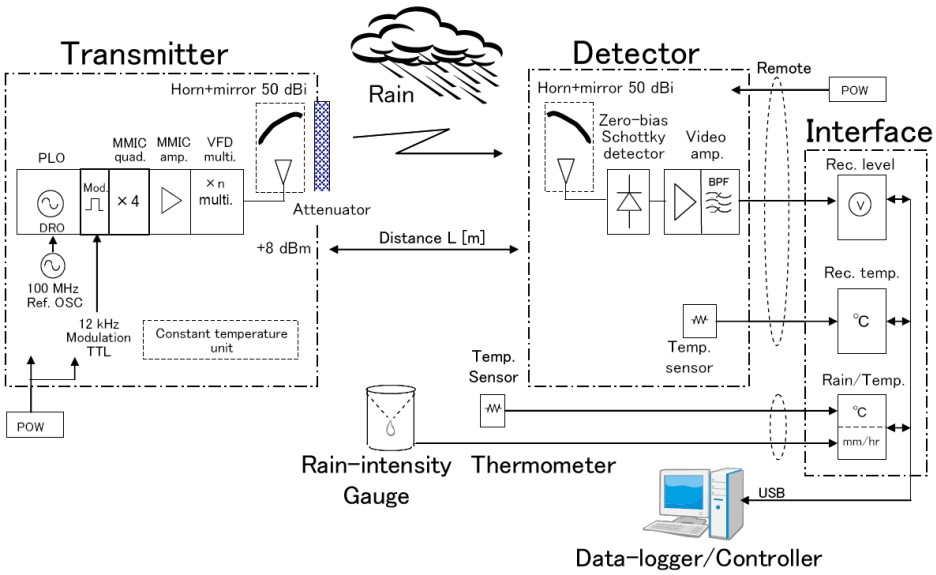

Figure 1: System for measuring rain attenuation in terahertz wave ranges.

Author Index